Abdelazim M. Negm
Rawya Y. Rizk
Rehab F. Abdel-Kader
Asmaa Ahmed   *Editors*

Engineering Solutions Toward Sustainable Development

Proceedings of 1st International Conference on Engineering Solutions Toward Sustainable Development

Springer

Earth and Environmental Sciences Library

Series Editors

Abdelazim M. Negm, Faculty of Engineering, Zagazig University, Zagazig, Egypt

Tatiana Chaplina, Antalya, Türkiye

Earth and Environmental Sciences Library (EESL) is a multidisciplinary book series focusing on innovative approaches and solid reviews to strengthen the role of the Earth and Environmental Sciences communities, while also providing sound guidance for stakeholders, decision-makers, policymakers, international organizations, and NGOs.

Topics of interest include oceanography, the marine environment, atmospheric sciences, hydrology and soil sciences, geophysics and geology, agriculture, environmental pollution, remote sensing, climate change, water resources, and natural resources management. In pursuit of these topics, the Earth Sciences and Environmental Sciences communities are invited to share their knowledge and expertise in the form of edited books, monographs, and conference proceedings.

Abdelazim M. Negm · Rawya Y. Rizk ·
Rehab F. Abdel-Kader · Asmaa Ahmed
Editors

Engineering Solutions Toward Sustainable Development

Proceedings of 1st International Conference
on Engineering Solutions Toward Sustainable
Development

Springer

Editors
Abdelazim M. Negm 🆔
Water and Water Structures Engineering
Department, Faculty of Engineering
Zagazig University
Zagazig, Egypt

Rehab F. Abdel-Kader 🆔
Faculty of Engineering
Port Said University
Port Fouad, Egypt

Rawya Y. Rizk 🆔
Faculty of Engineering
Port Said University
Port Fouad, Egypt

Asmaa Ahmed 🆔
Faculty of Engineering
Port Said University
Port Fouad, Egypt

Preface

It is with great pleasure that we present this conference book, showcasing research articles presented at the **"First International Conference on Engineering Solutions Toward Sustainable Development."** This conference book focuses solely on engineering solutions that promote sustainable development, encompassing the latest trends and advancements in sustainable engineering practices. Engineering Solutions Toward Sustainable Development (ESSD) is a comprehensive guide for engineers and professionals interested in sustainable development, covering a wide range of topics, including renewable energy, green building design, water conservation, and waste management. With practical examples and case studies, readers will learn how to apply engineering principles to develop sustainable solutions that balance economic, social, and environmental needs. Written by experts in the field, this book is a must-read for anyone interested in creating a sustainable future for our planet. The book takes an interdisciplinary approach, combining insights from engineering, environmental science, social science, and other relevant fields to comprehensively understand sustainable development, their challenges and proposed solutions.

The selected articles in ESSD reflect the high quality of research work accepted and presented at the conference, highlighting the innovative approaches and cutting-edge technologies researchers employ worldwide. The contributions cover various parts, addressing various challenges and opportunities in engineering solutions for sustainability.

The first part presented in this book is **"Clean Energy"**. Within this part, researchers examined the advancement of renewable energy sources, such as solar, wind, and hydroelectric power, to reduce our dependence on fossil fuels and lower greenhouse gas emissions. Another area of investigation is energy storage technologies, which can enhance the stability and reliability of renewable energy systems. Additionally, exploring sustainable urban planning and smart grid technologies is essential to optimize energy consumption, reduce waste, and foster environmentally friendly communities. Other research investigates bioenergy, including biofuels that play a crucial role in achieving sustainable energy solutions. Moreover, understanding and improving the life cycle assessment of clean energy technologies ensures that these technologies' overall environmental impacts are minimized.

The part **"Clean Water"** focuses on diverse studies related to water distillation, wastewater treatment, and environmental sustainability. Addressing water scarcity challenges through water reuse and desalination technologies is a critical area of research in this part. Research in this area focuses on developing efficient and eco-friendly treatment methods to remove pollutants and pathogens from wastewater before its safe release or reuse. Another research topic investigated in this part is sustainable water resource management aimed at developing innovative strategies to conserve and protect water sources, ensuring a reliable and clean water supply for present and future generations.

"Climate Action" is another part covered in ESSD, presenting research investigating climate-resilient infrastructure design: developing engineering practices to design and retrofit infrastructure, such as communities, buildings, and universities, to withstand changing climate conditions.

The part **"Smart Cities and Communities"** encompasses many critical topics aimed at harnessing technological advancements to create environmentally friendly and efficient urban environments. This includes recent technologies, concepts, and trends involved in green and sustainable building practices required to maximize resource efficiency, minimize environmental impact, and foster a high quality of life. One of the key areas of investigation is the development and integration of smart infrastructure and Internet of things (IoT) technologies to optimize energy consumption, resource management, communication systems, and healthcare services. Research also focuses on implementing data analytics and artificial intelligence to monitor and manage resources effectively. Another research area is the study of citizen engagement, participatory governance, and risk management in smart cities.

The final part of **"Industry, Innovation and Infrastructure"** encompasses studies on sustainable material processing, recyclable materials, innovation in developing eco-friendly materials and technologies. These studies tend to optimize resource utilization, reduce waste generation, and promote circular economy principles. Other studies investigate innovations in ship design to support green ship recycling and green gas reduction. Other studies explore optimizing the operation of Petroleum Refineries and Gas-Oil separation plants to develop cleaner refining processes, biofuels, and sustainable alternatives that can lead to more environmentally friendly solutions.

Last but not least, the editors want to extend their deepest gratitude to all the authors for their exceptional contributions to this conference book, as their unwavering dedication, expertise, and passion have rendered this publication an invaluable resource for researchers, practitioners, stakeholders, and enthusiasts alike. Their fervent aspiration is that the knowledge imparted within these pages will ignite inspiration for continued progress and foster fruitful collaborations in Engineering Solutions and Practices for Sustainability. We gratefully acknowledge the continuous help and support of the editor of the **"Earth and Environmental Sciences Library series," Prof. Abdelazim M. Negm** for their invaluable contributions, including the precise review of articles of the conference proceedings and unwavering support throughout the entire lifecycle of the conference proceeding publication. Thanks are

also extended to include Springer's team, starting from the evaluation of the proposal till the end of the publication processes.

Zagazig, Egypt   Abdelazim M. Negm
Port Fouad, Egypt   Rawya Y. Rizk
Port Fouad, Egypt   Rehab F. Abdel-Kader
Port Fouad, Egypt   Asmaa Ahmed
July 2023

Contents

Industry, Innovation, and Infrastructure

Clean Energy

Ventilation Systems for Efficient Energy Use

Asmaa Ahmed, Mohamed Elsakka, and Ayman Mohamed

1 Introduction

Any indoor space must be properly ventilated in order to maintain a healthy environment. During ventilation, contaminated indoor air is replaced with fresh air from outside to maintain good air quality by removing pollutants and circulating fresh air [1]. When airflow is inadequate, harmful gases and particles can build, causing headaches, dizziness, or respiratory problems [2]. Additionally, proper ventilation can help regulate temperature and humidity levels, creating a more comfortable and productive environment. This can be done by reducing the build-up of humidity and removing excess heat from the indoor environment. According to ASHRAE Standard 62.1 [3, 4], the amount of outdoor air required in the breezing zone should not be less than the minimum rate (V_{bz}) that is calculated by the following equation:

$$V_{bz} = R_p \times P_z + R_a \times A_z \tag{1}$$

where R_p, R_a, P_z, A_z are the outdoor airflow rate required per person, outdoor airflow rate required per area, number of people during space use, and floor area, respectively. The ventilation can be natural, mechanical, or a combination of both through cracks, windows, or openings in the building envelope (air infiltration) or persistently provided through natural or mechanical means (hybrid or mixed-mode ventilation)

A. Ahmed (✉) · M. Elsakka · A. Mohamed
Department of Mechanical Power Engineering, Port Said University, Port Said, Egypt
e-mail: asmaa_rady@eng.psu.edu.eg

M. Elsakka
e-mail: elsakka@eng.psu.edu.eg

A. Mohamed
e-mail: president@psu.edu.eg

A. Ahmed · M. Elsakka
Energy Research and Studies Centre, Port Said University, Port Said, Egypt

[5]. Mechanical ventilation distributes airflow throughout the building through fans and ductwork, with air terminals or diffusers conducting the air into the room. In some cases, however, this process requires high levels of energy consumption, particularly if mechanical systems are used as part of the process. This power is used to move air in and out of buildings and to condition that air to the desired temperature and humidity levels. Depending on the building's size and number of occupants, and the level of indoor air quality desired, the amount of energy required can vary. Properly designing and maintaining ventilation systems can minimize energy consumption, and adequate ventilation can still be provided. Consequently, balancing energy efficiency with adequate ventilation is essential. In some cases, providing the system with the needed energy requirements can be done by different types of renewable energy resources. The system can be supplied with the required energy levels in some cases using a variety of renewable energy resources. Renewable energy plays a crucial role in mitigating climate change. Unlike fossil fuels, renewable energy sources such as solar and wind do not emit greenhouse gases that contribute to global warming [6]. Additionally, renewable energy technologies have become more cost-effective and efficient in recent years, making them a viable, sustainable alternative. Several solar and wind energy technologies can be exploited for building ventilation [7–9]. In this paper, a comprehensive review of different types of ventilation methods that are being utilized in buildings is presented. This includes reviewing numerous types of natural ventilation systems, mechanical ventilation systems, hybrid ventilation systems, and renewable energy-based ventilation systems.

2   Natural Ventilation

Natural ventilation (NV) is the process of supplying and removing air from an indoor space without the use of mechanical systems [10]. It relies on natural forces such as wind and temperature differences to create airflow. This method can improve indoor air quality and reduce energy consumption. NV can be achieved by opening windows, using vents, and creating air pathways. However, it should be designed in accordance with the climate, orientation of the building, and needs of occupants [11]. Several decades ago, scientists studied, analysed, and refined natural ventilation techniques [12]. Pabiou et al. [13] mentioned in their study that natural cross-ventilation is considered a promising solution to fulfil thermal comfort conditions in the summer season. However, in order to utilize this technique in hot climatic regions, the heat rate that should be dissipated must be predicted first for system effectiveness. NV schemes are an effective way to improve indoor air quality and reduce energy depletion. They work by using natural airflow to circulate fresh air throughout a building, reducing the need for mechanical ventilation systems. This can lead to significant energy savings and a healthier indoor environment. Some common natural ventilation strategies include single-sided ventilation, high-level roof ventilation, cross-ventilation, and ventilation chimneys. Figure 1 shows schematic diagrams of each of those methods. The effectiveness of these strategies depends on factors such as

building design, climate, and occupancy patterns. However, when implemented properly, natural ventilation schemes can provide a cost-effective and sustainable solution for improving indoor air quality.
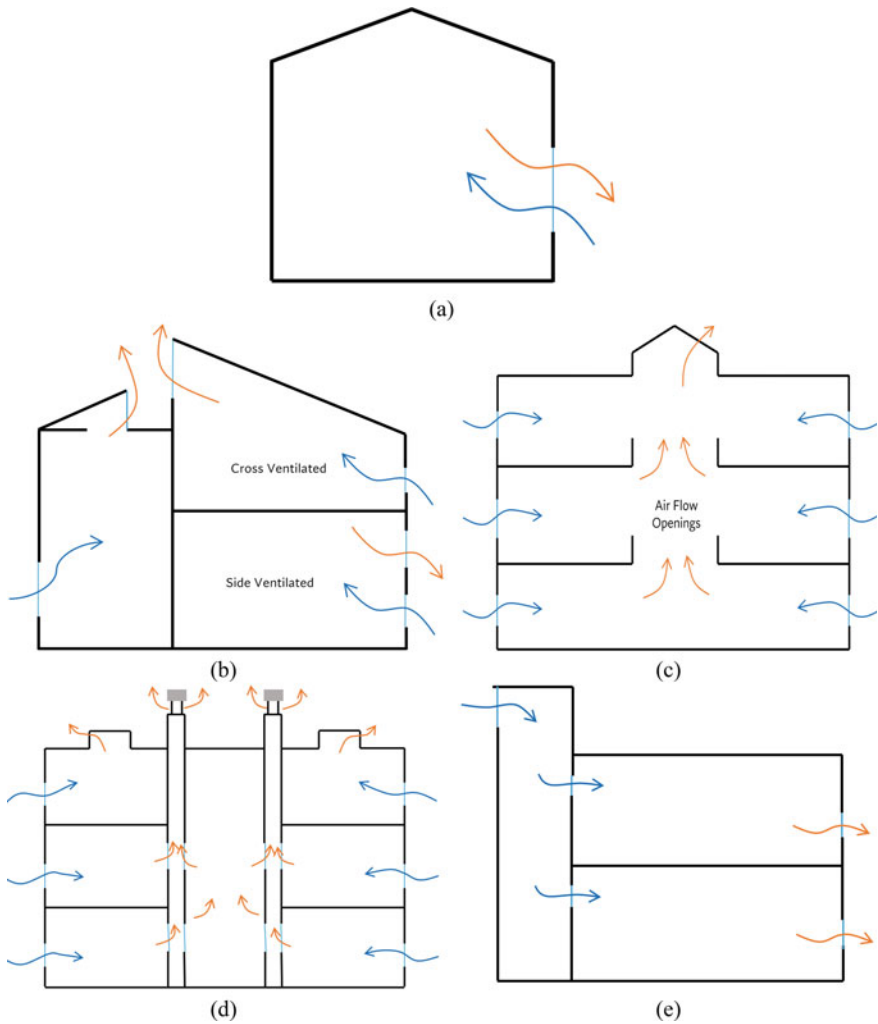
Fig. 1 Natural ventilation schemes: **a** single-sided ventilation, **b** high-level roof ventilation, **c** crossflow ventilation, **d** ventilation chimneys, **e** wind scoop

2.1　Single-Sided Ventilation

In single-sided ventilation, openings are generally placed on one side of the external wall, facing the wind as presented in Fig. 1a. This method can naturally ventilate spaces with limited areas [14]. Single-sided ventilation systems are commonly utilized in construction projects where cross-ventilation is not feasible due to various restrictions such as structural or environmental factors. These systems allow for satisfactory air circulation and exchange, ensuring a comfortable and healthy indoor environment. Additionally, single-sided ventilation systems are often more cost-effective and energy-efficient compared to other ventilation options. Gan [15] predicted theoretically the temperature distribution, airflow profile, and depth of air distribution of a single-sided ventilation scheme in a building. The findings revealed that the air distribution depth can be defined by using the internal heat of the building and outdoor temperature. Aflaki et al. [16] studied single-sided ventilation for high-level buildings in tropical climates as it is favourable in comparison with the crossflow type. The study considered the investigation of the impact of this scheme on the humidity, indoor temperature, and air velocity. At an air velocity of 0.52 m/s, the highest floor's thermal comfort conditions have been obtained by 90%.

2.2　High-Level Roof Ventilation

High-level roof ventilation is a system that is located in the upper part of a roof. It is designed to allow air to circulate through the roof space (Fig. 1b), which can help in reducing the temperature and humidity levels inside the building. The system typically consists of a series of vents or louvers that are placed at strategic locations along the roofline. These vents can be opened or closed, depending on the weather conditions and the needs of the building [17]. High-level roof ventilation effectively improves indoor air quality and reduces the risk of moisture damage to the roof structure.

2.3　Crossflow Ventilation

Crossflow ventilation is a method of natural ventilation that involves the movement of air through a building, from one side to the other [18]. It is achieved by opening windows or vents on opposite sides of the building (Fig. 1c), which allows air to enter one side and exit from the other. This method of ventilation is often used in buildings where mechanical ventilation is not practical or desirable, such as in residential homes or small commercial buildings. Crossflow ventilation can help to improve indoor air quality, reduce the risk of mould and mildew growth, and lower energy costs by reducing the need for air conditioning. It is important to ensure that

the windows or vents used for crossflow ventilation are properly sized and located to maximize airflow and minimize the risk of drafts. Chu and Chiang [19], investigated theoretically and experimentally the crossflow scheme of a building and the validation of a rule of thumb stating that the building length should be five times the building height for better ventilation rates. The findings revealed proof of the rule of thumb. However, ventilation rates decreased when increasing the building length further.

2.4 Ventilation Chimneys

The chimney effect, also called the stack effect, is constantly used in vertical buildings to provide ventilation through vertical airflow. It is a natural phenomenon that occurs in buildings. It is caused by the temperature, pressure, and densities differences between indoor and outdoor air [20]. It involves ushering cool air in and warm air out with help from strategically placed openings in a building. Warm air rises and escapes through openings in the upper part of the building (Fig. 1d), clerestory, zenithally openings, or wind exhausts. On the other hand, cooler air is drawn in through openings in the lower part of the building. This creates a continuous flow of air through the building and guarantees the building's natural ventilation. The chimney effect can positively and negatively affect a building's energy efficiency and indoor air quality. Proper ventilation and insulation can help to mitigate the negative consequences of the chimney effect. Ding et al. [21] studied theoretically and experimentally the possibility of integrating the solar chimney with a double-skin façade. The study revealed that increasing the solar chimney height would lead to rising the ventilation rate and ensure better pressure difference distribution. However, the authors recommended that the height should exceed two-floor high.

2.5 Wind Scoop

A Wind Scoop is a passive ventilation system that can be installed on the roof of a building to improve indoor air quality and thermal comfort. It captures the natural wind flow and directs it into the building, creating a cooling breeze [12] as presented in Fig. 1e. Wind Scoops are particularly effective in hot and dry climates, where air conditioning can be expensive and energy intensive. They are also environmentally friendly, as they do not require any electricity or mechanical components. Studies have shown that buildings with wind scoops have lower indoor temperatures and reduced energy consumption. Khan et al. [22] have reviewed various types of wind scoops in their recent study and suggested one with the ability to rotate with the wind direction. Overall, Wind Scoops are a cost-effective and sustainable solution for improving indoor air quality and thermal comfort in buildings.

3 Mechanical Ventilation

Mechanical ventilation (MV) is a system used in buildings to provide fresh air and remove stale air by means of mechanical devices [23, 24]. It is typically used in buildings where natural ventilation is not sufficient or not possible. Mechanical ventilation systems can be either central or local. Central systems are designed to serve the entire building, while local systems are designed to serve individual rooms or areas. The type of system used depends on the building's size, layout, and occupancy. They can be designed to provide a variety of airflows, depending on the building's needs. These systems are typically designed to meet specific standards and codes to ensure that they are safe and effective.

- Central ventilation systems are an imperative component of prevailing buildings. They serve to circulate fresh air throughout the building and remove stale air, odours, and pollutants. These systems typically consist of a network of ducts and vents that are connected to a central unit. A centralized ventilation system usually uses fewer, but larger, air handling units (AHUs) as shown in Fig. 2a. These are usually located on the roof of the building or indoors in technical rooms. The system's size and capacity depend on the building's size and the number of occupants. Regular maintenance and cleaning are essential to ensure the system operates efficiently and effectively.
- In terms of local ventilation systems, help to maintain a healthy and comfortable indoor environment by removing pollutants and excess moisture from the air. These systems are typically designed to meet specific requirements based on the size and usage of the building. They can be installed in a variety of locations, including bathrooms, kitchens, and industrial workspaces such as fans. Several points should be taken into consideration when selecting a suitable fan such as power consumption, current consumption, air volume, fan speed, noise, and the net fan weight. Proper maintenance and regular cleaning are necessary to ensure that these systems continue to function effectively.
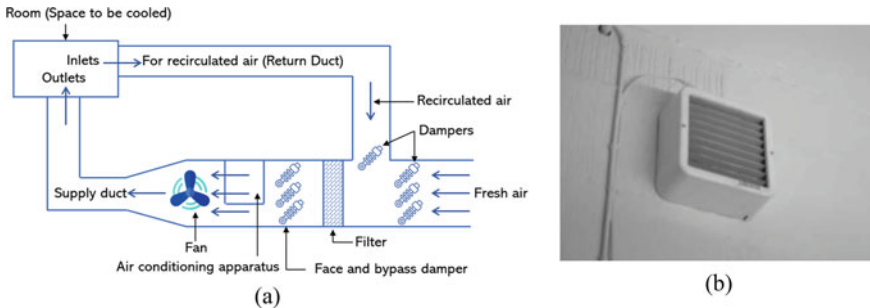
Fig. 2 **a** Central ventilation system, and **b** local system: wall-fan

4 Hybrid Ventilation Systems (Mixed Mode)

Hybrid ventilation (HV) technology depends on utilizing both natural and mechanical ventilation systems to ensure the thermal comfort conditions of the indoor space are met [24, 25]. Sometimes, a switch between different technologies can be made depending on the year's season. Therefore, by implementing this method, the capital cost and energy consumption can be reduced in comparison with the MV systems. In addition, vigorous indoor air quality (IAQ) and air conditioning conditions can be met. As a result, hybrid ventilation systems are becoming increasingly popular. Utilizing HV technologies in the building is subject to two main approaches. The contingency approach depends on the use of natural ventilation and utilizing mechanical systems to provide further cooling and ventilation to the building. Usually, this approach can be implemented when an old building is being renovated and strict policies should be met. On the other hand, a complementary approach is when both natural and mechanical systems are designed and integrated for operation. However, this approach takes the advantage of the outdoor ambient conditions to maintain the required indoor air quality and thermal conditions when the outside air conditions are not suitable. Figure 3 shows different configurations of HV systems for improving air quality.

5 Renewable Energy-Based Ventilation Systems

Renewable energy-based ventilation systems are becoming increasingly popular due to their many benefits. These systems use clean energy sources such as wind and solar power to operate, reducing reliance on non-renewable sources. Additionally, they are environmentally friendly as they do not emit harmful pollutants into the atmosphere. Furthermore, they can help reduce energy costs in the long run as they require less maintenance and have a longer lifespan compared to traditional ventilation systems. They are, also, a practical and sustainable solution for modern buildings. Figure 4 shows different possible renewable energy options that can be implemented for ventilating a building. However, a combination of these technologies can be used under specific design conditions. The next subsections will discuss different renewable energy applications for building ventilation.

5.1 Solar Energy Systems

5.1.1 Photovoltaics

Photovoltaics (PV) are semi-conductor devices that absorb incident solar energy and convert it into electrical energy [26–29]. The PV system consists of a PV panel,

Fig. 3 Different configurations of HV systems when utilizing **a** wall fan, **b** ceiling fan

(a)

(b)

Solar Chimney

Wind Turbine/Cowl

Photovoltaics

Glazed Balcony

Solar Wall/solar air collector/Photovoltaics
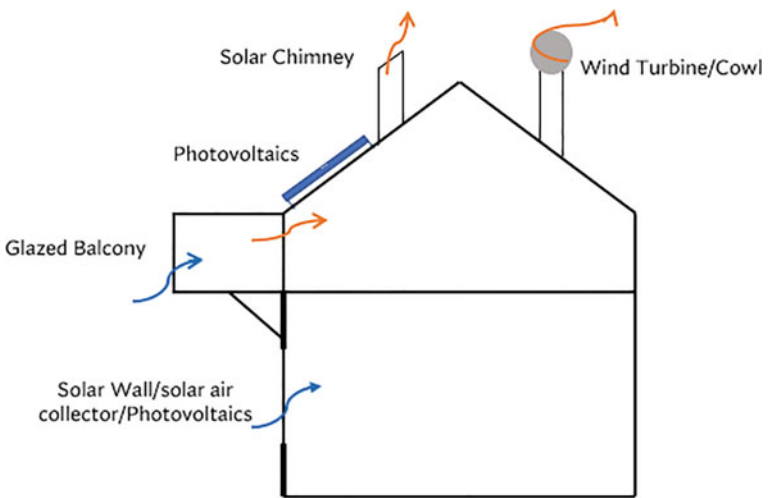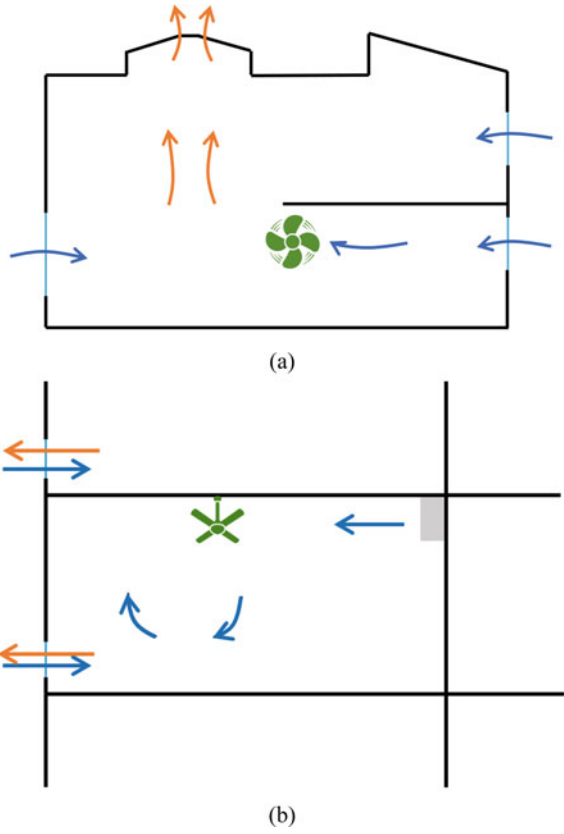
Fig. 4 Different scenarios of renewable energy-based ventilation systems
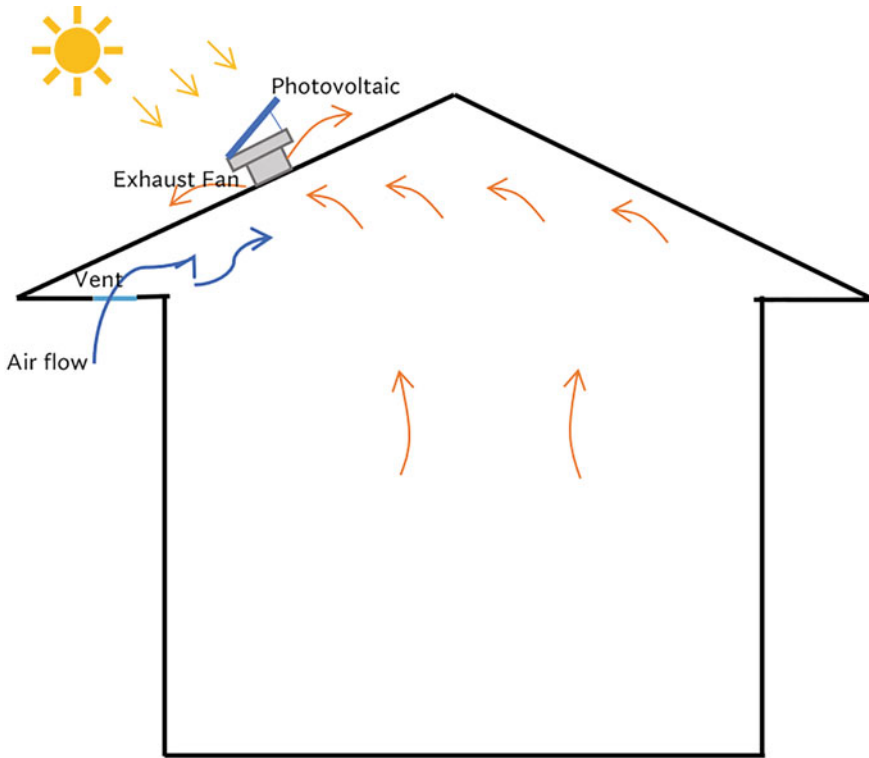
Fig. 5 Solar powered exhaust fan

inverter, and battery if it is not connected to the grid. This system is most suitable to be established in locations that have high levels of incident solar irradiances for reliable operation. The geographical location of the building, and PV installation to prevent the shadowing which may occur to the solar cells are crucial parameters for system feasibility. Overall, the best operating conditions are when the PV system faces the south and the optimum tilt angle is assured. Using the power produced by the PV system, some ventilation system components can be powered [30]. These components may be actuators as they require low energy demand. Therefore, small PV modules may be suitable. However, fans require high energy consumption, involving larger PV modules and a battery bank (Fig. 5).

5.1.2 Other Solar Systems

The ventilation system may involve different solar energy technology in addition to the photovoltaic technology discussed above [30, 31]. In glazed balconies, the air enters and is heated by the sun directly in a closed space. However, this method may cause air overheating especially in summer. Therefore, regions with shorter summer
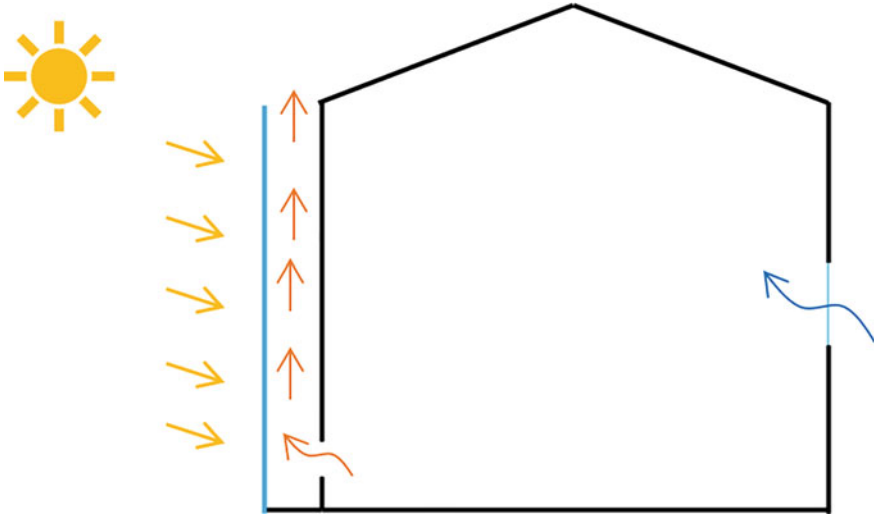
Fig. 6 Solar chimney concept

seasons are favourable for implementing this option. In addition, the heated moist air may be condensed on the building's window which is counted as an additional limitation. However, this method is believed to be a cost-effective option that doesn't require regular maintenance. Another option is by using a solar collector in which the air absorbs the heat of the incident solar energy. Usually, a fan is used to force the air to pass through the solar collector and is then reheated in the central heating system of the building to increase the heat further. The system cost depends mainly on the building location and the heating level requirements (Fig. 6).

5.2 Wind Energy Systems

By using a wind turbine, the kinetic energy due to the air movement can be converted into electrical power or mechanical energy [32–34]. This technique depends mainly on wind direction and speed. The enclosed space can be ventilated by placing this small wind turbine in the attic or the rooftop of the building. Fresh air can flow and enter through the building by using intake and exhaust vents as shown in Fig. 7a. This can reduce the temperature of the internal space, recirculate the air to ensure indoor air quality is obtained, and certain comfort conditions have been met. The type of intake vent that is used depends on the building structure, the system design criteria, and the area where the system is to be installed. To ensure a balanced process and a sufficient flow of air through an attic, exhaust vents must be applied simultaneously with intake vents.
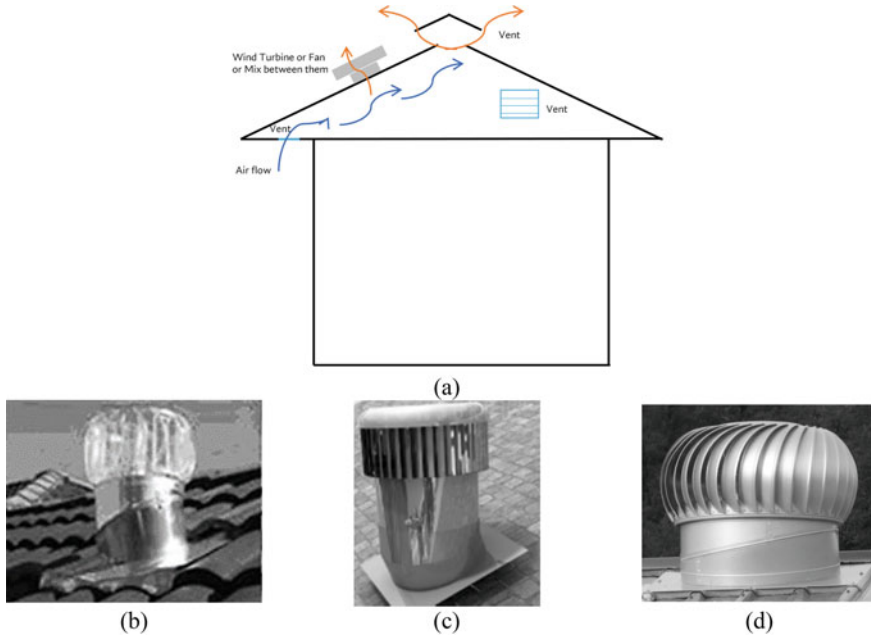
Fig. 7 **a** Principles of using wind turbine with or without a fan for air ventilation, examples of **b** straight vane turbines with a curved side [12], **c** straight vane turbines, and **d** curved vane turbines

Several types of wind turbines can be utilized in ventilation systems [35] such as straight vane turbines with a curved side, straight vane turbines, and curved vane turbines as shown in Fig. 7b–d. Designed for light winds, straight vane turbines with a curved side consist of polycarbonate blades with vertical vanes and an aluminium neck. On the other hand, straight vane turbines have a vertical design made from lightweight aluminium. They work efficiently for extracting smoke. Curved vane turbines are manufactured from galvanized mild steel or lightweight aluminium. A slight breeze or convection current will activate these types of vents. Sometimes these turbines cannot be effective in providing enough air circulation. Therefore, several researchers have proposed integrating wind turbines with a fan to increase the air change rate. In some cases, this may require a power supply that can be supplied by photovoltaic panels as presented in Fig. 8. In some scenarios, the wind turbine can be integrated with photovoltaics such as a study provided by [36]. The authors suggested this prototype to enhance the ventilation rate. The system consists of a wind turbine and an inner fan powered by a photovoltaic panel as shown in Fig. 8. This combination has been found to be more effective in low wind speeds than the original design, which relies solely on wind turbines. Another study was introduced by [37] where they developed a prototype of a conventional wind turbine with the integration of a solar-driven extractor fan. The results revealed that the air temperature was reduced by about 1 °C in comparison with the original case. Overall, it might

Fig. 8 Different
configurations of a
wind-solar ventilation
system [36]
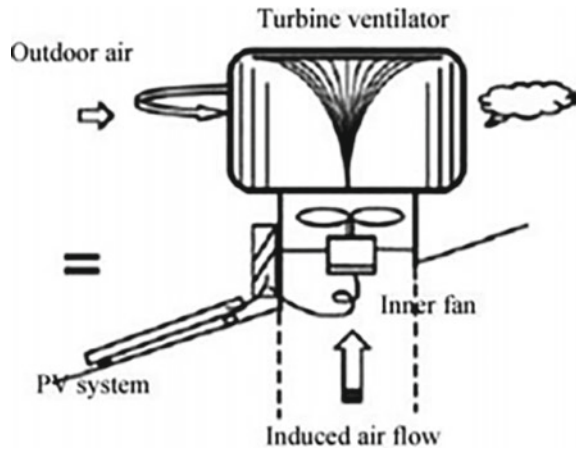
be the most efficient way to achieve energy efficiency is to integrate different types
of renewable energy for building ventilation which still needs further research.

6 Conclusion

This paper reviews air ventilation technologies to achieve proper indoor air quality
and reduce heat stress. Previous research studies of each ventilation method and
its working principles have been covered. From the literature, it seems that relying
on mechanical ventilation technologies alone may require high levels of energy
consumption. However, natural ventilation methods may also be not sufficient, partic-
ularly at low wind speeds. Therefore, a combination of these two methods may be
a more efficient and reliable option. However, for a more sustainable way to reduce
greenhouse gas emissions and save more energy. The paper has suggested that inte-
grating two or more renewable energy resources to provide electrical power for the
mechanical parts would be the best way as it saves energy, reduces carbon emissions,
and provides a uniform airflow and temperature distribution according to the season.
This is considered a new direction and reliable way to achieve energy efficiency in
buildings.

7 Recommendation

Based on this review, it is recommended to employ a combination of mechanical and
natural ventilation methods for efficient and reliable ventilation in buildings. Integra-
tion of multiple renewable energy resources to power the mechanical parts is the most
energy-efficient and eco-friendly option. To achieve sustainable ventilation, building

stakeholders must adopt integrated design and management practices that prioritize indoor air quality, energy consumption, and environmental impact. Implementing these recommendations can significantly contribute to the Sustainable Development Goal of affordable and clean energy.

References

1. Fan M, Fu Z, Wang J, Wang Z, Suo H, Kong X, Li H (2022) A review of different ventilation modes on thermal comfort, air quality and virus spread control. Build Environ 212:108831. https://doi.org/10.1016/J.BUILDENV.2022.108831
2. Elsaid AM, Mohamed HA, Abdelaziz GB, Ahmed MS (2021) A critical review of heating, ventilation, and air conditioning (HVAC) systems within the context of a global SARS-CoV-2 epidemic. Process Saf Environ Prot 155:230–261. https://doi.org/10.1016/J.PSEP.2021.09.021
3. Amende K, Keen J, Catlin L, Tosh M, Sneed A, Howell R (2021) Principles of heating, ventilating, and air conditioning, 9th edn
4. Hedrick RL, Thomann WR, Aguilar H, Damiano LA, Darwich AKH, Gress G, Habibi H, Howard EP, Petrillo-groh LG, Smith JK, Williams SD, Doppel PL, Davis HD, Fisher FJ, Morris WE, Olsen JWW, Hall RL, Reindl DT, Anderson JR, Barnaby CS, Clark JA, Graef PT (2015) Ventilation for acceptable indoor air quality
5. Oropeza-Perez I, Østergaard PA (2018) Active and passive cooling methods for dwellings: a review. Renew Sustain Energy Rev 82:531–544. https://doi.org/10.1016/J.RSER.2017.09.059
6. Suman A (2021) Role of renewable energy technologies in climate change adaptation and mitigation: a brief review from Nepal. Renew Sustain Energy Rev 151:111524. https://doi.org/10.1016/J.RSER.2021.111524
7. Ahmed A, Baig H, Sundaram S, Mallick TK (2019) Use of nanofluids in solar PV/thermal systems. Int J Photoenergy 2019:1–17. https://doi.org/10.1155/2019/8039129
8. Ahmed A (2021) Thermal management of high concentrating photovoltaic system. University of Exeter
9. Ahmed A, Shanks K, Sundaram S, Mallick T (2021) Energy and exergy analyses of new cooling schemes based on a serpentine configuration for a high concentrator photovoltaic system. Appl Therm Eng 199:117528. https://doi.org/10.1016/j.applthermaleng.2021.117528
10. Larsen TS, Heiselberg P (2008) Single-sided natural ventilation driven by wind pressure and temperature difference. Energy Build 40:1031–1040. https://doi.org/10.1016/J.ENBUILD.2006.07.012
11. Sakiyama NRM, Carlo JC, Frick J, Garrecht H (2020) Perspectives of naturally ventilated buildings: a review. Renew Sustain Energy Rev 130:109933. https://doi.org/10.1016/J.RSER.2020.109933
12. Khan N, Su Y, Riffat SB (2008) A review on wind driven ventilation techniques. Energy Build 40:1586–1604. https://doi.org/10.1016/J.ENBUILD.2008.02.015
13. Pabiou H, Salort J, Ménézo C, Chillà F (2015) Natural cross-ventilation of buildings, an experimental study. Energy Procedia 78:2911–2916. https://doi.org/10.1016/J.EGYPRO.2015.11.666

14. Albuquerque DP, O'Sullivan PD, da Graça GC (2021) Effect of window geometry on wind driven single sided ventilation through one opening. Energy Build 245:111060. https://doi.org/10.1016/J.ENBUILD.2021.111060

15. Gan G (2000) Effective depth of fresh air distribution in rooms with single-sided natural ventilation. Energy Build 31:65–73. https://doi.org/10.1016/S0378-7788(99)00006-7

16. Aflaki A, Mahyuddin N, Baharum MR (2016) The influence of single-sided ventilation towards the indoor thermal performance of high-rise residential building: a field study. Energy Build 126:146–158. https://doi.org/10.1016/J.ENBUILD.2016.05.017

17. Marley UK (2022) Roof ventilation. https://www.marley.co.uk/blog/why-is-roof-ventilation-important. Accessed 5 Apr 2023

18. Zhang X, Weerasuriya AU, Wang J, Li CY, Chen Z, Tse KT, Hang J (2022) Cross-ventilation of a generic building with various configurations of external and internal openings. Build Environ 207.https://doi.org/10.1016/J.BUILDENV.2021.108447

19. Chu CR, Chiang BF (2014) Wind-driven cross ventilation in long buildings. Build Environ 80:150–158. https://doi.org/10.1016/J.BUILDENV.2014.05.017

20. Chan HY, Riffat SB, Zhu J (2010) Review of passive solar heating and cooling technologies. Renew Sustain Energy Rev 14:781–789. https://doi.org/10.1016/J.RSER.2009.10.030

21. Ding W, Hasemi Y, Yamada T (2005) Natural ventilation performance of a double-skin façade with a solar chimney. Energy Build 37:411–418. https://doi.org/10.1016/J.ENBUILD.2004.08.002

22. Dehghani-Sanij AR, Soltani M, Raahemifar K (2015) A new design of wind tower for passive ventilation in buildings to reduce energy consumption in windy regions. Renew Sustain Energy Rev 42:182–195. https://doi.org/10.1016/J.RSER.2014.10.018

23. Izadyar N, Miller W (2022) Ventilation strategies and design impacts on indoor airborne transmission: a review. Build Environ 218:109158. https://doi.org/10.1016/J.BUILDENV.2022.109158

24. Peng Y, Lei Y, Tekler ZD, Antanuri N, Lau SK, Chong A (2022) Hybrid system controls of natural ventilation and HVAC in mixed-mode buildings: a comprehensive review. Energy Build 276:112509. https://doi.org/10.1016/J.ENBUILD.2022.112509

25. Brager G (2006) UC Berkeley envelope systems title mixed-mode cooling

26. Ahmed A, Shanks K, Sundaram S, Mallick TK (2020) Theoretical investigation of the temperature limits of an actively cooled high concentration photovoltaic system. Energies 13.https://doi.org/10.3390/en13081902

27. Ahmed A, Alzahrani M, Shanks K, Sundaram S, Mallick TK (2020) Effect of using an infrared filter on the performance of a silicon solar cell for an ultra-high concentrator photovoltaic system. Mater Lett 277:128332. https://doi.org/10.1016/j.matlet.2020.128332

28. Ahmed A, Zhang G, Shanks K, Sundaram S, Ding Y, Mallick T (2021) Performance evaluation of single multi-junction solar cell for high concentrator photovoltaics using minichannel heat sink with nanofluids. Appl Therm Eng 182:115868. https://doi.org/10.1016/j.applthermaleng.2020.115868

29. Ahmed A, Alzahrani M, Shanks K, Sundaram S, Mallick TK (2022) Reliability and temperature limits of the focal spot of a primary optical component for an ultra-high concentrated photovoltaic system. AIP Conf Proc 2550.https://doi.org/10.1063/5.0099091

30. Antvorskov S (2008) Introduction to integration of renewable energy in demand controlled hybrid ventilation systems for residential buildings. Build Environ 43:1350–1353. https://doi.org/10.1016/J.BUILDENV.2007.01.045

31. Wang H, Lei C (2020) A numerical investigation of combined solar chimney and water wall for building ventilation and thermal comfort. Build Environ 171:106616. https://doi.org/10.1016/J.BUILDENV.2019.106616

32. Ahmed NA (2010) Wind-solar driven natural electric hybrid ventilators. Wind Power. https://doi.org/10.5772/8349

33. Elsakka MM, Ingham DB, Ma L, Pourkashanian M (2021) Comparison of the computational fluid dynamics predictions of vertical axis wind turbine performance against detailed pressure measurements. Int J Renew Energy Res 11:276–293

34. Elsakka MM, Ingham DB, Ma L, Pourkashanian M (2020) Effects of turbulence modelling on the predictions of the pressure distribution around the wing of a small scale vertical axis wind turbine. In: Proceedings of the 6th European conference on computational mechanics: solids, structures and coupled problems, ECCM 2018 and 7th European conference on computational fluid dynamics, ECFD 2018, pp 3921–3931
35. Ishugah TF, Li Y, Wang RZ, Kiplagat JK (2014) Advances in wind energy resource exploitation in urban environment: a review. Renew Sustain Energy Rev 37:613–626. https://doi.org/10.1016/J.RSER.2014.05.053
36. Lai CM (2006) Prototype development of the rooftop turbine ventilator powered by hybrid wind and photovoltaic energy. Energy Build 38:174–180. https://doi.org/10.1016/J.ENBUILD.2005.06.004
37. Ismail M, Abdul Rahman AM (2010) Comparison of different hybrid turbine ventilator (HTV) application strategies to improve the indoor thermal comfort. Int J Environ Res 4:297–308. https://doi.org/10.22059/IJER.2010.22

A Comprehensive Review of Biomass Pyrolysis to Produce Sustainable Alternative Biofuel

Yasser Elhenawy, Kareem Fouad, Mohamed Bassyouni, Mamdouh Gadalla, F. H. Ashour, and Thokozani Majozi

1 Introduction

Affordable and clean energy is one of the major topics in the Sustainable Development Goals (SDGs), and the search for sustainable energy sources is a crucial concern [1]. At present, humanity suffers from two main issues; the first issue is

Y. Elhenawy (✉) · T. Majozi
School of Chemical and Metallurgical Engineering, University of the Witwatersrand, Johannesburg 2000, South Africa
e-mail: yasser.elhenawy@wits.ac.za

T. Majozi
e-mail: Thokozani.Majozi@wits.ac.za

Y. Elhenawy
Department of Mechanical Power Engineering, Faculty of Engineering, Port Said University, Port Said 42526, Egypt

K. Fouad
Department of Civil Engineering, Higher Future Institute of Engineering and Technology, El Mansoura, Egypt
e-mail: engkareem.s.civil@gmail.com

M. Bassyouni · M. Gadalla
Department of Chemical Engineering, Faculty of Engineering, Port Said University, Port Said 42526, Egypt
e-mail: m.bassyouni@eng.psu.edu.eg

M. Gadalla
e-mail: mamdouh.gadalla@yahoo.com

M. Bassyouni
Center of Excellence in Membrane-Based Water Desalination Technology for Testing and Characterization, Port Said University, Port Said 42526, Egypt

F. H. Ashour
Department of Chemical Engineering, Cairo University, Giza, Egypt
e-mail: fhashour@yahoo.com

19

the growing levels of pollution and waste generated, and the other is the increased need for energy sources [2–7]. Food waste for example has increased dramatically as the world population has grown. According to the United Nations, the estimated worldwide food loss at roughly 1.6 billion tons. This is predicted to rise by 32% during the following ten years [8–10]. Energy is considered a vital product, and its need has expanded with global economic activity and population growth, particularly in emerging countries [10–13]. Petroleum crude fuels provided barely 4% of the whole world's power requirements at the turn of the twentieth century. Nonetheless, crude fuels are now the utmost essential source of energy, accounting for around 40% of global power needs and generating 96% of all passage fuels. Even so, crude fuels are a non-renewable source, and fossil fuel supplies are rapidly diminishing. Furthermore, the usage of petroleum fuels has an impact on the environment by emitting large quantities of carbon dioxide and additional contaminants such as SOx and NOx. As a result, finding renewable and ecologically friendly feedstocks for a sustained supply of fuels and energy is critical [14–18]. Biofuels are environmentally friendly alternatives to fossil fuels, and their production is being pushed hard due to the hazard of climate change [15]. Table 1 shows the difference between the features of bio-oil and crude oil.

Of all renewable resources, biomass is desirable because it is a plentiful forestry resource that can be converted into biofuels, bio-based products, and chemicals using various operating technologies. Because of the diminution of fossil fuels and the effluence associated with their usage, the conversion of biomass into liquid fuels is gaining popularity [9]. Pyrolysis is a simple thermochemical method without the presence of oxygen that transforms solid biomass into non-condensable gases, charcoal, and a liquid product called bio-oil. Non-condensable gases are combustion and may be utilized as gaseous fuels to power the endothermic pyrolysis procedure [17, 18]. Table 2 illustrates the pyrolysis process operating parameters and the final products.

Biomass pyrolysis is frequently performed at or above 500 °C, providing adequate heat to degrade the previously stated strong bio-polymers. As a product, biomass

Table 1 Features of bio-oil and crude oil [16]

Composition	Crude oil	Bio-oil
pH	–	2.8–3.8
Viscosity 50 °C (cP)	180	40–100
Water (wt%)	0.1	15–30
HHV (MJ/kg)	44	16–19
Density (kg/L)	0.86	1.05–1.25
N (wt%)	< 1	< 0.4
H (wt%)	11–14	5–7
C (wt%)	83–86	55–65
S (wt%)	< 4	< 0.05
O (wt%)	< 1	28–40

Table 2 Operating parameters for the pyrolysis procedure and its final outputs [19]

Pyrolysis procedure	Solid retention time (s)	Heating rate (K/s)	Particle Size (mm)	Temp. (K)	Product yield (%)		
					Gas	Oil	Char
Flash	< 0.5	> 1000	< 0.2	1050–1300	13	75	12
Fast	0.5–10	10–200	< 1	850–1250	30	50	20
Slow	450–550	0.1–1	5–50	550–950	35	30	35

pyrolysis produces three products: one gaseous; syngas, one solid; bio-char, and one liquid; bio-oil. A variety of issues, such as feedstock structure and process situations, influence the percentage of these byproducts. Yet, if all other elements are equal, bio-oil generation is maximized in rapid pyrolysis conditions when the pyrolysis temperature is around 500 °C and the temperature range is high (1000 °C/s). Bio-oil yields of 60–70% from a common biomass feedstock are possible in these conditions, with bio-char yields ranging from 15 to 25 and 10–15% of syngas yields. Slow pyrolysis refers to procedures that use slower heating rates, and biochar is frequently the end product. Various substances such as plastic, tires, and wood may all be pyrolyzed [20]. In the pyrolysis process, raw materials are first dried before grinding to small particles to feed the pyrolysis reactor. After the chemical decomposition of biomass material, bio-oil, bio-char, and gases are produced as shown in Fig. 1.
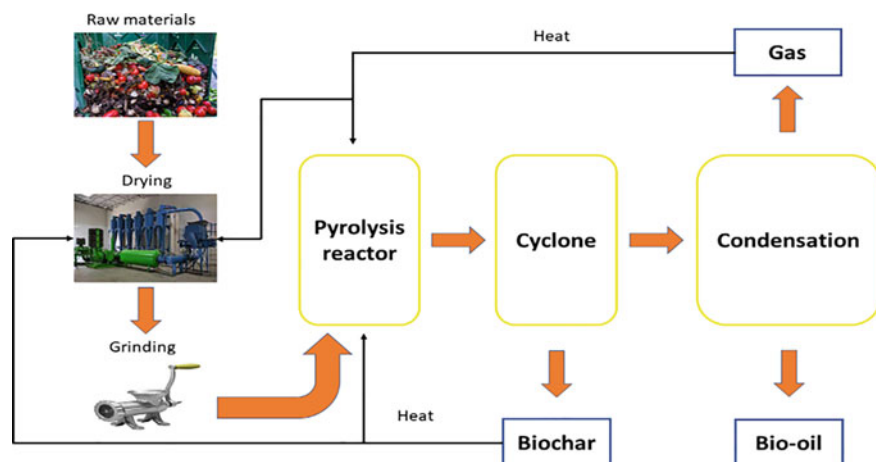
Fig. 1 Pyrolysis schematic diagram

2 Plastic

For further than 50 years, plastic has played an important part in improving people's level of living. It is a crucial driver of product innovation in numerous industries, including healthcare, automotive, electronics, construction, and packaging. The fast rise in the world population has raised the demand for commodity plastics. In 2013, worldwide plastic production reached approximately 299 million tons, a 4% increase over 2012 [21]. Plastic pyrolysis outputs vary depending on the type of plastic, reactor type, temperatures used, residence time, feeding arrangement, and condensation arrangement [22]. Pyrolysis degradation process can turn plastic trash into gases, liquid oil, and solid residue (char) at elevated heat ranging from 300 to 900 °C [23]. Pratama et al. [24] illustrated the pyrolysis of a combination of polypropylene plastic for generating fuel and gasoline with percentages of 10, 15, and 20% of the mixture. The resultant fuel was observed to examine a motor vehicle's engine power and torque. For every 10 kg of polypropylene waste, 1.5 L of gasoline, 0.5 L of kerosene, and 6 L of diesel fuel are produced. The initial testing resulted in torque and supreme force in the combination of 20% plastic trash fuel (Polypropylene) + 80% gasoline occurring at 3000 rpm and torque occurring at 3000 rpm 10.43 N m, but in the second examination, the resulted in torque and maximum power in the mixture of 20% occurring in 4.391 HP 3500 rpm and torque 10.28 N m in rpm 3000. There is an enhancement in torque and power as compared to the initial testing results. Moreover, when the PP (Polypropylene) liquid plastic fuel contains a mixture with gasoline, the torque and engine power value is likely to increase significantly. The experimental pyrolysis reactor is shown in Fig. 2. Firstly, plastic wastes were placed in a melting tank before interring the pyrolysis reactor. Then the resultant interring a catalytic reactor to enhance the output fuel products. Finally, a fractional tank was utilized to separate the bio-fuel products.

Setiawan et al. [25] studied pyrolysis to produce liquid oil from low-density polypropylene (PP) and polyethylene (LDPE) plastic waste. This paper has studied the impact of plastic-type changes on the results. After a reaction for 4 h is 325 °C, the resultant fuels were examined in nature for viscosity, density, and flash point. The fuel components were verified by using a GC–MS device. The viscosity reached (0.61 cSt) and the density was (820 K kg m^{-3}) with the pyrolysis of 100% PP plastic waste. The maximum produced liquid oil was achieved to be 26.23% with a 100% LDPE composition, while the maximum gas production was 64.44% with a 75% LDPE composition and 25% PP (64.44%). The results found that the thermal decomposition of LDPE and PP plastics produces a relatively low proportion of cyclohexanedione compound ($C_9H_{14}O_2$). In contrast, the viscosity and flash point values of wholly sample configurations are quite minor than diesel fuel requirements. According to the GC–MS data, whole models had a hydrocarbon makeup through carbon sequence spans ranging from C9 to C12, indicating that they comprise petrol (C4–C12) and diesel fuel constituents (C12–C24).

Bahri [26] investigates biomass pyrolysis through the additive of natural zeolite to calculate the enthalpy necessary to produce char, gas, and oil. Natural zeolite
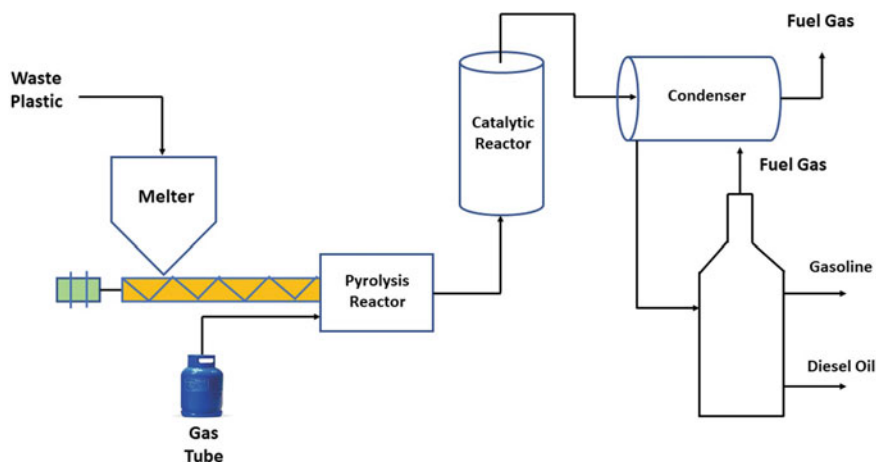
Fig. 2 Pyrolysis process

sorts Clipnotilolite (Z) and Sengon (S) sawdust were utilized. The results reveal that when Z increases, the enthalpy of pyrolysis S drops. The fall in enthalpy becomes steeper as the fraction of Z increases, whereas the mass decrease is minor. Martynis et al. [27] explored the features of pyrolysis liquid fuel (PLF) created from wastes of polypropylene plastic with temperature fluctuations were examined in this study. Pyrolysis was performed on 200 g of polypropylene trach polymers for 45 min at temperatures varying from (200 to 350 °C). As demonstrated in the data, the supreme liquid fuel output was 21.7% at a temperature of 350 °C. The pyrolysis procedure yielded an inverted solid to liquid products (char) (oil) ratio. The working groups found in pyrolytic oil are predominantly alkene, aromatic, and aliphatic hydrocarbon derivatives. The pyrolytic oil was discovered to include chemicals with carbon chain lengths ranging from C8 to C13. The density of the liquid fuel generated was 0.71–0.8 g/cm^3, comparable to gasoline's density. A simple batch pyrolysis process may transfer plastic cup trash to liquid hydrocarbons with temperature-dependent yields.

3 Tires

Tire pyrolysis is considered the greatest favorable possibility among management solutions, particularly for large-scale applications [28]. Numerous attempts have examined the thermal breakdown pathway of rubber tires. Rubber polymers can be depolymerized via chain and side-group scission [29]. In 2014, Alsaleh et al. [30] published a study demonstrating that unused tires are suitable applicants for pyrolysis to regain power and byproducts. Temperature is the most important element controlling the distribution and physical/chemical characteristics of solid phase, liquid, and gas pyrolysis yields. The flow rate of transferor gas/residence time of volatiles,

thermal rate, the occurrence of steam in the transferor gas, feedstock composition, particle size, pyrolysis time/tire residence time, and the presence of a catalyst are all important parameters. Pyrolytic oils derived from waste tires have been well burnt in examination furnaces and diesel engines, with roughly 40 MJ/kg of normal heating values. Pyrolysis oils can also give compounds valuable to the petrochemical sector, such as aromatics and light olefins. For pollution elimination, solid-phase pyrolysis char can be utilized to produce activated carbon or carbon black. The gases generated, which include hydrogen and other hydrocarbons, can be utilized to power the pyrolysis process. Neto et al. [31] researched the establishment of a reactor model for the pyrolysis of scrap tires to produce carbon black and additional byproducts. The research was carried out in Brazil, with the dual goal of decreasing environmental problems and establishing economic sustainability. The study's purpose was to support the growth and development of environmentally friendly processing technologies so that they can attain their full potential. By using a calorific value of 36 MJ/kg of the tire, the pyrolysis procedure yielded 8.9% steel waste, 38% carbon black, 12% gas, and. 41% pyrolytic oil. The carbon black had 90% carbon, while the pyrolytic oil included 66% gasoline and 33% other oils of sufficient superiority to be utilized as a fuel additive or as fuel for engines and furnaces. Consequently, the ecological benefits of the scrap tire pyrolysis process contain avoiding the straight discarding of tires into wastelands. So, this avoids soil contamination, water, and air owing to the release of chemical pollutants created through the breakdown of the scrap tires.

4   Wood

Pyrolysis is vital in the combustion of sawdust and wood because the products of this stage, especially volatiles, and char are then subjected to flame and glowing combustion to release thermal energy [32]. Chen et al. [33] investigated the effect of iron including petrochemical waste ash on pine wood pyrolysis. Thermal actions and kinetic factors were all used to confirm that they had specific advantages in the pyrolysis of pine wood. The trial loss in weight ranges was all greater than the parallel theoretical rates. Ning et al. [34] examined the temperature influence on the thermal decomposition of biochar blast boiler injection performance. The study revealed that the pyrolysis procedure can successfully rise biomass fuel performance. The carbonization degree steadily increases as the pyrolysis temperature rises, as does the fuel performance of biochar. Miranda et al. [35] assess the possibility of integrated power and heat generation from waste pequi seeds. The suggested energy extraction process relied on the gasification of charcoal for use in heat engines. During pyrolysis of entire and fragmented pequi seed trials at 2 °C min1, high quantities of charcoal and bio-oil were produced for retention durations of 3.5 and 7.0 h at 430 °C. At low temperatures, the cold gas efficiency was 90%, resulting in a fuel gas with a calorific value of 7259 kJ Nm^3. Chen et al. [36] investigated the impact of torrefied temperature and retention time on the thermal decomposition of

pine wood elements. The results showed that throughout the biomass gasification, wood torrefied at 275 and 300 °C had a reduced weight loss rate and a larger char percentage, and the pyrolysis conversion time was unaffected by torrefied conditions. The torrefaction parameters were discovered to affect the yields of liquid, gas, and char pyrolysis. The acid concentration of bio-oil derived from torrefied wood reduces with boosted torrefaction intensity, signifying improved bio-oil quality, according to GC/MS analysis. Figure 3 illustrates the experimental apparatus.

Nurhadi et al. [37] studied the optimal pyrolysis temperature of lamtoro wood to create acceptable biochar for coal mixtures as a steam power plant fuel in order to minimize CO_2 emissions. The best temperature for lamtaro wood pyrolysis was determined to be 450 °C. The production of biochar dropped as the pyrolysis temperature raised, while tar and non-condensed gases (NCG) increased. Also, the biochar matter of O, N, H, and S diminished with temperature increase, while carbon content increased from 16.35 to 61.82% at 450 °C, compared to 52.67% in bituminous coal. Mukhametzyanov et al. [38] investigate the influence of pre-heating grounded wood on mass production which is handled by rapid pyrolysis procedure. In order to intensify the superiority of the pyrolysis outcomes as basic resources for additional usage in chemical technologies. A hammer crusher is used to crush 2700 kg of wood fragments. Subsequently crushing, crushed fragments are dried in a rotating dryer till the moisture matter in the mass is 4%, and then heat treated for 2.5 h at 220–270 °C through an endless feed procedure.

El-Gamal et al. [39] investigated the physicochemical characteristics of biochar constructed from two feedstocks, rice husk feedstock (RHF), and sugarcane bagasse feedstock (SCBF). The original pyrolysis procedure was held at a temperature of roughly 500 °C. Nevertheless, pyrolysis temperatures were repeated under controlled
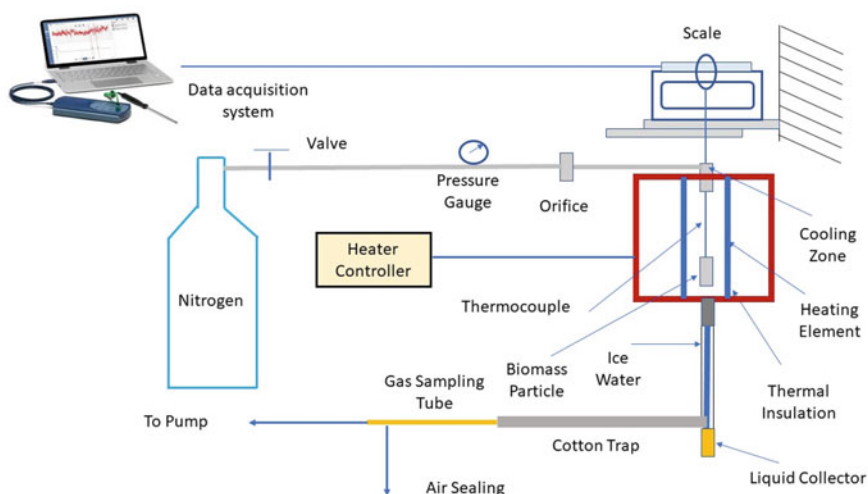
Fig. 3 Pyrolysis reactor

settings at 450 and 550 °C. In general, increasing the pyrolysis temperature lowered biochar output. In contrast, low temperature increases total surface area, total pore volume, and volatile matter.

5   Rubber

Rubber is widely employed in the manufacture of a variety of items, including tires, sealing strips, hoses, rubber-shell products, and so on. Increased rubber usage unavoidably leads to an increase in rubber trash. Scrap tires are one of the most common types of rubber waste, and they have been difficult to remove organically for years due to their resistance to biological decomposition. Several reprocessing plans as road paving, floor mats, derived fuel, and so on, have been suggested to reuse in various modes [40]. Yang et al. [41] investigated the molecular reaction dynamics were joined with experimental tests to achieve the pyrolysis gaseous generation products. The findings present that the pyrolysis temperature of NR steadily rises with the presence of SBR. Choi et al. [42] proposed a fixed bed reactor for waste tire rubber (WTR) pyrolysis at temperatures ranging from 500 to 800 °C. Pyrolysis oils outputs were investigated and the pyrolysis chars acquired were motivated via CO_2 at 950 °C for an activation time of 1–3 h. In the trials, the outputs of pyrolysis char and pyrolysis oil were 37 and 30–38 wt%, respectively. The main composition of pyrolysis oils was aromatic hydrocarbons like xylene, heteroatom-including mixtures like benzothiazole and 2,4-dimethylquinoline and limonene. Wang et al. [43] investigated improving the quality of oil from waste rubber pyrolysis by the addition of larch sawdust. Throughout the pyrolysis activity, the content of sawdust in the rubber steadily rose from 0 to 50, 100, and 200% (wt%) using a 1 kg/h stainless pyrolysis reactor. The results showed that as the percentage of sawdust grew, the effectiveness of pyrolysis enhanced and the remaining carbon decreased.

6   Municipal Solid Waste Pyrolysis

Municipal solid waste (MSW) treatment, management, and disposal are general challenges in each society. MSW pyrolysis is regarded as a pioneering method of processing MSW that yields various chemicals and fuels. Lower levels of nitrogen oxides (NOx) and sulfur oxides (SO_2) are fabricated due to the unmotivated environment in the pyrolysis operations and the ability to cleanse syngas before combustion a pyrolysis-involved process than in a standard MSW incineration facility. In addition to lower gas emissions, pyrolysis-involved MSW treatment can be predicted to improve solid residue quality [43, 44]. He [45] revealed the production of syngas from the pyrolysis of municipal solid waste (MSW at temperatures ranging from 750 to 900 °C. The effects of reactor temperature and weight hourly space velocity (WHSV) on product yields and gas composition have been investigated. Syngas

generation from MSW pyrolysis ranged from 47 to 67 mol%. The results showed that the presence of calcined dolomite substantially impacted product yields and gas composition in the pyrolysis process, with strong catalytic performance on raising gas yield while decreasing oil yield and char production when contrasted to the non-catalytic approach.

7 Conclusion

Pyrolysis technology has attracted the attention of many researchers recently due to the urgent need for energy sources. This study presented the pyrolysis of several potential materials and their resulting fuels. The effect of temperature and time was also discussed with many other parameters on production efficiency. Numerous studies have been discussed for focusing emphasis on the present state of pyrolysis substances and their prospective applicability. Various materials such as plastics, tires, wood, rubber, and municipal wastes were illustrated. Despite the success of many researches in reaching good results, it is important to increase the focus on industrial production so that a large amount of fuel can be produced that can be used economically. Also, attention must be paid to the storage of the resulting fuel so that it is kept for the longest possible period. This technology is suitable for developing countries and societies that suffer from the accumulation of degradable waste. Ultimately, pyrolysis technology may offer a suitable alternative to the huge fluctuation in fossil fuel prices.

8 Recommendation

Emphasis should be placed on the possibility of industrial production of large quantities of biofuel from waste. Also, studying the appropriate methods for storing the resulting fuel and its economic uses. Experimenting with new waste and studying the economic feasibility of converting it into biofuel. Establishing power plants in villages and rural areas, and using the resulting fuel to support agricultural production and economic activity.

References

1. Elhenawy Y, Fouad K, Bassyouni M, Majozi T (2023) Design and performance a novel hybrid membrane distillation/humidification–dehumidification system. Energy Convers Manag 286:117039. https://doi.org/10.1016/j.enconman.2023.117039
2. Fouad K, Gar Alalm M, Bassyouni M, Saleh MY (2021) Optimization of catalytic wet peroxide oxidation of carbofuran by Ti-LaFeO$_3$ dual photocatalyst. Environ Technol Innov 23:101778. https://doi.org/10.1016/j.eti.2021.101778
3. Fouad K, Bassyouni M, Alalm MG, Saleh MY (2021) The treatment of wastewater containing pharmaceuticals. J Environ Treat Tech 9:499–504. https://doi.org/10.47277/JETT/9(2)504
4. Fouad K, Gar Alalm M, Bassyouni M, Saleh MY (2020) A novel photocatalytic reactor for the extended reuse of W-TiO$_2$ in the degradation of sulfamethazine. Chemosphere 257:127270. https://doi.org/10.1016/j.chemosphere.2020.127270
5. El-Gamal H, Radwan K, Fouad K (2020) Floatation of activated sludge by nascent prepared carbon dioxide (Dept. C (Public)). Bull Fac Eng Mansoura Univ 40:21–29. https://doi.org/10.21608/bfemu.2020.101236
6. Fouad K, Bassyouni M, Alalm MG, Saleh MY (2021) Recent developments in recalcitrant organic pollutants degradation using immobilized photocatalysts. Appl Phys A Mater Sci Process 127:612. https://doi.org/10.1007/s00339-021-04724-1
7. Mansi AE, El-Marsafy SM, Elhenawy Y, Bassyouni M (2022) Assessing the potential and limitations of membrane-based technologies for the treatment of oilfield produced water. Alexandria Eng J 68:787–815. https://doi.org/10.1016/j.aej.2022.12.013
8. Makkawi Y, Hassan Pour F, Elsayed Y, Khan M, Moussa O, Masek O, Badrelzaman M, El Tahir W (2022) Recycling of post-consumption food waste through pyrolysis: Feedstock characteristics, products analysis, reactor performance, and assessment of worldwide implementation potentials. Energy Convers Manag 272:116348. https://doi.org/10.1016/j.enconman.2022.116348
9. Ahmed A, Abu Bakar MS, Sukri RS, Hussain M, Farooq A, Moogi S, Park YK (2020) Sawdust pyrolysis from the furniture industry in an auger pyrolysis reactor system for biochar and bio-oil production. Energy Convers Manag 226:113502. https://doi.org/10.1016/j.enconman.2020.113502
10. Elhenawy Y, Moustafa GH, Abdel-Hamid SMS, Bassyouni M, Elsakka MM (2022) Experimental investigation of two novel arrangements of air gap membrane distillation module with heat recovery. Energy Rep 8:8563–8573. https://doi.org/10.1016/j.egyr.2022.06.068
11. Aboelela D, Saleh H, Attia AM, Elhenawy Y, Majozi T, Bassyouni M (2023) Recent advances in biomass pyrolysis processes for bioenergy production: optimization of operating conditions. Sustainability 15(14):11238. https://doi.org/10.3390/su151411238
12. Hu X, Gholizadeh M (2019) Biomass pyrolysis: a review of the process development and challenges from initial researches up to the commercialisation stage. J Energy Chem 39:109–143. https://doi.org/10.1016/j.jechem.2019.01.024
13. Elsakka MM, Ingham DB, Ma L, Pourkashanian M, Moustafa GH, Elhenawy Y (2022) Response surface optimisation of vertical axis wind turbine at low wind speeds. Energy Rep 8:10868–10880. https://doi.org/10.1016/j.egyr.2022.08.222
14. Zakaria M, Sharaky AM, Al-Sherbini AS, Bassyouni M, Rezakazemi M, Elhenawy Y (2022) Water desalination using solar thermal collectors enhanced by nanofluids. Chem Eng Technol 45:15–25. https://doi.org/10.1002/ceat.202100339
15. Li H, Yan S, Song B, Hall P, Karnowo K, Gao W, Zhang H, Hu X, Zhang S (2022) Heavy bio-oils as bio-binders for rice husk densification: Parameter optimization, binding mechanisms and subsequent pyrolysis and combustion performances. Biofuels Bioprod Biorefining 16:1025–1037. https://doi.org/10.1002/bbb.2354
16. Dickerson T, Soria J (2013) Catalytic fast pyrolysis: a review. Energies 6:514–538. https://doi.org/10.3390/en6010514

17. Li C, Zhang C, Sun K, Zhang Z, Zhang L, Zhang S, Liu Q, Hu G, Wang S, Hu X (2020) Pyrolysis of saw dust with co-feeding of methanol. Renew Energy 160:1023–1035. https://doi.org/10.1016/j.renene.2020.06.080

18. Sait HH, Hussain A, Bassyouni M, Ali I, Kanthasamy R, Ayodele BV, Elhenawy Y (2022) Hydrogen-rich syngas and biochar production by non-catalytic valorization of date palm seeds. Energies 15:1–13. https://doi.org/10.3390/en15082727

19. Jahirul MI, Rasul MG, Chowdhury AA, Ashwath N (2012) Biofuels production through biomass pyrolysis—a technological review. Energies 5:4952–5001. https://doi.org/10.3390/en5124952

20. Mandal S, Kunhikrishnan A, Bolan NS, Wijesekara H, Naidu R (2016) Chapter 4—application of biochar produced from biowaste materials for environmental protection and sustainable agriculture production. In: Prasad MNV, Shih K (eds) Environmental materials and waste. Academic Press, pp 73–89

21. Anuar Sharuddin SD, Abnisa F, Wan Daud WMA, Aroua MK (2016) A review on pyrolysis of plastic wastes. Energy Convers Manag 115:308–326. https://doi.org/10.1016/j.enconman.2016.02.037

22. Kiran N, Ekinci E, Snape CE (2000) 00/03732 recycling of plastic wastes via pyrolysis. Fuel Energy Abstr 41:417–418. https://doi.org/10.1016/s0140-6701(00)94792-1

23. Miandad R, Barakat MA, Aburiazaiza AS, Rehan M, Nizami AS (2016) Catalytic pyrolysis of plastic waste: a review. Process Saf Environ Prot 102:822–838. https://doi.org/10.1016/j.psep.2016.06.022

24. Pratama AW, Winarko (2020) Performance test of A mixture of polypropylene plastic fuel from pyrolisis with gasoline to torque and engine power. J Phys Conf Ser 1569. https://doi.org/10.1088/1742-6596/1569/3/032045

25. Setiawan A, Setiani V, Mazdhatina OS (2021) Characterization of fuel oil from pyrolysis waste light density polyethylene (LDPE) and polypropylene (PP). IOP Conf Ser Mater Sci Eng 1034:012069. https://doi.org/10.1088/1757-899x/1034/1/012069

26. Bahri MH (2021) Effect of natural zeolite on biomass pyrolysis. IOP Conf Ser Mater Sci Eng 1034:012082. https://doi.org/10.1088/1757-899x/1034/1/012082

27. Martynis M, Mulyazmi M, Praputri E, Witri R, Putri N (2018) The influence of temperature on the formation of liquid fuel from polypropylene plastic wastes. IOP Conf Ser Mater Sci Eng 334. https://doi.org/10.1088/1757-899X/334/1/012014

28. Hita I, Arabiourrutia M, Olazar M, Bilbao J, Arandes JM, Castaño Sánchez P (2016) Opportunities and barriers for producing high quality fuels from the pyrolysis of scrap tires. Renew Sustain Energy Rev 56:745–759. https://doi.org/10.1016/j.rser.2015.11.081

29. Quek A, Balasubramanian R (2013) Liquefaction of waste tires by pyrolysis for oil and chemicals—a review. J Anal Appl Pyrolysis 101:1–16. https://doi.org/10.1016/j.jaap.2013.02.016

30. Alsaleh A, Sattler ML (2014) Waste tire pyrolysis: influential parameters and product properties. Curr Sustain Energy Rep 1:129–135. https://doi.org/10.1007/s40518-014-0019-0

31. Oliveira Neto G, Chaves L, Pinto L, Santana J, Amorim M, Rodrigues M (2019) Economic, environmental and social benefits of adoption of pyrolysis process of tires: a feasible and ecofriendly mode to reduce the impacts of scrap tires in Brazil. Sustainability 11:2076. https://doi.org/10.3390/su11072076

32. Cranford SW (2020) Modelling of pyrolysis in wood: a review. Matter 2:1–3. https://doi.org/10.1016/j.matt.2019.12.003

33. Chen J, Fang H, Xu F, Ren Y, Wang Z, Zhu Y, Mu L (2022) Influence of iron-containing petrochemical sludge ash on the pyrolysis of pine wood: thermal behaviors, thermodynamic analysis, and kinetic parameters. Bioresour Technol 345:126551. https://doi.org/10.1016/j.biortech.2021.126551

34. Ning X, Liang W, Wang G, Xu R, Wang P, Zhang J, Guo X, Jiang C, Li J, Wang C (2022) Effect of pyrolysis temperature on blast furnace injection performance of biochar. Fuel 313:122648. https://doi.org/10.1016/j.fuel.2021.122648

35. Miranda MRS, Veras CAG, Ghesti GF (2020) Charcoal production from waste pequi seeds for heat and power generation. Waste Manag 103:177–186. https://doi.org/10.1016/j.wasman. 2019.12.025

36. Chen Y, Cao W, Atreya A (2016) An experimental study to investigate the effect of torrefaction temperature and time on pyrolysis of centimeter-scale pine wood particles. Fuel Process Technol 153:74–80. https://doi.org/10.1016/j.fuproc.2016.08.003

37. Nurhadi N, Rianda S, Irawan C, Pramono GP (2021) Biochar production investigation from pyrolysis of lamtoro wood as a coal blend for fuel substitution in steam power plants. IOP Conf Ser Earth Environ Sci 749. https://doi.org/10.1088/1755-1315/749/1/012037

38. Mukhametzyanov SR, Safin RR, Ilalova GF, Khasanshin RR, Shaikhutdinova AR (2019) Improving the quality of pyrolysis products through preliminary thermal treatment of woody raw materials. IOP Conf Ser Mater Sci Eng 666. https://doi.org/10.1088/1757-899X/666/1/ 012082

39. El-gamal EH, Saleh M, Elsokkary I, Rashad M, El-latif MMA (2017) Comparison between properties of biochar produced by traditional and controlled pyrolysis. Alexandria Sci Exch J Int Q J Sci Agric Environ 38:412–425. https://doi.org/10.21608/asejaiqjsae.2017.3720

40. Ji J, Chen G, Zhao J, Wei Y (2020) Efficient removal of Pb (II) by inexpensive magnetic adsorbents prepared from one-pot pyrolysis of waste tyres involved magnetic nanoparticles. Fuel 282:118715. https://doi.org/10.1016/J.FUEL.2020.118715

41. Yang Q, Yu S, Zhong H, Liu T, Yao E, Zhang Y, Zou H, Du W (2021) Gas products generation mechanism during co-pyrolysis of styrene-butadiene rubber and natural rubber. J Hazard Mater 401:123302. https://doi.org/10.1016/j.jhazmat.2020.123302

42. Choi GG, Jung SH, Oh SJ, Kim JS (2014) Total utilization of waste tire rubber through pyrolysis to obtain oils and CO_2 activation of pyrolysis char. Fuel Process Technol 123:57–64. https:// doi.org/10.1016/j.fuproc.2014.02.007

43. Wang W, Chang J, Cai L, Shi SQ (2014) Quality improvement of pyrolysis oil from rubber by adding sawdust. Waste Manag 34:2603–2610. https://doi.org/10.1016/j.wasman.2014.08.016

44. Chen D, Yin L, Wang H, He P (2014) Pyrolysis technologies for municipal solid waste: a review. Waste Manag 34:2466–2486. https://doi.org/10.1016/j.wasman.2014.08.004

45. He M, Xiao B, Liu S, Hu Z, Guo X, Luo S, Yang F (2010) Syngas production from pyrolysis of municipal solid waste (MSW) with dolomite as downstream catalysts. J Anal Appl Pyrolysis 87:181–187. https://doi.org/10.1016/j.jaap.2009.11.005

Performance Analysis of a Green Hydrogen Production System in Several Coastal Locations in Egypt

Mohamed Mohamed Elsakka, Ahmed Refaat, Asmaa Ahmed, Ahmed Amer, Ahmed Elsheikh, Medhat Elfar, Yasser Elhenawy, Nidiana Rosado Hau, Thokozani Majozi, Islam Amin, Selda Oterkus, Erkan Oterkus, and Ayman Mohamed

1 Introduction

Green hydrogen is produced through electrolysis, a process that uses electricity from renewable sources such as solar and wind to split water molecules into hydrogen and oxygen. This process produces zero emissions and can be used to power vehicles, generate electricity, and store energy for later use [1]. Egypt has abundance of renewable energy resources that could be used to produce green hydrogen. There is an intensive research progress in developing renewable energy systems in the Egyptian environment [2–23]. The country has some of the world's highest levels of solar

M. M. Elsakka (✉) · A. Ahmed · A. Amer · A. Mohamed
Department of Mechanical Power Engineering, Faculty of Engineering, Port Said University, Port Said, Egypt
e-mail: elsakka@eng.psu.edu.eg

A. Ahmed
e-mail: asmaa_rady@eng.psu.edu.eg

A. Amer
e-mail: eng.ahmed_amer@eng.psu.edu.eg

A. Mohamed
e-mail: president@psu.edu.eg

M. M. Elsakka · A. Ahmed
Energy Research and Studies Unit, Faculty of Engineering, Port Said University, Port Said, Egypt

A. Refaat · M. Elfar
Department of Electrical Engineering, Faculty of Engineering, Port Said University, Port Said, Egypt
e-mail: ahmed_refaat_1984@eng.psu.edu.eg

M. Elfar
e-mail: mhelfar@eng.psu.edu.eg

31

radiation as it receives about 3050 h of sunlight annually, making it an ideal location for solar power plants. Also, Egypt has vast deserts with some regions well-suited for wind farms. Furthermore, several Egyptian coastal areas have a good wind potential and are suitable for wind turbine installations that could generate large amounts of electricity for electrolysis [24]. The Egyptian government is already taking significant steps to utilize this potential by investing in green hydrogen production projects. In 2022, the government announced plans to build a $1 billion green hydrogen plant near Cairo that would produce up to 1 gigawatt (GW) of power per year. The plant would use solar and wind energy to produce up to 500 tons of green hydrogen per day, enough to power more than 1 million homes or fuel thousands of cars and buses [25].

Overall, green hydrogen production has great potential in Egypt due to its abundance of renewable resources and strategic location. If properly developed, this technology could help to create new economic opportunities while reducing emissions from traditional energy sources.. With continued investment from both public and private entities, green hydrogen could become a major source of clean energy for Egypt in the near future. Egypt has the vision to produce 42% of its electricity from renewable resources to reduce greenhouse emissions by 10% by 2030–2035 [26].

Jang et al. [27] carried out a techno-economic analysis for the production of green hydrogen. They compared four different methods to find out the most economic technique. The authors compared proton exchange membrane electrolysis, alkaline water electrolysis, and solid oxide electrolysis with a waste heat source and with an electric heater. Results showed that solid oxide electrolysis with a waste heat

A. Elsheikh
Department of Production Engineering, Faculty of Engineering, South Valley University, Qena, Egypt
e-mail: ahmed.elsheikh@eng.svu.edu.eg

Y. Elhenawy · T. Majozi
Department of Chemical Engineering, Faculty of Engineering, University of the Witwatersrand, Johannesburg, South Africa
e-mail: yasser.elhenawy@wits.ac.za

T. Majozi
e-mail: thokozani.Majozi@wits.ac.za

N. R. Hau
Multidisciplinary Engineering, Faculty of Engineering, The University of Sheffield, Sheffield, UK
e-mail: n.rosadohau@sheffield.ac.uk

I. Amin · S. Oterkus · E. Oterkus
Department of Naval Architecture, Ocean and Marine Engineering, Faculty of Engineering, University of Strathclyde, Glasgow, UK
e-mail: i.amin@strath.ac.uk

S. Oterkus
e-mail: selda.oterkus@strath.ac.uk

E. Oterkus
e-mail: erkan.oterkus@strath.ac.uk

source gave the lowest price for 1 kg of hydrogen production for the price of 7.16 $/kgH$_2$. Mastropasqua et al. [28] investigated the economic feasibility of producing green hydrogen using a parabolic dish integrated with a high-temperature electrolysis system. The solar system provided electricity and thermal energy. The system could be operated with a cell efficiency of about 80%, and solar to hydrogen efficiency could reach 30%. Zhang et al. [29] investigated the performance of a solar-driven system for hydrogen production. They investigated the parameters that could affect the system's performance as operating temperature, inlet water rate, and leakage resistance. AlZahrani et al. [30] designed a system to generate hydrogen which has four subsystems: solar tower, thermal energy storage system, supercritical CO$_2$ Brayton cycle, and solid oxide steam electrolyzer. Results showed the overall efficiency of solar-hydrogen conversion of the integrated system reaching 12.7%. All systems were optimized to provide continuous operation and high overall efficiency. Lin et al. [31] carried out a techno-economic analysis of a solar-driven electrolysis system to produce hydrogen besides synthesis gas. They compared three different configurations to find the most economic one. The three systems had different technologies: solar concentration, photovoltaic, and a combination of both technologies.

Boudries [32] carried out a techno-economic study for hydrogen production using concentrated solar power. The solar system was used to heat the heat transfer fluid for steam production. A Rankine cycle power plant was employed for electricity generation to power the electrolysis unit for hydrogen production. Results showed that the cost of hydrogen depends on the cost of energy production. Normal solar irradiance was an important parameter for hydrogen cost. The system was economically feasible compared to PV based electrolysis system. Rahil et al. [33] investigated the economic feasibility of hydrogen production using a system operated by off-peak electricity. Results showed that the system reliability is low to some extent due to operation by off-peak electricity. Yadav et al. [34] carried out an economic assessment for hydrogen production using solar driven electrolyzer. The authors found that increasing current density improves efficiency. The system was cost-effective for long-term calculations. They depended on the reduction in equipment cost expected in 2030. Mohsin et al. [35] investigated the economic feasibility of producing hydrogen using wind energy in different sites. Air density, turbine size, and wind speed affected hydrogen production. Results showed that the cost of hydrogen varied from 5.30 to 5.80 $/kg H$_2$. Abdin et al. [36] presented an economic analysis of hydrogen production using renewable energy. They compared different locations. Optimization was performed for systems sizing depending on load demand as wind speed and solar radiation intensity were different in each location. It was concluded that better wind speed and radiation intensity could lead to reduced cost of energy for the system.

This paper aims to assess the performance of a solar-powered electrolysis system for green hydrogen production in several coastal locations in Egypt. The system incorporates a PV array with a maximum power point tracking controller, battery storage, and charge controller. A comparative study of the proposed system performance is conducted for a set of 25 different coastal sites considering a year-long dataset for each location.

2 Meteorological Data

In order to obtain a comprehensive assessment of the proposed green hydrogen system in different coastal environments in Egypt, 25 coastal sites have been considered. Figure 1 illustrates the locations of the selected sites on the Egyptian map. The detailed locations of these sites are presented in Table 1 based on the geographic coordinate system. These locations are categorized into three main coastal regions, namely, the Red Sea coast, the Sinai Peninsula coasts, and the Mediterranean Sea coast, as shown in Table 1. Furthermore, the year-averaged Global Horizontal Irradiation (GHI) in [kWh/m^2] for each site is presented in Table 1 based on the data from the Global Solar Atlas [37]. It is observed that Hurghada has the highest GHI among those considered locations with a value of almost 2321.5 [kWh/m^2]. On the other hand, Sidi Barrani possesses the lowest GHI of about 1981.9 [kWh/m^2].

Fig. 1 The map of Egypt with an illustration of the selected coastal cities under investigation. The map is captured from Google Earth Pro Software, with attribution: DATA SIO, NOAA, U.S. Navy, NGA, CEBCO, Image Landsat/Copernicus [38]

Table 1 A list of the selected coastal cities under investigation including their geographic coordinate, year-averaged global horizontal irradiation, and their specific coastal region

No.	City	Latitude	Longitude	Year-averaged global horizontal irradiation [kWh/m^2]	Region
1	Suez	29.97706	32.51149	2133.0	Red Sea coast
2	Ain Sokhna	29.65097	32.31112	2181.8	
3	Zaafarana	29.11065	32.66038	2195.8	
4	Ras Ghareb	28.35084	33.07536	2273.8	
5	Hurghada	27.1925	33.78171	2321.5	
6	Safaga	26.75296	33.93559	2315.5	
7	Marsa Alam	25.06842	34.88419	2312.6	
8	Halayeb	22.22043	36.64124	2237.5	
9	Taba	29.49346	34.89587	2199.8	Sinai Peninsula coast
10	Dahab	28.4956	34.50043	2276.0	
11	Sharm El-Sheikh	27.94671	34.34875	2294.5	
12	Al-Tor	28.23149	33.6375	2286.0	
13	Ras Abu Rudeis	28.90598	33.18981	2194.6	
14	Ras Sedr	29.59099	32.71954	2151.7	
15	Arish	31.11754	33.80462	2073.2	
16	Bir al-Abd	31.0196	33.00792	2114.1	
17	Port Said	31.23868	32.28517	2064.4	Mediterranean Sea coast
18	Gamasa	31.44123	31.53645	2021.9	
19	Rasheed	31.40101	30.41673	2031.1	
20	Alexandria	31.22411	29.95489	2034.1	
21	El-Alamein	30.82247	28.95431	2045.7	
22	El Dabaa	31.02236	28.44776	2063.9	
23	Marsa Matruh	31.33664	27.25533	2045.3	
24	Sidi Barrani	31.61058	25.93	1981.9	
25	El Salloum	31.575	25.15932	2016.5	

The National Solar Radiation Database (NSRDB) [39] is a comprehensive set of meteorological data and solar radiation measurements, including direct normal irradiance, global horizontal irradiance, and diffuse horizontal irradiance, that are available in the hourly form. This investigation utilizes the year-long historical data from the NSRDB to provide the input solar radiation to the system-level model. Spline interpolation is utilized to convert the hourly data from the NSRDB to instantaneous

interpolated data which is essential for system-level modeling. More details about
the proposed system-level model are available in Sect. 3.

3 Mathematical Modeling

MATLAB Simulink has been incorporated to build the system-level model. Figure 2
shows a schematic diagram of the Simulink model for the proposed solar-powered
green hydrogen system. The solar irradiance data from NSRDB is fed to the model
in hourly format. Then, a lookup table is used to provide the instantaneous data to
model each second based on the Spline interpolation. The Simulink model consists
of blocks, and each block represents an interconnected subsystem to form a system-
level model. These subsystems include the PV array, battery storage, and proton
exchange membrane (PEM) electrolyzer. The signals between the blocks represent
the system variable. While the system input is mainly the meteorological data, the
system output is mainly the hydrogen production quantity.

The PV array subsystem is one of the key subsystems. The PV array is repre-
sented by a double exponential diodes model that incorporates a current source that
provides the highest accuracy. This accurate model is formed by incorporating series
resistance, shunt resistance, and recombination into the simplest model. The series
resistance reflects the voltage drop that occurs due to the current path through the
semiconductor material, metal grid, contacts, and current-collecting bus. The shunt
resistance represents the current leakage to the ground at the edges of the cell. The
second diode signifies the recombination in the PV cell's depletion regionwhich
provides a non-resistive current path in parallel with the intrinsic PV cell [40]. The
PV array submodel is constructed with a Maximum Power Point Tracking (MPPT)
controller in order to ensure successful tracking of the maximum power under fast
changes in solar radiation. Cuckoo Search Algorithm is a bioinspired MPPT algo-
rithm that has been successfully employed in fast changes in solar radiation [41].
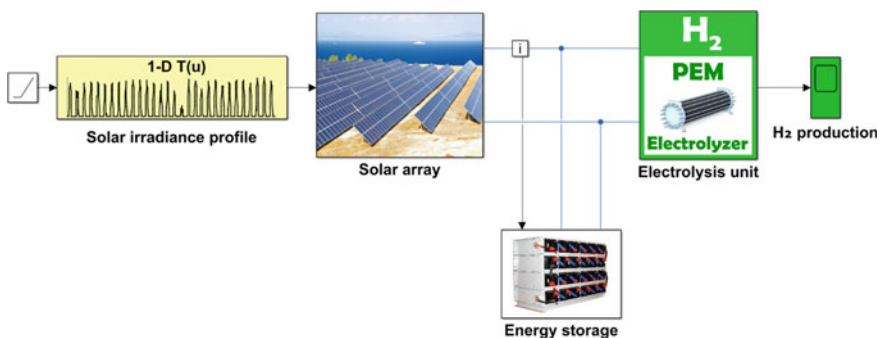
Fig. 2 A schematic diagram of the proposed solar-powered green hydrogen production system for
a coastal location

The Buck-boost DC–DC converter is used as a power conditioning unit between the PV source and the electrolyzer [42]. The MPPT controller regulates this Buck-boost converter to adjust its duty cycle.

The battery storage subsystem is implemented to model the storage of excess energy generated by the PV array. Energy management battery storage is important to ensure a stable, reliable, and cost-effective energy supply. The energy management battery storage is regulated by the energy balance based on the instantaneous energy stored in the battery, the initial energy stored in the battery, and the power input/output from the battery. The employed battery charger prevents the battery from overcharging as well as deep discharging. The battery is represented by a combination of a resistor in series and a voltage source that depends on the charge. To make the model more robust, an approximate correlation is employed between voltage and the remaining charge. This correlation mimics the faster decline in voltage as the charge decreases.

The electrolyzer is the key element in any green hydrogen production system. A PEM electrolyzer is one of the promising types of the electrolyzer. It uses a solid polymer electrolyte membrane to split water into hydrogen and oxygen gases. In the proposed system, the PEM electrolyzer is employed. PEM electrolyzers consist of several components, including an anode and a cathode, a proton exchange membrane, and an electrolyte. The Electrolyzer is modeled as an electric load that identifies the amount of hydrogen production based on the electricity provided considering the temperature of water in the tank. The electrolysis stack consists of series-connected individual electrolyzer cells that are modeled considering the ideal state with a constant pH.

The NSRDB's actual historical data from a full year was used to supply solar radiation data to the system-level model. The hourly data from NSRDB was transformed into instantaneously interpolated data using spline interpolation to ensure accurate system-level modeling. Figure 3 illustrates two examples of the annual historical data for two locations, namely Al-Tor and Ain Sokhna, based on the hourly data obtained from NSRDB [39].

4   Results and Discussions

The abovementioned MATLAB Simulink model is implemented to mimic the performance of the green hydrogen production system in the selected coastal locations that are specified in Table 1. The historical data of solar irradiance for each location from the NSRDB is fed to the model as an input. The model is capable to provide instantaneous hydrogen production with a 1-s resolution. However, the hydrogen production is then integrated to provide the annual hydrogen production for each of the considered locations. Figure 4 illustrates the annual output of green hydrogen production in kg for each of the considered coastal locations.

As mentioned before in Table 1, the considered 25 locations are categorized into three regions based on their geographical coastal area, particularly the Red Sea
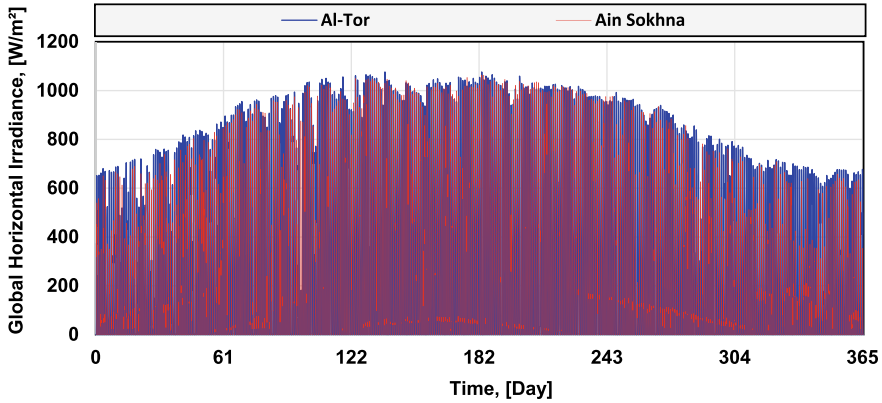
Fig. 3 Examples of the annual historical data for two locations, namely Al-Tor and Ain Sokhna. Data are obtained from NSRDB [39]
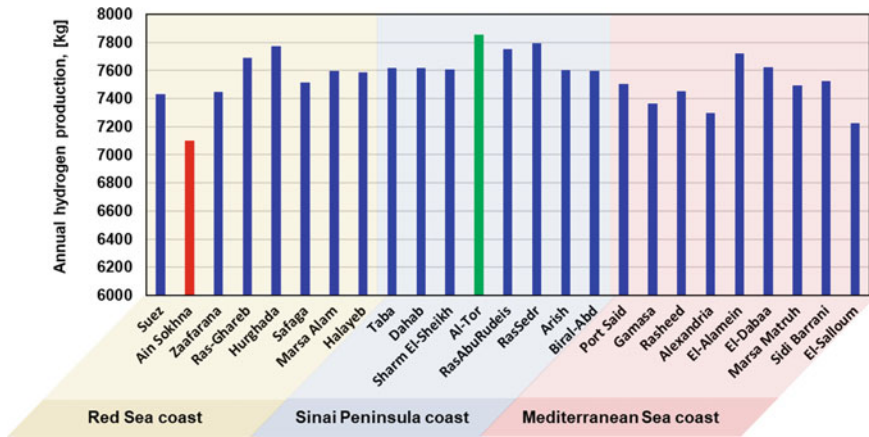
Fig. 4 An illustration of the annual hydrogen production for 25 selected locations over the three coastal regions in Egypt

coast, Sinai Peninsula coast, and Mediterranean Sea coast. These three regions are illustrated in Fig. 4 with different shading colors. Hurghada offers the best annual hydrogen production on the Red Sea coast while Ain Sokhna exhibits the lowest annual hydrogen production. Al-Tor has the highest hydrogen production rate among the other considered locations on the Sinai Peninsula coast. Considering the Mediterranean coast, it can be noticed that El-Alamein has the highest annual hydrogen production rate while El-Salloum is found to exhibit the lowest annual hydrogen production rate. It is well-known that Hurghada and Al-Tor have excellent wind potential which suggests that it would be worth studying the feasibility of green hydrogen production based on a hybrid solar/wind system.

Considering the 25 selected locations over the three coastal regions, Al-Tor, marked in green color in Fig. 4, shows the best performance with an annual hydrogen production rate of 7858 [kg/annum] and this is about 11% higher than Ain Sokhna, marked in red color in Fig. 4, that manifested the lowest annual hydrogen production rate about 7102 [kg/annum]. Overall, the locations in the Sinai Peninsula show a relatively close annual hydrogen production rate with relatively low variations in contrast with the other two coastal regions that exhibit considerable variations in the hydrogen production rates even between the close neighboring cities, such as Suez and Ain Sokhna. These considerable variations are due to the different topographic conditions that are expected to influence the clouds and shadings. In conclusion, this suggests that the Sinai Peninsula coast is promising in green hydrogen production based on solar energy.

In order to assess the effect of the seasonal variation of solar irradiance on the performance of the system production of green hydrogen, three coastal locations are considered including Ain Sokhna, Rashed, and Al-Tor. The hydrogen production of each site is illustrated as shown in Fig. 5 for each month over one year. It can be observed that the system hydrogen production in Rasheed in July outperforms the production in Al-Tor even though Al-Tor exhibits the highest annual hydrogen production. Also, in February and April, the production in Ain Sokhna outperforms the production in Rasheed even though Rasheed outperforms Ain Sokhna based on the annual hydrogen production. This illustrates the importance of considering the instantaneous data and the different seasonal conditions rather than the year-averaged solar irradiance in the investigation of green hydrogen production systems.
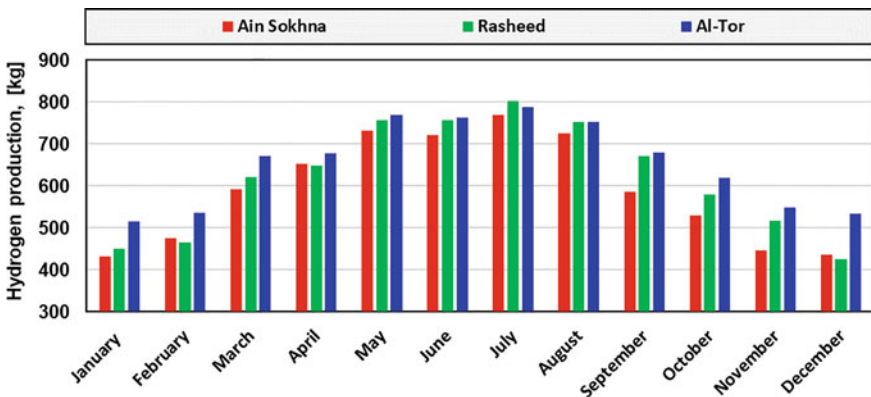
Fig. 5 The monthly hydrogen production of three selected sites over one year

5 Conclusion

This article explores the potential of producing green hydrogen in Egypt, which has ample renewable resources and a strategic location on the Sea. The study evaluates the performance of green hydrogen production in various coastal locations in Egypt, using a MATLAB Simulink simulation that considers 25 locations and their available solar irradiance. The analysis includes an assessment of a solar-powered green hydrogen system, using a historical year-long solar irradiance dataset for each location. The results indicate that the Sinai Peninsula coast is a promising area for green hydrogen production based on solar energy, with Al-Tor showing the best performance and an annual hydrogen production rate of 7858 kg. The study highlights the importance of considering instantaneous data and seasonal conditions for investigating green hydrogen production systems. It is suggested that future work should explore the feasibility of a hybrid solar/wind system for green hydrogen production in locations with high wind potential.

6 Recommendation

Based on the abovementioned findings, it is recommended to implement the proposed green hydrogen production system in Sinai coastal area. Furthermore, it is recommended to investigate the potential of hybrid PV-Wind utilization in green hydrogen production systems.

References

1. Shiva Kumar S, Lim H (2022) An overview of water electrolysis technologies for green hydrogen production. Energy Rep 8:13793–13813
2. Elbaz A, Elfar MH, Kalas A, Refaat A (2022) Maximum power extraction from polymer electrolyte membrane (PEM) fuel cell based on deterministic particle swarm optimization algorithm. In: Proceedings of the 2022 conference of russian young researchers in electrical and electronic engineering, ElConRus 2022. Institute of Electrical and Electronics Engineers Inc., pp 613–619
3. Refaat A, Elgamal M, Korovkin NV (2019) A novel photovoltaic current collector optimizer to extract maximum power during partial shading or mismatch conditions. In: Proceedings of the 2019 IEEE conference of russian young researchers in electrical and electronic engineering, ElConRus 2019, 407–412. https://doi.org/10.1109/EICONRUS.2019.8657173
4. Osman MH, Ahmed MK, Refaat A, Korovkin NV (2021) A comparative study of MPPT for PV system based on modified perturbation observation method. In: Proceedings of the 2021 IEEE

conference of Russian young researchers in electrical and electronic engineering, ElConRus 2021, 1023–1026

5. Refaat A, Abdel A, Shehata H, Elgamal M, Korovkin NV, Shehata AA, Korovkin NV (2020) Current collector optimizer topology with reconfiguration algorithm to harvest optimal power from nonuniform aged PV arrays. In: 2020 international multi-conference on industrial engineering and modern technologies (FarEastCon). https://doi.org/10.1109/fareastcon50210.2020.9271455

6. Elsakka MM, Ingham DB, Ma L, Pourkashanian M, Moustafa GH, Elhenawy Y (2022) Response surface optimisation of vertical axis wind turbine at low wind speeds. Energy Rep 8:10868–10880

7. Elsakka MM, Ingham DB, Ma L, Pourkashanian M (2020) Effects of turbulence modelling on the predictions of the pressure distribution around the wing of a small scale vertical axis wind turbine. In: Proceedings of the 6th European conference on computational mechanics: solids, structures and coupled problems, ECCM 2018 and 7th European conference on computational fluid dynamics, ECFD 2018, pp 3921–3931

8. Elsakka MM, Ingham DB, Ma L, Pourkashanian M (2021) Comparison of the computational fluid dynamics predictions of vertical axis wind turbine performance against detailed pressure measurements. Int J Renew Energy Res 11:276–293

9. Amin I, Elsakka M, Oterkus S, Nguyen CT, Ozdemir M, El-Aassar AH, Shawky H, Oterkus E (2022) Computational fluid dynamics-based design of anoxic bioreactor zone in wastewater treatment plant. Desalination Water Treat 253:9–23. https://doi.org/10.5004/dwt.2022.28300

10. Ahmed A, Alzahrani M, Shanks K, Sundaram S, Mallick TK (2022) Reliability and temperature limits of the focal spot of a primary optical component for an ultra-high concentrated photovoltaic system. AIP Conf Proc 2550. https://doi.org/10.1063/5.0099091

11. Ahmed A (2021) Thermal management of high concentrating photovoltaic system. University of Exeter

12. Ahmed A, Shanks K, Sundaram S, Mallick T (2021) Energy and exergy analyses of new cooling schemes based on a serpentine configuration for a high concentrator photovoltaic system. Appl Therm Eng 199:117528. https://doi.org/10.1016/j.applthermaleng.2021.117528

13. Ahmed A, Zhang G, Shanks K, Sundaram S, Ding Y, Mallick T (2021) Performance evaluation of single multi-junction solar cell for high concentrator photovoltaics using minichannel heat sink with nanofluids. Appl Therm Eng 182:115868. https://doi.org/10.1016/j.applthermaleng.2020.115868

14. Abuhashish MN, Daoud AA, Elfar MH (2022) A novel model predictive speed controller for PMSG in wind energy systems. Int J Renew Energy Res 12:170–180. https://doi.org/10.20508/IJRER.V12I1.12750.G8385

15. Amin I, Ali MEA, Bayoumi S, Balah A, Oterkus S, Shawky H, Oterkus E (2021) Numerical hydrodynamics-based design of an offshore platform to support a desalination plant and a wind turbine in Egypt. Ocean Eng 229:108598. https://doi.org/10.1016/J.OCEANENG.2021.108598

16. Bayoumi S, Ali MEA, Amin I, Torky RE, Oterkus S, Shawky H, Oterkus E, Bayoumi S, Ali MEA, Amin I, Torky RE, Oterkus S, Shawky H, Oterkus E (2021) Environmentally-driven design of a floating desalination platform (case study: reverse osmosis floating desalination platform of ras gharib, Egypt). AIMS Energy 9(3):623–650. https://doi.org/10.3934/ENERGY.2021030

17. Amin I, Ali MEA, Bayoumi S, Oterkus S, Shawky H, Oterkus E (2020) Conceptual design and numerical analysis of a novel floating desalination plant powered by marine renewable energy for Egypt. J Mar Sci Eng 8:95. https://doi.org/10.3390/JMSE8020095

18. Amin I, Eshra N, Oterkus S, Oterkus E (2022) Experimental investigation of motion behavior in irregular wave and site selection analysis of a hybrid offshore renewable power station for Egypt. Ocean Eng 249:110858. https://doi.org/10.1016/J.OCEANENG.2022.110858

19. Gharib-Yosry A, Blanco-Marigorta E, Fernández-Jiménez A, Espina-Valdés R, Álvarez-álvarez E (2021) Wind–water experimental analysis of small SC-darrieus turbine: an approach for energy production in urban systems. Sustainability 13:5256. https://doi.org/10.3390/SU1309 5256

20. Gharib Yosry A, Fernández-Jiménez A, Álvarez-Álvarez E, Blanco Marigorta E (2021) Design and characterization of a vertical-axis micro tidal turbine for low velocity scenarios. Energy Convers Manag 237

21. Amer AE, Lebedev VA (2020) Numerical investigations on latent heat storage unit using phase change material. J Phys Conf Ser 1565:012099. https://doi.org/10.1088/1742-6596/1565/1/012099

22. Amer AE, Elsakka MM, Lebedev VA (2021) Thermal performance of an accumulator unit using phase change material with a fixed volume of fins. Int J Energy Res 45:19089–19102. https://doi.org/10.1002/ER.7095

23. Refaat A, Khalifa AE, Elsakka MM, Elhenawy Y, Kalas A, Elfar MH (2023) A novel meta-heuristic MPPT technique based on enhanced autonomous group particle swarm optimization algorithm to track the GMPP under partial shading conditions—experimental validation. Energy Convers Manag 287:117124. https://doi.org/10.1016/J.ENCONMAN.2023.117124

24. Moharram NA, Tarek A, Gaber M, Bayoumi S (2022) Brief review on Egypt's renewable energy current status and future vision. Energy Rep 8:165–172

25. Egypt close to deals on 1GW of solar and wind projects|Reuters. https://www.reuters.com/business/cop/egypt-close-deals-1gw-solar-wind-projects-2022-11-17/. Accessed 10 Feb 2023

26. IRENA (2018) Renewable energy outlook. Egypt, Abu Dhabi

27. Jang D, Kim J, Kim D, Han WB, Kang S (2022) Techno-economic analysis and Monte Carlo simulation of green hydrogen production technology through various water electrolysis technologies. Energy Convers Manag 258

28. Mastropasqua L, Pecenati I, Giostri A, Campanari S (2020) Solar hydrogen production: Techno-economic analysis of a parabolic dish-supported high-temperature electrolysis system. Appl Energy 261

29. Zhang H, Su S, Chen X, Lin G, Chen J (2013) Configuration design and performance optimum analysis of a solar-driven high temperature steam electrolysis system for hydrogen production. Int J Hydrogen Energy 38:4298–4307

30. AlZahrani AA, Dincer I (2016) Design and analysis of a solar tower based integrated system using high temperature electrolyzer for hydrogen production. Int J Hydrogen Energy 41:8042–8056

31. Lin M, Haussener S (2017) Techno-economic modeling and optimization of solar-driven high-temperature electrolysis systems. Sol Energy 155:1389–1402

32. Boudries R (2018) Techno-economic study of hydrogen production using CSP technology. Int J Hydrogen Energy 43:3406–3417

33. Rahil A, Gammon R, Brown N (2018) Techno-economic assessment of dispatchable hydrogen production by multiple electrolysers in Libya. J Energy Storage 16:46–60

34. Yadav D, Banerjee R (2018) Economic assessment of hydrogen production from solar driven high-temperature steam electrolysis process. J Clean Prod 183:1131–1155

35. Mohsin M, Rasheed AK, Saidur R (2018) Economic viability and production capacity of wind generated renewable hydrogen. Int J Hydrogen Energy 43:2621–2630

36. Abdin Z, Mérida W (2019) Hybrid energy systems for off-grid power supply and hydrogen production based on renewable energy: a techno-economic analysis. Energy Convers Manag 196:1068–1079

37. Global Solar Atlas. https://globalsolaratlas.info/map. Accessed 22 Mar 2023

38. Google Earth Pro, DATA SIO, NOAA, U.S. Navy, NGA, CEBCO, Image Landsat/Copernicus. https://earth.google.com/intl/earth/. Accessed 12 Apr 2023

39. National Renewable Energy Laboratory National Solar Radiation Database: NSRDB. https://nsrdb.nrel.gov/. Accessed 2 Apr 2023

40. Vamsi Krishna Reddy AK, Venkata Lakshmi Narayana K (2022) Investigation of a social group assisted differential evolution for the optimal PV parameter extraction of standard and modified diode models. Energy Convers Manag 268:115955. https://doi.org/10.1016/J.ENCONMAN.2022.115955

41. Khalifa AE, Refaat A, Kalas A, Elfar MH (2022) Two bio-inspired MPPT algorithms to harvest the maximum power from partially shaded PV arrays. In: Proceedings of the 2022 conference

of russian young researchers in electrical and electronic engineering, ElConRus 2022. Institute of Electrical and Electronics Engineers Inc., pp 670–674

42. Osman MH, Refaat A (2019) Adaptive multi-variable step size P&O MPPT for high tracking-speed and accuracy. IOP Conf Ser Mater Sci Eng 643:012050. https://doi.org/10.1088/1757-899X/643/1/012050

Numerical and Experimental Investigation on Integrated Solar Chimney for Seawater Desalination System in Egypt

Mohamed Elsakka, Islam Amin, Erkan Oterkus, Selda Oterkus, Moustafa Aboelfadl, Mohamed Elsayed Abdelfattah, Omar Nimr, Amro Abdullateif, Dalia Abouzaid, and Hossam Shawky

1 Introduction

Water is essential for sustainable development and plays a crucial role in various aspects such as socio-economic progress, energy generation, food production, the well-being of ecosystems, and even human survival. Furthermore, water is of utmost importance in adapting to climate change, as it serves as the vital connection between

M. Elsakka (✉)
Mechanical Power Engineering Department, Port Said University, Port Said, Egypt
e-mail: Elsakka@eng.psu.edu.eg

Energy Research and Studies Unit, Faculty of Engineering, Port Said University, Port Said, Egypt

I. Amin
Department of Naval Architecture and Marine Engineering, Port Said University, Port Said, Egypt
e-mail: i.amin@strath.ac.uk

I. Amin · E. Oterkus · S. Oterkus
Department of Naval Architecture, Ocean and Marine Engineering, University of Strathclyde, Glasgow, UK
e-mail: erkan.oterkus@strath.ac.uk

S. Oterkus
e-mail: selda.oterkus@strath.ac.uk

M. Aboelfadl · M. E. Abdelfattah · A. Abdullateif · D. Abouzaid · H. Shawky
Egyptian Desalination Research Center (EDRC), Desert Research Center (DRC), Cairo, Egypt

O. Nimr
Ain Shams University, Cairo, Egypt
e-mail: omar.nemr@eng.asu.edu.eg

University of Antwerp, Antwerp, Belgium

society and the environment. [1]. Over the last century, power and fresh water production processes have dominantly been driven using fossil fuels. The use of fossil fuels has shown challenging issues, which are mainly the damage they cause to the environment and the depletion of their sources. Furthermore, attaining the worldwide intensive growing demand for those two crucial resources has necessitated switching to sustainable energy sources to produce them. Among various utilized sustainable and environmentally safe energy resources, solar energy has been found as the most dependable and affordable renewable energy resource [2]. Many studies were previously carried out to utilize the sustainable renewable energy to generate freshwater. Amin et al. proposed floating desalination plant powered by marine renewable energy [2–11]. Elminshawy et al. [12] proposed floating photovoltaics system to generate clean energy that can used to desalinate freshwater for remote rural areas. Eshra and Amin [8] developed a hybrid floating power station driven by renewable energy to generate freshwater for remote coastal areas. Amin et al. [9] developed wastewater treatment plant powered by renewable energy to generate freshwater.

Solar Energy is another important sustainable energy source, especially in sunbelt countries such as Egypt, where sunlight and higher radiation are available for longer time. The technology of solar energy has been considered as a sustainable and clean source of energy. The main advantage of solar chimney compared with photovoltaics system is that it is able to deploy all day not only during daylight [12]. The development at Solar updraft tower (SUT), or solar chimney power plant (SCPP), represents one of the means that have been developed and implemented to convert solar energy into electric power. Cuce et al. [10] presented the design and performance testing results of Manzanares pilot SCPP in Spain, which has been launched for operation in 1982. Those results have been considered as a foundation of this developing technology and benchmark for all the subsequent related studies.

To study the performance of solar chimney systems, computational fluid dynamics (CFD) was used based on different simulation codes. Bernardes et al. [13] used CFD to solve the energy and Navier–Stokes equations in a steady state for the natural convection using the finite volume method. Chung and Gholamalizadeh [14] developed a numerical-based model of a solar chimney power plant by performing a 3D simulation of the engineering standards for the Manzanares prototype coupled with a real turbine implemented using computational fluid dynamics (CFD). Bouabidi et al. [15] studied numerically the solar chimney power plant under the weather conditions of Tunisia. They performed many test simulations to analyze the effect of chimney diameter. They studied the characteristics of the flowing air with various diameters. Simulation results revealed that the air flow velocity increased with the chimney diameter. Ismail et al. [16] performed a computational analysis to examine possible changes to the properties of air flow and heat transfer in relation to a traditional solar chimney device by using unsuccessful (negative) flow control methods. This research found that the rise in the number of unsuccessful controllers contributed to a 7% increase in the maximum speed at the chimney entrance. Djaouida et al. [17] presented a numerical study of the station of the solar chimney. To test the air flow characteristics of the prototype power plant from the solar chimneys in Manzanares, Spain, numerical simulations were performed.

Hassan et al. [18] conducted a numerical analysis using the ANSYS Fluent software, which involved investigating the effects that occur when adjusting the slope of the solar collector of the device and also the angle of diffraction of the chimney on power output from the solar chimney device. Guo et al. [19] suggested a solar chimney three-dimensional numerical model with solar radiation, solar load, and a turbine model, and then tested it first using experimental data for Spain's original solar chimney model. Das and Chandramohan [20] developed a three-dimensional numerical model for a solar chimney station to estimate and evaluate flow and efficiency parameters. They studied the effects of geometric variables such as the chimney height and the solar collector roof angle.

Setareh [21] conducted an experiment to investigate the influence of geometric factors such as the roof collector angle (B), chimney divergence angle (A), and wind speed on the performance of the solar chemistry power plant (SCPP). The parametric research was conducted on different a and b components. The results demonstrated that the SCPP power output rose by b to a given a. It was also recommended that in the range of 0.7–0.85, the ratio of the decrease in the turbine pressure to the total pressure potential be chosen to achieve the optimal output of the SCPP. Singh et al. [22] examined the potential design changes to enhance their extremely poor energy conversion efficiency with a third component, called the bell-mount inlet, as well as two key components: a collector and a chimney, to improve the thermal performance of the system. The results showed that the air velocity might significantly increase by about 270% when the collector, the chimney, and efficient bell-mouth integration modifications are suitable and significantly improve the turbine power output compared to conventional power supplies.

The objectives of this work are to provide a proof of physical concept of operation of a novel solar-powered hybrid generator of power and sea water desalination experimentally and numerically where solar power system has been combined with liquid desiccant system to simultaneously produce power and fresh water. Numerical and experimental investigation on the proposed system is conducted to prove the concept.

2   Concept Description

A typical Solar updraft tower is shown in Fig. 1. For the Solar tower prototype in Egypt, the plant consists of three main components: solar collector, chimney tower and ducted type wind turbine. The collector is of a circular geometry and a canopy made of pellucid material fixed above the ground at a certain height. The chimney tower is a circular duct. The tower can be constructed as either steel or concrete structure. The wind turbine is typically of horizontal axis type (air flow is parallel to rotation axis), coupled to an electrical generator at its lower shaft end. The collector receives solar radiation, and due to greenhouse effects, the ground underneath the transparent canopy is heated. In the meantime, it heats the adjacent mass of air, which is induced to move, via natural convection mechanism, from collector perimeter

towards the plant tower inlet where the chimney pipe maintains a decreasing pressure gradient. In other words, the collector and chimney pipe complement each other to create and maintain the targeted air flow throughout the plant's passages, in such a manner that the collector provides the temperature rise required to make the flowing air stream lower in density as it advances towards chimney inlet, while the chimney pipe with the pressure difference between its top (outlet) and bottom (inlet), due to altitude difference, provides the needed decreasing pressure gradient. Moreover, at inlet of the chimney pipe where the wind turbine is located, the surge of the effectuated large volume of air will lead to a strong upwind. This upwind would drive the turbine, which then rotate a coupled electrical generator and thus produce electricity. Concerning water scarcity worldwide, desalination is the most widely used measure to help achieving possible quantities of the demanded fresh water. However, desalination process can only be used in coastal areas where the seawater is available. In addition, serious environmental and economic challenges are encountered in all types of desalination systems. Consequently, there have been strategic plans globally to develop freshwater generation technologies characterized of being environmentally safe, economically viable and renewable energy- sourced. Atmosphere represents a large reservoir with approximately 37.5×1015 gallons of water in an invisible vapour form [11].

Fig. 1 Solar tower prototype in Egypt

Table 1 Main geometric dimensions of the solar chimney power plant prototype

Geometric parameter	Value
Chimney height (m)	6.00
Chimney inner diameter (m)	0.12
Chimney thickness (m)	0.05
Cover of the heat collector (m)	0.06
Water tank height (evaporation tank) (mm)	0.30
Collector diameter (m)	2.60

3 Experimental Work

The pilot plant of solar chimney was fabricated and tested in outdoor site at Desert Research Center, Egypt, as shown in Fig. 1. The pilot main dimensions and components are listed in Table 1. The collector canopy of the built pilot plant was fabricated using a polyethylene transparent sheet of 1mm thickness. The canopy was designed to be fixed and fabricated using wooden frame and supports. However, the black pebble bed was selected to be the suitable collector ground material that can be used as an absorber for its affordable and good thermal storage effects. The black pebbles were designed with a depth of 0.2 m.

The solar irradiance was measured by DFY2 sky radiometer and radiation ammeter. The heated air flow speed will be measured by hot bulb anemometer. The ambient temperature will be measured automatically by Pt100 resistance which is placed in an instrument shelter. Multi-channel SWP inspection monitors were connected to the Pt100 resistances at each measuring point. And the network was connected to the serial port of a computer through converter, sending the collected data to the computer.

The pilot was tested on hourly basis over the daytime for ten randomly selected non-rainy days. At the beginning of each testing hour, the weather conditions were measured (solar irradiance, ambient temperature, relative humidity, and wind speed). At the same time, the SCPP collector ground temperature as well as its canopy film temperature would be measured. Right afterwards, the SCPP operating air velocity, temperature and density were recorded at different points across the collector flow field as well as at the inlet of the chimney pipe.

4 Numerical Modeling and Simulation

4.1 Numerical Model

Numerical simulation is an important tool for studying any transportation phenomenon involving heat, fluid, and mass flow [12]. The model of the presented solar chimney as shown in Fig. 2, corresponding to the dimensions of the prototype

pilot fabricated in Egypt was modeled in the Design Modular software of ANSYS Fluent. The computational domain was discretized with a structured mesh having fine elements. The computational model is illustrated in Fig. 3. The mesh was performed according to the model as in Fig. 4 in the same ANSYS Mesher software. Due to the size large model, generating mesh is a complicated task and requires a large number of elements and nodes, especially at some important locations such as the curved zone between the collector and the tower as shown in Fig. 5.

The simulation was carried out using the numerical finite volume method for solving Navier–Stokes equations and the laws of mass and energy conservation with a commercial software ANSYS Fluent, product of ANSYS. Furthermore, the COUPLE algorithm was used to describe the relationship between pressure and velocity; the RNG turbulence model k-e was selected to describe the flow, and the body force weighted algorithm was selected as a tool for estimating the pressure limit. As for the other equations, with second-order upwind algorithms, they were all considered. In order to obtain more accurate results, all numerical calculations were solved using double precision choice. For all equations, the iteration error was set to the 10^{-5} limit; for the energy equation, it is 10^{-8}.

Fig. 2 An illustration of the geometry of the solar chimney
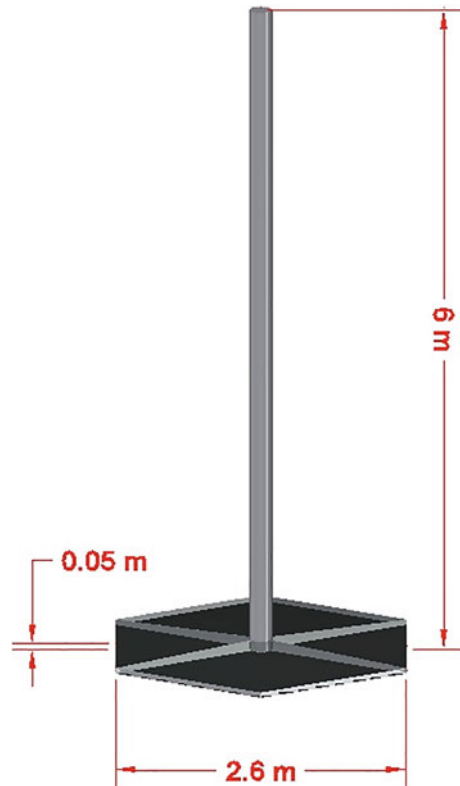
Fig. 3 An illustration of the 3D computational model
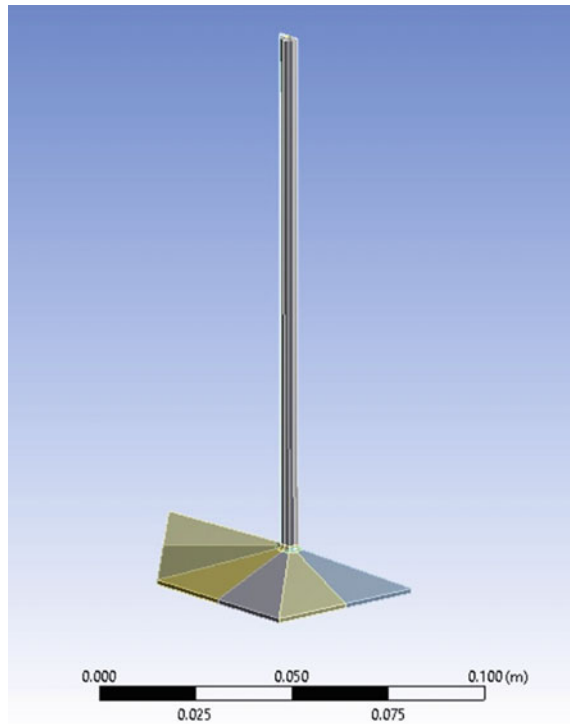
Fig. 4 A plot of the computational mesh
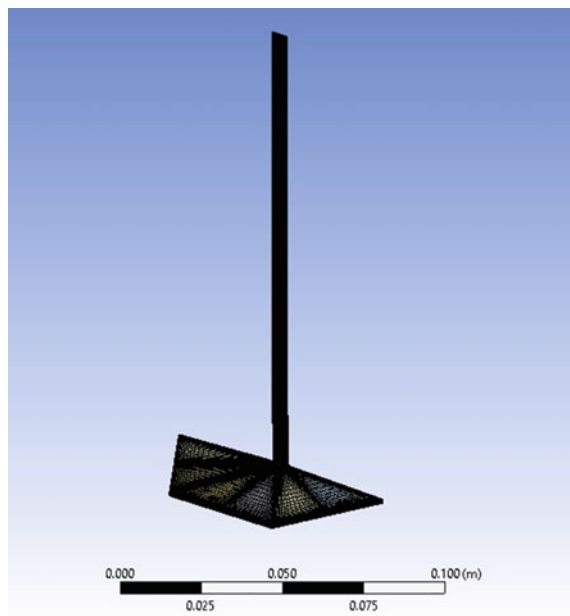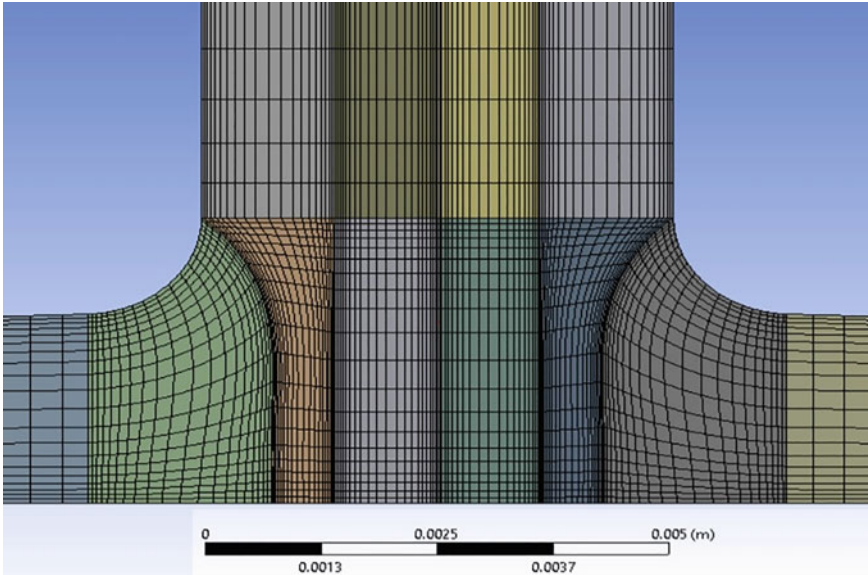
Fig. 5 An illustration of the mesh topology at the connection between the collector and the vertical chimney

4.2 Model Validation

The present numerical model was validated against the experimental test results. The temperature profile for numerical model prediction and experimental data of the flow temperature which were collected at the center of the vertical solar chimney was compared for different solar irradiance. The detailed experimental data from the solar chimney test rig are shown in Fig. 6. As shown in Fig. 7, good agreement between the numerical model prediction and experimental data are presented. Also, comparison between the numerical model prediction and the experimental test results for the flow velocity for different solar irradiance are shown in Fig. 8.

5 Results and Discussion

A numerical model was carried out to evaluate the possibility of producing electricity in Egypt from solar chimney. A three-dimensional (3D) simulation of the main geometric dimensions corresponding to the dimensions of the prototype pilot fabricated in Egypt, was performed using computational fluid dynamics (CFD). Three different solar radiation were examined; 463.6, 629.6 and 830 W/m^2. The selected solar radiations matching with experimental test results to facilitate validation and comparison process. Figure 9 illustrates the flow stream velocity for different solar
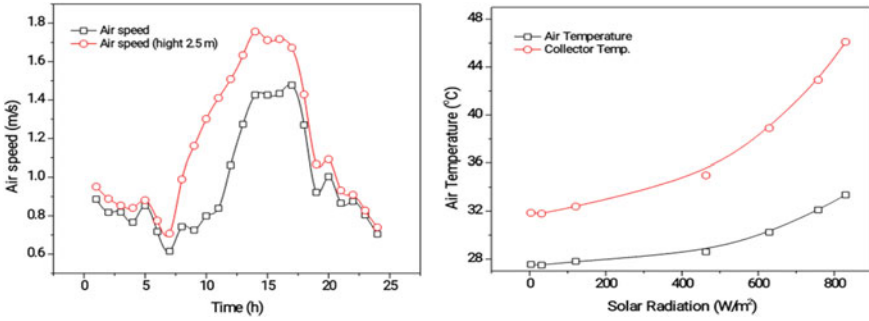
Fig. 6 Air speed and air temperature experimental test results for the solar chimney prototype
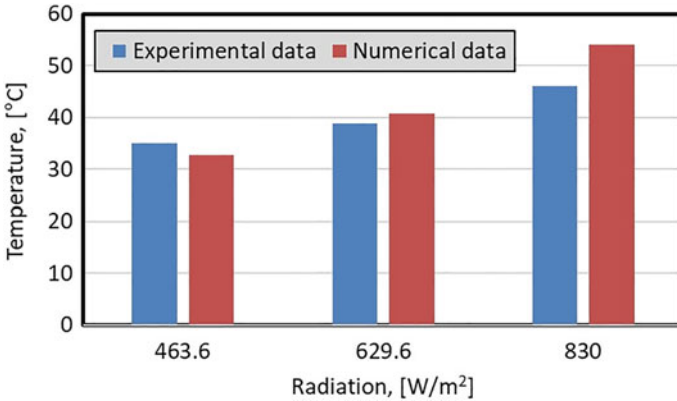
Fig. 7 A comparison between the numerical prediction and the corresponding experimental data for the flow temperature at the centerline of the vertical chimney for different solar irradiance
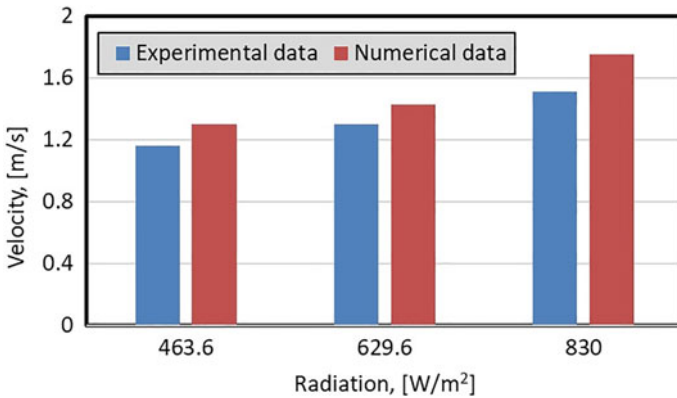
Fig. 8 A comparison between the numerical prediction and the corresponding experimental data for the flow velocity at the centerline of the vertical chimney for different solar irradiance

irradiation. It appears that the highest velocity is for radiation equal to 830 W/m^2 because the ambient air temperature that is entering the collector has the highest value due to the high amount of solar radiation absorbed in this case. The higher solar radiation means reduction in the air density which then means increment in the flow velocity. For this reason, the solar radiation has the main fundamental effect on the air velocity.

Velocity for radiation = 463.6 W/m2   *Temperature for radiation = 463.6 W/m2*

Velocity for radiation = 629.6 W/m2   *Temperature for radiation = 629.6 W/m2*

Velocity for radiation = 830 W/m2   *Temperature for radiation = 830 W/m2*
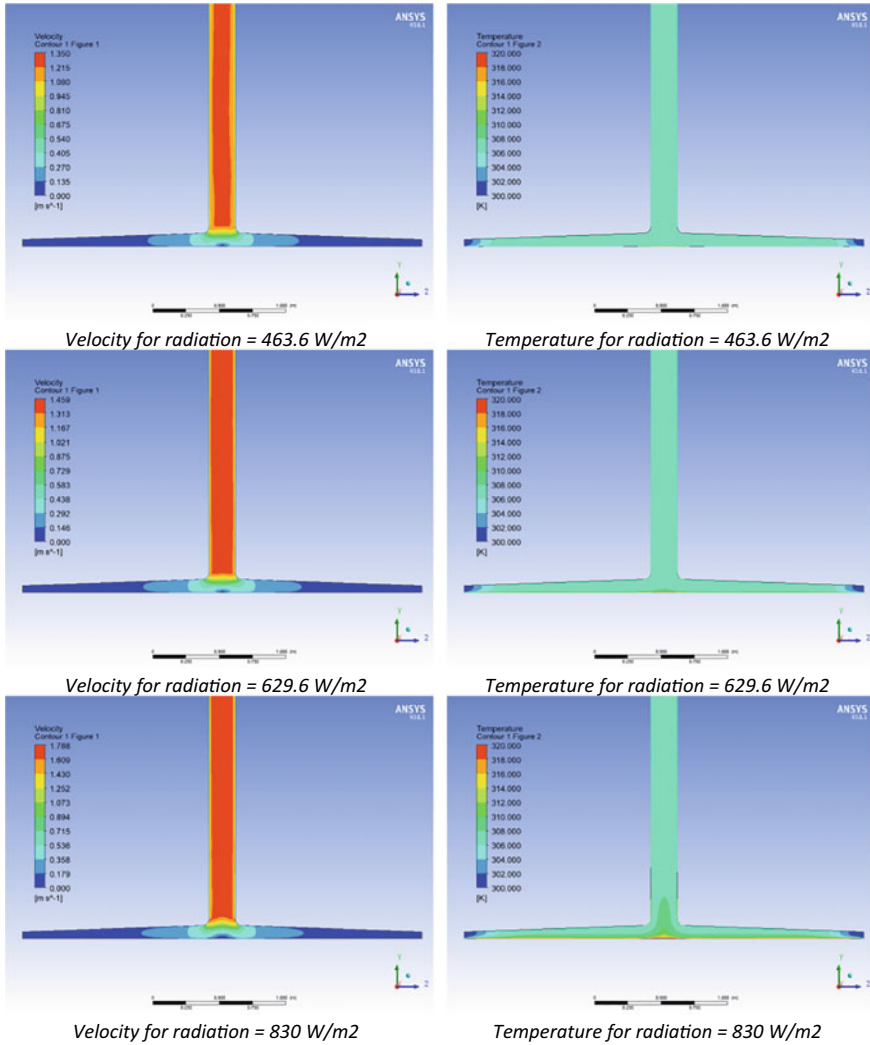
Fig. 9 Contours of velocity magnitude and static temperature at the midplane of the solar chimney for different solar irradiance

6 Conclusion

The solar chimney is one of the interested areas in renewable solar energy utilization, especially in sunbelt countries such as Egypt. Computational fluid dynamics can be utilized in designing a solar chimney and predicting its performance. In the present study, the performance assessment of solar chimney pilot was numerically and experimentally investigated. A pilot of solar chimney was fabricated and tested in outdoor site located at Desert Research Center, Egypt. By taking the real dimensions of the pilot main system, a model was designed in a three-dimensional form using the ANSYS Fluent software. The simulation was conducted by taking into consideration the atmospheric condition in the deployment area. Velocity and temperature distributions in the pilot from collector entry to chimney outlet were numerically simulated with respect to different solar intensity. The numerical simulation has shown a good agreement with the tested results of the pilot power plant. It was observed that the maximum stream velocity 1.7 m/s is achieved at highest solar radiation of 830 W/m^2 due to the high solar radiation and ambient temperature in this case.

7 Recommendation

Based on the above-mentioned discussions, it is recommended to utilize CFD simulations for optimizations of solar chimney systems. It is recommended to carry out sophisticated optimization of the solar chimney parameters in order to increase its performance.

References

1. Water. United Nations. Retrieved June 17, 2023, from https://www.un.org/en/global-issues/water

2. Amin I, Ali ME, Bayoumi S, Balah A, Oterkus S, Shawky H, Oterkus E (2021) Numerical hydrodynamics-based design of an offshore platform to support a desalination plant and a wind turbine in Egypt. Ocean Eng 229:108598

3. Sharbatiyan MH, Rashidi S, Mirhosseini M (2023) Experimental study on the performance of floating solar desalination system with porous absorbent plate. J Taiwan Inst Chem Eng: 104677

4. Amin I, Ali ME, Bayoumi S, Oterkus S, Shawky H, Oterkus E (2020) Conceptual design and numerical analysis of a novel floating desalination plant powered by marine renewable energy for Egypt. J Marine Sci Eng 8:95

5. Wang Y, Zhao J, Zhang Z, Xu J, Gao ZD, Song YY (2023) Water strider inspired floating solar evaporator with high salt-resistant ability for desalination of contaminated seawater. J Environ Chem Eng 11(3):109800

6. Amin I, Dai S, Day S, Ali ME, Balah A, Shawky H, Oterkus S, Oterkus E (2021) Experimental study on the motion response of an integrated floating desalination plant and offshore wind turbine on a non-ship platform. Ocean Eng 234:109275

7. Refaat A, Khalifa AE, Elsakka MM, Elhenawy Y, Kalas A, Elfar MH (2023) A novel meta-heuristic MPPT technique based on enhanced autonomous group particle swarm optimization algorithm to track the GMPP under partial shading conditions—experimental validation. Energy Convers Manage 287:117124

8. Amin I, Dai S, Oterkus S, Day S, Oterkus E (2020) Experimental investigation on the motion response of a novel floating desalination plant for Egypt. Ocean Eng 210:107535

9. Amer AE, Elsakka MM, Lebedev VA (2021) Thermal performance of an accumulator unit using phase change material with a fixed volume of fins. Int J Energy Res 45(13):19089–19102

10. Amin I, Eshra N, Oterkus S, Oterkus E (2022) Experimental investigation of motion behavior in irregular wave and site selection analysis of a hybrid offshore renewable power station for Egypt. Ocean Eng 249:110858

11. Amin I, Ali ME, Oterkus S, Shawky H, Oterkus E (2021) Experimental investigation on a towing assessment for a floating desalination plant for Egypt. Ocean Eng 238:109746

12. Elminshawy NA, Mohamed A, Osama A, Amin I, Bassam AM, Oterkus E (2022) Performance and potential of a novel floating photovoltaic system in Egyptian winter climate on calm water surface. Int J Hydro Energy 47:12798–12814

13. Eshra NM, Amin I (2020) Hybrid floating power station driven by renewable energy for Saudi Arabia coastal areas. In: 2020 international conference on electrical, communication, and computer engineering (ICECCE). IEEE, pp 1–6

14. Amin I, Elsakka M, Oterkus S, Nguyen Tien C, Ozdemir M, El-Aassar A, Shawky H (2022) Computational fluid dynamics-based design of anoxic bioreactor zone in wastewater treatment plant. Desalination Water Treatment

15. Cuce E, Cuce P, Sen H (2020) A thorough performance assessment of solar chimney power plants: case study for manzanares. Cleaner Eng Technol 1:100026

16. Mahal SK (2020) Experimental investigation on a novel integrated solar chimney and liquid desiccant system for simultaneous power and fresh water generation. 20, 67–86

17. Dhahri A, Omri A (2013) A review of solar chimney power generation technology. Int J Eng Adv Technol 2:1–17

18. Backström V, Gannon A (2004) Solar chimney turbine characteristics. Sol Energy 76:235–241

19. Gholamalizadeh E, Chung JD (2017) Analysis of fluid flow and heat transfer on a solar updraft tower power plant coupled with a wind turbine using computational fluid dynamics. Appl Therm Eng 126:548–558

20. Bouabidi A, Nasraoui H, Ayadi A, Driss Z, Abid MS (2019) Numerical analysis of chimney diameter effect on the fluid flow and the heat transfer characteristics within the solar tower. Energy Sources Part A Recover Util Environ Eff 41:2494–2506

21. Ismail A, Hamed AM, Hussin AMTAE (2019) Numerical modeling for a solar chimney. J Al-Azhar Univ Eng Sect 14:87–98
22. Djaouida B, Aouachria Z, Benmachiche AH, Ali S (2018) Controlling power output of solar chimney power plant according to demand. Int J Ambient Energy 41:1467–1481
23. Hassan A, Ali M, Waqas A (2018) Numerical investigation on performance of solar chimney power plant by varying collector slope and chimney diverging angle. Energy 142:411–425
24. Guo P, Li J-Y, Wang Y (2014) Numerical simulations of solar chimney power plant with radiation model. Renew Energy 62:24–30
25. Das P, Chandramohan VP (2018) CFD analysis on flow and performance parameters estimation of solar updraft tower (SUT) plant varying its geometrical configurations. Energy Sources Part A Recover Util Environ Eff 40:1532–1546
26. Setareh M (2021) Comprehensive mathematical study on solar chimney powerplant. Renew Energy 175:470–485
27. Singh AP, Kumar A, Singh O (2020) A novel concept of integrating bell-mouth inlet in converging-diverging solar chimney power plant. Renew Energy 169:318–334

An Efficient MPP Tracker Based on Flower Pollination Algorithm to Capture Maximum Power from PEM Fuel Cell

Ahmed Elbaz, Ahmed Refaat, Nikolay V. Korovkin, Abd-Elwahab Khalifa, Ahmed Kalas, Mohamed Mohamed Elsakka, Hussien M. Hassan, and Medhat H. Elfar

1 Introduction

Traditional power sources are mainly fossil fuels such as coal, oil and natural gas. They face several problems such as, they are non-renewable and can be depleted over time. They cause environmental pollution and health issues when burned. They require costly and invasive processes of extraction, transportation and combustion. Renewable energy is preferred over traditional power sources because it has many benefits, such as being cleaner and not emitting greenhouse gases or other pollutants. Furthermore, it is sustainable and will never run out unlike fossil fuels [1]. Although

A. Elbaz · A. Refaat (✉) · A.-E. Khalifa · A. Kalas · M. H. Elfar
Department of Electrical Engineering, Faculty of Engineering, Port Said University, Port Said, Egypt
e-mail: ahmed_refaat_1984@eng.psu.edu.eg

A. Elbaz
e-mail: ahmed.sabry@eng.psu.edu.eg

A.-E. Khalifa
e-mail: abedalwahab.alsayed@eng.psu.edu.eg

A. Kalas
e-mail: ahmed.kalas@eng.psu.edu.eg

M. H. Elfar
e-mail: mhelfar@eng.psu.edu.eg

N. V. Korovkin
Institute of Energy, Peter the Great Saint Petersburg Polytechnic University, Saint Petersburg, Russia

M. M. Elsakka
Department of Mechanical Power Engineering, Faculty of Engineering, Port Said University, Port Said, Egypt

the majority of the installed generation capacity currently is based on fossil fuels, there is a recent both market and research interest in the utilization of new and renewable energy including solar energy [2–7], wind energy [8–10], and fuel cells [11, 12].

Fuel cells (FCs) are electrochemical devices that convert chemical energy from a fuel into DC electricity besides producing heat and water as byproducts of the chemical reaction. FCs can help decrease CO_2 emissions since hydrogen can be produced from renewable sources. This may decrease CO_2 emissions by almost 90% compared to traditional electrical power plants. FCs possess several advantages such as high energy efficiency, low maintenance cost (no moving parts), high reliability, low noise pollution, low thermal pollution, designing is modular; therefore, the parts are exchangeable, and low air pollution [13].

Maximum power extraction for FCs is the process of achieving the optimal power output from the FCs under varying operating conditions. One of the challenges of this process is to design a maximum power point (MPP) tracker that can regulate the load impedance to match the FC internal impedance. Another challenge is dealing with the nonlinearity and uncertainty of the FC characteristics, which are influenced by gas pressure, working temperature, humidity, and aging [14]. A wide range of MPP tracking (MPPT) techniques has been proposed in the literature in order to cope with these challenges.

Incremental resistance-based-MPPT technique and Perturb and Observe (P&O) based-MPPT technique are suggested in [15–18]. These techniques have some merits such as the simplicity of the structure of the algorithms and easy implementation in low-cost hardware. Nonetheless, they suffer from high steady-state power fluctuations, low tracking speed, and may fail to trace the MPP under different operating conditions. Therefore, these techniques have low energy efficiency and low reliability. The MPPT controller based on Fuzzy Logic Control (FLC) is proposed in [19] to enhance the FCs' performance and efficiency. The FLC can track the MPP quickly and accurately without overshooting spikes. In addition, it can adapt to different working conditions (e.g., temperature, humidity, and load changes) [20]. However, the controller may require a large number of parameters and rules to cover all potential working conditions, which increases the complexity and cost of the tracking system.

Metaheuristic techniques are a class of optimization algorithms that are employed to solve complex problems that cannot be solved using traditional optimization techniques. They offer several advantages over classical optimization techniques

Energy Research and Studies Unit, Faculty of Engineering, Port Said University, Port Said, Egypt

M. M. Elsakka
e-mail: Elsakka@eng.psu.edu.eg

H. M. Hassan
Department of Naval Architecture and Marine Engineering, Faculty of Engineering, Port Said University, Port Said, Egypt
e-mail: Hussein.mohamed@eng.psu.edu.eg

for solving complex problems in various fields. Their flexibility, efficiency, robustness, global optimization capability, and independence from derivatives make them an attractive choice for many real-world applications [21]. Recently, metaheuristic algorithms-based MPPT controllers have been widely used to extract maximum power from the FCs such as Artificial Bee Colony (ABC) [14], differential evolution (DE) [22], golden section search (GSS) [23], bat optimizer[24], Cuckoo Search (CS) [25], Chicken Swam [26], and others. This work proposes an efficient MPP tracker based on the flower pollination (FP) algorithm to harvest the maximum power from a stand-alone PEMFC system. In order to demonstrate the feasibility and effectiveness of the proposed MPPT controller, the performance of the FP MPP tracker is compared with the PSO-based-MPPT controller under various operating conditions.

2 System Description

The schematic diagram of stand-alone PEMFC system is depicted in Fig. 1. As evident, the PEMFC system is composed of four main parts including the PEMFC stack, DC–DC power converter, resistive load, metaheuristic-based MPPT controller. Regarding the power circuit, a 1.2 kW PEMFC stack is connected to the resistive load via boost converter. The PEMFC stack and the parameters of boost converter are listed in Tables 1 and 2. The instantaneous power of the PEMFC stack is measured using current and voltage sensors. These signals are sent to the metaheuristic-based MPPT controller in order to extract the maximum power from PEMFC stack under different operating conditions. The MPPT controller produces the optimal duty cycle, considered the PWM generator's reference signal. This reference signal is compared with a high-frequency carrier signal to produce the boost switch trigger pulses.

In order to study the influence of the membrane water content (MWC) and the FC working temperature on the performance of the stand-alone PEMFC system,
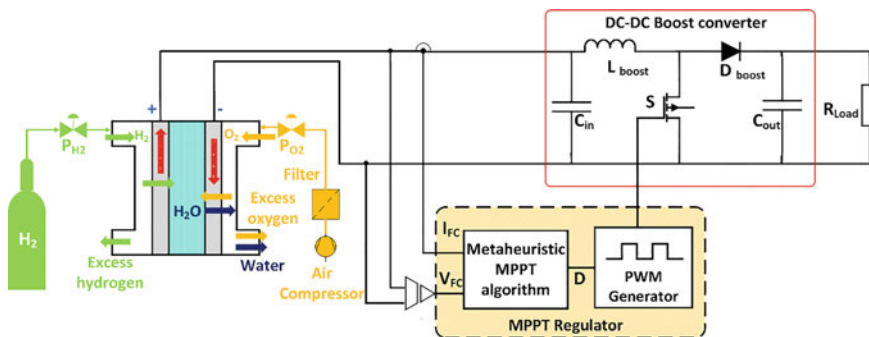
Fig. 1 The schematic diagram of stand-alone PEMFC system

Table 1 The parameters of the PEMFC stack

Symbol	Description	Value
i_l	The limiting current	2 A/cm^2
N_{FC}	No. of series FCs	32
t_m	The membrane thickness	0.0178 cm
τ_{H_2}	The time constant of H$_2$	3.37 s
A	The active area of FC	35 cm^2
$q_{H_2}^{in}$	The input flow rate of H$_2$	10 * 10^{-5} kmol/s
k_{H_2}	The molar constant of the H$_2$ valve	4.22 * 10^{-5} kmol/s A
α_1	Parametric coefficient 1	− 0.944
α_2	Parametric coefficient 2	0.00354
α_3	Parametric coefficient 3	8 * 10^{-8}
α_4	Parametric coefficient 4	− 1.96 * 10^{-4}
τ_{O_2}	The time constant of O$_2$	6.47 s
$q_{O_2}^{in}$	The input flow rate of O$_2$	5 * 10^{-5} kmol/s
k_{O_2}	The molar constant of the O$_2$ valve	2.11 * 10^{-5} kmol/s A
k_r	The coefficient of modeling	17 * 10^{-8} kmol/s A
n	No. of electrons participating in the reaction	2

Table 2 The designed parameters of the DC–DC converter

Symbol	Description	Value
l_{boost}	Boost chopper inductor	1 mH
f_{sw}	Switching frequency	20 kHz
C_{out}	output capacitor	500 uF
R_{Load}	Resistive load	2 Ω

numerous models based on the equivalent circuit are suggested in the literature [27–29]. A typical equivalent circuit that represents the practical PEMFC stack is shown in Fig. 2. This model considers different polarization voltages that occur inside the FC such as activation polarization, ohmic polarization, and concentration polarization. The basic equations expressing the nonlinear characteristics of the PEMFC stack taking into account the impact of MWC and FC operating temperature are as follows:

$$V_{cell} = E_N - V_a - V_c - V_\Omega \tag{1}$$

where V_{cell} represents the FC output voltage, E_N is open-circuit (OC) voltage, V_c refers to the concentration overvoltage. V_a is the activation overvoltage, and V_Ω represents the ohmic overvoltage.

The following Nernst equation represents the OC voltage.

Fig. 2 The equivalent
circuit of the PEMFC
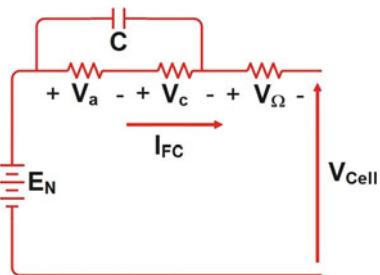
$$E_N = 1.229 - 8.5 \times 10^{-4}(T_{cell} - 298.15)$$
$$+ 4.308 \times 10^{-5} T_{cell} \left(\ln\left(P_{H_2}\right) + 0.5 \ln\left(P_{O_2}\right) \right) \tag{2}$$

where P_{O_2} and P_{H_2} refer to the partial pressures of O_2 and H_2; respectively, and T_{cell} represents the operating temperature of the FC.

Activation polarization V_a can be defined by Tafel equation.

$$V_a = -(\alpha_1 + \alpha_2 T_{cell} + \alpha_3 T_{cell} \ln\left(C_{O_2}\right) + \alpha_4 T_{cell} \ln(I_{FC}) \tag{3}$$

where α_1, α_2, α_3 and α_4 denote parametric constants, and C_{O_2} denotes the dissolved oxygen concentration.

$$C_{O_2} = \frac{P_{O_2}}{(5.08 \times 10^6) \exp\left(-498/T_{cell}\right)} \tag{4}$$

The ohmic polarization V_Ω is governed by ohm's law which is created by the electrode resistance, the bulk membrane resistance, and the interface contact resistance between the electrode and the membrane.

$$V_\Omega = I_{FC} R_m \tag{5}$$

$$R_m = \frac{\rho_m t_m}{A} \tag{6}$$

where ρ_m represents the membrane resistivity, t_m s the membrane thickness, A denotes the FC active area.

The resistivity of FC membrane is influenced by the humidity and FC temperature as given below:

$$\rho_m = \frac{181.6\left[1 + 0.03\left(I_{FC}/A\right) + 0.0062\left(T_{cell}/303\right)^2 \left(I_{FC}/A\right)^{2.5}\right]}{\left[\lambda_m - 0.634 - 3\left(\frac{I_{FC}}{A}\right)\right] \exp\left(4.18\left((T_{cell} - 303)/T_{cell}\right)\right)} \tag{7}$$

where λ_m refers to the MWC and its value belongs to [0,14] which represents the variation of humidity from $\lambda_m \in [0, 14]$ 0–100%.

The concentration polarization V_c can be calculated as (8).

$$V_c = -\frac{RT_{cell}}{nF} \ln\left(1 - \frac{I_{FC}}{i_l A}\right) \tag{8}$$

where n refers to the electron number participating during the reaction process, and i_l denotes the limiting current.

The output voltage and power of FC stack are given by:

$$V_{FC} = N_{FC} V_{cell} \tag{9}$$

$$P_{FC} = V_{FC} I_{FC} \tag{10}$$

The effect of the MWC variation on the characteristic curves of the PEMFC stack is illustrated in Fig. 3. Under an invariant FC working temperature, the output power of the PEMFC stack reduces as the MWC reduces. On the other hand, for a constant MWC, the output power of the PEMFC stack decreases with the decrease of the FC operating temperature as shown in Fig. 4. Furthermore, different locations of MPPs are observed under various operating conditions which explains the importance of employing the MPPT controller to trace the MPP.

3   Metaheuristic Algorithms Based-MPPT Controller

Metaheuristic algorithms are a class of optimization algorithms that are used to solve complex problems that cannot be solved using traditional optimization techniques. These algorithms are based on the principles of natural selection, swarm intelligence, and other biological processes. In recent years, metaheuristic algorithms have been used in various applications, including power electronics and renewable energy systems. They can be used to develop MPPT controllers for PEMFCs because they can handle complex nonlinearities and uncertainties associated with the system. This manuscript employs the Particle Swarm Optimization (PSO) algorithm and the Flower Pollination (FP) algorithm to obtain the maximum power yielded from PEMFC under different operating conditions. The following subsections cover the principle of operation for each algorithm.
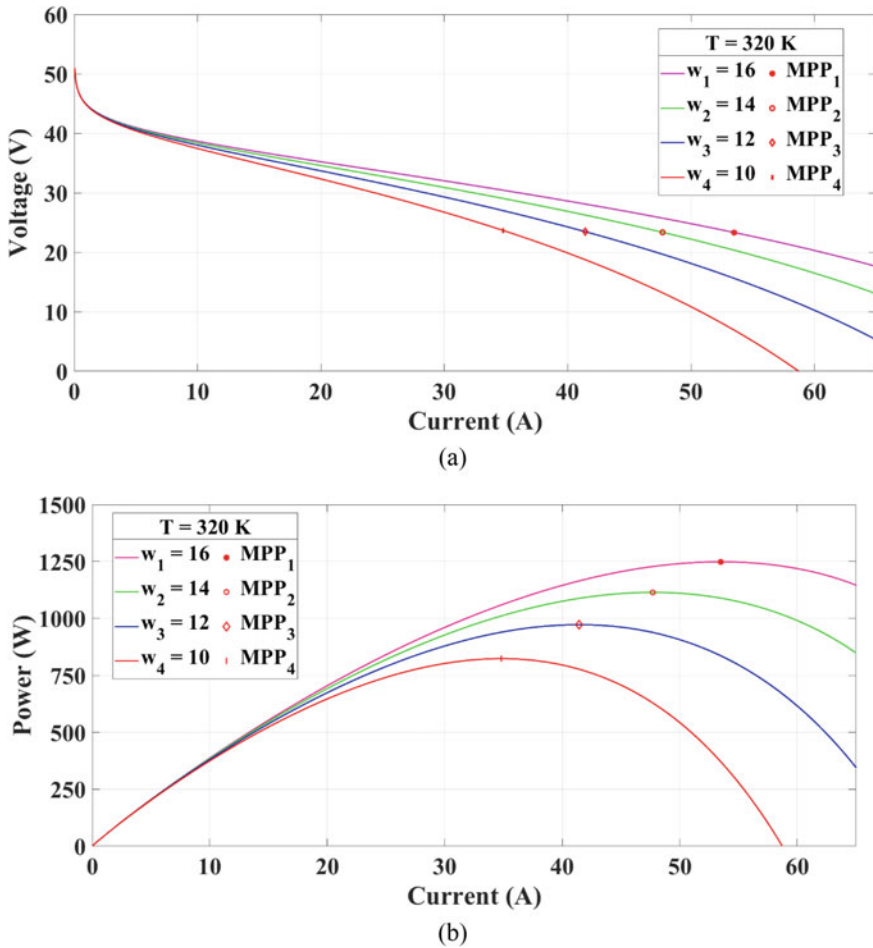
Fig. 3 The characteristic curves of the PEMFC stack with various MWC: **a** the I-V curves and **b** the I-P curves

3.1 PSO Algorithm

PSO is a metaheuristic-based optimization technique that simulates the behavior of a group of agents (known as particles) moving in a search space to find the optimal solution [30]. The movement of agents is guided by their best position as well as the overall group's best position as depicted in Fig. 5. The PSO algorithm can be employed as an MPPT technique for PEMFC system by adapting the duty cycle of the converter. The fitness function of the PSO is to maximize the output power of the PEMFC stack by regulating the optimal duty cycle that conforms to the MPP. The PSO algorithm can offer fast convergence speed and high tracking accuracy under
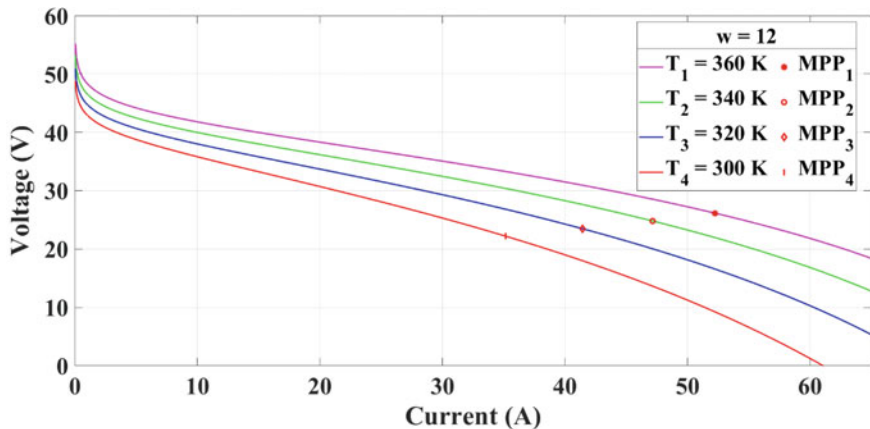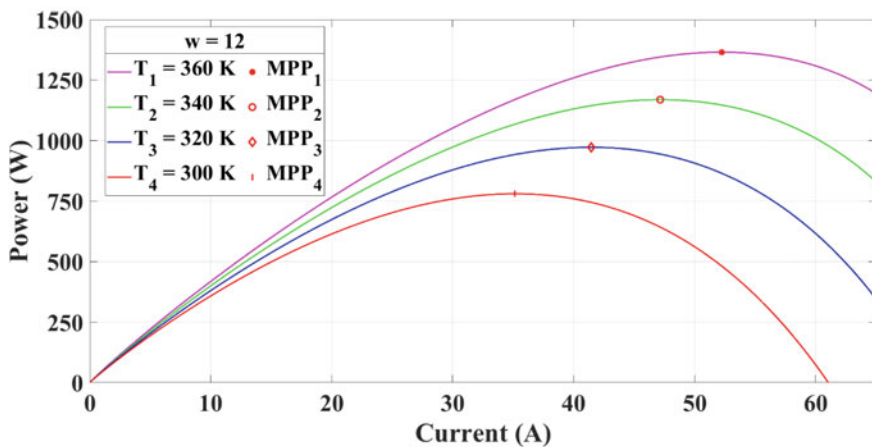
Fig. 4 The characteristic curves of the PEMFC stack with various cell temperature **a** the I-V curves and **b** the I-P curves

various operating conditions of the PEMFC stack [14, 31]. The flowchart of PSO-based-MPPT algorithm is depicted in Fig. 6. The mathematical model that represents the movement of the particles is as follows:

$$\Delta D(j)^{k+1} = \omega.\Delta D(j)^k + a_1 r_1 \big(P_{best}(j) - D(j)^k \big) + a_2 r_2 \big(G_{best} - D(j)^k \big) \quad (11)$$

$$D(j)^{k+1} = D(j)^k + \Delta D(j)^{k+1} \quad (12)$$

where $\Delta D(j)^k$ denotes the current step size of agent (j), k represents the current iteration, w denotes the inertia weight coefficient, a_1 and a_2 are the acceleration
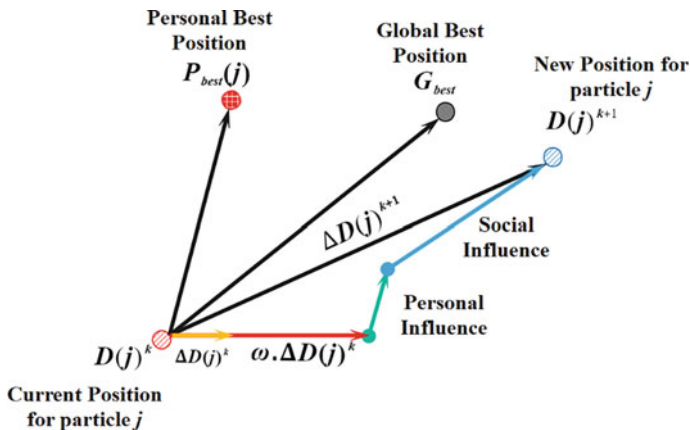
Fig. 5 The movement mechanism of agents in the PSO algorithm

constants, r_1 and r_2 are random values, G_{best} and $P_{best}(j)$ are the agent best global position and best personal position, and $D(j)^k$ denotes the current displacement vector of particle(j).

When the operating conditions of the PEMFC are changed, a new MPP is acquired. Therefore, the PSO-based-MPPT controller must be reinitialized to follow the new MPP as given by Eq. (13). If the reinitialization step is not executed correctly after changes in operating conditions, G_{best} and $P_{best}(j)$ will not be updated properly for the new MPP, leading to false tracking of the new MPP and in turn high power loss.

$$\frac{\left| P_{FC}^k - P_{FC}^{k-1} \right|}{P_{FC}^{k-1}} = \Delta P_{FC} \tag{13}$$

where ΔP_{FC} equals 5% as recommended in [32].

3.2 FP Algorithm

The flower pollination (FP) algorithm is a metaheuristic optimization algorithm that is inspired by the pollination process of flowers. FP has been applied to various types of problems such as optimization, image recognition, scheduling, and combinatorial optimization. Pollination process can be broken down into two types of pollination: global pollination and local pollination. Global pollination (also known as cross pollination) simulates the movement of pollen by insects or wind across long distances, while local pollination (also known as self-pollination) mimics the movement of pollen within the flower itself or near neighborhood of flower (Fig. 7).

The pollination process has a random switch probability to decide whether to use global or local pollination. In global pollination, a solution (or pollen) is updated by

Fig. 6 The flowchart of the
PSO MPPT algorithm
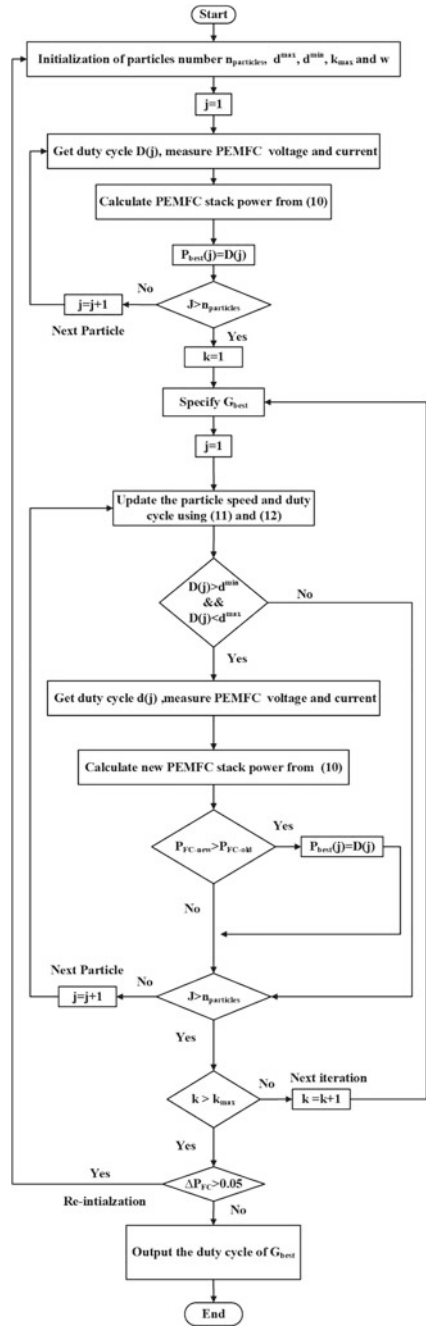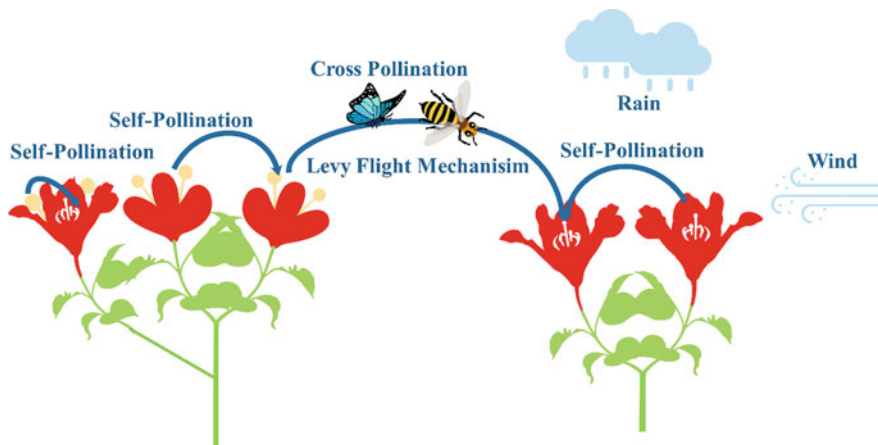
Fig. 7 The pollination process of flowers in nature

adding a Levy flight multiplied by the difference between the current solution and the best solution found so far. A Levy flight is a random walk that follows a heavy-tailed probability distribution. This allows the algorithm to explore a large search area and escape from local optimal [33].

$$D_i^{k+1} = D_i^k + \gamma \, L\acute{e}vy(\lambda)\big(D_{best} - D_i^k\big) \tag{14}$$

$$L\acute{e}vy(\lambda) \approx \frac{\lambda \Gamma(\lambda) \sin\left(\frac{\pi\lambda}{2}\right)}{\pi} \frac{1}{s^{1+\lambda}} (s \gg s_0 > 0) \tag{15}$$

where D_i^{k+1} refers to the updated position vector or duty cycle, D_i^k represents to *ith* pollen position vector for the flower at *kth* iteration, γ is a scaling factor to control the step size of duty cycle, D_{best} denotes the best duty cycle for the present pollen generation, λ denotes the variance, and is the levy distribution function.

In local pollination, a solution (or pollen) is updated by adding a uniform random number ψ multiplied by the difference between the current solution and another solution chosen randomly from among all solutions. This allows the algorithm to exploit a local region and refine the solutions. The flowchart of the FP MPPT algorithm is illustrated in Fig. 8.

$$D_i^{k+1} = D_i^k + \psi\big(D_j^k - D_g^k\big) \tag{16}$$

where D_j^k and D_g^k are the values of the duty cycles that represent pollen from different flowers of identical species.
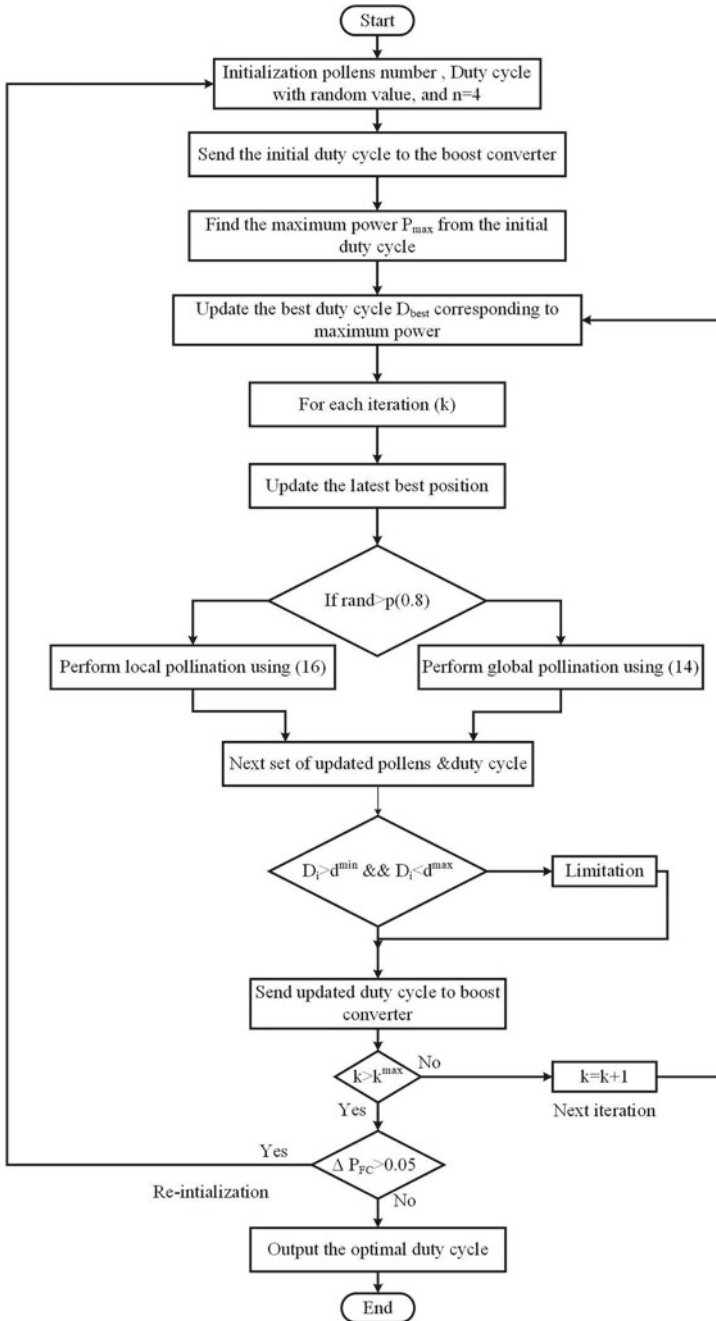
Fig. 8 The flowchart of FP MPPT algorithm

4   Results and Discussions

The stand-alone PEMFC system shown in Fig. 1 has been implemented on MATLAB for two cases in order to show the performance of the proposed FP MPPT controller compared to the PSO MPPT controller for different operating conditions. The first case tests the behavior of the PEMFC system under various MWCs with a constant cell temperature. While the second case tests the behavior of the PEMFC system under different cell working temperatures considering the MWC is constant. The control parameters for the two algorithms are detailed in Table 3.

In the first case, the PEMFC stack temperature is supposed to be invariant at 320 k during the simulation run. The MWC variation profile is depicted in Fig. 9. As can be seen, the MWC profile is divided into three periods, each of which is 2 s. At the beginning of the simulation, the value of MWC is 14. Then, the MWC suddenly dropped from 14 to 10 in the second period. After that, the MWC suddenly increased from 10 to 12 in the third period. The voltage, current, power, and duty cycle waveforms of both MPPT controllers based on the considered algorithms are illustrated in Fig. 10. As evident, the two algorithms can successfully track the MPP for each period with MPPT efficiency for the three successive periods of almost 99.88%, 99.74%, and 99.68%, respectively. This indicates the reliability and robustness of both algorithms to continuously track the maximum power under the MWC variation. However, the performance of the proposed FP-based-MPPT controller is superior to the PSO-based-MPPT controller. As shown in Fig. 10, the PSO suffers from steady-state voltage, current, and power fluctuations with frequent overshoots. In addition, the PSO controller has a lower convergence speed compared to the proposed FP controller. The tracking time of the proposed FP MPPT controller for the three successive periods is 0.279 s, 0.231 s, and 0.521 s, respectively, in contrast with 0.673 s, 0.496 s, and 0.616 s for the PSO MPPT controller. Figure 11 demonstrates the searching behavior of both algorithms for the three periods, confirming the higher fluctuations of the PSO algorithms to obtain the optimal duty cycle during the simulation run.

Table 3 A summary of the control parameters for the two algorithms

Symbol	Description	Value
PSO parameters		
ω	Inertia weight	0.5
a_1	Cognitive Constant	2
a_2	Social Constant	2
k_{max}	No. of iteration	100
N	No. of Particles	4
FP parameters		
p	Probability switch value	0.8
γ	Scaling factor	0.7
k_{max}	No. of iteration	100
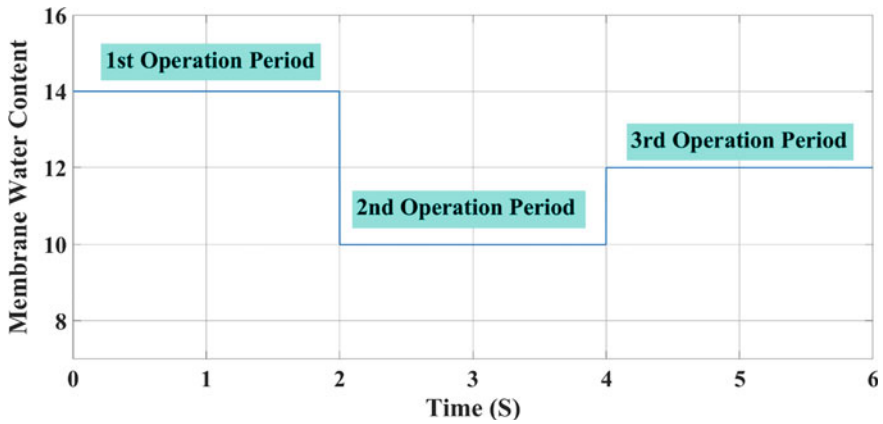
Fig. 9 The MWC variation profile

In the second case, the PEMFC stack MWC is assumed to be constant at 12 through the simulation run. The stack temperature variation profile is illustrated in Fig. 12. As shown, the stack temperature is changed for three periods, each of which is 2 s. In the first period, the stack temperature is 300 k. After that, the stack temperature abruptly increased from 300 to 340 k in the second period. Then, the stack temperature abruptly fell from 340 to 320 k in the third period. The corresponding waveforms of the voltage, current, power, and duty cycle of both MPPT controllers based on the tested algorithms are depicted in Fig. 13. As shown, both algorithms can follow the MPP for stack temperature with MPPT efficiency for the three successive periods of about 99.67%, 99.81%, and 99.75%, respectively. The performance of the proposed FP-based-MPPT controller outperforms the PSO-based-MPPT controller. The proposed FP controller offers lower convergence speed as well as lower steady-state fluctuations of the voltage, current, and power than the PSO controller. Under the second case, the tracking time of the proposed FP MPPT controller for the three successive periods is 0.541 s, 0.359 s, and 0.515 s, respectively, compared to 0.830 s, 0.638 s, and 0.672 s for the PSO MPPT controller.
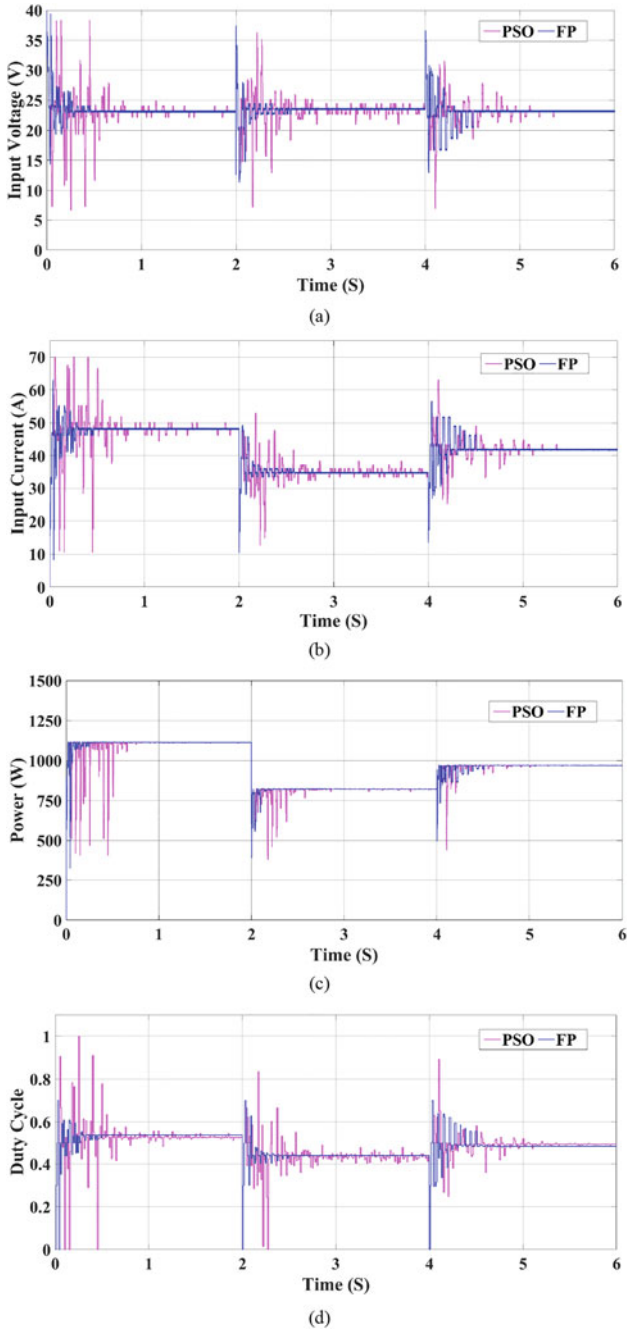
Fig. 10 The response of both algorithms for case1: **a** voltage, **b** current, **c** power, and **d** duty cycle
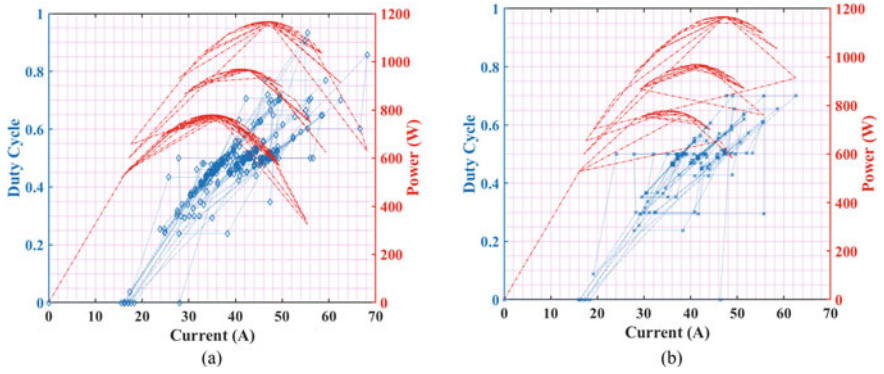
Fig. 11 The searching behavior of both algorithms **a** PSO algorithm and **b** FP algorithm
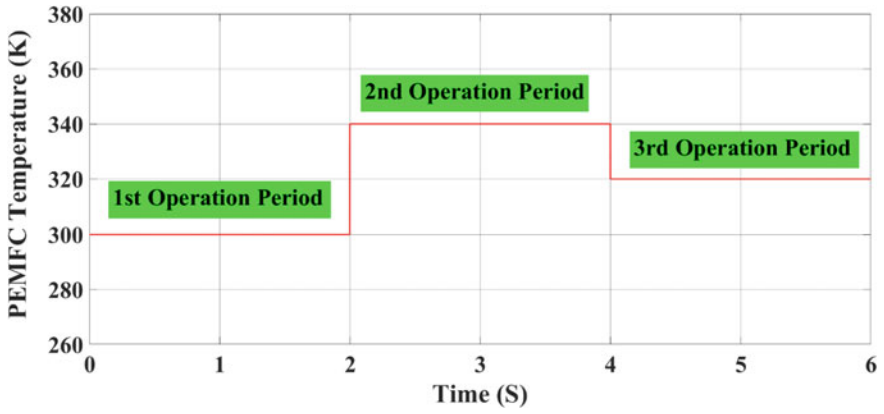
Fig. 12 The PEMFC stack temperature variation profile
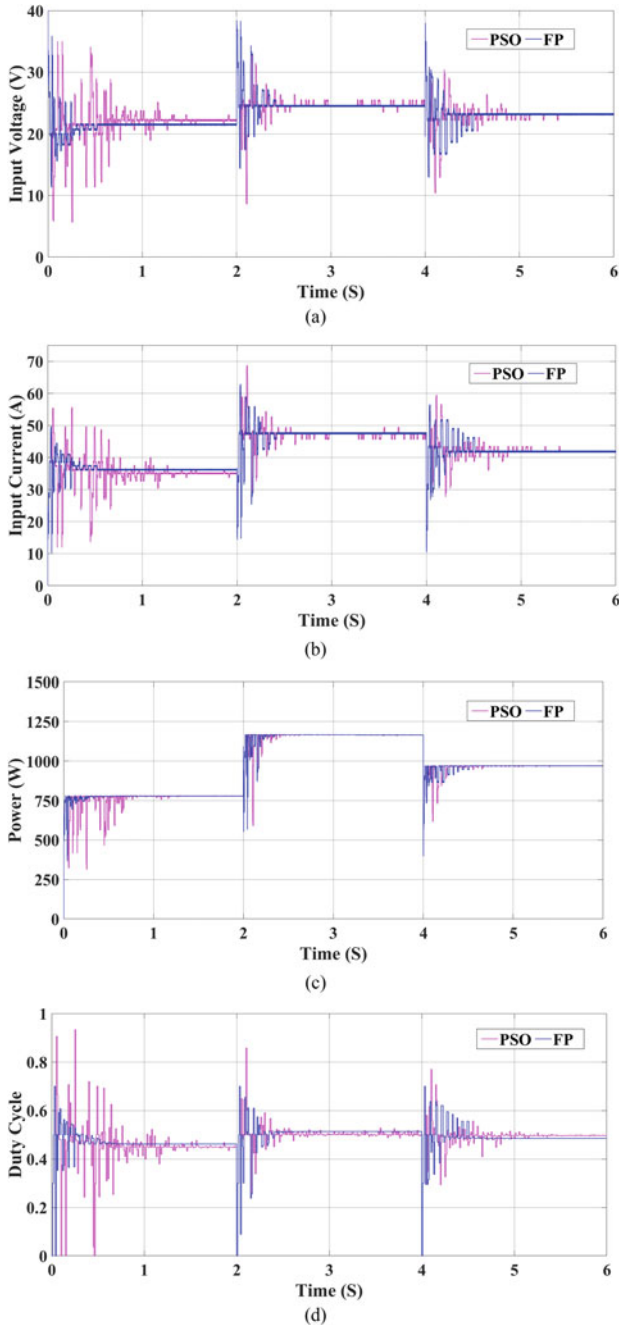
Fig. 13 The response of both algorithms for case2: **a** voltage, **b** current, **c** power, and **d** duty cycle

5   Conclusion

This article proposed an efficient MPP tracker based on the FP algorithm to capture maximum power from a stand-alone PEMFC system. Firstly, the PEMFC is accurately modeled on MATLAB based on the equivalent circuit of the FC stack. Then, a comparative study has been conducted to demonstrate the effectiveness of the proposed controller compared with the PSO-based-MPPT controller under various operating conditions. Simulation results have proven the reliability and robustness of both controllers as they continuously track the maximum power under the tested operating conditions. Nevertheless, the performance of the proposed FP-based-MPPT controller outperformed the PSO-based-MPPT controller. The proposed FP controller offered lower convergence speed in addition to lower steady-state fluctuations than the PSO controller under various MWCs and FC stack temperatures. Using the FP controller, the reduction of tracking time under various MWCs for the three successive periods was about 59%, 53%, and 15%, respectively. Additionally, the reduction of tracking time under different FC stack temperatures for the three successive periods was almost 35%, 44%, and 23%, respectively.

6   Recommendation

According to the previous results, it is recommended to implement an AI-based-MPPT algorithm in FC systems to track the maximum power under different operating conditions and therefore increase the system efficiency. This reinforces the endeavors of fulfilling SDG 7: Affordable and clean energy through maximizing the energy extraction from FC systems.

References

1. Elsakka MM, Ingham DB, Ma L, Pourkashanian M (2021) Comparison of the computational fluid dynamics predictions of vertical axis wind turbine performance against detailed pressure measurements. Int J Renew Energy Res 11:276–293
2. Amer AE, Elsakka MM, Lebedev VA (2021) Thermal performance of an accumulator unit using phase change material with a fixed volume of fins. Int J Energy Res 45:19089–19102. https://doi.org/10.1002/ER.7095
3. Refaat A, Osman MH, Korovkin NV (2020) Current collector optimizer topology to extract maximum power from non-uniform aged PV array. Energy 195. https://doi.org/10.1016/j.energy.2020.116995
4. Refaat A, Shehata AA, Elgamal M, Korovkin NV (2020) Current collector optimizer topology with reconfiguration algorithm to harvest optimal power from nonuniform aged PV arrays. In: 2020 international multi-conference on industrial engineering and modern technologies, FarEastCon 2020. Institute of Electrical and Electronics Engineers Inc.
5. Elfar M, Kalas AE, Sharaf SM, Sair KA, Sharaf S (2016) Hybrid photovoltaic battery (PVB) system for a desalination plant in sinai desert experimental and analytical investigation of

multi-phase induction machines view project experimental analysis of CHB-MLI induction motor drive view project hybrid photovoltaic battery (PVB) system for a desalination plant in sinai desert. J Electr Eng 14

6. Refaat A, Kalas A, Khalifa AE, Elfar MH (2023) A comparative study of two metaheuristic MPPT techniques to extract maximum power from PV array under different partial shading patterns. In: IEEE conference on power electronics and renewable energy, CPERE 2023. Institute of Electrical and Electronics Engineers Inc.

7. Refaat A, Khalifa AE, Elsakka MM, Elhenawy Y, Kalas A, Elfar MH (2023) A novel meta-heuristic MPPT technique based on enhanced autonomous group particle swarm optimization algorithm to track the GMPP under partial shading conditions—experimental validation. Energy Convers Manag 287. https://doi.org/10.1016/j.enconman.2023.117124

8. Abuhashish MN, Daoud AA, Elfar MH, Abu Hashish MN (2022) A novel model predictive speed controller for PMSG in wind energy systems

9. Elsakka MM, Ingham DB, Ma L, Pourkashanian M (2020) Effects of turbulence modelling on the predictions of the pressure distribution around the wing of a small scale vertical axis wind turbine. In: Proceedings of the 6th European conference on computational mechanics: solids, structures and coupled problems, ECCM 2018 and 7th European conference on computational fluid dynamics, ECFD 2018, pp 3921–3931

10. Elsakka MM, Ingham DB, Ma L, Pourkashanian M, Moustafa GH, Elhenawy Y (2022) Response surface optimisation of vertical axis wind turbine at low wind speeds. Energy Rep 8:10868–10880. https://doi.org/10.1016/J.EGYR.2022.08.222

11. Kanouni B, Badoud AE, Mekhilef S (2022) A SMC-based MPPT controller for proton exchange membrane fuel cell system. In: 2022 19th IEEE international multi-conference on systems, signals and devices, SSD 2022. Institute of Electrical and Electronics Engineers Inc., pp 527–531

12. Elbaz A, Elfar MH, Kalas A, Refaat A (2022) Maximum power extraction from polymer electrolyte membrane (PEM) fuel cell based on deterministic particle swarm optimization algorithm. In: Proceedings of the 2022 conference of Russian young researchers in electrical and electronic engineering, ElConRus 2022

13. Hai T, Zhou J, khaki M, (2023) Optimal planning and design of integrated energy systems in a microgrid incorporating electric vehicles and fuel cell system. J Power Sources 561:232694. https://doi.org/10.1016/j.jpowsour.2023.232694

14. Fan L, Ma X (2022) Maximum power point tracking of PEMFC based on hybrid artificial bee colony algorithm with fuzzy control. Sci Rep 12. https://doi.org/10.1038/s41598-022-08327-5

15. Osman MH, Ahmed MK, Refaat A, Korovkin N V. (2021) A comparative study of MPPT for PV system based on modified perturbation observation method. In: Proceedings of the 2021 IEEE conference of Russian young researchers in electrical and electronic engineering, ElConRus 2021. Institute of Electrical and Electronics Engineers Inc., pp 1023–1026

16. Mohamed SA, Abd El Sattar M (2019) A comparative study of P&O and INC maximum power point tracking techniques for grid-connected PV systems. SN Appl Sci 1. https://doi.org/10.1007/s42452-018-0134-4

17. Shang L, Guo H, Zhu W (2020) An improved MPPT control strategy based on incremental conductance algorithm. Protection Control Modern Power Syst 5. https://doi.org/10.1186/s41601-020-00161-z

18. Sun C, Ling J, Wang J (2022) Research on a novel and improved incremental conductance method. Sci Rep 12. https://doi.org/10.1038/s41598-022-20133-7

19. Aly M, Rezk H (2022) An improved fuzzy logic control-based MPPT method to enhance the performance of PEM fuel cell system. Neural Comput Appl 34:4555–4566. https://doi.org/10.1007/s00521-021-06611-5

20. Ali ZM, Al-Dhaifallah M, Al-Gahtani SF, Muranaka T (2023) A new maximum power point tracking method for PEM fuel cell power system based on ANFIS with modified manta ray foraging algorithm. Control Eng Pract 134:105481. https://doi.org/10.1016/j.conengprac.2023.105481

21. Rezk H, Olabi AG, Sayed ET, Wilberforce T (2023) Role of metaheuristics in optimizing microgrids operating and management issues: a comprehensive review. Sustainability 15:4982. https://doi.org/10.3390/su15064982

22. Hussaian Basha CH, Murali M, Rafikiran S, Mariprasath T, Bhaskara Reddy M (2022) An improved differential evolution optimization controller for enhancing the performance of PEM fuel cell powered electric vehicle system. Mater Today Proc: 308–314

23. Bahri H, Harrag A (2021) Ingenious golden section search MPPT algorithm for PEM fuel cell power system. Neural Comput Appl 33:8275–8298. https://doi.org/10.1007/s00521-020-055 81-4

24. Hu X, Jiang W, Ying X, Eslami M (2023) The application of a new design of bat optimizer for energy efficiency enhancement in PEMFCs based on fractional order theory. Sustain Energy Technol Assess 55. https://doi.org/10.1016/j.seta.2022.102904

25. İnci M, Caliskan A (2020) Performance enhancement of energy extraction capability for fuel cell implementations with improved Cuckoo search algorithm. Int J Hydrogen Energy 45:11309–11320. https://doi.org/10.1016/j.ijhydene.2020.02.069

26. Priyadarshi N, Azam F, Solanki SS, Sharma AK, Bhoi AK, Almakhles D (2021) A bio-inspired chicken swarm optimization-based fuel cell system for electric vehicle applications. In: Studies in computational intelligence. Springer, pp 297–308

27. Rezk H, Aly M, Fathy A (2021) A novel strategy based on recent equilibrium optimizer to enhance the performance of PEM fuel cell system through optimized fuzzy logic MPPT. Energy 234. https://doi.org/10.1016/j.energy.2021.121267

28. Ahmadi S, Abdi S, Kakavand M (2017) Maximum power point tracking of a proton exchange membrane fuel cell system using PSO-PID controller. Int J Hydrogen Energy 42:20430–20443. https://doi.org/10.1016/j.ijhydene.2017.06.208

29. Al-Baghdadi MARS (2005) Modelling of proton exchange membrane fuel cell performance based on semi-empirical equations. Renew Energy 30:1587–1599. https://doi.org/10.1016/j. renene.2004.11.015

30. Shehata AA, Refaat A, Ahmed MK, Korovkin NV. (2021) Optimal placement and sizing of FACTS devices based on autonomous groups particle swarm optimization technique. Arch Electr Eng 70:161–172. https://doi.org/10.24425/aee.2021.136059

31. Padmanaban S, Priyadarshi N, Bhaskar MS, Holm-Nielsen JB, Hossain E, Azam F (2019) A hybrid photovoltaic-fuel cell for grid integration with jaya-based maximum power point tracking: experimental performance evaluation. IEEE Access 7:82978–82990. https://doi.org/ 10.1109/ACCESS.2019.2924264

32. Mirhassani SM, Golroodbari SZM, Golroodbari SMM, Mekhilef S (2015) An improved particle swarm optimization based maximum power point tracking strategy with variable sampling time. Int J Electr Power Energy Syst 64:761–770. https://doi.org/10.1016/j.ijepes.2014.07.074

33. Khalifa AE, Refaat A, Kalas A, Elfar MH (2022) Two bio-inspired MPPT algorithms to harvest the maximum power from partially shaded PV arrays. In: Proceedings of the 2022 conference of russian young researchers in electrical and electronic engineering, ElConRus 2022. Institute of Electrical and Electronics Engineers Inc., pp 670–674

Experimental Investigation of Two Bio-inspired MPPT Algorithms for Partially Shaded PV Arrays

Abd-Elwahab Khalifa, Medhat H. Elfar, Qays Adnan Ali, Ahmed Elbaz, Ahmed Kalas, Mohamed Mohamed Elsakka, Nikolay V. Korovkin, and Ahmed Refaat

1 Introduction

The use of renewable energy resources (RERs) has been increasing around the world in recent decades due to concerns about carbon footprint and energy shortages. The most promising RER technology of the twenty-first century is solar photovoltaic (PV) energy since it has some advantages such as green energy, low operating cost, zero carbon emission, zero fuel consumption, low maintenance cost, low noise pollution, and can be established to any size depending on the energy requirements. However, it suffers from a considerably high capital cost and low energy efficiency. Therefore,

A.-E. Khalifa · M. H. Elfar · A. Elbaz · A. Kalas · A. Refaat (✉)
Department of Electrical Engineering, Faculty of Engineering, Port Said University, Port Said, Egypt
e-mail: ahmed_refaat_1984@eng.psu.edu.eg

M. H. Elfar
e-mail: mhelfar@eng.psu.edu.eg

A. Elbaz
e-mail: ahmed.sabry@eng.psu.edu.eg

A. Kalas
e-mail: ahmed.kalas@eng.psu.edu.eg

Q. A. Ali
Department of Fuel and Energy Techniques Engineering, Technical Engineering College, Northern Technical University, Kirkuk, Iraq
e-mail: alnajarqays@ntu.edu.iq

M. M. Elsakka
Department of Mechanical Power Engineering, Faculty of Engineering, Port Said University, Port Said, Egypt

Energy Research and Studies Unit, Faculty of Engineering, Port Said University, Port Said, Egypt

it is crucial to optimize the power generated from PV systems by utilizing suitable control schemes [1–6].

The key challenge for capturing the maximum power from the outdoor PV systems is the uneven fallen of solar irradiation on the upper surface of the PV array owing to the partial shading conditions (PSCs). The PSCs lead to the distortion of the P–V characteristic curves of the PV array where multiple peaks are emerged including one global peak (GP) beside one or more local peaks (LPs). Indeed, the connection of the bypass protective diodes across each panel in the PV array is the main reason for these distortions in the P–V curves. However, bypass protective diodes are mandatory in PV system installations to protect the PV panels that may be destroyed under the PSCs due to the hot-spot phenomenon [7, 8].

Classical algorithms-based-maximum power point tracking (MPPT) controllers such as incremental conductance (InC), perturb and observe (P&O), and their improved versions have been suggested in the literature [9–12]. Classical algorithms have relatively simple structures, easy to executions, and a low computation burden. Nevertheless, these algorithms suffer from a trade-off between tracking speed and tracking accuracy. For instance, if the step size in the algorithm is increased to obtain fast-tracking time, high steady-state power oscillations are observed that lead to low tracking accuracy. On the other hand, if the step size in the algorithm is reduced to acquire relatively low steady-state power oscillations, the convergence speed of the algorithms is slowed down resulting in a high tracking time. In addition, these algorithms are frequently trapped in LPs under the PSCs [13–15].

Recently, AI techniques are widely employed in the MPPT controllers for PV systems in order to guarantee the successful tracking of the GPs under the PSCs [16]. Many AI-based approaches have been introduced in the literature including Fuzzy Logic Control-based MPPT controllers [17], Deep Learning Techniques-based MPPT controllers, and Bio-inspired Algorithms-based MPPT controllers. Numerous bio-inspired algorithms have been developed by researchers to address the PSCs problems such as Ant-Lion Optimization (ALO) [18], Grasshopper Optimization (GHO) [19], Cuckoo Search (CS) [20], Search and Rescue Algorithm (SRA) [21], Bat Algorithm (BA) [22], Grey Wolf Optimization (GWO) [23], Sine Cosine Algorithm (SCA) [24], Yellow Saddle Goatfish Algorithm (YSGA) [25], Firefly Algorithm (FA) [26], Moth-Flame Optimization (MFO) [27], Earthquake Algorithm (EA) [28], Flower Pollination Algorithm (FPA) [29], Dragonfly Optimization Algorithm (DFOA) [30], Harris Hawk Optimization Algorithm (HHOA) [31], Hybrid Particle Swarm Optimization-Fireworks (PSO-FW) algorithm [32], Salp-Swarm Optimization Algorithm (SSOA) [33], Artificial Bee Colony (ABC) algorithm [34], Group Teaching Optimization Algorithm (GTOA) [35], and others.

M. M. Elsakka
e-mail: Elsakka@eng.psu.edu.eg

N. V. Korovkin
Institute of Energy, Peter the Great Saint Petersburg Polytechnic University, Saint Petersburg, Russia

This article introduces a comparative study between the performance of the Autonomous Group Particle Swarm Optimization (AGPSO) algorithm and the Cuckoo Search (CS) algorithm for partially shaded photovoltaic (PV) arrays. Firstly, the performance of the two algorithms is assessed under different weather conditions including STC and PSCs by using MATLAB/SIMULINK. Then, an experimental study is conducted to validate the obtained simulation results.

2 System Configuration

The entire PV system configuration is depicted in Fig. 1. The PV system under study composed of four main parts, including the PV array, power conditioning unit, load, and maximum power point tracking (MPPT) controller. A 450 W PV array is constructed by three parallel strings, each string consists of three series-connected PV panels. The PV panel produces a maximum power of about 50.04 W with a MPP voltage of 19.01 V and a MPP current of 3.16 A at the standard test conditions $\left(STC: T_{ref} = 25\,°C,\ G_{ref} = 1000\,\text{W/m}^2\right)$. A 50 Ω resistive load is interfaced with the PV array through a boost converter. The specifications of the boost converter design to work in continuous conduction mode have been listed in Table 1. The MPPT controller continually monitors the PV array power using current and voltage sensors and then regulates the duty cycle of the boost converter to assure that it operates at its MPP under various weather conditions. This ensures that maximum power is extracted from the PV array and delivered to the load.

In order to study the impact of weather conditions on the PV system performance, several mathematical models based on the equivalent circuits have been proposed in the literature [36]. A typical representation of the PV cell using a five-parameter model is illustrated in Fig. 2. This model presents an excellent balance between model complexity and accurateness, and its parameters $(I_{Ph}, I_0, R_{sh}, R_s, m)$ are numerically determined in accordance with previous literature [36].

The fundamental equations describing the characteristics of the PV array model taking into consideration the effect of solar radiation change and cells operating temperature are as follows:

$$
I_{PV} = I_{Ph} N_{pr}
$$
$$
- I_0 N_{pr} \left\{ \exp\left[\frac{V_{PV} + I_{PV} R_s \left(\frac{N_{sr}}{N_{pr}} \right)}{m V_t N_{sr}} \right] - 1 \right\} - \frac{V_{PV} + I_{PV} R_s \left(\frac{N_{sr}}{N_{pr}} \right)}{R_{sh} \left(\frac{N_{sr}}{N_{pr}} \right)} \quad (1)
$$

$$
I_{Ph} = \left[I_{Ph,T_{ref}} + \alpha_I \left(T_c - T_{ref} \right) \right] \left(\frac{G}{G_{ref}} \right) \quad (2)
$$

$$
I_{Ph,T_{ref}} = \frac{R_{sh} + R_s}{R_{sh}} I_{sc,T_{ref}} \quad (3)
$$
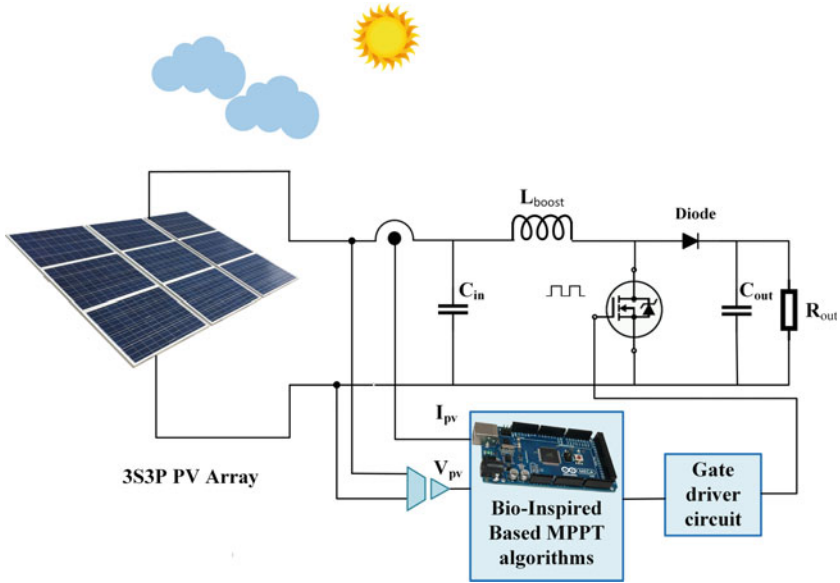
Fig. 1 The system configuration

Table 1 Specifications of boost converter

Component	Value
Input capacitor	100 μF
Output capacitor	500 μF
Boost inductor	1.5 mH
Switching frequency	10 kHz

Fig. 2 Equivalent circuit of the five-parameter model of a PV cell
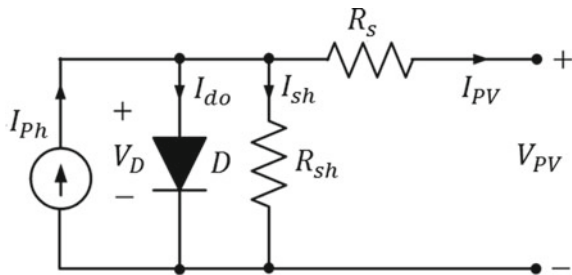
$$I_0 = \frac{I_{sc,T_{ref}} + \alpha_I\left(T_c - T_{ref}\right)}{\left\{\exp\left(\frac{V_{oc,T_{ref}} + \alpha_V\left(T_c - T_{ref}\right)}{m V_t}\right) - 1\right\}} \quad (4)$$

where I_{PV} denotes the array output current, V_{PV} denotes the array output voltage I_{Ph} denotes the photo-current, I_0 is the dark saturation current, q is the electron charge, N_{sr} is No. of series-connected panels, N_{pr} is the No. of parallel-connected strings, ($v_t = n_s K T_c / q$) is the panel thermal voltage, K denotes the Boltzmann constant, T_c is the panel temperature, m denotes the diode ideality factor $I_{Ph,T_{ref}}$ is the photo-current at STC, $V_{oc,T_{ref}}$ refers to the open-circuit voltage at STC, $I_{sc,T_{ref}}$ refers to the short circuit current at STC, α_V and α_I are the voltage and current temperature coefficients, respectively.

3 Bio-Inspired Optimization Algorithms

Bio-inspired techniques use algorithms that mimic natural processes such as genetic algorithms, neural networks, and swarm intelligence. These algorithms permit a more efficient and effective optimization process than traditional methods. In this article, the Autonomous Group Particle Swarm Optimization (AGPSO) algorithm and the Cuckoo Search (CS) algorithm are utilized to acquire the optimum duty cycle under different environmental conditions. This section provides an overview of the AGPSO and CS algorithms including the mechanism of operation, the mathematical model, and the MPPT flowchart for each algorithm.

3.1 AGPSO Algorithm

Particle Swarm Optimization (PSO) algorithm is widely utilized in various applications because of its simple structure, ease of establishment, and low computational cost. The PSO algorithm, however, has some drawbacks for MPPT applications, such as the challenge of adjusting its parameters under various environmental conditions, long convergence time, and the possibility of being trapped in LP under PSCs [37]. In order to tackle the issues related to the PSO algorithm, AGPSO algorithm is employed in this study.

Balancing between the exploration and exploitation phases during the search process is the main challenge for the classical PSO algorithm. The search behavior of particles in the search space for the PSO algorithm is dependent on the value of the cognitive and social parameters (c_1 and c_2). The particles have a high ability for local exploration throughout the search process if the cognitive parameter c_1 is relatively higher than the social parameter c_2. Conversely, if the parameter c_2 is relatively greater than c_1, then the particles search more globally, and exploit information compiled to converge towards the optimal solution [38].

The AGPSO is a bio-inspired algorithm that mimics the behavior of termite colonies in nature. Particles in a classical PSO algorithm may be considered as a group with a single strategy since all particles exhibit the same behavior in terms of local and global search. On the other hand, the particles in the AGPSO algorithm are

separated into four independent groups, each of which has a different strategy for searching both locally and globally. This led to the improvement of the algorithm performance since a better equilibrium between the exploration and exploitation phases is achieved during the search process [39].

In the AGPSO algorithm, the acceleration parameters are modeled by employing third root and cubic functions instead of using constant parameters as in classical PSO. These functions are chosen with various curvatures, intersection points, and slopes as shown in Fig. 3. The updating strategy of c_1 and c_2 for each group is provided in Table 2. In this work, the inertial weight parameter is decreased linearly from 0.9 to 0.4 as given in Eq. (5). Using the AGPSO algorithm as an MPPT controller, the mathematical equations to update the duty cycle of the DC–DC boost converter and its step size are as follows:

$$\omega^k = \omega_{\max} - (\omega_{\max} - \omega_{Min}).{k}/{k_{\max}} \tag{5}$$

$$\Delta D_i^{k+1} = \omega^k.\Delta D_i^k + c_1.r_1.\left(D_{Pbest} - D_i^k\right) + c_2.r_2\left(D_{Gbest} - D_i^k\right) \tag{6}$$

$$D_i^{k+1} = D_i^k + \Delta D_i^{k+1} \tag{7}$$

where k is the No. of iteration, i denotes the No. of particles, ω^k is value of the inertia weight at the iteration k, $\omega_{\max} = 0.9$ and $\omega_{\min} = 0.4$ are the upper and lower bounds of ω^k, D^i denotes the duty cycle of the i th-particle, ΔD_i is the perturbation step, c_1 and c_2 are the acceleration coefficients, r_1 and r_2 are random numbers $\in [0, 1]$ denotes the personal best position of the i th-particle, and D_{Gbest} is the global best position. The flow chart of the AGPSO MPPT algorithm is depicted in Fig. 4.

3.2   CS Algorithm

CS is a bio-inspired algorithm created by Xin-She Yang et. al in 2009 [40]. It is inspired by the parasitic behavior of cuckoo birds (CBs), which lay their eggs in the nests of other host birds instead of constructing their own nest as shown in Fig. 5. The CBs move around randomly, but they are also guided by an exploration–exploitation mechanism that encourages them to explore new nests in the search space while also exploiting promising nests they have already discovered.

The exploration–exploitation mechanism works by evaluating each cuckoo's current position in the search space and assigning it a fitness value based on how close it is to the optimal solution. The cuckoos with higher fitness values are more likely to be chosen for reproduction, while those with lower fitness values are more likely to be replaced by new cuckoos generated from random positions in the search space.

Fig. 3 The updating values of c1 and c2 for the four groups utilized in the AGPSO algorithm
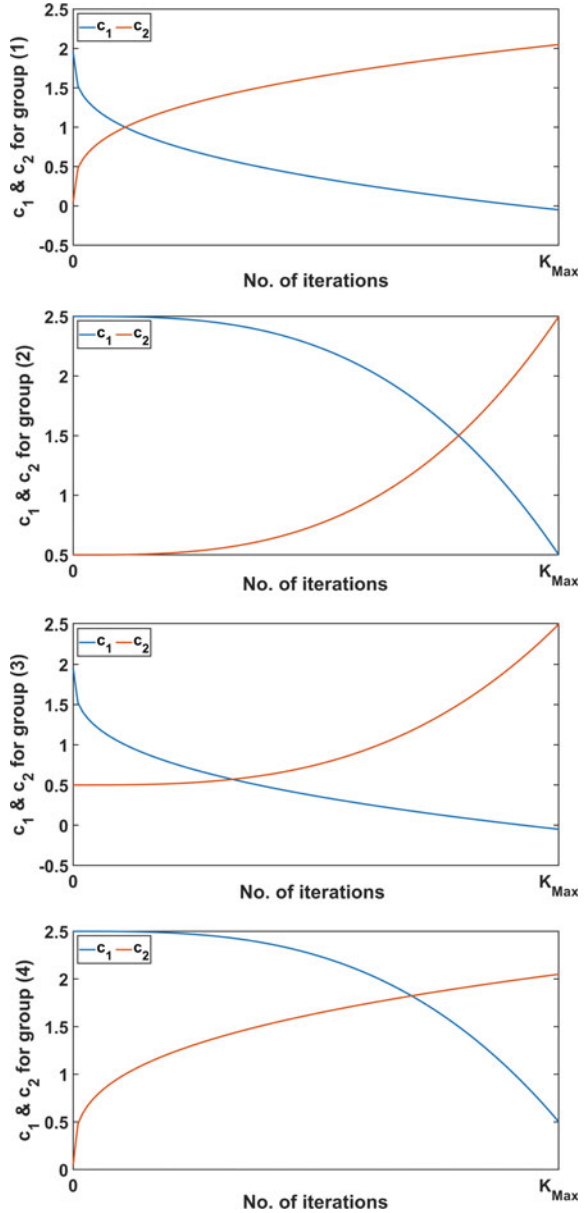
This process continues until the optimal solution is found or until all possible solutions have been explored. Hence, the CBs improve their opportunities of surviving by placing their eggs in numerous nests.

The reproduction behavior of the CBs is employed in the CS algorithm. Random movements based on the Lévy flight function enable CB a long jump in the search

Table 2 The updating strategies for c_1 and c_2

Group No.	Updating of c_1	Updating of c_2
(1)	$1.95 - \left(2k^{1/3}/k_{\text{Max}}^{1/3}\right)$	$\left(2k^{1/3}/k_{\text{Max}}^{1/3}\right) + 0.05$
(2)	$\left(-2k^3/k_{\text{Max}}^3\right) + 2.5$	$\left(2k^3/k_{\text{Max}}^3\right) + 0.5$
(3)	$1.95 - \left(2k^{1/3}/k_{\text{Max}}^{1/3}\right)$	$\left(2k^3/k_{\text{Max}}^3\right) + 0.5$
(4)	$\left(-2k^3/k_{\text{Max}}^3\right) + 2.5$	$\left(2k^{1/3}/k_{\text{Max}}^{1/3}\right) + 0.05$

space which enhances the algorithm performance and increases its convergence speed. The flow chart of the CS algorithm to obtain the optimal duty cycle for the MPPT controller of the PV system is depicted in Fig. 6. The following mathematical model is utilized to construct the algorithm.

$$D_i^{k+1} = D_i^k + \alpha \oplus L\acute{e}vy(\lambda) \tag{8}$$

$$L\acute{e}vy(\lambda) \approx \mathcal{X}\left(\frac{u}{|v|^{\frac{1}{\beta}}}\right)(D_{best} - D_i) \tag{9}$$

$$v \approx N\left(0, \sigma_v^2\right) \text{ and } u \approx N\left(0, \sigma_u^2\right) \tag{10}$$

$$\sigma_u = \left(\frac{\Gamma(1+\beta) \times \sin\left(\frac{\pi\beta}{2}\right)}{\Gamma\left(\frac{1+\beta}{2}\right) \times \beta \times 2^{\left(\frac{\beta-1}{2}\right)}}\right)^{\frac{1}{\beta}} \tag{11}$$

$$\sigma_v = 1 \tag{12}$$

where α is a scaling factor to adjust the step size, $L\acute{e}vy$ refer to the levy flights, λ is the variance, D_{best} denotes of the best duty cycle, Γ denotes the gamma function $\mathcal{X}$ denotes Lévy multiplication coefficient, $\beta = 1.5$ and u and v are calculated from the normal distribution curves.

4 Simulation Results

In order to evaluate the performance of both algorithms for MPPT application, the PV system in Fig. 1 has been carried out on MATLAB/SIMULINK. Four cases of weather conditions have been chosen to assess the performance of each algorithm in terms of tracking accuracy and speed. The pattern of the fallen solar irradiance on the surface of the PV array is presented in Table 3, and the associated P–V characteristic

Fig. 4 Flowchart of the
MPPT based on the AGPSO
algorithm
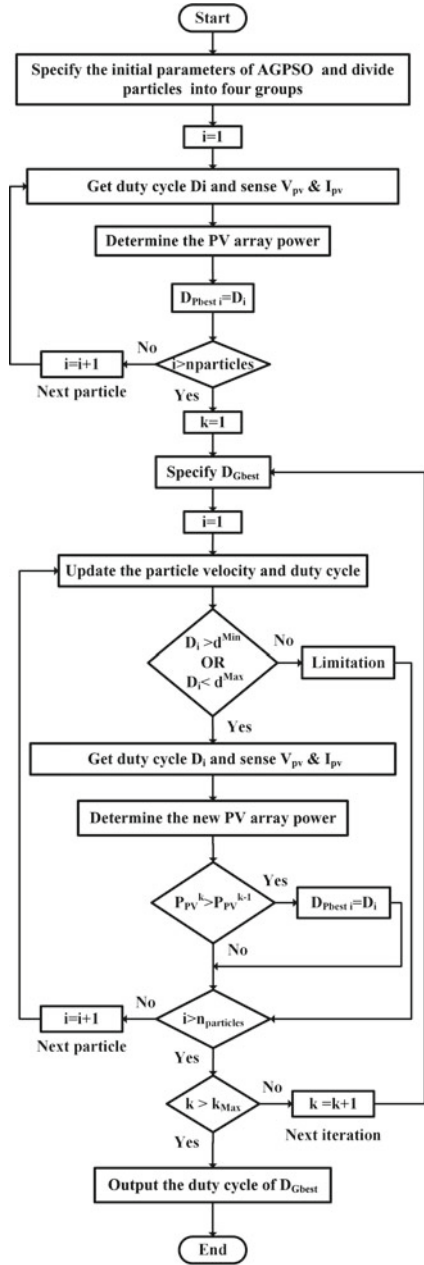
Fig. 5 The reproductive behavior of the CBs in nature

of the PV array for each case are shown in Fig. 7. Each case has a different MPP voltage and MPP power with a different curvature on the P–V characteristic. The first case handles the STCs which have a unique MPP, whereas the remaining cases address three dissimilar PSCs which have several MPPs. The three shaded patterns are more challenging for the MPPT controller since it must discriminate the GP among the other LPs to harvest the maximum power available.

The output power and duty cycle of both methods for considered weather patterns are illustrated in Figs. 8, 9, 10 and 11. The acquired power, tracking time, and MPPT efficiency for both techniques have been listed in Table 4. As shown, the maximum power that should be harvested for the GP1, GP2, GP3, and GP4 is 450.36 W, 149.98 W, 194.3 W, and 296.27 W, respectively.

Regarding the first case, the obtained numerical results of the PV system for both controllers under STCs are depicted in Fig. 8. As illustrated, CS and AGPSO algorithms have a maximum power of 449.25 W and 449.35 W with a tracking time of 0.163 s and 0.297 s, respectively. This indicates that the utilization of the CS algorithm reduces the tracking time by almost 82%. Furthermore, the CS algorithm has more tracking accuracy with an MPPT efficiency of 99.78% compared to 99.75% for the AGPSO algorithm.

Under the PSCs, three shaded patterns have been selected with different GP location on the P–V curve, particularly case 2, case 3, and case 4 that are corresponding to GP location at the left, middle, and right relative to the other MPPs; respectively,

Fig. 6 Flowchart of the
MPPT based on the CS
algorithm

Start

Initialization CS parameters n=4, α and β

Initialization duty cycle D with random value and
store this values in a matrix

Sense PV voltage and current store the measuring in a matrix

Calculate the yielded power by the PV system

Set the duty cycle D ,that corresponds to the MPP
and use it as the best

Worst nest are excluded

Update the latest best solution

The global best position is set to the PWM control circuit

Update the global best of duty cycle

$k > k^{Max}$

No

k = k+1

Next iteration

Yes

Output the optimal duty cycle

End

Table 3 The pattern of the fallen solar irradiance on the regarded PV array

Shading pattern	Solar irradiance (kW/m^2)		
Case 1	1.0	1.0	1.0
	1.0	1.0	1.0
	1.0	1.0	1.0
Case 2	1.0	1.0	1.0
	0.3	0.3	0.3
	0.2	0.2	0.2
Case 3	1.0	1.0	1.0
	0.6	0.6	0.6
	0.2	0.2	0.2
Case 4	1.0	1.0	1.0
	0.8	0.8	0.8
	0.6	0.6	0.6

as shown in Fig. 7. Simulation results show that the CS algorithm has a better performance than the AGPSO algorithm under all tested PSCs as demonstrated in Table 4. The reduction in the convergence time for GP_2, GP_3, and GP_4 is about 47.36%, 47%, and 60%, respectively. In addition, the CS algorithm has a higher tracking accuracy with MPPT efficiencies of 99.94%, 99.79%, and 99.84% in contrast with the AGPSO algorithm which has MPPT efficiencies of 99.93%, 99.52%, and 99.67% for GP_2, GP_3, and GP_4, respectively.

5 Experimental Results

In this section, experimental studies are conducted in order to validate the simulation results for both considered algorithms-based controllers under the PSCs. The experimental tests had been carried out on the selected PV testing site which is equipped with a pyranometer and provides easy access to the nearby solar energy laboratory. The selected test site is located on the roof of the teaching building in the Faculty of Engineering at Port Said. The exact location of the PV testing site is identified with Latitude: 31° 14′ 50.97″ N and longitude: 32° 18′ 44.63″ E. Figure 12 shows the experimental hardware setup for the considered PV system. The 3S3P PV array is mounted at a fixed tilt angle of 30° facing south. The PV panel temperature is measured by a thermocouple installed on the back surface of each panel. The shading pattern is constructed by employing opaque and semi-transparent sheets as depicted in Fig. 12. A data logger records the data about the weather condition to acquire the P–V curve of the PV array under the tested PSC.

The PV array is connected to the load via the boost converter. The specifications of the designed converter are $f_{sw} = 31.372$ kHz, $L_{boost} = 2.6$ mH, $C_{in} = 330 \, \mu F$, and $C_{out} = 1000 \, \mu F$. Two measurement circuits have been implemented to monitor
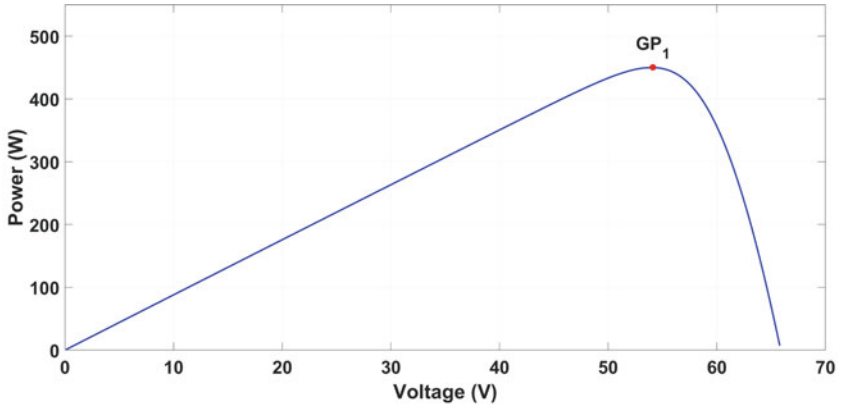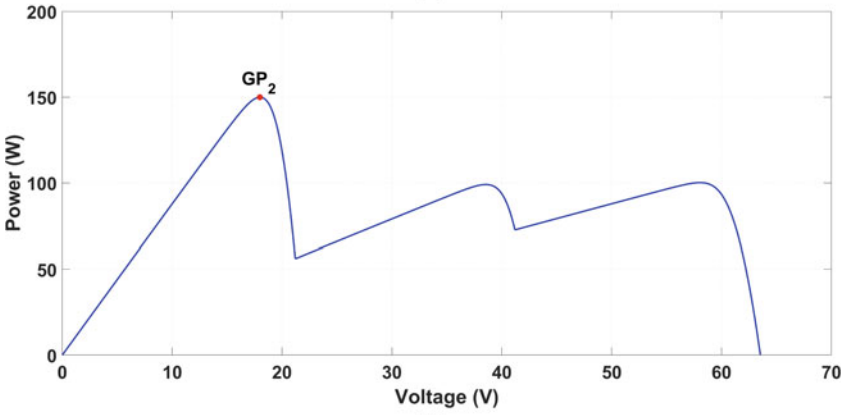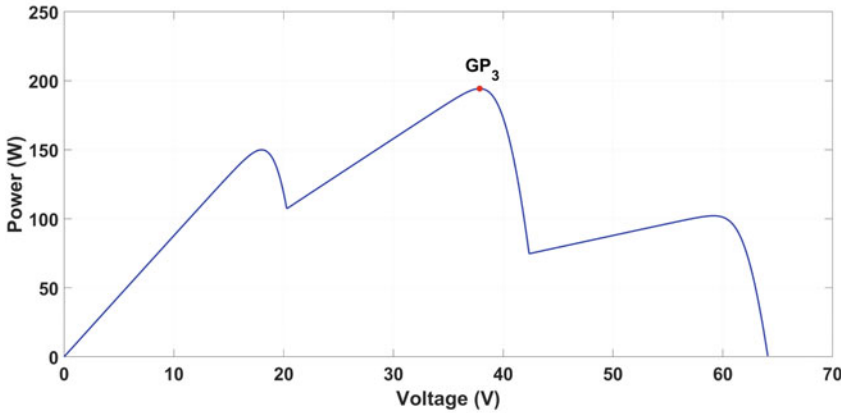
Fig. 7 The P–V curves of the PV array for various weather conditions: **a** case 1, **b** case 2, **c** case 3, and **d** case 4
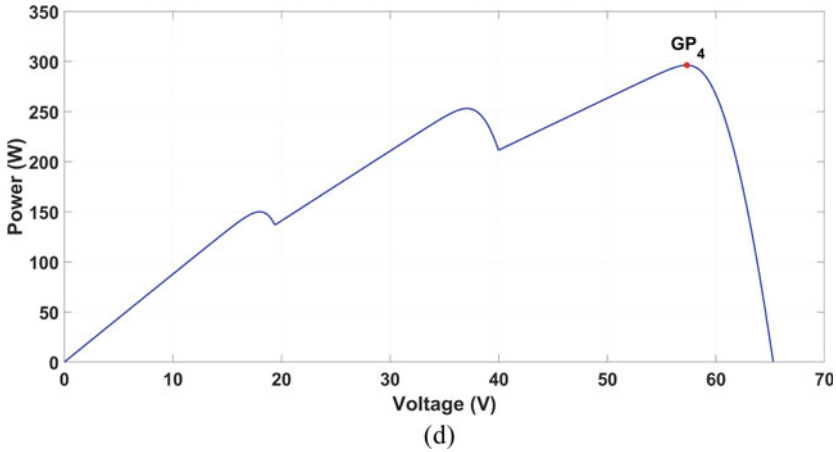
Fig. 7 (continued)

the output of the PV array and the load. The input sensors measure the array current and voltage and send the sensed signals to the controller. Arduino Mega 2560 is used in this study which is interfaced with MATLAB through a supported package. The tested algorithms are deployed on the controller that generates the optimal duty cycle and then sent its value to the TLP250 drive circuit. A digital oscilloscope has been employed to display the PWM signal.

The obtained P–V characteristic for experimental studies is illustrated in Fig. 13. As it is noticed, the characteristic curve displays numerous MPPs with the GP on the right side of the curve. The value of the power and voltage for the GP is 158.3 W and 54.53 V. The corresponding experimental results of the PV array power and voltage for the two algorithms are shown in Figs. 14 and 15. As can be seen from Fig. 14, the AGPSO algorithm reached a maximum power of about 155.72 W at an MPP voltage of 53.85 V and tracking efficiency of about 98.4%. It has an MPPT time of about 5 s with high power fluctuations of about 4.7 W at steady-state conditions. On the other hand, the CS algorithm has a maximum power of almost 156.02 W at an MPP voltage of 53.91 V and tracking efficiency of about 98.6% as shown in Fig. 15. It reached the MPP in just 2.9 s with lower power fluctuations of about 3.4 W at steady-state conditions. Overall, the experimental results indicate that the performance of the CS algorithm is better than the AGPSO algorithm in terms of tracking accuracy and speed.
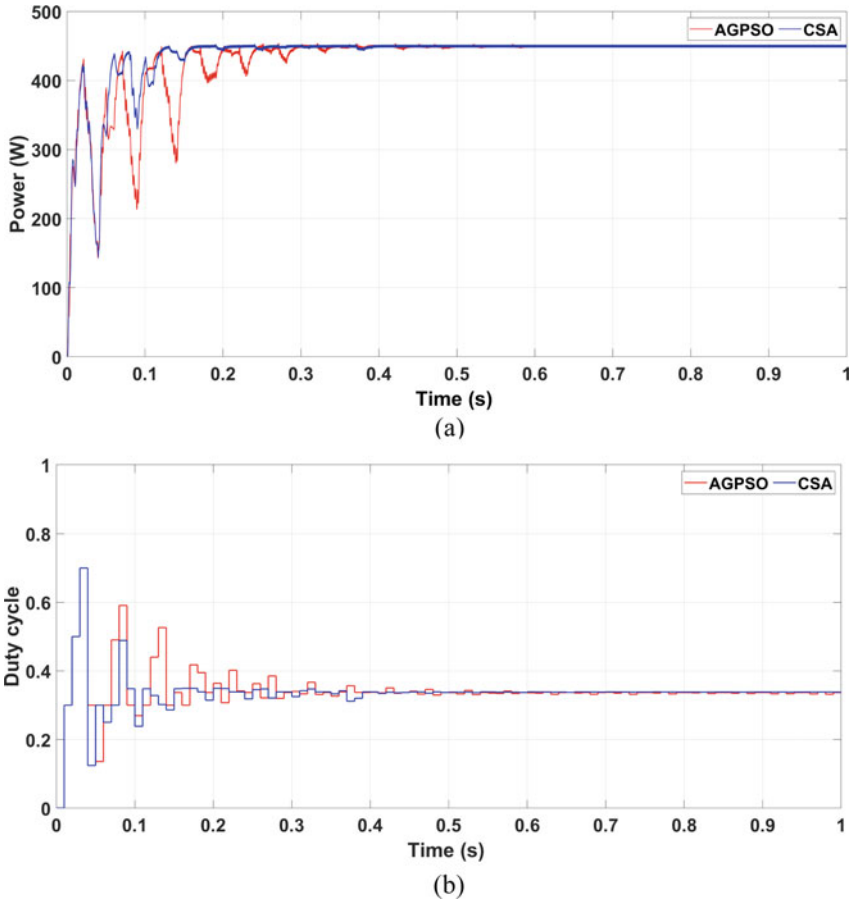
Fig. 8 The behavior of both algorithms for case 1: **a** output power and **b** duty cycle

6 Conclusion

This article presented a comprehensive comparison between AGPSO and CS algorithms for harvesting the maximum power from the PV system under the PSCs. The mechanism of operation, the mathematical model, and the MPPT flowchart for both considered bio-inspired algorithms were explained. MATLAB simulations and experimental tests were carried out to compare both algorithms' performance under various weather conditions.

From the obtained results, the two bio-inspired algorithms can follow the GP of the PV array under tested conditions with low convergence time and high MPPT accuracy. Although the AGPSO algorithm can successfully trace the GP, the CS algorithm outperforms it with a higher convergence speed and tracking accuracy. The simulation results demonstrated that using the CS algorithm decreased the MPPT time by 82%,
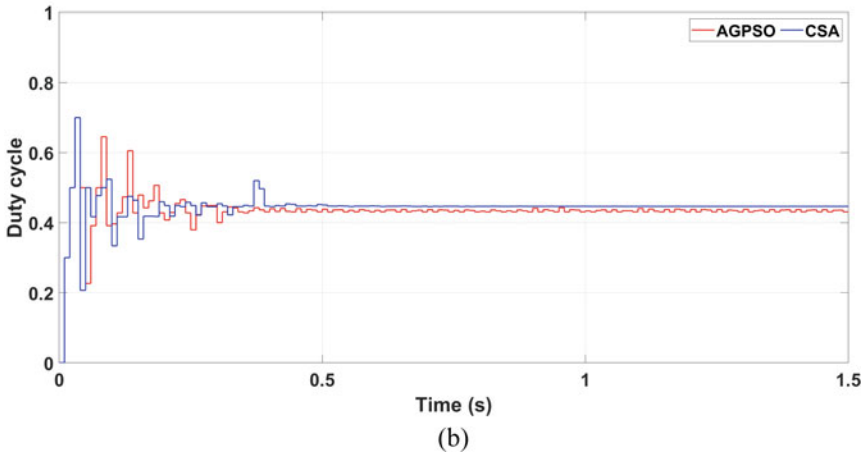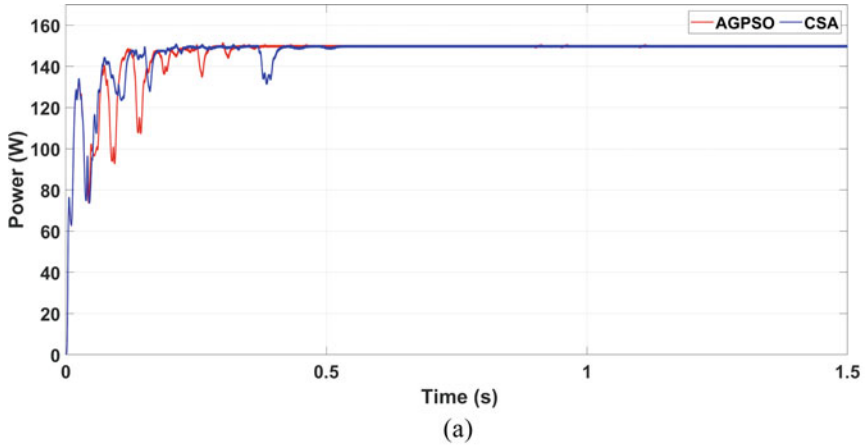
Fig. 9 The behavior of both algorithms for case 2: **a** output power and **b** duty cycle

47.36%, 47%, and 60% for GP$_1$, GP$_2$, GP$_3$, and GP$_4$, respectively. Furthermore, the tracking efficiency for the CS algorithm was higher than the AGPSO algorithm under various weather patterns. Experimental results confirmed the simulation results since the tracking time of the CS algorithm was reduced by almost 42% compared with the AGPSO algorithm. In addition, the CS algorithm was found to have lower power fluctuations and higher MPPT accuracy than the AGPSO algorithm counterpart.
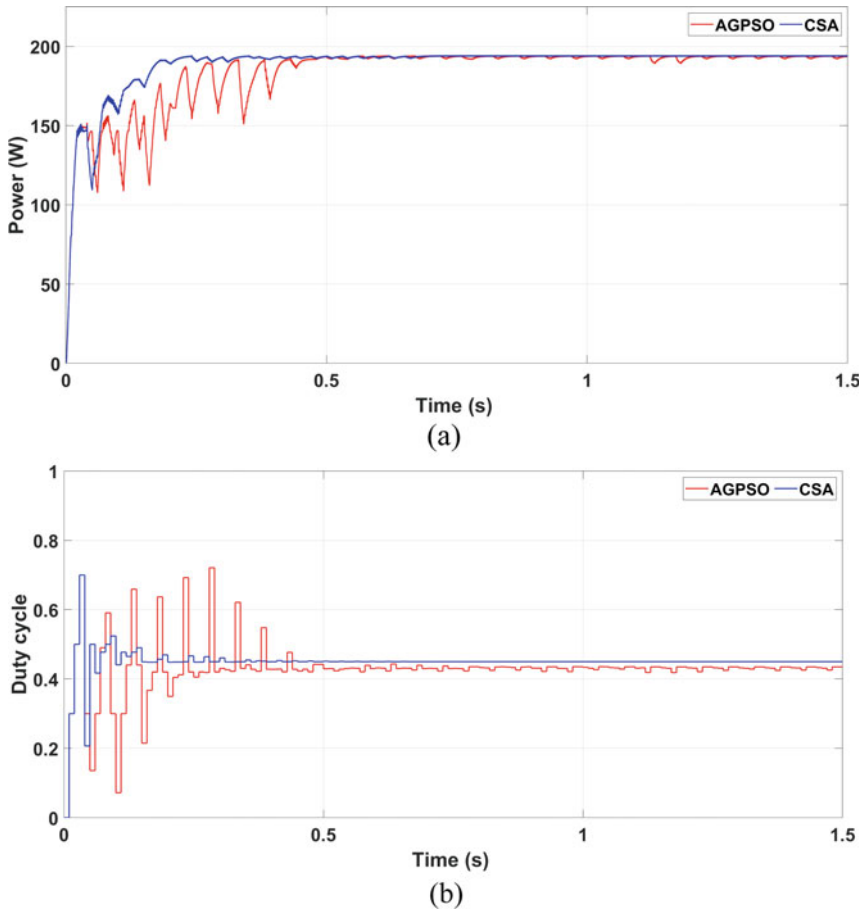
Fig. 10 The behavior of both algorithms for case 3: **a** output power and **b** duty cycle

7 Recommendation

Based on the previous findings, it is recommended to carry out a bio-inspired-based-MPPT algorithm in PV systems to extract the maximum power from PV systems under PSCs and hence improve the system efficiency. This enhances the endeavors of fulfilling SDG 7: Affordable and clean energy through optimizing the energy harvest from PV systems.
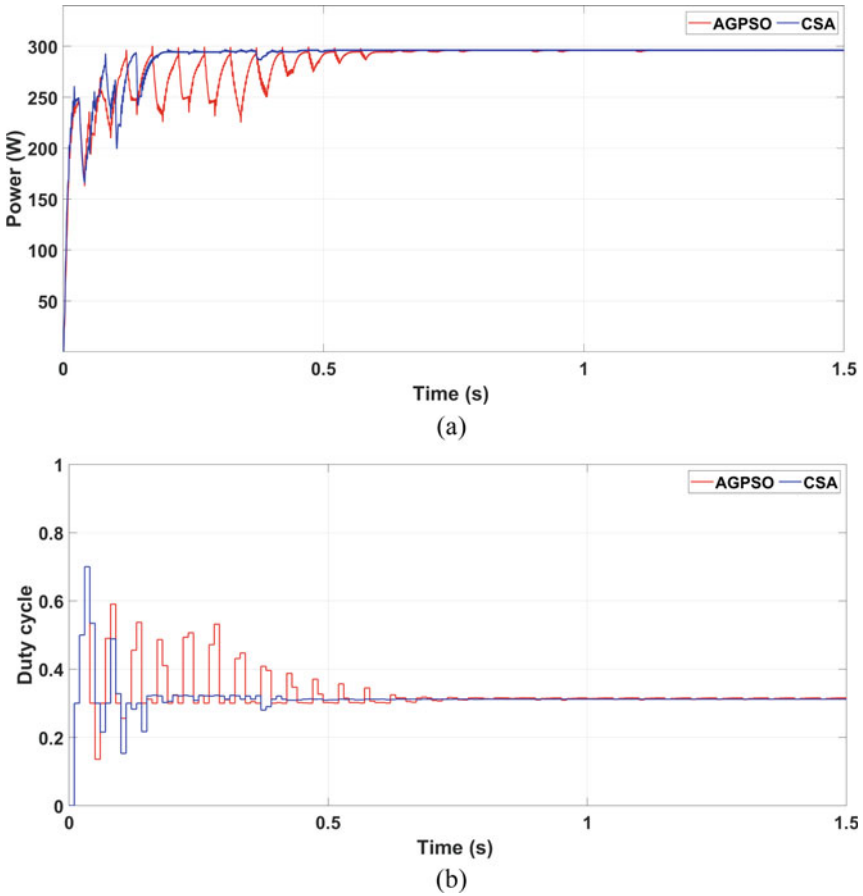
Fig. 11 The behavior of both algorithms for case 4: **a** output power and **b** duty cycle

Table 4 Performance of bio-inspired algorithms for different patterns of solar radiation

Pattern	Algorithm	Power (w)	Tracking time (s)	GP power (w)	MPPT Efficiency (%)
Case 1	AGPSO	449.25	0.297	450.36	99.75
	CS	449.35	0.163		99.78
Case 2	AGPSO	149.87	0.283	149.98	99.93
	CS	149.89	0.199		99.94
Case 3	AGPSO	193.36	0.494	194.3	99.52
	CS	193.9	0.336		99.79
Case 4	AGPSO	295.3	0.596	296.27	99.67
	CS	295.8	0.202		99.84
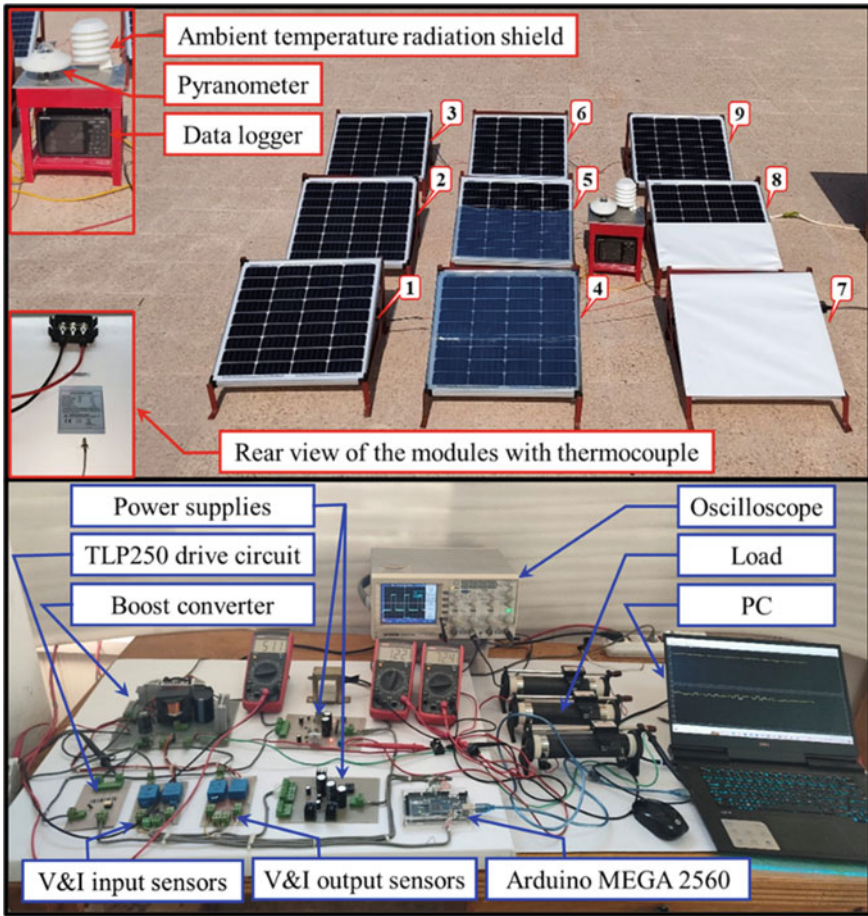
Fig. 12 Experimental hardware setup for the considered PV system
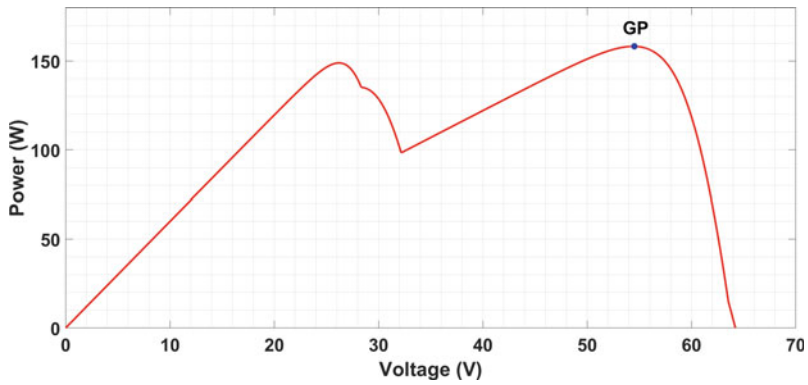
Fig. 13 The acquired P–V curve for the experimental test
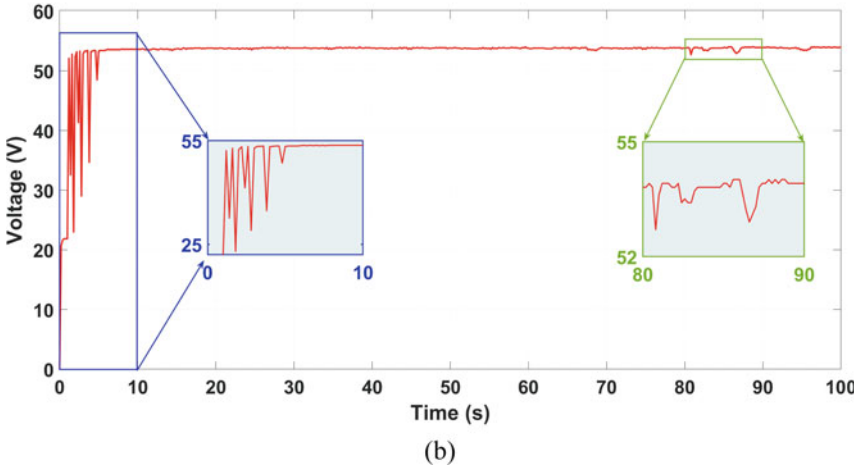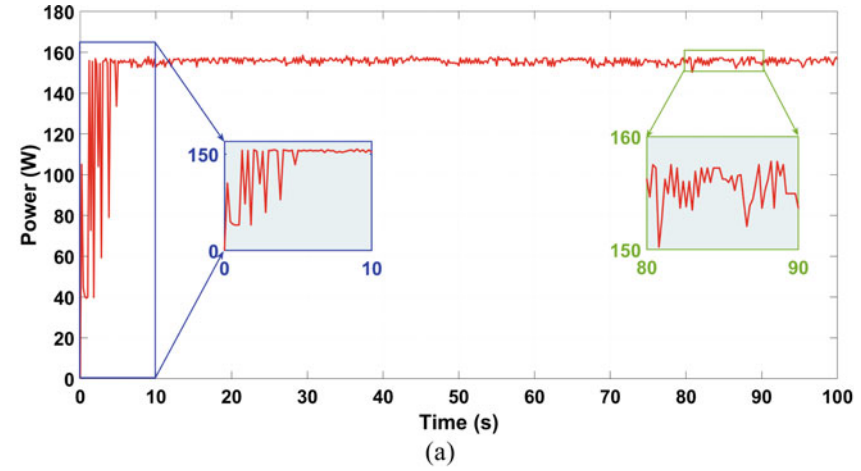
Fig. 14 Experimental results for the AGPSO algorithm: **a** power and **b** voltage
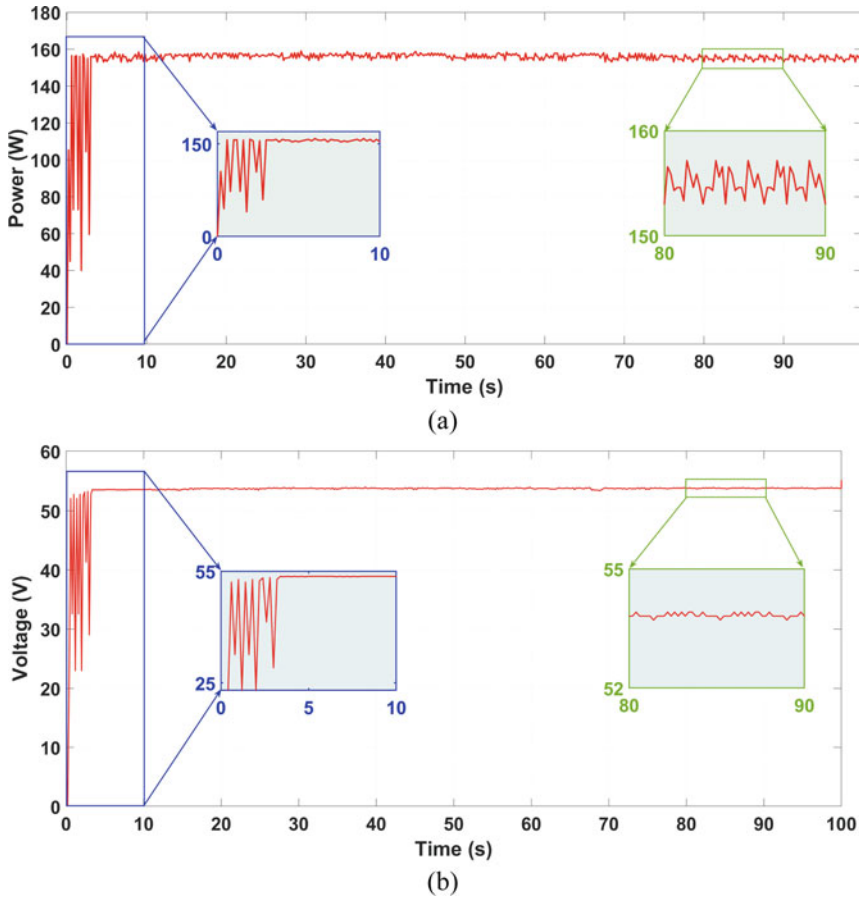
Fig. 15 Experimental results for the CS algorithm: **a** power and **b** voltage

References

1. Elsakka MM, Ingham DB, Ma L, Pourkashanian M (2021) Comparison of the computational fluid dynamics predictions of vertical axis wind turbine performance against detailed pressure measurements. Int J Renew Energy Res 11:276–293
2. Amer AE, Elsakka MM, Lebedev VA (2021) Thermal performance of an accumulator unit using phase change material with a fixed volume of fins. Int J Energy Res 45:19089–19102. https://doi.org/10.1002/er.7095
3. Abuhashish MN, Daoud AA, Elfar MH (2022) A novel model predictive speed controller for PMSG in wind energy systems. Int J Renew Energy Res 12:170–180. https://doi.org/10.20508/ijrer.v12i1.12750.g8385
4. Elsakka MM, Ingham DB, Ma L, Pourkashanian M (2020) Effects of turbulence modelling on the predictions of the pressure distribution around the wing of a small scale vertical axis wind turbine. In: Proceedings of the 6th European conference on computational mechanics: solids, structures and coupled problems, ECCM 2018 and 7th European conference on computational fluid dynamics, ECFD 2018, pp 3921–3931

5. Osman MH, Seify MAE, Ahmed MK, Korovkin NV, Refaat A (2022) Highly efficient MPP tracker based on adaptive neuro-fuzzy inference system for stand-alone photovoltaic generator system. Int J Renew Energy Res 12:209–217. https://doi.org/10.20508/ijrer.v12i1.12634.g8424

6. Elsakka MM, Ingham DB, Ma L, Pourkashanian M, Moustafa GH, Elhenawy Y (2022) Response surface optimisation of vertical axis wind turbine at low wind speeds. Energy Rep 8:10868–10880. https://doi.org/10.1016/j.egyr.2022.08.222

7. Refaat A, Osman MH, Korovkin NV (2020) Current collector optimizer topology to extract maximum power from non-uniform aged PV array. Energy 116995. https://doi.org/10.1016/j.energy.2020.116995

8. Refaat A, Shehata AA, Elgamal M, Korovkin N V. (2020) Current collector optimizer topology with reconfiguration algorithm to harvest optimal power from nonuniform aged PV arrays. In: 2020 international multi-conference on industrial engineering and modern technologies, FarEastCon 2020, p 9271455

9. Osman MH, Refaat A (2019) Adaptive multi-variable step size P&O MPPT for high tracking-speed and accuracy. IOP Conf Ser Mater Sci Eng

10. Chevtchenko SF, Barbosa EJ, Cavalcanti MC, Azevedo GMS, Ludermir TB (2022) Combining PPO and incremental conductance for MPPT under dynamic shading and temperature. Appl Soft Comput 131:109748. https://doi.org/10.1016/j.asoc.2022.109748

11. Bouarroudj N, Benlahbib B, Sedraoui M, Feliu-Batlle V, Bechouat M, Boukhetala D, Boudjema F (2022) A new tuning rule for stabilized integrator controller to enhance the indirect control of incremental conductance MPPT algorithm: Simulation and practical implementation. Optik (Stuttg) 268:169728. https://doi.org/10.1016/j.ijleo.2022.169728

12. Loukriz A, Haddadi M, Messalti S (2016) Simulation and experimental design of a new advanced variable step size Incremental Conductance MPPT algorithm for PV systems. ISA Trans 62:30–38. https://doi.org/10.1016/j.isatra.2015.08.006

13. Osman MH, Ahmed MK, Refaat A, Korovkin NV (2021) A comparative study of MPPT for PV system based on modified perturbation observation method. In: Proceedings of 2021 IEEE conference Russians young researchers in electrical and electronic engineering, ElConRus 2021, 1023–1026. https://doi.org/10.1109/ElConRus51938.2021.9396444

14. Refaat A, Khalifa A, Elsakka MM, Elhenawy Y, Kalas A, Hegazy M (2023) A novel meta-heuristic MPPT technique based on enhanced autonomous group particle swarm optimization algorithm to track the GMPP under partial shading conditions—experimental validation. Energy Convers Manag 287:117124. https://doi.org/10.1016/j.enconman.2023.117124

15. Refaat A, Kalas A, Khalifa AE, Elfar MH (2023) A comparative study of two metaheuristic MPPT techniques to extract maximum power from PV array under different partial shading patterns. In: IEEE conference on power electronics and renewable energy, CPERE 2023. IEEE

16. Refaat A, Elgamal M, Korovkin NV (2019) A novel photovoltaic current collector optimizer to extract maximum power during partial shading or mismatch conditions. In: Proceedings of the 2019 IEEE conference of Russian young researchers in electrical and electronic engineering, ElConRus 2019, pp 407–412

17. Abouobaida H, Mchaouar Y, Abouelmahjoub Y, Mahmoudi H, Abbou A, Jamil M (2023) Performance optimization of the INC-COND fuzzy MPPT based on a variable step for photovoltaic systems. Optik (Stuttg) 278:170657. https://doi.org/10.1016/j.ijleo.2023.170657

18. Abbass MJ, Lis R, Saleem F (2023) The maximum power point tracking (MPPT) of a partially shaded PV array for optimization using the antlion algorithm. Energies 16:1–13. https://doi.org/10.3390/en16052380

19. Mansoor M, Mirza AF, Ling Q, Javed MY (2020) Novel grass hopper optimization based MPPT of PV systems for complex partial shading conditions. Sol Energy 198:499–518. https://doi.org/10.1016/j.solener.2020.01.070

20. Ahmed J, Salam Z (2014) A maximum power point tracking (MPPT) for PV system using cuckoo search with partial shading capability. Appl Energy 119:118–130. https://doi.org/10.1016/j.apenergy.2013.12.062

21. Hamza Zafar M, Mujeeb Khan N, Feroz Mirza A, Mansoor M, Akhtar N, Usman Qadir M, Ali Khan N, Raza Moosavi SK (2021) A novel meta-heuristic optimization algorithm based

MPPT control technique for PV systems under complex partial shading condition. Sustain Energy Technol Assessments 47:101367. https://doi.org/10.1016/j.seta.2021.101367

22. da Rocha MV, Sampaio LP, da Silva SAO (2020) Comparative analysis of MPPT algorithms based on Bat algorithm for PV systems under partial shading condition. Sustain Energy Technol Assessments 40:100761. https://doi.org/10.1016/j.seta.2020.100761

23. Mohanty S, Subudhi B, Ray PK (2016) A new MPPT design using grey Wolf optimization technique for photovoltaic system under partial shading conditions. IEEE Trans Sustain Energy 7:181–188. https://doi.org/10.1109/TSTE.2015.2482120

24. Chandrasekaran K, Sankar S, Banumalar K (2020) Partial shading detection for PV arrays in a maximum power tracking system using the sine-cosine algorithm. Energy Sustain Dev 55:105–121. https://doi.org/10.1016/j.esd.2020.01.007

25. Azli H, Titri S, Larbes C, Kaced K, Femmam K (2022) Novel yellow saddle goatfish algorithm for improving performance and efficiency of PV system under partial shading conditions. Sol Energy 247:295–307. https://doi.org/10.1016/j.solener.2022.10.029

26. Abo-Khalil AG, Alharbi W, Al-Qawasmi AR, Alobaid M, Alarifi IM (2021) Maximum power point tracking of PV systems under partial shading conditions based on opposition-based learning firefly algorithm. Sustainability 13:1–18. https://doi.org/10.3390/su13052656

27. Aouchiche N, Aitcheikh MS, Becherif M, Ebrahim MA (2018) AI-based global MPPT for partial shaded grid connected PV plant via MFO approach. Sol Energy 171:593–603. https://doi.org/10.1016/j.solener.2018.06.109

28. Mendez-Flores E, Ortiz A, Macias I, Molina A (2022) Experimental validation of an enhanced MPPT algorithm and an optimal DC–DC converter design powered by metaheuristic optimization for PV systems. Energies 15:8043

29. Khalifa AE, Refaat A, Kalas A, Elfar MH (2022) Two bio-inspired MPPT algorithms to harvest the maximum power from partially shaded PV arrays. In: Proceedings of the 2022 conference of russian young researchers in electrical and electronic engineering, ElConRus 2022, pp 670–674

30. Mirza AF, Mansoor M, Ling Q (2020) A novel MPPT technique based on Henry gas solubility optimization. Energy Convers Manag 225:113409. https://doi.org/10.1016/j.enconman.2020.113409

31. Mansoor M, Mirza AF, Ling Q (2020) Harris hawk optimization-based MPPT control for PV systems under partial shading conditions. J Clean Prod 274:122857. https://doi.org/10.1016/j.jclepro.2020.122857

32. Chai LGK, Gopal L, Juwono FH, Chiong CWR, Ling HC, Basuki TA (2021) A novel global MPPT technique using improved PS-FW algorithm for PV system under partial shading conditions. Energy Convers Manag 246:114639. https://doi.org/10.1016/j.enconman.2021.114639

33. Mirza AF, Mansoor M, Ling Q, Yin B, Javed MY (2020) A salp-swarm optimization based MPPT technique for harvesting maximum energy from PV systems under partial shading conditions. Energy Convers Manag 209:112625. https://doi.org/10.1016/j.enconman.2020.112625

34. Gong L, Hou G, Huang C (2022) A two-stage MPPT controller for PV system based on the improved artificial bee colony and simultaneous heat transfer search algorithm. ISA Trans 132:428–443. https://doi.org/10.1016/j.isatra.2022.06.005

35. Zafar MH, Al-Shahrani T, Khan NM, Mirza AF, Mansoor M, Qadir MU, Khan MI, Naqvi RA (2020) Group teaching optimization algorithm based mppt control of pv systems under partial shading and complex partial shading. Electronics 9:1–24. https://doi.org/10.3390/electronics9111962

36. Vamsi Krishna Reddy AK, Venkata Lakshmi Narayana K (2022) Investigation of a social group assisted differential evolution for the optimal PV parameter extraction of standard and modified diode models. Energy Convers Manag 268:115955. https://doi.org/10.1016/j.enconman.2022.115955

37. Elbaz A, Elfar MH, Kalas A, Refaat A (2022) Maximum power extraction from polymer electrolyte membrane (PEM) fuel cell based on deterministic particle swarm optimization algorithm. In: Proceedings of the 2022 conference of Russian young researchers in electrical and electronic engineering, ElConRus 2022, pp 613–619

38. Shehata AA, Refaat A, Ahmed MK, Korovkin NV (2021) Optimal placement and sizing of FACTS devices based on autonomous groups particle swarm optimization technique. Arch Electr Eng 70:161–172. https://doi.org/10.24425/aee.2021.136059
39. Mirjalili S, Lewis A, Sadiq AS (2014) Autonomous particles groups for particle swarm optimization. Arab J Sci Eng 39:4683–4697. https://doi.org/10.1007/s13369-014-1156-x
40. Yang XS, Deb S (2009) Cuckoo search via Lévy flights. In: 2009 world congress on nature and biologically inspired computing, NABIC 2009—proceedings. IEEE, pp 210–214

A Modified Model Predictive Speed Control Based on Sensorless Hybrid MPPT Algorithm in Wind Turbine Systems

Mai N. Abuhashish, Ahmed A. Daoud, Ahmed Refaat, and Medhat H. Elfar

1   Introduction

Throughout the previous decades, electricity generation from renewable energy resources (RERs) has expanded significantly due to concerns about greenhouse gas emissions and energy shortages [1–3]. This leads to increasing research in wind turbine (WT) engineering [4–8]. Globally, the wind energy system integration in the electric utility network is gradually increasing, which raises the penetration level of WTs in the entire worldwide power generation [9]. According to [10], the worldwide installation of wind power capacity reached approximately 75 GW in the year 2022. Different types of wind energy conversion systems (WECS), using various mixtures of wind generators and power conditioning units, have been formed through the global wind power markets [11]. Type 4 WECS achieves the highest wind energy conversion efficiency, where full variable-speed operation is achievable in this configuration; accordingly, the maximum possible amount of power can be acquired at various wind speeds [12, 13]. The permanent magnet synchronous generator (PMSG) is highly favored in Type 4 WECS due to several reasons. These include direct-drive operation, less maintenance, no need for a DC excitation system, low rotor power loss, and high operating efficiency [14].

M. N. Abuhashish · A. A. Daoud · A. Refaat (✉) · M. H. Elfar
Department of Electrical Engineering, Faculty of Engineering, Port Said University, Port Said, Egypt
e-mail: ahmed_refaat_1984@eng.psu.edu.eg

M. N. Abuhashish
e-mail: mai.nasr@eng.psu.edu.eg

A. A. Daoud
e-mail: a.daoud@psu.edu.eg

M. H. Elfar
e-mail: mhelfar@eng.psu.edu.eg

Due to continuously changing wind speeds, maximum power point tracking (MPPT) has a crucial role in variable-speed WECS (VS-WECS) to maximize energy conversion efficiency. MPPT algorithms are applied to WT systems to ensure maximum wind power extraction. The optimum torque (OT) and optimum tip speed ratio (TSR) MPPT techniques are frequently employed in WECS, which provide the most favorable trade-off between the performance and the system complexity under various wind speeds [14–20]. In the TSR algorithm, accurate wind speed measurement is essential for proper generator speed adaptation with optimum rotor speed. To accomplish this, several mechanical sensors called anemometers are located at distinct places around the WT area [21]. To control the WT efficiently, it is necessary to have a trustworthy method of measuring wind speed. However, the traditional anemometer is not sufficient for this purpose. Wind speed estimation (WSE) algorithms are currently being utilized as a substitute for mechanical sensors to address this issue. These algorithms provide dependable wind speed estimates, simplify the WT system, and reduce costs. Numerous researchers have recommended the use of WSE methods to optimize wind power extraction, and many studies have demonstrated their effectiveness [21–23].

Generally, in VS-WECS with PMSG, voltage-oriented control (VOC) and field-oriented control (FOC) schemes are the most widely utilized linear control methods for grid-side converters (GSCs) and machine-side converters (MSCs), respectively. These control methods use a cascaded control structure consisting of PI controllers in both the inner and outer control loops and a modulation stage to produce the PWM signals for the power conditioning units [24–28]. The method used for controlling the current in the MSC involves a rapid internal loop that operates in a synchronized *dq*-axes reference frame. This allows for separate control of the generator currents, while a slower external loop regulates the generator speed to match its desired value. On the other hand, the GSC uses a different approach, with an external control loop that maintains the DC-link voltage at the intended level and an internal current loop that ensures the operation of the system at unity power factor (UPF) and injects real power from the MSC to the electrical network [29]. Several drawbacks associated with these control techniques have been addressed in the literature. The effectiveness of the linear controller heavily relies on the proper adjustment of numerous controller parameters within the PI cascaded control structure. The coupling effects of control variables, like *dq*-axes generator or grid currents, are noticeable, and it requires extra feed-forward terms to disentangle the *dq* components of the current, resulting in increased complexity of the control system [30, 31].

Recently, finite-control-set model predictive control (FCS-MPC) has shown numerous important features that render it a viable alternative technique for controlling power converters [32–37]. To name just a few, FCS-MPC has a straightforward concept and is suitable for many different systems. It can provide an excellent transient response compared with linear controllers [30, 34, 35]. Generally, in Type 4 WECS, model predictive current control (MPCC) has been applied to PMSG by just replacing the inner PI controller, resulting in an enhanced dynamic response for the control system [18, 38, 39]. However, it still uses a cascaded configuration that includes a PI speed controller, and there is potential for enhancing the dynamic

response of the outer speed loop. According to Mousa et al. [22], an MPC scheme is utilized only for MSC in VS-WECS with PMSG as a replacement for the outer loop PI controller, and the inner one uses a classical hysteresis controller for the current control. Therefore, the cascaded structure still exists in the control system of the MSC. The key feature of the MPC is the ability to incorporate different control variables employing a single multi-term cost function without using the cascaded configuration or outer PI controller. Model predictive speed control (MPSC) strategy has been implemented in a PMS motor (PMSM) in [34, 40–44], where simultaneous manipulation of the electrical variables and speed has been achieved in one control law. The authors proposed, in [45], an MPSC system for PMSG, nevertheless, the implemented control technique has not taken into account the characteristics of the WT systems. Abuhashish et al. [46] suggests an MPSC technique for PMSG in variable-speed WT (VSWT) systems. The suggested control technique is based on a hybrid MPPT (HMPPT) algorithm to assure maximum energy harvested from the wind. However, the measured value of wind speed is required to implement the proposed HMPPT. To this end, the authors are motivated to propose an efficient HMPPT without raising the system's complexity.

This paper proposes a modified MPSC technique for PMSG in VSWT system, where the value of wind speed is obtained via a WSE method. The modified MPSC is based on a sensorless HMPPT technique that calculates the wind speed without employing any sensors. This WSE method is polynomial-based estimation approach where the nonlinear power coefficient curve is approximated to a third-order polynomial. Therefore, the modified MPSC reduces the WT complexity, installation cost, and increases the total efficiency as well as reliability of the WT system. In addition, an MPCC scheme has been implemented to the GSC for injecting active power into the electrical network MATLAB simulations are used to assess the efficacy of the modified MPSC when subjected to fluctuations in wind speed, both in the form of sudden changes and random variations.

The following is the organization of this paper: Sect. 2 explains the modeling of the WT system. Section 3 provides an overview of the FCS-MPC principles in addition to the proposed MPSC and MPCC techniques. Section 4 involves testing the system's performance through simulations. Eventually, Sect. 5 concludes this study.

2 Wind Turbine System Modeling

The system configuration of VSWT with PMSG is shown in Fig. 1. It consists of a three-phase PMSG, which has a direct connection with the WT. The wind power is transferred to the electric utility network via the back-to-back (BTB) two-level voltage source converters (2L-VSCs). A DC-link capacitor links the identical MSC and GSC on either side, providing decoupling between the electrical network and the generator.
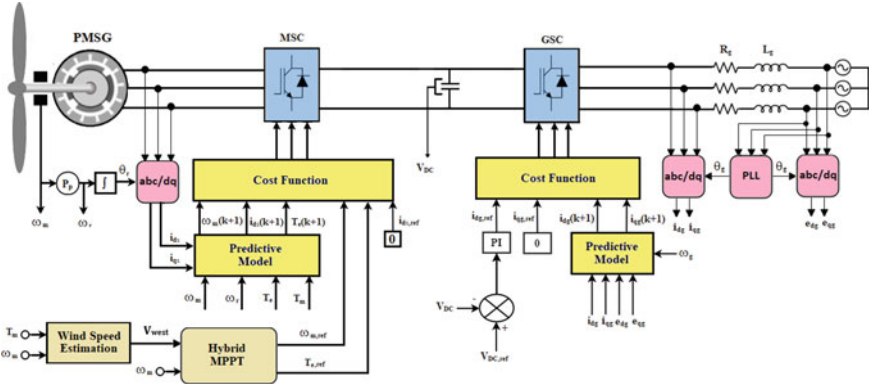
Fig. 1 The schematic diagram of grid-tied PMSG-based WT system

2.1 Wind Turbine Model

The wind energy is converted to mechanical energy through WTs, which then drive the generator rotor to generate electrical power. The following equation expresses the extracted output mechanical power from the wind [47]:

$$P_m = \frac{1}{2}\rho A C_p(\lambda, \beta) V_w^3 \tag{1}$$

where ρ refers to the air density, V_w denotes the wind speed, A denotes the WT blades swept area, C_p refers to the WT power coefficient as a function of blade pitch angle (β) and TSR (λ). The TSR is a crucial parameter for the WTs, representing the relationship between the incoming wind speed and the blade tip speed. It can be calculated using (2):

$$\lambda = \frac{\omega_m R}{V_w} \tag{2}$$

where R refers to the blade length and ω_m denotes the turbine rotor rotational speed. In this work, the C_p value is calculated as follows:

$$C_p(\lambda, \beta) = C_{w1}\left(\frac{C_{w2}}{\lambda_i} - C_{w3}\beta - C_{w4}\right)e^{\frac{-C_{w5}}{\lambda_i}} + C_{w6}\lambda \tag{3}$$

$$\lambda_i^{-1} = (\lambda + 0.08 \times \beta)^{-1} - 0.035 \times (1 + \beta^3)^{-1} \tag{4}$$

where the turbine coefficients $C_{w1} - C_{w6}$ are given as: $C_{w1} = 0.5176$, $C_{w2} = 116$, $C_{w3} = 0.4$, $C_{w4} = 5$, $C_{w5} = 21$, and $C_{w6} = 0.0068$ [25].

The developed mechanical torque by means of the WT can be mathematically expressed as follows:

$$T_m = \frac{P_m}{\omega_m} = \frac{1}{2} \frac{\rho A C_p(\lambda, \beta) V_w^3}{\omega_m} \tag{5}$$

2.2 Maximum Power Point Tracking Algorithms

The WTs have four distinct operating regions, which are outlined in [17]. This paper focuses on region 2, where the mechanical power exhibits a cubic correlation with wind speed. In this region, MPPT is activated to maximize power generation from the wind. The optimal TSR (λ_{opt}) is a crucial design parameter for WTs, for which the extracted power is maximized. In VS-WECS, WTs can adjust their rotational speed in response to instantaneous changes in wind speed to maintain the optimal TSR and generate the maximum amount of power at all times [16]. Figure 2 depicts the relationship between the power coefficient C_p and TSR (λ), assuming a pitch angle β of zero. Consistently operating of the WT at λ_{opt}, where C_p is maximum, ensures the maximum energy captured at any wind speed [16]. Figure 3 depicts the maximum power that can be acquired under wind speed variations. Tracking maximum power points (MPPs) is accomplished by controlling rotor speed in accordance with varying wind speeds to work at optimum value of C_p and λ_{opt}.
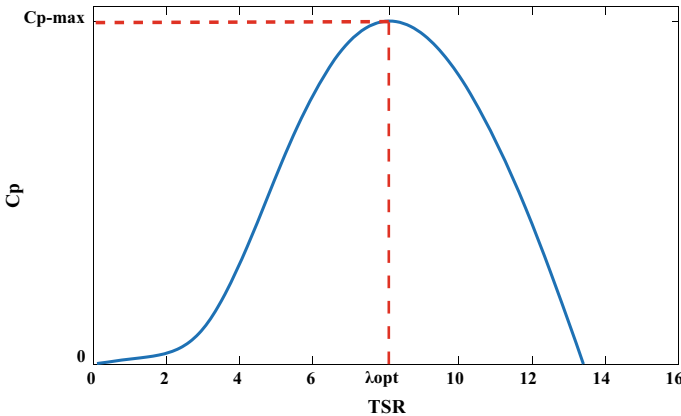
Fig. 2 Power coefficient versus TSR
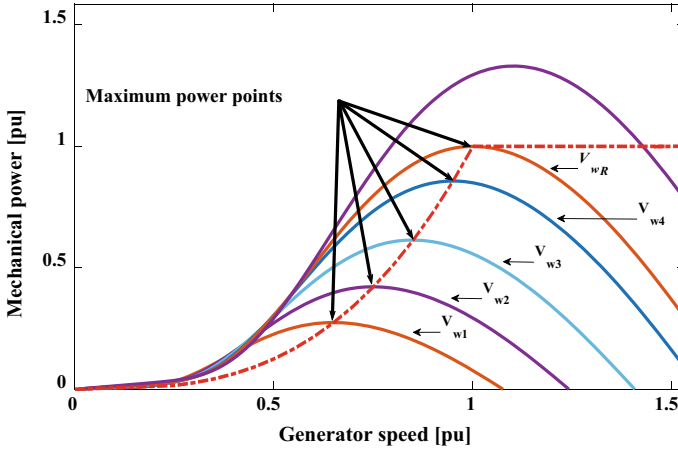
Fig. 3 Power characteristic of WT

2.3 Wind Speed Estimation Method

Without employing any mechanical wind speed sensors, the MPPT depending on the WSE approach has been utilized to estimate actual V_w. The V_w can be estimated using the measured rotational speed of rotor. The C_p for WSE is formulated by a third-order polynomial as follows [48]:

$$C_p = b_0 + b_1\lambda + b_2\lambda^2 + b_3\lambda^3 \tag{6}$$

where constants b_i for $i = 0, 1, 2, 3$ are listed in Table 1 in details.

From (1), (2), and (6), the mechanical power is given by:

$$P_m = \frac{1}{2}\rho A V_w^3\left(b_0 + b_1\frac{\omega_m R}{V_w} + b_2\left(\frac{\omega_m R}{V_w}\right)^2 + b_3\left(\frac{\omega_m R}{V_w}\right)^3\right) \tag{7}$$

Using (7), the estimated value of wind speed (V_{west}) can be derived as a function of (T_m, ω_m) as follows:

$$V_{west}^3 + b_1 b_0^{-1}\omega_m R V_{west}^2 + b_2 b_0^{-1}\omega_m^2 R^2 V_{west} + b_3 b_0^{-1}\omega_m^3 R^3 - T_m\omega_m(0.5\rho A)^{-1} = 0 \tag{8}$$

Table 1 Constants of C_p

$b_0 = 0.00715814$	$b_2 = 0.02899277$
$b_1 = -0.04454063$	$b_3 = -0.00202519$

Three roots for V_{west} are generated by the numerical solution for (8); Only one root is feasible.

The mechanical torque can be evaluated as follows:

$$T_e - T_m = J\frac{d}{dt}\omega_m + F\omega_m \tag{9}$$

2.4 Permanent Magnet Synchronous Generator Dynamic Model

A permanent magnet synchronous (PMS) machine can function as either a generator or a motor based on the sign of the shaft mechanical torque T_m. In VS-WECS, the PMS machine works as a generator by simply changing the T_m sign [32]. The *dq* reference frame stator voltage formulas of the three-phase surface-mounted PMSG (SPMSG) are given according to Youssef et al. [38]:

$$v_{ds} = R_s i_{ds} + L_s\frac{d}{dt}i_{ds} - \omega_r L_s i_{qs} \tag{10}$$

$$v_{qs} = R_s i_{qs} + L_s\frac{d}{dt}i_{qs} + \omega_r L_s i_{ds} + \omega_r \psi_r \tag{11}$$

where ω_r denotes the generator electrical angular speed, i_{ds} and i_{qs} are the *dq*-axes stator currents, ψ_r is the permanent magnet flux linkage, L_s and R_s refer to the stator winding inductance and resistance, respectively. The electromagnetic torque T_e of the SPMSG is as follows:

$$T_e = \frac{3}{2}P_p\psi_r i_{qs} \tag{12}$$

where P_p denotes the No. of pole pairs.

The mechanical formula of rotor speed dynamics can be rewritten from (9) as follows:

$$J\frac{d}{dt}\omega_m = T_e - T_m - F\omega_m \tag{13}$$

where J denotes the moment of inertia, ω_m denotes the generator mechanical angular rotational speed, and F denotes the friction factor.

The relationship between electrical and mechanical angular speed can be described as:

$$\omega_r = P_p\omega_m \tag{14}$$

3 Finite-Control-Set Model Predictive Control

The fundamental principle of FCS-MPC is based on the fact that a power converter can only produce a limited number of switching states. By using a discrete-time (DT) model of the system, the future behaviour of controlled variables can be predicted for each switching state. The best switching state is chosen by minimizing a cost function. The switching state that minimizes this cost function is then directly applied to the power converter without needing a modulation stage for generating the switching signals [34, 35]. This paper employs the FCS-MPC to implement the modified MPSC and MPCC for the MSC and GSC, respectively.

3.1 Modified Model Predictive Speed Control for MSC

Figure 1 shows schematic diagram for the modified MPSC at MSC. The key purpose of the MSC controller is to achieve optimal power generation at different wind speeds. In order to create the MPSC scheme, it is necessary to convert the continuous-time (CT) model of SPMSG into a predictive model by discretizing it. This predictive model is then utilized to foretell the future values of system variables at the next sampling point. The dynamics of the SPMSG's stator current in the dq-axes are derived from (10) and (11) as outlined below:

$$\frac{d}{dt}i_{ds} = -\frac{R_s}{L_s}i_{ds} + \omega_r i_{qs} + \frac{1}{L_s}v_{ds} \tag{15}$$

$$\frac{d}{dt}i_{qs} = -\frac{R_s}{L_s}i_{qs} - \omega_r i_{ds} + \frac{1}{L_s}v_{qs} - \frac{\omega_r \psi_r}{L_s} \tag{16}$$

According to [46], it is possible to discretize the first-order derivatives of the generator mechanical speed and stator currents in (13), (15), and (16) with a sampling time T_s using the forward Euler (FE) approximation method as demonstrated below:

$$i_{ds}(k+1) = \left(1 - \frac{R_s T_s}{L_s}\right)i_{ds}(k) + \omega_r(k)T_s i_{qs}(k) + \frac{T_s}{L_s}v_{ds}(k) \tag{17}$$

$$i_{qs}(k+1) = \left(1 - \frac{R_s T_s}{L_s}\right)i_{qs}(k) - \omega_r(k)T_s i_{ds}(k) + \frac{T_s}{L_s}v_{qs}(k) - \frac{\omega_r(k)\psi_r T_s}{L_s} \tag{18}$$

$$\omega_m(k+1) = \omega_m(k) + \frac{T_s}{J}(T_e(k+1) - T_m(k)) \tag{19}$$

In this work, the cost function is designed using a sensorless HMPPT. It is imperative to obtain the reference values of the electromagnetic torque $T_{e,ref}$ and the generator mechanical speed $\omega_{m,ref}$. The value of $\omega_{m,ref}$ can be computed using the

estimated value of wind speed V_{west} provided by the WSE method. The expressions of the $\omega_{m,ref}$ and $T_{e,ref}$ are given as follows:

$$\omega_{m,ref} = \frac{\lambda_{opt} V_{west}}{R} = K_1^{opt} V_{west} \tag{20}$$

$$T_{e,ref} = \frac{1}{2} \rho \pi R^5 \frac{C_{p-max}}{\lambda_{opt}^3} \omega_m^2 = K_2^{opt} \omega_m^2 \tag{21}$$

The cost function, g_M, is formulated as given below:

$$\begin{aligned} g_M = \lambda_\omega |\omega_{m,ref} - \omega_m(k+1)| + \lambda_c |i_{ds,ref} - i_{ds}(k+1)| \\ + \lambda_T |T_{e,ref} - T_e(k+1)| + g_c \end{aligned} \tag{22}$$

where

$$g_c = \begin{cases} \infty, & if \sqrt{i_{ds}(k+1)^2 + i_{qs}(k+1)^2} > i_s \\ 0, & otherwise \end{cases} + \begin{cases} \infty, & if \ \omega_m(k+1) > \omega_{m,rated} \\ 0, & otherwise \end{cases} \tag{23}$$

The weighting factors in (22) are adjusted as described in [46]. The mechanical reference speed is being tracked using the first term of g_M. The second term is employed to achieve zero direct axis current control technique for SPMSG (i.e., $i_{ds,ref} = 0$). The third term is used to regulate T_e with its reference value, such that T_e and T_m are equal at steady state. The last term is a constraint term that is normally zero but becomes infinite when the stator current amplitude or speed (i.e., i_s or $\omega_{m,rated}$) surpasses their rated values. This constraint ensures that voltage vectors resulting in a very high-cost function value will not be selected.

The MPSC scheme directly controls the mechanical and electrical variables in a single muti-term cost function. Seven different values of v_{ds} and v_{qs} can be generated utilizing the seven various switching states of 2L-VSC. The prediction models in (17), (18) and (19) employ these values to generate seven possible values for dq stator currents and generator mechanical speed. Following this step, the predicted values are used to assess a cost function for every switching state. The optimal action, which is made up of the switching signals that minimize this cost function, is then selected and applied to the MSC [32, 49].

3.2 Model Predictive Current Control for GSC

As shown in Fig. 1, the MPCC technique is applied for GSC to control active and reactive power injected into the electric network. The dq-axes GSC voltages are given below [32]:

$$v_{dg} = R_g i_{dg} + L_g \frac{d}{dt} i_{dg} - \omega_g L_g i_{qg} + e_{dg} \tag{24}$$

$$v_{qg} = R_g i_{qg} + L_g \frac{d}{dt} i_{qg} + \omega_g L_g i_{dg} + e_{qg} \tag{25}$$

where ω_g denotes the grid angular frequency, e_{dg} and e_{qg} denote the dq grid voltages, R_g and L_g refer to the grid filter resistance and inductance, respectively, and i_{dg} and i_{qg} refer to the dq grid currents.

The FE approximation technique is employed to derive the following DT model for grid currents:

$$i_{dg}(k+1) = \left(1 - \frac{R_g T_s}{L_g}\right) i_{dg}(k) + \omega_g T_s i_{qg}(k) + \frac{T_s}{L_g}\left(v_{dg}(k) - e_{dg}(k)\right) \tag{26}$$

$$i_{qg}(k+1) = \left(1 - \frac{R_g T_s}{L_g}\right) i_{qg}(k) - \omega_g T_s i_{dg}(k) + \frac{T_s}{L_g}\left(v_{qg}(k) - e_{qg}(k)\right) \tag{27}$$

The cost function for GSC is formulated as given below:

$$\begin{aligned} g_G = {} & \left| i_{dg,ref} - i_{dg}(k+1) \right| + \left| i_{qg,ref} - i_{qg}(k+1) \right| \\ & + \begin{cases} \infty, \ if \ \sqrt{i_{dg}(k+1)^2 + i_{qg}(k+1)^2} > i_g \\ 0, \quad otherwise \end{cases} \end{aligned} \tag{28}$$

The system includes a constraint that prevents the grid current from exceeding its rated value (i.e., i_g) by avoiding voltage vectors that may lead to such an event. The reference q-axis grid current $i_{qg,ref}$ is set to zero in order to achieve UPF operation. On the other hand, the reference d-axis grid current $i_{dg,ref}$ can be acquired from the outer DC-link voltage controller.

Likewise, the seven different switching state combinations of 2L-GSC result in seven different values for $i_{dg}(k+1)$ and $i_{qg}(k+1)$. The GSC optimum switching signals are then selected by evaluating the predicted grid currents that cause a minimization of the cost function in (28).

4   Simulation Results

In this section, a MATLAB/SIMULINK model is carried out in order to study and evaluate the proposed control schemes which are applied to VSWT with PMSG. Table 2 lists the specifications of the system parameters. Two scenarios are conducted to evaluate the dynamic performance of the implemented control based on the WSE method considering different wind speed profiles.

Table 2 Specifications of the system parameters [46]

Parameter	Symbol	Value
Maximum power coefficient	$C_{p\text{-}max}$	0.48
Blade radius	R	1.6 m
Optimal tip speed ratio	λ_{opt}	8.11
Rated wind speed	V_w	20 m/s
PMSG RMS line voltage	V_s	400 V
Pole pairs number	P_p	3
Stator resistance	R_s	0.2 Ω
Stator inductance	L_s	15 mH
Moment of inertia	J	0.01 kg m^2
Permanent magnet flux linkage	ψ_r	0.85 Wb
DC-link voltage	V_{dc}	700 V
Grid resistance	R_g	0.16 Ω
Grid inductance	L_g	10 mH
Capacitor of the DC-link	C	3 mF
Grid frequency	f	50 Hz

4.1 Step Change in Wind Speed

Figure 4 illustrates the wind speed variation in a stepped manner, initiated at 14 m/s, then raised to 20 m/s at t = 0.2 s, and finally reduced to 16 m/s at t = 0.3 s. The value of the estimated wind speed V_{west} is displayed and compared with the actual wind speed V_w profile. It is noticeable that an overshoot of about 21.1% exists in the V_{west}. However, the V_{west} follows the actual wind speed value with a very small difference that does not exceed 0.2 m/s.
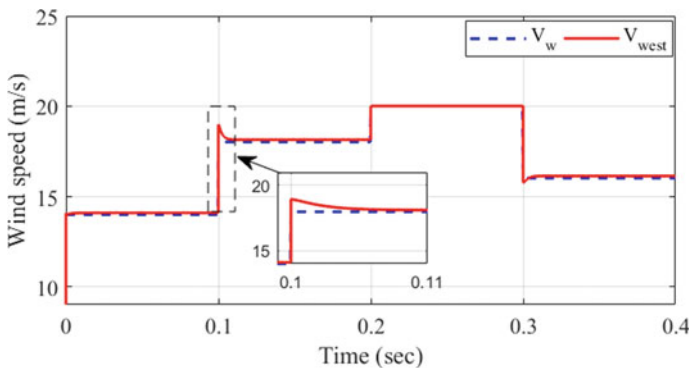
Fig. 4 Estimated and actual step wind speed
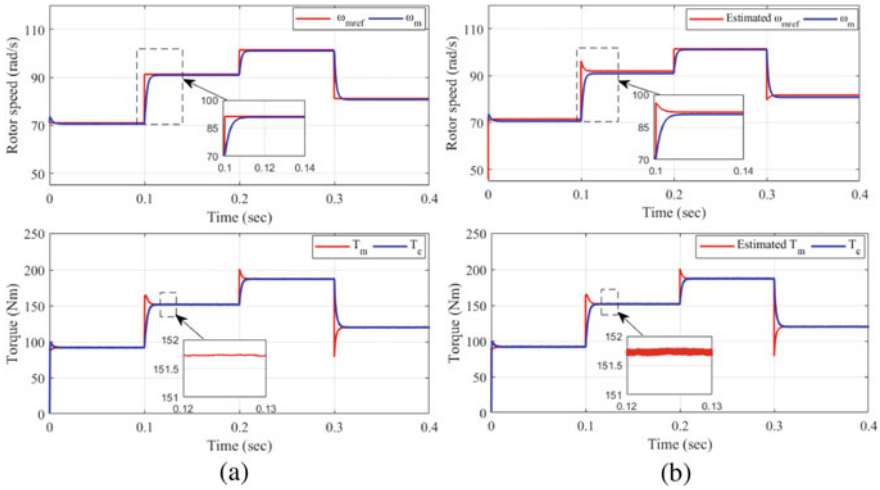
Fig. 5 Mechanical rotor speed and torque under step changes in wind speed: **a** measured wind speed and **b** estimated wind speed

Figure 5 displays the outcomes of MSC control under measured and estimated wind speed. As can be observed, the response of the estimated ω_{mref} is proportional to the variation in V_{west} as shown in Fig. 5b. Nevertheless, when wind speed changes, the controller forces the mechanical rotor speed ω_m to track its reference value. Moreover, the estimated T_m and T_m values have extremely similar dynamic response. In addition, for $V_w = 18$ m/s, the variation in the steady-state value of the estimated T_m is within the range of 0.15 Nm. The obtained average value of the estimated T_m is about 151.73 which is quite similar to the value of the T_m. Besides that, the T_e correctly tracks the estimated T_m according to the variations in wind speed.

Figure 6 depicts the GSC control simulation results. As evident, the DC-link voltage follows its reference closely as illustrated in Fig. 6a. The changes in the value of DC-link voltage does not surpass 4 V. Figures 6b shows that the d-axis current traces the grid real power with the wind speed variation and the q-axis current is forced to zero in order to achieve UPF operation.

4.2 Random Change in Wind Speed

The modified MPSC technique for MSC is also tested under random changes in wind speed. As evident from Fig. 7, the estimated wind speed V_{west} from the WSE method and actual wind speed V_w only slightly differ from one another. The wind speed difference does not exceed 0.13 m/s which is almost negligible. Figure 8 illustarates the values of ω_{mref} under the measured and estimated wind speed. The estimated ω_{mref} tracks the value of ω_{mref} using the measured value of wind speed with very
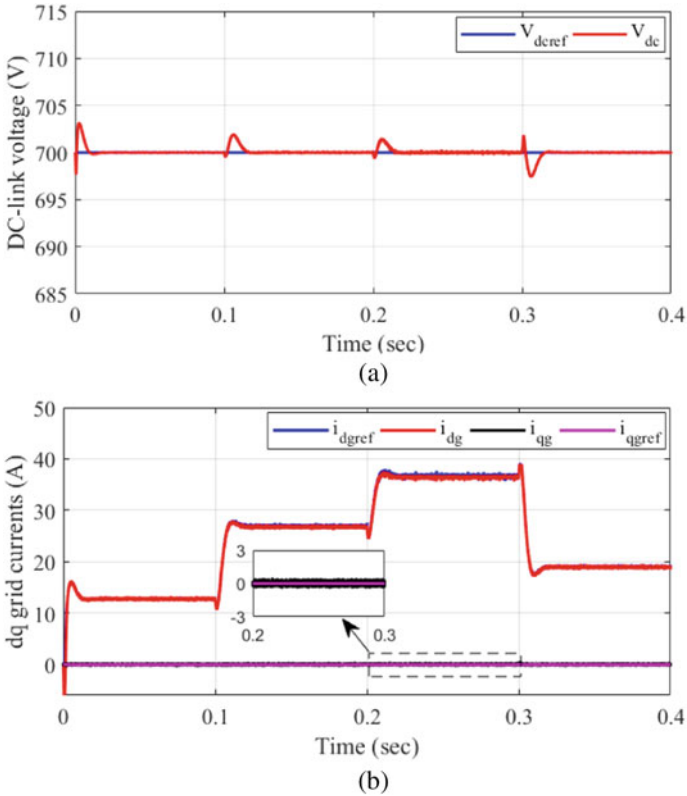
Fig. 6 Results from the grid side under step changes in wind speed: **a** DC-link voltage and **b** *dq* grid currents

small difference between them under random wind speed variations. Figure 9 shows that the response of the estimated T_m is remarkably similar to that of actual T_m. Therefore, the MSC gives an acceptable performance and sensorless HMPPT has been achieved.
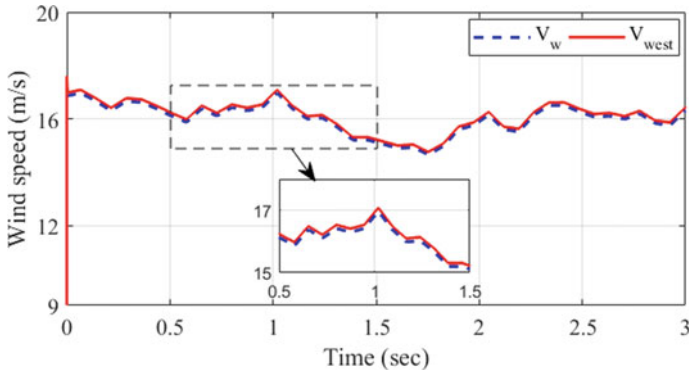
Fig. 7 Estimated and actual random wind speed
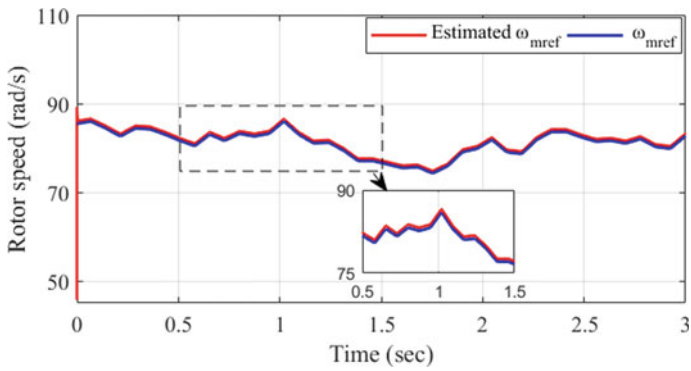
Fig. 8 Estimated and actual reference mechanical rotor speed under random changes in wind speed
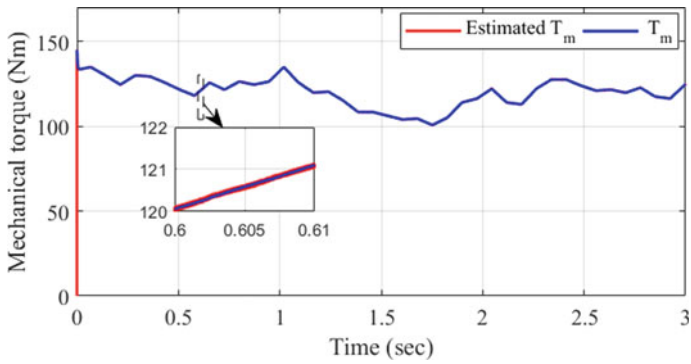
Fig. 9 Estimated and actual mechanical torque under random changes in wind speed

5 Conclusion

A modified MPSC strategy is presented in this paper for the MSC in VSWT with PMSG, which is based on sensorless HMPPT algorithm. The proposed sensorless HMPPT depends on the WSE method to estimate the wind speed and avoid using mechanical wind speed sensors, which increases the cost of the system. The effectiveness of the WSE method is about 98.9%. This results in improving the entire efficiency and reliability of the WT system and reducing the WT installation cost and complexity. The estimation of wind speed depends on the measured value of rotor speed and mechanical torque. Furthermore, an MPCC is applied to replace PI controllers in the inner current control loop for the GSC to control active and reactive power delivered to the electric utility grid. The performance of the system is examined under variations of wind speeds through MATLAB simulations. The results show that the executed control schemes have great capability to achieve the sensorless MPPT and operate at UPF at the grid side.

6 Recommendations

According to the above-mentioned findings, it is recommended to implement a sensorless hybrid MPPT algorithm in WT systems to reduce the WT complexity and installation cost while increasing the total efficiency as well as reliability of the WT system. This supports the endeavors of fulfilling SDG 7: Affordable and clean energy through maximizing the energy yield from WT systems.

References

1. Khalifa A-E, Refaat A, Kalas A, Elfar MH (2022) Two bio-inspired MPPT algorithms to harvest the maximum power from partially shaded PV arrays. In: 2022 conference of Russian young researchers in electrical and electronic engineering (ElConRus). IEEE, pp 670–674
2. Elsakka MM, Ingham DB, Ma L, Pourkashanian M, Moustafa GH, Elhenawy Y (2022) Response surface optimisation of vertical axis wind turbine at low wind speeds. Energy Rep 8:10868–10880
3. Refaat A, Osman MH, Korovkin NV (2020) Current collector optimizer topology to extract maximum power from non-uniform aged PV array. Energy 116995. https://doi.org/10.1016/j.energy.2020.116995
4. Elhenawy Y, Fouad Y, Marouani H, Bassyouni M (2021) Performance analysis of reinforced epoxy functionalized carbon nanotubes composites for vertical axis wind turbine blade. Polymers 13:1–16. https://doi.org/10.3390/polym13030422
5. Elsakka MM, Ingham DB, Ma L, Pourkashanian M (2020) Effects of turbulence modelling on the predictions of the pressure distribution around the wing of a small scale vertical axis wind turbine. In: Proceedings of the 6th European conference on computational mechanics: solids, structures and coupled problems, ECCM 2018 and 7th European conference on computational fluid dynamics, ECFD 2018, pp 3921–3931

6. Refaat A, Khalifa A, Elsakka MM, Elhenawy Y, Kalas A, Hegazy M (2023) A novel meta-heuristic MPPT technique based on enhanced autonomous group particle swarm optimization algorithm to track the GMPP under partial shading conditions—experimental validation. Energy Convers Manag 287:117124. https://doi.org/10.1016/j.enconman.2023.117124

7. Refaat A, Kalas A, Khalifa AE, Elfar MH (2023) A comparative study of two metaheuristic MPPT techniques to extract maximum power from PV array under different partial shading patterns. In: IEEE conference on power electronics and renewable energy, CPERE 2023. IEEE

8. Elsakka MM, Ingham DB, Ma L, Pourkashanian M (2021) Comparison of the computational fluid dynamics predictions of vertical axis wind turbine performance against detailed pressure measurements. Int J Renew Energy Res 11:276–293

9. Huang N (2013) Simulation of power control of a wind turbine permanent magnet synchronous generator system

10. IRENA (2023) Renewable capacity Statistiques De Capacité Estadísticas De Capacidad

11. Yaramasu V, Wu B (2017) Power electronics for high-power wind energy conversion systems

12. Yaramasu V, Wu B, Sen PC, Kouro S, Narimani M (2015) High-power wind energy conversion systems: state-of-the-art and emerging technologies. Proc IEEE 103:740–788

13. Errami Y, Ouassaid M, Maaroufi M (2013) Control of a PMSG based wind energy generation system for power maximization and grid fault conditions. Energy Procedia 42:220–229

14. Yaramasu V, Dekka A, Durán MJ, Kouro S, Wu B (2017) PMSG-based wind energy conversion systems: survey on power converters and controls. IET Electr Power Appl 11:956–968

15. Yaramasu V, Kouro S, Dekka A, Alepuz S, Rodriguez J, Duran M (2019) Power conversion and predictive control of wind energy conversion systems. In: Advanced control and optimization paradigms for wind energy systems. Springer, pp 113–139

16. Abdullah MA, Yatim AHM, Tan CW, Saidur R (2012) A review of maximum power point tracking algorithms for wind energy systems. Renew Sustain Energy Rev 16:3220–3227

17. Kumar D, Chatterjee K (2016) A review of conventional and advanced MPPT algorithms for wind energy systems. Renew Sustain Energy Rev 55:957–970

18. Abdelrahem M, Hackl C, Kennel R (2016) Model predictive control of permanent magnet synchronous generators in variable-speed wind turbine systems. In: Proceedings of power and energy student summit (PESS 2016)

19. Porate DK, Gawande SP, Munshi AP, Porate KB, Kadwane SG, Waghmare MA (2017) Zero direct-axis current (ZDC) control for variable speed wind energy conversion system using PMSG. Energy Procedia 117:943–950

20. Mousa HHH, Youssef A-R, Mohamed EEM (2018) Model predictive speed control of five-phase PMSG based variable speed wind generation system. In: 2018 twentieth international middle east power systems conference (MEPCON). pp 304–309

21. Youssef A-R, Sayed MA, Abdel-Wahab M (2015) MPPT control technique for direct-drive five-phase PMSG wind turbines with wind speed estimation. Variations 21:22

22. Mousa HHH, Youssef A-R, Mohamed EEM (2019) Model predictive speed control of five-phase permanent magnet synchronous generator-based wind generation system via wind-speed estimation. Int Trans Electr Energy Syst 29:e2826

23. Jena D, Rajendran S (2015) A review of estimation of effective wind speed based control of wind turbines. Renew Sustain Energy Rev 43:1046–1062. https://doi.org/10.1016/j.rser.2014.11.088

24. Tripathi SM, Tiwari AN, Singh D (2016) Optimum design of proportional-integral controllers in grid-integrated PMSG-based wind energy conversion system. Int Trans Electr Energy Syst 26:1006–1031

25. Alaboudy AHK, Daoud AA, Desouky SS, Salem AA (2013) Converter controls and flicker study of PMSG-based grid connected wind turbines. Ain Shams Eng J 4:75–91

26. Milev K, Yaramasu V, Dekka A, Kouro S (2020) Modulated predictive current control of PMSG-based wind energy systems. In: 2020 11th power electronics, drive systems, and technologies conference (PEDSTC), pp 1–6

27. Abdelrahem M, Hackl C, Zhang Z, Kennel R (2016) Sensorless control of permanent magnet synchronous generators in variable-speed wind turbine systems. In: Proceedings of power and energy student summit (PESS 2016)

28. Abdelrahem M, Hackl CM, Kennel R (2018) Implementation and experimental investigation of a sensorless field-oriented control scheme for permanent-magnet synchronous generators. Electr Eng 100:849–856
29. Li S, Haskew TA, Xu L (2010) Conventional and novel control designs for direct driven PMSG wind turbines. Electr Power Syst Research 80:328–338
30. Young HA, Perez MA, Rodriguez J, Abu-Rub H (2014) Assessing finite-control-set model predictive control: a comparison with a linear current controller in two-level voltage source inverters. IEEE Industr Electron Mag 8:44–52
31. Rodriguez J, Pontt J, Silva CA, Correa P, Lezana P, Cortés P, Ammann U (2007) Predictive current control of a voltage source inverter. IEEE Trans Industr Electron 54:495–503
32. Yaramasu V, Wu B (2016) Model predictive control of wind energy conversion systems. Wiley
33. Cortés P, Kazmierkowski MP, Kennel RM, Quevedo DE, Rodríguez J (2008) Predictive control in power electronics and drives. IEEE Trans Industr Electron 55:4312–4324
34. Rodriguez J, Kazmierkowski MP, Espinoza JR, Zanchetta P, Abu-Rub H, Young HA, Rojas CA (2012) State of the art of finite control set model predictive control in power electronics. IEEE Trans Industr Inf 9:1003–1016
35. Kouro S, Cortés P, Vargas R, Ammann U, Rodríguez J (2008) Model predictive control—a simple and powerful method to control power converters. IEEE Trans Industr Electron 56:1826–1838
36. Vazquez S, Rodriguez J, Rivera M, Franquelo LG, Norambuena M (2016) Model predictive control for power converters and drives: advances and trends. IEEE Trans Industr Electron 64:935–947
37. Ali AK, Omar RG (2021) Finite control set model predictive direct current control strategy with constraints applying to drive three-phase induction motor. Int J Electr Comput Eng (2088-8708) 11
38. Youssef A-R, Mohamed EEM, Ali AIM (2018) Model predictive control for grid-tie wind-energy conversion system based PMSG. In: 2018 international conference on innovative trends in computer engineering (ITCE), pp 467–472
39. Shehata EG (2017) A comparative study of current control schemes for a direct-driven PMSG wind energy generation system. Electr Power Syst Res 143:197–205
40. Fuentes EJ, Silva C, Quevedo DE, Silva EI (2009) Predictive speed control of a synchronous permanent magnet motor. In: 2009 IEEE international conference on industrial technology, pp 1–6
41. Fuentes EJ, Silva CA, Yuz JI (2011) Predictive speed control of a two-mass system driven by a permanent magnet synchronous motor. IEEE Trans Industr Electron 59:2840–2848
42. Preindl M, Bolognani S (2012) Model predictive direct speed control with finite control set of PMSM drive systems. IEEE Trans Power Electron 28:1007–1015
43. Gao J, Liu J (2019) A novel FCS model predictive speed control strategy for IPMSM drives in electric vehicles. In: IECON 2019–45th annual conference of the IEEE industrial electronics society, pp 3169–3173
44. Formentini A, Trentin A, Marchesoni M, Zanchetta P, Wheeler P (2015) Speed finite control set model predictive control of a PMSM fed by matrix converter. IEEE Trans Industr Electron 62:6786–6796
45. Abdelrahem M, Hackl C, Kennel R, Rodriguez J (2019) Sensorless predictive speed control of permanent-magnet synchronous generators in wind turbine applications. In: PCIM Europe 2019; international exhibition and conference for power electronics, intelligent motion, renewable energy and energy management, pp 1–8
46. Abuhashish MN, Daoud AA, Elfar MH (2022) A novel model predictive speed controller for PMSG in wind energy systems. Int J Renew Energy Res (IJRER) 12:170–180
47. Wu B, Lang Y, Zargari N, Kouro S (2011) Power conversion and control of wind energy systems. Wiley

48. Abdellatif WSE, Hamada AM, Abdelwahab SAM (2021) Wind speed estimation MPPT technique of DFIG-based wind turbines theoretical and experimental investigation. Electr Eng 103:2769–2781. https://doi.org/10.1007/s00202-021-01268-8
49. Kouro S, Perez MA, Rodriguez J, Llor AM, Young HA (2015) Model predictive control: MPC's role in the evolution of power electronics. IEEE Industr Electron Mag 9:8–21

Clean Water

A Review of Wastewater Treatment Using Biodegradable Polymers for Dyes Removal

Rana Gamal, Mohamed Bassyouni, Medhat M. H. ElZahar, and Mamdouh Y. Saleh

1 Introduction

Because of the rapidly rising population and their regular standard of living, freshwater shortages and resources are in grave danger. The removal of manufacturing waste materials and environmental effects like global industrialization are the main reasons for the rise in toxicity and population on a global scale [1–3]. As a result of manufacturing growth in textiles, tannery, plastics, and food, the clean water issue has become one of the greatest challenges threatening life in the entire world. Many industrial processes, such as those used to make leather, paper, and textiles, release extremely dangerous and cancer-causing chemicals into wastewater. Scientists estimate that 65% of the number of people worldwide will require tremendous quantities of water in their daily live, and millions of people will experience drinking water shortages [4, 5]. Human health is put at risk because of mismanagement and poor water supply management. In other words, water pollution caused by significant amounts of industrial effluents that are not properly cleaned before being released into sources of water creates a substantial threat to human beings.

The textile industries are receiving a lot of attention from water specialists and scientists due to a large amount of unwanted dye waste entering water bodies. The dyes are harmful to the ecosystem and do not constitute biodegradable. The biological

R. Gamal · M. M. H. ElZahar · M. Y. Saleh
Sanitary and Environmental Engineering, Civil Engineering Department, Faculty of Engineering, Port Said University, Port Said 42526, Egypt

M. Bassyouni (✉)
Department of Chemical Engineering, Faculty of Engineering, Port Said University, Port Said 42526, Egypt
e-mail: m.bassyouni@eng.psu.edu.eg

Center of Excellence in Membrane-Based Water Desalination Technology for Testing and Characterization (CEMTC), Port Said University, Port Said 42526, Egypt

East Port Said University of Technology, Saini, Port Said 45632, Egypt

treatment eventually decreases because of the dye effluents from textiles' ability to block sunlight from entering the aquatic environment, compete with oxygen transfer, and prevent the receiving water from reoxygenating. Therefore, it is inevitable for drinking water to become contaminated with numerous dangerous metal ions and dyes, which have a serious harmful effect [6–8]. Millions of dyes are used in a variety of industries, notably textiles, and most of them are extremely poisonous or even lethal to animals and humans, posing a significant barrier to the purification of the world's aquatic environment. Thus, removing dyes from wastewater is critical in large-scale applications to preserve human health. A range of water treatment procedures is available based on the application and potential of wastewater treatment.

Many methods for removing these compounds from unclean wastewater have been proposed, including flocculation, biodegradation, adsorption, improved oxidation, precipitation, ultrafiltration, ion exchange, electrochemical degradation, and coagulation [9]. Adsorption is regarded as the most promising and financially viable option. Unfortunately, due to reduced capacity of adsorption, sluggish adsorption movement, pricey and difficulty in implementation, many of them are limited. To solve these issues, new materials containing functional groups are constantly required to simplify the water treatment process [10]. Because of their simplicity, cost-effectiveness, and practicality, adsorption techniques have emerged as viable and sustainable alternatives in recent decades. To boost adsorption capabilities, a variety of active compounds have been utilized [7, 9, 11]. Biomaterials are gaining popularity because of their low cost and ability to be prepared from a variety of sources, including agricultural waste. Bio-adsorbents made from shells, lemon peels, maize cobs, mango seeds, tea trash, coconut shells, orange peels and biopolymers like chitosan and alginate are just a few recent discoveries in environmentally friendly products.

To remediate dye-induced wastewater, biodegradable polymers are utilized. These techniques offer various advantages, including simple design, cheap cost, fewer chemical needs, flexibility, and ease of operation. They have received a lot of attention in the latest generations for dye wastewater treatment because of their benefits such as regeneration, simplicity, flexibility, appealing features, and high efficiency. A key strategy for reducing the overuse of industrial activated carbon is the use of biodegradable polymers in water treatment [12, 13]. Even though activated carbon is the most utilized adsorbent, regeneration is difficult and expensive, especially for powdered activated carbon. Agricultural operations generate a substantial amount of garbage. It must be used with caution. It must be borne in mind that the ultimate objective is to rescue the planet. It must also incorporate biomass valorization. Considering these environmental concerns, our effort focused on the development of affordable adsorbents that were persuasive, cheap in cost, non-dirty, and easily disposed of away. Continuous adsorption researches have the potential to assist with the evaluation of processes. It enables us to appreciate and assess the elements, such as the pollutant feed concentration, contact time, solution pH, temperature, stirring rate, and adsorbent mass [14, 15], that have an impact on the phenomena. In

this review, we covered a variety of dyes, their impact on the well-being of individuals, parameters influencing this adsorption phenomenon, and a few biodegradable polymers to optimize the elimination of dyes by adsorption. We will offer an overview of the review and future projections for this subject. The use of biodegradable polymers in wastewater treatment aligns with several Sustainable Development Goals (SDGs) by promoting sustainable practices and addressing environmental challenges. Biodegradable polymers can play a role in improving water quality by aiding in the removal of pollutants from wastewater wgixh meets (SDG 6), (SDG 9) and (SDG 12).

2 Dyes in Wastewater

Water is a renewable resource that is required for all life on Earth. It is a "special gift of nature" used for everyday necessities, the timber industry, livestock production, farming, manufacturing processes and other purposes [16, 17]. All of these activities require water, but some dangerous compounds are found in water bodies that contaminate them and make them unusable for bathing, cooking, or other uses. "The water you pollute will always come back to bite you," is a proverb that perfectly captures the fact that humans are the ones who cause pollution, and as a result, they are suffering from several serious illnesses [18, 19]. Because businesses, industries, and mills release large amounts of dye, water is already polluted. Most of the industries producing dye wastewater are the textile, printing, paper, food processing, and tannery industries as shown in Fig. 1.

In addition to acids, glues, salts, and other contaminants, dye effluent also contains auxiliaries that are toxic, teratogenic, carcinogenic, and xenobiotic. The human body experiences these effects as eye burns, skin irritations, allergic conjunctivitis, and occupational asthma. Even though the dye industry produces a variety of pollutants in different amounts [20, 21]. As a result, dye effluent poses a risk to both aquatic and terrestrial environments as well as human health. Because of the tremendous increase in the number and variety of colors used in textile and other industries, dyes are also a significant source of water pollution. These dyes can be categorized as azo, Sulphur, indigo, phthalocyanine, anthraquinonoid, nitro, nitroso, and others, which we will discuss in more detail later in this book. These dyes also have a variety of functional groups. Several pharmaceutical companies poured waste into rivers, possibly triggering a variety of illnesses in those who drank and utilized the water.

Fig. 1 Pollutant types in wastewater
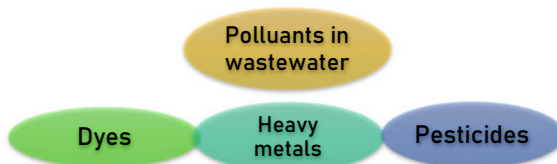
Fig. 2 Sources of dyes in
environment
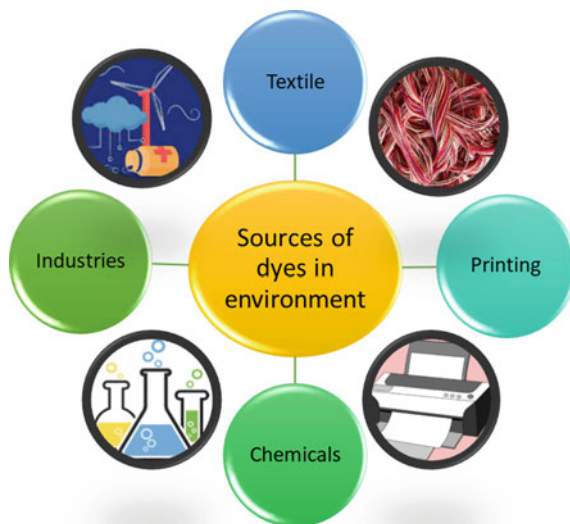
Water contamination is mostly caused by dyes, heavy metals, medications, bacteria, and others, are mentioned in Fig. 2.

3 Environmental and Health Effects of Dyes

Dyes are often used to improve a product's look and quality. As a result, dye production, processing, and use raise several health and environmental problems. Dye is widely used in the pharmaceutical, textile, food, lather, paint industries, household and wastewater treatment plant. When straight black, methyl red, acid red, acids blue, blue dye, methyl blue, hair products, mordant red dyes, and indigo are used and released into the environment, they damage the ecosystem [22, 23]. Dye effluent contains ammonia, leveling chemicals, hydrochloric acid, acetic acid, soap, formaldehyde, sulfur dioxide, organic polymer, softener, and other compounds [24, 25].

Long-term workers in these dye industries face health concerns when handling, processing, and transporting the colors. Breathing problems, pneumonia, burning, allergens, immune response loss, coughing, cardiovascular disease, skin rashes and itching, and other physical problems are frequently caused by inhalation and ingestion of pollutants. Additionally, dyes can negatively impact human health in several ways, including dermatitis, the central nervous system, the liver, the kidney, the skin, the enzymatic system, the reproductive system, human chromosomes, the neurological system, and the epidermis [26, 27].

Because animals and humans use water for everyday activities including bathing, cooking, drinking, and cleaning, the presence of synthetic dyes in freshwater

resources is undesirable. While some textile manufacturers filter their wastewater to dissolve and remove dyes and other industrial wastes, others released dyes and other manufacturing waste straight into sources of water, creating major ecotoxicological problems, inflicting environmental harm, and risking human health.

Because of the dye, sunlight becomes obstructed and is unable to penetrate the bottom of bodies of water, resulting in an oxygen deficit. If dye is present on the surface of water bodies, it is unsightly and produces a foul stench. Ultimately, dye degrades soil quality, productivity, and fertility while polluting the air quality [28, 29]. Wastewater, particularly untreated industrial effluent, was used by farmers in less developed countries to irrigate their crops, which harmed the integrity of the soil, crop growth, and the emergence of seed rates, ultimately harming people or animals. Furthermore, the deterioration of water quality could be caused by wastewater containing color.

Dyeing can obstruct access to the aquatic environment's photic domain, as well as the absorption and visible reflection of sunlight. As a result, potential ecological concerns include changed aquatic environments and diminished process of photosynthesis. On the other hand, if people consume colored fish and other aquatic foods, it could result in fever, cramps, hypertension, and other medical issues. Dyes can be detected in the environment because of their extensive use, and they physiologically increase in the aquatic ecosystem, including in fish and algal species.

The environment and human health could be harmed by dye wastewater. Therefore, it is important to manage dye-containing wastewater in a way that is both economical and responsible for the environment. A safe, acceptable, and sustainable dye wastewater treatment is critical for preserving human health, reducing environmental harm, and improving environmental protection [30]. The effects of dyes direct and indirect which impact various substrates are shown in Fig. 3.

4 Dye Classifications and Applications

One of the things we use the most in our daily lives is dyes, which can be either natural or artificial substances that can be found in many settings. Dyes are now widely used in a variety of sector-specific industries, such as textiles and clothing, personal care items, polymers, and printing [31].

Chromophores and auxochromes are the two main parts of dye molecules. Chromophores provide color, but auxochromes can help by boosting the chromophore's affinity for fibers and making it more water-soluble. Dyes are chemical substances that can bond to the outer layer of clothing to add color. Synthetic dyes are available in many different kinds of sizes and forms and are categorized according to their chemical composition, color, and purpose of use. Based on their solubility, colors may occasionally be categorized in different ways. Insoluble dyes include azo, dispersion, sulfur, solvent, and vat, while soluble dyes include acid, basic, direct, mordant, and reactive as it is shown in Fig. 4.
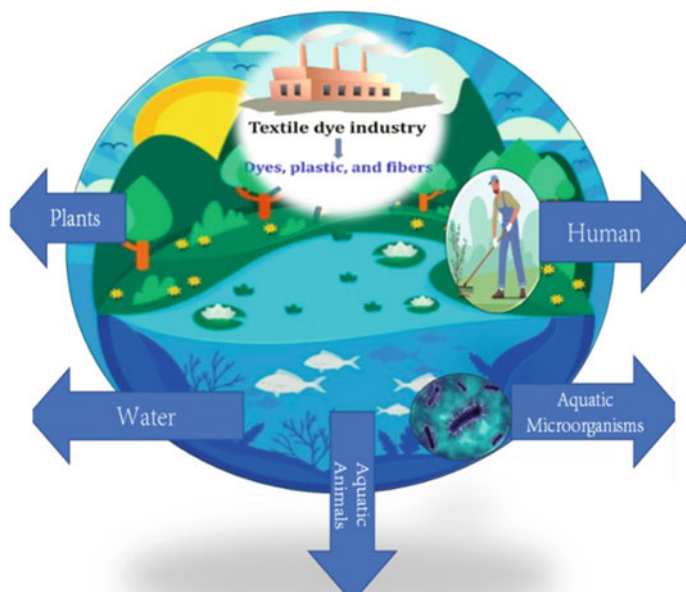
Fig. 3 Effects of dye on several substrates
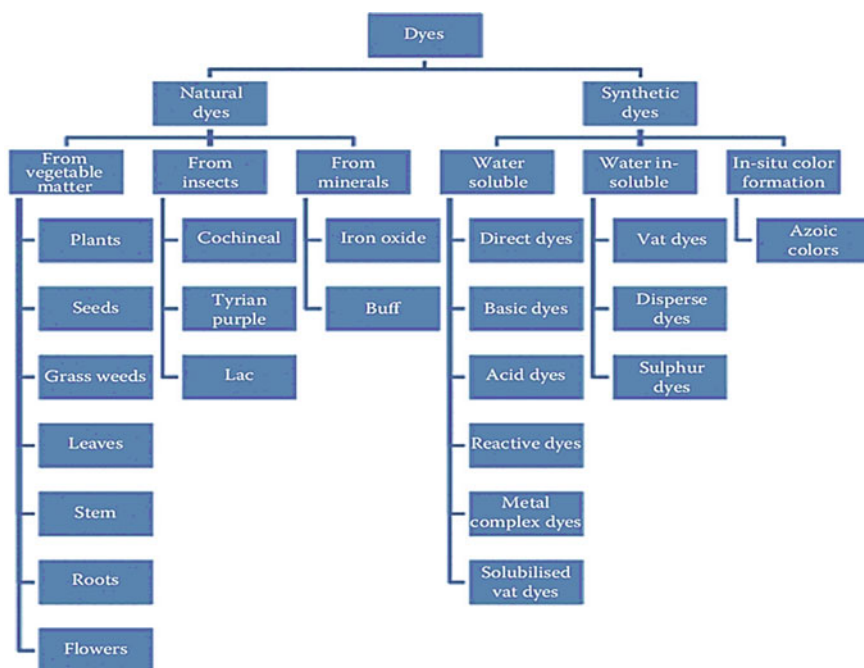
Fig. 4 Dyes classification based on the source of the material

Table 2 provides several examples of synthetic dyes and their possible applications, as well as the ingredients necessary and the chemical structure of different dyes as shown in Fig. 5. Dyes combined wastewater is a significant contamination as well as one of the world's current challenges and burning dilemmas. Dye wastewater is rising because of industrial expansion and human demands. According to the US EPA, 1 kg of fabric requires at least 40 L of clean water, which might vary depending on the textile material and coloring procedure [32, 33].

Untreated wastewater from many dye manufacturers has the potential to harm the environment and human health. Dyes have an impact on water quality by interfering with photosynthesis, slowing plant development, infiltrating the nourishment chains, causing accumulation in the body, and perhaps increasing poisoning. Dye effluent contains organic pollutants, hazardous colors, and heavy metals such as mercury, chromium, cadmium, lead, and arsenic. Azo dyes are the most widely used in the manufacturing of textiles, calculating more than 60% of all textile dyes [32, 33].

Azo dyes, such as diazo, monoazo, and triazo, are typically synthetic aromatic colors consisting of two or more N=N groups linked to benzene and naphthalene

Table 2 Applications and examples of dyes

Types	Applications	Constituent chemicals	References
Acid	Skincare products, nutrition, leather and suede, polyester, printing pigments for paper, natural fibers such as wool, silk, and paints	Azo, azine, nitro, xanthene	[30, 34]
Basic	Medical science, pigments, synthetic polyester, paper goods, polyester, fibers such as wool, silk and wood for its operations	Oxazine, azine, thiazine, triarylmethane, cyanine	[34]
Disperse	Acetate, acrylic fibers, cellulose, nylon, polyamide, polyester, cotton, plastic	Anthraquinonoid, benzo difuran, and styryl	[33, 35]
Direct	Leather, cotton, cellulose	Stilbenes, azo and poly azo	[30, 33]
Azo	Cellulosic materials, detergents	Ana phthalimides	[30, 36]
Mordant	Cotton, fibers, wool, leather, and hair	Azo and anthraquinone	[34, 37]
Sulphur	Paper, cotton, leather, rayon, wool, silk, and polyamide fibers	Thiazoles, thiazone, thianthrene, and phenothiazonethioanthrone subunits	[35, 36]
Solvent	The fats, varnishes, petrol, paints, fluids, lacquers, oily substances, spots polymers and waxes	Anthraquinone and phthalocyanine	[30, 33]
Vat	Rayon, cellulosic fibers, cotton, polyester-cotton, and wool	Anthraquinone, carbazole, indigoids	[34, 35]
Reactive	Cellulosic, nylon, cotton	Oxazine, anthraquinone, azo, basic, formazan, triphenylmethane, and phthalocyanine	[36, 37]
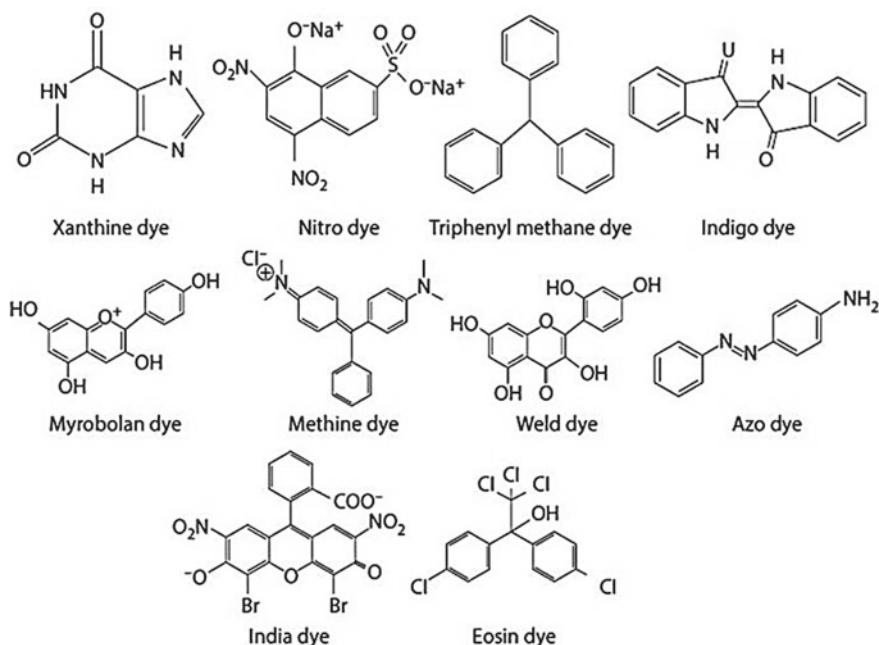
Fig. 5 Chemical structure of different dyes

rings. Azo dyes have a wide range of applications including medications, textiles dyeing, pharmaceuticals, and paper printing. Azo dyes are widely used in the textile industry because they are affordable, stable, and provide a wide range of colors. The following industries contribute to and release dye into the environment: textile businesses (54%), concurrent dyeing businesses (21%), paper and pulp companies (10%), paint and tanneries (8%), and dye producing facilities (7%) as shown in Fig. 6.

Figure 7 depicts the quantity of dye combinations ejected throughout the textile production process. Among the many different chemical combinations of the various substances used during manufacturing and processing are inorganic compounds, polymers, and natural products.

5 Biodegradable Polymers-Based Adsorbents for Dyes Removal

Researchers and scientists have employed biodegradable polymers extensively for the adsorption of many contaminants, including colors. Given that they feature a range of functional groups on their backbone, these combined polymers may be readily altered or changed to match the component's requirements. By effectively adsorbing specific metal ions, polymer selection can also increase selectivity. Due to
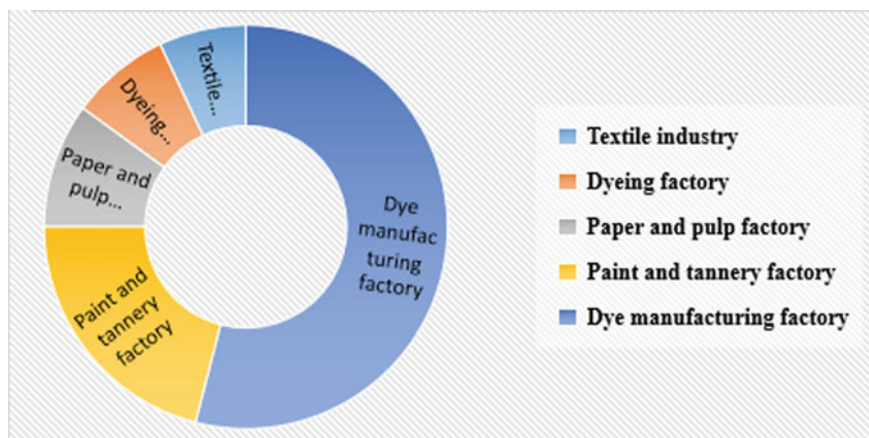
Fig. 6 Sector wise dye producing industries
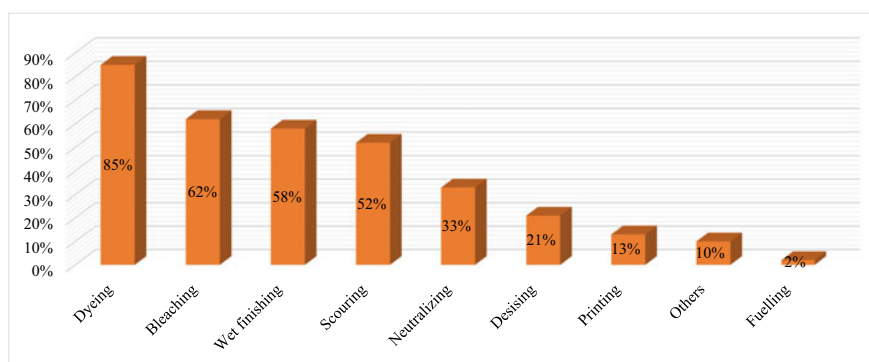
Fig. 7 Rate of dye granting in textile manufacturing processes

their simplicity in synthesis, lack of toxicity, low cost, structural strength, stability, high porosity, and low water solubility, conducting polymers have become more popular as adsorbents [25, 38].

Table 3 provides several examples of biodegradable polymers used as adsorbents in dye removal and shows their maximum capacity for adsorption and their condition for removing the specific dye with a specific polymer.

As indicated in Table 3, Bio-adsorbents derived from agricultural waste such as citrus fruits, olive kernels, shells of palm nuts, peach and apricot kernels, corn husk, coffee beans, fruit waste, nut shells, and biopolymers such as chitosan and alginate are now being studied. The use of biomass in wastewater treatment serves as a key alternative for minimizing the overuse of industrial activated carbon. Agricultural operations generate a substantial amount of garbage. It must be used with caution. It must be borne in mind that the ultimate objective is to rescue the planet. It must

Table 3 Biodegradable polymers-based adsorbents for dye removal

Adsorbent	Type of adsorbent	Adsorbate	Conditions	Removal performance	References
Cassava starch-based-polyacrylamide hydrogels	Agricultural biodegradable polymer	Methylene blue	40% of the MB was eliminated within 1 h and continued to decrease over time until a plateau was established at 10 h. 85% of MB was removed by the CS50 hydrogel before elimination leveled off	Highest adsorption capacity = 2000 mg/g	[39]
Aloe vera-acrylamide-acrylic acid-based interpenetrating polymer network	Agricultural biodegradable polymer	Malachite green	Time = 180 min pH = 4.5 Adsorbent dose = 5 g/l	97.3% dye removal efficiency	[40]
Gum ghatti-acrylamide-based hydrogel	Agricultural biodegradable polymer	Brilliant green, congo red, methyl orange and rhodamine B	At 25 °C, with concentrations ranging from 50 to 400 mg/l Using 40 mg of Gg-cl-PAAM resulted in the highest adsorption efficiency (94%) while using 50 mg of the adsorbent resulted in the adsorption efficiency for RhB (87%), CR (32%), and MO (30%)	Highest adsorption Capacity = 523.62 mg/g for BG Capacity = 421.60 mg/g for RhB Capacity = 179.09 mg/g for CR Capacity = 173.69 mg/g for MO	[41]

Table 3 (continued)

Adsorbent	Type of adsorbent	Adsorbate	Conditions	Removal performance	References
Unmodified citrus peels	Agricultural biodegradable polymer	Methylene blue dye	$C_o = 100$ mg/L $M = 10$ mg $V = 10$ mL Speed $= 200$ rpm $T = 24 \pm 1$ °C pH $= 6.4$	Q ads max $= 185.83$ mg/g	[42]
Rice flour (RF)	Agricultural biodegradable polymer	Methylene orange	pH $= 7:5.5$ In 20 ml solution Time $= 220$ min	Capacity $= 173.24$ mg/g	[43]
Pine leaves	Agricultural biodegradable polymer	Methylene blue	$T° = 30$ °C Speed $= 120$ rpm for a period of 240 min	Capacity $= 126.58$ mg/g	[44]
Mango seed	Agricultural biodegradable polymer	Orange 16	Biosorbent mass 50.0 mg; pH fixed at 2.0, contact time 6 h	Capacity $= 52.5$ mg/g	[45]
Graham flour (GF)	Agricultural biodegradable polymer	Methylene orange	pH $= 7:5.5$ In 20 ml solution Time $= 260$ min	Capacity $= 151.27$ mg/g	[43]
Alginate-activated lemon peels composite beads	Biodegradable polymer	Methylene blue dye	$C0 = 25–2200$ mg/L $V = 10$ mL $M = 10$ mg Speed $= 200$ rpm $T° = (24 \pm 1$ °C)	Q ads max $= 841.37$ mg/g	[46]

also incorporate biomass valorization. Considering these environmental concerns, our effort focused on the development of affordable adsorbents that were persuasive, cheap in cost, non-dirty, and easily disposed of away. Unending adsorption study results give valuable data for process analysis.

It enables us to understand and assess the many variables that affect the phenomena, including the impact of pollutant loading rate, contact length, solution pH, temperature, agitation speed, and adsorbent mass. Adsorption in both batch and continuous columns ought to be used as a method for treating industrial wastewater. In continuous adsorption systems, the concentration in the liquid and solid phases varies across time and space. The design and performance of fixed bed columns present specific problems in the absence of a quantitative approximation model.

For instance, in batch and bed column systems, the ability of citrus peel-alginate compound beads to remove methylene blue (MB) dye from an aqueous solution was investigated. To analyze breakthrough curves, a series of continuous adsorption experiments were conducted, considering three different factors: bed height, input feed flow rate, and feed MB dye concentration.

The results of the batch tests showed that dye adsorption is influenced by the pH of the solution. The high MB removal on UCP/A was found to be 93% at pH 7 [42]. On the other hand, nano-hydroxyapatite was incorporated into a starch-graft-poly(acrylamide)/graphene oxide network to create a nano-adsorbent composite for the removal of malachite green dye from aqueous solutions. The following parameters were used to achieve the highest dye adsorption (297 mg/g): agitation for 60 min, n-Hap content of 3 weight percent, solution pH of 10, and initial dye concentration of 100 mg/L [39]. Technology, natural carbohydrate polymeric materials, tunable materials, and sensitive materials would all benefit from another application of biodegradable polymers as adsorbents to efficiently remove toxins from wastewater at a variety of levels [43, 44].

Consequently, the methyl orange anionic color from contaminated water was removed using natural carbohydrate polymeric materials made from rice flour (RF) and graham flour (GF). In this study, the RF and GF adsorbents showed exceptional selectivity, enabling precise, targeted removal of dangerous dye with high efficacy under ideal experimental conditions. Because of the adsorbent charge reactivity, the pH of the solution was significantly altered. The best experimental technique was used to assess the influence of each influencing element and its interactions. According to the kinetic results, RF and GF adsorbents had slower kinetic capabilities than functional nanomaterials and ion exchange fibrous adsorbents [43, 45, 47].

The monolayer coverage adsorption findings showed a high adsorption capacity of 173.24 and 151.27 mg/g of RF and GF adsorbent, respectively, and were closely associated with the Langmuir isotherms. Foreign anions including chloride, nitrate, and sulfate had no impact on the RF and GF adsorbents' ability to bind dye. Additionally, during a few cycles, the adsorbed dye on the RF and GF was completely desorbed with ethanol and reconstituted back into its original form for the following removal process. This was done with no appreciable functional loss [46, 48, 49]. Based on the findings of reactivity, selectivity, and applicability, the RF and GF natural carbohydrate polymeric adsorbents may be employed to remove harmful

anionic pollutants [50–52]. Natural carbohydrate polymeric adsorbents RF and GF might be employed in large-scale applications to remove hazardous anionic dyes and other pollutants to start cleaning up wastewater to preserve population well-being [53–55].

6 Conclusion

This study aims to offer an overview of biodegradable polymer-based materials for dye adsorption to combat water pollution. Adsorption removal of contaminants from wastewater is a substantial substitute for cost-effective traditional procedures and the best solution for wastewater treatment as well as for businesses. Dye wastewater-producing enterprises are expanding and discharging more often across the world. Because there is no worldwide norm for wastewater discharge, each country has its own set of guidelines established by its government. Therefore, there are no distinctive, unique, or financially viable solutions to the wastewater curse. Moreover, multiple standard, advanced, and new ways to dye wastewater have been developed and tested. Taking into account neither the rate of dye removal nor the benefits and drawbacks, biodegradable polymers as adsorbents appear to be the most effective and sophisticated for dye removal. The results of this ongoing investigation and numerous model-predicted results demonstrated how toxic dyes are to our health and their influence on the environment, despite their widespread use in industry and other fields. The review also suggests the potential of biodegradable polymer adsorbents as efficient, cheap and environmentally friendly adsorbents for different types of dyes removal from wastewater, as well as how they show a high removal rate and worldwide acceptable that may be used to scale up the procedure to an industrial ecosystem because they performed well in various experiments. Consequently, this study will assist governments and entrepreneurs make the appropriate environmental decisions as it is also relevant to the sixth number of the sustainable development goals (Clean water and Sanitation).

7 Recommendation

Encourage the adoption and utilization of biodegradable polymers as adsorbents in water treatment processes. These polymers offer a more sustainable and environmentally friendly alternative to traditional adsorbents like activated carbon. Collaboration between researchers, policymakers, and industries is crucial to facilitate the implementation and scale-up of biodegradable polymer-based adsorption techniques. Invest in further research and development to explore and optimize the functionalization of biodegradable polymers for enhanced adsorption of dyes. This can include studying different types of biodegradable polymers, their modifications, and their

performance under various conditions. Additionally, investigate the use of agricultural waste as a source of biodegradable polymers to reduce costs and promote circular economy principles. The use of sustainable adsorption techniques, including biodegradable polymers, in water treatment processes. Provide incentives and support mechanisms for industries to adopt environmentally friendly practices and invest in.

References

1. Sahraei R, Sekhavat Pour Z, Ghaemy M (2017) Novel magnetic bio-sorbent hydrogel beads based on modified gum tragacanth/graphene oxide: removal of heavy metals and dyes from water. J Clean Prod 142:2973–2984. https://doi.org/10.1016/j.jclepro.2016.10.170
2. Marni Sandid A, Bassyouni M, Nehari D, Elhenawy Y (2021) Experimental and simulation study of multichannel air gap membrane distillation process with two types of solar collectors. Energy Convers Manag 243:114431. https://doi.org/10.1016/j.enconman.2021.114431
3. Elhenawy Y, Fouad K, Bassyouni M, Majozi T (2023) Design and performance a novel hybrid membrane distillation/humidification–dehumidification system. Energy Convers Manag 286:117039. https://doi.org/10.1016/j.enconman.2023.117039
4. Fouad K, Gar Alalm M, Bassyouni M, Saleh MY (2020) A novel photocatalytic reactor for the extended reuse of W-TiO$_2$ in the degradation of sulfamethazine. Chemosphere 257:127270. https://doi.org/10.1016/j.chemosphere.2020.127270
5. Elhenawy Y, Bassyouni M, Fouad K, Sandid AM, Abu-Zeid MA-R, Majozi T (2023) Experimental and numerical simulation of solar membrane distillation and humidification—dehumidification water desalination system. Renew Energy 118915. https://doi.org/10.1016/j.renene.2023.118915
6. Elhady S, Bassyouni M, Mansour RA, Elzahar MH, Abdel-Hamid S, Elhenawy Y, Saleh MY (2020) Oily wastewater treatment using polyamide thin film composite membrane technology. Membranes (Basel) 10:84. https://doi.org/10.3390/membranes10050084
7. Eteba A, Bassyouni M, Saleh M (2022) Modified coal fly ash for textile dye removal from industrial wastewater. Energy Environ 1–27. https://doi.org/10.1177/0958305X221130536
8. Eteba A, Bassyouni M, Saleh M (2022) Utilization of chemically modified coal fly ash as cost-effective adsorbent for removal of hazardous organic wastes. Int J Environ Sci Technol. https://doi.org/10.1007/s13762-022-04457-5
9. Malik LA, Bashir A, Qureashi A, Pandith AH (2019) Detection and removal of heavy metal ions: a review. Environ Chem Lett 17:1495–1521. https://doi.org/10.1007/s10311-019-00891-z
10. Eteba A, Bassyouni M, Saleh M (2021) Removal of hazardous organic pollutants using fly ash. Environ Ecol Res 9:196–203. https://doi.org/10.13189/eer.2021.090407
11. Fouad K, Bassyouni M, Alalm MG, Saleh MY (2021) Recent developments in recalcitrant organic pollutants degradation using immobilized photocatalysts. Appl Phys A Mater Sci Process 127:612. https://doi.org/10.1007/s00339-021-04724-1
12. Chai WS, Cheun JY, Kumar PS, Mubashir M, Majeed Z, Banat F, Ho SH, Show PL (2021) A review on conventional and novel materials towards heavy metal adsorption in wastewater treatment application. J Clean Prod 296:126589. https://doi.org/10.1016/j.jclepro.2021.126589
13. Bassyouni M, Zoromba MS, Abdel-Aziz MH, Mosly I (2022) Extraction of nanocellulose for eco-friendly biocomposite adsorbent for wastewater treatment. Polymers (Basel) 14. https://doi.org/10.3390/polym14091852

14. Zoromba MS, Ismail MIM, Bassyouni MI, Abdel-Aziz MH, Salah N, Alshahrie A, Memic A (2017) Fabrication and characterization of poly (aniline-co-o-anthranilic acid)/magnetite nanocomposites and their application in wastewater treatment. Colloids Surfaces A Physicochem Eng Asp 520:121–130. https://doi.org/10.1016/j.colsurfa.2017.01.075

15. Abdel-Aziz MH, Bassyouni M, Soliman MF, Gutub SA, Magram SF (2017) Removal of heavy metals from wastewater using thermally treated sewage sludge adsorbent without chemical activation. J Mater Environ Sci 8:1737–1747

16. Kumar R, Mathur S (2022) Natural reserves of water on earth. In: Handbook of research on water sciences and society. IGI Global, pp 699–721

17. Rashid R, Shafiq I, Akhter P, Iqbal MJ, Hussain M (2021) A state-of-the-art review on wastewater treatment techniques: the effectiveness of adsorption method. Environ Sci Pollut Res 28:9050–9066

18. Periyasamy S, Karthik V, Senthil Kumar P, Isabel JB, Temesgen T, Hunegnaw BM, Melese BB, Mohamed BA, Vo D-VN (2022) Chemical, physical and biological methods to convert lignocellulosic waste into value-added products. A review. Environ Chem Lett 20:1129–1152

19. Fouad K, Gar Alalm M, Bassyouni M, Saleh MY (2021) Optimization of catalytic wet peroxide oxidation of carbofuran by Ti-LaFeO$_3$ dual photocatalyst. Environ Technol Innov 23:101778. https://doi.org/10.1016/j.eti.2021.101778

20. Muhd Julkapli N, Bagheri S, Bee Abd Hamid S (2014) Recent advances in heterogeneous photocatalytic decolorization of synthetic dyes. Sci World J 2014. https://doi.org/10.1155/2014/692307

21. Mateo-Sagasta J, Zadeh SM, Turral H (2018) More people, more food, worse water?: a global review of water pollution from agriculture

22. Singh J, Yadav P, Pal AK, Mishra V (2020) Water pollutants: origin and status. Sensors Water Pollut Monit Role Mater 5–20

23. Borah P, Kumar M, Devi P (2020) Types of inorganic pollutants: metals/metalloids, acids, and organic forms. In: Inorganic pollutants in water. Elsevier, pp 17–31

24. Mekhilef S, Saidur R, Kamalisarvestani M (2012) Effect of dust, humidity and air velocity on efficiency of photovoltaic cells. Renew Sustain energy Rev 16:2920–2925

25. Uddin F (2021) Environmental hazard in textile dyeing wastewater from local textile industry. Cellulose 28:10715–10739

26. Nur ASM, Sultana M, Mondal A, Islam S, Robel FN, Islam A, Sumi MSA (2022) A review on the development of elemental and codoped TiO$_2$ photocatalysts for enhanced dye degradation under UV–vis irradiation. J Water Process Eng 47:102728

27. Ayodhya D, Veerabhadram G (2018) A review on recent advances in photodegradation of dyes using doped and heterojunction based semiconductor metal sulfide nanostructures for environmental protection. Mater Today Energy 9:83–113. https://doi.org/10.1016/j.mtener.2018.05.007

28. Al-Tohamy R, Ali SS, Li F, Okasha KM, Mahmoud YA-G, Elsamahy T, Jiao H, Fu Y, Sun J (2022) A critical review on the treatment of dye-containing wastewater: ecotoxicological and health concerns of textile dyes and possible remediation approaches for environmental safety. Ecotoxicol Environ Saf 231:113160

29. Yaseen DA, Scholz M (2019) Impact of pH on the treatment of artificial textile wastewater containing azo dyes using pond systems. Int J Environ Res 13:367–385

30. Sharma J, Sharma S, Soni V (2021) Classification and impact of synthetic textile dyes on Aquatic Flora: a review. Reg Stud Mar Sci 45:101802

31. Vikrant K, Giri BS, Raza N, Roy K, Kim K-H, Rai BN, Singh RS (2018) Recent advancements in bioremediation of dye: current status and challenges. Bioresour Technol 253:355–367

32. Kishor R, Purchase D, Saratale GD, Saratale RG, Ferreira LFR, Bilal M, Chandra R, Bharagava RN (2021) Ecotoxicological and health concerns of persistent coloring pollutants of textile industry wastewater and treatment approaches for environmental safety. J Environ Chem Eng 9:105012

33. Samsami S, Mohamadizaniani M, Sarrafzadeh M-H, Rene ER, Firoozbahr M (2020) Recent advances in the treatment of dye-containing wastewater from textile industries: overview and perspectives. Process Saf Environ Prot 143:138–163

34. Katheresan V, Kansedo J, Lau SY (2018) Efficiency of various recent wastewater dye removal methods: a review. J Environ Chem Eng 6:4676–4697
35. Ahmed SF, Mofijur M, Nuzhat S, Chowdhury AT, Rafa N, Uddin MA, Inayat A, Mahlia TMI, Ong HC, Chia WY (2021) Recent developments in physical, biological, chemical, and hybrid treatment techniques for removing emerging contaminants from wastewater. J Hazard Mater 416:125912
36. Shaikh MA, Weiguo S, Shahid MU, Ayaz H, Ali M (2018) An assessment of hazards and occupational health & safety practices for workers in the textile industry: a case study. J Acad Res Bus Soc Sci 8:333–347
37. Shahedi A, Darban AK, Taghipour F, Jamshidi-Zanjani A (2020) A review on industrial wastewater treatment via electrocoagulation processes. Curr Opin Electrochem 22:154–169
38. Taghizadeh A, Taghizadeh M, Jouyandeh M, Yazdi MK, Zarrintaj P, Saeb MR, Lima EC, Gupta VK (2020) Conductive polymers in water treatment: a review. J Mol Liq 312:113447
39. Junlapong K, Maijan P, Chaibundit C, Chantarak S (2020) Effective adsorption of methylene blue by biodegradable superabsorbent cassava starch-based hydrogel. Int J Biol Macromol 158:258–264
40. Kumar V, Rehani V, Kaith BS (2018) Synthesis of a biodegradable interpenetrating polymer network of Av-cl-poly (AA-ipn-AAm) for malachite green dye removal: kinetics and thermodynamic studies. RSC Adv 8:41920–41937
41. Mittal H, Kumar V, Alhassan SM, Ray SS (2018) Modification of gum ghatti via grafting with acrylamide and analysis of its flocculation, adsorption, and biodegradation properties. Int J Biol Macromol 114:283–294
42. Benhouria A, Islam MA, Zaghouane-Boudiaf H, Boutahala M, Hameed BH (2015) Calcium alginate–bentonite-activated carbon composite beads as highly effective adsorbent for methylene blue. Chem Eng J 270:621–630
43. Janarthanan P, Yunus WMZW, Bin AM (2003) Thermal behavior and surface morphology studies on polystyrene grafted sago starch. J Appl Polym Sci 90:2053–2058
44. Yagub MT, Sen TK, Ang HM (2012) Equilibrium, kinetics, and thermodynamics of methylene blue adsorption by pine tree leaves. Water Air Soil Pollut 223:5267–5282
45. Alencar WS, Acayanka E, Lima EC, Royer B, de Souza FE, Lameira J, Alves CN (2012) Application of Mangifera indica (mango) seeds as a biosorbent for removal of Victazol Orange 3R dye from aqueous solution and study of the biosorption mechanism. Chem Eng J 209:577–588
46. Belhouchat N, Zaghouane-Boudiaf H, Viseras C (2017) Removal of anionic and cationic dyes from aqueous solution with activated organo-bentonite/sodium alginate encapsulated beads. Appl Clay Sci 135:9–15
47. Saleh MY, Enany GEL, Elzahar MH, Elshikhipy MZ, Hamouda R (2014) Removal of lead in high rate activated sludge system. Int J Environ Ecol Eng 8:413–418
48. Abdel-Aziz MH, El-Ashtoukhy EZ, Bassyouni M, Al-Hossainy AF, Fawzy EM, Abdel-Hamid SMS, Zoromba MS (2021) DFT and experimental study on adsorption of dyes on activated carbon prepared from apple leaves. Carbon Lett 31:863–878
49. Saleh MY, El Enany G, Elzahar MH, Omran MH (2015) Industrial wastewater treatment improvements using activated carbon. In: International conference on energy, ecology, environment and sustainable development at: Miami, USA
50. Gutub SA, Bassyouni M, Abdel-Hamid SMS (2013) Dissolved solids adsorption of freshwater using synthesized bio-foam composite. Life Sci J 10:464–471
51. Hamdon RS, Salem A, Ahmed HGI, ElZahar MMH (2022) Use of chitosan for enhancing the process of surface water purification in Egypt. Int J Environ Sci Dev 13:26–34
52. Elshikhipy MZ (2014) Use of alum for removal of total dissolved solids and total iron in high rate activated sludge system

53. EL-Dosoky SH, El-Zahar MH, Saleh MY (2019) The usage of date pits for treatment of thickened sludge
54. Saleh M, El Enany G, Elzahar M, Omran M (2017) Industrial wastewater treatment improvements using limestone. J Environ Stud Res 7:910–918
55. Saleh MY, El Enany G, Elzahar MH, Elshikhipy MZ (2014) Industrial wastewater treatment using high rate activated sludge and alum additive. Int J Environ Sci Dev 5:551

Treatment of Printing Ink Wastewater Using Natural and Synthetic Coagulants

Menna Eid, S. M. El-Marsafy, and M. Bassyouni

1 Introduction

Water is one of the necessities of life, and preserving it and developing its sources deserves attention [1–4]. Numerous contaminants are found in our water sources due to the development of industry and the widespread usage of complicated chemicals. These compounds have a serious hazard to our ecology since they are difficult to break down. They have significantly grown in number over time, posing a grave threat to the next generations [5–7]. The procedures of printing, color matching, cleaning printing machines, etc. generate printing ink wastewater (PIW). The primary ingredients of ink are pigments, fillers, auxiliaries, solvents, and color carriers (often certain resin compounds with hydrophilic groups, etc.) [8] as shown in Fig. 1. Wastewater from printing ink comprises recalcitrant substances, traces of metals (such as Cd, Hg), adhesives, and pigments. In addition to their vibrant color, these wastewaters have high chemical oxygen demand (COD) values, typically up to 20,000 mg/L. To avoid major environmental issues, printing ink wastewater must be treated before being released [9–11]. Even very low concentrations of dyes in the effluent (less than 1 mg/L for some dyes, for example) cause the water to turn a highly noticeable and unwelcome shade of color. Additionally, it harms water bodies like rivers

M. Eid · M. Bassyouni (✉)
Department of Chemical Engineering, Faculty of Engineering, Port Said University, Port Said 42526, Egypt
e-mail: m.bassyouni@eng.psu.edu.eg

M. Eid · S. M. El-Marsafy
Department of Chemical Engineering, Faculty of Engineering, Cairo University, Giza 12613, Egypt

M. Bassyouni
Center of Excellence in Membrane-Based Water Desalination Technology for Testing and Characterization (CEMTC), Port Said University, Port Said 42526, Egypt

East Port Said University of Technology, Saini, Port Said 45632, Egypt

and lakes by obstructing sunlight or promoting eutrophication [12]. Effective treatment is required for (PIW) so it could be disposed of safely in aquatic systems. For the treatment of this sort of extremely colored wastewater, advanced oxidation processes (AOPs), electrochemical techniques, coagulation/sedimentation, and either separately or in combination with other physicochemical methods, are typically preferred [13, 14]. It was reported that utilizing coagulation/flocculation for processing wastewater showed satisfactory results using either organic or inorganic flocculants/coagulants such as aluminum, iron (III) salts, or organic polyelectrolytes [15]. Dyeing processes often involve the use of chemicals and may lead to changes in the pH range of the surrounding environment. Pipe lines and tanks made of aluminum alloys are more susceptible to corrosion in both highly acidic and highly alkaline environments. If the dyeing process alters the pH of the surrounding medium significantly, it could affect the corrosion rate of aluminum alloys. Water and wastewater treatment was conducted using flocculation and coagulation for a very long time. This treatment method is advantageous since it is inexpensive, simple to use, and effective at eliminating water contaminants. The type of coagulant has a significant impact on how well coagulation works. Wastewater treatment is essential for ensuring access to clean water and sanitation for all. By treating wastewater before its discharge into water bodies or reuse, water resources will be protected, improve water quality, and enhance sanitation achieving SDG (6).
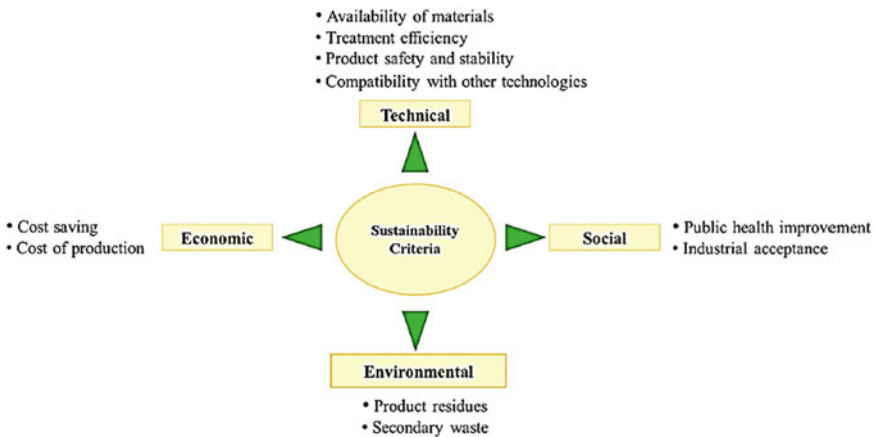
Fig. 1 Sustainability of natural coagulants

2 Printing Ink Wastewater Treatment Techniques

2.1 Coagulation

Chemical coagulation is often carried out in water treatment facilities by the addition of trivalent metallic salts such as ferric chloride ($FeCl_3$) or aluminum sulfate $Al_2(SO_4)_3$. Four mechanisms—ionic layer compression, adsorption and charge neutralization, sweep coagulation, and inter-particle bridging—are hypothesized to occur. Instead of utilizing a quantitative method, a jar test is used to choose the best coagulant dosages. Every water that needs to be coagulated must undergo the jar test, which must be repeated whenever a water's quality noticeably changes. The turbidity and chromaticity of ink wastewater can be decreased by coagulation. In the treatment of wastewater, coagulant selection is crucial [16]. It was found that COD treatment achieved 92.1%, decoloring rate obtained 97.4% following coagulation by polyferric chloride, taking sediment time, decoloring rate, and other aspects into consideration. Other study stated that employing ferrous sulfate as a coagulant resulted in low removal rates for both decoloring and COD, whereas polymerization aluminum chloride can produce decoloring removal rates of 99% and COD removal rates of 45–60% [17].

2.2 Adsorption

The findings showed that active carbon removes ogranic matters with good efficiency [18]. After adsorption, the wastewaters are transparent and colorless. Yet, active carbon is often expensive and saturated [19]. Remediate ink wastewater by first modifying zeolite with polyamidoamine (PAMAM). It was reported that fly ash and poly-dimethyl-diallylammonium chloride (PDMDAAC) were used in combination to treat ink wastewater and organic compounds with removal efficiency 94% and 74%, respectively [20].

2.3 Electrolysis Method

Iron was used as an anode and aluminum as a cathode in the electrolysis process to treat print ink wastewater. In the electrolytic process, iron gradually dissolved into Fe^{2+}, and hydrolysis produced Fe $(OH)_2$, which precipitated. After being removed, COD_{cr} accomplished 47% removal, BOD_5 60% removal, and decoloring 84% following treatment [21].

2.4 Oxidation

Chemical oxidation frequently uses the oxidants NaClO, KMnO$_4$, O$_3$, and C$_2$H$_2$O$_4$·H$_2$O. Most organic materials can be reduced, but not completely, and the cost of treatment process is a substantial factor. Coagulation and Fenton mixing were employed to treat ink wastewater. Chroma and COD$_{cr}$ can be completely removed at pH 4.5, H$_2$O$_2$, 4.5 mg/L, FeSO$_4$ 25 mg/L, and PAC 700 mg/L after a specified contact period. This is equivalent to 100% and 93.4% removal, respectively [22].

3 Biological Approach

Using biological methods for ink wastewater is a suitable approach considering the challenges associated with the biodegradability of ink compounds. The two-stage Sequencing Batch Reactor (SBR) is a commonly employed biological treatment process that can effectively remove organic contaminants from wastewater. The SBR process involves a sequence of fill, react, settle, and followed by decant phases within a single reactor. In the case of ink wastewater treatment, a two-stage SBR configuration is often applied to enhance the removal efficiency and achieve better treatment performance. In the pretreatment stage, physical and chemical processes are required to remove large particles, solids, and any potential inhibitors that could hinder the biological treatment. This step is required before biological treatment. The two-stage SBR method allows for a more comprehensive treatment of ink wastewater. The first stage focuses on the removal of easily biodegradable organic compounds and the initial reduction of chemical oxygen demand (COD). The wastewater is subjected to a controlled aerobic process where microorganisms metabolize the organic pollutants, breaking them down into simpler, more biodegradable forms. After the first stage, the wastewater undergoes a settling process to separate the biomass and any residual solids. The clarified wastewater is then transferred to the second stage, where more resistant and complex organic compounds are further degraded. This stage typically involves an anoxic or anaerobic process to target specific recalcitrant compounds, enhancing the overall removal efficiency. According to the findings, the COD removal rate stayed over 93% and the decoloring rate was 80% [23].

4 Ink Raw Materials

4.1 Pigments

The ink's color is a pigment's most evident function. Pigments can also be abrasive, glossy, and resistant to damage from light, heat, solvents, etc. Also, specialized pigments called extenders and opacifiers are utilized. Opacifiers are white pigments

that make the paint opaque so that the surface beneath the paint cannot be seen, whereas extenders are transparent pigments that make the colors of other pigments look less intense [24].

4.2 Resins

Resins are essentially binders; they combine the other ink components to form a coating that adheres the ink to the paper. They also support qualities like gloss and resistance. water, chemicals, and heat. There are many different types of resins utilized, and each ink often contains more than one resin. This is a list of resins that are most frequently used: Maleics, Formaldehydes, Phenolics, Acrylics, Alkyds, Cellulose derivatives, Rubber resins, and Ketones [25].

4.3 Solvents

When ink is put on a printing plate or cylinder, solvents are employed to maintain the ink's liquid state until it has been transferred to the surface that will be printed. The solvent must now separate from the ink body for the image to dry and adhere to the surface [26].

5 Chemical Coagulants and Flocculants

Chitosan, starch, cellulose, tannin, microbiological raw materials, animal glue, and gelatin are the main sources of natural flocculants. Three categories can be made out of them: Depending on the type of functional groups that make up its chemical structure, flocculants are classified as (i) cationic flocculant, (ii) anionic flocculant, and (iii) non-ionic flocculant. Such flocculants are also non-toxic and biodegradable. Natural flocculants are thought to be the greatest option for eliminating dyes and/ or heavy metals from wastewater because of their many inherent qualities. Long polymer chains and a high cationic charge density are some of these characteristics [27].

5.1 Inorganic Compounds

The TOC, AOX, and COD loading values supported the removal of turbidity and color as well as a significant portion of the inorganic content by adding aluminum and ferric chlorides to printing ink wastewater. From an economic and technological standpoint,

flocculation has been proven to be an appropriate, quick, and easy treatment for such effluent [28, 29] (Tables 1, 2 and 3).

Table 1 Values of water quality parameters for W1 and W2

Wastewater	COD, mg/L	BOD, mg/L	AOX, mg Cl/L	TOC, mg/L	pH
W1	3220	0.0896	9.323	941.971	7.6
W2	2320	0.0384	6.036	893.9	7.4

Table 2 Efficiency of studied flocculants expressed by the concentration of residual ink in treated water

	Flocculant, g/L	Turbidity, NTU[a]	Residual ink concentration, mg/L	pH	Sample of filtrate
$Al_2(SO_4)_3$					
W1	0.375	0.6	0.076	6.6	A
W2	0.450	0.69	0.08	6.6	B
$FeCl_3$					
W1	0.505	0.49	0	6.6	C
W2	0.650	0.39	0	6.5	D
$AlCl_3$					
W1	0.375	0.59	0	6.5	E
W2	0.415	0.49	0	6.4	F

Table 3 Treated water analysis

Sample of filtrate	COD mg/l	BOD_5 mg/l	TOC mg/l	AOX mg/l Cl_2	pH
W1					
A	840	0	313	2.102	6.7
C	740	0	323.1	1.398	6.6
E	560	0	305.7	1.955	6.6
W2					
B	220	0	146.4	0.674	6.6
D	160	0	139.3	0.510	6.5
F	110	0	118.2	0.474	6.4

5.2 Chitosan and Tannin

An effluent comprising ink that was created during the manufacturing of packaging was treated utilizing a coagulation/flocculation process using a variety of biopolymers (chitosan and tannin). The effectiveness of the procedure was examined in terms of how pH, coagulant and flocculant concentrations, and chitosan properties affected it (especially the molecular weight). The procedure was especially effective with acidic solutions since restricted the pH to 5 [30].

5.3 Fenton Oxidation

The Fenton process treated effluent was improved by the coagulation utilizing fenugreek and iron sulfate ($FeSO_4$) by reducing the flocs settling time, enhancing turbidity, and increasing COD and BOD removal. Under particular circumstances, the elimination of COD, BOD, and total turbidity was 99%, 63%, and 39.5%, respectively. As a result, this work may provide a practical method for the printing industry and manufacturers of water-based inks to treat their wastewater [31].

6 Mechanism of Coagulation by Natural Coagulants

Natural coagulants have a similar mechanism of action to polyelectrolytes and contain a variety of functional groups, including –OH, –COOH, and –NH_2. The red circles are the negatively charged colloidal particles, while the green circles are the positively charged coagulants. Natural coagulants can be classified according to their mechanism of action into four categories: sweep flocculation, charge neutralization, double-layer compression, and antiparticle bridging [32]. Sweep flocculation/coagulation is a method for removing colloids by trapping or entangling them in a net-like structure that contains precipitates of the amorphous metal hydroxide that are produced during the hydrolysis of the colloids. The flocs formed using this method are relatively smaller in size with adequate settling capacity, but they are distinguished by a slow rate of floc formation, according to several evaluations, including initial floc-aggregation, the relative settling factor, and the flocculation index [32]. The great fractal dimension of the floc created by sweep flocculation demonstrates the complexity of flocs [33]. The high fractal dimension has theoretically stronger flocs that can withstand breaking. Nevertheless, sweep flocculation produces big, easily broken flocs despite having a higher floc generation rate. Adsorption between the oppositely charged surfaces of the coagulants and the colloid results in charge neutralization [34]. Chemical coagulants are hydrolyzed to produce some cationic species before reacting with the colloids. For the charge neutralization procedure, an electrostatic patch mechanism, a patch-wise medium, is used. The surface of the

colloids will patch with different cationic species, resulting in particle surfaces with positive and negative charges. surfaces of colloids with a mixed charge will weaken repelling forces and strengthen van der Waals forces between the particles [35].

Double-layer compression is a technique that penetrates the double layer that surrounds the colloidal particles by using ions that have the opposite charge to that of the colloidal particles. The volume and thickness of the double layer will decrease due to the counterions. As the electrolyte is continuously compressed, electrostatic repulsion is decreased and van der Waals forces are increased, which makes it easier for the two destabilized colloids to unite.

7 Sustainability of Natural Coagulants

Sustainable development meets the demands of both present and future generations. According to the United Nations' idea of sustainability, the reliability of technology is just as important as performance efficiency when it comes to the treatment of water. As a result, the idea of sustainability combines social, environmental, and economic considerations [36] as shown in Fig. 1. Industrial acceptance and advancements in public health are two societal aspects of the sustainability of natural coagulants. The ability of natural coagulants to provide outcomes comparable to those of chemical coagulants and be employed as an alternative is a requirement for industrial accept-ability. Because there aren't any regulatory or approved standards for the treatment of potable water, Businesses are reluctant to use natural coagulants. Natural coagulants may help with health and cleanliness and raise everyone's standards of living, especially in rural regions. The technological side of sustainability includes product and treatment stability, material accessibility, and compatibility with other methods. The effectiveness of several natural coagulants in the treatment of water and wastewater has been well-established over time. Natural coagulants are regarded as harmless and non-toxic due to their natural origin. Organic coagulants' environmental safety needs to be confirmed because it is uncertain whether they are dangerous to humans and the environment [37].

Hence, careful choice and dose optimization of effective natural coagulants could offer encouraging outcomes in WT and possibly serve as a replacement for pharmaceutical coagulants. As was previously said, natural coagulants are readily available, reliable, resilient, and can be derived from a variety of sources, including plants, microbes, or animals [38–40]. Yet their vulnerability to microbial or other environmental biodegradation has a negative impact on their long-term storage (shelf life) and commercialization [41, 42]. Environmental sustainability criteria call for the use of plant-based, biodegradable coagulants that are safe for the environment and can produce biodegradable sludge [43], which can be used for a variety of other things like agricultural practices, landfills, and the civil engineering sector [44, 45].

8 Conclusion

The ink industry is one of the important industries at present, and despite its importance, the industry's output of liquids represents an environmental threat that must be addressed. The resulting wastewater contains many recalcitrant chemicals and heavy metals. Many researchers have dealt with the technology of removing these pollutants. One of the promising technologies for treatment is the use of the coagulation process. In this review, the composites of ink were discussed. Also, printing ink treatment technologies were illustrated.

9 Recommendation

The coagulation/flocculation technique is commonly used in water treatment and can be effective in removing pollutants from ink-contaminated water. However,, one of its significant drawbacks is that the pollutants are concentrated during the process, requiring a subsequent treatment method for their proper disposal. This emphasizes the need for a comprehensive approach that ensures the safe and complete removal of pollutants. To address this issue, researchers and scientists should focus on developing or improving post-treatment methods that can safely dispose of the concentrated pollutants. These methods could include techniques such as adsorption, advanced oxidation processes, membrane filtration, or biological treatments, depending on the specific characteristics of the concentrated pollutants and the environmental requirements. Furthermore, it's essential to study different types of dyes present in inks to understand the variations in their toxicity and identify the most appropriate treatment methods for each type. Some dyes may be more harmful to living organisms or more resistant to conventional treatment techniques than others. By evaluating the toxicity of various dyes and assessing their chemical composition, researchers can determine the most effective and environmentally friendly treatment options.

References

1. Elminshawy NAS, El-Ghandour M, Elhenawy Y, Bassyouni M, El-Damhogi DG, Addas MF (2019) Experimental investigation of a V-trough PV concentrator integrated with a buried water heat exchanger cooling system. Sol Energy 193:706–714. https://doi.org/10.1016/j.solener.2019.10.013
2. Elhenawy Y, Fouad K, Bassyouni M, Majozi T (2023) Design and performance a novel hybrid membrane distillation/humidification–dehumidification system. Energy Convers Manag 286:117039. https://doi.org/10.1016/j.enconman.2023.117039

3. Elhenawy Y, Bassyouni M, Fouad K, Sandid AM, Abu-Zeid MA-R, Majozi T (2023) Experimental and numerical simulation of solar membrane distillation and humidification—dehumidification water desalination system. Renew Energy 118915. https://doi.org/10.1016/j.renene.2023.118915

4. Marni Sandid A, Bassyouni M, Nehari D, Elhenawy Y (2021) Experimental and simulation study of multichannel air gap membrane distillation process with two types of solar collectors. Energy Convers Manag 243:114431. https://doi.org/10.1016/j.enconman.2021.114431

5. Fouad K, Gar Alalm M, Bassyouni M, Saleh MY (2020) A novel photocatalytic reactor for the extended reuse of W-TiO$_2$ in the degradation of sulfamethazine. Chemosphere 257:127270. https://doi.org/10.1016/j.chemosphere.2020.127270

6. Fouad K, Bassyouni M, Alalm MG, Saleh MY (2021) Recent developments in recalcitrant organic pollutants degradation using immobilized photocatalysts. Appl Phys A: Mater Sci Process 127:612. https://doi.org/10.1007/s00339-021-04724-1

7. Zampeta C, Paparouni C, Tampakopoulos A, Frontistis Z, Charalampous N, Dailianis S, Koutsoukos PG, Paraskeva CA, Vayenas DV (2022) Printing ink wastewater treatment using hydrodynamic cavitation and coagulants/flocculants. J Environ Manag 321:115975. https://doi.org/10.1016/j.jenvman.2022.115975

8. Ding C, Xie A, Yan Z, Li X, Zhang H, Tang N, Wang X (2021) Treatment of water-based ink wastewater by a novel magnetic flocculant of boron-containing polysilicic acid ferric and zinc sulfate. J Water Process Eng 40:101899. https://doi.org/10.1016/j.jwpe.2020.101899

9. Papadopoulos KP, Argyriou R, Economou CN, Charalampous N, Dailianis S, Tatoulis TI, Tekerlekopoulou AG, Vayenas DV (2019) Treatment of printing ink wastewater using electrocoagulation. J Environ Manag 237:442–448

10. Zampeta C, Mastrantonaki M, Katsaouni N, Frontistis Z, Koutsoukos PG, Vayenas DV (2022) Treatment of printing ink wastewater using a continuous flow electrocoagulation reactor. J Environ Manag 314:115033. https://doi.org/10.1016/j.jenvman.2022.115033

11. Zhang F, Li Y, Liang Z, Wu T, Huang Y (2021) Experimental investigation on the oxidation of printing ink wastewater under hydrothermal flames. J Environ Chem Eng 9:106745. https://doi.org/10.1016/j.jece.2021.106745

12. Zampeta C, Bertaki K, Triantaphyllidou IE, Frontistis Z, Vayenas DV (2021) Treatment of real industrial-grade dye solutions and printing ink wastewater using a novel pilot-scale hydrodynamic cavitation reactor. J Environ Manag 297:113301. https://doi.org/10.1016/j.jenvman.2021.113301

13. Zampeta C, Arvanitaki F, Frontistis Z, Charalampous N, Dailianis S, Koutsoukos PG, Vayenas DV (2022) Printing ink wastewater treatment using combined hydrodynamic cavitation and pH fixation. J Environ Manag 317:115404. https://doi.org/10.1016/j.jenvman.2022.115404

14. Fouad K, Gar Alalm M, Bassyouni M, Saleh MY (2021) Optimization of catalytic wet peroxide oxidation of carbofuran by Ti-LaFeO$_3$ dual photocatalyst. Environ Technol Innov 23:101778. https://doi.org/10.1016/j.eti.2021.101778

15. Shaheed H, Mohamed R, Al-Sahari M, Mohd-Zind NS, Al-Gheethi A, Alomari T (2020) Coagulation and flocculation of printing ink effluent using polyaluminium chloride (PAC): optimization and phytotoxicity study. Desalin Water Treat 208:303–311. https://doi.org/10.5004/dwt.2020.26408

16. Bassyouni M, Zoromba MS, Abdel-Aziz MH, Mosly I (2022) Extraction of nanocellulose for eco-friendly biocomposite adsorbent for wastewater treatment. Polymers (Basel) 14. https://doi.org/10.3390/polym14091852

17. Zoromba MS, Ismail MIM, Bassyouni MI, Abdel-Aziz MH, Salah N, Alshahrie A, Memic A (2017) Fabrication and characterization of poly (aniline-co-o-anthranilic acid)/magnetite nanocomposites and their application in wastewater treatment. Colloids Surf A: Physicochem Eng Asp 520:121–130. https://doi.org/10.1016/j.colsurfa.2017.01.075

18. Abdel-Aziz MH, Bassyouni M, Soliman MF, Gutub SA, Magram SF (2017) Removal of heavy metals from wastewater using thermally treated sewage sludge adsorbent without chemical activation. J Mater Environ Sci 8:1737–1747

19. Eteba A, Bassyouni M, Saleh M (2022) Modified coal fly ash for textile dye removal from industrial wastewater. Energy Environ 1–27. https://doi.org/10.1177/0958305X221130536
20. Eteba A, Bassyouni M, Saleh M (2022) Utilization of chemically modified coal fly ash as cost-effective adsorbent for removal of hazardous organic wastes. Int J Environ Sci Technol. https://doi.org/10.1007/s13762-022-04457-5
21. Abdel-Aziz MH, El-Ashtoukhy EZ, Bassyouni M, Al-Hossainy AF, Fawzy EM, Abdel-Hamid SMS, Zoromba MS (2021) DFT and experimental study on adsorption of dyes on activated carbon prepared from apple leaves. Carbon Lett 31:863–878
22. Amor C, Marchão L, Lucas MS, Peres JA (2019) Application of advanced oxidation processes for the treatment of recalcitrant agro-industrial wastewater: a review. Water (Switzerland) 11. https://doi.org/10.3390/w11020205
23. Elhady S, Bassyouni M, Mansour RA, Elzahar MH, Abdel-Hamid S, Elhenawy Y, Saleh MY (2020) Oily wastewater treatment using polyamide thin film composite membrane technology. Membranes (Basel) 10:84. https://doi.org/10.3390/membranes10050084
24. Koo H-S, Chen M, Pan P-C (2006) LCD-based color filter films fabricated by a pigment-based colorant photo resist inks and printing technology. Thin Solid Films 515:896–901
25. Sharma B, Singh S, Prakash B, Sharma H, Maji PK, Dutt D, Kulshreshtha A (2022) Effect of cellulose nanocrystal incorporated acrylic copolymer resin on printing properties of waterborne inks. Prog Org Coatings 167:106842
26. Brazeau L, Gaudreau M (2007) Ballpoint pen inks: the quantitative analysis of ink solvents on paper by solid-phase microextraction. J Forens Sci 52:209–215
27. Maddah HA, Alzhrani AS, Bassyouni M, Abdel-Aziz MH, Zoromba M, Almalki AM (2018) Evaluation of various membrane filtration modules for the treatment of seawater. Appl Water Sci 8:1–13. https://doi.org/10.1007/s13201-018-0793-8
28. Leach R (2012) The printing ink manual. Springer
29. Meteš A, Koprivanac N, Glasnovic A (2000) Flocculation as a treatment method for printing ink wastewater. Water Environ Res 72:680–688
30. Liu Z, Liu K (2022) Reproducing ancient Chinese ink depending on gelatin/chitosan and modern experimental methodology. Herit Sci 10:1–12
31. Khannous L, Elleuch A, Fendri I, Jebahi N, Khlaf H, Gharsallah N (2016) Treatment of printing wastewater by a combined process of coagulation and biosorption for a possible reuse in agriculture. Desalin Water Treat 57:5723–5729
32. Jiao Y-N, Chen H, Gao R-X, Zhu Y-G, Rensing C (2017) Organic compounds stimulate horizontal transfer of antibiotic resistance genes in mixed wastewater treatment systems. Chemosphere 184:53–61
33. Li YS, Yan L, Xiang CB, Hong LJ (2006) Treatment of oily wastewater by organic–inorganic composite tubular ultrafiltration (UF) membranes. Desalination 196:76–83
34. Miller SM, Fugate EJ, Craver VO, Smith JA, Zimmerman JB (2008) Toward understanding the efficacy and mechanism of *Opuntia* spp. as a natural coagulant for potential application in water treatment. Environ Sci Technol 42:4274–4279
35. Chong JWR, Khoo KS, Yew GY, Leong WH, Lim JW, Lam MK, Ho Y-C, Ng HS, Munawaroh HSH, Show PL (2021) Advances in production of bioplastics by microalgae using food waste hydrolysate and wastewater: a review. Bioresour Technol 342:125947
36. Kamali M, Suhas DP, Costa ME, Capela I, Aminabhavi TM (2019) Sustainability considerations in membrane-based technologies for industrial effluents treatment. Chem Eng J 368:474–494
37. Koul B, Bhat N, Abubakar M, Mishra M, Arukha AP, Yadav D (2022) Application of natural coagulants in water treatment: a sustainable alternative to chemicals. Water 14:3751
38. Saleem M, Bachmann RT (2019) A contemporary review on plant-based coagulants for applications in water treatment. J Ind Eng Chem 72:281–297
39. Kanmani P, Aravind J, Kamaraj M, Sureshbabu P, Karthikeyan S (2017) Environmental applications of chitosan and cellulosic biopolymers: a comprehensive outlook. Bioresour Technol 242:295–303
40. Do MH, Ngo HH, Guo WS, Liu Y, Chang SW, Nguyen DD, Nghiem LD, Ni BJ (2018) Challenges in the application of microbial fuel cells to wastewater treatment and energy production: a mini review. Sci Total Environ 639:910–920

41. Ho YC, Norli I, FM A, Morad N (2014) New vegetal biopolymeric flocculant: a degradation and flocculation study. Iran J Energy Environ 5
42. Abidin ZZ, Norhafizah M, Robiah Y, Aishah D (2019) Effect of storage conditions on *Jatropha curcas* performance as biocoagulant for treating Palm Oil Mill Effluent. J Environ Sci Technol 12:92–101
43. dos Santos JD, Veit MT, Juchen PT, da Cunha GG, Palacio SM, Fagundes-Klen M (2018) Use of different coagulants for cassava processing wastewater treatment. J Environ Chem Eng 6:1821–1827
44. Dezfooli SM, Uversky VN, Saleem M, Baharudin FS, Hitam SMS, Bachmann RT (2016) A simplified method for the purification of an intrinsically disordered coagulant protein from defatted *Moringa oleifera* seeds. Process Biochem 51:1085–1091
45. Barbosa AD, da Silva LF, de Paula HM, Romualdo LL, Sadoyama G, Andrade LS (2018) Combined use of coagulation (*M. oleifera*) and electrochemical techniques in the treatment of industrial paint wastewater for reuse and/or disposal. Water Res 145:153–161

Artificial Intelligence for Predicting the Performance of Adsorption Processes in Wastewater Treatment: A Critical Review

Mohammad Mansour, M. Bassyouni, Rehab F. Abdel-Kader, Yasser Elhenawy, Lobna A. Said, and Shereen M. S. Abdel-Hamid

1 Introduction

The quest to protect our planet and ensure the well-being of humanity demands the preservation of environmental quality and public health through the effective treatment of water. Conventional wastewater treatment methods can be a drag on time and resources [1]. The power of artificial intelligence (AI) has been harnessed to optimize the adsorption of pollutants and ensure a cleaner, healthier future for all. Removing dyes from wastewater is particularly important for environmental remediation [2]. Dyes, commonly used in industries like textile, leather, and paper manufacturing, can be toxic, carcinogenic, and persistent in the environment [3]. They can cause aesthetic problems and harm aquatic life and human health. Adsorption is one of the most effective methods for removing dyes from wastewater, and it involves attaching

M. Mansour · L. A. Said
Nanoelectronics Integrated Systems Center (NISC), Nile University, Giza 12588, Egypt
e-mail: mmansour@nu.edu.eg

L. A. Said
e-mail: lsaid@nu.edu.eg

M. Bassyouni (✉)
Department of Chemical Engineering, Faculty of Engineering, Port Said University, Port Said 42526, Egypt
e-mail: m.bassyouni@eng.psu.edu.eg

M. Bassyouni · Y. Elhenawy
Center of Excellence in Membrane-Based Water Desalination Technology for Testing and Characterization (CEMTC), Port Said University, Port Said 42526, Egypt
e-mail: yasser.elhenawy@wits.ac.za

R. F. Abdel-Kader
Electrical Engineering Department, Faculty of Engineering Port, Said University, Port Said 42526, Egypt
e-mail: rehabfarouk@eng.psu.edu.eg

dye molecules to the surface of solid adsorbent material, such as activated carbon, zeolites, or clay [4]. Modifying the adsorbent surface can enhance this process [5, 6]. The effectiveness of wastewater treatment has the potential to be increased by methods like machine learning, neural networks, and fuzzy neural networks [6]. AI techniques can optimize process parameters, such as pH, temperature, and adsorbent dosage, to improve efficiency and cost-effectiveness. AI can also develop predictive models for accurate prediction of the adsorption behavior of dyes on different types of adsorbents. Traditional methods of adsorption process design and optimization have relied on empirical models and trial-and-error approaches. However, recent advances in AI show promising results in optimizing pollutant adsorption processes [7].

The research presented in this study directly aligns with key Sustainable Development Goals (SDGs) established by the United Nations. Specifically, our focus on optimizing the pollutant adsorption process in wastewater treatment using artificial intelligence (AI) techniques contributes to achieving SDG 6: Clean Water and Sanitation. By enhancing the removal of toxic dyes from wastewater, we aim to improve water quality (SDG 6.3) and ensure the sustainable management of water resources. Furthermore, our work also supports SDG 9: Industry, Innovation, and Infrastructure by promoting the adoption of cutting-edge AI techniques within wastewater treatment systems. This contributes to sustainable industry practices, resource efficiency, and cleaner production technologies (SDG 9.4). Lastly, our efforts align with SDG 12: Responsible Consumption and Production as we strive to minimize the release of hazardous chemicals and promote the environmentally sound management of wastewater pollutants. By optimizing adsorption processes, we contribute to reducing the adverse impacts of pollutants on human health and the environment (SDG 12.4).

The main objective of this study is to offer a thorough examination of how artificial intelligence (AI) can be utilized to optimize the pollutant adsorption process in wastewater treatment. Cutting-edge AI techniques and their applications in pollutant adsorption optimization will be analyzed. The study continues to address the challenges and future research directions in this field. This review aims to provide valuable insights for researchers and practitioners to enhance the effectiveness of pollutant adsorption processes in wastewater treatment.

Y. Elhenawy

Department of Mechanical Power Engineering, Faculty of Engineering, Port Said University, Port Said 42526, Egypt

S. M. S. Abdel-Hamid

Chemical Engineering Department, Egyptian Academy for Engineering and Advanced Technology affiliated to Ministry of Military Production, Cairo 3066, Egypt
e-mail: shereenahmed@eaeat.edu.eg

2 Adsorption Process and Artificial Intelligence Techniques

The act of adsorption is a method of physicochemical treatment that involves attaching particles or molecules to a surface [8]. It encompasses various processes, such as molecule movement caused by concentration gradients, diffusion through a boundary layer, and movement into the material's interior. When adsorption occurs, the molecules being adsorbed move from the bulk solution to the adsorbent surface because of concentration gradients. The rate of adsorption is determined by the establishment of a concentration gradient, as well as other factors. Dye molecules may also penetrate the surface of the adsorbent material and enter the interior by diffusing through pores. The rate of diffusion depends on factors like pore size, temperature, and dye concentration. It's critical to consider the adsorption process's influencing factors, including the adsorbent material's properties, adsorbate molecule characteristics, and adsorption conditions [9]. One critical property is the adsorbent's surface area, which affects the number of available adsorption sites. The surface area can be increased using methods like surface modifications or increased material porosity [10]. The adsorbent material's surface chemistry is also vital, as surface functional groups like hydroxyl, carboxyl, or amine groups can interact with adsorbate molecules via hydrogen bonding, Van der Waals forces, or electrostatic interactions. The adsorbate molecule's size, shape, and polarity also play a significant role in determining adsorption behavior [11]. Conditions like pH, temperature, and adsorbate molecule concentration can impact the rate and capacity of adsorption. Increasing the temperature, for example, increases the adsorbate molecule's kinetic energy, leading at most cases to a higher rate of adsorption. When faced with the need to reduce treatment costs in competitive markets, accurately predicting pollutant removal and modeling treatment factors can offer economic benefits. Machine learning (ML) approaches, which can make complex decisions quickly, are particularly appealing in such scenarios. By employing ML models, researchers can enhance the efficiency and reliability of water pollutant treatment systems without needing to analyze intricate variables, thereby lowering experimental costs.

Artificial intelligence (AI) continues to evolve, with new techniques expected to emerge, and existing techniques set to become increasingly effective. This section will explore some widely used AI techniques, including their applications, strengths, and weaknesses, and address ethical considerations and challenges that arise when using AI in various domains.

3 Support Vector Machine

Support vector machine (SVM) is a commonly used technique in machine learning that employs supervised learning for both classification and regression tasks. Its main idea involves finding the best possible hyperplane that separates data points into their corresponding classes by maximizing the distance between the hyperplane and the

Fig. 1 SVM classification and hyperplane concept
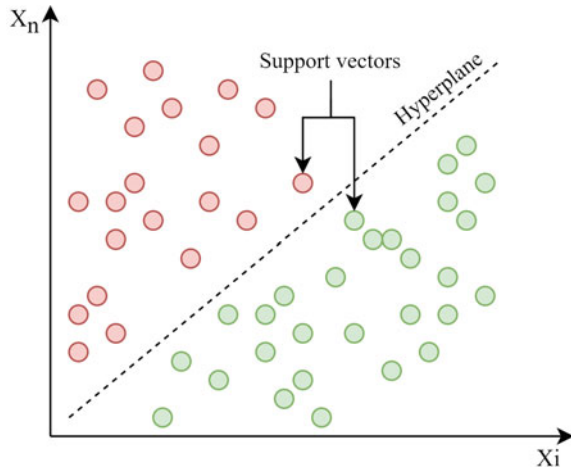
nearest data points on each side. In binary classification, a straight line is utilized as the hyperplane to distinguish the two classes (see Fig. 1). For multi-class classification, various approaches such as one-vs-all or one-vs-one are employed by SVM. By utilizing a kernel function, SVM transforms data points into a higher-dimensional space [12]. The kernel function is a mathematical function that calculates the dot product of two vectors without knowing their coordinates. This feature of SVM allows it to handle complex and nonlinear data distributions. After data points are transformed into the higher-dimensional space, SVM identifies the hyperplane that provides maximum margin between classes. Crucial to defining the hyperplane are support vectors, or the data points that are closest to it. SVM is capable of managing high-dimensional data and has less tendency to overfit compared to other classification methods. Despite its benefits, SVM can be sensitive to the choice of kernel function and hyperparameters, which necessitates thorough tuning. SVM has found applications in a variety of fields, including bioinformatics, image classification, and text classification.

3.1 K-Nearest Neighbor

K-Nearest Neighbors (KNN) is a machine learning technique that is commonly used for both classification and regression tasks. The idea behind KNN is that similar data points are typically located near each other in the feature space. To assign a label or value to a new data point, KNN finds the K nearest points and utilizes their labels or values to determine the label or value of the new point. The distance metric used to assess similarity can vary depending on the data and problem being solved [13]. KNN is a straightforward algorithm that can be executed quickly without the need for a training phase. However, it can be vulnerable to the choice of K and distance metric,

and it can face the curse of dimensionality when working with high-dimensional data.

KNN is a versatile approach that can be applied to various data types and problems. By adjusting the decision rule, KNN can also be utilized for clustering and outlier detection. However, the algorithm may be computationally challenging for larger datasets since it requires distance calculation between every pair of data points. Furthermore, KNN may be influenced by the data scaling, as the magnitude of prominent features can dominate the distance metric. Despite these limitations, KNN remains a prevalent and useful technique for data analysis and machine learning.

3.2 Decision Tree (DT)

Decision trees (DTs) are a widely used machine learning technique for both classification and regression tasks. Until a certain stopping criterion is reached, DTs are recursively partitioning the data into subsets based on specific features. This creates a tree-like structure that can be used for prediction by following the branches of the tree based on the input features. Decision trees are especially useful for analyzing data with a mixture of categorical and numerical features and can handle missing data and outliers effectively [14].

One of the benefits of decision trees is their interpretability, as the tree structure allows for easy visualization and understanding of the decision-making process. Decision trees can also provide insight into feature importance, which can help identify the most relevant features for prediction. However, decision trees are susceptible to overfitting, particularly when the tree is deep, or the number of features is high. This can be addressed through techniques such as pruning or using ensemble methods like Random Forest. Nevertheless, decision trees remain a valuable tool for machine learning and data analysis.

3.3 Random Forest

The Random Forest (RF) technique is a widely recognized machine learning method used for regression and classification purposes. It leverages a group of decision trees to achieve more reliable and accurate predictions. The technique is powerful because it constructs different decision trees, where each tree is trained using a distinct set of training data and attributes. The final forecast is made by averaging the predictions of all the trees for classification or averaging the projected output values for regression. One of the advantages of this approach is its capability to handle a vast number of features, as well as cope with missing data and anomalies. It also minimizes the risk of overfitting by decreasing the model's variance through the ensemble method, enhancing its generalization performance [15]. Additionally, this technique provides insight into the significance of features, aiding in the comprehension of data and

identifying critical features. This knowledge can be employed to improve model performance by concentrating only on the most important features.

3.4   Artificial Neural Network

Artificial neural network (ANN) was derived from biological neural network structural. Recently, it has grown in prominence, particularly for the modeling process. Currently, it has the potential to be a tool for process design, process analysis, and systems behavior prediction. An input layer (independent variables), several hidden layers, and an output layer (dependent variables) make up the basic ANN design. The input layer receives the input data, which is then processed through the hidden layers, with each layer extracting increasingly complex features from the input. The output layer produces the final prediction or classification. Each of these layers is made up of a number of linked processing units known as neurons [16]. Weighted connections between these neurons allow for the passage of data between them. Each neuron is linked to every other neuron at the level below it and the level above it, by adjusting the weights and biases of the neurons, the model's performance is tuned during the training phase. One of the benefits of ANNs is that they can discover complicated patterns and correlations in the data that conventional machine learning algorithms may struggle to understand [17]. ANNs can also handle noisy or incomplete data and can be trained on large datasets using parallel computing resources. However, ANNs can be computationally expensive to train, especially when dealing with large and complex networks. They can also be prone to overfitting, especially when the network is too large, or the training data is limited. Additionally, ANNs can be difficult to interpret, as the decision-making process of the network is not always transparent.

3.4.1   Deep Neural Network

Deep Neural Networks (DNNs) belong to a class of Artificial Neural Networks (ANNs) that excel at extracting complex patterns and relationships in vast datasets. Deep Neural Networks can have many layers of neurons, allowing them to discover the hierarchical combinations of the input data. At each successive layer, the output of the previous layer is nonlinearly transformed, enabling the network to learn increasingly abstract and complex features of the input data (Fig. 2). This unique ability to learn hierarchical representations makes Deep Neural Networks incredibly powerful in many tasks. Training a DNN involves adjusting the weights and biases of the neurons in the network to minimize a cost function that measures the difference between the network's predictions and its actual output. This is typically done using backpropagation, a mathematical algorithm that calculates the gradient of the cost function with respect to the weights and biases of the network. The gradient is then used to update the weights and biases to improve the network's predictions
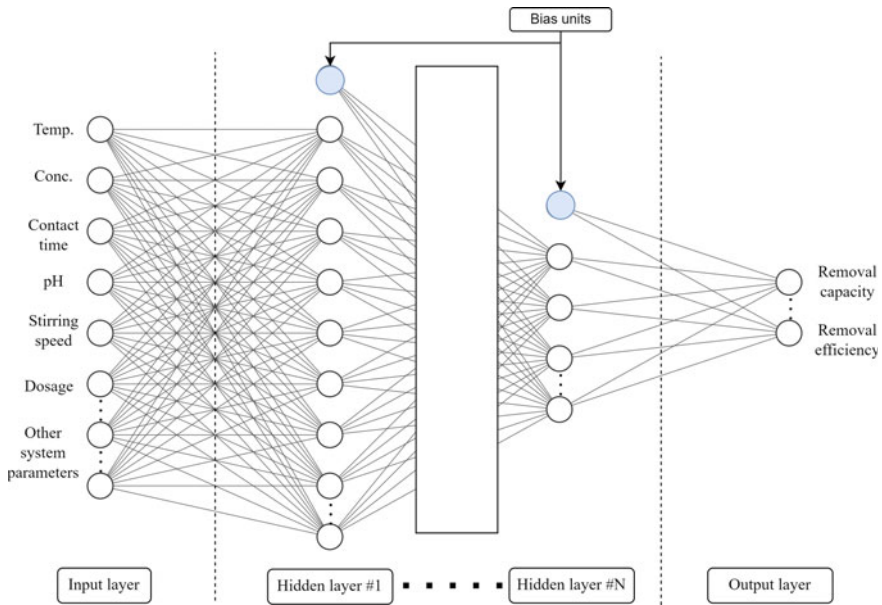
Fig. 2 ANN basic structure

based on the training data. In training DNNs, it is challenging to avoid overfitting, which occurs when the network learns to memorize the training data rather than generalize it to new data. Several techniques have been developed to address this issue, including dropout, early stopping, and regularization. DNNs have changed the machine learning landscape by producing industry-leading results across a broad variety of applications.

3.4.2 Adaptive Neuro-fuzzy Inference System

Adaptive Neuro-Fuzzy Inference System (ANFIS) is a hybrid AI method created by combining fuzzy logic with neural networks. It is designed to provide an adaptive and intelligent way of processing and analyzing data by incorporating the strengths of both fuzzy logic and neural network technology [18]. ANFIS consists of a set of fuzzy if–then rules that are learned from data using a combination of backpropagation and least squares methods. The input variables are first fuzzified, which means they are converted into fuzzy sets that represent the degree of membership of each value in the input variable. The fuzzy if–then rules are then generated based on the fuzzified inputs and the output variables [19]. Before mapping it to a neural network structure, the fuzzy rules are combined to form a fuzzy inference system. The neural network is trained using a combination of backpropagation and least squares methods, where the output of the fuzzy inference system is used as the target output. ANFIS can

handle complex and non-linear relationships in data and incorporate human expertise and domain knowledge into the system. Additionally, it can manage noisy and imperfect data and instantly adjust to changing situations. However, the requirements of a large amount of data for training still exist and it can be computationally expensive. Furthermore, the decision-making process may not be visible, and the system's interpretability may be constrained.

3.4.3 Recurrent Neural Networks

Rzecurrent Neural Networks (RNNs) are a class of artificial neural networks that are developed to handle sequential data, including time-series data or text. They can capture long-term dependencies and patterns in the input data. The key feature of RNNs is their ability to maintain a memory of previous inputs, which allows them to take into account the context of the current input. This memory is achieved through the use of "hidden" states, which are dynamically updated at each time step depending on the current input and the previously concealed state. The output of the RNN at each time step is a function of the current input and the current hidden state. In the training phase, RNNs still suffer from vanishing or exploding gradients. This can occur when the gradient signal that is propagated back through the network during training becomes too small or too large. Several techniques have been developed to address this issue, including gradient clipping and the use of specialized activation functions such as the long short-term memory (LSTM) and gated repeat recurrent unit (GRU) functions. Several fields have found usage for RNNs, including speech recognition, language translation, and image captioning. They have also been used to generate new text, music, and images and to model complex systems such as protein folding and climate dynamics.

3.5 Reinforcement Learning

Reinforcement learning (RL) is a type of machine learning based on an agent learning to make decisions based on feedback from its environment. RL is designed to make the agent to learn a policy that maximizes a reward signal over time. In real life, the agent interacts with the environment by taking action and receiving feedback in the form of a reward or punishment. The agent's objective is to maximize the cumulative reward over a sequence of actions. This requires the agent to learn a policy that maps the current state of the environment to the best action to take. RL algorithms typically use a value function to estimate the long-term reward of a given action in each state. The value function can be estimated through various methods, such as temporal difference learning, Monte Carlo methods, and Q-learning. RL still suffers from the exploration–exploitation tradeoff. The agent needs to balance between taking actions that it knows will yield a high reward (exploitation) and taking actions that may yield

a higher reward but are uncertain (exploration). RL has been successfully applied in a variety of domains, such as game-playing, navigation, and process control systems.

3.6 AI-Optimized Adsorption Process

The AI-Aided adsorption process involves data collection and cleaning to obtain relevant data for analysis. Feature engineering is then used to extract relevant features and prepare the data for modeling. Model selection is then done to select the best AI technique to use for modeling the adsorption process. Once the model is developed, metaheuristic algorithms, such as genetic algorithms, particle swarm optimization, or simulated annealing, can be used to optimize the adsorption process. Finally, model evaluation and assessment are carried out to ensure the model's accuracy and effectiveness in improving the adsorption process, as shown in Fig. 3. More details for each step are discussed in this section.
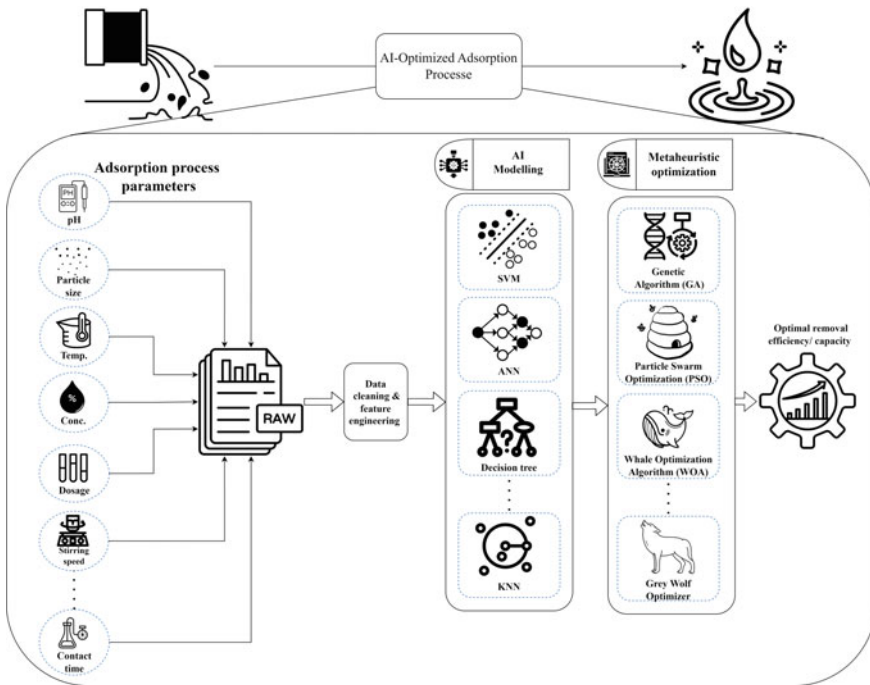
Fig. 3 AI-optimized adsorption process workflow

3.7   Data Collection and Cleaning

To develop an efficient AI-based model for water treatment optimization, it is crucial to carefully collect and clean the data. Firstly, the data requirements for the adsorption process should be defined, including the parameters that need to be measured, such as the adsorbent material properties, contaminant type and concentration, and process variables like pH, temperature, contact time, and mixing rate. Secondly, the data can be collected from experiments that are conducted in the laboratory using sensors automatically. The design of experiment (DoE) techniques are recommended to generate the experiment set. After data collection, cleaning is essential to remove any inconsistencies or errors by eliminating outliers, correcting mistakes, and filling in missing data. Finally, data preparation for modeling involves dividing the data into three sets for training, validation, and testing purposes. The training set is utilized to train the AI model, the validation set is used to refine the model, and the testing set is used to evaluate the performance of the model.

3.8   Feature Engineering

Feature engineering is a crucial step in the development of AI-based models for water treatment optimization with adsorption. It involves selecting the most relevant and informative features from the raw data and transforming and preparing them for input into the model [20]. Main steps involved in feature engineering can be described as follows:

Data cleaning: The first step in the feature engineering process is to clean the data. This involves removing any outliers or erroneous values and dealing with any missing data. The cleaned data is then prepared for further analysis. The process of feature selection is about identifying the most important and valuable features in a dataset. To accomplish this, various techniques can be used use such as statistical tests and domain knowledge. The features that have a strong relationship with the target variable and contribute significantly to the adsorption process should be chosen. Feature scaling is a technique for guaranteeing that all features are on the same scale. Techniques like normalization or standardization can be applied to this purpose. This helps to improve the model's performance by avoiding issues with variables that have vastly different ranges. Feature transformation: It is the process in which new features are extracted from existing ones. This improves the model's ability to capture non-linear relationships between variables. Polynomial expansion or logarithmic transformation is usually used in these scenarios. Feature encoding: Feature encoding is the process of converting categorical variables into numerical variables that can be used by the model. This can be done using techniques such as one-hot encoding or label encoding. Feature extraction: It is the process of reducing the dimensionality of the dataset by selecting a subset of relevant features. Principal component analysis (PCA) or linear discriminant analysis represents a viable option in this process.

3.9 Model Selection

After completing feature engineering, the subsequent step involves choosing a suitable AI model for optimizing water treatment with adsorption [21]. The methodology can be outlined as follows:

Problem type identification: The initial step in selecting an AI model involves identifying the problem type. The problem must be classified as either regression or classification. This categorization helps to narrow down the available model options.

Model family selection: Once the problem type is identified, the subsequent step is to choose a family of models that are appropriate for the problem at hand. For instance, linear regression, decision trees, or neural networks may be suitable for a regression problem. In contrast, logistic regression, decision trees, or support vector machines may be suitable for a problem that involves classification. The following step after selecting a model family is to assess its performance using a variety of measures, including precision, recall, accuracy, or mean squared error. Cross-validation can be employed to ensure that the performance is not biased by the training set. These metrics are further discussed in the next section.

Hyperparameter tuning: Once a set of candidate models is identified, hyperparameter tuning comes next. Hyperparameters control how the model learns and are set before training. Examples of hyperparameters include regularization, learning rate, and the number of layers in a neural network. Adjusting these parameters to find the best combination for optimal model performance constitutes hyperparameter tuning.

Final model selection: After evaluating candidate models and tuning their hyperparameters, the final step involves selecting the model that performs best. This model can then be utilized to optimize the water treatment process with adsorption.

3.10 Model Evaluation and Assessment

There are several evaluation metrics that can be used to assess the performance of an AI model for water treatment optimization with adsorption [22]. Some typical metrics are summarized in Table 1 and defined as follows:

Accuracy: This is the proportion of correct predictions out of all the predictions made by the model. It is a useful metric when the classes in the data are balanced. However, it can be misleading when the data is imbalanced.

Precision: This is the proportion of true positive (TP) predictions out of all positive predictions made by the model. It is statistically valuable when reducing false positives (FP) is the main objective, as it is when the expense of a false positive is considerable.

Recall: This is the proportion of true positive predictions out of all actual positive cases in the data. It is a useful metric when the focus is on minimizing false negatives (FN), such as in cases where missing a positive case is costly.

Table 1 Statistical metrics to evaluate the AI models

Accuracy metric	Equation
Correlation coefficient (R)	$\frac{\sum_{i=1}^{n} AB}{n\sigma_a \sigma_b}, A = a - \overline{a}, B = b - \overline{b}$
Coefficient of determination (R^2)	$(\frac{\sum_{i=1}^{n} AB}{n\sigma_a \sigma_b})^2$
Sum square of errors (SSE)	$(q_{exp} - q_{pre})^2$
Mean square error (MSE)	$\frac{1}{n} \sum_{i=1}^{n} (q_{exp} - q_{pre})^2$
Mean absolute error (MAE)	$\frac{1}{n} \sum_{i=1}^{n} |q_{exp} - q_{pre}|$
Root mean square error (RMSE)	$\sqrt{\frac{1}{n-2} \sum_{i=1}^{n} (q_{exp} - q_{pre})^2}$
Precision	$\frac{TP}{TP+FN}$
Recall	$\frac{TP}{TP+FN}$
F1-score	$\frac{2 \times Precision \times Recall}{Precision + Recall}$

The area under the Receiver Operating Characteristic Curve (ROC AUC): This is a measure of how well the model can distinguish between positive and negative cases. It plots the true positive rate against the false positive rate, and the area under the curve provides a single value that summarizes the model's performance.

F1-score: This is the harmonic mean of precision and recall and provides a balance between the two metrics. It is a statistically effective measure when both false positives and false negatives are significant.

Mean Squared Error (MSE): This is a measure of the average squared difference between the predicted values and the actual values. It is commonly used for regression problems and provides a measure of the model's accuracy. Root Mean Squared Error (RMSE): This is the square root of the MSE and provides a measure of the model's accuracy in the same units as the target variable. Mean Absolute Error (MAE): This metric measures the average absolute difference between expected and actual values. It is also commonly used for regression problems and provides a measure of the model's accuracy. The choice of evaluation metric will depend on the specific problem and the desired outcome. By carefully selecting and interpreting these metrics, it is possible to evaluate the performance of an AI model for water treatment optimization with adsorption and make informed decisions about model refinement and deployment.

4 Applications of AI-Enhanced Adsorption Processes

4.1 Dyes

Dyes are widely utilized in diverse industries like textiles, paper, and food production, and their waste discharged from industrial activities is a major contributor to water pollution. Because of their intricate molecular makeup, dyes are resistant to decomposition and can endure in the ecosystem for prolonged periods, presenting considerable health and environmental hazards [23]. The technique of adsorption, with its simplicity, effectiveness, and affordability, is widely adopted for eliminating dyes from wastewater. Many studies have examined different kinds of adsorbents for the removal of dyes from wastewater [24]. Activated carbon (AC) is one of the most effective adsorbents due to its large surface area and porous structure that allows for the effective absorption of dye molecules. Chitosan, zeolites, and clay minerals are additional materials that have been discovered to be efficient for dye removal [25].

4.2 Heavy Metals

One of the most harmful and long-lasting pollutants, heavy metals, is commonly discharged into the environment from industrial activities such as mining, electroplating, and battery production. These metals have the potential to cause significant health issues and ecological harm, and their removal from wastewater is a major environmental challenge [12].

In adsorption, the driving force behind the process is the attraction between the metal ions and the adsorbent surface. It is influenced by several conditions and parameters, including pH, temperature, and ionic strength. Multiple research studies have explored adsorption's potential in removing various heavy metals, including Lead, Zinc, Copper, Chromium, and Cadmium [26].

4.3 Organic Compounds, Nutrients, Pharmaceuticals, Drugs, and Pesticides

The presence of organic compounds, nutrients, pharmaceuticals, drugs, pesticides, and PCPs (Personal Care Products) in wastewater has become a significant environmental concern due to their potential adverse effects on human health and the environment. These pollutants are often resistant to conventional wastewater treatment techniques, and their removal has become a major challenge for environmental scientists and engineers [27]. Adsorption is a highly effective and widely used technique for the removal of these pollutants from the aqueous phase.

AI models can be used to maximize the removal efficiency and capacity of the adsorption process. This is accomplished by predicting the most effective adsorbent and the optimal conditions for adsorption such as pollutant initial concentration (IC), temperature, pH, stirring/mixing rate, contact time (CT), adsorbent dosage, pH, and the dosage of any additions. Several studies are collected to show the AI applications for the removal optimization as shown in Table 2.

5 Challenges and Future Research Directions

The use of AI in optimizing wastewater treatment through adsorption is still hampered by various constraints and challenges. This lack of accurate data leads to difficulties in building models that are precise enough. Another obstacle is the interpretability of AI models, particularly modern ones like Deep Neural Networks which are often opaque and prevent understanding of how the models arrive at their predictions, limiting the scope for enhancements. With the increasing amount of data produced by water treatment plants, scalable AI models capable of handling large datasets in real-time are becoming more critical, wide-scale variations particularly in operating conditions such as water quality, temperature, and pH necessitate that AI models should be resilient and general.

Data quality is another important factor to consider, as incomplete, inaccurate, or inconsistent data can have adverse effects on the performance of AI models. Hence, it is essential to have reliable data validation and cleaning processes when using data to train AI models. The integration of AI models with water treatment plant systems like data management systems, control systems, and sensors is a challenging task that requires close collaboration between water treatment professionals and AI experts. Employing state-of-the-art Internet of Things (IoT) protocols to organize the sensors transmission can be helpful in this case [38]. Additionally, AI optimization of the adsorption process in water treatment has the potential to increase energy consumption, making it essential to explore developing AI models that optimize the process while minimizing energy usage. Similarly, the cost of implementing AI models in water treatment can be high, especially for smaller plants. As such, exploring cost-effective AI solutions or finding ways to integrate AI models with existing systems can help to mitigate costs.

Collaborative research involving water treatment experts, AI professionals, and other stakeholders can help address these challenges and identify new opportunities for innovation in optimizing water treatment through adsorption. Furthermore, future directions for AI in water treatment could include developing explainable AI models that offer insight into the decision-making process, utilizing reinforcement learning to optimize adsorption processes in real-time, and creating AI models capable of predicting and preventing equipment failures. Despite the obstacles in applying AI models to enhance water treatment with adsorption, there are promising opportunities for progress and innovation. By overcoming these obstacles and pursuing novel AI-based solutions for water treatment, we can achieve more streamlined and robust

Table 2 Comparison of the AI modeling techniques for different pollutants adsorption and their corresponding accuracy

Pollutant	Adsorbent	Modelling technique	Input variables	Output variable	Evaluation	References
Cr (VI)	Algae–derived biochar	ANN	Conc., contact time	Removal efficiency	RMSE = 1.832, R^2 = 0.989	[28]
Copper ions	Attapulgite clay	ANN, SVM, RF	IC, dose, CT, pH, addition of NaNO$_3$	Removal efficiency	RMSE = 0.9283, R^2 = 0.9974	[29]
MB	Nano zero–valent aluminum (nZVAl)	ANN	Residence time, IC, temperature, pH, stirring rate, nZVI dosage, the concentration of two detergents (Ariel and Vanish), and the concentration of three salts: NaCl, Na$_2$CO$_3$, and Na$_2$SO$_4$	Removal efficiency	R^2 = 0.97	[30]
MB	Calcium alginate hydrogels reinforced with cellulose nanocrystals (CA/CNC)	ANN	IC, CT, shaking rate	Adsorption capacity	RMSE = 0.758, R^2 = 0.999	[31]
MO	Activated carbon made from date seeds (DPAC)	ANN	Adsorbent dosage, IC, pH, CT	Removal efficiency	RMSE = 0.0172, R^2 = 0.9971	[32]
Ammonia–nitrogen (A–N)	Waste crab shells (CS)	ANN, ANFIS	pH, dosage, IC, CT, temperature	Removal efficiency	R^2_{ANFIS} = 0.9998, R^2_{ANN} = 0.9025	[33]
MB	Residual agricultural biomass	RF, ANN	Temperature, pH, adsorbent dosage	Removal capacity	RMSE = 0.0007, R^2 = 0.991	[15]

(continued)

Table 2 (continued)

Pollutant	Adsorbent	Modelling technique	Input variables	Output variable	Evaluation	References
Arsenate [As(V)]	Metal organic frameworks (MOFs)	DT, RF	Dosage, CT, IC, surface area, temperature, pH, and the presence of anions	Removal efficiency	$R^2_{RF} =$ 0.9799, $R^2_{DT} =$ 0.9812, $RMSE_{RF} =$ 3.3845, $RMSE_{DT} =$ 2.9137	[34]
MB	Ultrasound-modified chitin (UM-chitin)	ANN	Initial concentration, temperature	Capacity	MSE = 0.0003 and R^2 = 0.9995	[35]
MB	Activated spent tea (AST)	ANN	Contact time, adsorbent dosage, initial dye concentration, temperature, and pH	Efficiency	R^2 = 0.999	[36]
CV	ZnO-NR-AC	ANN	Sonication time, adsorbent doses, pH, and initial	Capacity	RMSE = 0.0007, R^2 = 0.991	[37]

processes that deliver safe and trustworthy drinking water to communities across the globe. A summary of the challenges with their corresponding severity and proposed solutions discussed in this section is provided in Table 3.

6 Conclusion

In conclusion, this study has evaluated the current research on AI-aided adsorption processes for efficient wastewater pollutant removal. The results show that AI-aided adsorption processes have substantial potential in improving wastewater treatment efficiency and efficacy when used with various adsorbents. The study has also highlighted several challenges and limitations of AI-aided adsorption processes, such as inadequate data and the requirement for further research to optimize process parameters. Nonetheless, the use of AI-aided adsorption processes in wastewater treatment is expanding rapidly across industries such as petrochemical, pharmaceutical, and textile. These processes have exhibited better pollutant removal rates and lower operational expenses in comparison to traditional methods, which can significantly reduce environmental pollution and safeguard public health. The study suggests that reinforcement learning can be used to achieve context-aware systems in wastewater treatment applications. The scalability of AI-aided adsorption processes enables their deployment in diverse geographical areas, from densely populated urban centers to rural communities. This flexibility allows for tailored solutions that address specific regional challenges, optimizing resource utilization and minimizing the environmental footprint of wastewater treatment systems. Future Collaborative research between water treatment professionals, AI experts may focus on developing more cost-effective and scalable AI systems, optimizing process parameters, and assessing the long-term effectiveness of AI-aided adsorption processes under real-world conditions. In summary, the study concludes that AI-aided adsorption processes could revolutionize wastewater treatment and pollution control and could have a crucial role in achieving sustainable development goals.

7 Recommendations

Future research efforts should focus on addressing the existing challenges and limitations of AI-aided adsorption processes. This includes addressing issues related to the availability of adequate data for model training, optimizing process parameters, and developing context-aware systems. Continued research and innovation in these areas will contribute to further improving the efficiency and effectiveness of AI-aided adsorption processes.

Policymakers and decision makers should recognize the potential of AI-aided adsorption processes in wastewater treatment and actively support their implementation. This can be achieved by establishing supportive regulatory frameworks,

Table 3 Challenges facing deployment of AI models in the adsorption process and the proposed ways to tackle them

Challenge	Definition	Severity	Proposed solution
Lack of data	The availability of data for modeling is limited, and this can affect the accuracy and reliability of the model	High	Data augmentation techniques, such as generating synthetic data or transferring knowledge from similar processes
Data quality	Data can be incomplete, inaccurate, or inconsistent, which can affect the performance of AI models	High	Data validation and cleaning processes to ensure that the data used to train AI models is reliable
Model interpretability	Black-box models, such as deep learning models, can be difficult to interpret, limiting their practical application	Low	Collaborative research between water treatment professionals, AI experts
Scalability of deployment	The adsorption process in wastewater treatment plants involves large volumes of wastewater, and it can be challenging to scale AI models to handle such volumes	High	Developing distributed computing architectures to handle large volumes of data and provide real-time predictions. Using cloud-based solutions for scalability and ease of deployment. Developing models that can run on low-power edge devices for real-time monitoring and control
Model generalization	There is no general model for all types of adsorbents and pollutants. Each adsorbent material and type of pollutant has unique properties that can affect the adsorption process	High	Using transfer learning techniques to adapt models from similar systems. Incorporating experimental data to improve the accuracy of the models
Robustness	AI models need to be robust to different operating conditions and variations in input data to be reliable in practical applications	Medium to high	Developing models that can adapt to changing conditions and incorporating uncertainty analysis to quantify the model's reliability
Integration with existing systems	AI models need to be integrated with existing water treatment plant systems, such as control systems, sensors, and data management systems	Medium	Close collaboration between water treatment professionals and AI experts

providing incentives for the adoption of AI technologies, and promoting collaboration between water treatment professionals, AI experts, and relevant stakeholders.

Stakeholders, including industries and wastewater treatment facilities, should consider integrating AI-aided adsorption processes into their existing infrastructure. Pilot projects and feasibility studies can be conducted to assess the suitability and benefits of implementing AI technologies in different contexts. Sharing best practices and lessons learned can further facilitate the adoption of these processes on a larger scale.

International collaboration and knowledge-sharing platforms should be established to promote the exchange of expertise, data, and technological advancements in AI-aided adsorption processes. This will enable countries and regions to learn from each other's experiences, accelerate progress, and address water pollution challenges collectively.

Long-term monitoring and assessment of the performance and effectiveness of AI-aided adsorption processes under real-world conditions are essential. This will help ensure the reliability, sustainability, and long-term benefits of these technologies, enabling decision makers and stakeholders to make informed choices regarding their implementation.

By following these recommendations, future studies can continue to advance the field of AI-aided adsorption processes, while policy planners, decision makers, and stakeholders can actively contribute to the adoption and integration of these technologies in wastewater treatment practices. Together, these efforts will support the achievement of sustainable development goals related to water quality, environmental preservation, and public health.

References

1. Marni Sandid A, Bassyouni M, Nehari D, Elhenawy Y (2021) Experimental and simulation study of multichannel air gap membrane distillation process with two types of solar collectors. Energy Convers Manag 243:114431. https://doi.org/10.1016/j.enconman.2021.114431
2. Alam G, Ihsanullah I, Naushad M, Sillanpää M (2022) Applications of artificial intelligence in water treatment for optimization and automation of adsorption processes: recent advances and prospects. Chem Eng J 427:130011. https://doi.org/10.1016/j.cej.2021.130011
3. Momina AK (2023) Feasibility of the adsorption as a process for its large scale adoption across industries for the treatment of wastewater: research gaps and economic assessment. J Clean Prod 388:136014. https://doi.org/10.1016/j.jclepro.2023.136014
4. Zoromba MS, Ismail MIM, Bassyouni M, Abdel-Aziz MH, Salah N, Alshahrie A, Memic A (2017) Fabrication and characterization of poly (aniline-co-o-anthranilic acid)/magnetite nanocomposites and their application in wastewater treatment. Colloids Surf A Physicochem Eng Asp 520:121–130. https://doi.org/10.1016/j.colsurfa.2017.01.075

5. Bassyouni M, Zoromba MS, Abdel-Aziz MH, Mosly I (2022) Extraction of nanocellulose for eco-friendly biocomposite adsorbent for wastewater treatment. Polymers (Basel) 14. https://doi.org/10.3390/polym14091852

6. Solayman HM, Hossen MdA, Abd Aziz A, Yahya NY, Leong KH, Sim LC, Monir MU, Zoh K-D (2023) Performance evaluation of dye wastewater treatment technologies: a review. J Environ Chem Eng 11:109610. https://doi.org/10.1016/j.jece.2023.109610

7. Aghilesh K, Kumar A, Agarwal DS, Garg M, Joshi H (2021) Use of artificial intelligence for optimizing biosorption of textile wastewater using agricultural waste. Environ Technol 44:1–35. https://doi.org/10.1080/09593330.2021.1961874

8. Abdel-Aziz MH, Bassyouni M, Soliman M, Gutub S, Magram S (2017) Removal of copper from wastewater using thermally treated sewage sludge adsorbent without chemical activation. J Mater Environ Sci 21:1–10

9. Eteba A, Bassyouni, Saleh (2022) Utilization of chemically modified coal fly ash as cost-effective adsorbent for removal of hazardous organic wastes. Int J Environ Sci Technol 3. https://doi.org/10.1007/s13762-022-04457-5

10. Abdel-Aziz MH, El-Ashtoukhy EZ, Bassyouni M, Al-Hossainy AF, Fawzy EM, Abdel-Hamid SMS, Zoromba MS (2021) DFT and experimental study on adsorption of dyes on activated carbon prepared from apple leaves. Carbon Lett 31:863–878. https://doi.org/10.1007/s42823-020-00187-1

11. Gutub S, Bassyouni M, Hamid S (2013) Dissolved solids adsorption of freshwater using synthesized bio-foam composite. Life Sci J 10:464–471

12. González Costa JJ, Reigosa MJ, Matías JM, Covelo EF (2017) Soil Cd, Cr, Cu, Ni, Pb and Zn sorption and retention models using SVM: variable selection and competitive model. Sci Total Environ 593–594:508–522. https://doi.org/10.1016/j.scitotenv.2017.03.195

13. Kuhn M, Johnson K et al (2013) Applied predictive modeling. Springer

14. Burkov A (2019) The hundred-page machine learning book. Andriy Burkov, Quebec City, QC, Canada

15. De Miranda Ramos Soares AP, De Oliveira Carvalho F, De Farias Silva CE, Da Silva Gonçalves AH, De Souza Abud AK (2020) Random Forest as a promising application to predict basic-dye biosorption process using orange waste. J Environ Chem Eng 8. https://doi.org/10.1016/j.jece.2020.103952

16. Shojaeimehr T, Rahimpour F, Khadivi MA, Sadeghi M (2014) A modeling study by response surface methodology (RSM) and artificial neural network (ANN) on Cu^{2+} adsorption optimization using light expanded clay aggregate (LECA). J Ind Eng Chem 20:870–880. https://doi.org/10.1016/j.jiec.2013.06.017

17. Jadhav A, Pathak P, Raut R (2023) Water and wastewater quality prediction: current trends and challenges in the implementation of artificial neural network. Environ Monit Assess 195. https://doi.org/10.1007/s10661-022-10904-0

18. Buckley JJ, Yoichi H (1995) Neural nets for fuzzy systems. Fuzzy Sets Syst 71:265–276

19. Onu CE, Nwabanne JT, Ohale PE, Asadu CO (2021) Comparative analysis of RSM, ANN and ANFIS and the mechanistic modeling in eriochrome black-T dye adsorption using modified clay. S Afr J Chem Eng 36:24–42. https://doi.org/10.1016/j.sajce.2020.12.003

20. Wang Z, Xia L, Yuan H, Srinivasan RS, Song X (2022) Principles, research status, and prospects of feature engineering for data-driven building energy prediction: a comprehensive review. J Build Eng 58:105028. https://doi.org/10.1016/j.jobe.2022.105028

21. Cruz YJ, Rivas M, Quiza R, Haber RE, Castaño F, Villalonga A (2022) A two-step machine learning approach for dynamic model selection: a case study on a micro milling process. Comput Ind 143:103764. https://doi.org/10.1016/j.compind.2022.103764

22. Aydın Temel F, Cagcag Yolcu O, Turan NG (2023) Artificial intelligence and machine learning approaches in composting process: a review. Bioresour Technol 370. https://doi.org/10.1016/j.biortech.2022.128539

23. Eteba A, Bassyouni M, Saleh M (2022) Modified coal fly ash for textile dye removal from industrial wastewater. Energy Environ. 0958305X2211305. https://doi.org/10.1177/0958305X221130536

24. Jagadeesh N, Sundaram B (2023) Adsorption of pollutants from wastewater by biochar: a review. J Hazard Mater Adv 9:100226. https://doi.org/10.1016/j.hazadv.2022.100226
25. Taoufik N, Boumya W, Elmoubarki R, Elhalil A, Achak M, Abdennouri M, Barka N (2022) Experimental design, machine learning approaches for the optimization and modeling of caffeine adsorption. Mater Today Chem 23:100732. https://doi.org/10.1016/j.mtchem.2021.100732
26. Lemessa G, Gabbiye N, Alemayehu E (2023) Waste to resource: utilization of waste bagasse as an alternative adsorbent to remove heavy metals from wastewaters in sub-Saharan Africa: a review. Water Pract Technol 18:393–407. https://doi.org/10.2166/wpt.2023.011
27. Başer B, Yousaf B, Yetis U, Abbas Q, Kwon EE, Wang S, Bolan NS, Rinklebe J (2021) Formation of nitrogen functionalities in biochar materials and their role in the mitigation of hazardous emerging organic pollutants from wastewater. J Hazard Mater 416:126131
28. Khan AA, Naqvi SR, Ali I, Arshad M, AlMohamadi H, Sikandar U (2023) Algal-derived biochar as an efficient adsorbent for removal of Cr (VI) in textile industry wastewater: non-linear isotherm, kinetics and ANN studies. Chemosphere 316:137826. https://doi.org/10.1016/j.chemosphere.2023.137826
29. Bhagat SK, Pyrgaki K, Salih SQ, Tiyasha T, Beyaztas U, Shahid S, Yaseen ZM (2021) Prediction of copper ions adsorption by attapulgite adsorbent using tuned-artificial intelligence model. Chemosphere 276. https://doi.org/10.1016/j.chemosphere.2021.130162
30. Sadek AH, Mostafa MK (2023) Preparation of nano zero-valent aluminum for one-step removal of methylene blue from aqueous solutions: cost analysis for scaling-up and artificial intelligence. Appl Water Sci 13:34. https://doi.org/10.1007/s13201-022-01837-7
31. Soleimani S, Heydari A, Fattahi M, Motamedisade A (2023) Calcium alginate hydrogels reinforced with cellulose nanocrystals for methylene blue adsorption: synthesis, characterization, and modelling. Ind Crops Prod 192:115999. https://doi.org/10.1016/j.indcrop.2022.115999
32. Alardhi SM, Fiyadh SS, Salman AD, Adelikhah M (2023) Prediction of methyl orange dye (MO) adsorption using activated carbon with an artificial neural network optimization modeling. Heliyon 9. https://doi.org/10.1016/j.heliyon.2023.e12888
33. Ohale PE, Onu CE, Nwabanne JT, Aniagor CO, Okey-Onyesolu CF, Ohale NJ (2022) A comparative optimization and modeling of ammonia–nitrogen adsorption from abattoir wastewater using a novel iron-functionalized crab shell. Appl Water Sci 12. https://doi.org/10.1007/s13201-022-01713-4
34. Abdi J, Mazloom G (2022) Machine learning approaches for predicting arsenic adsorption from water using porous metal–organic frameworks. Sci Rep 12. https://doi.org/10.1038/s41598-022-20762-y
35. Pauletto PS, Dotto GL, Salau NPG (2020) Optimal artificial neural network design for simultaneous modeling of multicomponent adsorption. J Mol Liq 320:114418. https://doi.org/10.1016/j.molliq.2020.114418
36. Babaei AA, Khataee A, Ahmadpour E, Sheydaei M, Kakavandi B, Alaee Z (2016) Optimization of cationic dye adsorption on activated spent tea: equilibrium, kinetics, thermodynamic and artificial neural network modeling. Korean J Chem Eng 33:1352–1361
37. Dil EA, Ghaedi M, Ghaedi A, Asfaram A, Jamshidi M, Purkait MK (2016) Application of artificial neural network and response surface methodology for the removal of crystal violet by zinc oxide nanorods loaded on activate carbon: kinetics and equilibrium study. J Taiwan Inst Chem Eng 59:210–220. https://doi.org/10.1016/j.jtice.2015.07.023
38. Mansour M, Gamal A, Ahmed AI, Said LA, Elbaz A, Herencsar N, Soltan A (2023) Internet of Things: a comprehensive overview on protocols, architectures, technologies, simulation tools, and future directions. Energies (Basel) 16:3465. https://doi.org/10.3390/en16083465

A Critical Review of Sustainable Biodegradable Polymeric Reverse Osmosis Membranes

Check for updates

Kareem Fouad, Yasser Elhenawy, Medhat A. El-Hadek, and M. Bassyouni

1 Introduction

Clean water and sanitation are major Sustainable Development Goals (SDGs). Therefore, the search for multiple sources to obtain fresh water is a matter of interest to many researchers [1]. The shortage of freshwater and the significant increase of pollutants in natural water resources portend disasters for the coming decades [2–6]. Water desalination stands as a desirable procedure to provide freshwater to districts

K. Fouad
Civil Engineering Department, Higher Future Institute of Engineering and Technology, El Mansoura, Egypt

Y. Elhenawy
School of Chemical and Metallurgical Engineering, University of the Witwatersrand, Johannesburg, South Africa

Department of Mechanical Power Engineering, Faculty of Engineering, Port Said University, Port Said 42526, Egypt

Y. Elhenawy
e-mail: yasser.elhenawy@wits.ac.za

M. A. El-Hadek
Production Engineering and Mechanical Engineering Department, Faculty of Engineering, Port Said University, Port Said 42526, Egypt
e-mail: melhadek@eng.psu.edu.eg

M. A. El-Hadek · M. Bassyouni (✉)
East Port Said University of Technology, North Sinai, Port Said 45632, Egypt
e-mail: m.bassyouni@eng.psu.edu.eg

M. Bassyouni
Department of Chemical Engineering, Faculty of Engineering, Port Said University, Port Said 42526, Egypt

Center of Excellence in Membrane-Based Water Desalination Technology for Testing and Characterization, Port Said University, Port Said, Port Said 42526, Egypt

for various uses. Reverse osmosis (RO) is a pressure-driven membrane separation process that has been broadly utilized for handling saline water. It is also considered a highly effective desalination procedure for freshwater production. RO has many benefits as it requires a small footprint, flexible design, automatic process control, and a lower produced water cost. Figure 1 shows a schematic diagram of the RO process. As shown, a semi-permeable reverse osmosis membrane separates two solutions with different TDS concentrations. At present, RO systems represent about 93% of the total market of desalination plant installations and produce about 60% of the total desalinated water. In contrast, it is unable to manage highly concentrated brines due to physical restrictions forced by significant osmotic pressure. Furthermore, only 50% of freshwater could be recovered with a significant amount of highly concentrated brine as a byproduct. The discharge of by-products to the surrounding environment poses a clear danger to the ecosystem and existing organisms [7–12]. To reduce brine volume, several utilities aim to boost RO water recovery to > 95%. Achieving zero liquid discharge (ZLD) can diminish the cost of the RO procedure by avoiding the need to drain highly saline water from the desalination process [13]. The properties of semi-permeable polymers are the bases of reverse osmosis membranes. They have significant water permeability and low dissolved substances permeability. The existing water in the feed tank is pushed to pass via the membrane by providing a pressure difference across it.

The feed pressure needed to be high to get over the feed side osmotic pressure. Typically, the range in seawater desalination is between 55 and 68 bar. Operational pressures for brackish water purification are lower because of decreased osmotic pressure caused by the lower salinity of the feed water [14, 15]. As shown in Fig. 2, a pretreatment is employed on seawater before transferring it to the RO membrane. The resultant freshwater is utilized for post-treatment before its final delivery. However, the resultant brine was employed for post-treatment before its final disposal.

Fig. 1 Reverse osmosis schematic diagram
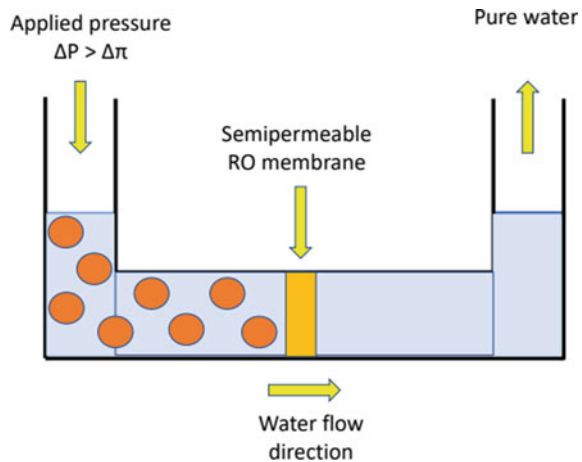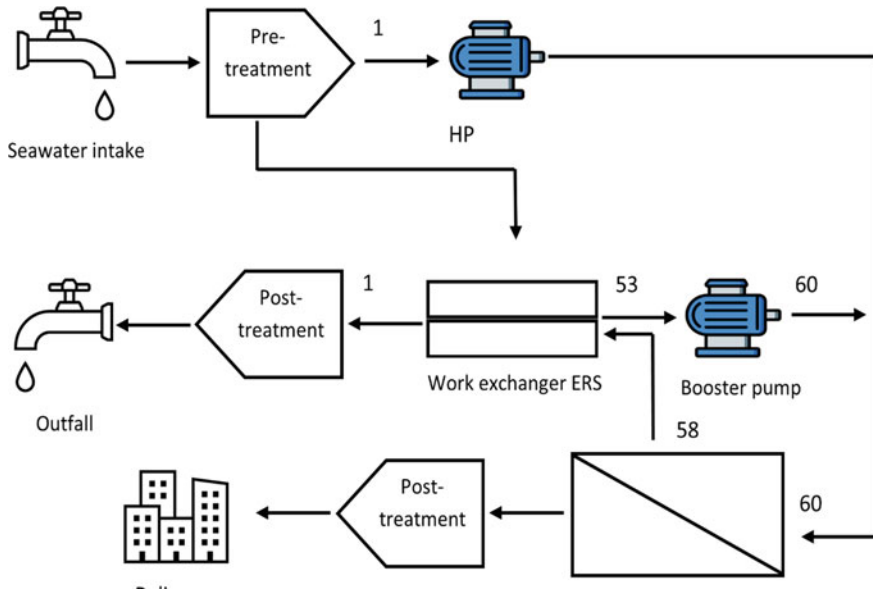
Fig. 2 Reverse osmosis desalination plant

As aforementioned, a standard RO procedure involves four main procedures: Pretreatment, high-pressure pumping, salt separation, and post-treatment [16]. Reverse osmosis technology has been developed to desalinate seawater or brackish water. In general, brackish water RO membranes require less operating pressure, have superior water productivity (permeate) flux, and reject less salt (owing to the minor osmotic pressures of fewer saline waters). The RO membrane employed operating pressure is utilized to reverse the solvent flow direction. The feed water leaves minerals and salts when passes through the membrane and is produced as purified water. This mechanism happens when the employed pressure exceeds the osmotic pressure ($\Delta P > \Delta \pi$). Salt rejection and water flux are the two constraints ruling the operation of the RO membrane [17] (1).

$$J = A(\Delta P - \Delta \pi) \tag{1}$$

where J is the water flux, $\Delta \pi$ is the variance of the osmotic pressure difference among the permeate water and feed water, Δp is the transmembrane pressure (TMP) difference, and A is an inherent coefficient of water permeability that illustrates the membrane

The first large-scale desalination RO plant was in Kuwait then desalination using RO membranes entered the desalination market at the end of the 1960s [18]. Based on the superiority of the input processed, there are two categories of RO processes: brackish water RO plants (BWRO), in which the salinity is between 500 and 10,000 mg/L, and seawater RO plants (SWRO), where the salinity is about

30,000 mg/L. RO efficiency depends on various parameters such as the characteristics of water feed, operational parameters, and membrane features [19].

1.1 Limitations Associated with the Reverse Osmosis Process

Reverse osmosis requires a significant amount of energy to operate. The process involves pushing water through a semi-permeable membrane against its natural flow, which requires a significant amount of pressure. This pressure must be generated by pumps, which consume a lot of energy. Over time, the membrane used in reverse osmosis can become fouled or clogged by impurities, which can reduce its effectiveness and require replacement. This can be costly and time-consuming. The initial capital costs associated with building a reverse osmosis plant can be high. This is because the process requires specialized equipment, such as pumps, membrane modules, and control systems. While reverse osmosis is effective at removing many types of contaminants, it is less effective at removing some contaminants, such as volatile organic compounds (VOCs) and certain types of bacteria and viruses. Reverse osmosis produces a significant amount of brine, which is a concentrated solution of salts and other impurities that must be disposed of properly. Disposal of brine can be challenging and expensive, particularly in areas where water resources are already scarce.

1.1.1 Fouling

Membrane fouling is a substantial obstacle to the long-term operation of the desalination system. Fouling resistance is needed to be improved for the desalination process and to improve energy efficiency [20, 21]. Surface modification has been used to develop fouling-resistant RO membranes by enhancing hydrophilicity, reducing surface roughness, and lowering concentration polarization at the membrane's surface. One of the major struggles for membrane manufacturers is still establishing a fouling-resistant membrane, although it is hoped that more creative approaches to reduce membrane fouling will be discovered in the future [22]. According to the aforementioned "fouling-resistant mechanism," there are the following modifying for anti-fouling [23]: (1) designing innovative membranes with specialized features, (2) hydrophilic substances including PVA, PEI, and zwitterionic polymer may be applied as a surface coating or graft to the RO membrane's PA selective layer, (3) integrating PA selective layer with hydrophilic organic or inorganic nanostructured materials. Figure 3 shows an aschematic diagram for parameters affecting RO fouling.
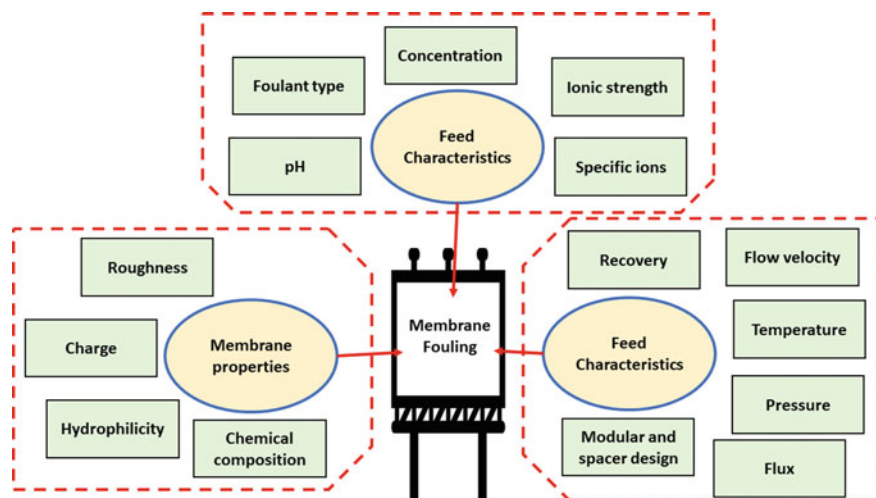
Fig. 3 RO fouling parameters diagram

1.1.2 Chlorination

Understanding the basic principles of chlorination is crucial for the improvement of RO membranes that are further unaffected by chlorine. Depending on the environmental conditions, chlorine gas (Cl_2) in water can produce hypochlorite ion (OCl^-) and hypochlorous acid ($HOCl$), which are able then to produce extra chlorine species [24]. For TFC RO membranes, amides placed on polyamide connections can be attacked by chlorine. Amidic nitrogen is first N-chlorinated, and then chlorine is replaced on an aromatic ring connected to amidic nitrogen via an intermolecular rearrangement, altering the thin-layer structure of the polyamide membrane and lowering membrane performance. Consideration of the drop in salt rejection and the decrease or rise in water flux in the RO operation may aid in highlighting this efficiency drop [25].

1.1.3 Brine Disposal

Even though desalination produces freshwater, the brine that is also produced during the process is a major environmental concern. Many different methods are used to dispose of brine in the environment, involving surface water flow, evaporation ponds, sewage flow, deep-well injection, and land purposes. Brine could include hazardous pretreatment chemicals, organic materials, and heavy metals in addition to its extreme salinity [26]. Brine waste fluid from the desalination process also contains a significant percentage of salt and heavy metals, such as As, Cd, Cu, Pb, U, Hg, Ni, and Cr [27]. Pretreatment technologies for seawater include the following [28]:

Table 1 Brine disposal methods [30]

Brine disposal method	Limitations and drawbacks
Deep well injection	Groundwater contamination and earthquake triggering
Evaporation ponds	Due to the high cost of land acquisition, capital costs are significant. Poor environmental impact, such as the poisoning of subsurface aquifers due to leakage issues, and difficulties for breeding and migrating birds
Land application	Soil salinization if the process is employed on a wide scale crop production
Sewer discharge	Reduce the performance of biological treatment processes when there is a considerable amount of brine
Zero liquid discharges	Capital costs are high. The initial and ongoing costs of these can sometimes outweigh the cost of the desalination unit
Seawater surface discharge	Marine contamination as a result of improper dilution
Seawater submerged discharge	Because of its excellent dilution capabilities, it is useful. Diffusers must be properly designed to achieve high dilution

- Chlorination
- Lime treatment
- Scale inhibitor
- Cartridge filtration
- pH control
- Alkalinity reduction
- UV radiation
- Clarification with flocculation

The method of brine disposal chosen mostly depends on the site; for example, all seawater desalination uses discharge into the sea, while inland desalination plants typically employ deep good injection. When choosing disposal technology, factors like quality and volume are just as significant as the location. Additionally, the price of brine disposal is taken into account, particularly in developing nations [29]. Table 1 shows the methods for brine disposal and its limitations.

1.1.4 Boron Removal

A crucial trace portion for organisms is boron. Boron intensity in saltwater is about 5 mg/L. Extreme boron consumption can also inhibit plant growth in addition to harming animal reproductive systems. Recently, numerous countries and governments have recognized standards for boron that should be present in water used for irrigation and drinking which must not exceed 0.5 mg/L. Hence, it is crucial to ensure

that the seawater desalination process uses RO membranes with a boron retention rate of at least 90%. Because of the electric neutrality and tiny molecular size of boric acid, which is the predominant form of boron compounds in the marine environment, TFC RO membranes struggle to retain boron (about 80–85%) [31]. Boron, in the condition of the negatively charged borate ion $B(OH)_4$, is removed easily by RO membranes in the same way as other dissolved ionic compounds are. Nevertheless, removing non-dissociated neutrally charged boric acid in saltwater by RO is problematic. Reported rejection rates vary depending on the membrane [32].

2 Reverse Osmosis Membranes

Among the viable methods for providing freshwater in dried and semi-dried environments is membrane-based seawater desalination. A broad variety of membranes were developed for the handling of seawater. Also, the generation of freshwater from varying salinities of feed water. Nanofiltration (NF), reverse osmosis (RO), and membrane distillation are now the utmost widely operated membrane methods for treating saline water (MD). Because it is reliable, has an extraordinary water recovery level, rejection salt rate, and can handle a wider variety of seawater concentrations, the RO procedure differs from other technologies in that it has several benefits that make it a desirable method for seawater desalination [33].

2.1 Membrane Modules

There are four types of RO desalination membranes: (1) tubular membranes, (2) spiral wound membranes, (3) plate, and frame membranes, and (4) hollow fiber membranes. To ensure process compactness, simplicity of membrane installment, washing, and substitution, as well as minimal capital costs, RO membrane modules for industrial applications must have a significant packing density. That allows a considerable membrane area to be arranged into a quite minor volume [19].

2.1.1 Frame and Plate Modules

One of the basic RO membrane modules is plate and frame modules. In such modules, a stiff plate constructed of solid plastic, reinforced porous paper, or porous fiberglass is linked to the two sides by a flat sheet RO membrane. Multiple plates are employed, which are placed inside a pressurized support structure. These plates have channels with grooves that function as a conduit for permeate flow. Water molecules pass through the membrane in which the feed solution crosses the unit from one end and are gathered as a filtered solution in a central permeate collection manifold. The module's opposite end is where the brine or concentrate solution exits. Due to

their laborious design and fabrication, frame and plate modules have poor packing density and are pricey. These modules also have dead zones inside of them, which sorts them vulnerable to fouling. However, the modules' ease of cleaning makes them appropriate for feed streams with an elevated proportion of suspended material [19].

2.1.2 Tubular Modules

The most straightforward reverse osmosis module is made of tubular modules. It has an interior diameter of 1/8 to 1 in (0.32–2.54 cm) porous tube, which is constructed of carbon, ceramic, or porous plastic. Moreover, the membrane is put into or glazed on the exterior of the tube. Usually, a module is created by joining many tubes in parallel or series. This resulted in water seeping across the porous tube, in which membrane as pressure feedwater is delivered into the module before collecting outdoors. However, the rejected stream leaves the tube at the opposite end. Tubular modules were widely used in the 1960s for chemical food and pharmaceutical separation and processing. However, because of their low packing density (approximately 100 ft^2/ft^3 or 328 m^2/ m^3), these units were not practical for usage on a large scale. Despite being still commercially available, tubular designs are typically exclusively utilized for high-end, low-volume purposes. A main benefit is that they would be utilized to clean up an incredibly turbid feed stream. Furthermore, tubular units maintain turbulence using a fluid velocity of 3–4 ft/s (0.9 to 1.2 ml s), limiting the development of dissolved salts at the membrane surface [34].

2.1.3 Hollow Fiber Modules

The DuPont Permease unit is an illustration of a hollow fiber module. These module's membranes are hollow, hair-like fibers manufactured of aromatic polyamide (discussed earlier). A bundle of these fibers can contain up to 4.5 million. The fiber bundles wound then around a support frame, with one end of the bundle being potted in epoxy to create a tube sheet while leaving the other end of the bundle's fibers uncapped. Epoxy is used to generate an epoxy nub at the other end of the fiber bundle, preventing quick circuiting of the feed to the brine exit. The membrane bundle is then placed in a pressure vessel with a diameter of 4–10 in. (10.2–25.4 cm) and a length of up to 4 ft (1.2 m) [34]. Due to their superior surface area per unit volume and recovery factor, hollow fiber modules are presently favored by many users [35].

2.1.4 Spiral Wound Modules

The module configuration scheme of the spiral wound models (SWMs) is utilized in RO desalination. Many benefits could be gained from this configuration such as interchangeability, low replacement costs, easy scale-up operation, significant specific membrane surface area, and less expensive to be produced from flat sheet polyamide thin film composite (TFC) membrane. With a 91% market share, polyamide spiral wound membranes are the industry standard for RO/Nano-filtration (NF). Also, there is symmetric cellulose acetate (CA) hollow fiber membrane [36, 37]. In SWMs, various RO membrane layers, feed and permeate spacers, and a perforated center pipe is alternately stacked and wrapped to create independent feed and permeate channels. The unit has a complicated geometry that might be challenging to represent in mathematical models because of the wrapping of membranes and spacers [38]. As a crucial component of these modules, the feed spacer plays a significant function in setting the pressure drop and crossflow velocity of the feed channel. The crossflow velocity and membrane fouling are typically linked to the pressure drop as well as the operational cost of the membrane. The adjustment of the feed spacer in RO has been restricted to only a slight increase in this component's thickness despite several studies being done on the feed spacer in various membrane applications [39].

3 Reverse Osmosis Membrane Materials

Considerable progress has been constructed in the creation of RO membranes from various substances over the past few decades. In spite of this, studies of RO membrane substances have been hard to come by, most likely as a result of the fact that most RO membranes that are currently important in practice are based on patents rather than standard research journal articles. The use of nanomaterials in RO processes is now possible thanks to nanotechnology, besides current studies into traditional polymeric RO membrane materials [36]. Superior RO membranes should have excessive separation performance (flux and such as salt rejection) beneath operational situations, appropriate mechanical stability, and resistance to microbial or chemical attack. Existing fabricated polymeric membranes require to be improved [40]. Since the 1970s, after the initial synthetic polymer was launched, polymers have been a part of the national economy and people's lives. This is due to their enormous variety, exceptional performance, low cost, and a variety of other useful applications. There are numerous sources of biodegradable plastics, ranging from natural to manmade polymers. Natural polymers are abundant and made from renewable resources, whereas synthetic polymers are made from nonrenewable petroleum resources. Several biodegradable polymers have recently been produced, and various microbes and/or microorganisms or enzymes capable of degrading them have been identified. Synthesis, characteristics, and modification of different polymers are discussed in the following sections, including those formed from petroleum sources, and bio-based sources.

3.1 Polymeric Membrane Materials

3.1.1 Petroleum-Based Polymers

Since the early 1960s, when phase inversion technology was developed, fossil polymers have predominated in membrane applications. Most petroleum polymers have inexpensive manufacturing costs, superior chemical and thermal stability, exceptional mechanical resilience, and high flexibility. These advantages make them suitable candidates for industrial separation processes. The production of membranes for water treatment using stretching, phase inversion, sintering, or track-etching processes is common. Hydrophilic materials include sulfonated polyetheretherketone (SPEEK), polysulfone (PSF), polyethersulfone (PES), and poly(viny1idene fluoride) (PVDF). However, hydrophobic materials include poly(viny1idene fluoride), poly(viny1idene) [41].

3.1.2 Bio-based Polymers

One of the markets for plastics with the greatest growth is biopolymers. Plastics which are called biopolymers (also known as bioplastics) can be made from renewable resources such as soy, sugar, and hemp. corn, and waste-captured methane. Various biopolymers produced today contain mixtures of conventional and renewable feedstocks, which do not necessarily have to be created from renewable materials. Additionally, some biopolymers, like Bio-PET, would be reused with equivalent-resin fossil-based plastics since they have the same polymeric structure as their conventional counterparts. Due to the wide range of feedstocks and manufacturing techniques, not all biopolymers are compostable or biodegradable.

In response to the growing desire to substitute petrochemical-based polymers, bio-based polymers are being promoted within the context of the innovative circular economy in the EU. The interest in preserving and enhancing the environment for the future has been sparked by green environmental initiatives and policies. Additionally, consumers are desired products with lower toxicity and environmental influence. The consumer pricing and ultimate operation, which should be comparable to those constructed on petrochemical products, will determine whether this scenario comes to pass. In this way, bioplastics can utilize biological resources to either replace or at least reduce the need for petrochemicals. Biobased and/or biodegradable terms are used to characterize bioplastics, depending on whether they are made from fossil (coal or petrochemical) or biological (biological) resources [41, 42]. Numerous studies have been conducted to create biodegradable films employing substances established in biological resources, such as lignin, cellulose, arabinoxylan, chitin, alginic acid, curdlan, soy protein, whey, starch, xanthan, xylan, and zein. This is because conventional plastic films have disposal issues. Currently,

biofilms are used in numerous products, containing coating and packaging materials, as well as agricultural applications including landscaping and greenhouse construction [43, 44].

The two primary groups of biodegradable polymers are (1) natural and (2) synthetic. While synthetic polymers are made from non-renewable petroleum resources, natural polymers can be found in enormous amounts from renewable sources. Numerous biodegradable polymers have been created or are made naturally during the life cycles of various organisms, including cellulose, chitin, starch, polyhydroxyalkanoates (PHAs), polylactide, poly(-caprolactone), collagen, and other polypeptides. Some certain known microbes and enzymes can break down these polymers [45].

Most biodegradable polymers fall into one of two categories [45].

A. Agro-polymers derived from natural sources:
- Polysaccharides (e.g., chitin, cellulose, starch, and lignin)
- Proteins (e.g., wool, wheat gluten, casein, and silk)
- Lipids (e.g., animal fats, and plant oils including plant oils castor oil)
- Polyesters generated by plants or microorganisms (e.g., poly-3-hydroxybutyrate and polyhydroxy-alkanoates)
- Synthetic polyesters made from bio-derived monomers (polylactic acid)
- Miscellaneous polymers (composites, natural rubbers)
B. Bio-polyesters derived from natural sources:
- Aliphatic polyesters (e.g., poly(ε-caprolactone), polyglycolic acid (PGA), and polybutylene succinate (PBS)
- Aromatic polyesters or mixtures of the two forms (e.g., polybutylene succinate terephthalate)
- Polyvinyl alcohols
- Modified polyolefins (polypropylene or polyethylene containing certain compounds that are temperature- or light-sensitive).

Table 2 illustrates the advantages and drawbacks of various polymer membranes.

3.1.3 Potentials and Limitations of Biodegradable Polymers

One potential biodegradable polymer that has been studied for RO membranes is poly(lactic acid) (PLA). It is a biodegradable thermoplastic that is made from renewable resources such as corn starch or sugarcane. It has been shown to have good membrane properties such as high permeability, low fouling, and good mechanical properties as shown in Figs. 4 and 5. As shown, the tensile strength of the membrane increases with the increases in the membrane density. Another biodegradable polymer that has been explored for RO membranes is polyhydroxyalkanoates (PHAs). PHAs are a family of biodegradable polymers that are synthesized by various microorganisms. Other biodegradable polymers that have been investigated for RO membranes include cellulose acetate, chitosan, and polyethylene glycol (PEG). These polymers

Table 2 Polymer membranes

Membrane origin	Polymer	Advantages	Limitations	References
Petroleum-based	PVDF	• High mechanical strength • Great resistance stability at low and high temperatures • Great resistance stability at radiation and UV • Low flammability and resistance to the growth of microbes • Good chemical resistance		[46, 47]
	PP	• High temperature • Excellent resistance • Low cost		[48]
	PTFE	• Outstanding thermal characteristics • High level of contamination resistance	Low strength and stiffness, very low surface hardness, high density for a thermoplastic (the highest). Poor radiation resistance, high thermal expansion (30% between room temperature and crystalline melting temperature). Limited resistance in some cases to fluorine, attacked by molten alkali metals	[49]
	PA	• Environmental production • Extreme efficiency • Resist biofouling	• Poor mechanical stability • Poor solubility in aprotic solvents	[50, 51]
	PVA	• Non-toxic • Biodegradable		[52]

Table 2 (continued)

Membrane origin	Polymer	Advantages	Limitations	References
	PAN	• Outstanding thermal and mechanical characteristics • Sufficient chemical stability		[53]
	PDMS	• High selectivity and permeability for gases that can condense, such as CO_2 • High permeability • Low-selectivity silicon rubber		[54]
	Teflon 2400	• High permeability • Minimal tendency to swell • Strong film characteristics • High chemical and thermal stability		[55]
Bio-based	Cellulosic-derived polymers	• Hydrophilicity • Mechanical strength • Availability • Chlorine tolerance • Fouling resistance • Low cost • Biodegradable	• Limited resistance to biological attack • Restricted operating pH and temperature ranges • Structural compaction at high operating pressure • Less resistance to chloride	[56]
	PLA	• Recyclable • Biodegradable		[57]
	PEEK, SPEEK and PEEK-WC	• Strong chemical and combustion properties • Withstand high temperatures • UV radiation resistant		[58]

Table 2 (continued)

Membrane origin	Polymer	Advantages	Limitations	References
	PHA	• Recyclable • Degradable into CO_2 and water		[41]
	PBS	• Acceptable level of heat and chemical resistance	• Low mechanical resistance and weak strength	[59]
	Alginate	• High biocompatibility • Minimal toxicity • Simple gelation when divalent cations are added		[60]
	Polyisoprene	• Softness • Elastic		[61]
	Starch	• Biodegradable • Low cost • Renewability		[62]
	Chitosan (CS)	• Biodegradable • Non-toxic • Natural		[63]
	Collagen and sericin	• Low toxicity		[64]

have shown promise for use in RO membranes due to their good membrane properties and biodegradability.

A few strategies can be used to improve the mechanical strength of biodegradable membranes; (i) Crosslinking can increase the stability and mechanical strength of polymer membranes. By adding crosslinking agents to the polymer matrix, the polymer chains can be linked together, making the membrane more resistant to deformation and damage, (ii) Blending different polymers with complementary properties can improve the mechanical strength of biodegradable polymer membranes. For example, blending a biodegradable polymer with a more rigid and strong polymer can improve the overall mechanical properties of the membrane (iii) Incorporating reinforcing materials such as fibers or nanoparticles can also improve the mechanical strength of biodegradable polymer membranes. These materials can provide additional strength and stability to the membrane, improving its durability and lifespan, (iv) Processing conditions: The processing conditions used to fabricate biodegradable polymer membranes can also impact their mechanical strength. By optimizing the processing parameters such as temperature, pressure, and stretching, the mechanical strength of the membrane can be improved.
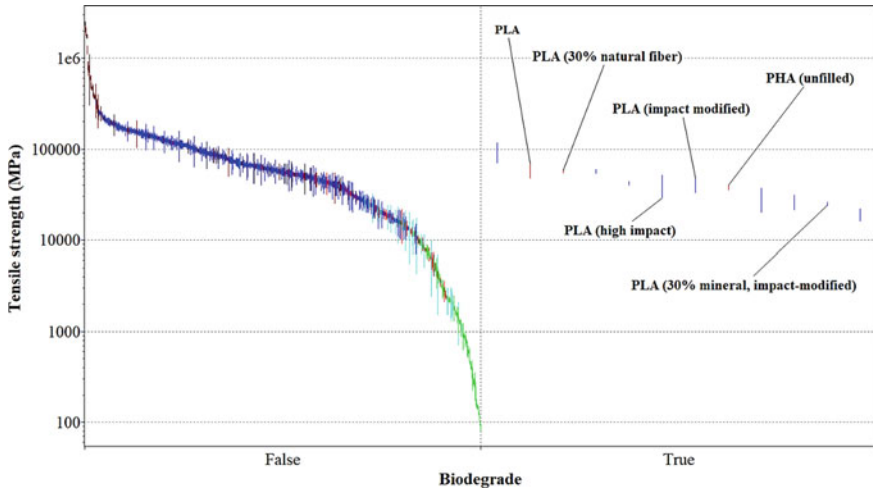
Fig. 4 Tensile strength of biodegradable polymer
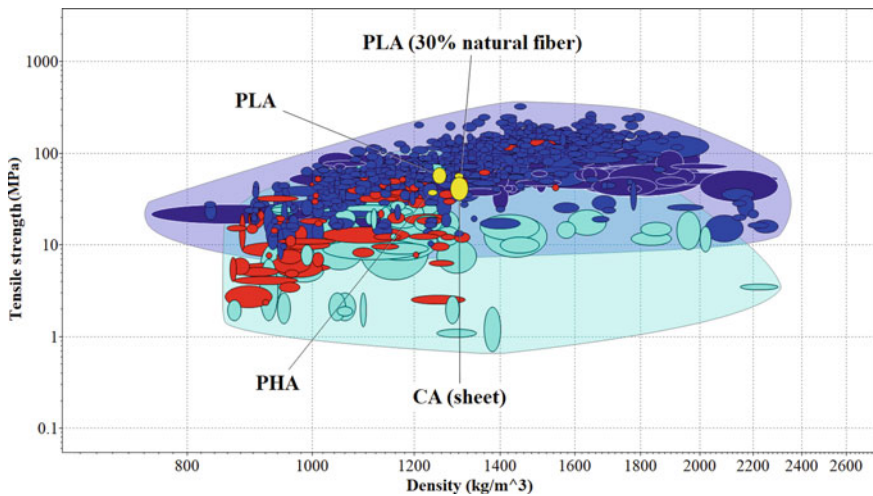
Fig. 5 Density versus tensile strength of biodegradable polymer

Overall, improving the mechanical strength of biodegradable polymer membranes is essential for their successful application in reverse osmosis water filtration. By using strategies such as crosslinking, blending, reinforcement, and optimizing processing conditions, the mechanical strength of these membranes can be improved, making them more durable and long-lasting.

4   Conclusion

Biodegradable polymer membranes offer a promising and sustainable alternative to traditional polymer membranes for reverse osmosis (RO) water filtration. In this study, the most important challenges facing reverse osmosis membranes were studied, in addition to the materials from which they are made, especially those that are biodegradable. While biodegradable polymer membranes have shown promising performance in laboratory studies, there are still challenges that need to be addressed before they can be widely used in commercial applications. The mechanical strength of biodegradable polymer membranes is one of the key challenges that need to be overcome, and researchers are exploring various strategies to improve their mechanical properties. Additionally, scaling up the production of biodegradable polymers and optimizing their performance in industrial conditions are important areas of research. Biodegradable polymer membranes for RO water filtration offer a potential solution for sustainable and environmentally friendly water treatment, but ongoing research is needed to address the remaining challenges and realize their full potential. These membranes are suitable for areas that consume large amounts of membranes for water desalination, such as the desert and tourist areas in the Arabian Peninsula.

5   Recommendation and Future Work

One major challenge is the relatively low mechanical strength and stability of biodegradable polymers compared to traditional RO membrane materials such as polyamide. Biodegradable polymers can be susceptible to degradation under harsh conditions such as high temperatures, high salinity, and exposure to certain chemicals, which can lead to reduced membrane performance and a shorter lifespan. Therefore, improving the stability and durability of biodegradable polymers is a crucial area of future research.

Another challenge is the scalability of biodegradable polymer production. Currently, the production of biodegradable polymers on a large scale is not as cost-effective as traditional polymers. Therefore, developing cost-effective methods for large-scale production of biodegradable polymers is another area for future work.

Additionally, the performance of biodegradable polymer membranes in real-world water treatment applications still needs to be extensively studied. While laboratory experiments have shown promising results, the performance of biodegradable polymer membranes in real-world water treatment conditions is influenced by various factors such as feedwater composition, fouling, and cleaning methods.

Future work in this field will focus on improving the properties and stability of biodegradable polymers, as well as optimizing their performance in real-world water treatment applications. This includes developing novel manufacturing processes, exploring new types of biodegradable polymers, and evaluating the long-term performance and sustainability of biodegradable polymer membranes.

References

1. Elhenawy Y, Fouad K, Bassyouni M, Majozi T (2023) Design and performance a novel hybrid membrane distillation/humidification–dehumidification system. Energy Convers Manag 286:117039. https://doi.org/10.1016/j.enconman.2023.117039

2. Fouad K, Bassyouni M, Alalm MG, Saleh MY (2021) Recent developments in recalcitrant organic pollutants degradation using immobilized photocatalysts. Appl Phys A Mater Sci Process 127:612. https://doi.org/10.1007/s00339-021-04724-1

3. Fouad K, Gar Alalm M, Bassyouni M, Saleh MY (2021) Optimization of catalytic wet peroxide oxidation of carbofuran by Ti-LaFeO3 dual photocatalyst. Environ Technol Innov 23:101778. https://doi.org/10.1016/j.eti.2021.101778

4. Fouad K, Gar Alalm M, Bassyouni M, Saleh MY (2020) A novel photocatalytic reactor for the extended reuse of W-TiO$_2$ in the degradation of sulfamethazine. Chemosphere 257:127270. https://doi.org/10.1016/j.chemosphere.2020.127270

5. Fouad K, Bassyouni M, Alalm MG, Saleh MY (2021) The treatment of wastewater containing pharmaceuticals. J Environ Treat Tech 9:499–504. https://doi.org/10.47277/JETT/9(2)504

6. El-Gamal H, Radwan K, Fouad K (2020) Floatation of activated sludge by nascent prepared carbon dioxide (Dept. C (Public)). Bull Fac Eng Mansoura Univ 40:21–29. https://doi.org/10.21608/bfemu.2020.101236

7. Zhu Z, Tan G, Lei D, Yang Q, Tan X, Liang N, Ma D (2021) Omniphobic membrane with process optimization for advancing flux and durability toward concentrating reverse-osmosis concentrated seawater with membrane distillation. J Memb Sci 639:119763. https://doi.org/10.1016/j.memsci.2021.119763

8. Eteba A, Bassyouni M, Saleh M (2022) Modified coal fly ash for textile dye removal from industrial wastewater. Energy Environ 1–27. https://doi.org/10.1177/0958305X221130536

9. Samir A, Ashour FH, Hakim AAA, Bassyouni M (2022) Recent advances in biodegradable polymers for sustainable applications. npj Mater Degrad 6. https://doi.org/10.1038/s41529-022-00277-7

10. Eteba A, Bassyouni M, Saleh M (2022) Utilization of chemically modified coal fly ash as cost-effective adsorbent for removal of hazardous organic wastes. Int J Environ Sci Technol. https://doi.org/10.1007/s13762-022-04457-5

11. Eteba A, Bassyouni M, Saleh M (2021) Removal of hazardous organic pollutants using fly ash. Environ Ecol Res 9:196–203. https://doi.org/10.13189/eer.2021.090407

12. Guo Y, Liu C, Liu H, Zhang J, Li H, Zhang C (2022) Contemporary antibiofouling modifications of reverse osmosis membranes: state-of-the-art insights on mechanisms and strategies. Chem Eng J 429:132400. https://doi.org/10.1016/j.cej.2021.132400

13. Alrehaili O, Perreault F, Sinha S, Westerhoff P (2020) Increasing net water recovery of reverse osmosis with membrane distillation using natural thermal differentials between brine and co-located water sources: impacts at large reclamation facilities. Water Res 184. https://doi.org/10.1016/j.watres.2020.116134

14. Fritzmann C, Löwenberg J, Wintgens T, Melin T (2007) State-of-the-art of reverse osmosis desalination. Desalination 216:1–76. https://doi.org/10.1016/j.desal.2006.12.009

15. Liu C, Rainwater K, Song L (2011) Energy analysis and efficiency assessment of reverse osmosis desalination process. Desalination 276:352–358. https://doi.org/10.1016/j.desal.2011.03.074

16. Shenvi SS, Isloor AM, Ismail AF (2015) A review on RO membrane technology: developments and challenges. Desalination 368:10–26. https://doi.org/10.1016/j.desal.2014.12.042
17. Hailemariam RH, Woo YC, Damtie MM, Kim BC, Park KD, Choi JS (2020) Reverse osmosis membrane fabrication and modification technologies and future trends: a review. Adv Colloid Interface Sci 276:102100. https://doi.org/10.1016/j.cis.2019.102100
18. Greenlee LF, Lawler DF, Freeman BD, Marrot B, Moulin P (2009) Reverse osmosis desalination: water sources, technology, and today's challenges. Water Res 43:2317–2348. https://doi.org/10.1016/j.watres.2009.03.010
19. Qasim M, Badrelzaman M, Darwish NN, Darwish NA, Hilal N (2019) Reverse osmosis desalination: a state-of-the-art review. Desalination 459:59–104. https://doi.org/10.1016/j.desal.2019.02.008
20. Tow EW, Warsinger DM, Trueworthy AM, Swaminathan J, Thiel GP, Zubair SM, Myerson AS, Lienhard VJH (2018) Comparison of fouling propensity between reverse osmosis, forward osmosis, and membrane distillation. J Memb Sci 556:352–364. https://doi.org/10.1016/j.memsci.2018.03.065
21. Tawalbeh M, Qalyoubi L, Al-Othman A, Qasim M, Shirazi M (2023) Insights on the development of enhanced antifouling reverse osmosis membranes: industrial applications and challenges. Desalination 553:116460. https://doi.org/10.1016/j.desal.2023.116460
22. Park K, Kim J, Yang DR, Hong S (2020) Towards a low-energy seawater reverse osmosis desalination plant: a review and theoretical analysis for future directions. J Memb Sci 595:117607. https://doi.org/10.1016/j.memsci.2019.117607
23. Chen D, Gao F, Liu T, Kang J, Xu R, Cao Y, Xiang M (2021) Fabrication of anti-fouling thin-film composite reverse osmosis membrane via constructing heterogeneous wettability surface. J Appl Polym Sci 138. https://doi.org/10.1002/app.51256
24. Lim YJ, Goh K, Kurihara M, Wang R (2021) Seawater desalination by reverse osmosis: Current development and future challenges in membrane fabrication—a review. J Memb Sci 629:119292. https://doi.org/10.1016/j.memsci.2021.119292
25. Gholami S, Rezvani A, Vatanpour V, Cortina JL (2018) Improving the chlorine resistance property of polyamide TFC RO membrane by polyethylene glycol diacrylate (PEGDA) coating. Desalination 443:245–255. https://doi.org/10.1016/j.desal.2018.06.004
26. Panagopoulos A, Haralambous KJ, Loizidou M (2019) Desalination brine disposal methods and treatment technologies - a review. Sci Total Environ 693:133545. https://doi.org/10.1016/j.scitotenv.2019.07.351
27. Alshahri F (2017) Heavy metal contamination in sand and sediments near to disposal site of reject brine from desalination plant, Arabian Gulf: assessment of environmental pollution. Environ Sci Pollut Res 24:1821–1831. https://doi.org/10.1007/s11356-016-7961-x
28. Jamaly S, Darwish NN, Ahmed I, Hasan SW (2014) A short review on reverse osmosis pretreatment technologies. Desalination 354:30–38. https://doi.org/10.1016/j.desal.2014.09.017
29. Shalaby SM, Sharshir SW, Kabeel AE, Kandeal AW, Abosheiasha HF, Abdelgaied M, Hamed MH, Yang N (2022) Reverse osmosis desalination systems powered by solar energy: Preheating techniques and brine disposal challenges—a detailed review. Energy Convers Manag 251:114971. https://doi.org/10.1016/j.enconman.2021.114971
30. Ahmad N, Baddour RE (2014) A review of sources, effects, disposal methods, and regulations of brine into marine environments. Ocean Coast Manag 87:1–7. https://doi.org/10.1016/j.ocecoaman.2013.10.020
31. Li X, Wang Z, Han X, Wang J (2022) Facile fabrication of hydroxyl-rich polyamide TFC RO membranes for enhanced boron removal performance. Desalination 531. https://doi.org/10.1016/j.desal.2022.115723
32. Hilal N, Kim GJ, Somerfield C (2011) Boron removal from saline water: a comprehensive review. Desalination 273:23–35. https://doi.org/10.1016/j.desal.2010.05.012
33. Altaee A, Zaragoza G, van Tonningen HR (2014) Comparison between forward osmosis-reverse osmosis and reverse osmosis processes for seawater desalination. Desalination 336:50–57. https://doi.org/10.1016/j.desal.2014.01.002

34. Corson MacNeil J (1988) Membrane separation technologies for treatment of hazardous wastes. Crit Rev Environ Control 18:91–131. https://doi.org/10.1080/10643388809388344
35. Marcovecchio MG, Scenna NJ, Aguirre PA (2010) Improvements of a hollow fiber reverse osmosis desalination model: analysis of numerical results. Chem Eng Res Des 88:789–802. https://doi.org/10.1016/j.cherd.2009.12.003
36. Lee KP, Arnot TC, Mattia D (2011) A review of reverse osmosis membrane materials for desalination—development to date and future potential. J Memb Sci 370:1–22. https://doi.org/10.1016/j.memsci.2010.12.036
37. Alsarayreh AA, Al-obaidi MA, Patel R, Mujtaba IM (2020) Scope and limitations of modelling, simulation, and optimisation of a spiral wound reverse osmosis process-based water desalination
38. Gu B, Xu XY, Adjiman CS (2017) A predictive model for spiral wound reverse osmosis membrane modules: the effect of winding geometry and accurate geometric details. Comput Chem Eng 96:248–265. https://doi.org/10.1016/j.compchemeng.2016.07.029
39. Shi W, Ren H, Huang X, Li M, Tang Y, Guo F (2020) Separation and Purification Technology Low cost red mud modified graphitic carbon nitride for the removal of organic pollutants in wastewater by the synergistic effect of adsorption and photocatalysis. Sep Purif Technol 237:116477. https://doi.org/10.1016/j.seppur.2019.116477
40. Li D, Wang H (2010) Recent developments in reverse osmosis desalination membranes. J Mater Chem 20:4551–4566. https://doi.org/10.1039/b924553g
41. Galiano F, Briceño K, Marino T, Molino A, Christensen KV, Figoli A (2018) Advances in biopolymer-based membrane preparation and applications. J Memb Sci 564:562–586. https://doi.org/10.1016/j.memsci.2018.07.059
42. Marni Sandid A, Bassyouni M, Nehari D, Elhenawy Y (2021) Experimental and simulation study of multichannel air gap membrane distillation process with two types of solar collectors. Energy Convers Manag 243:114431. https://doi.org/10.1016/j.enconman.2021.114431
43. Rosentrater KA, Otieno AW (2006) Considerations for manufacturing bio-based plastic products. J Polym Environ 14:335–346. https://doi.org/10.1007/s10924-006-0036-1
44. Maddah HA, Alzhrani AS, Bassyouni M, Abdel-Aziz MH, Zoromba M, Almalki AM (2018) Evaluation of various membrane filtration modules for the treatment of seawater. Appl Water Sci 8:1–13. https://doi.org/10.1007/s13201-018-0793-8
45. Ashter SA (2016) Types of biodegradable polymers
46. Cui Z, Drioli E, Lee YM (2014) Recent progress in fluoropolymers for membranes. Prog Polym Sci 39:164–198. https://doi.org/10.1016/j.progpolymsci.2013.07.008
47. Kang Gd, Cao Ym (2014) Application and modification of poly(vinylidene fluoride) (PVDF) membranes—a review. J Memb Sci 463:145–165. https://doi.org/10.1016/j.memsci.2014.03.055
48. Gryta M (2007) Influence of polypropylene membrane surface porosity on the performance of membrane distillation process. J Memb Sci 287:67–78. https://doi.org/10.1016/j.memsci.2006.10.011
49. Zhu H, Wang H, Wang F, Guo Y, Zhang H, Chen J (2013) Preparation and properties of PTFE hollow fiber membranes for desalination through vacuum membrane distillation. J Memb Sci 446:145–153. https://doi.org/10.1016/j.memsci.2013.06.037
50. Meeks D, Hottle T, Bilec MM, Landis AE (2015) Compostable biopolymer use in the real world: Stakeholder interviews to better understand the motivations and realities of use and disposal in the US. Resour Conserv Recycl 105:134–142. https://doi.org/10.1016/j.resconrec.2015.10.022
51. Elhady S, Bassyouni M, Mansour RA, Elzahar MH, Abdel-Hamid S, Elhenawy Y, Saleh MY (2020) Oily wastewater treatment using polyamide thin film composite membrane technology. Membranes (Basel) 10:84. https://doi.org/10.3390/membranes10050084
52. Yeom CK, Lee KH (1996) Pervaporation separation of water-acetic acid mixtures through poly(vinyl alcohol) membranes crosslinked with glutaraldehyde. J Memb Sci 109:257–265. https://doi.org/10.1016/0376-7388(95)00196-4

53. Scharnagl N, Buschatz H (2001) Polyacrylonitrile (PAN) membranes for ultra- and microfiltration. Desalination 139:191–198. https://doi.org/10.1016/S0011-9164(01)00310-1
54. Bernardo P, Drioli E, Golemme G (2009) Membrane gas separation: a review/state of the art. Ind Eng Chem Res 48:4638–4663
55. Polyakov AM, Starannikova LE, Yampolskii YP (2004) Amorphous Teflons AF as organophilic pervaporation materials: separation of mixtures of chloromethanes. J Memb Sci 238:21–32. https://doi.org/10.1016/j.memsci.2004.03.018
56. Li D, Yan Y, Wang H (2016) Recent advances in polymer and polymer composite membranes for reverse and forward osmosis processes. Prog Polym Sci 61:104–155. https://doi.org/10.1016/j.progpolymsci.2016.03.003
57. Djonlagic J, Nikolic MS (2011) Biodegradable polyesters: synthesis and physical properties
58. Kurtz SM, Devine JN (2007) PEEK biomaterials in trauma, orthopedic, and spinal implants. Biomaterials 28:4845–4869. https://doi.org/10.1016/j.biomaterials.2007.07.013
59. Ghaffarian V, Mousavi SM, Bahreini M, Jalaei H (2014) Polyethersulfone/poly (butylene succinate) membrane: effect of preparation conditions on properties and performance. J Ind Eng Chem 20:1359–1366. https://doi.org/10.1016/j.jiec.2013.07.019
60. Lee KY, Mooney DJ (2012) Alginate: properties and biomedical applications. Prog Polym Sci 37:106–126. https://doi.org/10.1016/j.progpolymsci.2011.06.003
61. Cornish K (2001) Similarities and differences in rubber biochemistry among plant species. Phytochemistry 57:1123–1134. https://doi.org/10.1016/S0031-9422(01)00097-8
62. Ahmed MJ, Hameed BH, Hummadi EH (2021) Insight into the chemically modified crop straw adsorbents for the enhanced removal of water contaminants: a review. J Mol Liq 330:115616. https://doi.org/10.1016/j.molliq.2021.115616
63. Wu P, Imai M (2012) Novel biopolymer composite membrane involved with selective mass transfer and excellent water permeability. Adv Desalin 57–81
64. Goissis G, Junior EM, Adriana, Rosemary Marcanto C, Carlos R, Lia C, Cancian DCJ, De Carvalho WM (1999) Biocompatibility studies of anionic collagen membranes with different degree of glutaraldehyde cross-linking. Biomaterials 20:27–34

A Critical Review of Bilgewater Treatment

Maggie Gad, A. E. Mansi, Noran Ashraf, Yasser Elhenawy, and M. Bassyouni

1 Introduction

According to estimates, 20% of the oily water that ships discharge into the world's seas each year comes from bilgewater, one persistent source of oil pollution [1]. Bilgewater, also known as shipboard wastewater, is a complicated mixture of seawater, different fuels, lubricants, cooling water, and other pollutants (such as detergents, solvents, and solid particulates) from a variety of sources, including equipment washes, condensation, leaks, and other activities [2]. Oil in bilgewater is most likely the result of motor oil, hydraulic fluid, and fuel line leaks. Large boats primarily consume bunker oil and use petroleum-based lubricating oils and hydraulic fluids. These oil sources most likely have more substantial, heavier constituents than would be anticipated for gasoline-fueled vehicles, and they have higher boiling points.

M. Gad · A. E. Mansi · N. Ashraf · M. Bassyouni (✉)
Department of Chemical Engineering, Faculty of Engineering, Port Said University, Port Said 42526, Egypt
e-mail: m.bassyouni@eng.psu.edu.eg

A. E. Mansi · M. Bassyouni
Center of Excellence for Membrane Testing and Characterization (CEMTC), Port Said University, Port Said 42526, Egypt

Y. Elhenawy
School of Chemical and Metallurgical Engineering, University of the Witwatersrand, Johannesburg, South Africa

Department of Mechanical Power Engineering, Faculty of Engineering, Port Said University, Port Said 42526, Egypt

Y. Elhenawy
e-mail: dr_yasser@eng.psu.edu.eg

M. Bassyouni
East Port Said University of Technology, North Sinai, Port Said 45632, Egypt

Various forms of oil can be found in bilgewater, mainly depending on the size of oil droplets: free, dispersed, and emulsified [3].

The type of materials released and their physicochemical characteristics determine the final composition of the bilgewater [4, 5]. Lighter, more flammable hydrocarbons tend to vaporize, while photosensitive hydrocarbons will be oxidized by sunlight. solidification of marine tar residuals may occur after interaction with suspended particulates. Oil-in-water emulsifications are commonly encountered in bilgewater, emulsion homogenization is expected to happen during the pumping and transport of bilgewater between holding tanks [6–8]. Surfactants are considered the primary factor in the stabilization of emulsions, and hydrophilic-lipophilic mutual attraction is deemed the dominant mechanism rather than charge attraction [9, 10]. Figure 1 illustrates the possible scenarios of oil pollution development after spills or discharge from ships. Minimization or elimination of ship fluids discharge to the ecosystem adheres to the Sustainable Development Goals (SDGs) by sustaining the marine life, the coastal plants, and the water ways (Goals No. 14, 15, and 6 respectively).

Numerous activities fall under the category of coastal and marine systems, all of which are vulnerable to the impacts of coastal oil spills [11]. Therefore, different treatment processes have been proposed for bilgewater treatment. In this work, a comprehensive review of the state of the art bilgewater treatment is developed. The general characteristics and composition of bilgewater are reviewed. The recent treatment efforts are investigated and the role of membrane-based technologies and their advantages and limitations in the treatment of bilgewater are assessed. Several types of membrane technologies can be used to treat bilgewater, including ultrafiltration (UF), nanofiltration (NF), and reverse osmosis (RO). Each of these technologies has its advantages and disadvantages, depending on the specific application and the level of treatment required [12–17].
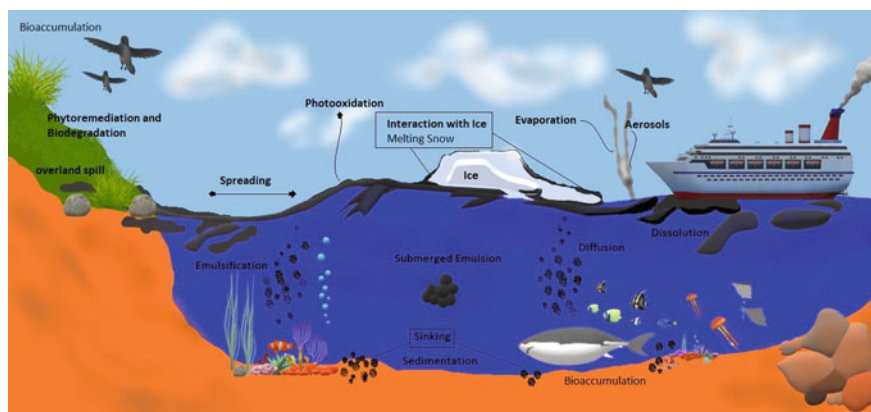
Fig. 1 A comprehensive diagram depicting all interactions oil spills have on the environment on a large scale. The behavior and environmental impacts of oil released into aqueous environments

2 General Bilgewater Characteristics

Numerous publications reported the characteristics of actual bilgewater. The characteristics of interest include oil and grease (O&G), pH, chemical oxygen demand (COD), total suspended solids (TSS), total organic carbon (TOC), and conductivity. Table 1 presents the typical range of bilgewater characteristics from various locations and different publications from the literature.

From the data in Table 1, it is observed that the range and average values of bilgewater are pH: 6.8–9.0, O&G: 0–976 ppm, COD: 20–12,800 ppm, TSS: 220–1760 ppm, and conductivity: 0.67–38.1 mS/cm.

Table 1 Characteristics of various bilgewater samples reported in the literature

Sample description	pH	O&G	COD	TSS	Conductivity	References
Stabilization tanks from the Haydarpasa Port waste acceptance plant	6.95	338	1033	295	31.7	[18]
Washings of bilges in Quebec Canada	7.09	800	3400	543	0.67	[19]
Bilgewater from Ecofuel Ltd. in Zygi, Cyprus	7.5–8	NA[a]	2900–12,800	800–1200	38.1	[20]
Bilgewater from small fishing vessels in Sing Amnuai Port, Thailand	6.8–7.4	58–976	NA	NA	4.22–6.25	[21]
Bilgewater from cargo ships at Amirabad port, Iran	8.0–9.0	–	20–200	220–1760	NA	[22]
Bilgewater from passenger ship, Milazzo harbor, Italy	6.9	36	NA	NA	8.4	[23]

All the concentrations are in ppm and the conductivity is in mS/cm
[a] NA: not available

3   State of the Art Bilge Water Treatment

Various treatment methods were proposed for the removal of oil impurities from bilgewater. electrical energy can be used to demulsify the oil from wastewater. The most-involved electrochemical strategies in the treatment of slick wastewater are electroflotation and electrocoagulation. Through the use of a membrane and pressure, the liquid content of a suspension is physically separated in membrane filtration. Ceramic and polymeric ultrafiltration and microfiltration membranes are the most widely used membranes. Additionally, oily wastewater has been treated with reverse osmosis (RO) membranes. Natural treatment includes the utilization of microorganisms that produce the lipase catalyst, which separates the biodegradable natural substances in sleek wastewater. It's important to note that using just one treatment method can be difficult and complicated for oily wastewater [24, 25]. The following sections highlight a number of contributions made by numerous scientists using various treatment strategies.

3.1   Electrochemical Process

Electrochemical processes are considered recent and efficient methods for treating oily wastewater is the electrochemical method. Oily wastewater from various sources can be treated using a variety of electrochemical techniques. Multi-electrode Electro-Fenton and electrochemical oxidation processes are two examples of these electrochemical technologies. Various materials have been tested in the literature as anodes for the electrochemical separation of oil from bilgewater. Common anode materials include aluminium, iron, iridium-platinum alloy, and titanium alloys [26].

A previous study investigated the effect of reaction temperature and current density on the treatment effectiveness of bilge water in a batch electrochemical reactor utilizing platinum–iridium electrodes. Results showed that the optimum conditions are a reactor temperature of 32 °C and a current density of 12.8 mA/cm^2 and 32 °C. The removal percentages at the optimum conditions were 91.1%, 99.2%, and 93.2%, of turbidity, COD, and O&G respectively with an average energy consumption of 119.7 MJ/kg COD removed [27].

Another study utilized lower-cost iron and aluminum electrodes for the treatment of oily bilge water. The electrodes were arranged in a monopolar or bipolar configuration in an electrolytic cell. Results showed that the optimum conditions are a current of 1.5 A and a retention time of 60–90 min. The removal percentages at the optimum conditions were 93.0 ± 3.3%, 95.6 ± 0.2%, and 78.1 ± 0.1% of BOD, O&G, and COD respectively [19].

Ulucan and Kurt (2015) tested a hybrid system combining electrochemical oxidation and electro Fenton processes to treat the bilge water from the waste-receiving facilities at Haydarpasa. Iron and aluminium electrodes were utilized in the hybrid

system. A comparison of the aluminium and iron electrodes showed COD removal efficiencies of 64.8% and 36.2% for aluminium and iron, respectively [28].

A hybrid system comprising nanofiltration and electrocoagulation was tested for the treatment of real bilgewater using two aluminium electrodes [29]. The distance between the electrodes were 8 cm. The optimum conditions were pH = 6.25, voltage = 15 V, and electrocoagulation time of 1.5 h. The proposed system achieved COD removal of 62.4%.

3.2   Biological Treatment Processes

In the biological treatment of bilgewater, the water is first screened to remove larger solids and debris. The water is mixed in the presence of microorganisms, that can consume and degrade the organic contaminants in the water. The source of microorganisms can be in the form of a culture or naturally occurring in the water. The biological treatment process typically takes place in a bioreactor, which provides an environment in which the microorganisms can thrive and grow. The bioreactor is designed to provide optimal conditions for the microorganisms' including temperature, pH, and oxygen levels. As the microorganisms consume the organic contaminants in the bilgewater, the products include carbon dioxide and water. Further treatment can be applied before discharging, such as filtration or disinfection, to remove any remaining contaminants before it is discharged into the environment. The advantages of biological treatment include its low cost, removal of a wide range of organic matter, and its ability to be scaled up or down depending on the volume of water being treated. However, biological treatment may not be effective for some contaminants, and it may require longer treatment times than other methods. Biological treatment can be a useful method for treating bilgewater, especially in hybrid systems with other methods such as membrane technology, to achieve higher levels of treatment and ensure the water is safe for the marine environment.

The treatment of oily wastewater with microorganisms has recently produced some remarkable results. Various microbes were utilized to eliminate certain pollutants from oily wastewater. A pervious study utilized an up-flow anaerobic sludge fixed film reactor to treat low-strength bilgewater obtained from Caspian Sea ships. The reaction time was varied between eight and ten hours and the oil loading rate was varied between 0.12 g COD/L.d and 0.6 g COD/L.d. Results showed high removal of COD (~ 75%) and ~ 100% TSS at a retention time of 8h and 0.6 g COD/L.d. The oil concentration of the product was below the international maritime organization's discharge limit standards of 15 ppm [30].

A study examined the biodegradation of undiluted bilge water (BW) and the production of methane utilizing a microbial electrolysis cell containing anaerobic granular sludge. Up to 70% COD removal was achieved and a maximum methane production of 142.2 ± 4.8 mL over 10 days of operation. The technology is highly promising however, the retention time required is excessively long [31].

3.3   Membrane Technologies

In the treatment of bilgewater, a combination of membrane technologies can be applied to achieve the desired quality of treatment. For example, a sequence of microfiltration, ultrafiltration, and nanofiltration can be designed and implemented to remove suspended solids, bacteria, and dissolved solids from the water [32, 33]. For high purification, to provide drinking water or reuse, reverse osmosis can be applied [33]. Membrane technology can be also used in combination with other treatment methods, such as biological treatment, to achieve high levels of treatment and ensure the water is safe for the marine environment. There are also specialized membranes that are specifically designed for the treatment of oily bilgewater. These membranes use specialized materials and coatings that can adsorb and remove oil and grease from the water. One example of a specialized membrane technology where it is used for bilgewater is the oleophobic membrane. This type of membrane has a surface that repels oil and grease, allowing the membrane to selectively remove these contaminants from the water. The oleophobic membrane can be used in combination with other membrane technologies, such as ultrafiltration or nanofiltration, to achieve high levels of treatment for oily bilgewater. Another advantage of membrane technology is that it can be used in a modular design, allowing for easy scalability and flexibility. The modular design allows the treatment system to be customized to the specific requirements of the application and allows for easy expansion or modification of the system as the volume of bilgewater being treated changes. One potential drawback of membrane technology is that the membranes can become fouled or clogged over time, reducing their effectiveness and requiring regular maintenance and cleaning [34, 35]. However, advances in membrane materials and designs have led to membranes that are more resistant to fouling and require less frequent cleaning. Membrane technology is a highly effective and versatile method for treating bilgewater, and its use can help to protect the marine environment by ensuring that discharged bilgewater meets regulatory standards for water quality.

The application of membrane technologies for large-scale oily-saline wastewater treatment had bottlenecks due to the constraints of irreversible fouling. To overcome this obstacle, different solutions have been proposed including the modification of the membrane, pre-treatment of the feed, or use of hybrid treatment technologies.

3.3.1   Mechanism of Membrane Fouling for Oily Wastewater Treatment

Membrane fouling involves the deposition or attachment of solid particles or oil droplets deteriorating the membrane separation effectiveness. Fouling causes the membrane to experience declining flux. The fouling mechanism may be classified into four types:

1. Cake formation.
2. Intermediate fouling which involves the continuous build-up of fouling on the membrane surface creating passages for effluent liquids to cross the membrane.

3. Standard blocking: partial blocking of the pores reducing the flux.
4. Complete blocking: the pores are completely blocked by a large particle consequently deteriorating the overall membrane performance

3.3.2 Membrane Surface Modification

The surface of a membrane can be altered through physical or chemical means. The surface of the membrane can be crosslinked in situ with multiple materials to enhance their secondary interaction and stability. The following techniques are used to modify the membrane's surface: surface grafting, surface coating, and blending are all examples of surface grafting. Plasma treatment and grafting are frequently used to modify the surface of polymers without affecting their bulk properties. To modify the surfaces of membranes, a variety of materials, such as TiO_2 nanotubes, graphene oxide (GO), carbon nanotubes (CNTs), and iron oxide particles (IOP), have been used [36]. Sun et al. (2010) studied the treatment of bilge water using a biofilm membrane bioreactor and flat sheet ceramic membrane under dead-end and recycle side stream configurations. Results indicated that a good permeate quality was obtained in both configurations with an oil content of 5 mg/L [37]. A recent study utilized a ceramic ultrafiltration membrane having a molecular weight cut off equal to 8 kDa to treat bilgewater containing TDS = 6519 ppm and oil content = 73.5 ppm. The permeate was oil-free with turbidity ~ 0.2 NTU. Membrane performance deterioration was observed due to fouling. However, the flux stabilized after 100 min and a steady-state flux of 69.5 l/m² h (Normalized flux = 70%) at a transmembrane pressure of 2.8 bar and crossflow velocity of 4.1 m/s [38].

3.3.3 Hybrid Technologies

The integration of different oily wastewater treatment technologies, to observe the overall impact of the combined technologies on the removal efficiencies of pollutants, has also been investigated. Microfiltration (MF) and ultrafiltration (UF) membranes are common pre-treatment steps to reverse osmosis (RO) and membrane distillation (MD). MF and UF membranes can remove suspended solids, bacteria, and colloidal particles. On the other hand, RO membranes can remove metal ions and aqueous salts including chloride, sodium, lead, copper, etc. A hybrid UF-RO system was studied for the treatment of bilgewater. The treatment was carried out in two stages. In the first stage using treatment the ultrafiltration process was applied. Such obtained UF permeate was subsequently used as a feed for the RO process [39]. An illustration of the process is given in Fig. 2. The process results are detailed in Table 2.

Fouling of membranes and the elevated operational cost are the major drawbacks of membrane technologies. As such, electrocoagulation can be used as a pre-treatment process for the effective removal of different wastewater pollutants, while
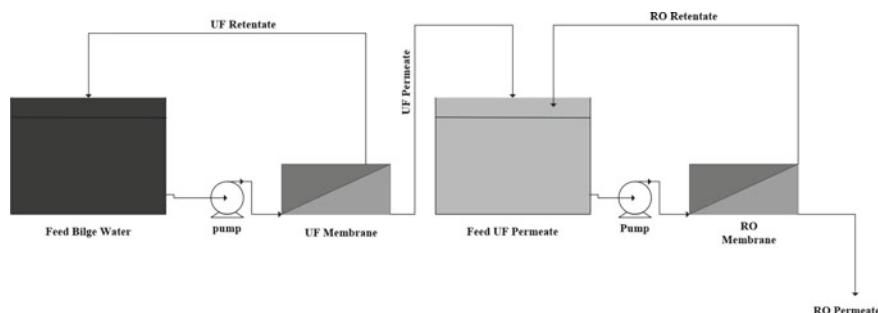
Fig. 2 Illustration of the UF-RO hybrid system

Table 2 A comparison of the effectiveness of two stages treatment of bilge water

Temperature 25 °C	Bilge water	Ultrafiltration		Reverse osmosis			
		FP 100		BW3040		SW30-4040	
		Permeate	Rejection %	Permeate	Rejection %	Permeate	Rejection %
Flux, dm^3/ m^2 h	–	27	–	35	–	54	–
Oil, ppm	107	8.2	92.3	0	100	0	100
TOC, mg/dm^3	1765	1345	23.8	115	93.5	61.7	95.3
TDS, ppm	1307	898.9	31.2	11.6	99.1	61.7	95.3
Conductivity, µS/cm	1817	0.561	99.7	18.3	99.0	96.03	94.7
Turbidity, NTU	200	0.561	99.7	–	–	–	–
Suspended solids, mg/dm	28	0	100	–	–	–	–

also reducing the overall operating cost of the combined process. Removal efficiencies of 100% COD, 99.9% turbidity, 98.9% TDS, and 99.6% Al ions were achieved. The permeate flux was found to be 20 L/m^2 h [40].

4 Conclusion

In this paper, the state of the art bilgewater treatment has been reviewed. The general characteristics and the factors affecting the composition of bilgewater has been introduced. The influence of the bilgewater components on the environment was discussed in detail. Bilgewater adversely affects the marine ecosystem, the coastal plants, and the humans that consume fish polluted by bilgewater. Various processes has

been proposed for the treatment of bilgewater. The most common processes include electro oxidation, biological processes, and membrane technologies. The electrochemical processes remove the organic matter effectively; however, the dissolved and suspended salts remain unaffected. The area footprint and retention time of biological processes are the main disadvantages. Membrane technologies offer superior efficiency in the removal of pollutants from bilgewater. The emerging membrane distillation technology can handle the complex nature of oil-saline water yet, membrane wetting can deteriorate the membrane performance severely. The best approach for bilgewater treatment was concluded to be hybrid systems that incorporates membrane technologies as a final treatment step.

5 Recommendations

Various technologies were tested for the treatment of bilgewater. The most common processes namely electrocoagulation and biological degradation have major drawbacks including the high energy demand and process instability. Membrane technologies exhibited promising performance in treating bilgewater. Despite the inherent drawback in membrane technologies (i.e. fouling), its lower cost and superior treatment efficiency urges the development of these technologies. The emerging membrane distillation technology can handle the complex nature of oil-saline water yet, membrane wetting can deteriorate the membrane performance severely. The literature data about utilizing membrane distillation in treating bilgewater is limited, so it is recommended to extend the research effort on this technology. Hybrid systems incorporating membrane technologies are the best approach for bilge water treatment.

References

1. Tomaszewska M, Orecki A, Karakulski K (2005) Treatment of bilge water using a combination of ultrafiltration and reverse osmosis. Desalination 185(1–3):203–212
2. Buck EH (2010) Ballast water management to combat invasive species
3. Albaigés J, Jimenez N, Arcos A, Dominguez C, Bayona JM (2013) The use of long chain alkylbenzenes and alkyltoluenes for fingerprinting marine oil wastes. Chemosphere 91(3):336–343
4. Fingas M (2016) Oil spill science and technology, 2nd edn. Gulf Professional Publishing, Boston
5. Palantzas G, Zafeirakou A, Samaras A, Karambas T, Koutitas C (2016) The use of oil spill trajectory models in oil pollution incidents response

6. Azevedo A, Oliveira A, Fortunato AB, Zhang J, Baptista AM (2014) A cross-scale numerical modeling system for management support of oil spill accidents. Mar Pollut Bull 80(1–2):132–147

7. Pichot R, Spyropoulos F, Norton IT (2010) O/W emulsions stabilised by both low molecular weight surfactants and colloidal particles: the effect of surfactant type and concentration. J Colloid Interface Sci 352(1):128–135

8. Tadros TF (2009) Emulsion science and technology: a general introduction. Emuls Sci Technol 1(1):1–55

9. Church J, Paynter DM, Lee WH (2017) In situ characterization of oil-in-water emulsions stabilized by surfactant and salt using microsensors. Langmuir 33(38):9731–9739

10. Church J, Lundin JG, Diaz D, Mercado D, Willner MR, Lee WH, Paynter DM (2019) Identification and characterization of bilgewater emulsions. Sci Total Environ 691:981–995

11. Zhang B, Matchinski EJ, Chen B, Ye X, Jing L, Lee K (2019) Marine oil spills—oil pollution, sources and effects. In: World seas: an environmental evaluation. Academic, pp 391–406

12. Sandid AM, Bassyouni M, Nehari D, Elhenawy Y (2021) Experimental and simulation study of multichannel air gap membrane distillation process with two types of solar collectors. Energy Convers Manag 243:114431

13. Maddah HA, Alzhrani AS, Bassyouni M, Abdel-Aziz MH, Zoromba M, Almalki AM (2018) Evaluation of various membrane filtration modules for the treatment of seawater. Appl Water Sci 8:1–13

14. Alhathal Alanezi A, Bassyouni M, Abdel-Hamid SM, Ahmed HS, Abdel-Aziz MH, Zoromba MS, Elhenawy Y (2021) Theoretical investigation of vapor transport mechanism using tubular membrane distillation module. Membranes 11(8):560

15. El-Mehalmey WA, Safwat Y, Bassyouni M, Alkordi MH (2020) Strong interplay between polymer surface charge and MOF cage chemistry in mixed-matrix membrane for water treatment applications. ACS Appl Mater Interfaces 12(24):27625–27631

16. Elrasheedy A, Rabie M, El-Shazly A, Bassyouni M, Abdel-Hamid SMS, El Kady MF (2021) Numerical investigation of fabricated MWCNTs/polystyrene nanofibrous membrane for DCMD. Polymers 13(1):160

17. Zakaria M, Sharaky AM, Al-Sherbini AS, Bassyouni M, Rezakazemi M, Elhenawy Y (2022) Water desalination using solar thermal collectors enhanced by nanofluids. Chem Eng Technol 45(1):15–25

18. Ulucan K, Kabuk HA, Ilhan F, Kurt U (2014) Electrocoagulation process application in bilge water treatment using response surface methodology. Int J Electrochem 9(5):2316

19. Asselin M, Drogui P, Brar SK, Benmoussa H, Blais JF (2008) Organics removal in oily bilgewater by electrocoagulation process. J Hazard Mater 151(2–3):446–455

20. Vyrides I, Drakou EM, Ioannou S, Michael F, Gatidou G, Stasinakis AS (2018) Biodegradation of bilge water: batch test under anaerobic and aerobic conditions and performance of three pilot aerobic Moving Bed Biofilm Reactors (MBBRs) at different filling fractions. J Environ Manag 217:356–362

21. Chanthamalee J, Wongchitphimon T, Luepromchai E (2013) Treatment of oily bilge water from small fishing vessels by PUF-immobilized Gordonia sp. JC11. Water Air Soil Pollut 224:1–13

22. Emadian SM, Rahimnejad M, Hosseini M, Khoshandam B (2015) Investigation on up-flow anaerobic sludge fixed film (UASFF) reactor for treating low-strength bilge water of Caspian Sea ships. J Environ Health Sci Eng 13:1–9

23. Santisi S, Gentile G, Volta A, Bonsignore M, Mancini G, Quatrini P, Cappello S (2015) Isolation and characterization of oil-degrading bacteria from bilge water. Growth 17:18

24. Elhady S, Bassyouni M, Mansour RA, Elzahar MH, Abdel-Hamid S, Elhenawy Y, Saleh MY (2020) Oily wastewater treatment using polyamide thin film composite membrane technology. Membranes 10(5):84

25. Mansi AE, El-Marsafy SM, Elhenawy Y, Bassyouni M (2022) Assessing the potential and limitations of membrane-based technologies for the treatment of oilfield produced water. Alexandria Eng J

26. Albaiges J, Jimenez N, Arcos A, Dominquez C, Bayona JM (2013) The use of long-chain alkylbenzenes and alkyltoluenes for fingerprinting marine oil wastes. Chemosphere 91(3):336–343

27. EPA (2010) Study of discharges incidental to normal operation of commercial fishing vessels and other non-recreational vessels less than 79 ft. Report to Congress. U.S., Environmental Protection Agency, Washington, DC

28. Ulucan K, Kurt U (2015) Comparative study of electrochemical wastewater treatment processes for bilge water as oily wastewater: a kinetic approach. J Electroanal Chem 747:104–111

29. Tahreen A, Jami MS, Ali F (2020) Role of electrocoagulation in wastewater treatment: a developmental review. J Water Process Eng 37:101440

30. Emadian SM, Rahimnejad M, Hosseini M, Khoshandam B (2015) Investigation on upflow anaerobic sludge fixed film (UASFF) reactor for treating low strength bilgewater of Caspian Sea ships. J Environ Public Health 13:23

31. Gatidou G, Samanides CG, Fountoulakis MS, Vyrides I (2022) Microbial electrolysis cell coupled with anaerobic granular sludge: a novel technology for real bilge water treatment. Chemosphere 296:133988

32. Eteba A, Bassyouni M, Saleh M (2022) Modified coal fly ash for textile dye removal from industrial wastewater. Energy Environ. 0958305X221130536

33. Fouad K, Alalm MG, Bassyouni M, Saleh MY (2020) A novel photocatalytic reactor for the extended reuse of W-TiO$_2$ in the degradation of sulfamethazine. Chemosphere 257:127270

34. Elhenawy Y, Moustafa GH, Attia AM, Mansi AE, Majozi T, Bassyouni M (2022) Performance enhancement of a hybrid multi effect evaporation/membrane distillation system driven by solar energy for desalination. J Environ Chem Eng 10(6):108855

35. Ali I, Bamaga OA, Gzara L, Bassyouni M, Abdel-Aziz MH, Soliman MF, Drioli E, Albeirutty M (2018) Assessment of blend PVDF membranes, and the effect of polymer concentration and blend composition. Membranes 8(1):13

36. Samuel O, Othman MHD, Kamaludin R, Kurniawan TA, Li T, Dzinun H, Imtiaz A (2022) Treatment of oily wastewater using photocatalytic membrane reactors: a critical review. J Environ Chem Eng 108539

37. Sun C, Leiknes T, Weitzenböck J, Thorstensen B (2010) Development of a biofilm-MBR for shipboard wastewater treatment: the effect of process configuration. Desalination 250(2):745–750

38. Tomczak W, Gryta M (2021) Application of ultrafiltration ceramic membrane for separation of oily wastewater generated by maritime transportation. Sep Purif Technol 261:118259

39. Eskandarloo H, Selig MJ, Abbaspourrad A (2018) In situ H$_2$O$_2$ generation for de-emulsification of fine stable bilge water emulsions. Chem Eng J 335:434–442

40. da Silva JRP, Merçon F, da Silva LF, Cerqueira AA, Ximango PB, da Costa Marques MR (2015) Evaluation of electrocoagulation as pre-treatment of oil emulsions, followed by reverse osmosis. J Water Process Eng 8:126–135

Utilization of Fly Ash in Wastewater Treatment: A Review

Medhat M. H. ElZahar, M. Bassyouni, Mayada M. Gomaa, Mohamed Z. El-Shekhiby, and Mamdouh Y. Saleh

1 Introduction

Surface water pollution is mostly results from industrial processes. The pollution includes those in the sectors of petrochemical, food, dye, chemical, and textile. The toxic pollutants in water have the potential to harm the environment. sources have generated considerable concern. Additionally, they can degrade the hue, flavor, and aroma of source waters [1]. The manufacture and use of colored dyes in the textile and associated industries directly result in the generation of colored dye wastewater. The processing of minerals, rubber, paper, plastics, leather, rubber, and textiles are just a few examples of the many industries that use dyes extensively. The textile industry finishing, in particular, consumes a lot of water, a lot of which is used for dying and rinsing [1]. In textile factories, large amounts of water and chemicals are used to produce fiber, fabric, and clothing, resulting in the discharge of numerous pollutants [2]. Colors, biological oxygen demand; BOD_5, dangerous chemicals, chemical

M. M. H. ElZahar · M. M. Gomaa · M. Z. El-Shekhiby · M. Y. Saleh
Sanitary and Environmental Engineering, Civil Engineering Department, Faculty of Engineering, Port Said University, Port Said 42526, Egypt
e-mail: melzahar@yahoo.com

M. Z. El-Shekhiby
e-mail: eng-moh-zak@hotmail.com

M. Y. Saleh
e-mail: mamsaleh29@yahoo.com

M. Bassyouni (✉)
Department of Chemical Engineering, Faculty of Engineering, Port Said University, Port Said 42526, Egypt
e-mail: m.bassyouni@eng.psu.edu.eg

Center of Excellence in Membrane-Based Water Desalination Technology for Testing and Characterization, Port Said University, Port Said 42526, Egypt

East Port Said University of Technology, Saini, Port Said 45632, Egypt

oxygen demand; COD, and dissolved salts are some of the pollutants found in textile wastewater (TDS and TSS). According to Egyptian law and national organizations, the percentage of pollution caused by dye effluent should be less than the amount permissible for release [2]. Toxic pollutants should never be released into the environment because of the disastrous consequences. As a result, wastewater decolonization has emerged as a major issue in wastewater pollution [2]. Treatment of dyes wastewater aids in sustaining the water resources and minimize pollution which follows the SDGs goal for clean water.

2 Environmental Impact of Dyes and Methods of Removal

2.1 Description of Dyes and Their Classification

Dyes are aromatic compounds with a variety of functional groups. The two types of dyes used in textiles are natural dyes (derived from plants and animals) and synthetic dyes (azo and non-azo). Synthetic dyes are classified into several types based on their molecular structure. Dyes can be categorized based on their use and/or solubility. Soluble dyes include but are not limited to, acid, basic, direct, mordant, and reactive hues. Azo, dispersion sulfur, and vat dyes are examples of insoluble dyes. Tables 1 and 2 provide a summary of the various types, substrates, applications, and examples of soluble and insoluble dyes [2, 3]. A complicated chemical structure and resistance to oxidizing chemicals, light, and heat characterize synthetic dyes. Nowadays, synthetic dyes are frequently used to color cosmetics, plastics, fabrics, and printed materials. This is because dyes are naturally resistant materials that cannot be easily or effectively degraded [2]. Because auxochromes (water-soluble bonding chemicals) and chromophores are used to create synthetic dye molecules, these molecules have complex and stable structures (color-giving compounds). Simple techniques of degradation are challenging because of this characteristic of dyes. By producing dyes in this manner, it is possible to prevent color fading in dyed materials. They're supposed to be sophisticated organic materials that don't break down when exposed to water, detergents, or other cleaning products [2]. All synthetic dyes have one disadvantage in common. As a result, untreated synthetic dyes should be avoided from entering the environment and mixing with water sources. Because of their toxicity, dyes have raised serious concerns among water consumers and environmentalists. It is highly considered that techniques and technologies are being developed to totally remove one or more color kinds from water bodies [1, 2].

Table 1 Applications, types, substrates, and examples of soluble dyes

Solubility in water	Water soluble				References
Type	Acidic	Basic	Direct	Reactive	
Substrate	Nylon, wool, inks, silk, paper, and leather	Paper, processed nylon, polyacrylonitrile, inks, and polyester	Nylon, rayon, paper, leather, and cotton	Cotton, silk, wool, and nylon	[2]
Dye application	In dye baths that range from neutral to acidic	In dye baths with acidic conditions	In neutral or slightly alkaline dye baths with additional electrolytes	The interaction between the functional group of the fiber and the active site of the dye. Covalent bonds form as a result of heat and an alkaline pH	[3]
Examples	Acid yellow 36 Acid orange 7 Acid blue 83 Acid blue 7	Methylene blue Basic red 1 or rhodamine 6G Basic yellow 2	Direct orange 26 Congo red (CR) Direct red 28 Direct black 38	C.I. reactive red 120, C.I. reactive red 147, C.I. reactive blue 19	[2, 3]

2.2 Toxicity Effects of Dyes

After dyes have served their purpose in coloring materials, they are typically stored as industrial waste. These wastes are then disposed of in the environment's water bodies, contaminating colorless clean water and converting it to contaminated colored water. These industries should treat the wastewater before releasing it into the environment. Because dyes are hazardous toxic substances, water pollution caused by dyes is unacceptable to environmentalists and the general public [1]. Skin irritation can occur when dye effluent comes into contact with the skin. If dye effluents come into contact with their eyes, both humans and animals risk having their eyes burned or permanently damaged. When dye effluents are dumped into water sources, chemicals from the effluents can evaporate into the air and cause breathing difficulties or shortness of breath when inhaled. Consuming dyes can cause vomiting, nausea, methemoglobinemia, mouth burns, and excessive sweating. Traditional carcinogens like dyes have unavoidable long-term effects on the body or fetus [2]. The clear, colorless water is then polluted with color by the injection of dye wastes into environmental bodies of water. High pH and temperature immediately released concentrated dye effluents are uncommon. The mechanism for transferring oxygen and the process

Table 2 Various types, substrates, applications, and examples of different insoluble dyes

Type	Solubility in water					References
	Water insoluble					
	Azo	Disperse	Solvent	Sulfur	Vat	
Substrate	Acetate, cellulose, cotton, rayon, and polyester	Polyamide, acrylic polyester, acetate, and plastics	Fatty substances, motor oil, paints, lacquers, lubricants, stains, varnishes, waxes, cants, and plastics	Rayon and cotton	Wool and cotton	[2, 3]
Dye application	A stabilized diazonium salt solution is used to treat the fiber after it has been impregnated with a coupling component	Padded on fabric, either baked or set in a thermos at high pressure and temperature or transported using low-temperature ways	Substrate dissolution	The re-oxidation of an aromatic substrate with sodium sulfide results in the formation of insoluble sulfur-containing products on fiber	Before being exhausted on fiber and re-oxidized, water-insoluble colors are solubilized with sodium hydrogen sulfite	[2, 3]
Examples	Reddish-blue azo dye, acid orange 20, direct black 22, disperse yellow 7, methyl red, methyl orange (MO), and trypan blue	Disperse violet 1, disperse blue 27, disperse red 4, disperse yellow 3, disperse red 9, and disperse red 60	Solvent red 26, Solvent blue 35	Leuco phthalic anhydride, sulfur brilliant green, sulfur blue, sulfur black 1, and sulfur black 1	Indanthrene-based vat blue 4, vat blue 1, and vat acid blue 74	[2, 3]

by which environmental water bodies purify themselves will be interfered with by this phenomenon. When these effluents are released into the environment after use, they endanger the ecosystem because they contaminate water sources and make it difficult to use water [2]. In addition to causing eye irritation, dye effluents that are combined with natural water sources give off a bad smell. Both aquatic and terrestrial animals and plants can be harmed by textile effluents. After use, these effluents put the ecosystem in danger by contaminating water sources and making it impossible to use water [2]. When dye effluents mix with natural water sources, a foul odor, and eye irritation follow. Textile effluents can affect both land-based and aquatic animals and plants. When dye effluents mix with water, they produce a visible layer above the surface of the water due to their lower density of 0.8 kg/m^3 compared to water's density of 1.0 kg/m^3. This causes turbidity to increase. This stops sunlight from reaching undersea living creatures, effectively destroying their existence [2]. The most significant and serious environmental issue with dyes is that they absorb and reflect sunlight that enters the water, blocking bacterial development or reducing it to insufficient levels to destroy pollutants biologically. Aesthetic concerns pale in comparison to environmental concerns [1].

2.3   Importance and Methods of Dyes Removal

Previously, it was not considered acceptable to discharge dye wastewater into the environment. This issue has only recently received the attention it deserves, as health issues have emerged. There is little doubt that for technical, economic, and environmental reasons, many nations value the removal of such colored compounds from aqueous effluents. Textile wastewaters have a high biodegradability due to the presence of dyes [3].

Therefore, the most urgent problem is still how to effectively and cheaply remove dyes from the textile business. Large volumes of dye should be quickly removed from wastewater using a process that produces no secondary contamination. Biological, chemical, and physical approaches can all be used to remove dye [2].

2.3.1   Biological Dye Removal Methods

Anaerobic and aerobic processes are combined prior to the release of dye effluents into the environment. Although this method reduces the wastewater's chemical oxygen demand, it does not render the water colorless or toxin-free [2]. Pure and mixed cultures, algae and enzyme breakdown, microbial biomass adsorption, fungal and microbial cultures, and fungal and microbial cultures are examples of traditional biological dye removal procedures. The biological dye-removal procedure involves the use of a living thing [2]. The main disadvantage of this procedure is that it progresses slowly because it involves living things. Because it can occasionally be

difficult to estimate their development rate and reactivity, biological dye removal procedures frequently experience system instability [2].

2.3.2　Methods of Chemical Dye Removal

Chemical dye removal procedures remove the dye using chemistry principles. Traditional chemical dye removal procedures include advanced oxidation, electrochemical destruction, Fenton reaction dye removal, oxidation, ozonation, photochemical irradiation, and ultraviolet radiation. The bulk of chemical dye removal processes, with the exception of electrochemical degradation dye removal, are more expensive than biological and physical dye removal approaches. Chemical color removal techniques necessitate costly equipment and a lot of energy, making them commercially unappealing. Electricity is needed in large quantities to power the machinery or reactors used to remove chemical dyes. Additionally, users of chemical dye removal methods frequently lament the high chemical and reagent consumption. Another drawback of this technology is the development of harmful secondary contamination following chemical color removal procedures, which creates a new disposal problem [2].

2.3.3　Methods of Physical Dye Removal

Physical dye removal is the most widely used of the three techniques (chemical, biological, and physical). The mass transfer mechanism is employed in the majority of straightforward physical dye removal methods. Adsorption, coagulation or flocculation, ion exchange, irradiation, membrane filtration, nanofiltration or ultrafiltration, and reverse osmosis are all traditional physical dye removal procedures. Due to their effectiveness and simplicity, these techniques are frequently used. This technique uses the least amount of chemicals when compared to biological or chemical dye removal techniques. This process is thought to be more dependable than the other two dye removal techniques because there are no living organisms present [2]. However, due to the high cost of each of these techniques, small businesses are unable to use them to treat a variety of wastewater. Adsorption, therefore, seems to be a better approach for handling effluents from the textile industry [2]. Adsorption has been shown to outperform alternative methods in terms of design simplicity and flexibility, up-front cost, sensitivity to toxic contaminants, constituent removal from organic waste, and ease of operation. Adsorption doesn't result in any toxic byproducts [3]. The cost of getting started and purchasing the land was lower. It is very effective, simple to use, and appropriate for a variety of absorbents. Surprisingly, the adsorption technique removes inorganic and organic complex metals that other treatment methods do not. However, because each of these methods is costly, small enterprises cannot utilize them to treat a variety of wastewater. Adsorption, therefore, seems to be a better approach for handling effluents from the textile sector [2]. In terms of starting cost, sensitivity to harmful contaminants, removal of organic waste

constituents, design flexibility, and simplicity, adsorption has been proven to be superior to alternative approaches. Adsorption does not produce any hazardous materials [3]. It needed less money and land investment up front. It is very effective, easy to use, and appropriate for a range of absorbents. Unexpectedly, the adsorption process successfully eliminates inorganic and organic complex metals that previous treatment techniques would not remove. Adsorption is a desirable method for cleaning up polluted waterways when the sorbent is affordable and does not necessitate a separate, costly pre-treatment operation [4].

2.4 Adsorption Using Fly Ash

During the adsorption process, materials accumulate at the interface between two phases, such as a liquid–liquid, gas–liquid, gas–solid, or liquid–solid contact. The adsorbate is the substance that is adsorbed, while the adsorbent is the material that conducts the adsorption. Adsorbates and adsorbents have different properties that are influenced by their ingredients.

The adsorption process is comprised of four steps, which are as follows: Adsorption between the adsorbate and the adsorbent's active sites can occur in four ways: (i) via bulk solution boundary layer diffusion, (ii) via film diffusion or external mass diffusion, (iii) via pore diffusion or intraparticle diffusion, and (iv) by physical and/or chemical interaction [4, 5].

If the interaction between the adsorbed molecules and the solid surface is physical in character, the process is known as physisorption. If chemical bonding is the cause of the attraction forces between adsorbed molecules and the solid surface, the adsorption method is known as chemisorption. Table 3 indicates the differences between chemisorption and physical sorption.

Because a homogenous distribution of adsorbent and adsorbate in a solution can lessen the influence of mass transfer resistance, the first bulk diffusion stage is typically avoided if the solution is agitated evenly. Because the physical/chemical reaction, the final step, occurs quickly, adsorption kinetics is dominated by film diffusion and/or pore diffusion.

Liquid concentration and adsorbent outer surface film diffusion rate are related (i.e., liquid membrane area). As the relative velocities of the liquid and particle increase, the fixed liquid film on the particle's outer surface thins, hastening the film's diffusion. The fluidity of the pollutants in the pores influences the pore diffusion rate, which is correlated with the pore structure and distribution of the adsorbents as well as the molecular size and structure of the adsorbates but is less influenced by the liquid concentration or the outer surface area of the adsorbent particle [5].

Table 3 Characteristics and differences between physisorption and chemisorption

Property	Physisorption	Chemisorption	Ref
Characteristics	Adsorption molecules and solid surfaces have weak wear-attractive forces. Adsorbent molecules are free to move across the surface because they are not attached to a particular size of the adsorbent particle. Electrostatic forces in physical sorption include dipole–dipole interactions, dispersion interactions, and hydrogen bonds between the adsorbate and the adsorbent	A dipole moment is formed when there is a net separation of positive and negative charges within a molecule. On the other hand, chemisorption involves the formation of chemical bonds between sorbent and sorbate molecules	[4, 6]
Type of bonding forces	Physisorption occurred as a result of weak Van der Waals attraction forces	Chemisorption results from stronger electrostatic forces, such as covalent or electrostatic chemical bonds, which are required for the attraction of the sorbent and sorbate. This relationship is more energetic and shorter	[4, 6]
Reversibility	Due to the nature of the weaker bonding forces and energies, this sorption is reversible. The adsorptive in the fluid surrounding the surface becomes less active, resulting in adsorbate desorption	This sorption is irreversible in nature. Desorbed compounds are different from adsorbed ones	[4, 6]
Adsorption heat	Low, 10–40 kJ mol^{-1}	High, 20–400 kJ mol^{-1}	[4, 6]
Energy activation	Very low (close to zero)	High, similar to a chemical reaction	[4, 6]
Required temperature	Low temperature required	High temperature is required	[4, 6]
Chemical change of adsorptive	None	A surface compound formation	[4, 6]
Specificity of adsorbate–adsorbent interactions	Very low	High	[4, 6]
Formation of multilayers	It results in multimolecular layers on the adsorbent surface	It results in a unimolecular layer	[4, 6]

2.4.1 Removal of Dyes Using Adsorption

Because of its amazing ability to eradicate practically any type of dyestuff, adsorption (physical approach) has become one of the most extensively used dye removal procedures among the various tried-and-true dye removal processes. This approach

can be used to clean both drinking water and industrial waste. Synthetic dyes cannot be completely removed from dye wastewater using standard methods. Adsorption is one of the most effective dye-removal processes currently in use. Adsorption dye effluent treatment generated higher-quality treated water than earlier dye removal technologies. This method's sole flaw was the high cost of the adsorbents, but after less expensive but equally efficient adsorbents were discovered, it was refined and is today a popular, reasonably priced method of color removal [2, 3]. Adsorbents are extremely minute porous substances. They act like sponges, adhering to other materials. Various industrial ecology segments can be cleaned or have contaminants removed using adsorbent components [4–7]. Adsorbents are often classified into five types: Activated carbons, activated alumina, and silica gel are examples of natural materials that have been processed to develop their structures and properties. Aluminosilicates, polymeric resins, and zeolites are examples of manmade materials. Bauxite, wood, fuller's earth, and sawdust are examples of natural materials [8–10]. Some examples of industrial byproducts include fly ash, date pits, and solid agricultural waste. agricultural wastes and industrial byproducts like fly ash, red mud, and date pits [11]; bio sorbents like chitosan or bacterial, fungal, or fungal biomass; and effluents from sewage treatment plants. The term "adsorption capacity" describes an adsorbent's capacity to bind a specific volume of adsorbate to its surface [12, 13]. The surface area is a crucial component of a good adsorbent. With increasing porosity, an adsorbent's surface area grows, leading to a high adsorption capacity [14, 15]. A good adsorbent should have a short adsorption period because the system needs time to reach equilibrium [16–18]. Fourth, the ability of an adsorbent to remove various types of contaminants must be considered [19, 20]. A good adsorbent should work at a variety of temperatures, pH levels, and dye concentrations. Adsorbents are the most important component of the adsorption process [21–23]. The cost of the adsorbent employed is a common issue with the adsorption process. Numerous research papers have identified and established less expensive adsorbents to address this issue [24–26]. To remove dyes from textile wastewater, natural and even waste materials can be converted into adsorbents [27–29]. It was reported that there are 185 different low-cost adsorbents can be used with different adsorption capacity [30].

2.4.2 Fly Ash Source and Generation

Combustion produces fly ash, also referred to as flue ash. Clay, feldspar, quartz, and shale are a few examples of the mineral impurities in coal that fuse in suspension during combustion and float out with exhaust gases. Depending on the source and makeup of the coal burned, fly ash's composition can vary greatly. SiO_2, Al_2O_3, Fe_2O_3, and CaO are all present in fly ash. To capture fly ash that has crystallized while still in the exhaust gases, electrostatic precipitators or filter bags are utilized. Fly ash particles are spherical, can range in size from 0.5 to 300 m, and solidify fast while suspended in exhaust gases [31].

Annually, thousands of tons of fly ash are produced as waste by power plants that use coal or sugar. Significant disposal and environmental problems result from it. A

waste product created by coal power plants when powdered lignite coal is burned in a fluidized bed combustion technology system to produce electricity is called coal fly ash. Significant environmental, disposal, and health problems are brought on by this powdered waste. Coal fly ash is a grey substance that is acidic, refractory, and abrasive in nature. It has a bulk density of 600–900 kg/m^3, a specific surface area of 2500–7000 cm^2/g, a porosity of 0.38%, a pore volume of 0.023 cm^3/g, a specific gravity of 2.3–2.5, and a specific surface area of 2500–7000 cm^2/g [32].

Classification and Properties of Fly Ash

The type of coal used to make fly ash determines its classification. Coal is classified into four types/ranks: lignite, bituminous, sub-bituminous, and anthracite. The majority of the constituents in bituminous coal fly ash include alumina, silica, calcium, iron oxide, and variable levels of carbon. Sub-bituminous and lignite coal fly ashes contain less silica and iron oxide, more calcium and magnesium oxide, and less carbon than bituminous coal fly ashes. Because anthracite coal is rarely used in utility boilers, there is extremely little anthracite coal fly ash. The physical/chemical properties of fly ash are affected by the type of coal used in a process, as well as the techniques utilized to burn the coal. Particularly influential on fly ash qualities are (i) boiler configuration, (ii) boiler burning condition and temperature, (iii) coal particle size, and (iv) gas cleaning equipment [33]. The minimum three categories into which fly ash can be classified are chemical composition, physical characteristics, and mineralogical composition [34].

Chemical Composition of Fly Ash

Two classification standards are mentioned for chemical composition (ASTM C618 and Canadian Standard, CAN/CSA-A3000-03. According to ASTM, the total silicon oxide (SiO_2) composition plus alumina oxide (Al_2O_3) plus iron oxide (Fe_2O_3) must be at least 70% (by weight) for class F fly ash and 50% (by weight) for class C fly ash [34].

Class C fly ashes contain more calcium (as CaO) than Class F fly ashes, according to ASTM. Class C fly ash includes more than 15% CaO, and Class F fly ash contains less than 5% CaO. When anthracite or bituminous coal is burned, Class F fly ash is usually produced. This fly ash has pozzolanic properties. Class F fly ash must be coupled with a cementing ingredient such as Portland cement, quicklime, or hydrated lime due to its pozzolanic qualities in order for glassy silica and alumina to react and generate cementitious compounds. A geopolymer can also be made using a Class F ash, such as sodium silicate, and a chemical activator (water glass). Typically, Class C fly ash is produced using lignite or sub-bituminous coal. In addition to having pozzolanic qualities, this fly ash also has some self-cementing qualities. Class C fly ash strengthens and hardens when exposed to water. In contrast to Class F fly ash, self-cementing Class C fly ash does not require an activator. Class C fly ashes contain

more sulfate (SO_4) and alkali than other types [35]. In addition to Class F and C fly ashes, the US ASTM C618 standard also lists Class N mineral admixtures. Some clays and shales, as well as raw or natural pozzolans such as diatomaceous earth, opaline cherts, and shales, as well as calcined or uncalcined volcanic ashes or pumicites, are examples of Class N mineral admixtures. These materials must be calcined to induce pozzolanic or cementitious qualities. The Canadian Standard, CAN/CSA-A3000-03, is another standard that classifies fly ash. These standards divide fly ash into three categories depending on the chemical component calcium oxide. Fly ash containing less than 8% calcium compound (by weight) is categorized as F, those containing 8–20% calcium compound (by weight) as CI, and those containing more than 20% calcium compound (by weight) as CH [34]. The chemical composition ranges of fly ash components employed in color removal are shown in Table 4.

Physical Properties of Fly Ash

Fly ash is made up of tiny, powdery, mostly spherical, hollow or solid, and amorphous particles. Coal ash has a specific gravity that ranges from 1.6 to 3.1, but it usually stays around 2.0.

A variety of factors influence this fluctuation, including particle form, gradation, and chemical makeup. Fly ashes are divided into two groups: sandy silt and silty sand, based on the distribution of their grain sizes. The coal ashes are primarily silt-sized with a small amount of clay-sized fraction, especially in India. Despite its low bulk density, fly ash has a significant specific surface area.

Fly ash can range in color from orange to deep red, brown, white, or yellow depending on the quantity of unburned carbon and iron present [33]. The quantity retained when wet-weight is one of the physical characteristics that both classes of fly ash must meet, according to ASTM C618.

In addition to fineness, ASTM also specifies requirements for soundness, uniformity, water requirement, and strength activity index. Despite the fact that the CAN/CSA-A3000-03 standard includes physical requirements such as restricting SO to 5% for all kinds, LOI to 8% for type F and 6% for type CI, and expanding to 0.8% [34, 35], the study employed five samples of fly ash from various coal-fired power plants.

Table 5 shows the fly ash code and physical properties. Dissolving 20 g of fly ash in 80 mL of deionized water yields the alkalinity (pH) of the fly ash. Particle size analysis (PSA) was performed on the fly ash to identify the gradation distribution of the fly ash type. Figure 1 depicts the color of fly ash. Samples were found to have different color and Fe_2O_3 wt.% [34].

In addition to its physical characteristics, fly ash also has aesthetic qualities, particularly color, which is frequently influenced by the amount of iron oxide and the amount of carbon. Additionally, the black or grey appearance of some concretes is due to the carbon percentage, which can range from 0.5 to 10 or 12% in some cases. The relationship between iron oxide levels and fly ash colour is supported by Fig. 1 [34].

Table 4 Chemical components of fly ash used in dye removal

Component (wt.%)	SiO$_2$	Al$_2$O$_3$	CaO	Fe$_2$O$_3$	MgO	SO$_3$	TiO$_2$	P$_2$O$_5$	Na$_2$O	K$_2$O	LOI	Application	References
A large-scale power plant in China supplied raw coal fly ash	47.2%	24.8%	(4.9%)	15.9%	–	–	–	–	–	–	–	Reactive red 23, reactive blue 171, and acid black 1	[36]
Raichur thermal power station (RTPS), a coal-fired power station in Karnataka, India, supplied the fly ash	63.55	22.71	5.66	3.72	1.48	1.34	0.60	0.46	0.26	0.11	–	Reactive blue 25 dye	[37]
Fly ash obtained from Lethabo, South Africa	52.59	34.59	4.08	3.15	1.06	–	–	0.28	0.17	0.60	1.4	Methylene blue	[38]
Fly ash from South African coal was obtained from the Lethabo power plant	52.59	34.59	4.08	3.15	1.06	–	–	0.28	0.17	0.60	1.4	Methyl orange	[39]

Table 4 (continued)

Component (wt.%)	SiO₂	Al₂O₃	CaO	Fe₂O₃	MgO	SO₃	TiO₂	P₂O₅	Na₂O	K₂O	LOI	Application	References
The coal fly ash utilized in this investigation was supplied by a power plant in Shandong, China	50.76	36.04	3.64	3.31	0.43	1.39	1.79	–	0.53	1.14	–	Methylene blue	[40]
The fly ash was from the thermal coal plant of Jorfasfar in Morocco	52.5	30.2	0.822	2.94	1.23	0.787	1.03	0.203	–	–	7.12	Indigo carmine and acid orange	[41]
The Tuticorin Thermal Power Plant in Tamil Nadu, India's electrostatic precipitator produced raw coal fly ash	53.3	29.5	7.6	10.7	–	1.8	–	–	–	–	0.33	Methylene blue	[42]

Table 4 (continued)

Component (wt.%)	SiO$_2$	Al$_2$O$_3$	CaO	Fe$_2$O$_3$	MgO	SO$_3$	TiO$_2$	P$_2$O$_5$	Na$_2$O	K$_2$O	LOI	Application	References
The Jorf Lasfar power plant in ELJaddida, Morocco, is where the fly ash was produced	52.5	30.2	0.822	2.94	1.23	0.719	1.03	0.203	0.719	2.08	7.12	Methylene blue	[43]
The fly ash came from an Indian thermal coal power plant in Panipat, Haryana	62.28	25.32	0.69	6.44	0.62	–	1.52	–	0.10	2.02	–	Methylene blue	[44]

Table 5 Physical properties and pH of the fly ash sample

Fly ash (Fe$_2$O$_3$%)	Source	pH	SSA (kg/m^2)	Dv(90) (μm)	Dv(50) (μm)	Dv(10) (μm)	Specific gravity
9.66	Tanjung Jati	10.6	2078	63.5	8.03	1.46	2.915
15.00	Paiton unit 1 & 2	10.3	1370	13.6	20.1	2.38	2.489
17.71	Paiton unit 5 & 6	9.8	1785	84.3	10.3	1.73	2.360
24.28	Rembang	9.6	1169	104	19.2	3.08	2.245
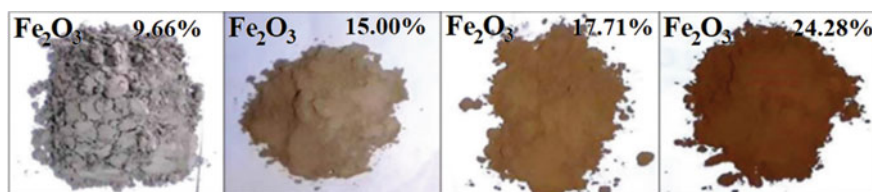
Fig. 1 The color of obtained fly ash from five different sources, each with different Fe$_2$O$_3$ contents

SEM, on the other hand, can be used to investigate the morphology and composition of fly ash particles affected by heating and cooling operations. A detailed examination of fly ash particles reveals that iron oxide exhibits a range of textures, both outwardly and inside [34, 45].

3 Batch Process and Fixed Bed Column

Based on how it functions, adsorption is divided into two categories: static and dynamic. In contrast to static adsorption, also known as batch adsorption, which occurs in a closed system with the desired amount of adsorbent contacting with a specific volume of adsorbate solution, dynamic adsorption typically occurs in an open system where adsorbate solution continuously passes through a column packed with adsorbent [46].

Batch mode or fixed bed column adsorption techniques can be employed in the lab to adsorb undesired contaminants such as heavy metals and synthetic colors on activated carbon. The use of adsorption to remove specific pollutant constituents can be learned from laboratory adsorption studies. However, the greatest practical use of the adsorption process in the treatment of wastewater is provided by continuous column research [29]. According to several scientific studies, the continuous adsorption method is more adaptable and acceptable in actual water treatment industries due to its cheap running costs and the columns' adaptability to varied procedures. However, for pilot-scale or commercial applications, batch reactors are not the best

option. For laboratory research, batch reactors are helpful. Batch mode approaches were used in most published investigations on the adsorption of dyes (and heavy metals) by activated carbon. The determination of the sorbent's sorption capacity in the batch equilibrium experiment reveals the effectiveness of the sorbate-sorbent system essentially. The data gained from such a technique, however, cannot be applied to most treatment processes (i.e., the column process) since the contact time in the batch process is insufficient to attain equilibrium in the continuous flow process [44]. Fixed-bed columns, on the other hand, are widely utilized in many chemical industries due to their ease of usage. When there is a high amount of wastewater to be treated, continuous treatment is also much more time-effective than batch-mode treatment [46]. The experimental breakthrough curve is calculated using the fixed-bed column technique. As shown in a number of scientific papers [45], fixed bed column adsorptions with activated carbon have been used for many years to remove organic contaminants. This is because high adsorption capacities are attained when the influent concentration is in equilibrium as opposed to the effluent concentration. The quantity of activated carbon adsorbent in contact with the same solution is fixed in batch mode (static mode) adsorption studies. The adsorption process must be continued in order to reach an equilibrium between the solute concentration in the solution and the solute adsorbed (i.e., synthetic dyes) per unit weight of the AC adsorbents. In this scenario, equilibrium is static, which means that it does not alter over time. Because the solution continuously enters and departs the column, dynamic column adsorption ensures that equilibrium is never reached. Because it must be established each time it reaches a fresh concentration, equilibrium in column mode is referred to as dynamic equilibrium [47]. Column treatment, also known as a fixed bed or continuous pack bed, is a typical adsorption technique in which an adsorbate solution is constantly fed through a column containing an adsorbent at a specified flow rate. Furthermore, the adsorbent and adsorbate are in constant contact. The advantage of fixed-bed operations is that all fluid that departs the column is contaminant-free for a short time. When complete removal is not required, batch or fixed-bed adsorption can be used to reduce the amount of adsorbent required for a given separation [48]. Comparisons of batch trials and fixed bed columns are shown in Table 6. This table demonstrates that a fixed bed column is superior and industrially practicable for removing various impurities from both simulated and real wastewater. There aren't many comparison studies between fixed-bed and batch processes in the early literature [49], compared to studies of each process alone. Table 6 lists studies on dye removal on various adsorbents using fixed bed column adsorption models and batch treatment.

4 Conclusions

Fly ash is a byproduct of coal combustion, and it has been found to be effective in wastewater treatment due to its adsorption and ion exchange properties. When used in conjunction with other treatment methods, fly ash can help to reduce the concentration

Table 6 Comparison between fixed bed column and batch experiments

	Fixed bed column	Batch process	References
Introduction	A fixed-bed system consists of an adsorbent through which adsorbate flows at a steady rate	• In a well-mixed system, the adsorbent and adsorbate are thoroughly combined in a diluted solution at a constant volume • The residual concentration in the adsorbent and the bulk eventually come to an equilibrium	[25]
Mechanism	A packed column of adsorbent is continuously fed contaminated fluid, and when the adsorbent and feed concentration reach equilibrium, the column is fully loaded with contaminants (i.e., adsorbate). Although a considerable amount of the column is in equilibrium with the feed, adsorbent use is limited by mass transfer and axial dispersion difficulties	Adsorption occurs after the adsorbent has been added to a specific volume of contaminated fluid because the adsorbent is now in equilibrium with the remaining concentration in the bulk	[26]
Advantages	• Very easy and cheap technique • Simplicity of scale-up process • Used for larger amounts of wastewater with a higher pollution load • Used extensively in industry • Compared with batch adsorption, the contact time is shorter • Equilibrium is not reached for certain adsorption	• Cheap and easy technique • Analyze the feasibility of adsorbent—adsorbate system • The performance of an adsorbent can be predicted before being applied on a larger scale thanks to studies of adsorption by equilibrium in batch mode	[25]

(continued)

Table 6 (continued)

	Fixed bed column	Batch process	References
Disadvantages	• Adsorbent attrition, feed channeling, and uneven adsorbent particle flow are issues with this sorption • It is difficult to carry out a priori design and optimization of fixed-bed columns without a quantitative methodology. Adsorbent exhaustion, inlet channeling, and unpredictable particle feed flow	• Small quantity of wastewater • Minimum pollution load • Scarcely used in industrial applications • Not suitable for real-scale application • Adsorbent is eliminated from the system using a straightforward filtration process	[26]
Isotherm models	• Bed depth service time model (BDST) • Thomas model (TM) • Clark model (CM) • Wolborska model (WM) • Adam and Bohart model (ABM) • Modified dose–response model (MDRM) • Yoon–Nelson model (YNM)	• Linear isotherm model (Henry's law) • Freundlich • Redlich&Peterson • Sips isotherm model • Toth isotherm model • Temkin isotherm model • Dubinin-Radushkevich (D-R) • Astakhov (D-A) models • Langmuir isotherm model • Volmer isotherm model • BET isotherm model ($n = \infty$) • Aranovich isotherm model • Homovalent Model • Monovalent and bivalent	[27]

of pollutants in wastewater. Studies have shown that fly ash can effectively remove pollutants such as heavy metals, dyes, and organic compounds from wastewater. It is also relatively inexpensive and widely available, making it an attractive option for wastewater treatment in developing countries and areas with limited resources to use it in industrial sector especially textile industry. However, it is important to note that fly ash is not a standalone solution for wastewater treatment. It should be used in conjunction with other treatment methods, such as coagulation, sedimentation, and filtration, to ensure the effective removal of pollutants. In conclusion, fly ash can be an effective and cost-efficient option for wastewater treatment when used in combination with other treatment methods. Its potential use in this field warrants further investigation and research to fully explore its capabilities and limitations.

5   Recommendation

Removal of dyes from wastewater is crucial for the environment and human health. Using fly ash as an adsorbent showed promising results in the treatment of the tested wastewater. It is also cost efficient. Also, it is recommended to use it in conjunction with other treatment methods. Therefore, it is recommended to do more research in the future to enhance and develop the adsorption process using fly ash to produce cleaner water that can be reused.

References

1. Noroozi B, Sorial GA (2013) Applicable models for multi-component adsorption of dyes: a review. J Environ Sci 25(3):419–429
2. Katheresan V, Kansedo J, Lau SY (2018) Efficiency of various recent wastewater dye removal methods: a review. J Environ Chem Eng 6(4):4676–4697
3. Yagub MT, Sen TK, Afroze S, Ang HM (2014) Dye and its removal from aqueous solution by adsorption: a review. Adv Coll Interface Sci 209:172–184
4. Patel H (2019) Fixed-bed column adsorption study: a comprehensive review. Appl Water Sci 9(3):1–17
5. Mishra A, Tripathi BD (2008) Utilization of fly ash in adsorption of heavy metals from wastewater. Toxicol Environ Chem 90(6):1091–1097
6. Hamdon RS, Salem A, Ahmed HG, ElZahar MM (2022) Use of chitosan for enhancing the process of surface water purification in Egypt. Int J Environ Sci Dev 13(2):26–34
7. Saleh MY, Enany GE, Elzahar MH, Elshikhipy MZ, Hamouda R (2014) Removal of lead in high rate activated sludge system. Int J Environ Ecol Eng 8(4):413–418
8. Saleh MY, El Enany G, Elzahar MH, Elshikhipy MZ (2014) Industrial wastewater treatment using high rate activated sludge and alum additive. Int J Environ Sci Dev 5(6):551

9. Saleh MY, El Enany G, Elzahar MH, Omran MH (2015) Industrial wastewater treatment improvements using activated carbon. In: International conference on energy, ecology, environment and sustainable development, Miami, USA

10. Saleh M, El Enany G, Elzahar M, Omran M (2017) Industrial wastewater treatment improvements using limestone. J Environ Stud Res 7(2):910–918

11. Wang L, Shi C, Pan L, Zhang X, Zou JJ (2020) Rational design, synthesis, adsorption principles and applications of metal oxide adsorbents: a review. Nanoscale 12(8):4790–4815

12. Králik M (2014) Adsorption, chemisorption, and catalysis. Chem Pap 68(12):1625–1638

13. Crini G, Lichtfouse E, Wilson LD, Morin-Crini N (2019) Conventional and non-conventional adsorbents for wastewater treatment. Environ Chem Lett 17(1):195–213

14. Saleh M, El Enanyb G, Elzaharc M, Elshikhipy M (2014) Use of alum for removal of total dissolved solids and total iron in high rate activated sludge system. Int J Environ Eng Sci Technol Res 2:1–12

15. Ahmaruzzaman M (2010) A review on the utilization of fly ash. Prog Energy Combust Sci 36(3):327–363

16. Blissett RS, Rowson NA (2012) A review of the multi-component utilization of coal fly ash. Fuel 97:1–23

17. Zhou J, Xia K, Liu X, Fang L, Du H, Zhang X (2021) Utilization of cationic polymer-modified fly ash for dye wastewater treatment. Clean Technol Environ Policy 23:1273–1282

18. Mushtaq F, Zahid M, Bhatti IA, Nasir S, Hussain T (2019) Possible applications of coal fly ash in wastewater treatment. J Environ Manag 240:27–46

19. Zoromba MS, Ismail MIM, Bassyouni M, Abdel-Aziz MH, Salah N, Alshahrie A, Memic A (2017) Fabrication and characterization of poly (aniline-co-o-anthranilic acid)/magnetite nanocomposites and their application in wastewater treatment. Colloids Surf A 520:121–130

20. Sandid AM, Bassyouni M, Nehari D, Elhenawy Y (2021) Experimental and simulation study of multichannel air gap membrane distillation process with two types of solar collectors. Energy Convers Manag 243:114431

21. Fouad K, Alalm MG, Bassyouni M, Saleh MY (2020) A novel photocatalytic reactor for the extended reuse of W-TiO$_2$ in the degradation of sulfamethazine. Chemosphere 257:127270

22. Elhady S, Bassyouni M, Mansour RA, Elzahar MH, Abdel-Hamid S, Elhenawy Y, Saleh MY (2020) Oily wastewater treatment using polyamide thin film composite membrane technology. Membranes 10(5):84

23. Abdel-Aziz MH, Bassyouni M, Zoromba MS, Alshehri AA (2018) Removal of dyes from waste solutions by anodic oxidation on an array of horizontal graphite rods anodes. Ind Eng Chem Res 58(2):1004–1018

24. Maddah HA, Alzhrani AS, Bassyouni M, Abdel-Aziz MH, Zoromba M, Almalki AM (2018) Evaluation of various membrane filtration modules for the treatment of seawater. Appl Water Sci 8:1–13

25. Gutub SA, Bassyouni M, Abdel-Hamid SMS (2013) Dissolved solids adsorption of freshwater using synthesized bio-foam composite. Life Sci J 10(2):464–471

26. Abdel-Aziz MH, Bassyouni M, Soliman MF, Gutub SA, Magram SF (2017) Removal of heavy metals from wastewater using thermally treated sewage sludge adsorbent without chemical activation. J Mater Environ Sci 8(5):1737–1747

27. Elhenawy Y, Moustafa GH, Abdel-Hamid SMS, Bassyouni M, Elsakka MM (2022) Experimental investigation of two novel arrangements of air gap membrane distillation module with heat recovery. Energy Rep 8:8563–8573

28. Sait HH, Hussain A, Bassyouni M, Ali I, Kanthasamy R, Ayodele BV, Elhenawy Y (2022) Anionic dye removal using a date palm seed-derived activated carbon/chitosan polymer microbead biocomposite. Polymers 14(12):2503

29. Eteba A, Bassyouni M, Saleh M (2021) Removal of hazardous organic pollutants using fly ash. Environ Ecol Res 9:196–203

30. Rafatullah M, Sulaiman RHO, Ahmad A (2010) Adsorption of methylene blue on low-cost adsorbents: a review. J Hazard Mater 177(1–3):70–80

31. Dabi N, Patwa N (2015) Flyash: an effective method for treatment of wastewater. Int J Eng Res Technol 3(23):1–3
32. Shah AK, Ali ZM, Laghari AJ, Shah SFA (2013) Utilization of fly ash as low-cost adsorbent for the treatment of industrial dyes effluents—a comparative study. Res Rev: J Eng Technol 2(1):1–10
33. Bhatt A, Priyadarshini S, Mohanakrishnan AA, Abri A, Sattler M, Techapaphawit S (2019) Physical, chemical, and geotechnical properties of coal fly ash: a global review. Case Stud Constr Mater 11:e00263
34. Wattimena OK, Antoni D, Hardjito (2017) A review on the effect of fly ash characteristics and their variations on the synthesis of fly ash based geopolymer. In: AIP conference proceedings, vol 1887, no 1. AIP Publishing LLC, p 020041
35. Dwivedi A, Jain MK (2014) Fly ash–waste management and overview: a review. Recent Res Sci Technol 6(1)
36. Sun D, Zhang X, Wu Y, Liu X (2010) Adsorption of anionic dyes from aqueous solution on fly ash. J Hazard Mater 181(1–3):335–342
37. Deshannavar UB, Katageri BG, El-Harbawi M, Parab A, Acharya K (2017) Fly ash as an adsorbent for the removal of reactive blue 25 dye from aqueous solutions: optimization, kinetic and isotherm investigations. Proc Estonian Acad Sci 66(3)
38. Potgieter JH, Pearson S, Pardesi C (2018) Kinetic and thermodynamic parameters for the adsorption of methylene blue using fly ash under batch, column, and heap leaching configurations. Coal Combust Gasif Prod 10(2):23–33
39. Potgieter JH, Pardesi C, Pearson S (2021) A kinetic and thermodynamic investigation into the removal of methyl orange from wastewater utilizing fly ash in different process configurations. Environ Geochem Health 43(7):2539–2550
40. Yuan N, Cai H, Liu T, Huang Q, Zhang X (2019) Adsorptive removal of methylene blue from aqueous solution using coal fly ash-derived mesoporous silica material. Adsorpt Sci Technol 37(3–4):333–348
41. El Alouani M, Alehyen S, Achouri ME, Taibi M (2017) Potential use of Moroccan fly ash as low cost adsorbent for the removal of two anionic dyes (indigo carmine and acid orange). J Mater Environ Sci 8:3397–3409
42. Murugan P, Ramesh ST, Biju VM (2020) Characterization, morphology and stability assessment of low-cost industrial by-product as an adsorbent for the removal of methylene blue from aqueous solution. Sep Sci Technol 55(3):471–486
43. Alouani MEL, Alehyen S, Achouri MEL, Taibi M (2018) Removal of cationic dye—methylene blue—from aqueous solution by adsorption on fly ash—based geopolymer. J Mater Environ Sci 9(1):32–46
44. Mor S, Chhavi MK, Sushil KK, Ravindra K (2018) Assessment of hydrothermally modified fly ash for the treatment of methylene blue dye in the textile industry wastewater. Environ Dev Sustain 20(2):625–639
45. Wijaya SW, Hardjito D (2016) Factors affecting the setting time of fly ash-based geopolymer. In: Materials science forum, vol 841. Trans Tech Publications Ltd., pp 90–97
46. Eteba A, Bassyouni M, Saleh M (2022) Utilization of chemically modified coal fly ash as cost-effective adsorbent for removal of hazardous organic wastes. Int J Environ Sci Technol 1–14
47. Eteba A, Bassyouni M, Saleh M (2022) Modified coal fly ash for textile dye removal from industrial wastewater. Energy Environ. 0958305X221130536
48. Abdel-Aziz MH, El-Ashtoukhy EZ, Bassyouni M, Al-Hossainy AF, Fawzy EM, Abdel-Hamid SMS, Zoromba MS (2021) DFT and experimental study on adsorption of dyes on activated carbon prepared from apple leaves. Carbon Lett 31:863–878
49. Bassyouni M, Zoromba MS, Abdel-Aziz MH, Mosly I (2022) Extraction of nanocellulose for eco-friendly biocomposite adsorbent for wastewater treatment. Polymers 14(9):1852

Assessing the Performance and Fouling of Polytetrafluorethylene Hydrophobic Membrane for the Treatment of Oil-Polluted Seawater Using AGMD

Check for
updates

A. E. Mansi, Y. Elhenawy, Maggie Gad, Noran Ashraf, Ahmed Eteba, and M. Bassyouni

1 Introduction

Bilgewater is a chronic source of oil pollution that is being increasingly discharged to the marine ecosystem. Bilgewater is complex shipboard wastewater comprising mainly seawater in addition to various ship pollutants (e.g., fuels, lubrication oils, solid particulates, etc.) [1]. The environmental and ecological impacts of ship fluids discharge into the ocean are very far-reaching. Coastal plants are very vulnerable to the hydrocarbon residues in the bilgewater. The heavy residues can accumulate in the

A. E. Mansi · M. Gad · N. Ashraf · M. Bassyouni (✉)
Department of Chemical Engineering, Faculty of Engineering, Port Said University, Port Said 42526, Egypt
e-mail: m.bassyouni@eng.psu.edu.eg

A. E. Mansi · M. Bassyouni
Center of Excellence in Membrane-Based Water Desalination Technology for Testing and Characterization, Port Said 42526, Egypt

Y. Elhenawy
School of Chemical and Metallurgical Engineering, University of the Witwatersrand, Johannesburg 2000, South Africa

Department of Mechanical Power Engineering, Faculty of Engineering, Port Said University, Port Said 42526, Egypt

Y. Elhenawy
e-mail: dr_yasser@eng.psu.edu.eg

A. Eteba
Civil Engineering Department, Higher Future Institute of Engineering and Technology, El Mansoura, Egypt

M. Bassyouni
East Port Said University of Technology, Saini, Port Said 45632, Egypt

soil and adversely affect its permeability. Marine mammals are as well threatened by the bilgewater pollutants, they are susceptible to accidental consumption of tar residuals and physical contact with oils all of which cause severe health conditions. Therefore, the treatment of bilgewater is mandatory for sustaining the ecosystem and for potential reutilization for the irrigation of coastal plants [2]. Minimization or elimination of ship fluids discharge to the ecosystem adheres to the Sustainable Development Goals (SDGs) by sustaining the marine life, the coastal plants, and the water ways (Goals No. 14, 15, and 6 respectively).

Various treatment technologies have been proposed for the treatment of oil-contaminated seawater including electrodialysis, adsorption, coagulation and floatation, photodegradation, and chemical oxidation [3, 4]. Among the proposed processes, membrane technologies exhibited outstanding performance in terms of effluent quality and process cost [5–7]. Pressure-driven membrane technologies such as ultrafiltration and reverse osmosis have been reported widely in the literature for the treatment of oil-polluted wastewater [8–11]. However, the presence of oil in water causes severe fouling and subsequent deterioration of the membrane performance [12–15]. Previous studies tested ultrafiltration units for the treatment of bilgewater. Crossflow pilot ultrafiltration experiments were conducted for the treatment of oily bilgewater containing 6100 Total dissolved solids (TDS) and 27.2 ppm oil. The oil content in the obtained permeates was reduced by 80% however, no considerable removal of salts was observed [16–18].

Membrane distillation processes are generally utilized for the elimination of salts from oily-saline wastewater. Membrane distillation is a thermally driven membrane process that can utilize waste energy or renewable energy to desalinate water [19, 20]. Capillary polypropylene commercial membrane (Accurel PP V8/2 HF) was tested in direct contact membrane distillation (DCMD) for the treatment of bilgewater from a port in the Baltic Sea (TDS ~ 6500 ppm, average oil = 40 ppm). Excellent separation efficiency was achieved, and the obtained distillate was practically freshwater [21, 22]. Treatment of high-oil content bilgewater can foul MD membranes and cause severe wetting. A recent study investigated the treatment of bilgewater containing 360 ppm oil and TDS of 3700 ppm using a capillary polypropylene membrane in DCMD configuration. Oil rejection was virtually 100% however, salt rejection was only ~ 10% indicating severe membrane wetting. The authors included an ultrafiltration pretreatment step to minimize the oil load on the MD module from 360 to 10 ppm. The permeate quality was enhanced greatly and freshwater was obtained [23, 24].

In this work, hydrophobic polytetrafluoroethylene membrane is—tested for the treatment of bilgewater from a ship berth in the Suez Canal using air gap membrane distillation (AGMD). Membrane characterization is carried out to assess the fouling behavior and separation efficiency of the membrane. To our knowledge, no previous study tested the treatment of bilgewater in AGMD configuration using polytetrafluoroethylene and investigated the fouling behavior on the membrane surface.

2　Materials and Methods

Polytetrafluoroethylene (PTFE) membrane was obtained from STERLITECH USA, the membrane characteristics are shown in Table 1. Bilgewater was collected from a ship berth in the city of Port Said, Egypt.

Membrane characterization was carried out to assess the fouling behavior of the membrane-bilgewater system. Surface morphology was analyzed by scanning electron microscopy (TESCAN MIRA). The samples were fixed on pieces of conductive carbon tape and coated with 10 nm of silver using argon plasma sputtering. Surface composition was detected before and after experimental bilgewater treatment by using energy dispersive X-ray (OXFORD Xplore) using a landing energy of 15 keV and a beam current of 100 picoamps. The active functional groups and organic fouling bonding to the membrane were detected by Fourier transform infrared spectroscopy (FTIR) (BRUKER ALPHA II equipped with ATR crystal). The surface roughness of the membrane was determined by atomic force microscopy (Nanosurf FlexAFM).

Membrane performance was tested using a pilot-scale AGMD system. A graphical illustration of the system is shown in Fig. 1 and a photograph of the actual system is shown in Fig. 2. The system comprises four main sections:

1. Hot feed cycle.
2. Cooling fluid cycle.
3. The membrane unit
4. Monitoring and control.

The separation efficiency of the PTFE membrane was tested in the system described. The membrane used was 10 cm × 10 cm. The feed temperature is 70 °C and the cooling temperature was fixed at 20 °C. The feed flow rate was 2 l/min.

The purification efficiency was determined by measuring the TDS, TSS, Turbidity, and chemical oxygen demand (COD) of the bilgewater before and after treatment. TDS and TSS were measured by conductivity measurement and gravimetric method respectively. The COD was measured by the dichromate method using spectrophotometry. The error in COD measurements due to the presence of a high concentration of chloride ion in bilgewater was compensated by diluting the sample and using a COD kit that contains mercuric (II) sulfate. The flux, J (l/m^2 h) was calculated using the following equation (Eq. 1):

Table 1 Characteristics of the membrane utilized in this study	Membrane material	Polytetrafluoroethylene
	Support layer material	Polypropylene
	Average pore size	0.45 µm
	Membrane porosity	65%
	Membrane thickness	127 µm
	Water contact angle	127°
	Liquid entry pressure	0.76 bar
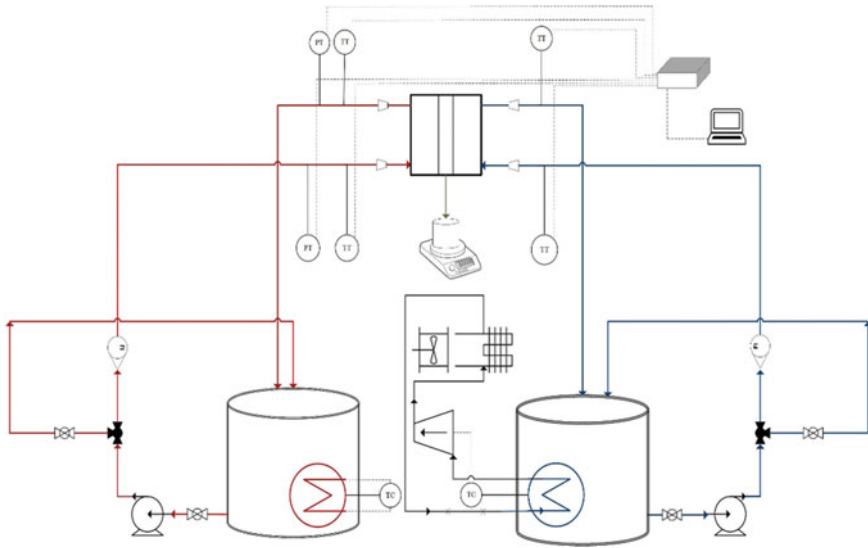
Fig. 1 Illustration of the pilot MD module utilized in this work. The red lines represent the hot fluid cycle, the blue lines represent the cold fluid cycle, and the dashed lines represent the electrical connections. The abbreviations "PT", "TT", "TC", and "FI" are "pressure transmitter", "temperature transmitter", "temperature control", and "rotameter", respectively

$$J = \frac{W}{\rho A \Delta t} \tag{1}$$

where (W) is the permeate mass, (ρ) is the density (A) is the area of the membrane, and (Δt) is the experiment time.

3 Results and Discussion

3.1 Surface Morphology and Surface Composition

Scanning electron microscope images of the PTFE membrane before and after the treatment of bilgewater are shown in Fig. 3. In MD operation, the surface hydrophobicity of the membrane is crucial to prevent the deposition of salts and membrane wetting. In addition to the presence of the hydrophobic C-F function group, the presence of a rough surface at the Cassie-Baxter state may capture micro air bubbles and minimize wetting (Fig. 3). However, higher roughness may induce the deposition of inorganic scales. The morphology of the PTFE membrane (Fig. 4, left) indicated the presence of surface roughness. Deposition of salts is obvious (Fig. 4 right) after the treatment of bilgewater. The size of the deposits is variable, coarse salt particles

Fig. 2 The actual experimental system utilized in this study; 1—synthetic PW tank, 2—feed pump, 3—rotameter, 4—thermocouples, 5—pressure transmitters, 6—membrane module, 7—cooling water pump, 8—cooling water tank, 9—refrigeration cycle, 10—data logger, 11—electricity panel

are observed at magnifications of 1 kx and 5 kx. At a magnification of 45 kx, the attachment of particles to the membrane surface is evident.

Energy dispersive X-ray analyses were performed to assess the nature of the deposited particles. EDS analyses of the PTFE membrane before and after treatment are given in Table 2. Elemental mapping of the membrane after treatment is shown in Fig. 5.

The Elemental analysis revealed the presence of a wide variety of salts and minerals in the bilgewater. Sodium and calcium are the most abundant cations while chloride is the most abundant anion. The presence of oxygen may be attributed to the presence of Silicates, iron oxides, or carbonate ions in the bilgewater. The elemental mapping illustrates that sodium ions (which represent the formation of NaCl scales) are distributed uniformly over the membrane surface. However, Calcium ions tend to be present in large deposits or particle aggregates, these observations suggest
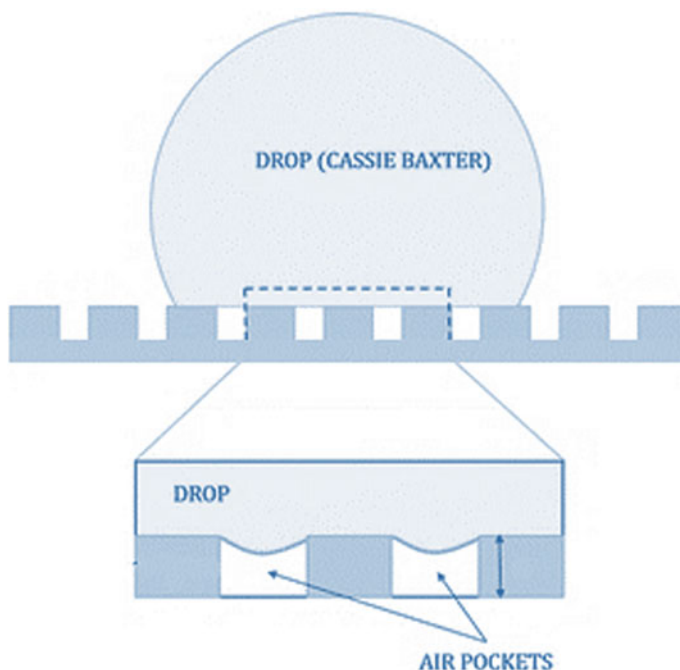
Fig. 3 Illustration of the underwater Cassie-Baxter state

two different scaling mechanisms. Sodium chloride precipitates due to the effect of concentration polarization, while calcium salts normally precipitate from water at higher temperatures and form salt clusters.

3.2 Chemical Structure

The FTIR spectrum was captured within the wave number region of 400–4000 cm^{-1} with a resolution of 4 cm^{-1}. The IR absorption spectrum for the PTFE membrane is shown in Fig. 6. The CF$_2$ characteristic peaks of the symmetric and asymmetric stretching of C–F are observed at 1204 cm^{-1} and 1148 cm^{-1} respectively. Lower wave number CF$_2$ characteristic peaks of the deformation and rocking modes are observed at 550 cm^{-1} and 640 cm^{-1} respectively. The C–H bending peak at 755 cm^{-1} and the strong C–H stretching peaks at 2850 and 2930 cm^{-1} represent the polypropylene support. The presence of noise in the FTIR chart is due to the trapping of air molecules between the very thin membrane coupon and the ATR crystal.

3.3　Membrane Surface Roughness

Numerous studies have established the relationship between surface roughness and the liquid-repel ability of the membrane surface. Surface roughness was determined by obtaining height images from atomic force microscopy. The membrane was imaged in dynamic force mode using a gold-coated silicone tip with an average resonance frequency of 191 kHz and height of 13 μm. The height color map and 3D height map for a sample area of 225 μm^2 are shown in Fig. 7.

The average line roughness parameter Ra and area roughness parameter Sa were 0.7 μm and 0.73 μm respectively. The height fluctuation ranged from − 0.9 to 2.8 μm.
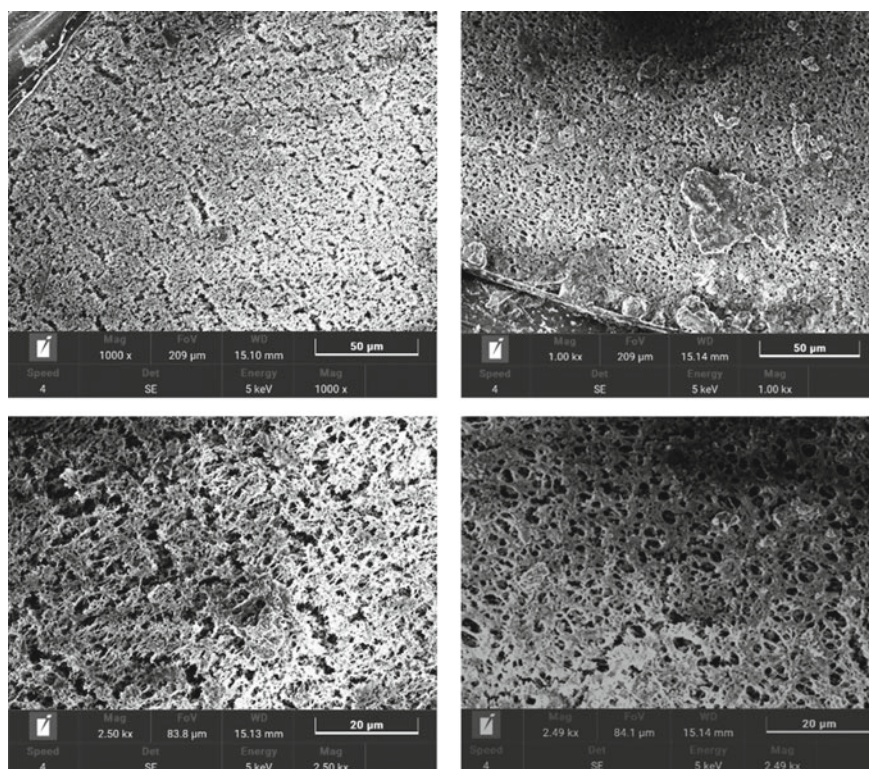
Fig. 4 Field-emission scanning electron microscope images of the pristine PTFE membrane (left) and images of the PTFE membrane after treatment of the bilgewater (right)
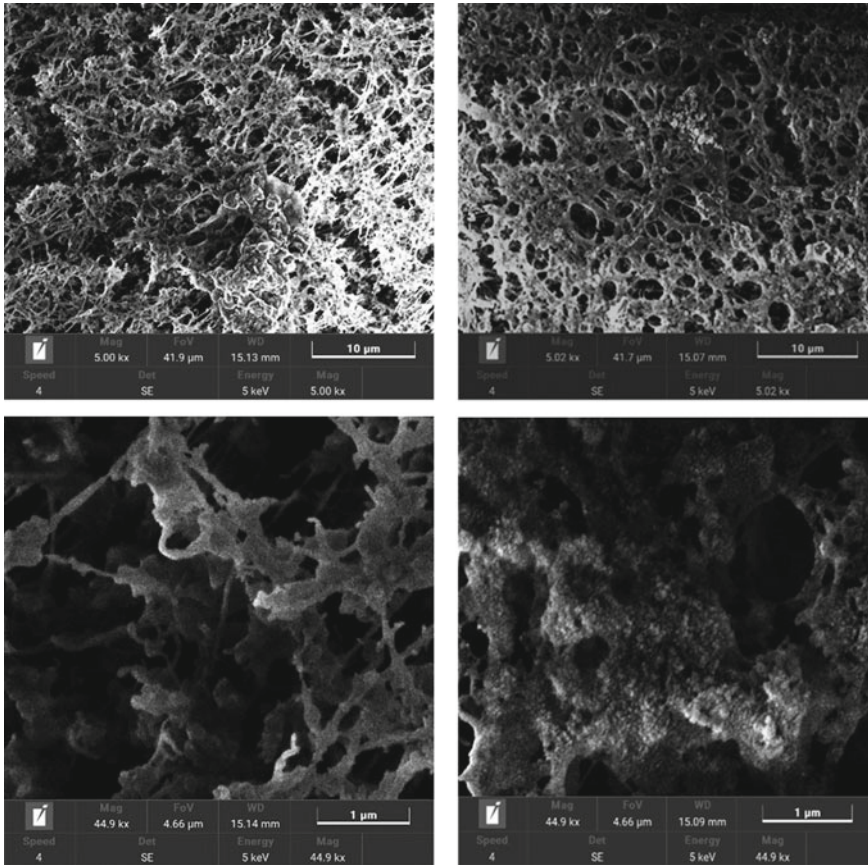
Fig. 4 (continued)

3.4 Membrane Testing Experiment

The membrane flux was approximately stable during the experiment with little fluctuations. The membrane flux and salt rejection percentage are plotted as a function of time and the results are presented in Fig. 8. The initial water flux was 4 l/m^2 h. The flux remained stable at 3.4 l/m^2 h during the first hour then deteriorated to 2.6 l/m^2 h and finally increased again to 3.3 l/m^2 h and remained stable. The initial deterioration in flux is attributed to the initial deposition of foulants on the membrane surface. However, the membrane flux increased again and stabilized due to the widening of pores which is obvious in the SEM images after treatment (Fig. 4, right). The increase in pore size is due to the simultaneous effect of the elevating membrane temperature and the passage of hot water vapor.

Salt rejection was always above 99%. The COD of the permeate was 70% less than that of the feed. The feed and permeate water qualities are given in Table 3.

Table 2 Elemental analysis of the PTFE membrane before and after treatment of bilgewater

Element	PTFE membrane before bilgewater treatment		PTFE membrane after bilgewater treatment	
	wt%	Atomic %	wt%	Atomic %
C	22.80	31.84	16.25	23.87
F	77.20	68.16	63.33	58.80
O	NA	NA	10.40	11.47
Na	NA	NA	3.05	2.34
Mg	NA	NA	0.38	0.28
Al	NA	NA	0.63	0.41
Si	NA	NA	0.99	0.62
Cl	NA	NA	2.03	1.01
Ca	NA	NA	2.27	1.00
Fe	NA	NA	0.68	0.21
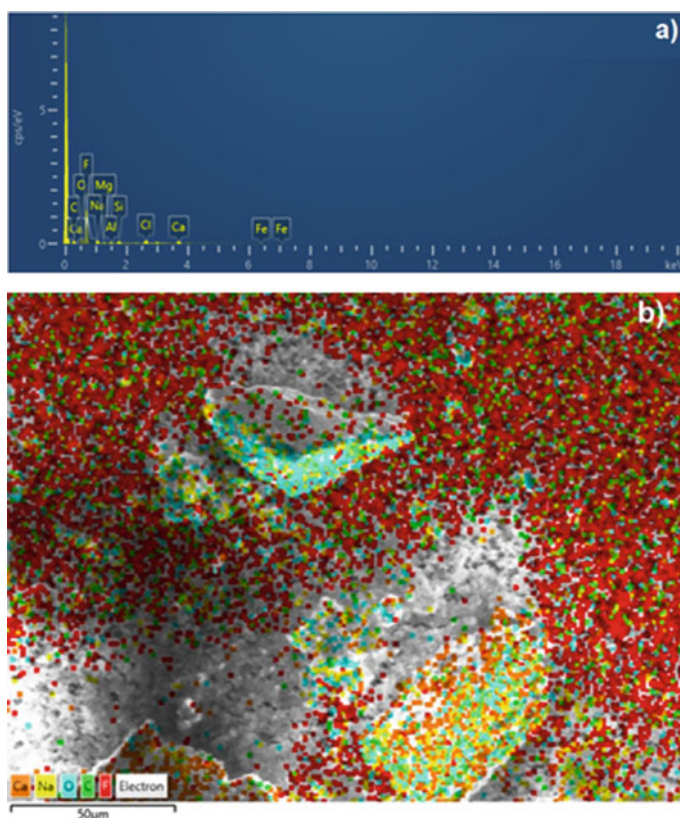
Fig. 5 Elemental distribution data of the PTFE membrane after bilgewater treatment. **a** The EDS intensity chart and **b** elemental mapping of the membrane surface
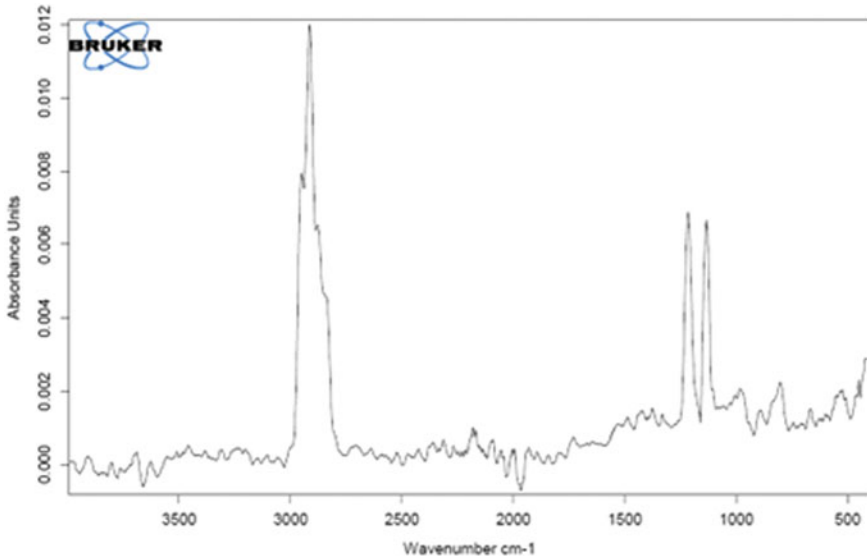
Fig. 6 FTIR absorbance spectrum of the polytetrafluoroethylene membrane

4 Conclusion

An experimental study was carried out to assess the effectiveness of using AGMD for treating saline oil-polluted seawater. Various membrane characteristics were measured and their influence on the membrane performance and fouling tendency were investigated. The membrane morphology was uniform with an equal distribution of pores. Elemental analysis revealed the deposition of inorganic monovalent and divalent salts in addition to a few metal oxides. Sodium and calcium were the most abundant cations and chlorine was the most abundant anion. Calcium formed large aggregates which on long-term operation will clog the pores and damage the membrane and is, therefore, recommend being removed in a pretreatment step. Surface topography showed high variation in features height which enhanced the roughness. The average linear roughness parameter was 0.7 μm. AGMD process using PTFE membrane showed an excellent solids rejection above 99% and COD minimization up to 70%. The membrane flux increased on increasing the membrane pore size and salt rejection was not affected considerably. The initial water flux was 4 l/m^2 h and the flux stabilized after 3 h at 3.3 l/m^2 h. The membrane distillation process is not energy intensive and can be driven by waste heat or renewable energy sources which renders the process applicable in ships, ports, or coastal treatment facilities. The process showed promising results in handling such a challenging feed and further elaboration of the process parameters and membrane materials is recommended.
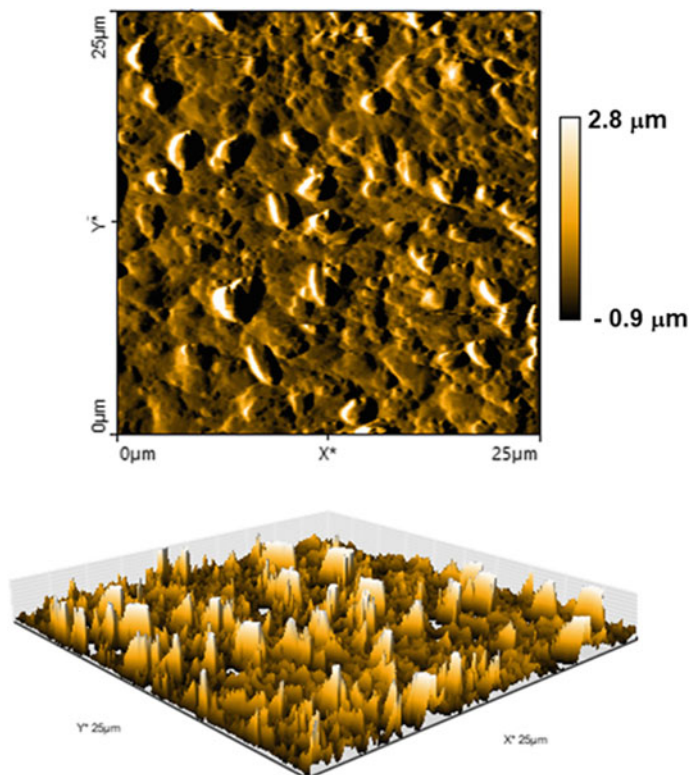
Fig. 7 Atomic force microscopy height images featuring the topography of the membrane surface
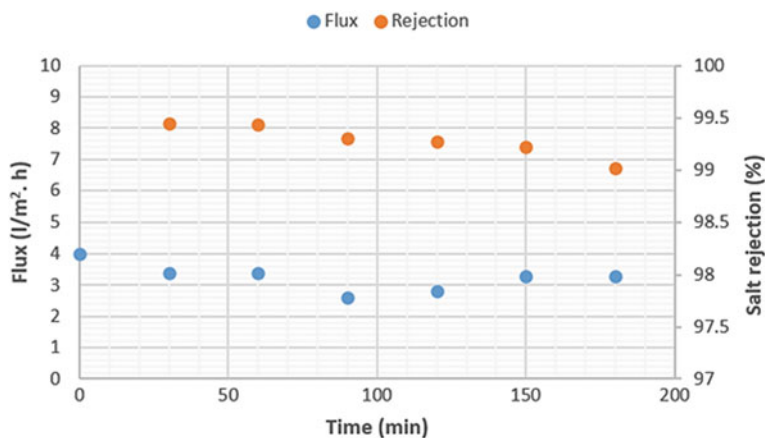
Fig. 8 AGMD performance of the PTFE membrane against the oily-saline bilgewater. The feed and cold temperatures were 70 ± 0.5 °C and 20 ± 0.5 °C respectively. The cross flow velocity of the feed was 0.167 m/s

Table 3 Water quality of the feed and the permeate

Parameter	Bilgewater	Permeate
TDS	16,046 ppm	130 ppm
TSS	1305.9 ppm	Not detected
Conductivity	15.73 ms/cm	115 μs/cm
Turbidity	4.4 NTU	0.8 NTU
COD	537 ppm	161 ppm

5 Recommendations

Membrane distillation is a recent technology that is still at its early stages. It is therefore recommended to test the AGMD system at different operating conditions (temperature, flow rate, etc.). Different membrane materials can yield distinctive results; PTFE membrane showed outstanding results however, modification to the intrinsic membrane characteristics (e.g. porosity, hydrophobicity, etc.) can improve the process sustainability. The AGMD system offers low thermal conduction losses, yet this comes at the expense of reducing the water flux. The air gap configuration should be compared with other configurations such as direct contact or vacuum membrane distillation to assess the most efficient configuration. The behaviour of the system varies greatly with the wastewater to be treated. Collecting different samples of bilge water from different locations and perform a comparative study should provide insights into the effect of feed characteristics on the process effectiveness.

References

1. Özkaynak ÖH, İçemer GT (2021) Determining the bilge water waste risk and management in the Gulf of Antalya by the Monte Carlo method. J Air Waste Manag Assoc 71(12):1545–1554
2. Fletcher LM, Zaiko A, Atalah J, Richter I, Dufour CM, Pochon X, Wood SA, Hopkins GA (2017) Bilge water as a vector for the spread of marine pests: a morphological, metabarcoding and experimental assessment. Biol Invasions 19(10):2851–2867
3. Eteba A, Bassyouni M, Saleh M (2022) Modified coal fly ash for textile dye removal from industrial wastewater. Energy Environ. 0958305X221130536
4. Fouad K, Alalm MG, Bassyouni M, Saleh MY (2020) A novel photocatalytic reactor for the extended reuse of W-TiO$_2$ in the degradation of sulfamethazine. Chemosphere 257(14):127270
5. Mansi AE, El-Marsafy SM, Elhenawy Y, Bassyouni M (2022) Assessing the potential and limitations of membrane-based technologies for the treatment of oilfield produced water. Alex Eng J 68(50):787–815
6. Elhady S, Bassyouni M, Mansour RA, Elzahar MH, Abdel-Hamid S, Elhenawy Y, Saleh MY (2020) Oily wastewater treatment using polyamide thin film composite membrane technology. Membranes 10(5):84

7. El-Mehalmey WA, Safwat Y, Bassyouni M, Alkordi MH (2020) Strong interplay between polymer surface charge and MOF cage chemistry in mixed-matrix membrane for water treatment applications. ACS Appl Mater Interfaces 12(24):27625–27631

8. Sandid AM, Bassyouni M, Nehari D, Elhenawy Y (2021) Experimental and simulation study of multichannel air gap membrane distillation process with two types of solar collectors. Energy Convers Manag 243(14):114431

9. Maddah HA, Alzhrani AS, Bassyouni M, Abdel-Aziz MH, Zoromba M, Almalki AM (2018) Evaluation of various membrane filtration modules for the treatment of seawater. Appl Water Sci 8(6):1–13

10. Elhenawy Y, Moustafa GH, Attia AM, Mansi AE, Majozi T, Bassyouni M (2022) Performance enhancement of a hybrid multi effect evaporation/membrane distillation system driven by solar energy for desalination. J Environ Chem Eng 10(6):108855

11. Ali I, Bamaga OA, Gzara L, Bassyouni M, Abdel-Aziz MH, Soliman MF, Drioli E, Albeirutty M (2018) Assessment of blend PVDF membranes, and the effect of polymer concentration and blend composition. Membranes 8(1):13

12. Elrasheedy A, Rabie M, El-Shazly A, Bassyouni M, Abdel-Hamid SMS (2021) El Kady, MF Numerical investigation of fabricated MWCNTs/polystyrene nanofibrous membrane for DCMD. Polymers 13(1):160

13. Alhathal Alanezi A, Bassyouni M, Abdel-Hamid SM, Ahmed HS, Abdel-Aziz MH, Zoromba MS, Elhenawy Y (2021) Theoretical investigation of vapor transport mechanism using tubular membrane distillation module. Membranes 11(8):560

14. Soliman MF, Abdel-Aziz MH, Bamaga OA, Gzara L, Sharaf F, Al-Sharif M, Bassyouni Z, Ahmad R (2017) Performance evaluation of blended PVDF membranes for desalination of seawater RO brine using direct contact membrane distillation. Desalin Water Treat 63(6):6–14

15. Tomczak W, Gryta M (2021) Application of ultrafiltration ceramic membrane for separation of oily wastewater generated by maritime transportation. Sep Purif Technol 261(9):118259

16. Gryta M (2020) Bilge water separation by membrane distillation. Sep Purif Technol 237(38):116332

17. Kalla S (2021) Use of membrane distillation for oily wastewater treatment—a review. J Environ Chem Eng 9(1):104641

18. Magnusson K, Jalkanen JP, Johansson L, Smailys V, Telemo P, Winnes H (2018) Risk assessment of bilge water discharges in two Baltic shipping lanes. Mar Pollut Bull 126(34):575–584

19. Bilgili MS, Ince M, Tari GT, Adar E, Balahorli V, Yildiz S (2016) Batch and continuous treatability of oily wastewaters from port waste reception facilities: a pilot scale study. J Electroanal Chem 760(1):119–126

20. Lu D, Liu Q, Zhao Y, Liu H, Ma J (2018) Treatment and energy utilization of oily water via integrated ultrafiltration-forward osmosis–membrane distillation (UF-FO-MD) system. J Membr Sci 548(32):275–287

21. Ahmad NA, Goh PS, Abdul Karim Z, Ismail AF (2018) Thin film composite membrane for oily waste water treatment: recent advances and challenges. Membranes 8(4):86

22. Andrés-Mañas JA, Ruiz-Aguirre A, Acién FG, Zaragoza G (2018) Assessment of a pilot system for seawater desalination based on vacuum multi-effect membrane distillation with enhanced heat recovery. Desalination 443(12):110–121

23. Couto CF, Lange LC, Amaral MCS (2018) A critical review on membrane separation processes applied to remove pharmaceutically active compounds from water and wastewater. J Water Process Eng 26(19):156–175

24. Damtie MM, Kim B, Woo YC, Choi JS (2018) Membrane distillation for industrial wastewater treatment: studying the effects of membrane parameters on the wetting performance. Chemosphere 206(33):793–801

Low-Cost Filter Media for Removal of Hazardous Pollutants from Industry Wastewater Effluents

Nehal Mossad Ashour

1 Introduction

Water is the most important human need to survive in this world [1, 2]. Water is necessary for all human activities and living organisms [3–5]. The problem of scarcity of potable water has become an important issue because most of the water on the planet is salt water [6], which represents more than 2/3 of the planet's surface. What increases the problem of water scarcity is the pollution of the little water available for drinking by some factors resulting from man-made factors [7, 8]. Urbanization [9–12], industrialization [10, 11, 13, 14], agricultural [13–15], surface runoff, and sediment transport [2]. It is one of the most important factors causing the deterioration of water quality standards that reach people. It is estimated that 4 billion people around the world do not have access to clean drinking water [16]. Pollution that reaches water leads to poor quality and makes it transmit to humans many diseases that affect human health, especially in developing countries that suffer from poor quality of drinking water [17–19].

To ensure the supply of water in appropriate quantities and high quality, waste water treatment techniques have been applied, which are divided into three main types: biological, chemical and physical treatment [20].

Physical treatment depends on separating the pollutants physically from the water only without a significant change in its chemical and biological properties. As for the chemical treatment, it depends on adding a specific chemical that targets a specific pollutant in order to remove it. Biological treatment uses microorganisms to biodegrade pollutants in wastewater that reduce organic and nutrient content in wastewater [21].

To choose the appropriate type, several factors must be taken into account, the most important of which is the effectiveness of the technology to remove the targeted

N. M. Ashour (✉)
Civil Engineering Department, Faculty of Engineering, Port Said University, Port Said, Egypt
e-mail: nehalashoor@eng.psu.edu.eg

pollutants in wastewater, ease of operation, low cost, and the labor required to operate this technology.

Industrial effluent is water generated from the use of water in the entire industrial process. One of the things that worries the world is the disposal of huge quantities of liquid waste in random and improper ways, which leads to high pollution of water and the environment and causes great health risks. Therefore, this waste must be disposed of in healthy and sound ways and by following sound economic techniques that adhere to certain standards [22].

wastewater are produced from domestic or industrial activities and constitute the main sources of pollution. This liquid waste is a great challenge because it has a serious impact on the environment and pollutes water sources and must be treated. The large expansion of industry has led to the deterioration of the environment in developing countries in the recent period, as this waste is disposed of in water bodies without proper treatment [23].

Environmental pollution with untreated industrial wastewater is a major problem facing developing countries in particular. It has become necessary to develop low-cost technologies and systems to treat industrial wastewater that is loaded with many harmful organic and inorganic pollutants, especially heavy metals. Period and adsorption are one of the most important technologies that are characterized by their ease of operation and low cost, in exchange for high efficiency in removing pollutants.

During the flotation process, wastewater containing suspended matter is added to the surface of the porous medium, where the suspended matter is removed as the wastewater filters through via several of different processes. These include straining, sedimentation, impaction, interception, adhesion, adsorption, focculation, and biological degradation, particularly for organic removals on the top of the filter material. The intrinsic characteristics of the filter media play a critical role in the efficacy of pollutant removal. Among these are effective size, size distribution, slope, density, and porosity [24].

Adsorption is one of the most used technologies in the treatment of industrial wastewater. In short, it depends on the transfer of a substance from one surface to the surface of another substance. Adsorption is divided into two types: chemical adsorption and physical adsorption [25]. The type of adsorption depends on the strength of attraction between the pollutant and the adsorbent. There are many factors that affect the adsorption process, including pH, temperature, and surface area [26].

Although the adsorption process has become an important and available process, the materials used as adsorbents are expensive. Therefore, many researchers tended to study low-cost and high-efficiency materials to achieve sustainability in nature [27].

Studying the ability of some low-cost adsorbents to remove pollutants from wastewater, and we reached excellent results that help in environmental sustainability and provide great advantages and opportunities for using these adsorbents commercially in the future. Therefore, it is crucial for tanning enterprises to properly practise environmental management that filter media that is possibly effective, affordable, and locally accessible be identified as an adsorbent. However, due to the country's rapid growth in construction and expansion, ordinary sand for filter media is

expensive, difficult to get, and ineffective at removing dangerous pollutants through adsorption; as a result, pottery filtration must be used in place of sand filtration [28].

Pottery clay was examined as a unique type of clay, with particular attention paid to the composition and characteristics of porcelain, rubber reinforcement, flame retardant additives, toxin adsorption in medicine, ornamental materials, geologic features, and mechanical qualities. Additionally, studies on the adsorption of Ni(II) and Cu(II) on pottery clay and glaze [29–31]. shown that the material has remarkable adsorption capabilities. However, because of the usual regional peculiarities of soil distribution, it is both economical and environmentally friendly to use local resources in engineering applications. In Egypt, ceramic clay is generally separated into white, red, and grey varieties, and the adsorption capacities for different heavy metals are different. The adsorption properties of pottery have only been the subject of a few number of research to date. In the current work, pottery was employed as a low-cost adsorbent and filter medium, and experiments were conducted to examine the effectiveness of the material for a variety of contaminants and the effect of fine pottery thickness on adsorption.

2 Material and Methods

2.1 Study Design

This research aims to study the efficiency of using different types of pottery in a filter to remove hazardous pollutants from industrial wastewater. The effect of the thickness of the pottery layer in the filter on the efficiency of removing pollutants was studied. Pottery was tested as a low-cost filter media for removal conductivity, TDS, TSS, COD, pH and Cr.

2.2 Filter Media

Pottery samples were collected from pottery workshops. The collection of samples of different types of pottery (red, white, gray) was considered. The different samples were crushed, classified, and the effictive size was determined by means of standard sieves suitable for the filter. Before placing these samples in the filter, they were washed with distilled water and dried by exposing them to the sun for four days.

Fig. 1 Section elevation of
the filter tank
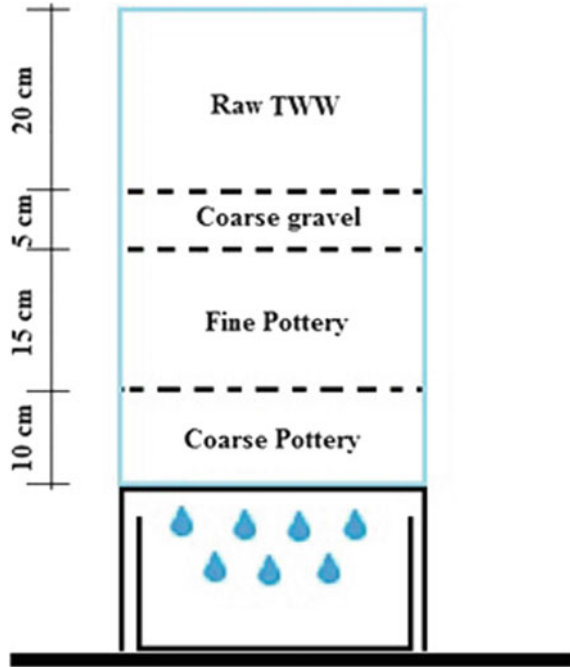
2.3 Design and Set Up of the Filter

A tank was made of glass as a filter. Its dimensions were as follows: 60 cm in height and 35 cm in length. Its square base was perforated from the bottom with 9 holes of 0.5 cm in diameter, to drain the treated water and collect it in a tank below the filter [32]. After the completion of making the filter, the filter layers were placed as follows: 10 cm of pottery with a size ranging from 10 to 25 mm, (4:15) cm of pottery with a size ranging from 1.5 to 4.5 mm, and the filter layers were topped with a layer of fat coarse gravel with a thickness of 5 cm [33] in order to protect The upper filter layer from corrosion as shown in Fig. 1.

2.4 Wastewater Sample Collection and Filtration

A composite sample of industrial wastewater was collected from textile factories and transported in plastic containers. An analysis of the physical and chemical properties of the composite sample was carried out before passing through the filter. The mean concentrations of selected physicochemical parameters were presented in Table 1. The combined wastewater sample was added to the filter, and the treated samples

Table 1 Charactristic of textile wastewater composte sample

S. No.	Parameter	Concentration (mg/l) Expect pH and T°
1	pH	10.4
2	T°	24
3	COD	865
4	Cr	1.7
5	TDS	2381
6	TSS	668
7	Conductivity	3721

coming out of the filter were subjected to laboratory measurements to determine their physical and chemical properties.

2.5 Wastewater Collection and Analysis

An analysis of the samples of the composite industrial wastewater and samples of the treated water coming out of the filter was carried out in order to study its physical and chemical properties and to determine the effectiveness of this filter for removing pollutants from the industrial wastwater. The effect of the depth of the fine layer of pottery with a size ranging from 1.5 to 4.5 mm was studied at heights of 40, 80, 120, 150 mm. The following parameters were measured for water samples conductivity, TDS, TSS, COD, pH and Cr. In this study, the characteristics of the liquid waste generated from the textile industry were determined before and after treatment and passing through the filter. To measure the characteristics of the treated water from the filter, a sample was collected within 24 h, three times throughout the day, and then mixed well before measurement.

3 Result and Disscussion

3.1 Effect of Pottery Type

As shown in Fig. 2, the efficiency of removing pollutants from wastewater with red pottery is often better than white and gray pottery. Red pottery, its efficiency in removing COD is much greater than white pottery, with a difference of up to twice. But The removal of Cr, the best type to remove was white pottery, followed by red pottery, then gray pottery.
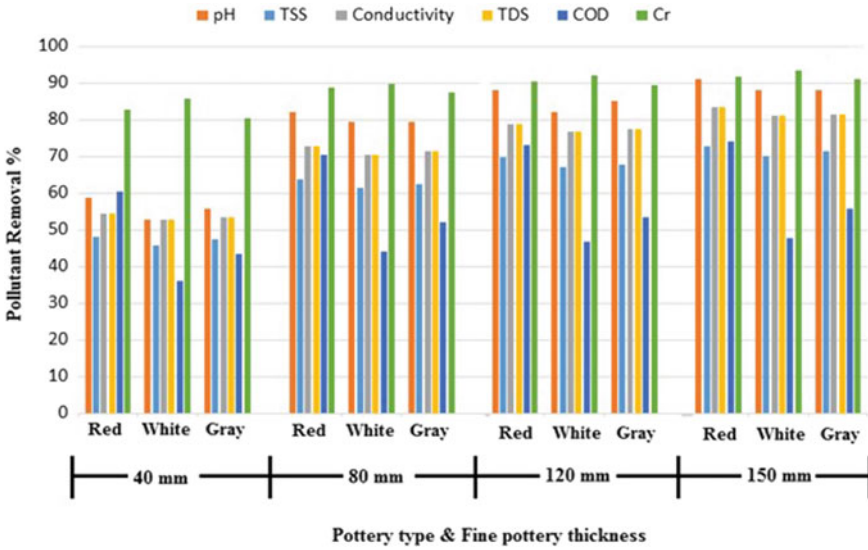
Fig. 2 Comparison of different type of pottery on the removal efficiency pH, TSS, conductivity, TDS, COD and Cr

3.2 Effect of Pottery Thickness

As shown in Fig. 2, the increasing in fine pottery layer thickness, the greater the percentage of pollutants will be removed, due to the increase in the surface area of the adsorbent to which pollutants are attracted. The maximum removal of pH, pH, TSS, conductivity, TDS, COD and Cr is reached 91.2, 72.9, 83.7, 83.7, 74.3 and 93.5% respectively at a thickness of 150 mm.

To measure the organic material and inorganic nutrients present in water samples such as nitrate or ammonia, we measure the amount of oxygen required to chemically oxidize these substances by estimating the chemical oxygen demand. The value decreased from 865 mg/L to the lowest value of 221 using red pottery with a thickness of 150 mm. Red pottery, its efficiency in removing COD is much greater than white pottery, with a difference of up to twice. Figure 2 shows a comparison between the removal of COD for different types of pottery and the thickness of the fine pottery layer 40, 80, 120 and 150 mm.

The element chromium (Cr) was found in wastewater samples. In the textile industry, heavy metals are widely employed to enhance and increase colour efficiency. Cr mean level in wastewater was 1.7 mg/L. Cr treatment value ranged from 0.33 to 0, 0.11. white pottery with thickness 150 mm was shown to be the best removal for Cr. The Cr was shown to be significant in the white pottery results. The best type to remove was white pottery, followed by red pottery, then gray pottery. Figure 2 shows a comparison between the removal of Cr for different types of pottery and the thickness of the fine pottery layer 40, 80, 120 and 150 mm.

Solids that pass through a filter with pores < 2 μm are called total dissolved solids. To measure the amount of TDS, the conductivity electrode is used and measured in ppm. The average TDS value for compost wastewater was found to be 2381, whereas treated values ranged from 1121 to 388. TDS removal was shown to be most effective with 150 mm thickness of red pottery. The results proved the effectiveness of using pottery as a filter media to remove TDS from the liquid waste of the textile industry. The results proved the effectiveness of using pottery as a filter media to remove total solids from the liquid waste of the textile industry. Figure 2 shows a comparison between the removal of TDS for different types of pottery and the thickness of the fine pottery layer 40, 80, 120 and 150 mm.

Traditional pollutants in water bodies are known as (TSS). TSS values for the untreated compost wastewater sample were found to be 668, whereas treated values ranged from 361 to 181. Disease-causing bacteria and toxicity may be present in the suspended solids. TSS may also cause an obnoxious odour to be released during anaerobic degradation. It's also used to assess the effluent and influent quality. It also has the ability to reduce oxygen consumption in plants [34]. Figure 2 shows a comparison between the removal of TSS for different types of pottery and the thickness of the fine pottery layer 40, 80, 120 and 150 mm.

When a sample of untreated wastewater was studied for pH measurement, the mean value of untreated effluents was shown to be 10.4. The values that were treated ranged from 8.6 to 7.3. Figure 2 shows a comparison between the removal of pH for different types of pottery and the thickness of the fine pottery layer 40, 80, 120 and 150 mm.

The untreated industrial wastwater sample had a mean electrical conductivity value (EC) of 3720, while the treated effluents had EC values ranging from 1752 to 606. Despite the fact that the results were within acceptable limits, red pottery was found to be the most effective treatment for EC removal. The higher EC value indicated that effluents contain a lot of salt [35], which causes salinity in soils and degrades natural water resources. Figure 2 shows a comparison between the removal of Conductivityfor different types of pottery and the thickness of the fine pottery layer 40, 80, 120 and 150 mm.

4 Conclusion

The investigation's findings have led to the following important conclusions: The characteristics of polluted textile effluent were very high strength wastewater and a variety of hazardous substances. The used approach gives a useful and efficient method for reducing pollutants. Red pottery had a strong chance of reducing TDS, pH, and conductivity pollutants from textile wastewater, but it had less of a chance of doing so for COD pollutants. The decrease of chromium from textile effluent also had encouraging results for white pottery. By employing various processes, such as filtration, all varieties of pottery have the ability to control high strength industrial wastewater, such as textile effluent, and can serve as an alternative to sand

filtration. White pottery has a greater ability to decrease chromium than red pottery, however when we examine the average efficiency to reduce those chosen wastewater characteristics, red pottery performed better than white pottery and grey pottery.

5 Recommendations

As a result, using low-cost adsorbents that are readily available locally might help develop a low-tech approach to sustainable wastewater management. Any company with an interest is allowed to employ these substrates as the filter medium in the filtration bed or alternatively change out the sand in the currently installed filtration bed for the treatment of wastewater.

References

1. Chandra DS, Asadi SS, Raju MVS (2017) Estimation of water quality index by weighted arithmetic water quality index method: a model study. Int J Civil Eng Technol 8(4):1215–1222
2. Gopal V et al (2018) Water quality of the Uppanar estuary, Southern India: implications on the level of dissolved nutrients and trace elements. Mar Pollut Bull 130:279–286
3. Ahmed S et al (2020) Water quality assessment of shallow aquifer based on Canadian Council of Ministers of the environment index and its impact on irrigation of Mathura District, Uttar Pradesh. J King Saud Univ Sci 32(1):1218–1225
4. Ebba M (2021) Application of electrocoagulation for the removal of color from institutional wastewater: analysis with response surface methodology. J Environ Treat Tech 9(2):470–479
5. Uddin MG, Nash S, Olbert AI (2021) A review of water quality index models and their use for assessing surface water quality. Ecol Ind 122:107218
6. Dinka MO (2018) Safe drinking water: concepts, benefits, principles and standards. In: Glavan M (eds) Water challenges of an urbanizing world. InTech, p 163
7. Soltani AA et al (2021) A new methodology for assessing water quality, based on data envelopment analysis: application to Algerian dams. Ecol Ind 121:106952
8. Liu S et al (2018) Characterisation of spatial variability in water quality in the Great Barrier Reef catchments using multivariate statistical analysis. Mar Pollut Bull 137:137–151
9. Giri S, Singh AK (2014) Assessment of surface water quality using heavy metal pollution index in Subarnarekha River, India. Water Qual Expo Health 5(4):173–182
10. Mahapatra SS et al (2012) Prediction of water quality using principal component analysis. Water Qual Expo Health 4(2):93–104
11. Rezaie-Balf M et al (2020) Physicochemical parameters data assimilation for efficient improvement of water quality index prediction: comparative assessment of a noise suppression hybridization approach. J Clean Prod 271:122576
12. Deepa S, Venkateswaran S (2018) Appraisal of groundwater quality in upper Manimuktha sub basin, Vellar river, Tamil Nadu, India by using Water Quality Index (WQI) and multivariate statistical techniques. Model Earth Syst Environ 4:1165–1180
13. Gibrilla A et al (2011) Seasonal evaluation of raw, treated and distributed water quality from the Barekese Dam (River Offin) in the Ashanti Region of Ghana. Water Qual Expo Health 3:157–174
14. Judran NH, Kumar A (2020) Evaluation of water quality of Al-Gharraf River using the water quality index (WQI). Model Earth Syst Environ 6(3):1581–1588

15. Chaudhary JK et al (2020) A comparative study of fuzzy logic and WQI for groundwater quality assessment. Proc Comput Sci 171:1194–1203
16. Biswas AK, Tortajada C (2019) Water quality management: a globally neglected issue. Int J Water Resour Dev 35(6):913–916
17. Kelly ER et al (2020) How we assess water safety: a critical review of sanitary inspection and water quality analysis. Sci Total Environ 718:137237
18. Abtahi M et al (2015) A modified drinking water quality index (DWQI) for assessing drinking source water quality in rural communities of Khuzestan Province, Iran. Ecol Indic 53:283–291
19. Li P, Wu J (2019) Drinking water quality and public health. Expo Health 11(2):73–79
20. Ang WL, Mohammad AW (2020) State of the art and sustainability of natural coagulants in water and wastewater treatment. J Clean Prod 262:121267
21. Moussa DT et al (2017) A comprehensive review of electrocoagulation for water treatment: Potentials and challenges. J Environ Manage 186:24–41
22. EPA (1993) Constructed wetlands for wastewater treatment and wildlife habitat. http://www.epa.gov/owow/wetlands/construct. Accessed 14 Jan 2014
23. Akaninwor JO, Anosike EO, Egwim O (2007) Effect of Indomie industrial effluent discharge on microbial properties of new Calabar River. Sci Res Essays 2(1):001–005
24. Boller MA, Kavanaugh MC (1995) Particle characteristics and headloss increase in granular media filtration. Water Res 29(4):1139–1149
25. Rao BH, Dalinaidu A, Singh DN (2006) Accelerated diffusion test on the intact rock mass. J Test Eval 35(2):111–117
26. Dąbrowski A (2001) Adsorption—from theory to practice. Adv Coll Interface Sci 93(1–3):135–224
27. Babel S, Kurniawan TA (2003) Low-cost adsorbents for heavy metals uptake from contaminated water: a review. J Hazard Mater 97(1–3):219–243
28. Bilal M, Ihsanullah I, Younas M, Shah MUH (2021) Recent advances in applications of low-cost adsorbents for the removal of heavy metals from water: a critical review. Sep Purif Technol 278:119510
29. Yu SY, Li JH, Yu SX (1998) Study on the treatment of nickel-bearing wastewater by pottery clay adsorption process. Environ Protect Chem Indus 4:7–10
30. Mazloom F et al (2016) Novel sodium dodecyl sulfate-assisted synthesis of $Zn_3V_2O_8$ nanostructures via a simple route. J Mol Liq 214:46–53
31. Rao RAK, Kashifuddin M (2012) Pottery glaze—an excellent adsorbent for the removal of Cu (II) from aqueous solution. Chin J Geochem 31:136–146
32. Ashour NM, Bassyouni M, Mamdouh YS (2021) Removal of TDS and TSS from industrial wastewater using fly ash. J Environ Treatment Tech 9(1):289–296
33. Aregu MB, Asfaw SL, Khan M (2018) Identification of two low-cost and locally available filter media (pumice and scoria) for removal of hazardous pollutants from tannery wastewater. Environ Syst Res 7(1):1–14
34. Eaton AD et al (2005) Standard methods for the examination of water and wastewater, 21st edn. American Public Health Association, Washington, DC
35. Rasool A et al (2016) Elevated levels of arsenic and trace metals in drinking water of Tehsil Mailsi, Punjab, Pakistan. J Geochem Explor 169:89–99

Saline Water Desalination Using Direct Contact Membrane Distillation: A Theoretical and Experimental Investigation

Yasser Elhenawy, Kareem Fouad, Thokozani Majozi, Shereen M. S. Majozi, and M. Bassyouni

1 Introduction

The increase of various pollutants in freshwater sources to unprecedented proportions with the limitations of these sources portends many problems in the future. Therefore, all countries seek to find alternative sources of pure water through the

Y. Elhenawy · T. Majozi
School of Chemical and Metallurgical Engineering, University of the Witwatersrand, Johannesburg 2000, South Africa
e-mail: yasser.elhenawy@wits.ac.za

T. Majozi
e-mail: Thokozani.Majozi@wits.ac.za

Y. Elhenawy
Mechanical Power Engineering Department, Port-Said University, Port Said 42526, Egypt

Y. Elhenawy · M. Bassyouni (✉)
Center of Excellence in Membrane-Based Water Desalination Technology for Testing and Characterization (CEMTC), Port Said University, Port Said 42526, Egypt
e-mail: m.bassyouni@eng.psu.edu.eg

K. Fouad
Civil Engineering Department, Higher Future Institute of Engineering and Technology, El Mansoura, Egypt
e-mail: engkareem.s.civil@gmail.com

S. M. S. Majozi
Chemical Engineering Department, Egyptian Academy for Engineering and Advanced Technology Affiliated to Ministry of Military Production, Cairo 3066, Egypt
e-mail: shereenahmed@eaeat.edu.eg

M. Bassyouni
Department of Chemical Engineering, Faculty of Engineering, Port Said University, Port Said 42526, Egypt

East Port Said University of Technology, Saini, Port Said 45632, Egypt

application of many technological methods [1–5]. Clean water and sanitation are major Sustainable Development Goals (SDGs). Consequently, many scholars are interested in discovering multiple sources of freshwater [6]. Egypt has over 2,400 km of shoreline on the Red Sea and the Mediterranean Sea, respectively. Desalination is employed as a sustainable water supply for residential purposes in various regions of the country. Desalination is now being used along the Red Sea coast to provide enough household water to tourist communities and resorts. This is since the economic price of a water unit in these places is significant enough to cover the expense of desalination [7]. Many approaches are available for the seawater desalination process. To isolate a solvent or specific solutes, semi-permeable or phase change membranes are employed in industrial desalination systems. Desalination techniques may thus be divided into two broad types [8–11]. The first type is the thermal or phase-change process in which the raw water is boiled or heated. Minerals, salts, and contaminants are extremely dense to be carried away by the steam created by boiling and hence persist in the raw water. In this process, the vapor is condensed and cooled. As known, the main thermal desalination techniques are multiple effect distillation (MED), vapor compression (VC), and multi-stage flash distillation (MSF). The second type is the single-phase membrane procedure, the salt rejection occurs without excessive energy or phase transition. Electrodialysis and reverse osmosis (RO) are the two most common membrane procedures (ED). These systems are costly for small volumes of freshwater and cannot be employed in areas with few maintenance facilities [12–15]. Since these systems are well-established, they are considered energy-intensive and ultimately related to non-renewable energy supplies. Also, they are considered complex and have numerous operational issues. Alternative methods, including forward osmosis (FO), and membrane distillation (MD) has been studied because of their potential benefits (produced water quality, simplicity, energy consumption, competence to be joined with renewable energies including solar energy, etc.) [16–19].

Membrane distillation (MD) is a thermal separation method that uses a hydrophobic membrane to aid phase change, allowing only vapor to pass through the membrane wall. This technique has the potential to be employed for the desalination of brackish water or saltwater. Also, it is employed for the enhancement of important compounds [20–22]. Trans-membrane distillation, capillary distillation, pre-evaporation, osmotic distillation, membrane distillation, and other terminology are used in the field of MD to identify the process [23, 24]. The phenomena of membrane distillation derive from the process's resemblance to conventional distillation. MD and conventional distillation depend on the equilibrium of vapor–liquid as the core for salt rejection, and they involve the latent heat of vaporization being provided to induce the phase change [25, 26]. Polyvinylidenefluoride (PVDF), polypropylene (PP), and polytetrafluoroethylene (PTFE) are the mainly utilized resources for MD membranes [27]. The membranes used have porosities ranging from 0.06 to 0.95, pore sizes ranging from 0.2 to 1.0 m, and thicknesses ranging from 0.04 to 0.25 mm [28, 29]. Table 1 offers a list of these materials' surface energies and thermal conductivities.

Table 1 Materials employed in MD and their reported surface energy and thermal conductivity [30]

Membrane material	Surface energy ($\times 10^{-3}$ N/m)	Thermal conductivity (W m^{-1} K^{-1})
PTFE	9.13	0.26
PP	30.2	0.18
PVDF	30.5	0.20

From table, PTFE has oxidation resistance, decent thermal and chemical stability with supreme hydrophobicity. In contrast, it has a significant conductivity in which a superior heat loss will happen through PTFE membranes. On the other hand, PVDF shows respectable mechanical strength, thermal resistance, and hydrophobicity, and could simply be equipped into membranes with adaptable pore assemblies via various methods. In the case of PP, it shows well chemical and thermal resistance [30]. Recently, novel membrane components, including fluorinated copolymers and carbon nanotubes [31, 32], have been created to create MD membranes with high porosity and hydrophobicity, and strong mechanical strength.

The estimated flow of flat sheet membranes is ~20–30 m^{-2} h^{-1} at input hot temperatures of 60 °C and cold temperatures of 20 °C [28]. In all MD designs, the water flow typically upsurges with the consumed temperature [33]. Whereas the contrast in vapor pressure across the membrane drives membrane distillation. A rise in feed temperature causes an increase in vapor pressure in the feed solution channel, which raises the trans-membrane vapor pressure. A theoretical model for forecasting the behavior of membrane distillation was investigated by Burgoyne et al. [34]. Permeating fluxes have been discovered using the mass and heat transfer equations, and they have been supported by experiments. The primary research looked at the impact of flat-plate module design in laminar flow regimes. It was discovered that a 50% reduction in membrane area tended to result in a 66% increase in water flow. This could be caused by the rapid liquid velocity, which thins the boundary layer. The water flux tends to increase with larger main channels, which enhances flow distribution throughout the membrane.

In the several described MD setups, the impact of the support temperature on the water flow has been extensively investigated. In all MD designs, the water flow usually upsurges with the feed temperature [33]. Although the temperature polarization effect rises with feed temperature, numerous research claim that it is preferable to operate at high feed temperatures due to the high evaporation efficiency and complete heat transfer from the feed to the permeate/cooling side [28, 33, 35–37]. However, it must be noted that operating at temperatures over 90 °C may result in a decrease in membrane selectivity and serious scaling issues. The majority of research [38, 39] shows that the influence of the supply flow rate is to enhance the water flux. This is because the integration effect brought on by the boosted confusion through the feed channel has reduced the temperature and concentration polarisation influences. As a consequence of the turbulence, the temperature at the membrane surface

approaches the bulk input temperature. Because of the larger trans-membrane temperature decrease at higher temperatures, the influence of the flow rate on the production is excluding than half that of the influence of the input temperature [40]. In general, up to a certain point, the relationship between the feed flow rate and the trans-membrane flux is linear [40]. Chan et al. [41] tested the membrane distillation crystallization procedure. This investigation shows that the MD can function at high concentrations with fluxes up to 20 l/h m^2 at feed temperatures of 50 and 60 °C. Working at batch concentration, the flux steadily decreases as a result of concentration polarisation and vapor pressure suppression. Due to temperature polarization, which prevents salt saturation and scale deposition, the investigations revealed that the membrane wall temperature is ~5–10 °C lower than the bulk temperature. Based on the aforementioned studies, this paper applied a theoretical and experimental investigation to study the effect of a PTFE direct contact membrane sheet's geometric dimensions on the water flux.

2   Methods

This section presents details of the experimental and theoretical work of the flat sheet membrane distillation unit. The experimental equipment design and operational characteristics are described for the water desalination system.

2.1   *Experimental Setup Description*

Figure 1 depicts a schematic representation of the flat sheet DCMD technique for PTFE membrane materials. In the existing experiments, a flat sheet membrane with dimensions of 20 cm × 20 cm and an operative membrane area of 15 cm × 15 cm is employed. The permeate streams are depicted in blue in Figs. 1 and 2, whereas the warm streams are denoted in red. The membrane module and the electrical heater (1) are connected by the hot water pump (2), which moves the heated fluid between them (6). Via the top port aperture, the hot fluid is sent to the membrane module. Due to the related energy being lost to the vapor passing through the membrane, the hot feed temperature drops in the feed channel. The electrical heater (1) makes up for the temperature loss by raising the temperature of the hot stream to its starting point. The temperature of the feed fluctuates from 40 to 80 °C. Between the membrane module and the chiller (7), the cold water pump (8) circulates the cold water (6). Condensate from the vapor permeate raises the temperature of the cooled water as it passes through the permeate channel. The chilled stream is brought back to the original permeate temperature using the chiller function. The permeate temperature is managed by the chiller and is typically kept between 20 and 30 °C. Rotameters are used to measure the feed and permeate flow rates. Pressure transducers and thermocouples of type T are used, respectively to detect pressure and temperature.
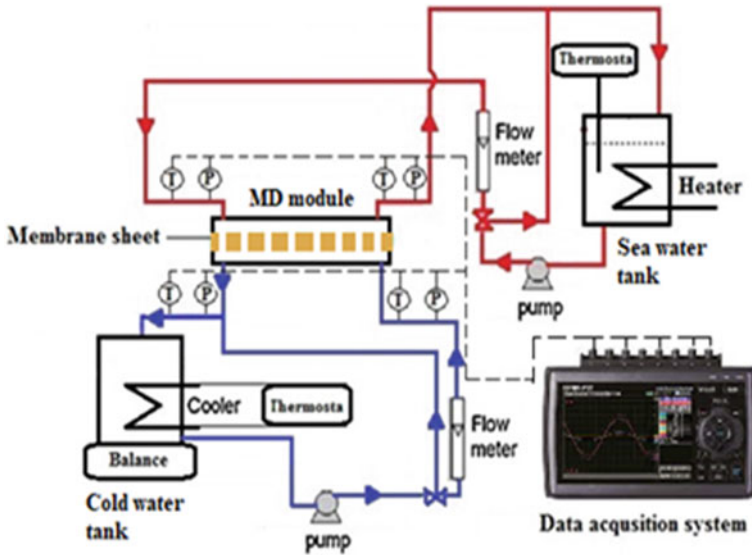
Fig. 1 A flow schematic of the DCMD unit

Using a weighing balance, the weight of the distillate is used to calculate the mass flow. The TDS meter model measures the brine and permeate concentrations. DATAQ Instruments (Graphtec Model: GL220 820APS, Graphtec) are used to record the data. NaCl with a salinity of 35 g/L is utilized as the feed solution in order to study the impact of feed salinity. The flow regime in the feed channel is laminar since the feed and permeate were set to the same flow rate and varied between 0.3 and 0.9 L/min (0.15 and 0.50 m/s).

The polypropylene non-woven layer utilized in experiments is laminated onto a membrane layer comprised of pure PTFE in the membrane flat sheet. The USA-based STERLITECH Company is where membranes are acquired. Table 2 lists the membrane's primary characteristics.

2.2 Heat and Mass Transfer of One-Dimension Model for DCMD

While the heat movement inside the MD unit is frequently described in three phases as illustrated in Fig. 3, water vapor transportation in membrane distillation may be a contemporaneous heat and mass transference process.

(I) The bulk input to the vapor–liquid membrane results in heat convection at the membrane exterior.
(II) Conductivity via the microporous membrane and evaporation.

Fig. 2 DCMD experimental unit: (1) heater supply basin, (2) supply pump, (3) filter, (4) rotameter, (5) thermocouple, (6) DCMD unit, (7) permeate tank (with chiller), (8) permeate pump, (9) electronic balance, (10) a pressure transducer, (11) DAQ scheme

Table 2 Properties of the PTFE membrane sheet

Description	Specification
Pore size	0.45 μm
Thickness	127 μm
porosity	60–70%
Dimension	300 × 300 mm

(III)   Heat convection, or the thermal physical phenomena of the permeate side, from the vapor/liquid boundary to the bulk, permeate at the membrane face [30].

It is assumed that the flux (J) depends on a variety of factors for a particular DCMD system, and a general connection may be expressed as

$$J = f\left(A, T_f, T_p, \dot{m}_f, \dot{m}_p, C_{membrane}, U\right) \tag{1}$$

Fig. 3 Mass and heat and transmission section of a parallel flow DCMD
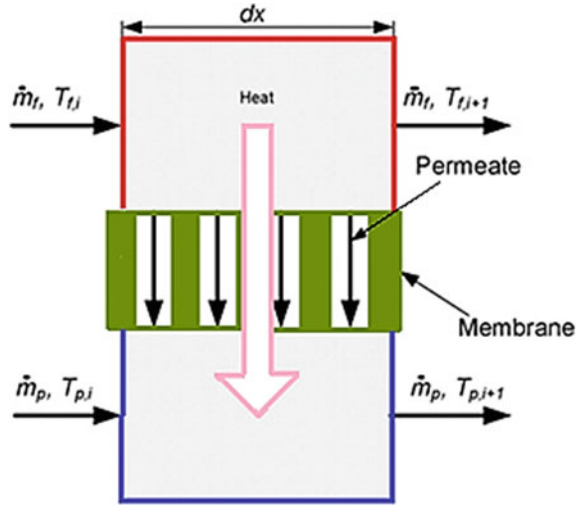
Here, $\dot{m}_p$ and $\dot{m}_f$ are the rates of mass flow for the cold face and feed side (hot flow). To further simplify the model, the following presumptions were also made:

1. There is no heat loss through the unit wall.
2. According to R. G. Lunnon's discovery [41], the specific heat of condensation and evaporation does not alter among concentrations.
3. Across the membrane, no temperature descent perpendicular to the flow guidance, and C_{global} and U remain constant for a given membrane at a given flow rate.
4. Typically, below 3% of the total apparent thermal energy transported by the vapor is delivered to the cold face, it is possible to ignore the sensible heat carried by the permeate when balancing the heat transfer.

These presumptions allow us to express the flow as:

$$J = C_{global}\left(P_{Tf} - T\,P_{Tp}\right) \tag{2}$$

where C_{global} involves the processes of mass transport in the membrane and the boundary layer.

Figure 3 depicts a parallel flow DCMD heat and mass transfer element in a flat sheet unit. Change in thermal energy on the hot face in this element may be stated as follows:

$$C_{p,f}\dot{m}_f\left(T_{f,i+1} + T_{f,i}\right) = -\left(J\,H_{latent}\,dA + U\left(T_f - T_p\right)dA\right) \tag{3}$$

where $T_{f,i}$ and $T_{f,i+1}$ are temperatures at the ith and (i + 1) th points, and $C_{p,f}$ is the specific heat of feed.

$dA = Wdx$, where W is the width of the membrane, the relation among the stream displacement and temperature difference can be stated as,

$$dT_f = -\frac{W\left(J_i H_{latent} + U\left(T_{f,i} - T_{p,i}\right)\right)}{C_{p,f}\dot{m}_f}dx \tag{4}$$

As a result, the input temperature change after the feed stream passes through each element can be stated as follows:

$$\Delta T_{f,i} = -\frac{C_{global}\left[EXP\left(23.1964 - \frac{3816.44}{T_{f,i}+227.02}\right) - EXP\left(23.1964 - \frac{3816.44}{T_{p,i}+227.02}\right)\right]H_{latent} + U\left(T_{f,i} - T_{p,i}\right)}{C_{p,f}\dot{m}_f}W\Delta x \tag{5}$$

Because C_{global} and U are supposed to be constants, the temperature of the input stream at $(i + 1)$th can be computed by

$$T_{f,i+1} = T_{f,i} - \Delta T_{f,i} \tag{6}$$

The permeate temperature may be determined similarly by

$$T_{p,i+1} = T_{p,i} - \frac{\dot{m}_f}{\dot{m}_p}\Delta T_{f,i} \tag{7}$$

Thus, the flux at $(i + 1)$th can be revealed as:

$$J_{i+1} = C_{global}\left(P_{Tf,i+1} - P_{T,i+1}\right) \tag{8}$$

This allows for the calculation of the membrane's overall flux as

$$J = \frac{\sum_{i=0}^{N} J_i W \Delta x}{A} - \frac{\sum_{i=0}^{N} J_i \Delta x}{L} \tag{9}$$

The aforementioned equations can be computationally solved.

3   Results and Discussions

This section illustrates the influence of the DCMD operating parameters on the system's productivity. The influence of feed inlet temperature, membrane effective length, velocity, temperature difference, and feed velocity on the final flux.

3.1   Model Validation

Figure 4 shows the anticipated derived flux, which is the outcome of a parallel flow DCMD. The model was run with a constant velocity of 0.35 m/s (0.7 L/min) with various hot inlet temperatures (40–80) °C. Increasing feed inlet temperature
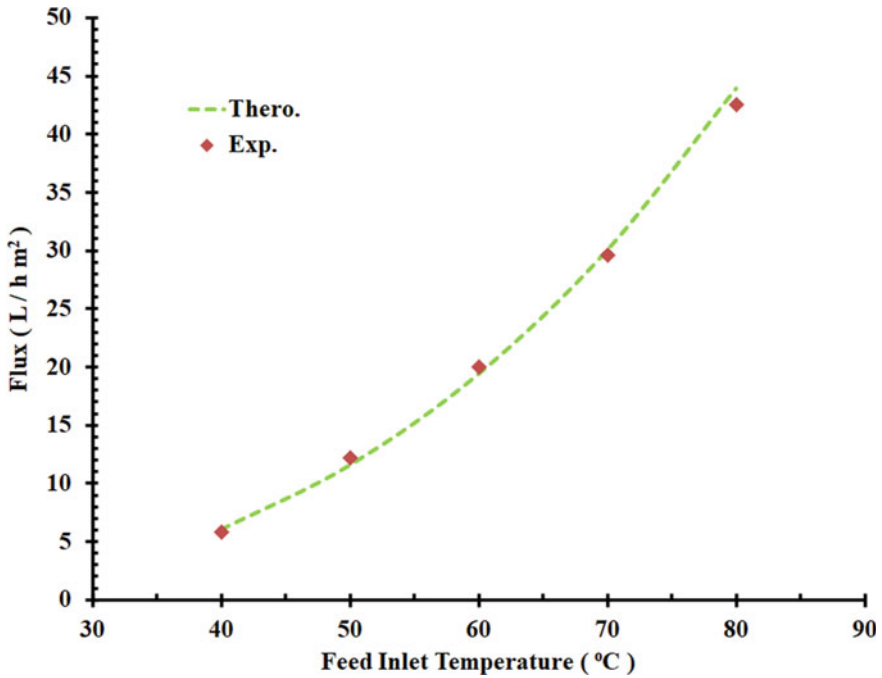
Fig. 4 Validation of experimental and theoretical results at different feed inlet temperatures

significantly boosts the output flux. This trend is the same as in a previous study [42]. Comparison between experimental and theoretical results shows that the simulation results well agree with the experimental outcomes and the maximum error is less than 1%, indicating that the proposed model is reliable and valid.

Figure 5 illustrates the comparison between experimental and theoretical results from parallel flow setups. Because a shorter membrane will result in a greater average temperature and differential through the membrane [43]. With a shorter retention period for mass and heat transfers, the membrane length influences the productivity of the membrane for certain stream velocities and intake temperatures. As a result, if the membrane size is not taken into account, it is inappropriate to assess the function of MD membranes by flux even when the inlet temperature and velocity are the same. Model validation shows that the maximum error is < 4% indicating that the proposed model is valid.

3.2 Temperature Distribution Along the Membrane Sheet

The temperature profiles predicted by parallel flow DCMD along the stream flow direction are shown in Fig. 6. Local temperatures on both faces of the membrane in
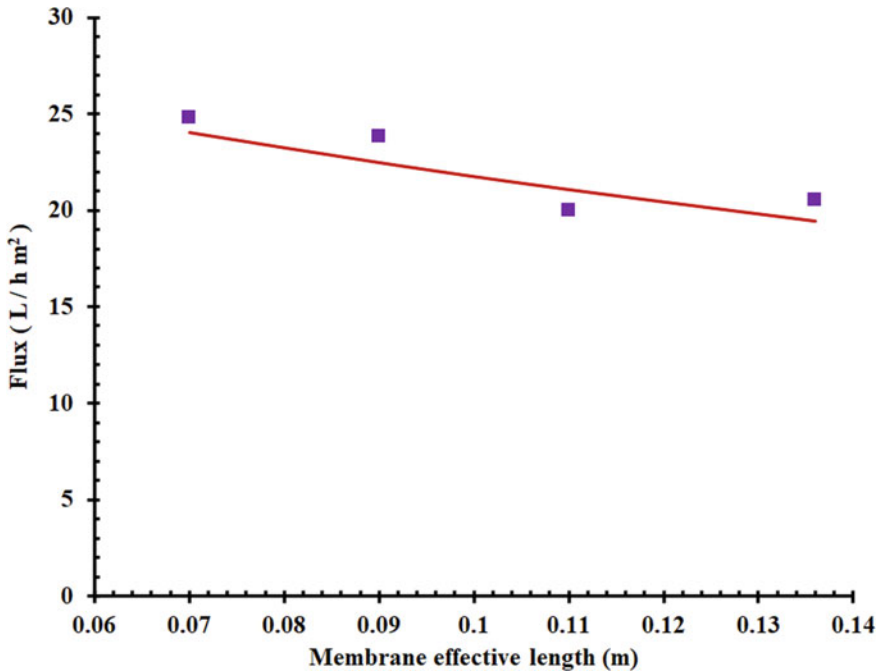
Fig. 5 Comparison between experimental and theoretical results for different membrane lengths

the parallel flow approach one another at points further from the entrance (origin). It is possible to predict that the flux of parallel flow mode would decrease laterally the feed low trend due to a smaller temperature variance based on the difference in the temperature profile [44].

3.3 Average Temperature Difference Across the Sides of the Membrane

Employing the computed heat and mass transfer coefficients from the created database was operated. Figure 7 illustrates the expected mean temperature difference across the membrane at various speeds. This chart showed that when the stream velocity decreased, the temperature differential enhanced. When the velocity increased from 0.2 to 0.45 m/s, the temperature difference decreased from 29 to 24 °C, which resulted in a temperature difference decrease of about 17%. This result is following a previous study [45].
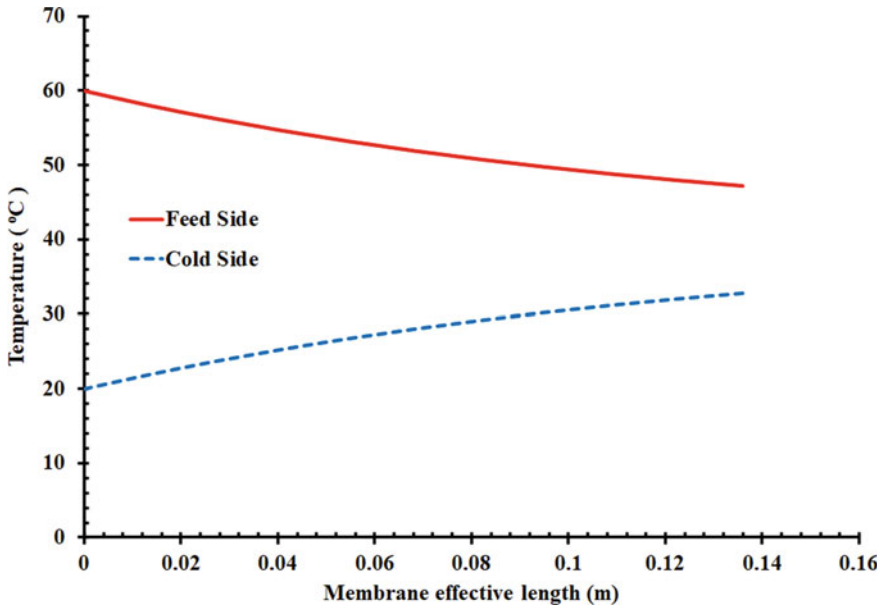
Fig. 6 Temperature distributions along the membrane sheet (supply velocity = 0.35 m/s, supply inlet temperature = 65 °C, cold inlet temperature = 20 °C)
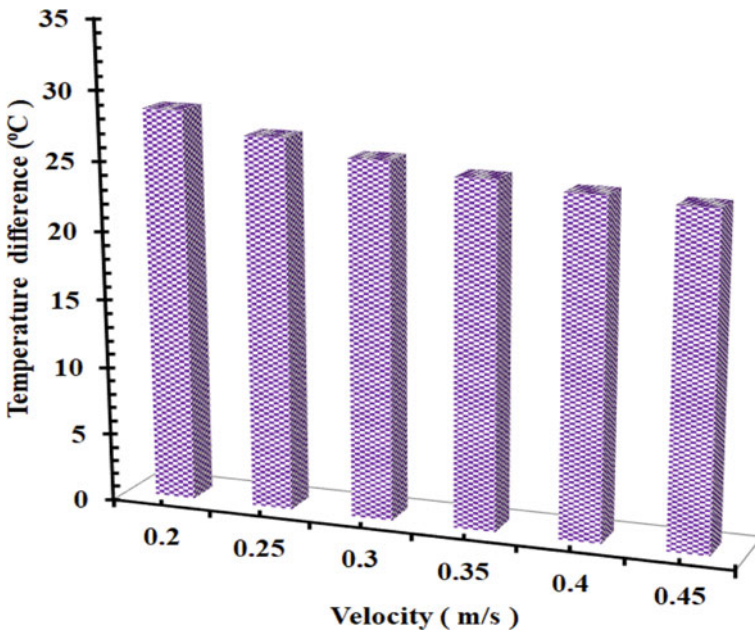
Fig. 7 Mean temperature differential across the membrane's sides at varying velocities (Membrane span = 0.145 m, supply inlet temperature = 65 °C, cold inlet temperature = 20 °C)
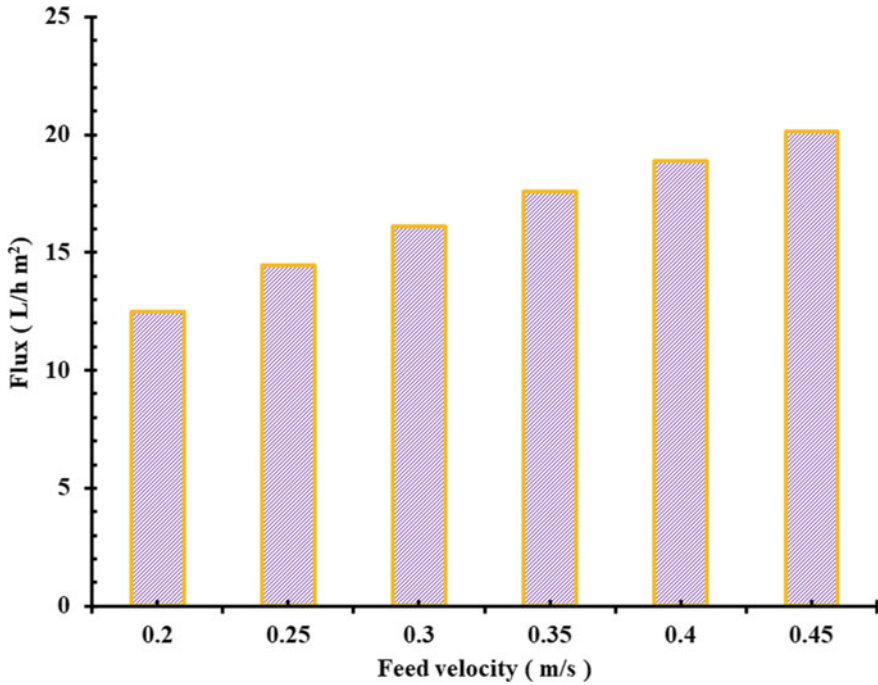
Fig. 8 Flux at different velocities (membrane length = 0.145 m, feed inlet temperature = 65 °C, cold inlet temperature = 20 °C)

3.4 Influence of Feed Velocity on Flux

Figure 8 illustrates the influence of feed velocity on the final flux. Increasing the feed velocity showed a significant boost in water productivity. This is due to the reduction in the residence time which is influenced by the boosted feed velocity [32]. The maximum flux reached about 20 L/h m^2 at a feed velocity of 0.45 m/s.

3.5 Influence of Membrane Different Effective Lengths on Flux

Figure 9 depicts the flow changes along the membrane's length at various speeds. When the velocity rose by around 0.065 m/s, the overall flux differential decreased from 4.6 to 2.3 L m^{-2} h^{-1}. The trustworthiness of the model predictions is further supported by the previously documented tendency of permeate flux with boosting feed flow rates. The figures also demonstrate that when longer membranes are utilized, the difference in flux at different speeds decreases. Hence, when larger
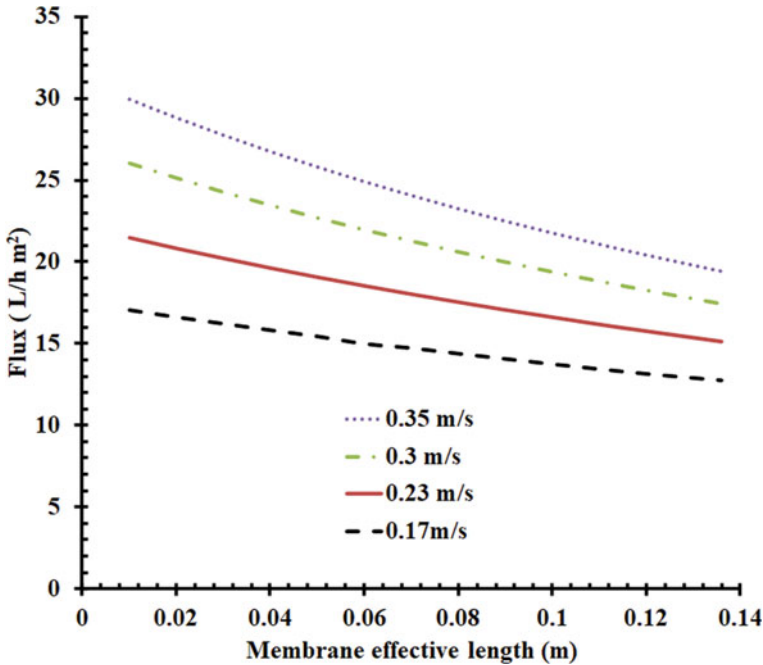
Fig. 9 Flux variance of parallel flow DCMD in the direction of the flow at various velocities (inlet feed temperature = 65 °C, inlet cold temperature = 20 °C)

membrane dimensions are used, the influence of feed velocity on flow will diminish [28].

4 Conclusions

This paper investigated experimentally and theoretically the desalination of saline water using direct contact membrane distillation. A polytetrafluoroethylene (PTFE) membrane was employed with a pore size of 0.45 µm and supported by a scrim layer in a desalination unit. The experimental results showed that the average overall mass and heat transfer coefficients slightly variate with changes in certain factors. These factors are the temperature difference between (40–80 °C) and membrane span variance, which serve as a basis for the simple model's validity. The basic model may be utilized to forecast productivity at various temperatures and membrane spans. Furthermore, the module flow channel structure's properties, such as the existence of a turbulence promoter (spacer) or the size of the flow channel cross-section, will have a substantial impact on the established boundary layer conditions. As a result, changes in these flow channel characteristics will invalidate the previous database at the same stream velocity. The model's predictions demonstrated that when the flow

rates on both sides are the same, the temperature profiles on the hot and cold sides approach one another. Also, MD flux is influenced by membrane length, therefore it is advised to employ a short, broad membrane for high production requests adequately extended, slim membrane scheme. The simulation findings demonstrated that for longer membranes, the supply velocity will have a lower impact on flow. Finally, the comparison between experimental and theoretical results shows that the simulation results well agree with the experimental outcomes indicating that the proposed model is reliable and valid.

5   Recommendations

Polytetrafluoroethylene (PTFE) membranes have proven to be highly efficient in operating as desalination membranes. The proposed simulation model has proven the predictability of desalination results by (PTFE) membranes. This model could be used for other types of membranes to get the best types and conditions. Also, the validation error could be reduced by improving the simulation inputs or by trying artificial intelligence methods.

References

1. Fouad K, Gar Alalm M, Bassyouni M, Saleh MY (2020) A novel photocatalytic reactor for the extended reuse of W-TiO_2 in the degradation of sulfamethazine. Chemosphere 257:127270. https://doi.org/10.1016/j.chemosphere.2020.127270

2. Fouad K, Bassyouni M, Alalm MG, Saleh MY (2021) Recent developments in recalcitrant organic pollutants degradation using immobilized photocatalysts. Appl Phys A Mater Sci Process 127:612. https://doi.org/10.1007/s00339-021-04724-1

3. Fouad K, Bassyouni M, Alalm MG, Saleh MY (2021) The treatment of wastewater containing pharmaceuticals. J Environ Treat Tech 9:499–504. https://doi.org/10.47277/JETT/9(2)504

4. Fouad K, Gar Alalm M, Bassyouni M, Saleh MY (2021) Optimization of catalytic wet peroxide oxidation of carbofuran by Ti-$LaFeO_3$ dual photocatalyst. Environ Technol Innov 23:101778. https://doi.org/10.1016/j.eti.2021.101778

5. El-Gamal H, Radwan K, Fouad K (2020) Floatation of activated sludge by nascent prepared carbon dioxide (Dept. C (Public)). Bull Fac Eng Mansoura Univ 40:21–29. https://doi.org/10.21608/bfemu.2020.101236

6. Elhenawy Y, Fouad K, Bassyouni M, Majozi T (2023) Design and performance a novel hybrid membrane distillation/humidification–dehumidification system. Energy Convers Manag 286:117039. https://doi.org/10.1016/j.enconman.2023.117039

7. Elsaie Y, Ismail S, Soussa H, Gado M, Balah A (2023) Water desalination in Egypt; literature review and assessment. Ain Shams Eng J 14:101998. https://doi.org/10.1016/j.asej.2022.101998

8. Elhenawy Y, Moustafa GH, Abdel-Hamid SMS, Bassyouni M, Elsakka MM (2022) Experimental investigation of two novel arrangements of air gap membrane distillation module with heat recovery. Energy Rep 8:8563–8573. https://doi.org/10.1016/j.egyr.2022.06.068

9. Mansi AE, El-Marsafy SM, Elhenawy Y, Bassyouni M (2022) Assessing the potential and limitations of membrane-based technologies for the treatment of oilfield produced water. Alexandria Eng J 68:787–815. https://doi.org/10.1016/j.aej.2022.12.013

10. Elhenawy Y, Moustafa GH, Mahmoud A, Mansi AE, Majozi T (2022) Performance enhancement of a hybrid multi effect evaporation/membrane distillation system driven by solar energy for desalination. J Environ Chem Eng 10:108855. https://doi.org/10.1016/j.jece.2022.108855

11. Zakaria M, Sharaky AM, Al-Sherbini AS, Bassyouni M, Rezakazemi M, Elhenawy Y (2022) Water desalination using solar thermal collectors enhanced by nanofluids. Chem Eng Technol 45:15–25. https://doi.org/10.1002/ceat.202100339

12. Alhathal Alanezi A, Bassyouni M, Abdel-Hamid SMS, Ahmed HS, Abdel-Aziz MH, Zoromba MS, Elhenawy Y (2021) Theoretical investigation of vapor transport mechanism using tubular membrane distillation module. Membranes (Basel). https://doi.org/10.3390/membranes11080560

13. Mabrouk A, Elhenawy Y, Mostafa G, Shatat M, El-Ghandour M (2016) Experimental evaluation of novel hybrid multi effect distillation–membrane distillation (MED-MD) driven by solar energy. Desalin Environ Clean Water Energy 2016, 22–26

14. Alanezi AA, Safaei MR, Goodarzi M, Elhenawy Y (2020) The effect of inclination angle and Reynolds number on the performance of a direct contact membrane distillation (DCMD) process. Energies 13(11):2824

15. Elhady S, Bassyouni M, Mansour RA, Elzahar MH, Abdel-Hamid S, Elhenawy Y, Saleh MY (2020) Oily wastewater treatment using polyamide thin film composite membrane technology. Membranes (Basel) 10:84. https://doi.org/10.3390/membranes10050084

16. Elhenawy Y, Fouad Y, Marouani H, Bassyouni M (2021) Performance analysis of reinforced epoxy functionalized carbon nanotubes composites for vertical axis wind turbine blade. Polymers (Basel) 13:1–16. https://doi.org/10.3390/polym13030422

17. Elsakka MM, Ingham DB, Ma L, Pourkashanian M, Moustafa GH, Elhenawy Y (2022) Response surface optimisation of vertical axis wind turbine at low wind speeds. Energy Rep 8:10868–10880. https://doi.org/10.1016/j.egyr.2022.08.222

18. Elhenawy Y, Hafez G, Abdel-Hamid S, Elbany M (2020) Prediction and assessment of automated lifting system performance for multi-storey parking lots powered by solar energy. J Clean Prod 266:121859. https://doi.org/10.1016/j.jclepro.2020.121859

19. Elbany M, Elhenawy Y (2021) Analyzing the ultimate impact of COVID-19 in Africa. Case Stud Transp Policy 9:796–804. https://doi.org/10.1016/j.cstp.2021.03.016

20. Marni Sandid A, Bassyouni M, Nehari D, Elhenawy Y (2021) Experimental and simulation study of multichannel air gap membrane distillation process with two types of solar collectors. Energy Convers Manag 243:114431. https://doi.org/10.1016/j.enconman.2021.114431

21. Elminshawy NAS, Gadalla MA, Bassyouni M, El-Nahhas K, Elminshawy A, Elhenawy Y (2020) A novel concentrated photovoltaic-driven membrane distillation hybrid system for the simultaneous production of electricity and potable water. Renew Energy 162:802–817. https://doi.org/10.1016/j.renene.2020.08.041

22. Elrasheedy A, Rabie M, El Shazly AH, Bassyouni M, El-Moneim AA, El Kady MF (2021) Investigation of different membrane porosities on the permeate flux of direct contact membrane distillation. Key Eng Mater Trans Tech Publ 889:85–90

23. Elrasheedy A, Rabie M, El-Shazly A, Bassyouni M, Abdel-Hamid SMS, El Kady MF (2021) Numerical investigation of fabricated MWCNTs/polystyrene nanofibrous membrane for DCMD. Polymers (Basel) 13:160. https://doi.org/10.3390/polym13010160

24. Bassyouni M, Abdel-Aziz MH, Zoromba MS, Abdel-Hamid SMS, Drioli E (2019) A review of polymeric nanocomposite membranes for water purification. J Ind Eng Chem 73:19–46. https://doi.org/10.1016/j.jiec.2019.01.045

25. Maddah HA, Alzhrani AS, Almalki AM, Bassyouni M, Abdel-Aziz MH, Zoromba M, Shihon MA (2017) Determination of the treatment efficiency of different commercial membrane modules for the treatment of groundwater. J Mater Environ Sci 8:2006–2012

26. Soliman MF, Abdel-Aziz MH, Bamaga OA, Gzara L, Al-Sharif SF, Bassyouni M, Rehan ZA, Drioli E, Albeirutty M, Ahmed I, Ali I, Bake H (2017) Performance evaluation of blended PVDF membranes for desalination of seawater RO brine using direct contact membrane distillation. Desalin Water Treat 63:6–14. https://doi.org/10.5004/dwt.2017.20175

27. Jiao B, Cassano A, Drioli E (2004) Recent advances on membrane processes for the concentration of fruit juices: a review. J Food Eng 63:303–324. https://doi.org/10.1016/j.jfoodeng.2003.08.003

28. Alklaibi AM, Lior N (2005) Membrane-distillation desalination: status and potential. Desalination 171:111–131. https://doi.org/10.1016/j.desal.2004.03.024

29. Zhang J, Dow N, Duke M, Ostarcevic E, De LJ, Gray S (2010) Identification of material and physical features of membrane distillation membranes for high performance desalination. J Memb Sci 349:295–303. https://doi.org/10.1016/j.memsci.2009.11.056

30. Curcio E, Drioli E (2005) Membrane distillation and related operations—a review. Sep Purif Rev 34:35–86

31. Dumee LF, Sears K, Schütz J, Finn N, Huynh C, Hawkins S, Duke M, Gray S (2010) Characterization and evaluation of carbon nanotube Bucky-Paper membranes for direct contact membrane distillation. J Memb Sci 351:36–43. https://doi.org/10.1016/j.memsci.2010.01.025

32. Zhang J, De LJ, Duke M, Xie Z, Gray S (2010) Performance of asymmetric hollow fibre membranes in membrane distillation under various configurations and vacuum enhancement. J Memb Sci 362:517–528. https://doi.org/10.1016/j.memsci.2010.07.004

33. El-Bourawi MS, Ding Z, Ma R, Khayet M (2006) A framework for better understanding membrane distillation separation process. J Memb Sci 285:4–29. https://doi.org/10.1016/j.memsci.2006.08.002

34. Burgoyne A, Vahdati MM, Priestman GH (1995) Investigation of flux in flat-plate modules for membrane distillation. Dev Chem Eng Miner Process 3:161–175. https://doi.org/10.1002/apj.5500030305

35. Izquierdo-Gil MA, García-Payo MC, Fernández-Pineda C (1999) Air gap membrane distillation of sucrose aqueous solutions. J Memb Sci 155:291–307. https://doi.org/10.1016/S0376-7388(98)00323-8

36. Ali A, Macedonio F, Drioli E, Aljlil S, Alharbi OA (2013) Experimental and theoretical evaluation of temperature polarization phenomenon in direct contact membrane distillation. Chem Eng Res Des 91:1966–1977. https://doi.org/10.1016/j.cherd.2013.06.030

37. Shirazi MMA, Kargari A, Tabatabaei M (2014) Evaluation of commercial PTFE membranes in desalination by direct contact membrane distillation. Chem Eng Process Process Intensif 76:16–25. https://doi.org/10.1016/j.cep.2013.11.010

38. Banat FA, Simandl J (1994) Theoretical and experimental study in membrane distillation. Desalination 95:39–52. https://doi.org/10.1016/0011-9164(94)00005-0

39. Bin AM, Wahab RA, Salam MA, Gzara L, Moujdin IA (2023) Desalination technologies, membrane distillation, and electrospinning, an overview. Heliyon 9:e12810. https://doi.org/10.1016/j.heliyon.2023.e12810

40. Lawson KW, Lloyd DR (1997) Membrane distillation. J Memb Sci 124:1–25. https://doi.org/10.1016/S0376-7388(96)00236-0

41. Chan MT, Fane AG, Matheickal JT, Sheikholeslami R (2005) Membrane distillation crystallization of concentrated salts—flux and crystal formation. J Memb Sci 257:144–155. https://doi.org/10.1016/J.MEMSCI.2004.09.051

42. Francis L, Ghaffour N, Alsaadi AA, Amy GL (2013) Material gap membrane distillation: a new design for water vapor flux enhancement. J Memb Sci 448:240–247. https://doi.org/10.1016/j.memsci.2013.08.013

43. Li G, Liu J, Zhang F, Wang J (2022) Heat and moisture transfer and dimension optimization of cross-flow hollow fiber membrane contactor for membrane distillation desalination. Sep Purif Technol 297:121576. https://doi.org/10.1016/j.seppur.2022.121576

44. Ghosh R, Madadkar P, Wu Q (2016) On the workings of laterally-fed membrane chromatography. J Memb Sci 516:26–32. https://doi.org/10.1016/j.memsci.2016.05.064
45. Hahne E, Chen Y (1998) Numerical study of flow and heat transfer characteristics in hot water stores. Sol Energy 64:9–18. https://doi.org/10.1016/S0038-092X(98)00051-6

Tanneries Wastewater Treatment by Coagulation and Reverse Osmosis

A. Essam, M. Bassyouni, Mamdouh A. Gadalla, and Fatma H. Ashour

1 Introduction

There are several techniques that can be used in wastewater treatment, including (i) Physical treatment that involves the removal of suspended solids and large particles from the wastewater through stages such as screening, sedimentation, and flotation [1–3], (ii) Chemical treatment that involves the use of chemicals to treat the wastewater such as coagulation and flocculation, (iv) Biological treatment, microorganisms are used to break down organic matter in the wastewater such as activated sludge, trickling filters, and rotating biological contactors, (v) Membrane filtration that involves the use of membranes to remove impurities from the wastewater. Microfiltration, ultrafiltration, nanofiltration, and reverse osmosis are common types of membrane filtration [4–8], (vi) Adsorption that refers to use an adsorbent material to remove pollutants from the wastewater. Activated carbon is a common adsorbent material [9, 10], (vii) Electrochemical treatment, the use of cathodes and anodes to treat the wastewater. Electrocoagulation and electro-oxidation are common electrochemical treatment techniques [11, 12], and (viii) Ion exchange: this involves the use of resins to remove ions from the wastewater.

Chromium is widely used in industries because it is an anticorrosive material. Chromium is mainly consumed in stainless steel fabrication which makes the steel

A. Essam · F. H. Ashour
Chemical Engineering Department, Faculty of Engineering, Cairo University, Giza 12613, Egypt

M. Bassyouni (✉) · M. A. Gadalla
Department of Chemical Engineering, Faculty of Engineering, Port Said University, Port Said 42526, Egypt
e-mail: m.bassyouni@eng.psu.edu.eg

M. Bassyouni
Center of Excellence in Membrane-Based Water Desalination Technology for Testing and Characterization (CEMTC), Port Said University, Port Said 42526, Egypt

East Port Said University of Technology, Saini, Port Said 45632, Egypt

anticorrosive and prevents the steel from losing its color. Chromium is also consumed in paints application to give a variety of colors by mixing with lead (Pb), zinc (Zn), and barium (Ba). These compounds are used to apply permanent colors to buildings, glass, and vehicles. Chromium is used in the formation of potassium dichromate ($K_2Cr_2O_7$) which helps to make waterproof inks for printing photos [13].

Chromium in industrial wastewater is one of the most crucial pollutants put into consideration as it severely affects the water quality of the environment [14, 15]. Cr^{+6} has a high oxidation potential, mobility, and solubility that is considered to be toxic and carcinogenic to the environment [16, 17]. Trivalent chromium is more stable than Cr^{+6} and known to be with less toxicity, and could be useful for humans and animals with specific concentrations for the metabolism. Although low concentrations of Cr^{+3} is important for metabolism, at higher concentrations it causes corruption to the DNA of the bodies [18, 19]. Trivalent chromium can be converted to Cr^{+6} by using an oxidizing agent as hydrogen peroxide in a basic solution. Hydrogen peroxide is mainly used in the sanitization of drinking water loops and this is where it might occur. Usually, industries spill their wastewater into rivers and drinking water networks that affect the water quality to contain Cr^{+3}, and in sanitization, Cr^{+3} converts to Cr^{+6} which reacts with calcium and magnesium to supply hazardous calcium chromate and magnesium chromate. Trivalent chromium can be converted to Cr^{+6} also by interacting with acids or bases along with the interaction with air [20, 21]. Treatment of tanneries wastewater aids in sustaining the water resourses and minimize pollution which follows the SDGs goal for clean water.

Hexavalent chromium can cause a variety of severe diseases such as skin cancer by directly interacting with the human skin that makes Cr^{+6} passes through the cell membrane due to its high solubility, ingestion by washing food with water containing Cr^{+6}, and inhalation. Cr^{+6} interacting results in a short duration when it reaches the kidney and might cause direct death. Chromium can also affect the human body to have the respiratory system and throat corrupted, irritation, skin and eyes enlargement, loss of smelling odors, and lung cancer. Chromium itself can be corrosive to metals, particularly in its hexavalent state (Cr^{6+}), which is more toxic and more corrosive than its trivalent state (Cr^{3+}) [22–24].

Chromium also affects agriculture by direct interaction with irrigation water and soil. When magnesium chromate is found in the soil, negative impacts will occur on the plantation by changing the environmental behavior of plants growth, venoming the seed generation, preventing enzymatic activities, mutagenesis, preventing photosynthesis, yield minimization, and in stabilizing in oxidation and nutrition [25].

Coagulation–flocculation and RO have revealed that they have the capability of treating various types of wastewater industrial, storm, and municipal wastewater [26]. Wastewater treatment systems are divided into two streams, which are surface or subsurface flow. In the surface flow stream (SF), the water table is preserved overhead the ground level unlike the subsurface flow stream (SSF) which contains a water table that is beneath the ground level [27].

2 Materials and Methods

Five samples of tanneries wastewater were tested with different TDS concentrations to evaluate the toxicity and treatment procedures of this wastewater. The main objective in tanneries wastewater treatment is to remove heavy metals composed of chromium, which is the most hazardous component found in the wastewater. The wastewater treatment results were determined and evaluated by using zeta-potential device, COD and BOD analyzers, ICP-MS spectrophotometer, SEM and EDX microscopes.

The research was divided to four phases as shown in Fig. 1. In phase I, the pH and TDS of the four wastewater samples were measured for neutralization process. The five industrial tanneries wastewater samples revealed a great TDS amount with acidic pH solution. pH adjustment process was done by using alkaline solution after testing the zeta-potential to ensure the decision of neutralization. In phase II, coagulation–flocculation process was done by using $FeSO_4$ and CaO as a coagulant and aiding coagulant respectively. Coagulation–flocculation process was a major procedure used to reduce organic matters and dissolved solids in the form of COD, BOD, TDS, and chromium concentrations in tanneries wastewater. In phase III, the filtration and adsorption process were done by the usage of melt-blown polypropylene (PP) water filters, carbon block (CB) filter, and granular activated carbon (GAC) filter. The PP filter was used to reduce the amount of suspended solids from wastewater. The CB filter was used to remove the turbidity and chlorine contents. The GAC filter was used to adsorb the organic matters from wastewater. Finally, in phase IV, RO membranes were used to capture heavy metals and to significantly reduce the TDS for further reuse of the treated wastewater such as irrigation water.
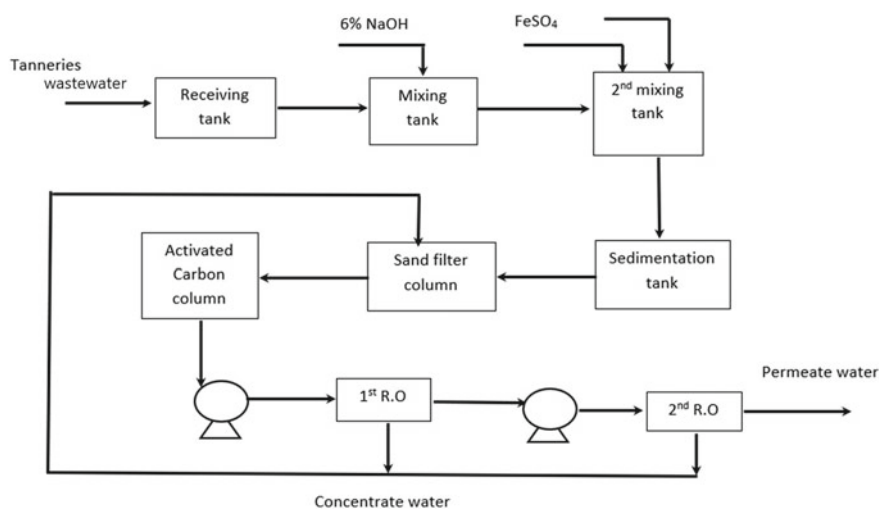
Fig. 1 Tanneries wastewater treatment block flow diagram

The block flow diagram identifies the sequence of tanneries wastewater treatment for reusing treated water in the irrigation. The receiving tank is the tank where the tanneries wastewater was gathered, and measured in pH and TDS. After TDS and pH measurements, it was noticed that the wastewater was acidic. Before applying the treatment process, neutralization procedure was taken into consideration by pH adjustment by using 6% (wt./wt.) NaOH to achieve the pH at 7.4–7.8. Coagulation–flocculation process was an important step that helps to the great minimization of the amount of COD, BOD, and heavy metals as Cr^{+3}. After neutralization, filtration process was applied by using melt-blown PP water filter, CB filter, GAC filter, 1st RO, and 2nd RO respectively. Melt-blown PP filter helped in capturing suspended particles. Carbon block filter was a pre-filter that reduce the concentrations of organics, and Cr^{+3}. Granular activated carbon filter was used to remove different types of contaminants, organic compounds, and heavy metals. Filtration process is a pretreatment stage that is essential to be used in order to ease the treatment process through reverse osmosis and to decrease the probability of scaling or fouling. Reverse osmosis membrane is a purification tool that is globally used to treat the water by applying high pressure to the water through a semi-permeable membrane that prevents solutes to pass with the solvents. The 2nd RO device was used to capture the remaining organics and heavy metals.

Scanning electron microscope was used to study the surface morphology of polypropylene, activated carbon and membranes. TESCAN MIRA's 4th generation Scanning Electron Microscope (SEM) with FEG Schottky electron emission source combines SEM imaging and live elemental composition analysis was used.

Energy dispersive X-ray is better device used to differentiate between atoms and quantify the weight and atomic percentage of atoms on the surface. The EDX was applied by using Oxford instrument provides AZtec, that gathers accurate data at the micro- and nanoscales attached to FE-SEM.

Zeta potential is a measurement tool that determines the sliding or clipping plane of colloids that move under the force of electric field. Zeta potential measurement has been applied by using (Zetasizer Ultra).

The COD was measured by heating the sample to 150 °C for 2 h by the addition of potassium dichromate and sulfuric acid. The COD measurement was done by using (Lamotte Smart COD Spectrophotometer).

The BOD test was conducted by using two samples to measure the amount of oxygen consumed in 5 days by reading the dissolved oxygen after 5 days of incubation. The BOD test was done by using (VELP Scientifica BOD Evo Sensor).

Inductively coupled plasma mass spectrometry (ICP-MS) is a device that is used to quantify the mass of elements through ion detection. In this research, (Shimadzu's ICPMS-2030) was used to measure the chromium concentration in each phase of the treatment process.

3   Results and Discussion

It was found that the treatment process provided significant results by extremely decreasing high loads of organic materials, dissolved solids, and chromium.

Coagulation–flocculation was applied by the usage of $FeSO_4$ powder and CaO as a coagulant and aiding coagulant respectively to form ferrous hydroxide to form chromium hydroxide to settle by applying Eqs. (1) and (2).

$$2FeSO_4(7H_2O) + 2CaO + 0.5O_2 \rightarrow 2Fe(OH)_3 + 2CaSO_4 + 4H_2O \quad (1)$$

$$CrCl_3 + Fe(OH)_3 \rightarrow Cr(OH)_3 + FeCl_3 \quad (2)$$
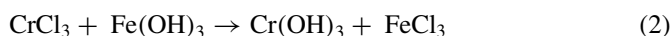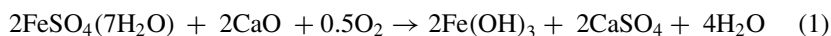
Table 1 shows the overall percentages of tanneries wastewater treatment using the coagulation–flocculation method in each sample. The COD removal in the 1st sample was 90.92%, the BOD removal was 92.15%, the TDS removal was 82.19, and the Cr^{+3} removal was 50.05%. The COD removal in the 2nd sample was 83.26%, the BOD removal was 90.81%, the TDS removal was 46.52%, and the Cr^{+3} removal was 50.05%. The COD removal in the 3rd sample was 74.45%, the BOD removal was 85.23%, the TDS removal was 46.98%, and the Cr^{+3} removal was 51.40%. The COD removal in the 4th sample was 44.72%, the BOD removal was 32.88%, the TDS removal was 17.40%, and the Cr^{+3} removal was 52.40%. The COD removal in the 5th sample was 76.96%, the BOD removal was 75.83%, the TDS removal was 11.43%, and the Cr^{+3} removal was 53.94%. Figure 2 reveals the average percentage of removal of each parameter in the five samples using the coagulation–flocculation method.

3.1   Reverse Osmosis Filtration

Table 2 shows the removal effectiveness in COD, BOD, TDS, and Cr ions after using the 1st RO in tanneries wastewater treatment in the five samples. In the 1st sample, the COD and BOD removal reached 93.47% and 100% respectively. The TDS

Table 1 Removal efficiency using coagulation–flocculation in five samples

Coagulation–flocculation effectiveness in TWW treatment			
Sample	COD (%)	BOD (%)	TDS (%)	Cr (%)
1	90.92	92.15	82.19	50.05
2	83.26	90.81	46.52	50.05
3	74.45	85.23	46.98	51.40
4	44.72	32.88	17.40	52.40
5	76.96	75.83	11.43	53.94
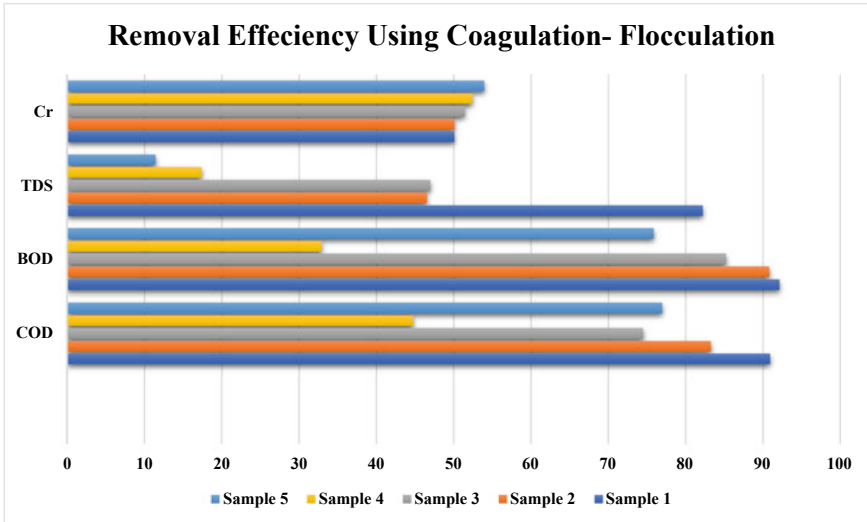
Fig. 2 Average removal efficiency graph using coagulation–flocculation

and Cr ions removal achieved 94.03% and 28.46% respectively. In the 2nd sample, the COD and BOD removal reached 86.69% and 100% respectively. The TDS and Cr ions removal reached 96.86% and 39.37% respectively. In the 3rd sample, the COD and BOD removal attained 83.79% and 84.19% respectively. The TDS and Cr ions removal attained 91.00% and 40.61%. In the 4th sample, the COD and BOD removal achieved 100%. The TDS and Cr ions removal reached 95.08% and 43.05% respectively. In the 5th sample, the COD and BOD removal attained 94.45% and 100% respectively. The TDS and Cr ions removal accomplished 98.55% and 56.10% respectively. Figure 3 clears the difference of percentages of removal in COD, BOD, TDS, and Cr from raw wastewater to passing through the 1st RO.

Table 3 shows the removal effectiveness in COD, BOD, TDS, and Cr after using the 2nd RO in tanneries wastewater treatment in the 5 tanneries wastewater samples. In the 1st sample, the COD removal reached 100%, and the BOD was eliminated by the 1st RO. The TDS removal achieved 61.76%, and the Cr removal accomplished

Table 2 Removal efficiency using 1st RO in five samples

1st RO effectiveness in TWW treatment				
Sample	COD (%)	BOD (%)	TDS (%)	Cr (%)
1	93.47	100	94.03	28.46
2	86.69	100	96.86	39.37
3	83.79	84.19	91.00	40.61
4	100	100	95.08	43.05
5	94.45	100	98.55	56.10
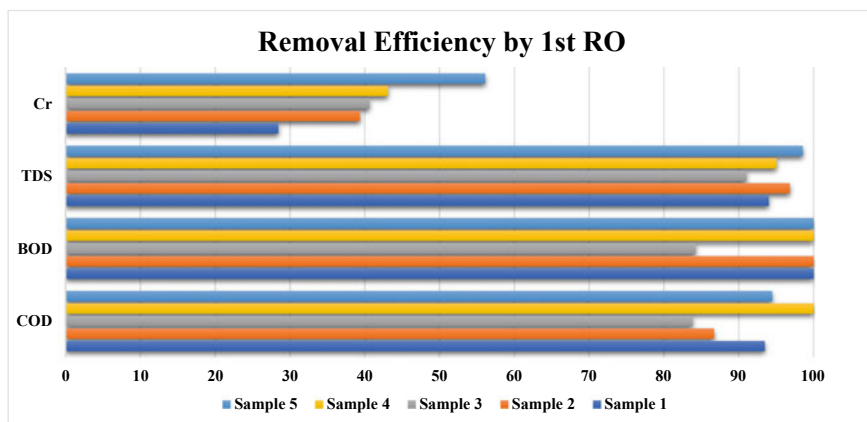
Fig. 3 Average removal efficiency plot using 1st RO in five samples

45.97%. In the 2nd sample, the COD and BOD removal were eliminated by the 1st RO. The TDS removal attained 70.73%, and the Cr removal accomplished 46.75%. In the 3rd sample, the COD removal reached 92.31% and the BOD removal achieved 100%. The TDS removal accomplished 78.43%, and the Cr removal attained 46.57%. In the 4th sample, the COD and the BOD were eliminated by the 1st RO. The TDS removal accomplished 57.76%, and the Cr removal reached 46.25%. In the 5th sample, the COD removal attained 70.83% and the BOD was eliminated by the 1st RO. The TDS removal reached 94.38%, and the Cr removal accomplished 43.48%. Figure 4 provides the removal percentages of COD, BOD, TDS, and Cr from raw wastewater to passing through the 2nd RO. The BOD was totally reduced through the 1st, 2nd, 4th, and 5th samples, but in the 3rd sample there was a low concentration of BOD that the 2nd RO had accomplished their total removal.

As shown in Fig. 5, the SEM was applied at the outer and inner surface of the RO membrane to reveal the difference between the cross-section and the outlet of the RO in order to evaluate the membrane performance.

The EDX showed the highly elemental distribution on the RO membrane as shown in Figs. 6, 7 and 8. The sodium atoms (Na) were found at the outlet of the treated

Table 3 Removal efficiency using 2nd RO in five samples

2nd RO effectiveness in TWW treatment				
Sample	COD (%)	BOD (%)	TDS (%)	Cr (%)
1	100	100	61.76	45.97
2	100	100	70.73	46.75
3	92.31	100	78.43	46.57
4	100	100	57.76	46.25
5	70.83	100	94.38	43.48
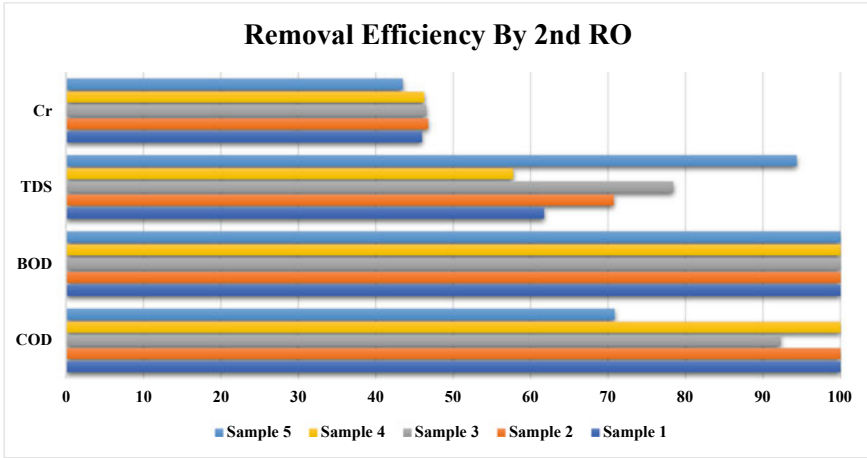
Fig. 4 Average removal efficiency plot using 2nd RO in five samples
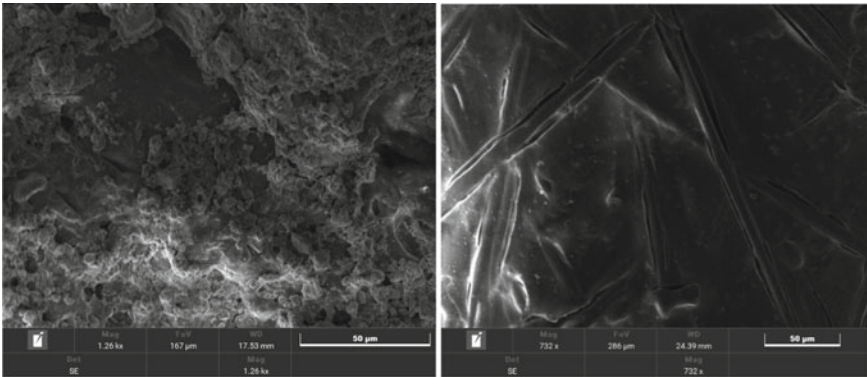
Fig. 5 Cross-section surface and inner surface view of RO membrane through SEM

wastewater with low concentrations after capturing great amount of Na atoms after the addition of NaOH solution in the pretreatment phase to TWW.

3.2 Chromium, COD, BOD, and TDS Removal

According to the results measured and plotted in Table 4 and Fig. 9 respectively, there is an effective and continuous performance in tanneries wastewater treatment. The organic matter removal in terms of COD ranged from 99.62 to 100%, BOD removal to 100%, TDS reduced up to 99.93%, and chromium removal up to 88.57%. The standard deviation of each parameter was calculated through excel to provide

Element	Weight %	Atomic %
C	74.09	79.43
O	24.78	19.94
Na	1.13	0.64
Total	100	100

Element	Weight %	Atomic %
C	76.11	80.93
O	22.86	18.73
Cr	1.03	0.34
Total	100	100
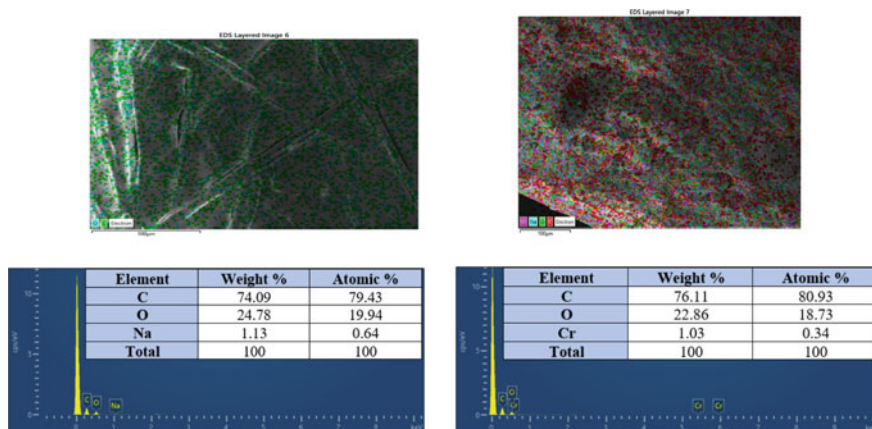
Fig. 6 EDX cross-section and inner surface view of RO membrane, and atomic and weight % of C, O, Cr, and Na atoms at both sides
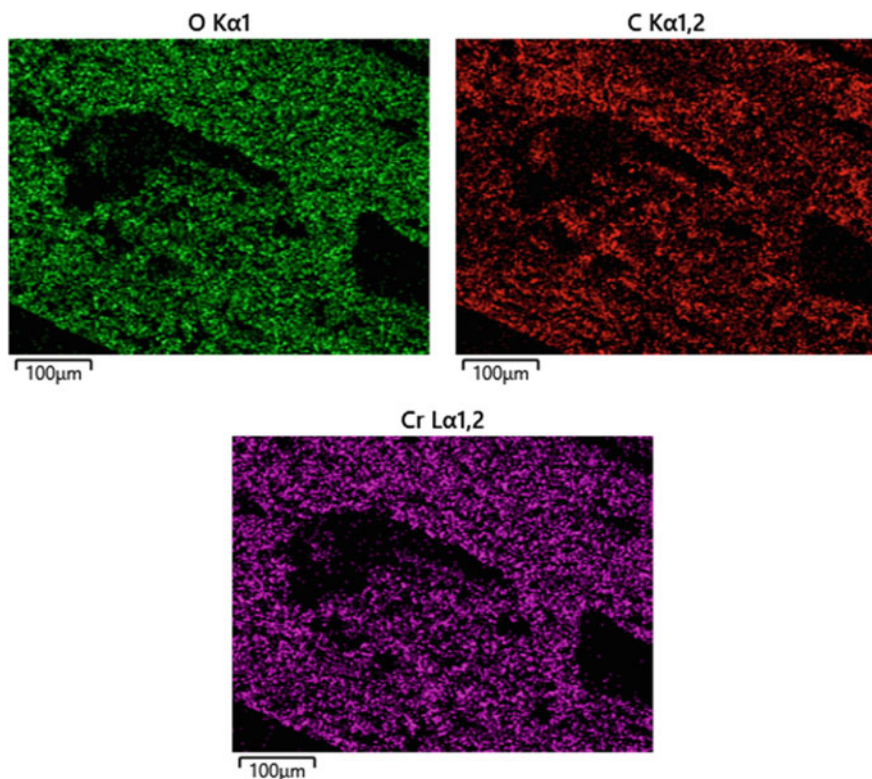
Fig. 7 EDX quantification of Cr, C, and O atoms at the cross-section surface of RO membrane
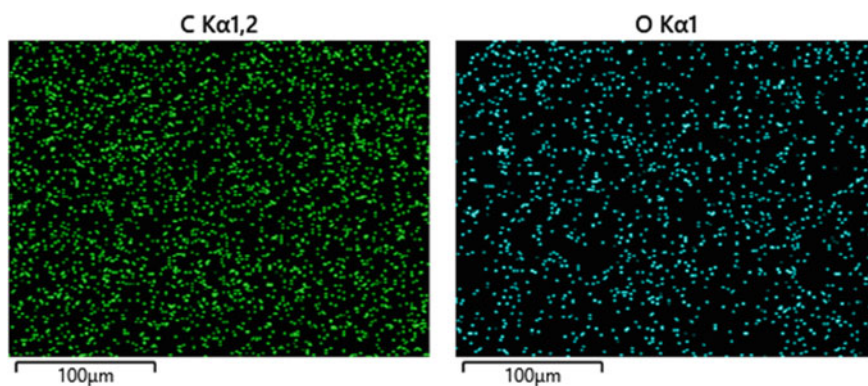
Fig. 8 EDX quantification of C, and O atoms at the inner surface of RO membrane

Table 4 Overall removal efficiency in five samples

Sample	COD (%)	BOD (%)	TDS (%)	Cr (%)
1	100.00	100.00	99.59	80.69
2	100.00	100.00	99.51	83.87
3	99.68	100.00	98.97	84.58
4	100.00	100.00	98.28	85.43
5	99.63	100.00	99.93	88.57
Average	99.86	100	99.26	84.63
STD	0.19	0	0.65	2.84

optimum results in COD, BOD, TDS, and chromium concentrations deviation. The highest standard deviation occurred in the chromium concentration reduction due to the difficulty of heavy metals reduction. Although, the heavy metals concentration reduction focusing on chromium was remarkable and could be considered as a great treatment process in order to reuse this treated wastewater.
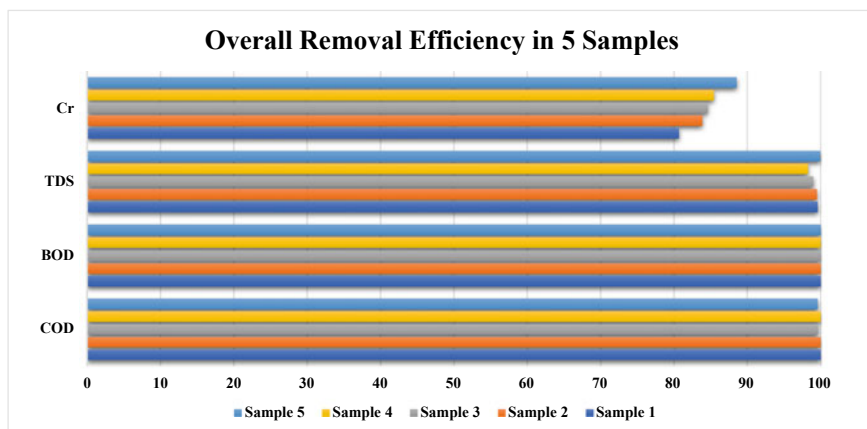
Fig. 9 Overall removal efficiency plot in five samples

4 Conclusion

Chromium sulfate is the major component used in leather production industries. Chromium sulfate is partially disposed with the wastewater in the form Cr^{+3} after the tanning process that will cause extremely negative environmental impacts if interacted without treatment. This research targets to find a solution to reuse this wastewater by applying a variety of treatment procedures. Chromium was the major parameter to be removed from tanneries wastewater due to its high toxicity to the environment and the human health. Chromium concentrations were ranging from 6.5 to 6.65 ppm from the five samples from different sources. The treatment process was done on the five samples and captured an average of 84.63%. The treatment process showed great results in organic materials removal by the reduction of the amount of COD and BOD. The COD and BOD were ranging from 1288 to 8434 ppm and 365 to 2960 ppm respectively. The treatment process accomplished 100% COD and BOD removal, which is the optimum result for reusing this wastewater safely. The TDS is an important parameter that can be measured instantly to evaluate the performance of the treatment process. The TDS in the five samples was ranging from 13,160 to 28,300 ppm. The treatment process provided impressive removal results with an average of 99.26%. The treated wastewater TDS was finally ranging from 12.6 to 226 ppm, which is safely complying with legal standards of treated wastewater qualifications. Applying the proposed hybrid system can offer a potential solution to the persisting problem of chromium pollution in the industrial sector. Treated wastewater can be more qualified by alternative coagulants and extra membranes in order to enable the use of this water to be drinking water. Ultrafiltration membrane can be replaced instead of granular activated carbon to extremely decrease the COD and BOD without the interaction with carbon atoms to the wastewater.

5 Recommendations

Treatment of Tannaries wastewater is crucial for environmental sustainability. The proposed system showed promising results in the treatment of the industrial wastewater. Therefore, the system could be instakked and fixed for tanning industries further to remove different concentrations of chromium.

References

1. Bassyouni M, Zoromba MS, Abdel-Aziz MH, Mosly I (2022) Extraction of nanocellulose for eco-friendly biocomposite adsorbent for wastewater treatment. Polymers 14(9):1852
2. Zoromba MS, Ismail MI, Bassyouni M, Abdel-Aziz MH, Salah N, Alshahrie A, Memic A (2017) Fabrication and characterization of poly (aniline-co-o-anthranilic acid)/magnetite nanocomposites and their application in wastewater treatment. Colloids Surf A 520:121–130
3. Abdel-Aziz MH, Bassyouni M, Soliman MF, Gutub SA, Magram SF (2017) Removal of heavy metals from wastewater using thermally treated sewage sludge adsorbent without chemical activation. J Mater Environ Sci 8(5):1737–1747
4. Mansi AE, El-Marsafy SM, Elhenawy Y, Bassyouni M (2022) Assessing the potential and limitations of membrane-based technologies for the treatment of oilfield produced water. Alex Eng J 68:787–815
5. Eteba A, Bassyouni M, Saleh M (2023) Utilization of chemically modified coal fly ash as cost-effective adsorbent for removal of hazardous organic wastes. Int J Environ Sci Technol 20(7):7589–7602
6. Abdel-Aziz MH, El-Ashtoukhy EZ, Bassyouni M, Al-Hossainy AF, Fawzy EM, Abdel-Hamid SM, Zoromba MS (2021) DFT and experimental study on adsorption of dyes on activated carbon prepared from apple leaves. Carbon Lett 31:863–878
7. Elminshawy NA, El-Ghandour M, Elhenawy Y, Bassyouni M, El-Damhogi DG, Addas MF (2019) Experimental investigation of a V-trough PV concentrator integrated with a buried water heat exchanger cooling system. Sol Energy 193:706–714
8. Sandid AM, Bassyouni M, Nehari D, Elhenawy Y (2021) Experimental and simulation study of multichannel air gap membrane distillation process with two types of solar collectors. Energy Convers Manage 243:114431
9. Fouad K, Alalm MG, Bassyouni M, Saleh MY (2020) A novel photocatalytic reactor for the extended reuse of W-TiO$_2$ in the degradation of sulfamethazine. Chemosphere 257:127270
10. Elhady S, Bassyouni M, Mansour RA, Elzahar MH, Abdel-Hamid S, Elhenawy Y, Saleh MY (2020) Oily wastewater treatment using polyamide thin film composite membrane technology. Membranes 10(5):84
11. Abdel-Aziz MH, Bassyouni M, Zoromba MS, Alshehri AA (2018) Removal of dyes from waste solutions by anodic oxidation on an array of horizontal graphite rods anodes. Ind Eng Chem Res 58(2):1004–1018
12. Maddah HA, Alzhrani AS, Bassyouni M, Abdel-Aziz MH, Zoromba M, Almalki AM (2018) Evaluation of various membrane filtration modules for the treatment of seawater. Appl Water Sci 8:1–13

13. Rodríguez MC, Barsanti L, Passarelli V, Evangelista V, Conforti V, Gualtieri P (2007) Effects of chromium on photosynthetic and photoreceptive apparatus of the alga *Chlamydomonas reinhardtii*. Environ Res 105(2):234–239. https://doi.org/10.1016/j.envres.2007.01.011
14. Wang Y (2019) Release of chrome in chrome tanning and post tanning processes (July 2012)
15. Oliveira H (2012) Chromium as an environmental pollutant: insights on induced plant toxicity. J Bot 2012:1–8. https://doi.org/10.1155/2012/375843
16. Stearns DM, Belbruno JJ, Wetterhahn KE (2018) A prediction of chromium(III) accumulation in humans from chromium dietary supplements. FASEB J 9(15):1650–1657. https://doi.org/10.1096/fasebj.9.15.8529846
17. Kolomaznik K, Adamek M, Andel I, Uhlirova M (2008) Leather waste-Potential threat to human health, and a new technology of its treatment. J Hazard Mater 160(2–3):514–520. https://doi.org/10.1016/j.jhazmat.2008.03.070
18. Khan SA, Ibrahim M, Jamil Y, Islam MS, Abbas F (2013) Spectrochemical analysis of soil around leather tanning industry using laser induced breakdown spectroscopy. J Chem. https://doi.org/10.1155/2013/894020
19. Cheng S, Grosse W, Karrenbrock F, Thoennessen M (2002) Efficiency of constructed wetlands in decontamination of water polluted by heavy metals. Ecol Eng 18(3):317–325
20. Eastlick BK (1995) Wetlands wastewater treatment for the Canadian prairies. Master, Environmental Design, University of Calgary
21. El-Hadek MA (2018) Dynamic equivalence of ultrasonic stress wave propagation in solids. Ultrasonics 83:214–221
22. El-Shamy AM, El-Hadek MA, Nassef AE, El-Bindary RA (2020) Box-Behnken design to enhance the corrosion resistance of high strength steel alloy in 3.5 wt% NaCl solution. Moroccan J Chem 8(4):4–8
23. Bassyouni M, Mansi AE, Elgabry A, Ibrahim BA, Kassem OA, Alhebeshy RJAPA (2020) Utilization of carbon nanotubes in removal of heavy metals from wastewater: a review of the CNTs' potential and current challenges. Appl Phys A 126:1–33
24. Nassef A, El-Hadek M (2016) Microstructure and mechanical behavior of hot pressed Cu-Sn powder alloys. Adv Mater Sci Eng 2016:1–10
25. Sobolewski A (1996) Metal species indicate the potential of constructed wetlands for long-term treatment of metal mine drainage. Ecol Eng 6(4):259–271
26. Wang L, Hung Y-T, Shammas N (2005) Physiochemical treatment processes. Human Press, New Jersey
27. Almuktar SAAAN, Abed SN, Scholz M (2017) Recycling of domestic wastewater treated by vertical-flow wetlands for irrigation of two consecutive *Capsicum annuum* generations. Ecol Eng 107:82–98

Removal of Methylene Blue from an Aqueous Solution Using a Surfactant-Modified Activated Carbon

Farid I. El-Dossoki [ID] **, Osama K. Hamza** [ID] **, and Esam A. Gomaa** [ID]

1 Introduction

The approach to this research project stems from our belief in a better tomorrow and in order to achieve the Sustainable Development Goals. It is not possible to achieve high and sustainable economic growth without considering its side effects that impede this growth. Here we are talking about water treatment as one of the most important and dangerous problems that threaten those economic entities and impede their progress. The development of human society, especially in the industrial field, is automatically associated with a significant rise in the general level of pollution if it is not confronted with the appropriate scientific method. The discharge of industrial wastewater is one of the most important of these examples, and we are here to talk about the treatment of this wastewater, which is polluted by dyes, as it is considered to be a remarkable source of its pollution [1]. Currently, the use of dyes has spread in various important industries, such as paper and textile production, hair dyes, food industries, leather tanning, and paints [2]. A number of toxicological and aesthetic problems are produced from the discharge of different types of dyes (methylene blue, methyl orange, gentian violet, rhodamine B, etc.) into the environment [3].

Methylene blue is a cationic dye that is commonly used as a biological dye, an acid–base indicator, and for its cardioprotective properties. The dye wastewater has different characteristics like a high concentration of organic substances, great

F. I. El-Dossoki (✉)
Chemistry Department, Faculty of Science, Port-Said University, Port-Said, Egypt
e-mail: feldossoki64@sci.psu.edu.eg

O. K. Hamza
Egyphar Company for Pharmaceutical Drugs, Cairo, Egypt
e-mail: osama.kamal@sci.psu.edu.eg

E. A. Gomaa
Chemistry Department, Faculty of Science, Mansoura University, Mansoura, Egypt
e-mail: esam2007@mans.edu.eg

285

discharge, and poor biodegradability. Finally, it significantly affects the health properties of water in general, including the photosynthesis of the microorganisms which are present in it [4].

For a long time until now, typical methods were used to treat the wastewater polluted by dyes. These methods include oxidation [5], membrane technology [6], flocculation [7], ozonation [8], photocatalytic degradation [9], and biodegradation. The previous classic methods are considered to be highly expensive and complicated techniques. As a result of that, it is necessary to search for effective and simple methods. The adsorption method has become a suitable technique due to its great effectiveness, inexpensiveness, ease of use, and lack of harmful components [10].

Activated carbon served as the most frequently utilized adsorbent because it is typically used to eliminate the inorganic and organic contaminations from the wastewater. Adsorption capacity is a significant index for evaluating the adsorption effect of an adsorbent. Different substitutional adsorbent sources are recommended for the treatment of wastewater to achieve low-cost properties [11–15].

Despite that, the most common activated carbon material is not used in the adsorption process of pollutants because it possesses a low adsorption capacity. Little surface area and inadequate adsorption performance selectivity are responsible for this flaw. In order to increase activated carbon's removal ability and adsorption capacity in the treatment of wastewater, it has become necessary to change the surface of the material. For instance, the chemical technology for Surf-C could be enhance the hydrophilic nature and distribution of activated carbon in water. Surfactants provide a number of benefits, including being inexpensive and having the ability to alter the charge characteristics of activated carbon surfaces. Finally, surfactants added more ionic adsorption sites, not only to promote the (Q_e) of ionic impurities on the Surf-C but also to enhance the adsorption selectivity [16, 17]. Several authors employed anionic surfactant-modified activated carbon to absorb cationic dyes and heavy metals from industrial wastewater [18–21] whereas others used cationic surfactant to modify activated carbon for removal various pollutants species (anionic dyes and salts) from the wastewater [22–25].

The word "surfactants" refers to surface active agents that consist of a hydrophobic part (non-polar part, usually a linear or branched hydrocarbon chain) attached to a polar part (hydrophilic). The hydrophilic part can be ionic, zwitterionic, or nonionic and is accompanied by counter ions. The surfactant category is divided into mainly four classes: anionic, cationic, nonionic, and amphoteric. The applications of surfactants are spread in our daily life, such as detergents, paints, dyestuffs, cosmetics, pharmaceuticals, fibers, and plastics [26].

This study aims to investigate the modification of activated carbon based on coconut shells by different surfactants for use in the removal of methylene blue from wastewater. The different variables that may have an impact on the cationic adsorption process were carefully examined.

Table 1 Type, physical appearance, purity and supplier of the chemicals under study

Item	Name	Physical appearance	Concentration (%)	CAS No.	Supplier
Carbon	AC	Granular	99.0	744044-0	AC Europe
Surfactants	BAC	Solution	50.0	68424-85-1	CISME Italy
	CTAC	Solution	30.0	112-02-7	CISME Italy
	SLES	Paste	70.0	9004-82-4	Royal Chemicals
	AOS	Powder	95.0	68439-57-6	Godrej ind.ltd
Dye	MB	Powder	82.0	122965-43-9	Sigma-Aldrich
Acids	HCl	Liquid	36.5	7647-01-0	CDH
Bases	NaOH	Pellets	98.5	1310-73-2	Scharlau

2 Experimental

2.1 Materials

All information about the chemicals under study was obtained in Table 1 and Fig. 1. The remaining percentages of the BAC, CTAC, and SLES (50%, 70%, and 30%, respectively) are water and were taken into account in the preparation of the stock solution. The solvent is bidistilled water from the central laboratory in the faculty of science of Port Said University.

Activated carbon is manufactured by high temperature steam activation from selected grades of coconut shell.

2.2 Formation of Activated Carbon Modified by Surfactants

First, a total of 5 g of virgin activated carbon was placed to a conical flask with 150 ml of surfactant aqueous solution (concentration = its CMC value) to produce a surfactant modified activated carbon compound. At a temperature of 301.15 K, the mixture was vibrated for 6 h, then a filtration step was made to extract the surfactant modified activated carbon. After being filtered, the Surf-C was rinsed with bidistilled water and dried in an air-dry oven for one day at 313.15 K. It was then placed in a clean and dry bottle for storage. According to recent studies, the optimal surfactant concentration for adsorption is that which matches its CMC [21]. The CMC values of BAC CTAC, SLES, and AOS at 298.15 K have been observed to be 0.00525, 0.001, 0.00079, and 0.0019 mol/L, respectively [27–29]. Virgin-C, BAC-C, CTAC-C, SLES-C and AOS-C are the acronyms for unmodified activated carbon and surfactant-modified activated carbon, respectively.

(a) Alkyl Benzyl Dimethyl Ammonium Chloride
(BAC)
$C_6H_5CH_2N(CH_3)_2C_{12}H_{25}Cl$

(c) Cetyl Trimethyl Ammonium Chloride
(CTAC)
$CH_3(CH_2)_{15}N(Cl)(CH_3)_3$

(b) Sodium Lauryl Ether Sulphate
(SLES)
$CH_3(CH_2)_{10}CH_2(OCH_2CH_2)_2\ OSO_3Na$

(d) Sodium Alpha Olefin Sulphonate
(AOS)
$CH_3(CH_2)_{10}(CH)_2CH_2SO_3Na$

(e) Methylene Blue (MB)
$C_{16}H_{18}ClN_3S.xH_2O$
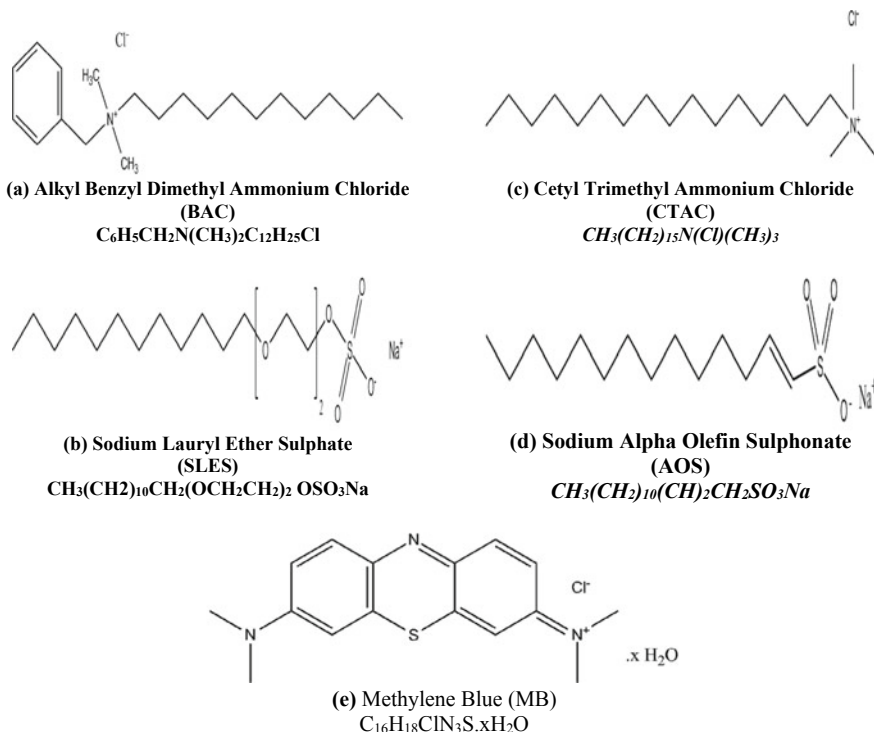
Fig. 1 The chemical structure of **a** BAC-C, **b** CTAC-C, **c** SLES-C, **d** AOS-C, and **e** MB

The functional groups on the surfaces of adsorbents were detected via a single-beam FT-IR (Bruker, Vertex70) in the wavenumber domain from 400 till 4000 cm^{-1}. The sample was prepared for analysis using the KBr disc.

The morphology of adsorbents was investigated using the SEM version (Quanta 250 FEG FEI Corporation, Holland) with an accelerating voltage of 30 kV. To decrease the impact of sample charging caused by the electron beam, a 3.5 nm coating of gold was applied to the samples' surfaces.

2.3   Testing for Adsorption

By examining various experimental variables, including surfactant concentration loaded, pH (1–12), contact time, the initial concentration of MB (10, 30, and 50 mg L^{-1}), and adsorbent dosage at room temperature (298.15 K), the adsorption capacity and removal percentage of methylene blue on Surf-C were calculated. The initial pH of the solution was adjusted using 0.1 M HCl and 0.1 M NaOH. A 100 mL of MB solution was mixed with a specified amount of Virgin-C or Surf-C

in a conical flask. Each combination was shaken at 160 rpm and 298.15 K for the predetermined amount of time. The specimens were filtrated and examined once the equilibrium point of the adsorption process had been reached.

2.4 Data Analysis

The absorbance of methylene blue in aqueous solutions was evaluated using the UV–visible spectrophotometer (HACH DR6000TM) at the peak of maximal absorption at MB 664 nm. The OriginLab software was used to show the concentration, adsorption capacity, and removal percentage of MB by drawing a relationship graph between concentration and absorbance of MB. The pH of the solution was determined by an AD1200 pH-ORP-ISE-TEMP Bench Meter. The removal % of MB on BAC-C, CTAC-C, SLES-C, and AOS-C adsorbents was investigated using the batch equilibrium method by analyzing the dye solution's absorbance before and after treatment. The capacity for adsorption and the rate of dye removal in an equilibrium condition were determined using Eqs. (1) and (2).

$$\text{Adsorption capacity } (Q_e) = \frac{(C_0 - C_e)V}{m} \tag{1}$$

$$\text{Removal percentage } (\%) = \frac{(C_0 - C_e)}{C_0} \times 100 \tag{2}$$

where C_0, C_e, V, and m refer to the initial and post-adsorption MB concentrations in mg/L, the volume in liter of adding methylene blue, and the weight of adsorbents in gram respectively.

All the adsorption analysis are carried out using the standard test methods for wastewater and water [30].

3 Results and Discussion

3.1 Investigation of the Surfactant Modified Activated Carbon

3.1.1 FT-IR Identifications

The surface characteristics of the adsorbent (Virgin-C and Surf-C) were detected by using FT-IR (Fourier transform infrared spectroscopy) as shown in Fig. 2 and Table 2.
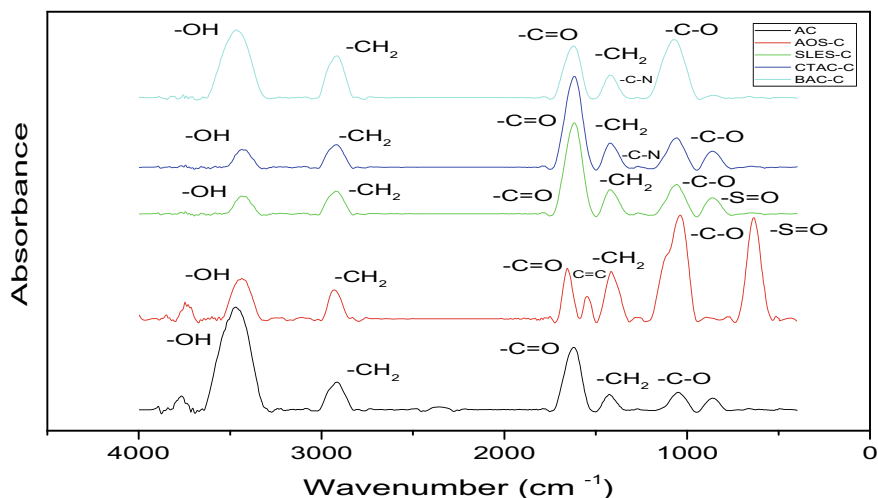
Fig. 2 FT-IR scanning for Virgin-C, BAC-C, CTAC-C, SLES-C and AOS-C

There were five significant absorption bands visible in the spectra of virgin activated carbon. The five peaks of 3469, 2916, 1618, 1425, and 1049 cm^{-1} may be correspond to the O-H stretching of carboxylic and phenolic groups, C-H stretching in aliphatic methyl group, C=O stretching conjugated to carboxylic group, bending in an alkane methyl group, and C-O stretching in a carboxylic group respectively. In the region of the fingerprint, the remaining peaks reflect the C-C bonds.

As a result of surfactants' modification of activated carbon, new bands were detected. For instance, the S-O stretching of sulphonate group, the S-O stretching of sulphonate group, and the C=C alkene may be referenced by the three bands in AOS-C at 1546 cm^{-1}, 1035 cm^{-1}, and 634 cm^{-1}, respectively.

In addition, three different bands at 1267, 1119, and 862 cm^{-1} in SLES-C were identified. These bands can be attributed to the C-O stretching in ether, S=O stretching of sulphate group, and S-O stretching of sulphate group, consecutively. The C-N stretching vibration of aliphatic amines in CTAC-C and BAC-C was represented by a new peak at 1276–1273 cm^{-1}. while the C=C stretching vibration aromatic ring in BAC-C was observed at 1427 cm^{-1}.

The intensity of OH absorption band was decrease in all case of Surf-c than the Virgin-C this may be related to effect of different function groups (sulphate, sulphonate, and amine) were found in surfactants structures.

3.1.2 SEM Identifications

The surface morphological appearances of activated carbon and surfactant modified activated carbon (AOS-C) is shown in Figs. 3 and 4 using SEM analysis.

Table 2 The functional groups for Virgin-C, BAC-C, CTAC-C, SLES-C, and AOS-C depending on FTIR scanning

Functional group		Wavenumber, cm^{-1}				
		AC	AOS-AC	SLES-AC	CTAC-AC	BAC-AC
-OH	Stretching	3469	3438	3435	3435	3468
-CH$_2$	Stretching in aliphatic (alkane)	2916	2918	2922	2918	2916
C=O	Stretching conjugated	1618	1654	1618	1618	1620
C=C	Stretching in alkene	–	1546	–	–	–
-CH$_2$	Bending in aliphatic (alkane)	1425	1411	1423	1423	1421
C-N	Stretching of alphatic amine	–	–	–	1273	1276
C-O	Ether group	–	–	1267	–	–
S=O	Sulphate/ sulphonate group	–	1035	1119	–	–
C-O	Stretching in carboxylic group	1049	1072	1059	1056	1072
C=C	Aromatic ring	–	–	–	–	856
S-O	Sulphate/ sulphonate group		634	862	–	–
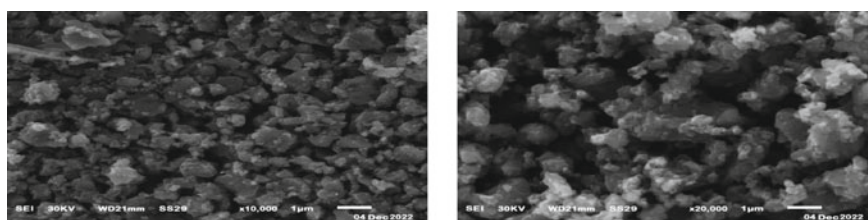
Fig. 3 SEM analysis for Virgin-C at different magnification

The image of coconut shell-based activated carbon showed irregular 2D sheets. The sheets are aggregated, and there are organic moieties on the surface of them. While in AOS-C sample There are sandy granules (organic material) irregularly distributed on the surface of the aggregated 2D sheets.
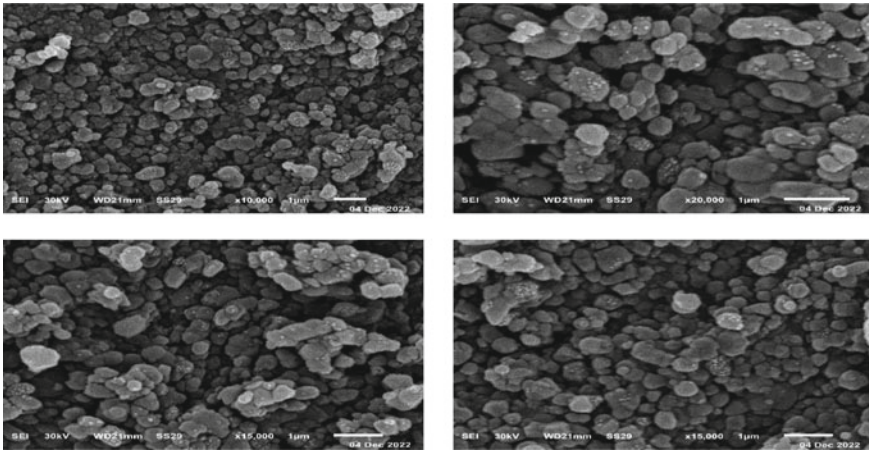
Fig. 4 SEM analysis for AOS-C at different magnification

The collected SEM images demonstrate clearly that modified active carbon adsorbents have distinct physico-chemical properties and larger surface area than unmodified activated carbon. All of these findings suggest that surfactants and activated carbon can interact effectively via hydrophobic contact.

The size of the sheets is in the range 105–800 nm with maximum at 210 nm as shown in Fig. 5.
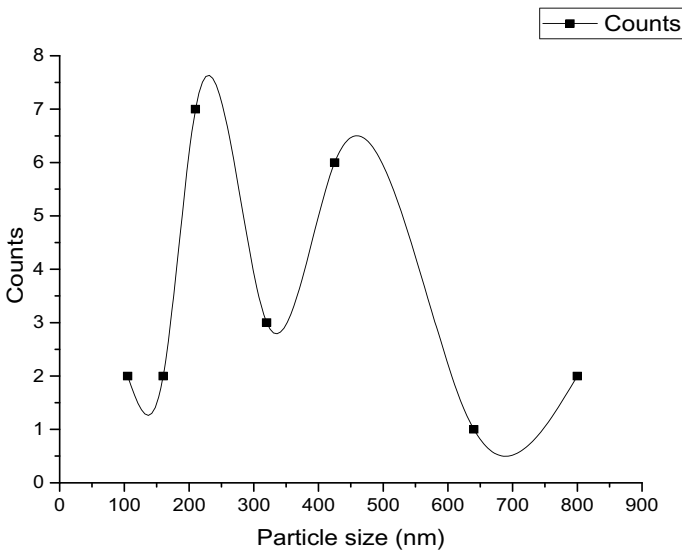
Fig. 5 The size of AOS-C sheet

3.2 Adsorption Measurements

3.2.1 Effect of Concentrations and Various Types of Surfactant Loading in the Modification Step

The first and most important step in the modification process of the activated carbon by surfactants is to choose the right and effective concentration of surfactants, so we use three concentrations of each surfactant (before its CMC, at its CMC, and finally after its CMC) as shown in Fig. 6. A relationship between the removal percentage and the three concentrations of surfactants was used. Also, three concentrations of initial MB were used to make a good coverage area from comparison.

The results revealed that the surfactant concentration equivalent to its CMC value is more efficient than the other two different concentrations. The removal percentage in the case of AOS-C and SLES-C increases as surfactant concentration increases, this may be correlated with the increase in net surface charges, both positive and negative. Whereas, on the contrary, the opposite happens in the case of BAC-C and CTAC-C did not increase remarkably, except for their CMC. The micropores were blocked when the surfactant molecules increased, resulting in a reduction in the surface area [31].

The analysis indicated that AOS-C, followed by SLES-C, Virgin-C, BAC-C, and CTAC-C, exhibit the maximum adsorption capacity of MB. Because the anionic and cationic systems (AOS-MB or SLES-MB) had a strong relationship, the anionic
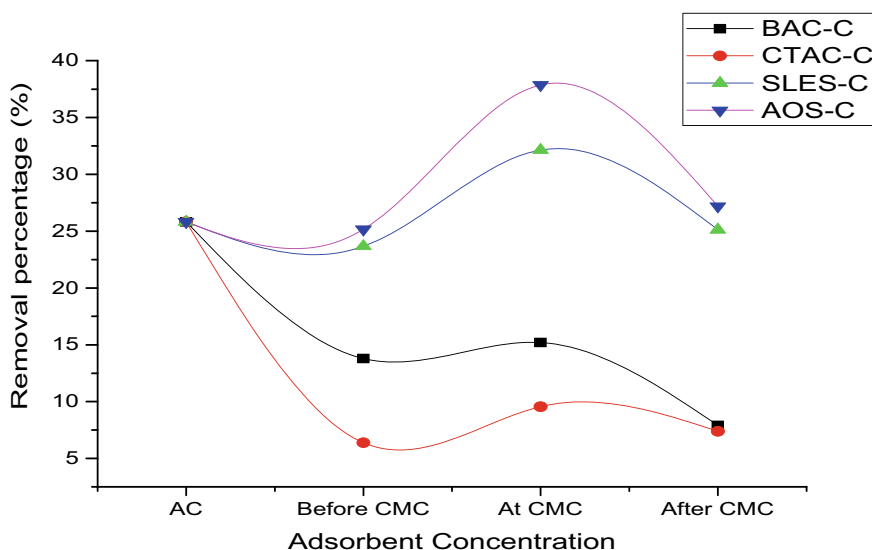
Fig. 6 Effect of concentrations and various types of surfactants on the percent removal of MB (S/L = 0.015 g L^{-1}, initial MB concentration = 10 mg L^{-1}, pH = 8.0, time = 120 min and T = 298.15 K)

surfactant-modified activated carbon demonstrated a strong adsorption capacity for MB. The chemistry of the functional groups in surfactants has a considerable impact on the adsorption mechanism. Strong acids are supposed to have conjugate bases in the sulphate (SO_4^-) and sulfite (SO_3^-). The sodium and hydrogen ions that are attached to these conjugated bases make the dissociation easy in an aqueous solution. Therefore, the MB ion can be easily exchanged [32, 33].

On the other hand, the activated carbon improved by BAC and CTAC exhibited the frailest adsorption capacity for the MB because of the repulsive force that occurred between the cationic surfactants and cationic dye. Moreover, the two cationic surfactants may clog the pores on the surface of the activated carbon when they are applied, which subsequently reduces its capability to adsorb MB compared with unmodified activated carbon [19].

3.2.2 Impacts of a pH Change in the Solution

Figure 7 display the percentage of methylene blue removed by Virgin-C, SLES-C, and AOS-C at various pH levels. These figures demonstrate that the basic medium became appropriate for the adsorption process.
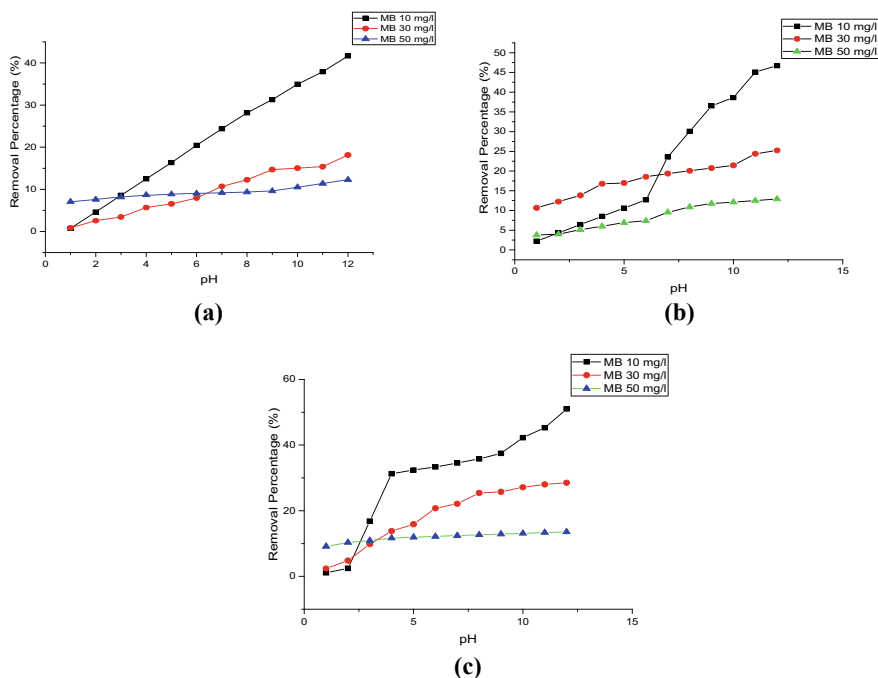
Fig. 7 Removal percentage of MB adsorption at different pH values by **a** Virgin-C **b** SLES-C, and **c** AOS-C (S/L = 0.015 g L^{-1}, time = 120 min, T = 298.15 K)

The Q_e of methylene blue were 2.39, 5.08, and 4.23 mg g^{-1}, respectively, at a pH equal to 8, and they were 3.40, 5.71, and 4.52 mg g^{-1} at a pH of 12.00 in the case of AOS-C, where the starting concentrations of the dye were 10, 30, and 50 mg L^{-1}. As a result, growing the pH value promote the adsorption removal % and the Q_e.

The surface charge of Virgin-C, SLES-C, and AOS-C is influenced by the pH of dye solutions, which also regulates the ionization of acids and bases. The total negative surface charge of virgin-C is improved by the anionic surfactant modification procedure. As the pH value increases, the surface charge becomes more negatively charged. Due to the attraction that develops between them as a result, the adsorption of MB by SLES-C and AOS-C grows with pH. At low pH values, the dissociation of (H$^+$) ions on SLES-C and AOS-C functional groups may be prevented. Consequently, the electronegativity of SLES-C and AOS-C as well as the electrostatic attraction force between SLES-C or AOS-C and MB cation, were comparatively weak. At higher pH, the concentration of (OH$^+$) ions in the solution is increased, which leads to the dissociation of dye cations becoming a little less rapid [34–36].

Kannan's research on the impact of pH on the MB adsorption by different ACs revealed that an increase in the initial pH improved the adsorption capacity of dye [37].

The point of zero charge (PZC) for activated carbon and surfactants-modified activated carbon was calculated as mention in the previous studies [38, 39].

As shown from Fig. 8, the pH of points of zero charge (PZC) for virgin-C, SLES-C, and AOS-C in 10 mg/L aqueous solution of methylene blue are 8.07, 8.6, and 9.6 respectively.
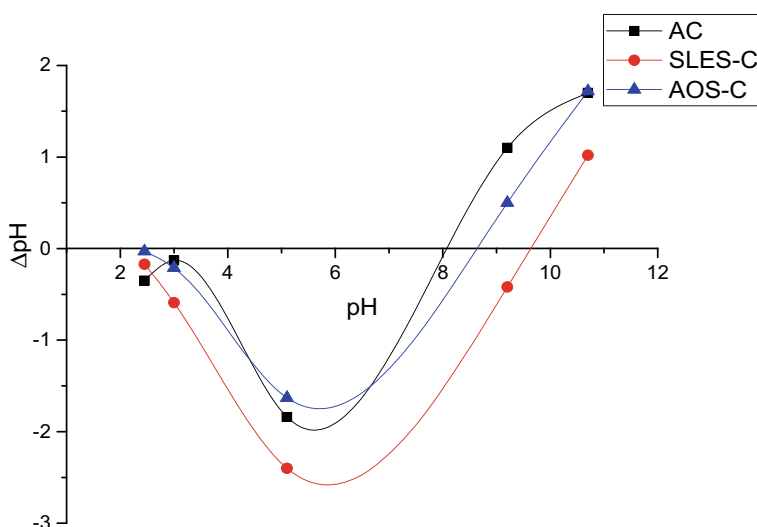
Fig. 8 Point of zero charge of Virgin-C, SLES-C, and AOS-C

These kinds of adsorbents exhibit excellent charge balance in the fundamental area, and their PZC values are over 8. The surface of these adsorbents is negatively charged and can attract cations.

3.2.3 Effect of Contact Time

The adsorption capacity and removal percentage of MB on anionic surfactants modified activated carbon in aqueous solutions through an interval of time have been reported in Table 3 and Fig. 9.

Figure 9 demonstrated that, as the duration of the encounter lengthened, the Q_e quantity of methylene blue by Virgin-C, SLES-C, and AOS-C was increased until it reached a maximum value, then it was stabilized. The process can be divided into two periods. The first one is called fast adsorption, which starts at 5–60 min until it reaches the adsorption equilibrium condition. This behavior is attributed to the good binding between the adsorption active sites on the SLES-C and AOS-C adsorbents and cationic dye, which reaches its highest value after all the adsorption active sites of the adsorbents are filled. the rate of dye adsorption for this phase is controlled by the MB ions which transferred to the surface of the adsorbents from the surround solution. After 60 min of contact time, we get to the second step, which is the slow growth adsorption process. At this stage, we did not see a noticeable increase in the rate of absorption with increasing time, but it did decrease and gradually stabilize. The surface saturation condition on the SLES-C and AOS-C adsorption active sites may be responsible for this performance. The factor controlling the rate of dye adsorption is the migration of the dye from the outside to the inner pore sites of the adsorbent

Table 3 The adsorption capacity of MB by Virgin-C, SLES-C, and AOS-C at different contact times (S/L = 0.015 g L^{-1}, pH = 8.0, T = 298.15 K)

Time (min)	Adsorption capacity (q_e) mg/g								
	MB = 10 mg/l			MB = 30 mg/l			MB = 50 mg/l		
	Virgin-C	SLES-C	AOS-C	Virgin-C	SLES-C	AOS-C	Virgin-C	SLES-C	AOS-C
5	0.72	0.75	0.73	1.44	2.60	2.09	1.78	1.32	2.12
10	0.82	0.85	0.88	1.55	2.70	2.35	1.90	1.55	2.49
15	0.92	0.97	1.03	1.67	2.79	2.61	2.03	1.79	2.87
20	1.02	1.10	1.17	1.78	2.88	2.86	2.15	2.02	3.25
30	1.21	1.34	1.47	2.01	3.07	3.37	2.40	2.49	4.00
60	1.80	2.07	2.36	2.70	3.63	4.91	3.15	3.89	6.27
90	1.80	2.07	2.37	2.74	3.66	5.08	3.18	3.84	6.32
120	1.80	2.08	2.39	2.78	3.68	5.26	3.22	3.80	6.37
150	1.81	2.08	2.40	2.82	3.71	5.43	3.25	3.75	6.42
180	1.81	2.08	2.42	2.86	3.73	5.60	3.29	3.71	6.47
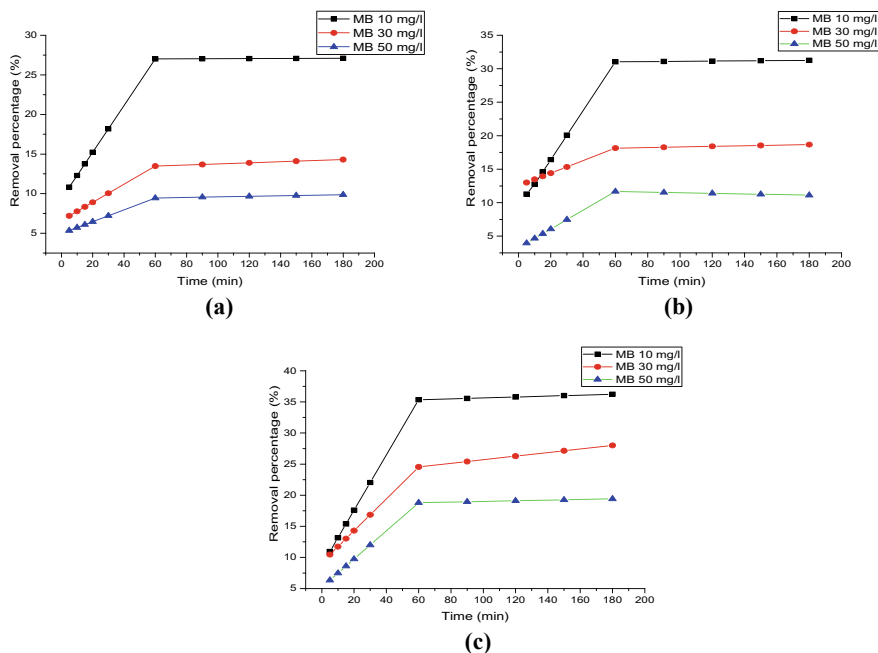
Fig. 9 Removal percentage % of MB adsorption at interval time by **a** Virgin-C, **b** SLES-C, and **c** AOS-C (S/L = 0.015 g L^{-1}, pH = 8.0, T = 298.15 K)

molecules [40]. Finally, the adsorption process also moves along faster with a lesser dye concentration. This the result was agreed with previous studies [41].

3.2.4 The Impact of Initial MB Concentration

The effect of various initial concentrations of MB dye was studied using the similar weight of the adsorbents (Virgin-C, SLES-C, and AOS-C) for 120 min at 298.15 K, keeping the solution pH at 8.0. As stated by results were collected in Table 4, a growth in the adsorption capacity at equilibrium (Q_e) of MB dye using SLES-C and AOS-C was observed when the initial concentration of MB was increased, reaching its maximum values of 4.01 and 5.08 mg g^{-1} for adsorbents SLES-C and AOS-C respectively, at the initial dye concentration of 30 mg L^{-1}. Then, a decrease in adsorption capacities occurs as the initial concentration of MB dye is increased from 30 to 50 mg L^{-1}. This could be because SLES-C and AOS-C have full active sites on their surfaces [32, 42, 43].

Table 4 The removal percentage and adsorption capacity of different initial concentration from MB by Virgin-C (S/L = 0.015 g L^{-1}, time = 120 min, pH = 8.0, T = 298.15 K)

MB initial concentration (mg/l)	Removal percentage (%)			Adsorption capacity (mg/g)		
	Virgin-C	SLES-C	AOS-C	Virgin-C	SLES-C	AOS-C
10	28.17	30.06	35.79	1.88	2.00	2.39
20	20.22	25.06	30.61	2.17	3.01	3.74
30	13.89	20.05	25.42	2.78	4.01	5.08
40	10.82	15.47	19.05	2.79	3.82	4.66
50	8.91	10.89	12.69	1.78	3.63	4.23

3.2.5 Effects of Adsorbent Dosage

Adsorbent dosage plays a significant effectiveness on adsorption efficacy. To find the optimal dose of adsorbent at different concentrations of the cationic dye, MB adsorption was investigated in relation to the influence of adsorbent dosage.

From Fig. 10, it was observed that with increasing adsorbent dose, the value of removal percentage increases until it reaches the highest value, then a relative stability occurs [44–46].

Table 5 contains the data that were gathered, and as an example at an initial MB concentration of 10 mg L^{-1}, it was found that when Virgin-C, SLES-C, and AOS-C doses increased from 0.05 to 0.2 g/l, the adsorption capacities of MB increased as follows: from 4.2 to 9.25 mg/g, from 5.2 to 13.35 mg/g, and from 5.6 to 10.4 mg/g, respectively. After that a decrease in the adsorption capacities of MB was found as the adsorbent dose increase. For a constant initial pollutant concentration, when the adsorbent concentration increases, the number of binding spots that are active and/or the surface area of the adsorbate may grow. A reduction for the specific ion absorption with an increase in adsorbent concentration may be caused by increased unsaturation and/or decreased utilization of the binding sites that are active at high adsorbent concentrations. Additionally, at high adsorbent concentrations, particles self-bind and agglomerate, which decreases the number of useful active binding sites that are accessible for adsorption. As a result, as the concentration of the adsorbent increases, the specific ion adsorbed decreases [47, 48].

3.3 Adsorption Kinetic and Isotherm Calculations

3.3.1 Adsorption Kinetic Studies

Adsorption kinetics data are used to describe the reaction rate between cationic dye and anionic surfactant-modified activated carbon in the adsorption process, besides studying different factors that could have an effect on the reaction rate. Four kinetic models were applied to assure the most effective equation in this study [38].

(a)

(b)

(c)
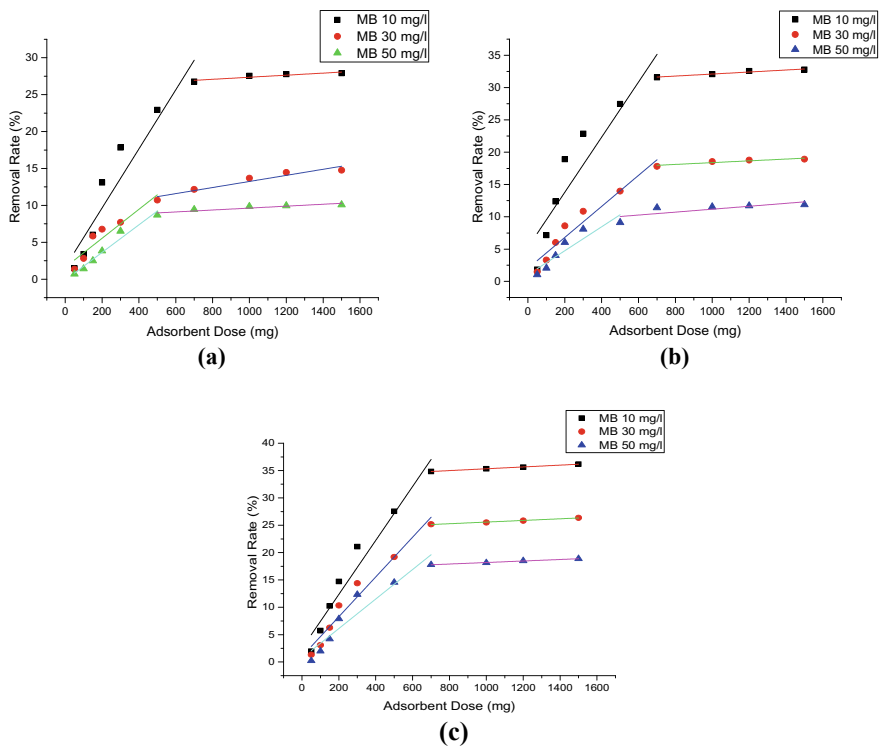
Fig. 10 Effect of adsorbent dose **a** Virgin-C, **b** SLES-C, and **c** AOS-C on MB adsorption (MB initial concentration = 10, 30 and 50 mg l^{-1}, time = 120 min, pH = 8, T = 298 K)

Table 5 Effect of adsorbent dose Virgin-C, SLES-C, and AOS-C on the adsorption capacity of different initial concentration from MB (MB initial concentration = 10, 30 and 50 mg l^{-1}, time = 120 min, pH = 8, T = 298 K)

Adsorbent dose (mg/L)	Adsorption capacity (mg/g)								
	Virgin-C			SLES-C			AOS-C		
	10 mg/l	30 mg/l	50 mg/l	10 mg/l	30 mg/l	50 mg/l	10 mg/l	30 mg/l	50 mg/l
50	4.20	7.40	6.60	5.20	8.00	9.80	5.60	7.20	2.20
100	4.80	7.60	6.70	10.10	8.90	9.70	8.10	8.30	9.40
150	5.67	10.47	7.87	11.67	10.80	12.60	9.67	11.27	13.20
200	9.25	9.10	9.04	13.35	11.55	14.20	10.40	13.90	18.60
300	8.40	6.90	10.22	10.77	9.73	12.70	9.93	12.90	19.37
500	6.48	5.76	8.18	7.76	7.52	8.58	7.78	10.32	13.72
700	5.40	4.67	6.36	6.37	6.84	7.67	7.03	9.67	11.97
1000	3.89	3.68	4.64	4.53	4.99	5.44	4.99	6.86	8.54
1200	3.27	3.24	3.91	3.83	4.21	4.59	4.19	5.79	7.26
1500	2.63	2.65	3.17	3.09	3.39	3.73	3.41	4.73	5.93

Depending on the pseudo-first-order kinetic model, the reaction rate is directly dependent on the proportion of the saturation concentration to the quantity of dye that SLES-C or AOS-C adsorbed over time. Steps in the diffusion process regulate the adsorption in this model [42]. The following integrated equation (3) is used to describe this model.

$$\ln(Q_e - Q_t) = \ln Q_e - k_1 t \tag{3}$$

where k_1 (min^{-1}), and Q_e and Q_t (mg g^{-1}) are rate constant, the quantities of MB adsorbed at equilibrium concentration and at various times t, respectively. The rate constant was calculated by plotting a relation between $\ln(Q_e - Q_t)$ and time (t). The calculated R^2 data was in the range of 0.886–0.954, 0.896–0.972, and 0.919–0.973 for Virgin-C, SLES-C, and AOS-C, respectively. Furthermore, the data in Table 6 showed that there are significant differences between $Q_{e,exp}$ and $Q_{e,cal}$ values, demonstrating that the pseudo-first order model was unable to accurately depict the adsorption process.

The pseudo-second-order kinetic model presupposes that the adsorption is managed by a chemical adsorption step and that the reaction rate is proportionate to the concentrations of the two reactants. Equation (4) can explain this model [49].

$$\frac{t}{Q_t} = \frac{1}{k_2 Q_e^2} + \frac{t}{Q_e} \tag{4}$$

where k_2 $(\text{g mg}^{-1}\,\text{min}^{-1})$ refers to the second order rate constant and can be measured using the linear plot of (t/Q_t) against (t) for different MB concentrations as shown in Fig. 11. The observed (R^2) values were found to be greater than 0.989, 0.994, and 0.989 for Virgin-C, SLES-C, and AOS-C, respectively. Also, there was good

Table 6 Pseudo (first and second) order models for the adsorption of MB by Virgin-C, SLES-C, and AOS-C

Adsorbent	C_0 mg L^{-1}	$Q_{e,exp}$ mg g^{-1}	Pseudo first order model			Pseudo second order model		
			k_1 min^{-1}	$Q_{e,cal}$ mg g^{-1}	R^2	k_2 g mg^{-1} min^{-1}	$Q_{e,cal}$ mg g^{-1}	R^2
Virgin-C	10	1.806	0.047	2.374	0.919	0.030	2.074	0.989
	30	2.820	0.027	4.025	0.973	0.031	3.038	0.993
	50	3.254	0.043	5.922	0.927	0.031	3.486	0.994
SLES-C	10	2.080	0.060	2.169	0.896	0.018	2.497	0.994
	30	3.708	0.036	1.425	0.946	0.014	3.840	0.998
	50	3.752	0.053	4.011	0.972	0.019	3.972	0.997
AOS-C	10	2.401	0.047	2.374	0.919	0.013	2.951	0.993
	30	5.430	0.027	4.025	0.973	0.011	5.757	0.989
	50	6.422	0.043	5.922	0.927	0.011	6.288	0.993
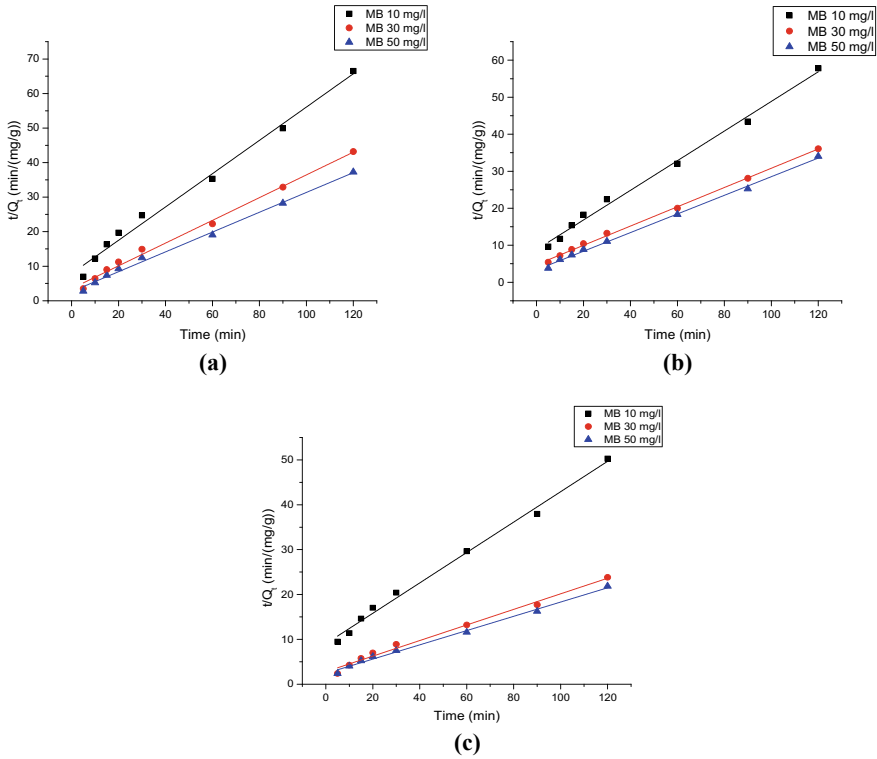
Fig. 11 Pseudo second order model for the adsorption of MB on **a** Virgin-C, **b** SLES-C, and **c** AOS-C (S/L = 0.015 g L^{-1}, pH = 8.0, T = 298 K)

agreement between both the experimental $Q_{e,cal}$ and $Q_{e,exp}$. Depending on this performance, the pseudo-second-order model was the most accurate model for describing the adsorption of MB on Virgin-C, SLES-C, and AOS-C.

The intra-particle diffusion and Weber-Morris intra-particle diffusion models also applied to more clarifications for the adsorption mechanism as obtained in Eq. 5 [50].

$$Q_t = k_{ip} t^{\frac{1}{2}} + C_i \tag{5}$$

where k_{ip} (mg g^{-1} $min^{-1/2}$) and C_i (mg g^{-1}) are the rate constant and constant of the intra particle diffusion model, which can be measured using a linear curve for the Q_t versus $t^{1/2}$, the data was collected in Table 7. It was found that the values of constant C_i increase when the MB dye concentration is increased, it can be related to the thickening of the boundary layer. On the other hand, the high C_i values indicated that the initial adsorption interval was greatly influenced by the exterior diffusion of the MB on virgin-C, SLES-A, and AOS-C. The close proximity of the R^2 values to 0.999 shows that the intra-particle model was successfully used in the sorption process.

Table 7 Intra-particle diffusion and Elovich models for the elimination of MB by Virgin-C, SLES-C, and AOS-C

Adsorbent	C_0 mg L^{-1}	Intra-particle diffusion model			Elovich model		
		k_{ip} mg g^{-1} min$^{-1/2}$	C_i	R^2	α g mg^{-1} min^{-1}	β mg g^{-1}	R^2
Virgin-C	10	0.164	0.310	0.990	0.311	2.339	0.898
	30	0.214	0.880	0.977	1.158	1.973	0.900
	50	0.235	1.164	0.976	1.869	1.817	0.899
SLES-C	10	0.209	0.218	0.946	0.289	1.904	0.890
	30	0.164	2.190	0.955	30.213	2.423	0.899
	50	0.371	0.432	0.956	0.531	1.065	0.917
AOS-C	10	0.257	0.090	0.951	0.269	1.546	0.898
	30	0.461	0.923	0.963	0.938	0.866	0.900
	50	0.658	0.476	0.951	0.798	0.605	0.898

Elovich's model of the adsorption process for a non-ideal condition is described in Eq. 6. In this model, the adsorption mechanism contains a fast and slow adsorption process.

$$Q_t = \frac{1}{\beta} \ln \alpha\beta + \frac{1}{\beta} \ln t \qquad (6)$$

where α (mg g^{-1} min^{-1}) and β (mg g^{-1}) represent the initial adsorption rate and the desorption coefficient, respectively. Plotting Q_t across ln(t) using $1/\beta$ for the slope and $1/\beta \ln(\alpha \beta)$ for the intercept allows for the calculation of this model. As presented in Table 7, the values of (R^2) for the initial MB concentrations (10, 30, and 50 mg L^{-1}) were (0.898, 0.900, and 0.899), (0.890, 0.899, and 0.917) and (0.898, 0.900, and 0.898) for virgin-C, SLES-C and AOS-C, respectively. The intra-particle diffusion mechanism is one of many that regulates the adsorption process, according to fitting data generated for the Elovich kinetic model [51].

3.3.2 Adsorption Isotherm Studies

Explaining the link between both the adsorption capacity and quantity of the dye at a dynamic equilibrium state with constant pH and temperature is crucial for researching adsorption isotherms. To explain the phenomena of adsorption isotherms, three models were utilized: Langmuir, Freundlich, and Temkin models [19]. The Langmuir isotherm can be measured using the following Eq. (7):

$$\frac{C_e}{Q_t} = \frac{1}{Q_{max}k_l} + \frac{C_e}{Q_{max}} \qquad (7)$$

where C_e (mg L^{-1}), Q_e (mg g^{-1}), Q_{max} (mg g^{-1}) and K_L (L mg^{-1}) are the equilibrium concentration, the amount of adsorbed dye at equilibrium, the Langmuir constants and the adsorption rate, respectively. The linear plot of C_e/Q_e against C_e yielded an R-squared value of 0.994, 0.996, and 1.000 for virgin-C, SLES-C, and AOS-C, respectively, demonstrating that the adsorption mechanism was consistent with the isotherm model proposed by Langmuir as shown in Fig. 12. The computed values of Q_{max} and K_L are collected in Table 8.

A dimension equilibrium variable can be used to express the key features of the Langmuir isotherm (R_L), it can be calculated by Eq. 8:

$$R_L = \frac{1}{1 + k_l C_O} \tag{8}$$

(a)

(b)

(c)
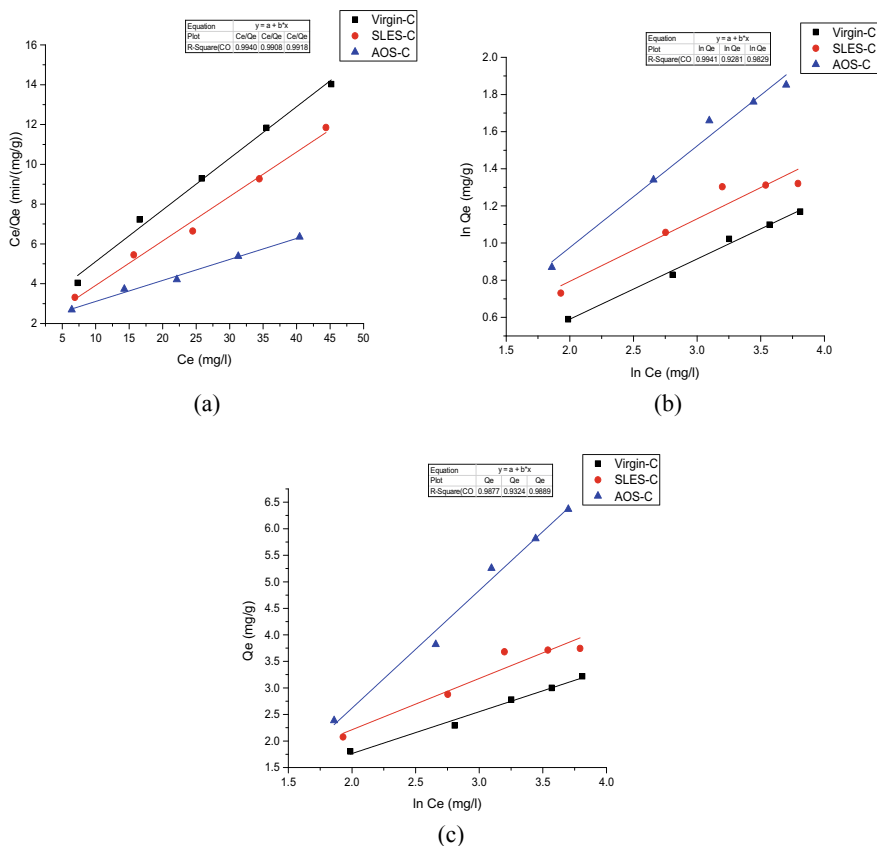
Fig. 12 Three isotherm graphs C **a** Langmuir, **b** Freundlich, and **c** Temkin for adsorption of MB on Virgin-C, SLES-C, and AOS-C

Table 8 The three isotherms characteristics for the MB adsorption on Virgin-C, SLES-C, and AOS-C

	Adsorption model									
	Langmuir			Freundlich			Temkin			
	Q_{max} mg g^{-1}	K_L L m^{-1} g^{-1}	R^2	K_f mg g^{-1}	1/n	R^2	B J mol^{-1}	A L g^{-1}	b L g^{-1}	R^2
Virgin-C	3.854	0.103	0.994	0.943	0.324	0.994	0.788	1.269	3145.739	0.988
SLES-C	4.395	0.130	0.996	1.128	0.337	0.928	0.966	1.337	2566.592	0.932
AOS-C	1.010	6.987	1.000	0.889	0.547	0.983	2.219	0.441	1117.292	0.989

According to the magnitude of R_L, the isotherm is either irreversible ($R_L = 0$), preferential ($0 < R_L < 1$), linear ($R_L = 1$), or unpalatable ($R_L > 1$).

For Virgin-C, SLES-C, and AOS-C, the MB adsorption procedure performed favorably since the R_L variable fell within the range of 0.003–0.493.

The second adsorption isotherm is the Freundlich model, it is an empirical formula describe in Eq. (9).

$$\ln Q_e = \ln k_f + \frac{1}{n} \ln C_e \tag{9}$$

where the parameter K_f (mg g^{-1}) is associated with the energy of adsorption. The values of correlation coefficients (R^2) produced from the linear plot that was drawn between $\ln Q_e$ and $\ln C_e$ were 0.994, 0.928, and 0.983. The Freundlich equation was less adequate for this adsorption cases than Langmuir equation, as seen in Fig. 12, when evaluating the R_2 values for both isotherm models. Table 8 contains the calculated values for 1/n and K_f. The adsorption intensity or surface heterogeneity was represented by the slope (1/n) data. A successful adsorption process is often considered to be one where the ratio of 1/n falls within the range of 0.1–1.0. The fact that the experiment's index value fell within the permitted region shows that the adsorption process worked effectively. This finding matched that of the Langmuir model.

Equations (10) and (11) illustrate the Temkin isotherm equation.

$$Q_e = \frac{RT}{b} \ln A + \frac{RT}{b} \ln C_e \tag{10}$$

$$B = \frac{RT}{b} \tag{11}$$

where B (J mol^{-1}) is a parameter associated with adsorption's heat, The Temkin isotherm equilibrium binding factor is A (L g^{-1}), and the Temkin isotherm characteristic b (mg L^{-1}). Table 8 displays the derived values for A, B, and b. Figure 12 illustrates the linearization of the isotherm data using the Langmuir formula. Table 8 displays the Langmuir isotherm's variables. The high value of R^2 demonstrated that the parameter estimates were in good agreement with each other. As determined by

Table 9 The dimension equilibrium parameter (R_L) of Langmuir model for adsorption of MB on Virgin-C, SLES-C, and AOS-C

The feasibility of adsorbent adsorption			
	R_L		
	$C_o = 10$ mg L^{-1}	$C_o = 30$ mg L^{-1}	$C_o = 50$ mg L^{-1}
Virgin-C	0.493	0.245	0.163
SLES-C	0.434	0.203	0.133
AOS-C	0.014	0.005	0.003

the fitting of the Langmuir adsorption isothermal equation, the theoretical extreme adsorption capacities of MB on Virgin-C, SLES-C, and AOS-C were up to 3.854, 4.395, and 1.010 mg g^{-1}, respectively.

The same data was also fitted using the Freundlich equation and Temkin equation, as seen in Figure 12. The concerning coefficients, like K_L, Q_{max}, R_L, K_f, n, A, B, and b, can be determined from the three previous isotherms. The calculated data were collected in Table 9.

According to that, the uniform surfactant molecule coverage of the AC surface for Virgin-C, SLES-C, and AOS-C produced homogeneous adsorption sites. Hence, it may be argued that Virgin-C, SLES-C, and AOS-C used the MB adsorption method, which involved both physical and chemical monolayer adsorption.

4   Conclusions

The optimum condition for the cationic dye which was adsorbed from aqueous solution by Virgin-C and Surf-C can be obtainable in Table 10.

It is possible to apply this study and benefit from it practically in textile factories.

Table 10 The optimum condition for the adsorption of MB from aqueous solution by Virgin-C and SLES-C, and AOS-C

Adsorbent	pH	Contact time min	[MB] mg/l	[Surfactant] mole/l
Virgin-C	≥ 8	60	30	
SLES-C	≥ 8	60	30	0.0008
AOS-C	≥ 8	60	30	0.0019

5 Recommendations

To improve efficiency, many factors can be investigated, including the following: studying the effect of temperature, adding inorganic salts to the solution (e.g., NaCl), and trying to make a nano sample.

References

1. Dutta S, Bhattacharjee J (2022) A comparative study between physicochemical and biological methods for effective removal of textile dye from wastewater. In: Development in wastewater treatment research and processes. Elsevier, Amsterdam, pp 1–21. https://doi.org/10.1016/b978-0-323-85657-7.00003-1

2. Alsantali RI, Raja QA, Alzahrani AYA, Sadiq A, Naeem N, Mughal EU, Al-Rooqi MM, El Guesmi N, Moussa Z, Ahmed SA (2022) Miscellaneous azo dyes: a comprehensive review on recent advancements in biological and industrial applications. Dye Pigment 199:110050. https://doi.org/10.1016/j.dyepig.2021.110050

3. Muthu SS, Khadir A, Materials SB (2022) In: Sarwar T, Khan S (eds) Textile wastewater treatment, vol 1, 1st edn. Springer, Singapore

4. Khan I, Saeed K, Zekker I, Zhang B, Hendi AH, Ahmad A, Ahmad S, Zada N, Ahmad H, Shah LA, Shah T, Khan I (2022) Review on methylene blue: its properties, uses, toxicity and photodegradation. Water (Switzerland) 1–30. https://doi.org/10.3390/w14020242

5. Liu X, Chen Z, Du W, Liu P, Zhang L, Shi F (2022) Treatment of wastewater containing methyl orange dye by fluidized three dimensional electrochemical oxidation process integrated with chemical oxidation and adsorption. J Environ Manag 311:114775. https://doi.org/10.1016/j.jenvman.2022.114775

6. Moradihamedani P (2022) Recent advances in dye removal from wastewater by membrane technology: a review. Polym Bull 79:2603–2631. https://doi.org/10.1007/s00289-021-03603-2

7. Ihaddaden S, Aberkane D, Boukerroui A, Robert D (2022) Removal of methylene blue (basic dye) by coagulation-flocculation with biomaterials (bentonite and *Opuntia ficus indica*). J Water Process Eng 49:102952. https://doi.org/10.1016/j.jwpe.2022.102952

8. Tanveer R, Yasar A, Tabinda A ul B, Ikhlaq A, Nissar H, Nizami AS (2022) Comparison of ozonation, Fenton, and photo-Fenton processes for the treatment of textile dye-bath effluents integrated with electrocoagulation. J Water Process Eng 46:102547. https://doi.org/10.1016/j.jwpe.2021.102547

9. Waghchaure RH, Adole VA, Jagdale BS (2022) Photocatalytic degradation of methylene blue, rhodamine B, methyl orange and eriochrome black T dyes by modified ZnO nanocatalysts: a concise review. Inorg Chem Commun 143:109764. https://doi.org/10.1016/j.inoche.2022.109764

10. Azam K, Shezad N, Shafiq I, Akhter P, Akhtar F, Jamil F, Shafique S, Park YK, Hussain M (2022) A review on activated carbon modifications for the treatment of wastewater containing anionic dyes. Chemosphere 306:135566. https://doi.org/10.1016/j.chemosphere.2022.135566

11. Prajapati AK, Mondal MK (2020) Comprehensive kinetic and mass transfer modeling for methylene blue dye adsorption onto CuO nanoparticles loaded on nanoporous activated carbon prepared from waste coconut shell. J Mol Liq 307:112949. https://doi.org/10.1016/j.molliq.2020.112949

12. Behloul H, Ferkous H, Bougdah N, Djellali S, Alam M, Djilani C, Sedik A, Lerari D, Jeon BH, Benguerba Y (2022) New insights on the adsorption of CI-reactive red 141 dye using activated carbon prepared from the $ZnCl_2$-treated waste cotton fibers: statistical physics, DFT, COSMO-RS, and AIM studies. J Mol Liq 364:119956. https://doi.org/10.1016/j.molliq.2022.119956

13. Gohr MS, Abd-Elhamid AI, El-Shanshory AA, Soliman HMA (2022) Adsorption of cationic dyes onto chemically modified activated carbon: kinetics and thermodynamic study. J Mol Liq 346:118227. https://doi.org/10.1016/j.molliq.2021.118227

14. Alardhi SM, Fiyadh SS, Salman AD, Adelikhah M (2023) Prediction of methyl orange dye (MO) adsorption using activated carbon with an artificial neural network optimization modeling. Heliyon 9(1):e12888. https://doi.org/10.1016/j.heliyon.2023.e12888

15. Raji Y, Nadi A, Mechnou I, Saadouni M, Cherkaoui O, Zyade S (2023) High adsorption capacities of crystal violet dye by low-cost activated carbon prepared from Moroccan *Moringa oleifera* wastes: characterization, adsorption and mechanism study. Diam Relat Mater 135:109834. https://doi.org/10.1016/j.diamond.2023.109834

16. Onuzulike CM, Aniagor CO, Modekwe GO, Ejimofor MI, Menkiti MC (2022) Remediation of lead ion contaminated stream using biosurfactant-functionalized mesoporous activated carbon. Chem Afr 1–8. https://doi.org/10.1007/s42250-022-00316-5

17. Asadullah, Kaewsichan L, Techato K, Qaisrani ZN, Chowdhury MS, Yilmaz M (2022) Elimination of selected heavy metals from aqueous solutions using biochar and bentonite composite monolith in a fixed-bed operation. J Environ Chem Eng 10(1):106993. https://doi.org/10.1016/j.jece.2021.106993

18. Deniz F (2021) An economical and effective alternative to commercial activated carbon for treatment of synthetic dye pollution in aquatic environment: surfactant modified waste product of *Zostera marina*. Int J Phytoremediation 23(5):530–538. https://doi.org/10.1080/15226514.2020.1833301

19. Kuang Y, Zhang X, Zhou S (2020) Adsorption of methylene blue in water onto activated carbon by surfactant modification. Water (Switzerland) 12(2):587. https://doi.org/10.3390/w12020587

20. Azmi NM, Mohamed M, Lazim AM, Bakar MBA, Sobri SA, Masri MN, Janvekar AA, Zakaria H (2022) Modification of activated carbon with cationic surfactant for heavy metals removal. In: AIP conference proceedings, vol 2454. American Institute of Physics Inc. https://doi.org/10.1063/5.0078636

21. Goswami R, Dey AK (2022) Use of anionic surfactant-modified activated carbon for efficient adsorptive removal of crystal violet dye. Adsorpt Sci Technol 2022. https://doi.org/10.1155/2022/2357242

22. Mondal S, Majumder SK (2021) Cationic surfactant-aided surface modification of the activated carbon-based materials for the enhancement of phenol adsorption-capacity determined by ultraviolet-visible spectroscopy. J Dispers Sci Technol 1–15. https://doi.org/10.1080/01932691.2021.1884089

23. Patra C, Gupta R, Bedadeep D, Narayanasamy S (2020) Surface treated acid-activated carbon for adsorption of anionic azo dyes from single and binary adsorptive systems: a detail insight. Environ Pollut 266:1–39. https://doi.org/10.1016/j.envpol.2020.115102

24. Zhang LL, Zaoui A, Sekkal W, Zheng YY (2023) Interlayer adsorption of cationic dye on cationic surfactant-modified and unmodified montmorillonite. J Hazard Mater 442:130107. https://doi.org/10.1016/j.jhazmat.2022.130107

25. Karaman C, Karaman O, Show PL, Karimi-Maleh H, Zare N (2022) Congo red dye removal from aqueous environment by cationic surfactant modified-biomass derived carbon: equilibrium, kinetic, and thermodynamic modeling, and forecasting via artificial neural network approach. Chemosphere 290:133346. https://doi.org/10.1016/j.chemosphere.2021.133346

26. Abdolla N, El-Dossoki F, Hamza OK, Gomaa EA (2023) Measurements and modelling of the micellization of alkyl benzyl dimethyl ammonium chloride and cetyl trimethyl ammonium chloride in various aqueous media at 298.15°K. Egypt J Chem. https://doi.org/10.21608/EJCHEM.2023.193054.7589

27. El-Dossoki F, Gomaa E, Hamza O (2019) Solvation thermodynamic parameters for alkyl benzyl dimethyl ammonium chloride and cetyl trimethyl ammonium chloride surfactants in water and alcoholic-water solvents. J Chem Eng Data 64(10):4482–4492. https://doi.org/10.1021/acs.jced.9b00527

28. El-Dossoki FI, Gomaa EA, Hamza OK (2019) Solvation thermodynamic parameters for sodium dodecyl sulfate (SDS) and sodium lauryl ether sulfate (SLES) surfactants in aqueous

and alcoholic-aqueous solvents. SN Appl Sci 1(8):1–17. https://doi.org/10.1007/s42452-019-0974-6

29. Harutyunyan LR, Harutyunyan RS (2019) Effect of amino acids on micellization and micellar parameters of anionic surfactant alpha olefin sulfonate C 14–C 16 in aqueous solutions: surface tension, conductometric, volumetric, and fluorescence studies. J Chem Eng Data 64(2):640–650. https://doi.org/10.1021/acs.jced.8b00886

30. Baird RB, Eaton AD, Rice EW (2017) Standard methods for the examination of water and wastewater, 23rd edn. American Public Health Association, American Water Works Association, Water Environment Federation, Washington, DC

31. Farooq W, Hong H-J, Kim EJ, Yang J-W (2012) Removal of bromate (BrO^{-3}) from water using cationic surfactant-modified powdered activated carbon (SM-PAC). Sep Sci Technol 47(13):1906–1912. https://doi.org/10.1080/01496395.2012.664232

32. Lee W, Yoon S, Choe JK, Lee M, Choi Y (2018) Anionic surfactant modification of activated carbon for enhancing adsorption of ammonium ion from aqueous solution. Sci Total Environ 639:1432–1439. https://doi.org/10.1016/j.scitotenv.2018.05.250

33. Malovanyy A, Sakalova H, Yatchyshyn Y, Plaza E, Malovanyy M (2013) Concentration of ammonium from municipal wastewater using ion exchange process. Desalination 329:93–102. https://doi.org/10.1016/j.desal.2013.09.009

34. Wu SH, Pendleton P (2001) Adsorption of anionic surfactant by activated carbon: effect of surface chemistry, ionic strength, and hydrophobicity. J Colloid Interface Sci 243(2):306–315. https://doi.org/10.1006/jcis.2001.7905

35. Zhang R (2011) Adsorption of dye by modified activated carbon and heavy and heavy metals by rice husk-based activated carbon. Nanjing Agricultural University

36. Wang C (2017) Fabrication of polyacrylonitrile-based activated carbon fibers functionalized sodium dodecyl sulfate for the adsorptive removal of organic dye from aqueous solution. Hunan University

37. Kannan N, Sundaram MM (2001) Kinetics and mechanism of removal of methylene blue by adsorption on various carbons—a comparative study. Dye Pigment 51(1):25–40. https://doi.org/10.1016/S0143-7208(01)00056-0

38. Ibrahim AH, Lyu X, ElDeeb AB (2023) Synthesized zeolite based on Egyptian boiler ash residue and kaolin for the effective removal of heavy metal ions from industrial wastewater. Nanomaterials 13(6):1091–1117. https://doi.org/10.3390/nano13061091

39. Ederer J, Ecorchard P, Slušná MŠ, Tolasz J, Smržová D, Lupínková S, Janoš P (2022) A study of methylene blue dye interaction and adsorption by monolayer graphene oxide. Adsorpt Sci Technol 2022. https://doi.org/10.1155/2022/7385541

40. Amin NK (2008) Removal of reactive dye from aqueous solutions by adsorption onto activated carbons prepared from sugarcane bagasse pith. Desalination 223(1–3):152–161. https://doi.org/10.1016/j.desal.2007.01.203

41. Choi HD, Shin MC, Kim DH, Jeon CS, Baek K (2008) Removal characteristics of reactive black 5 using surfactant-modified activated carbon. Desalination 223(1–3):290–298. https://doi.org/10.1016/j.desal.2007.01.224

42. Plazinski W, Rudzinski W, Plazinska A (2009) Theoretical models of sorption kinetics including a surface reaction mechanism: a review. Adv Colloid Interface Sci 152(1–2):2–13. https://doi.org/10.1016/j.cis.2009.07.009

43. Xiang Y, Gao M, Shen T, Cao G, Zhao B, Guo S (2019) Comparative study of three novel organo-clays modified with imidazolium-based Gemini surfactant on adsorption for bromophenol blue. J Mol Liq 286:1–9. https://doi.org/10.1016/j.molliq.2019.110928

44. Jafari AJ, Kakavandi B, Kalantary RR, Gharibi H, Asadi A, Azari A, Babaei AA, Takdastan A (2016) Application of mesoporous magnetic carbon composite for reactive dyes removal: process optimization using response surface methodology. Korean J Chem Eng 33(10):2878–2890. https://doi.org/10.1007/s11814-016-0155-x

45. Ahmadi M, Foladivanda M, Jaafarzadeh N, Ramezani Z, Ramavandi B, Jorfi S, Kakavandi B (2017) Synthesis of chitosan zero-valent iron nanoparticles-supported for cadmium removal: characterization, optimization and modeling approach. J Water Supply Res. Technol Aqua 66(2):116–130. https://doi.org/10.2166/aqua.2017.027

46. Salam KA (2019) Assessment of surfactant modified activated carbon for improving water quality. J Encapsul Adsorpt Sci 09(01):13–34. https://doi.org/10.4236/jeas.2019.91002
47. Babaei AA, Kakavandi B, Rafiee M, Kalantarhormizi F, Purkaram I, Ahmadi E, Esmaeili S (2017) Comparative treatment of textile wastewater by adsorption, Fenton, UV-Fenton and US-Fenton using magnetic nanoparticles-functionalized carbon (MNPs@C). J Ind Eng Chem 56:163–174. https://doi.org/10.1016/j.jiec.2017.07.009
48. Rezaei Kalantry R, Jonidi Jafari A, Esrafili A, Kakavandi B, Gholizadeh A, Azari A (2016) Optimization and evaluation of reactive dye adsorption on magnetic composite of activated carbon and iron oxide. Desalin Water Treat 57(14):6411–6422. https://doi.org/10.1080/194 43994.2015.1011705
49. Ho YS, McKay G (1999) Pseudo-second order model for sorption processes. Process Biochem 34(5):451–465. https://doi.org/10.1016/S0032-9592(98)00112-5
50. Feng M, You W, Wu Z, Chen Q, Zhan H (2013) Mildly alkaline preparation and methylene blue adsorption capacity of hierarchical flower-like sodium titanate. ACS Appl Mater Interfaces 5(23):12654–12662. https://doi.org/10.1021/am404011k
51. Mahmoud ME, Amira MF, Seleim SM, Mohamed AK (2017) Adsorption isotherm models, kinetics study, and thermodynamic parameters of Ni(II) and Zn(II) removal from water using the LbL technique. J Chem Eng Data 62(2):839–850. https://doi.org/10.1021/acs.jced.6b00865

Textile Wastewater Treatment Using a Modified Coal Fly Ash as a Low-Cost Adsorbent

Ahmed Eteba, Mohamed Bassyouni, Amr Mansi, and Mamdouh Saleh

1 Introduction

Synthetic dyes are commonly used in various industries, such as textiles, paper and tannery, due to their vibrant colors, low manufacturing costs, and durability against environmental factors [1]. However, the excessive use of these dyes has led to the generation of substantial volumes of polluted liquid waste, containing both organic and inorganic compounds [2]. It was estimated that, textile industry consumes almost 3×10^3 m^3 of water per day to produce 20 tons of textiles [3]. These discharges are highly contaminated with hazardous dyes and chemicals that exceed permissible limits, necessitating high-efficiency treatment technologies before discharging into water bodies. To this end, various methods have been investigated for removing dyes from industrial wastewater, such as coagulation, photo-degradation, nanofiltration, photocatalysis, adsorption, and cation-exchange membrane. Nevertheless, these techniques have limitations, including poor efficacy in removing various contaminants, high costs, large reagent requirements, and the production of toxic waste products that require safe disposal [4].

A. Eteba · M. Saleh
Civil Engineering Department, Faculty of Engineering, Port Said University, Port Said 42526, Egypt
e-mail: ahmed.Eteba@eng.psu.edu.eg

M. Bassyouni (✉) · A. Mansi
Chemical Engineering Department, Faculty of Engineering, Port Said University, Port Said 42526, Egypt
e-mail: m.bassyouni@eng.psu.edu.eg

A. Mansi
e-mail: amrmansi24@gmail.com

A. Eteba · M. Bassyouni · A. Mansi
Center of Excellence in Membrane-Based Water Desalination Technology for Testing and Characterization, Port Said University, Port Said 42526, Egypt

Adsorption is considered one of the most versatile methods for removing dyes due to its simplicity, high removal efficiency, minimal secondary pollution, and ability to treat highly concentrated solutions [4, 5]. The most common application of adsorption is for removing colorants from industrial wastewater, using appropriate adsorbents. Adsorption is an effective and desirable alternative to traditional methods for treating industrial wastewater, especially when the adsorbent is readily available, inexpensive, and reusable. Many studies have investigated the use of industrial or agricultural waste materials as adsorbents, and the results have shown that these wastes have varying levels of adsorption capacity [6–8].

In recent years, the disposal of solid wastes has become a major environmental issue [9]. Coal fly ash (CFA) is a by-product of coal combustion that is primarily composed of unburned carbon, iron oxides, and aluminosilicate. It is commonly disposed of in landfills as an industrial solid waste [10]. To address this problem, researchers have explored alternative uses for CFA to ensure proper disposal, management, and utilization. Despite some advantageous properties such as desirable particle size, large specific area, and metal oxy-ide components, CFA can be used as an adsorbent for industrial wastewater treatment [11]. To improve its adsorption characteristics, physical and/or chemical methods can be used to increase its particle surface area, pore volume, and surface morphology. Treated fly ash has been successfully used as an economical adsorbent for the removal of dyes and heavy metals [12–16].

According to a report, fly ash can serve as an inexpensive adsorbent that efficiently removes toxic dyes with 99% effectiveness [4]. However, the required adsorption time of 1 h is longer than that of commercial adsorbents. To address this issue, several studies have been conducted to activate the fly ash using chemical methods that enhance its adsorption capacity and decrease the required contact time. For instance, treating fly ash with an acidic solution was found to increase its surface area from 13 to 58 $m^2 g^{-1}$ [17]. Although previous studies have examined the ability of coal fly ash for dye removal, research on the direct dye adsorption technique onto coal fly ash is still limited. The novelty of this research is to improve the adsorption characteristics of coal fly ash by using a thermos-chemical treatment method to enhance its surface area and morphology and make it a cost-effective adsorbent for textile industrial wastewater treatment.

This research directly contributes to several Sustainable Development Goals (SDGs). It aligns with SDG 6 by improving water quality and sanitation through the removal of pollutants from textile wastewater. Additionally, it supports SDG 9 by promoting innovation and sustainable infrastructure within the textile industry. SDG 12 is addressed by reducing the environmental impact of textile production through responsible consumption and production patterns. Feasible targets and indicators include improving water quality, reducing pollution, and minimizing hazardous waste generation.

2 Materials and Methods

2.1 Preparation of Activated Fly Ash (AFA)

Coal fly ash (CFA) used in this study was taken from a coal-based cement factory in eastern Egypt, which relies on coal as a source of energy in one of the production lines. The fly ash samples were taken into a 500 mL distilled water, the solution was stirred 4 h with speed 250 r.p.m at 25 °C for washing, filtered and left to dry at 120 °C for 24 h using a thermal furnace. In order to activate the raw fly ash, the samples were subjected to a microwave-chemical activation process. Fly ash samples were activated by dipping a 20 g of onto a 300 mL from HCl solution with concentration 30%, then the solution was placed into a domestic microwave (frequency 2.45 GHz and power 600 W) for contact time 5 min. At the end of activation process the mixture was filtrated, washed using a distilled water and left to dry at 110 °C for 12 h (Fig. 1).

The dye applied in the dyeing process was direct blue 78 (DB78), which has a maximum wavelength of 604 nm, a relative molecular mass of 1059.95, and a solubility of up to 10 g/L at 25 °C. This dye was selected due to its common use in the textile industry. The structure of direct blue 78 is depicted in Fig. 2.
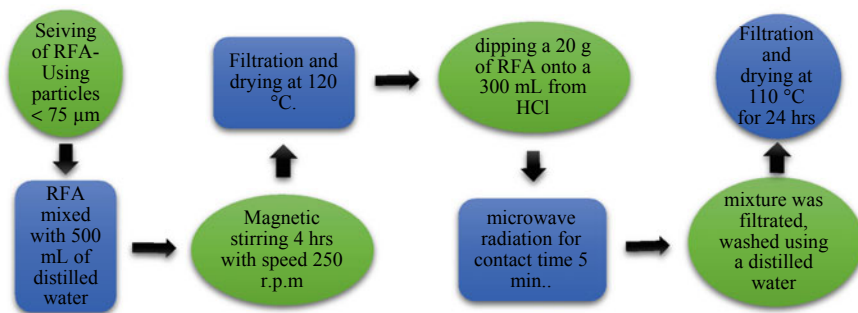
Fig. 1 The preparation process of activated fly ash
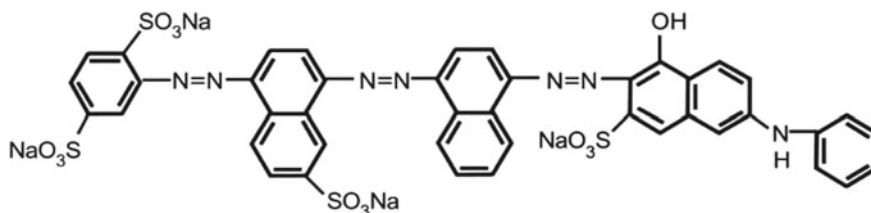
Fig. 2 The chemical structure of DB78 dye
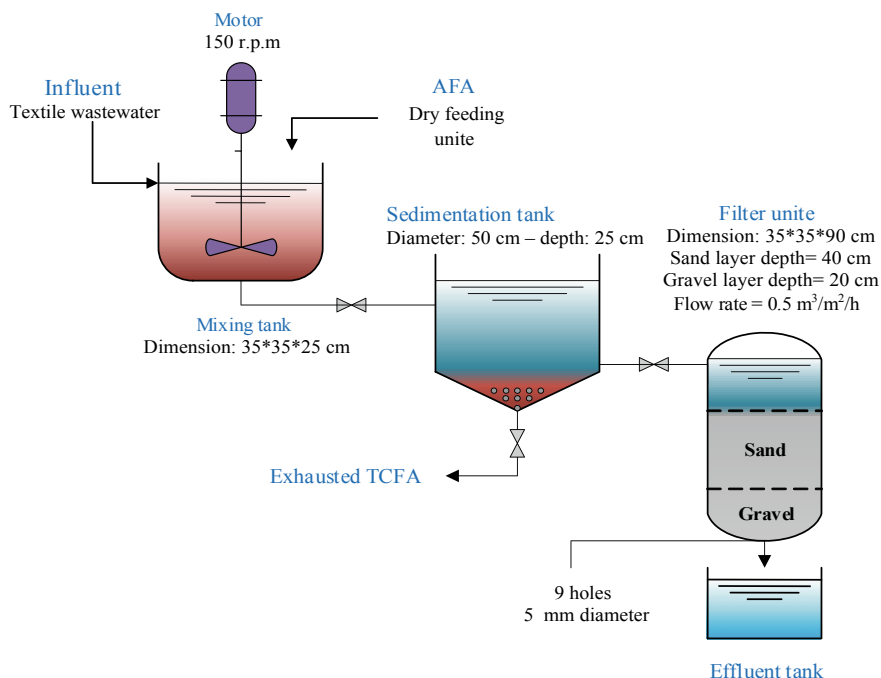
Fig. 3 Pilot plant used for wastewater treatment

2.2 Sources of Wastewater

In order to evaluate the AFA as a low-cost adsorbent and investigate its effect on chemical oxygen demand (COD), total dissolved solids (TDS), and biological oxygen demand (BOD_5), a lab scale pilot plant consists of three stages (mixing, sedimentation and filtration) was designed as shown in Fig. 3. The influent wastewater to the pilot plant was obtained from a wastewater collection sump in a textile factory—investment industrial zone—Port Said government—Egypt.

2.3 Characterization of Materials

The activated fly ash was diluted in water and ultrasonicated for 10 min in an ultrasonic bath at 5% (w/v). Model USC-1400 is one-of-a-kind (40 kHz of ultrasound frequency). The Malvern 3000 Zetasizer NanoZS was used to make the measurements (Malvern Instruments, UK).

Prior to adsorption studies, the samples were degasified at 200 °C for 4 h then the surface area was measured in the presence of N_2 adsorption at $-$ 195.65 °C using surface area analyzers (Autosorb-l-C-8, Quantachrome, USA).

FTIR studies for the used materials were observed using (VERTEX 80v vacuum FTIR Spectrometer, Bruker corporation, Germany).

The surface morphology and porous micro-structure for materials samples were investigated by SEM analysis using (TESCAN MIRA-High Resolution scanning electron microscope, Tescan Essence company, Brno, Czech Republic).

The chemical composition of coal fly ash was determined using XRF analysis (Axios advanced, Sequential WD_XRF Spectrometer, Panalytical 2005, Malvern, UK).

Elemental analysis for samples were performed using field-emission scanning electron microscopy (TESCAN MIRA-High Resolution scanning electron microscope, Tescan Essence company, Brno, Czech Republic) coupled with an energy dispersive X-ray (EDX) (Oxford instrument nano analysis detector, UK).

3 Results and Discussion

3.1 Characterization of Adsorbent

3.1.1 Particle Size Distribution Analysis

To investigate the impact of the activation process, size distribution analysis was conducted on fly ash particles, as shown in Fig. 4. The results showed that all RFA particles fell within a size range of 0.9–2.1 μm with an average size of 1.25 μm, while 13.65% of AFA particles fell within a size range of 0.1–0.3 μm with an average size of 0.25 μm. Moreover, 86.35% of AFA particles fell within a size range of 0.55–1.2 μm with an average size of 0.92 μm. This decrease in particle size was attributed to the erosion of fly ash particle surfaces caused by thermo-chemical treatment during the activation process. It has been reported that using fly ash with a small particle size and high surface area can enhance its adsorption capacity [18].

3.1.2 X-Ray Fluorescence (XRF) Analysis

In order to investigate the chemical composition of RFA, the XRF analysis was conducted and the results showed that, The chemical compositions of RFA are 33.1% lime, 2.35% silica, 0.44% alumina, 0.04% titanium dioxide, 6.73% magnesium oxide, 0.43% hematite, 3.41% sodium oxide, 8.42% potassium oxide, 3.59% phosphorus pentoxide, 2.22% sulfur trioxide, 2.61% chlorine and LOI (36.16%). Trace elements include MnO, NiO, CuO, ZnO, PbO and SrO as shown in Table 1.
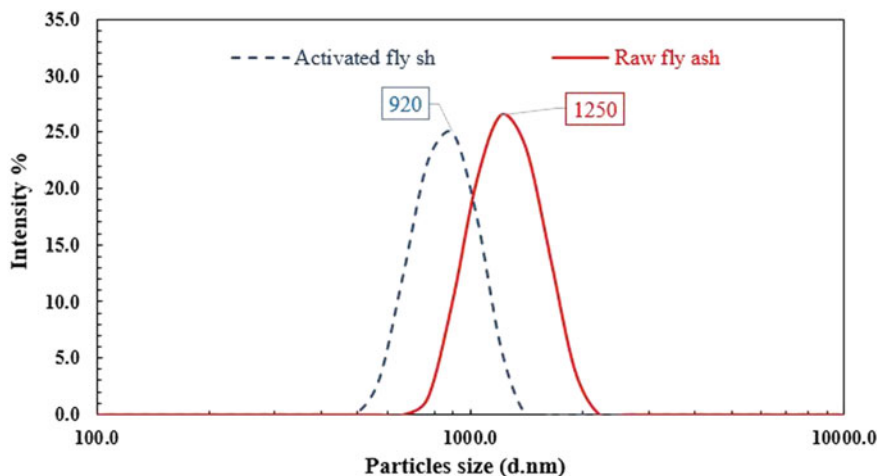
Fig. 4 Particles size distribution analysis

Table 1 XRF analysis results for raw coal fly ash sample

Main constituents	% weight
SiO_2	2.35
TiO_2	0.04
Al_2O_3	0.44
Fe_2O_3	0.43
MgO	6.73
CaO	33.14
Na_2O	3.41
K_2O	8.42
P_2O_5	3.59
SO_3	2.22
Cl	2.61
LOI	36.16

3.1.3 FTIR Analysis

FTIR analysis was conducted on AFA before and after the adsorption process as shown in Fig. 5, to identify the primary peaks of minerals and organics. The FTIR spectrum showed nine main peaks with higher transmittance (%) at various wave numbers (cm^{-1}). The first peak at 445 cm^{-1} indicated the bending of the Si-O-Si bonds, while peaks 2–4 at 565, 605, and 711.6 cm^{-1}, respectively, showed the stretching of the Si-O-Si and Al-O-Si bands. The fifth peak at 871 cm^{-1} indicated the loss of $CaCo_3$, and peaks 6 and 7 at 1024 and 1400 cm^{-1}, respectively, indicated the rise of Si-O-Si bond. Peak 8 at 1639 cm^{-1} indicated the presence of organic matter
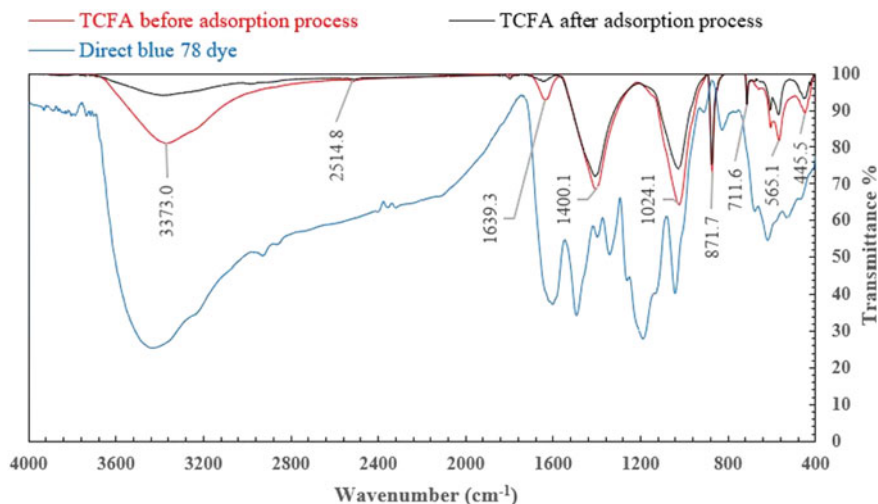
Fig. 5 FTIR analysis for activated fly ash before and after adsorption process

(C=O carboxylate group), and the last peak at 3337 cm^{-1} indicated the strongly hydrogen bond Si-OH group and adsorbed molecules of water H-O-H bonds. The chemical structure analysis showed a difference in the FTIR spectra when comparing AFA with exhausted fly ash, indicating additional bonds resulted due to the accumulation of dye molecules on AFA surface. These results suggested that the adsorption mechanism is chemical adsorption.

3.1.4 Surface Morphology Analysis

SEM analysis was conducted to examine the impact of activation process on RFA surface morphology. Figure 6 shows that raw fly ash particles have aggregated in irregular surfaces with a significant number of macropores and crevices of different sizes. The particles have unique size distribution and distinct shapes. The SEM image in Fig. 6a reveals that RFA particles have a rough surface with a constrained porosity structure. After activation process, the surface of the fly ash changed significantly, with a substantial improvement in the porous structure. The surface changed from being smooth to eroded and rough, and the particles became relatively smaller in size due to chemical degradation in the presence of acidic solution as observed in SEM image Fig. 6b.

3.1.5 XRD Analysis

According to the diffraction curve obtained from X-rays for RFA with a particle size equal to or less than 75 μm, as shown in Fig. 7, it was discovered that the RFA

(a)   (b)
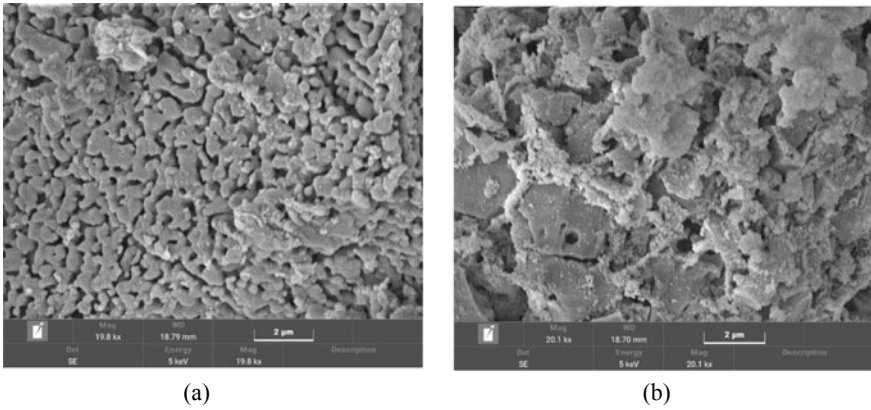
Fig. 6 SEM analysis for **a** RFA and **b** AFA
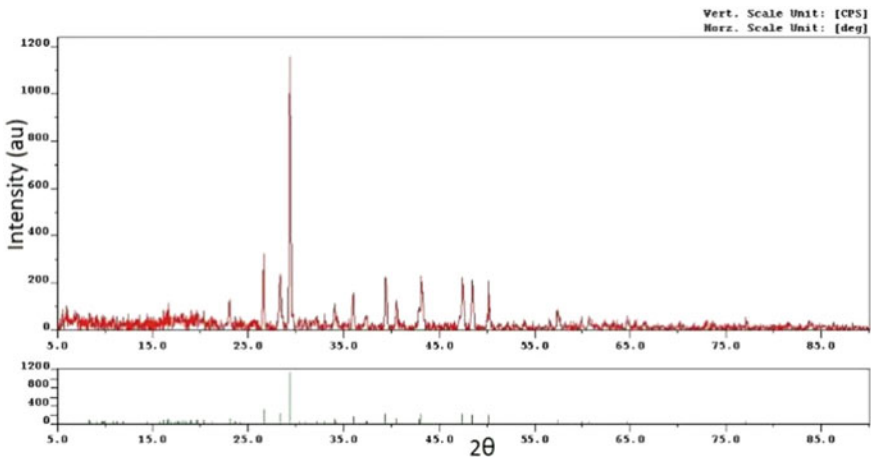
Fig. 7 XRD pattern for RFA

sample comprises a number of distinct crystalline peaks arising from the presence of minerals like quartz, mullite, hematite, and lime, as well as some amorphous phases that result from the formation of a stable glassy surface layer formed by quartz. This layer is characterized by an extremely strong intensity, as well as mullite.

3.2 Textile Wastewater Treatment

The experiments were conducted over a period of 15 days, divided into three separate runs. The first run, lasting for 3 days, involved starting the filter. The second and third

Table 2 Chemical composition of industrial wastewater

Pollutant	Average dye concentration (mg/L)	Average COD values (mg/L)	Average BOD$_5$ values (mg/L)	Average TDS values (mg/L)
Second run analysis	18.85	1312	126	2667
Third run analysis	19.50	1209	160	2306

runs lasted approximately 6 days each, with the first and second weeks analysed separately.

During the treatment process, industrial wastewater was mixed with an optimal dose of AFA until equilibrium conditions were reached. The fly ash particles exhibited high efficiency in removing various adsorbates, including complex dyes and other dissolved solids. The adsorbates were transported from the liquid boundary layer to the surface of the particles, and then into the pores and micropores. This adsorbate movement was achieved due to the driving force created by the concentration difference between the adsorbates in the liquid and on the surface of the particles.

Once adsorption equilibrium was reached, the wastewater was subjected to a sedimentation stage to remove the exhausted AFA particles from the treated wastewater. Finally, the treated wastewater was filtered using a sand filter to remove AFA fine particles with low sedimentation ability and to improve the elimination of other suspended solids. Table 2 shows the chemical composition of industrial wastewater.

3.2.1 Effect of Treatment Process on Dye Removal

Based on the second and third run analyses showed in Fig. 8, it can be concluded that the treatment process using AFA was effective in reducing the concentration of dyes in the industrial wastewater. The achieved removal efficiency for dyes was high, with an average of 89% in the second run and 86.5% in the third run. The AFA dose used in both runs was similar, with an average of 3.0 g/L in the second run and 3.1 g/L in the third run. The influent concentration values for dyes were slightly different between the two runs, with an average value of 19.3 mg/L in the second run and 19.7 mg/L in the third run. Overall, the results suggest that AFA can be used as an effective adsorbent for the removal of dyes from industrial wastewater with maximum capacity 5.73 mg/g.

3.2.2 Effect of Treatment Process on COD Removal

Based on the second and third run analyses, the treatment process demonstrated a significant reduction in COD concentration of the industrial wastewater. The average
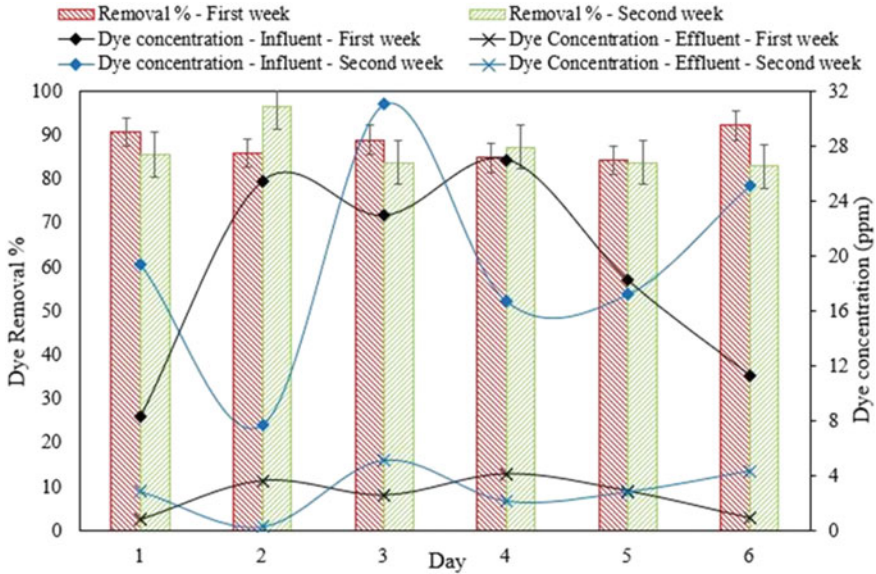
Fig. 8 Effect of treatment process on dyes removal

removal efficiency for COD was found to be 85.4% and 83.3% for the second and third runs, respectively. The influent COD concentrations were found to be in the range of 775–2226 mg/L and 781–1602 mg/L for the second and third runs, respectively. The effluent COD concentrations were significantly reduced and ranged from 82 mg/L to 442 mg/L and 79 mg/L to 291 mg/L for the second and third runs, respectively. The average AFA dose used in both runs was 3.0 g/L and 3.1 g/L, respectively. Figure 9 depicts the effect of the treatment process on the COD concentration values and removal efficiency.

3.2.3 Effect of Treatment Process on TDS Removal

Based on the second and third run analysis, the influent TDS concentration values ranged from 986 to 3660 mg/L, with an average of 2667 mg/L in the second run, and ranged from 1165 to 3045 mg/L, with an average of 2307 mg/L in the third run. The effluent TDS concentration values ranged from 106 to 733 mg/L, with an average of 424 mg/L in the second run, and ranged from 164 to 744 mg/L, with an average of 447 mg/L in the third run. The average achieved removal efficiency for TDS was 85.3% with an average AFA dose of 3.0 g/L in the second run, and 80% with an average AFA dose of 3.1 g/L in the third run. The effect of the treatment process on TDS values and removal efficiency is shown in Fig. 10.

The utilization of AFA can effectively reduce the concentrations of various pollutants such as BOD_5, COD, TDS and color in textile wastewater. The mechanism
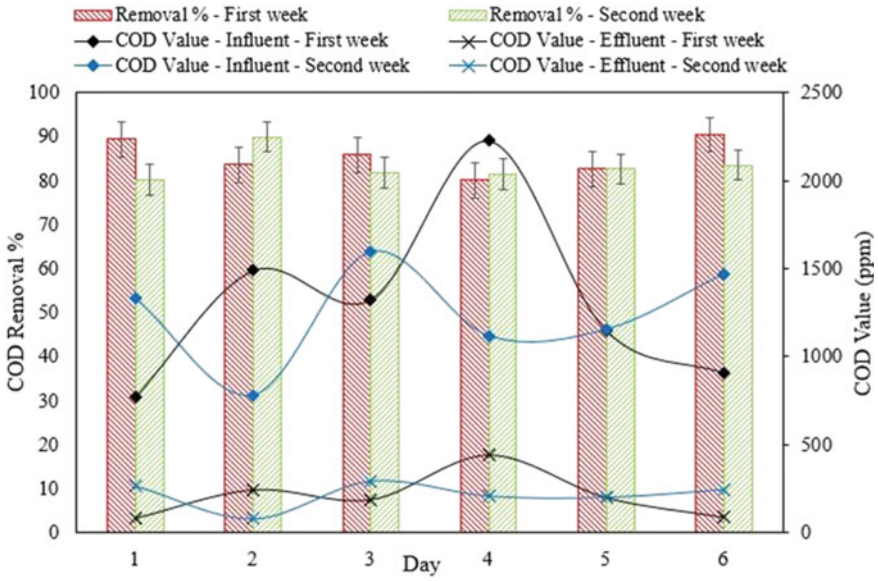
Fig. 9 Effect of treatment process on COD removal
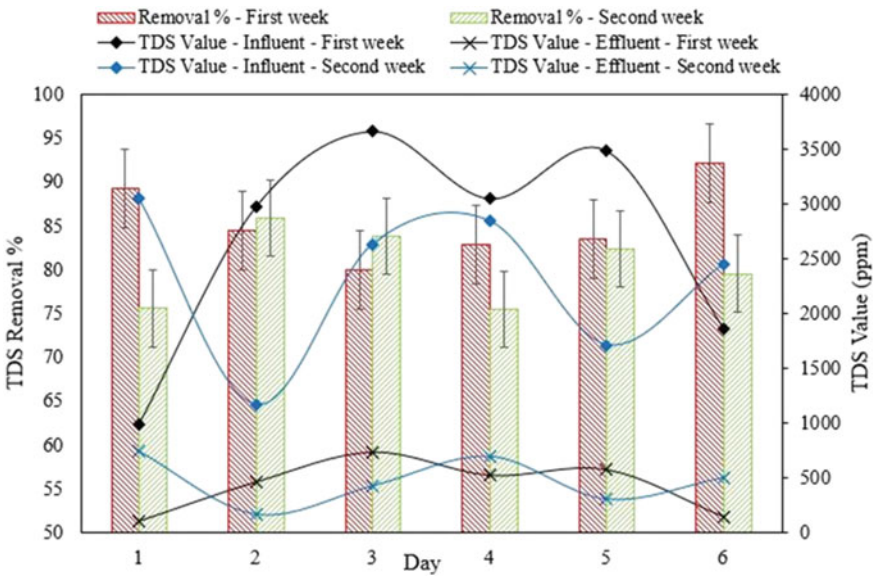
Fig. 10 Effect of treatment process on TDS removal

of pollutants adsorption onto absorbents can be explained by two basic concepts: intrinsic adsorption and coulombic interaction, which are influenced by the electrostatic energy between the adsorbent and adsorbate. The size of adsorbent particles and their specific surface area also affect the adsorption capacity. Increasing the specific surface area of an adsorbent increases its adsorption capacity, and this trend can be expressed as $BOD_5 > COD > TDS$, which can be explained by solubility and diffusion mechanisms [19, 20].

4 Conclusion

The use of AFA as an adsorbent for textile wastewater treatment has shown promising results. The thermos-chemical treatment of RFA significantly enhances its surface morphology and pore structure, thereby increasing its adsorption capacity. The pilot plant model, consisting of three stages (mixing, sedimentation, and filtration), effectively reduces COD, TDS, and dye concentration values from influent wastewater. These results suggest that AFA has great potential as a low-cost adsorbent for the treatment of industrial wastewater. However, further studies are needed to optimize the operating parameters and investigate the feasibility of scaling up the process for commercial use.

5 Recommendation

This study on Textile Wastewater Treatment using a Modified Coal Fly Ash as a Low-Cost Adsorbent has provided valuable insights into the potential of utilizing coal fly ash as an adsorbent for textile wastewater treatment. However, further research and development are recommended to advance this area of study and address certain aspects that remain unexplored. The following recommendations outline the future directions for this research: optimization of modification techniques: Investigate and optimize various modification techniques for coal fly ash to enhance its adsorption capacity, selectivity, and stability towards textile wastewater contaminants. This could involve surface modification methods such as chemical treatments, heat treatments, and activation processes. Comparative studies should be conducted to evaluate the effectiveness of different modification approaches and their impact on the adsorbent's performance. Furthermore, Perform a comprehensive life cycle assessment (LCA) to evaluate the environmental impact of the modified coal fly ash adsorbent compared to conventional treatment methods. Additionally, conduct an economic analysis to determine the cost-effectiveness of implementing the adsorbent in textile wastewater treatment plants. Consider factors such as adsorbent production costs, adsorption capacity, operational expenses, and potential revenue from recovered pollutants.

References

1. Leng Q, Wu X, Xu S, Wang S, Jin D, Wang P, Dong F, Wu D (2022) Numerical simulation of dyeing wastewater treated by a multi-stage reverse electrodialysis reactor series system. Energy Environ. 0958305X221112909
2. Pathak AK, Tyagi VV, Anand S, Kothari R (2022) Experimental investigation of designed solar parabolic concentrator based desalination system for textile industry wastewater treatment. Energy Environ 33(5):870–896
3. Bassyouni M, Zoromba MS, Abdel-Aziz MH, Mosly I (2022) Extraction of nanocellulose for eco-friendly biocomposite adsorbent for wastewater treatment. Polymers 14(9):1852
4. Eteba A, Bassyouni M, Saleh M (2022) Modified coal fly ash for textile dye removal from industrial wastewater. Energy Environ. 0958305X221130536
5. Abdel-Aziz MH, El-Ashtoukhy EZ, Bassyouni M, Al-Hossainy AF, Fawzy EM, Abdel-Hamid SM, Zoromba MS (2021) DFT and experimental study on adsorption of dyes on activated carbon prepared from apple leaves. Carbon Lett 31:863–878
6. Sardar M, Manna M, Maharana M, Sen S (2021) Remediation of dyes from industrial wastewater using low-cost adsorbents. Green adsorbents to remove metals, dyes and boron from polluted water, pp 377–403
7. Ibrahim AH, Lyu X, ElDeeb AB (2023) Synthesized zeolite based on Egyptian boiler ash residue and kaolin for the effective removal of heavy metal ions from industrial wastewater. Nanomaterials 13(6):1091
8. Zoromba MS, Ismail MI, Bassyouni M, Abdel-Aziz MH, Salah N, Alshahrie A, Memic A (2017) Fabrication and characterization of poly (aniline-co-o-anthranilic acid)/magnetite nanocomposites and their application in wastewater treatment. Colloids Surf A: Physicochem Eng Asp 520:121–130
9. Darmayanti L, Kadja GT, Notodarmojo S, Damanhuri E, Mukti RR (2019) Structural alteration within fly ash-based geopolymers governing the adsorption of Cu^{2+} from aqueous environment: effect of alkali activation. J Hazard Mater 377:305–314
10. Qi L, Teng F, Deng X, Zhang Y, Zhong X (2019) Experimental study on adsorption of Hg (II) with microwave-assisted alkali-modified fly ash. Powder Technol 351:153–158
11. Ramanathan S, Gopinath SC, Arshad MM, Poopalan P (2020) Nanostructured aluminosilicate from fly ash: potential approach in waste utilization for industrial and medical applications. J Clean Prod 253:119923
12. Zhang L, Zhao Y, Mu C, Zhang X (2020) Selective adsorption for Ag (I) from wastewater by carbon-magnetic fly ash beads modified with polydopamine and thiourea. Sustain Chem Pharm 17:100287
13. Visa M (2016) Synthesis and characterization of new zeolite materials obtained from fly ash for heavy metals removal in advanced wastewater treatment. Powder Technol 294:338–347
14. Visa M, Chelaru AM (2014) Hydrothermally modified fly ash for heavy metals and dyes removal in advanced wastewater treatment. Appl Surf Sci 303:14–22
15. Nowak B, Aschenbrenner P, Winter F (2013) Heavy metal removal from sewage sludge ash and municipal solid waste fly ash—a comparison. Fuel Process Technol 105:195–201
16. Salam OEA, Reiad NA, ElShafei MM (2011) A study of the removal characteristics of heavy metals from wastewater by low-cost adsorbents. J Adv Res 2(4):297–303

17. Abdel-Aziz MH, Bassyouni M, Soliman MF, Gutub SA, Magram SF (2017) Removal of heavy metals from wastewater using thermally treated sewage sludge adsorbent without chemical activation. J Mater Environ Sci 8(5):1737–1747
18. Ahmaruzzaman M (2008) Adsorption of phenolic compounds on low-cost adsorbents: a review. Adv Colloid Interface Sci 143(1–2):48–67
19. Eteba A, Bassyouni M, Saleh M (2022) Utilization of chemically modified coal fly ash as cost-effective adsorbent for removal of hazardous organic wastes. Int J Environ Sci Technol 1–14
20. Igwe JC, Onyegbado CO, Abia AA (2010) Adsorption isotherm studies of BOD, TSS and colour reduction from palm oil mill effluent (POME) using boiler fly ash. Eclética Química 35:195–208

Contrasting the Water Consumption Estimation Methods: Case of USA and South Africa

E. A. Feukeu and L. W. Snyman

1   Introduction

Water is an essential component of any living being on earth and more than 65% of the human being is made of water. Water is incredibly important and vital for the human body. However, despite its influential importance to the wellbeing of the human being, because of its presence in many parts of the world, its preservation, storage, and management has been very well neglected in the past until the apparition of a fast desertification compounded with the global climate change pattern. This change of the climatic characteristics resulted in an unbalanced global water demand and supply system. These signals alerted the world on the essence of this vital, precious liquid (water). Thereafter, several worldwide actions and strategies have been setup to promote any action contributing to the preservation, maintenance, and protection of the planetarium eco-system. Based on the current statistics, the global water demand is expected to increase to 40% by 2030. Furthermore, under the "business-as-usual" approach, more water demand pressure is still ahead because the world's population is predicted to reach 9.1 billion people by 2050 [1] from the current eight billion [2]. In view to contribute to the conservation of the water in the world, most action and activities related to the water daily usage guided by the water reticulation infrastructure must be well planned prior distribution to the water reticulation network. However, beside the technological and scientific advancement, a standardized and harmonised accurate estimation technique and prediction model

E. A. Feukeu (✉)
Department of Electrical Engineering, CSET, University of South Africa, Florida Campus, Pretoria, South Africa
e-mail: feukeu@gmail.com

L. W. Snyman
Institute for Nanotechnology and Water Sustainability, CSET, University of South Africa, Florida Campus, Pretoria, South Africa
e-mail: snymalw@unisa.ac.za

is still a challenge nowadays. Most classical models in use till today for peak water demand calculation is some sort of improvement of the probabilistic model proposed by Hunter [3]. Water demand estimation is particularly important because it helps the water supply company to well plan future water demand forecast while maintaining lower operating cost. It was proved by Ghiassi et al. [4, 5] that good water demand estimation associated with optimal operation planning can result in a substantial saving amounting to a value of 25–30% of operating cost saving due to the reduction of the consumed electricity and the treatment inputs. Not only does good water estimation contribute to direct money saving, but it also helps reduce related water losses and thereby addressing the 6th Sustainable development goal of the United Nations 2030 agenda [1]. In general, an accurate water estimation method is a bit challenging because, numerous factors are involved in the calculation. Some most key factors include: the water pressure in the network, the losses in the system, the climatic conditions (temperature), the relative humidity and the precipitation, the size of the population, the price structure (residential, commercial, industrial, and public), the household income, size, and outdoor space [6–8].

In the field of on-demand water estimation, forecast and prediction, numerous works have already been published in the literature. A special case of Feed Forward architecture (FFNN) was improved to develop a Dynamic Artificial Neural Network (DAN2) in [4]. The DAN2 was thereafter used to predict daily, weekly, and monthly water demand forecast, and the result demonstrated the effectiveness and accuracy of the DAN2 in comparison to other methods such as Auto Regressive Integrated Moving Average (ARIMA) and ANN. It was also proved that an excellent adjustment can be achieved even when only the water demand data are employed. This method proved to be efficient in performing water demand estimation for all time horizons. In [9], two types of Fuzzy Inference System (FIS): a Mandami Fuzzy Inference System (MFIS) and an Adaptive Neuro-fuzzy Inference System (ANFIS) were used to predict the time series of urban water demand. To evaluate the best forecast method, the performance of the two methods (ANFIS and MFIS) were analysed in the training and test stage of the water demand. All levels of threshold statistics employed in the study demonstrated the higher accuracy of the M5-ANFIS model over the M5-MFIS model. The M5 model comprises a Fuzzy Inference System with five-month lags. Therefore, the results showed that the M5-ANFIS method is superior to the M5-MFIS method for forecasting monthly demand series and can be applied successfully for predicting water consumption. Authors in [10] described and compared various methods for predicting water demand in a city in the south of Spain. The methods used were Support Vector Regression (SVR), FFNN employing the Error Back propagation learning method, Projection Pursuit Regression (PPR), Multivariate Adaptive Regression Splines (MARS), and Random Forest (RF). In addition to these methods, researchers proposed a simple method based on the demand profile, using weighted results from exploratory data analysis (WPatt). The results obtained identified the SVR as the most accurate method, followed closely by the MARS, PPR and RF methods. In [11], a short-term water demand forecasting method based on the Markov Chain (MC) statistical concept was proposed. The proposal used two methods, one based on Homogeneous Markov Chains (HMC) and one based on

Non-Homogeneous Markov Chains (NHMC). These methods were applied to three District Metered Areas (DMA) located in Yorkshire (UK), in order to predict water demands from 1 to 24 h later. Subsequently, the results were compared with the predictions of the two methods used as benchmarks (ANN, Naive Bayes). The results show that the HMC method provides more accurate short-term predictions than NHMC. Both methods provide probabilistic information on stochastic demand forecasting with reduced computational effort, as compared with most existing methods. Although most related works were conducted under a prescribed single standard or guidelines, there is still a considerable variance in term of achieving results especially while dealing with different standards.

In an attempt to demonstrate the disparity which may exist in different model and standards, the work presented in this study contrast and analyse the inconsistency of the available water estimation methods presented in literature. Two applicable methods from two standards (USA and South Africa) are investigated in the study and compared to the recommended South African (SA) standard. The result exploration demonstrated that if the methods are used interchangeably, unreliable, and significant inaccurate result will occur over a long run.

The remainder of this work is organized as follows; the methods exploration is presented in Sect. 2. The result discussion is presented in Sect. 3 and finally the conclusion in Sect. 4.

2 Methods Exploration

In order to explore the two selected methods used in the two countries, some preliminary information related to the user's daily water utilisation is required. Based on the user's information gathered and consolidated from various sources [12, 13], a list of a 3 user's daily activities requiring water as a main entrant are recapitulated in Table 1. This table summarises some activities performed by everyone several time in a week to keep its basis hygienic state in order. In all figures and tables, GPM stand for Gallon per Minute while LPM stands for litre per minute.

Making use of the information available from Table 1, considering the case where the shower, dishwasher and the laundry only work for a period of 1 h. The water consumption for each fixture is evaluated for the period of 1 h. Then total water flow rate for a period of 1 min was computed as

$$\text{FR}_{\text{emp}} = \frac{\left(\sum_{i=1}^{N} Li \right)}{60} \qquad (1)$$

where Li is the individual fixture water consumption over a period of 1 h and FR_{emp} is the empirical water flow rate computation.

After this step, an analytical flow rate calculation was evaluated using the Bernoulli equation. Since a Flow Rate (FR) describes how many cubic meters (in case of

Table 1 Daily water activities

Bathroom water use
How many showers per day on average does each member of your household take? What is the average length *(in minutes)* of each shower? *(10 min is average) 2-min shower = 20 l*
Washing dishes
Do you wash your dishes by hand? If yes, how many times and for how long do you wash your dishes every day? Do you use a dishes washer to wash your dishes? If yes, for how long do you use a dishwasher every day? In general, 25 L of water are used per load of the dishwasher
Laundry water use
Do you wash your laundry by hand? If yes, how many times and for how long do you wash your laundry every day? Do you use a laundry washing machine to wash your laundry? If yes, for how long do you wash your laundry every day? In general, a new top loader washing machine use 50 L of water per load while the old one take 100 L of water per load

volumetric FR) or how many kilograms (in case of the mass FR) flow through one point of the pipe at a given time, since the FR is directly related to the pipe cross sectional size, for conformity [14], the pipe size of 15 mm was selected for this study.

$$FR = 3600\pi v \left(\frac{d}{2}\right)^2 \tag{2}$$

where v is the water velocity (m/s), d the pipe inner diameter (m) and FR the water Flow Rate (m³/h).

The South Africa (SA) water reticulation standard suggested the water velocity of 0.6, 1 and 1.5 m/s for the minimum, recommended and maximum water velocity in a SA reticulation system [15].

To conclude the investigation, the Exhaustive Enumeration Method (EEM) for automatic Water Demand Calculator (WDC) proposed by the USA's special task group of the International Association of Plumbing and Mechanical Officials (IAPMO) was also employed to evaluate the water FR (Fig. 1).

The proposed WDC derivation builds upon the work performed by Hunter [3] and Wistort method [16] to propose a Zero-Truncated Binomial Distribution (ZTBD) which describe the conditional probability distribution of busy fixtures in any building, including single family homes. The IAPMO method makes use of the recommended probability fixture as well as the fixture FR depicted in Table 2 on its derivation.

Based on the water reticulation fixture of concern (dishwasher, shower, and laundry), the water FR was evaluated using the proposed EEM model of WDC developed by the IAPMO [17]. The WDC was downloaded and modified in line with our scenario.
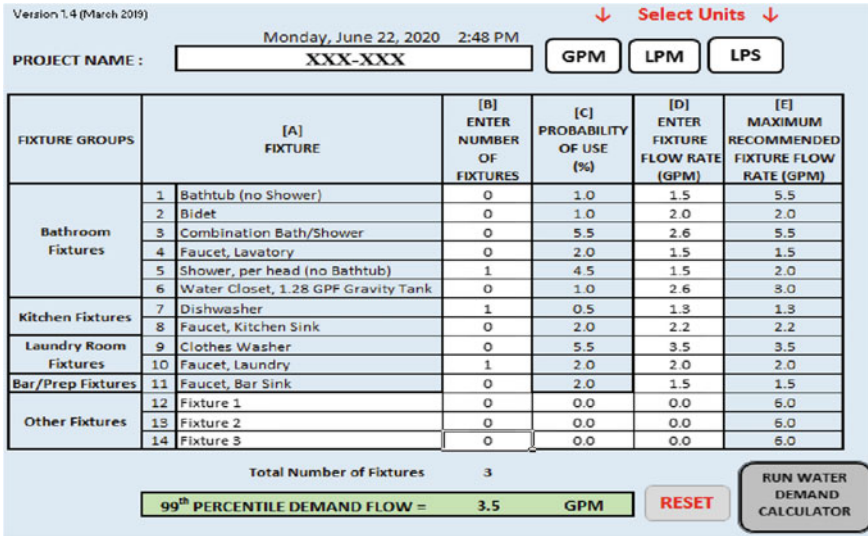
Fig. 1 Water demand calculator (WDC) [17]

Table 2 Recommended probability of fixture

Fixtures	Design P value (%)	Maximum recommended design flow rate (GPM)
Bar sink	2.0	1.5
Bathtub	1.0	5.5
Bidet	2.0	1.5
Clothes washer	1.0	5.5
Combination bath/shower	2.0	1.5
Dishwasher	1.0	5.5
Kitchen faucet	2.0	1.5
Laundry faucet	1.0	5.5
Lavatory faucet	2.0	1.5
Shower, per head	1.0	5.5
Water closet, 1.28 GPF gravity tank	2.0	1.5

3 Result and Discussion

After running the WDC, the result in term GPM is depicted in Fig. 2; the total water consumed over a period of 10 h using the two prescribed methods and concept was computed and presented in Fig. 2.

This figure is made of three graphs named Empirical (Emp), Analytical (Ana) and Water Demand Calculator (WDC) representing the consumed water volume using
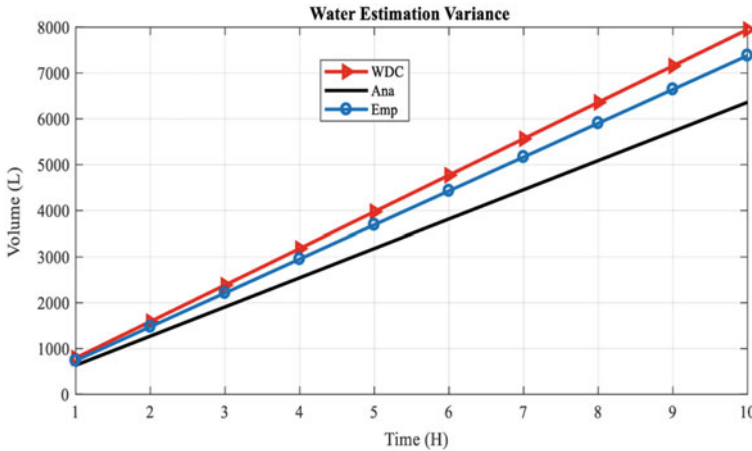
Fig. 2 SA versus USA method comparison

Eqs. 1 and 2 and the IAPMO WDC, respectively. It is to note that the Analytic (Ana) was computed using the recommended SA standard velocity value of 1 m/ s as suggested in [14]. Looking at this figure, it can be observed that at the first running hour, the difference between the three different curves is not really perceptible. However, as the running time increase, it becomes obvious that a considerable discrepancy exists between the three graphs. This deviation in value just over 10 h of utilisation demonstrates the incoherence and the complexity faced by the any person or entity who is trying to theoretically estimate the customer water consumption and prediction. To further clarify and evaluate this calculation discrepancy, Table 3 was populated with the corresponding values. In this table, it can be noticed that although the difference in terms of FR calculation is less than 3% in all cases at the first minute, if evaluated over long run hours, a very important deviation can be observed especially in terms of consumed water volume where a difference of up to 1800 L is clearly perceptible. If after only 10 h of operation this type of discrepancy can be observed, what about 24 h, a month, and a year of operation! It became obvious and evident that continuing using mixture of methods for future water provision is really misleading and prone of significant inaccuracy and errors. The main problem here is that beside all underline theories used to perform the water estimation, there isn't any realistic mean or criteria which can allow one to certainly confirm the accuracy of any of these three methods without proper physical direct measurement of the consumed water with a calibrated system. This result also raises the concern of the water reticulation standard conversion between the South Africa (SA) and the USA. In the USA, the correct prediction will be that achieved with the WDC (WDC) while in SA the correct prediction will be the recommended (Ana). The lesson here is that none of the method is false because they are all based on solid fundamental water measurement theory. But the problem only arises when instead of performing all measurements using the same concept or methods, a variety of methods are used

Table 3 Comparative discrepancy

	Volume (L) after 10 h	Flow rate (LPM)	Discrepancy against Ana (%)
WDC	43,721	13.248	**24.96**
Emp	40,590	12.3	**16**
Ana	34,989	10.6	**0**

Bold indicates the comparative results of the two methods

interchangeably. It is obvious that this type of problem is not only perceptible in water environment. However, in other engineering field, there is a standardisation and harmonisation which helps minimise the error when a variety of methods are used to estimate a certain quantity of product, material, or resources. But in water FR estimation environment, consistency is a key for a successful prediction. The same method needs to be used throughout in order to expect reliable result.

4 Conclusion

This work demonstrates the complexity and the challenge faced by the Water Supply Company, entity or individual during estimation and prediction of a possible water provision. The work makes use of the available data and information to estimate the total water consumed by a group of three fixtures using SA and USA standard. All methods, calculation and derived results were based on well-known water estimation concepts and theories. However, the result obtained after a long simulation period of 10 h proved that as the running time increases, the discrepancy between the obtained results also increases considerably. As a result of this effect, it was suggested to stick to one method throughout and use it consistently in order to expect reliable end-result. The study also demonstrates that if different standards originated from different countries are used interchangeably, a high probability of error and misleading results can be obtained in the absence of the un-calibrated water measurement device.

Future work will consider investigating and developing a conversion curve or coefficients to enable any user to work in both standards interchangeably.

References

1. WWAP (United Nations World Water Assessment Programme) (2023) The United Nations World Water Development Report 2015: Water for a Sustainable World. UNESCO, Paris. [Online]. Available at: https://sdgs.un.org/2030agenda. Accessed 3 July 2023
2. United Nations Population Division (2019) World population prospects: the 2019 revision. [Online]. Available at: https://www.worldometers.info/world-population/. Accessed 3 July 2023
3. Hunter RB (1940) BMS65 methods of estimating loads on plumbing systems. US NBS, Washington, DC
4. Ghiassi DK, Zimbra, Saidane H (2008) Urban water demand forecasting with a dynamic artificial neural network model. J Water Resour Plan Manag 134(2):138–146. https://doi.org/10.1061/(ASCE)0733-9496(2008)134:2(138)
5. Odan FK, Reis LFR (2012) Hybrid water demand forecasting model associating artificial neural network with Fourier series. J Water Resour Plan Manag 138:245–256. https://doi.org/10.1061/(ASCE)WR.1943-5452.000017
6. Schleich J, Hillenbrand T (2009) Determinants of residential water demand in Germany. Ecol Econ 68:1756–1769. https://doi.org/10.1016/j.ecolecon.2008.11.012
7. Nauges C, Whittington D (2010) Estimation of water demand in developing countries: an overview. The World Bank Research Observer 25(2):263–294
8. De Maria André D, Carvalho JR (2014) Spatial determinants of urban residential water demand in Fortaleza. Brazil, Water Resources Management 28:2401–2414. https://doi.org/10.1007/s11269-014-0551-0
9. First M, Turan ME, Yurdusev MA (2009) A Comparative analysis of fuzzy inference systems for water consumption time series prediction. J Hydrol 374:235–241. https://doi.org/10.1016/j.jhydrol.2009.06.013
10. Herrera M, Torgo L, Izquierdo J, Pérez-García R (2010) Predictive models for forecasting hourly urban water demand. J Hydrol 387:141–150. https://doi.org/10.1016/j.jhydrol.2010.04.005
11. Gagliardi F, Alvisi S, Kapelan Z, Franchini M (2017) A probabilistic short-term water demand forecasting model based on the Markov Chain. Water 9:507. https://doi.org/10.3390/w9070507
12. City of Cape Town/Thinkwater, Calculate Your Daily Use. [Online]. Available at: http://coct.co/thinkwater/calculator.html. Accessed 17 July 2023
13. MrFIXIT. Water usage calculator. [Online]. Available at: https://www.mrfixitbali.com/water/water-usage-bills-and-charges/water-usage-calculator.html. Accessed 3 July 2023
14. SANS10252-1, SANS10400-W, SANS10252-2, SANS102400-P. Water reticulation and drainage in buildings 2001. [Online]. Available at: http://www.msunduzi.gov.za/site/search/downloadencode/SANS_10252_Water_Reticulation.pdf. Accessed 3 July 2023
15. King T (2015) Design Guidelines and Minimum Standards for Civil Engineering Services: Revision no: 0. Development Services and Project Management Engineering Services Directorate, Stellenbosch Municipality
16. Wistort RA (1994) A new look at determining water demands in building: ASPE direct analytic method. In: Technical proceedings. American Society of Plumbing Engineers convention. ASPE, Kansas City, MO, pp 17–34
17. Buchberger S, Omaghomib T, Wolfec T, Hewittd J, Colee D (2023) Peak water demand study: probability estimates for efficient fixtures in single and multi-family residential buildings. [Online]. Available at: https://www.iapmo.org/media/3857/peak-water-demand-study-executive-summary.pdf. Accessed 3 July 2023

Climate Action

Sustainability Research at Port Said University Towards the Achievement of the Sustainable Development Goals

Mohamed M. Elsakka, Mohamed Bassyouni, Rawya Y. Rizk, and Ayman M. I. Mohamed

1 Introduction

Port Said University (PSU) pays great attention to research aimed at fulfilling Sustainable Development Goals (SDGs). The SDGs represent a set of 17 global goals that have been adopted by the United Nations since 2015. These goals aim to protect the planet and end poverty in addition to ensuring prosperity for all. Figure 1 illustrates the 17 sustainability goals of the United Nations, also known as SDGs. Figure 2 presents an illustration of the University's contributions towards the SDGs. However, this paper shed more light on the research aspects of the PSU contributions towards the achievements of the SDGs. Although the SDGs appear to be distinguishable, the majority of the SDGs have a significant and strong correlation with the other SDGs [1]. For example, SDG 1: Poverty elimination and SDG 3: Good health and well-being (SDG 3) show synergetic relationships with the majority of the other goals. Also, SDG 7: Affordable and clean energy provides strong support to some other SDGs, particularly, SDG 1: No poverty, SDG 2: Zero hunger, SDG 3: Good health and

M. M. Elsakka (✉) · A. M. I. Mohamed
Mechanical Power Engineering Department, Faculty of Engineering, Port Said University, Port Said, Egypt
e-mail: elsakka@eng.psu.edu.eg

M. Bassyouni
Department of Chemical Engineering, Faculty of Engineering, Port Said University, Port Said, Egypt

Center of Excellence in Membrane-Based Water Desalination Technology for Testing and Characterization, Port Said University, Port Said, Egypt

M. Bassyouni
e-mail: m.bassyouni@eng.psu.edu.eg

R. Y. Rizk
Electrical Engineering Department, Faculty of Engineering, Port Said University, Port Said, Egypt
e-mail: r.rizk@eng.psu.edu.eg

well-being, SDG 8: Decent work and economic growth, and SDG 13: Climate action [1]. Although sustainability action has been active since the United Nations (UN) Sustainable Development Goals were announced in 2015, the COVID-19 pandemic has been found to threaten the global commitment to 2030 sustainable development [2]. SciVal [3] is an evaluation tool provided by Elsevier that assists in visualizing the organization's research performance and benchmarking it relative to peers in addition to identifying and analyzing emerging research trends. SciVal can also be used to provide data-driven insights to evaluate research and monitor research progress. In this paper, the SciVal database is utilized to assess the sustainability research at PSU toward the Achievement of Sustainable Development Goals. Figure 3 presents a comparison between the worldwide research contribution to sustainable development and the specific contributions from the PSU based on SciVal database [3]. It is observed that PSU has produced impactful world-leading research outputs in the fields of SDG 6: Clean water and sanitation, SDG 7: Affordable and Clean Energy, and SDG 14: Life below water. Figure 4 illustrates the number of research papers and the Field-Weighted Citation Impact for PSU publications for each SDG. It is depicted that SDG 3: Good Health and Well-being acquires the highest number of publications. However, the research output in SDG 5: Gender equality and SDG 13: Climate action has the highest citation impact.

Port Said University acknowledges that scientific research has played a crucial role in accomplishing these SDGs through the development of knowledge and solutions that would influence real-life practices and policies. This paper provides a deeper insight into the recent research progress at PSU towards the fulfillment of the emerging SDGs while highlighting some of its key achievements and initiatives.

2   Sustainable Development Goals in Port Said University

Achieving the Sustainable Development Goals (SDGs) is a complex and multi-faceted task. Leaders, researchers, instructors, students, and employees at PSU have worked together toward achieving the SDGs. Strategies that PSU has employed towards the SDGs included:

1. Integration of SDGs into PSU policies: the SDGs were integrated into PSU's policies, including strategic plans, academic programs, and research agendas leading to create a culture of sustainability throughout the institution.
2. Collaborative research: PSU engaged in collaborative research with other local and international institutions, and organizations to address the challenges posed by the SDGs. This collaboration included research on sustainable development, climate change, clean water, and other related topics.
3. Community engagement: PSU has engaged with its local communities to promote sustainable development. It involved working with community organizations, local governments, and businesses to address local sustainability challenges.

Fig. 1 An illustration of the 17 sustainability goals of the United Nations

4. Curriculum development: PSU has developed curricula in several programs that focus on sustainability and the SDGs including courses in environmental engineering, sustainable development, and social entrepreneurship.
5. Sustainable campus practices: PSU has implemented sustainable practices on its campuses, such as reducing energy and water consumption, promoting recycling and waste reduction, and promoting sustainable transportation options.
6. Capacity building: PSU has engaged in capacity-building activities to help communities build the skills and knowledge needed to achieve sustainable development. This strategy includes training programs, workshops, and other educational activities.

One key strategy is to integrate the SDGs into institutional policies. This can involve developing a sustainability plan that outlines specific targets and goals for the institution to work towards. For example, PSU has developed a Sustainability Strategy that sets out specific targets for reducing carbon emissions, increasing energy efficiency, and low-cost production of desalinated water.

In addition to developing a sustainability plan, PSU has also incorporated the SDGs into its academic programs and research agendas. This can involve developing

Fig. 2 University contributions towards the SDGs
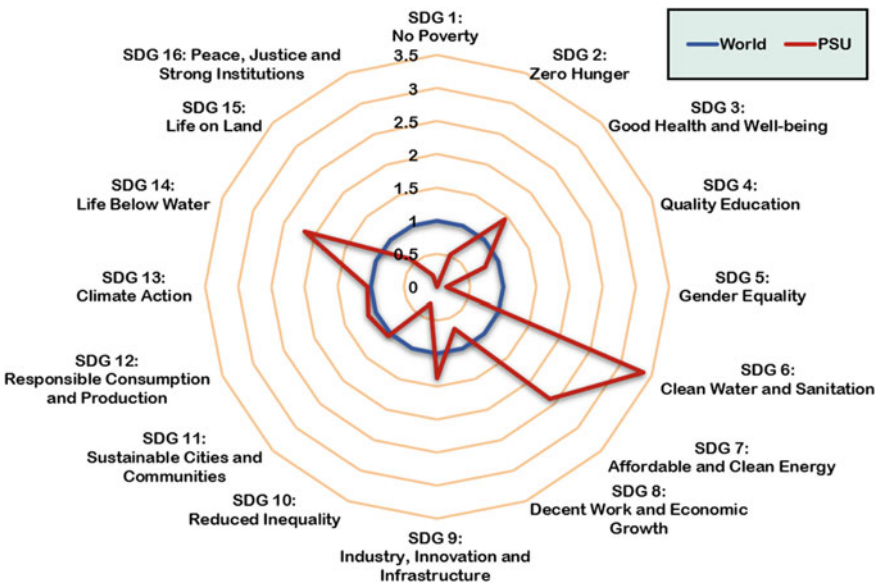
Fig. 3 A comparison between the worldwide research contribution to sustainable development and the specific contributions from the Port Said University based on SciVal database [3]
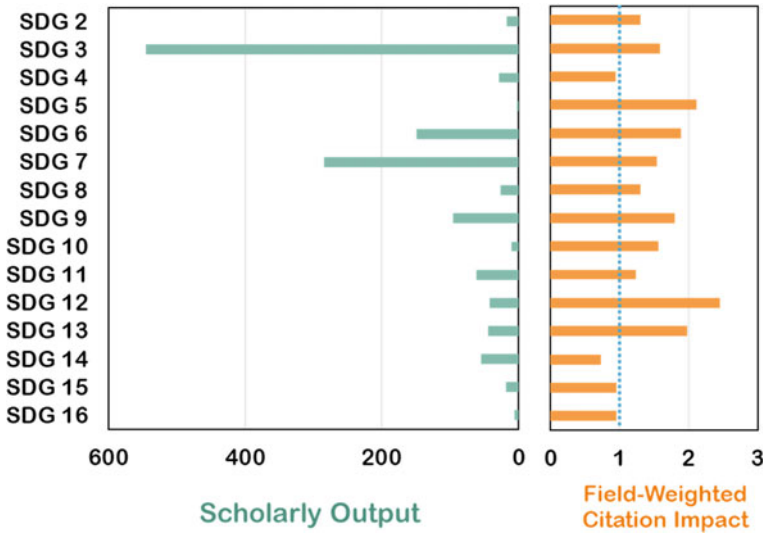
Fig. 4 An illustration of the number of research papers and the field-weighted citation impact for Port Said University publications for each SDG based on SciVal database [3]

new courses and programs that focus on sustainability and the SDGs, as well as conducting research on topics related to sustainable development. For example, the Faculty of Engineering at PSU has several courses covering SDGs studies such as Water treatment and desalination, fuel and combustion technology, air pollution and treatment, renewable energy technology, and environmental management systems that allow students to explore environmental and sustainability issues across a range of disciplines.

Community engagement is another key strategy for PSU to achieve the SDGs. This involved working with local communities to identify sustainability challenges and develop solutions that are tailored to the specific needs of the community. For example, PSU has established a Community Engagement and Outreach that works with local communities for medical examinations and COVID-19 tests.

Sustainable campus practices are also an important strategy to achieve the SDGs. This can involve reducing energy and water consumption, promoting sustainable transportation options, and implementing waste reduction and recycling programs. For example, PSU has a Sustainable Energy Initiative that aims to reduce the university's energy consumption through a combination of energy efficiency measures and the use of renewable energy sources.

Finally, capacity building is another important strategy to achieve the SDGs. This involved providing training and education programs to help communities build the skills and knowledge needed to achieve sustainable development. For example, PSU has a Centre of Excellence in water desalination that provides training and support to educators and students on topics related to clean water and energy (SDG 6 and SDG 7).

2.1 Recent Progress in PSU Research Towards the Fulfillment of SDG 1

Port Said University contributed to reducing the poverty (SDG 1) by providing education and training opportunities to individuals living in poverty or at risk of poverty. By offering affordable and accessible education, the university helped the community acquire the skills and knowledge they need to improve their economic situation and lift themselves out of poverty. Ibrahim et al. [4] studied the impact of a mother education programme at PSU on her knowledge and practices related to the prevention of sudden infant death syndrome (SIDS). They found that more than 75% of the mothers had little to no knowledge about SIDS before the programme. Furthermore, prior to the training, almost half of the moms had an unacceptable level of SIDS prevention practice. After completing the program, the majority of them had enough knowledge and practice levels.

In addition to education, PSU also supported SDG 1 by engaging in research and development activities that focused on poverty reduction. This included studying the causes and impacts of poverty, developing innovative solutions to alleviate poverty, and working with local communities and organizations to implement poverty reduction initiatives. Furthermore, the university can also promote sustainable development practices that contribute to poverty reduction, such as promoting sustainable agriculture, energy efficiency, and access to clean water and sanitation. By taking a holistic approach to poverty reduction and promoting sustainable development, PSU can contribute to achieving SDG 1 and creating a more equitable and prosperous future for all.

2.2 Recent Progress in PSU Research Towards the Fulfillment of SDG 2

Overcoming hunger and providing practical solutions to avoid hunger and supply sufficient amounts of food are crucial for the welfare of human beings, many researchers at PSU introduced solutions to face hunger fulfilling SDG 2. Selim et al. [5] investigated the results of the COVID-19 lockdown on small-scale farms in the North-eastern Nile Delta. They found that the income of small farm owners decreased to some extent. If smart irrigation was adopted, a considerable amount of water would be saved, but the farmers couldn't afford to use this technology despite this technology having a positive impact on crop productivity. Suleiman et al. [6] examined ethanol extract as a biocontrol agent to eliminate post-harvest diseases of potatoes and tomatoes. As plant diseases are considered a major threat to global food security, El-Saadony et al. [7] investigated the challenges and the mechanisms of plant growth microorganisms as a biocontrol agent to resist plant diseases. The authors proved that these microorganisms were efficient from an economic perspective besides suppressing plant diseases producing inhibitory chemicals as immune

responses in plants to resist phytopathogens. Shahda et al. [8] studied if skyscrapers integrated with vertical farming could solve the environmental and social issues that appeared as result of COVID-19. Results showed that skyscrapers integrated with vertical farming could be considered as closed ecosystem securing food and improving air quality. It also helps in improving physical and psychological health in addition to reducing greenhouse emissions. Eltarabily et al. [9] investigated the possibility of using groundwater for irrigation in El Moghra, Egypt. They recommended planting highly salt-tolerant crops and short intervals between irrigations were important to ensure wet soil and avoid soil dryness.

2.3 Recent Progress in PSU Research Towards the Fulfillment of SDG 3

By targeting a healthier life for Egyptian citizens, the researchers at PSU highlighted health care and well-being research with active research studies that aims to fulfil the SGD 3. Megahed et al. [10] evaluated the effect of building design on indoor air quality. COVID-19 pandemic showed how poor air quality could amplify airborne viruses effects, so the authors thought that air quality must be considered when a building is designed in the future as it didn't be a luxury parameter anymore. Refat et al. [11] investigated new drug therapy for pulmonary dysfunction and ameliorate glucometabolic control in diabetes mellitus. Results showed that the potential of a combination therapy with MSCs and Q/Zn. Better insulin secretion and decreased cellular inflammation were achieved by using the combination rather than using each drug alone. Therapy was promising in mitigating the symptoms of COVID-19. Elmaaty et al. [12] revised some glucocorticoids activity as a potential inhibitor of SARS-CoV-2 main protease. Results showed some glucocorticoids had priority over others for inflammation treatment accompanied by COVID-19.

2.4 Recent Progress in PSU Research Towards the Fulfillment of SDG 4

Enhancing education quality is considered the key to success and progress. High-quality education always assists in forming brilliant and creative future generations. Many researchers at PSU directed their efforts for education development fulfilling SDG 4. Abdulaal et al. [13] compared dynamic and non-dynamic assessments and how they influenced EFL learners. They concluded dynamic assessments improve the listening and reading skills of the learners. Megahed et al. [14] investigated the influence of Ai empowered education in engineering. The study provided a vision about how AI could affect the educational processes. Hosni et al. [15] provided a virtual learning environment with different learning styles. It recommended study

materials depending on the student education field. Megahed et al. [16] studied the transformation from traditional learning to e-learning and focused on the e-learning ecosystem to build sustainable education to face crises such as COVID-19.

2.5 Recent Progress in PSU Research Towards the Fulfillment of SDG 5

Port Said university has shown its commitment to SDG 5 at both research, education, and administration levels. The university believes in the importance of promoting gender equality and empowering all women and girls. Zahra [17] discussed the vision of UNESCO to promote the dimensions of global citizenship in education. One of the goals of global citizenship education according to the 2030 agenda is emphasizing gender quality in education as there is gender disparities in the education system and girls had fewer opportunities to complete their education. During the investigation of human capital upgrading in the Suez Canal region, Biltagy et al. [18] found there was a lack of gender gap in the educational profile of the region. The number of women unemployed is remarkably high as men's employment rate is about three times women's employment rate. Elsayed et al. [19] studied women empowering effect of high education. They found that women's empowerment had a positive effect on labour market outcomes, especially for women. Well-educated women had chances to get married to better-educated men leading to getting empowered in their households.

2.6 Recent Progress in PSU Research Towards the Fulfillment of SDG 6

The SDG 6 concerns about Clean Water and Sanitation, the researchers at PSU have been active in investigating novel methods for wastewater treatment for domestic and industrial usage. Several types of membranes were fabricated from nano-based materials for water purification [20–24]. They evaluated the performance of the membranes and their fouling resistance. They found that nanosilica/PSF membrane resisted fouling and its tensile force was tolerant. Amin et al. [25] conducted an experimental study to investigate the motion response of a floating desalination plant powered by wind turbines. Experimental results were obtained for two models with and without the turbine to understand the motion behavior of the two models and study the possibility of using different types of wind turbines for the same platform. Elhenawy et al. [26] investigated a desalination module with a corrugated feed channel with a new air gap membrane. The experiment was conducted to evaluate the performance of the module with the two new feed channels and the effect of the new channels on the thermal boundary of the membrane sheet. Rizk et al. [27]

investigated the effect of heavy metal contamination in the aquatic ecosystem in lake Nasser. They found that the quality of lake Nasser water was excellent, and the dissolved metals were absorbed by the sediment, so water quality was preserved. Elwakeel et al. [28] investigated the performance of beach bivalve shells to absorb methylene blue from aqueous solutions Elgarahy et al. [29] reviewed heavy metals and organic dyes removal by biomaterials due to their low cost and eco-friendly.

Several studies have utilized the state-of-the-art Computational Fluid Dynamics (CFD) simulation for the design and optimization of water channels [30, 31]. Amin et al. [31] designed an anoxic bioreactor based on computational fluid dynamics in the wastewater treatment plant. They compared three different models to find the optimum design. They found the orbital bioreactor had the optimal design as it drove the flow field with more uniform flow patterns at variance with the other designs. El-Sayed et al. [32] investigated a novel nanomaterial for toxic substances removal. The new material had rapid adsorption properties and the maximum capability was 79.20 mg/g. Elhady et al. [33] treated oily wastewater using a polyamide thin film composite membrane. Oily wastewater with a 99% concentration could be improved by about 99%. Eltarabily et al. [34] modeled groundwater found in agriculture watersheds under variable conditions of charging and discharging for a quaternary aquifer located in the eastern Nile Delta.

2.7 Recent Progress in PSU Research Towards the Fulfillment of SDG 7

Numerous researchers at PSU have dedicated their efforts to developing new ways to provide affordable and clean energy fulfilling SDG 7. The majority of energy research focuses on solar photovoltaics and wind turbine. However, there is an increasing research interest in green hydrogen and fuel cells. Green hydrogen production recently become one of the most attractive research topics in the continuous efforts to mitigate the alarming climate change. Elgarahy et al. [35] carried out a critical review regarding the production of hydrogen from wastewater. Their review has been extended to cover the storage, economical evaluations, and applications of hydrogen produced from wastewater. They expected that hydrogen production will be economically competitive and that the cost of hydrogen production will fall after 2030 [35]. In light of the increasing attention towards green hydrogen, fuel cell technology is very important as a primary device to convert hydrogen directly to useful electricity. Albaz et al. [36] investigate the performance of Polymer Electrolyte Membrane (PEM) fuel cells. They found that the Deterministic Particle Swarm Optimization (DPSO) technique has an outstanding performance in capturing the maximum power point and this enables maximizing the electricity generation in fuel cells [36].

Photovoltaic (PV) panels have excellent potential in providing affordable and clean energy for everyone [37–39]. It is expected to be the major energy source

in the future energy mix [40–42]. However, large PV systems suffer from some issues regarding partial shading [43] and non-uniform aging [44]. Khalifa et al. [45] investigated the performance of several bio-inspired algorithms in order to track the maximum power point of PV arrays at several partial shading conditions. Their investigations concluded that the Cuckoo Search (CS) algorithm has a superior performance in terms of accuracy and short convergence time [45]. Yosry et al. [46] carried out a detailed experimental investigation that aimed to design and characterize a small-scale low-speed tidal turbine. The additive manufacturing technique is utilized for prototyping. They concluded that increasing the blockage ratio leads to a significate increase in the power coefficient [46]. Concentrated PV systems aim to focus the solar irradiance onto a solar cell by means of a set of optical components and this increases the energy produced from the solar panels while rising some challenges regarding the cooling of the panels. Several experimental investigations were carried out to improve the performance of high and ultra-high concentrator PV systems [47–49].

Egypt has limited regions with very good wind speeds in which large wind turbines have been installed. However, there is a need to develop new wind turbines that can work effectively in locations with low and moderate wind speeds. Several investigations have been conducted to investigate the aerodynamics of wind turbines [50, 51]. Gharib-Yosry et al. [52] evaluated the applicability of the Darrieus turbine in urban environments by carrying out experimental investigations in both the wind tunnel and the water current channels. They found that the blockage corrections are essential for the experimental data from confined test sections. Elsakka et al. [53] carried out a response surface optimization study in order to select the optimal design for small-scale vertical axis wind turbines at low and moderate wind speeds. The optimization study leads to an improvement of about 34.5% in the power coefficient in contrast with the initial design.

Due to the continuous increase in renewable energy utilization, there is an increasing interest in energy storage research. Amer et al. [54] investigated the effects of the number of fins on the performance of thermal energy accumulator units using the computational fluid dynamics numerical simulations. Furthermore, the researchers at PSU are actively investigating novel techniques for improving the energy efficiency in wireless sensor networks [55, 56], LTE-advanced networks [57, 58], computation offloading algorithm in industry 4.0 [59] and Joint channel assignment and power allocation [60].

2.8   Recent Progress in PSU Research Towards the Fulfillment of SDG 8

Decent work and economic growth are the main targets of SDG 8. Protecting workers' rights and fostering safe and secure workplaces for all employees, including those in precarious jobs and migratory workers, particularly women migrants are one of the

most important pillars in achieving SDG 8. Abuwarda et al. [61] developed wearables to monitor workers' fatigue. The previous scheduling algorithms physiological factors of humans led to unrealistic schedules. This work provided monitoring physiological changes of workers during their work allowing them to set their activities up according to the collected data.

2.9 Recent Progress in PSU Research Towards the Fulfillment of SDG 9

Port Said University has been encouraging research seeking to find ways for sustainable industry. Various research investigated how to improve access to modern energy services and establish sustainable transport systems. Moshiri et al. [62] introduced a smart production system for the process chain to manufacture small lot size tooling. The production line of the proposed system was fully digitized. The system provided full traceability and flexibility. Salama et al. [63] developed industrial internet of things solution to monitor various manufacturing processes such as the nozzle temperature and filament runout. Charles et al. [64] used machine learning to develop additive manufacturing processes. The system guaranteed high quality of the printed products and efficient resource usage by preventing loss of material caused by defected parts. Mohsen et al. [65] introduced three models to recognize the daily activities of humans. The most accurate model was the combined long short-term memory and convolutional neural network with an accuracy of about 97%. Elkaseer et al. [66] investigated the effect of specified parameters that could affect the part quality and resource usage efficiency. Results showed that part quality decreased with increasing thickness layer as it spread out.

In addition, the temperature had a remarkable effect on the dimensional errors as it regulated the used material viscosity. Also, high printing speed led to inaccurate deposition of the material. Bayomie et al. [67] introduced a new model of the crude distillation unit. They adopted a pinch analysis technique to assure heat transfer with high efficiency. The proposed system reduced CO_2 emissions by 45%. Ibrahim et al. [68] investigated the improvement of combustion characteristics using an industrial air-blast atomizer. Alhajri et al. [69] introduced a new concept for designing heat recovery systems by relating heat duty to the heat exchange area. They found that a system with a high Q/A value -which is the new parameter- transfers heat more efficiently. Tayeb et al. [70] introduced a new sustainable material used in oil spill removal. However, rice straw was an agricultural waste, the authors proved that it could be used for oil removal with an efficiency reached 94.7%. Another study was conducted for noise reduction. The KNN-KF algorithm was suggested to improve the accuracy of data streams from Industrial Internet of Things (IIoT) sensors in cloud storage and fog node architecture [71].

2.10 Recent Progress in PSU Research Towards the Fulfillment of SDG10

Fulfilling SDG10, researchers at PSU are pursuing their research studies aiming to reduce social and economic inequality based on religion or sex. Mohamed et al. [72] investigated the relationship between the nurses' gender and their perception of organizational justice at selected hospitals in Port Said. They found no significant effect of gender on the nurses' perception of organizational justice. Mohamed et al. [73] studied how urban planning could affect the social sustainability of the residential neighborhood. Considering Salam's new city as a case study, they found that social interaction improved by 48% from the base case.

2.11 Recent Progress in PSU Research Towards the Fulfillment of SDG11

Citizen's safety and comfort are major concerns according to SDG11. Researchers at PSU have conducted several studies on sustainable cities and communities that serve to fulfil SDG11. Eltarabily et al. [74] developed a model to evaluate groundwater resources in Western Nile Delta and Examine variable management alternatives in the region. Elqattan et al. [75] employed a PV system to drive system used to cool pavement to improve outdoor climate, hence reducing energy consumption in buildings. Abdelmohsen et al. [76] conducted a study to optimize highway work zones to reduce traffic crashes and provide safety to individuals. Elrayies [77] discussed the role of microalgae in obtaining green buildings. The author summarized the challenges in obtaining these buildings as high capital cost and the positive impacts of these buildings as reducing greenhouse emissions, improving air quality, and water treatment. The VANET, also known as the Vehicular Ad hoc NETwork, has been utilized to create Intelligent Transportation Systems (ITSs) with a fast and ever-changing network structure. The outcomes of simulations verify that the suggested protocol effectively handles both Vehicle to Vehicle and Vehicle to Infrastructure scenarios. Moreover, it significantly enhances the packet delivery ratio and reduces delays, while maintaining an acceptable level of overhead and number of hops across all vehicles [78]. Other studies showed that navigation in a vehicular ad hoc network (VANET) is used today to provide communications between nearby vehicles and between vehicles and fixed infrastructure on the roadside as well as to provide road safety, driving comfort, and infotainment due to the rapid growth of technology involved in smart city networks [79, 80].

2.12　Recent Progress in PSU Research Towards the Fulfillment of SDG12

The university encouraged research to investigate new approaches for responsible consumption and production to reduce waste and eliminate pollution which fulfilled SDG12. Aboelazayem et al. [81] investigated waste cooking oil conversion into biodiesel. The produced diesel matched the standards of biodiesel providing a solution for sustainable biofuel production. Eladl et al. [82] proposed an optimization model for dispatch for multi energy power sources. Taha et al. [83] experimentally studied biochar usage in the industrial field by employing biochar for pollutants removal from phosphoric acid.

2.13　Recent Progress in PSU Research Towards the Fulfillment of SDG13

Reducing greenhouse emissions by having cleaner energy resources was extensively investigated by researchers at PSU. All these efforts sought to face climate change and fulfill SDG13 [84, 85]. Moneim et al. [86] investigated a new approach to obtain hydrocarbon gases from solid agriculture waste especially rice straw. They did an optimization analysis to find the proper operating condition that provided the lowest possible cost. The findings revealed that the optimum operating temperature was 250 °C which allowed proper gas composition with the highest rate of gas production. Eloffy et al. [87] studied the conversion of biomass into hydrogen. They evaluated the feasibility of the production of hydrogen and found the optimum operation by optimizing the main parameter that controlled the hydrogen production. Nabil et al. [88] examined CO_2 with water conversion into fuel using a continuous-flow photochemical reactor. Various catalysts are tested and compared in the performance of the reduction process of CO_2.

2.14　Recent Progress in PSU Research Towards the Fulfillment of SDG14

Aiming to protect aquatic systems and ensure sustainable use of marine resources, PSU has numerous pieces of research in this field fulfilling SDG14. Awad et al. [89] investigated the effect of acidification on the grooved carpet shell clam. They found that there were no recent threats to the organism despite the current level of acidification of the Mediterranean Sea. They concluded that risk assessment will be important in the future to assure that the organisms can adapt to the incoming climate changes. Al-Zaydi et al. [90] carried out an experimental study to treat contaminated water with ultrasound. This innovative method treated water contaminated by polycyclic

aromatic sulfur hydrocarbons such as benzothiophene. These hydrocarbons were common impurities in water because of the oil industry. This method could convert the pollutant into small chain pollutants and less harmful pollutants allowing more efficient treatment. Abu El-Regal et al. [91] conducted an investigation discussing the first time when the Schindler's fish was recorded in the red sea. Shaltout et al. [92] described plant diversity in the coastal lakes of Egypt. Nevertheless, the area of the lakes is about < 0.003 of the total area of Egypt, they are considered the most important hot spots for the Egyptian flora. Elgarahy et al. [93] published a review shedding the light on microplastic and its effect on the aquatic environment. The authors studied the interaction between microplastic waste and aquatic organisms and how it could accumulate through the chain of food affecting both the aquatic ecosystem and humans.

2.15 Recent Progress in PSU Research Towards the Fulfillment of SDG15

SDG15: life on land: this goal aims to protect and promote sustainable use of terrestrial ecosystems and manage combat desertification. The researchers at PSU carried out several studies aiming at fulfilling this goal. Abdelhady et al. [94] ranked selected invertebrate fossils Stratigraphically. Results showed the Jurassic ammonite had the lowest species duration meanwhile the benthic foraminifers and bivalves had longer species durations. Assaeed et al. [95] studied the mechanisms of invasive species to control them in the arid ecosystem. Results showed that the aboveground phenological features such as plant height, leaf dry mass and leaf area reached their highest value in the wadi channels while the lowest values were attained in the mountain ranges. Yahia et al. [96] studied the intraspecific differences in functional and molecular traits of near-endemic *Onopordum alexandrinum* Boiss. in anthropogenic and natural habitats along the Western Mediterranean coast of Egypt. The results indicated that plant functional traits related to high rates of growth occurred in populations located in abandoned fields and rich soil resources.

2.16 Recent Progress in PSU Research Towards the Fulfillment of SDG16

For promoting development and providing justice for all, the university promotes research practices to ensure public access to information and sustainable development fulfilling SDG16. Abdou et al. [97] discussed the relationship between earnings management and corporate governance. The authors concluded that firms had low earning management if they had larger boards in Egypt. Governance quality had a major effect on earnings management.

3 Conclusions

The United Nations SDGs have been adopted by the researchers at PSU in their endeavors towards pursuing their intensive sustainability research activities. This paper provides a deeper insight into the recent research progress at PSU toward the fulfillment of the emerging SDGs. The SciVal database has been found as a powerful evaluation tool for visualizing the university research performance. In this paper, the data provided by SciVal has been utilized to analyze sustainability research at PSU. It is observed that some of the SDGs are in a strong correlation with the other SDGs. Based on this review of the sustainability research at PSU, it is concluded that PSU has delivered world-leading research outputs in the fields of SDG 6: Clean water and sanitation, SDG 7: Affordable and Clean Energy, and SDG 14: Life below water. Furthermore, it is depicted that SDG 3: Good Health and Well-being acquires the highest number of publications from PSU. Also, the research output in SDG 5: Gender equality and SDG 13: Climate action has the highest citation impact. It is concluded that the researchers at PSU have carried out substantial efforts in the research topics related to SDG 2 to SDG 16. However, there are still areas for potential improvement, such as SDG 1: and SDG 17: in which the researchers at PSU need to put more effort.

4 Recommendations

It is recommended to utilize the SciVal database for evaluating the university sustainability research. For researchers at PSU, it is recommended to put more efforts on the research topics related to SDG 2 to SDG 16.

References

1. Fonseca LM, Domingues JP, Dima AM (2020) Mapping the sustainable development goals relationships. https://doi.org/10.3390/su12083359
2. Shulla K, Voigt B-F, Cibian S, Scandone G, Martinez Edna, Nelkovski F, Salehi P (2021) Effects of COVID-19 on the sustainable development goals (SDGs). Discov Sustain 2:15. https://doi.org/10.1007/s43621-021-00026-x
3. SciVal. https://www.scival.com/home. Accessed 21 Mar 2023
4. Ibrahim AM, Sobeh Sobeh DE, Elsaid Fathi Zaghamir D (2023) Mothers' knowledge and practices regarding preventing poor Egyptian infant death syndrome. J Neonatal Nurs 29:341–349. https://doi.org/10.1016/J.JNN.2022.07.019
5. Selim T, Eltarabily MG (2022) Impact of COVID-19 lockdown on small-scale farming in Northeastern Nile Delta of Egypt and learned lessons for water conservation potentials. Ain Shams Eng J 13. https://doi.org/10.1016/j.asej.2021.11.018
6. Suleiman WB, El Bous MM, El Said M, El Baz H (2019) In vitro evaluation of *Syzygium aromaticum* L. ethanol extract as biocontrol agent against postharvest tomato and potato diseases. Egypt J Bot 59:81–94. https://doi.org/10.21608/ejbo.2018.3838.1180

7. El-Saadony MT, Saad AM, Soliman SM, Salem HM, Ahmed AI, Mahmood M, El-Tahan AM, Ebrahim AAM, Abd El-Mageed TA, Negm SH, Selim S, Babalghith AO, Elrys AS, El-Tarabily KA, AbuQamar SF (2022) Plant growth-promoting microorganisms as biocontrol agents of plant diseases: mechanisms, challenges and future perspectives. Front Plant Sci 13

8. Shahda MM, Megahed NA (2022) Post-pandemic architecture: a critical review of the expected feasibility of skyscraper-integrated vertical farming (SIVF). Archit Eng Des Manag

9. Eltarabily MG, Moghazy HEM (2021) GIS-based evaluation and statistical determination of groundwater geochemistry for potential irrigation use in El Moghra, Egypt. Environ Monit Assess 193.https://doi.org/10.1007/s10661-021-09058-2

10. Megahed NA, Ghoneim EM (2021) Indoor Air Quality: rethinking rules of building design strategies in post-pandemic architecture. Environ Res 193.https://doi.org/10.1016/j.envres.2020.110471

11. Refat MS, Hamza RZ, Adam AMA, Saad HA, Gobouri AA, Al-Harbi FS, Al-Salmi FA, Altalhi T, El-Megharbel SM (2021) Quercetin/zinc complex and stem cells: a new drug therapy to ameliorate glycometabolic control and pulmonary dysfunction in diabetes mellitus: structural characterization and genetic studies. PLoS One 16.https://doi.org/10.1371/journal.pone.0246265

12. Elmaaty AA, Alnajjar R, Hamed MIA, Khattab M, Khalifa MM, Al-Karmalawy AA (2021) Revisiting activity of some glucocorticoids as a potential inhibitor of SARS-CoV-2 main protease: theoretical study. RSC Adv 11:10027–10042. https://doi.org/10.1039/d0ra10674g

13. Al-Dawoody Abdulaal MA, Ramadan Khalil N, Heji Alenazi M, Robso Wodajo M (2022) Dynamic vs nondynamic assessments: impacts on intermediate EFL learners' receptive skills. Educ Res Int 2022. https://doi.org/10.1155/2022/5372929

14. Megahed NA, Abdel-Kader RF, Soliman HY (2022) Post-pandemic education strategy: framework for artificial intelligence-empowered education in engineering (AIEd-Eng) for lifelong learning. In: Lecture notes on data engineering and communications technologies. Springer, pp 544–556

15. Hosni H, El-Dosuky M, Eisa M (2020) Virtual learning environment and learning styles. J Theor Appl Inf Technol 198:3595–3606

16. Megahed NA, Ghoneim EM (2022) E-learning ecosystem metaphor: building sustainable education for the post-COVID-19 era. Int J Learn Technol 17:133–153. https://doi.org/10.1504/IJLT.2022.125075

17. Zahra A (2022) UNESCO's vision to promote the dimensions of global citizenship in education "analytical study in light of the 2030 agenda for sustainable development." Port Said J Educ Res 1:1–35

18. Biltagy M, Nassar H (2020) Human capital upgrading, social inclusion and New Suez canal economic zone. Econ Reg 16:962–974. https://doi.org/10.17059/ekon.reg.2020-3-22

19. Elsayed A, Shirshikova A (2023) The women empowering effect of higher education

20. Bassyouni M, Abdel-Aziz MH, Zoromba MS, Abdel-Hamid SMS, Drioli E (2019) A review of polymeric nanocomposite membranes for water purification. J Ind Eng Chem 73:19–46

21. Marni Sandid A, Bassyouni M, Nehari D, Elhenawy Y (2021) Experimental and simulation study of multichannel air gap membrane distillation process with two types of solar collectors. Energy Convers Manag 243:114431. https://doi.org/10.1016/J.ENCONMAN.2021.114431

22. Maddah HA, Alzhrani AS, Bassyouni M, Abdel-Aziz MH, Zoromba M, Almalki AM (2018) Evaluation of various membrane filtration modules for the treatment of seawater. Appl Water Sci 8:1–13. https://doi.org/10.1007/S13201-018-0793-8/FIGURES/16

23. Elrasheedy A, Rabie M, El-Shazly A, Bassyouni M, Abdel-Hamid SMS, El Kady MF (2021) Numerical investigation of fabricated MWCNTs/polystyrene nanofibrous membrane for DCMD. Polymers 13:160. https://doi.org/10.3390/POLYM13010160

24. Alhathal Alanezi A, Bassyouni M, Abdel-Hamid SMS, Ahmed HS, Abdel-Aziz MH, Zoromba MS, Elhenawy Y (2021) Theoretical investigation of vapor transport mechanism using tubular membrane distillation module. Membranes 11:560. https://doi.org/10.3390/MEMBRANES11080560

25. Amin I, Dai S, Day S, Ali MEA, Balah A, Shawky H, Oterkus S, Oterkus E (2021) Experimental study on the motion response of an integrated floating desalination plant and offshore wind turbine on a non-ship platform. Ocean Eng 234

26. Elhenawy Y, Moustafa GH, Abdel-Hamid SMS, Bassyouni M, Elsakka MM (2022) Experimental investigation of two novel arrangements of air gap membrane distillation module with heat recovery. Energy Rep 8:8563–8573. https://doi.org/10.1016/J.EGYR.2022.06.068

27. Rizk R, Juzsakova T, Ben Ali M, Rawash MA, Domokos E, Hedfi A, Almalki M, Boufahja F, Shafik HM, Rédey Á (2022) Comprehensive environmental assessment of heavy metal contamination of surface water, sediments and Nile Tilapia in Lake Nasser, Egypt. J King Saud Univ Sci 34

28. Elwakeel KZ, Elgarahy AM, Mohammad SH (2017) Use of beach bivalve shells located at Port Said coast (Egypt) as a green approach for methylene blue removal. J Environ Chem Eng 5:578–587

29. Elgarahy AM, Elwakeel KZ, Mohammad SH, Elshoubaky GA (2021) A critical review of biosorption of dyes, heavy metals and metalloids from wastewater as an efficient and green process. Clean Eng Technol 4

30. Selim T, Hesham M, Elkiki M, Elsakka MM (2023) Numerical analysis of sediment transport and depth averaged flow velocity in non-prismatic compound channels. Ain Shams Eng J. https://doi.org/10.1016/J.ASEJ.2023.102229

31. Amin I, Elsakka M, Oterkus S, Nguyen CT, Ozdemir M, El-Aassar AH, Shawky H, Oterkus E (2022) Computational fluid dynamics-based design of anoxic bioreactor zone in wastewater treatment plant. Desalin Water Treat 253:9–23. https://doi.org/10.5004/dwt.2022.28300

32. El-Sayed WN, Elwakeel KZ, Shahat A, Awual MR (2019) Investigation of novel nanomaterial for the removal of toxic substances from contaminated water. RSC Adv 9:14167–14175

33. Elhady S, Bassyouni M, Mansour RA, Elzahar MH, Abdel-Hamid S, Elhenawy Y, Saleh MY (2020) Oily wastewater treatment using polyamide thin film composite membrane technology. Membranes (Basel) 10

34. Eltarabily MG, Negm AM, Yoshimura C, Takemura J (2018) Groundwater modeling in agricultural watershed under different recharge and discharge scenarios for Quaternary aquifer Eastern Nile Delta, Egypt. Environ Model Assess 23:289–308

35. Elgarahy AM, Eloffy MG, Hammad A, Saber AN, El-Sherif DM, Mohsen A, Abouzid M, Elwakeel KZ (2022) Hydrogen production from wastewater, storage, economy, governance and applications: a review. Environ Chem Lett

36. Elbaz A, Elfar MH, Kalas A, Refaat A (2022) Maximum power extraction from polymer electrolyte membrane (PEM) fuel cell based on deterministic particle swarm optimization algorithm. In: Proceedings of the 2022 conference of Russian young researchers in electrical and electronic engineering, ElConRus 2022. Institute of Electrical and Electronics Engineers Inc., pp 613–619

37. Osman MH, Ahmed MK, Refaat A, Korovkin NV (2021) A comparative study of MPPT for PV system based on modified perturbation observation method. In: Proceedings of the 2021 IEEE conference of Russian young researchers in electrical and electronic engineering, ElConRus 2021, pp 1023–1026

38. Osman MH, Refaat A (2019) Adaptive multi-variable step size P&O MPPT for high tracking-speed and accuracy. IOP Conf Ser Mater Sci Eng 643:012050. https://doi.org/10.1088/1757-899X/643/1/012050

39. Refaat A, Khalifa AE, Elsakka MM, Elhenawy Y, Kalas A, Elfar MH (2023) A novel meta-heuristic MPPT technique based on enhanced autonomous group Particle Swarm Optimization Algorithm to track the GMPP under partial shading conditions—experimental validation. Energy Convers Manag 287:117124. https://doi.org/10.1016/J.ENCONMAN.2023.117124

40. Elminshawy NAS, Mohamed AMI, Morad K, Elhenawy Y, Alrobaian AA (2019) Performance of PV panel coupled with geothermal air cooling system subjected to hot climatic. Appl Therm Eng 148:1–9. https://doi.org/10.1016/J.APPLTHERMALENG.2018.11.027

41. Elminshawy NAS, Osama A, El-Damhogi DG, Oterkus E, Mohamed AMI (2021) Simulation and experimental performance analysis of partially floating PV system in windy conditions. Sol Energy 230:1106–1121. https://doi.org/10.1016/J.SOLENER.2021.11.020

42. Elminshawy NAS, Mohamed AMI, Osama A, Amin I, Bassam AM, Oterkus E (2022) Performance and potential of a novel floating photovoltaic system in Egyptian winter climate on calm water surface. Int J Hydrogen Energy 47:12798–12814. https://doi.org/10.1016/J.IJHYDENE.2022.02.034

43. Refaat A, Elgamal M, Korovkin NV (2019) A novel photovoltaic current collector optimizer to extract maximum power during partial shading or mismatch conditions. In: Proceedings of the 2019 IEEE conference of Russian young researchers in electrical and electronic engineering, ElConRus, pp 407–412. https://doi.org/10.1109/EICONRUS.2019.8657173

44. Refaat A, Abdel A, Shehata H, Elgamal M, Korovkin NV, Shehata AA, Korovkin NV (2020) Current collector optimizer topology with reconfiguration algorithm to harvest optimal power from nonuniform aged PV arrays. In: 2020 international multi-conference on industrial engineering and modern technologies (FarEastCon). https://doi.org/10.1109/fareastcon50210.2020.9271455

45. Khalifa AE, Refaat A, Kalas A, Elfar MH (2022) Two bio-inspired MPPT algorithms to harvest the maximum power from partially shaded PV arrays. In: Proceedings of the 2022 conference of Russian young researchers in electrical and electronic engineering, ElConRus 2022. Institute of Electrical and Electronics Engineers Inc., pp 670–674

46. Gharib Yosry A, Fernández-Jiménez A, Álvarez-Álvarez E, Blanco Marigorta E (2021) Design and characterization of a vertical-axis micro tidal turbine for low velocity scenarios. Energy Convers Manag 237

47. Ahmed A, Alzahrani M, Shanks K, Sundaram S, Mallick TK (2022) Reliability and temperature limits of the focal spot of a primary optical component for an ultra-high concentrated photovoltaic system. AIP Conf Proc 2550.https://doi.org/10.1063/5.0099091

48. Alzahrani M, Ahmed A, Shanks K, Sundaram S, Mallick T (2021) Optical component analysis for ultrahigh concentrated photovoltaic system (UHCPV). Sol Energy 227:321–333. https://doi.org/10.1016/J.SOLENER.2021.09.019

49. Ahmed A, Shanks K, Sundaram S, Mallick T (2021) Energy and exergy analyses of new cooling schemes based on a serpentine configuration for a high concentrator photovoltaic system. Appl Therm Eng 199. https://doi.org/10.1016/J.APPLTHERMALENG.2021.117528

50. Elsakka MM, Ingham DB, Ma L, Pourkashanian M (2021) Comparison of the computational fluid dynamics predictions of vertical axis wind turbine performance against detailed pressure measurements. Int J Renew Energy Res 11:276–293

51. Elsakka MM, Ingham DB, Ma L, Pourkashanian M (2020) Effects of turbulence modelling on the predictions of the pressure distribution around the wing of a small scale vertical axis wind turbine. In: Proceedings of the 6th European conference on computational mechanics: solids, structures and coupled problems, ECCM 2018 and 7th European conference on computational fluid dynamics, ECFD 2018, pp 3921–3931

52. Gharib-Yosry A, Blanco-Marigorta E, Fernández-Jiménez A, Espina-Valdés R, Álvarez-álvarez E (2021) Wind–water experimental analysis of small SC-Darrieus turbine: an approach for energy production in urban systems. Sustainability 13:5256. https://doi.org/10.3390/SU13095256

53. Elsakka MM, Ingham DB, Ma L, Pourkashanian M, Moustafa GH, Elhenawy Y (2022) Response surface optimisation of vertical axis wind turbine at low wind speeds. Energy Rep 8:10868–10880

54. Amer AE, Elsakka MM, Lebedev VA (2021) Thermal performance of an accumulator unit using phase change material with a fixed volume of fins. Int J Energy Res 45:19089–19102. https://doi.org/10.1002/ER.7095

55. Rizk R, Magdy SM, Zaki FW (2015) Energy efficiency of virtual multi-input, multi-output based on sensor selection in wireless sensor networks. Commun Mob Comput 15:1–15. https://doi.org/10.1002/wcm.2310

56. Rizk R, Farouk F, Fayez, Zaki W (2017) Towards energy efficiency and stability in heterogeneous wireless sensor networks. Wirel Pers Commun 96. https://doi.org/10.1007/s11277-017-4390-1

57. Abohashish SMM, Rizk RY, Zaki FW (2019) Towards energy efficient relay deployment in multi-user LTE-A networks. https://doi.org/10.1049/iet-com.2018.5034

58. Abohashish SMM, Rawya, Rizk Y, Fayez, Zaki W (2019) Energy efficiency optimization for relay deployment in multi-user LTE-advanced networks. Wirel Pers Commun 108:297–323. https://doi.org/10.1007/s11277-019-06404-z

59. Abdel-Kader RF, El-Sayad NE, Rizk RY (2021) Efficient energy and completion time for dependent task computation offloading algorithm in industry 4.0. PLoS One 16:e0252756. https://doi.org/10.1371/JOURNAL.PONE.0252756

60. Salah A, Abdel-Atty HM, Rizk RY (2018) Joint channel assignment and power allocation based on maximum concurrent multicommodity flow in cognitive radio networks. Wirel Commun Mob Comput 2018.https://doi.org/10.1155/2018/3545946

61. Abuwarda Z, Hegazy T, Oetomo A, Morita PP (2023) Using wearables to monitor and mitigate workers' fatigue. In: Lecture notes in civil engineering. Springer, pp 587–597

62. Moshiri M, Charles A, Elkaseer A, Scholz S, Mohanty S, Tosello G (2020) An industry 4.0 framework for tooling production using metal additive manufacturing-based first-time-right smart manufacturing system. In: Procedia CIRP. Elsevier B.V., pp 32–37

63. Salama M, Elkaseer A, Saied M, Ali H, Scholz S (2019) Industrial internet of things solution for real-time monitoring of the additive manufacturing process. In: Advances in intelligent systems and computing. Springer, pp 355–365

64. Charles A, Salem M, Moshiri M, Elkaseer A, Scholz SG (2021) In-process digital monitoring of additive manufacturing: proposed machine learning approach and potential implications on sustainability. In: Smart innovation, systems and technologies. Springer, pp 297–306

65. Mohsen S, Elkaseer A, Scholz SG (2021) Industry 4.0-oriented deep learning models for human activity recognition. IEEE Access 9:150508–150521

66. Elkaseer A, Schneider S, Scholz SG (2020) Experiment-based process modeling and optimization for high-quality and resource-efficient FFF 3D printing. Appl Sci (Switzerland) 10

67. Bayomie OS, Abdelaziz OY, Gadalla MA (2019) Exceeding Pinch limits by process configuration of an existing modern crude oil distillation unit—a case study from refining industry. J Clean Prod 231:1050–1058

68. Ibrahim IA, Elzallat AM, Elsakka MM, Farag TM, Gad HM (2022) Numerical study of kerosene spray and combustion characteristics using an air-blast atomizer. Energy Rep 8:5974–5986. https://doi.org/10.1016/J.EGYR.2022.04.046

69. Alhajri IH, Gadalla MA, Elazab HA (2021) A conceptual efficient design of energy recovery systems using a new energy-area key parameter. Energy Rep 7:1079–1090

70. Tayeb AM, Farouq R, Mohamed OA, Tony MA (2020) Oil spill clean-up using combined sorbents: a comparative investigation and design aspects. Int J Environ Anal Chem 100:311–323

71. Abdel-Kader RF, El-Sayad NE, Rizk RY (2022) Efficient noise reduction system in industrial IoT data streams. Lect Notes Data Eng Commun Technol 100:219–232. https://doi.org/10.1007/978-3-030-89701-7_20/FIGURES/7

72. Salah S, Eldossoqi E, Abd S, Moniem Zahran E, Rashwan T, Abd-El Hady M (2021) Organizational justice perception and job burnout among nurses at port said selected hospitals. Port Said Sci J Nurs 8:22–51. https://doi.org/10.21608/PSSJN.2021.53400.1072

73. Mohamed AN, Elmokadem AAE, Ali SM, Badawey N (2022) Improve urban form to achieve high social sustainability in a residential neighborhood Salam new city as a case study. Buildings 12.https://doi.org/10.3390/buildings12111935

74. Eltarabily MGA, Negm AM (2019) Groundwater management for sustainable development plans for the western Nile delta. In: Handbook of environmental chemistry. Springer, pp 709–727

75. Elqattan AA, Elrayies GM (2021) Developing a novel solar-driven cool pavement to improve the urban microclimate. Sustain Cities Soc 64.https://doi.org/10.1016/j.scs.2020.102554

76. Abdelmohsen AZ, El-Rayes K (2018) Optimizing the planning of highway work zones to maximize safety and mobility. J Manag Eng 34.https://doi.org/10.1061/(asce)me.1943-5479.0000570

77. Elrayies GM (2018) Microalgae: prospects for greener future buildings. Renew Sustain Energy Rev 81:1175–1191

78. Attia R, Hassaan A, Rizk R (2021) Advanced greedy hybrid bio-inspired routing protocol to improve IoV. IEEE Access 9:131260–131272. https://doi.org/10.1109/ACCESS.2021.311 4646

79. Alkady Y, Rizk R (2022) Location privacy-preserving of vehicular ad-hoc network in smart cities. Lect Notes Data Eng Commun Technol 113:532–543. https://doi.org/10.1007/978-3-031-03918-8_44/FIGURES/5

80. Farouk F, Alkady Y, Rizk R (2020) Efficient privacy-preserving scheme for location based services in VANET system. IEEE Access 8:60101–60116. https://doi.org/10.1109/ACCESS.2020.2982636

81. Aboelazayem O, Gadalla M, Saha B (2018) Valorisation of high acid value waste cooking oil into biodiesel using supercritical methanolysis: experimental assessment and statistical optimisation on typical Egyptian feedstock. Energy 162:408–420. https://doi.org/10.1016/j.energy.2018.07.194

82. Eladl AA, ElDesouky AA (2019) Optimal economic dispatch for multi heat-electric energy source power system. Int J Electr Power Energy Syst 110:21–35. https://doi.org/10.1016/j.ijepes.2019.02.040

83. Taha MH, Abdel Maksoud SA, Ali MM, El Naggar AMA, Morshedy AS, Elzoghby AA (2019) Conversion of biomass residual to acid-modified bio-chars for efficient adsorption of organic pollutants from industrial phosphoric acid: an experimental, kinetic and thermodynamic study. Int J Environ Anal Chem 99:1211–1234

84. Fouad K, Bassyouni M, Alalm MG, Saleh MY (2021) Recent developments in recalcitrant organic pollutants degradation using immobilized photocatalysts. Appl Phys A 2021 127:1–28. https://doi.org/10.1007/S00339-021-04724-1

85. Sait HH, Hussain A, Bassyouni M, Ali I, Kanthasamy R, Ayodele BV, Elhenawy Y (2022) Hydrogen-rich syngas and biochar production by non-catalytic valorization of date palm seeds. Energies 15:2727

86. Moneim MA, El Naggar AMA, El Sayed HA, Mostafa MS, Khalil NM, Hassan MED (2018) Direct conversion of an agricultural solid waste to hydrocarbon gases via the pyrolysis technique. Egypt J Pet 27:991–995

87. Eloffy MG, Elgarahy AM, Saber AN, Hammad A, El-Sherif DM, Shehata M, Mohsen A, Elwakeel KZ (2022) Biomass-to-sustainable biohydrogen: insights into the production routes, and technical challenges. Chem Eng J Adv 12

88. Nabil S, Hammad AS, El-Bery HM, Shalaby EA, El-Shazly AH (2021) The CO_2 photoconversion over reduced graphene oxide based on Ag/TiO$_2$ photocatalyst in an advanced meso-scale continuous-flow photochemical reactor. https://doi.org/10.1007/s11356-021-13090-7

89. Awad ME, Shaltout NA, Madkour FF, Abu El-Regal M, El-Sayed HS, El-Wazzan E (2019) Ocean acidification impact on the grooved carpet shell clam (*Ruditapes decussatus*). Egypt J Aquat Biol Fish 23:169–182

90. Al-Zaydi KM, Petrier C, Mousally SMM, Arab ST, Refat MS (2019) Sonochemical degradation of benzothiophene (BT) in deionized water, natural water and sea water. Molecules 24

91. Abu El-Regal MA, Kon T (2019) First record of the Schindler's fish, *Schindleria praematura* (Actinopterygii: Perciformes: Schindleriidae), from the red sea. Acta Ichthyol Piscat 49:75–78

92. Shaltout K, El-Bana M, Galal T (2019) Coastal lakes as hot spots for plant diversity in Egypt. In: Handbook of environmental chemistry. Springer, pp 129–146

93. Elgarahy AM, Akhdhar A, Elwakeel KZ (2021) Microplastics prevalence, interactions, and remediation in the aquatic environment: a critical review. J Environ Chem Eng 9

94. Abdelhady AA, Seuss B, Hassan HF (2019) Stratigraphic ranking of selected invertebrate fossils: a quantitative approach at different temporal and geographic scales. Palaeontol Electron 22. https://doi.org/10.26879/912

95. Assaeed AM, Al-Rowaily SL, El-Bana MI, Hegazy AK, Dar BA, Abd-Elgawad AM (2020) Functional traits plasticity of the invasive herb *Argemone ochroleuca* sweet in different arid habitats. Plants 9:1–16. https://doi.org/10.3390/plants9101268

96. Yahia A, Mashaly I, El-Bana M, Rizk R, El-Sherbeny G (2020) Intraspecific variations in functional and molecular traits of near-endemic *Onopordum alexandrinum* Boiss. in natural and anthropogenic habitats along the western Mediterranean coast of Egypt: implications for conservation. Plants 9:1–19. https://doi.org/10.3390/plants9081041
97. Abdou HA, Ellelly NN, Elamer AA, Hussainey K, Yazdifar H (2021) Corporate governance and earnings management nexus: evidence from the UK and Egypt using neural networks. Int J Financ Econ 26:6281–6311. https://doi.org/10.1002/ijfe.2120

An Overview of LCA Integration Methods at the Early Design Stage Towards National Application

Sally Rashad Hassan [iD]**, Naglaa Ali Megahed** [iD]**,**
Osama Mahmoud Abo Eleinen, and Asmaa Mohamed Hassan [iD]

1 Introduction

The construction sector is responsible for 36% of final energy consumption and 39% of energy-related greenhouse gas (GHG) emissions in 2018, 11% of which came from the production of building products and materials [1]. It is also in charge of 40% of natural resource depletion and 25% of waste generation [2]. Therefore, the architecture, engineering, and construction (AEC) sector started to adopt strategies, methodologies, and technologies that minimize these percentages and promote sustainable development [3–8].

The life cycle assessment (LCA) is a methodology that evaluates the environmental impact of a process or product over its entire life cycle [9] and has lately proven its reliability in the construction field. Integrating LCA in the early design stage can support the decision-making process and enable designers and stakeholders to determine the building's shape, components, materials, and features based on scientific methodology measuring the environmental impact. Research interest in that field is growing and presenting frameworks, methodologies, approaches, and tools. The UN's Sustainable Development Goals (SDGs) can be reinforced by integrating LCA into the design process. That possibly contributes to at least four SDGs; Sustainable Cities and Communities, Responsible Consumption and Production, Climate Action, and Affordable and Clean Energy. The presented study is driven by research questions as follows:

- What is the situation in Egypt regarding LCA studies?

S. R. Hassan (✉) · N. A. Megahed · O. M. A. Eleinen · A. M. Hassan
Architectural Engineering and Urban Planning Department, Faculty of Engineering, Port Said University, Port Said, Egypt
e-mail: sally.rashad@eng.psu.edu.eg

N. A. Megahed
e-mail: naglaaali257@eng.psu.edu.eg

- What are the current methods used to integrate LCA at the early design stage and how it is implemented?

This paper aims to present an overview of studies and attempts regarding the integration of LCA at the initial design stage to reach a method for a national early decision tool facilitating environmentally responsible choices from designers. The first two sections present background and LCA studies related to buildings in Egypt, then the used methodologies for the study are clarified. Afterward, the subsequent results section first offers the bibliometric analysis, then the integration methods. In the end, the conclusion and recommendations are outlined.

2 Background

Publications in the last decade regarding the LCA of building at the design stage are rapidly increasing (see Fig. 1). The design stage is more covered in research than the early stage or streamlined LCA. The integration of building LCA and early design stages was briefly covered in publications. Three review articles investigated Building Information Modelling (BIM)-LCA integration as Soust et al. [10] reviewed the recent studies which used BIM-based LCA focusing on how can BIM simplify data input, and optimize output data and results during the LCA application in buildings, taking advantage of data exchange and facilitating interoperability between different software. The study proposed the challenges and recommendations for BIM and LCA tools to be developed. Another review paper on BIM-LCA integration by Obrecht et al. [11] identified the current integration methods, shedding the light on positives and negatives of the integration process, 60 case studies were analyzed and 16 of which are during the early design stage. Moreover, Safari and AzariJafari [2] sought to promote the progress of BIM-based LCA by proposing research opportunities in the conducted systematic review. By analyzing the published articles from many aspects based on the ISO framework, BIM-based LCA was found to be lacking automation of data exchange. It also revealed areas of interest such as the opportunity to develop a local LCA database adapted to the level of development (LOD) models, involving sensitivity analysis in the design process, and comparing different LODs serve as a benchmark for early-stage decision-making.

Jusselme et al. [12] presented methods to improve the usability of LCA at the initial design stage by addressing the three primary problems with the application of LCA (time consumption, lack of design details, and the non-reproducibility of results) and the techniques that can currently deal with them. In the end, the paper outlines the composition and structure of an LCA-based data-driven design approach. Pomponi and Moncaster [13] took a quite different perspective in reviewing LCA studies as their article investigated in detail embodied carbon assessments in some case studies considering the used data and assumptions finding out fundamental limitations in comparing results and drawing conclusions due to variations of the applied methods, they recommend for more transparency of LCA studies.
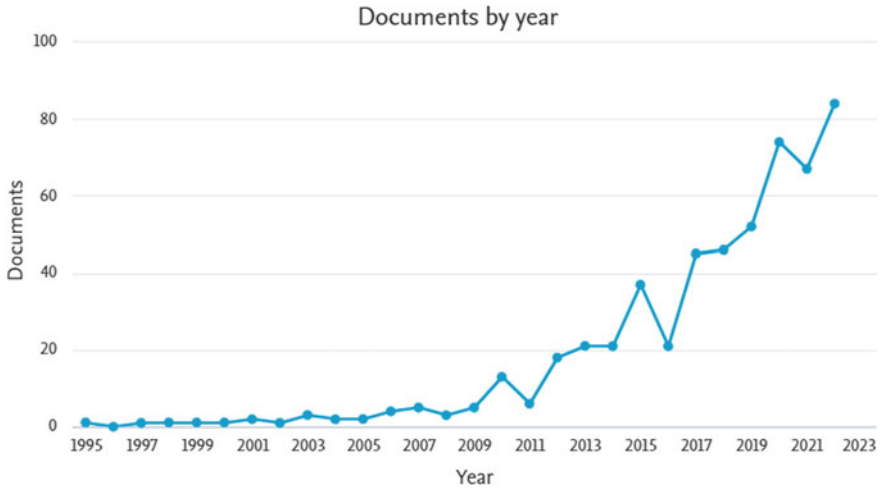
Fig. 1 The increase of publications over the years (1995–2022) (*source* Scopus)

Roberts et al. [14] conducted a systematic review to determine how life cycle assessment (LCA) is combined at various stages of the building design process by reviewing 108 publications. Finding out that LCA is generally used late in the design process also the review demonstrated that LCA still faces some challenges and limitations. Three main trends have also formed the results, the first two are coupling LCA with BIM or Life Cycle Costing (LCC) and the third promising trend is the parametric methods. Furthermore, The IEA-EBC Program, an international energy research and innovation program in the buildings and communities field, Launched Annex 72 project (2016–2022),which mission is to establish guidelines, standards, and tools for building design and planning that fit different regions integrating LCA [15]. Liying Li's review [16] discussed the integration of climate change impact in the new building design process to propose recommendations for LCA tool developers, researchers, and policy-makers.

The current published literature review revealed that there are still issues and gaps with implementing LCA at the early design stage, national studies are very constrained, and parametric methods can be advantageous for the early stage because they offer and compare a variety of options in addition to issues that should be geared towards interoperability facilitation with BIM. The next section will discuss national studies pertaining to LCA for buildings, but among the few presented national publications, only two are related to the design stage.

3   LCA Studies Related to Buildings in Egypt

According to a review of LCA studies carried out in Africa, there aren't even half as many publications on the entire continent as there are in Germany, a developed country [17]. Only 8% of all LCA publications (199 publications) deal with construction, and in Egypt, there have been about ten LCA publications in the past ten years that consider buildings [17, 18]. This section reviews LCA studies related to buildings in Egypt and discusses the local constraints or boundaries like the country codes.

Few publications discussed LCA concerning buildings and building materials in Egypt, Ali et al. [19] implemented an initiative LCA of a typical residential building in Egypt and carried out a comprehensive building LCA in accordance with ISO 14040 standards. Two additional studies looked at the impact of structural and construction systems, as Morsi et al. [20] conducted an LCA of an Egyptian residential building using the Tally plugin to look at the stages and components that had the biggest influence, while Abouhamad and Abu-Hamd [21] developed a life cycle assessment framework for embodied environmental impacts of building construction systems to aid in decision-making during the early design phase. On the other hand, four publications provided LCA studies related to materials and components of buildings as Dabaieh et al. [22] compared the embodied energy of two kinds of bricks, and Ali et al. [23] investigated the LCA of the cement industry in Egypt, while Elkhayat et al. [24] used LCA to compare the energy performance and the environmental impacts of three glazing systems for office buildings in the hot desert climate zone. Ay-Eldeen and Negm [25] assessed the GWP of a pile foundation construction stage. On the other hand, another study by Ali et al. [26] suggested a framework to develop a national life cycle inventory (LCI) database. Furthermore, in the construction management scope, Morsi et al. [27] examined the potential and difficulties of using an LCA-BIM integration technique to create a sustainable management process. The results or outcome of these studies might support the design process but it is clear that there is no national study that investigated the architectural design concerning LCA as a guide, also Abouhamad and Abu-Hamd [21] or Gomaa et al. [28] research concerned early design but neglected national codes [29, 30].

National building codes in Egypt related to energy efficiency are "The Egyptian code for improving energy efficiency use in buildings," ECP 306/1-2005 (Part one: residential buildings) [29] followed by a version for commercial buildings, ECP 306/2-2009 (Part two: commercial buildings) [30]. They divide the area of Egypt into eight regions and determine the requirements for each region based on a group of factors. Other codes related to the material properties of external walls [31, 32] can also form constraints. The results of this review opened the door for a framework of a national LCA prototype tool that employ generative design during the early stage to support decisions for exterior walls of residential buildings in Egypt [33].

4 Methodology

The methodology used for this research can be divided into three steps. The first step is using Preferred Reporting Items for Systematic Reviews and Meta-Analysis (PRISMA) for database development. The second step is using the Biblioshiny tool for bibliometric analysis of the results. After filtering the data, the third step is a literature review performed on the final elected publications arranged and classified from the author's point of view.

First, a thorough literature search was conducted on Scopus and the WoS core collection to find terms associated with the topic. The used keywords for the research are "LCA" OR "life cycle assessment" AND "building" AND "design" AND "stage" within titles, abstracts, and keywords and filters were used for subject areas, source type, and language. The total number of publications after removing duplicates is 648, then to make sure that only studies met the goals and parameters of the micro-scale, the titles and abstracts of the publications were manually screened, resulting in 264 publications. The screening step filtered the results, and records related to manufacturing, civil, infrastructure, and assessment at other stages than design were excluded, as the focus is the decision support during the design phase, including embodied impact and choosing between alternatives.

Lastly, to determine which studies should continue as part of the analysis, the full texts of 264 articles were examined, which led to 72 publications related to the topic, as shown in (Fig. 2).

5 Results and Discussion

5.1 Overall Bibliometric Analysis

The Biblioshiny tool's results can give a general overview of the bibliometric analysis. Since the number of publications is not that vast, insightful information on research progress, trends, and opportunities is provided using author keywords and a thematic map. Then a literature review of the selected studies is presented and discussed.

Investigating the trending topics is essentially based on analysis of keywords used by authors in the field for their publications. In this context, the most frequent keywords over the last years in publications related to the topic are presented in Fig. 3. It visualizes the word cloud of the authors' most used keywords in LCA and building design publications. Around 2010, the majority of these keywords started to show up significantly in academic fields, and they have since increased.

The four quadrants (the niche themes, emerging or declining themes, motor themes, and basic themes) of the thematic map can be used to intuitively plot and group the keywords to understand research themes (Fig. 4).

The keywords "recycling," "building material," and "construction and demolition waste" present niche themes, which means express the extreme specialty of these
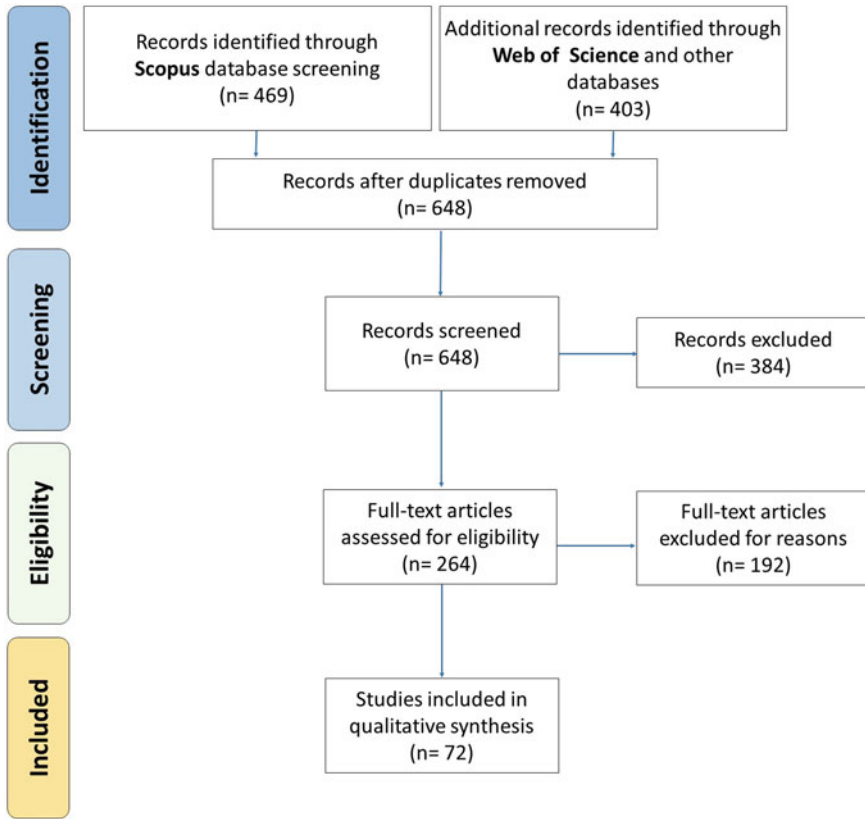
Fig. 2 Flowchart for the selection process based on the PRISMA method (*source* The authors)

themes. However, the keywords "life-cycle assessment," "early stage," "emissions," "framework," and "environmental impacts" are considered emerging or declining themes, even though their important. On the other hand, the keywords "life cycle assessment," "architectural design," "environmental impacts," and "eco-design" are considered motor themes, which demonstrate a well-developed and vital themes. The keywords "life cycle analysis," "building," "environmental impacts assessment," "construction material," and "design stage" appears to be trapped between basic and motor themes, which means they are significant and leading theme in the research field. Some emerging or declining themes (Q3) cross over into basic themes (Q4), indicating that some of the themes' components are fundamental and essential for the field's development.

According to thematic analysis, upcoming work are required to evolve themes like "design stage" and "construction material" aligned with life cycle analysis. Also, the dimensions of demolition, waste, and recycling need consideration at the design stage. Therefore, further research should adopt and address such themes.

Fig. 3 A word cloud showing a graphic of the most popular keywords in the 264 publications (*source* Biblioshiny tool)
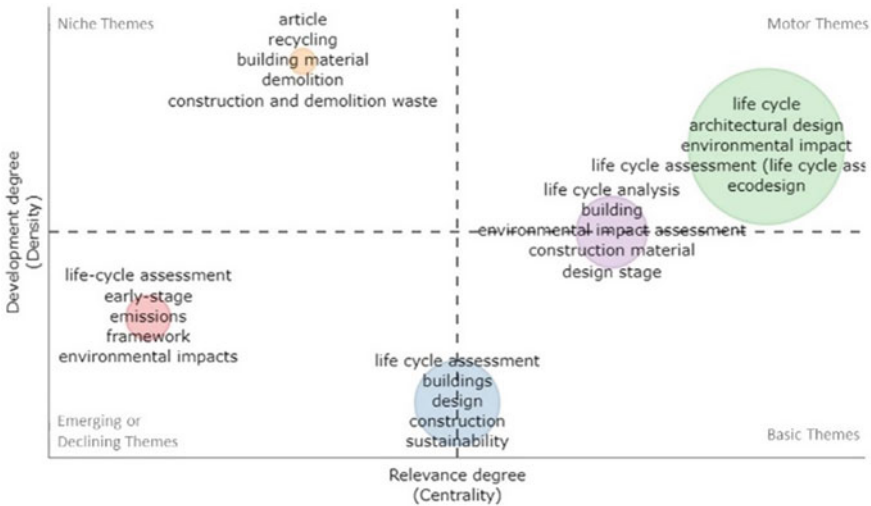
Fig. 4 Thematic map of the most frequent keywords (*source* Biblioshiny tool)

According to countries, Fig. 5 presents the countries' scientific production, which illustrates the leading nations in that scientific field. The results show that China accomplished 65 documents, Switzerland 60 documents, and England 57 documents.
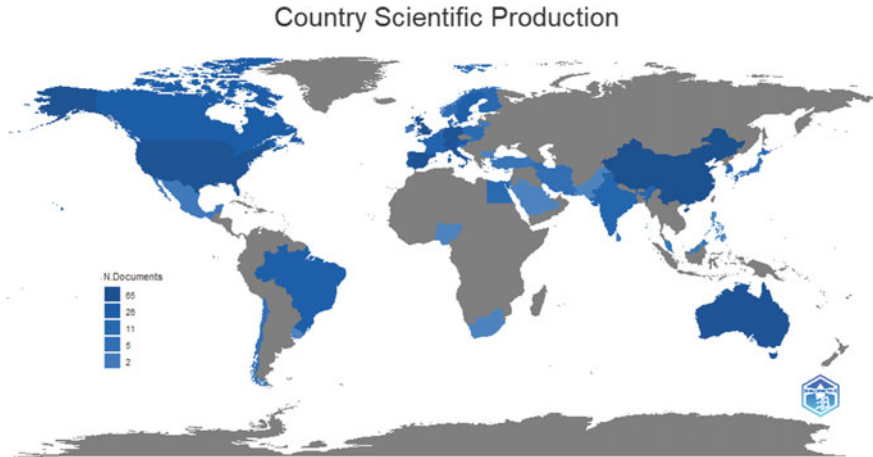
Fig. 5 Map visualization for the number of documents per country (*source* Biblioshiny tool)

5.2   LCA Integration Methods

The output of the bibliometric analysis emphasized the importance of that trending topic worldwide, and the objective of this review is to extract the experience of international trials to see the potential of application on the national level. The selected publications representing the research results are divided into two main sections. The first section handled the BIM and LCA integration, it proposes the attempts of early design stage integration. The second section reviews parametric methods used for conducting LCA (see Fig. 6).

5.2.1   BIM and LCA Integration

The previous studies on BIM-LCA integration during the design stage are mainly targeting the following purposes:

- Revealing challenges and research gaps in the integration of BIM-LCA approaches [2, 10, 34–37].
- Case studies analysis by interpretation or evaluation [11, 34–36, 38].
- Establishing a framework, method, or tool for BIM and LCA integration [38–40].
- Simplifying LCA application or facilitating interoperability and data exchange [2, 10, 11, 40, 41].

Early design decisions have a significant effect on a building's environmental impact, and designers need to be directed to which decisions are preferable [42]. Integrating LCA in the building design process is an increasing research field, which is aiming at the evaluation and improvement of the life cycle performance of buildings [43]. BIM offers quantities for Life Cycle Inventory (LCI) used in LCA, which gives
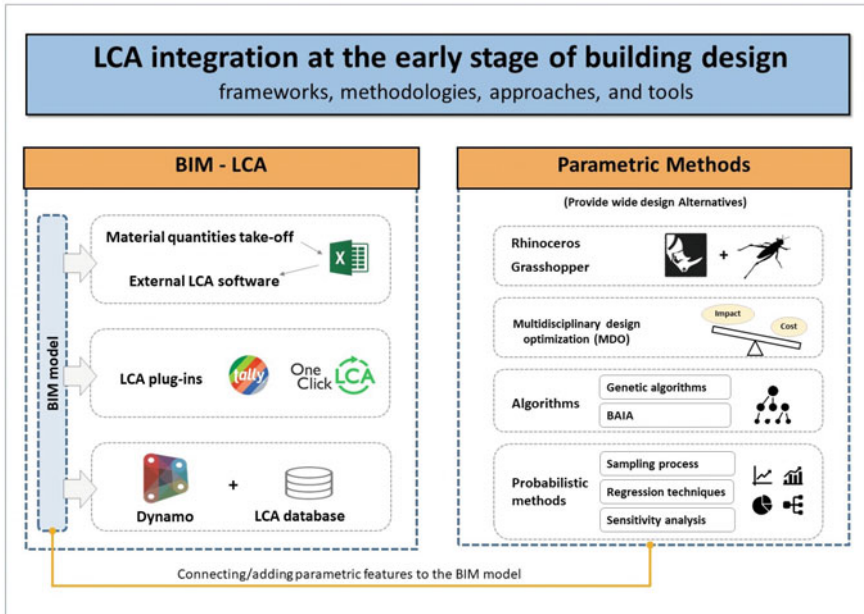
Fig. 6 LCA integration at the early stage of building design (*source* The authors)

a good and easy potential for impact calculations, either by using a plugin tool like Tally and One Click or by data extraction and exportation to an external LCA software.

The approach of integrating Life Cycle Assessment (LCA) in the early design phase has been introduced in previous studies through many aspects. For instance, Röck et al. [43] proposed an approach using BIM to assess a wide variety of construction options and their embodied environmental impact mainly focused on materials, the approach enables communication of LCA results and visual design to offer assistance during the design stage. Rezaei et al. [44] investigated the integration of BIM and LCA in both early and detailed design stages of a residential building in Quebec, Canada by developing a framework and applying it to the case study then the environmental impacts of the building stages and components were calculated to decide the best building assembly options from an environmental standpoint. Hollberg et al. [45] evaluated BIM-based LCA results for building design mainly concentrated on the embodied global warming potential (GWP) throughout the entire design process of an existing building, offering the first application of a BIM-LCA tool as environmental performance assessments during the entire design process. Cavalliere et al. [46] suggested a novel approach to evaluate the flexibility level of buildings within a BIM environment leading to more flexible and sustainable design choices, Cavalliere et al. [47] also proposed a new method for applying LCA repeatedly over the entire building design process to assess the embodied environmental impacts by using the BIM data. Basbagill et al. [42] method targeted BIM design choices at the early

design stage, taking into consideration: building shape, material options, and thicknesses; it used sensitivity analysis which will be discussed later. Shadram et al. [48] offered a framework that supports design decisions while facilitating interoperability between BIM and LCA and it was also tested by a developed prototype. Shadram et al. [49] also presented a BIM-based method to manage the trade-off between embodied and operational energy at early stages. Santos et al. developed and tested a tool (BIMEELCA) for both streamlined and complete LCA coupled with LCC through several articles [3, 50, 51].

On the national level, Eichner and Elsharawy [52] proposed an iterative design method for buildings based on LCA with the goal of establishing a path toward low or zero environmental impact levels during the concept phase in their conference paper "Life cycle assessment (LCA) based concept design method for potential zero-emission residential building".

No doubt that BIM facilitated the LCA process by providing an easy material take-off, but the main common observation of studies that attempt to integrate LCA and BIM at early design using a plugin or data extraction is the limited options of design alternatives. Uncertainties are not significantly considered as well. Most of the studies are classified as conventional or static LCA; only a few studies offered parametric methods through a suggested approach or framework that connects the BIM model with an external parametric tool.

5.2.2 Parametric Methods and LCA

Much interest is recently dedicated to generative processes in design [53]. New technologies in the field of artificial intelligence and computational tools made new horizons in the interaction between computers and the design process [54–57]. Minimizing the environmental impacts of buildings using the parametric design where design alternatives are available for designers [14]. Using the parametric design exceeds traditional LCA tools in the early design process in both matters of time and determining optimal design solutions [58].

Hasik et al. [59] classified parametric and sensitivity LCA studies into two categories, the first category try to investigate the effect of LCA methods, assumptions, and other boundaries on the study results and outcome while the second category goal is to improve the selection of the building design.

Grasshopper

Reviewed literature about combining LCA with the parametric methods during the design presented publications that used Grasshopper to conduct a parametric design for buildings [58, 60–63] by integrating a simplified LCA with the design process. On the national level, Gomaa et al. [28] developed a framework that integrates LCA with the conventional design process to be applied at the early design stages using Grasshopper with Bombyx [63] plugin for embodied energy calculations, and other

plugins for the operational energy calculations, Then testing it on a case study in Alexandria, Egypt. But Roberts et al. [14] consider that using Grasshopper for parametric design needs to be further developed. Another method that uses a set of parameters or variables to simplify the design process is using algorithms. The following subsections will unveil the used types of algorithms for LCA.

Multidisciplinary Design Optimization (MDO)

Initially developed in the aerospace industry in the 1970s, multidisciplinary design optimization (MDO) techniques have since been applied to a variety of other disciplines. Architectural design is one such example. Designers can navigate a wide range of design options using MDO methods, quickly assess a large number of design options, and identify optimal or nearly optimal solutions [64]. It was also used by some studies [65, 66] to investigate the conflicts and trade-offs between life-cycle environmental impact and cost but like any other method, it has limitations [64]. Basbagill et al. [64] proposed a multi-objective feedback approach to evaluate sequential design choices. The suggested method uses probability distribution functions to assist sequential decision-making processes, which sets it apart from other MDO methods.

Genetic Algorithms

Genetic algorithms were early used in green building design optimization by Caldas and Norford who proposed a computer tool that applies genetic algorithms to find the best window placement and size options for office buildings, focusing on thermal and lighting performance in a building [54]. Further LCA was integrated into the parametric design process. Several studies used a multi-objective genetic algorithm for solving the trade-offs between cost and environmental impacts to support the design decision for example the presented framework by Inyim and Zhu [67] study allowing the selection of the best possible alternatives during the entire design phase. Wang et al. [68] identified several optimal solutions for green building design. Schwartz et al. [69] presented a decision support tool for building design balancing Life Cycle Carbon Footprint (LCCF) and Life Cycle Costs (LCC) using a type of genetic algorithm. Genetic algorithm is also used for optimization in the refurbishment and renovation of buildings [70, 71]. Flager et al. [72] used it as well for building envelope optimization while Azari et al. [73] investigated the ideal building envelope design focusing on energy use and LCA. Not only genetic algorithms are used in LCA studies, but also other algorithms and probabilistic methods. The two following subsections will discuss these methods.

Building Attribute to Impact Algorithm (BAIA)

"BAIA is a streamlined LCA method that incorporates uncertainty and probabilistic triage to calculate impact predictions and to identify influential attributes for the whole building life-cycle" [74]. Using Monte Carlo simulation, BAIA employs algorithms to reduce the building design process to a set of parameters or variables [14].

Hester et al. [74] demonstrated that the use of streamlined probabilistic LCA at the primary stages of the design process by analyzing twelve design options for a hypothetical single-family residential building using the available level of details can inform decision-making to choose the preferred design. Going further with BAIA, Hester et al. [75] tested it coupled with two design guidance methods to identify the features of buildings with near optimum impacts and costs to reveal that genetic optimization is most efficient leading to more optimal solutions with better flexibility by analyzing design variables related to geometry, systems, and occupants behavior.

Uncertainties and Sensitivity Analysis

Using sampling process, sensitivity analysis, regression techniques, or any other probabilistic methods became very effective at early LCA as it assists users to try a significant number of solutions by iteratively testing design variables.

Tecchio et al. [76] demonstrated that even at low levels of accuracy, users could statistically resolve a significant number of comparisons and options by proposing a streamlined LCA approach (structured under-specification). Their approach can be conducted even when only a few details about the design are decided, then Tecchio et al. [77] further tested the method combined with probabilistic triage on a series of building typologies. Basbagill et al. [42] presented a method for applying LCA at the early design stage. It employs sensitivity analysis to guide the reduction of the embodied impacts of building components, considering materials and dimensioning options. Hester et al. [78] used quantitative, probabilistic analyses (regression-based energy metamodel) for estimating the energy consumption at the initial stages of the design process while Xikai et al. [79] compared four regression models for the estimation of carbon emissions during a building's lifecycle using designing aspects. Some studies also used sensitivity analysis to determine the domain factors that affect LCA results [80, 81].

6 Conclusion and Recommendations

An overview of the Life Cycle Assessment (LCA) of buildings at the early design stage was conducted to investigate the potential of implementation in the Egyptian environment. The introduction and background on the topic and publication of LCA related to buildings in Egypt and national codes prefaced the study. The LCA studies

in Egypt related to building appeared to be limited. The methodology first applied PRISMA for database development, and the results were fed into the Biblioshiny tool for the bibliometric analysis, then the main used methods and attempts of early integration were classified, discussed, and analyzed to understand the potential of national application. Summary of main findings can be summed up as follows:

- Bibliometric analysis results provided insightful data on research progress, trends, and possibilities. It revealed the frequently used keywords and each country's scientific production.
- Results on BIM and LCA integration at the design and early design stage were discussed to confirm the obvious contribution of BIM on the LCA implementation and development, but the need for comparing various scenarios at the initial design stage requires more enhancements, as most of this method application can be described as traditional or static.
- Parametric LCA illustrates a beneficial influence on the early design process of buildings, as revealed by the reviewed and analysis studies. The results presented various methods by the selected publications, including Grasshopper, Multidisciplinary design optimization (MDO), algorithms, Sensitivity analysis, and other probabilistic methods.

The impact of using LCA on the design process, especially at the initial design stages, can significantly affect many aspects of building design and material selection; the study provided a comprehensive understanding of the current integration methods and the situation in Egypt to be the first step for national application.

Recommendations for future studies related to LCA in Egypt will first comprise a national database containing environmental data on building materials and products as well as building codes; then facilitate the application of LCA at the early building design by developing a tool that uses input parameters and generative algorithms methods to inform architects and designers with the environmental impact or make suggestions based on it. An initiative toward developing such a tool for exterior walls of residential buildings in Egypt, is conducted by the authors in their publication [33].

References

1. Global Alliance for Buildings and Construction IEA and the UNEP (2019) 2019 global status report for buildings and construction: towards a zero-emission, efficient and resilient buildings and construction sector
2. Safari K, AzariJafari H (2021) Challenges and opportunities for integrating BIM and LCA: methodological choices and framework development. Sustain Cities Soc 67
3. Santos R, Aguiar Costa A, Silvestre JD, Pyl L (2020) Development of a BIM-based environmental and economic life cycle assessment tool. J Clean Prod 265. https://doi.org/10.1016/j.jclepro.2020.121705
4. Megahed NA, Hassan AM (2022) Evolution of BIM to DTs: a paradigm shift for the post-pandemic AECO industry. Urban Sci 6

5. Noaman DS, Moneer SA, Megahed NA, El-Ghafour SA (2022) Integration of active solar cooling technology into passively designed facade in hot climates. J Build Eng 56:104658. https://doi.org/10.1016/J.JOBE.2022.104658

6. Sameer H, Behem G, Mostert C, Bringezu S (2022) Comparative analysis of resource and climate footprints for different heating systems in building information modeling. Buildings 12.https://doi.org/10.3390/buildings12111824

7. da Costa TP, Gillespie J, Pelc K, Adefisan A, Adefisan M, Ramanathan R, Murphy F (2023) Life cycle assessment tool for food supply chain environmental evaluation. Sustainability 15.https://doi.org/10.3390/su15010718

8. Hassan AM (2023) UMC-based models: an integrating UMC performance analysis and numerical methods. Renew Sustain Energy Rev 181:113307. https://doi.org/10.1016/J.RSER.2023.113307

9. ISO (2006) 14040: Environmental management—life cycle assessment—principles and framework. International Organization for Standardization

10. Soust-Verdaguer B, Llatas C, García-Martínez A (2017) Critical review of BIM-based LCA method to buildings. Energy Build 136

11. Obrecht TP, Röck M, Hoxha E, Passer A (2020) BIM and LCA integration: a systematic literature review. Sustainability 12

12. Jusselme T, Rey E, Andersen M (2018) An integrative approach for embodied energy: towards an LCA-based data-driven design method. Rene. Sustain Energy Rev 88

13. Pomponi F, Moncaster A (2018) Scrutinising embodied carbon in buildings: the next performance gap made manifest. Renew Sustain Energy Rev 81

14. Roberts M, Allen S, Coley D (2020) Life cycle assessment in the building design process—a systematic literature review. Build Environ 185:107274. https://doi.org/10.1016/j.buildenv.2020.107274

15. The International Energy Agency's Energy in Buildings and Communities Annex 72

16. Li L (2021) Integrating climate change impact in new building design process: a review of building life cycle carbon emission assessment methodologies. Clean Eng Technol 5:100286. https://doi.org/10.1016/J.CLET.2021.100286

17. Karkour S, Rachid S, Maaoui M, Lin C (2021) Status of life cycle assessment (LCA) in Africa

18. Yacout DMM (2019) Assessing status of life cycle assessment studies in Egypt. Curr Appl Sci Technol 19

19. Ali AAMM, Negm AM, Bady MF, Ibrahim MGE (2015) Environmental life cycle assessment of a residential building in Egypt: a case study. Procedia Technol 19:349–356. https://doi.org/10.1016/j.protcy.2015.02.050

20. Morsi DMA, Ismaeel WSE, El-Hamed AEA (2020) Life cycle assessment of a residential building in Egypt: a case study. IOP Conf Ser Mater Sci Eng 974.https://doi.org/10.1088/1757-899X/974/1/012028

21. Abouhamad M, Abu-Hamd M (2021) Life cycle assessment framework for embodied environmental impacts of building construction systems. Sustainability 13.https://doi.org/10.3390/su13020461

22. Dabaieh M, Heinonen J, El-Mahdy D, Hassan DM (2020) A comparative study of life cycle carbon emissions and embodied energy between sun-dried bricks and fired clay bricks. J Clean Prod 275:122998. https://doi.org/10.1016/j.jclepro.2020.122998

23. Ali AAMM, Negm AM, Bady MF, Ibrahim MGE, Suzuki M (2016) Environmental impact assessment of the Egyptian cement industry based on a life-cycle assessment approach: a comparative study between Egyptian and Swiss plants. Clean Technol Environ Policy 18:1053–1068. https://doi.org/10.1007/s10098-016-1096-0

24. Elkhayat YO, Ibrahim MG, Tokimatsu K, Ali AAMM (2020) A comparative life cycle assessment of three high-performance glazing systems for office buildings in a hot desert climate zone. Clean Technol Environ Policy 22:1499–1515. https://doi.org/10.1007/s10098-020-01891-2

25. Ay-Eldeen MK, Negm AM (2015) Global warming potential impact due to pile foundation construction using life cycle assessment. Electron J Geotech Eng 20

26. Ali AAMM, Negm AM, Bady MF, Ibrahim MGE (2014) Moving towards an Egyptian national life cycle inventory database. Int J Life Cycle Assess 19:1551–1558. https://doi.org/10.1007/s11367-014-0760-z

27. Morsi DMA, Ismaeel WSE, El Hamed AEA, Othman AAE (2020) Applying LCA-BIM integration for a sustainable management process. In: ARCOM 2020—Association of researchers in construction management, 36th annual conference 2020—proceedings

28. Gomaa M, Farghaly T, El Sayad Z (2021) Optimizing a life cycle assessment-based design decision support system towards eco-conscious architecture. In: Computational methods and experimental measurements, vol XX

29. The Egyptian Code Permanent Committee (2005) The Egyptian code for improving energy efficiency use in buildings (Part one: residential Buildings). Housing and Building National Research Center, Egypt

30. The Egyptian Code Permanent Committee (2009) The Egyptian code for improving the efficiency of energy use in buildings (Part two: commercial buildings). Housing and Building National Research Center, Egypt

31. The Egyptian Code Permanent Committee (2005) The Egyptian code for masonry design and execution. Housing and Building National Research Center, Egypt

32. The Egyptian General Standards Permanent Committee (1998) Specifications for thermal insulation: design and execution requirements. Housing and Building National Research Center, Egypt

33. Hassan SR, Megahed NA, Abo Eleinen OM, Hassan AM (2022) Toward a national life cycle assessment tool: generative design for early decision support. Energy Build 267:112144. https://doi.org/10.1016/J.ENBUILD.2022.112144

34. Obrecht TP, Röck M, Hoxha E, Passer A (2020) The challenge of integrating Life Cycle Assessment in the building design process—a systematic literature review of BIM-LCA workflows. IOP Conf Ser: Earth Environ Sci

35. Mora TD, Bolzonello E, Cavalliere C, Peron F (2020) Key parameters featuring BIM-LCA integration in buildings: a practical review of the current trends. Sustainability 12.https://doi.org/10.3390/su12177182

36. Teng Y, Xu J, Pan W, Zhang Y (2022) A systematic review of the integration of building information modeling into life cycle assessment. Build Environ 221:109260. https://doi.org/10.1016/J.BUILDENV.2022.109260

37. Tam VW, Zhou Y, Illankoon C, Le KN (2022) A critical review on BIM and LCA integration using the ISO 14040 framework. Build Environ 213:108865. https://doi.org/10.1016/J.BUILDENV.2022.108865

38. Nilsen M, Bohne RA (2019) Evaluation of BIM based LCA in early design phase (low LOD) of buildings. IOP Conf Ser: Earth Environ Sci

39. Alwan Z, Nawarathna A, Ayman R, Zhu M, ElGhazi Y (2021) Framework for parametric assessment of operational and embodied energy impacts utilising BIM. J Build Eng 42:102768. https://doi.org/10.1016/j.jobe.2021.102768

40. Kotula BM, Kamari A (2020) Development of a BIM-based LCA tool to support sustainable building design during the early design stage. In: Proceedings of the international conference of Architectural Science Association

41. Sobhkhiz S, Taghaddos H, Rezvani M, Ramezanianpour AM (2021) Utilization of semantic web technologies to improve BIM-LCA applications. Autom Constr 130:103842. https://doi.org/10.1016/j.autcon.2021.103842

42. Basbagill J, Flager F, Lepech M, Fischer M (2013) Application of life-cycle assessment to early stage building design for reduced embodied environmental impacts. Build Environ 60:81–92. https://doi.org/10.1016/j.buildenv.2012.11.009

43. Röck M, Hollberg A, Habert G, Passer A (2018) LCA and BIM : Visualization of environmental potentials in building construction at early design stages. Build Environ 140:153–161. https://doi.org/10.1016/j.buildenv.2018.05.006

44. Rezaei F, Bulle C, Lesage P (2019) Integrating building information modeling and life cycle assessment in the early and detailed building design stages. Build Environ 153:158–167. https://doi.org/10.1016/j.buildenv.2019.01.034

45. Hollberg A, Genova G, Habert G (2020) Evaluation of BIM-based LCA results for building design. Autom Constr 109:102972. https://doi.org/10.1016/j.autcon.2019.102972
46. Cavalliere C, Dell'Osso GR, Favia F, Lovicario M (2019) BIM-based assessment metrics for the functional flexibility of building designs. Autom Constr 107.https://doi.org/10.1016/j.autcon.2019.102925
47. Cavalliere C, Habert G, Dell'Osso GR, Hollberg A (2019) Continuous BIM-based assessment of embodied environmental impacts throughout the design process. J Clean Prod 211:941–952. https://doi.org/10.1016/j.jclepro.2018.11.247
48. Shadram F, Johansson TD, Lu W, Schade J, Olofsson T (2016) An integrated BIM-based framework for minimizing embodied energy during building design. Energy Build 128.https://doi.org/10.1016/j.enbuild.2016.07.007
49. Shadram F, Mukkavaara J, Schade J, Sandberg M, Olofsson T (2017) A BIM-based method for analyzing the trade-off between embodied and operational energy. In: ICCREM 2017: industry regulation and sustainable development—proceedings of the international conference on construction and real estate management 2017
50. Santos R, Costa AA, Silvestre JD, Vandenbergh T, Pyl L (2020) BIM-based life cycle assessment and life cycle costing of an office building in Western Europe. Build Environ 169:106568. https://doi.org/10.1016/j.buildenv.2019.106568
51. Santos R, Costa AA, Silvestre JD, Pyl L (2019) Integration of LCA and LCC analysis within a BIM-based environment. Autom Constr 103:127–149. https://doi.org/10.1016/j.autcon.2019.02.011
52. Eichner MJ, Elsharawy HH (2020) Life cycle assessment (LCA) based concept design method for potential zero emission residential building. IOP Conf Ser Earth Environ Sci 410:012301. https://doi.org/10.1088/1755-1315/410/1/012031
53. Hassan AM, Megahed NA (2022) Improving urban energy resilience with an integrative framework based on machine learning methods. Archit Eng 7. https://doi.org/10.23968/2500-0055-2022-7-4-17-35
54. Caldas LG, Norford LK (2002) A design optimization tool based on a genetic algorithm. Autom Constr 11:173–184. https://doi.org/10.1016/S0926-5805(00)00096-0
55. Shehata AO, Megahed NA, Shahda MM, Hassan AM (2022) (3Ts) Green conservation framework: a hierarchical-based sustainability approach. Build Environ 224:109523. https://doi.org/10.1016/J.BUILDENV.2022.109523
56. El-Mowafy BN, Elmokadem AA, Waseef AA (2022) Evaluating adaptive facade performance in early building design stage: an integrated daylighting simulation and machine learning. In: Hassanien AE, Rizk RY, Snášel V, Abdel-Kader RF (eds) The 8th international conference on advanced machine learning and technologies and applications (AMLTA2022). Springer, Cham, pp 211–223
57. Hassan AM, Megahed NA (2022) Urban planning and development improving urban energy resilience with an integrative. Archit Eng. https://doi.org/10.23968/2500-0055-2022-7-4-17-35
58. Hollberg A, Ruth J (2016) LCA in architectural design—a parametric approach. Int J Life Cycle Assess 21:943–960. https://doi.org/10.1007/s11367-016-1065-1
59. Hasik V, Ororbia M, Warn GP, Bilec MM (2019) Whole building life cycle environmental impacts and costs: a sensitivity study of design and service decisions. Build Environ 163:106316. https://doi.org/10.1016/j.buildenv.2019.106316
60. Davis D (2013) Modelled on software engineering: flexible parametric models in the practice of architecture
61. Lobaccaro G, Wiberg AH, Ceci G, Manni M, Lolli N, Berardi U (2018) Parametric design to minimize the embodied GHG emissions in a ZEB. Energy Build 167:106–123. https://doi.org/10.1016/j.enbuild.2018.02.025
62. Wiberg AH, Wiik MK, Auklend H, Slake ML, Tuncer Z, Manni M, Ceci G, Hofmeister T (2019) Life cycle assessment for Zero Emission Buildings—a chronology of the development of a visual, dynamic and integrated approach. IOP Conf Ser Earth Environ Sci 352:012054. https://doi.org/10.1088/1755-1315/352/1/012054

63. Basic S, Hollberg A, Galimshina A, Habert G (2019) A design integrated parametric tool for real-time Life Cycle Assessment—Bombyx project. IOP Conf Ser Earth Environ Sci 323:012112. https://doi.org/10.1088/1755-1315/323/1/012112

64. Basbagill JP, Flager FL, Lepech M (2014) A multi-objective feedback approach for evaluating sequential conceptual building design decisions. Autom Constr 45:136–150. https://doi.org/10.1016/j.autcon.2014.04.015

65. Wright JA, Loosemore HA, Farmani R (2002) Optimization of building thermal design and control by multi-criterion genetic algorithm. Energy Build 34:959–972. https://doi.org/10.1016/S0378-7788(02)00071-3

66. Geyer P (2009) Component-oriented decomposition for multidisciplinary design optimization in building design. Adv Eng Inform 23:12–31. https://doi.org/10.1016/j.aei.2008.06.008

67. Inyim P, Zhu Y (2013) A framework for integrated analysis of building designs using a life-cycle assessment and energy simulation. In: ICCREM 2013: construction and operation in the context of sustainability—proceedings of the 2013 international conference on construction and real estate management

68. Wang W, Zmeureanu R, Rivard H (2005) Applying multi-objective genetic algorithms in green building design optimization. Build Environ 40:1512–1525. https://doi.org/10.1016/j.buildenv.2004.11.017

69. Schwartz Y, Raslan R, Korolija I, Mumovic D (2021) A decision support tool for building design: an integrated generative design, optimisation and life cycle performance approach. Int J Archit Comput 19.https://doi.org/10.1177/1478077121999802

70. Schwartz Y, Raslan R, Mumovic D (2016) Implementing multi objective genetic algorithm for life cycle carbon footprint and life cycle cost minimisation: a building refurbishment case study. Energy 97:58–68. https://doi.org/10.1016/j.energy.2015.11.056

71. Sharif SA, Hammad A (2019) Simulation-based multi-objective optimization of institutional building renovation considering energy consumption, life-cycle cost and life-cycle assessment. J Build Eng 21:429–445. https://doi.org/10.1016/j.jobe.2018.11.006

72. Flager F, Basbagill J, Lepech M, Fischer M (2012) Multi-objective building envelope optimization for life-cycle cost and global warming potential. In: eWork and eBusiness in architecture, engineering and construction—proceedings of the European conference on product and process modelling 2012, ECPPM 2012

73. Azari R, Garshasbi S, Amini P, Rashed-Ali H, Mohammadi Y (2016) Multi-objective optimization of building envelope design for life cycle environmental performance. Energy Build 126:524–534. https://doi.org/10.1016/j.enbuild.2016.05.054

74. Hester J, Miller TR, Gregory J, Kirchain R (2018) Actionable insights with less data: guiding early building design decisions with streamlined probabilistic life cycle assessment. Int J Life Cycle Assess 23:1903–1915. https://doi.org/10.1007/s11367-017-1431-7

75. Hester J, Gregory J, Ulm FJ, Kirchain R (2018) Building design-space exploration through quasi-optimization of life cycle impacts and costs. Build Environ 144:34–44. https://doi.org/10.1016/j.buildenv.2018.08.003

76. Tecchio P, Gregory J, Ghattas R, Kirchain R (2019) Structured under-specification of life cycle impact assessment data for building assemblies. J Ind Ecol 23:319–334. https://doi.org/10.1111/jiec.12746

77. Tecchio P, Gregory J, Olivetti E, Ghattas R, Kirchain R (2019) Streamlining the life cycle assessment of buildings by structured under-specification and probabilistic triage. J Ind Ecol 23:268–279. https://doi.org/10.1111/jiec.12731

78. Hester J, Gregory J, Kirchain R (2017) Sequential early-design guidance for residential single-family buildings using a probabilistic metamodel of energy consumption. Energy Build 134:202–211. https://doi.org/10.1016/j.enbuild.2016.10.047

79. Xikai M, Lixiong W, Jiwei L, Xiaoli Q, Tongyao W (2019) Comparison of regression models for estimation of carbon emissions during building's lifecycle using designing factors: a case study of residential buildings in Tianjin, China. Energy Build 204:109519. https://doi.org/10.1016/j.enbuild.2019.109519

80. Rodrigues C, Freire F (2021) Environmental impacts and costs of residential building retrofits—what matters? Sustain Cities Soc 67:102733. https://doi.org/10.1016/j.scs.2021.102733
81. Pannier ML, Schalbart P, Peuportier B (2018) Comprehensive assessment of sensitivity analysis methods for the identification of influential factors in building life cycle assessment. J Clean Prod 199:466–480. https://doi.org/10.1016/j.jclepro.2018.07.070

How Urban Morphology Affects Energy Consumption and Building Energy Loads? Strategies Based on Urban Ventilation

Sarah G. Aboria, Osama M. Abo Eleinen, Basma N. El-Mowafy, and Asmaa M. Hassan

1 Introduction

Climate change is, in general, one of the most significant concerns that the globe has faced since the turn of the century [1–9] and has a significant influence on the performance of buildings and their energy consumption [10, 11]. It is expected that an increase in maximum temperatures in urban areas will reach 6° by 2100 [12]. As well population growth forecast, which put the numbers between 8.01 and 8.26 billion by 2025, and 9.15–11.03 billion by 2050 [13], which in turn led to an increase in residential units [14], besides the attendant impact on the microclimate and energy consumption inside buildings [15, 16]. In developed countries, buildings account for about half of all energy used for heating, cooling, and lighting [9] and the attendant emissions of CO_2 and greenhouse gases [17–19].

Whereas, in hot regions, keeping cool has become a topic of public concern and action in recent decades, affecting entire urban populations. Refrigeration's energy and greenhouse gas emissions are similarly significant, but they have human effects. Due to high temperatures and heat waves, such greenhouse gases cause high heat stress and mortality; this is therefore a public health policy issue, as is low productivity [20–22].

As is well known, the occurrence of UHI, in which temperatures within cities are often several degrees higher than in the surrounding countryside, leads to increased energy requirements for cooling in hot climes [12, 23–33], both passive design

S. G. Aboria · O. M. A. Eleinen · B. N. El-Mowafy (✉) · A. M. Hassan
Architectural Engineering and Urban Planning Department, Faculty of Engineering, Port Said University, Port Said, Egypt
e-mail: basma_nashaat@eng.psu.edu.eg

A. M. Hassan
Department of Architectural Engineering, College of Engineering and Information Technology, Buraydah College, Buraydah, Saudi Arabia

and natural ventilation have become prominent sectors nowadays; passive cooling provides outstanding thermal comfort and indoor air quality while consuming very little energy to improve the microclimate and combat pollution [32, 34–41], as well as a healthy indoor environment. In hot and humid areas, passive cooling via natural ventilation is the most effective way [42–45], especially in residential buildings [46].

The heating, cooling, lighting, and urban ventilation of individual buildings, as well as the microclimate of the streets, are all affected by urban morphology [47–50]. One of the most significant challenges of urban design is predicting the effect of urban shape on the microclimate, which affects not only the external thermal comfort of buildings but also their energy performance [51].

This study aims to provide a comprehensive analysis of studies related to urban morphology and its impact on providing urban ventilation and reduction of energy consumption and building energy loads under various climatic regions and buildings' heights based on the proposed matrix. Such aim can contribute to providing Sustainability Development Goals (SDGs), like goal number 11 considering sustainable cities and communities. Therefore, the next section presents a background of related studies. Then the used method of bibliometric analysis is clarified to present the results afterward then the proposed matrix. Finally, the conclusion is drawn.

2 Background

In the last few years, much more studies indicated the influence of urban morphology on energy in the building, for instance, Santamouris et al. [52] discuss the energy impact of rising temperature levels in city centers [53]. In addition, recent literature [15, 23, 52, 54] highlights the influence of urban geometry on urban ventilation and wind speed in urban canyons and UHI [17, 18, 24–26, 46, 55, 56], especially in a hot and humid climate [57], and their interrelationships with energy performance [58]. The findings were examined and analyzed in terms of natural ventilation passive cooling and its impact on human comfort [58] and health [14]. Such studies provide the potential for energy savings owing to the appropriate design of urban morphology [59].

Various variables can influence UHI effects, such as aspect ratio (H/W) [21], sky view factor (SVF), albedo [60, 61], orientation, site coverage ratio (ρ), average building height (H), density [62], plan area ratio [63], surface-to-volume ratio, obstruction angle [64] in changing the climate state and improving urban ventilation [65]. In this context, Table 1 sheds light on related studies with their tools, variables, and main findings.

Table 1 Related studies with their tools, variables, and main findings

References	Description		Location	Main findings
	Tools	Variables		
[70]	Coupled ENVI-met and EnergyPlus	• Street orientation • H/W	• Taiwan	• The largest influence on building energy consumption is H/W, followed by street direction and roadside vegetation density
[60]	ArcGIS	• Urban porosity • Albedo • SVF	• Seoul/ Korea South Korea	• SVF can minimize the duration of hot air in both low and high albedo urban environments
[71]	URBSIM	• H/W	–	• Shortwave radiation, which is the principal source of energy in canyons, is affected by low H/W and can be higher due to multiple reflections than in flat terrain
[62]	BPS with TRNSYS	• ρ • H	• Rome/Italy • Antofagasta/ Chile	• The density of urban texture determines annual energy demand depending on the temperature of the location
[63]	Theoretical	• H • Plan area ratio	• Hong Kong	• Building patterns can influence solar radiation gain and redistribution in sub-aspects, indirectly altering urban air temperature • The ventilation rate, building height, and plan area ratio all have an impact on the daily cycle of urban air temperature

(continued)

Table 1 (continued)

References	Description		Location	Main findings
	Tools	Variables		
[61]	KRLS model	• Albedo • SVF	• Seoul/South Korea	• High albedo helps with intensive cooling in urban areas
[64]	Building energy consumption data	• Surface-to-volume ratio • Orientation • Obstruction angle	• Seoul/South Korea	• Both the surface-to-volume ratio and the obstruction angle are critical

3 Method

This research is divided into two parts: database construction and the selection of the VOSviewer tool. The recommended reporting items for systematic reviews and meta-analysis (PRISMA) technique was used to create the database [66]. The sections that follow go over these stages in further detail.

3.1 Database Development

This study is based on numerous criteria to construct the database, which represents an important phase in conducting scientific reviews due to its direct impact on the quality of results [67]. Whereas Scopus and the Web of Science Core Collection (WoSCC) present the most accessible bibliometric sources, their coverage varies, altering search results [67–69]. First, the topic was utilized to conduct the search, titles, abstracts, and keywords of "urban morphology", "urban strategies" and energy from the first published article in 1981 to 2023. 473 documents were identified by Scopus on the 16th of November 2022 including 313 articles, 109 conference papers, 19 book chapters, 10 reviews, 7 conference reviews, and 2 books.

Following that, three filters were applied to limit relevant in-scope publications, including Scopus categories, publication type, and language. This analysis focused on the Scopus categories "engineering", "environmental science", and "energy". This study is based on certified information in "articles", "review articles", and "book chapters" according to publishing kind. Finally, publications printed in languages other than English were barred. As a result, 458 papers matching the initial filters were discovered. These publications were then transferred to the VOSviewer tool for analysis.

To ensure that no material appropriate for inquiry was overlooked, WoSCC offered additional searches with comparable keywords, yielding 410 more publications, which were then deleted, yielding 603 publications. The titles and abstracts
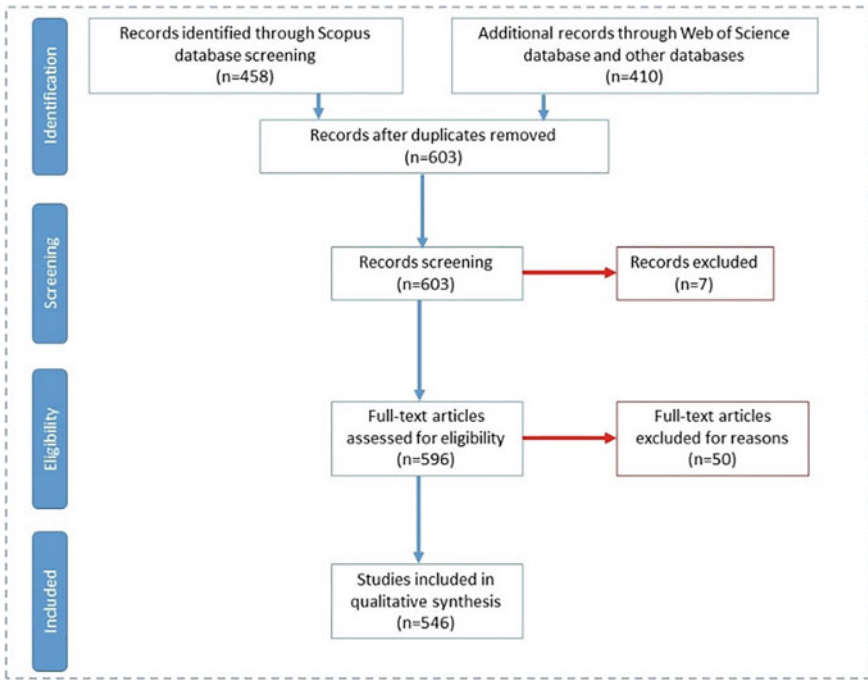
Fig. 1 Workflow of the PRISMA-based selection mechanism.

of the publications were manually checked to ensure that only research that fulfilled the objectives and scope of the study were included, resulting in 596 publications. Finally, the whole text of 596 publications was reviewed to determine their suitability for retaining material related to the research topic. As a consequence, 546 were identified as relevant to the goal of this bibliometric analysis s, as shown in Fig. 1.

3.2 Selection of VOSviewer Tool for Data Analysis

Over the last two decades, several software tools have been developed to map and visualise bibliometric data in order to properly analyse the literature, including VOSviewer, Biblioshiny, CiteSpace, Gephi, CitNeTExplorer, VantagePoint, and BibExcel [67]. Such tools are designed to visualise the complicated interactions that exist between things in research disciplines such as documents, keywords, authors, journals, references, nations, and so on. VOSviewer (version 1.6.18) was used to visualise "co-occurrence", "co-citation", "co-authorship", "bibliographic coupling", and "citation" analyses in this context.

Documents by year
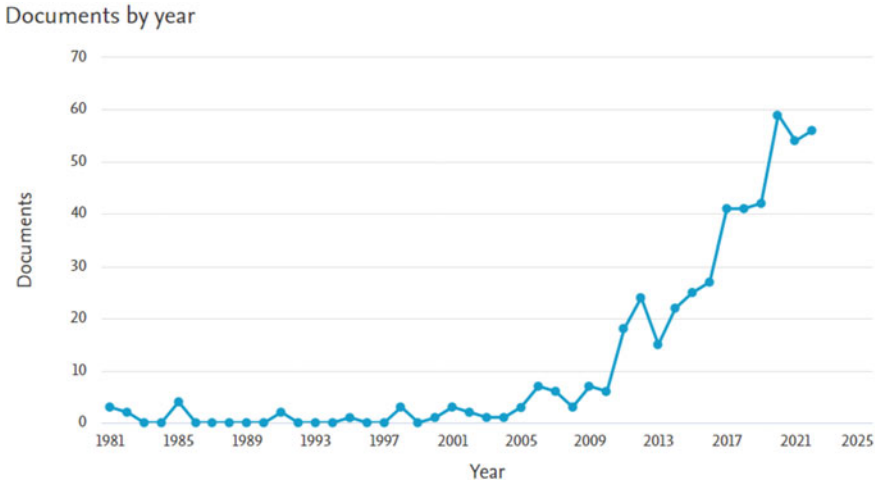
Fig. 2 Annual number of articles published

4 Results and Discussions

4.1 General Information

The total number of publications is an essential indicator of the state of scientific research. As shown in Fig. 2, the number of linked publications has grown year after year. The increase in the published literature year after year suggests that scholarly efforts have been made to apply concepts, technologies, and models of urban morphology and urban strategies to the creation of sustainable construction.

4.2 Bibliometric Analysis

4.2.1 Co-occurrence Network

Co-occurrence network visualization of the 546 papers identified nine different color clusters, as shown in Fig. 3. The keyword "urban morphology" occupies the largest node. Green Cluster focuses on the application of urban morphology, including climate change, cities, energy, energy efficiency, green infrastructure, land use, solar access, sustainable cities, and sustainable urban design. Brown Cluster is mainly related to the topic of UHI, including local climate zones, urban meteorology, and WRF. The red cluster is associated with urban form and urban sustainability. Orange Cluster includes the technical requirements for achieving their goals of building energy simulation and CFD. Purple Cluster reflects the microclimate, including UHI

and urban density that are related to outdoor thermal comfort. The dark blue cluster emphasizes the impact of such a city and its forms on buildings. The light blue cluster focuses on the street canyon, and urban ventilation, aiming at design and addressing the challenge of energy optimization. The pink cluster focuses on sustainable urban development, and the energy performance of buildings, including solar potential. The yellow cluster features advanced technologies and systems, such as urban form, density, and renewable energy, which are used to develop urban sustainability projects and energy consumption.

Figure 4 illustrates a keyword network visualization on the theme of urban strategies, which mainly includes urban morphology, green infrastructure, and thermal comfort, as applied to sustainable urban development. Among these themes, links between urban morphology and thermal comfort, such as green infrastructure, albedo, and natural ventilation are highlighted. However, energy fails to form effective links with urban strategies. The keywords urban form interlinked with other areas, focusing on energy, building performance optimization, and environmental impact. However, sustainable urban development is only linked to urban morphology.

The clustering keywords that are most closely related to urban morphology, urban strategies, and energy are urban morphology, UHI, urban form, GIS, urban planning, energy, energy efficiency, urban climate, sustainability, urban design, microclimate, solar potential, energy consumption, and climate change. Table 2 shows the high-frequency keywords identified from the VOSviewer software keyword co-occurrence

Fig. 3 Co-occurrence map

Fig. 4 Keyword network visualization of urban form

analysis, which specifies at least 15 keyword occurrences, also including color representation, clusters, the frequency of occurrences, and the total link strengths to the keywords.

Table 2 High-frequency keywords

Color	Cluster	Keyword	Occurrences	Total link strength
	1	Urban morphology	148	181
	2	UHI	47	63
	3	Urban form	30	37
	3	GIS	21	30
	3	Urban planning	20	22
	1	Energy	15	29
	8	Energy efficiency	15	19
	9	Urban climate	15	11
	6	Sustainability	14	28
	4	Urban design	14	27
	4	Microclimate	14	23
	8	Solar potential	14	15
	9	Energy consumption	13	19
	1	Climate change	13	16
	3	Solar energy	13	11

4.2.2 Co-occurrence Overlay

The temporal overlay graphic can show prominent study topics by year and can also reveal future research trends. Figure 5 illustrates the keyword co-occurrence overlay network map for urban morphology, urban strategies, and energy, with colours ranging from dark blue to yellow for the years 1981 to 2022. The colour of the circle corresponds to the emerging years for the various keywords.

As indicated in Table 3, the study hotspots regarding urban morphology, urban strategies, and energy from the year 2014 to 2021, have been summarized as the following five schemes:

(1) Cutting-edge concept: energy, urban morphology, and urban strategies.
(2) Urban sustainability: urban climate, urban planning, and sustainability.
(3) Factors influencing: albedo, natural ventilation, and street canyon.
(4) Activity for outdoor thermal comfort, and energy.
(5) Emerging technology: numerical analysis and simulation.
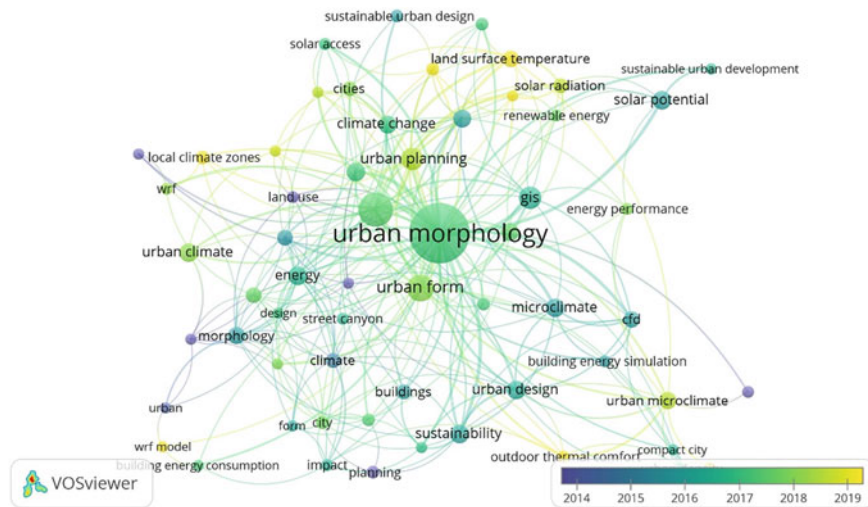
Fig. 5 Keyword overlay visualization from the year 2014 to 2021

Table 3 Popular research keywords in the past eight years via overlay visualization

Year	Color	Keywords
2014		Urban, planning, land use, natural ventilation.
2016		Urban design, sustainability, morphology, climate, energy efficiency.
2018		Urban morphology, UHI, climate change.
2020		Urban planning, urban form, energy efficiency.
2022		Local climate zones, outdoor thermal comfort, green infrastructure.
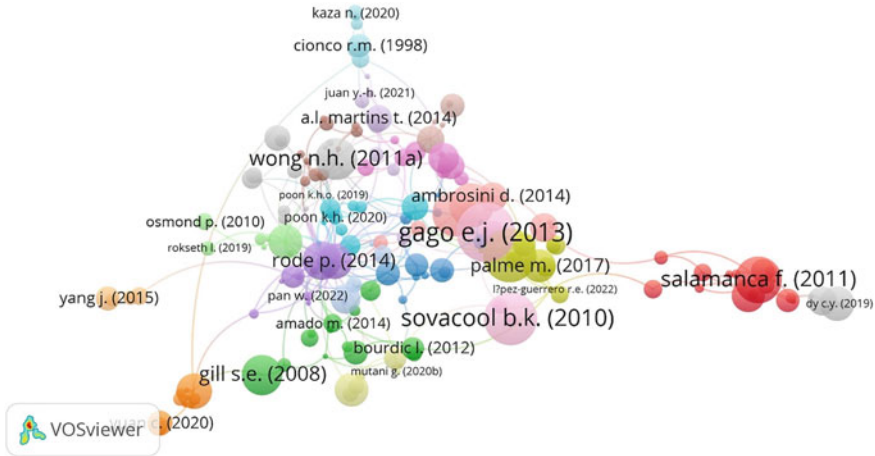
Fig. 6 Most cited publications

4.2.3 Most Cited Publications

Co-citation analysis was carried out in order to identify the most cited papers, which is one of the most essential markers in an academic subject [72]. As shown in Fig. 6, the results were identified for a minimum of 20 citations.

Furthermore, Table 4 summarises the top ten referenced papers, with 80% of the top ten cited publications including urban morphological aspects of case studies. However, only the third and fourth rankings are based on UHI, and they span a variety of techniques, including morphology, SVF, and UHI intensity [73, 74].

4.2.4 Most Productive Sources

In addition, the top 10 most productive sources for the subject are visualized in Fig. 7 and listed in Table 5. Among the sources, Sustainable Cities And Society is the most productive journal with 28 articles, followed by Energy And Buildings, Building And Environment, Sustainability Switzerland, Energy Procedia, Urban Climate, Wit Transactions On Ecology And The Environment, Energies, IOP Conference Series Earth And Environmental Science, and Applied Energy. The top ten most productive sources serve a key role in establishing for future studies on "urban morphology", "urban strategies" and energy.

Table 4 Top-ten most-cited publications

	Publication title	Scope	Citations	Year
1st	A GIS tool for the calculation of solar irradiation on buildings at the urban scale, based on Italian standards	Energy efficiency and urban solar irradiation	676	2018
2nd	Boosting solar accessibility and potential of urban districts in the Nordic climate: A case study in Trondheim	Solar potential and urban planning	658	2017
3rd	Building neighborhood emerging properties and their impacts on multi-scale modeling of building energy and airflows	Building energy simulation, urban neighborhood, and urban scale modeling	424	2015
4th	Characterizing urban heat island in Montreal (Canada)—Effect of urban morphology	Morphology, UHI intensity, urban canopy, and WRF	423	2015
5th	Analysis of temperature variability within outdoor urban spaces at multiple scales	Thermal comfort; climate, design, performance, hot and morphology	274	2019
6th	A Mechanical Drag Coefficient Formulation and Urban Canopy Parameter Assimilation Technique for Complex Urban Environments	Mesoscale models and urban canopy parameters	233	2015
7th	Cross-indicator analysis between wind energy potential and urban morphology	Morphological indicator, urban form, and urban wind energy	219	2017
8th	A Conceptual Framework for Assessment of Urban Energy Resilience	Absorption, adaptation, planning, recovery, resilience and urban energy	219	2015
9th	CFD assessment of wind energy potential for generic high-rise buildings in close proximity: Impact of building arrangement and height	Building arrangement, urban morphology, urban physics, urban planning, urban wind energy, and wind resource assessment	202	2022
10th	Application of MORUSES single-layer urban canopy model in a tropical city: Results from Singapore	Tropical city, urban canopy parametrization, and urban morphological parameters	201	2020

5 Proposed Matrix

Based on earlier studies, the research highlights the most related subjects between active and passive design, as demonstrated in Fig. 8. As seen in the illustration, passive design values strategies such as green infrastructure, square and plaza, urban ventilation potential, renewable morphological changes, and building typology, which contains potentials like albedo, building envelope design, the complexity of building
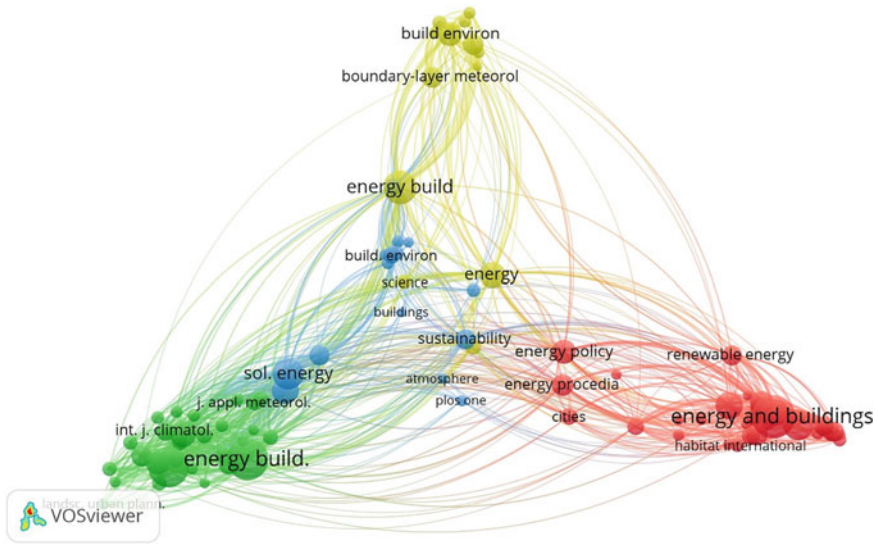
Fig. 7 Most productive sources

Table 5 Top 10 most productive sources

	Source titles	Number of publications
1st	Sustainable Cities And Society	28
2nd	Energy And Buildings	26
3rd	Building And Environment	19
4th	Sustainability Switzerland	16
5th	Energy Procedia	12
6th	Urban Climate	12
7th	Wit Transactions On Ecology And The Environment	11
8th	Energies	9
9th	IOP Conference Series Earth And Environmental Science	8
10th	Applied Energy	7

cluster, and courtyard/patio aspect ratio. While renewable energy systems are the only ones active design considers.

The research focuses on urban ventilation potential as its main theme. Figure 9 illustrated the possibilities of passive strategies that enhance urban ventilation potential in different climate zones; hot humid, hot dry, hot arid, tropical, temperate, temperate-humid, cold-desert, desert, and cold. The matrix categorizes the potential of every technique into three levels: weak, moderate, and high potential. The potential for urban ventilation is then shown in Fig. 10 for various building types, including low-rise, midrise, high-rise, planned, and unplanned.
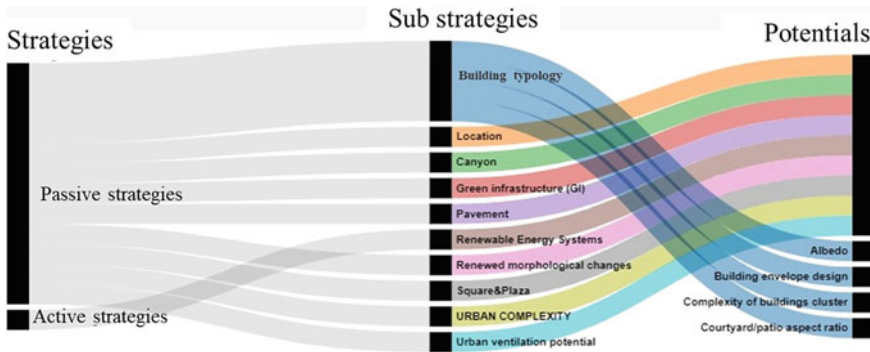
Fig. 8 Sub strategies associated with active and passive design

Based on the literature review, the proposed matrix proved that the highest possible techniques in all climate zones are urban density, roofing morphology, building porosity, and building layout (i.e. building void and separation) as illustrated in Fig. 11. Also, a Hot humid climate allows most techniques that can increase the potential of urban ventilation. Then, Fig. 12 confirms that a planned layout permits achieving most of the techniques that can enhance urban ventilation.

6 Conclusion and Recommendation

This study conducted a comprehensive review of studies related to urban morphology and its impact on providing urban ventilation and reduction of energy consumption and building energy loads. Since 1981, the number of publications linked to the scope of the study has increased, indicating a positive tendency. A bibliometric study based on filtered articles using the VOSviewer tool within the scope of "urban morphology," "urban strategies," and energy to visualise "co-occurrence" and "co-citation" analyses was also performed. VOSviewer software is used to provide the current status of research hotspots as well as future upcoming research hotspots. The following five schemes can be used to summarise the research hotspots in urban morphology, urban strategies, and energy: (a) cutting-edge concept: energy, urban morphology, and urban strategies, (b) urban sustainability: urban climate, urban planning, and sustainability, (c) factors influencing: albedo, natural ventilation, and street canyon, (d) activity for outdoor thermal comfort, and energy, and finally (e) emerging technology: numerical analysis and simulation. Both active and passive strategies were indicated to highlight their effects in the reduction of energy consumption and building energy loads. The proposed matrix emphasized passive strategies of urban morphology and urban ventilation potentials like; road orientations, building layout, porosity ratio, aspect ratio, frontal area density, building frontal area index, urban pattern, relative buildings height, urban block type under various climatic regions,
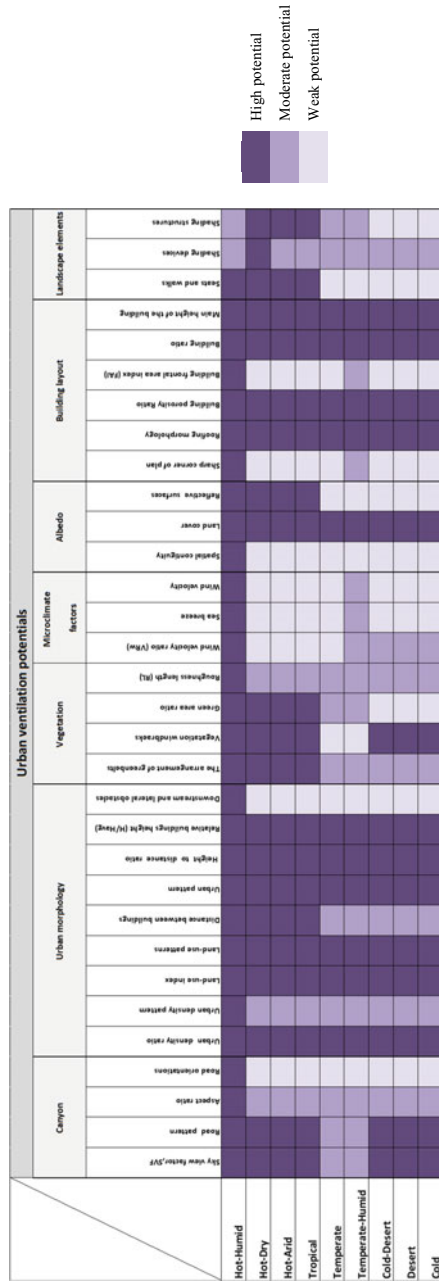
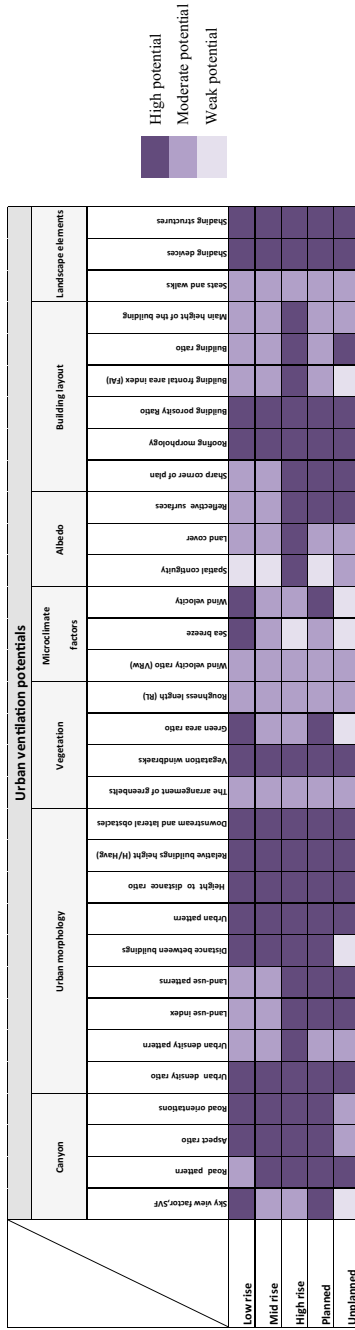**Fig. 9** The potentials of urban ventilation techniques in different climate zones

Fig. 10 The potentials of urban ventilation techniques in different building types
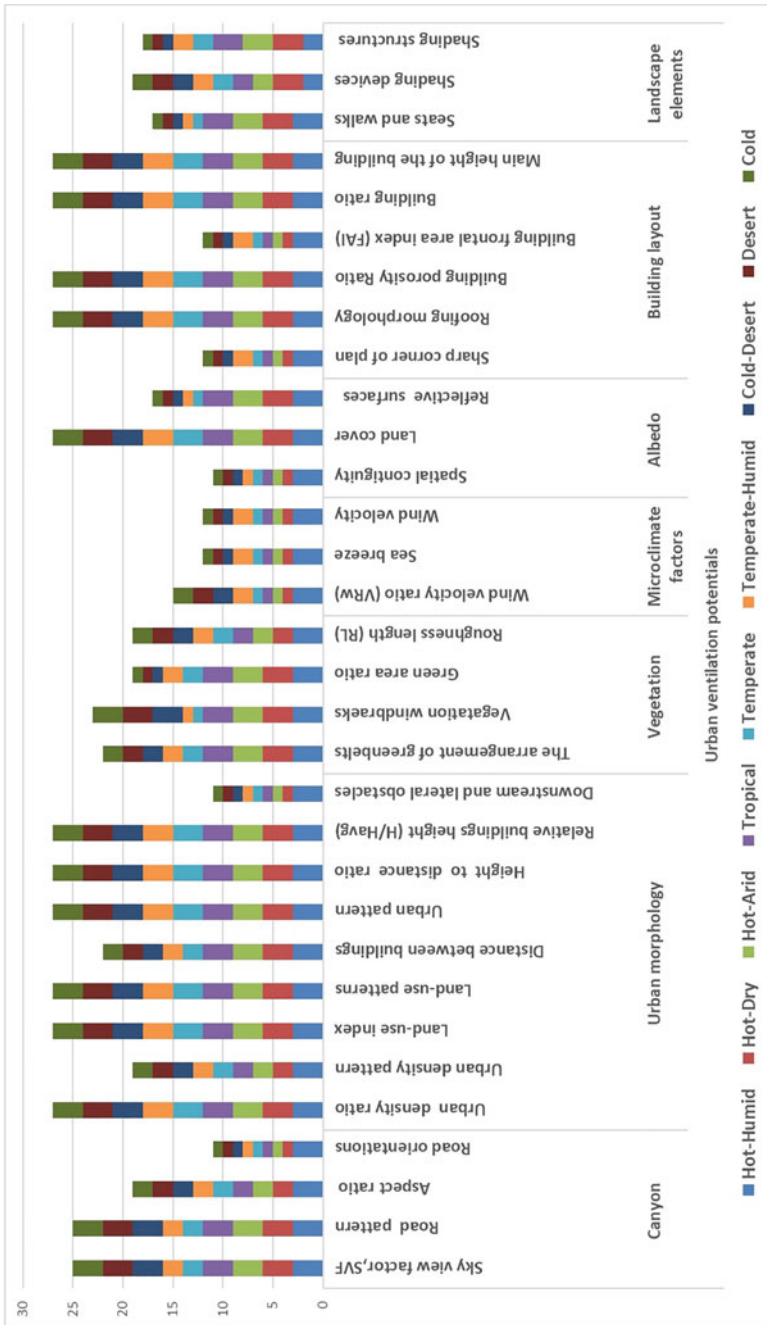
Fig. 11 The most effective techniques of urban ventilation in various climate zones
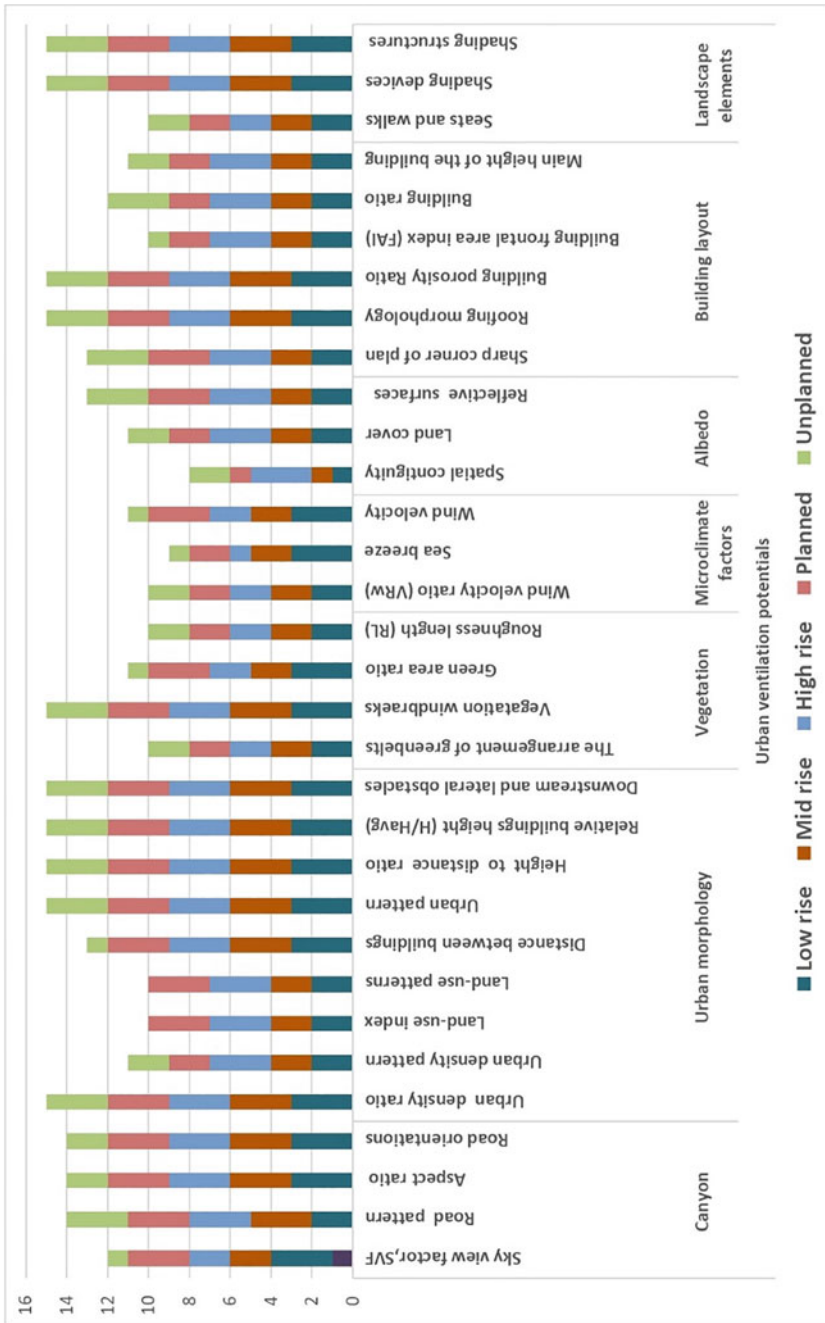
Fig. 12 The most effective techniques of urban ventilation in various building designs

and buildings' heights. Such strategies contribute to urban ventilation, which impacts the performance and building energy consumption and the prevalence of urban heat islands (UHI). Further computational and generative investigations can be conducted to validate such proposed matrix and optimize such urban potentials with various implications.

References

1. Noaman D, Moneer SA, Megahed N, El-Ghafour S (2022) Integration of active solar cooling technology into passively designed facade in hot climates. J Build Eng 104658
2. Hassan AM, Megahed NA (2022) Urban planning and development improving urban energy resilience with an integrative. Archit Eng
3. Elzeni MM, ELMokadem AA, Badawy NM (2022) Impact of urban morphology on pedestrians: a review of urban approaches. Cities [Internet] 129:103840. Available from: https://www.sciencedirect.com/science/article/pii/S0264275122002797
4. Shehata AO, Megahed NA, Shahda MM, Hassan AM (2022) (3Ts) Green conservation framework: a hierarchical-based sustainability approach. Build Environ [Internet] 224:109523. Available from: https://www.sciencedirect.com/science/article/pii/S0360132322007533
5. Hassan SR, Megahed NA, Abo Eleinen OM, Hassan AM (2022) Toward a national life cycle assessment tool: generative design for early decision support. Energ Build [Internet] 112144. Available from: https://www.sciencedirect.com/science/article/pii/S0378778822003152
6. Shahda M, Megahed N (2022) Post-pandemic architecture: a critical review of the expected feasibility of skyscraper-integrated vertical farming (SIVF). Archit Eng Des Manag
7. Abd Elraouf R, Elmokadem A, Megahed N, Eleinen O, Eltarabily S (2022) The impact of urban geometry on outdoor thermal comfort in a hot-humid climate. Build Environ 225:109632
8. Abd Elraouf R, Elmokadem A, Megahed N, Eleinen O, Eltarabily S (2022) Evaluating urban outdoor thermal comfort: a validation of ENVI-met simulation through field measurement. J Build Perform Simul 15:268–286
9. Yao R (2013) Design and management of sustainable built environments. Des Manag Sustain Built Environ
10. Nashaat B, Elmokadem A, Waseef A (2022) Evaluating adaptive facade performance in early building design stage: an integrated daylighting simulation and machine learning, pp 211–23
11. Abdallah ASH (2015) The influence of urban geometry on thermal comfort and energy consumption in residential building of hot arid climate, Assiut, Egypt. Procedia Eng 121:158–166
12. Cheshmehzang A, Butters C (eds) (2018) Cooler cities
13. Yao R (2013) Design and management of sustainable built environments, Chap. 1. In: Yao R (ed) Sustainability in the built environment
14. Abdelrahman MM et al (2016) The role of CFD simulation software in improving residential buildings' efficiency: case study on Youth Housing in New Damietta. 1:1–21
15. Papadopoulos AM, Moussiopoulos N (2004) Towards a holistic approach for the urban environment and its impact on energy utilisation in buildings: the ATREUS project. J Environ Monit 6:841–848
16. Javanroodi K, Mahdavinejad M, Nik V (2018) Impacts of urban morphology on reducing cooling load and increasing ventilation potential in hot-arid climate. Appl Energ 231:714–746
17. Ihara T, Kikegawa Y, Asahi K, Genchi Y, Kondo H (2008) Changes in year-round air temperature and annual energy consumption in office building areas by urban heat-island countermeasures and energy-saving measures. Appl Energ 85:12–25
18. Vuckovic M, Maleki A, Mahdavi A (2018) Strategies for development and improvement of the urban fabric: a Vienna case study. Climate 6:1–13

19. Eicker U, Monien D, Duminil É, Nouvel R (2015) Energy performance assessment in urban planning competitions. Appl Energ 155:323–333
20. Zhou X, Carmeliet J, Sulzer M, Derome D (2020) Energy-efficient mitigation measures for improving indoor thermal comfort during heat waves. Appl Energ 278:115620
21. Martins T, Adolphe L, Bonhomme M, Faraut S, Ginestet S, Michel C (2015) Creating urban cool islands effects for summer season in Toulouse new area, pp 8–13
22. Aktuğlu Aktan EÖ (2014) Wind ventilation in the built environment. WIT Trans Ecol Environ 190:749–62
23. Geros V, Santamouris M, Karatasou S, Tsangrassoulis A, Papanikolaou N (2005) On the cooling potential of night ventilation techniques in the urban environment. Energ Build 37:243–257
24. Kolokotroni M, Giannitsaris I, Watkins R (2006) The effect of the London urban heat island on building summer cooling demand and night ventilation strategies. Sol Energ 80:383–392
25. Shahmohamadi P, Che-Ani AI, Maulud KNA, Tawil NM, Abdullah NAG (2011) The impact of anthropogenic heat on formation of urban heat island and energy consumption balance. Urban Stud Res 2011:1–9
26. Allegrini J (2012) Urban climate and energy demand in buildings. PhD thesis, p 188
27. Ramponi R, Gaetani I, Angelotti A (2014) Influence of the urban environment on the effectiveness of natural night-ventilation of an office building. Energ Build 78:25–34
28. Toparlar Y, Blocken B, Vos P, Van Heijst GJF, Janssen WD, van Hooff T et al (2015) CFD simulation and validation of urban microclimate: a case study for Bergpolder Zuid, Rotterdam. Build Environ 83:79–90
29. Vallati A, De Lieto VA, Golasi I, Barchiesi E, Caranese C (2015) On the impact of urban micro climate on the energy consumption of buildings. Energ Procedia 82:506–511
30. Allegrini J, Carmeliet J (2018) Simulations of local heat islands in Zürich with coupled CFD and building energy models. Urban Clim 24:340–359
31. Liu J, Heidarinejad M, Guo M, Srebric J (2015) Numerical evaluation of the local weather data impacts on cooling energy use of buildings in an urban area. Procedia Eng 121:381–388
32. AbdelRahman MM, Moustafa WS, Farag OM (2017) Modelling of Egyptian low-cost-housing natural ventilation: integration of geometry, orientation and street width optimization. Urban Clim 21:318–331
33. Hassan AM (2023) UMC-based models: an integrating UMC performance analysis and numerical methods. Renew Sustain Energ Rev [Internet] 181:113307. Available from: https://www.sciencedirect.com/science/article/pii/S1364032123001636
34. Gao Y, Yao R, Li B, Turkbeyler E, Luo Q, Short A (2012) Field studies on the effect of built forms on urban wind environments. Renew Energ 46:148–154
35. Ramponi R (2014) Computational modeling of urban wind flow and natural ventilation potential of buildings
36. Huang H, Li X, Li K (2012) Study on the impact of the residential building shape on natural ventilation. In: 10th international conference on healthy buildings 2012, vol 3, pp 1988–96
37. Santamouris M, Kolokotsa D (2013) Passive cooling dissipation techniques for buildings and other structures: the state of the art. Energ Build 57:74–94
38. Wen CY, Juan YH, Yang AS (2017) Enhancement of city breathability with half open spaces in ideal urban street canyons. Build Environ 112:322–336
39. Hassan AM, ELMokadem AA, Megahed NA, Abo Eleinen OM (2020) Urban morphology as a passive strategy in promoting outdoor air quality. J Build Eng 29:101204
40. Hassan AM, Megahed NA (2021) COVID-19 and urban spaces: a new integrated CFD approach for public health opportunities. Build Environ [Internet] 204:108131. Available from: https://www.sciencedirect.com/science/article/pii/S0360132321005321
41. Hassan AM, El Mokadem A, Megahed NA, Abo Eleinen OM (2020) Improving outdoor air quality based on building morphology: numerical investigation. Front Archit Res [Internet] 9:319–34. Available from: https://linkinghub.elsevier.com/retrieve/pii/S2095263520300030
42. Al-Sallal KA, Al-Rais L (2011) Outdoor airflow analysis and potential for passive cooling in the traditional urban context of Dubai. Renew Energ 36:2494–2501

43. Yang F, Qian F, Lau SSY (2013) Urban form and density as indicators for summertime outdoor ventilation potential: a case study on high-rise housing in Shanghai. Build Environ 70:122–137
44. Access O (2019) Effects of street geometry on airflow regimes for natural ventilation in three different street configurations in Enugu City, pp 0–16
45. Xie AC, Cooler Cities L (2013) Chap. 3 Reducing cooling loads in hot-humid climates: a best practice research building in China
46. Palme M, Carrasco C, Ángel Gálvez M, Inostroza L (2017) Natural ventilation: a mitigation strategy to reduce overheating in buildings under urban heat island effect in South American cities. IOP Conf Ser Mater Sci Eng 245:0–9
47. Beygo K, Yüzer MA (2017) Early energy simulation of urban plans and building forms. A/Z ITU J Fac Archit 14:13–23
48. Sharmin T, Steemers K (2019) Impact of urban geometry on indoor air temperature and cooling energy consumption in traditional and formal urban environments. In: Comfort at the extremes: energy, economy and climate
49. Zhang J, Wong NH, Hii DJC (2015) The relationship between building form typology and cooling loads in the tropical climatic context. Plea
50. Musy M, Huang Y, Athamena K (2011) Mitigating urban heat island effect by urban design: forms and materials. In: Fifth urban research symposium, pp 1–15
51. Mosteiro-Romero M, Maiullari D, Pijpers-van Esch M, Schlueter A (2020) An Integrated microclimate-energy demand simulation method for the assessment of urban districts. Front Built Environ 6:1–18
52. Santamouris M, Papanikolaou N, Livada I, Koronakis I, Georgakis C, Argiriou A et al (2001) On the impact of urban climate on the energy consumption of building. Sol Energ 70:201–216
53. Perini K, Magliocco A (2014) Effects of vegetation, urban density, building height, and atmospheric conditions on local temperatures and thermal comfort. Urban Urban Green 13:495–506
54. Santamouris M, Klitsikas N, Niahou K (2002) Ventilation of street canyons and its impact on passive cooling design, p 8
55. Maragogiannis K, Kolokotsa D, Maria EA (2011) Study of night ventilation efficiency in urban environment: technical and legal aspects. Environ Clim Technol 6:49–56
56. Salvati A, Palme M, Chiesa G, Kolokotroni M (2020) Built form, urban climate and building energy modelling: case-studies in Rome and Antofagasta. J Build Perform Simul 13:209–225
57. Du X (2019) Space design for thermal comfort and energy efficiency in summer (a Chinese vernacular house case)
58. Ali-toudert F (2009) Energy efficiency of urban buildings: significance of urban geometry, building construction and climate conditions. In: The seventh international conference on urban climate, Yokohama, Japan, pp 29–32
59. Ignatius M, Wong NH, Jusuf SK, Hii DJC (2016) Holistic method on performing microclimate analyses of an urban area in the tropics holistic method on performing microclimate analyses of an urban area in the tropics
60. Choi Y, Lee S, Moon H (2018) Urban physical environments and the duration of high air temperature: focusing on solar radiation trapping effects
61. Choi Y, Lee S (2020) The impact of urban physical environments on cooling rates in summer: focusing on interaction effects with a kernel-based regularized least squares (KRLS) model. Renew Energ 149:523–534
62. Salvati A, Palme M, Chiesa G, Kolokotroni M (2020) Built form, urban climate and building energy modelling: case-studies in Rome and Antofagasta, p 1493
63. Xue Y, Wang Y, Peng H, Wang H, Shen J (2020) The impact of building configurations and anthropogenic heat on daily urban air temperature cycles. Build Environ 169:106564
64. Oh M, Moon K, Kim Y (2021) Energy and buildings empirical analysis of building energy consumption and urban form in a large city: a case of Seoul, South Korea. Energ Build 245:111046
65. Wong NH, Jusuf SK, Syafii NI, Chen Y, Hajadi N, Sathyanarayanan H et al (2011) Evaluation of the impact of the surrounding urban morphology on building energy consumption. Sol Energ 85:57–71

66. Chen Y, Huang D, Liu Z, Osmani M, Demian P (2022) Construction 4.0, industry 4.0, and building information modeling (BIM) for sustainable building development within the smart city. Sustainability 14
67. Omrany H, Chang R, Soebarto V, Zhang Y, Ghaffarianhoseini A, Zuo J (2022) A bibliometric review of net zero energy building research 1995–2022. Energ Build [Internet] 262:111996. Available from: https://www.sciencedirect.com/science/article/pii/S0378778822001670
68. Olawumi TO, Chan DWM (2018) A scientometric review of global research on sustainability and sustainable development. J Clean Prod [Internet] 183:231–50. Available from: https://www.sciencedirect.com/science/article/pii/S095965261830475X
69. Megahed NA, Hassan AM (2022) Evolution of BIM to DTs: a paradigm shift for the post-pandemic AECO industry. Urban Sci
70. Huang K-T, Li Y-J (2017) Impact of street canyon typology on building's peak cooling energy demand: a parametric analysis using orthogonal experiment. Energ Build [Internet] 154:448–64. Available from: https://www.sciencedirect.com/science/article/pii/S0378778817318340
71. Schrijvers PJC, Jonker HJJ, De Roode SR, Kenjere S (2020) On the daytime micro-climatic conditions inside an idealized 2D urban canyon, p 167
72. Ampese LC, Sganzerla WG, Di Domenico Ziero H, Mudhoo A, Martins G, Forster-Carneiro T (2022) Research progress, trends, and updates on anaerobic digestion technology: a bibliometric analysis. J Clean Prod [Internet] 331:130004. Available from: https://www.sciencedirect.com/science/article/pii/S095965262104172X
73. Touchaei AG, Wang Y (2015) Characterizing urban heat island in Montreal (Canada)—effect of urban morphology. Sustain Cities Soc 19:395–402
74. Srebric J, Heidarinejad M, Liu J (2015) Building neighborhood emerging properties and their impacts on multi-scale modeling of building energy and airflows. Build Environ 91:246–262

Parametric Urbanism in Optimising Outdoor Thermal Comfort of Urban Spaces

Maram Waleed Rezk, Ashraf Elmokadem, Nancy Badawy, and Heba Adel

Abbreviation

OTC   Outdoor thermal comfort
MRT   Mean radiant temperature
SVF   Sky view factor
FAR   Floor area ratio
BCR   Building coverage ratio
PMV   The predict mean vote index
PET   The physiological equivalent temperature index
UTCI   The universal thermal climate index

M. W. Rezk (✉) · A. Elmokadem · N. Badawy · H. Adel
Architectural Engineering and Urban Planning Department, Faculty of Engineering, Port Said University, Port Said, Egypt
e-mail: m.rezk@eng.psu.edu.eg

A. Elmokadem
e-mail: elmokadem1@eng.psu.edu.eg

N. Badawy
e-mail: n.badawy@eng.psu.edu.eg

H. Adel
e-mail: heba.adel@eng.psu.edu.eg

1 Introduction

According to United Nations estimations, the global urban population will expand by 80% by 2050, to reach 6.4 billion from 3.9 billion in 2014 [1]. With such rapid global urbanisation, the environmental optimization concept has become an increasingly important driver of the urbanization process. In urbanism, environmental optimization refers to the process of developing or recreating habitable and sustainable urban places using optimal criteria [2]. Numerous environmental concerns, such as urban microclimates, have an impact on urban development processes. Urbanisation negative environmental effects have drawn more attention about how to make cities more resilient and livable in the present and the future [3]. The attention paid to outdoor thermal comfort as the most important key performance factor for urban environmental evaluation has increased over the last three decades [4, 5]. The main goal of masterplans is typically to produce ecologically suitable physical urban spaces [6]. As a result, environmental impacts must be carefully taken into account during the urbanisation process [7]. However, most researches deal with the urban canyon thermal comfort and a few number of researches deal with the thermal comfort in the urban spaces such as courtyards where most of social activities occur [8]. By improving thermal comfort in the urban spaces, the indoor thermal performance improves accordingly, which results in a reduction in energy consumption and helps in making the urban environment more sustainable [9, 10]. In this regard, this research study how can parametric urbanism be used in optimising the outdoor thermal comfort in the urban spaces.

1.1 Urban Geometry

Urban geometry is considered one of the most important components of the urban environment and contributes significantly to the formation of urban fabric [11–13]. The design geometries or building complex is a synthetic process, and the main driver is the design concept, which is established to achieve specific objectives that could be functional, environmental or social [6]. Urban geometry indicators can be divided into three main groups as shown in Fig. 1: density indicators such as floor area ratio and building coverage ratio, space enclosure indicator, and building layout indicators [11].

Perini and Magliocco studied the influence of BCR indicator on OTC in Italy, concluded that increasing BCR results in a rise in air temperature [14]. Skarbit et al. also found that areas with higher BCR in Szeged, Hungary have higher minimum and mean air temperatures [15]. Petralli et al. studied the impact of various density indicators on temperature in summer and they found that increasing BCR by 10% raises the air temperature by 0.36 °C [16]. In contrast, Lin et al. found that higher BCR and FAR areas in Hong Kong caused a reduction in air temperature [17].
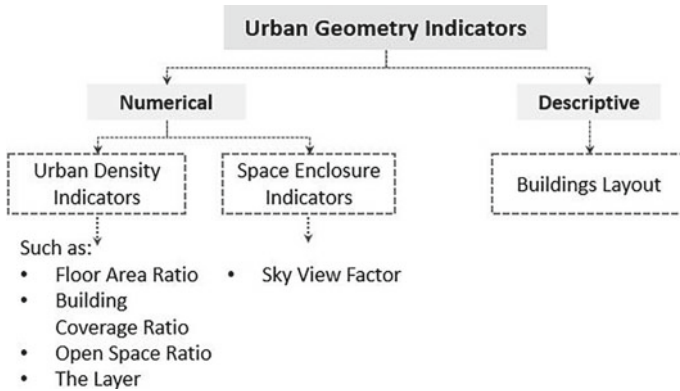
Fig. 1 Urban geometry indicators. *Source* By Authors

Lin et al. in a study in Taiwan found that a high sky view factor in summer causes discomfort [18]. Another study by Hwang et al. agreed with these findings [19]. From the above the selected indicators to be studied in this research are:

- SVF = non-dimensional number ranging from 0 to 1, illustrates the percentage of the sky occupied in the overlaying hemisphere [20].
- FAR = Gross Floors Area/Site Plan Area.
- BCR = Foot Print Area/Site Plan Area.

1.2 Thermal Comfort

The American Society of Heating, Refrigerating and Air-Conditioning Engineers (ASHRAE) defines comfort as 'that state of mind which expresses satisfaction with the thermal environment' [21]. Although thermal comfort depends on microclimatic parameters and other parameters related to the human, microclimatic factors are the most considered because they are more solid and measurable, and they are [22–24]:

- Air temperature.
- Mean radiant temperature.
- Wind speed.
- Relative humidity.

The definition of thermal comfort emphasizes that comfort evaluation is considered as a cognitive process that includes many factors, Physical, Physiological and psychological factors [25–27]. In this regard, there are 2 approaches for assessing thermal comfort, the adaptive approach which is very hard to predict as it based on surveys and questionnaires, and the rational approach which have many heat balance models with many indices such as PMV, PET, UTCI, etc. [25, 26, 28–30].

1.3 Research Problem and Objectives

The Egyptian government unveiled a long-term road map in 2015 for the physical growth of current cities and the development of new urban areas. Accordingly, the research problems are:

- The inability of traditional design methods to deal with the number of complications that affect outdoor thermal comfort in urban spaces.
- The efforts in Egypt to implement environmental performance evaluation are currently entirely voluntary.
- The Regulations of Construction Act only specify spatial guidelines rather than requirements for designing urban forms that are climate-responsive, as same urban forms can be found in different climates.
- The disconnect between research on outdoor thermal comfort and design practise, which prevents cities from improving their microclimates, besides worsens people's well-being and health.

From the above, the research objective is to suggest design considerations to help optimise outdoor thermal comfort in urban spaces in Egypt.

2 Methodology

To achieve the aim of the study, a hypothetical urban model was created and simulated in three successive phases as shown in Table 1. Design parameters thresholds were established according the Egyptian construction laws and regulations.

The case study consists of 12 buildings surrounding a 100 m × 100 m urban space in hot climate in Cairo. Density in each case does not exceed 50% following the executive regulation, number of floor varies from G+3 to G+7, and spaces between buildings varies from 6 to 12 m.

The first phase of the simulation is done by changing the heights of the buildings and the spacing between them symmetrically for the four building arrays as shown in Table 2 and deducing average UTCI, average MRT, FAR, BCR and SVF in each case to conclude the relationship between UTCI and MRT with the selected urban indicators which are SVF, FAR, and BCR. UTCI is calculated at each point on a 5 m grid on the urban space, and recorded from 7 am to 5 pm to represent most of the diurnal of the day. Calculating the average UTCI offers a better overall perspective for the OTC in the urban space. Additionally, calculating average MRT explains the relationship between solar radiation and OTC and the importance of it on thermal performance in summer.

In the second phase, a surrounding urban environment was added to the virtual model by repeating the virtual complex with average values for floor numbers and spacing between buildings, to create a residential neighborhood, and the average UTCI was also calculated in the same way as in the first phase from 7 am to 5 pm as

shown in Table 2. The aim of this phase is to study the impact of urban context on OTC.

In the third phase of simulation, the change is made in the number of floors and spacing between buildings for each array individually, with the rest of the arrays being fixed with average values in the number of floors and spacing between buildings, and then the change in the thermal comfort values and the rest of the outputs is deduced. This process was repeated 4 times for each array separately as shown in Table 3 and the results of the 4 arrays were compared to each other. The aim of this phase is to conclude the most influential array on outdoor thermal comfort and the least effect on it. The case study components are separated into two groups: generators (constraints) and parameters (variables), either dependent or independent, and each of them can also be divided environmentally and geometrically, as shown in Fig. 2.

Table 1 Shows the methodology of the research consisting of 3 phases of simulation, description, and aim for each phase

	Configuration	No. of cases	Description	Aim
Phase 1		20 cases	The changes in variables are made for the four arrays symmetrically around the urban space	The aim of this phase is to study the relationship between thermal comfort and other geometrical indicators such as SVF, FAR, and BCR
Phase 2		20 cases	There is an urban context added surrounding the studied model, the changes in variables are done symmetrically as in phase 1	The aim of this phase is to study the impact of adding surrounding urban context on microclimate and outdoor thermal comfort
Phase 3		80 cases	The changes are made individually in each array while the rest of array fixed in average numbers	The aim of this phase is to conclude the most influential direction (east, west, north, south) on the outdoor thermal comfort and the least effect on it

Table 2 The independent parameters (variables) steps for Phases 1 and 2 of the simulation

Parameters (variables)	Min	Max	Steps
Building heights	G+3	G+7	1 Floor
Spacing (m)	6	12	2
Hours	7 am	5 pm	1 h

Source By Authors

Table 3 The independent parameters (variables) steps for Phase 3 of the simulation

Parameters (variables)	Min	Max	Steps
Array A (Western direction)			
Building heights (array A)	G+3	G+7	1 Floor
Spacing (array A) (m)	6	12	2
Hours	7 am	5 pm	1 h
Array B (Northern direction)			
Building heights (array B)	G+3	G+7	1 Floor
Spacing (array B) (m)	6	12	2
Hours	7 am	5 pm	1 h
Array C (Eastern direction)			
Building heights (array C)	G+3	G+7	1 Floor
Spacing (array C) (m)	6	12	2
Hours	7 am	5 pm	1 h
Array D (Southern direction)			
Building heights (array D)	G+3	G+7	1 Floor
Spacing (array D) (m)	6	12	2
Hours	7 am	5 pm	1 h

Source By Authors

2.1 Simulation Workflow

The ladybug-tools model is a collection of plugins used to assess OTC and visualize the data and results. This model is based on connecting already validated engines with the grasshopper to calculate UTCI that represents the outdoor thermal comfort. The UTCI in the ladybug model is calculated by several other factors such as air temperature, relative humidity, wind speed, and the Mean radiant temperature as shown in Table 4. The Urban Weather Generator (UWG) by Dragonfly plugin used to calculate the relative humidity and the air temperature according to climate change factors. The component collects a number of inputs, such as building function, average heights and other factors, to produce a new 'urban' weather file from the original 'rural' one with adjusted hourly relative humidity and air temperature [4]. Using butterfly plugin, wind speed can be simulated, but it takes a very long time, so the wind speed was used directly from the weather file. MRT is calculated as the sum of three components:

- The long-wave radiation from the surfaces.
- The quantity of sky long-wave radiation that the human body absorbed.
- The additional quantity of solar short-wave radiation absorbed.
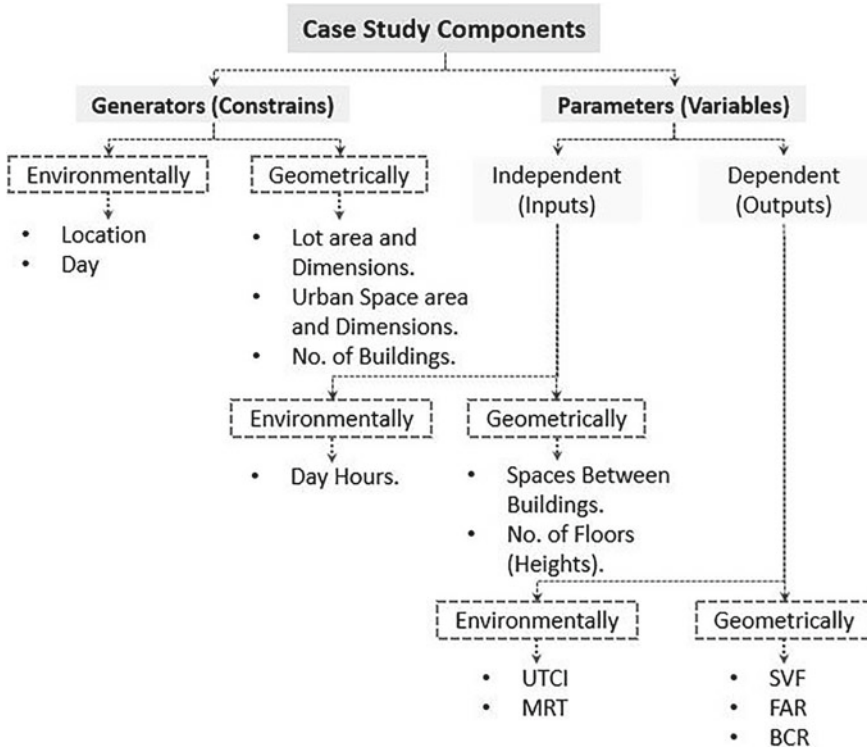
Fig. 2 Case study components. *Source* By Authors

Table 4 Each outdoor thermal comfort components source in the case study

OTC components	Tool of calculating
Air temperature	Calculated via UWG in Phase 2 and, while retrieved from the weather file in Phase 1
Relative humidity	
Wind speed	Retrieved from weather file
Mean radiant temperature	Calculated via Ladybug components

Source By Authors

The Colibri component of the TT-Toolbox [31] was applied to repeat a total number of 120 cases for the three phases, 20, 20 and 80 cases respectively. The simulation workflow can be summarised as shown in Fig. 3.
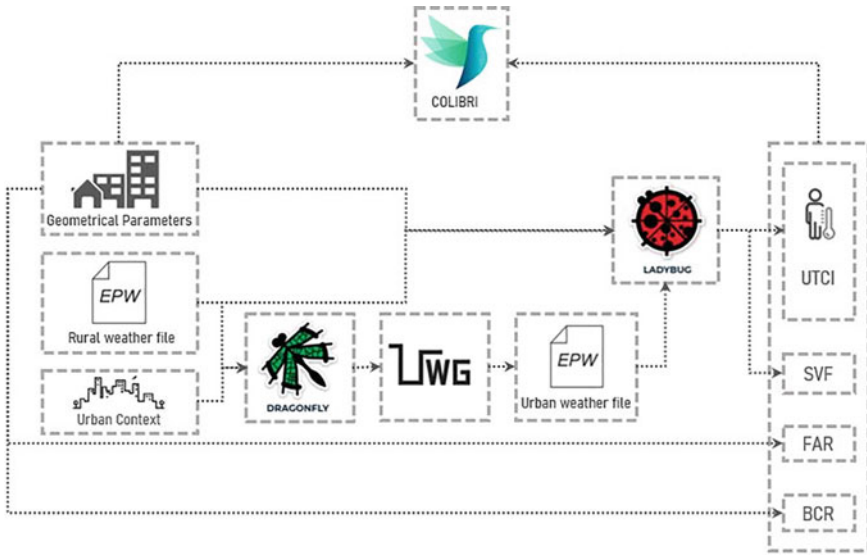
Fig. 3 The simulation map between plugins. *Source* By Authors

2.2 Workflow Validation

The simulation workflow is based on engines that have already been validated utilized to calculate MRT and UTCI. Bueno et al. validated urban weather generator in various climates: Singapore, Toulouse in France, and Basel in Switzerland by field measurements [32, 33]. The process must next be validated is how MRT equations been applied in the workflow, and how it integrates the various UTCI components. Evola et al. in a recent research validated the ladybug tool process in Italy, a Mediterranean climate, using experimental measurements, the study findings showed a good match with the measured data, with a determination coefficient R2 = 0.92 [34].

Furthermore, Ibrahim et al. validated the process against ENVI-met, the modelling package of CFD in two locations, Cairo in Egypt and London in UK [35, 36]. The results of Cairo case study for the average UTCI and MRT of all the points on grid demonstrate a parallel behaviour in UTCI and MRT (R2 = 0.96 and 0.94, respectively) [35, 36].

Ibrahim et al. also validated the workflow against field measurements in Cairo, Egypt, and the findings show a good agreement in MRT and UTCI values, noting that the ladybug-tools simulation workflow did not including CFD wind analysis [4]. Natanian et al. used the same simulation workflow in hot dry climates to perform an analysis of wind and solar parameters to calculate UTCI. The study concluded that the UTCI most influenced by MRT and the use of wind data directly from the weather file rather than simulating it had a minimal effect on the UTCI value [37].

Fig. 4 The calculated points on 5 m grid inside the urban space. *Source* By Authors
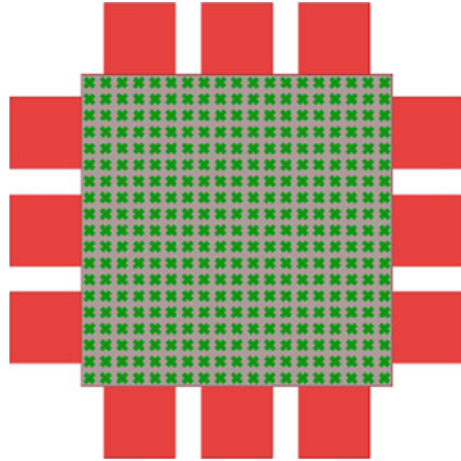
2.3 Hypothetical Study Modelling

A hypothetical urban geometry was built with the configuration of a square urban space of 100 m * 100 m surrounded by buildings on 4 sides as shown in Fig. 4, each side with 3 buildings of the same shape and dimensions. The shape was decided to be square to allow comparison between the four arrays representing the four main directions and to study the effect of each of them on outdoor thermal comfort.

2.4 Simulation Setup

The simulation was done using the weather file of 'One building' with the extension TMYx derived from the last 15 years (2007–2021), it was extracted from Cairo International Airport station. The simulation was done on July 16th as the hottest day of the year, according to the weather file, and throughout diurnal hours (10 h) from 7 am to 5 pm, by calculating the values of UTC for all the point distributed over the urban space on a 5 m grid as shown in Fig. 4 with a height 1.1 m representing human body gravity center, and taking the average UTCI for all points in every hour, then the average UTCI over the hours of the diurnal, to deduce the degree of thermal comfort expressing the specific case and compare it with the rest of the cases.

In the second and third phases, the complex was repeated to form an urban context with average values for the number of floors and the spacing between buildings as G+Five and 9 m, respectively. For the inputs of UWG in Dragonfly plugin, the building programme set as "mid-rise apartments", climate zone in construction set climate set to "Hot", and conditioned set to "False". In the MRT component, the ground reflectance should be a number between 0 and 1, and it was defined as the default value which is 0.25 and it expresses outdoor grass or dry bail soil (Fig. 5).

Fig. 5 Urban context added to the studied area. *Source* By Authors
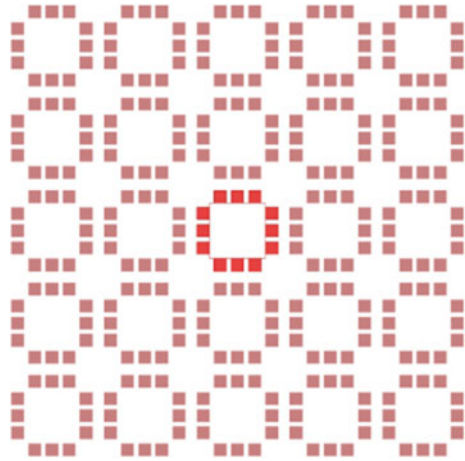
2.5 Climate Context

Egypt has a variety of climate conditions; nevertheless, based on Köppen-Geiger climate classification Egypt's climate is considered a hot desert climate [4]. This climate is defined as hot dry summer and mild winter with little precipitation. The highest temperatures are usually recorded in July, and the lowest are recorded in January. A weather file from one building with the extension TMYx extracted over the past 15 years from Cairo International Airport Station was used in this research.

3 Result and Discussion

3.1 Phase 1

The results of the first phase of simulation showed a noticeable reduction in the MRT values reached 4.2 ˚C, between the best and worst cases, the highest value of MRT was recorded at 55.6 ˚C, and the lowest value reached was recorded at about 51.4 ˚C, as for the reduction in the UTCI, it was very impressive, as it moved a level down on the UTCI assessment scale. The highest UTCI value reached 38.4 ˚C while the lowest recorded 37.4 ˚C, which is considered A noticeable difference in relation to the size of the urban space.

The case that achieved the highest value of MRT and UTCI, i.e. the worst thermal performance, was the lowest case in the number of floors and the largest in the spacing between buildings, while the best thermal performance and the lowest value of MRT and UTCI was in the highest case in the number of floors and the least in the distances between buildings (Figs. 6, 7 and 8).
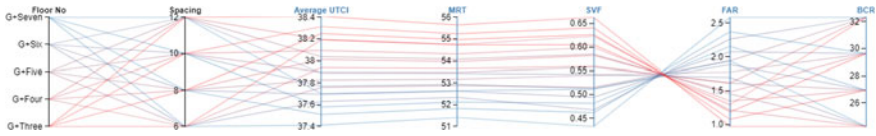
Fig. 6 A graph shows the relations between inputs and outputs for Phase 1. *Source* By Authors
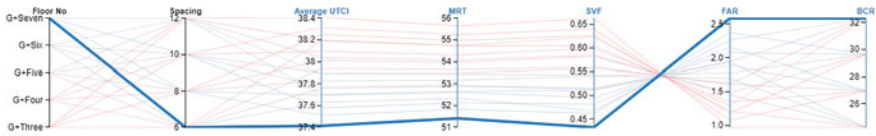
Fig. 7 A graph shows the statics of the case of the lowest UTCI achieved in Phase 1. *Source* By Authors
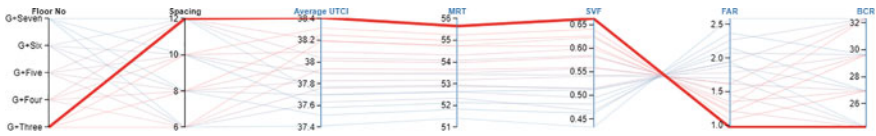
Fig. 8 A graph shows the statics of the case of the highest UTCI achieved in Phase 1. *Source* By Authors

And through the previous results, it was found that the difference in the UTCI values when fixing the spacing between buildings and changing the floor numbers reach 0.8 ˚C, while when fixing the floor numbers and changing the spacing between buildings, the difference ranges from 0.2 to 0.3 ˚C in UTCI. Therefore, the effect of height on OTC is stronger than the effect of spacing between buildings as shown in Fig. 9.

Accordingly, a simulation was made for an additional case outside the framework of building laws, so the number of floors was placed to G+Ten, there was a dramatic
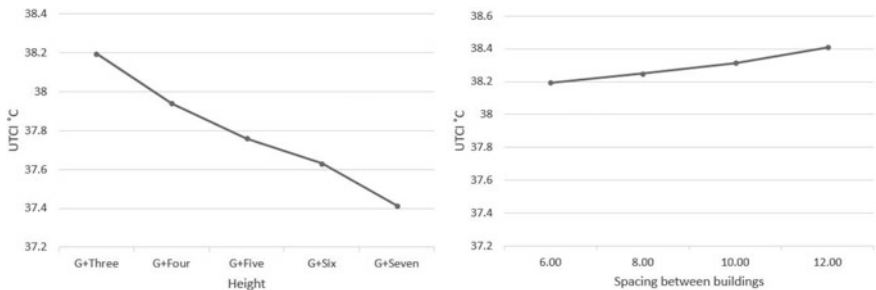
Fig. 9 The relationship between UTCI and heights, resulted from Phase 1 (left), the relationship between UTCI and spacing between buildings resulted from Phase 1 (right). *Source* By Authors

reduction in UTCI reached 60% from the G+Seven case. As the difference between UTCI values between the best and the worst case reached 1.6 °C instead of 1.0 °C, with a value of 36.8 °C. The decrease in the MRT value reached almost 6.6 °C, as it recorded 49.0 °C.

The value of SVF recorded downward, reaching 0.36, and FAR recorded 3.55. On the other hand, BCR remained the same because the change was in the height not in the spacing between buildings and the area of the ground floor.

3.1.1 Sky View Factor (SVF)

SVF has a significant impact on OTC. The following graph shows the values of the inputs of the 20 cases in phase 1, the values of SVF and average resulted UTCI. The graphs show that the relationship between SVF and UTCI is completely direct. The lower the value of the SVF and the higher the enclosure rate, the lower the degree of UTCI and the better thermal performance. The higher the value of SVF and the less enclosure, the higher the UTCI value and the worse the thermal performance. This is due to the increase in the percentage of shading and the reduction of solar radiation, which positively affects OTC (Figs. 10 and 11).
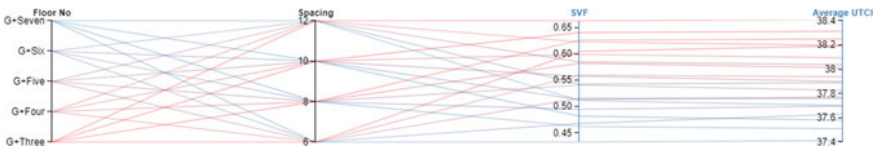
Fig. 10 A graph shows the values of inputs and the resulting SVF and UTCI for the 20 cases in Phase 1
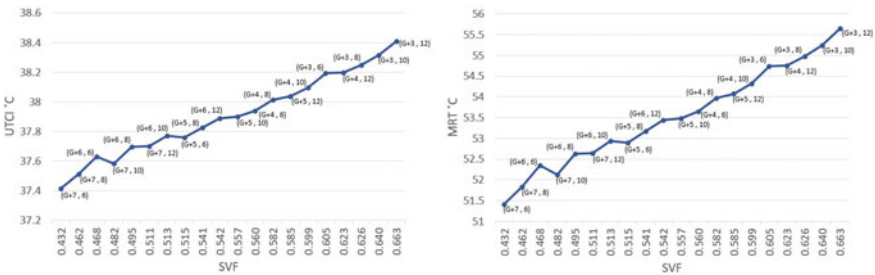
Fig. 11 The relationship between UTCI and SVF resulting from Phase 1 (left), the relationship between MRT and SVF resulting from Phase 1 (right). *Source* By Authors
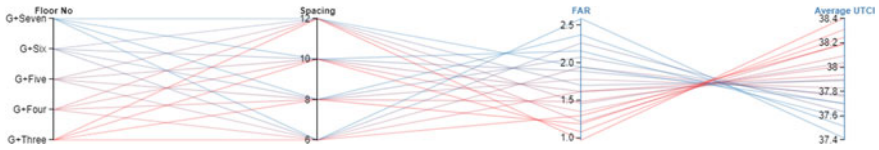
Fig. 12 A graph shows the input values and the resulting FAR and UTCI for the 20 cases in Phase 1. *Source* By Authors
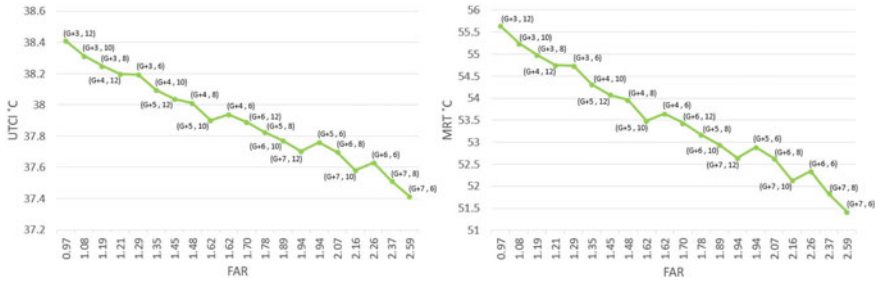
Fig. 13 The relationship between UTCI and FAR resulted from Phase 1 (left), the relationship between MRT and FAR resulted from Phase 1 (right). *Source* By Authors

3.1.2 Floor Area Ratio (FAR)

The change in the number of floors of buildings and the spacing between buildings both affect FAR, since the distances between buildings change by changing the width of the buildings. Through the results of phase 1, the following graph shows the values of the inputs of the 20 cases in phase 1, FAR values and the UTCI values, and the graphs show that FAR also has a strong effect on OTC, but with an inverse relationship. The higher the FAR, the lower the UTCI is and the better the thermal performance, and the lower the FAR, the higher the UTCI value and the worse the thermal performance. This is due to the increase in enclosure percentage by increasing the number of floors and reducing the distances between buildings, thus reducing solar radiation, which positively affects OTC (Fig. 12 and 13).

3.1.3 Building Coverage Ratio (BCR)

The spacing between buildings was the only factor that affected BCR, as it changes by the change of building widths, and the number of floors is not included in the calculation of BCR. The results of phase 1 is shown in the following graph, which illustrates the input values for the different cases and the values of the BCR and the corresponding UTCI, showed that the relationship between BCR and OTC is an irregular relationship that cannot be relied upon when designing for the purpose of environmental optimisation. It could be shown that there are some BCR values
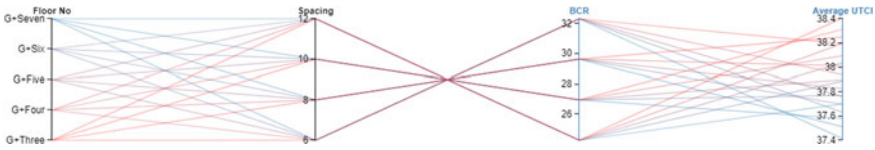
Fig. 14 A graph shows the input values and the resulting BCR and UTCI for the 20 cases in Phase 1. *Source* By Authors
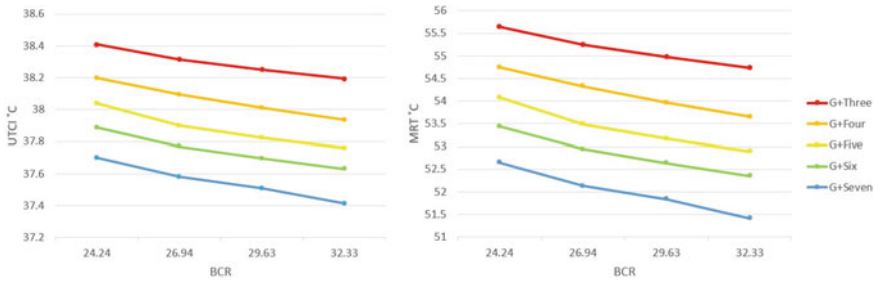
Fig. 15 The relation between UTCI and BCR resulted from Phase 1 (left), the relation between MRT and BCR resulted from Phase 1. *Source* By Authors

that give different results for UTCI, and the reason here is due to the fact that when increasing the number of floors, the thermal performance improves, but the value of BCR remains constant. And vice versa, when reducing the number of floors, the thermal performance deteriorates at the same value as BCR (Figs. 14 and 15).

3.2 Phase 2

In this phase UWG used to show the effect of the urban heat island by produces modified values for the air temperature, relative humidity and wind speed after adding the urban context.

The results of this phase showed a noticeable difference in UTCI values for all cases compared to their counterparts in phase 1, and the decrease is estimated about 0.4 °C. This is due to the changes in air temperature, wind speed and relative humidity values. The MRT values were not affected because they are related to solar radiation.

From these results, it was concluded that adding an urban context have a great impact on OTC and deducing the urban weather file through UWG gives more accurate values with a noticeable difference and helps to significantly improve OTC.

As for the relationship between UTCI and the rest of the factors such as SVF, FAR, and BCR, the results of the second phase showed the same relationships, but with a slight change in the UTCI values as it mentioned. The relationship between UTCI

and SVF was completely direct, inversely with FAR, and an irregular relationship with BCR.

3.3 Phase 3

The third phase of the simulation consists of 4 parts, in each part, the number of floors and the spacing between buildings are changing, while fixing the rest of the three arrays with average values for the number of floors and the distances between buildings as G+five and 9 m respectively, and repeat these cases 4 times as follows:

- Array A, in the western direction.
- Array B, in the northern direction.
- Array C, in the eastern direction.
- Array D, in the southern direction.

3.3.1 Part 1 (Array A—Western Direction)

The results of this part show that the western direction is one of the directions that has the most impact on OTC, and the change in it shows a noticeable difference in the values of MRT reached 1.8 and 0.4 ˚C in UTCI. The highest value of UTCI was 37.6 ˚C, and it was for the lowest case in floor numbers and the largest in spacing between buildings, as is the case in the previous phases. The lowest value of UTCI and the best thermal performance was 37.2 ˚C for the case with the highest number of floors and the lowest in the spacing between buildings also as before, so the difference between the highest and lowest value of UTCI is about 0.4 ˚C when changing the western array and fixing the rest of the arrays.

This is due to the fact that the sun's path is a long high path in summer, and the sun rises in the NE and sets in the NW. Therefore, the duration of the day becomes longer and the eastern and western directions receive the greatest amount of solar radiation as shown in Fig. 17. Additionally, the altitude angle of the sun decreases in the early morning and late afternoon (Fig. 16). Thus, increasing buildings heights and decreasing the spacing between them in the western direction can block solar radiation and provide a large amount of shading, which improves OTC.

3.3.2 Part 2 (Array B—Northern Direction)

The results of this part show a negligible difference in the values of the UTCI, and therefore the change in the northern side has a weak effect on OTC.

This is because the sun path is from the NE direction to the NW, passing through the south, which makes the solar radiation in the northern direction the lowest; throughout the year and not only in the summer, compared to the other directions.
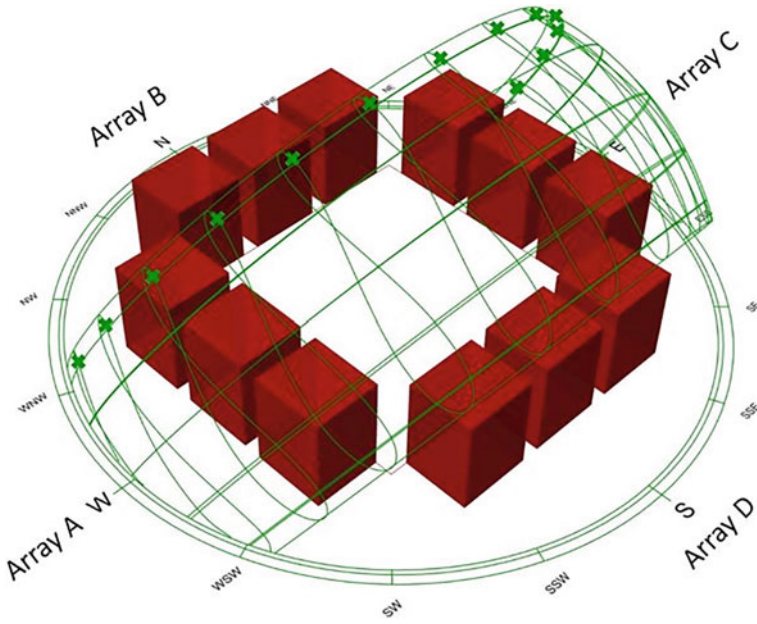
Fig. 16 Original directions to the 4 arrays of the model. *Source* By Authors
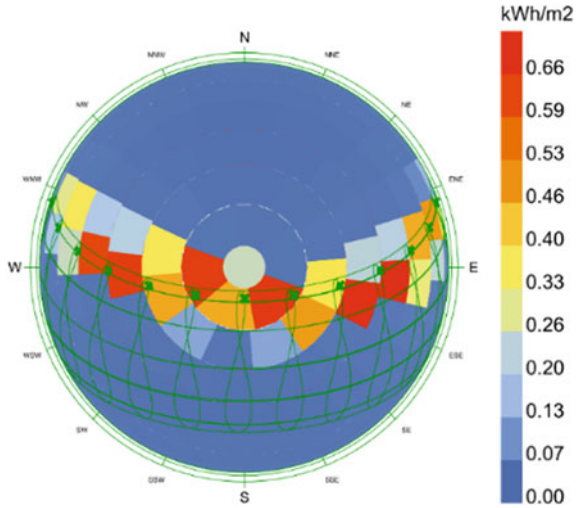
Fig. 17 The direction of the total radiation is on the path of the sun, 16 July. *Source* By Authors

Therefore, increasing the buildings heights and decreasing the spacing between them do not significantly affect the shading and their effect on OTC is very weak.

3.3.3 Part 3 (Array C—Eastern Direction)

The results of this part showed a significant difference in the MRT and UTCI values by 2.1 ˚C and 0.5 ˚C respectively. As the highest value reached by UTCI, which represents the worst performance for OTC, is 37.8 ˚C for the case had the lowest number of floors and the most spacing between buildings, while the lowest value reached by UTCI and the best performance of outdoor thermal comfort amounted to 37.3 ˚C for the case with the highest number of floors and the lowest in the spacing between buildings. From this it is concluded that the eastern direction is influential direction among the four directions on OTC.

This is consistent with the sun's path and its altitude angle as mentioned in Part 1. It is worth mentioning that, the intensity of solar radiation in the eastern side is stronger than its intensity in the western side. Therefore, the effect of the eastern side in blocking the solar radiation and improving OTC is greater than the western side.

3.3.4 Part 4 (Array D—Southern Direction)

The results of this part show a very weak difference between the highest value reached by UTCI and the lowest value, from which we conclude that the southern direction does not have a noticeable effect on OTC in summer.

This is because the sun's path is almost perpendicular in summer. Additionally, in the south direction, the sun reaches its highest altitude. Thus, neither increasing the buildings heights nor decreasing the spacing between them can block solar radiation or provide shading effectively, which explains why OTC is slightly affected by the change in the southern side.

Figure 18 shows the difference between the 4 arrays in UTCI and MRT values in the 20 cases of each part.

4 Conclusions

The results of the first phase showed a strong direct relationship between SVF and UTCI, while the relationship was inverse between UTCI and FAR, and an irregular relationship with BCR. The difference in UTCI values reached 1.0 ˚C for the case that the number of floors was G+Seven in compliance with the building codes, but when the height was increased to G+Ten, the difference in the UTCI reached 1.6 ˚C in a significant improvement in the outdoor thermal comfort. The difference increases as the number of floors increases.
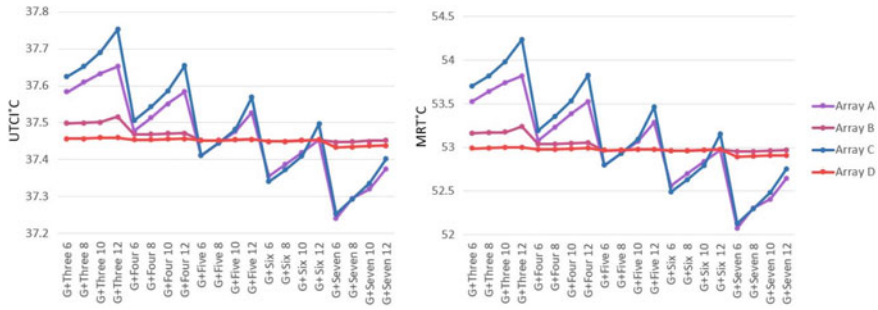
Fig. 18 A Line graph shows the difference in UTCI acting between the four arrays in Phase 3 (left), the difference in MRT acting between the four arrays in Phase 3 (right). *Source* By Authors

The results of the second phase showed that the urban context have a great impact on OTC and the importance of using the UWG to obtain more accurate results, as the difference in the values of UTCI reached 0.4 °C between the cases in phase 2 and their counterparts in phase 1, which is considered a noticeable value. As for the relationships between UTC and MRT with each of SVF, FAR, and BCR, it showed the same relationships as phase 1 results.

The results of the third phase showed that the buildings in the eastern and western directions have the most impact on OTC, whereas the northern and southern directions have a weak effect on OTC, because the percentage of solar radiation in the eastern and western directions constitutes most of the solar radiation in the summer.

5 Recommendations

Based on the foregoing, this research recommends decision makers to amend the building codes to allow for higher heights to provide a higher percentage of shading and thus improve OTC, as most of the new cities in Egypt have a hot arid climate and lack shading. It recommends the designers trying to reach a lower SVF and a higher FAR to improve the outdoor thermal comfort in the hot dry climate by increasing buildings' heights and increasing the side compactness of the urban space. It is also recommended for designers to design higher buildings in the eastern and western directions to reach higher shading ratios, as most of the solar radiation is concentrated in these two directions in summer. Table 5 shows a summary for the main result, conclusions, recommendation for the three phases of simulation.

Table 5 The results of the three phases with their conclusions and recommendations

	Results	Conclusions	Recommendations
Phase 1	The difference between the cases of higher and lower thermal performance in the values of MRT reached 4.2 and 1.0 ˚C in UTCI moving a level down on the UTCI assessment scale The best thermal performance was in the case with the lowest number of floors and the largest in spacing between buildings The best thermal performance was in the case with the highest number of floors and least in the distances between buildings The difference in the UTCI values when fixing the spacing between buildings and changing the floor numbers reach 0.8 ˚C, while when fixing the floor numbers and changing the spacing between buildings, the difference ranges from 0.2 to 0.3 ˚C	SVF has a significant impact on OTC and the relation between UTCI and SVF is completely direct FAR has a great impact on OTC with an inverse relationship between UTCI and FAR BCR has a little impact on OTC with irregular relationship The effect of height on OTC is stronger than the effect of spacing between buildings	To design urban areas with low SVF and high FAR
Phase 2	UTCI values reduced by 0.4 ˚C for the 20 cases compared with their counterparts in phase 1 MRT values was same as in phase 1	The surrounding urban context has a great impact on OTC	To use UWG in simulating OTC to achieve accurate results
Phase 3	Array A—Western direction: The difference between the cases of higher and lower thermal performance in the values of MRT reached 1.8 and 0.4 ˚C in UTCI Array B—Northern direction: The difference in values of UTCI and MRT between the higher and lower cases in terms of thermal performance is negligible Array C—Eastern direction: The difference between the cases of higher and lower thermal performance in the values of MRT reached 2.1 and 0.5 ˚C in UTCI Array D—Southern direction: The difference in values of UTCI and MRT between the higher and lower cases in terms of thermal performance is negligible	The western direction is one of the directions that has the most impact on OTC The northern and southern directions have a negligible impact on OTC The eastern direction has the most influence on OTC	To increase the heights of buildings in the eastern and western directions and reduce the spacing between buildings in those directions

Credit Authorship Contribution Statement Maram W. Rezk: Generating the idea, Collecting data, Methodology, Original draft preparation and Editing.

Ashraf A. Almokadem: Reviewing and Supervision.
Nancy M. Badawy: Editing, Reviewing and Supervision.
Heba A. Ahmed: Editing, Reviewing and Supervision.

References

1. Tumini I et al (2016) Urban microclimate and thermal comfort modelling: strategies for urban renovation. 7(1):22–37
2. Zhang Y, Liu C (2021) Parametric urbanism and environment optimization: toward a quality environmental urban morphology. IJERPH 18(7):3558
3. Basaly LG et al (2019) Improving the functional performance of outdoor spaces in hot arid region using photovoltaics systems. In: 2019 Advances in science and engineering technology international conferences (ASET). IEEE
4. Ibrahim Y et al (2021) A parametric optimisation study of urban geometry design to assess outdoor thermal comfort. Sustain Cities Soc 75:103352
5. Elzeni MM, ELMokadem AA, Badawy NM (2022) Impact of urban morphology on pedestrians: a review of urban approaches. JC 129:103840
6. Saleh M (2012) Using the tools of parametric urbanism toward a more responsive environmental urban morphology. University of Alexandria Alexandria, VA, USA
7. Çalışkan O (2017) Parametric design in urbanism: a critical reflection. JPPR 32(4):417–443
8. Ibrahim Y et al (2022) Multi-objective optimisation of urban courtyard blocks in hot arid zones. 240:104–120
9. Mohamed AN et al (2022) Improve urban form to achieve high social sustainability in a residential neighborhood Salam new city as a case study. 12(11):1935
10. Basaly LG et al (2021) Improvement of outdoor space microclimate in hot arid regions using solar pavilions. 147(3):05021027
11. Mahmoud H, Ghanem H (2019) Urban geometry mitigation guidelines to improve outdoor thermal performance in Egyptian hot arid new cities. JES 47(2):172–193
12. Jafari M et al (2018) Characteristics of arid and desert ecosystems, pp 21–91
13. Shafaghat A et al (2016) Street geometry factors influence urban microclimate in tropical coastal cities: a review. 17(1):61–75
14. Perini K, Magliocco A (2014) Effects of vegetation, urban density, building height, and atmospheric conditions on local temperatures and thermal comfort. JUFUG 13(3):495–506
15. Skarbit N et al (2017) Employing an urban meteorological network to monitor air temperature conditions in the 'local climate zones' of Szeged, Hungary. 37:582–596
16. Petralli M et al (2014) Urban planning indicators: useful tools to measure the effect of urbanization and vegetation on summer air temperatures. 34(4):1236–1244
17. Lin P et al (2017) Effects of urban planning indicators on urban heat island: a case study of pocket parks in high-rise high-density environment. 168:48–60
18. Lin T-P et al (2010) Shading effect on long-term outdoor thermal comfort. 45(1):213–221
19. Hwang R-L et al (2011) Seasonal effects of urban street shading on long-term outdoor thermal comfort. 46(4):863–870
20. Wei R et al (2016) Impact of urban morphology parameters on microclimate. Procedia Eng 169:142–149
21. Handbook, A.J.V. and A.-C. Engineers, Fundamentals, ASHRAE–American society of heating (2017)
22. Achour-Younsi S, Kharrat F (2016) Outdoor thermal comfort: impact of the geometry of an urban street canyon in a Mediterranean subtropical climate—case study Tunis, Tunisia. Procedia-Soc Behav Sci 216:689–700

23. Yang F et al (2011) Urban design to lower summertime outdoor temperatures: an empirical study on high-rise housing in Shanghai. 46(3):769–785
24. Aljawabra F (2014) Thermal comfort in outdoor urban spaces: the hot arid climate. University of Bath
25. A review of thermal comfort. TU Delft (2019)
26. Kumar P, Sharma A (2020) Study on importance, procedure, and scope of outdoor thermal comfort—a review. Sustain Cities Soc 61:102297
27. Coccolo S et al (2016) Outdoor human comfort and thermal stress: a comprehensive review on models and standards. 18:33–57
28. Ghani S et al (2021) Assessment of thermal comfort indices in an open air-conditioned stadium in hot and arid environment. 40:102378
29. Lin T-P et al (2019) The potential of a modified physiologically equivalent temperature (mPET) based on local thermal comfort perception in hot and humid regions. 135:873–876
30. Honjo T (2009) Thermal comfort in outdoor environment. Glob Environ Res 2009(13):43–47
31. Tomasetti T (2020) Core Studio
32. Bueno B et al (2013) The urban weather generator. 6(4):269–281
33. Bueno B et al (2014) Computationally efficient prediction of canopy level urban air temperature at the neighbourhood scale. 9:35–53
34. Evola G et al (2020) A novel comprehensive workflow for modelling outdoor thermal comfort and energy demand in urban canyons: results and critical issues. 216:109946
35. Ibrahim YI, Kershaw T, Shepherd P (2020) A methodology for modelling microclimate: a Ladybug-tools and ENVI-met verification study. In: 35th PLEA conference sustainable architecture and urban design: planning post carbon cities
36. Ibrahim Y et al (2020) Improvement of the Ladybug-tools microclimate workflow: a verification study
37. Natanian J et al (2020) From energy performative to livable Mediterranean cities: an annual outdoor thermal comfort and energy balance cross-climatic typological study. 224:110283

Field Measurements Used to Validate Envi-MET and Conduct Sensitivity Analysis in Egypt

Esraa Ebrahiem Salim, Naser Fawzy Ramadan, and Mohamed Saad

1 Introduction

Today's population is confronted with unfamiliar human changes in the lower and middle atmosphere of various other natural systems and global depletion. Apart from recognizing that these changes would affect economic activity, infrastructure and ecosystems managed at an early stage; global climate change is now recognized as a risk for population health. Globalization has created new, broad-based effects on patterns of human health. Some global changes are associated (in particular climate), including changes in regional food crops, the emergence of infectious diseases, the prevalence of cigarette smoking, various economic, social, demographic and environmental conditions, and health disparities.

Primary prevention from these global impacts is an enormous challenge at source to reduce health risks.

Conceptual perspectives are needed which go beyond the traditional understanding of causation and prevention. The challenge of mitigation strategies for climate change is clear. In the meantime, new instruments and policies will be required to reduce the health risks, which were or cannot be prevented as a result of global change. In order to redefine human society's plans, development, transportation, development, use, exchanges, and resources to support human lives sustainably and in long-term health, the health sector needs to work with other sectors.

E. E. Salim (✉) · N. F. Ramadan
Department of Architecture, Higher Institutes of Engineering and Technology, km 21, Cairo, Belbeis, Egypt
e-mail: esraa.ebrahiem@oi.edu.eg

M. Saad
Architecture and Building Technology at Architecture Department, Higher Institutes of Engineering and Technology, km 21, Cairo, Belbeis, Egypt
e-mail: M.saad@oi.edu.eg

Urban design factors can affect public health in several ways, including physical activity, traffic accident risk and sound level, pollution exposure, access to health resources, mental health and affordability, which affect household's ability to affordability.

The impact of the physical environment on health and well-being has become a common concern of the "new urbanism" called for the reintegration of public health and urban design. The application of human needs in the urban space which include air and water clean, safety, transportation, social interaction, and open space for leisure. Can lead to environmental space through:

- Reduction of urban fabric imbalances.
- Car use, air and noise pollution.
- Quality of public spaces, social cohesion.
- Healthy lifestyles and increase employment opportunities

As a result, environmental impacts must be considered during the design phase. The influence of space design on internal climate can be monitored before implementation using simulations such as the ENVI-met program to assure the best space design before the implementation phase on the site.

This research aims to covering some aspects of the environmental impacts of socio-economic development. Sustainable use of land, water, energy and biological resources to develop good health and wellbeing, global sustainability—the obstacles and ways in which they could be overcome.

2   Problem Definition

1. Public health research indicates that heat extreme affects human health.
2. Planning policies are incompatible with human health, in particular rigid standards of zoning and design.
3. Urban ratios effects climate change which affects urban spaces efficiency.

3   Methodology

This study validates the Envi-met software using measured and predicted air temperatures, relative humidity, wind speed in a residential area in El Obour city. The study's objective is to check the performance efficiency of the software using statistical analysis.

4 Validation of Envi-Met Software Using Measured and Predicted Air Temperatures, Relative Humidity and Wind Speed in Obour City

Obour city is the second-generation Satellite city located around and close to Cairo with a short and middle term objective of minimizing population density and benefiting from the available basic structures such as services and labour in attracting population, activities, creating new job opportunities, and economic elements that are associated with the mother city.

This study validates the Envi-met software using measured and predicted air temperatures, relative humidity, wind speed in a residential area in El Obour city. The study's objective is to check the performance efficiency of the software using statistical analysis.

Air temperature, relative humidity, and wind speed measured at the height of 1.8 m above the ground took 2 h from 3 to 4 pm at date 12/4/2021 used as the variables for the simulation validation (Fig. 1; Table 1).

4.1 Air Temperature Validation

See Figs. 2 and 3; Table 2.

4.2 Relative Humidity Validation

See Figs. 4 and 5; Table 3.

4.3 Wind Speed Validation

See Table 4; Fig. 6.

5 Results Ratios of Relationship Between Program Simulation and Site Measures

- Air temperature, the difference about 0.35 and 0.65 °C.
- Relative humidity, the difference about 0 and 1%.
- Wind speed, the difference about 0.08 and 0.58%.
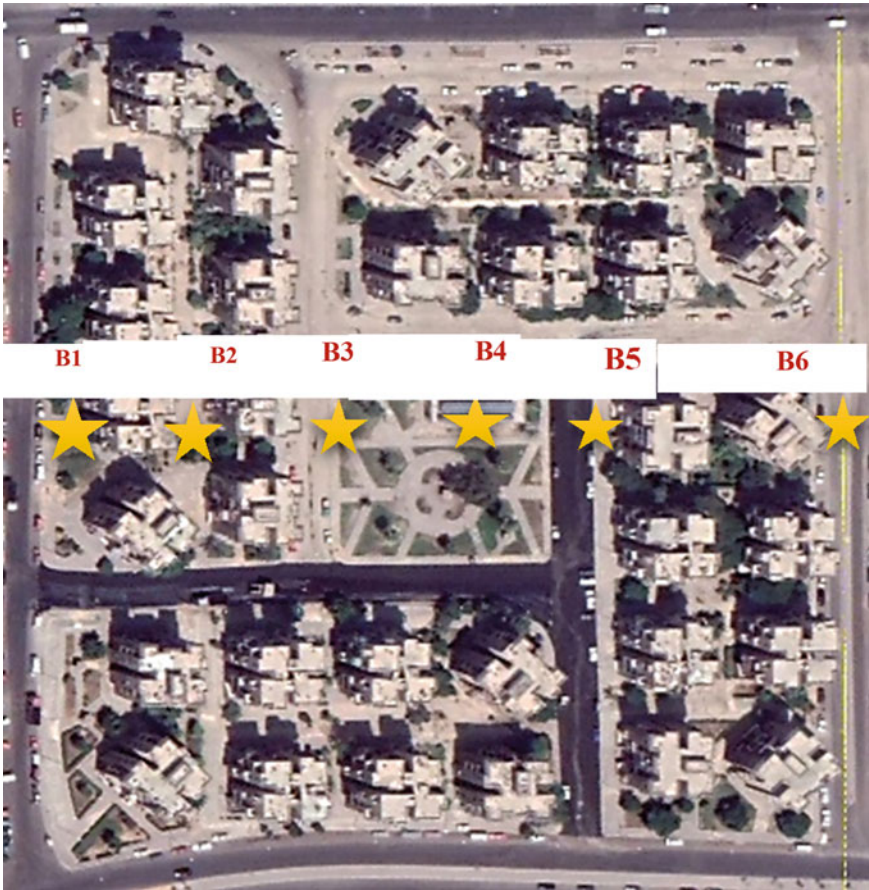
Fig. 1 Shows the points were measured in the location. *Source* Google earth

Table 1 The simulation data

Date	12/4/2021
Time	3 pm
Temperature	25.3 °C
Relative humidity	31%
Wind speed	3.3 m/s

6   Conclution

This study presents the verification of measured and predicted air temperatures, relative humidity and wind speed in Obour City using the Envi-met program. Measured and forecast data was taken for 2 h, and simulations were performed; the degree of
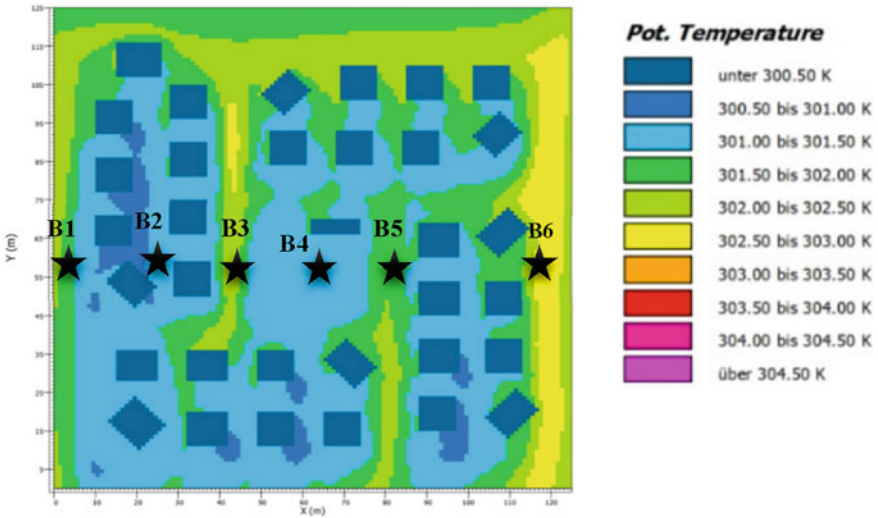
Fig. 2 Shows the measure points on the simulation results. *Source* Envi-mat program

Fig. 3 The graph shows the relationship between program simulation and measured air temperature, about 0.35 and 0.65 °C. *Source* The researcher
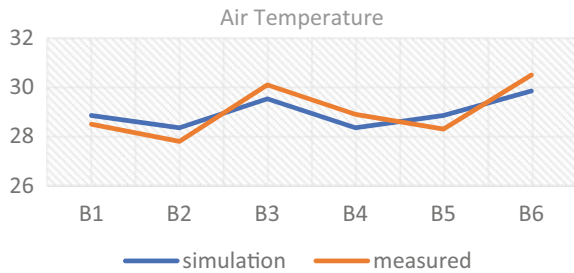
Table 2 Show the field measures and the simulation result of air temperature

Air temperature	B1	B2	B3	B4	B5	B6
Simulation	28.85	28.35	29.53	28.35	28.85	29.85
Measured	28.5	27.8	30.1	28.9	28.3	30.5

agreement was signed. Our study shows that the Envi-met software is well validated for further analysis because all parameters behave well.

We can use Envi-Met simulation programe to examine urban spaces design applied on a global scale or in various geographical areas by choosing the project location on the programe and choose the best design that provides thermal comfort to users prior to implementation.
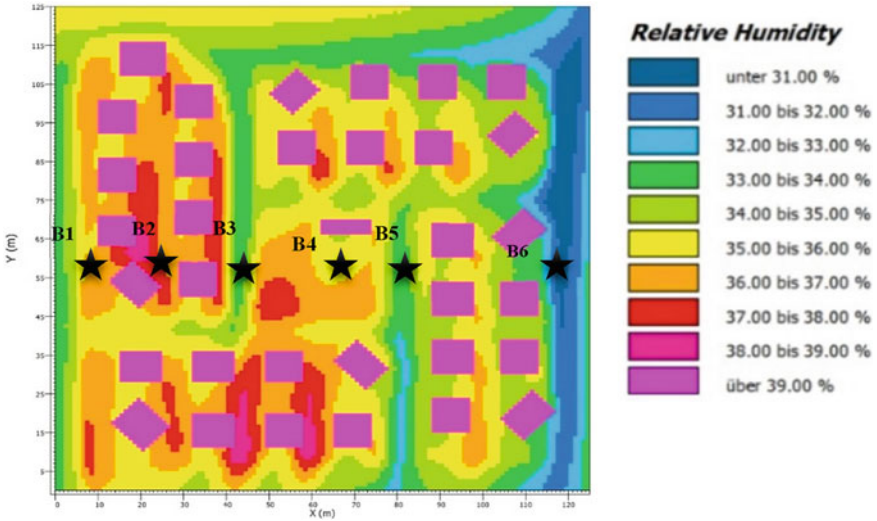
Fig. 4 Shows the shows the measure points on the simulation results. *Source* Envi-mat program

Fig. 5 Graph showing the relationship between program simulation and measured relative humidity, the difference about 0 and 1%. *Source* The researcher
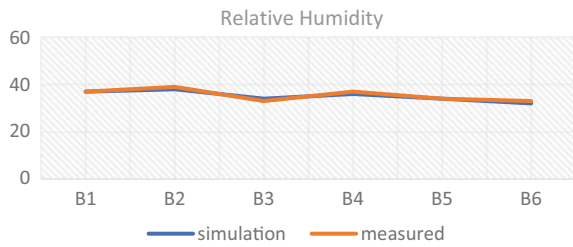
Table 3 Show the field measures and the simulation result of relative humidity

Relative humidity	B1	B2	B3	B4	B5	B6
Simulation	37	38	34	36	34	32
Measured	37	39	33	37	34	33

Table 4 Show the field measures and the simulation result of wind speed

Wind speed	B1	B2	B3	B4	B5	B6
Simulation	2.52	2.02	3.02	2.02	2.52	3.02
Measured	3.1	2.5	3.6	2.6	2.6	3.6
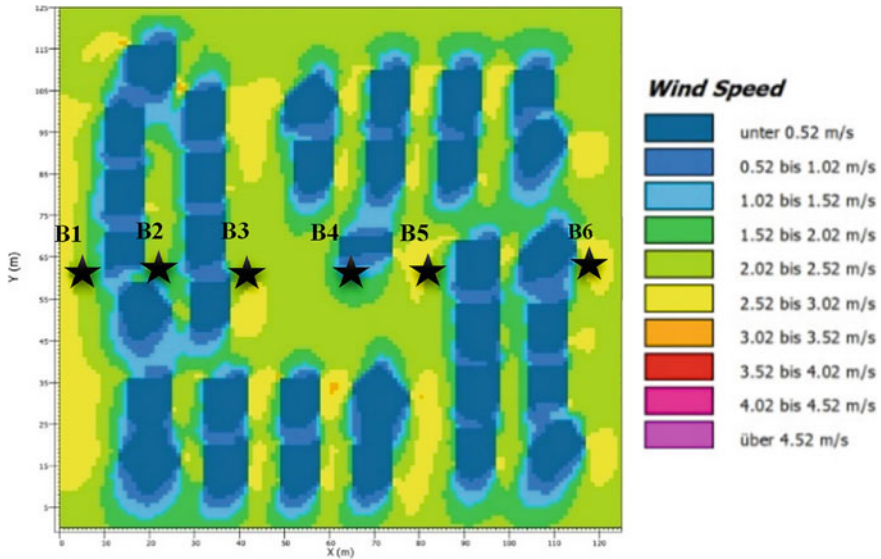
Fig. 6 Shows the measure points on the simulation results. *Source* Envi-mat program

7 Recommendation

Now, we must take care of our urbanity because everything around us affects climate change, especially extreme heat and wind speed, which impacts our health and lives. The world is now suffering from the problem of disease spread, which we can reduce with our designs and stop with appropriate decisions in our new urbanism.

Future developments of our urbanity are in the hand of researchers, professionals, the public.

- Researchers, must continue work on this field to achieve more details about the relation between the urban environment and our health, and continue the study of finishing materials' effect on the environment.
- Professional people need to remind the public and their work partners of the value of taking into account balanced ratios when designing every place for people in order to build comfortable places that are walking able and healthy.
- The general public should be mindful of the advantages and health effects of metropolitan environments. The public alone will have sufficient leverage to get politicians to promote and demand new urban leaders and to take part in urban initiatives to learn how their urban spaces can be preserved.

References

1. McMichael AJ (2013) Globalization, climate change, and human health. New England J Med Global Health. Massachusetts Medical Society
2. Alberti M, Derek B, Kristina H, Coburn B, Christina A (2003) The impacts of urban patterns on aquatic ecosystems, An empirical analysis in Puget Lowland Sub-Basins. Seattle, Department of Urban Design and Planning, University of Washington
3. Nicola D, Caroline B, Shibu R, Sergio P, Bramley G (2010) Elements of urban form. Oxford Institute for Sustainable Development, Oxford Brookes University, Oxford, UK
4. Huddleston NF, Laurie G, Sally T, Tracey E (2013) Climate change evidence and causes, an overview from the Royal Society and the US National Academy of Sciences
5. Public Health Advisory Committee, healthy places, healthy lives: urban environments and wellbeing. A report to the Minister of Health, Wellington, New Zealand, April 2010. http://www.phac.health.govt.nz
6. Witten K, Exeter D, Field A (2003) The quality of urban environments: mapping variation in access to community resources. Urban Stud
7. VicHealth (2016) Planning and designing healthy new communities: Selandra rise: research summary. Melbourne
8. https://en.climate-data.org/africa/egypt/qalyubia-governorate/al-obour-3828/
9. Human Development Report. Uncertain times, unsettled lives: Shaping our future in a transforming world, 08 Sept 2022
10. Racha R (2021) The state of the Sustainable Development Goals in Egypt: focus on poverty and inequality. Sustainable development report

Smart Cities and Communities

Sustainable Development: A Review of Concepts, Domains, Technologies, and Trends in Smart Cities

Mohamed Elnahla and Hossam Wefki

1 Introduction

Sustainable development is a complex and multidimensional concept that aims to balance human well-being's economic, social, and environmental aspects. According to World Commission on Environment and Development, sustainable development is defined as "a development that meets the needs of the present without compromising the ability of future generations to meet their own needs" [1]. This definition implies two key principles: first, recognizing the basic needs of the people living in poverty and their right to a decent quality of life, and second, acknowledging the limits of natural resources and ecosystems to support human activities. However, achieving sustainable development in an era of rapid urbanization and technological change poses significant challenges for policymakers, planners, and practitioners [2]. The United Nations Department of Economic and Social Affairs expects the number of people living in urban areas to increase to 68% by 2050, up from more than half of the world's population currently living in urban areas [3]. Urbanization brings opportunities for economic growth, social inclusion, and cultural diversity but also generates pressures on land use, infrastructure, energy, water, waste management, and climate change. Some megacities such as Tokyo, Delhi, Shanghai, and Cairo have reached unprecedented population density and complexity levels, requiring innovative solutions for urban governance and service delivery.

Smart cities are one of the emerging paradigms. Based on the United Nations Economic Commission for Europe, a smart city can be defined as "an innovative city that uses information and communication technologies (ICTs) and other means to

M. Elnahla (✉) · H. Wefki
Civil Engineering Department, Faculty of Engineering, Port Said University, Port Fouad, Egypt
e-mail: mohamed.elnahla@eng.psu.edu.eg

H. Wefki
e-mail: hossam.wefki@eng.psu.edu.eg

improve quality of life, the efficiency of urban operation and services, and competitiveness, while ensuring that it meets the needs of present and future generations concerning economic, social, cultural and environmental aspects" [4]. However, smart cities are not homogeneous; they can vary in their domains, technologies, and trends depending on their context, vision, and goals [5].

This research paper provides a review of the existing literature on the sustainable development of smart cities, focusing on four main dimensions:

(a) the conceptualization and definition of smart cities.
(b) the domains of smart city.
(c) the technologies and applications that enable smart city solutions.
(d) the current and future trends in smart city development.

This paper aims to provide a comprehensive overview of the state-of-the-art knowledge on smart cities and identify gaps and challenges for future research by examining the evolution of smart cities using in-depth network analysis on relevant Scopus database papers published between 1997 and 2023 Q1. The network analysis allows us to capture the main themes, trends, and relationships among the publications and reveal how the concept of smart cities has changed over time. The study is organized as follows: The study methodology, including the steps for gathering and analyzing data, is described in Sect. 2. The results are presented in Sect. 3. The findings are discussed in Sect. 4, together with study implications for smart cities. Section 5 shows the recommendations for further research on smart cities while, Sect. 6 concludes by outlining the study's primary contributions, and shortcomings.

As this paper is studying Smart Cities so it targets the following Sustainable Development Goals (SDGs):

• Goal 3: Good health and well-being.
• Goal 6: Clean water and sanitation.
• Goal 7: Affordable and clean energy.
• Goal 9: Industry, innovation, and infrastructure.
• Goal 11: Sustainable cities and communities.
• Goal 12: Responsible consumption and production.
• Goal 13: Climate action.

Goal 11 is considered the main target in this study, but other mentioned goals are also covered.

2 Materials and Methods

This study conducted a scientometric study based on [6, 7] to understand the smart city literature. This review aims to present a thorough, organized analysis of the idea of smart cities, along with the technologies and applications surrounding them. The review takes a two-step approach to accomplish this goal.

First, it identifies and examines the main keywords associated with smart cities in the literature using an Analysis of the keyword co-occurrence network. This analysis includes the following steps:

(a) choosing the database and keywords for the search.
(b) performing initial data analytics.
(c) analyzing the leading data indicators.
(d) creating the keyword co-occurrence network.
(e) discussing the topics uncovered by keyword co-occurrence clustering.

Second, by investigating each year, it determines and evaluates the domains of smart cities proposed in studies. This analysis involves repeating the same steps used to create the co-occurrence network to create a network for each year.

This study seeks to give a complete overview of smart cities by following this two-step approach.

The next subsections cover in full the methodological procedure.

2.1 Database Selection and Search

The primary data source for this study was the Scopus database, which is widely regarded as a comprehensive and reliable repository of scholarly publications from prominent worldwide publishers. Among the publishers included in the Scopus database are Emerald Insight, IEEE, Elsevier, Springer, and Taylor & Francis. The Scopus database offers a robust indexing system that facilitates the retrieval of relevant articles on various topics. To maintain high standards of quality and academic rigor in the data, the selection criteria for this study restricted inclusion to journal articles only. The study was centered on examining published articles that explore the topic of smart cities from various contexts and perspectives.

A rigorous and systematic search strategy was employed to reduce the likelihood of including irrelevant or inaccurate papers in the analysis. The main keyword used for the search was "smart cit*", which captured variations such as "smart city", and "smart cities". The search was conducted in English-language journals only. No filters were applied based on the publication date or subject area to avoid missing any important or recent publications on the topic. The search returned 12,148 papers.

2.2 Initial Data Analytics

The bibliographic is exported to record the selected publications and analyze them using descriptive statistics and bibliometric methods. The distribution of publications was examined by year, subject area, keyword, country, source, author, and affiliation to identify the main trends and patterns in smart city research. Table 1 summarizes the main features of smart city articles derived from the Scopus database.

Table 1 The main features of smart city articles

Documents	12,148
Subjects areas	26
Sources	160
Keywords with 100+	160
Countries	133
Time frame	1997–2023 (Q1)

2.3 Analysing the Leading Data Indicators

The leading data indicators are filtered and exported from Scopus by merging the main keywords corresponding to the same topic. Then, these main keywords were categorized for further analysis.

Using PowerBI to visualize the filtered general indicators regarding geographic and chronological information, the subject area, and keyword statistics. Then, a subjective mapping is created using an alluvial diagram between the top 50 keywords and their categories, following the same procedures of [7, 8].

2.4 The Keyword Co-occurrence Network (KCN)

The citation network and the Keyword Co-occurrence Network (KCN) are two network-based methodologies extensively utilized in bibliometric analysis. A citation network identifies popular research based on the frequency of its citations. It investigates the transmission of scientific information by focusing on the relationships between publications cited. However, it does not reveal new patterns in literature. On the other hand, a KCN is a valuable technique for scientometric analysis that examines the keywords in scientific papers to understand the knowledge components and display the major study subjects in a scientific discipline. Keywords provide a quick summary of the main points of the scientific study [7]. The KCN collects relationships between distinct knowledge components. It quantifies the relative relevance of each element within the network based on the density and centrality metrics of keywords. It also incorporates methodologies from co-word networks and portfolio analysis [6]. The KCN approach is more relevant for the present research than citation network methods since authors are interested in analyzing the knowledge components of the articles rather than determining the value and popularity of articles. KCNs are used in this research to analyze the development of subjects in scientific studies on smart cities.

To generate the KCN, the data is split by year to examine the themes and trends of smart city research in different periods. Then a keyword co-occurrence network was created using VOSviewer software, in which nodes correspond to keywords, and the

distance between each pair of nodes is defined by density. The degree of association and interaction between keywords is represented by density. The density-based approach minimizes the weighted sum of the squared Euclidean distance between each pair of nodes. As a result, a high-density number suggests a short distance between two nodes.

3 Results and Discussion

3.1 Geographic and Chronological Information

The analysis began by tracing the evolution of scholarly research into smart cities. Figure 1 depicts the annual propagation of papers in this discipline, exhibiting a spectacular long-term growth pattern. The time range is divided into three periods based on the volume and frequency of publications. The first period, which lasted from 1997 to 2012, was distinguished by a low level of research activity, with only a few articles produced each year. From 2013 to 2016, the second period showed substantial growth in research production as more scholars got interested in the smart city topic. The third period, from 2017 through 2022, had exponential publication growth, peaking in 2022. Based on presently published articles, the expected number of articles published this year will exceed that of the previous year by March 2023. This study analysis confirms the outcomes of [9], which evaluated the literature on smart cities from a computer science and information technology standpoint, and the findings of [10], who studied the smart city literature between 1990 and 2019.

Figure 2 depicts the provenance of research (country contributions); China is the most significant contributor, accounting for 2.5K publications, followed by India (1.5K), the United States (1.5K), the United Kingdom (1000), and Italy (0.9K). The figure depicts the remaining countries with a logarithmic scale bubble to represent each country's contribution and a bar chart representation to better demonstrate the number of publications.
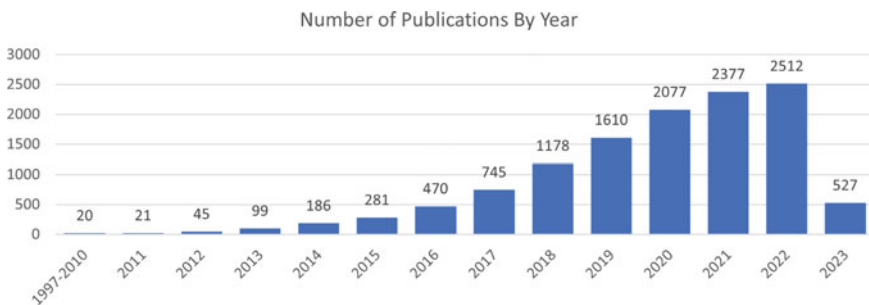
Fig. 1 Number of publications by year
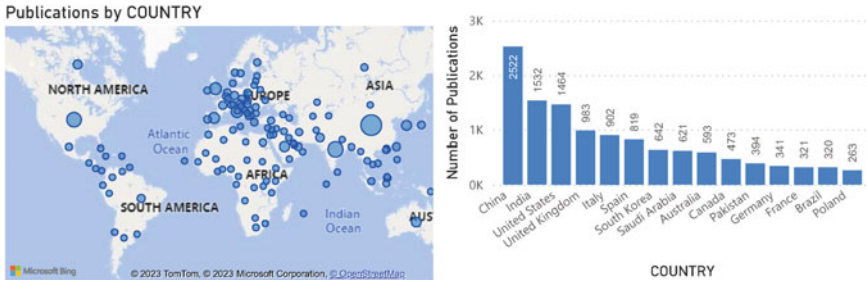
Fig. 2 The origin of research (countries' contributions)

3.2 The Subject Area

Figure 3 discovered that computer science has the most interest with 6725 articles, followed by engineering with 5934 articles, the social sciences with 3347 articles, environmental science with 1495 articles and energy with 1486 articles.

Fig. 3 Subjects of publications
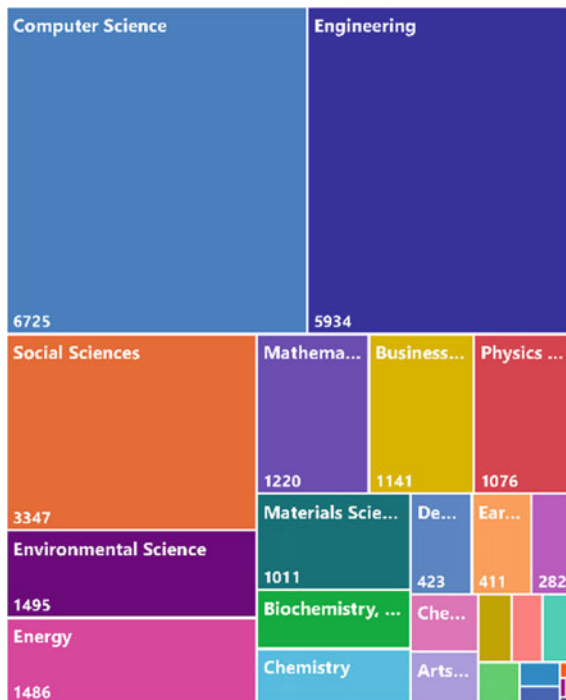
3.3 Keyword Statistics

By investigating the keywords provided by authors in the database and starting by getting the statistics, it was found that some keywords like smart city and smart cities are general and won't help in data analysis. Also, some keywords like "IoT", "Internet of Things", and "Internet of Things (IoT)" are the same, but because authors wrote them differently, the statistics show them as many entities.

So to address this issue, the data is filtered, and keywords with similar meanings are merged. As shown in Fig. 4, IoT was the most used keyword, accounting for 4487 papers, followed by Sustainable Development (654 articles) and Machine Learning (652 articles); these findings confirm the outcomes of [11] who studied the factors of the net zero smart city.

Keywords categorized for better understanding into (communication, environment, data processing, data security, application, testing, data storage, country,

Fig. 4 Author keywords (filtered)—Top 50

factors, data collection, and regulation) as shown in Fig. 5. Applications of Smart Cities are at the top, followed by Data Processing, Data Collection, Data Security, Communication, Environment, and Factors, then Data Storage.

Figure 6 shows a subjective mapping using an alluvial diagram between the top fifty keywords (right) and their categories (left) to show correlations between categorical dimensions, representing them as flows. The number next to the keyword indicates the number of publications that have used this keyword in the Scopus database. This figure helps further investigation of the categorized author keywords by providing a better understanding of the main keywords related to each category.
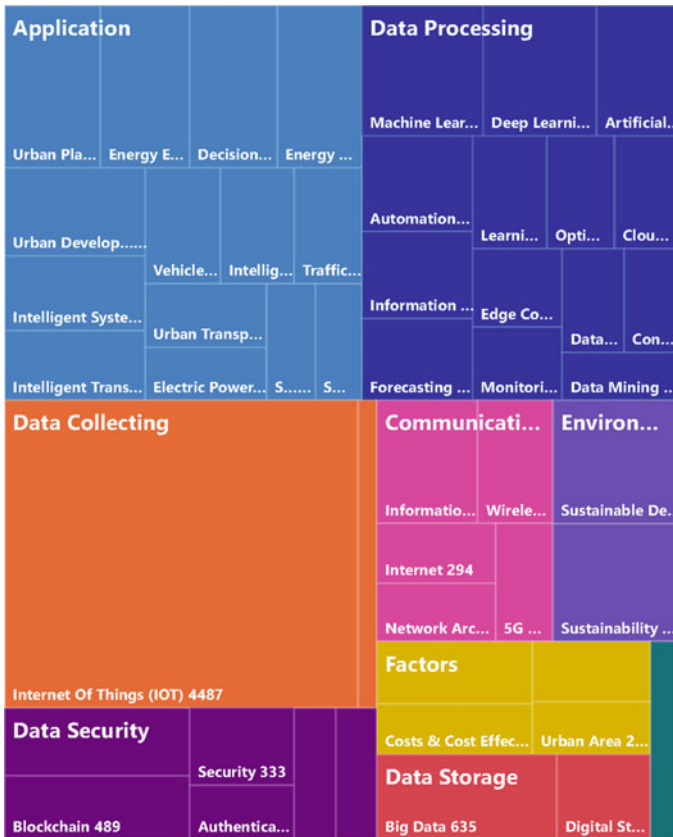
Fig. 5 Author keywords (categorized)
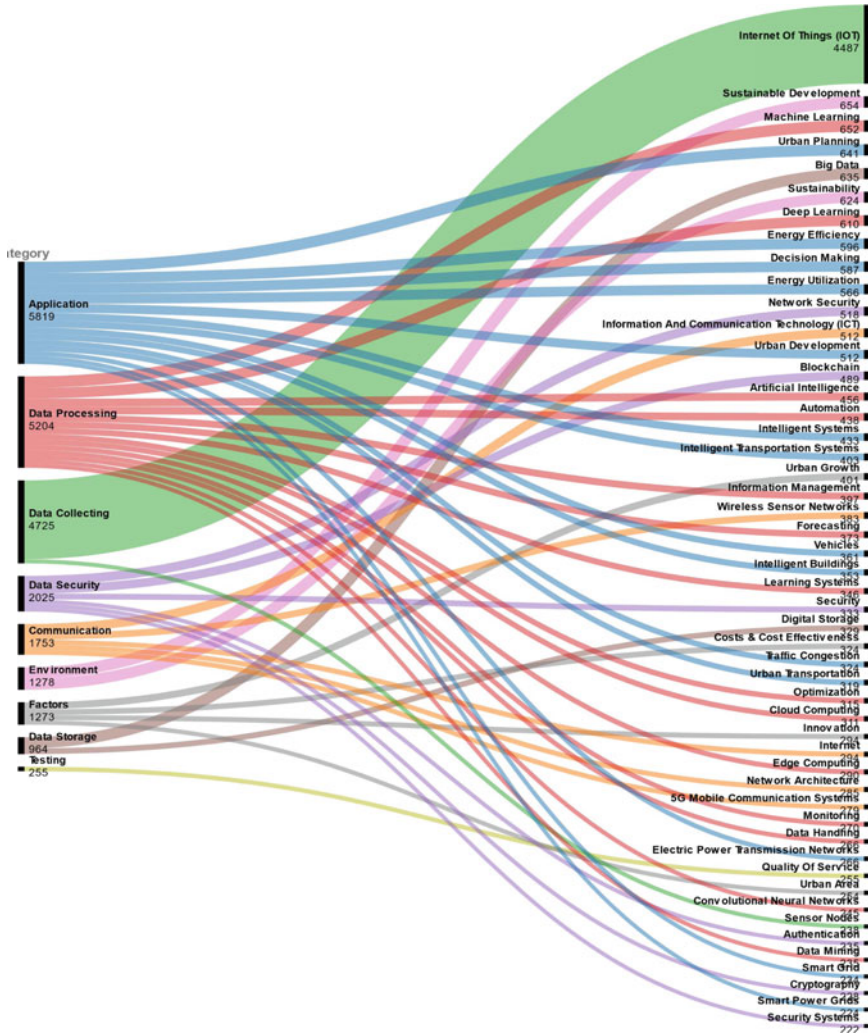
Fig. 6 Subjective mapping using an alluvial diagram between the top fifty keywords (right) and their categories (left)

3.4 Keyword Co-occurrence Networks

To fully understand the evolution of smart cities, this study generated research co-occurrence networks and summarized the development of the field and future trends using the links between keywords and clusters.

3.4.1 An Overview on the Full Period

First, a network is investigated for the full period (1997-2023Q1), as shown in Fig. 7. This network shows the co-occurrence of keywords and their relationships. Through it, the leading technologies and trends governing smart city research can be identified, as they have a bigger node size and more links to other nodes like the Internet of Things, big data, machine learning, blockchain, deep learning, security, and cloud computing.

Moreover, for more accurate detection of the main keywords, the density map in Fig. 8 can show, with a clearer vision, the keywords with the most significant impact.

Also, using a timeline network in Fig. 9 that highlights, with different colors, the nodes of keywords based on the year they first appeared, and detect which of these technologies started from the beginning of research and continued till now, like (the Internet of Things, energy efficiency, big data, cloud computing), and which are new trends that appeared recently and showing better solutions that will continue to improve through years to come, like (artificial intelligence, blockchain).

Although this analysis managed to get a more fabulous look at trends and technologies of smart cities through the entire period network, till further analysis needs to be performed to understand the domains and concept evolution of smart cities for each year of research to find the common theme of the period and the main parts proposed through that time.

So, the database is divided into three periods and a small part of 2023 Q1 as it was evolving while performing the study. These three periods were created based on the annual distribution of journal articles shown in Fig. 1.
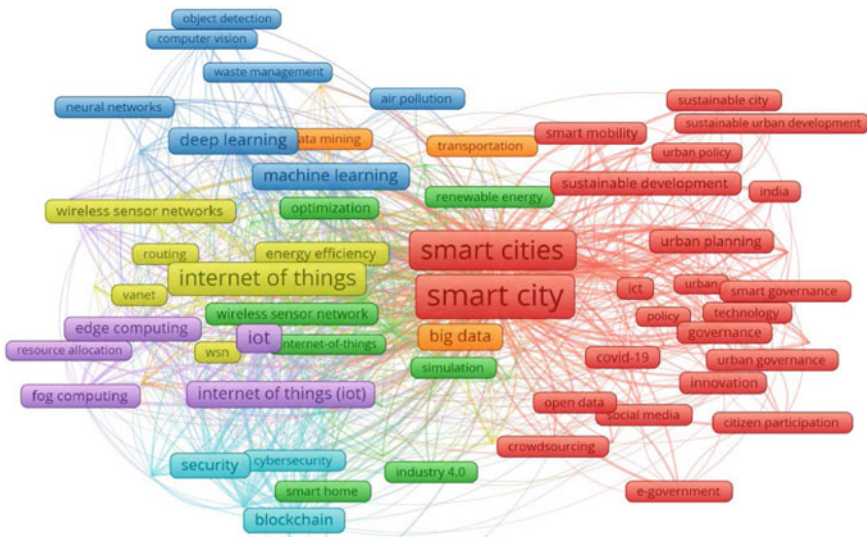
Fig. 7 Keywords co-occurrence network (1997-2023Q1)
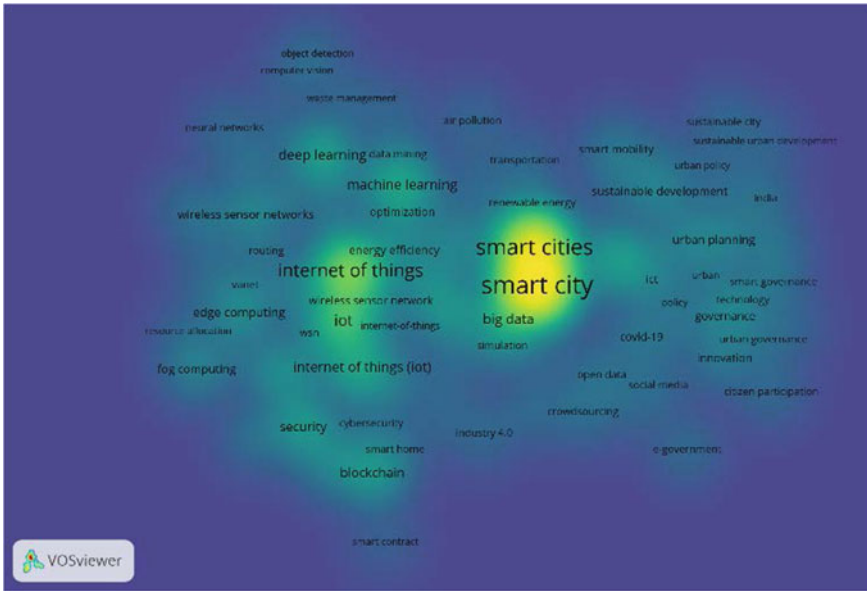
Fig. 8 Keywords co-occurrence density map (1997-2023Q1)
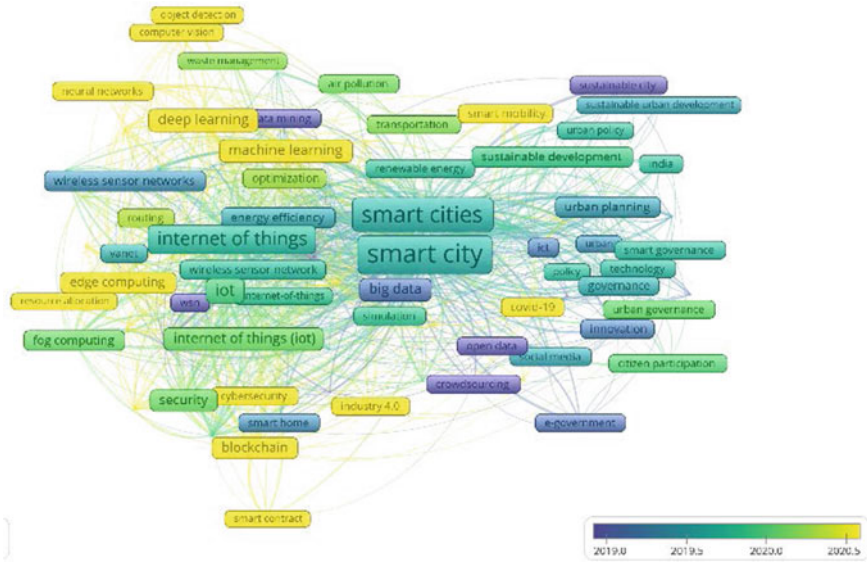
Fig. 9 Keywords co-occurrence network time based (1997-2023Q1)
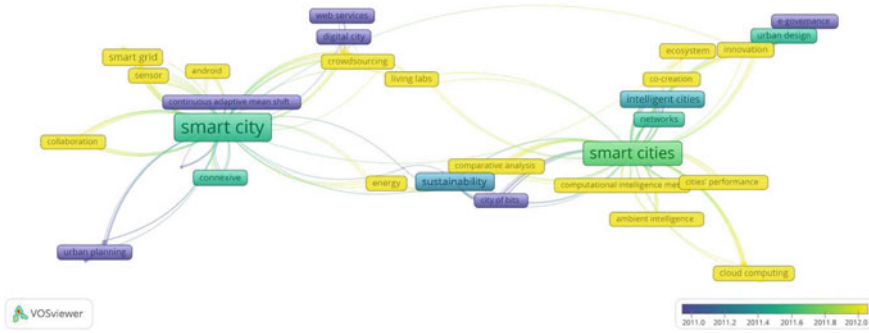
Fig. 10 Keywords co-occurrence network time based (1997–2012)

- The first period (1997–2012)
- The second period (2013–2016)
- The third period (2017–2022)
- At the time of the study (2023 Q1).

3.4.2 First Period (1997–2012)

In this period, authors observed that the first published paper about smart cities in the Scopus database was in 1997, and until 2010, just 20 articles were published. During this very early stage, the longest connected series of keyword nodes show that the concept of smart cities revolved around finding sustainable solutions using knowledge management and data security. The possible applications targeted by smart cities were infrastructure, urban transportation, energy use, and urban growth.

By the end of 2011, the network expanded, and some technologies like GIS started to appear, but no main target or technology was forming the main shape of the smart city till that time.

In 2012, the shape and target of smart cities started to be more apparent by targeting sustainability and using Big Data for the first time; meanwhile, data collection technologies like sensors or Android phones began to gain the interest of researchers.

Figure 10 shows the network from 1997 to 2012.

3.4.3 Second Period (2013–2016)

By entering the second period starting in 2013, smart city research jumped. In 2013, 99 research projects were independently created, nearly the number of all publications produced in the first period. When investigating the network of 2013, Fig. 11 clarifies the reason behind this huge increase as the Internet of Things (IoT) started to be the main technology of smart cities. With its ability to collect huge amounts of
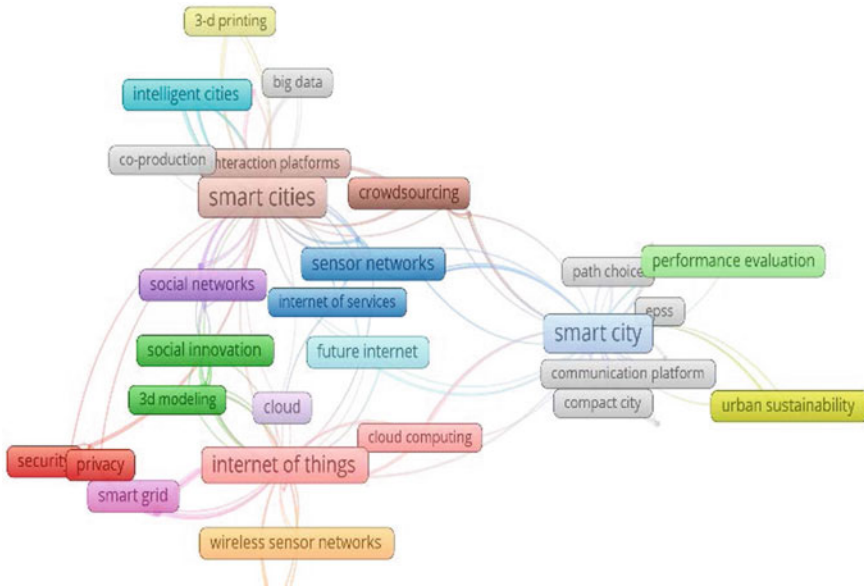
Fig. 11 Keywords co-occurrence network (2013)

information and store it in big data, smart cities can start to be more practical and efficient.

In 2014, as shown in Fig. 12, IoT and big data in smart cities continued to be the leading research topic with the emergence of new aspects like using social media platforms and developing some machine learning algorithms under the name "context-awareness".

In 2015, and by investigating the network in Fig. 13, the network stayed with the same theme as in 2014, but some aspects regarding interoperability and cybersecurity started to gain more interest, and some applications like smart parking evolved.

In 2016, the network of 2015 expanded, and new interests appeared, as shown in Fig. 14, as cloud computing became one of the essential topics and smart grids meant that machine learning started to play a massive role in the structure of smart cities while applications expanded to urban transport and planning and supported decision making. Also, blockchain started to appear in smart city research.

3.4.4 Third Period (2017–2022)

At the beginning of the third period, research in smart cities had its central theme oriented toward the Internet of Things. It focused on big data, machine learning, and artificial intelligence, with the blockchain aspect evolving. Figure 15 shows the network of 2017.
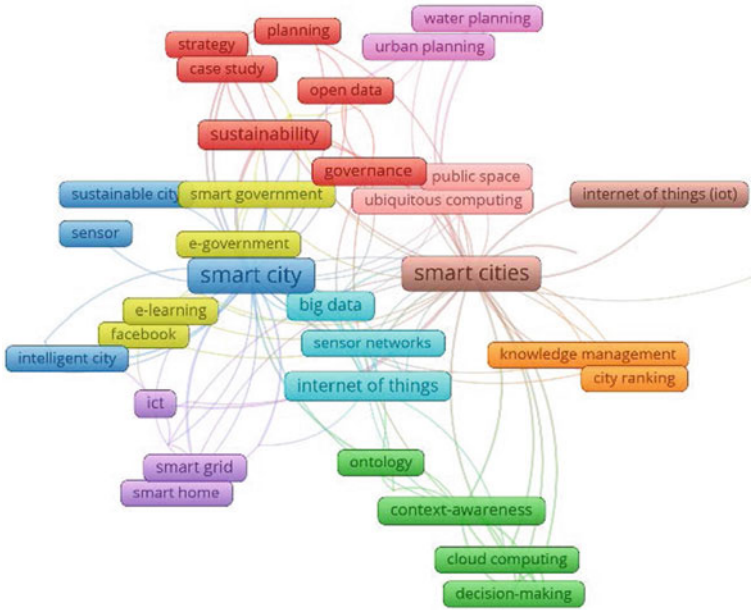
Fig. 12 Keywords co-occurrence network (2014)
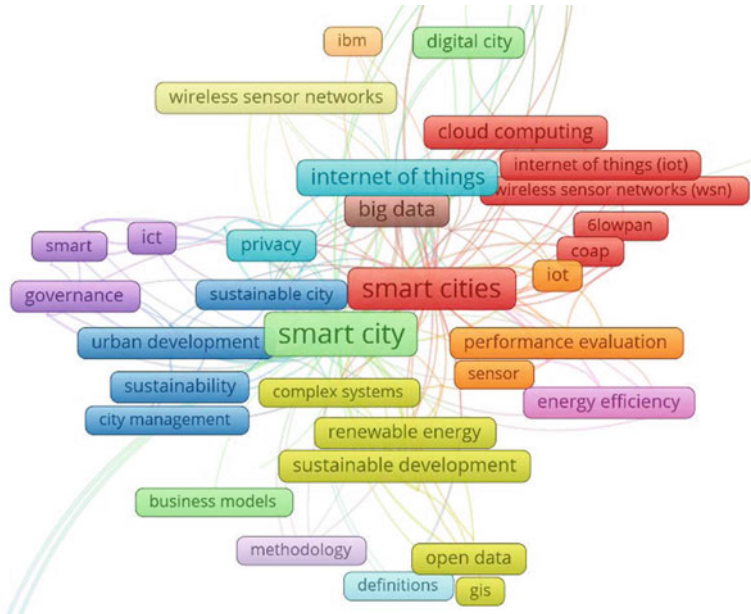
Fig. 13 Keywords co-occurrence network (2015)
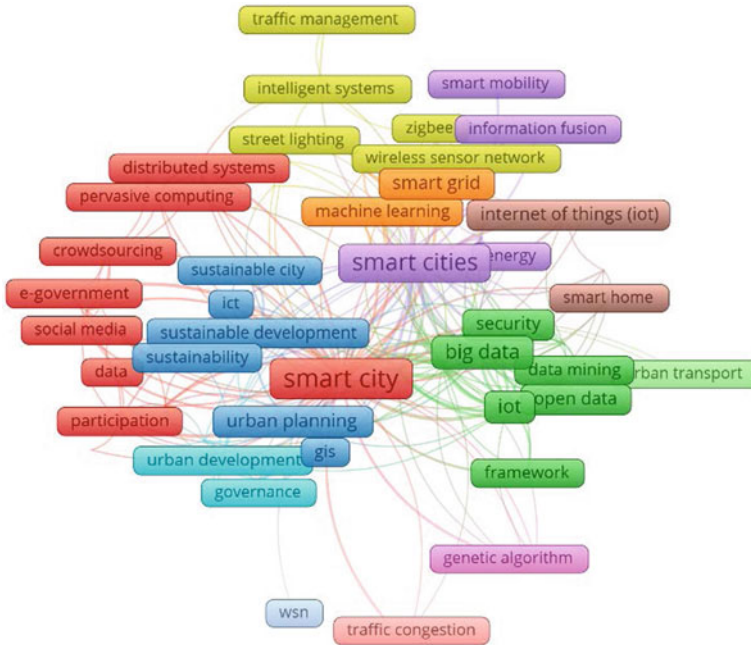
Fig. 14 Keywords co-occurrence network (2016)

In 2018, the network shown in Fig. 16 was the same as in 2017, but a new trend towards the uses of 5G started to gain more interest and helped develop more smart city applications and solutions while providing more data.

In 2019, the network shown in Fig. 17 showed a huge increase in research on Blockchain and more focus on privacy and Industry 4.0 than before.

In 2020, as shown in Fig. 18, during the COVID-19 Pandemic, the focus of most of the studies stayed the same as in 2019. However, new aspects of education, health informatics, and risk assessment started to be taken into consideration by some researchers.

In 2021, as shown in the network in Fig. 19, new trends started to appear as 6G and Society 5.0. Meanwhile, there was greater interest in industry 4.0, digital twins, 3D city models, and genetic algorithms. Also, some devices like drones captured greater interest in studies this year.

Meanwhile, security and Blockchain have become the focal point of much research.

The network of 2022, shown in Fig. 20, shows the same interests as in 2021 but with a focus on AI and deep learning.
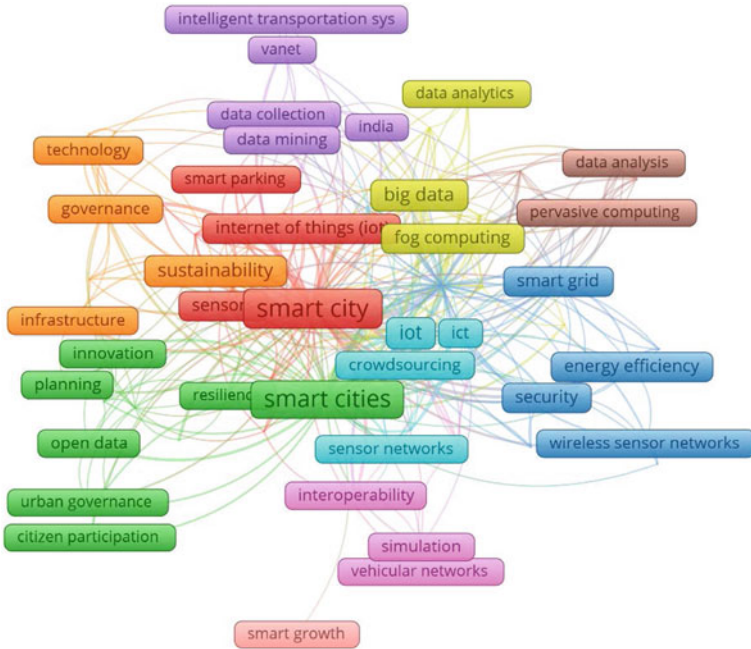
Fig. 15 Keywords co-occurrence network (2017)
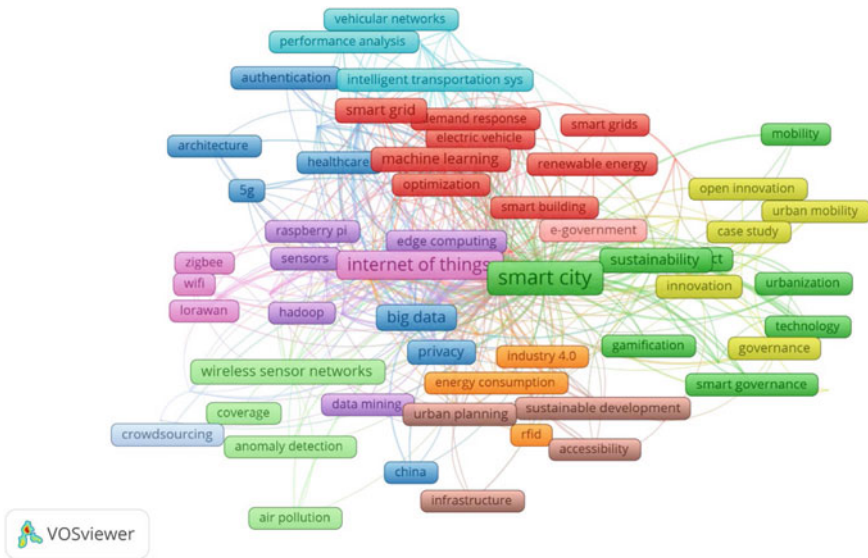
Fig. 16 Keywords co-occurrence network (2018)
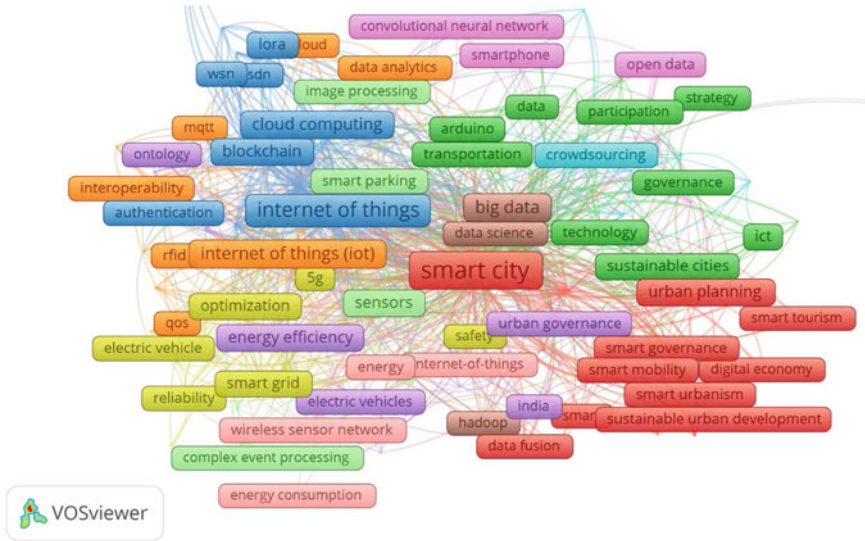
Fig. 17 Keywords co-occurrence network (2019)
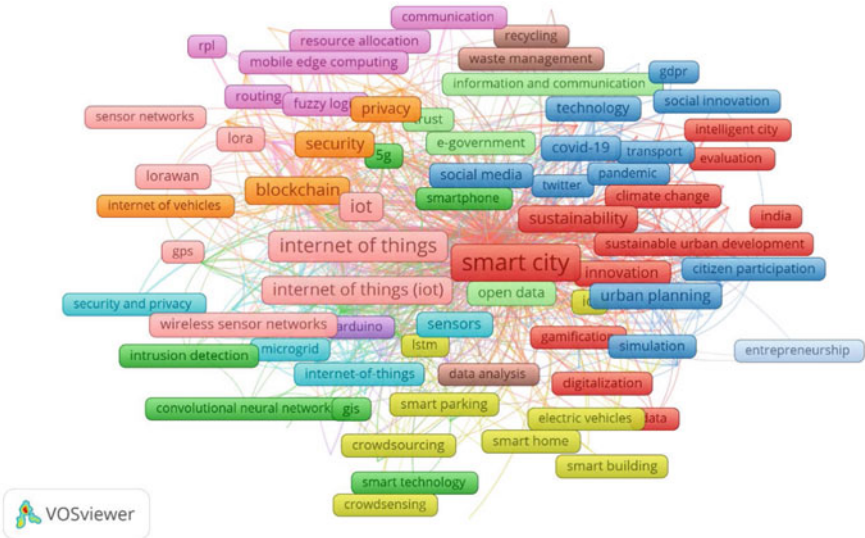
Fig. 18 Keywords co-occurrence network (2020)
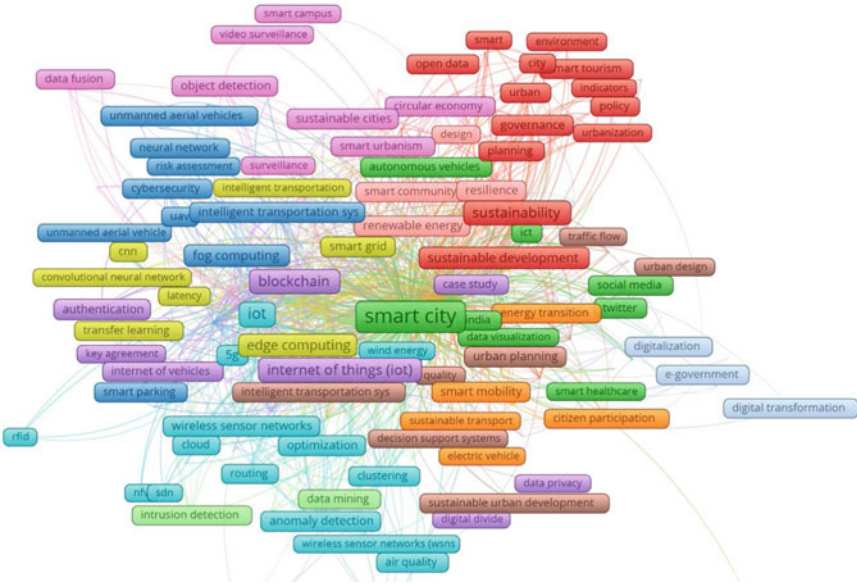
Fig. 19 Keywords co-occurrence network (2021)
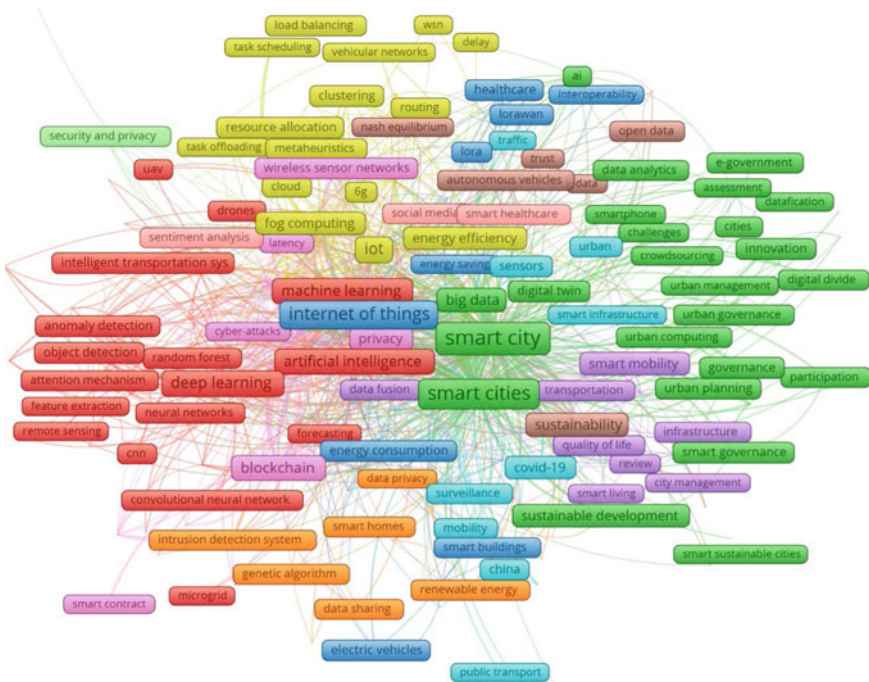
Fig. 20 Keywords co-occurrence network (2022)

3.4.5 At the Time of Research (2023-Q1)

As shown in Fig. 21, by investigating the network of the current year 2023 up until the date of typing this paper, it is found that IoT is still the main topic, while AI, blockchain, machine learning, deep learning, and big data are the focus of most studies. Also, some trends started to appear, like the metaverse.

4   Findings

4.1   The Evolution of the Concept of Smart Cities

According to network analysis, the early stages of the development of smart cities lacked a clear theme or technology that governs smart city applications till IoT was introduced into the field of smart city research. IoT has managed to become the central component of smart cities as almost all technologies and applications since 2013 show a relation with IoT either based on it or linked to it. Thus, a smart city can be defined as a framework that utilizes ICT to improve operational efficiency,
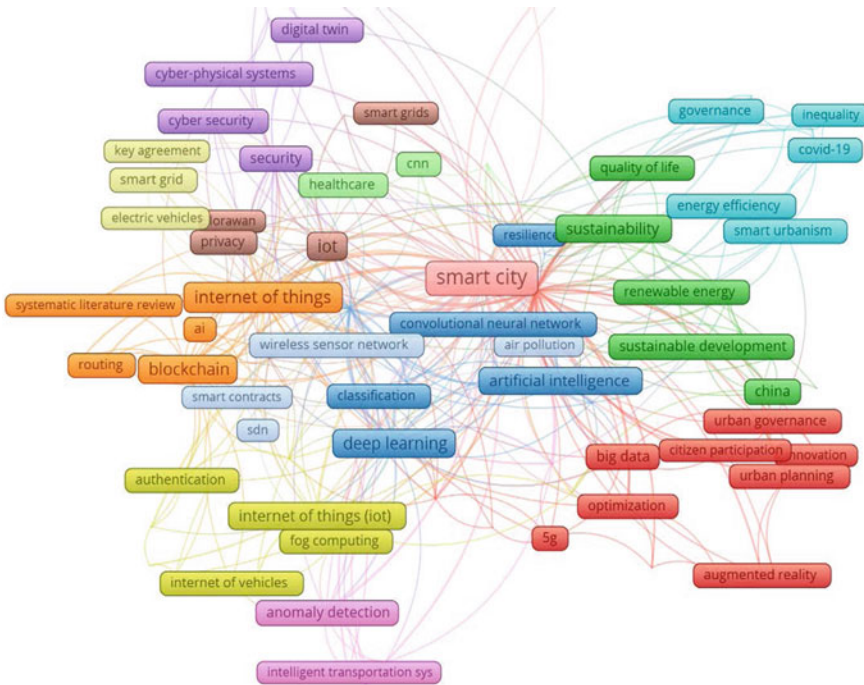
Fig. 21 Keywords co-occurrence network (2023 Q1)

public services, and the quality of life for its residents. A fundamental component of this architecture is the IoT, a network of interconnected objects that can interact and share data. IoT devices may include automobiles, sensors, household appliances, streetlights, and meters, among other things. By collecting and analyzing data from these devices, smart cities may enhance their infrastructure, transportation, energy distribution, waste management, and environmental sustainability. Smart cities seek to use technology and data to solve the urban issues and possibilities resulting from growing urbanization [5].

4.2   The Domains of Smart Cities

By analyzing the keywords and the networks, the smart city research has split the main domains governing the smart city applications into five main domains:

1. Data collection: Devices using sensors and other means of data collection, like surveys, are used to collect data on smart cities. Mostly these devices are connected and share data in IoT.
2. Communications: A fast connection method is needed to send this data from devices to storage systems, especially to collect vast amounts of information and process it in real time. For this, 5G and 6G are the targets in many recent research papers.
3. Data Storing: The data collected usually have different structures and needs to be processed to organize it before storing it to be used later for applications of smart cities. To cover this domain, studies of smart cities focus on Big Data and algorithms to organize this data.
4. Data Processing: For end applications to give users useful information and help in decision-making or main life sectors like education or health, the stored data needs to be processed using AI, Machine Learning (ML), and deep learning.
5. Security: Either it is about the connection between collecting Data devices, processing, and storing methods, or end applications receiving these processed data; a secure transfer and sharing of data are required to maintain smart cities. Many methods have been used, but the blockchain is the most effective one that is becoming the leading research focus in recent years and is expected to continue for subsequent years, as it is decentralized and peer-to-peer in nature [12].

4.3   Main Smart City Applications

The main applications of smart cities, as found by research, are Energy Management, Waste-Management, Water Management, Education, Economy, Health, Communication, Environment, Transportation, Safety and security, Infrastructure, City Resilience, and Construction.

These findings regarding the applications of smart cities confirm the findings of [2], while expanding the areas of applications to cover more applications found in the analysis.

4.3.1 Energy Management

One of the main objectives of smart city research is to optimize energy consumption in urban areas. By using a smart grid system that regulates the power supply and monitors energy consumption through intelligent meters and streetlights, smart cities can ensure that the resources are used efficiently and reduce wastage. Data collection related to bills, usage patterns, and other indicators should be done with care and supervision. This approach should also encourage more adoption of solar energy and other green projects to create sustainable buildings and residences. Moreover, smart cities should have a system that can manage renewable resources effectively and balance them with conventional sources [13].

4.3.2 Water Management

The essential component of life for all living things is water. Since life on Earth cannot exist without water, it should be used responsibly. Smart meters must be installed in homes, businesses, and factories to control usage and reduce waste. Digital management using autosensed leakage detection should be used for water supply management to cut down on waste [14].

4.3.3 Waste Management

Containers and trash cans need to be tracked in real time. As a result, if bins are too full, the system should notify the appropriate team right away so that an unoccupied bin can be used in their place. Waste classification, collection, and disposal should be scheduled carefully. Implementing resource optimization mechanisms based on actual needs will increase the effectiveness of the intelligent waste-management system.

4.3.4 The Environment

A smart city's efficient and environmentally friendly architecture is essential. In addition to creating intelligent buildings, minimizing the waste of non-renewable resources is crucial. Sustainable data centers are required to manage and store the data needed for various smart city applications. It is necessary to construct a pollution-control system with air toxicity monitoring capabilities. For the city's various applications to use weather data, an intelligent network of meteorological stations may be

necessary for an innovative environment. Automatic forest fire detection and prevention, intelligent earthquake early detection, and an intelligent meteorological system are all possible combinations.

4.3.5 Communication

Applications for the smart city can be supported by optical fiber, citywide Wi-Fi connectivity, and 5G/6G systems. These systems play the leading role in expanding applications of smart cities by providing faster connections to collect and transfer the most significant amounts of data. This connectivity enables using sensors, cameras, and other IoT devices to gather real-time data that can be analyzed to improve city services and infrastructure. As a result, smart cities can enhance the quality of life for citizens and promote sustainable development [15].

4.3.6 Healthcare

E-health and enhanced therapeutic workflow in smart hospitals can greatly enhance healthcare services. Utilizing various applications made specifically for smart healthcare systems can improve patient interaction. Smart healthcare may include updated healthcare information systems, M-Healthcare, and certified smart card readers for patient data security. In the meantime, sensors placed throughout the city can help gather information about the spread of viruses, assisting in the early detection and prevention of pandemics.

4.3.7 Education

Smart education and an intelligent educational environment have educated students and researchers throughout the pandemic. Various online learning platforms have made many courses available to sharpen skills. Webinars and online seminars have played an important role in knowledge sharing. Virtual class management systems and virtual labs have guaranteed no impediment to knowledge acquisition when educators and learners cannot interact face-to-face. Also, It provides learners with new tools and opportunities, such as using digital twins and smart learning indicators [16].

4.3.8 The Economy

With vast amounts of data collected in smart cities and stored and processed, applications can use this data to build better plans and business decisions that can result in overall economic growth. However, it is essential to ensure that this data is collected and used ethically and securely to protect citizens' privacy. Additionally, smart city

initiatives should prioritize inclusivity and accessibility to ensure all community members benefit from these advancements [17].

4.3.9 Transportation

By tracking the usage of means of transportation and the level of service also the quality of roads and record of crashes and their causes through sensors, cameras, smartphones, digital twin, and smart cars, the smart city applications can provide better plans regarding the maintenance of roads or adding new transportation method some places or increasing the number of buses in sometimes of the day in some places. Moreover, using self-driving cars or smart cars connected applications can eliminate crashes or traffic jams [18].

4.3.10 Infrastructure

The city can improve sewage, identify any capacity issues, and provide upgrade plans using the data collected by sensors and other devices in the IoT network of smart cities. Additionally, it can use metrology data to predict rain so that the city can be ready with a place to deal with these enormous amounts of water without flooding sewage systems. In the meantime, the city can identify the severity of road flaws and cracks so that timely maintenance can be performed.

4.3.11 Security and Surveillance

Security cameras and control station analytics should be handled carefully to reduce crime. An intelligent system must monitor the smart home safety system and the traffic system so that police can take appropriate action on time.

4.3.12 City Resilience

Using the smart city data, the city can predict natural disasters and create prevention methods that can be automatically operated using the smart city systems based on conditions detected by sensors and real-time data processing. Meanwhile, the city can monitor the virus spread and air quality to prevent pandemics and possible dangerous impacts on health. This application of smart cities gained more interest after the COVID-19 pandemic, and researchers started to investigate its relation to sustainability in smart cities, as performed by Lopez and Castro [19].

4.3.13 Construction

Construction is considered a high resource usage process with high negative environmental impacts while evolving high risks and safety hazards. Smart city systems can improve this industry sector by implementing the Construction 4.0 concept.

Based on [20], the applications of smart city technologies in the construction process are:

- Generative Design, especially in architectural designs, is enabled through Generative deep learning models and used to provide conceptual designs, generating floor plans or indoor designs.
- Structural Analysis through deep learning and machine learning models.
- Material Selection and Optimization, using Machine Learning algorithms to predict the properties of construction materials and provide the most optimum solution regarding cost, sustainability, and strength.
- Smart Modular systems manufacturing, using AI and 3D printing to provide a better-manufactured Modular part, while providing robotic arms, the steps to assembly it in the site.
- Digital Twin, in the operational phase, provides a considerable amount of data that ensure the reduction of emissions, the efficiency of the energy system, and the best user experience throughout the building [21].

4.4 Challenges of Smart Cities

Data analytics, accessibility, and affordability are the fundamental issues that all smart city systems face. Some of the major challenges are as follows:

4.4.1 Big Data Sources

Diverse data is produced from multiple sources in various forms, such as text, pictures, clips, sound, and social media data. To transform unstructured data into structured data and manage this varied data, big data technologies must be employed by developers. Conventional data mining techniques and software tools need to be improved to deal with the vast amounts and intricacies of data generated by various end devices and applications. Overcoming the obstacles associated with data management, system design, data analysis, distributed big data mining, continuous data generation, data compression, data visualization, and data security.

4.4.2 Data Filtration

As smart city applications are expected to generate substantial data volumes, developers should monitor and validate relevant and reliable information. Redundant or

insignificant data must be discarded to ensure efficient data storage and retention, which requires significant resources. To maintain data effectively, only high-quality data should be preserved in distributed databases. Developers face the challenge of maintaining high data consistency, integrity, and heterogeneity levels.

4.4.3 Data Exchange and Accessibility

The biggest challenge for development companies facing and managing the exchange of information among diverse and ever-changing users of various smart city applications. It is widely known that government officials maintain their own secure storage systems for confidential, sensitive, and personal information. Sharing such sensitive data across multiple applications poses a severe issue for developers, who must ensure the utmost security of private data. Nowadays, many users store their private information on their mobile devices. Citizens' personal information, including personal identification, addresses, contact details, etc., is highly confidential and cannot be revealed or used for any other purposes without the consent of the individuals concerned. Governments must devise a method to guarantee the privacy and security of individuals' data.

4.4.4 Safety and Privacy

As discussed in the previous section, ensuring safety and privacy is the most significant hurdle to overcome in a smart city that utilizes big data. Keeping personal information confidential and safeguarding it against harmful attacks and unauthorized access is essential. A smart system comprises several systems interconnected across multiple networks, which requires a high degree of security as data travels through different network types [17].

4.4.5 Affordability

The cost factor is fundamental, as separating valuable data from irrelevant data requires significant effort. Approximately 85% of the data generated needs to be more useful or noisy, making it challenging to verify, isolate, and refine the valuable data from the garbage. Nowadays, all enterprises depend on well-established traditional data management techniques, but advancements like cloud storage and virtualization demand more resources at a higher cost. As data overgrows, organizations strive to identify effective data management approaches to minimize the overall cost of maintaining large datasets. Innovative tools and technologies are necessary to provide efficient big data solutions. Smart city planners require state-of-the-art equipment and software, but the cost is delicate as it determines the viability of a program aimed at the people. The government must devise cost-effective strategies to develop successful solutions.

5   Conclusion

Smart cities offer an opportunity to manage population growth and rapid urbanization by establishing a data infrastructure. The primary objective of this study is to consolidate the progress made in the field of smart cities and enhance the current knowledge base. By conducting a bibliometric analysis and qualitatively assessing selected publications, the study can identify the most common topics in current research and suggest new and intriguing directions for future investigation. This study reviewed 12,148 journal articles from Scopus Database. The findings of this review can be beneficial to scholars actively studying the context of smart cities. This study provides valuable insights into this field's current state of research and highlights areas for future exploration.

Based on the study it was found that:

First, research on smart cities started in 1997, but it was in 2013 that it took its shape and formed the main targets and applications due to implementing IoT and big data as the core of smart city applications. These technologies shaped the concept of smart cities that has continued until now and will continue for years.

Then the study found the domains of smart cities to be Data collection, communication, data storing, data processing, and security. In contrast, the main application areas were Energy Management, Waste Management, Water Management, Education, Economy, Health, Communication, Environment, Transportation, Safety and security, Infrastructure, City Resilience, and construction. The study also found that AI, Machine learning, deep learning, Blockchain, big data, and IoT are the leading technologies shaping the future of smart city research. While, 5G and 6G communication technologies are the keys to expanding smart city applications.

When deeper investigating the applications of smart cities in construction, it was found that Generative Design, Structural Analysis through deep learning and machine learning models, Smart Modular-systems manufacturing, and Digital Twin in the operational phase are the main and most promising applications.

Meanwhile, the fundamental problems all smart city systems share are data analytics, accessibility, and affordability.

6   Recommendations

This Review of literature on smart cities has highlighted the main domains of smart cities and the key technologies and trends evolving to shape the future of smart cities. It has also highlighted the challenges of smart cities, and it turns out that the main challenge is the structure and clearance of collected data, so it is recommended that future studies find a new solution to standardize the structure of data collected in cities to help in reducing the time and cost of data filtration and processing. It is also recommended that future studies focus more on the trends emerging in each domain to accelerate the evolution of smart cities, especially in the security domain.

References

1. Environment WCo, Development, Brundtland GH (1987) Opening address by Gro Harlem Brundtland... on the occasion of the launch of the report "our common future", London, England, 27 April 1987. World Commission on Environment and Development
2. Malik S, Gupta K (2021) Smart city: a new phase of sustainable development using fog computing and IoT. IOP Conf Ser Mater Sci Eng 1022(1):012093
3. UNDESA P (2018) World urbanization prospects: the 2018 revision, vol 26. Retrieved Aug 2018
4. ECOSOC U (2015) The UNECE–ITU smart sustainable cities indicators
5. Belli L, Cilfone A, Davoli L, Ferrari G, Adorni P, Di Nocera F et al (2020) IoT-enabled smart sustainable cities: challenges and approaches. Smart Cities 3(3):1039–1071
6. Rejeb A, Rejeb K, Simske S, Treiblmaier H, Zailani S (2022) The big picture on the internet of things and the smart city: a review of what we know and what we need to know. Internet Things 19:100565
7. Weerasekara S, Lu Z, Ozek B, Isaacs J, Kamarthi S (2022) Trends in adopting Industry 4.0 for asset life cycle management for sustainability: a keyword co-occurrence network review and analysis. Sustainability 14(19):12233
8. Yuan C, Li G, Kamarthi S, Jin X, Moghaddam M (2022) Trends in intelligent manufacturing research: a keyword co-occurrence network based review. J Intell Manuf 33(2):425–439
9. Camero A, Alba E (2019) Smart City and information technology: a review. Cities 93:84–94
10. Zheng C, Yuan J, Zhu L, Zhang Y, Shao Q (2020) From digital to sustainable: a scientometric review of smart city literature between 1990 and 2019. J Clean Prod 258:120689
11. Barbhuiya MR, Kulkarni K (2022) Use of IoT in net-zero smart city concept in the Indian context: a bibliographic analysis of literature. In: Nath Sur S, Balas VE, Bhoi AK, Nayyar A (eds) IoT and IoE driven smart cities. Springer International Publishing, Cham, pp 235–251
12. Singh S, Sharma PK, Yoon B, Shojafar M, Cho GH, Ra I-H (2020) Convergence of blockchain and artificial intelligence in IoT network for the sustainable smart city. Sustain Cities Soc 63:102364
13. Verhulsdonck G, Weible JL, Helser S, Hajduk N (2023) Smart cities, playable cities, and cybersecurity: a systematic review. Int J Human-Comput Interact 39(2):378–390
14. Talebkhah M, Sali A, Marjani M, Gordan M, Hashim SJ, Rokhani FZ (2021) IoT and big data applications in smart cities: recent advances, challenges, and critical issues. IEEE Access 9:55465–55484
15. Puliga G, Bono F, Gutiérrez Tenreiro E, Strozzi F (2023) Bibliometric analysis of scientific publications and patents on smart cities
16. Tham JCK, Verhulsdonck G (2023) Smart education in smart cities: layered implications for networked and ubiquitous learning. IEEE Trans Technol Soc 4(1):87–95
17. Alam T (2022) Blockchain cities: the futuristic cities driven by Blockchain, big data and internet of things. GeoJ 87(6):5383–5412
18. Jafari M, Kavousi-Fard A, Chen T, Karimi M (2023) A review on digital twin technology in smart grid, transportation system and smart city: challenges and future. IEEE Access 11:17471–17484
19. Ramirez Lopez LJ, Grijalba Castro AI (2021) Sustainability and resilience in smart city planning: a review. Sustainability 13(1):181
20. Baduge SK, Thilakarathna S, Perera JS, Arashpour M, Sharafi P, Teodosio B et al (2022) Artificial intelligence and smart vision for building and construction 4.0: machine and deep learning methods and applications. Autom Constr 141:104440
21. Wang H, Chen X, Jia F, Cheng X (2023) Digital twin-supported smart city: status, challenges and future research directions. Exp Syst Appl 217:119531

Questions Concerning the Role of the Skycourt as a Passive Strategy to Enhance Energy Efficiency

Rasha A. Ali, Naglaa A. Megahed, Asmaa M. Hassan, and Merhan M. Shahda

1 Introduction

Buildings are responsible for 46.7% of the world's energy consumption and responsible for 40–50% of global carbon dioxide emissions [1, 2]. Heating, ventilation, and air conditioning (HVAC) systems account for more than 60% of the total energy use in buildings around the world [3]. Hence, increasing energy efficiency in buildings and providing a comfortable and healthy indoor environment has become a major challenge in the construction sector [4, 5]. This also represents the achievement of one of the Sustainable Development Goals (SDGs), which includes seventeen goals, including sustainable cities and communities [6, 7].

Several studies conducted to study the role of building form as a passive design element that helps reduce energy consumption [8–11]. The courtyard has been addressed as an important passive design element that has significant environmental, social, and economic benefits [12, 13]. Then other forms emerged that resulted from the development of the courtyard, such as the atrium. However, with the rapid spread of multi-story buildings around the world, designers began to develop these forms for the vertical level of buildings, and other configurations known as skycourt appeared [3].

R. A. Ali (✉) · N. A. Megahed · A. M. Hassan · M. M. Shahda
Department of Architectural Engineering and Urban Planning, Faculty of Engineering, Port Said University, Port Said, Egypt
e-mail: rasha.adel@eng.psu.edu.eg

N. A. Megahed
e-mail: naglaaali257@eng.psu.edu.eg

A. M. Hassan
e-mail: assmaa.mohamed@eng.psu.edu.eg

M. M. Shahda
e-mail: m.shahda@eng.psu.edu.eg

457
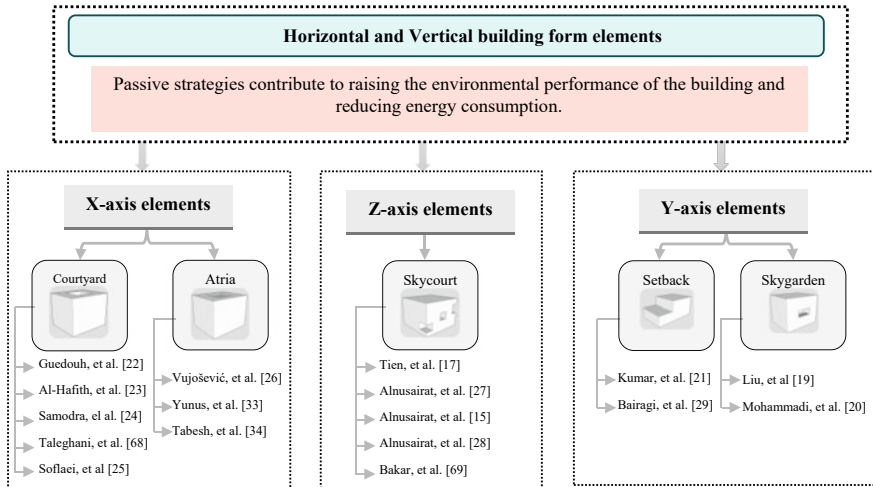
Fig. 1 Passive design strategies related to building envelope design. *Source* The Authors, adapted from [15, 17, 19–29, 33, 34, 68, 69]

Skycourt is a transitional space that can offer a variety of social, environmental, and economic benefits while improving the overall performance of buildings and saving energy consumption [14, 15]. The concept of skycourts arose from adapting traditional elements of low-rise buildings, such as courtyards and atriums, which have great potential in dealing with the building's surrounding climate [16]. Skycourts can provide passive designs for high-rise and mid-rise buildings by allowing natural light to penetrate deeply into indoor spaces and enhancing ventilation while avoiding unwanted solar gain [15].

There are different types of skycourts such as the skygardens and the setbacks [3]. Figure 1 shows examples of previous studies that have examined these passive forms.

The current research aims to study the role of skycourt as a passive design strategy that contributes to providing more sustainable cities and communities and providing clean energy as part of the Sustainable Development Goals (SDGs). This goal is achieved through a comprehensive study of previous research that dealt with this element that acts as a buffer between the interior and exterior spaces from an environmental point of view.

Table 1 shows the previous studies that dealt with the above-mentioned forms. In the study of Tien and Calautit [17], the objective was based on verifying the thermal air comfort in the different designs of a skycourt; the results indicated that the effect of skycourts on temperature is minimal, especially when vegetation cover is not considered. Alnusairat and Jones [14] investigated the potential of skycourts as ventilated buffer zones and reported that the construction of a ventilated skycourt exerts a significant impact on annual energy consumption. Alnusairat and Jones [18] also investigated skycourts as ventilated buffer spaces in high-rise buildings and

explored their effect on reducing energy demand. They found that incorporating skycourts as ventilated buffer spaces can reduce annual heating and cooling demand. As for skygardens, which are skycourts provided with implants, Liu and Huang [19], studied their effects on improving natural ventilation. They found that skygardens offer an effective way to mitigate the effect of heat, which is important for improving the quality of urban living. In addition, Mohammadi et al. [20] revealed that plants can provide a slight decrease in temperatures. The appropriate composition and proportions of these elements can help generate aerodynamic comfort across skygardens. As for the effect of setbacks on indoor daylight in residential buildings, Kumar and Kranthi [21] demonstrated that a small setback leads to poor lighting. Meanwhile, Guedouh and Inmmouri [22] studied the effect of the morphology of courtyard buildings on thermal and luminous environments in hot and dry regions. The results indicated that using a deep, sheltered void tends to improve daylight and sun exposure. Omar et al. [23] examined the effect of courtyard transactions on the level of shading and proved that the geometry of a courtyard greatly affects the level of shading. Moreover, the most effective parameter is the ratio of the width of the courtyard to its height. Focusing on the effect of courtyards with atriums, Samodra et al. [24] established that the use of an open courtyard from May to October and the use of the lobby for the rest of the year results in an optimal balance between energy use and summer comfort. In addition, Soflaei et al. [25] demonstrated that increasing the height of a courtyard improves shading performance and consequently the comfort temperature. As for the effect of lobbies on energy performance, Vujošević and Krstić [26] confirmed that atriums contribute to saving heating and cooling energy but that they require a great amount of energy for air conditioning.

Following the review of the previous studies, it becomes clear to us the large gap in the study of strategies (skycourts, skygardens, and setbacks). Therefore, the current research sheds light on verifying this gap.

This research follows a new methodology in scientific research that includes dividing the main subject of the study into several questions and answering them based on previous research to achieve the goal of the current research, this methodology is adopted here. The rest of the paper is organized as follows: Sect. 2 presents questions related to the research topic and strategies outlined above, as well as corresponding answers. Section 3 comprehensively presents conclusions about these answers.

2 Research Questions

Considering the current research gap described earlier, this study developed questions whose answers could contribute to providing a theoretical background on skycourt voids and their role as architectural spaces that provide comfort for occupants and help in energy saving.

Table 1 Collection of objectives of previous studies that dealt with skycourts, skygardens, setbacks, courtyards, and atriums

	Refs.	Year	Research objectives
Skycourt	[17]	2019	Investigate the aerothermal comfort in different skycourt designs
	[14]	2019	Examine the potential of skycourts as ventilated buffer zones
	[27]	2020	Explore skycourts as ventilated buffer spaces in high-rise buildings and investigate their impact on reducing energy demand
	[28]	2017	Outline the methodology for examining the performance of the basic spatial configurations of skycourts in high-rise office buildings
Skygarden	[19]	2020	Investigate the influence of skygardens on natural ventilation improvement
	[20]	2020	Investigate the effects of three common wind buffers (railing, hedges, and trees) on the performance of skygardens in occupants' wind comfort
Setback	[21]	2017	Examine the impact of building setbacks on indoor daylighting
	[29]	2018	Investigate the aerodynamic coefficient and structural behavior of setbacks in tall buildings
Courtyard	[30]	2022	Investigate the effects of courtyard envelope design on the energy performance in the hot summer–cold winter region
	[31]	2023	Identify the optimal configuration to enhance the environmental conditions of a terrace house courtyard in a hot-humid climate
	[24]	2018	Investigate the sustainability design performances of courtyards and atriums designs based on recommended site space
	[25]	2017	Identify the best design model for courtyards in terms of geometrical properties and orientation to improve thermal comfort in desert houses
Atrium	[32]	2021	Investigate the impact of glazed balconies and atriums on reducing the energy consumption of buildings with a cold semi-arid climate
	[33]	2019	Study the daylight availability in an atrium using different techniques and models
	[34]	2016	Investigate the integrated usage of an atrium and a courtyard for energy efficiency

As shown in Fig. 2, the questions are divided into 3 main groups. The first group, which includes the first and second questions, deals with the theoretical background of design forms through definitions and comparisons (skycourts, courtyards, and atriums). The second group, which consists of the third question, deals with the different configurations and designs of skycourt voids. The third group, which consists of the fourth and the fifth questions, deals with the role of these formations from an environmental, economic, and social perspective, and their impact on saving energy consumption. Research conclusions shed light on answers to questions.
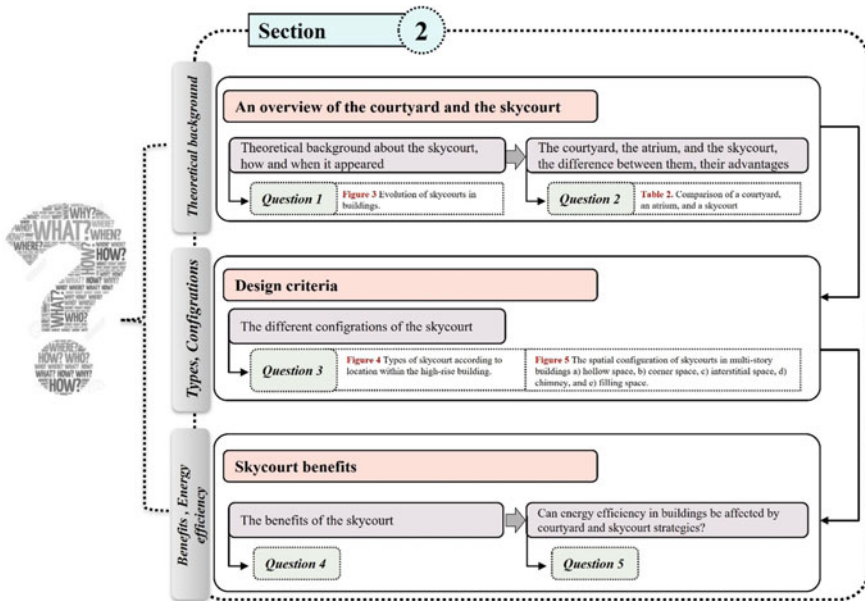
Fig. 2 Schematic overview of research questions. *Source* The Authors

2.1 What Are Skycourts and How and When Did They Transform into Buildings?

Architects have recently attempted to integrate solutions and introduce elements that can improve the quality of the indoor environment and provide beneficial effects for occupants [35–42]. One of those elements is the skycourt, which can be considered a transitional space that can provide a variety of social, environmental, and economic benefits and improve the overall performance of buildings [43, 44]. The concept of a skycourt originated from the adaptation of traditional (vernacular) elements of low-rise buildings, such as courtyards and atriums which have great potential in dealing with the surrounding climate [45].

Skycourts in high-rise and mid-rise buildings can provide a contemporary alternative to courtyards by allowing natural light to penetrate deep into indoor spaces and enhancing ventilation while avoiding unwanted solar gain [46]. This strategy can lead to a significant reduction in energy consumption and great improvement in occupants' health, well-being, and productivity [47].

Skycourts are increasingly being included in multistory buildings. These spaces serve as areas for social gatherings and transitional zones. In addition, they have the potential to provide environmental and economic benefits. Skycourts were developed from the well-known shape of courtyards and atriums [48].
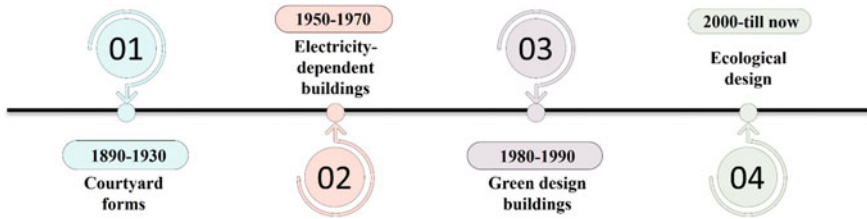
Fig. 3 Evolution of skycourts in buildings. *Source* The Authors

As shown in Fig. 3, skycourts were included in buildings between 1890 and 1930 as courtyard forms within U-, H-, E-, and O-shaped building plans to enhance ventilation and lighting [48]. Multistory buildings based on mechanical systems became increasingly common between 1950 and 1970 with the invention of air conditioning [49]. After the oil crisis in 1973, new mechanisms to reduce energy consumption for heating, ventilation, cooling, and lighting emerged. Skycourt has been reintroduced as a passive design strategy. Skycourts are incorporated as hollow multistory transitional zones located between the indoor and exterior walls of multistory buildings [43]. They have the potential to conserve energy and improve passenger satisfaction [50]. They have also been used as open spaces to divide buildings into vertical sectors [51].

2.2 What Is the Difference Between Courtyards, Atriums, and Skycourts?

Courtyards, atriums, and skycourts are traditional architectural forms that have contributed to improving the climatic environment inside buildings [52]. Table 2 shows a comparison of these architectural elements in terms of definition, image, and environmental benefit.
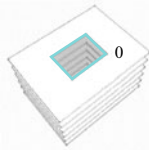
2.3 What Are the Different Skycourt Forms?

As shown in Fig. 4, skycourt voids can be located at the lower part of the buildings as a skyentrance, between the middle floors of the buildings as a skycourt, and at the top of the buildings as a skyroof. Skycourt voids spaces can be of two-floor height or more, linked with the surrounding indoor and outdoor spaces by open or enclosed walls [3, 15].

Skycourt is classified into five models that are used in multi-story buildings. As shown in Fig. 5, the skycourt can be (a) a hollow space with only one side connected to the outside, (b) a corner space with two sides connected to the outside, (c) an

Table 2 Comparison of a courtyard, an atrium, and a skycourt. *Source* The Authors, adapted from [14, 22, 28, 43, 53, 70, 71]

Definition		Image	Environmental benefit
Courtyard	The courtyard is a space of the building on the horizontal plane exposed to the open air and the architectural voids are built around this open space. It is also defined as an unroofed area that is totally or partially surrounded by walls or buildings. The courtyard has many forms such as U-, H-, E-, and O-shaped building plans		• Enhance natural ventilation and daylight in the middle of a house • Provide an outdoor area to the interior of the building
Atrium	The atrium is an evolution of the courtyard known for its traditional form but is covered with a glass roof providing an open view of the sky and weather protection. It is also defined as a building of two or more floors with high open spaces enclosed by a roof and vertical volumes enclosed by usable areas		• Promote impressive aesthetic space • Expose adjacent indoor spaces to daylight • Increase benefits from direct solar gain • Provide air circulation and communication among different stories of the building
Skyucourt	The skycourt is also considered a development of the courtyard but on the vertical level of the facades of the buildings. Skycourt began to appear with the spread of multi-story buildings. Skycourts in high-rise and mid-rise buildings can provide a contemporary alternative to patios		• Allow air and light to penetrate the interior • Reduces the effect of solar radiation and glare • Enhance thermal comfort

interstitial space with the building in the middle and the skycourt area enclosed by it as outer space, (d) chimney, similar to the case of a traditional courtyard in that the void is in the middle of the building and (e) filled space, which is similar to the previous case, but the void is the entire width of the building [3, 15].
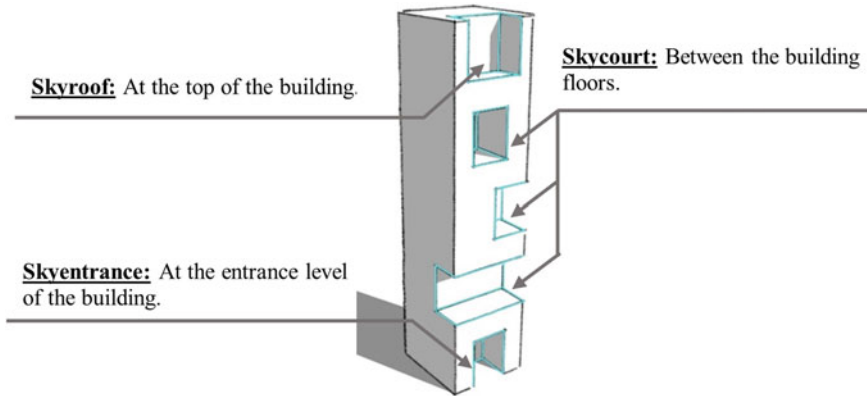
Fig. 4 Types of skycourt according to location within the high-rise building. *Source* The Authors, adapted from [3]
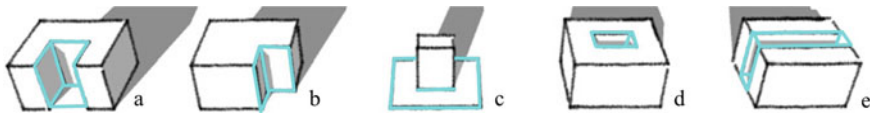
Fig. 5 The spatial configuration of skycourts in multi-story buildings **a** hollow space, **b** corner space, **c** interstitial space, **d** chimney, and **e** filling space. *Source* The Authors, adapted from [3]

2.4 What Are the Benefits of Skycourts in Multistory Buildings?

The main functions of skycourts in multistory buildings can be divided into environmental, social, and economic functions [53, 54].

Regarding environmental benefits: the skycourt serves as heat storage to mediate the temperature between the outside and the inside. It allows the air to penetrate inside and reduces the effect of solar radiation. These features provide positive effects on the thermal conditions inside spaces and on occupants as they provide a comfortable indoor environment in terms of air temperature, relative humidity, and air velocity [55, 56]. Additionally, skycourts can allow daylight to permeate the indoor environment [43]. Furthermore, green spaces in skycourts can enhance air quality by filtering polluting organisms [57]. Skygardens on top of buildings can reduce room temperature under the structure by 10% and surface heat loss during cold days in winter in hot climates [58, 59].

Considering social benefits: skycourts can provide a medium for different levels of social interactions between people [43]. They enhance the psychological well-being of occupants and thus improve their quality of life [60]. They also allow social interaction, which in turn affects users' sense of belonging and security. Furthermore, they can enhance exposure to natural features, such as air, daylight, views, and

greenery. These benefits improve the quality of architectural spaces, which in turn exert beneficial psychological effects on occupants [61].

Concerning economic benefits: skycourts act as a productivity enhancer. A direct relationship exists between productivity and the internal environment. Evidence shows that productivity can be improved by 4–10% by improving environmental conditions such as indoor air quality and pollution [62]. As a healthy work environment stems from natural light, good ventilation, the absence of organic compounds, and the right temperature, skycourts can lead to happier and healthier workers [63]. Skycourts act as a means to reduce energy consumption and thus reduce the economic aspect [64].

2.5 Can Energy Efficiency in Buildings Be Affected by Courtyard and Skycourt Strategies?

Courtyards and skycourts are traditional design metrics that can be used to reduce energy consumption in buildings [14, 65]. Several studies have indicated that the courtyard as a climatic modifier helps to improve the thermal environment and enhance the daylight in the indoor depth thus reducing the energy consumption of the building [65, 66]. The integrated use of the courtyard and atrium can save energy in all climates if the placement of the courtyard is adopted during the summer and the architectural style of the hall is used in the colder months. The results of this research showed that the use of the passive properties of courtyards and atriums and their integration affect energy consumption [34, 67].

By using a skycourt as a ventilated, heat- and cooling-free buffer zone, heating and cooling energy consumption can be significantly reduced, resulting in more than 55% energy savings per year. In addition, thermal comfort conditions are achieved in the occupied areas of skycourts [14]. The co-exhaust strategy, which involves ventilating skycourts using air emitted from adjacent void spaces, is an effective approach. This strategy can provide heating and cooling for multistory buildings relative to typical air conditioning strategies and provide thermal comfort to occupants in enclosed transition buffer areas, such as skycourts [17]. Alnusairat [3] demonstrated that the skycourt as an unheated and uncooled place in multi-story buildings, and ventilated based on a combined exhaust ventilation strategy, has a positive impact on reducing the total energy demand for heating and cooling of the building by more than 65% annually in the future.

3   Conclusions

Multistory buildings have become very popular nowadays for several reasons, but they are responsible for high energy consumption. One reason is the extensive use of air conditioning systems to provide thermal comfort to occupants. Skycourt has become increasingly integrated into the design of multistory buildings to provide ecologically designed and livable environments. This feature acts as a transition node and space for social interaction. Previous literature indicated that skycourts could play a promising role in reducing the energy consumption of buildings. Therefore, the research answered some of the questions related to the skycourt and its role in multistory buildings (Fig. 6). It was found that it contributes to providing natural ventilation, which leads to a reduction in energy consumption for cooling. It also has a role in providing natural lighting in addition to its social role. However, few studies provide evidence of its effect on the total energy demand of buildings. Hence, this research recommends further research related to the study of skycourt and the design indicators on which these designs can be based.

This research contributed to providing a large amount of information related to skycourt and its benefits from several aspects. The idea of skycourt can be applied on a global scale and not only in a specific geographical area, because the benefits related to it are not only from the environmental side but from the social and economic side as well. Undoubtedly, this contributes to the achievement of the Sustainable Development Goals at the global scale.
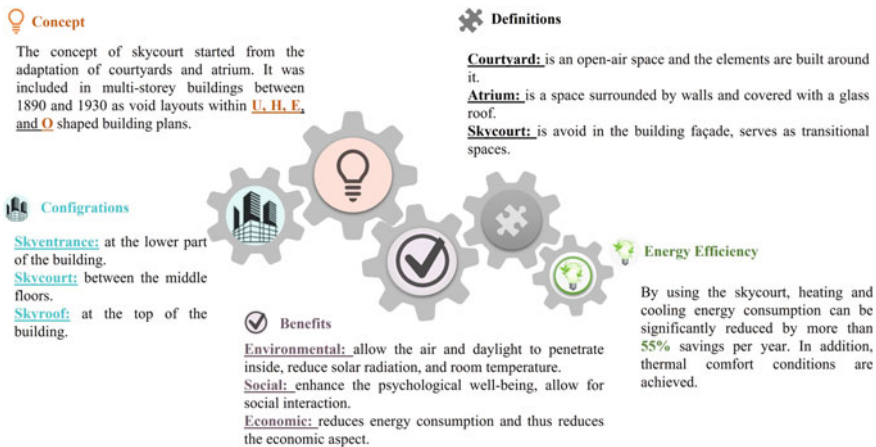
Fig. 6 Summarizing the answers to the research questions

4 Recommendations

The research recommends more future studies on the idea of a skycourt and the most important design criteria for a skycourt in each regional climate. The research also recommends studies related to the possibility of benefiting from the skycourt spaces in providing clean energy for buildings by cultivating these spaces, and this thus contributes to achieving the Sustainable Development Goals.

References

1. Li B, You L, Zheng M, Wang Y, Wang Z (2020) Energy consumption pattern and indoor thermal environment of residential building in rural China. Energy Built Environ 1:327–336
2. Pérez-Lombard L, Ortiz J, Pout C (2008) A review on buildings energy consumption information. Energy Build 40:394–398
3. Alnusairat S (2018) Approaches to skycourt design and performance in high-rise office buildings in a temperate climate. Cardiff University
4. Abo EL, Einen O, Shahda MM, Rasha A (2019) Effect of mass formation on indoor thermal performance in the Arab region. Port-Said Eng Res J 23:1–9
5. Hassan AM, Megahed NA (2022) Urban planning and development improving urban energy resilience with an integrative. Archit Eng 2022
6. Bali Swain R, Yang-Wallentin F (2020) Achieving sustainable development goals: predicaments and strategies. Int J Sustain Dev World Ecol 27:96–106
7. Schleicher J, Schaafsma M, Vira B (2018) Will the sustainable development goals address the links between poverty and the natural environment? Curr Opin Environ Sustain 34:43–47
8. Birkha Mohd Ali S, Hasanuzzaman M, Rahim NA, Mamun MAA, Obaidellah UH (2021) Analysis of energy consumption and potential energy savings of an institutional building in Malaysia. Alexandria Eng J 60:805–820
9. Shehata AO, Megahed NA, Shahda MM, Hassan AM (2022) (3Ts) green conservation framework: a hierarchical-based sustainability approach. Build Environ 224
10. Hassan SR, Megahed NA, Abo Eleinen OM, Hassan AM (2022) Toward a national life cycle assessment tool: generative design for early decision support. Energy Build: 112144
11. Ismail RM, Megahed NA, Eltarabily S (2022) Numerical investigation of the indoor thermal behaviour based on PCMs in a hot climate. Archit Sci Rev: 1–21
12. Safarzadeh H, Bahadori MN (2005) Passive cooling effects of courtyards. Build Environ 40:89–104
13. Toris-Guitron MG, Esparza-López CJ, Luna-León A, Pozo CE (2022) Evaluation of the thermal performance of traditional courtyard houses in a warm humid climate: Colima, Mexico. Herit Sci 10:187
14. Alnusairat S, Jones P (2019) Ventilated skycourts to enhance energy savings in high-rise office buildings. Archit Sci Rev 63:1–19
15. Alnusairat S, Jones P, Hou S (2017) Skycourt as a ventilated buffer zone in office buildings: assessing energy performance and thermal comfort. In: Design to thrive, PLEA 2017 conference. Edinburgh, pp 4901–4908
16. Pomeroy J (2008) Skycourts as transitional space: using space syntax as a predictive theory. In: Congress proceedings, tall green typology a sustain urban future
17. Tien P, Calautit JK (2019) Numerical analysis of the wind and thermal comfort in courtyards "skycourts" in high rise buildings. J Build Eng 24:100735
18. Alnusairat S, Jones P (2017) The influence of skycourt as part of combined ventilation strategy in high-rise office buildings. In: European conference on sustainability energy environment 2017. The International Academic Forum

19. Liu S, Huang G (2020) The ventilation improvement assessment of sky gardens—a case study of Hysan place. IOP Conf Ser Earth Environ Sci 440:52033
20. Mohammadi M, Tien P, Calautit JK (2020) Influence of wind buffers on the aero—thermal performance of skygardens. Fluids 5:160
21. Kumar M, Kranthi N (2017) Impact of setbacks on interior daylighting in residential buildings: a case study of Vijayawada, India. Indian J Sci Technol 10:1–10
22. Guedouh MS, Zemmouri N (2017) Courtyard building's morphology impact on thermal and luminous environments in hot and arid region. Energy Procedia 119:153–162
23. Al-Hafith O, Satish BK, Bradbury S, Wilde P (2017) The impact of courtyard parameters on its shading level an experimental study in Baghdad, Iraq. Energy Procedia 134:99–109
24. Samodra FXT, Defiana I, Setyawan W (2018) Researching for sustained translation from site cluster permeability into building courtyard and interior atrium. IOP Conf Ser Earth Environ Sci 126:12139
25. Soflaei F, Shokouhian M, Abraveshdar H, Alipour A (2017) The impact of courtyard design variants on shading performance in hot-arid climates of Iran. Energy Build 143:71–83
26. Vujosevic M, Krstic-Furundzic A (2017) The influence of atrium on energy performance of hotel building. Energy Build 156:140–150
27. Alnusairat S, Jones P (2020) Ventilated skycourts to enhance energy savings in high-rise office buildings. Archit Sci Rev 63:175–193
28. Alnusairat S, Hou S, Jones P (2017) Investigating spatial configurations of skycourts as buffer zones in high-rise office buildings: coupling building energy simulation (BES) and computational fluid dynamic (CFD). In: Conference on 5th eCAADe regional international symposium 2017. Cardiff, UK
29. Bairagi A, Dalui S (2018) Comparison of aerodynamic coefficients of setback tall buildings due to wind load. Asian J Civ Eng 19:205–221
30. He C, Tian W, Shao Z (2022) Impacts of courtyard envelope design on energy performance in the hot summer–cold winter region of China. Buildings 12
31. Gunasagaran S, Saw ES, Mari T, Srirangam S, Ng V (2023) Courtyard configuration to optimize shading, daylight and ventilation in a tropical terrace house using simulation. Int J Archit Res Archnet IJAR 17:109–123
32. Farivar S, Agharabi A (2021) Impact of Atrium and Glazed balcony on residential building energy consumption in cold semi-arid climate: case study in Mashhad, Iran. J Sol Energy Res 6:726–739
33. Yunus J, Ahmad S, Zain AA (2019) Daylight performances of atrium buildings for different roof configuration under Malaysia sky conditions. MATEC Web Conf 266:1001
34. Tabesh T, Sertyesilisik B (2016) An investigation into energy performance with the integrated usage of a courtyard and atrium. Buildings 6:21
35. Parker D, Wood A (2013) The tall buildings reference book. Routledge
36. Elmokadem A, Ekram M, Waseef A, Nashaat B (2018) Licensed under creative commons attribution CC BY kinetic architecture: concepts, history and applications. Int J Sci Res 7:750–758
37. Shahda M, Megahed N (2022) Post-pandemic architecture: a critical review of the expected feasibility of skyscraper-integrated vertical farming (SIVF). Archit Eng Des Manag
38. Megahed NA, Hassan AM (2022) Evolution of BIM to DTs: a paradigm shift for the post-pandemic AECO industry. Urban Sci
39. Hassan AM, ELMokadem AA, Megahed NA, Abo Eleinen OM (2020) Urban morphology as a passive strategy in promoting outdoor air quality. J Build Eng 29:101204
40. Hassan AM, El Mokadem A, Megahed NA, Abo Eleinen OM (2020) Improving outdoor air quality based on building morphology: numerical investigation. Front Archit Res 9:319–334
41. Elgheznawy D, Enein O, Shalaby G, Seif A (2022) An experimental study of indoor air quality enhancement using breathing walls. Civ Eng Archit 10:194–209
42. Noaman D, Moneer S, Megahed N, El-Ghafour S (2022) Integration of active solar cooling technology into passively designed facade in hot climates. J Build Eng: 104658
43. Pomeroy J (2013) The skycourt and skygarden: greening the urban habitat. Routledge

44. Aldawoud A (2008) Thermal performance of courtyard buildings. Energy Build Energy BLDG 40:906–910
45. Aldawoud A (2013) The influence of the atrium geometry on the building energy performance. Energy Build 57:1–5
46. Johnson T, Partner N (2015) How new generations, industries and workplace paradigms are redefining the commercial high-rise. Counc Tall Build Urban Habitat/Timothy Johnson, pp 310–317
47. Pomeroy J (2007) The sky court: a viable alternative civic space for the 21st century? CTBUH J: 14–19
48. Sev A, Aslan G (2014) Natural ventilation for the sustainable tall office buildings of the future. Int J Archit Environ Eng 8:897–909
49. Al-Kodmany K (2015) Eco-towers: sustainable cities in the sky. WIT Press
50. Zhou C, Wang Z, Chen Q, Jiang Y, Pei J (2014) Design optimization and field demonstration of natural ventilation for high-rise residential buildings. Energy Build 82:457–465
51. Pomeroy J (2012) Room at the top—the roof as an alternative habitable/social space in the Singapore context. J Urban Des 17:413–424
52. Abass F, Ismail LH, Solla M (2016) A review of courtyard house: history evolution forms, and functions. ARPN J Eng Appl Sci 11:2557–2563
53. Taib N, Aldrin A, Ali Z, Syed Fadzil S, Foong SY (2014) Trends in the air temperature of transitional spaces of a high-rise office building: the effects of season and location. Indoor Built Environ 23:1117–1128
54. Honold J, Lakes T, Beyer R, van der Meer E (2015) Restoration in urban spaces: nature views from home, greenways, and public parks. Environ Behav 48:796–825
55. Ismail L, Abd Wahab I, Sibley M (2012) Bioclimatic technology in high rise office building design: a comparison study for indoor environmental condition. J Sci Technol 3:89–103
56. Hassan AM (2023) UMC-based models: an integrating UMC performance analysis and numerical methods. Renew Sustain Energy Rev: 181
57. Lovell ST, Johnston DM (2009) Designing landscapes for performance based on emerging principles in landscape ecology. Ecol Soc 14:24
58. Wong NH, Tan A, Tan P, Chiang K, Wong N (2010) Acoustics evaluation of vertical greenery systems for building walls. Build Environ BLDG Env 45:411–420
59. Jaffal I, Ouldboukhitine S-E, Belarbi R (2012) A comprehensive study of the impact of green roofs on building energy performance. Renew Energy 43:157–164
60. Bay J (2004) Sustainable community and environment in tropical Singapore high-rise housing: the case of Bedok Court condominium. Archit Res Q 8:333–343
61. Altomonte S (2009) Daylight and the occupant. Vis physio-psychological well-being built Environ PLEA. Quebec City, Canada, pp 22–24
62. Clements-Croome D, Baizhan L (2000) Productivity and indoor environment. Proc Heal Build: 629–634
63. Miller N, Pogue D, Gough QD, Davis SM (2009) Green buildings and productivity. J Sustain Real Estate 1:65–89
64. Jahnkassim PS, Ip K (1988) Linking bioclimatic theory and environmental performance in its climatic and cultural context—an analysis into the tropical highrises of Ken Yeang. In: PLEA2006—23rd conference Passive low energy architecture. Citeseer, Geneva, Switzerland, p 9
65. Kumar R (2009) Effects of courtyard on thermal performance of commercial buildings in hot-dry climate, Ahmedabad, India. In: ICEBO—international conference on enhancement build operation. Energy Systems Laboratory, Austin, Texas
66. Al-Masri N, Abu-Hijleh B (2012) Courtyard housing in midrise buildings: an environmental assessment in hot-arid climate. Renew Sustain Energy Rev 16:1892–1898
67. Sharples S, Lash D (2007) Daylight in atrium buildings: a critical review. Archit Sci Rev 50:301–312
68. Taleghani M, Sailor DJ, Tenpierik M, van den Dobbelsteen A (2014) Thermal assessment of heat mitigation strategies: the case of Portland State University, Oregon, USA. Build Environ 73:138–150

69. Bakar MEA, Majid RA, Dzahir MAM (2020) Building information modelling analysis of proposed skycourt apartment prototype and conventional affordable apartment in Malaysia. J Crit Rev 7:811–824
70. Lau SSY, Yang F (2009) Introducing healing gardens into a compact University Campus: design natural space to create healthy and sustainable campuses. Landsc Res 34:55–81
71. Asfour O (2020) A comparison between the daylighting and energy performance of courtyard and atrium buildings considering the hot climate of Saudi Arabia. J Build Eng 30:101299

Utilizing Deep Reinforcement Learning for Resource Scheduling in Virtualized Clouds

Mona Nashaat and Heba Nashaat

1 Introduction

In cloud environments, clients can request processing, storage, and services from cloud computing over the Internet. As a result, operators and users produce massive volumes of data on various services in cloud environments, steadily demonstrating all of the general features of big data. Modern features, including flexibility, scalability, accessibility, and reliability, are advantageous to the cloud [1]. As a result, switching to the cloud from private internal IT infrastructures is a desirable option. Governments, corporations, and research organizations can use the cloud to handle their expanding storage and computing problems. Recent examples of successful commercial cloud providers include Microsoft Azure Services Platform, IBM "Blue Cloud," GoGrid, Google App Engine, and Amazon EC2. Cloud environment primarily offers three service models [2], which are Infrastructure as a Service (IaaS), Platform as a Service (PaaS), and Software as a Service (SaaS). IaaS offers cloud users the infrastructure for several purposes, such as computing resources and storage systems. Alternatively, PaaS gives clients access to platforms so they may build their apps there. Finally, SaaS makes software available to customers so they may get it straight from the cloud and avoid installing it on their computers [3].

In the context of cloud computing environments, users have access to endless resources. However, commercial cloud providers frequently bill customers on an hourly basis. As a result, rather than considering the number of resources used, the cost is calculated using the time unit model. As a result, Cloud Service Providers (CSPs) require large-sized data centers to organize the services provided to cloud

M. Nashaat (✉) · H. Nashaat
Department of Electrical Engineering, Faculty of Engineering, Port Said University, Port Said, Egypt
e-mail: MonaNashaat@eng.psu.edu.eg

H. Nashaat
e-mail: HebaNashaat@eng.psu.edu.eg

clients under the per-pay-usage model. Furthermore, to fulfill the ever-increasing demands of cloud consumers, CSPs must also continuously grow the number of servers, network devices, storage, cooling infrastructure, and other components in their data centers [3, 4]. Scheduling is therefore used to effectively distribute cloud applications among cloud servers while considering several crucial factors (such as processing power, memory, network bandwidth, deadline, and so forth) and consuming the least amount of energy possible. The most effective computer resources can be selected using efficient scheduling techniques based on performance, job makespan, system throughput, and energy efficiency. To maximize profits, efficient scheduling is currently combined with virtualization and migration strategy.

Virtualization is the leading cloud computing technology that can offer energy savings. With the use of virtualization technology, it is possible to separate the primary hardware and system resources from the Operating System (OS). By running a significant number of Virtual Machines (VM) on a single physical server, the number of physical servers required for operation can be decreased. As a result, a drop in the number of active servers could save money and reduce energy usage [5]. With a single virtualized server running multiple virtual servers, several physical servers can be combined into a single server with numerous OS on a virtual layer that can run concurrently. Different OSs can be separated from the essential server functionality via a virtual layer [6]. Since numerous VMs on a single server may share workloads, this dramatically increases server utilization while lowering energy consumption. Virtualization can avoid node under-utilization and mitigate energy usage as the under-utilized resources tend to draw more energy in their idle state.

Additionally, VM migration techniques are put into practice to help balance the workloads across the various nodes. These techniques involve moving VMs from a server that is severely loaded to a less laden server. There are two categories of migration techniques: cold migration and live migration. Cold migration involves shutting down the machine first before moving it to a different host, while hot migration occurs while the VM is running [7]. Migration helps to prevent any performance degradation brought on by a node that is overloaded. With advancements in virtualization and load balancing, there is a reduction in energy usage, resource utilization, as well as carbon footprints, and the resulting performance.

Alternatively, machine learning aims at teaching computers to predict events without explicit programming [8, 9]. Machine learning algorithms can be categorized into supervised [10], unsupervised [11], and semi-supervised learning [12] based on the learning techniques [11, 13]. Reinforcement learning is one of the unsupervised learning methods. Similarly, deep reinforcement learning (DRL) [8, 14] is the intersection of deep learning and reinforcement learning. DRL combines the perception of deep learning and the decision-making capacity of the RL [8]. However, two new technologies, DRL and cloud computing [15, 16], still need to intersect sufficiently. Recent years have seen an increase in the use of DRL to overcome scheduling issues in the cloud computing [8]. Following that, DRL demonstrated superior performance in the most recent study on using Cloud computing resource scheduling. Moreover, the global sustainable development goals aim to reach an affordable, reliable, and

sustainable energy system. SDG 7 calls to reduce unnecessary power consumption and target to increase power efficiency by at least 32.5% by 2030. This could be realized through energy consumption reductions in various domains. Therefore, this paper presents a DRL-based scheduling algorithm in cloud computing that aims to enhance power efficiency. The algorithm aims at optimizing dynamic resource allocation for large-scale cloud computing environments. The algorithm considers several policy parameters, such as system throughput and power usage. The algorithm then gathers metrics from the cluster using its monitor module before using a Deep Q learning network as its decision function to decide the following action.

The paper is structured as follows: Sect. 2 presents the background related to scheduling problems in cloud environments and virtualization, while Sect. 3 discusses related work. The proposed algorithm is presented in Sect. 4. Section 5 summarizes the experimental results, while Sect. 6 concludes the paper.

2 Resource Scheduling in Cloud Environment

This section discusses the cloud computing environment, task model, and methods.

2.1 Cloud Environments

Large-scale and complicated computations can now be carried out using the cloud [1, 2]. It makes it possible to quickly and instantly access a shared pool of configurable computing resources over the network. These resources can be quickly deployed and released without administration work or service provider involvement. The most important characteristics of cloud systems are flexibility and scalability, which make them highly complex and widely dispersed. Massive amounts of data can be computed and processed thanks to cloud computing. Task scheduling mechanisms play a crucial role in cloud computing settings as millions of users submit their computing jobs to the system.

Task scheduling refers to the process of assigning incoming tasks to all available resources. The primary objective of the task scheduling algorithm [17] is to maximize resource consumption while maintaining the cloud service parameters [3]. The fundamental scheduling procedure carried out in a cloud environment is depicted in Fig. 1. As the figure shows, there are three distinct approaches to task scheduling. The task scheduler gathers task and resource information from the task manager and resource manager in the first procedure, known as information provisioning. The second method is a selection procedure in which the target resource is chosen based on particular resource and task factors. The scheduling process considers different parameters such as task size, task priority, reliability factor, activity-based cost, and
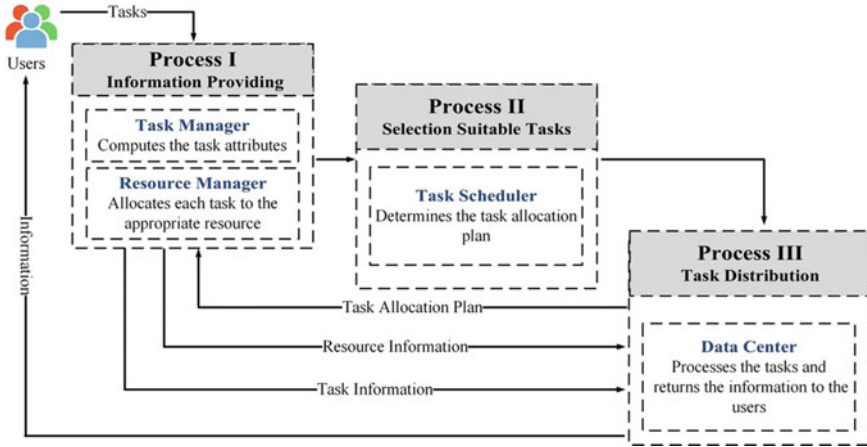
Fig. 1 Task scheduling in cloud environments

dynamic slotted length of the tasks. The resource manager receives the task alloca-
tion plan from the task scheduler. The task distribution process is the last step. The
task manager assigns each task to the relevant resources during this procedure.

As would be assumed, scheduling many jobs reduces computing effectiveness.
This causes lengthy maketime, extended waits, and exorbitant expenditures. As a
result, it can be challenging to assign many tasks to the right Virtual Machines
(VMs).

2.2 Deep Reinforcement Learning

Reinforcement Learning (RL) is a type of machine learning algorithm that falls
somewhere between supervised and unsupervised learning. Since it relies not only
on a set of labeled training data, it cannot be categorized as supervised learning. On
the other hand, the reinforcement learning agent aims to maximize a reward, hence;
it cannot be classified as unsupervised learning. The agent is trained to choose the
"right" actions in many scenarios to accomplish its main objective. The autonomous
agent observes a state from the environment at timestep. The agent engages in envi-
ronmental interaction by acting at state. Based on the current state and the selected
action, the agent and environment move to a new state when an action is taken. The
rewards that the environment offers define the optimum sequence of action. Every
time the environment changes states, it also gives the agent feedback as a scalar
reward. The agent aims to discover a policy that maximizes the predicted return.

Deep learning allows RL to scale to unsolvable decision-making problems, such
as situations with high-dimensional states and action spaces. DRL algorithms have
already been used to solve various problems, including robotics [8], where robot

Fig. 2 Overview of DRL
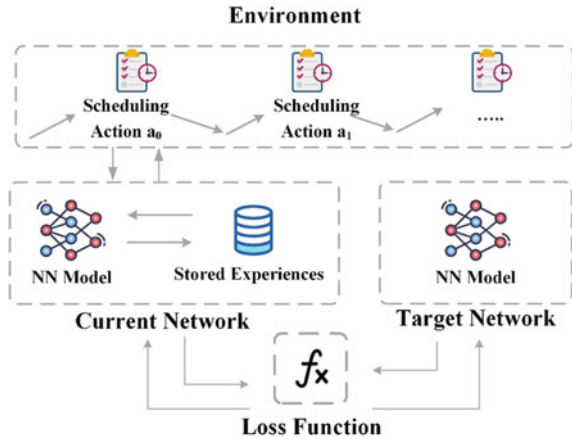
control policies can now be learned directly from camera inputs in the real world, replacing controllers that were previously hand-engineered or learned from low-dimensional features of the robot's state. Additionally, an overview of the DRL model is illustrated in Fig. 2. DRL has been used to develop agents that can meta-learn (or "learn to learn") [8], enabling them to generalize to complicated visual environments they have never seen before. This is a step towards ever more capable agents.

In contrast to tabular and conventional non-parametric approaches, DRL may effectively address the curse of dimensionality through the use of representation learning [8]. For example, convolutional neural networks (CNNs) can be included in RL agents to enable learning directly from unprocessed, high-dimensional visual inputs. DRL generally relies on deep neural network training to approximate the best possible policy and value functions.

3 Related Work

Scheduling algorithms assign workflow jobs to resources while still adhering to user-defined QoS constraints and data requirements. Different techniques have been investigated to provide scheduling solutions in cloud environments. Table 1 summarizes the state-of-the-art scheduling techniques. As the table shows, recent research has utilized different algorithms to obtain scheduling decisions. For instance, recent research [18] proposed a normalization-based budget constraint workflow scheduling algorithm for scheduling workflows using dynamic resource provisioning in the IaaS cloud.

Similarly, other research [8, 19] offer heuristic algorithms for scheduling Big Data workflow to achieve the deadline constraints. Most of these efforts [8, 19] aim to enhance the energy efficiency by minimizing the runtime of the proposed scheduler.

Table 1 Summary of related work

Authors	Techniques	Merits	Demerits
Chakravarthi et al. [18]	NBWS and ERB	To minimize the schedule length and execution time	Budget constraints and the makespan mitigation
Garg et al. [7]	DEAS and DVFS	Energy-efficiency	Average energy consumption
Ahmad et al. [19]	DCEDA	Better performance	Overheads and extra costs
Hussain et al. [20]	EPETS	Reduction in execution time and energy usage	Deadline constraints
Haidri et al. [21]	CEDA	Optimization of the total execution time	Deadline and priority constraints
Kalra and Singh [22]	HAED and GA	Better quality with regards to accuracy as well as diversity	Utilization of hyper-volume as well as set coverage
Nanjappan and Albert [23]	MCFCMA and PSO	Reduces load balancing	Load balancing and load scheduling
Kchaou et al. [26]	IT2FCM and PSO	To minimize data movements	Workflow scheduling problem
Supreeth and Patil [25]	GA-MPSO	Reduced energy consumption, SLA violation, and cost reduction	It is not easy to allocate the computational resources efficiently

Alternatively, several research [20, 21] focuses on minimizing the execution time. For example, authors in [21] proposed a scheduling technique that prioritizes the tasks with the highest upward rank to optimize the total execution time.

Likewise, Kalra and Singh in [22] emphasize satisfying QoS requirements by developing a hybrid technique that uses smart water drops and genetic algorithms to reduce the schedule length, execution time, and energy consumption. Like [22], another hybrid algorithm is proposed in [23], which utilizes a particle swarm-based optimization algorithm [24] with MCFCMA to cluster the available tasks and schedule them to virtual machines. Also, another research [25] applies the genetic algorithm along with a modified version of Particle Swarm Optimization to satisfy QoS parameters like reduced energy consumption cost.

Another scheduling algorithm is proposed in [26] to reduce data movements. The work utilizes the fuzzy clustering methods and the meta-heuristic optimization technique Particle Swarm Optimization (PSO) to minimize data movements throughout the workflow's execution. However, none of these efforts have utilized deep learning or reinforcement learning to obtain the scheduling decision, which is what this research aims to investigate.

4   The Proposed Solution: DRL Scheduler

In this section, we first describe an overview of the proposed solution. Then, we present the implementation details used to architect the proposed network.

4.1   DRL Scheduler Overview

The proposed algorithm utilizes a reward function, defined as the minimization of a user-defined policy function that expresses the user preferences for the system's behavior. To meet the user needs, the policy function combines the throughput, latency, and number of VMs per timestep parameters. With DRL's ability to handle high-dimensional states and action spaces, the agents are successful in obtaining better and more accurate results as the number of our input parameters increases, which corresponds to an increase in the number of input states. Also, since the input space is much less than other deep RL algorithms, the proposed solution can utilize a neural network solution with few hidden layers. As a result, the used Q tables are smaller, and our space complexity is much lower [8].

Afterward, the algorithm employs its monitor function to gather metrics from the cluster once every ten seconds. The metrics include a wide range of factors, including the cluster's throughput, latency, number of virtual machines, and power consumption. The algorithm uses 13 different parameters to describe the current state. Then, the framework applies its decision network, which is a Deep Q learning agent, to resolve the following action. We employ the Bellman equation to define the Q targets as:

$$Q(s, a) = r(s, a) + \gamma \max Q(s^*, a^*|s, a) \tag{1}$$

where r(s, a) represents the reward the agent will benefit if it takes action *a* from state *s* and Q(s*, a*|s, a) is the Q function given that the agent is currently on state *s* and takes action *a*, and γ is the discount factor that represents the impact of the subsequent rewards to the taken decision.

The algorithm utilizes the neural network as a function approximator that calculates the output based on a given input. The network output is then evaluated against a specified target. As we want our output to be as near to the objective as possible, we are utilizing the backpropagation [10] to change the weights in the network to make future outputs similar to the desired target. Backpropagation is used to find the minimum of a function using gradient descent [10], a first-order iterative optimization approach. The primary operation of the neural network is to multiply an input by the network weights to produce an output. Alternatively, in deep reinforcement learning, there are no predetermined targets. Instead, we construct our targets by computing the Bellman equation [10] for each state using the network. Therefore, the Q target obtained from the Bellman equation serves as the model's objective. The

r(s, a) factor represents the reward function. Our reward function is described as a function that evaluates a state's "goodness" depending on user-specified criteria.

At the beginning of training, the agent behaves erratically in the environment, especially in its early stages. The number of steps that our agent must take before decreasing the likelihood of making a random decision and raising the probability of making the best choice is the number of annealing steps. The algorithm decides to adopt a random action with probability 1 after i annealing steps rather than action a, where action $a = \arg\max_{a} Q(s, a)$. All of the agent decisions are optimal if i-annealing steps are equal to or larger than the training steps (i represents the iteration index). Moreover, the proposed algorithm uses a memory buffer to get better results. The buffer retains some previous output which consists of a state s, an action a, the reward r received from this action a, and the resulting state s. Therefore, during training, the model utilizes these experiences in various weight updates.

4.2 Network Architecture

To build the network, we used Google's TensorFlow framework [27] to build and train our neural network agent. The network has three hidden layers. Instead of a convolutional neural network, we utilize a fully connected neural network. A state s, an action a, the reward r obtained for an action a, and the state s that the agent finds after taking action a. (s, a, r, s′) are the components of the experience replay buffer employed in the proposed solution. During the first steps of training, the buffer is filled with memories which we refer to as pre-train steps. Following that, we feed the agent as many historical data points as our batch size suggests. We employ the TensorFlow RMSPropOptimizer as a trainer[27]. As a generalization of Rprop [27], RMSProp can deal with smaller batches in addition to complete batches.

5 Experimental Evaluation

The section presents the experimental results of comparing the proposed solution (DRL scheduler) against popular scheduling algorithms, including the shortest processing time first (SPF), and longest processing time first (LPF). The CloudSim platform was used to conduct the experiments. Section 5.1 describes the cloud environment employed in detail, while Sect. 5.2 describes the obtained results.

Table 2 Simulation environment

Type	No.	Parameters	Value
VM	10	Processor speed	9726 MIPS
		Memory	0.5 GB
		Bandwidth	1 GB/s
		Image size	10 GB
		Number of PEs	1
		VM monitor	Xen
Data center	1	Arch	x86
		Operating system	Linux
		VM monitor	Xen
		Cost	3.0
		Cost per memory	0.05
		Cost per storage	0.001
Host	20	MIPS	177,730
		Storage	4.0 TB
		VM monitor	Xen
		RAM	16.0 GB
		Bandwidth	15 GB/s
		Cores	6
DRL		Number of hidden layers	3
		Training steps	[2000, 5000, 10,000, 20,000, 500,000]
		Evaluation steps	2000
		Max error	10^6
		Loss function	Loss = ((target − prediction)2)

5.1 Experimental Setup

Cloud computing has become a powerful architecture for large-scale and complex computing. CloudSim [28] is a simulation tool used to evaluate the proposed algorithm's performance and compare the results with the other algorithms in terms of latency, resource utilization, and energy consumption. Table 2 shows the simulation parameters of the cloud environment used in the experiments.

5.2 Experimental Results

The proposed algorithm is compared against the shortest processing time and longest processing time scheduling algorithms with a large number of tasks to show the

Table 3 Performance of DLR, SPF, and LPF in terms of latency

Number of tasks	DLR scheduler	SPF	LPF
5000	80	82	84
7500	79	81	83
10,000	80	86	82
12,500	75	79	83
15,000	73	81	83
17,500	74	82	83
20,000	76	83	89

effect of the proposed algorithm. The number of tasks varies from 5000 to 2000. Table 3 compares the proposed algorithm with SPF and LPF regarding latency. It shows that the latency of the DLR scheduler decreases by about 10% relative to the SPF algorithm when it works with 17,500 tasks. The performance results regarding latency are illustrated in Fig. 3.

When compared with SPF and LPF, the proposed algorithm attained the highest resource utilization across all task numbers. The results of the comparison in terms of resource utilization are presented in Table 4 and Fig. 4. As the table show, when the number of tasks increases, the proposed method could enhance resource utilization by 13% and 11% when compared to SPF and LPF, respectively, when the number of tasks reaches 2000.

Finally, Table 5 shows the experimental results of energy savings enhancement achieved by the DRL scheduler and LPF compared to SPF. As the results, shown in Fig. 5, depict, DLR could reduce energy consumption, especially with higher task numbers. For instance, with 15,000 tasks, the DRL scheduler could enhance energy saving by 5% while LPF could only enhance the energy saving by 2.3%. overall, the
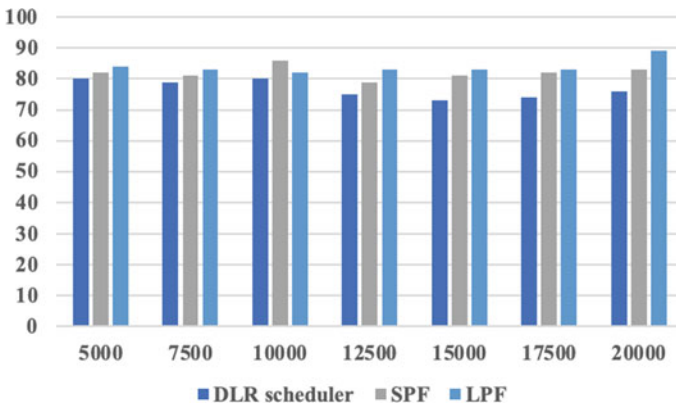
Fig. 3 Experimental results in terms of latency

Table 4 Performance of DLR, SPF, and LPF in terms of resource utilization

Number of tasks	DLR scheduler	SPF	LPF
5000	65.2	58.3	58.3
7500	69.3	63.7	64.5
10,000	79.2	74	74.4
12,500	81.3	72.5	73.5
15,000	84.1	74.9	76.1
17,500	82.12	76.3	76.6
20,000	83.3	73.9	75
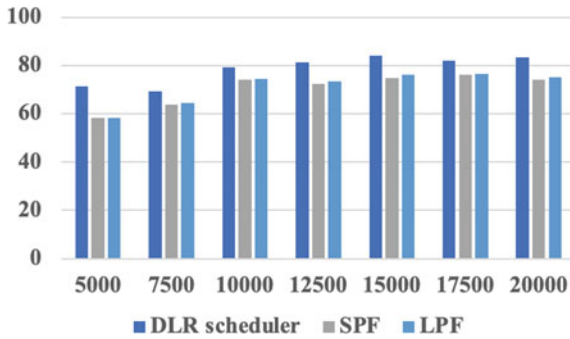
Fig. 4 Experimental results in terms of resource utilization

Table 5 Performance of DLR, SPF, and LPF in terms of energy savings

Number of tasks	DLR scheduler	LPF
5000	3.41	2.75
7500	4.21	3.34
10,000	4.04	3.03
12,500	3.34	2.95
15,000	4.91	2.37
17,500	3.02	2.83
20,000	3.01	2.53

results depict that the proposed solution sustains the highest quality of services (e.g., latency) while achieving the lowest energy consumption.

Fig. 5 Performance of DLR, SPF, and LPF in terms of energy savings
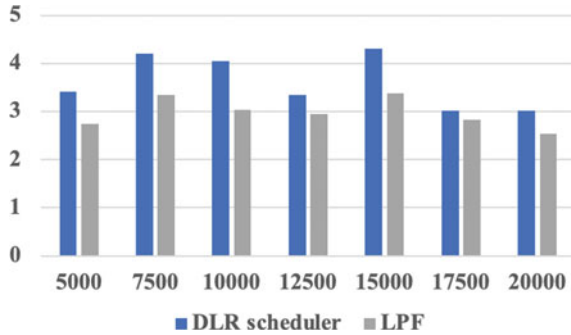
6 Conclusion

Resource scheduling is an important and developing topic of research in cloud computing. In this paper, we present deep reinforcement learning approaches as a suitable solution for scheduling problems in cloud environments that can successfully integrate the areas of cloud computing and DRL. Therefore, the paper proposes a DLR scheduler to accomplish automated elasticity. The scheduler employs Deep Reinforcement learning algorithms to process the multidimensional state of a cluster as input and learns and converges to the ideal elasticity behavior after a limited number of training steps. The algorithm considers reducing the task response and maintaining a satisfying Quality of Service while reducing energy consumption. To evaluate the proposed solution, we compare the proposed agent against popular scheduling algorithms and demonstrate that it achieves better rewards by up to 15% over different task numbers. To further evaluate our approach on a global scale, we next put our methodology to the test in a real-world cluster setting, demonstrating how the system resizes clusters in real time and responds to changing input and training loads and performance demands.

7 Recommendations

As the next step of this research, we aim to obtain a real-world dataset to test the proposed model in real-world situations with different traffic loads and task numbers. The dataset is collected with the help of the information technology center at Port Said University, which can provide us with a real-world dataset from their data centers located on campus. Another direction of this research is to investigate applying representation learning techniques to the input data so the model can learn the features automatically instead of engineering the input features. Finally, we also plan to conduct a feasibility study on the model parameters to investigate their effect on the overall performance.

References

1. Li Z, Ge J, Hu H, Song W, Hu H, Luo B (2018) Cost and energy aware scheduling algorithm for scientific workflows with deadline constraint in clouds. IEEE Trans Serv Comput 11:713–726. https://doi.org/10.1109/TSC.2015.2466545
2. Kumar P, Verma A (2012) Scheduling using improved genetic algorithm in cloud computing for independent tasks. In: Proceedings of the international conference on advances in computing, communications and informatics Association for Computing Machinery, New York, NY, USA, pp 137–142. https://doi.org/10.1145/2345396.2345420
3. Senthil Kumar AM, Venkatesan M (2019) Task scheduling in a cloud computing environment using HGPSO algorithm. Clust Comput 22:2179–2185. https://doi.org/10.1007/s10586-018-2515-2
4. Garg R, Rani R (2019) State-of-the-art energy-efficient thermal-aware scheduling in cloud. In: Fong S, Akashe S, Mahalle PN (eds) Information and communication technology for competitive strategies. Springer, Singapore, pp 157–164
5. Tarafdar A, Debnath M, Khatua S, Das RK (2021) Energy and makespan aware scheduling of deadline sensitive tasks in the cloud environment. J Grid Comput 19:19. https://doi.org/10.1007/s10723-021-09548-0
6. Zhang Y, Cheng X, Chen L, Shen H (2018) Energy-efficient tasks scheduling heuristics with multi-constraints in virtualized clouds. J Grid Comput 16:459–475. https://doi.org/10.1007/s10723-018-9426-6
7. Garg N, Singh D, Goraya MS (2021) Energy and resource efficient workflow scheduling in a virtualized cloud environment. Clust Comput 24:767–797. https://doi.org/10.1007/s10586-020-03149-4
8. Dong T, Xue F, Xiao C, Li J (2020) Task scheduling based on deep reinforcement learning in a cloud manufacturing environment. Concurr Comput Pract Exper 32:e5654. https://doi.org/10.1002/cpe.5654
9. El-Shekheby S, Abdel-Kader RF, Zaki FW (2019) Spatially varying blur estimation from a single image. IET Image Proc 13:746–753
10. Wang B, Liu F, Lin W (2021) Energy-efficient VM scheduling based on deep reinforcement learning. Futur Gener Comput Syst 125:616–628. https://doi.org/10.1016/j.future.2021.07.023
11. Nashaat M, Miller J (2021) Improving news popularity estimation via weak supervision and meta-active learning
12. Nashaat M, Ghosh A, Miller J, Quader S (2020) WeSAL: applying active supervision to find high-quality labels at industrial scale
13. Nashaat M, Ghosh A, Miller J, Quader S (2021) Semi-supervised ensemble learning for dealing with inaccurate and incomplete supervision. ACM Trans Knowl Discov Data 16. https://doi.org/10.1145/3473910
14. Nashaat M, Shaalan IE, Nashaat H (2022) LTE downlink scheduling with soft policy gradient learning. In: The 8th international conference on advanced machine learning and technologies and applications (AMLTA2022). Springer, pp 224–236
15. Rizk R, Nashaat H (2018) Smart prediction for seamless mobility in F-HMIPv6 based on location based services. China Commun 15:192–209. https://doi.org/10.1109/CC.2018.8357696
16. Hashem W, Nashaat H, Rizk R (2017) Honey bee based load balancing in cloud computing. KSII Trans Internet Inf Syst 11
17. Nashaat H, Refaat O, Zaki FW, Shaalan IE (2020) Dragonfly-based joint delay/energy lte downlink scheduling algorithm. IEEE Access 8:35392–35402
18. Kalyan Chakravarthi K, Shyamala L, Vaidehi V (2020) Budget aware scheduling algorithm for workflow applications in IaaS clouds. Clust Comput 23:3405–3419. https://doi.org/10.1007/s10586-020-03095-1
19. Ahmad W, Alam B, Ahuja S, Malik S (2021) A dynamic VM provisioning and de-provisioning based cost-efficient deadline-aware scheduling algorithm for Big Data workflow applications

in a cloud environment. Clust Comput 24:249–278. https://doi.org/10.1007/s10586-020-031 00-7

20. Hussain M, Wei L-F, Lakhan A, Wali S, Ali S, Hussain A (2021) Energy and performance-efficient task scheduling in heterogeneous virtualized cloud computing. Sustain Comput Inform Syst 30:100517. https://doi.org/10.1016/j.suscom.2021.100517

21. Haidri RA, Katti CP, Saxena PC (2020) Cost effective deadline aware scheduling strategy for workflow applications on virtual machines in cloud computing. J King Saud Univ Comput Inf Sci 32:666–683. https://doi.org/10.1016/j.jksuci.2017.10.009

22. Kalra M, Singh S (2021) Multi-objective energy aware scheduling of deadline constrained workflows in clouds using hybrid approach. Wireless Pers Commun 116:1743–1764. https://doi.org/10.1007/s11277-020-07759-4

23. Nanjappan M, Albert P (2022) Hybrid-based novel approach for resource scheduling using MCFCM and PSO in cloud computing environment. Concurr Comput Practice Exper 34:e5517. https://doi.org/10.1002/cpe.5517

24. Abdel-Kader RF, Atta R, El-Shakhabe S (2014) An efficient eye detection and tracking system based on particle swarm optimization and adaptive block-matching search algorithm. Eng Appl Artif Intell 31:90–100. https://doi.org/10.1016/j.engappai.2013.06.017

25. Supreeth S, Patil K (2022) Hybrid genetic algorithm and modified-particle swarm optimization algorithm (GA-MPSO) for predicting scheduling virtual machines in educational cloud platforms. Int J Emerg Technol Learn 17:208–225. https://doi.org/10.3991/ijet.v17i07.29223

26. Kchaou H, Kechaou Z, Alimi AM (2022) A PSO task scheduling and IT2FCM fuzzy data placement strategy for scientific cloud workflows. J Comput Sci 64:101840. https://doi.org/10.1016/j.jocs.2022.101840

27. Pattanayak S (2023) Introduction to deep-learning concepts and TensorFlow. In: Pro deep learning with TensorFlow 2.0: a mathematical approach to advanced artificial intelligence in python. Apress, Berkeley, CA, pp 109–197. https://doi.org/10.1007/978-1-4842-8931-0_2

28. Hussain A, Aleem M, Iqbal MA, Islam MA (2019) Investigation of cloud scheduling algorithms for resource utilization using CloudSim. Comput Inform 38

Enhanced COVID-19 Classification Using Ensemble Meta-Algorithms on Chest X-ray Images

Lamiaa Menshawy, Ahmad H. Eid, and Rehab F. Abdel-Kader

1 Introduction

Medical imaging of the chest is a critical tool for the detection, diagnosis and treatment of a wide range of medical conditions, including lung cancer, pneumonia, COVID-19, and tuberculosis. Through imaging techniques such as X-rays, computerized tomography (CT), and magnetic resonance imaging (MRI) it is possible to visualize the internal structures within the chest, and detect abnormalities or changes that may indicate the presence of a disease [1–5]. In addition to diagnosis, chest imaging enables early detection of diseases, which is crucial for effective treatment and improved patient outcomes. Furthermore, it is essential for monitoring the progress of a disease or a treatment and evaluating the effectiveness of interventions.

The use of medical imaging for COVID-19 detection has attracted the attention of researchers in recent years. One of the early symptoms of COVID-19 is respiratory distress, which can be detected through chest imaging. A CT scan of the chest can reveal characteristic features of COVID-19, such as ground-glass opacities and consolidations, which can help healthcare professionals diagnose the disease and distinguish it from other respiratory conditions. Moreover, chest imaging can also

L. Menshawy (✉)
Department of Technology and Information System, Faculty of Management Technology and Information System, Port Said University, Port Said, Egypt
e-mail: lamyaa_menshawy@himc.psu.edu.eg

A. H. Eid · R. F. Abdel-Kader
Department of Electrical Engineering, Faculty of Engineering, Port Said University, Port Said, Egypt
e-mail: ahmad.eid@eng.psu.edu.eg

R. F. Abdel-Kader
e-mail: rehabfarouk@eng.psu.edu.eg

help identify asymptomatic carriers of the virus, who may not show any symptoms but are still contagious which is essential to prevent the spread of the disease. The use of CT scans to diagnose COVID-19 retains many difficulties as it requires expensive equipment that is not usually available in many medical institutions, the need to accurately interpret the images, and the potential for radiation exposure. In contrast, the use of X-ray images is affordable, can provide results quickly, and is less dangerous than CT. As a result, the issue of categorizing COVID-19 using X-ray images is a research topic that is widely investigated in the literature [1].

Ensemble learning is a Machine Learning (ML) paradigm that combines the advantages of the base learners (weak learners) and uses them as building blocks to improve the overall performance of a predictive model [6]. Ensemble methods tend to reduce bias and/or variance of such weak learners by properly combining several of them. The ensemble construction process involves two main steps. First, multiple base learners are generated, which can be created either in parallel or sequential manner. Afterwards, predictions from the different learners are merged to produce a single prediction.

Tree-based ensemble algorithms for supervised ML have multiple advantages compared to other algorithms. This includes ease of use, they are non-parametric, can handle different datatypes, and robustness against multicollinearity, noise and overfitting. Bagging and boosting are two well-known tree-based ensemble models [6] as shown in Fig. 1. Bagging also called *bootstrapping* is a non-sequential learning ensemble. Initially, several sets of random samples are taken from the training dataset, and these subsets are utilized to train several base learners that are of the same type and are independent of each other. To produce predictions, an individual learner processes a test sample, and the outcomes are averaged (for regression) or voted (for classification) to generate the final result. On the other hand, the core idea of boosting is to implement homogeneous ML algorithms in a sequential manner. Boosting makes predictions for multiple rounds on the entire training sample and iteratively improves the performance of the boosting algorithm with the information from the prior round's prediction. The methodology by which each base learner's error improves with the next base learner in the sequence is the fundamental difference between all boosting approaches.

The detection of COVID-19 using chest X-ray images has been explored extensively in the literature. Some of these studies classify COVID-19 images based on deep learning [2, 7]. In [2], a deep neural network-based model for performing binary and multiclass classification was proposed with a classification accuracy of 98.08% and 87.02%, respectively. Badawi and Elgazzar [7] proposed a deep-learning model for identifying COVID-19 from X-ray images based on DenseNet201, VGG16, and VGG19. Aslan [8] presented a robust semantic lung segmentation study for CNN-based COVID-19 diagnosis. Ohata et al. [9] uses Convolution Neural Networks (CNNs) to extract features and classify them using various machine-learning techniques. In [10], two pre-trained CNN models, AlexNet and Xception, are used to merge features obtained from input X-rays using a deep feature concatenation mechanism. A voting ensemble strategy is proposed in [11] to create an ensemble framework using three classifiers: GoogLeNet, ResNet-18 and DenseNet-121. Authors in
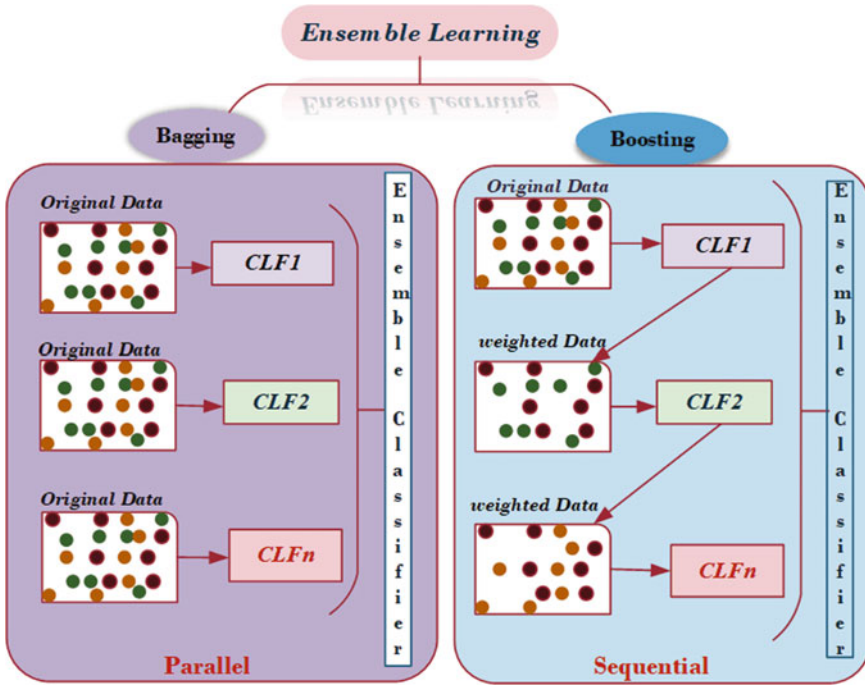
Fig. 1 Bagging and boosting algorithms

[12] use SVMs trained on deep networks to identify Covid-19 from chest X-rays images. The maximum accuracy is 96.16%, which is achieved by the proposed SVM on deep networks. Another approach is the use of deep convolutional neural networks (CNNs), such as in the work of Narin et al. [13] and Gupta et al. [14], who developed deep neural networks for COVID-19 detection using chest X-ray images. Another approach involves data augmentation using the auxiliary classifier GAN, as implemented in the CovidGAN by Waheed et al. [15]. Dhanapala and Sotheeswaran [16] proposed a transfer learning technique with SVM for COVID-19 disease prediction based on chest X-ray images.

Other studies have used ensemble models and ML to detect COVID-19 [1, 17–20]. Menshawy et al. [1] proposed two ensemble-based models that contrast deep learning (DL) approaches with traditional ML approaches. The first approach combines the results of different classifiers using two different decision fusion techniques: majority voting and bayes optimal. The second approach uses various deeplearning models for feature extraction. Subsequently, a voting classifier is employed to calculate the average outcome of the various classifiers.

In the study by Saha et al. [17], a deep learning model called EMCNet was proposed for automated COVID-19 diagnosis from X-ray images using a CNN and an ensemble of ML classifiers. The proposed model achieved an accuracy of 96.44%, a sensitivity of 95.67%, and a specificity of 97.20. Rahimzadeh and Attar

[18] proposed a modified deep CNN for detecting COVID-19 and pneumonia from chest X-ray images based on the concatenation of Xception and ResNet50V2. The proposed model achieved an accuracy of 97.08%, a sensitivity of 98.33%, and a specificity of 94.77% in detecting COVID-19. Huang and Liao [19] proposed a stacking ensemble and ECA-EfficientNetV2 CNN for the classification of multiple chest diseases, including COVID-19. Kumar [20] proposed a ML-based ensemble approach for predicting the mortality risk of COVID-19 patients. The proposed model used demographic and clinical features of patients to predict mortality risk. The model achieved an accuracy of 88.89% and an F1 score of 0.77, demonstrating its potential for predicting the mortality risk of COVID-19 patients.

The primary contributions of this study are outlined as follows:

- Various models are proposed to evaluate the effectiveness of bagging and boosting ensemble learning algorithms in the detection of COVID-19 form chest X-rays. The two boosting- based models utilize VGG-16, DenseNet201, and ResNet50V2 for feature extraction. Feature vectors obtained from these models are concatenated to provide feature sets. Instead of selecting only one classifier, boosting algorithms are utilized to estimate the average of all classifier outcomes.
- A comparison of the performance of the proposed models is investigated. Experimental results demonstrate that the proposed models outperform the performance of the individual base learners in multiclass covid-19 classification. Boosting yields better than that of the bagging-based model.

AI-powered algorithms and advanced diagnostic tools, play a crucial role in the early identification and tracking of Covid-19 cases, enabling prompt interventions and effective containment strategies. By leveraging technology to swiftly identify infected individuals, these detection mechanisms contribute to Sustainable Development Goal 3: Good Health and Well-being, as they help mitigate the spread of the virus and minimize its impact on communities. Moreover, the automatic detection of Covid-19 supports other Sustainable Development Goals, such as Goal 9: Industry, Innovation and Infrastructure, by fostering the development of cutting-edge technologies and improving healthcare infrastructure. Furthermore, it aligns with Goal 17: Partnerships for the Goals, as international collaboration and knowledge-sharing, are essential for the successful implementation of automatic detection systems worldwide.

The remainder of this paper is structured as follows: In Sect. 2, the proposed models are presented. In Sect. 3, the classification performance analysis of the suggested models is evaluated and discussed. Finally, the paper is concluded in Sect. 4.

2 The Proposed Models

2.1 Boosting Ensemble Proposed Model

Two variants of the Boosting Ensemble Model (BEM) were introduced, both consisting of four main stages. The first three stages are identical in both models, while the fourth stage differs between the two models, as illustrated in Fig. 2. The initial stage is the data augmentation phase that involves generating new images from the original dataset. The deep feature extraction phase uses popular Deep CNN models, such as VGG-16, DenseNet201, and ResNet50V2, to extract features. The feature fusion stage combines these extracted features to form a fused feature vector. Assuming that DenseNet201, ResNet50V2, and VGG-16 extract m-dimensional, n-dimensional, and v-dimensional vectors, respectively, concatenating them yields an (m + n + v) dimensional vector representing the fused feature vector.

In the fourth phase, Boosting Decision Fusion is utilized to enhance classification performance. BEM1 uses AdaBoost (Adaptive Boosting) while BEM2 uses the XGBoost classifier. The default weak classifier for AdaBoost is typically decision trees, but BEM1 uses different ML classifiers like K-Nearest Neighbor (KNN) and Logistic Regression (LR) to augment traditional AdaBoost.

2.2 The Proposed ML Feature and Decision Fusion (MLFDF) Model

The model shown in Fig. 3 is ML Feature and Decision Fusion (MLFDF) Model that consists of four phases. It shares similarities with BEM1 and BEM2 in terms of data augmentation, feature extraction, and feature fusion. In the fourth phase, the Decision Fusion phase, the final classification score is achieved by combining a SVM Classifier, a KNN Classifier, and LR classifier using a majority voting classifier.

3 Results and Discussion

3.1 Data Description

In this study, the performance of the proposed systems was examined using the COVID-ChestXray-15 k dataset. The dataset contains chest X-ray images of patients with COVID-19, pneumonia, and other respiratory and cardiovascular diseases [7]. The dataset is designed to aid researchers and healthcare professionals in the diagnosis and management of COVID-19 cases, especially in the early stages of the pandemic when access to COVID-19-specific datasets was limited. This dataset has

Fig. 2 The proposed
boosting ensemble models
(BEMs)
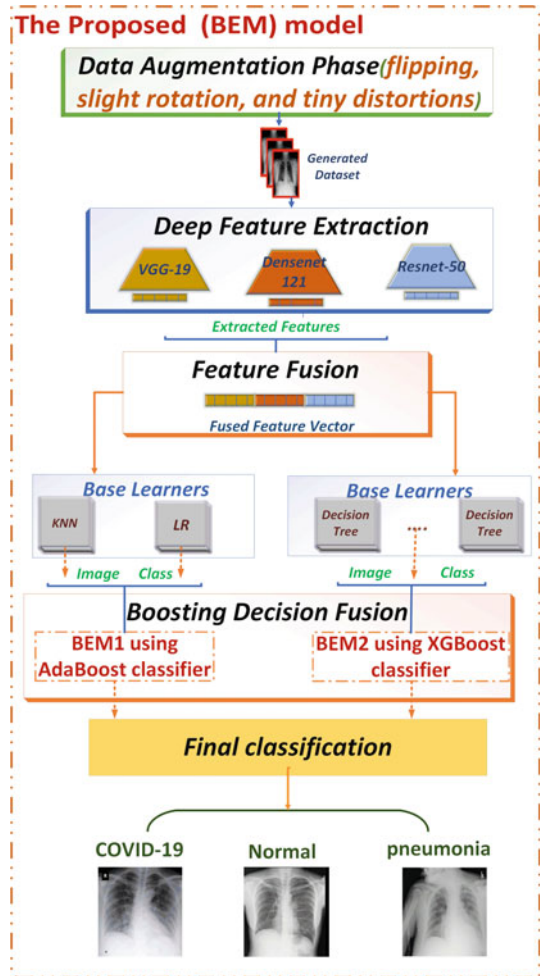
addressed important concerns such as the data imbalance as the dataset consists of over 15,000 images, with approximately 4420 images labelled as COVID-19 positive, 5000 images as pneumonia positive, and 5000 images as negative for both COVID-19 and pneumonia. The images are collected from various sources, including public datasets and hospitals worldwide. Images sizes of 128 × 128 were used and data set was divided as 70% for training, 15% validation and 15% for testing. All experimental simulations were carried out on TPUs with 16 GB of RAM using Google Colab.

Fig. 3 The proposed ML
feature and decision fusion
(MLFDF) [1]
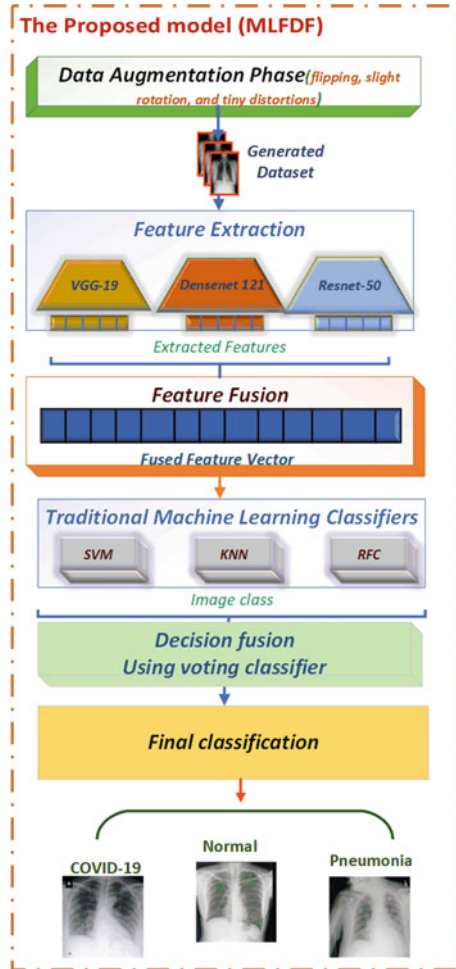
3.2 Performance of Multi-Class Classification

A confusion matrix is a table used in ML to evaluate the performance of a classification model. The matrix compares the predicted classes against the actual classes and provides a summary of the model's performance. The multiclass confusion presented in Fig. 4 is an N × N dimension matrix, where N is the number of distinct class labels C_0, C_1, C_N and with rows and columns representing the actual and predicted classes, respectively. In the diagonal of the matrix, the true positive (TP) and true negative (TN) values are represented, which are the cases where the model correctly predicted the class. In the off-diagonal cells, the false positive (FP) and false negative (FN) values are represented, which are the cases where the model made a mistake in its

Fig. 4 Multiclass classification confusion matrix [21]

prediction. A confusion matrix provides useful information such as accuracy, precision, recall, and F1 score, which are common metrics for the assessment of the performance of classification algorithms.

The proposed models perform multi-class classification to distinguish between normal, COVID-19, and pneumonia cases, with class 0 representing normal, class 1 representing COVID-19, and class 2 representing pneumonia. Figures 5 and 6 present confusion matrices that illustrate the test results for COVID-19, normal, and pneumonia cases. Table 1 summarizes the performance of the proposed models on the testing dataset by reporting accuracy, precision, recall, and F1 scores. The best-performing model for each metric is highlighted in bold font. The terms used in this table, including Accuracy (Acc), Recall (Rec), Precision (Pre), and F1-Score (F1), are defined mathematically as shown in reference [21].

$$Acc = \frac{\sum_{i=1}^{N} TP(\text{Ci})}{\sum_{i=1}^{N} \sum_{j=1}^{N} \text{Ci.j}} \tag{1}$$

$$Rec(\text{Ci}) = \frac{TP(\text{Ci})}{TP(\text{Ci}) + FN(\text{Ci})} \tag{2}$$

$$Pre(\text{Ci}) = \frac{TP(\text{Ci})}{TP(\text{Ci}) + FP(\text{Ci})} \tag{3}$$

$$F1(\text{Ci}) = 2 \times \left(\frac{Rec(\text{Ci}) \times Pre(\text{Ci})}{Rec(\text{Ci}) + Pre(\text{Ci})} \right) \tag{4}$$

Additionally, we compared the performance of the proposed models with other base learners, such as decision trees, KNN, Enhanced VGG16, Enhanced VGG19, Enhanced DenseNet201, and traditional bagging [7].

The Decision tree showed the lowest performance with a recall value of 82.43%. Furthermore, the KNN and traditional Bagging classifiers showed slightly improved results, with recall values of 91.2% and 90.33% respectively.

Fig. 5 The confusion
matrices obtained using;
a decision tree classifier,
b KNN, **c** bagging classifier
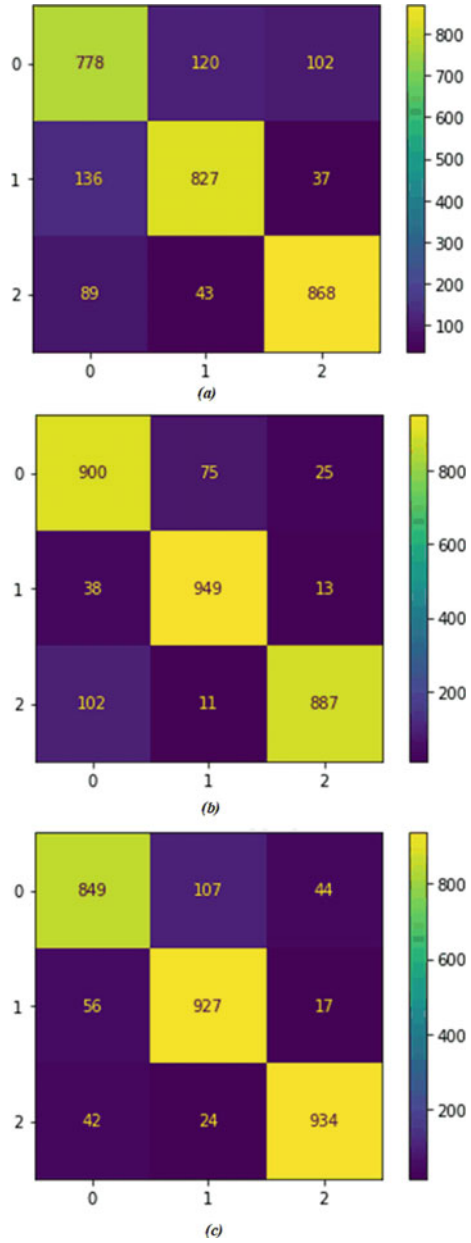
Fig. 6 The confusion matrices obtained using: **a** MLFDF, **b** proposed BEM1, **c** proposed BEM2
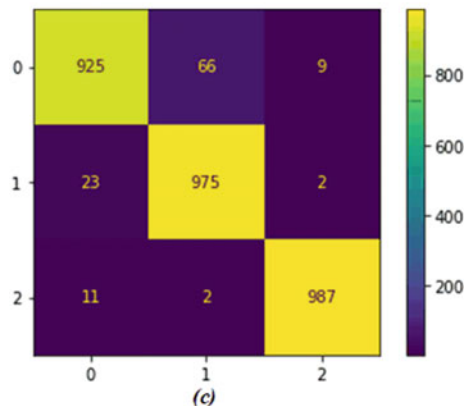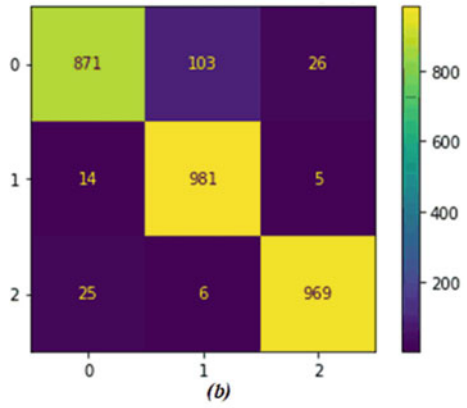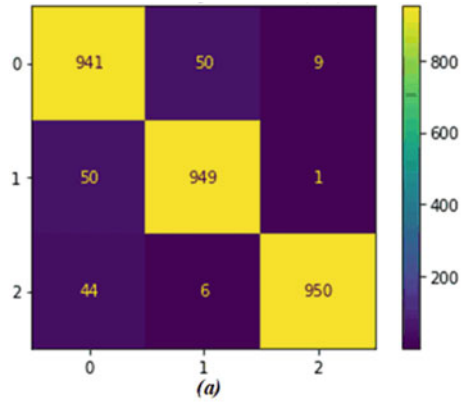
Table 1 Multi-class classification performance for the various models

Models	Acc	Rec	Pre	F1
Decision tree	82.43	82.43	82.43	82.43
KNN	91.2	91.2	91.37	91.2
Bagging classifier	90.33	90.33	90.37	90.31
Enhanced VGG16 [7]	95.48	95.41	95.48	95.41
Enhanced VGG19[7]	95.03	94.95	95.01	94.96
Enhanced DenseNet201[7]	91.97	88.30	94.07	89.44
Proposed MLFDF [1]	94.5	95.6	96.12	95.8
Proposed BEM1	94.03	94.03	94.2	93.99
Proposed BEM2	**96.2**	**96.23**	**96.27**	**96.22**

Bold indicates Proposed BEM2 achieved the best performance

Finally, the proposed MLFDF, BEM1 and BEM2 achieved recall values 95.6%, 94.03% and 96.2% respectively. When comparing BEM2 proposed model with the enhanced models in [7] it is shown that our model yield better performance compared to enhanced DenseNet201, VGG19, and VGG16.

The test results demonstrate that ensemble learning outperforms other models in terms of generalization performance. By combining the strengths of the base learner models, the final model yields superior performance. Moreover, model combination can effectively reduce training time, subject to the availability of hardware for model execution.

Among the various Machine learning algorithms and enhanced models, BEM2 achieved the highest performance with an accuracy of 96.2%, recall of 96.23%, and precision of 96.8%. This is attributed to BEM2's utilization of XGBoost, which is known to perform well with complex datasets.

4   Conclusion

This study aimed to develop multi-class classification models for detecting COVID-19 in chest X-rays. The COVID-Chest Xray-15k dataset was used, which consists of 15,000 radiographs. A voting classifier-based model was proposed for the bagging method, while AdaBoost and XGBoost algorithms were used for boosting. A comprehensive experimental analysis was conducted to evaluate the performance of the proposed models on the test dataset. The proposed ensemble models outperformed individual machine learning methods in the multiclass classification problem. The proposed bagging model achieved a recall of 0.956. The proposed AdaBoost and XGBoost-based models achieved recall scores of 0.94 and 0.962, respectively. XGBoost demonstrated the best performance among all ensemble methods and individual base learners in all experiments.

This paper can be applied in various geographical areas by providing insights into the development and implementation of COVID-19 classification methods. By understanding the strengths and limitations of various classification and detection methods, countries can develop strategies to effectively detect and control the spread of COVID-19.

Future research could focus on expanding the dataset to include chest radiographs from other classes of illnesses and other types of scans. Additionally, it may be possible to apply the proposed models to other imaging modalities.

5 Recommendation

This study suggests additional investigation into ensemble learning techniques for classifying COVID-19 patients according to their chest X-rays. It also advises working together globally to exchange knowledge and resources, as well as creating standardised datasets to compare the effectiveness of various machine learning models. The use of machine learning models in healthcare should also be made more widely known and understood by the general public, according to healthcare organizations. The final recommendation made by this study is to assess the utility of ensemble learning techniques in other healthcare applications.

References

1. Menshawy L, Eid AH, Abdel-Kader RF (2023) Ensemble deep models for covid-19 pandemic classification using chest x-ray images via different fusion techniques. Int J Adv Intell Inform 9(1)
2. Ozturk T, Talo M, Yildirim EA, Baloglu UB, Yildirim O, Rajendra Acharya U (2020) Automated detection of COVID-19 cases using deep neural networks with X-ray images. Comput Biol Med 121:103792
3. Chowdhury, Muhammad EH, Rahman T, Khandakar A, Mazhar R, Kadir MA, Mahbub ZB, Islam KR et al (2020) Can AI help in screening viral and COVID-19 pneumonia? IEEE Access 8:32665–132676
4. Lalmuanawma S, Hussain J, Chhakchhuak L (2020) Applications of machine learning and artificial intelligence for Covid-19 (SARS-CoV-2) pandemic: a review. Chaos Solitons Fractals 139:110059
5. Liu Y, Chen X, Wang Z, Jane Wang Z, Ward RK, Wang X (2018) Deep learning for pixel-level image fusion: recent advances and future prospects. Inf Fusion 42:158–173
6. Ganaie MA, Hu M, Malik AK, Tanveer M, Suganthan PN (2022) Ensemble deep learning: a review. Eng Appl Artif Intell 115:105151
7. Badawi A, Elgazzar K (2021) Detecting coronavirus from chest X-rays using transfer learning. Covid 1(1):403–415
8. Aslan MF (2022) A robust semantic lung segmentation study for CNN-based COVID-19 diagnosis. Chemometrics Intell Lab Syst 231:104695
9. Ohata EF, Bezerra GM, das Chagas JVS, Neto AVL, Albuquerque AB, De Albuquerque VHC, Filho PPR (2020) Automatic detection of COVID-19 infection using chest X-ray images through transfer learning. IEEE/CAA J Automatica Sinica 8(1):239–248

10. Ayadi M, Ksibi A, Al-Rasheed A, Soufiene BO (2022) COVID-AleXception: a deep learning model based on a deep feature concatenation approach for the detection of COVID-19 from chest X-ray images. Healthcare 10(10):2072
11. Agrawal K, Kumar R, Jain S (2022) An efficient ensemble model for diagnosing covid-19 and pneumonia using chest x-ray images. Indian J Sci Technol 15(38):1900–1906
12. Do T-N, Le V-T, Doan T-H (2022) SVM on top of deep networks for covid-19 detection from chest X-ray images. J Inf Commun Converg Eng 20(3):219–225
13. Narin A, Kaya C, Pamuk Z (2021) Automatic detection of coronavirus disease (covid-19) using x-ray images and deep convolutional neural networks. Pattern Anal Appl 24:1207–1220
14. Gupta RK, Kunhare N, Pateriya RK, Pathik N (2022) A deep neural network for detecting coronavirus disease using chest X-ray images. Int J Healthcare Inf Syst Inform (IJHISI) 17(2):1–27
15. Waheed A, Goyal M, Gupta D, Khanna A, Al-Turjman F, Pinheiro PR (2020) CovidGAN: data augmentation using auxiliary classifier GAN for improved covid-19 detection. IEEE Access 8:91916–91923
16. Dhanapala GH, Sotheeswaran S (2022) Transfer learning techniques with SVM for covid-19 disease prediction based on chest X-ray images. In: 2022 2nd international conference on advanced research in computing (ICARC). IEEE, pp 72–77
17. Saha P, Sadi MS, Islam MM (2021) EMCNet: automated COVID-19 diagnosis from X-ray images using convolutional neural network and ensemble of machine learning classifiers. Inform Med Unlock 22:100505
18. Rahimzadeh M, Attar A (2020) A modified deep convolutional neural network for detecting COVID-19 and pneumonia from chest X-ray images based on the concatenation of Xception and ResNet50V2. Inform Med Unlock 19:100360
19. Huang M-L, Liao Y-C (2022) Stacking ensemble and ECA-EfficientNetV2 convolutional neural networks on classification of multiple chest diseases including COVID-19. Acad Radiol
20. Kumar K (2021) Machine learning-based ensemble approach for predicting the mortality risk of COVID-19 patients: a case study. In: Intelligent data analysis for COVID-19 pandemic. Springer, Singapore, pp 1–25
21. Markoulidakis I, Kopsiaftis G, Rallis I, Georgoulas I (2021) Multi-class confusion matrix reduction method and its application on net promoter score classification problem. In: The 14th pervasive technologies related to assistive environments conference, pp 412–419

Epileptic Seizure Detection Contribution in Healthcare Sustainability

Saly Abd-Elateif El-Gindy, Ayman Ahmed, and Saad Elsayed

1 Introduction

Recently, sustainable development has gained increasing importance and plays a major role in the wise use of resources. It is worth noting that 17 major sustainable development Goals (SDGs) were proposed by the United States of America to address the most important global issues. These issues are about sustainable development and guiding countries in the economic, social and environmental aspects [1]. There is no doubt that health care plays a major role towards sustainable development, in that it guarantees the well-being of individuals and the health of societies and this can be achieved by diagnosis, detection and prediction of diseases as earlier as possible [2].

Electroencephalography is a medical signal acquisition system, which is utilized to read scalp electrical activities resulting from various brain functions. The electroencephalogram (EEG) in a simple word that refers to the recording of electrical activities, which contain useful information of different human states. Therefore, these recordings not only can be used to diagnose various brain disorders such as Alzheimer's disease and epilepsy, but it can also be used to monitor patterns of consciousness (such as feelings and emotions) or unconsciousness (such as sleep state and comma) of a human [3, 4]. Specialists have shown that epilepsy characterization is the most prevalent and dominant in the field of processing of electrical EEG signals [5].

S. A.-E. El-Gindy (✉) · A. Ahmed · S. Elsayed
Department of Electronics and Electrical Communications Engineering, High Institute for Engineering and Technology, AlObour, K 21Cairo/Belbeis Rd, Obour, Egypt
e-mail: eng.saly.elgindy@gmail.com

A. Ahmed
e-mail: ayman.mahmoud@oi.edu.eg

S. Elsayed
e-mail: s.elsayed8585@oi.edu.eg

Epilepsy is one of the most serious, acute and chronic brain disorders that cause an imbalance in the human nervous system. It should be noted that epilepsy patients face many challenges and risks in their daily lives, especially when dealing with heavy machinery or driving vehicle, due to the loss of control over most of the nervous organs [6]. Recent studies have shown that approximately more than 65% of epilepsy patients can control seizures through anti-epileptic drugs, and approximately 10% could befit from surgery. The remaining 25% have drug resistant and experience sudden symptoms. Therefore, it is necessary to notify the patient's medication-resistant epileptic seizure to the caretaker and analyze the pattern of related signals before, during, and after the seizure onset [7].

The most effective method for epileptic activity analysis among diagnostic imaging methods is the analysis of electrical EEG signals. These signals give a description of the voltage fluctuations, which result from ionic current within the brain [8]. Hence, there was a need for seizure detection and seizure prediction strategies, where seizure detection deals with recognition of seizures that occurring (or have occurred) through analysis of biologic signals recorded from a patient with epilepsy.

The rest of this paper is organized as follows. Section 2 presents the description of experimental materials and utilized methods. This section includes a brief description of the FWHT algorithm, the EEG signal attributes and the performance metrics. Section 3 investigates the simulation results and discussion. Finally, Sect. 4 gives the conclusion remarks.

2 Materials and Methods

2.1 Description of the Dataset

To evaluate the proposed approach, we used the CHB-MIT dataset, which was acquired at the Children Hospital Boston. It is also referred to as the Physio Net EEG dataset [9], which is composed of EEG recordings for pediatric individuals with intractable seizures. These recordings are public, available, and widely-used in the detection and prediction of epileptic seizures. It is grouped into 23 cases with various genders and different ages. It contains5 males, ages 3–22; and 17 females, ages 1.5–19. The standard 10–20 electrode system has been used to collect the EEG recordings in this dataset, which is sampled with a sampling rate of 256 Hz. The brief description of these datasets is illustrated in Table 1. This table includes all cases of patients, showing their age, gender and number of seizures for each case, in addition to the time taken during the measurement.

Table 1 Cases considered for seizure detection on CHB-MIT dataset [9]

Patient no.	Gender	Age	Seizure
1	F	11	3
2	M	11	7
3	F	14	4
4	M	22	5
5	F	7	10
6	F	15	3
7	F	14.5	5
8	M	3.5	4
9	F	10	7
10	M	3	3
11	F	12	7
12	F	22	10
13	F	3	8
14	F	9	20
15	M	16	8
16	F	7	3
17	F	12	6
18	F	18	3
19	F	19	8
20	F	6	4
21	F	13	3
22	F	9	7
23	F	6	7
24	F	–	16

2.2 Proposed Method

The proposed method depends mainly on the FWHD for discrimination between seizure and healthy epochs. The main idea of the proposed method is based on the decomposition of EEG signals into Hadamard coefficients, and then extraction of a certain attribute from decomposed EEG signals. Finally, the classification stage is performed based on a feature ranking method with a single attribute statistic as shown in Fig. 1. In this method, the Receiver Operating Characteristic (ROC) curve is utilized for performance assessment according to the selected attribute. The ROC curve is a relation between sensitivity and 1-specificity, for various values of the threshold. Ranking in general is executed depending on the area under the ROC curve [10–12].
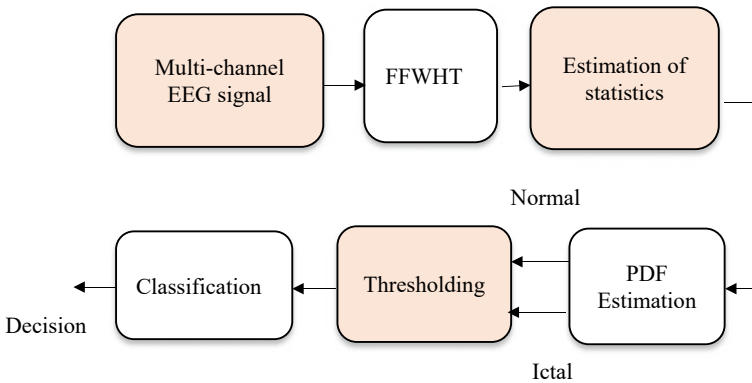
Fig. 1 Block diagram of the proposed method

The detection results are obtained for a selected attribute. The considered attributes include Kurtosis, Skewness, mean curve length, and Hjorth activity are estimated for decomposed Hadamard coefficients.

The classification strategy is performed based on a thresholding technique in which an optimum threshold is determined first on each attribute after PDF estimation of normal and seizure epochs, and then the threshold used in the classification process. Each threshold value is obtained at the intersection point between two PDF curves for normal and seizure activities as illustrated in Fig. 2. The distributions are obtained for groups of segments for normal and seizure activities to obtain the PDFs of FWHT coefficients. We clarify the values of thresholds for all attributes for all cases of CHB-MIT dataset in Tables 3, 4, 5 and 6.

The EEG seizure detection performance based on a single attribute is evaluated depending on five important metrics, which are optimum threshold Sensitivity (SEN), optimum threshold Specificity (SPE), obtained maximum Accuracy (ACC), Positive Predicted Value (PPV), Negative Predicted Value (NPV). These results are given in Tables 3, 4, 5 and 6. The steps of the proposed method are illustrated in Algorithm 1 for the detection of normal and seizure activities for epilepsy patients.

Algorithm 1

PDF of patient 1 for mean curve length feature	AROC of patient 1for mean curve length feature
PDF of patient 2 for mean curve length feature	AROC of patient 2 for mean curve length feature
PDF of patient 3 for mean curve length feature	AROC of patient 3 for mean curve length feature
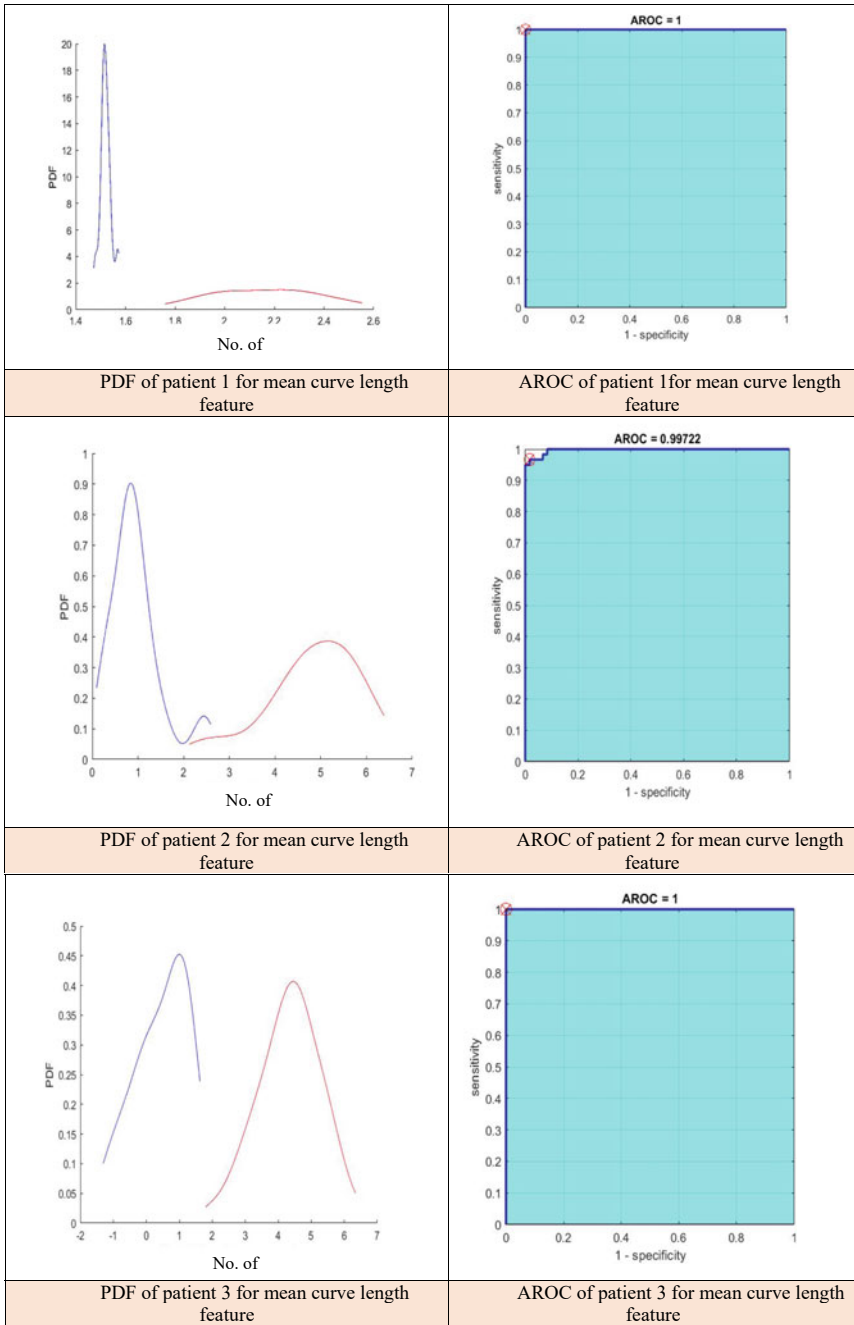
Fig. 2 PDFs and AROCs of samples patients for mean curve length feature

| PDF of patient 4 for mean curve length feature | AROC of patient 4 for mean curve length feature |
| PDF of patient 5 for mean curve length feature | AROC of patient 5 for mean curve length feature |
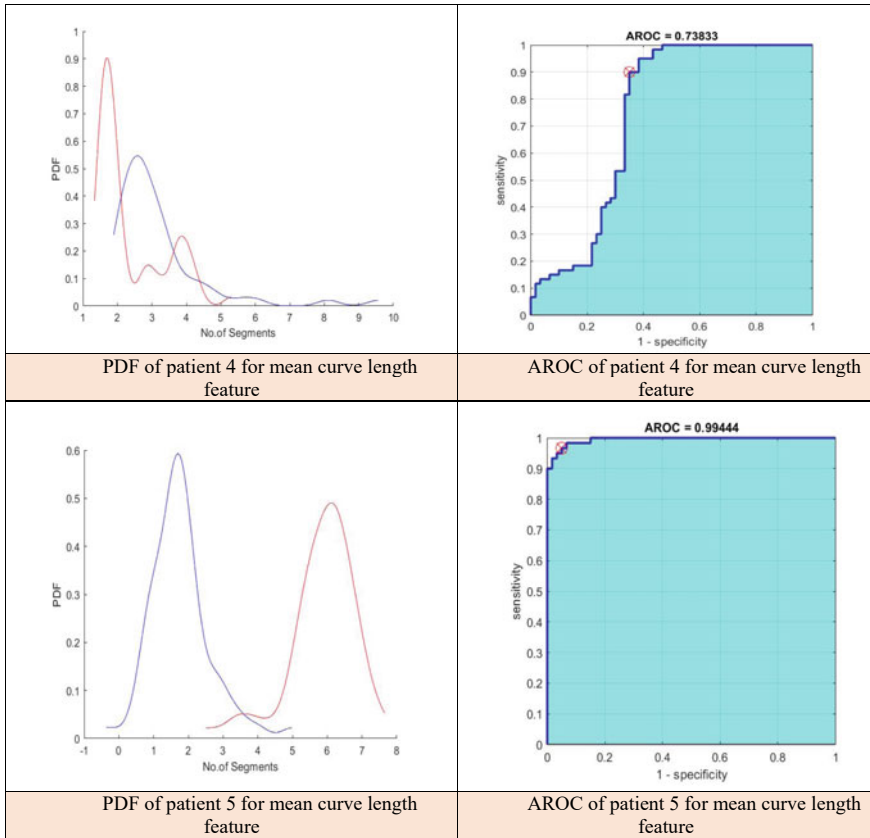
Fig. 2 (continued)

Detection of normal and seizure activities for epilepsy patients

---

Input: multi-channel EEG signal
Procedure
1. Apply FWHT on EEG signals
2. Extract one of the following attributes, namely Kurtosis, Skewness, mean curve length, Hjorth activity from decomposed EEG coefficients for several normal and seizure waveforms
3. Estimate PDFs of the selected attribute for several normal and seizure waveforms
4. Estimate the intersection point of the PDFs
5. Apply a ranking step for new incoming segments to perform classification
6. Obtain ROC curve and calculate area under ROC curve
7. Obtain SEN, SPE, ACC, PPV, and NPV for all segments
Output: ACC and FAR

2.2.1 Fast Walsh Hadamard Transform (FWHT)

The FWHT is an efficient methodology, which depends mainly on transformation of signals from time domain to frequency domain. It is worth monitoring that Walsh Hadamard transform is defined as being sequence oriented [13]. In addition to providing spectral representation, Hadamard transform is also essential for describing certain types of systems and their properties in the frequency domain. It has a high efficiency to identify the signals that have sharp disturbances in a more accurate way [14]. The FWHT of a signal $x(n)$ for $n= 1, 2, \ldots N$ can be computed according to this equation.

$$X_w(k) = \sum_{n=1}^{N} x(n) W_n, \quad k = 1, 2, \ldots N \tag{1}$$

where N indicates the total number of samples and Wn represents the Walsh matrix, which is given by the following equation:

$$W_n = \frac{1}{2^{\frac{n}{2}}} \begin{pmatrix} W_{n-1} W_{n-1} \\ W_{n-1} - W_{n-1} \end{pmatrix} \tag{2}$$

The basic benefit of this transformation is the high speed in performance, and it requires less storage memory to store decomposed coefficients.

2.2.2 EEG Signal Attributes

- **Hjorth Activity**

It is one of Hjorth's parameters, which define amplitude of EEG signal [15]. It can be determined according to the following equation:

$$m_0 = \int_{-\infty}^{\infty} S(w)dw = \frac{1}{T} \int_{t-T}^{t} f^2(t)dt \tag{3}$$

where $S(w)$ represents the power density spectrum and f(t) denotes as EEG signal (function of bio-signal). The activity parameter indicates the signal power, the variance of a time function $m_0 = \sigma_0^2$.

- **Kurtosis**

It is one of the high-level statistics, which are recommended in the recognition of EEG signals. It provides a measure of sharpness of the probability distribution of EEG signals. These distributions may have positive or negative values [16, 17]. The positive value is denoted as Kurtosis super-Gaussian, while the negative one is

labeled as Kurtosis sub-Gaussian. The normalized Kurtosis of random value can be determined according to the following equation

$$K_c(z) = \frac{E\{|z|^4\}}{(E\{|z|^2\})^2} - \frac{|E\{z^2\}|^2}{(E\{|z|^2\})^2} - 2 \tag{4}$$

where the first term indicates the fourth-order moment, while the second term represents the circulatory coefficients.

- **Skewness**

It is another complex static metric, which has high competency in the field of detection and prediction of EEG signals. It provides a measure of symmetry or asymmetry of the probability distribution of EEG signals. These distributions may have positive or negative values [18, 19]. Skewness of a signal $x(n)$ can be determined according to the following equation:

$$\boldsymbol{Skewness} = \frac{\boldsymbol{E}\big[(\boldsymbol{x(n)} - \boldsymbol{\mu})^3\big]}{\boldsymbol{\sigma}^3} \tag{5}$$

where μ indicates the mean of the signal, σ represents the standard deviation and E is the expected value of the signal.

- **Mean Curve Length (MCL)**

It is one of the prominent features in the field of recognition of EEG signals, as it reduces the computational cost and leads to better performance. It provides a measure of signal complexity depending on Katz fractal dimension [20, 21]. The Curve Length (CL) can be defined as the sum of linear distances between successive points on the curve. In the case of EEG signals, it can be defined for a time series as the sum of the absolute value of the first order finite difference. The MCL can be determined as the average of CL values. The MCL of a signal $x(n)$ for length N can be obtained according to the following equation:

$$MCL = \frac{1}{N-1} \sum_{n=0}^{N-2} |x(n+1) - x(n)| \tag{6}$$

2.2.3   Performance Metrics

The performance of the proposed method is evaluated depending on six metrics as follows [20] as tabulated in Table 2.

where TP is the true positives, FP is the false positives, FN is the false negatives, and TN is the true negatives.

Table 2 Performance metrics of the proposed approach

Performance metric	Equation
Sensitivity (SEN %)	$SEN = \frac{TP}{TP+FN} \times 100$ (7)
Specificity (SPE %)	$SPE = \frac{TN}{TN+FN} \times 100$ (8)
Accuracy (ACC %)	$ACC = \frac{TP+TN}{TP+TN+FP+FN)} \times 100$ (9)
Positive prediction value (PPV %)	$PPV = \frac{TP}{TP+FP} \times 100$ (10)
Negative prediction value (NPV %)	$NPV = \frac{TN}{TN+FN} \times 100$ (11)
ROC	It is created by plotting sensitivity versus 1-specificity at various values of the threshold

$$FN = L - TP \tag{12}$$

$$TN = L - FP \tag{13}$$

where L is the data class length.

3 Simulation Results and Discussion

Simulation experiments have been carried out on the whole CHB-MIT dataset as tabulated in Table 1. For each case, we apply the FWHT to analyze the EEG signals in frequency domain. Several attributes are considered including, kurtosis, skewness, mean curve length, and Hjorth activity.

Simulation results of the detection process for all patients are illustrated in Tables 3, 4, 5 and 6. The majority voting strategy is applied on the results of all attributes for efficient detection results. It is clear from all obtained results that the majority voting gives the best detection results. Moreover, working on MCL with FWHT gives the best results compared to the results obtained with other features achieving an average sensitivity of 98.59%, an average specificity of 96.26% and an average accuracy of 96.83%. Samples of MCL feature with the FWHT is illustrated in Fig. 2, which indicates the PDFs and area under the ROC curve for all patients.

One of the advantages of the proposed approach is avoiding the over-training problem, which is a major concern in modeling of data in several fields due to using a statistical model that contains more parameters than can be justified by the data. Unlike other techniques, one of the reasons that make our approach far from the over-training is that we do not use a noisy or unknown dataset. The dataset we use is well prepared as a standard benchmark for many years of research. In addition, we do not have a training process in which over-training may occur, but it is a direct detection technique (online technique) based on different metrics, statistical analysis and similarity measures. It avoids the training process, testing and then over-training problem.

Table 3 Results of Hjorth activity with FWHT for all patients

For all patient	Result of Hjorth with FWHT
Average SEN (%)	92.6984
Average SPE (%)	92.19697
Average AROC	0.9201641
Average ACC (%)	90.37879
Average PPV (%)	86.02868
Average NPV (%)	85.45591

Table 4 Results of mean curve length activity with FWHT for all patients

For all patient	Result of MCL with FWHT
Average SEN (%)	*98.59206*
Average SPE (%)	96.26984
Average AROC	0.9617989
Average ACC (%)	96.83333
Average PPV (%)	90.41736
Average NPV (%)	88.2364

Table 5 Results of kurtosis activity with FWHT for all patients

For all patient	Result of kurtosis with FWHT
Average SEN (%)	93.43136
Average SPE (%)	95.39216
Average AROC	0.9314705
Average ACC (%)	93.82353
Average PPV (%)	92.35181
Average NPV (%)	89.37992

Table 6 Results of skewness activity with FWHT for all patients

For all patient	Result of skewness with FWHT
Average SEN (%)	*95.93751*
Average SPE (%)	94.89584
Average AROC	0.9265799
Average ACC (%)	*95.88541*
Average PPV (%)	86.38388
Average NPV (%)	82.53691

In addition to the accuracy of the proposed approach in detecting epileptic seizures, it also saves a lot of time as it avoids the time consumed in the training process. In addition, the time of the proposed approach is very short ranging from 2 to 3 min using the same machine specifications. All of these benefits make the proposed approach

Table 7 Comparison of performance for the existing with the proposed method

Author	Dataset	Subject	Features	Classifier
Tsiouris et al. [20]	CHB-MIT	24 patients 181 seizures	Spectral analysis, variation in EEG energy distribution over the delta, theta, and alpha rhythms	Subset selection method (SSM)
Prathap and Aswathy [21]	CHB-MIT	17 patients 78 seizures	Spectral power and spectral power ratios	Kernel sparse representation classifier
Behnam and Hossein [22]	CHB-MIT	23 patients 163 seizures	Arithmetic mean, geometric mean, variance, COV, mode, median, Pearson and Bowley's, and moment measure of skewness, kurtosis, and negative entropy	Bayesian classifier
Janjarasjitt [23]	CHB-MIT	12 patients	Wavelet-based spectral features	No classifier
Proposed method	CHB-MIT	23 patients 174 seizures	Kurtosis, skewness, mean curve length, and Hjorth activity	Thresholding strategy

more effective in comparison with other previous methods. A comparison study with the existing state-of-the-art algorithms is given in Table 7.

4 Conclusion

The proposed approach adopted in this paper depends on using the FWHT, and hence statistical analysis of decomposed coefficients. Different statistical attributes are estimated for them. A thresholding strategy is applied on each attribute. Hence, a decision is taken based on that attribute. The main advantage of this approach is the avoidance of the classification problems represented in training, testing and overfitting problems. In addition, the results prove that mean curve length with FWHT demonstrates the best performance in comparison.

5 Recommendations

A growing body of evidence suggests that EEG analyses can be used in the early detect of Alzheimer's and may even allow for the diagnosis for different dementia subtypes. Most of the research has been done in academic environments, however

there could be the potential to develop low-cost medical testing devices which achieve sustainability in healthcare systems.

References

1. Gulis G, Krishnankutty N, Boess ER, Lyhne I, Kørnøv L (2022) Environmental impact assessment, human health and the sustainable development goals. Int J Publ Health

2. Wang EY, Zafar JE, Lawrence CM, Gavin LF, Mishra S, Boateng A, Thiel CL, Dubrow R, Sherman JD (2021) Environmental emissions reduction of a preoperative evaluation center utilizing telehealth screening and standardized preoperative testing guidelines. Resour Conserv Recycl

3. Niknazar H, Maghooli K, Nasrabadi AM (2015) Epileptic seizure prediction using statistical behavior of local extrema and fuzzy logic system. Int J Comput Appl (2)

4. Riney K, Bogacz A, Somerville E, Hirsch E, Nabbout R, Scheffer IE, Zuberi SM, Alsaadi T, Jain S, French J, Specchio N (2022) International League Against Epilepsy classification and definition of epilepsy syndromes with onset at a variable age: position statement by the ILAE task force on nosology and definitions. Epilepsia 63(6):1443–1474

5. Alickovic E, Kevric J, Subasi A (2018) Performance evaluation of empirical mode decomposition, discrete wavelet transforms, and wavelet packed decomposition for automated epileptic seizure detection and prediction. Biomed Signal Process Control 39:94–102

6. Ullah I, Hussain M, Aboalsamh H (2018) An automated system for epilepsy detection using EEG brain signals based on deep learning approach. Expert Syst Appl 107:61–71

7. Peng P, Song Y, Yang L, Wei H (2022) Seizure prediction in EEG signals using STFT and domain adaptation. Front Neurosci 15

8. Teplan M (2002) Fundamentals of EEG measurement. Measur Sci Rev 2(2):1–1

9. The CHB-MIT database (online). https://physionet.org/content/chbmit/1.0.0/. Accessed 4 Apr 2021

10. Duch D, Wieczorek T, Biesiada J, Blachnik M (2004) Comparison of feature ranking methods based on information entropy. IEEE Int Joint Conf Neural Netw 2(4):1415–1419

11. Hussain L (2018) Detecting epileptic seizure with different feature extracting strategies using robust machine learning classification techniques by applying advance parameter optimization approach. Cognitive Neuro-Dyn 12(3):271–294

12. Sharma R, Ram PB, Rajendra UA (2015) An integrated index for the identification of focal electroencephalogram signals using discrete wavelet transform and entropy measures. Entropy 17(8):5218–5240

13. Shakya N, Rahul D, Laxmi S (2021) Stress detection using EEG signal based on fast Walsh Hadamard transform and voting classifier

14. Subathra MSP, Mohammed MA, Maashi MS, Garcia-Zapirain B, Sairamya NJ, George ST (2020) Detection of focal and non-focal electroencephalogram signals using fast Walsh-Hadamard transform and artificial neural network. Sensors 17

15. Oh SH, Yu-Ri L, Hyoung NK (2014) A novel EEG feature extraction method using Hjorth parameter. Int J Electron Electr Eng 2:106–110

16. Büyükçakır B, Furkan E, Mutlu AY (2020) Hilbert vibration decomposition-based epileptic seizure prediction with neural network. Comput Biol Med

17. Mudhiganti PR (2012) A comparative analysis of feature extraction techniques for EEG signals from Alzheimer patients

18. Yahyaei R (2022) Fast EEG based biometrics via mean curve length. MS thesis. Middle East Technical University

19. Paranjpe MJ, Kakatkar MN (2013) Automated diabetic retinopathy severity classification using support vector machine. Int J Res Sci Adv Technol 3:86–91

20. Tsiouris KM, Markoula S, Konitsiotis D, Fotiadis DI (2018) A robust unsupervised epileptic seizure detection methodology to accelerate large EEG database evaluation. Biomed Signal Process Control 40:275–285
21. Prathap P, Aswathy TD (2017) EEG spectral feature-based seizure prediction using an efficient sparse classifier. In: IEEE international conference on intelligent computing, instrumentation and control technologies (ICICICT)
22. Behnam M, Hossein P (2016) Real-time seizure prediction using RLS filtering and interpolated histogram feature based on hybrid optimization algorithm of Bayesian classifier and Hunting search. In: Computer methods and programs in biomedicine, pp 115–136
23. Janjarasjitt S (2017) Performance of epileptic single-channel scalp EEG classifications using single wavelet-based features. Austr Phys Eng Sci Med 1:57–67

Performance Analysis of Emerging Waveforms for 6G Wireless Communications

Walid Raslan and Heba Abdel-Atty

1 Introduction

The next generation of wireless systems and standards (beyond 5G/6G) will need to accommodate extremely high mobility scenarios such as high-speed railway systems, vehicle-to-infrastructure, and vehicle-to-vehicle. Orthogonal frequency division multiplexing (OFDM) is currently used in 5G cellular systems and performs well in time-invariant frequency selective channels. However, in high-mobility scenarios, the large Doppler frequency shifts break orthogonality between subcarriers in OFDM, resulting in significant performance degradation. To address this issue, new waveforms are being investigated for fast time-varying channels [1].

Orthogonal chirp division multiplexing (OCDM) based on the discrete Fresnel transform (DFnT) performs better than OFDM in terms of bit error rate (BER) in multipath channels. However, OCDM does not achieve full diversity in general time-varying channels [2]. The orthogonal time frequency space (OTFS) was proposed in the delay-Doppler (DD) domain and shows superior performance to OFDM in time-varying channels but lacks its own orthogonal transmission pulse in the DD domain. Other modulation waveforms implemented in different domains are also proposed, such as orthogonal time sequency multiplexing (OTSM) which utilize the Walsh Hadamard transform (WHT) and the discrete Mellin transform (DMT), respectively [3].

To determine which waveform is most suitable for next-generation wireless communications, a thorough comparison of their performance is necessary. This

W. Raslan (✉)
Electronics and Communication Engineering Department, Faculty of Engineering, Delta University for Science and Technology, Gamasa, Egypt
e-mail: Walid.Raslan@deltauniv.edu.eg

H. Abdel-Atty
Electrical Engineering Department, Faculty of Engineering, Port Said University, Port Said, Egypt
e-mail: heba_atty@ieee.org

involves analyzing the correlations between the waveforms from the perspective of their modulation domain and obtaining a unified framework by discussing their system models [4, 5].

The BER performance of each waveform is then analyzed and compared through simulations. Based on these analyses and demonstrations, candidate waveform suggestions for future wireless communications are provided.

The study's emphasis on high-speed railway systems, vehicle-to-infrastructure, and vehicle-to-vehicle communications aligns with SDG 11. By optimizing waveforms for high-mobility scenarios, the research contributes to building smarter and more sustainable cities and communities. Reliable wireless communication is vital for efficient transportation systems, traffic management, and enhanced connectivity in urban environments [6].

The rest of the paper is organized as follows. In Sect. 2, we discuss the system model for four modulation techniques. The simulation results are provided in Sect. 3. Section 4 contains our concluding remarks.

2 System Model

In this section, we provide the overview and system model of the waveforms including OFDM, OCDM, OTFS, and OTSM. We classify them according to their modulation domain, i.e., time frequency (TF), delay-Doppler, delay-sequence, and delay-scale domain. Figure 1 illustrates the relationships between different domains (time, frequency, delay, Doppler, scale and sequence) [7]. The domains can be classified into three types: information symbol, channel, and transition. Each domain can be transformed using specific mathematical techniques Discrete Fourier Transform (DFT)/ Inverse Discrete Fourier Transform (IDFT), Discrete Multitone (DMT)/Inverse Discrete Multitone (IDMT), and Walsh-Hadamard Transform (WHT)/Inverse Walsh-Hadamard Transform (IWHT). For example, in the OTFS system, information symbols are multiplexed in the DD domain and then transferred to the TF domain through the Inverse Symplectic Finite Fourier Transform (ISFFT), which involves applying a Discrete Fourier Transform (DFT) along the delay axis and an inverse DFT (IDFT) along the Doppler axis. The TF domain is then converted to the delay-time domain using IDFT along the frequency axis, and the signal is transmitted in the delay-time domain. It is worth noting that the channel plays a critical role in the transformation of relations described above.
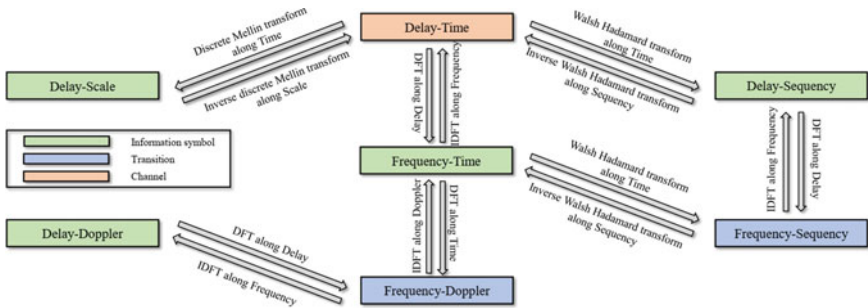
Fig. 1 Relation between the different discrete information symbol domains (time, frequency, delay, Doppler, scale and sequence) and the corresponding modulation transforms [7]

2.1 Orthogonal Frequency Division Multiplexing (OFDM)

OFDM can be seen as a chirp-based modulation waveform with a linearly varying instantaneous frequency of zero. OFDM is a widely used digital modulation technique in modern wireless communication systems. OFDM is a multicarrier modulation scheme that divides the high-speed data stream into multiple subcarriers and transmits them simultaneously in parallel. OFDM has become popular due to its ability to mitigate the effects of multipath fading, increase spectral efficiency, and provide robustness against interference [8].

The basic idea behind OFDM is to divide the high-speed data stream into multiple parallel subcarriers that are orthogonal to each other. The orthogonality between subcarriers eliminates the need for a guard interval between symbols, which reduces the bandwidth overhead and improves the spectral efficiency. OFDM also allows for the use of advanced error-correction codes, such as forward error correction (FEC), which further improves the reliability of the communication [9].

OFDM has been adopted in several wireless communication standards such as Digital Video Broadcasting (DVB), Wi-Fi, Long-Term Evolution (LTE), and 5G [10]. OFDM has also been used in other applications such as digital audio broadcasting, powerline communication, and optical communication. OFDM has become a popular multi-carrier modulation technique in various industries. The OFDM method involves dividing the available frequency band into multiple sub-bands, known as subcarriers, to enable parallel transmission of data. A baseband OFDM modulation and demodulation are functionally illustrated in Fig. 2 [11].
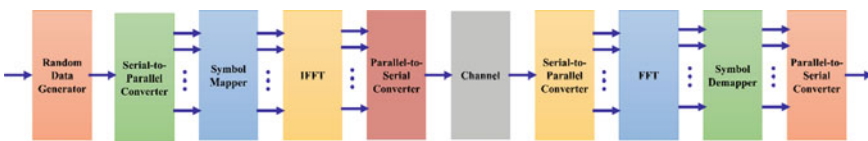
Fig. 2 Block diagram of OFDM modulation and demodulation [11]

OFDM can be understood as a chirp-based modulation waveform with a linearly varying instantaneous frequency of zero. Other modulation techniques, such as OCDM are also based on chirp modulation waveforms in the time–frequency domain as chirp-based waveforms The expression of data symbols X can be represented in the case of OFDM as follows.

$$\mathbf{X} = [\mathbf{X}(0), \mathbf{X}(1), \ldots, \mathbf{X}(M-1)]^T \tag{1}$$

where $X(m) = [X(m, 0), X(m, 1), \ldots, X(m, N-1)]^T$. Figure 2 illustrates that $X(n; m)$ represents the data symbol transmitted on the *m-th* subcarrier of the *n-th* OFDM symbol. The data symbols X are transmitted on each *m-th* OFDM symbol and are represented as $X = [X(0), X(1), \ldots, X(N-1)]^T$. These data symbols are then processed by the IDFT block, and the resulting time-domain signal can be expressed as:

$$s[n] = \frac{1}{\sqrt{N}} \sum_{m=0}^{N-1} X[m] e^{i\frac{2\pi}{N}nm} \tag{2}$$

In matrix form, (4) can be rewritten as

$$\mathbf{s} = \mathbf{F}^H \mathbf{X}, \tag{3}$$

The DFT matrix, with entries $e^{-j2\pi mn/N}/\sqrt{N}$, is denoted by F. The signal is then subjected to the addition of a cyclic prefix (CP) before being transmitted into the channels [12].

2.2 Orthogonal Time Frequency Space (OTFS)

OTFS is a novel modulation technique that has recently gained popularity in wireless communication systems. OTFS is a non-linear modulation technique that aims to overcome the limitations of traditional modulation schemes, such as OFDM, in dynamic and challenging wireless environments. OTFS operates in a two-dimensional time–frequency space, where the signal is spread across multiple time and frequency dimensions, rather than being confined to a single dimension [13].

The basic idea behind OTFS is to encode information in the delay-Doppler domain, which describes the changes in signal propagation caused by motion or reflections in the wireless channel. The delay-Doppler domain can be represented as a two-dimensional matrix, where the rows represent the signal delay and the columns represent the Doppler shift. OTFS spreads the signal energy across this matrix, making it resilient to fading and multipath effects, as well as Doppler shifts caused by the motion of the transmitter or receiver [14, 15].
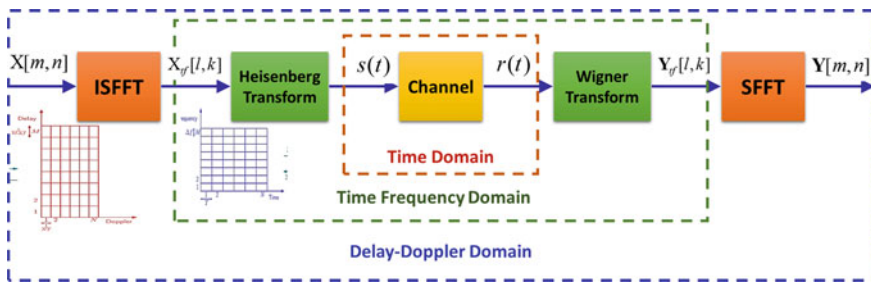
Fig. 3 The block diagram of OTFS modulation and demodulation [17]

OTFS has several advantages over traditional modulation techniques. It provides high spectral efficiency, robustness against channel variations, and low latency, making it suitable for a wide range of applications, including autonomous vehicles, 5G networks, and satellite communication systems. OTFS also provides high accuracy in channel estimation, which is critical for beamforming and other advanced signal processing techniques [16].

Figure 3 illustrates the modulation and demodulation process of the OTFS system. At the transmitter, the delay-Doppler information matrix $X[m, n]$ is utilized, which comprises NM symbols that map from modulation symbols. The number of subcarriers and time slots are denoted by M and N, respectively. The discrete-time domain OTFS frame contains NM samples, and as a result, the OTFS frame duration is given by $T_f = NMT_s = NT$ with the sampling frequency $f_s = B = \frac{1}{T_s}$.

The modulator applies the inverse symplectic fast Fourier transform (ISFFT) to transform the symbols from the delay-Doppler domain to the time–frequency domain $X_{tf}[l, k]$, as shown in Fig. 3 [17].

$$X_{tf}[l, k] = \frac{1}{\sqrt{NM}} \sum_{n=0}^{N-1} \sum_{m=0}^{M-1} X[m, n] e^{i2\pi \left(\frac{nk}{N} - \frac{ml}{M} \right)} \tag{4}$$

where $l = 0, \ldots, M - 1, k = 0, \ldots, N - 1$.

The inverse symplectic fast Fourier transform (ISFFT) is used to convert the symbols from the delay-Doppler domain to the time–frequency domain $X_{tf}[l, k]$. The ISFFT involves two operations: first, performing an M-point discrete Fourier transform (DFT) on the columns of X, and second, performing an N-point inverse DFT on the rows of X. A pulse shaping waveform $g_{tx}(t)$. is used to produce the transmitted signal $s(t)$ through the Heisenberg transform.

$$s(t) = \sum_{n=0}^{N-1} \sum_{m=0}^{M-1} X_{tf}[l, k] g_{tx}(t - kT) e^{i2\pi \Delta f(t-kT)} \tag{5}$$

Let's consider a high mobility communication scenario with a bandwidth of B and P channel paths. The delay and Doppler shift of the channel can be represented by the variables τ and ν, respectively, as shown in the following equation [18]:

$$\tau_i = \frac{\ell_i}{M\Delta f} \leq \tau_{\max} = \frac{\ell_{\max}}{M\Delta f}, \ \nu_i = \frac{\kappa_i}{NT} \ |\nu_i| \leq \nu_{\max} \tag{6}$$

The normalized delay and Doppler shift are represented by ℓ_i and κ_i, respectively. The received signal $r(t)$ in continuous time is expressed as follows:

$$r(t) = \int g(\tau, \nu) s(t - \tau) d\tau \tag{7}$$

where $g(\tau, t)$ is the delay-time channel response

$$g(\tau, t) = \int_\nu h(\tau, \nu) e^{j2\pi\nu(t-\tau)} d\nu \tag{8}$$

where $h(\tau, \nu)$ is the high mobility channel response. The discrete-time form of the received is expressed as

$$r[q] = \sum g^s[l, q] s[q - l], \quad q = 0, \ldots, NM - 1, \tag{9}$$

where $g^s[l, q]$ is the discrete delay-time channel response.

$$g^s[l, q] = \sum_{i=1}^{P} g_i z^{\kappa_i(q-l)} \delta[l - l_i] \tag{10}$$

The channel gain of the multipath channel is represented by g_i, and $z = e^{\frac{j2\pi}{NM}}$. It is assumed that the delay-Doppler channel is constant over the duration of T_f. In order to maintain this, N may need to be reduced, which would result in a decrease in Doppler shift resolution.

At the receiver end, the received signal $r(t)$ is converted to the time–frequency domain using the Wigner transform, as shown below [19]:

$$\mathbf{Y}_{tf}[l, k] = \int r(t') g_{rx}^*(t' - t) e^{-j2\pi f(t'-t)} dt' \tag{11}$$

The received matched filter g_{rx} is used to obtain the delay-Doppler domain samples. To achieve this, the time-domain received samples are transformed using symplectic fast Fourier transform (SFFT), which is a 2D transformation involving an M-point inverse discrete Fourier transform (IDFT) of the columns of Y and an N-point discrete Fourier transform (DFT) of the rows of $\mathbf{Y}$.

2.3 Orthogonal Time Sequency Multiplexing (OTSM)

OTSM is a single-carrier modulation scheme, which offers similar BER to OTFS. The information symbols are multiplexed in the delay-sequency domain using WHT. Note that sequency is the number of zero-crossings per unit interval. Since WHT does not require multiplicative operations and requires only addition and subtraction operations, the OTSM modulation/demodulation complexity is significantly low as compared to OFDM and OTFS modulation [18].

we will adopt the matrix and vector notation as follows: x and y, both of size $NM \times 1$, represent the transmitted and received information symbols, respectively. The duration of the transmitted OTSM signal frame, denoted as $T_f = NT$, while the bandwidth is $B = M\Delta f$, where N is a power of 2. We assume that $T\Delta f = 1$, which implies that the OTSM signal is critically sampled for any pulse shaping waveform. The operation of the OTSM transceiver is illustrated in Fig. 4 [20].

The transmitter splits the information symbols $x = [x_0^T, \dots, x_{M-1}^T]^T$ into vectors xm. These symbol vectors are organized into a matrix $X \in C^{M \times N}$ by placing each symbol vector x_m in the m-th row. The indices of the columns and rows indicate the delay and sequency indices, respectively, of the delay-sequency grid [20].

$$X = [x_0, x_1, \dots, x_{M-1}]^T \tag{12}$$

The final l_{max} symbol vectors, which refers to x_m for $m \geq M - l_{max}$ M, are set to zero vectors. The reason behind this is to avoid inter-block interference caused by channel delay spread. This is illustrated in Fig. 4.

By performing zero padding (ZP) along the delay domain, the signal is protected from this type of interference.

Afterward, a N-point Walsh-Hadamard transform is performed on each symbol vector to convert it into the delay-time domain.

$$\tilde{X} = X \cdot \mathbf{W}_N \tag{13}$$

The delay-time samples are stored in a matrix called $\tilde{X}$, which is then converted into time-domain samples s by vectorizing it. These time-domain samples s are
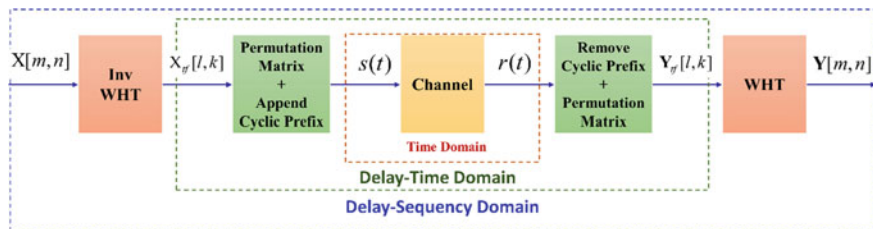
Fig. 4 The block diagram of OTSM modulation and demodulation [20]

then transmitted into the physical channel. The entire operation performed by the transmitter can be represented in a concise matrix form.

$$\mathbf{s} = \mathbf{P} \cdot (\mathbf{I}_M \otimes \mathbf{W}_N) \cdot \mathbf{x} \tag{14}$$

The above equation describes a matrix operation that involves a row-column interleaver matrix P. This permutation matrix is called a perfect shuffle and is used to rearrange the elements of two matrices A and B. The property of a perfect shuffle is described as follows: if A and B are both square matrices of equal size, then their perfect shuffle using the permutation matrix P results in a new matrix that has the same size as A and B combined.

$$\mathbf{A} \otimes \mathbf{B} = \mathbf{P} \cdot (\mathbf{B} \otimes \mathbf{A}) \cdot \mathbf{P}^T \tag{15}$$

Additionally, as P is a matrix of permutation, $P^{-1} = P^T$. By employing the perfect shuffle property given in (5), the operation of the transmitter in (4) can be simplified as:

$$\mathbf{s} = (\mathbf{W}_N \otimes \mathbf{I}_M) \cdot (\mathbf{P} \cdot \mathbf{x}) \tag{16}$$

The time-domain samples are pulse shaped, and digital to analog converted, and transmitted into the wireless channel as $s(t)$.

After the time-domain samples are shaped by pulses, converted to digital signals, they are transmitted as $s(t)$ into the wireless channel. At the receiver, the received time-domain vector $r(t)$ undergoes analog to digital conversion and sampling, and the steps taken by the transmitter are reversed to demodulate the received time-domain samples. The received information symbols y are arranged into the matrix $\tilde{Y}$ by folding the symbols column-wise, where M and N denote the number of delay and sequency bins respectively. The symbols can be converted from the DS domain to the DT domain by applying the N-point inverse WHT, represented by WN.

$$\tilde{\mathbf{Y}} = vec^{-1}_{M,N}(\mathbf{r}) \tag{17}$$

The received information symbols are obtained by taking a N-point WHT of the received delay-time samples $\tilde{Y}$ as

$$\mathbf{Y} = [\mathbf{y}_0, \mathbf{y}_1, \ldots, \mathbf{y}_{M-1}]^T = \tilde{\mathbf{Y}} \cdot \mathbf{W}_N \tag{18}$$

The receiver operation can be simplified in the matrix form as

$$\mathbf{y} = (\mathbf{I}_M \otimes \mathbf{W}_N) \cdot \left(\mathbf{P}^T \cdot \mathbf{r}\right) \tag{19}$$

where

$$\mathbf{Y} = [\mathbf{y}_0^T, \dots, \mathbf{y}_{M-1}^T]^T \qquad (20)$$

2.4 Orthogonal Chirp Division Multiplexing (OCDM)

Orthogonal Chirp Division Multiplexing (OCDM) is a modulation scheme that has gained significant attention in recent years due to its potential to provide high data rates and robustness against interference in wireless communication systems.

OCDM is a form of time division multiplexing (TDM) that uses orthogonal chirp signals to modulate multiple data streams onto the same frequency band. In OCDM, each data stream is modulated into a separate chirp signal, and the chirp signals are spaced so that they are orthogonal to each other. This allows for multiple data streams to be transmitted simultaneously without interfering with each other, thus increasing the data rate and robustness against interference as shown in Fig. 5 [21].

OCDM has several advantages over other modulation schemes, including its ability to provide high spectral efficiency, resistance to multipath fading and frequency-selective fading, and low power requirements. These features make OCDM an attractive option for high-speed data transmission in wireless communication systems, especially in challenging environments [22].

OCDM has been implemented in several communication standards, such as the IEEE 802.15.3c standard for high-speed wireless personal area networks (WPANs) and has also been proposed for use in fifth generation (5G) cellular networks. To introduce the Fresnel transform in the optics for OCDM, some constraints are raised.
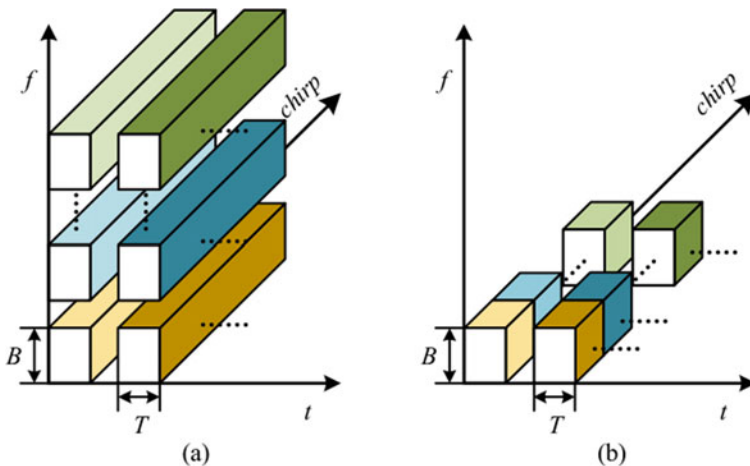
Fig. 5 **a** the multi-code chirp waveform and **b** the digital implemented OCDM signal in the temporal frequency-chirp dimension [2]

Firstly, the chirped waveform for modulation is time limited. Secondly, the spatial Talbot effect is adapted into the temporal counterpart for OCDM.

The OCDM system model combines the advantages of both OCDMA (Optical Code Division Multiple Access) and CSS (Chirp Spread Spectrum) techniques for secure and efficient communication. It uses chirp signals for spreading the spectrum of the signal, which provides secure and robust communication for military, underwater, and aerospace scenarios.

The chirp signal is conventionally generated by analog devices using filtering or frequency-modulation approaches. In the CSS system, a broad spectrum is occupied for modulating information, sacrificing spectral efficiency for high processing gain, multipath resolution, and other merits of the chirp signal. In a given period and bandwidth, only one modulated chirp is present, and interference occurs if multiple chirp signals are present in the same period and bandwidth. Thus, chirp is attractive for low data rate applications where reliability is a priority [23].

OCDM adds the benefit of OCDMA, which uses orthogonal codes for multiple access, allowing multiple users to share the same bandwidth without interference. In OCDM, the spreading codes are orthogonal chirp signals, and each user is assigned a unique orthogonal chirp code. This allows multiple users to share the same bandwidth while avoiding interference, increasing spectral efficiency. OCDM has potential applications in optical fiber communication systems, where multiple users can share the same fiber without interference, increasing the capacity of the system [23].

According to [2], $x(m)$ can be extracted by the matched filter to the $m\text{-}th$ chirp as shown in Fig. 6, as

$$
\begin{aligned}
x'(m) &= \int_0^T s(t)\, \psi_m^*(t)\, dt \\
&= \sum_{k=0}^{N-1} x(k)\, \delta(m-k) = x(m)
\end{aligned}
\tag{21}
$$

where $\psi(t)$ is the root chirp. The analog OCDM signal is transmitted within a bandwidth ranging from $-B$ to B, where B is equal to N divided by T. The digital implementation of the OCDM signal based on DFnT which demonstrates that the digital OCDM generates the OCDM signal with wrapped spectra in accordance with the sampling theory. The spectrum of the digital OCDM signal can be limited within the bandwidth of $-0.5B$ to $0.5B$. Furthermore, digital filters can effectively manage the out-of-band aliasing signal in chirp-based systems, such as CSS.

The discrete-time OCDM signal is equivalent to the continuous-time OCDM signal but with a wrapped spectrum. It is worth noting that there are two types of DFnT matrix. Therefore, the discrete OCDM signal can be expressed as:

$$
s(n) = s(t)\big|_{t=n\frac{T}{N}} = \sum_{k=0}^{N-1} x(k)\, \psi_k\left(n\frac{t}{N}\right)
$$
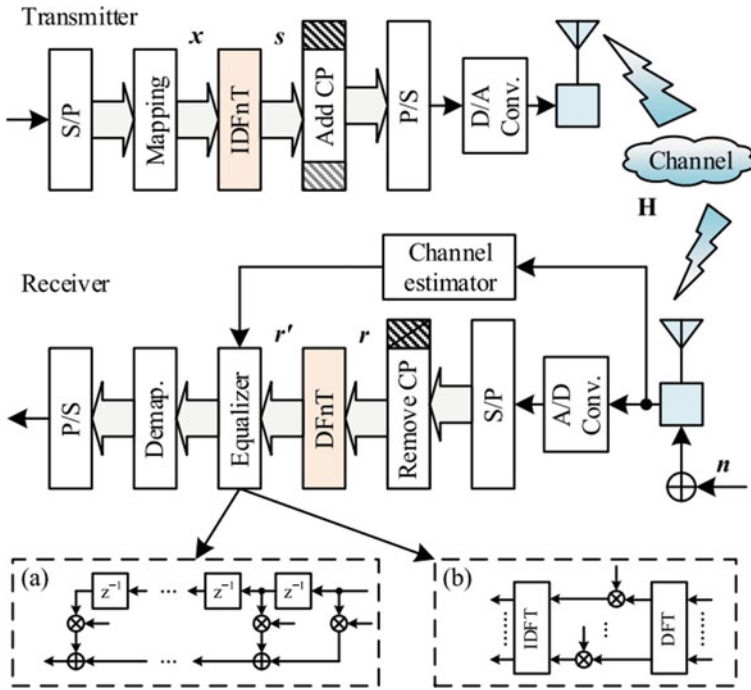
Fig. 6 The block diagram of OCDM modulation and demodulation [2]

$$= e^{j\frac{\pi}{4}} \sum_{k=0}^{N-1} x(k) e^{-j\frac{\pi}{N}(n-k)^2} \tag{22}$$

For even N, or

$$s(n) = s(t)|_{t=(n+\frac{1}{2})\frac{T}{N}} = \sum_{k=0}^{N-1} x(k)\, \psi_k\left(n\frac{T}{N} + \frac{T}{2N}\right)$$

$$= e^{j\frac{\pi}{4}} \sum_{k=0}^{N-1} x(k) e^{-j\frac{\pi}{N}(n-k+\frac{1}{2})^2} \tag{23}$$

Upon examining Eqs. (22) and (23), one can observe that they resemble the definition of DFnT, and are precisely the IDFnT. Hence, the synthesis of a series of discretized modulated chirp waveforms can be achieved using the IDFnT. thereby obtaining the discrete time-domain OCDM signal [2].

$$\mathbf{s} = \mathbf{\Phi}^H \mathbf{x} \tag{24}$$

Given that the DFnT matrix is unitary, the transmitted symbols can be retrieved at the receiver through the inverse operation, namely DFnT. The symbols obtained through this process are:

$$\mathbf{x}' = \Phi \mathbf{s} = \mathbf{x} \tag{25}$$

3 Simulation Results and Discussion

This section provides simulation outcomes that assist in evaluating the effectiveness of the proposed waveforms. The assessment is conducted by examining three different waveforms techniques and comparing them to the OFDM system within the extended vehicular channel (EVA).

In order to maintain simplicity in the OFDM system, only the ZF equalizer is employed, as both the ZF and MMSE equalizers exhibit identical bit-error-rate (BER) performance within the OFDM system. For the processing of OTFS and OTSM, a frequency domain equalizer is utilized, which implements a single tap and linear mean square error (LMMSE). In OCDM, both the zero-forcing (ZF) and minimum mean squared error (MMSE) equalizers are employed. All considered waveforms occupy the same resources, and the simulation parameters can be found in Table 1.

Figures 7, 8 and 9 show the bit error rate (BER) performance of OFDM, OCDM, OTFS, and OTSM, respectively, under the standard EVA Channel model. The modulation orders of 4-QAM, 16-QAM, and 64-QAM are used, and the receiver speed is set at 350 km/h. The channel delay model is generated in accordance with the standard EVA model (with a speed of 350 km/h) as described in [24], where the Doppler shift for the i-th path is produced from a uniform distribution $U(0, \nu_{max})$,, with ν_{max} representing the maximum Doppler shift.

In the OFDM system, only the ZF equalizer is used due to its simplicity. Both ZF and MMSE equalizers achieve the same BER performance in the OFDM system. However, the performance of OFDM is the worst in high-mobility scenarios due

Table 1 Simulation parameters

Simulation parameters	Value
Modulation order	QPSK, 16 and 64 QAM
Number of symbols (N)	64
Number of subcarriers (M)	64
Subcarrier spacing (Δf)	15 kHz
Number of frames	300
Carrier frequency (fc)	4 GHz
Channels model	EVA (9 taps)
Speed	350 km/h
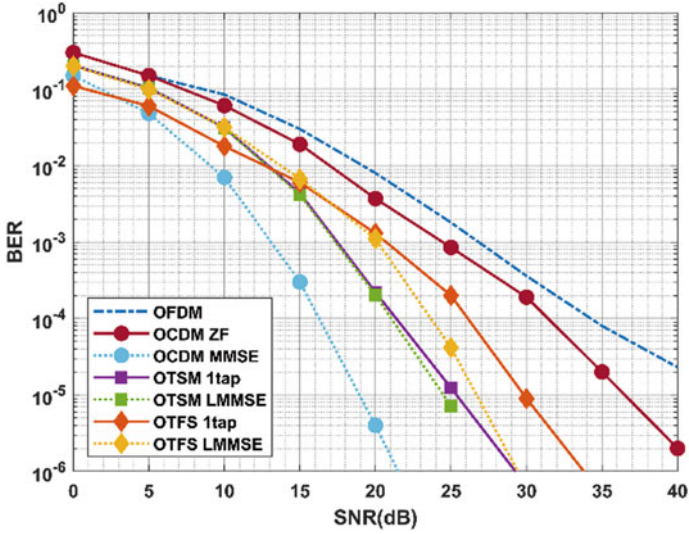
Fig. 7 BER performance of OFDM, OCDM, OTFS, and OTSM for 4 QAM in EVA Channel model (350 km/h)
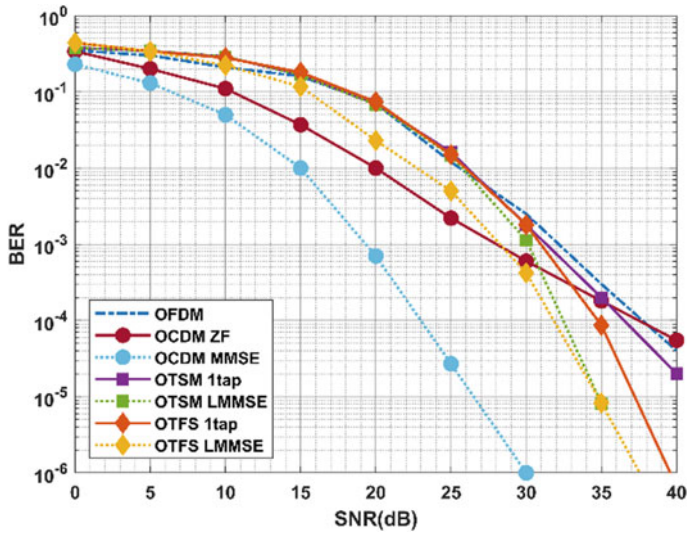
Fig. 8 BER performance of OFDM, OCDM, OTFS, and OTSM for 16 QAM in EVA Channel model (350 km/h)
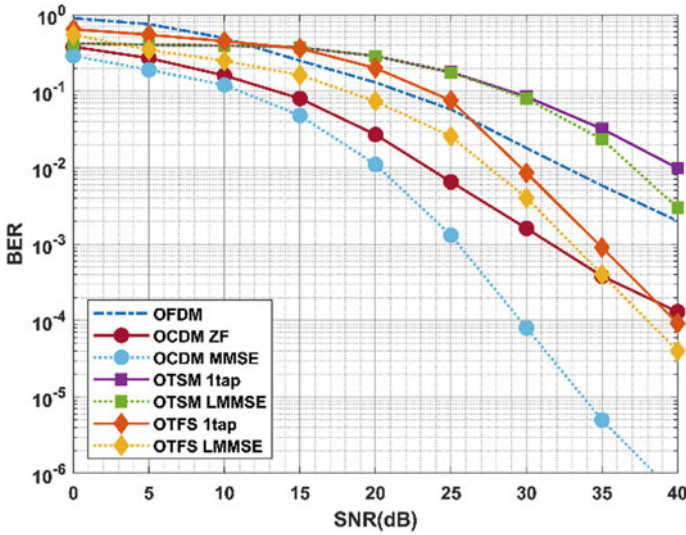
Fig. 9 BER performance of OFDM, OCDM, OTFS, and OTSM for 64 QAM in EVA Channel model (350 km/h)

to large Doppler frequency shifts and loss of orthogonality among subcarriers, resulting in inter-carrier interference. In contrast, OCDM has better performance than OFDM, thanks to its superior path separation capabilities. Similarly, OTFS outperforms OFDM because it operates in the DD coordinate system, allowing it to extract full channel diversity even under limited SNR. OTSM and OTFS have nearly identical performances as both maintain good orthogonality of subcarriers in the corresponding domain to carry information symbols. In the OCDM system with ZF equalizer, higher SNR is required to achieve the same BER compared to OFDM, especially in low SNR regions.

However, BER curves of OCDM and OFDM approach each other as SNR increases. Noise enhancement of the ZF equalizer causes the degradation of the BER performance of OCDM, which becomes smaller as SNR increases. The OCDM with MMSE equalizer outperforms that with the ZF equalizer, as the MMSE equalizer balances channel compensation and noise enhancement, and contributes to superior performance over OFDM due to multipath diversity. However, the MMSE equalizer is slightly degraded in low SNR regions. This degradation is more pronounced as the modulation level increases from 4 and 16 to 64-QAM, as high-level modulation formats are sensitive to noise.

OTSM uses a single tap equalizer whose performance can be improved by increasing the sub-carrier spacing Δf. When the channel Doppler spread is a small fraction of the sub-carrier spacing, time–frequency domain samples remain roughly orthogonal. This is useful for low-latency and delay-critical wireless applications.

OTSM also offers similar performance to OTFS but at significantly lower transmitter and receiver complexity.

The BER performance of the systems with 64-QAM modulation is shown in Fig. 8. The BER of OTFS with LMMSE equalization is the lowest among all the systems, followed by OTSM with LMMSE and 1-tap equalization. The BER of OCDM with ZF equalization is the highest among all the systems, and the BER of OFDM is higher than that of OTFS and OTSM. The results indicate that the BER performance of the systems depends on the modulation order and choice of equalization method. In most cases, OTFS with LMMSE equalization outperforms the other systems in terms of BER. However, OCDM with ZF equalization has the highest BER among all the systems. The simulation results provide insights for selecting suitable communication systems for high-speed mobile applications.

The simulation results indicate that OFDM is the worst-performing system in high-mobility scenarios, while OCDM has better performance than OFDM due to its superior path separation capabilities. OTFS outperforms OFDM, and OTSM offers similar performance to OTFS with significantly lower transmitter and receiver complexity. The choice of equalization method is crucial, with MMSE equalizer outperforming ZF equalizer in most cases. However, high-level modulation formats are sensitive to noise, and the performance of OCDM with MMSE equalizer is slightly degraded in low SNR regions. The results suggest that OTFS with LMMSE equalization is the best option for high-speed mobile communication applications.

4   Conclusion

In this paper, a comprehensive overview of the emerging multi-carrier waveforms for 6G wireless communications was presented. The performances of three promising multi-carrier waveforms, namely OTFS, OTSM, and OCDM, were analyzed and compared over doubly dispersive channels. Simulation results revealed that OTFS, OTSM, and OCDM are all waveforms techniques used in modern communication systems.

OTFS modulation is a recent technique that maps symbols to the time–frequency domain of a signal. The unique mapping technique used by OTFS transforms the time-varying channel into a static channel, making it highly resilient to channel impairments. It is particularly useful in high-speed mobility scenarios like autonomous vehicles, where the channel has a high Doppler spread.

OTSM is a well-established technique that uses the principles of time-domain and frequency-domain orthogonal codes to transmit multiple signals over a single channel. It utilizes a set of orthogonal waveforms to transmit symbols over time slots, which are then transmitted over different subcarriers in the frequency domain. OTSM is widely used in wireless communication systems such as cellular networks.

OCDM is another multicarrier technique that uses a set of orthogonal chirp waveforms to transmit multiple signals simultaneously over a single channel. It utilizes the principles of spread spectrum communication, where a unique code is assigned to each user to separate their data from others in the same channel. OCDM is primarily

used in satellite communication systems and has the advantage of being highly resistant to interference and jamming.

The global applicability of these waveforms lies in their ability to enhance wireless communication systems' performance in various geographical areas. The challenges posed by high-mobility scenarios are not limited to specific regions but are encountered worldwide. By adopting OTFS, OTSM, or OCDM in the design of 6G wireless systems, countries and regions can improve their communication infrastructure and provide reliable and efficient connectivity to their populations.

In summary, the choice of which technique to use depends on the specific application requirements and the characteristics of the communication channel. Overall, this paper provides insights into the benefits and drawbacks of the three multi-carrier waveforms and how they can be applied in different scenarios.

5 Recommendations

The recommendations for future studies, policy planners, decision makers, and stakeholders regarding emerging waveforms for 6G wireless communications are as follows: Future studies should focus on evaluating these waveforms in real-world scenarios, exploring optimization techniques and signal processing methods, and conducting comparative studies. Policy planners and decision makers should stay informed about advancements, make informed decisions on spectrum allocation and regulatory frameworks, and engage with relevant stakeholders. Stakeholders should consider the benefits and challenges of adopting these waveforms, contribute to standardization efforts, and invest in research and development. Standardization bodies should include emerging waveforms in their efforts, ensure interoperability with existing technologies, and collaborate with industry, academia, and regulatory authorities. Following these recommendations will foster the development, deployment, and standardization of emerging waveforms, leading to improved performance and reliability in high-mobility scenarios in the context of 6G wireless communications.

References

1. Salameh AI, El Tarhuni M (2022) From 5G to 6G challenges, technologies, and applications. Futur Internet 14:117. https://doi.org/10.3390/FI14040117
2. Ouyang X, Zhao J (2016) Orthogonal chirp division multiplexing. IEEE Trans Commun 64:3946–3957. https://doi.org/10.1109/TCOMM.2016.2594792
3. Thaj T, Viterbo E, Hong Y (2021) Orthogonal time sequency multiplexing modulation: analysis and low-complexity receiver design. IEEE Trans Wirel Commun 20:7842–7855. https://doi.org/10.1109/TWC.2021.3088479
4. Elaraby S, Soliman HY, Abdel-Atty HM, Mohamed MA (2017) Joint 2D-DOA and carrier frequency estimation technique using nonlinear kalman filters for cognitive radio. IEEE Access 5:25097–25109. https://doi.org/10.1109/ACCESS.2017.2768221

5. Ahmed S, Heba MA-A, Rawya YR (2018) Joint channel assignment and power allocation based on maximum concurrent multicommodity flow in cognitive radio networks. Wirel Commun Mob Comput. https://doi.org/10.1109/GLOCOM.2014.7036919

6. Huawei; ITU; GeSI. ICT Sustainable Development Goals Benchmark: Accelerating SDGs through ICT. Available online: https://bit.ly/3WWKeGX (accessed on 6 December 2022)

7. Zhou Y, Yin H, Xiong J, Song S, Zhu J, Du J, Chen H, Tang Y (2023) Overview and performance analysis of various waveforms in high mobility scenarios

8. Raslan WA, Mohamed MA, Abdel-Atty HM (2022) Deep-BiGRU based channel estimation scheme for MIMO-FBMC systems. Phys Commun 51:101592. https://doi.org/10.1016/J.PHYCOM.2021.101592

9. Kebede T, Wondie Y, Steinbrunn J, Kassa HB, Kornegay KT (2022) Multi-carrier waveforms and multiple access strategies in wireless networks: performance, applications, and challenges. IEEE Access 10:21120–21140. https://doi.org/10.1109/ACCESS.2022.3151360

10. Ezz-Eldien NA, Abdelkader MF, Abdalla MI, Abdel-Atty HM (2020) Handover performance improvement in heterogeneous wireless network. In: IEEE 11th annual information technology, electronics and mobile communication conference IEMCON 2020, pp 821–830. https://doi.org/10.1109/IEMCON51383.2020.9284906

11. Mrinalini (2018) A survey paper on multicarrier modulation techniques. In: 2018 5th IEEE Uttar Pradesh section international conference on electrical, electronics and computer engineering UPCON 2018. https://doi.org/10.1109/UPCON.2018.8597168

12. Stüber GL, Barry JR, Mclaughlin SW, Li YE, Ingram MA, Pratt TG (2004) Broadband MIMO-OFDM wireless communications. Proc IEEE 92:271–293. https://doi.org/10.1109/JPROC.2003.821912

13. Hadani R, Rakib S, Tsatsanis M, Monk A, Goldsmith AJ, Molisch AF, Calderbank R (2017) Orthogonal time frequency space modulation. IEEE Wirel Commun Netw Conf WCNC. https://doi.org/10.1109/WCNC.2017.7925924

14. Thaj T, Viterbo E (2022) Low-complexity linear diversity-combining detector for MIMO-OTFS. IEEE Wirel Commun Lett 11:288–292. https://doi.org/10.1109/LWC.2021.3125986

15. Thaj T, Viterbo E (2022) Unitary-precoded single-carrier waveforms for high mobility: detection and channel estimation. IEEE Wirel Commun Netw Conf WCNC, pp 962–967. https://doi.org/10.1109/WCNC51071.2022.9772003

16. Raslan WA, Abdel-Atty HM (2023) Performance evaluation of data detection methods for orthogonal time frequency space modulation. Delta Univ Sci J 6:162–180. https://doi.org/10.21608/DUSJ.2023.291035

17. Eldemiry A et al (2022) Overview of the orthogonal time-frequency space for high mobility communication systems. In: 2022 5th international conference on communications, signal processing, and their applications (ICCSPA). IEEE

18. Thaj T, Viterbo E (2021) Orthogonal time sequency multiplexing modulation. In: IEEE wireless communications and networking conference, WCNC. Institute of Electrical and Electronics Engineers Inc.

19. Hong Y, Thaj T, Viterbo E (2022) Delay-Doppler communications principles and applications. Academic Press (an imprint of Elsevier)

20. Neelam SG, Sahu PR (2023) Joint compensation of TX/RX IQ imbalance and channel parameters for OTSM systems. IEEE Commun Lett 27:1–1. https://doi.org/10.1109/lcomm.2023.3234538

21. Savaux V (2022) Flexible communication system for 6G based on orthogonal chirp division multiplexing. In: 2022 1st international conference 6G networking, 6GNet 2022. https://doi.org/10.1109/6GNET54646.2022.9830497

22. Singh MK, Goel A (2022) Orthogonal chirp division multiplexing: An emerging multi carrier modulation scheme. In: Communications in computer and information science. Springer Science and Business Media Deutschland GmbH, pp 236–246

23. Huan S, Chen W, Peng Y, Yang C (2020) Orthogonal chirp division multiplexing waveform for mmwave joint radar and communication. In: IET international radar conference (IET IRC 2020). Institution of Engineering and Technology (IET), pp 1222–1226

24. 3rd Generation Partnership Project (3GPP) TR 36.104 (2017) Technical specification group radio access network; evolved universal terrestrial radio access: base station radio transmission and reception

Post-pandemic Active Learning (PPAL): A Framework for Active Architectural Education

Asmaa M. Hassan and Basma N. El-Mowafy

1 Introduction

Integrating artificial intelligence (AI) applications and information, communication technology (ICT) provides a significant approach in many fields [1–7], in particular, sustainability to promote human–environment interactions on social, economic, and environmental levels to especially provide adapting to vulnerabilities, unprecedented changes, and unforeseen circumstances [8–12]. The COVID-19 pandemic affected all aspects of daily life [13–17], including university operations, especially the teaching and learning sections [18–20]. Therefore, several studies globally have discussed the transformation from conventional learning in physical settings to e-learning through virtual classes [17, 21, 22]. E-learning supports personalized, productive, and collaborative learning experiences and distance learning [1–3]. E-learning enables the integration of ICT to organize communication processes during instructional activities via innovative technology platforms [23].

Architectural education has attracted attention owing to the special category of pedagogy strategies [24, 25]. Conventional architectural education is based on face-to-face lectures and design studios [26], including desk critique and design juries [27–41].

The COVID-19 pandemic has posed several challenges in content delivery, assessments, and interrelations of students in a post-pandemic scenario [42, 43] to consider the requirements of mass gathering and social distancing [42, 44–50].

A. M. Hassan · B. N. El-Mowafy (✉)

Architectural Engineering and Urban Planning Department, Faculty of Engineering, Port Said University, Port Said, Egypt
e-mail: basma_nashaat@eng.psu.edu.eg

A. M. Hassan
Department of Architecture Engineering, College of Engineering and Information Technology, Buraydah colleges, Buraydah, Saudi Arabia

Recognizing the significance of e-learning in response to the post-pandemic scenario, this study addresses the following research gaps: post-pandemic architectural education, considering the special category of architectural education in e-learning. In addition, the necessity to develop conceptual frameworks considering the requirements of active learning environments, each architectural course, and its teaching methods and strategies. To bridge these gaps, this study contributes to identifying active learning approaches, teaching methods, and strategies by classifying architectural courses in terms of content delivery, assessments, and interrelations in a post-pandemic scenario, and a post-pandemic active learning (PPAL) framework is developed as an appropriate methodology to realize an active learning environment. Therefore this study can help to achieve the Sustainable Development Goals (SDGs), such as Goal 4 regarding quality education. The paper is organized as follows: Sect. 2 discusses the transformation from conventional to e-learning based, the innovative modes of content delivery, its ability the motivation of students, and blended learning in particular. Section 3 identifies the approaches of active learning and their teaching methods, and strategies. Section 4 presents the shift in post-pandemic architectural education, focusing on the proposed PPAL framework, which provides active learning strategies through both synchronous and asynchronous learning, according to the classification of architectural courses. Section 5 discusses the proposed framework, and Sect. 6 concludes the paper and presents future research directions to enhance future studies on post-pandemic architectural education applications.

2   Transition from Conventional to E-Learning

Several studies discuss the e-learning modes of content delivery, such as synchronous and asynchronous delivery types, as well as its ability to motivate students, with a particular focus on blended learning owing to its integration of conventional and e-learning. Geng et al. [51] compared conventional and blended learning and demonstrated that blended learning can promote involvement and collaboration among students in a class. In addition, Zhou et al. [52] reported that blended learning can be adapted to combine the advantages of conventional learning and e-learning to achieve student interaction and meet their individual needs to ensure an active learning process. Moreover, various previous studies have emphasized the concept of the blended learning methodology, as summarized in (Table 1).

3   Approaches to Active Learning Process

Current best practice approaches for teaching and learning emphasize the importance of student engagement in learning processes [53]. Figure 1 identifies the engagement of students with their own learning processes, which is considered the main pillar of active learning processes. Active learning processes are based on

Table 1 Previous studies conducted on blended learning and flipped classroom

	References	Field	Method	Evaluation
Integration of flipped classroom	[54]	Medicine	*Pre-class:* • Online lectures; and videos *In-class:* • A patient case with slides • Several relevant questions were presented • Small groups presentation	Pre-class: quiz In-class: quiz
	[55]	Nursing	*Pre-class:* • Textbook • Recorded lectures, and videos *In-class:* • Small group discussions • Clinical scenario	In-class: quiz After-class: Questionnaire
	[3, 56]	Computer Science	*Pre-class:* • Electronic documents, or videos *In-class:* • Problem-solving, • Small group activities, discussions, and feedback	After-class: Questionnaire
	[52] [57] [58] [59] [3]	Engineering	*Pre-class:* • Hstar teaching platform *In-class:* • Intelligent classroom *Pre-class:* • Course documents • YouTube links • Course books *In-class:* • Interaction around collaborative problem solving • Integrated questions	

Fig. 1 Pillars of the active learning process. *Source* The authors after [3, 53, 60–66]

attaining a balance between the following three pillars: teacher-centered learning (TCL), pedagogy-space-technology (PST), and student-centered learning (SCL) to exploit their individual advantages [3].

4 Active Learning Strategies

Various strategies have been implemented to provide active learning, which differs according to the used teaching pedagogies (Fig. 2). To enable students to become learners, creators, and directors of content via active learning methods and strategies, the matrix between active learning methods and strategies are shown in (Fig. 3). Students can learn more effectively and flexibly and achieve academic goals, such as improving their achievement, productivity, self-confidence, independence, and autonomy.

5 Architectural Education

Architectural education is based on interpersonal interactions between teacher and student or student and student to implement the approach of "learning by design" or "learning by trial and error." Such an approach needs cognitive processing, mental images, affect relationships, functional, technical, performance, aesthetic, cultural,
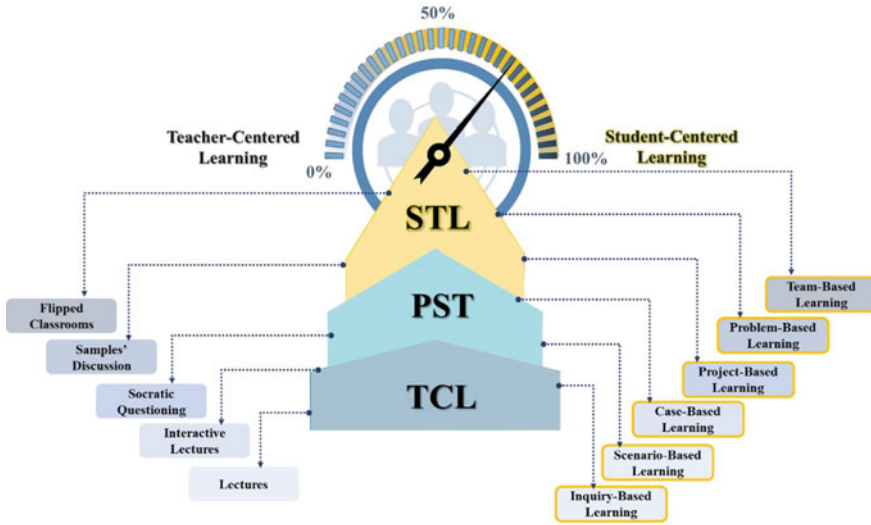
Fig. 2 Active learning strategies. The authors after [67–69]

and physical aspects [62]. In particular, the learning environment affects architectural student creativity, which requires group activities, sketch images, and visual references [70]. However, architectural education during the COVID-19 pandemic challenges academic staff to develop effective and technical ways of teaching and learning.

According to several researchers, e-learning at the outbreak of the COVID-19 pandemic does not meet the requirements of architectural education and requires new reform and change of curriculum. Therefore, we develop a conceptual framework that provides the shift toward architectural education in response to the COVID-19 pandemic, promoting key opportunities and considering threats related to such transformation.

6   PPAL Framework

Regarding the challenges related to the post-pandemic and special category of architectural education, we developed a conceptual framework, called PPAL. The PPAL framework provides an architectural active learning environment considering not only the learning environment but also the social and cognitive environments. In addition, key required skills and levels of cognitive activities are considered (Fig. 4). The proposed framework is based on the four interrelated pillars to support active learning related to post-pandemic architecture education: (a) the overall and specified skills of architectural courses; (b) the associated cognitive activities of Bloom's
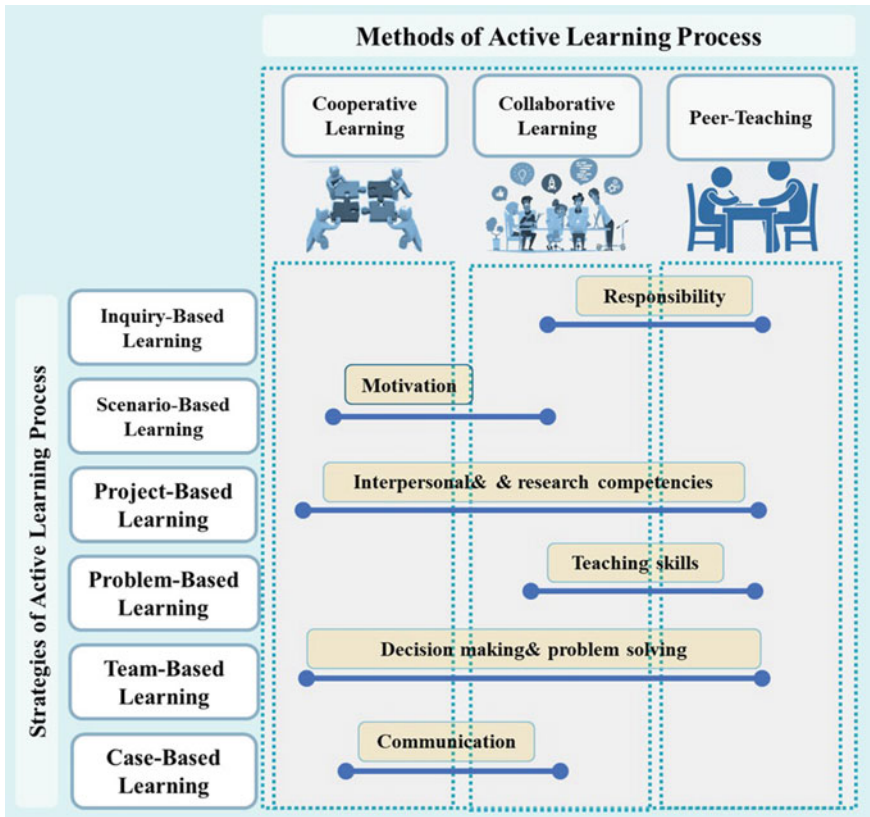
Fig. 3 Matrix between the methods and strategies of active learning toward a shift in post-pandemic

Taxonomy, with their four dimensions; (c) the approaches of active learning environment with their strategies and methods; (d) mode of delivery and assessment related to three classifications of architectural courses. The proposed framework illustrates the stages of required key skills related to each classification of architectural courses, whether design, skills, and knowledge, and the specifying skills of each classification. According to the overall skills, the proposed framework is based on the three domains of twenty-first-century skills; cognitive, interpersonal, and intrapersonal skills [71]. The framework determines the disparity between these skills according to the main classification of architectural courses and specifies skills that correspond to each classification.

For design courses, intrapersonal skills are key, this is followed by interpersonal and cognitive overall skills. In particular, design courses provide the following specified skills: creativity, innovation, decision-making, presentation, problem-solving, communication, and time management. The knowledge courses, interpersonal, cognitive, and intrapersonal skills are key, and research skills, critical thinking,
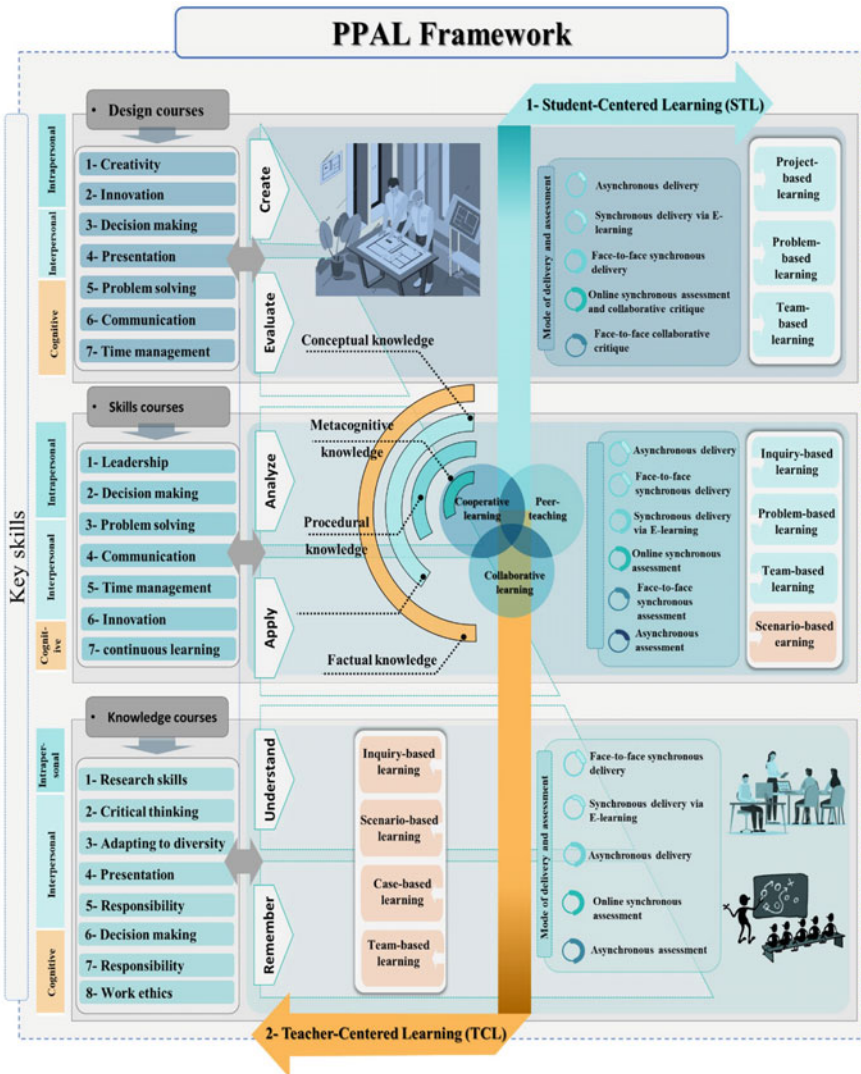
Fig. 4 Proposed conceptual framework

adapting to diversity, presentation, responsibility, decision-making, and work ethics are specified skills.

Implementing previous skills is associated with Bloom's Taxonomy, in which cognitive activities are categorized into six hierarchical levels, including remembering, understanding, applying, analyzing, evaluating, and creating. These cognitive activities can be developed to support an active learning environment via four

knowledge dimensions [72]: factual, conceptual, procedural, and metacognitive knowledge.

Considering the third pillar of the active learning process, the active learning approaches can provide three classifications of architectural courses via SCL and TCL. Active learning processes include the cognitive activities of Bloom's Taxonomy with their four dimensions through active strategies and methods, which can be involved via collaborative learning, cooperative learning, and peer teaching. Active learning is a gradient scale that starts with the basic fractal knowledge in knowledge courses and conceptual, procedural, and metacognitive knowledge in skills and design courses. Various strategies can be implemented to provide active learning, considering the pillars of key skills and Bloom's Taxonomy of the three classifications of architectural courses. For design courses, project, problem, and team-based learnings present the main strategies to support design conception via active learning by either face-to-face or online meetings. Skill courses can also be based on inquiry-based learning, problem, team, and scenario-based learning. Nevertheless, inquiry, scenario, case, and team-based learning can support the active learning process in knowledge courses.

Finally, the last pillar concerning the mode of delivery and assessment is related to three classifications of architectural courses. Blended learning demonstrates a vital need to provide both synchronous interactions in face-to-face or online meetings and asynchronous learning environments to verify the key skills and outcomes in architectural courses. In design courses, synchronous delivery shows the main delivery mode, including face-to-face and online meetings, and the asynchronous mode. Face-to-face or physical meetings exceed online meetings in promoting the quality of design products and the performance of students in their work. However, in skill courses, synchronous delivery is the main delivery mode, which includes face-to-face and online meetings. For knowledge courses, synchronous and asynchronous modes can be equal, and teachers can use brainstorming, question and answer, mimesis, pair and group work, role-playing, and creative drama techniques to promote active learning and student engagement. Notably, the goals of courses, learning roadmap, general procedures, and assessment criteria should be explained to support the outcomes of courses and prepare students for interactive and intensive online synchronous or asynchronous learning modes.

7 Discussion

Although the COVID-19 pandemic has considerably affected several activities worldwide in late 2019, the post-pandemic learning process is under ongoing development owing to investigations, analyses, and studies. The proposed PPAL framework can provide students' engagement in learning processes in general, and in architectural education particularly. The PPAL framework promotes active learning using specified strategies and methods, considering the category of courses and their required goals, outcomes, and skills. In the proposed framework, the instructor or teacher of a course

is considered an organizer or facilitator to direct the learning process toward active learning using the SCL approach to ensure the engagement of students, especially during e-learning.

The proposed framework has confirmed previous research regarding the active learning process with the SCL approach [63] and contributes as an appropriate methodology to attain active collaborative and cooperative learning environments by involving the basic applied strategies and methods according to their suitability with the classification of architectural courses. In addition, instructors integrate active learning approaches and levels of cognitive activities with their dimensions of knowledge, considering post-pandemic challenges in content delivery, assessments, and interrelations. Considering that the proposed framework emphasizes a general vision toward integrating active learning and post-pandemic architectural education, more inquiries and assessments are required on specified courses that can improve students' active participation in post-pandemic architectural education.

8   Conclusion

This study has highlighted the significance of active learning and SCL in particular, because of the COVID-19 lockdown. All aspects of life, including learning, have transformed, shifting the world into a new paradigm of the post-pandemic learning environment. Herein, we established a PPAL framework to bridge the gaps in previous studies conducted regarding the possibilities and threats of post-pandemic scenarios and e-learning in general and to determine how specialists can analyze such transformation. Furthermore, architectural education as a special category under e-learning faced several challenges during the COVID-19 lockdown.

The proposed framework emphasizes the active learning environments and SCL in particular as the key to verifying the required skills (cognitive, interpersonal, and intrapersonal skills), of each classification of each architectural course through several active teaching methods and strategies. Inquiry, scenario, project, problem, team, and case-based learning strategies can support the active learning process, which can be involved via collaborative learning, cooperative learning, and peer-teaching methods.

The proposed framework promotes students' engagement in learning processes via either face-to-face or online meetings, which can improve their motivation and attain the cognitive activities of Bloom's Taxonomy, with their four dimensions: factual, conceptual, procedural, and metacognitive knowledge.

Finally, this study serves as the first step, and various surveys need to be considered to verify the importance of active learning in post-pandemic architectural education, which needs continuous evaluation. There is a need for assessment and investigation to verify and develop the proposed framework for future studies.

References

1. Le Bot G, Xue L, Petegem W, van Wieringen A (2015) Interdisciplinary E-learning: an engineering perspective. https://doi.org/10.13140/RG.2.1.3731.8168
2. Al Musawi A, Raja Hussain RM, Alshuaili K (2020) The effectiveness of using augmented reality in teaching geography curriculum on the achievement and attitudes of Omani 10th grade students. Multidiscip J Educ Soc Technol Sci 7:20–29. https://doi.org/10.4995/muse.2020.13014
3. Urquiza-Fuentes J (2020) Increasing students' responsibility and learning outcomes using partial flipped classroom in a language processors course. IEEE Access 8:211211. https://doi.org/10.1109/ACCESS.2020.3039628
4. El-Mowafy BN, Elmokadem AA, Waseef AA (2022) Evaluating adaptive facade performance in early building design stage: an integrated daylighting simulation and machine learning BT. In: Hassanien AE, Rizk RY, Snášel V, Abdel-Kader RF (eds) The 8th international conference on advanced machine learning and technologies and applications (AMLTA2022). Springer International Publishing, Cham, pp 211–223
5. Abo El-Einen O, Ahmed M, Megahed N, Hassan A (2015) Interactive-based approach for designing facades in digital era. Port-Said Eng Res J 19:72–81
6. Megahed NA, Hassan AM (2022) Evolution of BIM to DTs: a paradigm shift for the post-pandemic AECO industry. Urban Sci 6. https://doi.org/10.3390/urbansci6040067
7. Megahed N, Abdel-kader R, Soliman H (2022) Post-pandemic education strategy: framework for artificial intelligence-empowered education in engineering (AIEd-Eng) for lifelong learning, pp 544–556. https://doi.org/10.1007/978-3-031-03918-8_45
8. Melkunaite L, Guay F (2016) Resilient city: opportunities for cooperation (Quelle überprüfen), pp 11–14
9. Shehata AO, Megahed NA, Shahda MM, Hassan AM (2022) (3Ts) Green conservation framework: a hierarchical-based sustainability approach. Build Environ 224. https://doi.org/10.1016/j.buildenv.2022.109523
10. Hassan SR, Megahed NA, Abo Eleinen OM, Hassan AM (2022) Toward a national life cycle assessment tool: generative design for early decision support. Energy Build 267:112144. https://doi.org/10.1016/j.enbuild.2022.112144
11. Hassan AM, Megahed NA (2022) Urban planning and development improving urban energy resilience with an integrative. Archit Eng. https://doi.org/10.23968/2500-0055-2022-7-4-17-35
12. Hassan AM (2023) UMC-based models: an integrating UMC performance analysis and numerical methods. Renew Sustain Energy Rev 181:113307. https://doi.org/10.1016/j.rser.2023.113307
13. Elgheznawy D, Eltarabily S () Post-pandemic cities—the impact of COVID-19 on cities and urban design 10:75–84. https://doi.org/10.5923/j.arch.20201003.02
14. Megahed N, Abdel-kader R (2022) Smart cities after COVID-19: building a conceptual framework through a multidisciplinary perspective. Sci Afr 17:e01374. https://doi.org/10.1016/j.sciaf.2022.e01374
15. Megahed N, Ghoneim E (2020) Indoor air quality: rethinking rules of building design strategies in post-pandemic architecture. Environ Res 193. https://doi.org/10.1016/j.envres.2020.110471
16. Hassan AM, Megahed NA (2021) COVID-19 and urban spaces: a new integrated CFD approach for public health opportunities. Build Environ 204:108131. https://doi.org/10.1016/j.buildenv.2021.108131
17. Franchi T (2020) The impact of the Covid-19 pandemic on current anatomy education and future careers: a student's perspective. Anat Sci Educ 113:312–315. https://doi.org/10.1002/ase.1966
18. Allu-kangkum ELA (2021) Covid-19 and sustainable architectural education: challenges and perceptions on online learning
19. El-Mowafy BN, Hassan AM (2023) Post-pandemic adopted learning approach to promote architectural education: statistical approach. High Educ Ski Work Learn (ahead-of-print). https://doi.org/10.1108/HESWBL-05-2022-0099

20. El-Mowafy BN, Hassan AM (2023) A problem and project-based learning strategy to promote students' motivation in post-pandemic graduation design studio: a prospective comparative study BT. In: Hassanien AE, Snášel V, Tang M, Sung T-W, Chang K-C (eds) Proceedings of the 8th international conference on advanced intelligent systems and informatics. Springer International Publishing, Cham, pp 89–106
21. Salama A, Crosbie M (2020) Educating architects in a post-pandemic world
22. Kavas K, Bakir İ, Oktay E, Danaci H, Unvan M (2021) Virtual education trials and evaluation process in architecture. J Qual Res Educ 9:302–315. https://doi.org/10.14689/enad.25.13
23. Sukendro S, Habibi A, Khaeruddin K, Indrayana B, Syahruddin S, Makadada FA et al (2020) Using an extended technology acceptance model to understand students' use of e-learning during Covid-19: Indonesian sport science education context. Heliyon 6:e05410. https://doi.org/10.1016/j.heliyon.2020.e05410
24. Allu E (2021) Covid-19 and sustainable architectural education: challenges and perceptions on online learning
25. Jabbar A, Gauci CG, Anstead CA (2021) Parasitology education before and after the COVID-19 pandemic. Trends Parasitol 37:3–6. https://doi.org/10.1016/j.pt.2020.10.009
26. Utaberta N, Hassanpour B, Handryant A, Che-Ani A (2013) Upgrading education architecture by redefining critique session in design studio. Proc Soc Behav Sci 102:42–47. https://doi.org/10.1016/j.sbspro.2013.10.711
27. Megahed N (2017) Reflections on studio-based learning: assessment and critique. J Eng Des Technol 16. https://doi.org/10.1108/JEDT-08-2017-0079
28. Çıkış Ş, Çil E (2009) Problematization of assessment in the architectural design education: first year as a case study. Proc Soc Behav Sci 1:2103–2110. https://doi.org/10.1016/j.sbspro.2009.01.369
29. Sidawi B (2015) The use of e-learning system in learning about architecture: obstacles and opportunities. https://doi.org/10.1109/ECONF.2015.13
30. Ghonim M (2016) Design thinking in architecture education: issues, limitations and suggestions
31. Ghonim M, Eweda N (2017) The graduation projects in architectural education: an analytical comparative study. Int J Architecton Spat Environ Des 11:15–34. https://doi.org/10.18848/2325-1662/CGP/v11i01/15-34
32. Soliman AM (2017) Appropriate teaching and learning strategies for the architectural design process in pedagogic design studios. Front Archit Res 6:204–17. https://doi.org/10.1016/j.foar.2017.03.002
33. Ghonim M, Eweda N (2018) Investigating elective courses in architectural education. Front Archit Res 7:235–256. https://doi.org/10.1016/j.foar.2018.03.006
34. Ghonim M, Eweda N (2018) Best practices in managing, supervising, and assessing architectural graduation projects: a quantitative study. Front Archit Res 7:424–439. https://doi.org/10.1016/j.foar.2018.06.002
35. Abdelmohsen S, Omar M, Kamal D, Kamel S (2019) Biomimetic approaches in architectural design education
36. Amer N (2019) Biomimetic approach in architectural education: case study of 'biomimicry in architecture' course. Ain Shams Eng J 10:499–506. https://doi.org/10.1016/j.asej.2018.11.005
37. Shahda M (2019) Biomimicry as a tool to enhance the skills of architecture students in understanding construction systems. https://doi.org/10.5923/j.arch.20190905.02
38. El-Latif MA, Al-Hagla KS, Hasan A (2020) Overview on the criticism process in architecture pedagogy. Alexandria Eng J 59:753–762. https://doi.org/10.1016/j.aej.2020.01.019
39. Laovisutthichai V, Lu W, Xue F (2020) Modular construction: design considerations and opportunities
40. Taneri B, Dogan F (2021) How to learn to be creative in design: architecture students' perceptions of design, design process, design learning, and their transformations throughout their education. Think Ski Creat 39:100781. https://doi.org/10.1016/j.tsc.2020.100781
41. Megahed N (2013) Towards math-based architectural education in Egyptian engineering faculties. Nexus Netw J 15:565–581. https://doi.org/10.1007/s00004-013-0159-3

42. Jafri MS, Varma A (2020) COVID-19 responsive teaching of undergraduate architecture programs in India: learnings for post-pandemic education. Archnet-IJAR Int J Archit Res (ahead-of-print). https://doi.org/10.1108/ARCH-10-2020-0234

43. Megahed N, Hassan A (2021) A blended learning strategy: reimagining the post-Covid-19 architectural education. Archnet-IJAR Int J Archit Res (ahead-of-print). https://doi.org/10.1108/ARCH-04-2021-0081

44. Bachiri H, Sahli R (2020) The need of distance learning in the wake of COVID-19 in Morocco. Int J Lang Lit Stud 2:240–256. https://doi.org/10.36892/ijlls.v2i3.326

45. Zheng F, Khan NA, Hussain S (2020) The COVID 19 pandemic and digital higher education: exploring the impact of proactive personality on social capital through internet self-efficacy and online interaction quality. Child Youth Serv Rev 119:105694. https://doi.org/10.1016/j.childyouth.2020.105694

46. Alsaywid B, Lytras M, Abuzenada M, Lytra H, Housawi A, Abuznadah W et al (2021) Effectiveness and preparedness of institutions' e-learning method during COVID-19 pandemic for residents' medical training in Saudi Arabia: a pilot study. https://doi.org/10.21203/rs.3.rs-270326/v1

47. Das P, Das K, Bordoloi R (2021) Perception towards online/blended learning at the time of Covid-19 pandemic: an academic analytics in the Indian context. Asian Assoc Open Univ J (ahead-of-print). https://doi.org/10.1108/AAOUJ-09-2020-0079

48. Peimani N, Kamalipour H (2021) Online education and the COVID-19 outbreak: a case study of online teaching during lockdown. Educ Sci 11. https://doi.org/10.3390/educsci11020072

49. Mok KH, Xiong W, Ke G, Cheung JOW (2021) Impact of COVID-19 pandemic on international higher education and student mobility: student perspectives from mainland China and Hong Kong. Int J Educ Res 105:101718. https://doi.org/10.1016/j.ijer.2020.101718

50. Muthuprasad T, Aiswarya S, Aditya KS, Jha GK (2021) Students' perception and preference for online education in India during COVID-19 pandemic. Soc Sci Humanit Open 3:100101. https://doi.org/10.1016/j.ssaho.2020.100101

51. Geng S, Law K, Niu B (2019) Investigating self-directed learning and technology readiness in blending learning environment. Int J Educ Technol High Educ 16. https://doi.org/10.1186/s41239-019-0147-0

52. Zhou X, Kong D, Zhang Z, Shu J, Cao T (2017) Cloud-class blended learning pattern innovation and its applications. https://doi.org/10.1109/ISET.2017.13

53. Duvivier R (2018) How to 'future-proof' the use of space in universities by integrating new digital technologies. Perspect Policy Pract High Educ 23:1–6. https://doi.org/10.1080/13603108.2018.1486894

54. Hu X, Zhang H, Song Y, Wu C, Yang Q, Shi Z et al (2019) Implementation of flipped classroom combined with problem-based learning: an approach to promote learning about hyperthyroidism in the endocrinology internship. BMC Med Educ 19. https://doi.org/10.1186/s12909-019-1714-8

55. Dehghanzadeh S, Jafaraghaee F (2018) Comparing the effects of traditional lecture and flipped classroom on nursing students' critical thinking disposition: a quasi-experimental study. Nurse Educ Today 71:151–156. https://doi.org/10.1016/j.nedt.2018.09.027

56. Gren L (2020) A flipped classroom approach to teaching empirical software engineering. IEEE Trans Educ PP:1–9. https://doi.org/10.1109/TE.2019.2960264

57. Kanelopoulos J, Papanikolaou K, Zalimidis P (2017) Flipping the classroom to increase students' engagement and interaction in a mechanical engineering course on machine design. Int J Eng Pedagog 7:19. https://doi.org/10.3991/ijep.v7i4.7427

58. Oliver J, Lloberas-Valls O (2017) Innovative experiences in civil engineering education at UPC-BarcelonaTec: continuum mechanics flipped classroom project

59. Suwapaet N (2017) Introducing a flipped classroom to engineering students: a case study. Mech Mater Course 1941. https://doi.org/10.1063/1.5028099

60. Veenman S, van Benthum N, Bootsma D, van Dieren J, van der Kemp N (2002) Cooperative learning and teacher education. Teach Teach Educ 18:87–103. https://doi.org/10.1016/S0742-051X(01)00052-X

61. Mascolo M (2009) Beyond student-centered and teacher-centered pedagogy: teaching and learning as guided participation. Pedagog Hum Sci 1:3–27
62. Khodeir L, Nessim A, Maguid D (2020) Tracing the impact of teaching sustainable design on design projects in architectural freshman level. Archit Urban A Smart Outlook 33–48. https://doi.org/10.1007/978-3-030-52584-2_3
63. Meulenbroeks R (2020) Suddenly fully online: a case study of a blended university course moving online during the Covid-19 pandemic. Heliyon 6:e05728. https://doi.org/10.1016/j.heliyon.2020.e05728
64. Pan X, Zhu L (2020) An e-learning space for the economics experimental teaching based on pedagogy-space-technology framework. https://doi.org/10.2991/assehr.k.200727.015
65. Zhao W, He L, Deng W, Zhu J, Su A, Zhang Y (2020) The effectiveness of the combined problem-based learning (PBL) and case-based learning (CBL) teaching method in the clinical practical teaching of thyroid disease. BMC Med Educ 20:381. https://doi.org/10.1186/s12909-020-02306-y
66. Peña-Ayala A (2021) A learning design cooperative framework to instill 21st century education. Telemat Inf 262:101632. https://doi.org/10.1016/j.tele.2021.101632
67. Rosson MB, Carroll JM (2002) Usability engineering: scenario-based development of human computer interaction
68. Jamkar A, Burdick W, Morahan P, Yemul V, Sarmukadum, Singh G (2007) Proposed model of case based learning for training undergraduate medical student in surgery. Indian J Surg 69:176–83. https://doi.org/10.1007/s12262-007-0016-2
69. Megahed NA (2014) Heritage-based sustainability in port said: classification of styles and future development. Archnet-IJAR 8:94–107. https://doi.org/10.26687/archnet-ijar.v8i1.299
70. Baghaei Daemei A, Safari H (2018) Factors affecting creativity in the architectural education process based on computer-aided design. Front Archit Res 7:100–106. https://doi.org/10.1016/j.foar.2017.09.001
71. Khodeir LM, Nessim AA (2020) Changing skills for architecture students employability: analysis of job market versus architecture education in Egypt. Ain Shams Eng J 11:811–821. https://doi.org/10.1016/j.asej.2019.11.006
72. Blignaut S, du Plessis A (2021) Offline–online information and communication technology (ICT) teaching and learning strategy in the age of COVID-19 and Beyond André du Plessis

Real-Time Facial Emotion Recognition Using Haar-Cascade Classifier and MobileNet in Smart Cities

Shereen El-Shekheby

1 Introduction

Facial emotion recognition (FER) has become a significant issue in many smart city applications. Facial expressions are forms of nonverbal communication, providing hints for human emotions. For decades, decoding expressions of emotion has been an interesting research topic in the field of human–computer interaction (HCI). Recently, the widespread availability of cameras and technological advances in biometric analysis, machine learning, and pattern recognition have played a prominent role in the development of FER technology [1–9]. FER is beneficial in several applications such as predictive teaching and learning for students, healthcare, driving, security, customer satisfaction, and marketing as shown in Fig. 1.

Due to the increase in connectivity and availability of advanced tools and sensors, smart cities have the potential to provide healthcare services that can truly meet the demands of citizens. Hence, an intelligent healthcare system in the smart city based on facial expression recognition was introduced in [10]. The proposed system allows registered physicians and caregivers to monitor patients' feelings remotely and take appropriate action as needed.

In the smart city, to enhance the driver's ability to think, perceive, and judge, it is necessary to detect the driver's negative emotions because negative emotions increase the risk of traffic accidents. In this paper [11], the Intelligent Vehicle Alert System (IVAUT) relies on the emotional identification of the driver. Proposed system is based on a convolutional neural network (CNN) along with a transformer network for smart vehicle alarms.

Measuring Customer Satisfaction (CS) has become one of the strategic tools for any smart city business. A comprehensive method for measuring customer satisfaction based on the most important facial emotions was proposed in [12].

S. El-Shekheby (✉)
Electrical Engineering Department, Faculty of Engineering, Port Said University, Port Said, Egypt
e-mail: SherenZakaria@eng.psu.edu.eg

Fig. 1 Facial emotion recognition applications

Another scoring system for a restaurant based on facial emotion recognition has been proposed in [13]. FER is used to stimulate the customer's interest. The CNN model was used to automatically detect the features of interest without any human supervision.

Nethravathi [14] developed a quantifiable system for measuring customer interest. This system recognizes significant facial expressions and describes a deep learning-based system for monitoring customers' actions. The proposed approach determines the client's attention by estimating the position of the head. The system detects facial expressions and informs about customers' interest. The proposed method identifies frontal facial positions, and then cuts out facial mechanisms that are critical to identifying facial expressions and creating an iconized face image. Finally, the values obtained from the resulting image are combined with the original value of facial sentiment analysis. This method combines local, fragment-based features with comprehensive facial information.

In the educational classroom, student participation leads to effective learning and increased success rates. Therefore, Smart Attendance Management (SAMS) application is proposed in [15]. The system is developed to manage student attendance using face recognition.

In fact, better services can be provided to citizens in smart cities if their personal experience is effectively evaluated and that experience is utilized in making the necessary adjustments to improve services and accordingly achieve a high-level quality of life for all citizens.

In this paper, the emotions of citizens' faces are subjective data that can be utilized to enhance smart city services and achieve SDG 11. For example, citizens' emotions could be analyzed in a smart store to assess a potential customer's appreciation towards certain products or, in terms of public safety, to assess whether someone is getting seriously angry. Therefore, the proposed approach identifies citizens' facial

emotions by combining the OpenCV Haar-Cascade classifier for automatic real-time facial detection and MobileNet as an emotion detection model. A performance comparison of the proposed model was investigated. Experimental results show that the proposed model is superior to other models.

The remainder of this paper is organized as follows: In Sect. 2, the research methodology is presented. In Sect. 3, the recognition performance analysis of the proposed approach is evaluated. In Sect. 4, the research is concluded. Finally, research recommendations are presented in Sect. 5.

2 Research Methodology

Facial emotion recognition mainly consists of three steps as follows: image acquisition, face detection, and facial emotion recognition. In this study, first Haar-Cascade classifier is applied to automatically detect the face in captured images. Then the MobileNet model trained on FER2013 [16] is used in the emotion recognition process to employ these emotions as indicators to achieve citizen satisfaction and improve the quality of services in the smart city.

2.1 Haar-Cascade Classifier

Object detection using Haar-Cascade classifier [17] is a powerful method introduced by Viola-Jones. It is a machine learning based method in which the cascade function is trained from various positive and negative images. Then, it is used to identify objects in an image or video in real-time. In this paper, OpenCV Haar-Cascade classifier is used to automatically detect the face in the captured images in real-time.

2.2 MobileNet

In this study, MobileNet [18, 19], which is a class of CNN architecture with a small model size and few trainable parameters, is used. MobileNets are great deep learning models for use on mobile devices, hence called "mobile". CNN results in higher performance but requires large GPU memory and computational time. Therefore, MobileNet was developed where it uses depth wise separable convolutions instead of the standard convolutions used in previous architectures to build lighter models. It introduces two global hyperparameters (width multiplier and resolution multiplier) that allow model developers to trade off latency or accuracy to reduce speed and scale according to their requirements [18].

MobileNet is built on deep, separable convolutional layers except the first layer, which is a full convolution. All layers are followed by nonlinear batchnorm and ReLU
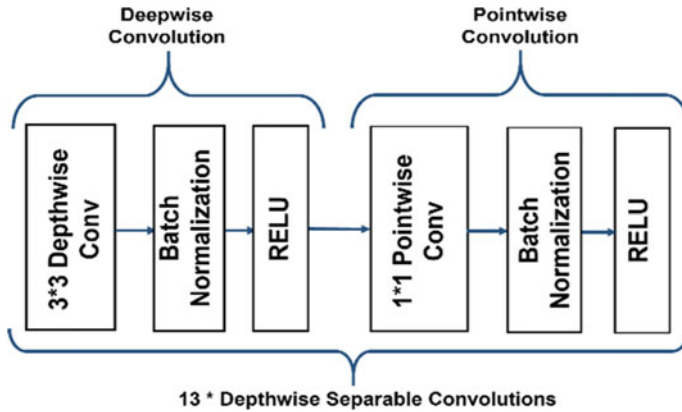
Fig. 2 MobileNet depthwise separable convolutions

except for the ending fully connected layer which does not contain nonlinearity and feeds into the softmax layer for classification. Each depthwise detachable convolution layer is composed of a depthwise convolution and a pointwise convolution as shown in Fig. 2. When calculating depthwise and pointwise convolutions as separate layers, MobileNet contains 28 layers. The original MobileNet has 4.2 million parameters which can be minimized by modifying the width multiplier hyperparameter properly [18].

In the proposed approach, it is better to use the SoftMax activation function together with the categorical crossentropy loss function. The loss function measures how far an estimated value is from its true value and evaluates how well the given algorithm models the given data. If predictions deviate too much from actual results, the loss function will be a very large number. Gradually, with some optimization function, the loss function learns to reduce the prediction error. There are several types of loss functions, but for this case of emotion identification the categorical crossentropy is used which is a loss function for multiclass classification tasks.

3 Results and Discussion

The dataset used in this study is FER2013 facial expression dataset [16]. The training set contains 28,709 images, and the validation set contains 7179 images. All images belong to the 7 classes: (Angry, Disgust, Fear, Happy, Neutral, Sad, Surprise).

The experiments were based on the Keras framework and were implemented in Python 3.9.7. The SoftMax classifier is used together with the categorical crossentropy loss function. Optimizers are used to change the attributes of the model such as weights to reduce losses, therefore, Adam optimizer which is an adaptive learning rate approach is used for training. The size of the input image is $224 \times 224 \times 3$. The

Table 1 Parameters used during MobileNet model training

Parameter	Value
Input image size	(224, 224, 3)
Epochs	30–60
Batch size	64
Classifier	Softmax
Optimizer	Adam
Loss function	Categorical_crossentropy
Dropout	0.5
Regularization	Batch Normalization

Table 2 Training accuracy and validation accuracy

Epoch	Training accuracy %	Validation accuracy %
30	80.22	65
50	88.2	66.08
60	91	66.58

batch size is 64 with epochs ranging from 30 to 60. The proposed model parameters are presented in Table 1.

In experiments, high accuracy is achieved in the training set but accuracy in the validation set is limited to 66.58% as shown in Table 2 and Fig. 3. It has been observed that there are unbalanced sample sets in the FER2013 dataset. The images are misplaced and grouped into the wrong category, and dataset also contains non-facial images, which leads to a decrease in the accuracy of human emotion recognition.

In Table 3 the proposed method is compared with the existing methods. The comparative analysis shows that the proposed model presents a slightly higher accuracy than the other comparative models with prediction accuracy of 66.58%.

In order to validate the proposed model, it was tested using a computer camera, and face detection was initially performed using OpenCV Haar-Cascade classifier. The MobileNet classification model is then used to predict the facial emotion in the captured image and the predicted emotion is added to the image as shown in the real-world example in Fig. 4. The future scope of this work is to increase its efficiency for the unbalanced sample sets by exploring the use of ensemble learning to handle the inaccurate supervised FER2013 dataset [24].
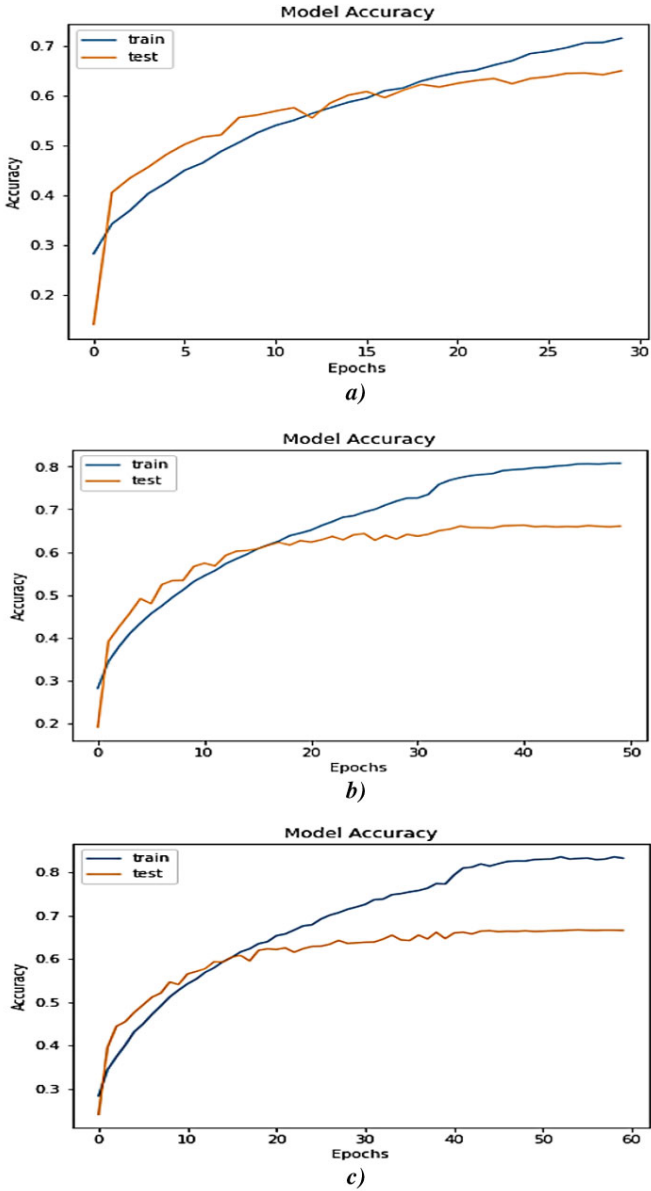
Fig. 3 MobileNet model accuracy results using different epochs **a** 30 epochs, **b** 50 epochs and **c** 60 epochs

Table 3 Accuracy comparison of the proposed emotion recognition and baseline methods

Method	Accuracy %
Transfer learning [20]	48.5
Multiple deep network [21]	52.29
FN2EN [22]	55.15
ZFER [23]	65
Proposed MobileNet	66.58
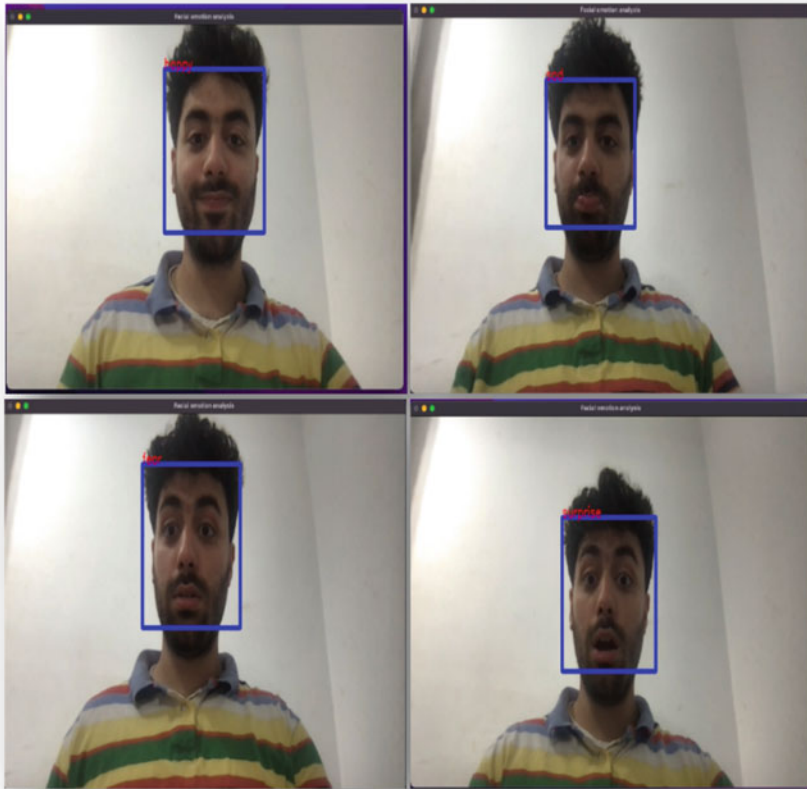
Fig. 4 Facial emotion recognition for images taken from a computer's webcam

4 Conclusion

In a smart city, citizens can enjoy a variety of modern technologies in many areas, such as smart healthcare, smart homes, smart traffic, smart buildings, smart community, smart education, and many other areas that are all essential for a smart city. Citizens' facial emotions are subjective data that need to be managed properly to enhance many

services in a smart city and achieve SDG 11. Proposed approach determines the citizens' facial emotions by combining OpenCV Haar-Cascade classifier for automatic face detection in real-time and MobileNet model for the emotion detection. The proposed model is superior to other comparative models with a prediction accuracy of 66.58%. The experimental results showed that the proposed approach is applicable in a real-world scenario.

5 Recommendations

Future research can focus on using other datasets and enabling data-driven rectification and ensemble learning to handle the inaccurate FER2013 dataset.

Author Contribution The main contribution of this research was equally contributed by all authors. The work has been read and approved by all authors.

References

1. Mehendale N (2020) Facial emotion recognition using convolutional neural networks (FERC). SN Appl Sci 2:1–8
2. Ko BC (2018) A brief review of facial emotion recognition based on visual information. Sensors 18(2):401
3. Rizk R, Nashaat H (2018) Smart prediction for seamless mobility in F-hmipv6 based on location based services. China Commun 15(4):192–209
4. Domínguez-Jiménez JA, Campo-Landines KC, Martínez-Santos JC, Delahoz EJ, Contreras-Ortiz SH (2020) A machine learning model for emotion recognition from physiological signals. Biomed Signal Process Control 55:140990–141020
5. Ozdemir MA, Elagoz B, Alaybeyoglu A, Sadighzadeh R, Akan A (2019) Real time emotion recognition from facial expressions using CNN architecture. In: 2019 medical technologies congress (TIPTEKNO). Izmir, Turkey, pp 1–4
6. Alankar B, Ammar MS, Kaur H (2021) Facial emotion detection using deep learning and Haar Cascade Face Identification algorithm. In: Advances in intelligent computing and communication: proceedings of ICAC 2020. Springer, Singapore, pp 163–180
7. De Simone F, Presta R (2022) A song can do that: an emotion induction study for the development of intelligent emotion-aware systems. In: Intelligent systems and applications: proceedings of the 2022 intelligent systems conference (IntelliSys), vol 2, pp 363–377
8. Nashaat M, Miller J (2021) Improving news popularity estimation via weak supervision and meta-active learning. Hawaii International Conference on System Sciences, pp 2918–2919
9. El-Sayad, NE, Abdel-Kader RF, Mahmoud IM (2013) Face recognition as an authentication technique in electronic voting. Int J Adv Comput Sci Appl 4(6):66–71

10. Muhammad G, Alsulaiman M, Amin SU, Ghoneim A, Alhamid MF (2017) A facial-expression monitoring system for improved healthcare in smart cities. IEEE Access 5:10871–10881

11. Wu L, Liu M, Li J, Zhang Y (2022) An intelligent vehicle alarm user terminal system based on emotional identification technology. Sci Program 2022:1–11

12. Slim M, Kachouri R, Atitallah AB (2018) Customer satisfaction measuring based on the most significant facial emotion. In: 2018 15th international multi-conference on systems, signals & devices (SSD), pp 502–507

13. Shylaja R, Megha Sai Sree P, Rishika P, Sreeja T, Srilekha M (2022) Facial emotion recognition based scoring system. In: Proceedings of third international conference on intelligent computing, information and control systems, vol 1415, pp 193–205

14. Nethravathi PS, Aithal PS (2022) Real-time customer satisfaction analysis using facial expressions and head pose estimation. Int J Appl Eng Manage Lett 6(1):301–312

15. Bhattacharya S, Nainala GS, Das P, Routray A (2018) Smart attendance monitoring system (SAMS): a face recognition based attendance system for classroom environment. In: 2018 IEEE 18th international conference on advanced learning technologies (ICALT), pp 358–360

16. Fer2013 [Internet]. Kaggle, 2020 [cited 2023 March 15]. https://www.kaggle.com/datasets/msambare/fer2013

17. Viola P, Jones M (2001) Rapid object detection using a boosted cascade of Simple features. In: Proceedings of the 2001 IEEE computer society conference on computer vision and pattern recognition, CVPR 2001

18. Howard AG, Zhu M, Chen B, Kalenichenko D, Wang W, Weyand T, Andreetto M, Adam H (2017) Mobilenets: efficient convolutional neural networks for mobile vision applications, arXiv preprint arXiv:1704.04861

19. Nan Y, Ju J, Hua Q, Zhang H, Wang B (2022) A-MobileNet: an approach of facial expression recognition. Alex Eng J 61(6):4435–4444

20. Ng HW, Nguyen VD, Vonikakis V, Winkler S (2015) Deep learning for emotion recognition on small datasets using transfer learning. In: Proceedings of the 2015 ACM on international conference on multimodal interaction, pp 443–449

21. Yu Z, Zhang C (2015) Image based static facial expression recognition with multiple deep network learning. In: Proceedings of the 2015 ACM on international conference on multimodal interaction, pp 435–442

22. Ding H, Zhou SK, Chellappa R (2017) Facenet2expnet: regularizing a deep face recognition net for expression recognition. In: 2017 12th IEEE international conference on automatic face & gesture recognition (FG 2017), pp 118–126

23. Shahzad T, Iqbal K, Khan MA, Iqbal N (2023) Role of zoning in facial expression using deep learning. IEEE Access 11:16493–16508

24. Nashaat M, Ghosh A, Miller J, Quader S (2021) Semi-supervised ensemble learning for dealing with inaccurate and incomplete supervision. ACM Trans Knowl Discov Data 16(3):1–33

Parametric Form-Finding in Architecture: Dimensions Classification and Processes Guidelines

Lina A. Ramadan, Ashraf El Mokadem, and Nancy Badawy

1 Introduction

The introduction of new digital tools to the architectural design process has always affected the architectural practice [1]. This development of the digital tools has shifted the design paradigm from being a traditional representational process to being a contemporary complex generative digital process based on simulation and evaluation [2]. Accordingly, parametric architecture emerged and caused the emergence of the other design approaches related to it, such as: generative design, performance-based parametric design [3], etc. In these design approaches, architects no longer create forms by pen on paper, or by mouse in CAD program, instead they define parameters and control procedures to generate forms which is called "form-finding".

There are many aspects/dimensions (tools, decisions, methods, processes, etc.) to consider in the process of parametric form-finding in order to achieve the desired design requirements, such as: sustainability, functional, structural, fabrication, etc. As a result, a designer may initially have an incomplete or unclear vision of the whole design process. Therefore, it is important to have a better understanding for the parametric form-finding process and its different aspects in order to aid the architects in managing their design process. However, only very few studies mentioned a guide or a classification for the whole dimensions of digital form-finding.

The main objectives of this research is to propose a classification that sums up the different dimensions of parametric form-finding process, including the ones that

L. A. Ramadan (✉) · A. El Mokadem · N. Badawy
Architectural Engineering and Urban Planning Department, Faculty of Engineering, Port Said University, Port Said, Egypt
e-mail: lina.ahmed@eng.psu.edu.eg

A. El Mokadem
e-mail: elmokadem1@eng.psu.edu.eg

N. Badawy
e-mail: n.badawy@eng.psu.edu.eg

support sustainability (optimization, performance, simulation, etc.). In addition to providing architects with some guidelines that can be used by them in designing parametric forms. Thus, enhancing the design of parametric buildings and contributing in achieving the UN SDG number 11: Sustainable Cities and Communities, which intends to make cities and human settlements inclusive, safe, resilient, and sustainable. The paper will discuss in detail the parametric form-finding. A classification of the different dimensions of parametric form-finding will be proposed. It will also categorize the current practices of parametric form-finding processes, giving some guidelines for the architects regarding designing parametric forms.

1.1 History of Digital Tools

During last years, computation tools introduced new innovative methods of designing and generating architectural forms that are based on specific requirements. Limitations that affected the architectural practice before are now starting to disappear. Evolution of design software throughout the years can be categorized as follows [2, 4]:

- The first category is the **2D processing software**, including technical CAD software and other programs used for graphics and communication of the project (Photoshop, Illustrator, etc.).
- The first commercially successful software, AutoCAD was released in 1982. Early versions of the software basically provided the designers a digital version of their conventional drawings. Later in the 90 s, it included some powerful spline modelers allowing architects to create unfamiliar designs.
- The second category is the **3D graphic based software**, which was initially used at the entertainment world of movies. However, it was later used in the modeling and rendering of architecture.
- The third category is the **BIM (Building Information Modeling) software**, in which the 3D model is extended to more than visual purposes only, to include the economic aspects and the construction phases of large and complex projects, facilitating the control of different aspects of the entire process.
- The fourth category is **parametric modeling** software and plugins (i.e.: Grasshopper for Rhinoceros) that enable the design of 3D models using parameters defined by the designer.
- The fifth category is the **analytical software** for different aspects (environmental, structural, etc.), that helps to create informed models and to work with **algorithmic and scripting-based software** by using the analysis results linking the shape of an architectural element to the studied performance. It is clearly associated with the previous parametric modeling category.
- As a result of these last two categories, new significant design trends appeared such as: **performance-based design approaches** and **generative processes** which are the processes of identifying the best design options for a number of different

objectives and constraints using the power of computation to explore a wide range of design solutions. They form promising opportunities for exploration in the current architectural research.

1.2 Parametric Architecture

Parametric architecture was defined by many researchers. Woodbury defined it as "a constraint modeling in which parts of a design, relate and change together in a coordinated way. It explores associative geometric relationships to support the creation, management, and organization of complex digital design models" [5]. Aish et al. defined it as "an approach which increases complexity of both designer task and interface as designers must model not only the artifact being designed, but a conceptual structure that guides variation. The designed artifact that is represented parametrically admits rapid change of design dimensions and structure" [6].

This research gives a very simple definition to parametric architecture as follows: "Parametric architecture is designing with the use of parameters and relations between them to generate architectural forms". Where the parameters are variable attributes for the properties of a design's geometrical entities. Values of these parameters are plugged into multiple equations defining the relationship between them in an algorithmic logic [7]. They are defined by the designer in the beginning of searching for a design solution. Manipulation of these parameters inform the design of architectural forms, as the model responds to the changes by adapting or reconfiguring to the new values of the parameters without erasing or redrawing the design. In parametric architecture, parameters determine the relationship between design intent and design outcomes, in contrast to the direct traditional design approach.

The use of parametric design does not necessarily lead to any specific style, it is just an efficient way of flexibly describing forms [8]. Parametric design as a design methodology based on parametric modeling and scripting techniques is equally applicable to any architectural style [9]. The strength of parametric design lies in generating highly specific, differentiated, rule-based designs [10].

1.3 From Form-Generation to Parametric Form-Finding

Form Generation is the process of producing new forms in architecture. It is the main aim of any architectural design process. With the huge advancements in computational tools, form generation is shifted from the traditional methods of form-making which used to have a static design target to new innovative techniques of digital form-finding where the design target is not a target, but a logical sequence connecting a variety of aspects of the architectural design [11, 12].

Agkathidis et al. defined form-finding as "a design method where generation of form is based on rules or algorithms, often deriving from computational tools, such as

Processing, Rhinoceros, Grasshopper and other scripting platforms" [13]. Parametric form-finding is simply the process which uses rules and parameters to find forms that offer solutions to spatial problems. It is common that parametric form-finding is also described by other terms such as: parametric design, generative design, evolutionary design, and algorithmic design.

1.4 Evolution of Parametric Architecture and Form-Finding

Parametric design is familiar for architects. From ancient pyramids to contemporary buildings, they have been designed and constructed in relationship to a variety of changing factors including climate, technology, usage, character, setting, culture, etc. [1]. Reviewing the history of parametric design, we can find that its evolution took many phases. Each phase somehow contributed in shaping the parametric form-finding practices that we know nowadays. Some of these phases are analogue and others are digital as shown in Fig. 1. The phases and their corresponding effect on the way of performing the form-finding process are listed as follows:

Analogue Phases

- Form-Finding **Through Mathematical Equations**

  The term parametric design was first used by Luigi Moretti in the 1940s as he studied the relationship between parametric equations and architectural design [14].

- Form-Finding **Through Physical Experiments**

  One of the earliest analogue examples of parametric design was Antonio Gaudi's upside down model of churches late in the nineteenth century. He created a model for **the Church of Colònia Güell** that consisted of strings weighted down with birdshot in order to create complex vaulted ceilings and arches. By manipulating the position of the weights, the length of the strings changed, this change affected the arches connected to it [15].

  The method of analogue computing was enlarged by Frei Otto in the 1960s, where he used soap bubbles to find optimal shapes of tensed structures in the design of **Munich Olympic Stadium**, designed for the 1972 Summer Olympics in Munich.

Digital Phases

- Form-Finding **Through 2D Parametric Modelling Software**

  In 1963, Ivan Sutherland used the computational power of the computer to create "**Sketchpad**", the first interactive computer-aided design program. Using a pen, a designer could draw simple two-dimensional shapes/models [16]. The architect's control of Sketchpad was similar to the idea of most of the parametric modelling software. They not only control the parameters of the model but also the model's underlying relationships [17].

Fig. 1 Evolution of parametric architecture throughout history. *Source* Author

- Form-Finding **Through 3D Parametric Modelling Software**

  In 1985, the mathematics professor Samuel Geisberg founded Parametric Technology Corporation. They created what would become the first commercially successful parametric software, "**Pro/ENGINEER**", in 1988. Pro/ENGINEER is a feature-based, parametric solid modeling system with many extended design and manufacturing applications. Like with Sketchpad, users could connect parts of the drawing models together using various parametric relations (equations), but the geometry here was three-dimensional [17].

  Also, Ghery Technology Company which was incorporated in 2001, released the parametric modelling software "**Digital Project**" in 2004. Digital Project took the parametric engine of CATIAv5 (computer-aided three-dimensional interactive application), an engine that enables architects to revise the parameters and equations defining their geometry, and combined it with tools tailored to architects to be able to rationalize complicated models as Frank Ghery's projects [17]. Among the changes made by Gehry Technologies to CATIA is a new visual interface suitable for architecture work.

- Form-Finding **Concept in BIM Software**

  The original software of "**Revit**" was developed by Revit Technology Corporation. The initial release of the software was in April, 2000. The authors of Revit website define parametric as an object based on parametric equations that the designer can adjust for particular circumstances. They later explained how a designer might adjust an object and how Revit in turn will revise instantly all plans, elevations, sections, schedules, dimensions and other elements of the model.

- Form-Finding **Through Innovative Visual-Scripting Parametric Modelling Software**

  In the twenty-first century, the visual interface emerged, which is a new type of scripting interface. In 2003, architects got their first visual-scripting interface, "**Generative Components**", which is a parametric CAD software developed by Bentley Systems. It uses graphs to map the flow of relations from parameters through user-defined functions, leading to the generation of geometry [17].

  Later in 2007, Robert McNeel and Associates assigned developer David Rutten to develop the visual scripting interface, "**Grasshopper".** The release of Generative Components in 2003 and Grasshopper in 2007 helped computational and parametric modelling to evolve and expand [4]. These tools are widely used in parametric design recently, and are being developed every day.

- Form-Finding **Introduction to the Traditional CAD Software**

  In AutoCAD2010, they published on their website that "Autodesk Takes 3D Design and Documentation to Next Level with AutoCAD 2010". Parametric functionality was finally introduced.

  It is obvious that computers did not invent parametric design, nor did it redefine the architectural profession. However, it did provide treasured tools that has enabled

architects to design and construct innovative buildings with more challenging qualitative and quantitative conditions [1]. The use of parametric design tools has opened new opportunities on how the designers work and think. It has significant impact on architecture [7].

2 Methodology (Dimensions of Digital Form-Finding in the Previous Work)

The research follows an analytical approach where it will conduct a review on the previous work related to the topic digital form-finding in order to clearly understand its different dimensions and to be able to develop a classification for the dimensions of parametric form-finding that can be used by architects in their future designs. The methodology which will be followed in this paper consists of five steps as shown in Fig. 2. The steps are represented as follows:

- Gathering the previous work related to the topic of digital form-finding.
- Analyzing the gathered work with respect to five different sub-topics.
- Suggesting a new classification for the dimensions of parametric form-finding based on the previous analysis.
- Evaluating the efficiency of the proposed classification by analyzing its relation with the reviewed work.
- Further analysis of the proposed classification to conclude a categorization for the main types of parametric form-finding processes currently used in the parametric design practice.
- Giving some guidelines to the architects who are willing to develop their own workflow/framework for their design process regarding the specific type of parametric form-finding process they are going to deal with.

After gathering and reviewing the previous work related to the topic of digital/parametric form-finding, the research will analyze these works in detail with respect to five sub-topics which were found to be common in most of these works. These five sub-topics are: approaches to generating forms, sources of making design decisions, design methods and processes, tools of designing parametric forms, implementation of designed forms. The analysis will be represented in the following sections discussing the sub-topics in the reviewed related work.

2.1 Approaches to Generating Forms

Many different approaches to designing a form were mentioned in the reviewed work. Kourkoutas in their thesis analyzed some of the pieces of contemporary architecture and found that generally the architectural forms consists of some two dimensional
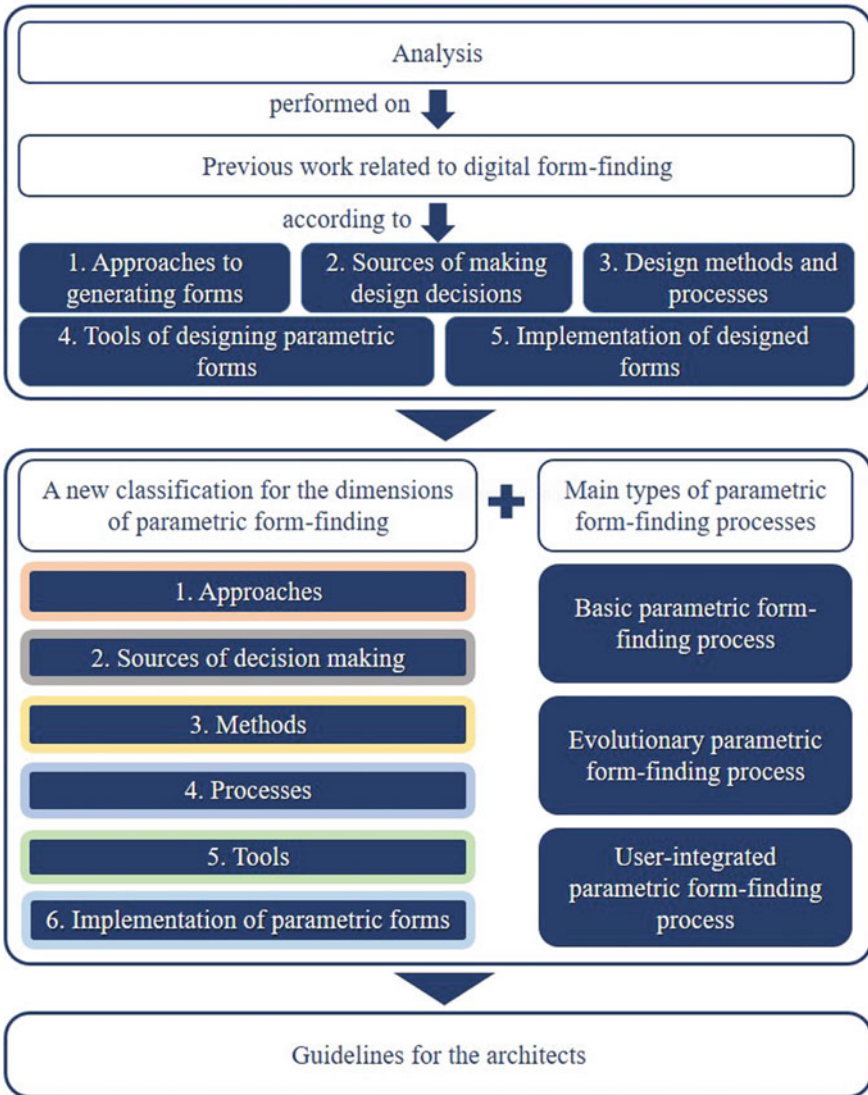
Fig. 2 Research methodology

shapes created using Nurbs Curves, and a skinning or an operation connecting those curves such as: sweep, loft, extrude, etc. [18]. They considered that these 2D initial geometries are the main approach to designing a form.

Also Agkathidis et al. studied some strategies for defining forms in architecture on a number of students' projects. The used strategies were some forming techniques (spatial and organizational principles for different types of geometries), such as: accumulation, constraint folding, knotting, linear dynamics, modularity, nodal

points, and surface fusion. The main concept was to diverge from the traditional ways of thinking and design, allowing for new innovative forms to emerge [19]. Later, Agkathidis et al. extended their limited idea about form-finding in which they discussed four different philosophies for form-finding in their book about generative design. The first is design processes driven by nature, in which they gain inspiration for the new forms form nature and science. The second is design processes driven by geometry, in which they follow geometric rules and proportions to produce new forms. The third is design processes driven by context, where the morphology and topology of the site are the main drivers of the new forms. The fourth is design processes driven by performance, where the different performance aspects of the new forms are the main focus of the design [13].

Another example for this extended idea about form-finding is the work of Oxman et al. who discussed computational processes, dividing form and generation into six models; mathematical form generation which use mathematical formulae as the base of the generative process, tectonic form generation that consider the use of tectonic patterns as the base of form generation, material form generation which are based on material structures and properties, natural or neo-biological form generation which rely on a specific natural form or phenomenon or process or principle for the generation of forms, fabricational form generation that use fabrication logics and techniques in the form generation, performative form generation where analysis is used along with the generation process in order to focus on the needed performance [20].

In some later work, the idea about form-finding was again limited to a specific approach. However, that approach wasn't limited to geometries and organizational principles. Schaur et al. highlighted the concept of self-generating forms, one of the most interesting formation processes of forms, which they defined as the visible result of equilibrium of all acting forces on a form in its generation process. They mentioned the huge interdependence of the shape and the structure of the form, which can also be seen as the connection between the visual aspect and the structural aspect of forms [21]. Their main approach for the form-finding was the structural logic.

Another example is the work of Ibrahim who explored the potential of applying new innovative methods of formation to ordinary materials like concrete. The resulted form was optimized for minimum used of concrete material. The research showed that form explorations with the new innovative tools can generate unexpected forms from ordinary materials which were only used before in producing traditional buildings [22]. His main approach for the form-finding was the properties of the used material.

2.2 Sources of Making Design Decisions

Sources of making design decisions were not directly mentioned in any of the reviewed work. However in most of the cases we can conclude them from the context of the work. In [13, 18, 19], the designer was the main source of making design decisions. In [21, 23–25], the design decisions were left to be done by the computer

which we consider as a rational source of decision. While in [26, 27], they relied on both the designer and the computer in making the design decisions.

An exception to this is the work of Al-Kazzaz, who directly introduced two main sources of decision making in his framework for digital form-finding in architecture. The first is intuitive guided design which is an interactive way that allows the user/ designer to interact with the process while it is running. The second is rational guided design where a form is designed or found on the basis of design requirements provided at the beginning of the design process through data and analysis [29].

While a unique direction was found in the work of Muehlbauer et al. where they represented a way of integrating the user in the evolutionary cycle of design. Their framework supported the collaborative decision making allowing users to be engaged with the designer and the computer in making some decisions during the design process through an aesthetic evaluation of some design alternatives [28].

2.3   Design Methods and Processes

Some of the reviewed work mainly focused on the design method. They described the whole method for the form-finding such as: self-generating forms, iterative process, etc. However, we still can conclude the processes which are underlying these design methods form the context of most of these works. Bohnacker et al. introduced the generative design as a process based on an initial idea, which is then applied to a rule or algorithm, then translated into a source code, producing a design output, the output returns to the designer where they can then modify the source code, and so on [26]. It is clearly an iterative design process. We can see that they used the generation process at the beginning, then the modification process, and finally the evaluation process. Also, Agkathidis et al. introduced a method of form-finding based on three phases. The first phase is the analysis, which focuses on the collection of data from different sources and the definition of design rules. The second phase is morphogenesis, which targets the generation of an abstract prototype based on some spatial and organizational principles. The third phase is metamorphosis, which is the transformation of the previous prototype into an architectural building [13]. It is mainly a one-way design process method.

Similar to that one-way process is the work of Zhang, who introduced four steps of a form-finding process. First step was gathering information. Second step was defining relationships between the different parameters and setting the algorithm to control them, then forming an initial model. In the third step, modifications were made to the initial model based on feedback. The fourth step was preparing the final model for fabrication and construction [27]. They obviously performed a generation process at the beginning, then evaluation process, then modification according to feedback. Also in the work of Kourkoutas, two methods of parametric form-finding were presented and explained in detail. The main steps of the faster method are: defining variables, creation of bounding volume, selecting the starting curve and additional curves if exist, form-finding using the selected starting curve, then the

selected additional curve if exist, and selecting a skinning technique to connect all the generated curves [18]. It is a one-way process. We can see that they used the generation process, then they mentioned that the form can undergo a modification process later if the designer decided to after conducting their evaluation process.

A unique design method was presented in the work of Schaur et al. where they conducted many studies about the concept of self-generating forms in relation to different topics; biology, non-planned settlements, and the phenomena of irregularity. They found that all the elements they studied follow the same structural principle of the self-generating forms. They came to the discovery of multi-layer membranes which follows the same phenomena of self-generation [21]. It is definitely a one-way process. We can see that they relied on the process of form imitation to generate forms from a phenomena found in nature. Another unique study was performed by Ibrahim, where they conducted a research that consisted of three steps. The first step was the form generation using a technique that converts two-dimensional images into three-dimensional geometries. In the second step, the generated forms were structurally analyzed. Finally, the resulted structural analysis was optimized for minimum use of concrete material [22]. It is an iterative process that uses both imitation and optimization.

Mainly focusing on the design method, Lee et al. introduced two parametric design strategies. Problem forwarding strategy, which focuses on decomposing the initial problem into algorithmic and geometric sub problems, forwarding them, resulting in a sequential synthesis until the final design is reached. Solution reflecting strategy, in which many variations of forms are generated, each generated form is reflected to new sub problems, producing a new form, and so on. They compared the two strategies and the results showed that the later strategy was the highest in terms of creativity [24].

Only in one of the reviewed works, they just focused on the processes themselves which are underlying the method for the form-finding such as: generation, optimization, etc. This can be seen in the work of Adriaenessens et al. who described the process of form-finding as controlling different parameters starting with an initial geometry, then the resulting shapes can be optimized for three main aspects. First, shape optimization, which affect the main geometry. Second, topology optimization, which affect the topology itself. Third, size optimization, which change the dimensions and proportions of a design, keeping its geometry and topology [25]. They mentioned the form generation process, with a huge focus on the optimization process.

However, some of the works clearly mentioned both the methods and the processes underlying them. Al-Kazzaz presented a framework for digital form-finding. He classified the digital form-finding methods into two methods; process-driven method, and outcome-driven method. He also mentioned some of the digital form-finding processes; generative process, and modification process. Finally, he applied the framework on some of existing contemporary tower designs through analyzing their design processes. The results showed that the different approaches of digital form finding have the ability to generate a wide variety of efficient complex forms [29]. Also, Anil Kumar et al. divided the parametric design process into three

stages; defining data sources, establishing relations between the data sources and defining parameters, and changing the parameters as per requirement to regenerate the designed form. It is obvious that they considered a one-way design process. They also classified the approaches to parametrization into three processes based on their purpose; form imitation (a source that inspired the architect searching for a new form), form optimization (a previously designed constrain-dependent form refined itself to solve a specific problem), and form-finding (an explorative approach of finding an internal generative logic that produces a range of possible forms that the designer can choose between them) [23].

2.4   Tools of Designing Parametric Forms

The tools that were used for designing were not directly mentioned in the reviewed work. However, they can be extracted from the context of the work. They mainly vary between parametric tools, simulation software, algorithms, and optimization tools. Only Al-Kazzaz directly presented some design tools in his framework for digital form-finding in architecture. He referred to them as the techniques of digital form-finding which are simulation-based, parametric-based, algorithmic-based, mathematic-based, and digital sketching and sculpting based [29].

2.5   Implementation of Designed Forms

Generally, in all of the reviewed work the bigger attention was given to the design and the form-finding process itself. Just a few of them considered how these designed forms will be implemented. Oxman et al. presented three digital technologies related to the implementation of the digitally designed forms. First one is materialization, which was defined as the translation of a former design in to its material state using computational tools. Second one is fabrication, where they highlighted the derivation of architectural forms through the potential of fabrication tools. Finally, the responsive technology which is the ability to react with the surrounding environment, it is also known as: interactive and dynamic [20]. Agkathidis et al. in their proposed design process, gave a huge focus to the materiality in design. They claimed that working with physical models in the design process was very crucial for more sensing of the produced forms, even in today's digital climate [19].

Ibrahim considered in his work an important aspect of implementation. Where the last step of his design method was the optimization of the designed forms for the minimum use of concrete material [22]. Also in the work of Zhang, they mentioned that the last step of their proposed design method was all about preparing the final designed model for fabrication and construction [27]. Also Agkathidis et al. who mentioned in their design method that the generation of the prototype forms can be done either in a digital or a physical way. They also explained that the last phase of

their design method is the transformation of the previous prototype into an actual architectural building which is implementation [13].

As we can find in the previous analysis for the related work, many aspects/dimensions of digital form-finding were considered. However, some studies focused on one or more dimensions, giving less focus to the other dimensions or neglecting them. This confirms that it is very important to have a classification that sums up the different dimensions of form-finding to be able to perform the whole process without forgetting any important aspect of it.

3 Findings (Proposed Classification for the Dimensions of Parametric Form-Finding)

Based on the aforementioned studies and analysis for the work related to the topic of digital form-finding in literature, we suggest a classification that sums up the different dimensions of parametric form-finding process in architecture, as shown in Fig. 3. The classification includes six dimensions as follows:

3.1 Approaches (Sources of Inspiration)

The approach is basically the main idea that inspired the initial shape of the form such as:

A. Nature

Forms are inspired by processes or materials or other forms from nature, mimicking them into new architectural forms.

B. Mathematics

Forms are inspired by theories or laws of mathematics, such as: fractals, golden ratio, etc.

C. Geometry

Forms are inspired by different geometries, being them simple or complex.

D. Spatial and Organizational Principles

Forms are generated by the spatial and organizational principles that connect different shapes and geometries together in a space, forming new complex forms.

E. Context

Forms are inspired by the topology or the morphology of the context or the social and cultural characteristics of that context in some cases.

F. Performance
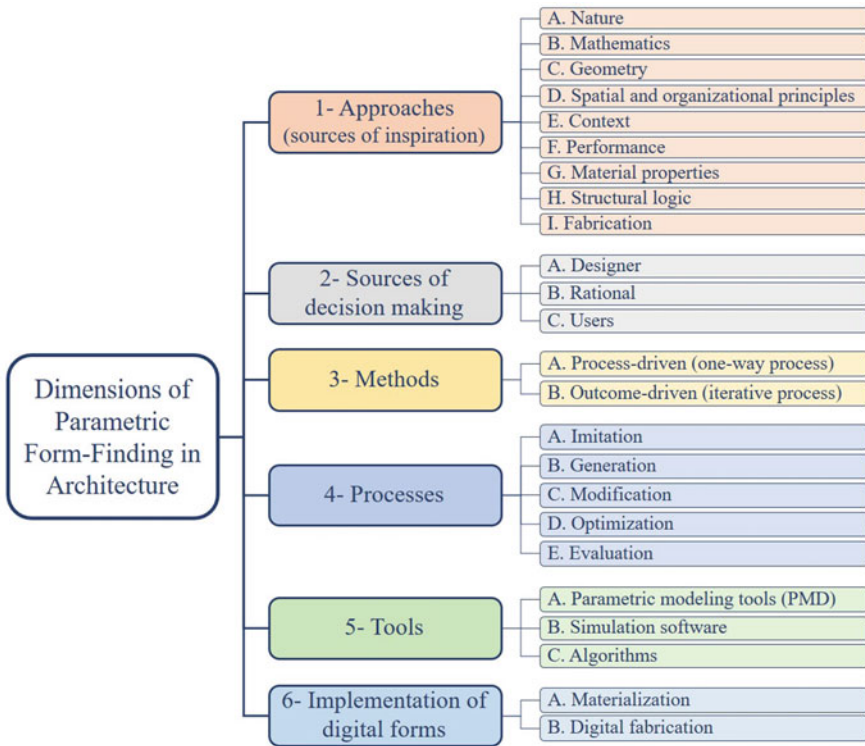
Fig. 3 The proposed classification for the dimensions of parametric form-finding in architecture. *Source* Author

Forms are generated considering the analysis and simulation results regarding their performance in a pre-specified aspect. These aspects can include: energy, structure, cost, etc.

G. Material Properties

The specific materials' structure and properties drives the generation of forms.

H. Structural Logic

The structural composition is what generates the forms, such as: self-generating forms.

I. Fabrication

The use of a specific fabrication design logic or technique in generating forms.

3.2   Sources of Decision Making

During the form-finding process, different sources can contribute in the decision making such as:

A. Designer

   The designer is the one who makes the major decisions in the design process according to his intention.

B. Rational

   Major decisions are automatically made as a result of a certain logic or target identified at the beginning of the design process, these decisions usually follow functional and design requirements for a design.

C. Users

   The main focus in the design process is the users themselves and their own needs, where designers adjust their design to satisfy them. Sometimes users are asked to support in making some design decisions. This is described as: user centric design.

3.3   Methods

There are two different methods for the process of form-finding:

A. Process-Driven Method (One-Way Process)

   A certain targeted process is set at the beginning, then the process runs until it produces any form, which is considered a final form. Here, the main focus is on the process itself.

B. Outcome-Driven Method (Iterative Process)

   A main target for the design outcome is set at the beginning of the process, where the process begins to run and many iterations can happen until that final target is achieved. Here, the main focus is on the design outcome.

3.4   Processes

Many sub-processes lie under the major form-finding process either contributing in generating the form or editing it such as:

A. Imitation

   It is one of the very first sub-processes where the forms are inspired from any source of inspiration mimicking it such as: nature, art, etc. An initial form is generated.

B. Generation

It is also one of the very first sub-processes where data about the design is collected as input parameters, then the process runs to generate the form according to the collected data. An initial form is generated.

C. Modification

After the form is generated, aesthetic or simulation feedback about that form is collected. It can then be modified according to the collected feedback until the designer is satisfied with the result or until it meets a specific objective.

D. Optimization

It is trying to find the best possible solution from a wide range of solutions for a given problem. It is an iterative process where values of different design parameters are varied until the form reaches the solution with the optimum values of these parameters that meet a pre-specified objective or objectives. When these optimum values are achieved, the process is done and the design result is extracted.

E. Evaluation

It is using a specific criteria to evaluate the design result/results in order to choose a final result or even modify the design.

Both processes of modification and optimization can contribute in achieving the UN sustainable development goal (SDG) number 11: Sustainable Cities and Communities, especially when the design objective is decided to be sustainability related.

3.5 Tools

We have a lot of computational design tools that are being developed every day and of course can be used in the digital form-finding process such as:

A. Parametric Modeling Tools (PMT)

Parametric modeling programs such as: Rhinoceros with its virtual programming environment: Grasshopper. In addition to the plug-ins associated with them such as: Ladybug, Kangaroo, etc.

B. Simulation Software

Software that is used to simulate various conditions related to the designed forms. An example to that are the software used for simulating environmental conditions, such as: Energy Plus, Radiance, Ecotect, etc.

C. Algorithms

Algorithms are a finite sequence of rules that are followed by the computer to solve a design problem. They define the logical process behind design decisions.

They also can be used to find the optimum solution for a specific problem. There are various types of algorithms, such as Genetic algorithms (Galapagos, Octopus, etc.).

3.6 Implementation of Digital Forms

For implementing/constructing a digital form after its design, we need to proceed with the following processes:

A. Materialization

Assigning materials to the generated forms.

B. Digital Fabrication

Deciding which fabrication technique will be used to create the generated forms and prepare the forms to be ready for fabrication.

4 Discussion

4.1 Efficiency of the Proposed Classification

To demonstrate the efficiency of the proposed classification, the research analyzes its relation with the existing related work. Table 1 shows an analysis of the reviewed previous work in relation to the proposed classification.

It is clear that each of the previous work used different approaches for form-finding, some of them mentioned many approaches, while others mentioned only one approach, and others didn't mention any. The most common approaches were: Geometry, spatial and organizational principles, and material properties. For the sources of decision making, most of the previous work focused whether on the designer or the rational sources or both of them together during the process, while in [20] none of the sources of decision making was mentioned. Only in [28] users were also incorporated in making design decisions together with both the designer and the rational sources. Users source of decision making is still a novel direction in design.

It is shown that both methods of form-finding were likely mentioned in the previous work. In the form-finding processes, generation process was the most mentioned, then imitation and modification processes, while optimization process was the least mentioned. In general, two of the previous work [19, 20] didn't mention neither the methods nor the processes of form-finding in their work.

We can notice that the most common of all of the form-finding tools are the parametric tools. Many of the previous work didn't consider the implementation of digital forms in their work, while others focused on both the materialization and the digital fabrication in their processes of form-generation, only in [27] digital

Table 1 Dimensions of form-finding in the related work

Related work	Approaches	Sources of decision making	Methods	Processes	Tools	Implementation of digital forms
[13]	Nature Geometry Spatial and organizational principles Context Performance	Designer	Process-driven	Imitation Generation Modification	PMT Simulation software	Materialization Digital fabrication
[20]	Nature Mathematics Performance Material properties Fabrication	N/A	N/A	N/A	PMT Simulation software Algorithms	Materialization Digital fabrication
[26]	N/A	Designer Rational	Outcome-driven	Imitation Generation Modification Evaluation	PMT Algorithms	N/A
[23]	N/A	Rational	Process-driven	Imitation Generation Optimization Evaluation	PMT Simulation software Algorithms	N/A
[19]	Spatial and organizational principles Material properties	Designer	N/A	N/A	Parametric tools	Materialization Digital fabrication
[29]	Mathematics Performance Spatial and organizational principles	Designer Rational	Process-driven Outcome-driven	Generation Modification	PMT Simulation software Algorithms	N/A
[24]	N/A	Rational	Process-driven Outcome-driven	Generation Modification	PMT Algorithms	N/A
[21]	Structural logic	Rational	Process-driven	Imitation	N/A	N/A
[25]	Geometry	Rational	Process-driven	Generation Optimization	PMT Algorithms	N/A
[27]	N/A	Designer Rational	Outcome-driven	Generation Evaluation Modification	PMT Algorithms	Digital fabrication

Table 1 (continued)

Related work	Approaches	Sources of decision making	Methods	Processes	Tools	Implementation of digital forms
[22]	Material properties Structural logic	Rational	Process-driven	Imitation Optimization	PMT Simulation software Algorithms	Materialization Digital fabrication
[18]	Context Geometry	Designer	Outcome-driven	Generation Evaluation Modification	PMT	N/A
[28]	Nature	Designer Rational Users	Outcome-driven	Imitation Optimization	PMT Simulation software Algorithms	N/A

fabrication was mentioned along with construction, but materialization process was not mentioned.

It is found that each of the previous work considered some of the dimensions of form-finding, while giving less focus to some other important dimensions or neglecting them. This can affect the designers' visions resulting in an incomplete or unclear vision during the design of new architectural forms. It can also affect the time and money spent on the process of form-finding, making it harder and slower for designers to design new architectural forms. The proposed classification of the dimensions of form-finding which was shown in Table 1, connects the different dimensions of form-finding. Following this classification will make it easier for the designers to organize their thoughts and ideas in the generating of architectural forms.

4.2 Categorization for the Current Practices of Parametric Form-Finding Processes

Analyzing the proposed classification of the dimensions of parametric form-finding, we can obtain three main types of parametric form-finding processes that are currently used by architects in their practice. These types can be explained as follows:

- **Basic** Parametric Form-finding Process

  It refers to the normal parametric design workflow, where the designer generates an initial form, then that form is being simulated with respect to a specific aspect using a simulation design program. After that, the simulation results are being used as feedback so that the designer can modify the design. The process runs again and again until the designer is satisfied with the simulation results, then the final design outcome is obtained. The process is shown in Fig. 4.
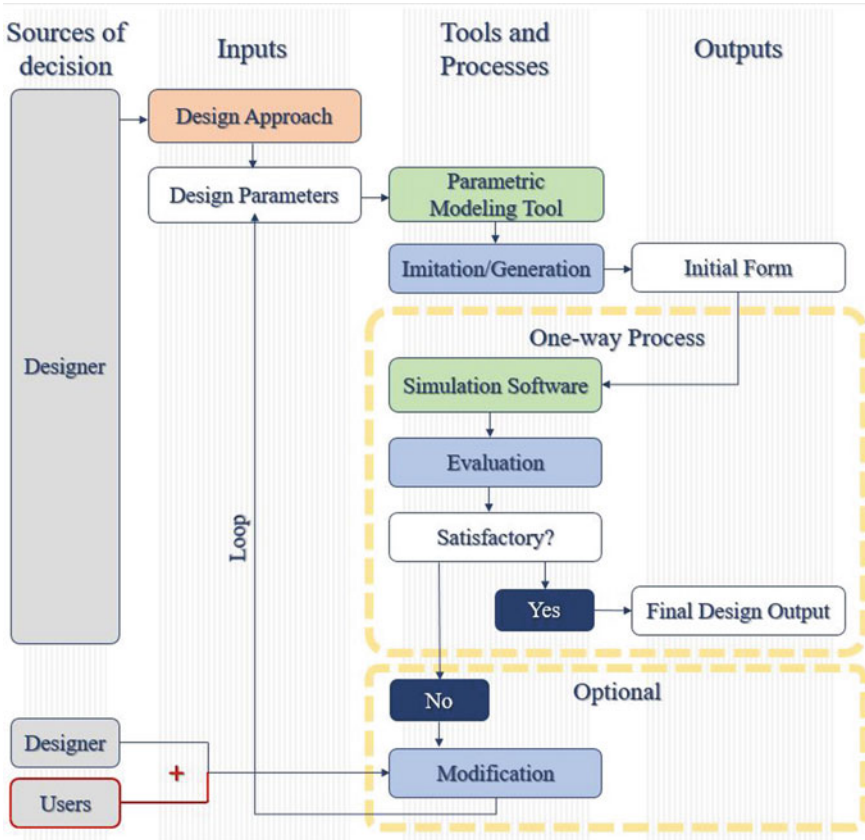
Fig. 4 Basic parametric form-finding process. *Source* Author

- **Evolutionary** Parametric Form-finding Process

  It is the design process where an evolutionary algorithm is integrated in the process of form-finding. The designer creates an initial design. Both the parameters of the initial design, and design objectives are introduced to the algorithm. Then the algorithm runs and starts to produce generations eliminating some design alternatives and keeping some others according to their fitness values. This process keeps running iteratively until the design objectives are satisfied, then the algorithm produces the final design alternative/alternatives. It is also known as generative parametric form-finding process. The process is shown in Fig. 5.

- **User-integrated** Parametric Form-finding Process

  In some practices, the designer may give users the chance to contribute with their choices regarding a specific design's alternatives or modifications. The designer then takes the user's choices into consideration producing a final outcome that meets their opinion and satisfy the other design objectives at the same time. This
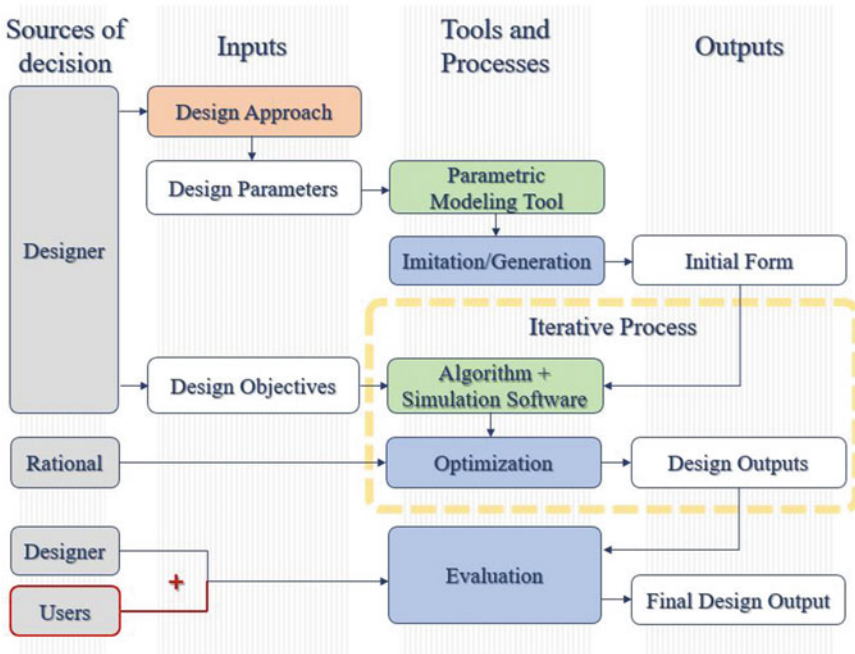
Fig. 5 Evolutionary parametric form-finding process. *Source* Author

type of process can be a part integrated to any of the other two types of processes mentioned above. The process is shown in both Figs. 4 and 5, represented in the parts outlined in the red color.

4.3 Guidelines for Architects in Designing Parametric Forms

As we notice in the previous figures, Figs. 4 and 5, each of the mentioned types of the parametric form-finding processes is related to different dimensions of parametric form-finding. This can be further demonstrated to be a guide for architects in designing parametric forms as shown in the following Fig. 6.

Any of the previously mentioned types of parametric form-finding processes can be used by architects in their practice. Therefore, it would be easier for them to follow the guidelines presented in Fig. 6 in order to only consider the specific dimensions related to the type of the process they are willing to use in their form-finding. This will direct them to efficiently create their own parametric design workflows/frameworks based on these guidelines.

Fig. 6 A guide matrix for the dimensions of the different types of parametric form-finding processes. *Source* Author

The table groups columns under **Related Dimensions**: *Approaches* (Nature, Mathematics, Geometry, Spatial and organizational principles, Context, Performance, Material properties, Structural logic, Fabrication), *Sources of decision making* (Designer, Rational, Users), *Methods* (Process-driven method (one-way process), Outcome-driven method (iterative process)), *Processes* (Imitation, Generation, Modification, Optimization, Evaluation), *Tools* (Parametric modeling tools, Simulation software, Algorithms), *Implementation of digital forms* (Materialization, Digital fabrication).

Process Type	Nature	Mathematics	Geometry	Spatial and organizational principles	Context	Performance	Material properties	Structural logic	Fabrication	Designer	Rational	Users	Process-driven method (one-way process)	Outcome-driven method (iterative process)	Imitation	Generation	Modification	Optimization	Evaluation	Parametric modeling tools	Simulation software	Algorithms	Materialization	Digital fabrication
Basic parametric design process	✓	✓	✓	✓	✓	✓	✓	✓	✓	✓			✓		✓	✓	✓			✓	✓	✓	✓	✓
Evolutionary parametric design process	✓	✓	✓	✓	✓	✓	✓	✓	✓	✓	✓			✓		✓	✓	✓		✓	✓	✓	✓	✓
User-integrated parametric design process — Basic	✓	✓	✓	✓	✓	✓	✓	✓	✓	✓		✓	✓		✓	✓	✓			✓	✓	✓	✓	✓
User-integrated parametric design process — Evolutionary	✓	✓	✓	✓	✓	✓	✓	✓	✓	✓	✓	✓		✓		✓	✓	✓		✓	✓	✓	✓	✓

5 Conclusion

The paper presented parametric architecture, parametric form-finding, and their evolution. A review was conducted for some of the existing related work which focused on the dimensions of digital form-finding, it was analyzed with respect to five sub-topics found to be common in most of these works: approaches to generating forms, sources of making design decisions, design methods and processes, tools of designing parametric forms, implementation of designed forms. Then, a classification for the dimensions of parametric form-finding was proposed (Fig. 3). The reviewed work was then analyzed for its relation with the proposed classification to demonstrate its efficiency (Table 1). It was found that each of the previous work considered some of the dimensions of form-finding, while giving less focus to some other important dimensions or neglecting them. The proposed classification was further analyzed to obtain a categorization for the main types of parametric design processes that are currently used in the practice of parametric form-finding (Figs. 4 and 5). Some guidelines regarding which dimensions of parametric form-finding are used in each of the different types of the mentioned parametric form-finding processes were given for architects to support them in designing their future designs (Fig. 6).

The proposed classification of the dimensions of form-finding can make it easier for the designers to consider the different dimensions of form-finding and organize their process accordingly. Thus, saving time and effort throughout the whole process, and cutting costs related to major design modifications (as a result of non-well planned design process) or fabrication applicability issues in some cases. Also, the presented guidelines mainly direct architects to efficiently create their own design

workflows/frameworks in the future based on them. In general, the work presented in this paper is applicable anywhere around the world. The paper mainly addressed enhancing the design process of parametric architectural forms. This in turn can have a great influence on the UN SDG number 11: Sustainable Cities and Communities, which intends to make cities and human settlements inclusive, safe, resilient, and sustainable.

6 Recommendations

It is important to consider that as the technologies around us continue to develop every day, more things can be added to the proposed classification in the future, especially for the tools and implementation methods which are strongly related to the technological advancement. Accordingly, new types of parametric form-finding processes may be introduced in future studies and be used by architects in their practices.

We recommend that architects, who are the main design decision makers, should always refresh their knowledge and stay up to date with the upcoming innovative trends in our digital world in order to make the best use of it in the architectural realm.

References

1. Phillips S (2010) Parametric design: a brief history. arcCA Digest 10.1:24–28, 2010
2. Marino D, Berizzi C (2020) New design methodologies between research and practice in digital fabrication of wooden architecture. IN_BO: Ricerche E Progetti Per Il Territorio La Città E l'architettura 11(5):32–43
3. Keshavarzi M, Hotson C, Cheng CY, Nourbakhsh M, Bergin M, Asl MR (2021) SketchOpt: sketch-based parametric model retrieval for generative design. In: Extended abstracts of the 2021 CHI conference on human factors in computing systems (CHI EA'21), pp 1–6
4. Hautala A (2021) An insight to computation: a study of the potentials of computation as well as digital fabrication in architectural design. School of Arts, Design and Architecture, Aalto University
5. Woodbury R (2010) Elements of parametric design, 1st edn. Routledge, pp 1–312
6. Aish R, Woodbury R (2005) Multi-level interaction in parametric design. In: Butz A, Fisher B, Krüger A, Olivier P (eds) Smart graphics, lecture notes in computer science, vol 3638. Springer, pp 151–162
7. Gu N, Yu R, Behbahani PA (2021) Parametric design: theoretical development and algorithmic foundation for design generation in architecture. In: Handbook of the mathematics of the arts and sciences, pp 1361–1383
8. Frazer J (2016) Parametric computation: history and future. Archit Des 86(2):18–23
9. Schumacher P (2015) Design parameters to parametric design. In: The Routledge companion for architecture design and practice. Taylor and Francis Group
10. Wortmann T, Tunçer B (2017) Differentiating parametric design: digital workflows in contemporary architecture and construction. Des Stud 52:173–197

11. El Iraqi A, El Daly H (2017) Architectural forming between form making and form finding towards form follows parameters. J Al-Azhar Univ Eng Sector 12(43):577–596
12. Kolarevic B (2003) Architecture in the digital age: design and manufacturing, 1st edn. Taylor & Francis Group
13. Agkathidis A (2016) Generative design: form-finding techniques in architecture (form + technique). Laurence King Publishing
14. Gallo G, Pellitteri G (2018) Luigi Moretti, from History to parametric architecture. In: Proceedings of 23rd international conference on computer-aided architectural design research in Asia (CAADRIA)
15. Burry M (2007) Gaudi unseen: completing the Sagrada Familia, Jovis
16. Sutherland IE (1963) Sketchpad a man-machine graphical communication system. In: Proceedings of the spring joint computer conference (AFIPS'63 (Spring)). Association for Computing Machinery, New York, NY, pp 329–346
17. Davis D (2013) A history of parametric. https://www.danieldavis.com/a-history-of-parametric/. Accessed 28 Mar 2022
18. Kourkoutas V (2007) Parametric form finding in contemporary architecture. TU Wien Organization
19. Agkathidis A, Hudert M, Schillig G (2009) Form defining strategies: experimental architectural design, 2nd illustrated edn. Distributed Art Pub Incorporated
20. Oxman R, Oxman R (2014) Theories of the digital in architecture. Routledge
21. Schaur E (2016) Forms, their aspects and their formation processes in architecture and nature. Int J Space Struct 31(1):31–42
22. Ibrahim M (2018) Form exploration with optimized three-dimensional printed architecture. In: GA2018 XXI generative art conference, pp 195–208
23. Anil Kumar K, Chani PS (2017) Approaches to parameterization in architectural design. In: Smart innovation, systems and technologies. Springer Science and Business Media Deutschland GmbH, pp 629–641
24. Lee J, Gu N, Williams AP (2014) Parametric design strategies for the generation of creative designs. Int J Archit Comput 12(3):263–282
25. Adriaenssens S, Block P, Veenendaal D, Chris W (2014) Shell structures for architecture: form finding and optimization. Routledge, pp 1–323
26. Bohnacker H, Groß B, Laub J (2009) Generative Gestaltung: Entwerfen. Programmieren. Visualisieren. Mit internationalen Best-Practise-Beispielen, Grundlagen, Programmcodes und Ergebnissen. Schmidt Hermann Verlag
27. Zhang B (2014) Emergence: form finding in nonlinear architecture. Int Sci J Arch Eng, 1(1):15–21
28. Muehlbauer M, Burry J, Song A (2020) An aesthetic-based fitness measure and a framework for guidance of evolutionary design in architecture. Lecture notes in computer science (including subseries lecture notes in artificial intelligence and lecture notes in bioinformatics). Springer, Cham, pp 134–149
29. Al-Kazzaz DA (2019) Form-finding in digital architecture—a case study of tower designs. Zanco J Pure Appl Sci 31(s3):121–130

Risk Categorization for Various Project Delivery Methods in Construction Sector

Ibrahim Mahdi, Ahmed Mohamed Abdelkhaleq, Hassan Mohamed Hassan, Ehab Rashad Tolba, and Lamisse Raed

1 Introduction

Delivery of a construction project or service is facilitated by a project delivery method, which is a strategy for planning and carrying out the phases of planning, designing, building, operating, and maintaining [1].

The selection of an appropriate project delivery method (PDM) greatly influences the project outcome. Design-Build, Design-Bid-Build and Construction Management represent the three traditional methods. Each PDM has its own advantages and disadvantages which suit various construction projects in different circumstances [21].

The selection of the appropriate PDM is one of the most important managerial decisions since it has a direct impact on the success of any project, it affects the project objectives such as cost, quality, schedule and safety. Indeed, PDMs have developed over the years, and there have been alternatives introduced in the construction industry to meet various demands [3].

Mitkus and Mitkus [29] Indicated that about 90% of the construction claims and disputes are caused by poor communication between the project stakeholders. Many authors underlined the importance of collaboration and partnership between all the parties involved in a project, which is supposedly established by the choice of the

I. Mahdi · A. M. Abdelkhaleq · H. M. Hassan · E. R. Tolba
Structural Engineering and Construction Management Department, Faculty of Engineering and Technology, Future University in Egypt, Cairo, Egypt

E. R. Tolba · L. Raed (✉)
Civil Engineering Department, Faculty of Engineering, Port Said University, Port Said, Egypt
e-mail: lamees.raad@eng.psu.edu.eg

L. Raed
Structural Engineering Department, Faculty of Engineering, Port Said University, Port Said, Egypt

PDM. The selection of a suitable PDM for a particular project is vital process to adopt a procurement and contracting method that is suitable for the project.

Because sustainable building delivery processes are more complex than traditional counterparts, there is still a lag in incorporating the concept of sustainability into fundamental management practices [9].

Ahmed and El-Sayegh [5] produced a list of applicable selection criteria to assist decision-makers in selecting the optimum project delivery method for sustainable construction projects and assessing the impact of those selection factors on the success of such projects. According to the findings, the most important factors are level of integration, green contract, green liability, green team, technology, and innovation.

The findings indicated that level of integration and green contract clauses are the most important relevant factors that influence the choice of PDM. For instance, in order to meet sustainability goals, the payment provisions should be carefully drafted.

The decision should be made in the project initiation phase and certainly before the final design phase begins. Although the purpose and needs must be clear in the scoping stage.

Ahmed and El-Sayegh [4] stated that to ensure that the suppliers chosen for sustainable building projects are adequate in considering the challenges associated with sustainable materials and technology, critical selection criteria for green suppliers should be created. In addition, there should be contractual incentives to promote the adoption of sustainable building and the use of an integrated team approach in order to address the contractual problems.

The purpose of this study is to identify the major risks present in various project delivery methods rather than focusing on all the risks at the same time as it is time-consuming as well as very complicated.

The results of this study will help construction practitioners to identify risks related to project delivery methods during project' s life cycle before commencement of the projects. Risk identification will enhance the capability of managing risk in construction projects. Further categorization of risks is done which will help in better allotment of risk responsibilities.

Traditional ways of managing projects, like Design Bid Build, Design Bid, Design Build, or EPC project delivery methods, are becoming less popular because of the way they work [1].

Molenaar [30] stated that sustainability goals are more likely to be met when the scope and cost of a project are discussed, like in a Guaranteed Maximum Price (GMP) with shared risks and rewards clauses.

This includes the overall responsibility for achieving sustainable goals, the communication strategies employed by project participants to ensure that everyone fulfils their part in achieving this responsibility, as well as the stage in the project delivery process at which the responsibility for obtaining a green certification is being assigned.

The "green guarantee" is the term used to describe the point at which the owner is legally obligated to receive the necessary green certification. The success rate

of sustainable construction projects will ultimately be impacted by the important selection criterion of selecting a delivery strategy that offers an early green assurance [30].

Understanding the risk involved in different project delivery methods at different phases of projects at such an early stage (commencement) of the project will help construction practitioners to manage it in such a way that it has the least negative effect on project targets and the most positive results possible.

2 Theoretical Background

2.1 Project Delivery Methods

There are various delivery methods available in the construction industry, from the traditional design-bid-build (DBB) to other alternative methods such as design-build (DB) and construction manager at risk (CMR) [20].

Traditional project delivery methods are described as forms of procurement that tends to separate the design and delivery, typically Design-Bid-Build (DBB) [16].

Traditional project delivery is also characterized by a large degree of responsibility for the owner. These methods focus on the integration between design and delivery processes mainly through contractual or physical planning and control systems. As opposing to methods that segregates the Design and Delivery processes. Integrated forms of project delivery are often aligned towards the formation of one project team to deliver both design and construction [16].

Traditional project delivery system has a linear flow of work processes which consists of decision, design, bidding and construction phases [17] (Fig. 1).

2.1.1 Design-Bid-Build

In the traditional project delivery method known as design-bid-build (DBB), the owner retains a designer to provide all design services and then awards a construction contract based on the designer's drawings and specifications. The owner "owns"
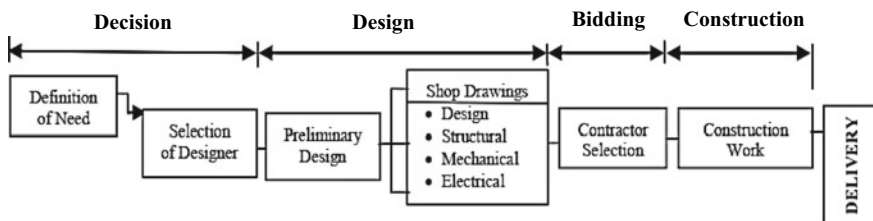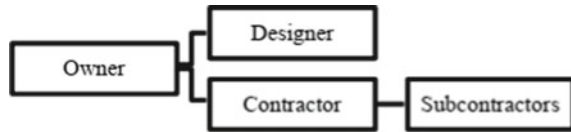

Fig. 1 Workflow Scheme of traditional project delivery system [8]

Fig. 2 Design bid build
delivery method [10]

Fig. 3 Design build delivery
method [10]

the design details and bears the financial burden of any mistakes made during
construction in DBB [28].

In DBB, there is no direct relationship between the designer and the builder, They
communicate only through the owner as shown in the following Fig. 2 [14].

2.1.2 Design-Build

In recent years, DB projects have become increasingly common in both the private
and public sectors. The primary reason is that Design-Build project delivery is a
viable option if the owner wishes to rely on a single source of responsibility for
design and construction in an effort to reduce unnecessary delays and extra expenses
caused by claims and counterclaims [38].

In DB method, In DB project structure, a single organization is ultimately respon-
sible for both design and construction (Fig. 3). A DB project begins with the owner
devising a conceptual design that describes the functional or performance require-
ments of the proposed project but does not specify its form or construction [7, 14,
22].

2.1.3 Construction Management (CM)

During the design phase and beyond, the construction manager (CM) takes on the
responsibility of analyzing the facility's budget, schedule, potential effects on other
designs and systems, and materials. The construction manager acts as the general
contractor in this delivery method, much like in the more conventional design-bid-
build method [25].

Agency-CM is a fee-based service in which the construction manager (CM) is
solely accountable to the agency and represents the agency throughout the whole
project.

While the CM may collaborate with the designer or contractor to lower costs, it
does not provide price assurance or assume contractual responsibility for construction
[40].
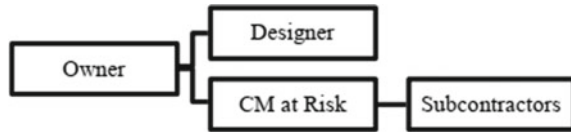
Depending on the contract provisions with the Construction Manager, the Owner may or may not negotiate directly with contractors. The Construction Manager (CM) delivery method is characterized by the owner's collaboration with a consultant and construction manager to achieve efficiency in time, constructability, and costs, especially during the pre-construction phase of a project, when the construction manager is not responsible for the construction but only manages it [27].

2.1.4 Construction Management at Risk (CMR)

While the owner may have signed separate contracts with the CM and designer, this approach allowed for team integration due to the CMR's early integration with the designer [18]. The owner could use the contractor's expertise to better estimate costs, create a work schedule, assess the engineer's framework, source and negotiate bids, and coordinate various aspects of the project [7].

CMR was established with the goal of supplying owners whose organizations lack such capabilities with expert management throughout the entirety of their projects [35]. A CMR project using this delivery method requires the execution of two contracts. Preconstruction services are provided during the design phase in the former, while construction is carried out in the latter. If the project's scope does not change after the GMP is established, as is often the case, the owner is relieved of any further financial responsibility under the CMR (Fig. 4).

2.1.5 Integrated Project Delivery

In order to supply accurate information and cutting-edge technologies in a collaborative team setting, Integrated Project Delivery (IPD) is introduced as a new delivery system. IPD promotes high efficiency. In this regard, the research sought to analyze the IPD principles and their primary categories, including contract, process, information and modeling (I&M), team, and communication. It also performed a qualitative analysis to show the current trends in research [41].

There is a lack of understanding about the integrated project delivery systems (IPD). That affects the lack of project environment, supply chain relationships, and possible project outcomes. Despite the fact that the IPD system is intended as a solution to the design and construction industry's performance problems [26].

The reluctance to implement IPD could be the result of practitioners lacking in the necessary knowledge, abilities, and/or experience, as well as the presence of company-specific technical challenges. Managers may move slowly through the

transformation process due to a lack of information. Professional skills in a multi-disciplinary setting, BIM-relevant skills, and integrated experience are now seen as essential for success in an IPD context at the implementation level [13].

The sustainability component is served by the IPD principles. When people respect and trust each other, it helps the project reach its goals, encourages creativity, and lets ideas run. This, in turn, will affect the business side of the project and help find new ways to save energy and cut pollution to save the environment. It will also make it possible for more projects to happen, which will help people socially [2].

The adoption and use of the integrated project delivery method is for sustainable building projects. But the standard Design-Bid-Build method is still the most used way to get projects done [11].

2.1.6   Public Private Partnerships (PPP)

The public and private sectors often work together on infrastructure projects through Public–Private Partnerships (PPP), which has received a lot of attention recently [37].

Several types of infrastructure have benefited from the use of PPP, including but not limited to: the construction of power plants and distribution networks; the building of hospitals, schools, airports, and prisons; the construction of railways, roads, and highways; and the construction of stadiums and telecommunications facilities. With a PPP delivery approach, the government and private enterprise may share risks and rewards equally and make full use of each other's strengths [32].

2.1.7   Build-Operate-Transfer (BOT)

Build-Operate-Transfer is one of the most promising new methods of funding construction projects (BOT). In the case of a shortage of building funds, it allows the client to gain access to the necessary capital. Concessions on project design, planning, funding, implementation, and management are all elements of this public–private financing model. The approach allows for post-completion project management, giving proponents a chance to recoup their initial investment [10, 43].

The Build-Operate-Transfer (BOT) model is an example of a public–private partnership (PPP), which is an arrangement whereby the government and private companies work together to supply goods and services for public infrastructure [12].

2.1.8   Engineering–Procurement–Construction (EPC)

In this delivery method, general contractor plans and executes the project, acquires all necessary materials, and hands over a completed building to the developer [19]. Simply said, the general contractor is in charge of nearly every aspect of a construction project.

When it comes to organizing and carrying out building projects, the Engineering-Procurement-Construction (EPC) model is widely recognized as the best practice [42].

Consequently, implementing the EPC mode is a strategic approach to overcoming the challenges associated with developing prefab structures.

In Zhao [44] study on the management of prefabricated buildings, he stated that the use of EPC as a delivery methods allows for systematic consideration of manufacturing and assembly procedures during the design phase. Furthermore, general contract management organization ensures prefabricated building design, production, and constructions are integrated, which is helpful in realizing lean construction [44].

Some very large construction projects in the engineering field feature complex technology, challenging management, and high management risk. The EPC project contractor must assume additional risk because the contractor is the sole party to the contract [36]. The logistics of engineering construction is a crucial guarantee for companies to participate in international engineering projects, as large-scale construction projects often require the joint completion of multiple companies.

2.2 Risk Management

Throughout the lifecycle of a project, risk management plays a vital role by identifying and addressing any threats that could derail progress toward the project's goals [8].

The term "risk management" refers to the procedure of systematically assessing, naming, and dealing with potential threats to a project's success. In order to achieve the project's goals, it entails increasing the likelihood and significance of favorable outcomes while decreasing those of unfavorable ones [23].

Due to the qualitative and quantitative analysis, risk management is an integral part of any decision-making process, whether in personal life, business, industry, or at different stages of the business cycle. The goal of risk management is to systematically examine a variety of relevant factors in order to estimate the likelihood of problems arising, to characterize the nature and likely consequences of these problems, and to consider how they might be avoided or at least mitigated [24].

The purpose of a risk assessment is to investigate potential causes of hazardous events.

The next step is to assess the potential dangers and weigh the likelihood of each against the potential harm they could cause.

The different uncertainties or assumptions must be accounted for, and a plan must be identified to decide whether a risk is acceptable or what should be done to make it acceptable. In addition, this method should aid in determining the likelihood of occurrence and the effects of known, unknown, and unexpected events [6].
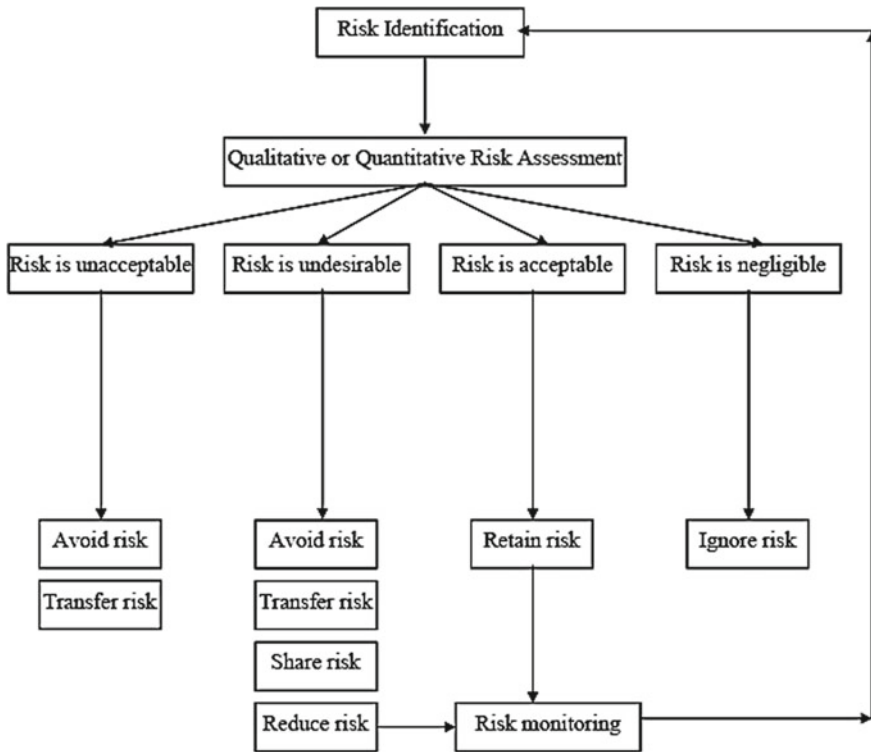
Fig. 5 RM process [38]

Typically, this RM framework has four main phases; hazard identification, risk assessment, risk mitigation and risk monitoring [31]. A schematic of (RM) is shown in Fig. 5

2.2.1 Risk Management Over Project Life Cycle

All stages of a project's life cycle carry some degree of danger, and some threats may manifest themselves in multiple stages. Academics can't agree on how dangerous each step of the building process actually is.

Ehi-Uujamhan [15] proposed establishing a risk plan during the planning and design phase; the plan should detail how to deal with all the potential problems that could arise during those steps. They also brought up the idea that all project stakeholders need to participate in risk planning at that stage, as doing so can help resolve problems before they progress to the mitigation stage.

Smith et al. [34] emphasized the importance of monitoring and controlling processes during the execution phase to ensure that activities were carried out as planned and that risks identified in earlier phases were mitigated.
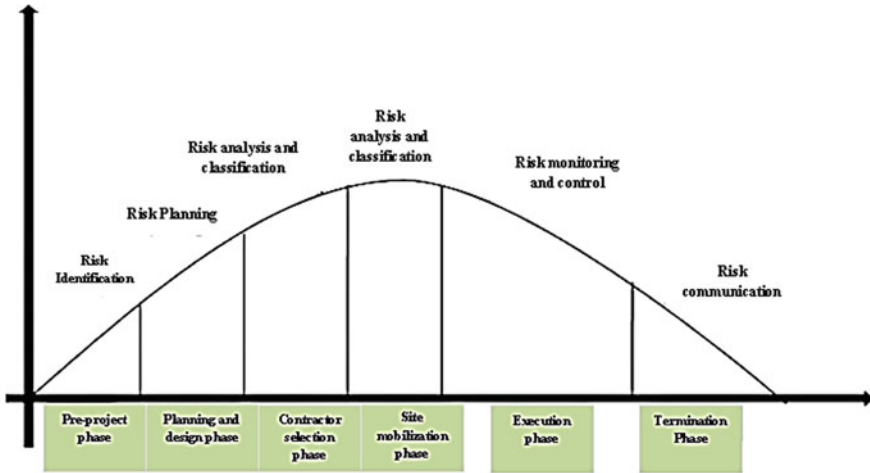
Fig. 6 Utilizing RM elements over PLC [41]

The following Fig. 6 by Shawish [33] showed the utilization of risk management over project life cycle.

3 Methodology

This research surveyed existing literature in order to learn more about the potential dangers of using different approaches to delivering projects at different stages. Project delivery methods, risk management, and life cycle management were some of the keywords used to search online databases and Google Scholar for relevant articles. These supplementary works were located by following references provided in the previously cited works.

The articles were selected from 126 articles published in high-quality, peer-reviewed journals over the past three decades and subjected to a thorough content analysis review. Content analysis showed that most of the articles selected identified risks for various delivery methods used in the construction industry around the world, and that these risks were typically categorized based on risk categorization throughout the life cycle of the project. Choosing a delivery method is often done without a clear understanding of how it will affect the overall budget or the distribution of risks in the project [39].

At the beginning of the project, all parties involved in the project want to see it through to a successful conclusion as quickly and cheaply as possible without sacrificing quality. Because of the number of people and factors involved, it may be challenging for the owners in particular to accomplish these aims, and they may encounter a number of obstacles along the way [17].

Table 1 Risk categorization

ID	Risk category
R1	Market risk and production competition (R1)
R2	Planning (R2)
R3	Government (R3)
R4	Management risks (R4)
R5	Stakeholders (R5)
R6	Financial and economical risk (R6)
R7	Tendering and contractual (R7)
R8	Design risks (R8)
R9	Time and cost (R9)
R10	Construction and technical (R10)
R11	Quality (R11)
R12	Operation and maintenance (R12)
R13	HSE (R13)
R14	Other risks (R14)

Possible risk categories which can be found in the literature are combined in Table 1. It was found 14 key risks categories related to different phases of project life cycle for various project delivery methods.

More effective management of risks would be possible if these risks are managed from the perspective of a project life cycle.

The foregoing 14 key risks categories are allocated into different project phases as per their possible time of occurrence. Many risks may arise in more than one phase of a construction project and hence they need to be considered in more than one phase.

Table 1 contains a list of potential dangers, and Table 2 provides a concise summary of how these threats relate to each of the four phases in the construction process. Risk decision-making relies heavily on assessing the influence level, which varies greatly across lifecycles.

It is crucial to anticipate potential problems at each stage and take corrective measures as needed. However, as these threats are all stakeholder-centric, the success of the project hinges on how well various stakeholders are engaged in risk

Table 2 Risk categorization over PLC

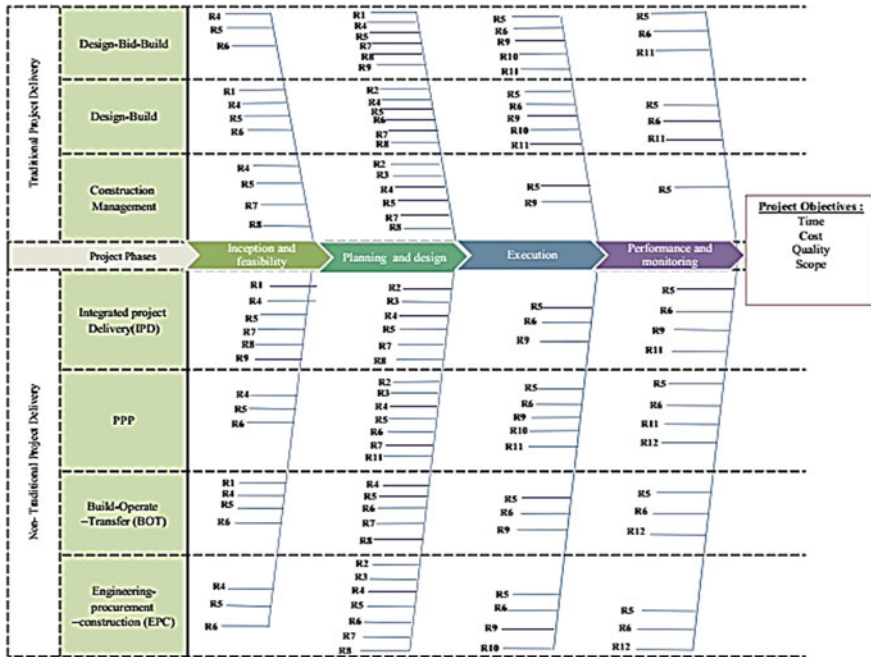| Project phase	Risk category
Inception and feasibility	R1, R4, R5, R6, R15
Planning and design	R2, R3, R4, R5, R6, R8, R9, R12, R15
Execution	R5, R6, R10, R11, R12, R15
Performance and monitoring	R5, R6, R12, R13, R14, R15

Fig. 7 Consolidation of key risk categories, delivery methods and PLC

management throughout the project's life cycle. Figure 7 is a fish-bone diagram that summarizes the project life cycle, PDMs, and key risks in a single visual.

4   Conclusions

The risk management-based selection of project delivery methods in sustainable construction can have a significant impact on the global construction industry. The selection of a project delivery method that prioritizes risk management can ensure that these sustainable practices are carried out effectively, thereby contributing to the growth of the sustainable construction sector.

Adopting risk management-based selection methods also helps avoid project delays, and related costs, enabling contractors to complete projects on schedule, within the budget, and to the satisfaction of all stakeholders. By adopting sustainable construction practices and the risk management-based selection of project delivery methods, the industry can mitigate these risks and deliver better projects.

This study provides a comprehensive literature for exploring the performance of project delivery systems. This literature allows for a better knowledge for traditional methods such as Design-Bid Build (DBB), Design-Build (DB), Construction Manager (CM), and non-traditional methods Integrated project delivery (IPD),

Public–Private-Partnership (PPP), Build-Operate-Transfer (BOT) and Engineering, Procurement and Construction (EPC) along the project life cycle starting from inception and feasibility and ended by performance and monitoring systems operate in terms of their organizational structure and contractual relationships.

The purpose of this research was to identify the most pressing threats to meeting the project's financial, schedule, quality, and scope goals.

This preliminary investigation is founded entirely on a survey of previous research and expert opinion. The findings determined the causes of Project Delivery Methods (PDMs) risk factors, which were categorized into15 major groups. They are Market risk and Production Competition (R1), Planning (R2), Government (R3), Management Risks (R4), Stakeholders (R5), Financial and Economical risk (R6), Tendering and Contractual (R7), Design Risks (R8), Time and cost (R9), Construction and Technical (R10), Quality (R11), Operation and maintenance (R12), Health and safety risks (R13) and Other Risks (R14).

It has been evident that the Tendering and contractual risks for various PDMs in project development and planning have been widely studied. However, how construction risks, operational performance over post construction phase associated to various types of PDMs have not been the focus in the past studies.

Overall, the risk management-based selection of project delivery methods in sustainable construction has the potential to enhance the construction industry's sustainability, profitability, and reputation.

5   Recommendations

Future research must be focused on qualitative and quantitative risk analysis on various PDMs and their effect on the project life cycle. The findings can help the scholars and practitioners in the construction sector advance their knowledge on risk management for various PDMs, as well as provide direction for future research.

References

1. Adamtey SA (2021) A case study performance analysis of design-build and integrated project delivery methods. Int J Constr Educ Res 17(1):68–84
2. Adel G, Othman AAE, Harinarain N (2022) Integrated project delivery (IPD): an innovative approach for achieving sustainability in construction projects. In: Construction in 5D: deconstruction, digitalization, disruption, disaster, development: proceedings of the 15th built environment conference. Springer
3. Ahmed S, El-Sayegh S (2021) Critical review of the evolution of project delivery methods in the construction industry. Buildings 11(1):1–25
4. Ahmed S, El-Sayegh S (2022) The challenges of sustainable construction projects delivery—evidence from the UAE. Arch Eng Des Manage 18(3):299–312
5. Ahmed S, El-Sayegh S (2023) Relevant criteria for selecting project delivery methods in sustainable construction. Int J Constr Manage 23:1–9

6. Aven T (2017) Improving risk characterisations in practical situations by highlighting knowledge aspects, with applications to risk matrices. Reliab Eng Syst Safety 167: 42–48

7. Azhar N, Kang Y, Ahmad IU (2014) Factors influencing integrated project delivery in publicly owned construction projects: an information modelling perspective. Proc Eng 77:213–221

8. Badiru A, Osisanya S (2016) Project management for the oil and gas industry: a world system approach

9. Banihashemi S, Hosseini MR, Golizadeh H, Sankaran S (2017) Critical success factors (CSFs) for integration of sustainability into construction project management practices in developing countries. Int J Project Manage 35(6):1103–1119

10. Chege LW, Rwelamila P (2000) Risk management and procurement systems-an imperative approach. CIB REPORT, pp 373–386

11. Chen Z, Liu P, Yang Y (2017) Integrated project delivery method to sustainable construction. In: 7th international conference on education, management, information and mechanical engineering (EMIM 2017). Atlantis Press

12. Cheng C, Wang Z (2009) Public private partnerships in China: making progress in a weak governance environment. Briefing Series 56

13. Cheng R (2012) IPD case studies

14. Darwish M (2017) Construction project delivery methods. www.researchgate.net/publication/320165827_Construction_Project_Delivery_Methods

15. Ehi-Uujamhan O (2016) The complements towards developing a new risk management framework and Its applicability to the Nigerian power sector (Doctoral dissertation, Aston University)

16. Engebø A, Lædre O, Young B, Larssen PF, Lohne J, Klakegg OJ (2020) Collaborative project delivery methods: a scoping review. J Civil Eng Manage 26(3):278–303

17. Erbas I (2016) Barriers of traditional project delivery system in achievement of project goals

18. Fong CK, Avetisyan HG, Cui Q (2014) Understanding the sustainable outcome of project delivery methods in the built environment. Org Technol Manage Constr 6(3):1141–1155

19. Guo Q, Xu Z, Zhang G, Tu T (2010) Comparative analysis between the EPC contract mode and the traditional mode based on the transaction cost theory. In: 2010 IEEE 17th international conference on industrial engineering and engineering management. IEEE

20. Hale D, Shrestha P, Gibson G, Migliaccio G (2009) Empirical comparison of design/build and design/bid/build project delivery methods. J Constr Eng Manage 135:579–587

21. Hosseini A, Lædre O, Andersen B, Torp O, Olsson N, Lohne J (2016) Selection criteria for delivery methods for infrastructure projects. Proc-Social Behav Sci 226:260–268

22. Katar I, Howeidy D (2018) Effective construction utilizing design-build vs. design-bid-build methods; 5-feature appraisal (timedrawings-calendar-communication-changes. Int J Civil Eng Technol 9:921

23. Luka G, Ibrahim Y (2015) Identification and assessment of key risk factors affecting public construction projects in Nigeria: stakeholders perspectives. The Nigerian Institute of Quantity Surveyors: 2nd research conference

24. Lyons T, Skitmore M (2004) Project risk management in the Queensland engineering construction industry: a survey. Int J Project Manage 22:51–61

25. Mahdi IM, Alreshaid K (2005) Decision support system for selecting the proper project delivery method using analytical hierarchy process (AHP). Int J Project Manage 23(7):564–572

26. Mesa HA, Molenaar KR, Alarcón LF (2016) Exploring performance of the integrated project delivery process on complex building projects. Int J Project Manage 34(7):1089–1101

27. Mesfin A (2014) A study on construction contract risk management practices in Ethiopian building construction projects. Addis Ababa university, Ethiopia

28. Mitchell BP (1999) The applicability of the Spearin doctrine: do owners warrant plans and specifications? Find Law for Legal Professionals

29. Mitkus S, Mitkus T (2014) Causes of conflicts in a construction industry: a communicational approach. Proc Soc Behav Sci 110:777–786

30. Molenaar K, Sobin N, Gransberg D, McCuen T, Korkmaz S, Horman M (2009) Sustainable, high performance projects and project delivery methods: a state-of-practice report. White Paper for the Design-Build Institute of America and the Charles Pankow Foundation, published September 1, 2009 (online). Retrieved November 17, 2009 from http://www.dbia.org/NR/rdonlyres/AA033026-60BF-495B9C9C-51353F744C71/0/Sep2009ReportPankowDBIA.pdf
31. Parra N, Nagi A, Kersten W (2018) Risk assessment methods in seaports: a literature review
32. Ramli NH, Adnan H, Azrin Baharuddin HE, Bakhary NA, Rashid ZZA (2022) Financial risk in managing public-private partnership (PPP) project. IOP Conf Ser Earth Environ Sci 1067(1):012074
33. Shawish WA (2018) The study of project risk management implementation critical success factors and construction project success: a correlation Study, The British University in Dubai (BUiD)
34. Smith NJ, Merna T, Jobling P (2014) Managing risk in construction projects. Wiley
35. Strang W (2002) The risk in CM "at-risk." Des Build 4:19
36. Sun C, Wang M, Zhai F (2021) Research on the collaborative application of BIM in EPC projects: the perspective of cooperation between owners and general contractors. Advances in Civil Engineering
37. Tang L, Shen G, Cheng EWL (2010) A review of studies on Public-Private Partnership projects in the construction industry. Int J Project Manage 28:683–694
38. Tariku R (2016) Project delivery systems and their effects on cost and time overrun on ethiopian road authority projects
39. Tran DQ, Molenaar KR (2015) Risk-based project delivery selection model for highway design and construction. J Constr Eng Manage 141(12):04015041
40. Trauner Consulting Services (2007) I. Construction project delivery systems and procurement practices: considerations, alternatives, advantages, disadvantages
41. Viana M, Bonaventura H, Mohammad M, Kahvandi Z (2020) Integrated project delivery (IPD): an updated review and analysis case study. J Eng Project Prod Manage 10:147–161
42. Wang T, Tang W, Du L, Duffield CF, Wei Y (2016) Relationships among risk management, partnering, and contractor capability in international EPC project delivery. J Manage Eng 32(6):04016017
43. Zhang X (2005) Criteria for selecting the private-sector partner in public-private partnerships. J Constr Eng Manage 131(6):631–644
44. Zhao Q (2017) Key points of precast structure construction deep design. Constr Technol 46(4):21–24

A Strategy to Create a City Brand as a Tool to Achieve Sustainable Development (Case Study: Branding of Port-Said City-Egypt)

Shaimaa R. Nosier and Nancy M. Badawy

1 Introduction

According to Egypt's 2030 vision and 17 sustainable development goals, City branding has become one of the main objectives of regeneration for many cities, as it aims to put a trademark for cities to attract foreign direct investment support, develop tourism and advance the city [1] cultural heritage can help shape a city's identity through city branding [2]. Heritage buildings can be used to create a sense of identity and belonging for citizens, as well as attract tourists and investors to the city [3, 4] Limited research has been done on how heritage buildings can be used as a key element in city branding and how it promotes the sense of nationalism and patriotism among the population and increases the attraction of tourist locations [5]. Meanwhile, economic interests in urban tourism and related cultural sectors coexist peacefully with social and cultural goals of maintaining national heritage [6].

City branding impacts the three-axis economic, social, and environmental [7, 8]. First, the economic axis. by maximizing the economic value of city marketing and complete reliance on the continuation of the economy, as well as by utilizing everything genuine and readily available in the city, as well as by ensuring the sustainability of investment sources and tourist attractions that sustain the city development [9], second, the social axis and the goal of the citizen through the revival of cultural and moral legacy, customs and traditions And raise the standard of living and the rate of employment, then enhance the culture and identity of each city and establish celebrations, seminars, conferences, etc., and publish the image of the city around the world, and the integration of the national cultural heritage with other cities in the

S. R. Nosier (✉) · N. M. Badawy
Architectural Engineering and Urban Planning Department, Faculty of Engineering, Port Said University, Port Said, Egypt
e-mail: shaimaa.nosier@eng.psu.edu.eg

N. M. Badawy
e-mail: n.badawy@eng.psu.edu.eg

593

cultural system of the country [10], third, the environment axis, especially the development of the urban environment of the city through interest in heritage buildings. The distinction is for every city in addition to caring for modern urban growth in a framework that serves the city's identity [11].

The concept of city branding has been gaining increasing attention in recent years, as cities around the world have sought to differentiate themselves from their competitors and create a unique identity. This has led to a growing body of research on the various frameworks and strategies used to achieve successful city branding. There is an increasing focus on the role of heritage buildings in city branding, as these can be used to create a sense of place and evoke positive emotions in potential visitors [12, 13]. Furthermore, studies have highlighted the importance of incorporating local culture and history into city branding initiatives [14, 15]. Also, Garcia-Lopez et al. explored how digital technologies can be used to enhance city branding efforts [16, 17].

To reach the city branding, procedures for choosing all positive factors for the place, then distinguishing between them, then promoting its new image through geographical characteristics of the place [18]. The city's marketing process means designing a place that meets the needs of the targeted markets. The brand system succeeds when it meets the needs of citizens and companies in their societies and meets the expectations of visitors and investors in the city [19].

The goal of this paper is to investigate the steps of successful city branding and put a framework for implementation in Port-said city in Egypt. This paper contributes to a clear framework for comprehensive and sustainable development contributing to Sustainable Development Goal 11 (SDG 11) Smart Cities and Communities in its economic, social, environmental, and urban aspects. It also contributes to achieving the purpose of political practice, which is serving the individual, achieving equality, social justice, and equal opportunities. The research consists of three parts, steps for reaching successful city branding, a comprehensive theoretical framework to city branding, and a case study for implementation in Port-said in Egypt, as shown in Fig. 1

2   Literature Review

188 relevant city branding research studies were found and obtained through iterative searches in various databases of the literature Scopus and Wos over years 2013–2023. Figure 2 mentions the keywords of topics related to city branding as analyzed by the VOS viewer, as shown in Fig. 2.

Culture heritage, heritage conservation, economic development, sustainable development, tourism, and brand equity were the keywords mentioned in the city branding. The studies most mention countries with heritage and historical cities, as illustrated in Fig. 3 were the ancient countries, with significant increase in numbers of city branding projects in Europe, regardless of the Middle East and Africa cities.
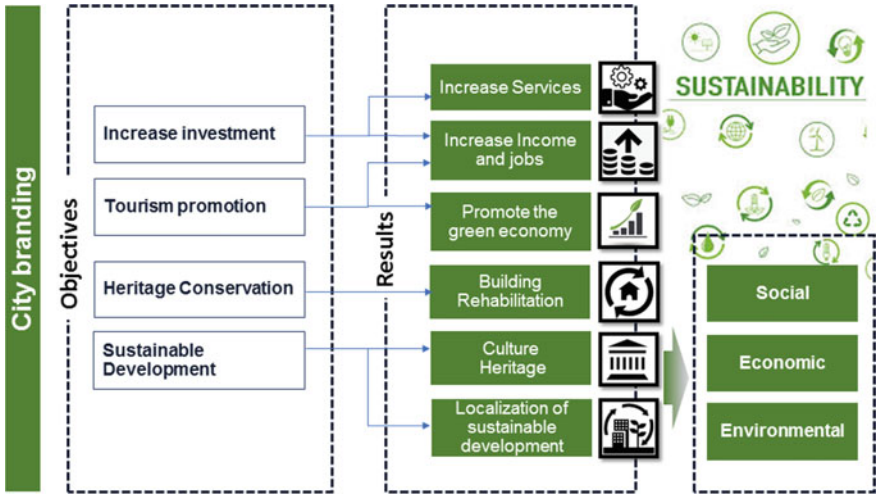
Fig. 1 Graphical abstract of research goals, objectives, and results. *Credit* The authors
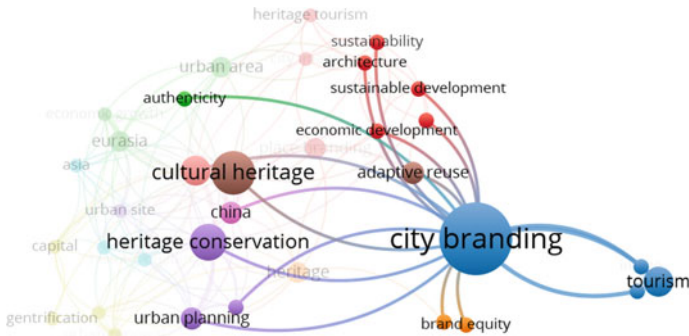

Fig. 2 Analysis of the keywords of Scopus research on city branding using the VOS viewer. *Credit* The authors
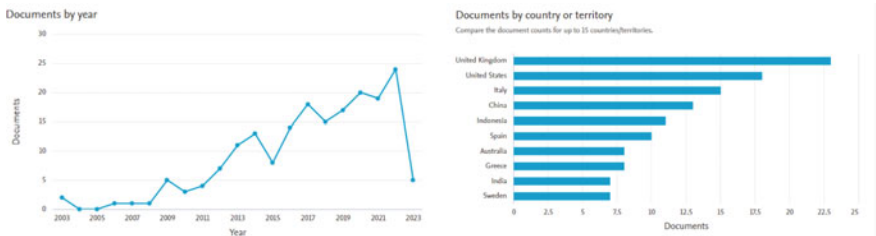

Fig. 3 Scopus analysis of research on city branding. *Credit* The authors

Researchers generally tend to heavily rely on case studies as methodology employed rather than comparative and multi-case studies, there is three main emerging perspectives can be seen when it comes to the current theoretical framework of the research field of city branding: (1) branding as production (with a focus on how to produce, create, and manage a brand as well as how to organize and govern a branding process); (2) Critical studies of city branding as a positive or negative influence on the economic, social, and cultural environment; and (3) branding as appropriation with emphasis on the reception, use, and consumption of the brand, as well as on the interpretation and utilization of the branding process [20]. Some studies were selected and divided into four categories based on steps to build city identity, Emotive visual city image, Existential Genuineness, Sense of community identity and Local culture and city development history.

Researchers generally tend to heavily rely on case studies as methodology employed rather than comparative and multi-case studies, there is three mains.

Emerging perspectives can be seen when it comes to the current theoretical framework of the research field of city branding: (1) branding as production (with a focus on how to produce, create, and manage a brand as well as how to organize and govern a branding process); (2) Critical studies of city branding as a positive or negative influence on the economic, social, and cultural environment; and (3) branding as appropriation with emphasis on the reception, use, and consumption of the brand, as well as on the interpretation and utilization of the branding process [20]. Some studies were selected and divided into four categories based on steps to build city identity, Emotive visual city image, Existential Genuineness, Sense of community identity and Local culture and city development history.

2.1 Emotive Visual City Image

The emotive city image describes how people see the city according to personal experience. According to Sahin and Baloglu [21], it is essential to include the affective component of a city's image while assessing it. The emotive city image is also treated by Ekinci and Hosany as a factor in predicting people's impressions of a city and their propensity to suggest it. The construct known as the "affective image of a city" has been extensively accepted and used to describe an individual's [22].

2.2 Existential Genuineness

Ram et al. describe Existential genuineness as how visitors felt during visiting the city. Existential authenticity refers to a feeling of pleasure and escape in a place [23]. Domnguez-Quintero et al. mention it as existential authenticity, which he describes as the process of discovering one's true self in a strange place and the relationships between existential authenticity and visitor feelings [24].

2.3 Sense of Community Identity

Sense of community is defining as "a feeling of belonging, a feeling that members matter to one another and to the group" [25] characterized by Los as the social construction influenced by contemporary political, economic, and social issues [5]. A heritage site can serve as a common link for people to their ancestry. It aids in the growth and enrichment of people's cultural identities as cohesive groupings within many contexts, including geography, history, aesthetics, and religious beliefs [26].

2.4 Local Culture and History of Development of the City

Preservation of historic sites can aid in the creation of urban areas' place-specific characteristics [2]. Understanding the healthy co-existence of the ancient and the new is crucial for maintaining local culture and features [27]. People's sense of place and identity is negatively impacted when historic buildings are demolished and replaced with new ones, as this fails to preserve the social and cultural essence of certain locations [28]. Maintaining traditional identity operations in local communities undergoing urban transformation is particularly difficult.

3 Research Methodology

Many Egyptian cities lack the attractions that encourage attracting investments and enhancing their economy, in addition to placing them on the ranks of tourist cities, which negatively affects their residents despite owning especial identity.

Comprehensive approach: City branding in heritage cites requires a comprehensive approach that considers the history, culture, and identity of the area.

- The first step is to identify the unique characteristics of the heritage site and the values that it holds. This can be done through research and consultation with local stakeholders (different participants). Once the values have been identified, the next step is to develop a brand strategy that reflects these values and communicates them to the public. This can include creating a logo, slogan, and other visuals that represent the heritage site.
- The second step is to create a marketing plan that outlines how the brand will be communicated to the public. This plan should include a mix of traditional and digital marketing tactics such as advertising, public relations, social networks, and events. It should also include a budget and timeline for use empirical study, a variety of mixed data collection techniques will be used: visualization techniques, structural observations, descriptive analysis, and case study in respect for this the research uses three questions:

A. How can cities compete globally in attracting investments and marketing themselves through their tourism, cultural, commercial, industrial, and environmental characteristics?
B. How can the buildings of the city branding contribute to highlighting its advantages?
C. What is the impact of establishing the city brand on the location of sustainable development and the achievement of its social, environmental, and economic aspects?

4   Definitions of City Branding

First, you should know that the identity of the city refers to the unique characteristics, values, and culture that define a city and differentiate it from other destinations. It is the core of the city's branding and marketing efforts and is a key factor in attracting visitors, investors, and residents [29]. Three terms in this aspect must be distinguished: City branding, city marketing, and city promotion are related concepts that are used to promote a city and attract visitors, investors, and residents. However, each have distinct roles and objectives.

City branding is a strategic process that involves creating and managing a unique identity and image for a city [30]. The goal of city branding is to differentiate the city from other destinations and create a compelling message that resonates with the target audience. City branding is a long-term process that requires a comprehensive strategy and a commitment to building the city's brand and reputation [31].

City marketing is a tactical process that involves promoting the city's attractions, events, and offerings to the target audience [32]. The goal of city marketing is to generate interest and awareness of the city and encourage visitors, investors, and residents to engage with the city. City marketing is typically focused on short-term campaigns and initiatives that support the overall brand strategy [33].

City promotion is a specific type of city marketing that involves promoting the city's attractions and events to potential visitors, investors, and residents [34]. City promotion can include a range of tactics such as advertising, public relations, events, and digital marketing. The goal of city promotion is to generate interest and awareness of the city and encourage people to visit, invest, or live in the city [14].

Overall, city branding is the strategic process of creating and managing a unique identity and image for a city, city marketing is the tactical process of promoting the city's offerings, and city promotion is a specific type of city marketing that focuses on promoting the city's attractions and events. All three concepts are important to promote a city and attract visitors, investors, and residents, the relationship between them is sequential and overlapping, as shown in the Fig. 4.

And effective city branding, marketing, and promotion require a comprehensive and integrated approach that involves collaboration between various stakeholders, including city officials, tourism boards, business owners, and marketing professionals. It is important that all these activities are aligned with the city's overall
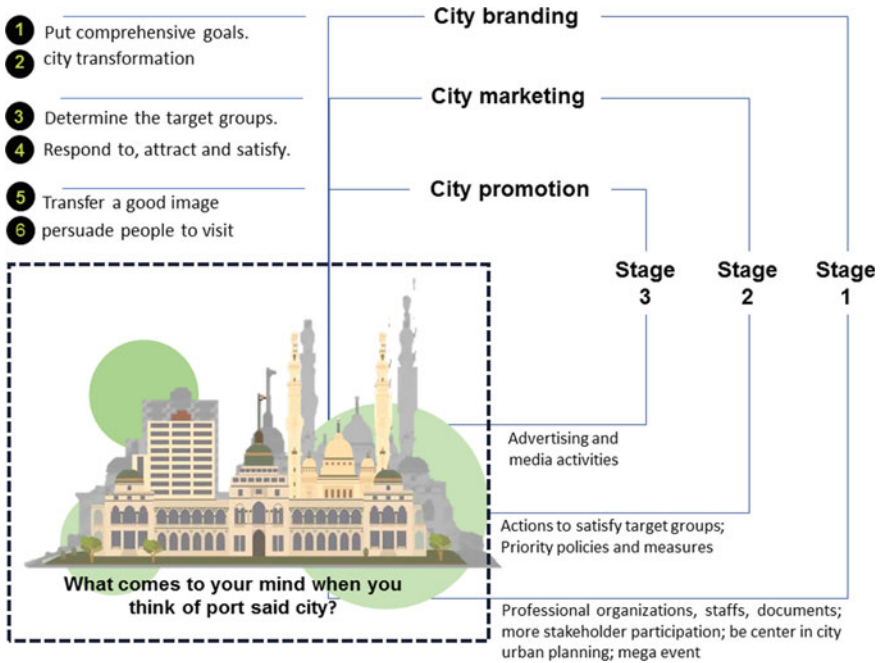
Fig. 4 Main stages of the strategy of city branding city promotion, city marketing and city branding. *Credit* The authors, after [36]

goals and objectives and are designed to create a positive image of the city and enhance its reputation. And city identity is a crucial component of city branding and promotion. By developing a strong and authentic city identity, cities can enhance their reputation, attract visitors, investors, and residents, and improve their economic and social well-being.

5 Steps Towards City Branding

The steps in the city branding process can vary depending on the specific context and goals of the branding initiative; in Egypt, our goals are closely related to Egypt's Vision 2030 and the seventeenth Sustainable Development Goals through the realization of three main aspects [35].

1. **The economy axis**: Enhancing the economic value through marketing the city and relying entirely on the continuity of the economy by exploiting everything that is authentic and available in the city. With the sustainability of the sources of investment and points of attraction for tourism, the economy and all its consequences will be sustainable.

2. **The social axis**: reviving cultural and ethical legacy—customs and traditions—folklore—raising the standard of living—raising employment rates—paying attention to the historical heritage of the place and raising the sense of identity and belonging—the openness of Egyptian culture to the world—the integration of the Egyptian cultural heritage into the international cultural system.
3. **The environmental axis**: the urban development of the city through paying attention to the heritage and distinctive buildings of each city, in addition to paying attention to urban growth in a framework that serves to highlight the city's identity.

6   Stakeholders in City Branding

Stakeholders are groups or individuals who are interested in the success of a city branding initiative. Effective city branding requires collaboration and engagement with a range of stakeholders to build support for the brand and ensure its success. Some of the key stakeholders in city branding may include.

1. City officials, city officials such as mayors, city council members, and economic development officers, play a crucial role in city branding. They are responsible for establishing policies and strategies that support the city's economic development and reputation [37].
2. Local businesses: local businesses are important stakeholders in city branding, as they are key contributors to the city's economy and can help promote the city to their customers and clients. They may also be involved in the sponsoring of events and initiatives that promote the city [38].
3. Residents: residents are important stakeholders in city branding, as they are the ones who live and work in the city and can help promote it to others. Engaging residents in the branding process can help build support for the brand and create a sense of community pride [39].
4. Tourism industry: the tourism industry is a key stakeholder in city branding, as it is responsible for promoting the city as a destination to visitors. Tourism boards, hotels, and other tourism-related businesses can help promote the city's brand and attract visitors [40].
5. Educational institutions: educational institutions such as universities and colleges are important stakeholders in city branding, as they attract students and faculty to the city and can help promote it as a center for education and innovation.
6. Community organizations: Community organizations such as chambers of commerce, nonprofit organizations, and cultural groups can play an important role in city branding by promoting the city's culture, heritage, and attractions [41].

In general, effective city branding requires collaboration and engagement with a range of stakeholders to build support for the brand and ensure its success. By involving key stakeholders in the branding process, cities can create a sense of community pride and build support for their economic and social development.

7 Building Strategy of Port Said Branding and Marketing Framework

Developing a city branding strategy for Port Said would involve several key steps, which include a strategic approach that incorporates the commercial, social, and environmental aspects as follows and illustrated in Fig. 5.

Seven key steps for implement sustainable development:

1. **Define a clear objective after research**: Conduct research to understand Port Said's unique identity [43], strengths, weaknesses, opportunities, and threats. This can include Port Said's geographic features, heritage cultural elements, tourism features, and industrial ingredients.

Port Said has several unique characteristics and strengths that can be leveraged in its branding efforts, including Geographical Characteristics: Strategic Location, which is located at the entrance of the Suez Canal, making it a key hub for global trade and transportation.in addition to Mediterranean Sea. Cultural Heritage: the Suez
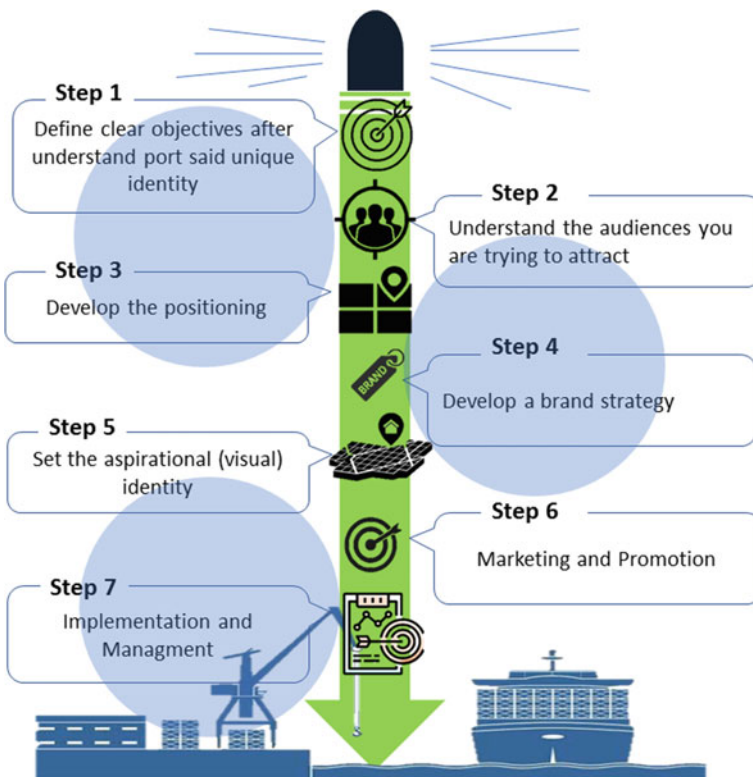
Fig. 5 Key steps of City branding strategy for Port Said. Credit: the authors, after, [14, 29, 37, 42]

Canal Authority building—the base of the Deleseps Statue—the Military Museum—the memorial—Port Said Lighthouse—640 heritage buildings, including ancient religious ones such as cathedrals, churches, mosques, consulates, villas and residential buildings—the historic island of Tennis and a nature reserve—Ashtoum Aljamil Reserve. Tourism Potential: fishing areas for amateurs—the coastal walkway—tourist villages—the new fish market, which has become a major destination for visitors to Port Said. Industrial ingredients: fisheries—industrial zone. Economic Potential: Port Said has the potential to become a major center for logistics and industry, with several large-scale projects underway to develop the city's infrastructure and attract investment. Goals can be formulated initially as follows:

- Competition on both the local and global levels
- Transition to a sustainable green economy
- Stimulating and encouraging tourism and investment
- Raising the standard of living

2. **Understand the audience**: selecting the right target audiences and prioritized According to importance, such as domestic and foreign tourists.
3. **Develop Positioning**: Based on the research, develop a positioning statement that captures the essence of Port Said and differentiates it from other destinations. The positioning statement should be unique, compelling, and relevant to the target audience. We can take several steps as:

   (a) Investing in tourism infrastructure to accommodate the expected tourist traffic and increase hotel capacity from 10 hotels with a capacity of 1750 beds, plus 3 youth hostels, to double that capacity as a first stage.
   (b) Repurposing the nearby tourist villages, such as Al-Jamil and others, to attract more visitors to the region.
   (c) Activating Al-Jamil Airport in the west of Port Said to encourage companies to include the governorate in their tourism programs.
   (d) Promoting the concept of one-day tourism (locally and through international tourist ships) and creating a varied program for Port Said's landmarks.
   (e) Offering sea tourism trips in the canal, establishing a marina for yachts on the beaches, and revitalizing amateur fishing activities.
   (f) Utilizing the investment area in South Port Said.
   (g) Focusing on the production resulting from the fish wealth, such as establishing a canned fish industry.

4. **Brand strategy**: Develop a brand strategy that include the three main axis, the economic axis, the social axis, the environmental axis and outlines key elements of Port Said's brand, including its positioning, personality, values, and messaging. The brand strategy should provide a clear direction for all city branding and promotion activities, as illustrated in Fig. 7.
5. **Visual identity**: Create a visual identity for Port Said that includes the design of a logo, color scheme, typography, and other visual elements that will be used to represent the city. The visual identity should be memorable and reflect the

brand's positioning and personality. The following Fig. 6 is a presentation of an experiment carried out by Port Said University- College of Engineering to create a logo that embodies the identity of the city of Port Said and circulate as a logo for the Engineering Department of Architectural and urban planning, and so was the competition at the Arab academy for science, technology and maritime transport. It can be applied to:

- Main transportation means taxis and buses of the governorate.
- Advertising billboards in various locations in the city, in addition to the possibility of seeing them during the passage of ships through the Suez Canal.
- Promotion on social media and various websites.
- Advertising brochures—printing on clothing.

6. **Marketing and promotion**: Develop a comprehensive marketing plan that includes a range of tactics such as advertising, public relations, events, and digital marketing. The marketing plan should be adapted to the specific needs and preferences of the target audience.
7. **Implementation and management**: Implement and manage the city branding and promotion initiatives effectively to ensure that the branding is consistent and aligned with the brand strategy. This may involve working with various stakeholders, including city officials, tourism boards, business owners, and marketing professionals (Fig. 7).
8. **Evaluation**: Regularly evaluate the success of the city branding and promotion initiatives to determine their effectiveness and identify areas for improvement. This can include tracking metrics such as website traffic, visitor numbers, and economic impact.

These steps provide a general framework for city branding in Port Said, but the specific process can vary depending on the goals and context of the initiative. Successful city branding requires a strategic approach, long-term commitment, and collaboration between various stakeholders.

Table 1 describe the implementation of the intensive framework to achieve sustainability through city branding steps, the participants and each one role.

The implementation of the intensive framework that includes social, economic, and environmental axis to achieve sustainability through city branding steps involves various participants and their respective roles. The social axis focuses on improving the quality of life of citizens through community engagement, cultural preservation, and social inclusion. The economic axis aims to promote economic growth and development by attracting investments, creating job opportunities, and supporting local businesses. The environmental axis prioritizes sustainable practices such as reducing carbon emissions, promoting renewable energy sources, and preserving natural resources. Participants in this framework include city officials, community leaders, business owners, environmental advocates, and citizens themselves. Each participant plays a crucial role in implementing sustainable practices within their respective areas of expertise to achieve a more sustainable future for the city.
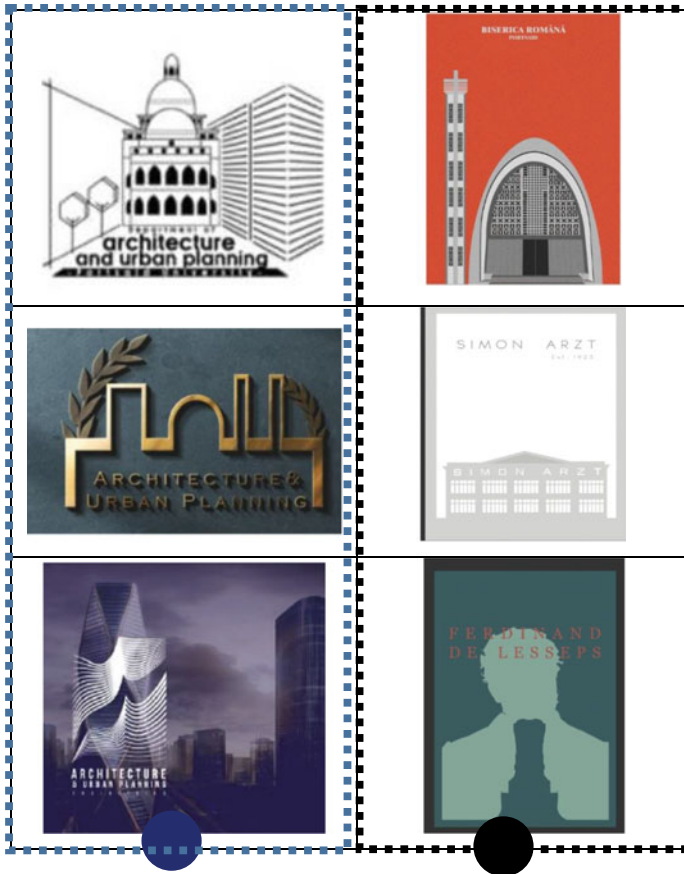
Fig. 6 Faculty of Engineering, Port-Said University. Arab Academy for Science, Technology and maritime transport. *Credit* PSU, AAST

8 Discussions and Recommendations

The branding strategy should address the commercial, social, and environmental aspects of the city. For example, the commercial axis can focus on promoting Port Said as a hub for trade, tourism and investment. The social axis can aim to improve the quality of life for residents and promote social cohesion and inclusivity. The environmental axis can focus on sustainability and preserving the city's natural and cultural heritage.

To implement the branding strategy, a dedicated team can be formed to oversee the branding process and ensure its effective implementation. The team can include representatives of the government, the business community, and civil society organizations.

Fig. 7 Building strategy of port-said branding and marketing framework. *Credit* The authors

The branding strategy can include various initiatives to promote Port Said and enhance its image.

There are some key steps that help create a successful city brand. A seven-step process can be followed to develop a city brand:

Step 1: Set clear goals; It is essential that decision makers understand the goals and objectives of the marketing initiative and what the primary objective of it is.

Step 2: Understand the audience you are trying to attract. Audiences should be kept to a minimum and prioritized based on importance.

Step 3: Determine the current brand image of the venue; The goal is to understand how the target audience perceives the place today so that the gap between the current state and the desired state can be assessed and bridged.

Step 4: Determine the desired location identity; It is how you want your target audience to see the brand and the benefits they expect to get from it. It should influence business and community decisions in the future.

Step 5: Create value propositions for priority target sectors; Once a site is defined, it is important to make it actionable for each of the target audiences. Specifically, what does brand positioning mean to this audience and what are the key messages that need to be communicated to influence their perceptions.

Step 6: Implementation of the strategy; It is essential to think about every point at which your target audience might meet your brand. Focal points may include items such as the airport, street signs, advertisements, brochures, website, events, media, and even the position of residents.

Table 1 The role of organizations and stakeholders in the building of branding steps

	Steps	Participants
1. Define clear objectives after understand port said unique identity and determine the characteristics of the city	The administrative authorities of the city are responsible for determining the characteristics of the city through the elements that characterize the city (tourist, agricultural, industrial, and commercial) also, able to determine these characteristics by conducting surveys and sharing the opinions of the community in the city	The administrative authorities of the governorates
2. The media (logo design—advertising campaigns)	Creating youth competitions for designs that are useful in advertising campaigns, such as designing slogans inspired by the city to capture the basic values of the city for the world to see. Modern advertising campaigns such as the use of mobile screens in vital places such as (squares, sporting events, historical places) and the use of social media platforms to create electronic propaganda for the city's fame and reach it to a greater number of people	Department of Public Relations in the Governorate in cooperation with colleges of applied arts (through competitions)
3. Public utilities	Community participation to know the needs of citizens and to know the facilities to be established or developed. Improving infrastructure (roads, electricity and water) to encourage investments and industries	The Ministry of Planning Ministry of Housing Governorate Ministry of Transportation Members of Parliament

(continued)

Table 1 (continued)

	Steps	Participants
4. The urban aspect and the preservation of heritage buildings	Identifying heritage places, knowing their importance, and protecting urban and historical heritage Conducting workshops and competitions to educate the community about the importance of heritage and historical places Using heritage buildings in advertising campaigns to enhance their importance Exploiting heritage buildings for important events	The National Organization for Urban Harmony (represented by heritage preservation committees in governorates) Ministry of Urban Development and Slums Departments of Architecture in faculties of engineering
5. Cultural activities	Work on developing creative industries and cultural arts Conduct workshops to promote and develop the distinctive cultural arts in the city	The Ministry of Culture and its affiliated cultural palaces
6. Investments	Facilitating laws and regulations to encourage foreign and domestic investment Facilitating procedures (banking, government, tax, manpower) for investors Training the manpower necessary for investment projects Providing places (industrial, commercial, agricultural, and tourism) ready to receive various investment sites	
7. Community participation	By involving citizens in all marketing stages through questionnaires for each stage to find out their satisfaction with it	The Ministry of Manpower Professional unions Political parties
8. Products and services	Providing the necessary markets to market the products of local and investment projects Providing the necessary services for tourism projects	The Ministry of Planning Governorate

Credit The authors

Step 7: Measure Success; The relationship between business strategy and brand becomes apparent as the return on investment is measured and the positive economic, social, and political impacts are measured over time.

Port Said city branding aimed to create an identity for the city that would attract visitors and investors and promote sustainable development. The branding strategy included developing a visual identity, creating a website, organizing events, and establishing partnerships with local businesses and stakeholders. The branding efforts have helped increase tourism to the city and have contributed to its economic growth. However, there is still room for improvement in terms of building a stronger sense of community and engaging residents in the branding process.

References

1. El-Megharbel N (2015) Sustainable development strategy: Egypt's vision 2030 and planning reform, vol 27. Minister of Planning, Monitoring, Administration and Reform, Integration Approaches to Sustainable Development of Planning and Implementation, New York
2. Yung EHK, Zhang Q, Chan EHW (2017) Underlying social factors for evaluating heritage conservation in urban renewal districts. Habitat Int 66:135–148. https://doi.org/10.1016/j.habitatint.2017.06.004
3. Al-Hinkawi WS, Zedan SK (2021) Branding for cities: the case study of Baghdad. IOP Conf Ser Earth Environ Sci 779(1):12. https://doi.org/10.1088/1755-1315/779/1/012037
4. Shahda M, Noseir S (2021) Traditional environmental treatments in Arab architecture: as a guide to contemporary architecture. Port-Said Eng Res J. https://doi.org/10.21608/pserj.2021.72763.1106
5. U. M. D. E. C. D. E. Los (2019) Study of heritage and sustainable tourism. Organization of World Heritage Cities (OWHC), Rakow, Poland
6. Dai T, Li J, Aktürk G, Jiao J (2022) The overlooked contribution of national heritage designation in city branding and tourism management. Sustain 14(14):1–17. https://doi.org/10.3390/su14148322
7. Rehan RM (2014) Urban branding as an effective sustainability tool in urban development. HBRC J 10(2):222–230. https://doi.org/10.1016/j.hbrcj.2013.11.007
8. Mohamed M (2021) Human poverty in rural communities in Egypt. A case study of Al-Sharkia Province. Sociol URBANA E Rural no. 124
9. Licciardi R, Amirtahmasebi G (2012) The economics of uniqueness: investing in historic city cores and cultural heritage assets for sustainable development. World Bank Publications. World Bank Publications. https://books.google.com.eg/books?hl=en&lr=&id=foEBbviH1-kC&oi=fnd&pg=PR5&dq=the+economic+axis.+by+maximizing+the+economic+value+of+city+marketing+and+complete+reliance+on+the+continuation+of+the+economy,+as+well+as+by+utilizing+everything+genuine+and+rea
10. Bendix R (2008) Heritage between economy and politics: an assessment from the perspective of cultural anthropology, 1st edn. Taylor& Francis
11. Bicakci A (2012) Branding the city through culture: Istanbul, European. Int J Hum Sci 9(1):13–17
12. Shamsuddin S, Ujang N (2008) Making places: the role of attachment in creating the sense of place for traditional streets in Malaysia. Habitat Int 32(3):399–409. https://doi.org/10.1016/j.habitatint.2008.01.004
13. Powell K (2010) Making sense of place: mapping as a multisensory research method. Qual Inq 16(7):539–555. https://doi.org/10.1177/1077800410372600

14. Ashworth M, Kavaratzis G (2010) Towards effective place brand management: branding European cities and regions. Edward Elgar Publishing
15. Rein I, Shields B (2007) Place branding sports: strategies for differentiating emerging, transitional, negatively viewed and newly industrialised nations. Place Brand Public Dipl 3:73–85
16. De-Marcos L, Garcia-Lopez E, Garcia-Cabot A (2016) On the effectiveness of game-like and social approaches in learning: comparing educational gaming, gamification & social networking. Comput Educ 95:99–113
17. Warnaby G, Medway D (2013) What about the 'place' in place marketing? Mark Theory 13(3):345–363. https://doi.org/10.1177/1470593113492992
18. Kavaratzis M, Ashworth GJ (2005) City branding: an effective assertion of identity or a transitory marketing trick? Tijdschr voor Econ en Soc Geogr 96(5):506–514. https://doi.org/10.1111/j.1467-9663.2005.00482.x
19. Turok I (2009) The distinctive city: Pitfalls in the pursuit of differential advantage. Environ Plan A 41(1):13–30. https://doi.org/10.1068/a37379
20. Lucarelli A, Olof Berg P (2011) City branding: a state-of-the-art review of the research domain. J Place Manag Dev 4(1):9–27. https://doi.org/10.1108/17538331111117133
21. Sahin S, Baloglu S (2011) Brand personality and destination image of Istanbul. Anatolia 22(1):69–88. https://doi.org/10.1080/13032917.2011.556222
22. Ekinci Y, Hosany S (2006) Destination personality: an application of brand personality to tourism destinations. J Travel Res 45(2):127–139. https://doi.org/10.1177/0047287506291603
23. Ram Y, Björk P, Weidenfeld A (2016) Authenticity and place attachment of major visitor attractions. Tour Manag 52:110–122. https://doi.org/10.1016/j.tourman.2015.06.010
24. Domínguez-Quintero AM, González-Rodríguez MR, Paddison B (2020) The mediating role of experience quality on authenticity and satisfaction in the context of cultural-heritage tourism. Curr Issues Tour 23(2):248–260
25. McMillan DW, Lorion RP (2020) Sense of community, pathway to, or bridge from alienation? J Commun Psychol 48(6):1706–1714. https://doi.org/10.1002/jcop.22406
26. Msengana NW (2006) The significance of the concept 'Ubuntu' for educational management and leadership during democratic transformation in South Africa. https://scholar.suCn; http://scholar.sun.ac.za/handle/10019.1/1192%5Cn; https://scholar.sun.ac.za/bitstream/10019.1/1192/1/msengana_significance_2006.pdf
27. Dutta MJ, De Souza R (2008) The past, present, and future of health development campaigns: reflexivity and the critical-cultural approach. Health Commun 23(4):326–339. https://doi.org/10.1080/10410230802229704
28. Said SY, Aksah H, Ismail ED (2013) Heritage conservation and regeneration of historic areas in Malaysia. Proc. Soc Behav Sci 105:418–428. https://doi.org/10.1016/j.sbspro.2013.11.044
29. Kavaratzis M (2004) From city marketing to city branding: towards a theoretical framework for developing city brands. Place Brand 1(1):58–73. https://doi.org/10.1057/palgrave.pb.5990005
30. Zenker S, Braun E (010) The place brand centre—a conceptual approach for the brand management of places. In: 39th European marketing academy conference, Copenhagen, Denmark, pp 1–8
31. Govers R, Go FM (2009) Tourism destination image formation. In: Handbook of tourist behavior. Routledge, pp 53–67
32. Zenker S, Erfgen C (2014) Let them do the work: a participatory place branding approach. J place Manag Dev 7(3):225–234
33. Pike S, Page SJ (2014) Destination marketing organizations and destination marketing: a narrative analysis of the literature. Tour Manag 41:202–227
34. Anholt S (2007) Nation-brands and the value of provenance. In: Destination branding. Routledge, pp 41–54
35. De Matteis S et al (2017) Current and new challenges in occupational lung diseases. Eur Respir Rev 26(146)

36. Ma W, de Jong M, Hoppe T, de Bruijne M (2021) From city promotion via city marketing to city branding: examining urban strategies in 23 Chinese cities. Cities 116:103269
37. Hanna R, Rohm A, Crittenden VL (2011) We're all connected: the power of the social media ecosystem. Bus Horiz 54(3):265–273
38. Warren G, Dinnie K (2018) Cultural intermediaries in place branding: who are they and how do they construct legitimacy for their work and for themselves? Tour Manag 66:302–314
39. Maignan I, Ferrell OC, Ferrell L (2005) A stakeholder model for implementing social responsibility in marketing. Eur J Mark 39(9/10):956–977
40. Raub SP, Martin-Rios C (2019) 'Think sustainable, act local'—a stakeholder-filter-model for translating SDGs into sustainability initiatives with local impact. Int J Contemp Hosp Manag 31(6):2428–2447
41. Karabağ SF, Yavuz MC, Berggren C (2011) The impact of festivals on city promotion: a comparative study of Turkish and Swedish festivals. Tour Int Interdisc J 59(4):447–464
42. Sameh H, El-Aziz A, Mohamed H, Hefnawy NH (2018) Building a successful city branding case study: Dubai. J Al-Azhar Univ Eng Sect 13(48):1058–1065
43. Gordon CS et al (2016) Characterization of *Triticum aestivum* abscisic acid receptors and a possible role for these in mediating Fusairum head blight susceptibility in wheat. PLoS ONE 11(10):e0164996

Towards an Action Plan to Improve the Role of Perforated Building Envelopes in Sustainable Design

Marwa Fawaz ⓘ**, Naglaa Ali Megahed** ⓘ**, Basma N. El-Mowafy** ⓘ**, and Dalia Elgheznawy** ⓘ

1   Introduction

As a result of the growing awareness of the importance of taking urgent action to combat climate change and its impact on indoor environmental quality (IEQ) and sustainability in accordance with the 13th goal of the Sustainable Development Goals (SDGs) on climate change, there have been many studies and recent techniques for breathing building envelopes, including the use of perforated envelopes to create a second-skin façade used by architects and designers [1–3]. Perforated building envelopes can be defined as facades or exterior walls of buildings that feature a series of small openings, or perforations, that allow air and light to pass through while still providing a barrier against wind, rain, and other weather elements [4, 5]. Moreover, these perforations can be of varying sizes and shapes and can be arranged parametrically in a pattern or random configuration [5, 6]. Furthermore, they are used through adaptations of traditional techniques to improve natural ventilation and daylighting, reduce energy consumption, and create a visually exciting street view [7, 8]. Today, perforated building envelopes are used in a variety of building types, including commercial, residential, and institutional structures [6, 9]. Additionally, new materials and manufacturing processes have enabled greater customization and

M. Fawaz (✉) · N. A. Megahed · B. N. El-Mowafy · D. Elgheznawy
Architecture and Urban Planning Department, Faculty of Engineering, Port-Said University, Port Said 42526, Egypt
e-mail: marwa.fawaz@eng.psu.edu.eg

N. A. Megahed
e-mail: Naglaaali257@eng.psu.edu.eg

B. N. El-Mowafy
e-mail: basma_nashaat@eng.psu.edu.eg

D. Elgheznawy
e-mail: dalia_elgheznawy@eng.psu.edu.eg

flexibility in perforation patterns, shapes, and sizes, giving designers and architects new opportunities for creativity and innovation [1, 10, 11].

Conversely, Sustainable design seeks to reduce negative impacts on the environment and the health and comfort of building occupants, thereby improving the building's performance [12, 13]. The basic objectives of sustainability are to reduce the consumption of non-renewable resources, minimize waste, and create healthy, productive environments [14, 15]. As a result, perforated building envelopes are becoming increasingly popular in sustainable design because of their ability to benefit the environment by lowering carbon emissions associated with energy consumption, reducing environmental impact, and improving indoor comfort [14, 16]. To that end, buildings with perforated envelopes can significantly reduce their carbon footprint by utilizing natural light and ventilation rather than artificial sources such as artificial lighting and HVAC (Heating, ventilation, and air conditioning) systems [2, 14]. Furthermore, perforated building envelopes can aid in temperature regulation is accomplished by lowering heat gain in the summer and heat loss in the winter. This can lead to improved health outcomes for building occupants as well as higher productivity [2, 14].

This research paper aims to explore the role of perforated building envelopes in sustainable design by providing an overview of the history of perforated building envelopes and their recent popularity in sustainable design. The paper examines how perforated building envelopes can contribute to sustainable design by improving IEQ, energy efficiency, and occupant comfort. The paper further explores the design considerations that should be considered when designing perforated building envelopes for sustainable design. An action plan is provided for creating perforated building envelopes that include design, material selection, and construction considerations. The paper investigates that perforated building envelopes have the potential to greatly contribute to sustainable design and should be carefully considered in building design. Figure 1 illustrates a graphical abstract for the research framework.

2   Overview of Perforated Building Envelopes Throughout History

Perforated building envelopes have been used in architecture for centuries, with their popularity and development changing over time [5, 13]. Furthermore, perforated building envelopes have long been used in architectural design, from their functional use in ancient Islamic architecture to their decorative use in modernism and contemporary designs [1]. To that end, this section will look briefly at the history and evolution of perforated building envelope roles, from the earliest examples in ancient Islamic architecture to nowadays contemporary designs, which will be investigated in Table 1 regarding their various definitions and roles.
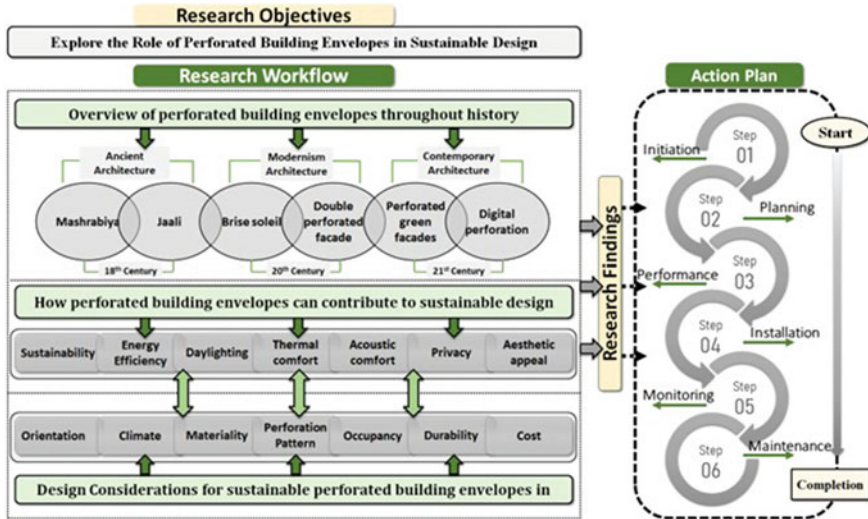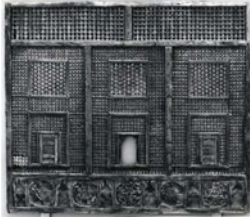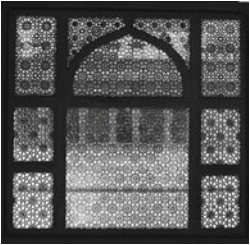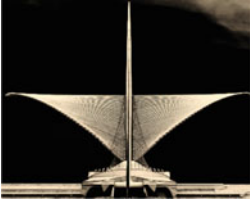
Fig. 1 Research framework, adapted by the authors

3 How Perforated Building Envelopes Can Contribute to Sustainable Design

Recently, the perforated building envelope design has numerous advantages and is highly significant, making it an excellent choice for contemporary buildings to contribute to sustainable design by developing several key factors [14, 23].

A study by [24], found that perforated screens can affect daylight penetration and natural ventilation. Another study by [25] investigated two parameters of daylight incidences to understand the daylight performance of a high-rise residential building. Also, studies by [18, 26] found that building envelope design, as determined by an appropriate assessment method, plays a significant role in building sustainability because it regulates all other factors including building element performance, thermal processes, transmission processes, and material properties. Moreover, a study carried out by [27] found that a sustainable building should be built with materials that have low life-cycle environmental impacts such as global warming, resource depletion, and human health. Furthermore, [28] also found that a sustainable building should be constructed of materials that minimize life-cycle environmental impacts such as global warming, resource depletion, and human health. Lastly, [29] discusses how perforated metal sheet facades can reduce energy costs by maintaining internal temperature, maximizing natural airflow and ventilation, and controlling solar heat.
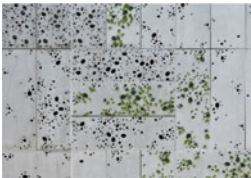
So, it can be concluded that perforated building envelopes can make a substantial contribution to sustainable design by improving IEQ, occupant comfort, and aesthetics, which will be described in points as follows:

Table 1 Development of perforated building envelopes among ages, the authors after [17–22]

Age	Element	Definition	Role	Sketch
Ancient Architecture	Mashrabiya	A wooden lattice screen with small openings in a geometric pattern to cover windows, balconies, and other building openings, used in traditional Arab Islamic architecture, particularly in the Middle East	Provide shade and privacy while also allowing air to circulate reflect the cultural and artistic heritage of the country	Mashrabiya Screen with Medallions/eighteenth century
	Jaali	A perforated stone screen or latticework in geometric shapes or calligraphy can be found in a variety of structures, such as windows, doors, balconies, and walls, and are used in Indian architecture	Allows indoor cross-ventilation and outdoor privacy while still letting light in	Jaali screens in the tomb of Salim Chishti, Fatehpur Sikri, India
Modernist Architecture mid-twentieth century	Brise soleil	A sunshade made of horizontal or vertical slats	Allow light and air to pass through while blocking direct sunlight	Art museum in Milwaukee, Wisconsin
	Double-skin perforated facades	A type of outer skin with small holes, or perforations, on the surface with an air gap between the cladding and the insulation layer	Allows for natural ventilation and moisture control	Ring-shaped 'Orange Village' in Côte d'Ivoire

(continued)

Table 1 (continued)

Age	Element	Definition	Role	Sketch
Contemporary Architecture twenty-first century	Perforated green facades	Vegetation-covered building envelopes through perforated cutouts	Help regulate temperature, improve air quality, and reduce noise pollution	 San Telmo Museum in Spain
	Digital perforation	A modern technology that uses computer-controlled laser cutting or water jetting to create intricate patterns with small holes punched into building facades made from aluminum, stainless steel, galvanized steel, copper or brass and usually designed using digital parametric tools	Add visual interest while also serving functional purposes such as shading or ventilation	 Laser cutter metal sheet

Sustainability: by reducing its environmental impact and building's carbon footprint to help create a more sustainable built environment [14, 23].

Energy Efficiency: by lowering the use of artificial lighting and mechanical ventilation, resulting in lower energy consumption and cost savings [14, 23].

Daylighting: by allowing natural light to pass through, improving occupant visual comfort and reducing the need for artificial lighting [30, 31].

Thermal comfort: by allowing ventilation and air to pass through, which can help regulate a building's temperature resulting in reducing the necessity for heating and cooling systems, and lowering the risk of indoor pollutants [24, 32].

Acoustic comfort: by reducing sound transmission between spaces and improving indoor acoustic performance [11, 17, 32].

Privacy: by obscuring the view into a building while still allowing light and air to pass through, depending on the size and location of the perforations [11, 17, 32].

Aesthetic appeal: by adding a distinctive aesthetic to a building's identity and creating a visually appealing and dynamic appearance [24, 32].

Overall, perforated building envelopes can contribute to the sustainability of a building by lowering energy consumption, material waste, and environmental impact. Designers and architects can create perforated building envelopes that are both aesthetically pleasing and environmentally responsible by considering the design of the perforations and the materials used.

4   Design Considerations for Perforated Building Envelopes in Sustainable Design

Designers and architects must consider several key factors when implementing this theoretical basis of perforated building envelopes to achieve the required sustainable design as illustrated in Fig. 2, such as:
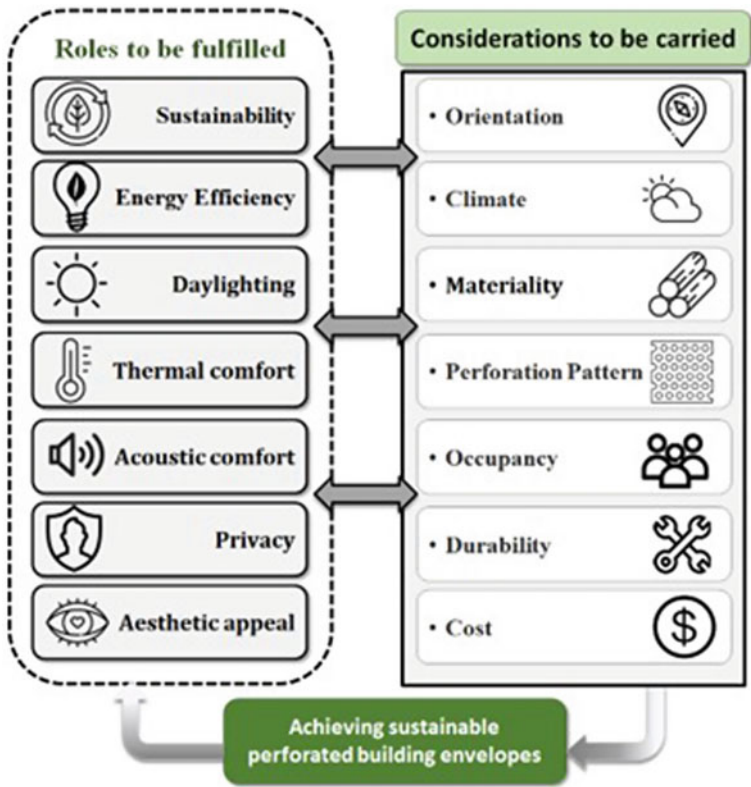
Fig. 2 Considerations for Architects and Engineers to achieve sustainable perforated building envelopes, adapted by the authors

Orientation: when determining the size and placement of perforations, designers should consider the orientation of the building to influence the amount of daylighting and air that can enter through the perforations [24, 32].

Climate: the perforation design may be influenced by the climate of the region in which the building is located. Designers in hot and humid climates, for example, should consider the possibility of moisture penetration and cast growth [27, 30, 33].

Materiality: the perforated building envelope's materials considerations and compatibility with the overall design of the building. These envelope materials can be made from sustainable materials such as like wood, bamboo, recycled steel, or low-carbon concrete, lowering their environmental impact even further [27, 30, 33].

Perforation pattern: the perforation pattern chosen will be determined by several factors, including the desired aesthetic effect, functional requirements such as ventilation or shading, and building envelope performance goals. Furthermore, the size and spacing of the perforations must also be carefully considered to ensure adequate IEQ [24, 32].

Occupancy: the type of occupancy in the building can influence the perforation design. A building used for manufacturing, for example, may require more ventilation than a building used for office space [33, 34].

Durability: the design of the perforations should consider the building envelope's durability, stability, and maintenance requirements [1, 35]. The size and placement of perforations, for example, should be designed to minimize the accumulation of debris and dirt.

Cost: the cost of a perforated building envelope must be considered, as it may be higher than that of a traditional building envelope regarding the materials and design used. This can have an impact on the project's overall budget and may limit its feasibility [2, 34].

Overall, the theoretical basis for perforated building envelopes should consider the impact of building orientation, climate, occupancy, and maintenance requirements on perforation design. By taking these factors into account, designers and architects can create sustainable perforated building envelopes that improve IEQ and provide occupants with a more comfortable and healthier indoor environment.

5 Results and Discussion

Overall, the development of perforated building envelope roles has been fueled by a growing recognition of the value of IEQ, sustainability, reduced environmental impact, and aesthetics. As these priorities shift, the use of perforated building envelopes will likely shift as well.

Furthermore, the overview of perforated building envelopes throughout history revealed that perforated facades have been utilized by many cultures to control light,

heat, and air movement in buildings. The use of perforated building envelopes in contemporary architecture has evolved to incorporate a sustainable design approach with energy optimization.

As, sustainable perforated building envelopes can range from simple openings in walls or roofs to more complex systems that include features such as louvers, screens, or shading devices. To that end, a step-by-step action plan for a sustainable perforated building envelope is extracted based on [5, 6, 31, 36], as described in Table 2.

In conclusion, according to the above steps in Table 2, developing a successful action plan for implementing perforated building envelopes for different climates requires careful consideration of a range of aspects, including design objectives, temperature and weather conditions, site analysis, material selection, perforation pattern design, testing, fabrication, installation, and maintenance. By considering these aspects, working with a qualified design professional and installer can help ensure that the perforated building envelope meets all relevant requirements while also meeting the desired aesthetic and functional goals and contribute to sustainable design.

Furthermore, this introduced action plan for implementing perforated building envelopes provides a comprehensive guide for architects and engineers to incorporate perforated facades into their designs. The plan emphasizes the importance of collaboration, effective communication, and continuous evaluation to ensure the successful implementation of perforated building envelopes in sustainable building design. Finally, it can be expected that even greater advancements in sustainable construction practices in the coming years as more architects and builders embrace these innovative designs.

6   Conclusions

Perforated building envelopes are an important component of sustainable design because they provide numerous benefits such as energy efficiency, improved IEQ, thermal comfort, and aesthetic appeal. That can achieve SDGs 13th goal with more sustainable buildings that promote environmental conservation and human well-being, architects and designers must consider incorporating these elements into their designs.

Overall, studying perforated building envelopes is important because it can lead to more efficient, sustainable, and aesthetically pleasing building designs that improve occupant quality of life while minimizing environmental impact.

One of the primary advantages of perforated building envelopes is that they allow for natural ventilation and daylighting. Designers can promote natural airflow and reduce the need for mechanical HVAC systems by incorporating openings or perforations in the building envelope. This can result in significant energy savings and lower operating costs over the building's life.

Table 2 Step-by-step guide for sustainable perforated building envelopes, the authors after [6, 31]

The main objective of the plan

Implementing sustainable perforated building envelopes

Task	Action step 1 initiation	Action step 2 planning	Action step 3 performance	Action step 4 installation	Action step 5 monitoring	Action step 6 maintenanc
Description	Conduct a thorough site analysis to decide on the best building orientation and placement, as well as the size and location of the perforations	Incorporate renewable energy sources such as integrating solar panels, wind turbines, or bio-reactive facades Use static or dynamic perforations according to the site analysis Select eco-friendly envelope materials	Model the envelope within a building Simulate building performance to consider passive ventilation and natural daylight to reduce the need for mechanical systems	Fabricate and install the perforated panels ensuring that the building envelope meets all applicable building codes and regulations	Test and monitor the perforated building envelope performance and controls to make any necessary adjustments	Monitor and maintain and clean up to ensure that the perforations continue to function properly and look good over time
Responsibility	Site Engineer	Architect and Construction Engineer	Architect and Environmental Engineer	Construction Engineer	Environmental Engineer and Mechanical Engineer	Mechanical Engineer and Maintenance Team
Resources	Site visits Simulation-based digital tools	Cost Durability Availability Sustainability Aesthetics	Modelling digital tools Simulation-based digital tools	Laser cutter for the used materials	On-site environmental analysis tools	On-site monitoring tools

Another advantage of perforated building envelopes is their ability to reduce construction's environmental impact. Designers can reduce the embodied energy and carbon footprint of a building by using lightweight materials and minimizing the amount of material required. Furthermore, perforated building envelopes can be designed to allow for easy disassembly and reuse, which can reduce the building's environmental impact over its lifetime.

Furthermore, the roles of perforated building envelopes have evolved, from functional openings for ventilation and light in classical architecture to decorative elements in modern architecture to high-performance building envelopes. As the priorities of building design evolve, the roles of perforated building envelopes will likely evolve as well.

To that end, while perforated building envelopes can provide several sustainability benefits, designers and architects should carefully consider the potential drawbacks and limitations before implementing this action plan. Designers can create perforated building envelopes that balance sustainability, functionality, and cost-effectiveness by carefully considering the design of the perforations and the materials used as introduced in the proposed action plan.

7 Recommendations

Further studies could be done to research the optimal design properties, number and area of perforations for different climate condition and buildings types. Furthermore, it is recommended that the design of a perforated building envelope should take local building codes and regulations into account. Based on factors such as fire safety and structural integrity, these regulations may dictate the size and placement of perforations. As well as working with a qualified design professional can help ensure that the perforated building envelope design complies with all applicable codes and regulations.

References

1. Taveres-Cachat E, Favoino F, Loonen R, Goia F (2021) Ten questions concerning co-simulation for performance prediction of advanced building envelopes. Build Environ 191:107570. https://doi.org/10.1016/j.buildenv.2020.107570
2. Di Turi S, Ronchetti L, Sannino R (2023) Towards the objective of Net ZEB: detailed energy analysis and cost assessment for new office buildings in Italy. Energy Build 279:112707. https://doi.org/10.1016/j.enbuild.2022.112707
3. Habibi S, Valladares OP, Peña DM (2022) Sustainability performance by ten representative intelligent Façade technologies: a systematic review. Sustainable Energy Technol Assess 52:102001. https://doi.org/10.1016/j.seta.2022.102001
4. Taylor M, Brown NC, Rim D (2021) Optimizing thermal comfort and energy use for learning environments. Energy Build 248:111181. https://doi.org/10.1016/j.enbuild.2021.111181

5. Pelletier K, Wood C, Calautit J, Wu Y (2023) The viability of double-skin façade systems in the 21st century: a systematic review and meta-analysis of the nexus of factors affecting ventilation and thermal performance, and building integration. Build Environ 228:109870. https://doi.org/10.1016/j.buildenv.2022.109870

6. Mohanta A, Das S, Mohanty RN (2021) Building envelope trade-off method integrated with BIM-based framework for energy-efficient building envelope. Arch Eng Des Manage 17(5–6):516–536. https://doi.org/10.1080/17452007.2021.1941741

7. Liao W, Wen C, Luo Y, Peng J, Li N (2022) Influence of different building transparent envelopes on energy consumption and thermal environment of radiant ceiling heating and cooling systems. Energy Build 255:111702. https://doi.org/10.1016/j.enbuild.2021.111702

8. Hagentoft C-E, Pallin S (2021) A conceptual model for how to design for building envelope characteristics. Impact of thermal comfort intervals and thermal mass on commercial buildings in U.S. climates. J Build Eng 35:101994. https://doi.org/10.1016/j.jobe.2020.101994

9. Xue F, Zhao J (2021) Building thermal comfort research based on energy-saving concept. Adv Mater Sci Eng 2021:7132437. https://doi.org/10.1155/2021/7132437

10. Webb M (2022) Biomimetic building facades demonstrate potential to reduce energy consumption for different building typologies in different climate zones. Clean Techn Environ Policy 24:493–518. https://doi.org/10.1007/s10098-021-02183-z

11. Ge J, Li S, Chen S, Wang X, Jiang Z, Shen C (2021) Energy-efficiency strategies of a residential envelope in China's Hot Summer-Cold Winter Zone based on intermittent thermal regulation behavior. J Build Eng 44:103028. https://doi.org/10.1016/j.jobe.2021.103028

12. Shehata AO, Megahed NA, Shahda MM, Hassan AM (2022) (3Ts) Green conservation framework: a hierarchical-based sustainability approach. Build Environ 224:109523. https://doi.org/10.1016/j.buildenv.2022.109523

13. Song K, Li D, Zhang C, Liu T, Tang Y, Xie YM et al (2023) Bio-inspired hierarchical honeycomb metastructures with superior mechanical properties. Compos Struct 304:116452. https://doi.org/10.1016/j.compstruct.2022.116452

14. Elshafei M, Abdelaziz H (2023) Responsive buildings envelope integration in sustainable new cities planning strategies. Eng Res J 177:145–58. https://doi.org/10.21608/erj.2023.289032

15. Aruta G, Ascione F, Bianco N, Iovane T, Mauro GM (2023) A responsive double-skin façade for the retrofit of existing buildings: analysis on an office building in a Mediterranean climate. Energy Build 284:112850. https://doi.org/10.1016/j.enbuild.2023.112850

16. Xiang C, Matusiak BS (2022) Façade integrated photovoltaics design for high-rise buildings with balconies, balancing daylight, aesthetic and energy productivity performance. J Build Eng 57:104950. https://doi.org/10.1016/j.jobe.2022.104950

17. Bagasi A, Calautit JK, Karban A (2021) Evaluation of the integration of the traditional architectural element Mashrabiya into the ventilation strategy for buildings in hot climates. Energies 14:530. https://doi.org/10.3390/en14030530

18. Shahda MM, Noseir S (2021) Traditional environmental treatments in Arab architecture: as a guide to contemporary architecture. Port-Said Eng Res J 25(2):38–52. https://doi.org/10.21608/pserj.2021.72763.1106

19. The MET Museum https://www.metmuseum.org/art/the-collection Accessed 2023

20. SanTelmo Museoa. https://www.santelmomuseoa.eus/index.php?lang=en. Accessed 2023

21. mam: Milwaukee Art Museum. https://mam.org/. Accessed 2023.

22. Elengical J (2022) Ring-shaped 'Orange Village' in Côte d'Ivoire has a perforated double skin façade. https://www.stirworld.com/see-features-ring-shaped-orange-village-in-cote-divoire-has-a-perforated-double-skin-facade#:~:text=Said%20to%20resemble%20the%20dimples,from%20glare%20and%20solar%20gain. Accessed 2023

23. Sawantt S (2021) Blending parametric design with sustainability

24. M. ElBatran R, Ismaeel WSE (2021) Applying a parametric design approach for optimizing daylighting and visual comfort in office buildings. Ain Shams Eng J. https://doi.org/10.1016/j.asej.2021.02.014

25. Zheng Z, Zhang Y, Mao Y, Yang Y, Fu C, Fang Z (2021) Analysis of SET* and PMV to evaluate thermal comfort in prefab construction site offices: case study in South China. Case Stud Thermal Eng 26:101137. https://doi.org/10.1016/j.csite.2021.101137

26. Shahda MM, Megahed NA (2022) Post-pandemic architecture: a critical review of the expected feasibility of skyscraper-integrated vertical farming (SIVF). Arch Eng Des Manage 2022:1–22. https://doi.org/10.1080/17452007.2022.2109123

27. Hinkle LE, Wang J, Brown NC (2022) Quantifying potential dynamic façade energy savings in early design using constrained optimization. Build Environ 221:109265. https://doi.org/10.1016/j.buildenv.2022.109265

28. Hassan SR, Megahed NA, Abo Eleinen OM, Hassan AM (2022) Toward a national life cycle assessment tool: generative design for early decision support. Energy Build 267:112144. https://doi.org/10.1016/j.enbuild.2022.112144

29. Zhang J, Liu N, Wang S (2021) Generative design and performance optimization of residential buildings based on parametric algorithm. Energy Build 244:111033. https://doi.org/10.1016/j.enbuild.2021.111033

30. Zhao B, Wang C, Hu M, Ao X, Liu J, Xuan Q et al (2022) Light and thermal management of the semi-transparent radiative cooling glass for buildings. Energy 238:121761. https://doi.org/10.1016/j.energy.2021.121761

31. Le DM, Park DY, Baek J, Karunyasopon P, Chang S (2022) Multi-criteria decision making for adaptive façade optimal design in varied climates: energy, daylight, occupants' comfort, and outdoor view analysis. Build Environ 223:109479. https://doi.org/10.1016/j.buildenv.2022.109479

32. Wang L, Zhang H, Liu X, Ji G (2022) Exploring the synergy of building massing and façade design through evolutionary optimization. Front Arch Res 11(4):761–780. https://doi.org/10.1016/j.foar.2022.02.002

33. Zaera-Polo A, Anderson J (2021) The ecologies of the building envelope: a material history and theory of architectural surfaces. Actar Publishers

34. Wang Y, Wei C (2021) Design optimization of office building envelope based on quantum genetic algorithm for energy conservation. J Build Eng 35:102048. https://doi.org/10.1016/j.jobe.2020.102048

35. Abdel-Rahman WSM (2021) Thermal performance optimization of parametric building envelope based on bio-mimetic inspiration. Ain Shams Eng J 12(1):1133–1142. https://doi.org/10.1016/j.asej.2020.07.007

36. Zapico A, Egiluz Z, García Frómeta Y, Cuadrado J (2022) Mechanical characterization of double-skin perforated-sheet façades. J Build Eng 56:104750. https://doi.org/10.1016/j.jobe.2022.104750

An Efficient Deep Deblurring Technique Using Dark and Bright Channel Priors

Nouran Ali, Asmaa Abdallah , I. F. Elnahry, and Randa Atta

1 Introduction

Image blur is a distortion in the image mostly caused by camera movement, object motion, missed focus, or insufficient depth of field. The image blur problems/cases can be classified into: uniform and non-uniform blur [1, 2]. The uniform blur is caused from camera movement while the scene is static, i.e., it is modeled by single blur kernel for the whole image, while non-uniform blur happens as a result of the objects motion whereas camera is fixed.

In general, the blurred image can be formulated as

$$B = k * X + a. \tag{1}$$

where X denotes to the sharp image, B is the blurred image, k is the blur kernel, and a is an additive noise; the convolution operator '*' shows that the inverse operation is highly ill-posed problem.

Image de-blurring is an image processing method that aims to recover a sharp latent image from a blurry one; the de-blurring procedures could be either blind when the blur kernel k is assumed to be unknown, or non-blind with known k value [3, 4].

N. Ali (✉) · A. Abdallah · I. F. Elnahry · R. Atta
Electrical Engineering Department, Faculty of Engineering, Port Said University, Port Said, Egypt
e-mail: noran.elaraby@eng.psu.edu.eg

A. Abdallah
e-mail: asmaa.refaat@eng.psu.edu.eg

I. F. Elnahry
e-mail: ibrahim.farouk@eng.psu.edu.eg

R. Atta
e-mail: r.atta@eng.psu.edu.eg

There are many applications for image deblurring, such as medical imaging [5], astronomy, underwater imaging, face recognition, and surveillance cameras. As one of Sustainable Development Goals (SDGs), image deblurring techniques are utilized in surveillance and face recognition services for smart cities.

Given the blurred image B, the information is not sufficient to estimate the blur kernel k and consequently to recover the latent sharp image X; many different pairs k and X can bring to the same B.

To address this problem, several optimization-based de-blurring approaches that exploit priors and constraints to regularize the solution space of blur kernel and latent image have been introduced. These approaches use different types of priors, such as sparse gradients [6], spatial prior [7], hyper-Laplacian prior [8], dark channel prior [9], combination of dark and channel prior [10], L0 approximation prior [11], and Normalized Sparsity [12]. However, previously proposed optimization techniques have two main drawbacks: they are time consuming procedures, additionally they simplify the assumption on the blur kernel.

Then, Convolutional Neural Networks (CNN) and deep learning related techniques have been proposed as blind end-to-end de-blurring solutions that can be either kernel-free or kernel estimation.

In [13–15], kernel estimation techniques use deep learning for estimating blur kernel and subsequently restoring the latent sharp image. While kernel-free end-to-end de-blurring models are presented in [16–20]; these models recover the estimated sharp image directly without kernels estimation.

In this paper, we introduce an end-to-end training multiscale framework using combination of dark and bright channel priors as loss function. Our model uses deep learning techniques with traditional knowledge to enhance the performance; it also follows kernel-free end-to-end de-blurring strategy to avoid articrafts induced by an inadequate blur kernel.

The remaining of the paper is organized as follows. Section 2 reviews the related work. Section 3 presents our proposed network. In Sect. 4, we analyze the experiments and evaluate the performance of our scheme. Section 5 concludes the paper. Section 6 presents recommendations.

2   Related Work

This section reviews the preceding work on the blind image motion de-blurring methods through deep learning strategies and via dark and bright channel priors.

2.1   Image Deblurring Through Deep Learning Techniques

The first category of the blind image motion de-blurring methods employs various deep learning strategies. Sun et al. [13] use CNN to estimate the non-uniform motion

blur kernel and then deconvolve the blurry image to estimate the sharp image. According to Gong et al. [14], they use fully-convolutional deep neural network (FCN) to estimate the blur motion flow field; then, they use non-blind deconvolution technique to recover the deblurred image. While [15] creates a network that consists of feature extraction module, kernel estimation module, and image estimation module and then trains the network from coarse-to-fine manner.

Other recent works train the kernel-free end-to-end network to restore the latent image from the blurry one directly to avoid the problem of kernel estimation. Nah et al. [16] adopt the multi-scale network that uses a specific coarse-to-fine deblurring approach with independent parameters. Tao et al. [17] introduce a multi-scale coarse-to-fine network that utilizes the recurrent feature strategy with shareable learning weights. Kupyn et al. [18] propose DeblurGAN, which is based on single-scale network and conditional generative adversarial network using multicomponent loss function. Zhang et al. [19] applies conditional general adversarial network using dark channel prior as loss function to render articrafts supressed. Liu et al. [20] introduces a recurrent conditional generative adversarial network in a coarse-to-fine scheme.

2.2 Image Deblurring Via Dark and Bright Channel Priors

2.2.1 Dark Channel

According to [21], the dark channel is the minimum intensity values in an image patch. The dark channel of an image can be represented as

$$DC(I)(m) = min_{n\varepsilon\Omega(m)}\big(min_{c\varepsilon\{r,g,b\}}I^c(n)\big).$$ (2)

where I is a given image, n and m are pixel locations, $\Omega(m)$ denotes the image patch which is centered at m, and I^c represents the c-th color channel.

He et al. [21] observe that the dark channel map $DC(I)$ in the dehazing image tends to be zero. However, Pan et al. [9] detect that the values of most pixels of the clear images are zero while most pixels in the dark channel of blurred images are non-zero. Furthermore, Pan et al. demonstrate that the dark channel map of blurred images is less sparse; they enforce sparsity in the deblurring process utilizing L0 norm, the count of non-zero values.

2.2.2 Bright Channel

Bright channel represents the maximum pixels values in an image patch. The bright channel of an image can be defined as [21]

$$BC(I)(m) = max_{n\varepsilon\Omega(m)}\big(max_{c\varepsilon\{r,g,b\}}I^c(n)\big).$$ (3)

Yan et al. [10] notice that the bright pixels values in clean image are diminished by blur process; they utilize this observation to combine the dark channel and bright channel priors (DCBP) in the deblurring operation. Moreover, in [24], a low-light image enhancement method based on maximum colour channel and bright channel prior is proposed.

3 Proposed Network

3.1 Model Architecture

Our model is a deep multi-scale network that follows a coarse-to-fine scheme to gradually recover the latent sharp image. Our network takes a set of blurry input images at different scales as an input and produces the sharp images at corresponding scale as an output. The final deblurred image will be the sharpest one at the finest scale.

The proposed model consists of three scale levels. Each level is a sub-network that contains three essential parts: input/output, Encoder/Decoder, and recurrent term.

Input/output block: Three different scale blurry images-blurry 64×64, blurry 128×128, and blurry 256×256-are entered as original input to the three scale levels: blurry 64×64 at level 1, blurry 128×128 at level 2, and blurry 256×256 at level 3. Moreover, the output latent image from the previous level is inserted. For instance, the network concatenates the initial output deblurred images from the first scale level, i.e., latent 64×64, and add them as an input to the second scale level with its original blurry image, blurry 128×128. Similarly, the network concatenates the output deblurred images from the scale level 2, i.e., latent 128×128, and add them as an input to the third scale level with its original blurry image, blurry 256×256.

Encoder/decoder Network: The encoder is responsible for picking the content abstraction and it is located after the input block while the decoder is used for recovering image details after the process ends. ResBlocks [16] is embedded in our encoder and decoder. ResBlocks consists of one convolution layer, followed by rectified linear unit, and finally one convolution layer.

The encoder block consists of one convolutional layer followed by three stacked ResBlocks. On the other hand, the decoder block contains three stacked ResBlocks followed by a deconvolution layer; as the decoder and decoder are symmetric.

There is skip connections between the convolution and deconvolution layers. Skip connections are responsible for avoiding the vanishing gradient problem that counteracts the changing of weight values. Likewise, skip connections helps the feature maps to pass through with image details that assists the deconvolution layer to reconstruct the sharp image in higher quality.

Recurrent term: long short term memory (LSTM) is a special case of recurrent neural network. We use convolutional LSTM [22] to make the convergence more fast,
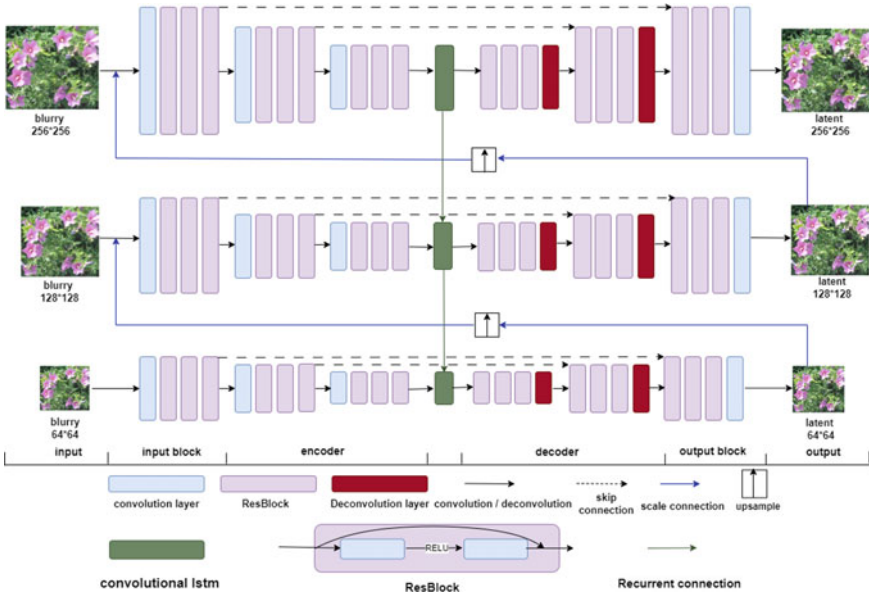
Fig. 1 Proposed network architecture

as convolutional LSTM shares information between different scale levels; it picks useful information from previous scale. As illustrated in Fig. 1, our network contains an input block followed by two stacked encoders blocks, next a convolutional lstm that is followed by two stacked decoders and finally one output block. Kernel size = 5×5 is used for every convolutional kernel.

3.2 Loss Function

Our network uses multicomponent loss function through every level. The total loss function is formulated as a combination of content, dark channel, and bright channel loss functions as

$$Total\_Loss = L_{content} + L_{dark\_channel} + L_{bright\_channel} \qquad (4)$$

Content loss: the content loss is computed using mean of the squared differences between the deblurred image and ground truth image through each scale level.

$$L_{content} = \sum_{j=1}^{3} \frac{1}{h_j \times w_j \times c_j} \left(||O_j - X_j||_2 \right) \qquad (5)$$

where h_j denotes *jth* scale level height, w_j *is jth* scale level width, c_j *is jth* level number of channels while h_j, w_j and, c_j are the components that normalize the loss function. O_j and X_j represent our network output and ground truth at each scale level j.

Dark channel loss: We choose dark channel as a loss-function component to make ringing articraft suppressed through each level scale. We aim to minimize the distance between the dark channel map of the estimated image and the ground truth image.

Dark channel loss is formulated as

$$L_{dark\_channel} = \sum_{j=1}^{3} \frac{1}{h_j \times w_j \times c_j} ||DC(O_j) - DC(X_j)||_2 \qquad (6)$$

$DC(.)$ represents the dark channel map of an image. We utilize L2 norm rather than L0 norm as L0 norm is not differentiable and cannot deal with neurons [6].

Bright channel loss: Our model utilizes a combination of bright and dark channel priors for deblurring operation, we add bright channel to the loss function.

Bright channel loss is formulated as

$$L_{bright\_channel} = \sum_{j=1}^{3} \frac{1}{h_j \times w_j \times c_j} ||BC(O_j) - BC(X_j)||_2 \qquad (7)$$

$BC(.)$ represents the bright channel map of an image.

4   Simulation Results

4.1   *Experiments Parameters*

Our experiments are done on a PC with GPU TYPE T4. Our model is implemented using tensorflow version2. The training batch size $= 16$, and number of epochs $= 500$, which takes 30 h. We randomly crop the input training pair to patches with the size of 256×256. Our optimization solver is Adam Optimizer.

Implemented Datasets: We use Gopro dataset [16] for both training and evaluation practices. Gopro dataset consists of 3214 image pairs of blurred and sharp image. We use 2103 pairs for training and 1111 pairs for testing. Gopro dataset simulates realistic blurring, as it handles dynamic scene motion blur. We use Gopro for both quantitative and qualitative results. Kohler dataset [23] is utilized in comparison and evaluation for quantitative results. Kohler dataset contains 12 different blur kernels that are used for blurring 4 sharp images.

Table 1 Gopro quantitative results according to different patch sizes

Measure	Patch size		
	3×3	5×5	7×7
PSNR	29.23	28.73	28.54
SSIM	0.9219	0.9140	0.9093
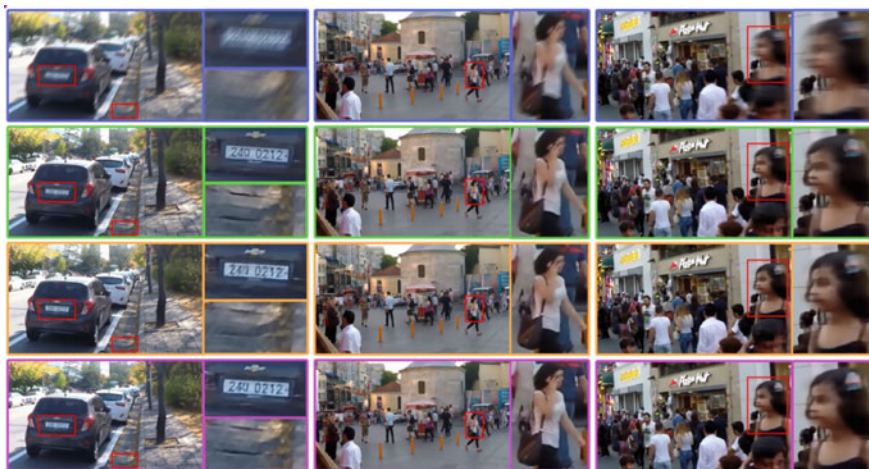
Fig. 2 Visual results on GOPRO testing dataset from top to bottom: blurry images, results by Tao et al. [14], results by Nah et al. [13], and our resulted images

4.2 Experimental Evaluation

4.2.1 Dark and Bright Channels Patch Size

We consider image patch size as a hyper parameter. For each image, dark and bright channels have been calculated based on different patch sizes ad shown in Table 1.

It has been observed that the patch size = 3×3 has achieved better performance than 5×5 and 7×7 for PSNR and SSIM term. Figure 2 show the visual results for different patches size.

4.2.2 Comparison

Our network has applied on both Gopro and Kohler datasets; the model performance is evaluated and compared with three previous state-of-the-art image deblurring approaches Sun et al. [13], Nah et al. [16], and Tao et al. [17]. We exploit the Gopro and Kohler datasets for quantitative results in terms of PSNR and SSIM. As shown in Table 2, we achieve the best performance.

Table 2 Quantitative comparison on Gopro and Kohler dataset

	GOPRO		KOHLER		TIME
	PSNR	SSIM	PSNR	MSSIM	
Sun et al.	24.64	0.8429	25.22	0.7735	20 min
Nah et al.	29.08	0.9135	26.48	0.8079	3.09 s
Tao et al.	28.95	0.9163	26.4617	0.8245	1.87 s
Ours	29.23	0.9219	26.5193	0.8304	1.87 s

Our proposed scheme testing time is much faster than [10, 13] and equivalent to [14] but our model performs better in terms of PSNR and SSIM. We compare our visual results with [13, 14] as shown in Fig. 2. It has been found that adding a combination of dark and bright channels to loss function makes the image more sharp and avoids ringing articrafts (Fig. 3).

Fig. 3 Results using different patch size; **a** patch size = 3 × 3, **b** patch size = 5 × 5, **c** patch size = 7 × 7, **d** blurry input image

5 Conclusion

In this paper, we introduce an efficient multi-scale network deblurring system with shareable weights for dynamic scene. Our propped incorporates traditional knowledge prior to achieve better performance. The applied learning operation is based on a combination of dark and bright channel priors and content loss. Using the dark and bright channel priors together with the effective multi-scale network architecture, the quantitative and qualitative evaluations on the GoPro and Kohler datasets show that our proposed outperforms the previous dynamic scene deblurring networks. The model can be applied on other image processing applications, such as image matting and super resolution.

6 Recommendations

In future work, we aim to enhance our model performance by reducing the number of trainable parameters, which consequently saves memory loss and produces more light-weight network.

References

1. Fergus R, Singh B, Hertzmann A, Roweis S, Freeman W (2006) Removing camera shake from a single photograph. ACM Trans Graphics 25:787–794
2. Hirsch M, Schuler C, Harmeling S, Scholkopf B (2011) Fast removal of non-uniform camera shake. In: Proceeding international conference on computer vision, (ICCV '11), USA, pp 463–470
3. Zhang K, Ren W, Luo W, Lai WS, Stenger B, Yang MH, Li H (2022) Deep image deblurring: a survey. Int J Comput Vision 130(9):2103–2130
4. Li C (2022) A survey on image deblurring. arXiv preprint arXiv:2202.07456
5. Rong R, Wang S, Zhang X, Wen Z, Cheng X, Jia L, Yang DM, Xie Y, Zhan X, Xiao G (2023) Enhanced pathology image quality with restore-generative adversarial network. Am. J. Pathol 193:404–416
6. Shan Q, Jia J, Agarwala A (2006) High-quality motion deblurring from a single image. ACM Trans Graph 27(3):1–10
7. Xu L, Jia J (2010) Two-phase kernel estimation for robust motion deblurring. In: Proceedings of Europe conference on computer vision, Greece
8. Krishnan D, Fergus R (2009) Fast image deconvolution using hyperLaplacian priors. In: Proceedings of advance neural information processing system, Canada
9. Pan J, Sun D, Pfister H, Yang MH (2016) Blind image deblurring using dark channel prior. In: Proceedings of IEEE conference on computer vision and pattern recognition conference (CVPR), USA
10. Yan Y, Ren W, Guo Y, Wang R, Cao X (2017) Image deblurring via extreme channels prior. In: Proceedings of IEEE conference on computer vision and pattern recognition, USA
11. Xu L, Zheng S, Jia J (2013) Unnatural l0 sparse representation for natural image deblurring. In: Proceedings of IEEE conference on computer vision and pattern recognition conference (CVPR), USA

12. Krishnan D, Tay T, Fergus R (2011) Blind deconvolution using a normalized sparsity measure. In: Proceedings of conference on computer vision and pattern recognition conference (CVPR), USA
13. Sun J, Cao W, Xu Z, Ponce J (2015) Learning a convolutional neural network for non-uniform motion blur removal. In: Proceedings IEEE conference on computer vision and pattern recognition, USA
14. Gong D, Yang J, Liu L, Zhang Y, Reid I, Shen C, Hengel AVD, Shi Q (2017) From motion blur to motion flow: a deep learning solution for removing heterogeneous motion blur. In: Proceedings of IEEE conference on computer vision and pattern recognition, USA
15. Xu L, Jia J (2010) Two-phase kernel estimation for robust motion deblurring. In: Lecture notes in computer science, artificial intelligence and bioinformatics, Springer
16. Nah S, Kim TH, Lee KM (2017) Deep multi-scale convolutional neural network for dynamic scene deblurring. In: Proceedings of computer vision and pattern recognition conference (CVPR), pp 3883–3891
17. Tao X, Gao H, Shen X, Wang J, Jia J (2018) Scale-recurrent network for deep image deblurring. In: Proceedings of IEEE computer society conference on computer vision and pattern recognition, USA
18. Kupyn O, Budzan V, Mykhailych M, Mishkin D, Matas J (2018) DeblurGAN: blind motion deblurring using conditional adversarial networks. In: Proceedings of computer vision and pattern recognition conference (CVPR), USA
19. Zhang S, Zhen A, Stevenson R (2019) Gan based image deblurring using dark channel prior. In: Proceedings of IS&T international symposium on electronic imaging, USA
20. Liu J, Sun W, Li M (2019) Recurrent conditional generative adversarial network for image deblurring. IEEE Access 7:6186–6193
21. He, K, Sun, J and Tang, X., Single image haze removal using dark channel prior, In proc. IEEE Conference in Computer Vision and Pattern Recognition Conference (CVPR), USA,2009.
22. Shi X, Chen Z, Wang H, Yeung DY, Wong WK, Woo WC (2015) Convolutional lstm network: a machine learning approach for precipitation nowcasting. In: Proceedings of neural information processing systems conference (NIPS 2015), Canada
23. Köhler R, Hirsch M, Mohler B, Schölkopf B, Harmeling S (2012) Recording and playback of camera shake: benchmarking blind deconvolution with a real-world database. In: Proceedings of the European conference on computer vision (ECCV), Italy
24. Sandoub G, Atta R, Ali HA, Abdel-Kader RF (2021) A low-light image enhancement method based on bright channel prior and maximum colour channel IET Image Processing 15(8):1759–1772 https://doi.org/10.1049/ipr2.v15.8, https://doi.org/10.1049/ipr2.12148

Industry, Innovation, and Infrastructure

Survey and Evaluation of Applied Modern Engineering Pedagogy

Omer Alkelany, Hatem Khater, Mohamed Kamal, and Hosam E. Mostafa

1 Introduction

Engineering education is the process of educating and training individuals to become engineers. It encompasses a wide range of disciplines, including mechanical, electrical, and computer engineering, and is designed to prepare students for careers in the engineering field. The goals of engineering education include providing students with a strong foundation in the principles of engineering, as well as the knowledge and skills needed to design and innovate new technologies. It is well known that engineering education aims to develop students' critical thinking and problem-solving abilities, and enhance their communication skills which are all essential for the success in the engineering field. Actually, engineering education has evolved over time, with the introduction of new technologies and changing societal needs [1]. The first engineering schools were established in the nineteenth century, and since then, engineering education has continued to adapt and evolve in response to advances in technology and changing industry needs.

Today, engineering education faces a number of challenges, including increasing enrollment, student diversity, and demanding accreditation standards. Additionally,

O. Alkelany (✉) · H. Khater · M. Kamal
Mechanical Engineering-Mechatronics Department, Faculty of Engineering, Horus University-Egypt, New Damietta, Egypt
e-mail: oalkelalny@horus.edu.eg

H. Khater
e-mail: hkhater@horus.edu.eg

M. Kamal
e-mail: mkhassan@horus.edu.eg

H. E. Mostafa
Faculty of Engineering, Alexandria University, Alexandria, Egypt
e-mail: hossam.mostafa@alexu.edu.eg

there is an increasing emphasis on interdisciplinary collaboration and industry partnerships, as well as the integration of technology in the classroom. Pedagogy plays a critical role in shaping engineering education. It is about the method and practice of teaching. It involves the way that curriculum, instruction, and assessment are designed, delivered, and evaluated. Different pedagogical approaches can lead to different learning outcomes and student engagement; thus it is important to choose the right pedagogy to achieve the desired goals of the education.

The research presented targets the Sustainable Development Goals (SDGs), on Quality Education. As will be shown, experiential learning method shows enhancements on engineering education when applied in higher education.

1.1 Scope of the Paper

This paper compares the conventional pedagogy as it relates to three main active learning in engineering education; namely project based learning, flipped-classroom, and experiential learning. Although other education pedagogies are of importance, such as: online education or virtual laboratories, their analysis is beyond the scope of this paper.

1.2 Conventional Pedagogy

Conventional pedagogy refers to traditional teaching methods that have been widely used in schools for many decades. These methods typically involve a teacher-centered approach, where the teacher is the primary source of knowledge and the students are passive recipients of that knowledge. Conventional pedagogy is often characterized by a focus on rote learning and memorization, as well as a limited use of technology in the classroom. This model emphasized strict discipline, a rigid curriculum, and a focus on memorization and rote learning. Conventional pedagogy was widely adopted in schools throughout the twentieth century and remains a common approach to teaching in many countries today. However, in recent years, there has been growing criticism of this approach and a growing interest in alternative forms of pedagogy [2–4].

Conventional pedagogy often provides limited opportunities for student engagement and creativity. Students are typically expected to sit quietly, listen to the teacher's lectures, and complete worksheets or exams. There is often little room for students to ask questions, express their own ideas, or engage in hands-on activities. This usually makes the students disengaged and uninterested in the learning process.

Conventional pedagogy provides a structured learning environment where students know what to expect and what is expected of them. This can be beneficial for students who thrive in a structured environment and need clear expectations

for behavior and learning. It also can be effective in teaching certain subjects such as mathematics and science, where a lot of factual information needs to be learned and retained. Memorization and rote learning can be particularly useful for these subjects. On the other hand, it often stifles student creativity and critical thinking and can be boring to those disengaged students.

1.3 Alternative Pedagogy

Alternative pedagogy refers to teaching methods that differ from conventional pedagogy. These methods are often characterized by a student-centered approach, where the students are actively engaged in the learning process and take more responsibility for their own learning [5–10]. Alternative pedagogy also emphasizes critical thinking, problem-solving, and creativity. This approach is often referred to as the "guide on the side" model, where the teacher acts as a facilitator and guide, rather than the primary source of knowledge. This approach allows students to ask questions, express their own ideas, and engage in hands-on activities.

Alternative pedagogy places a strong emphasis on critical thinking, problem-solving, and creativity. This approach is based on the idea that students should be encouraged to think for themselves and develop their own ideas, rather than simply memorizing facts and information. Alternative pedagogy often incorporates the use of technology in the classroom. This can provide opportunities for interactive and engaging learning, as well as giving students access to a wide range of resources and tools to support their learning. To make the most of both approaches, it is recommended to integrate elements of alternative pedagogy into a conventional classroom.

2 Active Learning in Engineering Education

Active learning is a teaching method that emphasizes student engagement and participation in the learning process. Unlike traditional passive learning, which relies on lectures and traditional teaching methods, active learning encourages students to take an active role in their own education through hands-on activities, group work, and problem-solving exercises. Active learning has been found to be a highly effective approach for improving student learning outcomes and engagement in engineering education. Studies have shown that active learning methods, such as flipped classroom and project-based learning, can lead to better retention of information, improved problem-solving skills, and greater student engagement [11].

One strategy for active learning is project-based learning, in which students work on a project that addresses a real-world problem or challenge. This method allows students to apply what they have learned to a real-world scenario, and it promotes creativity, critical thinking, and problem-solving skills. Another instructional strategy

is flipped classrooms, in which, students watch video lectures and complete interactive activities outside of class, and then use class time for hands-on, collaborative learning activities and discussions with the teacher and classmates. The goal of the flipped classroom is to make better use of class time and to increase student engagement and understanding of the material.

Hands-on activities and labs are also an effective way to engage students in active learning. Hands-on activities provide students with the opportunity to physically manipulate and experiment with materials, which can help them to better understand and retain the information they are learning. Additionally, group work and peer-to-peer teaching can also be effective strategies for active learning. Group work allows students to collaborate and learn from one another, and it promotes teamwork, communication, and leadership skills. Peer-to-peer teaching allows students to take on the role of teacher and present information to their peers, which can help to solidify their understanding of the material.

2.1 Project-Based Learning

Project-based learning (PBL) is an active learning approach that uses real-world projects or challenges as the starting point for learning. This student-centered method emphasizes creativity, critical thinking, and problem-solving skills and it is particularly well-suited for engineering education. In this methodology, students work in small groups or individually to research and analyze a project or challenge, and then develop a solution. This process is guided by a facilitator or instructor, who acts as a coach or mentor rather than a traditional lecturer. It is designed to mimic the process that engineers use in the real world, and it provides students with a more authentic and engaging learning experience. It can be used in a variety of settings, such as in the classroom, laboratory, or through online learning. It can be applied in any engineering discipline, including mechanical, electrical, and computer engineering.

When designing Project-Based Learning activities, it is important to start with a well-defined project or challenge that is relevant to the course content and that aligns with the learning objectives. *The project or challenge should be complex and open-ended, and it should require students to use creativity, critical thinking, and problem-solving skills.* The project or challenge should also be structured in a way that guides students through the project-solving process. This can be achieved by breaking the project down into smaller, manageable parts, and by providing students with a clear set of steps or guidelines to follow. It is also important to consider the resources and support that will be needed for students to successfully complete the PBL activity. This can include access to relevant literature, equipment, or software, as well as guidance from a facilitator or instructor [12–14].

When implementing this technique in the classroom, it is important to have a clear understanding of the project-solving process and the role of the facilitator or instructor. The facilitator should act as a coach or mentor, rather than a traditional lecturer, and should provide guidance and support to the students throughout

the project-solving process. Managing the project-solving process can also be challenging, especially when working with a large group of students. It is important to establish clear expectations and guidelines for the students, as well as to provide regular feedback and progress checks. It is important to assess not only the final solution that the students develop, but also the process of project-solving and the skills that the students have developed along the way [15–17].

Case studies are an effective way to see Project-Based Learning in action and to learn from the experiences of other educators. These case studies will provide the teacher with examples of how the technique has been implemented in different engineering disciplines, such as mechanical, electrical, and computer engineering. They will also give him a better understanding of the potential benefits and challenges, and will provide you with ideas for how to implement PBL in your own teaching practice.

One example of Project-Based Learning in engineering education is a project in which engineering students worked in teams to design and build a solar-powered irrigation system. The project required students to research and analyze the problem, and then develop a solution that incorporated sustainable energy principles. The project was designed to promote creativity, critical thinking, and problem-solving skills. Another example that can be implemented in a mechanical engineering course, students worked individually to design and build a robotic arm that can perform specific tasks (such as sorting and classifying fruits).

2.2 Flipped Classrooms

Also known as inverted classrooms, is a modern pedagogy that has been gaining wide popularity in recent years [18–28]. The basic concept of a Flipped Classroom (FC) is to have students watch videos or read materials at home before class, and then use class time for more interactive activities such as discussions, problem-solving, and hands-on projects. The idea behind flipped classrooms is to use technology to make the most of classroom time. Instead of lecturing for an hour, teachers can use video lectures or readings as homework, and then use class time for more interactive activities. This allows for a more personalized learning experience, as students can watch the videos or read the materials at their own pace and come to class with questions and ideas.

One of the main benefits of flipped classrooms is that they *allow for more active learning*. Instead of sitting and listening to a lecture, students are engaged in activities that help them understand and apply the material. This can lead to better retention of the material and a deeper understanding of the subject. Flipped classrooms also allow for more collaboration and peer-to-peer learning. By using class time for activities and discussions, students have the opportunity to work together and learn from each other. This can be especially beneficial for subjects such as science and math, where working through problems and discussing them with others can be a powerful learning tool.

Another benefit of flipped classrooms is that they can be *more inclusive for students with different learning styles.* By providing video lectures and readings, students who may not be comfortable speaking up in class or who prefer to learn at their own pace can still participate and benefit from the class. However, it's important to note that flipped classrooms are not a one-size-fits-all solution. They require a significant amount of planning and preparation, and may not be suitable for all subjects or all students. Additionally, students will need access to technology and internet at home to be able to access the video lectures and readings.

2.3 Experiential Learning

Experiential learning (EXL) requires that instructors just give guided instructions of what the aim is, without giving full details of how to reach it [29]. It gives students the opportunity to draw conclusions, and helps them to be more involved in their own learning process. Experiential Learning is thus considered as Learning by reflection on Doing [30–38] It was conceptualized by Aristotle about Ethics as "for the things we have to learn before we can do them, we learn by doing them (first!)" [39]. However, in the 1970s, Kolb had developed a fundamental modern model of experiential learning [40]. According to Kolb [41, 42], the learner must be actively involved in the experience; reflect on the experience; analyze the outcomes; and perform decision making and problem-solving skills in order to use the new ideas gained from the prior experience. In this process, instructors to give constructive feedback to the learners, but they should not rush to provide the answer [43–45], especially when creative abilities are to be developed (critical thinking, design, synthesis, etc.), and particularly when there is not a single right answer. Students/learners will use their experience to judge or evaluate an outcome of a targeted component and share it with the learners [46, 47].

In the Engineering domain, experiential learning is used in different ways. For example, in [48], it was used via hardware emulators, and Field Programmable Gate Arrays (FPGA)s were used in latter stage of complex multi-part designs. Also, in 2020, two different comparative studies for experiential learning were done in two different universities in China, and New Zealand considering virtual reality applications, concluded that it enhances learning experience [49, 50]. Furthermore, more researchers investigated the incorporation of experiential learning at a Canadian university, in 2017, but they implemented it in a single engineering course, without FPGAs, and thus their results were limited [51]. It is worth mentioning that EXL allows for sustainable learning experience, since the FPGA boards can be used for various hardware design, and no new hardware need to be purchased.

3 Incorporating Technology in Engineering Education

In engineering education, technology can be used to support a variety of teaching and learning methods, such as online learning, virtual labs, and simulations. Online learning platforms, for example, allow students to access course materials and resources at any time, and to interact with their peers and instructors in a virtual environment. Virtual labs and simulations provide students with hands-on experience in a safe and controlled environment, which can be especially useful for students who are unable to access physical labs or equipment. Technology can also be used to assess student learning, through the use of online quizzes, tests, and assignments. This can help instructors to quickly and easily evaluate student understanding and progress, and to provide timely feedback [52–54].

One popular technology tool in engineering education is Computer-Aided Design (CAD) software. CAD software allows students to create and edit 3D models, which can be used to design and analyze engineering projects. Many CAD software packages also include simulations, which can be used to test and evaluate designs before they are built. Another useful technology tool is simulation software. Simulation software allows students to model and test complex systems and processes in a safe and controlled environment. This can be particularly useful for students who are unable to access physical labs or equipment.

Online learning platforms, such as Blackboard, Canvas, and Moodle, are also commonly used in engineering education. These platforms provide students with access to course materials and resources, and allow for interaction with their peers and instructors in a virtual environment.

Case studies are an effective way to see technology integration in action and to learn from the experiences of other educators. These case studies will provide students with examples of how technology has been used in different engineering disciplines, such as mechanical, electrical, and computer engineering. They will also give them a better understanding of the potential benefits and challenges of technology integration, and will provide you with ideas for how to integrate technology in your own teaching practice.

One example of technology integration in engineering education is a course that used virtual reality (VR) technology to simulate real-world engineering scenarios. Students were able to interact with virtual environments and equipment, which allowed them to gain practical experience and develop technical skills in a safe and controlled environment. Another example is a course that used online learning platforms to deliver course materials and resources, and to facilitate online discussions and collaborations between students and instructors. The use of online learning platforms enhanced the learning experience and provided students with a more flexible and convenient way of learning. Tables 1 and 2 summarize the benefits and challenges of the three main active learning pedagogies discussed in this paper.

More details on our analysis of the relevant techniques in the scope of this survey. These details are presented in the next section (Sect. 4 Assessment in in Table 3). In

Table 1 Benefits of common active learning pedagogies

Benefits	PBL	FC	EXL
Better retention of information	✓	✓	✓
Improved problem-solving skills	✓	✓	✓
Greater student engagement	✓	✓	✓
More inclusive for students with different learning styles		✓	✓
Enhances creativity and critical thinking skills	✓	✓	✓
Works well with hands-on experience	✓	✓	✓
Empowers students to draw conclusions			✓
Good for sustainable hardware-based learning experience			✓
Empowers hardware-based experimentation	✓		✓

Table 2 Challenges of common active learning pedagogies

Challenges	PBL	FC	EXL
Instructors do not give details on how to learn	–	–	α
Cost of hardware for each project	α	–	
Online, video material needed	α	α	α
Divide class into small groups	α	α	α

Table 3, we also focus on the skill used as it relates to advantages and disadvantages of the technique in Engineering education.

Table 3 Detailed comparisons between different learning strategies in engineering education

Strategy used	Skill used										Advantages	Disadvantages
	Listen	Follow instructions	Solve problems	Comprehend	Analyze	Synthesize	Model	Verify	Teamwork	reflect/Think		
Lecture instructions	√										Easy, traditional	Lacks engagement, creativity, limited retention
Lab assignments		√			√	√					Relatively cheap	equipment dependent
Homework problems			√								Quick test of understanding	Lacks compressive assessments
Reports (technical/research)				√	√						Exposure to contemporary topics	Industry distant
Analysis surveys				√	√						Conclusion by analysis	limited to target
Simulations				√			√	√			Equipment not needed	Can be misleading, involves software licensing costs
Synthesis (discrete components)						√		√	√		Ready to acquire	Involves purchase of parts & equipment, Limited or hard part reuse, technology distant, subject to obsolescence., low performance
Projects/ Group work			√		√	√	√	√	√		Teamwork learning, learn together	May have non-active members, involves purchase of parts
Use of microcontroller boards/single board computers	√	√	√	√	√	√	√	√	√		Can be reused at software desing level only, learn by doing, improve retention, Technology empowered, room to involve all team members, medmm performance	Involves purchase of microcontroller boards, idle (non-programmed) microcontrollers are useless, training is required
EXL FPGA based, proposed	√	√	√	√	√	√	√	√	√	√	Can be reused at both software and hardware design level, learn by doing, improve retention, apply verify & simulate models, Technology empowered, obsolescence protected, room to involve all team members	Require well-built teaching components, blank (non-configured) FPGAs are useless, training, some available solutions are very expensive, with limited performance

4 Assessment and Evaluation in Modern Engineering Pedagogy

Assessment and evaluation are crucial components of engineering education, they provide instructors with the necessary information to determine student understanding and progress, and to identify areas where additional instruction or support may be needed. Assessment and evaluation also help to ensure that students are meeting the learning objectives of the course, and that they are developing the knowledge and skills necessary to succeed in the field of engineering.

There are many different forms of assessment and evaluation, including traditional methods such as exams and quizzes, as well as more modern methods such as performance assessments and self-assessments. Traditional methods, such as exams and quizzes, are useful for measuring student understanding of course content and for identifying areas where additional instruction may be needed. Performance assessments, on the other hand, provide an opportunity for students to demonstrate their understanding of the course content through hands-on projects and tasks. Self-assessments, provide students with the opportunity to reflect on their own learning and to identify areas for improvement.

Another important aspect of designing assessments for modern engineering pedagogy is to incorporate formative assessments, which are used to provide ongoing feedback to students and to identify areas where additional instruction or support may be needed. Formative assessments can be used in conjunction with summative assessments, which are used to evaluate student understanding at the end of a course or unit.

One key aspect of designing assessments for modern engineering pedagogy is to focus on higher-order thinking skills, such as critical thinking and problem-solving. This can be achieved through the use of performance assessments, such as open-ended questions, projects, and presentations. These assessments provide students with the opportunity to demonstrate their understanding of the course content through hands-on projects and tasks, rather than through multiple-choice questions.

Implementing assessments in the engineering classroom requires careful planning and organization. It is important to provide clear instructions and guidelines for students, and to communicate the purpose and objectives of the assessment.

It is crucial to provide adequate time for students to prepare for assessments, and to schedule them at appropriate times. One important aspect is to ensure that assessments are fair and unbiased. This can be achieved by using a variety of assessment methods, such as multiple-choice questions, short-answer questions, and open-ended questions, and by using a rubric to grade assessments. Another important aspect is to provide timely and constructive feedback to students. Feedback should be specific, objective and actionable, and should provide students with clear information on their strengths and weaknesses, and areas for improvement. Table 3 shows a detailed comparative study between the different techniques used in engineering education.

While evaluating the effectiveness of modern pedagogy in engineering education, researchers need to follow a systematic and evidence-based approach. This can be

achieved through the use of formative and summative evaluations, as well as through the use of student learning outcomes data. Formative evaluations, such as observations and focus groups, provide ongoing feedback on the effectiveness of modern pedagogy in the classroom. Summative evaluations, such as pre- and post-tests, can be used to measure student learning outcomes and to determine the effectiveness of modern pedagogy over time. Consequently, further assessments of the listed learning strategies is the subject of future research.

5 Future Directions for Modern Engineering Pedagogy

As technology continues to advance, and new research emerges in the field of education, the way engineering is taught is also evolving. One trend that is becoming increasingly popular is the use of virtual and augmented reality in the classroom. This technology allows students to visualize complex engineering concepts and systems in a more interactive and engaging way. By providing students with virtual experiences, this technology can help to enhance their understanding of engineering principles and improve their problem-solving abilities. Another trend in modern engineering pedagogy is the integration of entrepreneurship and innovation. This approach encourages students to think outside the box and to apply their engineering knowledge and skills to real-world problems. This type of education helps students to develop critical thinking skills, creativity and the ability to work in multidisciplinary teams. Another important trend is the integration of sustainability and environmental education in engineering education. This approach helps students to understand the importance of sustainable practices and to develop solutions that minimize the impact of engineering on the environment.

6 Conclusions

In this paper, the importance of modern pedagogy in engineering education has been discussed. It has been shown how it shapes the curriculum, instruction, and assessment. The paper has discussed conventional pedagogy and alternative pedagogy, highlighting the characteristics, advantages, and disadvantages of each approach. Conventional pedagogy is based on a teacher-centered approach, with a focus on memorization and rote learning, while alternative pedagogy is based on a student-centered approach, emphasizing critical thinking, problem-solving, and creativity. The paper has also compared the effectiveness of both approaches and provided recommendations for how to integrate elements of alternative pedagogy into a conventional classroom. It is important to note that there is no one-size-fits-all approach to teaching, and the most effective method will depend on the subject matter and the needs of the students.

The teaching methods surveyed can be applied on a global scale in any geographical area.

7 Recommendations

Future research can focus on developing strategies to effectively blend both approaches to enhance student learning.

Conflict of Interest All authors declare that they have no conflict of interest regarding this research paper and that they comply with research ethics.

References

1. Diaz Lantada A (2020) Engineering education 5.0: continuously evolving engineering education. Int J Eng Educ 36:1814–1832. https://www.researchgate.net/publication/345141439_Engineering_Education_50_Continuously_Evolving_Engineering_Education. Accessed Dec 2022
2. Gaffney J, Gaffney J (2016) Conventional pedagogy and the socially constructed classroom. J Educ Res 109(4):314–322
3. Kohn A (2017) Rethinking homework: best practices that support diverse needs. Association for Supervision and Curriculum Development, Alexandria, VA
4. Aziz A, Islam SN (2022) Impact of mixed pedagogy on engineering education. IEEE Trans Educ 65(1):56–63. https://doi.org/10.1109/TE.2021.3088808
5. King I, Saxena C, Pak C, Lam C, Cai H (2021) Rethinking engineering education: policy, pedagogy, and assessment during crises. In: IEEE signal processing magazine, vol 38, no 3, pp 174–184. https://doi.org/10.1109/MSP.2021.3059243
6. Tkacheva T, Sazonova Z (2015) Interactive educational methods of engineering pedagogy against technical teachers emotional Burnout. In: 2015 international conference on interactive collaborative learning (ICL). Firenze, Italy, pp 477–486. https://doi.org/10.1109/ICL.2015.7318076
7. Rüütmann T, Kipper H (2015) Klagenfurt school of engineering pedagogy by Adolf Melezinek as the basis of teaching engineering at Tallinn University of Technology. In: 2015 international conference on interactive collaborative learning (ICL). Firenze, Italy, pp 1102–1111. https://doi.org/10.1109/ICL.2015.7318186
8. Andres P, Dobrovská D (2014) Managing interaction skills in the engineering pedagogy programme. In: 2014 international conference on interactive collaborative learning (ICL). Dubai, United Arab Emirates, pp 112–116. https://doi.org/10.1109/ICL.2014.7017756
9. Dahnoun N (2020) Pedagogy for engineering and digital pedagogy, pp 1–1. https://doi.org/10.1109/MECO49872.2020.9134311
10. Darling-Hammond L (2018) Teacher education and the future of work. J Educ 198(2):5–26
11. Anderson LW, Krathwohl DR (2018) A taxonomy for learning, teaching, and assessing: a revision of Bloom's Taxonomy of educational objectives. Routledge

12. Passos AC, Junior FL, de Arruda HH (2022)Project-based learning activity with robotics: a low-cost case study. In: 2022 Latin American robotics symposium (LARS), 2022 Brazilian symposium on robotics (SBR), and 2022 workshop on robotics in education (WRE). São Bernardo do Campo, Brazil, pp 360-365. https://doi.org/10.1109/LARS/SBR/WRE56824.2022.9995849

13. Sanchez-Romero JL, Jimeno-Morenilla A, Pertegal-Felices ML, Mora-Mora H (2019) Design and application of project-based learning methodologies for small groups within computer fundamentals subjects. In IEEE Access, vol 7, pp 12456–12466

14. Banakhr FA, Iqbal MJ, Shaukat N (2018)Active project based learning pedagogies: learning hardware, software design and wireless sensor instrumentation. In: 2018 IEEE global engineering education conference (EDUCON). Santa Cruz de Tenerife, Spain, pp 1870–1874. https://doi.org/10.1109/EDUCON.2018.8363463

15. Tharakan JP (2022)A methodology for integration of project based learning into core engineering courses. In: 2022 IEEE IFEES world engineering education forum—global engineering deans council (WEEF-GEDC). Cape Town, South Africa, pp 1–3. https://doi.org/10.1109/WEEF-GEDC54384.2022.9996217

16. Barab SA, Squire KD (2018) Design-based research: putting a stake in the ground. J Learn Sci 27(1):3–56

17. Morais P, Ferreira MJ, Veloso B (2021) Improving student engagement with project-based learning: a case study in software engineering. IEEE Revista Iberoamericana de Tecnologias del Aprendizaje 16(1):21–28. https://doi.org/10.1109/RITA.2021.3052677

18. Nadarajan K et al (2023) The effectiveness of a technology-based isometrical transformation flipped classroom learning strategy in improving students' higher order thinking skills. IEEE Access 11:4155–4172. https://doi.org/10.1109/ACCESS.2022.3230860

19. Azizah N, Nisa J, Bahar S, Ardiansyah AN, Rozak A (2022) The influence of blended learning with flipped classroom model on motivation in learning geography. In: 2022 seventh international conference on informatics and computing (ICIC). Denpasar, Bali, Indonesia, pp 1–4. https://doi.org/10.1109/ICIC56845.2022.10006936

20. Wen X, Dawod AY (2022) Post-covid teaching of physics experiments through flipped classroom & blended teaching practice at college. In: 2022 international conference on engineering and emerging technologies (ICEET). Kuala Lumpur, Malaysia, pp 1–6. https://doi.org/10.1109/ICEET56468.2022.10007197

21. Do Nascimento Neto GS, Da Paz Silva MA, De Lima Teixeira LR, Do Nascimento Araújo Maia CJ, Chiesa ER, Lima CHJ (2022)Development of an introduction to robotics course for 9th-grade students of public schools using the flipped classroom methodology. In: 2022 Latin American robotics symposium (LARS), 2022 Brazilian symposium on robotics (SBR), and 2022 workshop on robotics in education (WRE). São Bernardo do Campo, Brazil, pp 1-6. https://doi.org/10.1109/LARS/SBR/WRE56824.2022.9995924

22. Elgrably IS, Ronaldo Bezerra Oliveira S (2022)Using flipped classroom to promote active learning and engagement in a Software Testing subject remotely during the COVID-19 pandemic. In: 2022 IEEE frontiers in education conference (FIE). Uppsala, Sweden, pp 1–6. https://doi.org/10.1109/FIE56618.2022.9962379

23. Zhang L, Niu J (2022)Research to practice in computer programming course using flipped classroom. In: 2022 IEEE frontiers in education conference (FIE). Uppsala, Sweden, pp 1–7. https://doi.org/10.1109/FIE56618.2022.9962430

24. Marqués Andrés M, Contelles JMB (2022) What students say about the flipped classroom. In: IEEE Revista Iberoamericana de Tecnologias del Aprendizaje, vol 17, no 3, pp 235–244. https://doi.org/10.1109/RITA.2022.3191470

25. Troya J, Parejo JA, Segura S, Gámez-Díaz A, Márquez-Chamorro AE, del-Río-Ortega A (2021). Flipping laboratory sessions in a computer science course: an experience report. IEEE Trans Educ 64(2):139–146. https://doi.org/10.1109/TE.2020.3016593

26. Parejo JA, Troya J, Segura S, del-Río-Ortega A, Gámez-Díaz A, Márquez-Chamorro AE (2020) Flipping laboratory sessions: an experience in computer science. In: IEEE Revista Iberoamericana de Tecnologias del Aprendizaje, vol 15, no 3, pp 183–191. https://doi.org/10.1109/RITA.2020.3008132

27. Gren L (2020) A flipped classroom approach to teaching empirical software engineering. IEEE Trans Educ 63(3):155–163. https://doi.org/10.1109/TE.2019.2960264
28. Kim Y, Ahn C (2018) Effect of combined use of flipped learning and inquiry-based learning on a system modeling and control course. IEEE Trans Educ 61(2):136–142. https://doi.org/10.1109/TE.2017.2774194
29. Hawtrey K (2007) Using experiential learning techniques. J Econ Educ 38(2):143–152
30. Felicia P (2011) Handbook of research on improving learning and motivation. ISBN 978-1609604967
31. MIT Sloan Management (2016) Action learning—how does it work in practice? Why back mission site
32. MIT Sloan Management (2016) The power of experiential learning, 4-H cooperative curriculum system
33. MIT Sloan Management (2014) The out of eden walk: an experiential learning journey from the virtual to the real. http://www.edutopia.org/blog/out-of-eden-experiential-learning-homatavangar. Accessed 3 Jan 2014 (Retrieved 2020)
34. MIT Sloan (2021) Action learning—how does it work in practice? http://mitsloan.mit.edu/mba/program-components/hands-on-learning/ (retrieved 2021)
35. MIT Sloan (2020) The power of experiential learning, 4-H cooperative curriculum system. http://njaes.rutgers.edu/learnbydoing/ (retrieved 2020)
36. Beard C (2010) The experiential learning toolkit: blending practice with concepts, p 20. ISBN 9780749459345. https://books.google.com/books?id=DAhYlaZhRI8C&pg=PA20 (retrieved 2020)
37. Itin CM (1999) Reasserting the philosophy of experiential education as a vehicle for change in the 21st century. J Phys Educ 22(2):91–98
38. Breunig MC (2009) Teaching Dewey's experience and education experientially. In: Stremba B, Bisson CA (eds) Teaching adventure education theory: best practices, p 122. ISBN 9780736071260
39. Nicomachean Ethics (1911) Aristotle, Book 2, D.P. Chase translation
40. Dixon NM, Adams DE, Cullins R (1997) Learning style. In: Assessment, development, and measurement, p 41. ISBN 9781562860493
41. Kolb D (1984) Experiential learning: experience as the source of learning and development. Prentice Hall, Englewood Cliffs, NJ, p 21
42. Kolb D (2012) http://www2.le.ac.uk/departments/gradschool/training/resources/teaching/theories/kolb
43. Merriam SB, Caffarella RS, Baumgartner LM (2007) Learning in adulthood: a comprehensive guide. John Wiley & Sons Inc., San Francisco
44. Moon J (2004) A handbook of reflective and experiential learning: theory and practice. Routledge Falmer, London, p 126
45. Kolb D (1984) Experiential learning as the science of learning and development. Prentice Hall, Englewood Cliffs, NJ
46. Chickering A (1977) Experience and learning. Change Magazine Press, New York, p 63
47. Hutton M (1980) Learning from action: a conceptual framework. In: Warner Weil S, McGill M (eds) Making sense of experiential learning. SRHE/Open University Press, Milton Keynes, pp 50–99
48. Hamblen JO, Owen HL, Yalamanchili S, Dao B (1999) An undergraduate computer engineering rapid systems prototyping design laboratory. In: IEEE transactions on education, vol 42, no 1, pp 8–14. https://doi.org/10.1109/13.746325
49. Zhou C, Li H, Bian Y (2020) Identifying the optimal 3D display technology for hands-on virtual experiential learning: a comparison study. IEEE Access 8:73791–73803. https://doi.org/10.1109/ACCESS.2020.2988678
50. Rho E, Chan K, Varoy EJ, Giacaman N (2020) An experiential learning approach to learning manual communication through a virtual reality environment. In: IEEE transactions on learning technologies, vol 13, no 3, pp 477–490. https://doi.org/10.1109/TLT.2020.2988523

51. Hajshirmohammadi A (2017) Incorporating experiential learning in engineering courses. In: IEEE communications magazine, vol 55, no 11, pp 166–169. https://doi.org/10.1109/MCOM.2017.1700373
52. Kirschner PA, Gerards M (2017) Three worlds of CSCL: a review of the literature. J Comput Supp Collab Learn 12(1):3–23
53. Kupperman J, Figg C (2018) The experimental college: an innovation in American higher education. University of California Press
54. Mitchell S (2018) The role of experimentation in the development of educational technology. J Educ Technol Dev Exchange 11(1):1–8

Preliminary Evaluation of Experiential Learning in Engineering Pedagogy for Undergraduate Students Learning Logic Design Concepts

Omer Alkelany, Hatem Khater, Mohamed Kamal, and Hosam E. Mostafa

1 Introduction: Experiential Learning Overview

Experiential learning requires the showing of the directions by the instructor, and not giving the learners all the details of how to take the route to the desired destination [1]. Thus, it makes learning an experience that moves beyond the classroom instruction and allows students the opportunity to draw conclusions. It also allows students to be more involved in their own learning process.

Experiential Learning is sometimes classified as learning by reflection on doing [2–10]. It is not a new concept, and various philosophers stressed it in their teachings. For example, it was conceptualized by Aristotle about Ethics as "for the things we have to learn before we can do them, we learn by doing them (first!)" [11]. However, in the 1970s, Kolb developed a fundamental modern model of experiential learning [12]. According to Kolb, [13, 14] the learner must be actively involved in the experience; reflect on the experience; analyze the outcomes; and perform decision making and problem-solving skills in order to use the new ideas gained from the prior experience. In this process, instructors give constructive feedback to the learners, but they should not rush to provide the answer [15–17], especially when creative abilities are to be developed (critical thinking, design, synthesis, etc.), and particularly when there is not a single right answer. Learners should use their experience to judge or evaluate an outcome of a targeted component and share it with the learners [18, 19].

O. Alkelany (✉) · H. Khater · M. Kamal
Mechanical Engineering-Mechatronics Department, Faculty of Engineering, Horus University-Egypt, New Damietta, Egypt
e-mail: oalkelalny@horus.edu.eg

H. Khater
e-mail: hkhater@horus.edu.eg

H. E. Mostafa
Faculty of Engineering, Alexandria University, Alexandria, Egypt
e-mail: hossam.mostafa@alexu.edu.eg

Experiential learning is used in different aspects of engineering education. For example [20], it was used via hardware emulators, and FPGA were used in latter stage of complex multi-part designs. FPGAs are configurable logic chips founded in 1985. FPGA key feature is that it allow the designer to describe logic circuits (hardware) in code, test it, and implement it on the lab without having to use a manufacturer for each circuit. Also, in 2020, two different comparative studies for experiential learning were done in two different universities in China, and New Zealand considering virtual reality application. These comparative studies concluded that experiential learning enhances learning experience [21, 22]. Furthermore, other researchers investigated the incorporation of experiential learning at a Canadian university, in 2017, but they implemented it in a single engineering course, without FPGAs, and their results were limited [23].

The research presented targets the Sustainable Development Goals (SDGs), on Quality Education. As will be shown, it improves the preliminary assessment results show improvement on education when the techniques proposed are used.

2 A Proposed Multi-Level Preliminary Logic-Design-Project Using FPGA

In a typical Digital and Logic Design course, the instructor may wish to have his/her students experience the design of a two packed BCD inputs to a seven-segment display decoder. This problem is so simple that can be designed with a few discrete components. But the students will need to go through the typical design process, decide on which components to use (buy parts), connect the parts, and test the final product before the semester ends. Afterwards, students typically spend significant amount of time to perform proper wiring to connect project components. Even when they succeed in doing so, they usually feel that what they implemented is so tedious and frustrating at times. Because of that, the appreciation of learning may be so limited. In such approach, the opportunity for innovation, or expansion is very low, or none.

To illustrate, a block diagram of a given preliminary problem can be seen in the Fig. 1. The students will need to design a four-bit binary adder, an overflow detector, then use it to provide inputs to the second stage adder. Finally, they will need to design a BCD to seven-segment decoder. It is well known, that there are parts that students can buy such as the 74,283-adder chip, and the BCD to Seven-Segment 7447 decoder chip, and discrete NAND gate chips for the overflow detection logic.

In such approach, not only the appreciation of learning may be limited, but also, the majority of time they spent was on none major tasks, (e.g. buying parts, wiring components, and so on).

So, what we propose is this research is the use of FPGA technology instead. FPGA development tools with the board will allow the students to design and test various circuits (from simple to complex) in different courses.
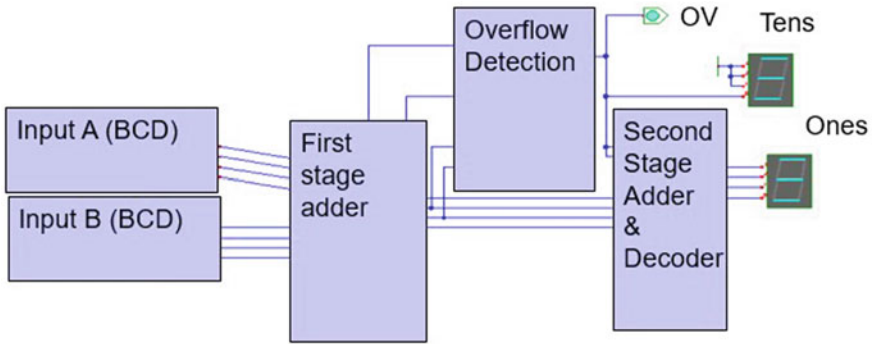
Fig. 1 Block diagram of the BCD circuit
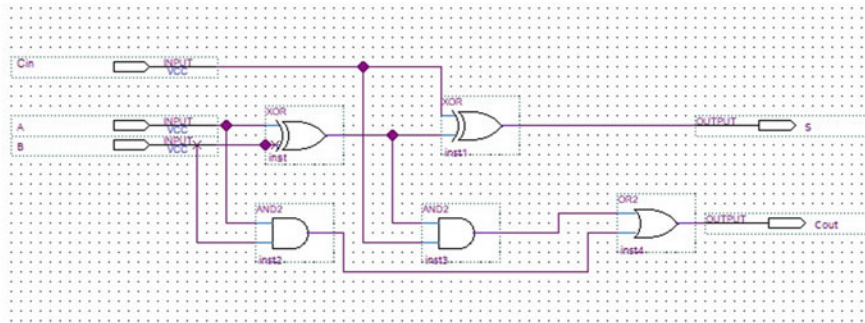
Fig. 2 Schematic entry of a 1-bit Full adder

To illustrate this further, a schematic entry of parts of the mentioned circuit can be inserted in a schematic editor such as that found in Quartus II package for the Intel FPGA as shown in Fig. 2.

Once the students design one small part, they can assign input and output pins to specific board input pins (e.g. switches) and board output pins (e.g. LEDs). Then, they can simulate the design and verify its functionality. An example of simulation result of a two input XOR gate, which is used in the full adder circuit students have just designed is shown in Fig. 3.

It is worth mentioning that students will not need to go through any difficulty of buying any hardware, or checking the proper wiring. Wiring is actually done at the chip level (internally), and reconfigurations are done by the development tool. So, the student time can be directed to useful learning. Especially when what they will learn is what the industry is using in FPGA design. Eventually, students will appreciate the learning experience since it is via the state-of-the-art technology.

It is known that a successful experience will lead to another. Instructors can demonstrate how students can avoid the frustration of spending too much time on trivial errors. In the example here, note that four 1-bit full adders, can be used to
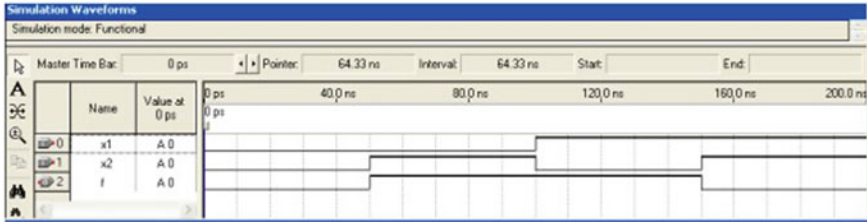
Fig. 3 Example of functional simulation
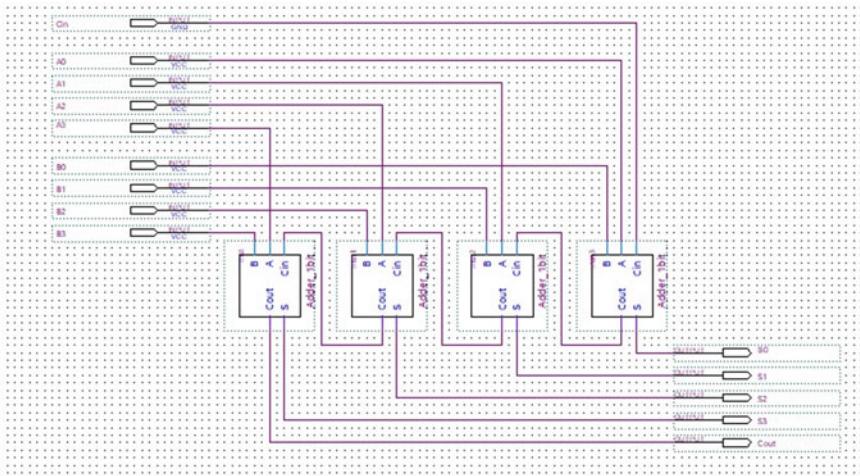
Fig. 4 The 4-bit adder circuit in schematic editor

develop one 4-bit Adder as shown in Fig. 4. So, the students can learn (incrementally) how to use prior parts in designing bigger parts.

The next step is the schematic entry of the overflow detection as shown in Fig. 5. But it is known that the BCD to seven-segment display circuit, has 4 inputs, 7 and outputs. So, it will be useful to students in this stage to design it using Hardware Description Language (e.g. Verilog HDL) to design such decoder. Figure 6 shows the code for such decoder.

Once all parts of the BCD Adder to seven-segment display are designed, they can be integrated as shown in Fig. 7. At this moment, the students can test the whole circuit via the use of on-board toggle switches and seven segments for the output in this illustration. Finally, Fig. 8 shows the result of providing A = 0110 or 6, B = 1000 or 8, for the summation to yield 14 as shown on the two right most seven-segments.

Using the same example problem, the instructor may further challenge the students by requesting that the inputs come from a keyboard, and the outputs go to LCD instead. Thus, students will need to use microcontrollers to connect to such interfaces and so on. Also, for advanced courses, the same project can be extended to send the
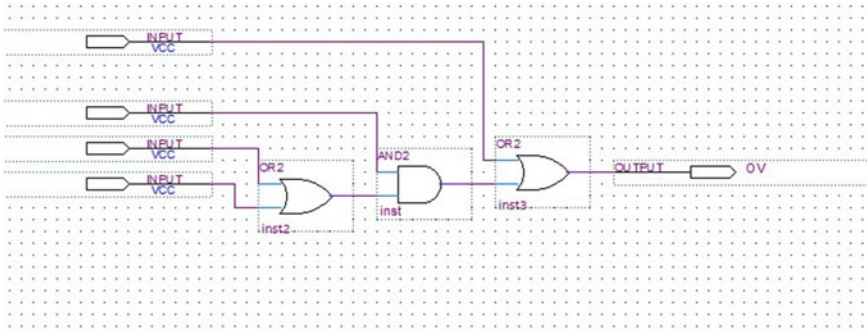
Fig. 5 BCD overflow detection circuit

```
1    module seg7_lut (Seg,BCD0,BCD1,BCD2,BCD3);
2    input BCD0,BCD1,BCD2,BCD3;
3    wire [3:0] BCD;
4    output [6:0] Seg;
5    reg [6:0] Seg;
6
7    assign BCD={BCD3,BCD2,BCD1,BCD0};
8
9    always @ (BCD)
10   begin
11   case (BCD)
12       4'h0:Seg=7'b1000000; //0
13       4'h1:Seg=7'b1111001; //1
14       4'h2:Seg=7'b0100100; //2
15       4'h3:Seg=7'b0110000; //3
16       4'h4:Seg=7'b0011001; //4
17       4'h5:Seg=7'b0010010; //5
18       4'h6:Seg=7'b0000010; //6
19       4'h7:Seg=7'b1111000; //7
20       4'h8:Seg=7'b0000000; //8
21       4'h9:Seg=7'b0011000; //9
22       default:Seg=7'b1111111; //off
23   endcase
24   end
25   endmodule
26
```

Fig. 6 Verilog HDL code for the BCD decoder

outputs to a network interface, thus using a web browser, and a microprocessor on the FPGA chip and so on. In those later experiences, students will need to learn other design entry methods such as Hardware Description Languages (HDL), such as Verilog or VHDL together with Schematic editors.
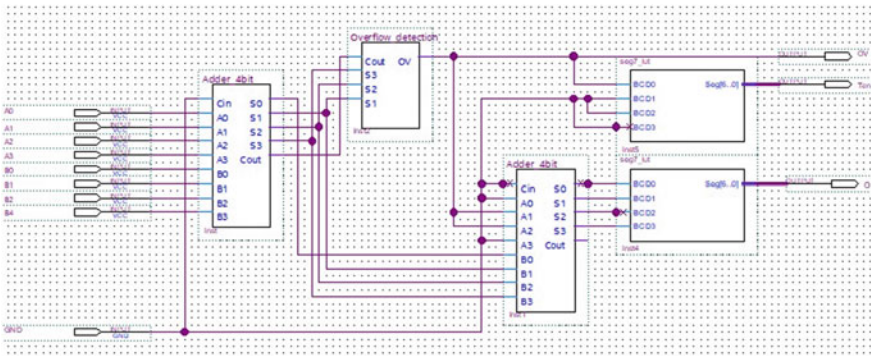
Fig. 7 Integrating all parts to build full logic circuit
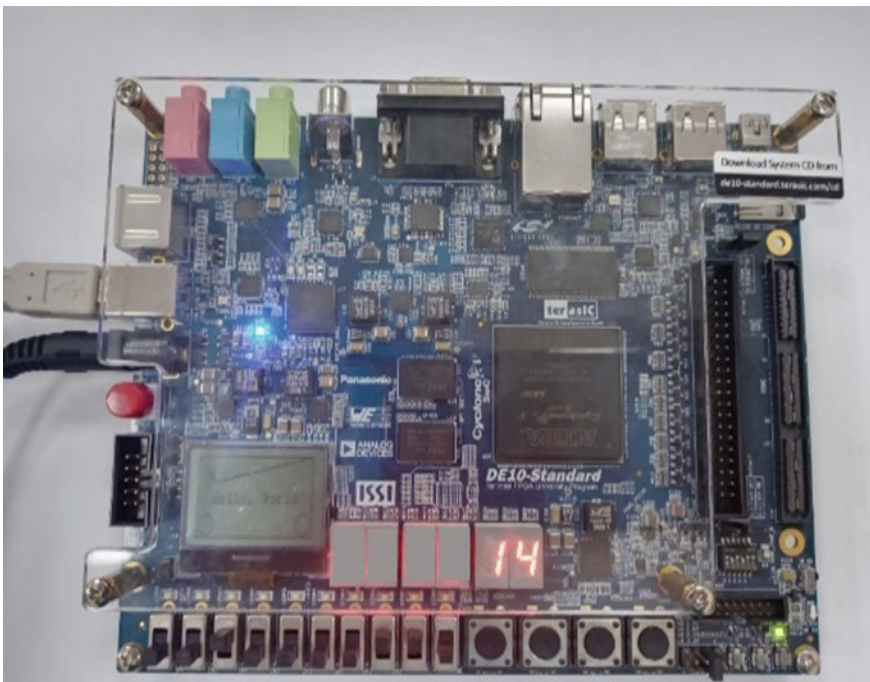
Fig. 8 DE10-Standard FPGA board configured to BCD circuit. Inputs provided by toggle switches, and outputs displayed on Seven-segments, and overflow detection output on the green LED at the bottom right corner (leftmost 4 seven segments not used)

Table 1 T-test analysis (done in Microsoft Excel)

	Pre-FPGA (59 students)	Post-FPGA (same students who took the PRE-FPGA quiz, count 59)
Mean	11.78	19.83
Variance	24.80	14.63
Hypothesized mean difference	0	
t Stat	− 9.611680299	
P(T ≤ t) one-tail	6.59511E−14	
P(T ≤ t) two-tail	1.319022E−13	

3 Experiential Learning Preliminary Evaluation and Numerical Results

To quantize the effectiveness of experiential learning, we've developed a preliminary evaluation setup to test the hypothesis: Experiential learning in engineering education improves learners' retention of knowledge, and provides better opportunity of innovation and creativity. So, we conducted a test on same set of students (i.e., a small group of 59 students) and provided them with instruction about FPGA devices, their applications in logic design, and their internal structures. There were similar conceptual problems given to the same set of the students before and after this phase of the test. Then we used an opposite null hypothesis of: There was no difference in the students' understanding of the logic design concepts before and after the exposure to given learning material. The T-test showed (via both the one-tailed and the two-tailed test) that there is a significant statistical difference and the null-hypothesis failed. Table 1 shows the statistical details of the two-group (same) different mean T-test for preliminary evaluation.

Null Hypothesis was that: The two methods are same, i.e. no difference between means. If the p-value is less than the significance level, the difference between means is statistically significant. Excel provides p-values for both one-tailed and two-tailed t-tests. One-tailed t-tests can detect differences between means in only one direction. For example, a one-tailed test might determine only whether Method B is greater than Method A. Two-tailed tests can detect differences in either direction—greater than or less than.

4 Conclusions

In this paper, the preliminary evaluation of the experiential learning pedagogy was performed.

To evaluate Experiential learning, we perform numerical/experimental analysis of an existing FPGA board and proposed how it can be used in a step-by-step multi-level undergraduate engineering education. Furthermore, a two-tailed T-test analysis statistically showed that there is a significant statistical difference in students' understanding of logic design concepts comparing their answers to basic similar concepts, but different questions *prior-to* and *after* exposure to FPGA devices, their applications in logic design, and their internal structures. In this preliminary analysis, and since the null-hypothesis we made failed significantly, we stated that experiential is a promising alternative to enhance students' learning. More analysis comparing the outcomes of experiential learning in logic-design-based courses is the subject of an on-going research project STDF#45945.

The experiential learning method used can be applied on a global scale in any geographical area. A survey is done separately by the authors [24] comparing this method with other methods used in the engineering education.

5   Recommendations

Due to its favorable comparison results, experimental learning is recommended in the engineering education, in particular when hands on experiences are used in teaching the courses.

References

1. Hawtrey K (2007) Using experiential learning techniques. J Econ Educ 38(2):143–152
2. Felicia P (2011) Handbook of research on improving learning and motivation. ISBN 978-1609604967
3. MIT Sloan Management (2016) "Action learning—how does it work in practice?", Why back mission site
4. MIT Sloan Management (2016) The power of experiential learning. 4-H Cooperative Curriculum System
5. MIT Sloan Management (2014) The out of eden walk: an experiential learning journey from the virtual to the real. http://www.edutopia.org/blog/out-of-eden-experiential-learning-homa-tavangar. Accessed 2020.
6. MIT Sloan. Action learning—how does it work in practice? http://mitsloan.mit.edu/mba/program-components/hands-on-learning/. Accessed 2021.
7. MIT Sloan. The power of experiential learning. 4-H Cooperative Curriculum System. http://njaes.rutgers.edu/learnbydoing/. Accessed 2020
8. Beard C (2010) The experiential learning toolkit: blending practice with concepts. p 20. ISBN 9780749459345. https://books.google.com/books?id=DAhYlaZhRI8C&pg=PA20. Accessed 2020

9. Itin CM (1999) Reasserting the philosophy of experiential education as a vehicle for change in the 21st century. J Phys Educ 22(2):91–98
10. Breunig, Mary C (2009) Teaching Dewey's experience and education experientially. In: Stremba B, Bisson CA (eds) Teaching adventure education theory: best practices, p 122. ISBN 9780736071260
11. Nicomachean Ethics (1911) Aristotle, Book 2. D.P. Chase translation
12. Dixon NM, Adams DE, Cullins R (1997) Learning style. Assessment, Development, and Measurement, p 41. ISBN 9781562860493
13. Kolb D (1984) Experiential learning: experience as the source of learning and development. Prentice Hall, Englewood Cliffs, NJ, p 21
14. Kolb D (2012) http://www2.le.ac.uk/departments/gradschool/training/resources/teaching/theories/kolb
15. Merriam SB, Caffarella RS, Baumgartner LM (2007) Learning in adulthood: a comprehensive guide. John Wiley & Sons Inc., San Francisco
16. Moon J (2004) A handbook of reflective and experiential learning: theory and practice. Routledge Falmer, London, p 126
17. Kolb D (1984) Experiential learning as the science of learning and development. Prentice Hall, Englewood Cliffs, NJ
18. Chickering A (1977) Experience and learning. Change Magazine Press, New York, p 63
19. Hutton M (1980) Learning from action: a conceptual framework. In: Warner Weil S, McGill M (eds) Making sense of experiential learning. Milton Keynes: SRHE/Open University Press, pp 50–59
20. Hamblen JO, Owen HL, Yalamanchili S, Dao B (1999) An undergraduate computer engineering rapid systems prototyping design laboratory. IEEE Trans Educ 42(1):8–14. https://doi.org/10.1109/13.746325
21. Zhou C, Li H, Bian Y (2020) Identifying the optimal 3D display technology for hands-on virtual experiential learning: a comparison study. IEEE Access 8:73791–73803. https://doi.org/10.1109/ACCESS.2020.2988678
22. Rho E, Chan K, Varoy HJ, Giacaman N (2020) An experiential learning approach to learning manual communication through a virtual reality environment. IEEE Trans Learn Technol 13(3):477–490. https://doi.org/10.1109/TLT.2020.2988523
23. Hajshirmohammadi A (2017) Incorporating experiential learning in engineering courses. IEEE Commun Mag 55(11):166–169. https://doi.org/10.1109/MCOM.2017.1700373
24. Alkelany O, Khater H, Kamal M, Mostafa HE (2023) Survey and evaluation of applied modern engineering pedagogy. Accepted by the First international conference on engineering solutions toward sustainable development (ESSD-2023)

Analysis of the Time Multiplexed Sampling and a Proposed Prototype for Effective Heterogenous Data Acquisition Systems

Omer Alkelany

1 Introduction

Data Acquisition systems are needed for almost all everyday systems we interact with. Multi-channel systems work with multitude of analog inputs. Typically, homogenous, i.e. a constant sampling period for all channels is used, due to the complexity of heterogenous sampling and data reconstruction. In our prior work, we presented a complex problem of Same-Time-Sampling conflict, for such heterogenous data acquisition systems, and presented a preliminary solution to avoid such conflict. This conflict, if happens, would cause failure of the schedule, thus lead to data loss, or data corruption. Most of the signals that are used in industrial control or automation are analog signals. But, analog signals cannot be used for digital instrumentation and control except after conversion to digital form. A plethora of Data Acquisition Systems (DAQs) are available today which vary in their number of input channels, sampling rate, and resolution. However, they inefficiently allocate ADC resources and generate redundant data when a set of heterogeneous signals, i.e. both low frequency and high frequency signals, is connected. In this thesis, we present a novel algorithm, namely the Heterogeneous Time-Multiplexed Sampling (HTMS) algorithm, which solves for a schedule pattern that allows a single multiplexed ADC to sample a heterogeneous set of input signals and enables (in many cases) each channel to have a different sampling rate. This reduces the amount of redundant (more samples taken than needed) data generated and increases the amount of hardware utilization which means that the same DAQ with HTMS can sample more input signals than one without HTMS.

The algorithm presented targets the Sustainable Development Goals (SDGs), on industry-innovation and infrastructure. As will be shown, it improves the design

O. Alkelany (✉)

Mechanical Engineering-Mechatronics Department, Faculty of Engineering, Horus University-Egypt, New Damietta, Egypt
e-mail: oalkelalny@horus.edu.eg

quality of multi-channel data aquisition systems, which are widely used in the industry.

1.1 Conventional Data Acquisition Systems

In today's world of technology, data acquisition is everywhere, to sample analog signals, process them, and present them in useful digital formats [1, 2]. The Nyquist-Shannon sampling theorem states that a signal with maximum frequency component of f Hz, cannot be reconstructed unless the sampling frequency is at least 2f Hz [1]. In sophisticated bioinformatic heterogenous data acquisition system applications such as in [2–7], homogenous channels are not expected unlike most signal processing algorithms which make the assumption that samples of a signal are equally spaced.

If it is desired to sample multiple signals simultaneously, it is possible to purchase multiple single-channel DAQs, but this is usually an expensive approach. Thus, a multi-channel DAQ can be used instead. Consequently, one DAQ can process the data for multiple channels at once, leading to a lower cost.

General purpose multi-channel DAQs [3–7] on the market today make use of a simple sampling technique called Round-robin to time-multiplex the sampling of all connected signals. When using the Round-robin sampling technique, the minimum sampling frequency of any channel is limited by the minimum required sampling frequency of the highest frequency input signal. If the input signals contain a heterogeneous mix of both high frequency and low frequency signals, the low frequency signals are oversampled. This results in redundant data and uses up ADC resources that could be used to sample additional signals.

1.2 Alternative Technologies

Numerous alternative technologies can be found which aid in the alleviating some of the disadvantages of conventional DAQs [9–22]. Non-uniform sampling techniques exist that relax the uniform interval restriction. One such technique is called Weighted Periodic None-uniform Sampling (WPNS) [8]. Using two A/D converters, the WPNS can estimate the frequency spectrum of a signal that has a higher bandwidth than the A/D converters [8].

The Weighted Round-Robin (WRR) [9] algorithm cycles through a list of processes and allocates multiple blocks of time to each process for its continuous execution behavior based on its priority. Priorities can be translated into weights, where a high priority process can be given a higher weight. For example, if a process is given a weight of 30,000, it can get 30,000 consecutive blocks of time when assigned to a CPU. Thus, processes with higher weights get more CPU time and the algorithm is successful as long as the sum of the weights does not exceed the maximum number of time-blocks a CPU can serve per second.

In this research paper, a novel sample scheduling algorithm, namely the Heterogeneous Time-Multiplexed Sampling (HTMS) algorithm, is proposed that optimizes the sample rate of each channel allowing (in many cases) each channel to be sampled at a different rate. HTMS increases the sampling capability of a DAQ with a single multiplexed ADC connected to a heterogeneous set of input signals by efficiently allocating ADC resources. A heterogeneous set of signals is a set in which the required sampling rates for each channel vary. HTMS also reduces the amount of redundant data acquired. Less redundant data leads to lower storage requirements, lower power usage, and less required CPU time. This is the key to the design of our novel HTMS based DQA, presented in brief in Fig. 1 [23].

A multi-channel standalone DAQ prototype implementing HTMS for quasi-simultaneous time-multiplexed sampling of a heterogeneous set of up to 32 signals is presented. The prototype DAQ features a learning mode to automatically determine the sample frequencies of the connected signals. It can also be used in standalone mode to save data to an SD Card or in peripheral mode where data is sent to a host via an Ethernet interface. Tests are performed using the prototype DAQ and a heterogeneous set of input signals. A comparison is made between the prototype DAQ and two current commercial DAQs. Finally, problems with the prototype and possible solutions are presented along with future opportunities for further research.
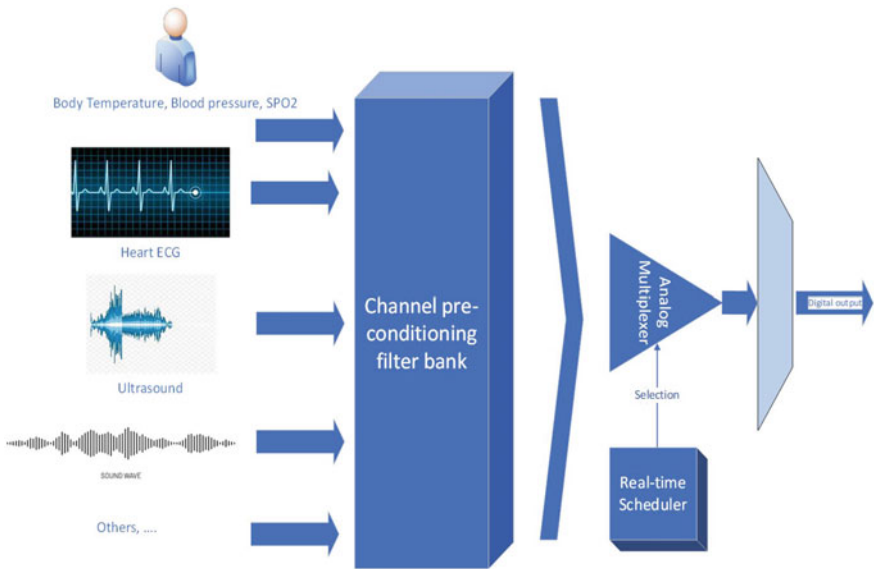
Fig. 1 Illustration of a HTMS-based DAQ with multichannel heterogenous Data Acquisition and a single A/D converter, (biomedical analog input signals are presented as examples)

2   Proposed HTMS Algorithm and Design

The purpose of HTMS is to optimally allocate ADC samples to multiplexed channels to maximize the number of signals that can be sampled with any given ADC and reduce the amount of redundant data required. Using HTMS to efficiently maximize ADC utilization can lower the cost for a DAQ compared to one using conventional scheduling methods by lowering the required ADC performance.

Given a set of channels with desired sampling frequencies, each channel's sampling rate is quantized (rounded) up to a factor of both the ADC's sampling rate and all previously chosen sampling rates. The first channel to be quantized has the highest desired sampling rate and we continue in descending order until all channels are quantized. The minimum desired frequency is called the minimum frequency and the quantized frequency is called the chosen frequency.

Next, the minimum schedule length is determined by finding the Least Common Multiple (LCM) of the quantized sample periods of all channels.

Finally, each channel's sampling pattern must be shifted to avoid STS events. This is done by letting the highest frequency channel have a shift of zero and assigning each consecutive channel the shift corresponding to the first open sample period with respect to previously assigned channels. Given that the sum of all chosen frequencies doesn't exceed the maximum sample rate of the ADC, we will not have a CSP problem caused by incorrect shifts.

The HTMS algorithm can run on-the-fly or can be used to generate a full schedule in advance.

The more factors the ADC's sampling frequency has, the more options the HTMS algorithm has when choosing a channel's sampling frequency. The HTMS algorithm chooses the sampling frequency as the least factor of the ADC's sampling frequency that is larger than the desired sampling frequency.

A preliminary prototype is designed and tested to demonstrate the merits of the HTMS algorithm. Figure 2 demonstrates the block diagram of the designed prototype.

After initial examination of the proposed design, a printed circuit board was fabricated and examined. Figures 3 and 4 demonstrate the top and bottom view of the developed board.

3   Preliminary Assessment and Evaluation of the Prototype Design

The more heterogeneous the input signal set is (the larger the difference between the minimum sampling frequencies of the channels in the set), the better the algorithm will perform at reducing redundant data and allocating ADC resources.

Since each signal may require a different minimum sampling rate, an optimized sampling rate can be chosen for it.
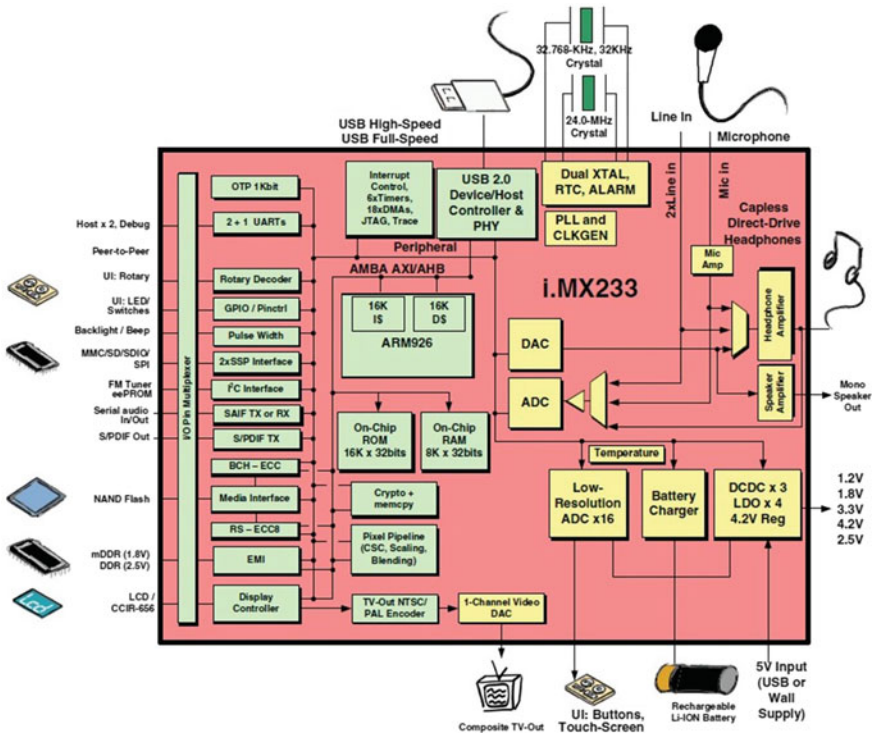
Fig. 2 HTMS based DAQ, block diagram
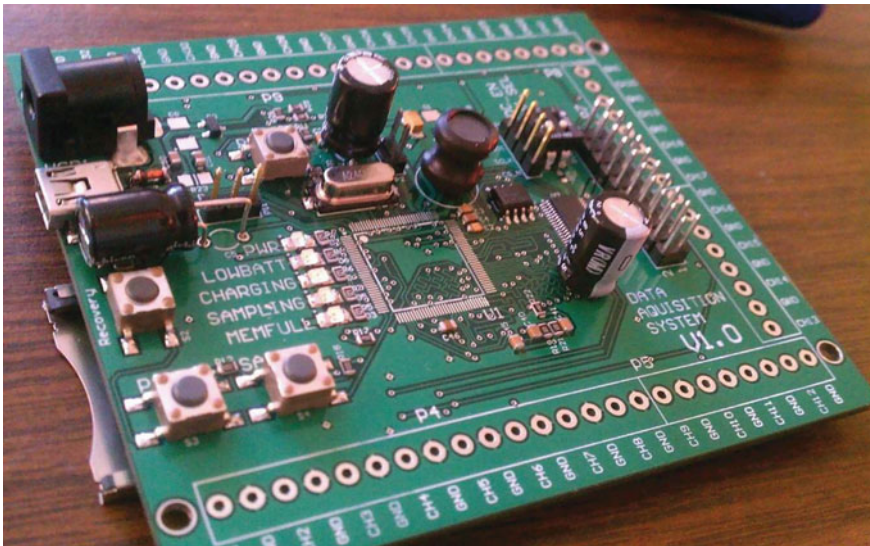
Fig. 3 HTMS based DAQ, top view
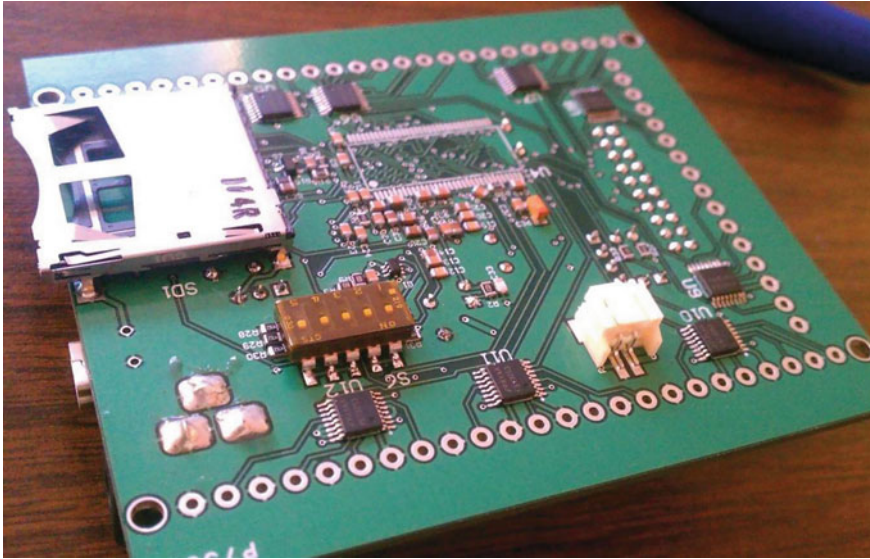
Fig. 4 HTMS based DAQ, bottom view

The ability to execute an optimized sampling schedule means that sample periods of the ADC are not wasted on channels that don't require them. This allows the quasi-simultaneous sampling of more signals than possible with a classic round-robin scheduling technique.

Since each channel is sampled at a close to optimal rate, there is very little redundant data. The output data size is optimized based on the sampling requirements of the input signal. This leads to reduced storage requirements and lower overall system cost.

Because redundant data is reduced, less time is spent processing redundant data which yields lower power consumption.

The HTMS algorithm generates a schedule that is repeatable. This yields the capability of continuous sampling for an arbitrary amount of time.

However, the sum of all chosen frequencies must be less than or equal to the sampling frequency of the ADC. There is a case when the sum of the Nyquist rates of all channels is less than the ADC's sampling rate but after quantization the sum of the chosen rates exceeds the ADC's sampling rate.

If the sampling frequency of the ADC has only a few factors then the quantization of desired sampling frequencies could result in less than optimal sampling.

The chosen frequencies are not absolutely optimal. If the minimum frequency lies between two factors it will be rounded up. This will cause some oversampling but it is better than round-robin. Finally, the frequency spectrum of any given input signal is assumed to be constant.

An input signal was acquired simultaneously on 5 different channels of the proposed HTMS based DAQ and the NI USB-6211 industrial counterpart at the

Table 1 HDAQ and NI USB-6211 comparison (10 ms)

Channel	Sampling frequency (Hz)	RMS (v)
0	477,204	0.027782
1	238,602	0.033302
2	119,301	0.026714
3	39,767	0.027038
4	5681	0.029125
Average		0.0287922

same time. The signal was a 1 kHz sinusoid with 1.8 V peak-to-peak and a 1.15 V DC offset generated by a GW Instek GFG-8250A function generator. The NI USB-6211 sampled the signal at 250 kSa/s. The HDAQ sampled the signal at the rates shown in Table 8.4. Due to frequency calibration error, only 10 ms of the signal is compared. For each channel, the DAQ data with the slower sampling rate is re-sampled to match that of the DAQ with the higher sampling rate. Table 1 summarizes the results of this comparison by calculating the root-mean-square error between both captured signals. All 5 channels satisfy the minimum sampling rate required in [1]. It is worth mentioning that even though the proposed solution is capable of improving the quality of sampling, but excessive over sampling requires also excessive storage memory.

To analyze the effect of excessive over sampling, let us assume that the 1 kHz signal, which has a minimum sampling frequency of 2000 samples per second according to [1], is excessively over sampled at 12 kHz. This yields 10,000 extra samples where 2000 may have sufficed (e.g. if the signal was a single tone sine wave). This is equivalent to 83.3% excessive data. So, it is not always wise to excessively over sample all channels to guarantee ability of reconstruction of all inputs, particularly when inputs have different frequency characteristics.

Consider a heterogenous set of inputs with frequencies equal to 1, 2, 3, and 8 kHz. An industrial counter part to the proposed DAQ will sample each input using at least 16 kHz, generating lots of redundant data for lower frequency inputs. However, the HTMS based DAQ will create the following schedule as mentioned before to avoid the STS problem [23], and avoiding the redundant sampling (Table 2).

Table 2 Generated schedule for the HTMS algorithm for a given set of inputs with heterogenous frequencies

Channel	Minimum sampling frequency (Hz)	HTMS calculated sampling frequency (Hz)
0	2	2
1	4	4
2	6	8
3	16	16

4 Conclusions

In a heterogeneous environment, the novel HTMS algorithm presented in this thesis yields better sampling capability, less redundant data, lower data storage requirements, and less required ADC and CPU performance than other methods, leading to a lower overall system cost and improved efficiency.

This paper demonstrated a detailed description of the proposed HTMS algorithm and a comparison to existing scheduling techniques. It also presented a prototype DAQ and used example cases of the algorithm in action. With a homogeneous set of input signals, we demonstrated that the HTMS based DAQ prototype is at least as capable as existing commercial DAQs with the same sampling rate. However, with a heterogeneous set of input signals, we show that the prototype DAQ's sampling capability increases while existing commercial DAQs have fixed sampling capability. In addition, no extra hardware is needed. The prototype DAQ uses common components, many of which are already used with commercial DAQs. Preliminary quantitate comparisons show that the HTMS based DAQ is comparable to industrial counter parts in capturing the original analog input. Furthermore, it is shown that the HTMS based DAQ outperforms traditional DAQs because it avoids redundant sampling by solving the STM scheduling conflict [23] via the proposed algorithm. The algorithm presented and the protype design shown can be applied on a global scale in any geographical area.

5 Recommendations

Further assessments of the developed HTMS prototype will be conducted and presented in the future. It is desired to compare its total cost with the cost of traditional DAQs such as those in [24–26].

References

1. Tsui JB (2004) Analog-to-digital converters. In: Digital techniques for wideband receivers. IET Digital Library, pp 155–217
2. Somappa L, Baghini MS (2022) Continuous-time hybrid delta sigma modulators for sub-mu W power multichannel biomedical applications. In: IEEE transactions on very large scale integration (VLSI) systems. https://doi.org/10.1109/TVLSI.2022.3140222

3. Moon J, HenkHunt R, Kenneth M, Devin D, Marshal SB, Matthew J (2021) Body-worn vital sign monitor. USA Patent US-11096596
4. Ryu J, Kim D, Kim Y, Seo M, Lee J (2021) Ultrasound diagnosis apparatus for self-diagnosis and remote-diagnosis, and method of operating the ultrasound diagnosis apparatus. USA Patent US-11123041
5. Banet M, Pede S, Meeks D, Marshal SH, Kenneth R (2021) Body-worn sensor for characterizing patients with heart failure. USA Patent US-11129537
6. Islam MN (2021) Multi-wavelength wearable device for non-invasive blood measurements in tissue. USA Patent US-11160455
7. Minas G, Rocha JG (2007) Sigma-delta analog to digital converter for use in lab-on-a-chip devices for biochemical clinical analyses. ECS Trans 4(171):2007
8. Ma B, Zhou J, Qu D (2010) Optimal weighted periodic nonuniform sampling sequences for digital alias-free signal processing. In: IEEE 10th international conference in signal processing (ICSP). Dalian
9. Wu J, Liu J-C, Zhao W (2007) Utilization-bound based schedulability analysis of weighted round robin schedulers, real-time systems symposium, pp 435–436
10. Imori M (1983) HReal time event selection and flash analog-to-digital converters. Jpn J Appl Phys 22:1427
11. Niu G, Cong L, Zhang J, Li X, Luo X (2021) Research progress of time-interleaved analog-to-digital converters. Integration 81:313–321. ISSN 0167-9260. https://doi.org/10.1016/j.vlsi.2021.08.007
12. D'Arco M, Napoli E, Zacharelos E, Angrisani L, Strollo AGM (2021) Enabling fine sample rate settings in DSOs with time-interleaved ADCs. Sensors 22(1). https://doi.org/10.3390/s22010234
13. Petrinovic D (1998) High efficiency multiplexing scheme for multi-channel A/D conversion. In: Midwest symposium on circuits and systems, pp 534–537
14. David L-G, Carlos P-P, Caballero S, Jesus J, Diaz I, Enrique G-C (1997) Simultaneous sampling by digital phase correction. Simultaneous sampling by digital phase correction June 1997 conference record—IEEE instrumentation and measurement technology conference 2:980–984, vol. 2. https://doi.org/10.1109/IMTC.1997.610287
15. Meurer RRM (2000) Enhancement of multichannel A/D conversion by a code division multiplex approach. In: IEEE 6th international symposium
16. Liu JWLCL (1973) Scheduling algorithms for multiprogramming in a hard-real-time environment. J ACM 20(1):46–61
17. Khramov KK, Romashov VV (2018) Operational modes of high-speed DACs: analysis and mathematical modelling. J Phys Conf Ser 1096:012158
18. RomashovVV et al (2020) Application high-speed digital-to-analog converters for direct digital synthesis of high-frequency radio signals. J Phys Conf Ser 1632:012023
19. Adimulam MK, Srinivas MB (2022) A 12-bit, 1.1-GS/s, low-power flash ADC. In: IEEE transactions on very large scale integration (VLSI) systems. https://doi.org/10.1109/TVLSI.2021.3138538
20. Li X, Zhou L (2020) A survey of high-speed high-resolution current steering DACs. J Semicond 41:111404
21. Saeed M, Martens Q, Larras O, Frappe B, Cardiff A, John BD (2021) Evaluation of level-crossing ADCs for event-driven ECG classification. In: IEEE transactions on biomedical circuits and systems. https://doi.org/10.1109/TBCAS.2021.3136206
22. Chen D, Cui XZ, Li Q, Cheng D, Fei W, Yang C, Yintang (2022) A survey on analog-to-digital converter integrated circuits for miniaturized high resolution ultrasonic imaging system. J Micromach 13(1). https://doi.org/10.3390/mi13010114
23. Alkelany O (2021) Simultaneous time sampling for heterogenous multichannel data acquisition. Int J Adv Sci Res Innov 4(2):39–52. ISSN: 2785-9541
24. National Instruments (2022) NI 9215 measurement system. https://sine.ni.com/nips/cds/view/p/lang/en/nid/209871. Accessed 2022

25. DATAQ, DATAQ DI-155, DATAQ. http://www.dataq.com/products/startkit/di155.htm. Accessed 2022
26. DATAQ, DATAQ DI-710, DATAQ. http://www.dataq.com/products/hardware/di710.htm Accessed 2022

A Comparative Study of Three Winding Configurations for Six-Phase Induction Motors

Basant A. Kalas, Ahmed Refaat, Mahmoud Fawzi, and Ayman Samy Abdel-Khalik

1 Introduction

Higher efficiency electric motors can lead to significant reductions in energy consumption and in turn reduce the environmental impact. Therefore, the mainstream of research nowadays is to replace conventional three-phase induction motors (3PIMs) with multi-phase induction motors (MPIMs) that possess a higher number of phases ($m > 3$). A six-phase induction motor (6PIM) refers to an induction motor (IM) with two sets of three-phase currents, which is essentially like connecting two 3PIMs in parallel [1]. By using a single dual stator winding IM instead of two separate 3PIMs, the cost is reduced, the power rating is increased, efficiency is increased, torque pulsation amplitude is reduced [2], reliability is improved with fault-tolerance capabilities [3–5], and low carbon emissions are obtained.

One of the main criteria for raising the efficiency of motors is the use of specially treated materials for motor manufacturing as in [6]. These materials are designed to have desirable properties that reduce energy loss and increase the overall efficiency of the motor. For example, high-quality magnetic materials such as neodymium iron boron (NdFeB) and samarium cobalt (SmCo) can be used to create stronger and more efficient magnetic fields. These materials are known for their high magnetic

B. A. Kalas · A. Refaat (✉) · M. Fawzi
Electrical Engineering Department, Faculty of Engineering, Port Said University, Port Said, Egypt
e-mail: ahmed_refaat_1984@eng.psu.edu.eg

B. A. Kalas
e-mail: basant.kalas@eng.psu.edu.eg

M. Fawzi
e-mail: mah_fawzi@eng.psu.edu.eg

A. S. Abdel-Khalik
Electrical Engineering Department, Faculty of Engineering, Alexandria University, Alexandria, Egypt
e-mail: ayman.abdel-khalik@alexu.edu.eg

strength, resistance to demagnetization, and thermal stability, all of which contribute to improved motor performance. Other materials that can be treated to enhance motor efficiency include copper, aluminum, and various types of steel. The manufactures aim to optimizing the composition and processing of these materials. Which in turn leads to reduction in the electrical resistance of motor components, minimize energy loss due to eddy currents, and increase the thermal conductivity of the motor. These factors all contribute to fewer carbon emissions, more efficiency, and higher reliable motors [7].

In addition to material treatments, the IMs efficiency can also be improved through careful design and engineering. This includes optimizing the size and shape of motor components, selecting appropriate winding configurations, and minimizing the use of materials that contribute to energy loss. A novel winding designs for the nine-phase induction motors (9PIMs) have been evaluated in [2]. The authors have found that using the 9PIMs, the phase currents are substantially decreased compared to the 3PIMs resulting in lower power losses and consequently higher motor efficiency. The optimal selection of the number and shape of the rotor bars has been suggested in [8, 9] to improve the performance of the IMs. In [6], Joksimović et al. proposed a general formula for the optimal selection of the number of rotor bars in multiphase cage IMs which can be applied to any number of phases. The optimal selection of rotor bars can eliminate the current and torque ripples according to the proposed formula even if the rotor bars are not skewed. In [7], the authors introduced a comparative study of different rotor slot geometry including various shapes of slots as well as different materials of rotor bars (i.e., copper and aluminum cages) in order to acquire the optimal design geometry that can be considered as a guide for designers to satisfy any requirements of specific applications for utilizing the IMs.

With the modern designs of the MPIMs, the attention to the requirement for innovative control techniques in both current control [10, 11] and speed control [12] has emerged. However, these modern designs require complex control schemes that increase the complexity of the motor drive and raise its cost. This may constrain the best options in the majority of real-world applications to a limited range of phase numbers. On the one hand, machines with prime phase orders may have several appealing advantages over those with composite phase orders, but they require a custom converter design [13]. Nevertheless, stators with numerous three-phase winding designs can just use the commonly accessible, commercially available three-phase power converters [14]. The extensive use of six-phase machines in several vital industrial fields was mostly due to this.

As the complexity of the system and manufacturing costs grow with the number of phases increases and also because having more than six phases does not greatly enhance system efficiency, the 6PIMs are studied in this work. Different winding configurations of the 6PIMs have been proposed and developed in the previous literature [15–19]. The aim of this work is to provide a comparative study of three different winding configurations of the 6PIMs. These configurations are carried out on the Ansys Motor-Cad software program. Then, the models have been exported to ANSYS Maxwell software for validation and extract the simulation results.

The structure of this paper is organized as follows: Sect. 1 presents the introduction, paper organization, and literature review. Section 2 presents the three different winding configurations for 6PIMs with winding structure and the phasor diagrams for each. Section 3 represents the modelling of the prototype motor calculating the motor main dimensions, stator slots and rotor bars dimensions. Section 4 simulation results for the comparative study of the different configurations of the 6PIMs. Section 5 provides conclusion.

2 MPIMs Winding Configurations

MPIMs contain a certain number of phases chosen according to the application for which they are designed. If this number of phases is a multiple of the number three, each three-phase winding is identified by the term "set". Therefore, the IMs which have two or more sets of three-phase winding are called multi-three-phase-induction motors (M-3PIMs). In this work, 6-PIMs which have two sets of three-phase winding are chosen for the modeling. The three different winding configurations of 6PIMs are identified according to the phase displacement between the two winding sets.

Figure 1 presents three different winding configurations of the 6PIMs which indicate the phase shift between the three-phase winding sets. The phase displacement between the two winding sets determines the 6PIM configuration type. If the phase displacement between two consecutive sets of windings is $(2\pi/m)$, then they can be arranged symmetrically. In the case of symmetrical six-phase induction machines (S-6PIMs), the two sets of three-phase windings can be positioned 60° apart from each other, as shown in Fig. 1a. This arrangement ensures that the phase displacement within each set of three-phase windings remains constant at 120° electrical. For asymmetrical configuration, π/m represents the phase displacement between the two sets of three-phase windings. In the case of asymmetrical six-phase induction machines (A-6PIMs), they are displaced by 30° between the phase winding and 120° between the phases in one set as shown in Fig. 1b. [2]. If the phase displacement between two sets of the phase winding is 0°, it can be called double three-phase induction motors (D-3PIMs) as depicted in Fig. 1c.

There are three main steps for designing AC windings. Firstly, allocating coils to the specific phases in the stator slots. If the slots have one side of the coil, in this case, the motor has a single-layer stator winding. On the other hand, if the slots have two sides of two different coils, subsequently, the motor has a double-layer stator winding. Secondly, for each phase, specify the direction of currents in coil sides and coil connections according to the types of winding (e.g., lap, wave, or concentric). The last step is to calculate the number of turns per coil and the size of the conductor.
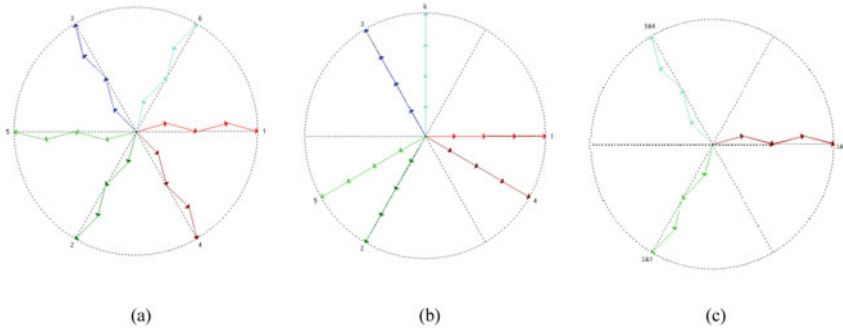
Fig. 1 Phasor diagrams of three different winding layouts for six phase induction motor: **a** S-6PIMs. **b** A-6PIMs. **c** D-3PIMs

Most practical 6PIMs use a 12-slot/pole pair stator or one of its multiples to implement the standard double-layer winding distribution by dividing the 60° phase belt of a conventional three-phase winding into two halves. A typical winding pitch of 5/6 is employed to guarantee a high-quality flux distribution and reduce the stator leakage inductance. In this work, the motor under investigation is a 4-pole, 6-phase having 24 stator slots. A double-layer machine with a short pitch winding of 5/6 coil span is utilized. Figures 2, 3 and 4 represent the winding distribution in the slots for the three winding configurations including linear and radial patterns.
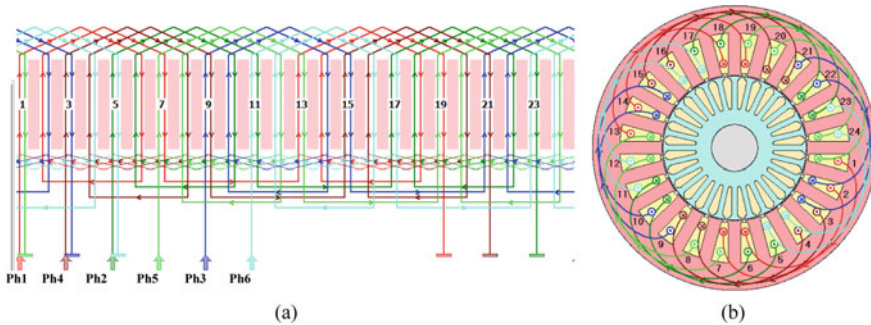
Fig. 2 The S-6PIM winding configuration: **a** linear pattern, **b** radial pattern
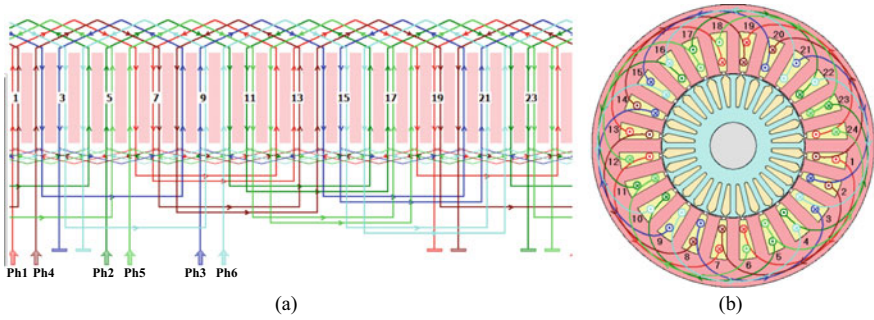
Fig. 3 The A-6PIM winding configuration: **a** linear pattern, **b** radial pattern
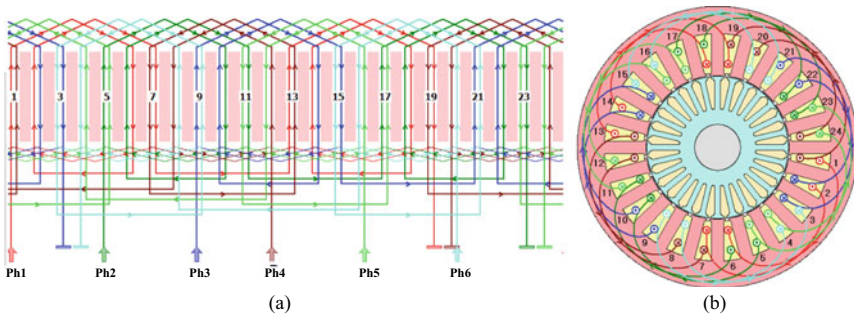
Fig. 4 The D-3PIM winding configuration: **a** linear pattern, **b** radial pattern

3 Modeling of 6PIMs

During the design process of a motor, various factors such as stator and rotor diameters, number of slots, length of the iron core, dimensions of the stator and rotor slots, winding, size of the IM, and type of material need to be taken into consideration. Generally, a larger diameter motor generates higher torque while producing lower speed, whereas a smaller diameter motor produces higher speed but lower torque. As the flux density increases, the motor size decreases. However, if the flux density goes beyond the rated value, the magnetic core gets saturated, and the resulting heat can cause motor failure. Moreover, higher flux density leads to a smaller motor diameter, which in turn requires careful consideration of cooling-related factors when choosing the diameter. To ensure the motor meets operational temperature limits, it may need to be extended. Therefore, the operating temperature, wire size, torque, and speed must be balanced to compromise the motor's diameter and length. The application type also has a significant impact on the design of the motor [6].

The following crucial formulas are applied to design excellent MPIM models. The subsequent section provides a comprehensive evaluation and computation of the primary dimensions for the stator, including the inner and outer diameter, the length of the core, and the dimensions of the slots for both the stator and rotor.

Input power in kVA in general form for MPIM is:

$$S_i = m V_{ph} I_{ph} 10^{-3} \tag{1}$$

where m denotes the total No. of phases, V_{ph} denotes the phase voltage, and I_{ph} denotes the phase current.

$$V_{ph} = 4.44 f \phi k w N_{ph} \tag{2}$$

where f is frequency, ϕ denotes the flux per pole, kw denotes the winding factor, and N_{ph} denotes the No. of conductors per phase.

The frequency can be calculated as the follows:

$$f = n_{sn} p / 2 \tag{3}$$

where n_{sn} is synchronous speed in rps and p is number of poles.

Hence, Eq. 1 becomes,

$$S_i = m(4.44 \times \left(n_{sn} \frac{p}{2} \right) \times (\phi k w N_{ph}) \times I_{ph} \times 10^{-3} \tag{4}$$

Equation (4) can be rewritten as follows,

$$S_i = 1.11 \times (\phi p) \times (2m I_{ph} N_{ph}) \times k w n_{sn} \tag{5}$$

The term ϕp indicates to the magnetic loading of IM and for AC machines. Also, the magnetic loading is equal to $\pi D L B a v$, where D is the stator inner diameter, L is the motor core length, and Bav is specific magnetic loading. While the term $2m I_{ph} N_{ph}$ indicates to the total electric loading for IM, also total electrical loading for AC machines can be calculated as $(\pi D \times ac)$, where ac is specific electrical loading, this can lead to rearranging the Eq. (5) to be as follows,

$$S_i = 1.11 \times \pi^2 B a v \, ac \, k w \, n_{sn} D^2 L \times 10^{-3} \tag{6}$$

Therefore, the input power depends on majorly the stator geometry dimensions D and L.

The next formulas give the dimensions of the stator slot. If the number of conductors per slot is known, the stator slot's approximate area can be calculated. The ratio of the copper area of the slot to the slot fill factor is used to calculate stator slot's area [20].

$$A_{\text{ss}} = \frac{Acon\,Ncst}{kff} \text{ and } Acon = \frac{S_{\text{i}}}{6 \times V_{\text{ph}}J_{\text{s}}} \text{ and } Ncst = \frac{2 \times N_{\text{ph}}}{pq} \tag{7}$$

where $Acon$ denotes the stator conductor cross section area, Nst denotes the number of conductors per stator slot, kff denotes the slot fill factor, and J_{s} denotes the current density passing through the stator slot conductors.

The depth of the stator core is the solid area below the slots sector. Half of the flux per pole flows via the stator core,

$$\phi sc = 1/2\phi \tag{8}$$

where ϕsc is the stator core magnetic flux.

Area of stator core is estimated as follows,

$$Asc = \phi/2Bsc = Ldsc \tag{9}$$

$$dsc = \frac{\phi}{2 \times BscL} \tag{10}$$

where dsc is minimum stator core depth that acquires maximum core flux density Bsc.

The Stator slot depth (dss) is obtained in terms of outer stator diameter (Do), inner stator diameter (D), and the slot core depth (dsc).

$$dss = \frac{1}{2} \times (Do - D - dsc) \tag{11}$$

The tooth width should be greater than the minimum acceptable width (wst) to prevent the occurrence of tooth saturation [6].

$$wst = \frac{\pi D}{Nss} \times \frac{Bg}{Bst\,kfl} \tag{12}$$

where Bg and Bst are the air gap flux density and maximum of stator slot flux density, respectively. Nss is the number of stator slots and kfl is the influence of lamination thickness factor.

In the following formulas, the geometry dimensions of rotor bars are discussed. The rotor diameter (Dr) is obtained as follows,

$$Dr = D - 2lg \tag{13}$$

where lg is the air gap length. For calculating the appropriate value of the cross-sectional area of the rotor bars, the proper value of the rotor bar current density is chosen.

$$Arb = Irb/Jrb = \frac{2m\,Krs\,N_{ph}\,Kw\,Irat}{Nrb\,Jrb} \tag{14}$$

where Krs is the constant MMF ratio of the rotor to stator, Jrb is the rotor bar current density, and Irb and $Irat$ are the nominal values for rotor bars current and stator winding current, respectively.

The minimum width of the rotor bar is given as follows,

$$wrb = \frac{\pi\,Dor}{Nrb} \times \frac{Bg}{Brb\,kfl} \tag{15}$$

where Dor is the rotor bore diameter, Brb is the maximum of rotor bar flux density, and Nrb is the number of rotor bars.

4   Simulation Results and Discussions

This research employs Ansys-Motor-Cad to create and simulate an initial design for the motor because it is user-friendly and straightforward. The resulting model is subsequently validated and analyzed using ANSYS Maxwell. Table 1 lists the specifications of the 6PIM design, while Table 2 shows the stator's geometry dimensions. Table 3 lists the dimensions of the rotor (squirrel cage rotor). Based on the earlier mathematical modeling, Fig. 5 depicts the resultant model.

Figure 5 illustrates the mechanical dimensions of the induction motor's stator and rotor in their preliminary design which includes the stator and rotor slot shapes, and the data from Tables 1, 2 and 3 have been utilized to complete an initial design

Table 1 Specification of the utilized IM

Parameter	Value
Power rating	1 kW
Voltage (max)	150 V
Current (max)	4 A
Poles	4
Speed	1400 rpm
Frequency	50 Hz
Motor length	220 mm
Number of turns per slot	100
Number of layers	2

Table 2 The stator geometry dimensions

Parameter	Value
Number of stator slots	24
Stator skew angle	15°
Rotor lamination length	80 mm
stator lamination outer diameter	135 mm
Stator bore diameter	69 mm
Slot type	Parallel teeth
Tooth width	6 mm
Slot depth (bore to slot bottom)	20 mm
Base slot corner radius	0
Tooth dip length (depth of slot opening from bore to tooth taper region)	1 mm
Slot opening	1.5 mm

Table 3 The rotor geometry dimensions

Parameter	Value
Number of rotor bars	28
Stator skew angle	0°
Rotor lamination length	80 mm
Rotor lamination outer diameter	68 mm
Shaft diameter	22 mm
Slot type	Parallel tooth pear
Bar opening	1.0 mm
Bar opening depth	0.7 mm
Rotor lamination tooth width	2.7 mm
Bar depth	15 mm
Air gap	0.5 mm

of the six-phase induction motor, using ANSYS Moror-Cad software. The winding architectures shown in Figs. 2, 3 and 4 describe the layout of winding distribution in stator slots for S-6PIM, A-6PIM, and D-3PIM, respectively. The ANSYS Moror-Cad environment is employed to produce a prototype model of the 6PIM types under investigation. Then, the model is exported to the ANSYS Maxwell software to acquire the simulation results.
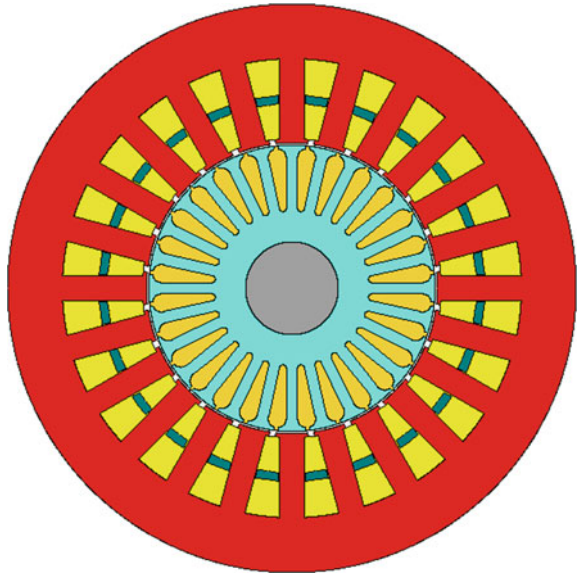
The best numerical technique used for electrical machine simulation is finite element analysis (FEA). Results from this technique may be quite accurate and closely resemble those from experiments. Therefore, Ansys Maxwell (FEA software tool) is utilized for the validation and simulation results of three models of the 6PIMs. Three machine models with various winding layouts are compared. The windings are supplied by voltage excitation taking into consideration the eddy current effect. The FEA model is shown in Fig. 6. It should be noticed that the three considered models have the same parameters and specifications.

Fig. 6 FEA model of
(6PIMs) via ANSYS
Maxwell platform
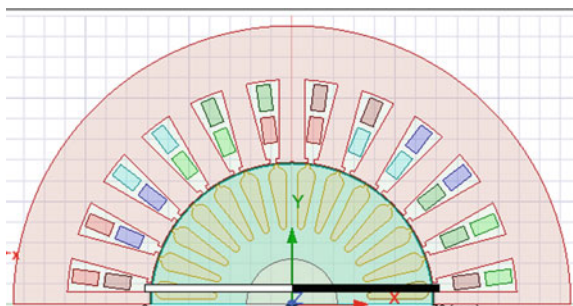
Figure 6 illustrates the FEA 6PIMs model using the ANSYS Maxwell platform. Figures 7, 8 and 9 show the induced torque and the phase currents waveforms as a function of time for the S-6PIMs, A-6PIMs, and D-3PIMs, respectively. It is clear from the figures that the rms current drawn in the case of A-6PIMs is less than the other two configurations. Consequently, the A-6PIM model has the lowest stator copper losses among the three winding layouts as illustrated in Table 4. According to the Torque-time graphs, the A-6PIMs starting torque can approximately reach 10 Nm which is higher than the starting torque produced by the S-6PIMs and D-3PIMs.

A comparative study is conducted for the three 6PIMs configurations including the RMS current, average torque, output power, input power, and efficiency as depicted in Figs. 10, 11, 12, 13 and 14. A comparison between the performance of the three different configurations of the 6PIMs at a nominal speed point is shown in Table 4. As can be observed from the figures, the output power of the A-6PIM is less than the two other configurations. However, the RMS current and the input power of A-6PIMs are also lower than the others. In addition, the A-6PIM possesses the lowest core and stator copper loss of almost 9.11 W and 235.25 W, respectively. As a result, the A-6PIM has the highest efficiency of about 81.41% compared to 76.35% and 76.9% for the S-6PIM and D-3PIM, respectively. This implies that the efficiency of
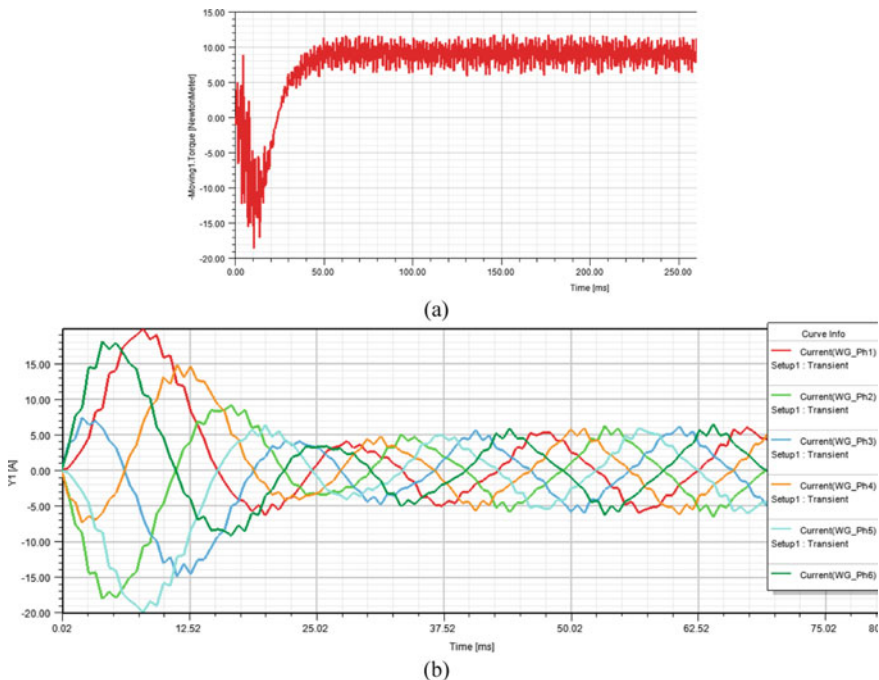
Fig. 7 The ANSYS Maxwell results for the S-6PIM: **a** the induced torque and **b** the phase currents

(a)

(b)
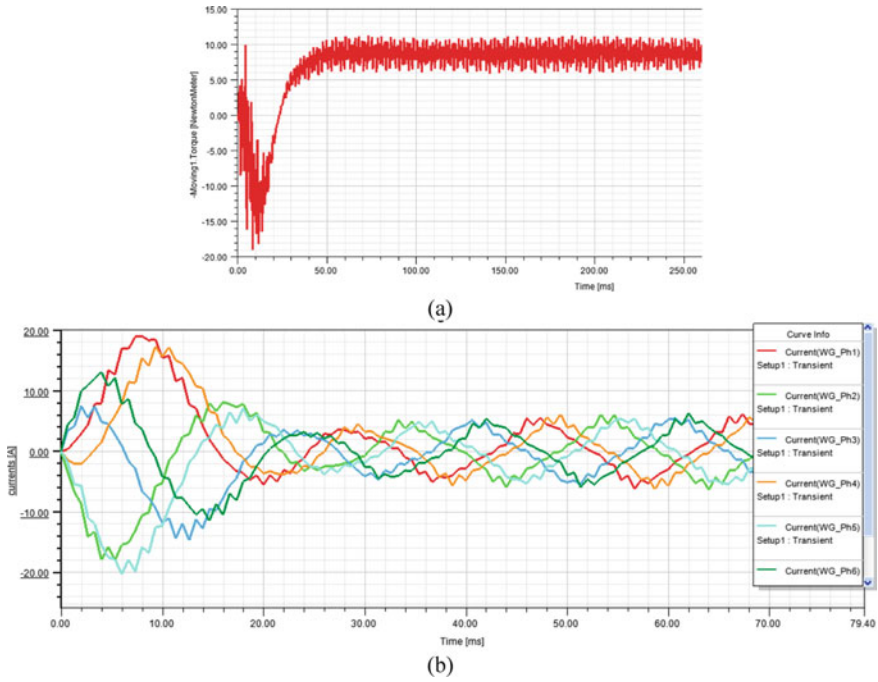
Fig. 8 The ANSYS Maxwell results for the A-6PIM: **a** the induced torque and **b** the phase currents

the IM is inversely proportional to the losses, based on the output results. And it also turns out that the S-6PIM and the D-3PIM have convergent performance in general conditions.

(a)

(b)
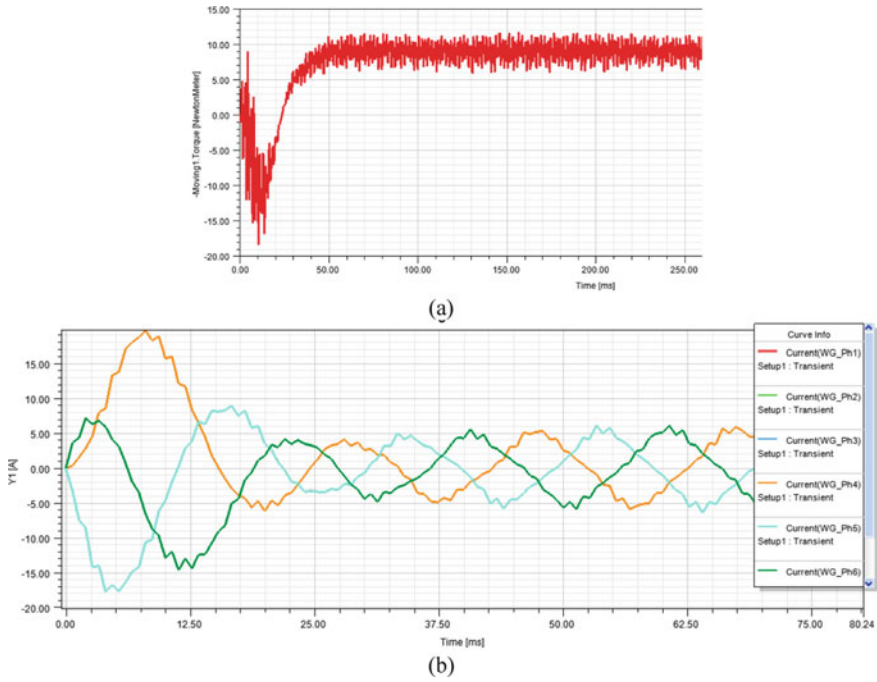
Fig. 9 The ANSYS Maxwell results for the D-3PIM: **a** the induced torque and **b** the phase currents

Table 4 Comparison between the performance of the three different configurations of the 6PIMs at a nominal speed point

Quantity	S-6PIM	A-6PIM	D-3PIMs
RMS current (A)	3.735	3.355	3.568
Output power (W)	970.34	932.86	974.14
Input power (VA)	1530.44	1441.37	1525.44
Average torque (Nm)	6.77	6.5	6.79
Efficiency %	76.35	81.41	76.9
Core loss (W)	9.8257	9.11	9.8093
Stator copper loss (W)	269.74	235.25	269.74

Fig. 10 FEA comparative
current-speed characteristics
for the three configurations
of the 6PIMs
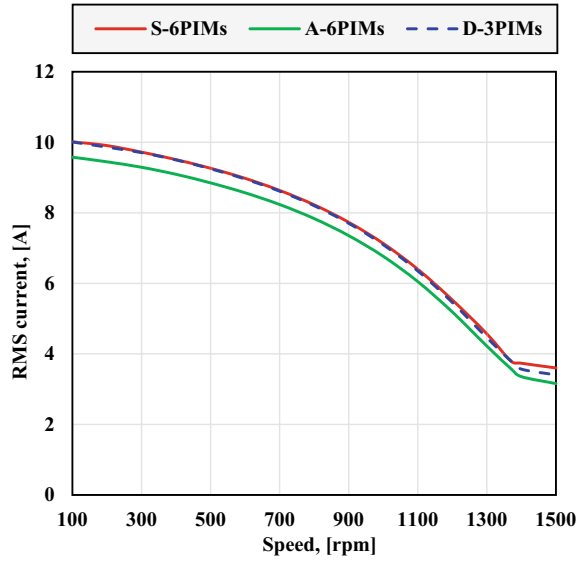
Fig. 11 FEA comparative
Torque-speed characteristics
for the three configurations
of the 6PIMs
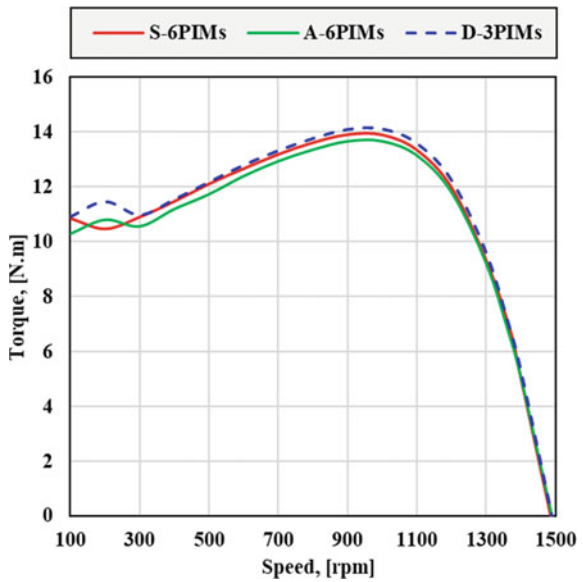
Fig. 12 FEA comparative output power-speed characteristics for the three configurations of the 6PIMs
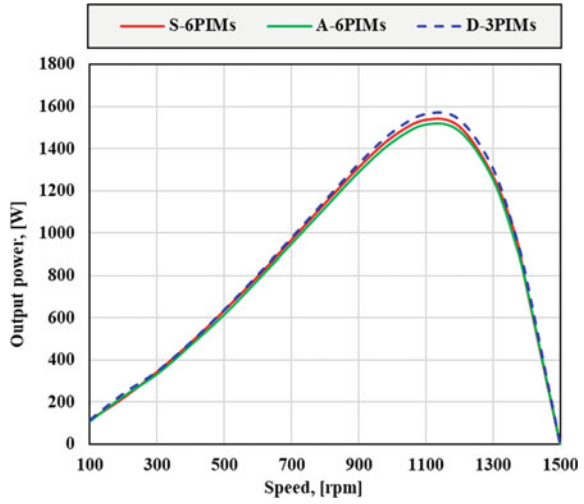
Fig. 13 FEA comparative input power-speed characteristics for the three configurations of the 6PIMs
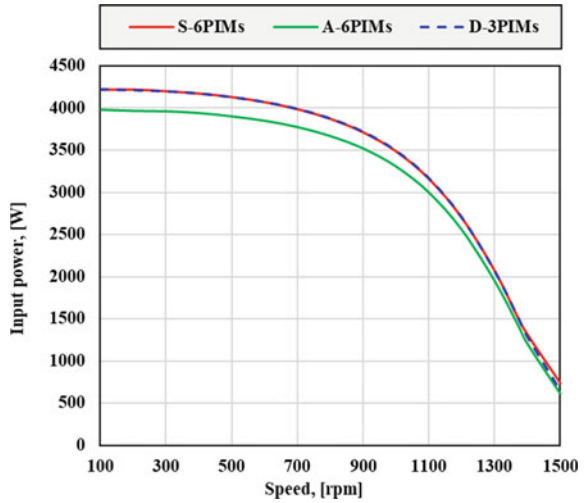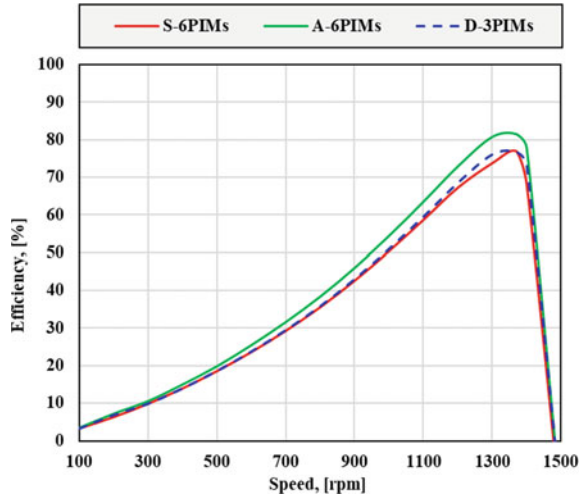
5   Conclusion

Continuous research that keeps pace with modern and innovative requirements in designing and controlling motors endeavors to utilize energy efficiently and save the environment from carbon emissions. ANSYS Maxwell software is a valuable tool in this pursuit, as it employs FEA to precisely simulate electrical machines, and produces results that are comparable to experimental data, thus increasing the efficiency of motor manufacturing. In this work, the 6PIMs are chosen for increasing motor efficiency compared to the traditional 3PIMs, and the ANSYS Maxwell is used to simulate and evaluate the 6PIMs with different types of winding configurations using the same parameters. A comparison among the three different configurations of 6PIMs is conducted in order to show the best performance among them. The results demonstrate that the A-6PIM has the highest efficiency of almost 81.41% with the lowest core and stator copper loss of about 9.11 W and 235.25 W, respectively. Thus, employing the A-6PIMs configuration shows potential in industrial and traction applications as a means to improve the performance of AC motors while also reducing carbon emissions. Consequently, future work will consider the optimal design of the number of rotor bars for the A-6PIMs in order to obtain more efficient performance for industrial and traction applications.

References

1. Wogi L, Thelkar A, Tahiro T, Ayana T, Urooj S, Larguech S (2022) Particle swarm optimization based optimal design of six-phase induction motor for electric propulsion of submarines. Energies 15. https://doi.org/10.3390/en15092994

2. Fleitas A, Ayala M, González O, Delorme L, Romero C, Rodas J, Gregor R (2022) Winding design and efficiency analysis of a nine-phase induction machine from a three-phase induction machine. Machines 10. https://doi.org/10.3390/machines10121124

3. Abdel-Mageed BS, Shalaby MSA, Seoudy HM (2020) Study of broken rotor bar fault for asymmetrical six-phase induction motor. In: 9th IEEE international conference on power electronics, drives and energy systems, PEDES 2020. Institute of Electrical and Electronics Engineers Inc

4. Shata AM, Abdel-Khalik AS, Hamdy RA, Mostafa MZ, Ahmed S (2021) Improved mathematical modeling of six phase induction machines based on fractional calculus. IEEE Access 9:53146–53155. https://doi.org/10.1109/ACCESS.2021.3069963

5. Pacheco I (2022) Romance and assonance in the German Calderón. Anuario Calderoniano 15:449–470. https://doi.org/10.13039/501100011033

6. Aishwarya M, Brisilla RM (2022) Design of energy-efficient induction motor using ANSYS software. Results Eng 16. https://doi.org/10.1016/j.rineng.2022.100616

7. Bonfante MC, Raspini JP, Fernandes IB, Fernandes S, Campos LMS, Alarcon OE (2021) Achieving sustainable development goals in rare earth magnets production: a review on state of the art and SWOT analysis. Renew Sustain Energy Rev 137. https://doi.org/10.1016/j.rser.2020.110616

8. Joksimovic G, Mezzarobba M, Tessarolo A, Levi E (2020) Optimal selection of rotor bar number in multiphase cage induction motors. IEEE Access 8:135558–135568. https://doi.org/10.1109/ACCESS.2020.3004685

9. Di NM, Marfoli A, Degano M, Gerada C, Chen W (2021) Rotor design optimization of squirrel cage induction motor—part II: results discussion. IEEE Trans Energy Convers 36:1280–1288. https://doi.org/10.1109/TEC.2020.3020263

10. Kali Y, Saad M, Doval-Gandoy J, Rodas J (2021) Discrete terminal super-twisting current control of a six-phase induction motor. Energies 14. https://doi.org/10.3390/en14051339

11. Romero C, Delorme L, Gonzalez O, Ayala M, Rodas J, Gregor R (2021) Algorithm for implementation of optimal vector combinations in model predictive current control of six-phase induction machines. Energies 14. https://doi.org/10.3390/en14133857

12. Chand Modi Rajeev Chaturvedi SK (2016) Implementation of prototype six phase induction motor and its speed control by vector control method

13. Abdel-Khalik AS, Abdel-Majeed MS, Ahmed S (2020) Effect of winding configuration on six-phase induction machine parameters and performance. IEEE Access 8:223009–223020. https://doi.org/10.1109/ACCESS.2020.3044025

14. Paredes J, Prieto B, Satrústegui M, Elósegui I, González P (2021) Improving the performance of a 1-MW induction machine by optimally shifting from a three-phase to a six-phase machine design by rearranging the coil connections. IEEE Trans Indus Electr 68:1035–1045. https://doi.org/10.1109/TIE.2020.2969099

15. Iduh SE, Omugbe SE (2020) The design and practical implementation of a six-phase induction motor. J Adv Sci Eng 3:1–77. https://doi.org/10.37121/jase.v3i1.95

16. Sarigül I, Özdemir M (2021) Comparative analysis of six phase induction motor. Eur J Tech. https://doi.org/10.36222/ejt.811334

17. Abdel-Mageed BS, Shalaby MSA, Ali KF, Morsy MA (2019) Coupled finite element-circuit modelling and parameter estimation of six-phase induction motor. In: 2019 21st international middle east power systems conference, MEPCON 2019—proceedings, pp 645–649. https://doi.org/10.1109/MEPCON47431.2019.9008048

18. Echagüe G, Ayala M, Rodas J (2020) Design, analysis and validation of a six-phase induction machine from a commercial three-phase for academic research. IEEE Lat Am Trans 18:1943–1952. https://doi.org/10.1109/TLA.2020.9398636

19. Caruso M, Di Tommaso AO, Marignetti F, Miceli R, Galluzzo GR (2018) A general mathematical formulation for winding layout arrangement of electrical machines. Energies 11. https://doi.org/10.3390/en11020446

20. Rezazadeh G, Tahami F, Capolino G-A, Nasiri-Gheidari Z, Henao H, Sahebazamani M (2021) Improved design of a six-phase squirrel cage induction motor with pseudo-concentrated windings. IEEE J Emerg Selected Topics Indus Electr 3:1187–1194. https://doi.org/10.1109/jestie.2021.3137056

Materials Selection and Performance of Fiber-Reinforced Plastic Poles

M. Bassyouni, Yasser Elhenawy, Yuliya Kulikova, Olga Babich, and Medhat A. El-Hadek

1 Introduction

Fiber reinforced plastics (FRP) light poles have become increasingly popular in outdoor lighting applications due to their lightweight, corrosion resistance, and high strength-to-weight ratio [1, 2]. Fiber reinforced plastics light poles are commonly used in areas with harsh environmental conditions, such as coastal regions, where

M. Bassyouni (✉)
Department of Chemical Engineering, Faculty of Engineering, Port Said University, Port Said 42526, Egypt
e-mail: m.bassyouni@eng.psu.edu.eg

M. Bassyouni · Y. Elhenawy
Center of Excellence in Membrane-based Water Desalination Technology for Testing and Characterization, Port Said University, Port Said 42526, Egypt
e-mail: yasser.elhenawy@wits.ac.za

M. Bassyouni · M. A. El-Hadek
East Port Said University of Technology, North Sinai 45632, Egypt
e-mail: melhadek@eng.psu.edu.eg

Y. Elhenawy
Department of Mechanical Power Engineering, Faculty of Engineering, Port Said University, Port Said 42526, Egypt

School of Chemical and Metallurgical Engineering, University of the Witwatersrand, Johannesburg 2000, South Africa

Y. Kulikova · O. Babich
Institute of Living Systems, Immanuel Kant Baltic Federal University, Kaliningrad 236016, Russia
e-mail: olich.43@mail.ru

M. A. El-Hadek
Production Engineering and Mechanical Engineering Department, Faculty of Engineering, Port Said University, Port Said 42526, Egypt

conventional metal poles are prone to corrosion [3, 4]. However, like any other material, FRP light poles can fail under certain conditions, which can pose a significant safety risk to the public and property [5, 6]. Therefore, it is essential to conduct a failure analysis of FRP light poles to ensure their safety and reliability [7, 8].

Fiber reinforced plastics (FRP) light poles are commonly used in outdoor lighting applications due to their lightweight, corrosion resistance, and high strength-to-weight ratio [9, 10]. However, like any other material, FRP light poles can fail under certain conditions [11, 12]. Here are some potential reasons for FRP light pole failure and their possible solutions (i) Overloading: Overloading of the light pole can cause it to fail. The load on the pole can come from various sources such as wind, ice, snow, or equipment mounted on the pole. The pole should be designed to withstand the maximum expected load in the area where it will be installed. The pole should also be periodically inspected to ensure that it is not overloaded [13, 14]. (ii) Impact damage: The light pole can also fail due to impact damage from a vehicle, equipment, or other objects. Solution: The pole should be designed with enough strength to resist impact damage. If the pole is damaged, it should be immediately replaced or repaired [15, 16]. (iii) Material degradation: The material used to make the pole can degrade over time due to exposure to UV radiation, moisture, and other environmental factors. The pole should be made from high-quality materials that are resistant to degradation. The pole should also be coated with a UV-resistant finish to protect it from the sun's rays [16, 17]. (iv) Manufacturing defects: Manufacturing defects such as voids, delaminations, and inconsistent fiber orientation can weaken the pole and cause it to fail. The pole should be manufactured using quality control measures to ensure that it is free of defects. The manufacturer should also conduct regular testing to ensure that the poles meet the required strength and quality standards [18, 19]. (v) Improper installation: Improper installation of the pole can also lead to failure [20, 21]. The pole should be installed according to the manufacturer's guidelines. The installation should be done by trained professionals who have experience in installing FRP poles [22, 23]. There are several standards which manufacutrers can used for fiber-reinforced plastics (FRP) testing ASTM D3754—standard specification for Fiberglass (Glass-Fiber-Reinforced Thermosetting-Resin) Sewer and Indusrial Pressure Pipe—This standard provides criteria for the manufacture of glass fiber pipe, which may be applicable to the manufacture of light poles made from FRP. ASTM D638—standard test method for mechanical testing. This standard provides a method for determining the tensile strength and other mechanical properties of polymers and FRPs. ASTM D790—standard test Methods for flexural properties of FRPs and electrical properties. This standard provides a method for determining the flexural properties of FRP materials. AASHTO standard specification for structural supports for highway signs, Luminaires, and traffic signals. This standard provides standards for the design and manufacture of structural supports for highway signs, luminaires, and traffic signals. ISO 10406-1—Fiber-reinforced plastic composites—to determine tensile properties—Part 1: General principles—this International Organization for Standardization (ISO) standard provides general principles for measuring the tensile properties of FRP materials, which may be useful for evaluating the strength of light poles made from FRP.

Fiber reinforced plastics (FRPs) offer lightweight and high-strength properties, making them suitable for innovative applications in construction. This promotes the development of sustainable infrastructure and encourages technological advancements (SDG 9). This can lead to energy-efficient structures and improved urban planning, contributing to the goal of creating sustainable cities and communities (SDG 11). They are known for their durability, corrosion resistance, and low maintenance requirements. These properties can extend the lifespan of products, reduce material waste, and minimize the need for frequent replacements, aligning with the principles of responsible consumption and production (SDG 12).

The objective of this study is to provide an overview of failure analysis of FRPs light poles, including the materials used, characterization techniques, common failure modes, and causes of failure.

2 Materials

Fiber reinforced plastics (FRPs) light poles are made by reinforcing a polymer matrix with high-strength fibers. The polymer matrix can be made from various resins, such as polyester, vinyl ester, or epoxy, while the fibers can be made from materials such as glass, carbon, or aramid.

The selection of the matrix and fiber materials depends on various factors such as the environmental exposure, mechanical properties required, and the manufacturing process used. For example, polyester resin is often used for low-cost applications due to its lower mechanical strength and stiffness compared to epoxy resins. In contrast, epoxy resins are preferred for high-performance applications due to their high strength, stiffness, and excellent resistance to moisture and chemical degradation.

The fiber reinforcement also plays a crucial role in determining the mechanical properties of the FRPs light poles. Glass fibers are commonly used due to their low cost, high strength, and stiffness, while carbon fibers are used for high-performance applications where weight reduction is critical (Fig. 1). Aramid fibers are used in applications that require impact resistance and high energy absorption.

In summary, the selection of materials for FRPs light poles must take into consideration the intended use, environmental conditions, and mechanical requirements.

3 Characterization

To evaluate the mechanical properties and potential failure modes of FRPs light poles, a range of characterization techniques was employed. Materials testing techniques, such as dynamic mechanical analysis (DMA), Fourier transform infrared spectroscopy (FTIR), and thermogravimetric analysis were utilized to evaluate the chemical and physical properties of the polyester and glass and natural fibers as

Fig. 1 Light poles made of FRPs

shown in Fig. 2. Dynamic mechanical analysis measures the viscoelastic properties of the polyester composites [24, 25]
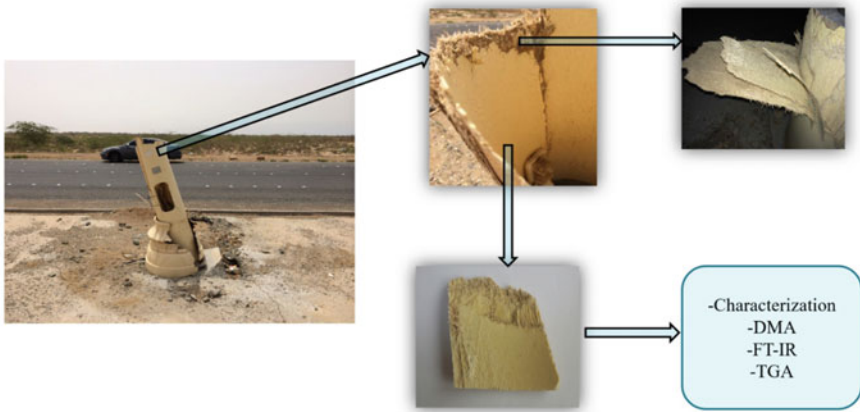
Fig. 2 Methodology of light pole failure characterization and analysis

4 Results and Discussion

4.1 Dynamic Mechanical Analysis

In DMA analysis, the FRPs were subjected to a sinusoidal deformation, and the resulting stress and strain were tested as a function of temperature and frequency. The analysis typically involved measuring the storage modulus (E'), which reflects the material's ability to store energy elastically, and the loss modulus (E''), which refers to the ability to dissipate energy viscoelastically. Tan (d) is the ratio of E''/E' which is known as the damping factor or tan delta, which is an indication of the material's ability to absorb energy [26–29]. The glass transition temperature (T_g) can be defined through onset of storage modulus curve, peak temperature of loss modulus or peak temperature of tan delta. Storage modulus onset is usually the most low value and peak temperature tan (d)—the most high. This information can be used to optimize the design and performance of GFRP using polyester for light pole applications. Figure 3 shows that the glass transition temperature is 76.2 °C according to the loss modulus.
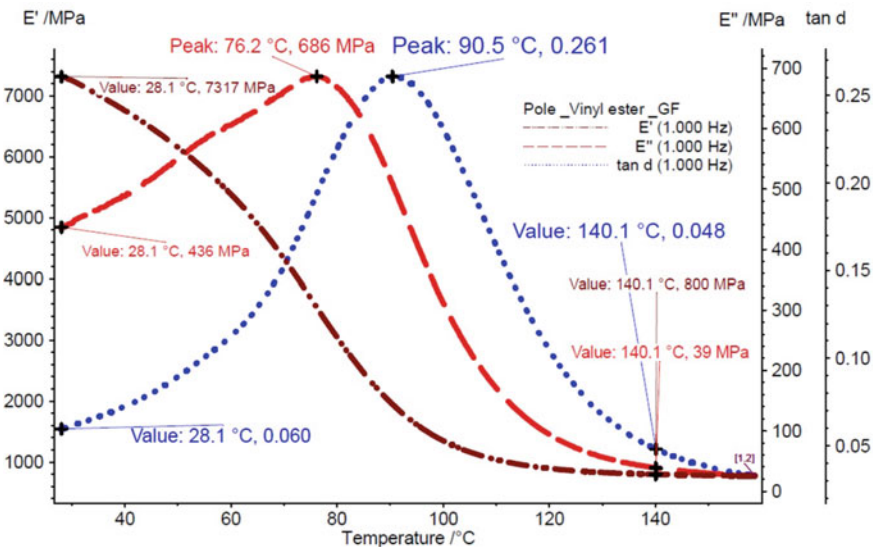
Fig. 3 DMA of FRPs
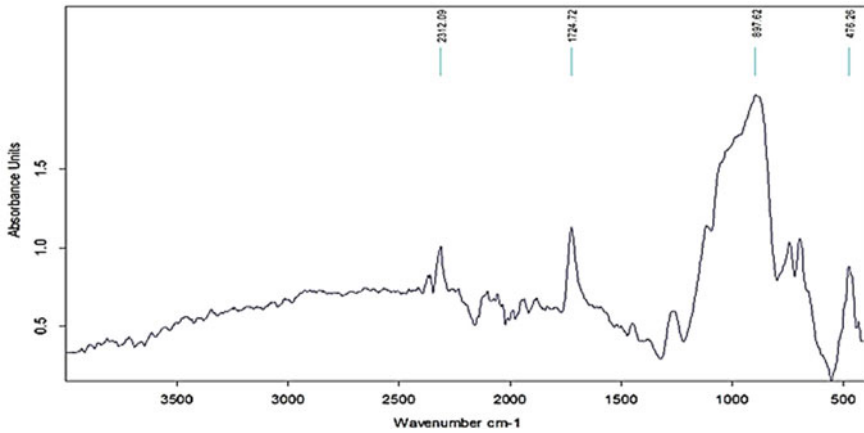
Fig. 4 FTIR of FRPs

4.2 Chemical Analysis

Figure 4 shows the FTI-IR analysis of FRPs of light pole composite material. The band at 1735 cm^{-1} corresponds to the stretching vibrations of C–O in ester or carbonyl group. The bands around 1100 cm^{-1} are arise due to stretching vibrations of C–O and Si–O, which might indicate the presence of polyethyl and/or a silane. The band at 426 cm^{-1} also show the presence of Si–O–Si bond which confirms the presence of silane. The silane used is expected to be N (beta-aminoethyl) gamma aminopropyltrimethoxy-silane. It is also found that feldspar ($K_2OAl_2O_3.6SiO_2$) is used as a filler material which is confirmed by the resemblance of strong peak of spectra at 1000 cm^{-1}. Presence of cellulose is detected which is assumed to be the presence of natural fibres in the composite.

4.3 Thermal Stability

The thermal stability of FRPs can be determined using the thermogravimetric analysis (TGA). Fiber reinforced plastic sample was heated in a controlled environment from room temperature to 900 °C. The weight loss of the material was measured as a function of temperature. The analysis typically involved measuring the onset temperature of decomposition, the temperature at which the maximum rate of decomposition occured, and the residual weight of the material after heating to certain temperature.

For FRP, TGA analysis can reveal the effect of temperature on thermal stability and degradation behavior of FRPs, which indicated the temperature at which the FRPs started to degrade, and the residual weight of the material after heating, which reflected the thermal stability of the polyester and the glass fiber and natural fiber.
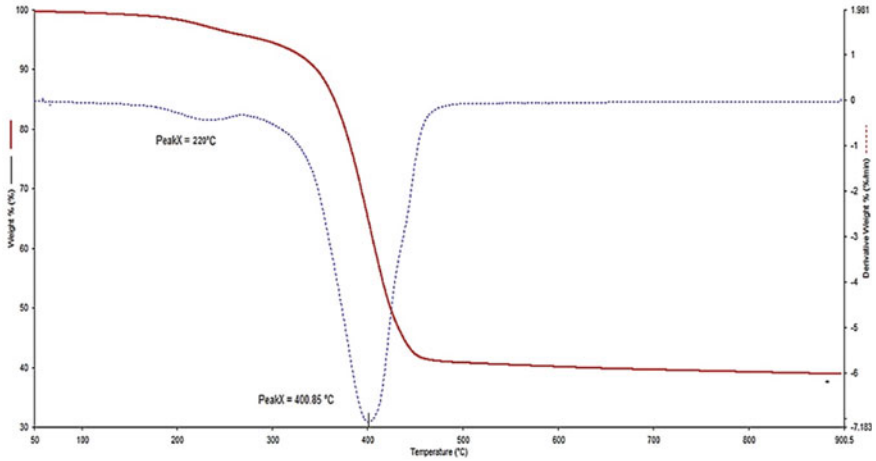
Fig. 5 TGA of FRPs

Figure 5 shows two major peaks. The first peak was found at 220 °C which indicated the degradation of natural fiber. The second peak was determined at 400 °C which was assigned to polyester. The weight % remaining was 40% wt./wt. which referred to the glass fiber contents in the FRPs sample.

This information can be used to optimize the design and performance of FRPs for light pole application where the FRPs are subjected to sun light and thermal stresses.

4.4 Mechanical Analysis

The effect of glass fiber loading on the yield strength and Young's modulus of polyester is shown in Fig. 6. It was found that the yield strength of polyester increased from 90 to 400 MPa with increasing GF loading from 10 v to 70% v/v. Modulus of elasticity of polyester improved significantly to 17 GPa as a result of increasing GF loading to 70% v/v.
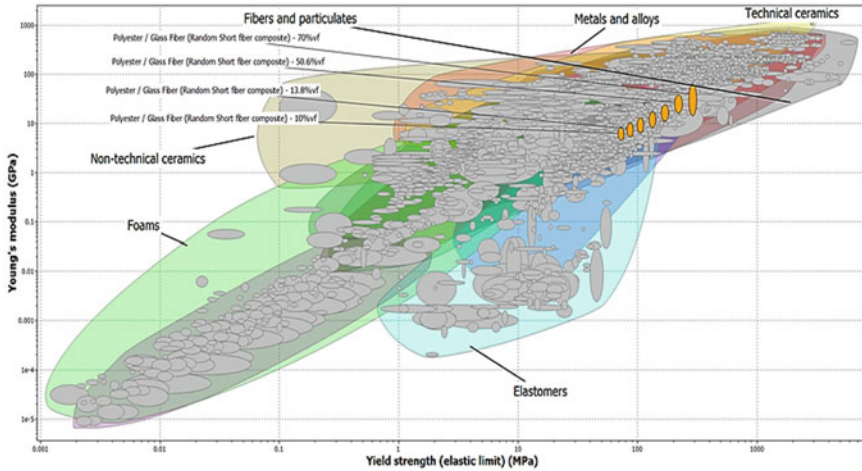
Fig. 6 Mechanical properties of fiber reinforced polyester

5 Conclusion

In conclusion, FRPs light poles are made by reinforcing a polymer matrix with high-strength fibers, and the selection of materials depends on various factors such as environmental exposure and mechanical requirements. To evaluate the mechanical properties and potential failure modes of FRP light poles, a range of characterization techniques were employed including dynamic mechanical analysis (DMA), FTIR, and TGA. Dynamic mechanical analysis was a valuable technique in the characterization of FRP light poles, providing information on the viscoelastic properties of the material and potential failure modes and glass transition temperature. Through comprehensive characterzation and failure analysis, it was possible to identify potential design and manufacturing improvements to increase the safety and reliability of FRPs light poles.

6 Recommendation

It is important to enhance the interfacial bonding between the polyester and glass fibers. This can be achieved by using compatible coupling agents or surface treatments to improve the adhesion between the fibers and the matrix. This study indicated that glass fiber-PE composites are suitable for light pole manufacture based on material index and wind load with a safety factor of 4. It is important to continue exploring and optimizing the material selection process to ensure the chosen materials have the required mechanical properties, durability, and resistance to environmental conditions.

References

1. Javaid U, Khan ZM, Khan MB, Bassyouni M, Abdel-Hamid SM-S, Abdel-Aziz MH, ul Hasan SW (2016) Fabrication and thermo-mechanical characterization of glass fiber/vinyl ester wind turbine rotor blade. Compos Part B Eng 91:257–266
2. Bassyouni M, Waheed Ul Hasan S (2015) The use of rice straw and husk fibers as reinforcements in composites. In: Biofiber reinforcements in composite materials, Woodhead Publishing, pp 385–422
3. Elhenawy Y, Fouad Y, Marouani H, Bassyouni M (2021) Performance analysis of reinforced epoxy functionalized carbon nanotubes composites for vertical axis wind turbine blade. Polymers 13(3):422
4. Iqbal N, Sagar S, Khan MB, Bassyouni MI, Khan ZM (2013) Aluminum silicate fibers impregnated acrylonitrile butadiene rubber composites: ablation, thermal transport/stability, and mechanical inspection. J Appl Polym Sci 130(6):4392–4400
5. Nawar MT, Kaka ME, El-Zohairy A, Elhosseiny O, Arafa IT (2022) Effect of supporting base system on the flexural behavior and toughness of the lighting GFRP poles. Sustainability 14(19):12614
6. Si J, Qiu S, Feng S, Chen J, Wang Z (2022) Experimental study on axial compression buckling of glass fiber reinforced plastics solid pole with circular cross-section. Adv Struct Eng 25:913–924
7. Bassyouni M (2018) Dynamic mechanical properties and characterization of chemically treated sisal fiber-reinforced polypropylene biocomposites. J Reinf Plast Compos 37(23):1402–1417
8. Elhenawy Y, Fouad Y, Marouani H, Bassyouni M (2021) Simulation of glass fiber reinforced polypropylene nanocomposites for small wind turbine blades. Processes 9(4):622
9. Samir A, Ashour FH, Abdel Hakim AA, Bassyouni M (2022) Recent advances in biodegradable polymers for sustainable applications. Npj Mat Degrad 6(1):68
10. Nassef A, El-Hadek M (2016) Microstructure and mechanical behavior of hot pressed Cu-Sn powder alloys. Adv Mat Sci Eng 2016(14)
11. El-Shamy AM, El-Hadek MA, Nassef AE, El-Bindary RA (2020) Box-Behnken design to enhance the corrosion resistance of high strength steel alloy in 3.5 wt.% NaCl solution. Moroccan J Chem 8(4):8–4 14
12. El-Hadek MA (2018) Dynamic equivalence of ultrasonic stress wave propagation in solids. Ultrasonics 83(13):214–221
13. Gan Y, El-Hadik M, Aglan H, Faughnan P, Bryan C (1999) Fatigue crack growth analysis of polymonochlorotrifluoroethylene (CTFE). J Elastomers Plast 31(2):96–129
14. Dimopoulos CA, Gantes CJ (2012) Experimental investigation of buckling of wind turbine tower cylindrical shells with opening and stiffening under bending. Thin-Walled Struct. 54:140–155
15. Arbelo MA, Herrmann, A, Castro SG, Khakimova R, Zimmermann R, Degenhardt R (2022) Investigation of buckling behavior of composite shell structures with cutouts. Appl Compos Mater 22(6):623–636
16. Jullien JF, L imam A (1998) Effects of openings of the buckling of cylindrical shells subjected to axial compression. Thin-Walled Struct 31(1–3):187–202
17. Metiche S, Masmoudi R (2007) Full-scale flexural testing on fiber-reinforced polymer (FRP) poles. Open Civ Eng J 1(1):37–50
18. Metiche S, Masmoudi R, Baky H (2009) New design procedure for FRP composites pole. Open Civ Eng J 4:2540–2552. Available online: https://www.researchgate.net/publication/283487870. Accessed on 02 Apr 2023

19. Broniewicz M, Broniewicz F, Broniewicz E (2021) Full-scale experimental investigation and structural assessment of GFRP poles. Materials 14(23):7398
20. Saboori B, Khalili S (2011) Static analysis of tapered FRP transmission poles using finite element method. Finite Elem Anal Des 47(3):247–255
21. Khalili S, Saboori B (2010) Transient dynamic analysis of tapered FRP composite transmission poles using finite element method. Compos Struct 92(2):275–283
22. Nassiraei H, Rezadoost P (2021) Stress concentration factors in tubular T/Y-connections reinforced with FRP under in-plane bending load. Mar Struct 76:102871
23. Nassiraei H, Rezadoost P (2021) SCFs in tubular X-connections retrofitted with FRP under in-plane bending load. Compos Struct 274(2021):114314
24. Urgessa G, Mohamadi S (2016) Structural assessment of fiber-reinforced polymer composite electric poles. Procedia Eng 145(2016):707–714
25. Ud Din I, Panier S, Hao P, Franz G, Bijwe J, Hui L (2019) Finite element modeling of indentation and adhesive wear in sliding of carbon fiber reinforced thermoplastic polymer against metallic counterpart. Tribol Int 135:200–212
26. Nawar MT, Kaka ME, El-Zohairy A, Elhosseiny O, Arafa IT (2022) Effect of supporting base system on the flexural behavior and toughness of the lighting GFRP poles. Sustainability 14:12614
27. ISO 527-4 (1997) Plastics—determination of tensile propertiess—part 4: test conditions for isotropic and orthotropic fibre reinforced plastic composites. ISO, London
28. ISO 14125(1998) Fibre-reinforced plastic composites—determination of flexural properties. ISO, London, 1997
29. ISO 2602 (1980) Statistical interpretation of test results—estimation of the mean—confidence interval. ISO, London, 1997

Optimal Design of Container Ships Geometry Based on Artificial Intelligence Techniques to Reduce Greenhouse Gases Emissions

Hussien M. Hassan, Mohamed M. Elsakka, Ahmed Refaat, Ahmed E. Amer, and Rawya Y. Rizk

1 Introduction

Several marine regulations and rules are incentivized to increase the ship's energy efficiency through ship hull enhancements in the design stage and reduce CO_2 emissions in operation. Hence, mandatory compliance for new and existing ship designs with the Energy Efficiency Design Index (EEDI) is required to achieve sustainability [1]. Broadly speaking, the EEDI is estimated based on the amount of CO_2 emissions due to the transport of the cargo through the ship trip. Therefore, the EEDI legislation obliges ship designers to design their models in a way that achieves the least total resistance possible. Ship designers have many tools to test their new models and predict the total ship resistance by empirical regression method, Computational Fluid Dynamics (CFD), and Artificial Intelligence (AI) [2]. Today, the latter (AI) tool is expected to become the most widely used in the creation of optimal 3D ship models

H. M. Hassan
Naval Architecture and Marine Engineering Department, Faculty of Engineering, Port Said University, Port Said, Egypt
e-mail: hussein.mohamed@eng.psu.edu.eg

M. M. Elsakka (✉) · A. E. Amer
Mechanical Power Engineering Department, Faculty of Engineering, Port Said University, Port Said, Egypt
e-mail: elsakka@eng.psu.edu.eg

A. E. Amer
e-mail: eng.ahmed_amer@eng.psu.edu.eg

A. Refaat · R. Y. Rizk
Electrical Engineering Department, Faculty of Engineering, Port Said University, Port Said, Egypt
e-mail: ahmed_refaat_1984@eng.psu.edu.eg

R. Y. Rizk
e-mail: r.rizk@eng.psu.edu.eg

that comply with EEDI regulations. In addition, the AI uses a prominent design tool to mimic and simulate the human brain called an Artificial Neural Network (ANN). Clausen et al. [3] is the first researcher that used the ANN for the determination of the main dimensions of the container ships model [3].

In 2005, Mason et al. [4] used various types of ANN to calculate the total resistance of the ship model. The study was created to illustrate the effect of the hidden layers number on the results. The ANN architecture was established with a range of hidden layers between 1 and 4 with 4 inputs and one output. It was shown that the optimum number is one hidden layer to reach minimum error. In 2009, Ortigosa et al. [5] applied the ANN technique for calculating the total hull resistance coefficient. They chose the Broyden algorithm to train the data with a sigmoidal function as a transfer function with one hidden layer. It was illustrated that the optimal ANN architecture was 5 inputs and 2 outputs through 9 hidden neuron layers. The ANN output was compared with the statistical Holtrop's method for estimating the total hull resistance. In 2014, Arslan et al. [6] used data from seven different tankers. The ANN architecture was created through MATLAB NNTool code for 6-inputs and one output. The input data were draft, ship speed, the number of main engine revolutions (rpm), sea state, the quantity of cargo, and fuel consumption as output. The ANN was constructed for 3646 samples of the dataset with 70% for training and 30% for validation. The type of ANN used was a Feed-Forward ANN (FFANN) with one hidden layer.

Gurgen et al. [7] applied the ANN model to predict the main principal dimensions of the chemical tanker. The inputs were deadweight and ship's speed of 100 tanker models, and they were trained through a Backpropagation learning algorithm. Cepowski et al. [8] used the ANN to develop the main dimensions of container models based on the number of containers and ship velocity as inputs. Also, the output ANN results were compared to the Multiple Nonlinear Regression (MNLR) results. It is illustrated that the ANN results were more accurate than the MNLR. Yang et al. [9] used the Radial Basis Function Neural Network (RBFNN) to predict the resistance of a container ship at different drafts. Abramowski [10] used artificial neural networks for the optimization of the cargo ship model and recommended a mathematical artificial model for predication effective power. Mosaad et al. [11] used a FFANN to predict the total resistance in a calm and regular wave of the combatant DTMB 5415 model. Ekinci et al. [12] applied about 18 computational intelligence methods to estimate the main design parameters of tanker ships and recommended that the use of artificial neural networks offers perfect results. The CFD simulations have been successfully utilized in thousands of fluid flow systems. Furthermore, CFD has been utilized along with several optimization techniques for the optimal design of fluid flow systems [13–23]. Furthermore, there is an increasing research interest in the implementation of AI and machine learning [24–30]. This paper aims to incorporate CFD and ANN-based AI in the development of a Graphical User Interface (GUI) software to draw the optimum 3D container model at a specified speed automatically.

The structure of the paper is as follows: Sect. 2 shows the main particular of chosen KCS container model with a 3D geometrical model. Section 3 presents the generating database based on the permutation matrix of different models' lengths, breadth, and drafts of the KCS model. Section 4 illustrates the different data of total
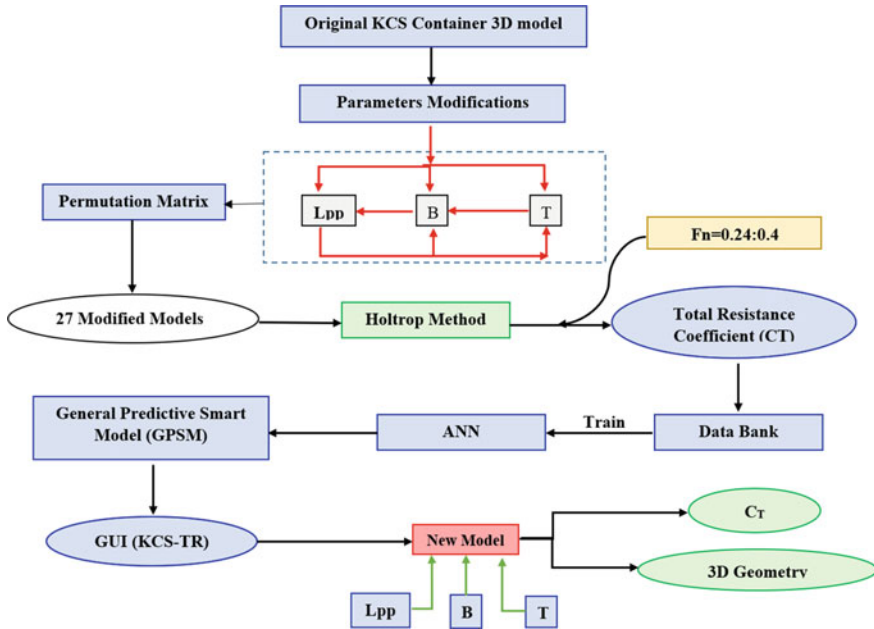
Fig. 1 A schematic diagram of the workflow of this study

KCS model resistance at each permutation case. Section 5 provides the details of the artificial neural architecture and its components. Section 6 shows the results of training the data to produce the General Predictive Smart Model (GPSM). Section 7 illustrates the use of the GPSM to create desktop software for automatic estimation of the total resistance of the KCS model and its 3D geometrical model, while in Sect. 8 the conclusions are established. Figure 1 shows the sequential steps of this paper.

2 Ship Features

In this study, The Korea Research Institute of Ships and Ocean (KRISO) Container Ship (KCS) model is selected for generating the resistance data with different model dimensions with different speed cases in calm water [31]. The KCS model is considered a benchmark test case that is used widely with the ship hydrodynamic scientific community for experimental tests and CFD validation. The hull represents a modern commercial container model with a bulbous bow and flare fore above the load waterline without a rudder. The original KCS 3D geometry model is illustrated in Fig. 2 and the main dimensions are presented in Table 1.

Fig. 2 3D geometry of KCS container hull

Table 1 Main principal dimensions

Main particulars	Value	Unit
Length between perpendicular (Lbp)	7.2789	m
Breadth (B)	1.019	m
Depth (D)	0.6013	m
Draft (T)	0.3418	m
Displacement (Δ)	1.649	ton
Wetted surface area (S)	9.4379	m^2
Block coefficient (C$_B$)	0.6505	–

3 Database Features for Neural Network Training

The aim of this section is to create different 3D geometrical models based on changing the original KCS model's dimensions and loading conditions. The created models result from changing the original length of the KCS model with its breadth and draft to produce three different groups (A), (B), and (C). The group (A) produced with the original KCS model length (i.e., 100%Lbp) with the different breadth 100B, 75B, and 50%B. Also, group (A) includes the changes of the draft as 100T, 75T, and 50%T. Group (B) focuses on generating the models at 75%Lbp with a range of breadth and draft. The breadth is varied as 100B, 75B, and 50%B. Also, the draft is varied as 100T, 75T, and 50%T. Group (C) has 50% Lbp with a change in the breadth by 100%B, 75B, and 50%B with permutation changes of the draft including 100T, 75T, and 50%T. The percentage of change in the KCS's model length is to be 75 and 50% of the original length. The original mode (i.e., 100%Lbp). Figure 3 shows the change of the original length parameter for the KCS model at different breadth and draft. Figure 4 shows the change of the original breadth parameter for the KCS model at 100B, 75B, and 50%B. Figure 5 shows the permutation matrix of different change parameters (Lbp, B, and T) with the total resistance coefficient (CT) as a target.

4 Data Generation

This section illustrates the data of total resistance coefficient (C$_T$) estimation for the various modified 3D KCS models by using Holtrop and Mennen's method. This method was created by Netherlands Ship Model Basin based on the multi-regression statistical analysis. The estimation is carried out considering the calm water state and

100%Lbp

75%Lbp

50%Lbp
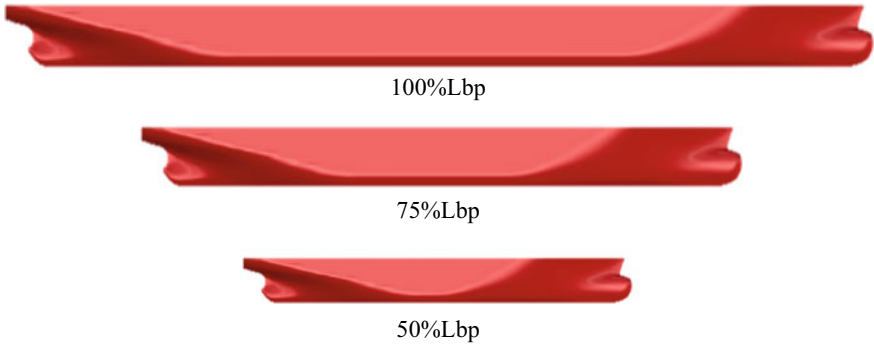
Fig. 3 The change of the length parameter for the KCS model

Fig. 4 The change of the breadth parameter for the KCS model

100%B

75%B

50%B
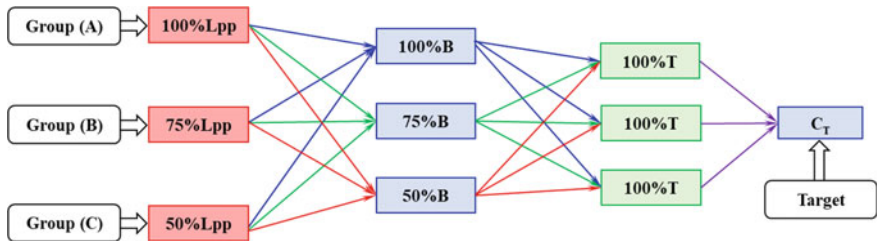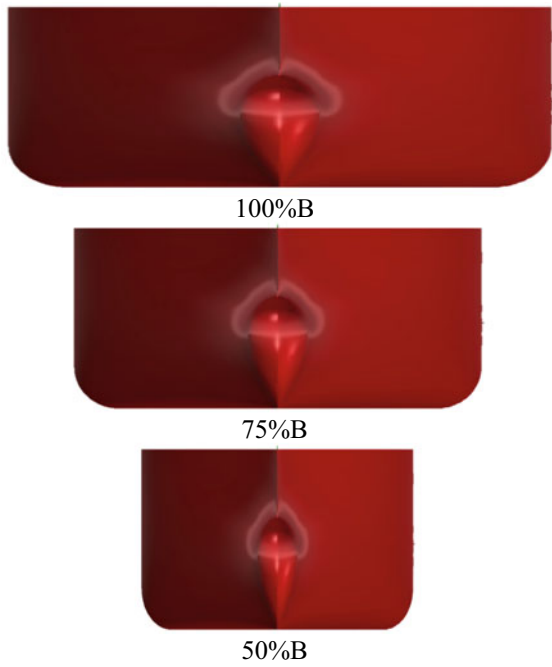
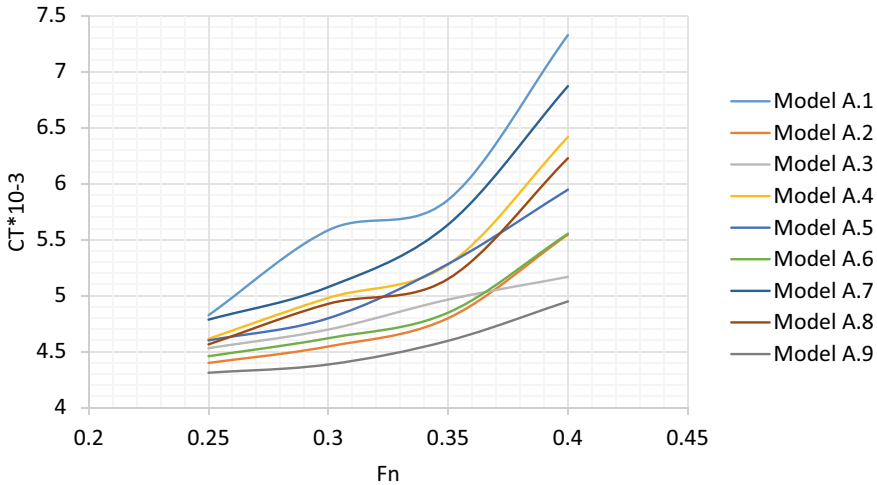**Fig. 5** The permutation matrix of different change parameters

Fig. 6 Total resistance coefficient versus Froude number of group (A)

at different speed ranges based on the Froude number definition (F_n). The tests are carried out at Fn = 0.25 to 0.4 with 0.05 intervals. The total resistance coefficient is generally determined as:

$$C_T = \frac{R_T}{0.5 \times \rho \times S \times V^2} \tag{1}$$

where R_T is the total resistance,

S is the wetted surface area as defined in Table 1,

V is the KCS model's speed,

Fn is Froude number $= \frac{V}{\sqrt{g \times Lpp}}$.

Figure 6 illustrates the results of total resistance for group (A) at different Froude numbers. Figures 7 and 8 show the results of total resistance versus Froude number of group (B) and group (C), respectively. Appendix 1 represents all data of the 27 model with their dimensions and the corresponding total resistance coefficients at different Froude numbers in the range (0.25: 0.4).

5 Artificial Neural Network Architecture

ANN is a way to mimic human thinking, and a technical system to simulate the structure and functional characteristics of the human brain neural network by means of engineering technology. In essence, it is a massively parallel nonlinear dynamic system [32]. The modified parameter of the KCS model and total resistance coefficient data are trained through the ANN code. In this paper, The MATLAB ANN
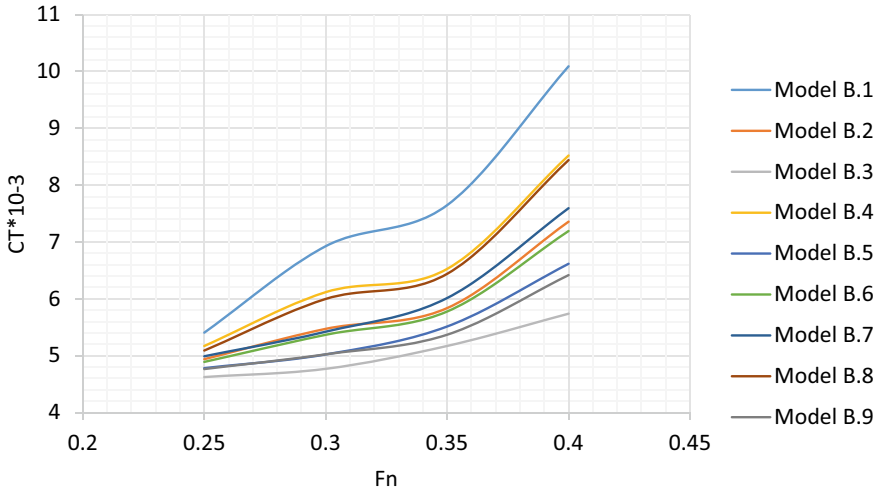
Fig. 7 Total resistance coefficient versus Froude number of group (B)
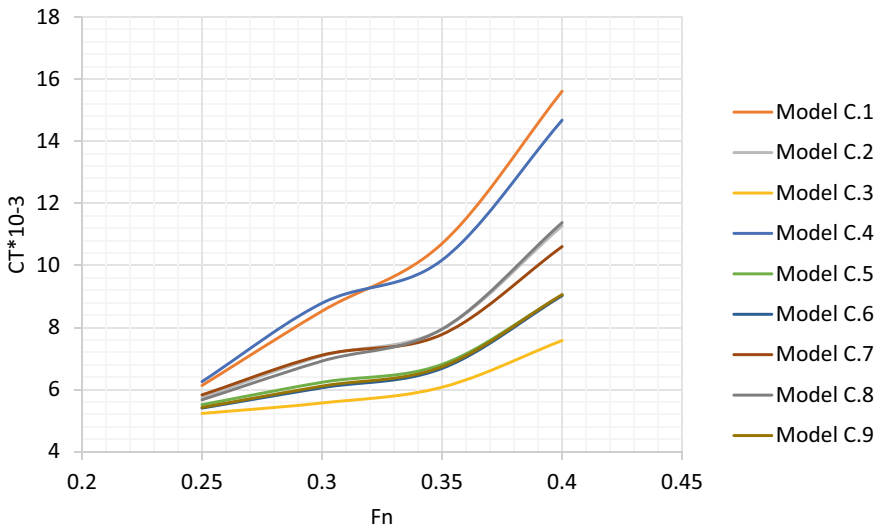
Fig. 8 Total resistance coefficient versus Froude number of group (C)

code is used for training and creating the smart artificial model. The ANN is created as a Multi-Layer Perceptron (MLP) that consists of input layers, hidden layers, and an output layer. The six input layers include the parameters of (Lbp, B, T, S, Δ, and C_B) of original and modified models of KCS. The output layer represents the target of one layer of the total resistance coefficient. The neuron number of the hidden layer can be estimated bas on the following Eq. 2.

$$N_H = \sqrt{N_I * N_O^{-2}} \tag{2}$$

where: N_H is the number of neurons of hidden layers

N_i is the number of neurons of input layers

N_o is the number of neurons of output layers

The architecture of the artificial neural network is created as Feed-Forward ANN (FFANN) with levenberg-marquette algorithm used as the training algorithm. Figure 9 shows the multilayer perceptron of FFAN architecture of the original and modified models' data training. The sigmoid function is used as an activation function and can be calculated as on the following Eq. 3.

$$\text{sig(x)} = \frac{1}{1 + e^{-x}} \tag{3}$$

The Sum of Square Error (SSE) is used to calculate the error between the actual value and the predicted value with the artificial neural network. It can be estimated by the sum of square differences between the target value and observed neural network output as the following Eq. 4.
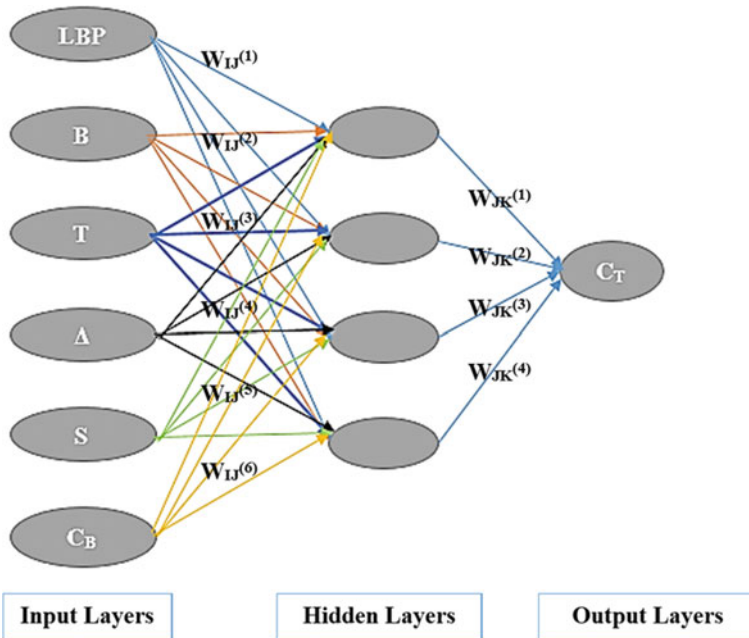
Fig. 9 Feed Forward propagation architecture of KCS model data

$$\text{SSE} = \sum_{I}^{N} (X_A^2 - X_N^2) \tag{4}$$

Where X_A is the actual value

X_N is the estimated value by the neural network.

The neural network mathematical form is obtained as the following relations:

$$Sig(X_n \times W_{ij}) + Sig(Sig(X_n \times W_{ij}) + W_{jk}) + b = Y \tag{5}$$

where

Sig is a sigmoid transfer function.

X_n is input feature.

Y is the output feature.

W_{ij} is the weight from the input layer to the hidden layer.

W_{jk} is the weight from the hidden layer to the output layer.

b is the biases.

6 Smart Model

In this study, artificial neural networks were trained and tested by using the MATLAB-ANN code, [32]. The constructed artificial MATLAB model includes input, an output layer, and output as shown in Fig. 10. The number of samples used is about 30,000, 70% of the sample for training, 15% for validation, and 15% for testing data. The data extracted from training data are used to enerate a General Predictive Smart (GPSM) model form with its variable of the input matrix, bias matrix, and balancing weight matrix. Figure 11 illustrates the results of training, validation, and test data of relations between the target data (actual data) and the output where R^2 is close to one. The numerical data of the input matrix, bias matrix, and balancing weight matrix are shown in Appendix 2.

Fig. 10 Artificial MATLAB model
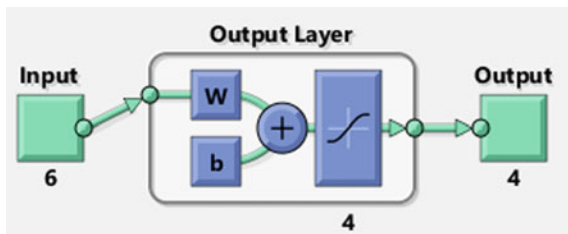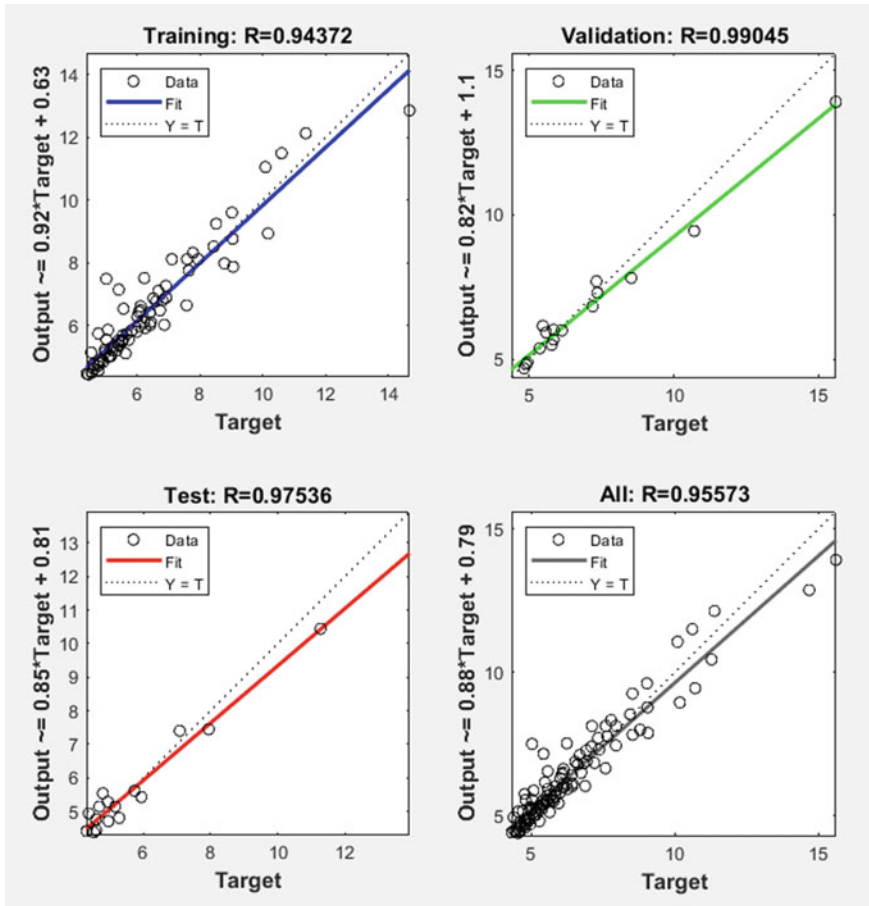
Fig. 11 Relation between the target data at training, test and validation

7 Graphical User Interface

MATLAB software is utilized to create a Graphical User Interface (GUI) as ready desktop software for non-experienced users. In this present work, the GUI is established by the APP Designer plugin of MATLAB SIMULINK Toolbox [33]. The authors created a computer program called KCS-TR based on the GPSM model. The KCS-TR estimates the KCS model's total resistance and auto-generating optimal 3D geometry model for specified speed utilization. Figure 12 represents the GUI of KCS-software including the input data and the KCS total resistance curve at different Froude number ranges.
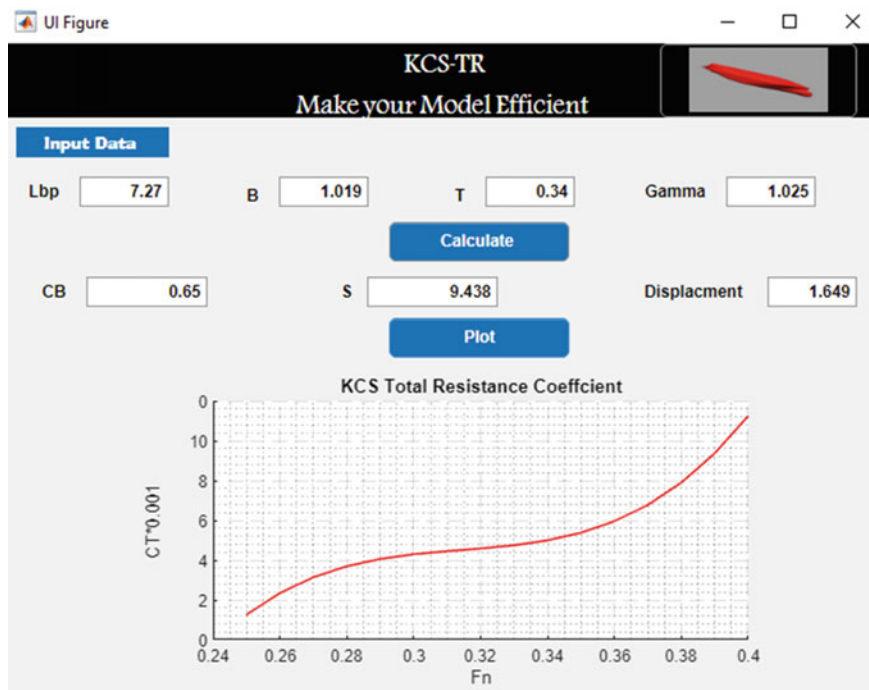
Fig. 12 Graphical user interface of KCS-TR software

8 Conclusion

The ANN is a good tool for predicting the total resistance coefficient of KCS models through the prepared database for training. The prepared database was investigated by changing the main dimension (Lbp, B, T) of the KCS model to create 27 new modified models. The modified models were tested by using the statistical Holtrop-Menan method for estimating the total resistance coefficient at different Froude number ranges from 0.25 to 0.4. The collected data were trained by using MATLAB NNTool code through a feed-forward artificial neural network (FFAN) with 6 input layers, 4 hidden layers, and one output layer with the levenberg-marquette training algorithm. The data produced from training data are used to create a general predictive smart (GPSM) model for a general solution and predicate the total resistance for non-defined data. The GPSM is used to create a graphical user interface (GUI) with the name KCS-TR for non-experienced users for automatic estimation of the total resistance of the KCS model. By optimizing the ship hull, the fuel consumption, and the greenhouse gases emissions. This would assist in the fulfillment of SDG13: Climate Action.

9   Recommendations

It is recommended to implement the CFD simulations for the optimization of ship hulls. Furthermore, it is recommended to utilize the ANN in optimizing the ship hulls in order to reduce the fuel consumbtion and reduce the greenhouse gases emissions.

Appendix 1

The data bank of input and output data at different speed ranges (Fn) for different KCS model dimensions.

Model Code	Input features data						$CT \times 0.001$ (Output data) Fn			
	L	B	T	Δ	S	CB	0.25	0.3	0.35	0.4
A.1	7.2	1.01	0.34	1.675	6.08	0.64	4.8252	5.5845	5.8552	7.3264
B.1	5.4	1.09	0.34	1.257	5.51	0.64	5.4058	6.9264	7.6478	10.090
C.1	3.6	1.01	0.34	0.829	4.80	0.64	6.1336	8.5286	10.703	15.604
A.2	7.2	0.76	0.25	0.882	6.55	0.612	4.398	4.5462	4.7986	5.5454
B.2	5.4	0.76	0.25	0.662	4.93	0.612	4.9387	5.4720	5.8371	7.3573
C.2	3.6	0.76	0.25	0.440	3.31	0.612	5.7464	7.0860	7.9451	11.272
A.3	7.2	0.51	0.17	0.363	4.13	0.564	4.5310	4.6974	4.9647	5.1677
B.3	5.4	0.51	0.17	0.272	3.10	0.564	4.6237	4.7684	5.1709	5.7384
C.3	3.6	0.51	0.17	0.181	2.07	0.564	5.2330	5.5707	6.0773	7.5806
A.4	7.2	0.76	0.34	1.56	8.71	0.62	4.6187	4.9033	5.2704	6.4169
B.4	5.4	0.76	0.34	0.942	6.15	0.642	5.171	6.1176	6.5263	8.5207
C.4	3.6	0.76	0.34	0.621	4.1	0.642	6.2575	8.7846	10.171	14.672
A.5	7.2	0.51	0.25	0.584	5.45	0.612	4.6032	4.793	5.289	5.947
B.5	5.4	0.51	0.25	0.441	2.02	0.612	4.7811	5.0194	5.51	6.6165
C.5	3.6	0.51	0.25	0.293	2.74	0.612	5.5161	6.2360	6.86	9.0441
A.6	7.2	1.01	0.17	0.727	6.26	0.564	4.4589	4.6200	4.848	5.5528
B.6	5.4	1.01	0.17	0.545	4.71	0.564	4.8906	5.3675	5.772	7.1926
C.6	3.6	1.01	0.17	0.333	3.16	0.564	5.4004	6.0154	6.642	9.029
A.7	7.2	0.51	0.34	0.838	6.89	0.64	4.7859	5.0770	5.63	6.8701
B.7	5.4	0.51	0.34	0.628	5.18	0.64	4.9897	5.4220	6.014	7.5941
C.7	3.6	0.51	0.34	0.418	3.47	0.64	5.8312	7.1111	7.77	10.603
A.8	7.2	1.01	0.25	1.177	7.74	0.612	4.5698	4.9217	5.1497	6.2266
B.8	5.4	1.01	0.25	0.882	5.86	0.612	5.0907	5.9984	6.4396	8.4399
C.8	3.6	1.01	0.25	0.587	3.93	0.612	5.6723	6.920	7.9480	11.375

(continued)

(continued)

Model Code	Input features data						CT × 0.001 (Output data)			
							Fn			
	L	B	T	Δ	S	CB	0.25	0.3	0.35	0.4
A.9	7.2	0.76	0.17	0.545	5.17	0.564	4.3116	4.3853	4.5969	4.9484
B.9	5.4	0.76	0.17	0.491	3.89	0.564	4.7657	5.0282	5.3865	6.4692
C.9	3.6	0.76	0.17	0.224	2.67	0.564	5.4263	6.1115	6.7311	9.0861

Appendix 2

$$\text{Input Matrix} = \begin{matrix} x1 \\ x2 \\ x3 \\ x4 \\ x5 \\ x6 \end{matrix} = \begin{matrix} Lpp \\ B \\ T \\ \Delta \\ S \\ CB \end{matrix}.$$

$$\text{Weight Matrix} = \begin{matrix} -0.20996 & 0.81581 & 0.35186 & 0.95122 & -0.7154 & -0.92804 \\ -0.2564 & 0.6785 & 1.0583 & 0.30792 & 0.35783 & -1.1146 \\ 1.0824 & 1.2061 & -0.19185 & -0.49619 & 0.35946 & -0.27009 \\ -0.42052 & 0.012983 & -1.0134 & 1.1447 & -0.25971 & -0.72761 \end{matrix}.$$

$$\text{Bias Matrix} = \begin{matrix} 1.7639 \\ 0.58796 \\ 0.58796 \\ -1.7639 \end{matrix}.$$

References

1. Hou YH (2017) Hull form uncertainty optimization design for minimum EEOI with influence of different speed perturbation types. Ocean Eng 140:66–72. https://doi.org/10.1016/j.oceaneng.2017.05.018
2. Abramowski T (2010) Application of artificial intelligence methods for improving ship transport efficiency. Sci J Marit Univ Szczecin 21:5–11
3. Clausen HB, Lu¨tzen M, Friis-Hansen A, Bjørneboe N (2001) Bayesian and neural networks for preliminary ship design. SNAME News 38:268–277
4. Mason A, Couser P, Couser P, Mason G, Smith CR, Von Konsky BR (2005) Optimisation of vessel resistance using genetic algorithms and artificial neural networks. In: 4-th international conference on computer applications and information technology in the maritime industries, pp 8–11
5. Ortigosa I, López R, García J (2009) Prediction of total resistance coefficients using neural networks. J Marit Res VI No III:15–26

6. Arslan O, Besikci E, Olcer A (2014) Improving energy efficiency of ships through optimization of ship operations
7. Gurgen S, Altin I, Ozkok M (2018) Prediction of main particulars of a chemical tanker at preliminary ship design using artificial neural network. Ships Offshore Struct 13:459–465. https://doi.org/10.1080/17445302.2018.1425337
8. Cepowski T, Chorab P (2021) Determination of design formulas for container ships at the preliminary design stage using artificial neural network and multiple nonlinear regression. Ocean Eng 238:109727 https://doi.org/10.1016/j.oceaneng.2021.109727
9. Yang Y, Tu H, Song L, Chen L, Xie D, Sun J (2021) Research on accurate prediction of the container ship resistance by RBFNN and other machine learning algorithms. J Mar Sci Eng 9(4):376. https://doi.org/10.3390/jmse9040376
10. Abramowski T (2018) Application of artificial intelligence methods to preliminary design of ships and ship performance optimization. Nav Eng J 125:87–98
11. Mosaad MA, Yehia W, Hussein AW, Hassan HM (2020) Proposed naval bow form for minimum wave resistance. In: International conference on science, technology, engineering and management (ICSTEM)
12. Ekinci S, Celebi UB, Bal M, Amasyali MF, Boyaci UK (2011) Predictions of oil/chemical tanker main design parameters using computational intelligence techniques. Appl Soft Comput J 11(2):2356–2366
13. Mabrouk AN, Elhenawy Y, Abdelkader M, Shatat M (2017) The impact of baffle orientation on the performance of the hollow fiber membrane distillation. Desalin Water Treat 58:35–45
14. Elsakka MM, Ingham DB, Ma L, Pourkashanian M, Moustafa GH, Elhenawy Y (2022) Response surface optimisation of vertical axis wind turbine at low wind speeds. Energy Rep 8:10868–10880
15. Abdelhamed AS, Yassen YES, Elsakka MM (2015) Design optimization of three dimensional geometry of wind tunnel contraction. Ain Shams Eng J 6:281–288. https://doi.org/10.1016/J.ASEJ.2014.09.008
16. Amer AE, Elsakka MM, Lebedev VA (2021) Thermal performance of an accumulator unit using phase change material with a fixed volume of fins. Int J Energy Res 45:19089–19102. https://doi.org/10.1002/ER.7095
17. Selim T, Hesham M, Elkiki M, Elsakka MM (2023) Numerical analysis of sediment transport and depth averaged flow velocity in non-prismatic compound channels. Ain Shams Eng J. https://doi.org/10.1016/J.ASEJ.2023.102229
18. Elsakka MM, Ingham DB, Ma L, Pourkashanian M (2020) Effects of turbulence modelling on the predictions of the pressure distribution around the wing of a small scale vertical axis wind turbine. In: Proceedings of the 6th European conference on computational mechanics: solids, structures and coupled problems, ECCM 2018 and 7th European conference on computational Fluid dynamics, ECFD, pp 3921–3931
19. Ibrahim IA, Elzallat AM, Elsakka MM, Farag TM, Gad HM (2022) Numerical study of kerosene spray and combustion characteristics using an air-blast atomizer. Energy Rep 8:5974–5986. https://doi.org/10.1016/J.EGYR.2022.04.046
20. Amin I, Elsakka M, Oterkus S, Tien Nguyen C, Ozdemir M, El-Aassar A-H, Shawky H, Oterkus E (2022) Computational fluid dynamics-based design of anoxic bioreactor zone in wastewater treatment plant. Desalin Water Treat 253:9–23. https://doi.org/10.5004/dwt.2022.28300
21. Mosaad MA, Hassan HM, Yehia W (2020) Improving ship wave resistance by optimal bulb configuration. Sylwan pp 1–12
22. Mosaad MA, Gafaary MM, Yehia W, Hassan HM (2017) On the design of X-bow for ship energy efficiency. Influence EEDI Ship Des Oper 22(12)
23. Hassan HM (2021) Optimal ship form based on artificial neural network. Port Said University
24. Saleh H, Saber W, Rizk R (2022) Mobile computation offloading in mobile edge computing based on artificial intelligence approach: a review and future directions. Lect Notes Data Eng Commun Technol 113:593–603. https://doi.org/10.1007/978-3-031-03918-8_49/TABLES/2
25. Mohammed NH, Nashaat H, Abdel-Mageid SM, Rizk RY (2021) A machine learning-based framework for efficient LTE downlink throughput. Stud Comput Intell 912:193–218. https://doi.org/10.1007/978-3-030-51920-9_10/FIGURES/15

26. Mohammed NH, Nashaat H, Abdel-Mageid SM, Rizk RY (2021) A framework for analyzing 4G/LTE-a real data using machine learning algorithms. Adv Intell Syst Comput 1261AISC:826–838. https://doi.org/10.1007/978-3-030-58669-0_73/TABLES/4
27. El-Baz A, Saber W, Rizk RY (2021) LWCOV: lightweight deep convolutional neural network for COVID-19 detection. Adv Intell Syst Comput 1339:12–22. https://doi.org/10.1007/978-3-030-69717-4_2/FIGURES/4
28. Hashem W, Attia R, Nashaat H, Rizk R (2022) Advanced deep reinforcement learning protocol to improve task offloading for edge and cloud computing. Lect Notes Data Eng Commun Technol 113:615–628. https://doi.org/10.1007/978-3-031-03918-8_51/TABLES/2
29. Moussa W, Nashaat M, Saber W, Rizk R (2022) Comprehensive study on machine learning-based container scheduling in cloud. Lect Notes Data Engin Commun Technol 113:581–592
30. Gamal M, Rizk R, Mahdi H, Elhady B (2019) Bio-inspired based task scheduling in cloud computing. Stud Comput Intell 801:289–308
31. Holtrop J, Mennen GGJ (1982) An approximate power prediction method. Int Shipbuild Prog 29:166–170
32. MathWorks (2017) MATLAB for NNtool reference manual, USA
33. MathWorks (2017) MATLAB for app designer reference Manual, USA

Ship Design for Green Ship Recycling: A New Approach

Walid M. Bahgat, El-Sayed Hegazy, Heba S. El-Kilani, Amman Ali, and M. M. Moustafa

1 Introduction

Ship breaking, dismantling, scraping, demolition and ship disposal are expressions with the same meaning which ends at ship recycling yards [1]. The ship recycling industry is a vigorous market which offers a huge profit to the ship owner, ship brokers and the cash buyers from selling ships as scrap. At the end of this loop between the ship owner, ship broker and the cash buyer, the ship recycling yard buys the ship according to its light weight or light ship displacement from the cash buyer.

The volume of ships recycled globally is expected to rise sharply in the near future, which will benefit the circular economy. Thus, it is essential to create a framework for ship recycling that would serve as a road map for establishing a circular economy [2].

Being on the agenda of numerous parties which include non-governmental organizations (NGOs), government agencies, and international organizations as International Maritime Organization (IMO) and International Labor Organization (ILO),

W. M. Bahgat (✉) · A. Ali
Institute of Maritime Upgrading Studies, Arab Academy for Science, Technology and Maritime Transport, Alexandria, Egypt
e-mail: wbahgat1971@aast.edu

A. Ali
e-mail: amman_aly@aast.edu

E.-S. Hegazy · H. S. El-Kilani · M. M. Moustafa
Naval Architecture and Marine Engineering Department, Faculty of Engineering, Port Said University, Port Said, Egypt
e-mail: elsayed.hesen@eng.psu.edu.eg

H. S. El-Kilani
e-mail: Hebaelkilani@eng.psu.edu.eg

M. M. Moustafa
e-mail: moustafa3875@eng.psu.edu.eg

the ship recycling has become an issue. Indeed, NGOs such as Greenpeace and NGO Ship breaking platform have posted a lot of reports pointing out the concerns associated with the environment and insecure condition of workers in ship recycling facilities [3–5]

In ship recycling industry, there are a variation between the green ship scraping (standard) yards that comply with the international regulations and safety standards requirements (e.g., Hong Kong convention and European union recycling regulation), and non-complied or substandard yards which offers more price for the scraped ship than the standard ship recycling yards. This condition occurs due to the high cost of applying health, safety and environmental standards and the exploitation in recycling yards and the workers welfare required for the standard ship recycling yards. So, this gap in price leads to the ship owners not thinking of selling their ships to standard ship recycling yards. In a nutshell, to fill this gap, the total cost of ship recycling process must be less than the revenue for the ship recycling yard.

Many aspects relate ship recycling industry to Sustainable Development Goals (SDGs); namely, the health of workers engaged in ship recycling process and subjected to hazardous materials contained on board ship is an objective of "GOAL 3"(Good Health and Well-being). Also, contamination of sea water due to residues of fuel oil, lubricating oil and sludge if tanks are not cleaned before ship recycling process is a concern of "GOAL 14" (Life Below Water).

The variables affecting environmentally friendly ship recycling that are related to organizational and management have the biggest overall effects [6].

In the process of recycling ships, ship scrapping contributes significantly to marine pollution. This includes poisonous substances that could leak into the environment or human health and present a serious risk to both [7].

The issuing of the Hong Kong convention and the European Union recycling regulations is an admission from the IMO that the ship recycling is the best solution to get rid from the old ships because it is considered to contribute to the economic and sustainable development of the society [8]. Additionally, the admission of IMO means that the ship recycling industry will provide hundreds of thousands of jobs to skilled, semi-skilled and unskilled workers in developing countries such as China, India, Pakistan, and Bangladesh [9, 10]. Moreover, ship recycling recovers millions of tons of scrap which include steel and other metals for recycling and different types of machinery, equipment, and other fittings for reutilizing from ship's end life annually [11–14].

2   Concept of Ship Design for Recycling

There is a relation between ship breaking and ship design, this relationship can encourage safe and ecologically stable ship recycling. The ship design cycle is principally affected by operation requirements specified by the shipowner, well-being prerequisites specified by international regulations, for example, MARPOL,

SOLAS, IMO codes, and production requirements indicated by the shipyard. Unfortunately, the last stage of a ship's lifecycle, namely recycling, is not involved in this cycle, chiefly considering the absence of coordination between different partners associated with various phases of a ship's lifecycle. These incorporate ship owners, ship designers, shipyards, classification societies, ship scrapping yards, and governmental authorities [15]. The designer should keep in mind that it is essential to build ecologically friendly ships that are easy to recycle in order to promote safe and environmentally sound ship recycling, in addition to raising the standards of recycling facilities [16]. In fact, the fundamental goal of ship recycling is to help sustainability by recycling vast quantities of materials from retired ships, but the industry's actual practices counteract this goal's beneficial impacts [17]. End-of-life ship demolition in unsafe conditions has several negative consequences on the environment, labor rights, and safe working conditions [18].

According to IMO guiding rules, design for ship recycling is a set of design tips which include suitable design/selection of structural parts, equipment, material and knowledge base that will facilitate clean and safe partial/full dismantling of ships, maximum use of recycled products/parts in ship production, and reduction in number of inseparable components/parts in on board equipment gatherings [19]. Major areas of concern within ship recycling industry causing health and environmental impacts include the use of hazardous materials such as asbestos and PCBs (Polychlorinated biphenyls) within the design and construction of a vessel. These also include toxicity of paints and coatings used on ships and the complexity in design and layout of overall ship structure, especially machinery compartment and oil tanks which must be manually cleaned before subjected to cutting operation. The concept of design for recycling requires documenting all the hazardous materials used in ship construction so that a relevant plan can be made to recycle the ship based on this inventory of hazardous materials [20].

3   Proposed Approach

The following four main issues would direct the ship design toward green recycling that comply with HKC and EU SRR:

1. Cutting the ship into small blocks to avoid using large floating or dry docks to dismantling the complete ship as required by HKC. If possible, a clear indication of where the original construction blocks were assembled during ship construction would enable recyclers to apply reverse block dismantling approach to identify elements such as access points to hazardous materials. The approach proposed in the present paper and illustrated in the following case study focuses on this issue.
2. Make the ship easy to dismantle:

Many critical items can be included in the detailed structural design stage to achieve this objective. Among these are standardization of all the parts and the concept of using modules that would provide easy access for maintenance and removal. Moreover, the use of the same type of stiffeners for hull structure and reduction in the variety of materials in insulation, paneling etc. within appropriate rules would make ship recycling a lot easier. The inclusion of properly designed lifting supports for future handling of the dismantled structural parts and onboard equipment is an effective requirement to minimize accidents due to falling components during ship dismantling phase. Reduced height of piping installation or strategically designed location of pipes within engine room would also minimize the accidents such as falling from heights during ship recycling. It would also allow an easier approach for gas cutting torches.

3. Reduce or replace hazardous materials:

Recently, suitable non-hazardous alternatives are available; for instance, certain hazardous materials such as asbestos, tributyltin (TBT) in antifouling paints, and chlorofluorocarbons (CFCs) in refrigerants are nowadays replaced in new designs after they were banned by IMO regulations.

4. Provide an accurate inventory of equipment and hazardous materials onboard ship. This step would be implemented in several stages of the design spiral, such as machinery selection, cargo handling, outfitting and equipment.

The present approach is herein proposed to minimize the gap in scrap ton price between the green ship scrapping yards and the sub-standard or non-complied scrapping yards which is offered to the shipowner. The method begins by dismantling the scrapped ship when afloat alongside by cutting it transversely at certain location into partitions and transferring every partition through the cradle to the cutting workshop without occupation to the slipway dock. This method relies on performing proper stability calculations to deduce the equilibrium condition of each partition being cut from the hull separately. "MAXSURF" software package is used starting from the available hull weight distribution, the weight and center of gravity of each partition is determined. Each partition is treated as a separate unit considering the space between two bulkheads as intact compartments and the other two spaces open to the sea forward and aft of this compartment as damaged compartments [21].

The intended calculations are like damage stability calculations, and the aim is to find out if the suggested separated partition will remain afloat and to determine its equilibrium condition. This will help setting the towing plan required to transfer the dismantled partition to a slipway in the scrapping yard. The basic input data required for this proposal consist of the ship like stability booklet, light weight distribution, loading manual, offset table, and ship's lines. The essential ship's documents must be held on the ship to be useful for the shipowner and the ship recycling yard at ship's end of life. Based on main technical information available in ship's documents, the proposed technique for breaking the scrapped ship can be done to facilitate the ship scrapping process complying with the ship breaking yard or the shipbuilding yard. This ship breaking process should be assessed and taken into consideration during the design stage.

The vessel could be broken into multiple smaller units, in which each unit can be individually moved into the cutting workshop or dock by any lifting facility in the shipyard whether it is crane, mechanical slipway, regular slipway, travel lift, synchro-lift, or small drydock. The outdated ship is then brought into the cutting workshop if this could not be possible with the ship as a whole unit.

4 Case Study

The case study is a multipurpose ship called "Prince Basel," with 4800-ton deadweight, the ship has length 100.6 m, breadth 16.2 m, depth 8.2 m and draft 6 m. It has five bulkheads dividing the ship into six compartments, namely the aft peak, engine room, holds No.1, 2, 3 and 4, as shown in Fig. 1. Figure 2 shows the lightweight distribution for the case study ship.

The stability booklet, light weight distribution, loading manual, offset table, lines plan and ship's capacity plan of Prince Basel are available to apply damage stability calculations for each proposed partition to determine its possible afloat condition.

To study the possibility of dividing the ship into partitions, one or more compartments are assumed to be damaged and lost. The number of the remaining intact compartments must be more than the number of compartments in the separated partition. For instance, since "Prince Basel" has six compartments, if the ship is divided into three units, two compartments are lost leaving four intact and hence the number of intact compartments is more than sectioned off compartments. But if the ship is to be cut into four units, three compartments are damaged, leaving three intact which are not enough to keep all three partitions afloat.

Therefore, the number of possible partitions may be expressed as:

$$No.\,of\,partitions = No.\,of\,Bulkheads - 2$$

Two scenarios are proposed and indicated Case A and Case B as shown in Fig. 3. The vessel could be broken into multiple smaller units depends on the number of
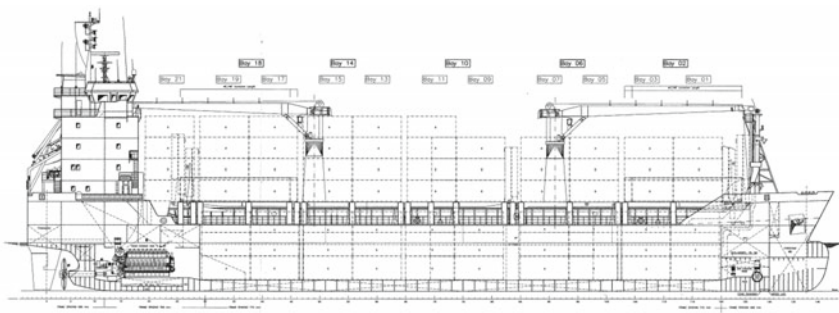
Fig. 1 "Prince Basel" cargo ship
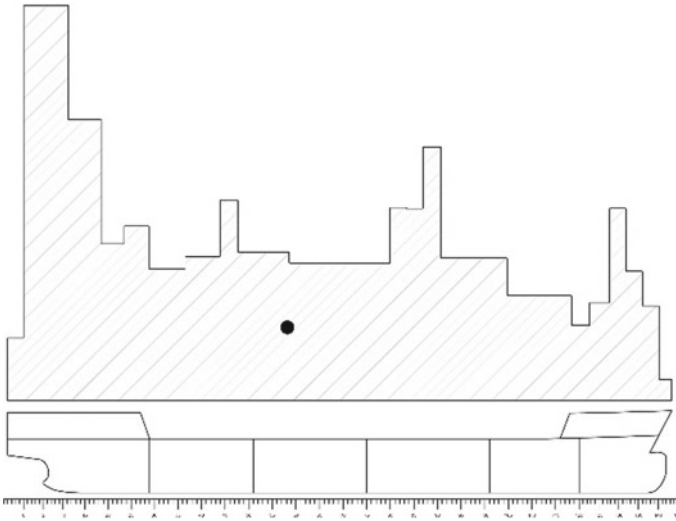
Fig. 2 Lightweight distribution for "Prince Basel"

intact watertight compartments of the ship and/or number of watertight bulkheads in a way that every partition or unit has at least one intact compartment that could provide enough buoyancy to keep the whole partition afloat.

The cutting must take place such that not only the partition is afloat but also it has sufficient stability to be towed to the nearest slipway or anchored waiting to be lifted by cranes on quay without sinking or capsizing.

Table 1 shows the results calculated for each partition. Each partition is treated as if it was an individual ship with the sectioned off compartment considered as a damaged compartment. The table shows the assessment of the ship transverse
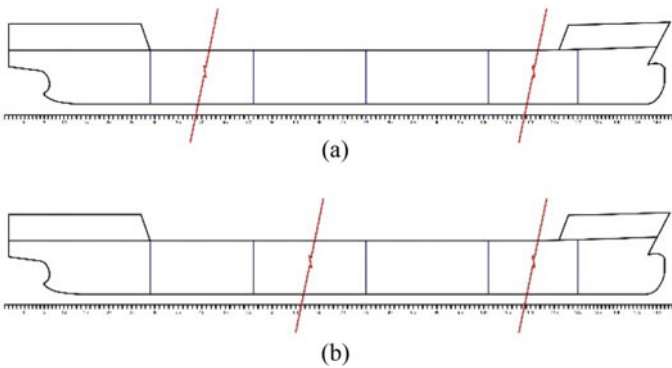
Fig. 3 Proposed cutting location: **a** Case A, **b** Case B

stability according to IMO MSC 267(85) Ch2—General Criteria used for all ships
[22].

The criteria are as follows:

- The area under the GZ curve should not be < 0.055 m rad up to θ = 30°.
- The area under the GZ curve should not be < 0.09 m rad up to θ = 40°.
- The area under the GZ curve should not be < 0.03 m rad between θ = 30° and θ = 40°.
- The righting arm should be at least 0.2 m at an angle of heel equal to or > 30°.
- The maximum righting arm should occur at an angle θ > 30°.
- The initial metacentric height GM should not be < 0.15 m.

Figures 4, 5 and 6 for Case A show that the longest partition is the middle one
which also has the largest weight. However, the aft partition shows a slightly smaller
weight despite it is only 60% of the middle length and the forward partition has the
least weight.

Figures 7, 8 and 9 for Case B show that the aft partition is the longest one and
represents more than 50% of the ship weight while the fore partition is the same. While
the aft partition has a large trim, the middle and fore partitions have respectively lower
trim in both studied cases. It can be noticed that both cases offer the possibility of

Table 1 Hydrostatics and stability of proposed sectioned off partitions

Results	Scenario					
	Case A			Case B		
	Aft partition	Middle partition	Fore partition	Aft partition	Middle partition	Fore partition
Length (m)	29.36	50.4	20.8	45.79	33.87	20.8
Displacement (tonnes)	988	1172	330.5	1373	787	330.5
LCG from aft end (m)	10.04	24.8	10.1	17.008	16.64	10.1
LCF from aft end (m)	8.84	25.9	9.65	16.73	17.78	9.65
Draft at fore end (m)	0.717	1.624	5.975	−1.328	1.524	5.975
Draft at aft end (m)	9.898	2.691	5.110	8.489	4.087	5.110
Trim (+ve by stern) m	9.181	1.067	−0.864	9.817	2.563	−0.864
Trim angle (+ve by stern) deg	18.8	1.213	−2.84	12.75	4.32	−2.84
IMO MSC267(85) Ch2—general criteria	Pass	Pass	Pass	Pass	Pass	Pass

Fig. 4 Case A—aft partition
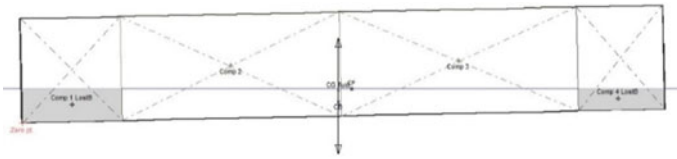
Fig. 5 Case A—middle partition
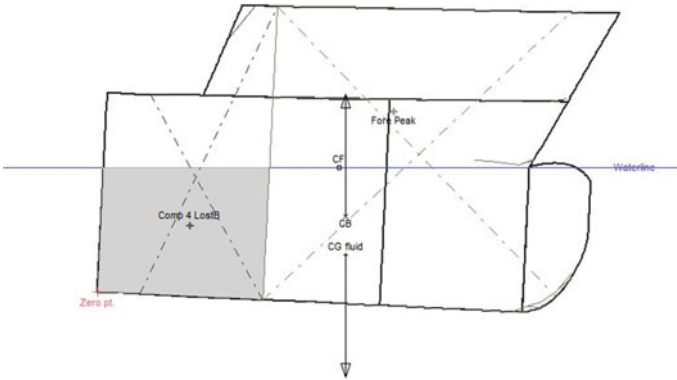
Fig. 6 Case A—forward partition

obtaining stable partitions, however the decision would rely on assessing the stability of the partitions during towing.
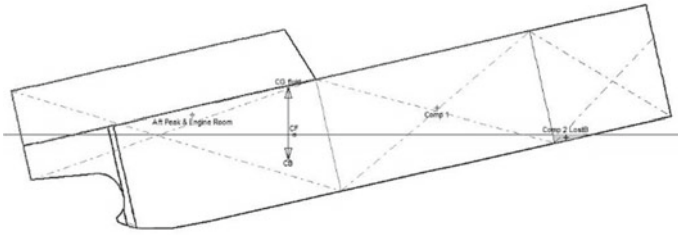
Fig. 7 Case B—aft partition
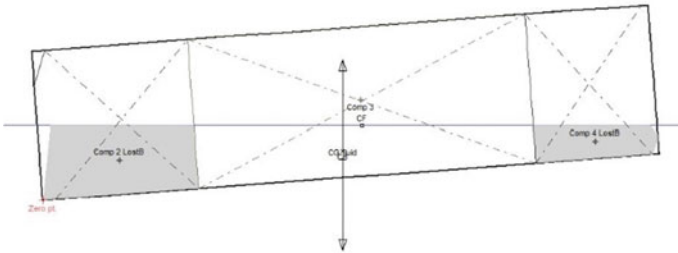
Fig. 8 Case B—middle partition
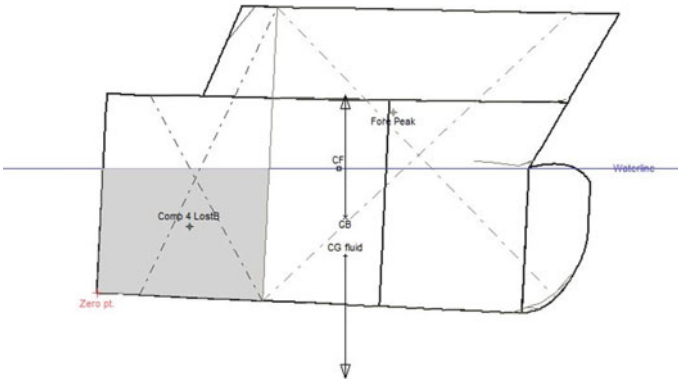
Fig. 9 Case B—forward partition

5 Conclusion

The design for recycling concept is aimed at maximizing the value of an end-of-life ship by minimizing the recycling costs. The proposed approach is considered as an alternative method to cutting the ship in the dock so that the costs can be reduced. It consists of determining the optimum cutting locations of the scrapped ship while alongside according to the shipyard facilities and/or towing options. The essential

part of this decision making is to perform the hydrostatic and stability calculations for each partition separately to ensure an adequate afloat condition. The proposed calculation process, if carried out during the design stage of a new ship, would be considered in all structural plans and details to facilitate the green recycling process. A shipbuilding yard may be therefore employed as a scrapping yard at the same time in which the scrapped ship will be cut into separate partitions that may be transferred by tug without crane assistance, to the slipway dock through the cradle and by a winch to the cutting workshop to complete the cutting process, the slipway dock would not be occupied and can be used for docking maintenance or new building. Study the ability of reducing the number of separated partitions according to the weight with the ship recycling yard facilities. Green ship recycling may be implemented in many developing countries that have limited shipbuilding potential. Egypt, for instance, is a promising location for such investment due to favorable weather conditions and coasts as well as abundant labor. Old slipways and floating or dry docks that are not fully complying to growing and contemporary shipbuilding market may be utilized in ship recycling according to the proposed approach.

6 Recommendation for Future Work

The proposed approach adopted stability analysis to judge the suitability of the cutting scenario to perform green ship recycling. However, many other aspects may affect the required decision. The structural and strength assessment of the resulting blocks should be studied to avoid undesirable collapse during handling of large blocks before entering the dock or slipway. The formulation of a method to evaluate the economic aspects of the process to select the cheaper scenario would also be a useful topic. Green ship recycling may benefit from a tailored optimization software that takes into account all objectives and constraints to set the best cutting and breaking scenario.

References

1. Mikelis N (2012) The Emergence of an International Regulatory regime for the Ship Recycling Industry. Lloyd's Maritime Academy Sale & Purchase Conference, London
2. Mannan B, Rizvi MJ, Dai M (2022) Developing a MCDM-based framework for achieving circular economy through sustainable ship recycling. In: Proceedings of the International Conference on Marine Technology MARTEC. University of Plymouth, Dhaka
3. Iqbal KMJ, Heidegger P (2013) Pakistan shipbreaking outlook: the way forward for a green ship recycling industry—environmental, health and safety conditions. In: Sustainable Development Policy Institute and NGO Shipbreaking Platform Joint Position Paper
4. Vardar E, Kumar R, Dao R, Harjono M, Besieux M, Brachet I, Wrzoncki E (2005). End of the human cost of ship breaking: a greenpeace-FIDH report in cooperation with YPSA. YPSA
5. Elias D (2004) Impacts and challenges of a large coastal industry: Alang-Sosiya ship-breaking yard Gujarat. UNESCO, India

6. Zhou Q, Liang J, Du Z, Zhu H, Jiao Y (2021) A study on factors affecting workers' safety during ship recycling. Ocean Eng 239:109910
7. Wan Z, Wang L, Chen J, Sperling D (2021) Ship scrappage records reveal disturbing environmental injustice. Mar Policy 130:104542
8. IMO (2009) International Convention for the Safe and Environmentally Sound Recycling of Ships adopted in Hong Kong, China
9. Dev AK (2010) Various aspects of sound ship recycling in South Asia: a compromise not a confrontation. In: Proceedings of MARTEC 2010 the International Conference on Marine Technology, Dhaka
10. Sarraf S-L, Dyoulgerov F, Bloch M, Wingfield R, Roy SW (2010) The ship breaking and recycling industry in Bangladesh and Pakistan. The World Bank, Washington, DC
11. Crang M, Hughes A, Gregson N, Norris L, Ahamed F (2013) Rethinking governance and value in commodity chains through global recycling networks. Trans Inst Br Geogr 38:12–24
12. Gregson N, Crang M, Ahamed FU, Akter N, Ferdous R, Foisal S, Hudson R (2011) Territorial agglomeration and industrial symbiosis: Sitakunda-Bhatiary, Bangladesh, as a secondary processing complex. Econ Geogr 88(1):37–58
13. Hiremath AM, Tilwankar AK, Asolekar SR (2015) Significant steps in ship recycling vis-a-vis wastes generated in a cluster of yards in Alang: a case study. J Clean Prod 87:520–532
14. Mizanur Rahman SM, Mayer AL (2015) How social ties influence metal resource flows in the Bangladesh ship recycling industry. Resour Conserv Recycl 104:254–264
15. Jain KP (2017) Improving the competitiveness of green ship recycling. Delft University of Technology, Delft
16. Jain KP, Pruyn JFJ, Hopman JJ (2016) Improving ship design process to enhance ship recycling. In: Conference: 3rd International Conference on Maritime Technology and Engineering (MARTECH2016. Taylor & Francis Group, Lisbon
17. Jain KP, Pruyn JFJ, Hopman JJ (2013) Critical analysis of the Hong Kong International. World Acad Sci Eng Technol Int J Environ Ecol Geol Mining Eng 7:684–692
18. Solakivi T, Kiiski T, Kuusinen T, Ojala L (2021) The European ship recycling regulation and its market implications: ship-recycling capacity and market potential. J Clean Prod 294:126235
19. IMO (2008) Resolution A. 962(23), Guidelines on Ship Recycling. London
20. Jayaram S, Sivaprasad K, Nandakumar CG (2018) Strategic guidance plan for recycling of ships in India. Int J Adv Res Sci Eng Technol 9(4):91–101
21. Bentley Systems Incorporated (2018) User Manual MAXSURF Modeler
22. IMO (2008) Resolution MSC.267(85). Adoption of the International Code on intact stability. International Maritime Organization, London

Enhanced Performance of Propane Refrigerant at LNG Plant in Hot Climate: Case Study

Usama N. Eldemerdash, Belal M. Abdel Aziz, Naser Safa, and Taha E. Farrag

1 Introduction

The C3-MR liquefaction process has established itself as the top option for the vast majority of operating companies in the LNG Industry during the past 30 years [1]. The APCI Technology is used to create LNG in 90% of LNG plants worldwide. It's crucial to take air temperature variations into consideration while using air coolers to condense propane, as is the case at the SEGAS LNG Plant [2]. Although adding more air coolers would be the simple solution, this study is interested in investigating a cost-effective alternative by making better use of the plant's existing equipment to boost condensation duty. Using the condensing duty of the propane compressor recycle cooler to increase the condensing duty of the propane condenser is the method that is investigated in this study. The performance of the propane refrigerant in terms of compressor power consumption, heat exchanger UA values, and air cooler duty is also being examined in this study.

U. N. Eldemerdash
Chemical and Petrochemical Engineering Department, Egypt Japan University of Science and Technology, Borg Al Arab Al Gadida, Egypt

Faculty of Engineering, Benha University, Benha, Egypt

U. N. Eldemerdash
e-mail: usama.nour@ejust.edu.eg; usama.nour@bhit.bu.edu.eg

U. N. Eldemerdash · B. M. Abdel Aziz
Department of Chemical Engineering, Universiti Teknologi Petronas, Bandar Seri Iskander, Malaysia

N. Safa
Spanish Egyptian Gas Co. (SEGAS), Damietta, Egypt

T. E. Farrag (✉)
Chemical Engineering Department, Faculty of Engineering, Port Said University, Port Said, Egypt
e-mail: tahafarrag70@eng.psu.edu.eg

725
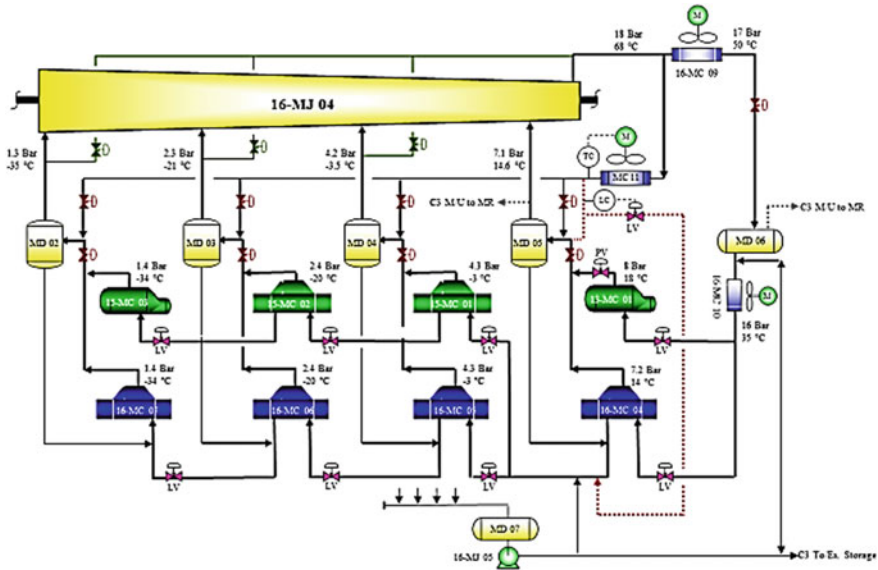
Fig. 1 Propane refrigeration process

2 SEGAS Propane Refrigerant Unit

The propane refrigeration system in SEGAS uses propane that vaporizes at four distinct pressure levels to four different compressor stages. Condensed compressed propane then provides cooling to the feed circuit and the MR circuit. For a diagram of the propane refrigeration process (see Fig. 1). In the Propane Condenser, ambient air de-super heats and condenses propane from the discharge of the Propane Compressor (16-MJ04) (16-MC09). The Propane Accumulator is where the condensed propane is collected (16-MD06). Before being fed to the evaporators, the propane liquid from 16-MD06 is sub-cooled in the Propane Sub-cooler (16-MC10). The Propane Compressor Recycle Cooler (16-MC11) has two main purposes: to cool the compressor discharge when it is operating in recycle mode and to supply feed to the compressor to prevent surge. Recycle Cooler is a different kind of air cooler [3, 4].

3 Study Background

A. *Problem Identification*

The design of the Propane Condenser 16-MC09 is based on an ambient air temperature of 24 °C. The plant is receiving natural gas in settings with greater temperatures throughout the summer when the ambient air temperature climbs to 30 °C⁺. The rate of propane vaporization in the chillers and the suction temperature of each

compressor stage both increase as a result of the rising ambient temperature. Higher temperatures cause the compressor to discharge more propane, but not all of that propane condenses since ambient air temperature also affects how quickly the air cooler cools the propane being discharged from Compressor 16-MJ04. There will be two main implications as more vapors do not condense:

1. Increases in temperature and pressure above 18.0 bars in the propane compressor discharge make condensing the propane practically difficult given the capacity of the air fan coolers.
2. Head Pressure on the propane compressor would cause the anti-surge streams to open, which would make the issue worse by recycling more propane into the compressor's outflow.

In order to redirect the cooling load to the Mixed Refrigerant, the DCS operator will need to reduce the quantity of propane going into the compressor's suction by lowering the level in the chillers (MR). The MR may only be chilled to −35 °C or greater using propane refrigerant as opposed to being cooled to −37 °C. That suggests that additional MR is needed to liquefy the natural gas (NG) [3]. Less chilled MR refrigerant directly translates to less Natural Gas being liquefied in the Main Cryogenic Heat Exchange (MCHE), which slows down plant production and prevents it from running at full capacity.

B. *Objective of the Study*
1. To construct and test the Aspen HYSYS powered propane refrigeration unit at SEGAS.
2. To determine how well the propane refrigerant performs when condensing in a hot climate while using a recycle cooler as a stage.
3. To examine the performance of the propane refrigerant in terms of compressor power consumption, heat exchanger UA and Air cooler duty by adding lighter component to the refrigerant.

C. *Two Stages Condensing Approach*

When the compressor is operating normally, the recycling cooler is employed as a safety feature to recycle the flow from the suction to the compressor's inlet after it has been partially cooled to prevent surge circumstances. The recycle cooler is often operated over empty flow to be prepared to manage any surge that might develop even though the compressor is not anticipated to go for surge during optimal performance at full load (Fig. 2).

The modification suggests that the compressor's discharge will initially be partially cooled in the propane recycle cooler 16-MC11 before being redirected to the compressor's propane condenser 16-MC09. This method enables summing up to the Air cooler's total condensing workload. We'll be looking at whether or not this sum is adequate given the hot weather circumstances.

D. *Modifying the Refrigerant Composition*

Methane or ethane is typically employed at cryogenic temperatures, while propane is typically used at chiller temperatures above −40 °C [5]. Due to its accessibility,
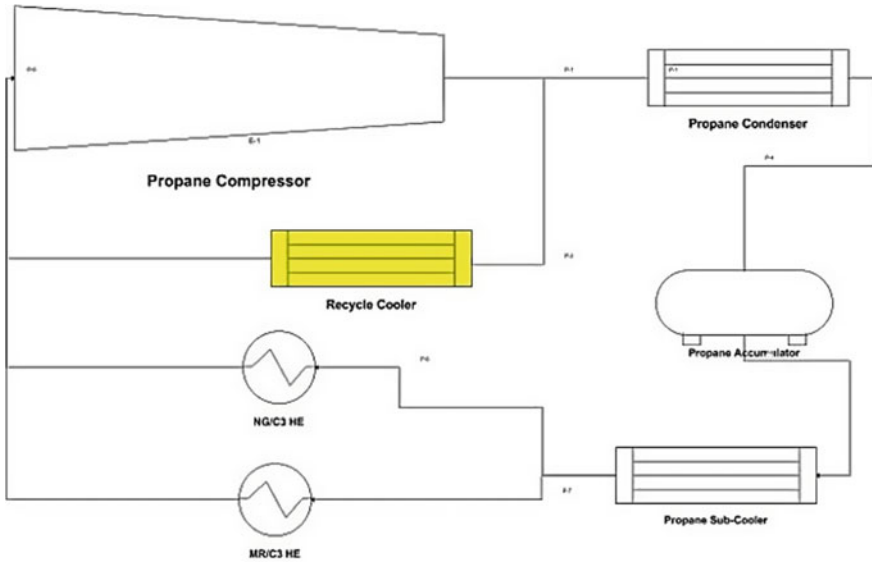
Fig. 2 A simplified schematic of the propane refrigerant process

low cost, and favorable vapor pressure curve, propane is a preferred choice in gas processing applications [6–8]. Our second method for evaluating the performance of the propane refrigerant involves evaluating how the propane performs when small amounts of lighter components are added to the propane refrigerant composition. We shall evaluate the performance in relation to: compressor power consumption, heat exchangers UA and air coolers duty (Fig. 3).

4 Results and Discussion

A. *Validating the Simulation Model*

Aspen HYSYS was used to simulate the propane unit, and real data was used to validate the results. The following factors were considered since the simulation was run as a steady state case:

1. A mixer was placed before each step of a four-stage propane compressor simulation to combine the flow from the chillers with the flow from the preceding stage.
2. To replicate a kettle-shaped heat exchange, a typical heat exchanger was used, followed by a separator to prevent liquid leakage into the compressor.
3. Discharge of each Heat Exchanger in each stage is sent to a separator where the vapor stream is sent to the Compressor suction and the liquid stream is sent to the next chiller stage.
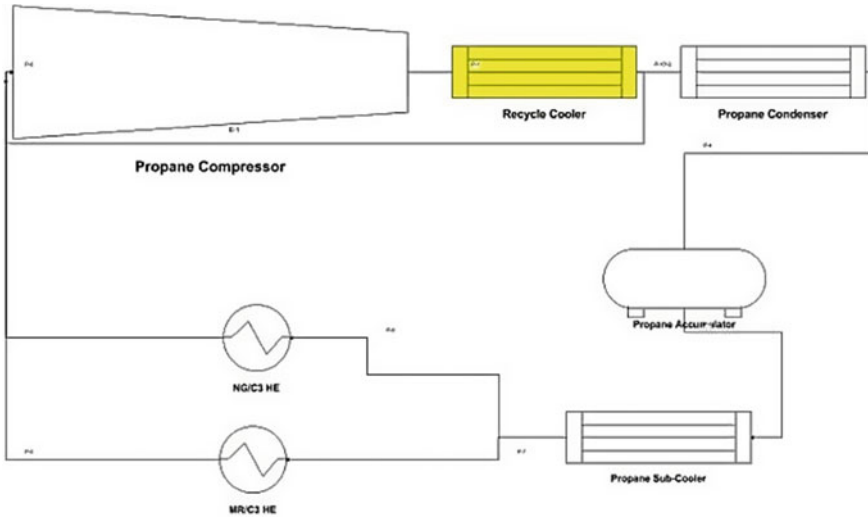
Fig. 3 A simplified schematic of the two stages condensing approach

By increasing the outlet design temperature of the propane condenser by 10 °C, we were able to mimic the hot climate situation in the steady state in HYSYS. Given that the PFD is set to 25 °C, a 10 °C increase in the outflow temperature will enable simulation of a hot climate up to 35 °C.

B. *Two Stages Condensing Approach*

When a hot climate is present and the recycle cooler is not being used as a stage in the propane condensing process, the system will not be able to maintain a Propane vapour fraction of zero, as indicated in Fig. 4. This will prevent a full propane condensation from occurring.
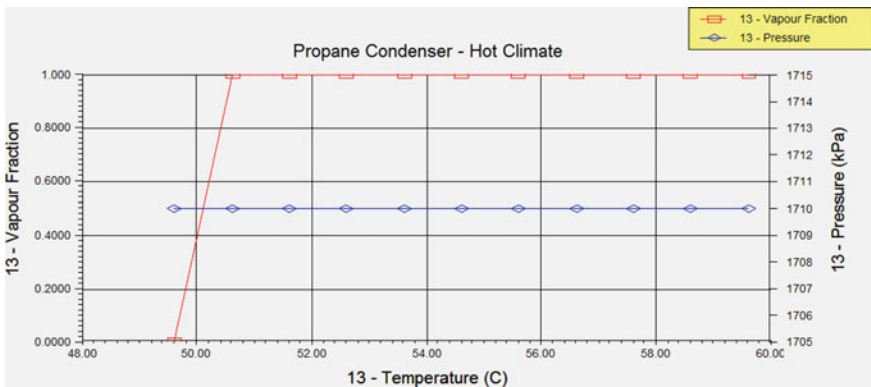
Fig. 4 Propane vapor fraction at normal operation

However, as shown in Fig. 5, adding up the cooling duty of the recycling cooler enables maintaining the propane vapour percentage at (0) zero during the hot climate range of 25–35 °C. The safety of the compressor is a problem because the results indicate that it is successful to maintain the propane totally condensed over a hot climate condition. Since the Recycle cooler's primary function is to recycle the flow to the compressor's inlet, it is crucial that there be no liquid at the exit of the Recycle cooler that could harm the compressor. To check if there is liquid at the output, the recycling cooler's outlet flow data from HYSYS was obtained. The vapour fraction is kept at one, as shown in Fig. 6. Based on this, the Two Stages Condensing technique succeeds in sustaining a full condensation of the propane over hot temperature conditions from a process perspective.

C. *Propane Operating Line*

We can determine where to operate to keep the propane in a liquid form by drawing the phase envelop for propane. Figure 7 compares the performance of propane in a
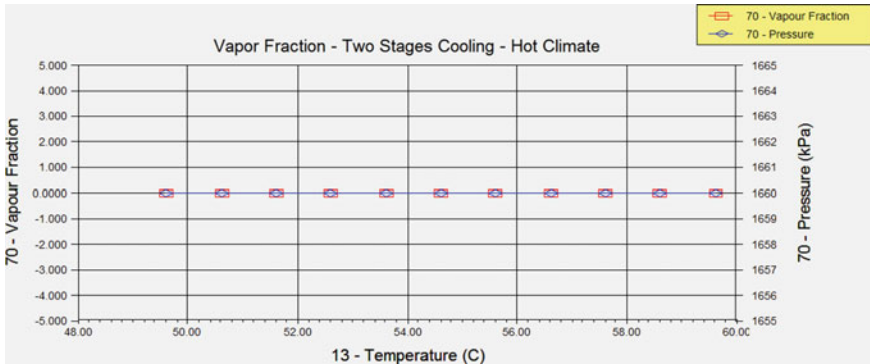
Fig. 5 Propane vapor fraction when using the two stages condensing approach
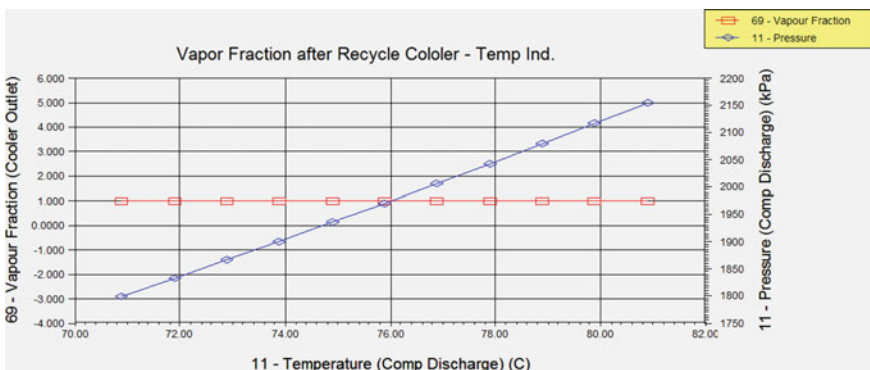
Fig. 6 Vapor fraction after recycle cooler

Fig. 7 The performance of propane in a hot region
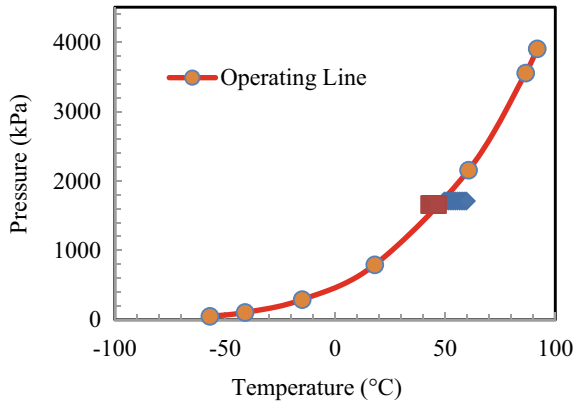
hot region with and without a two-stage condensing system. We can see from the image that the two-stage condensation system was able to completely condense the propane and move the line to a liquid condition.

D. *Modifying the Propane Refrigerant Composition*

We examined five alternative refrigerant formulations in our investigation, always keeping the propane level over 95% mole. Table 1 lists the various compositions that are being considered.

The five compositions were tested in Aspen HYSYS so that the data of air cooler duty, heat exchanger UA and Compressor Power consumption can be analyzed. Figures 8, 9, 10, 11 and 12 show the comparison of the data obtained for the different compositions configuration. Because lighter components demand a higher heat of condensation, adding them to the refrigerant enhanced the Air Cooler's condensation duty (Fig. 7). However, due to a decreased Specific Heat Capacity (Cp), the Air Sub-duty cooler's was decreasing as the proportion of lighter components increased (Fig. 8).

When methane was added to the refrigerant, SEGAS LNG Plant's total air cooler duty decreased to meet the required condition (Fig. 9). As the composition changes, a new mass flow of refrigerant is necessary, which explains the change.

Table 1 Refrigerant composition

Case composition	Propane (mol%)	Ethane (mol%)	Methane (mol%)
Case 1	100	0.0	0.0
Case 2	98.2	1.8	0.0
Case 3	97.0	3.0	0.0
Case 4	98.2	1.2	0.6
Case 5	98.2	0.6	1.2

Fig. 8 Air cooler duty across condenser
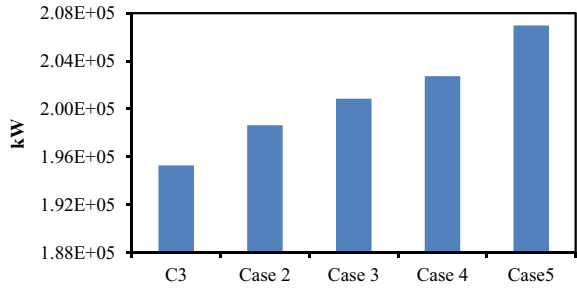
Fig. 9 Air cooler duty across sub-cooler
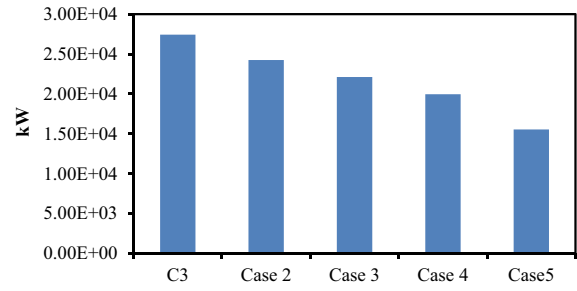
Fig. 10 Total air cooler duty
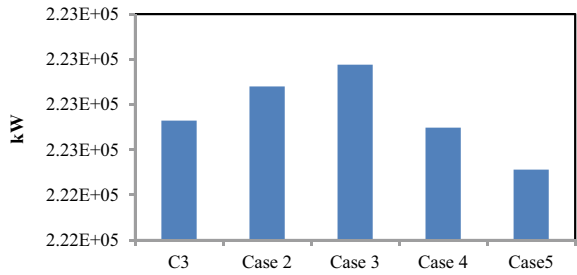
Fig. 11 Total heat exchangers UA
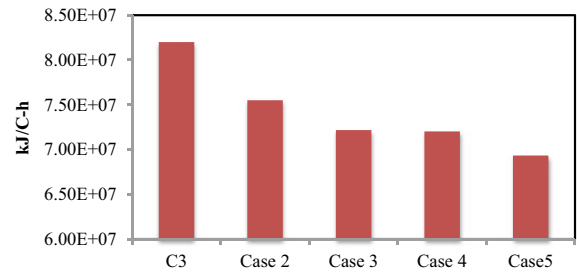
Fig. 12 Compressor power consumption
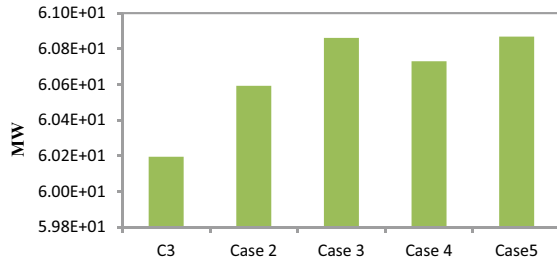
1. In compared to other refrigerant compositions, pure propane refrigerant demonstrated higher heat flow or UA values through the heat exchangers. The total heat flow decreased as the percentage of lighter components increased (Fig. 10).
2. Compared to the other compositions, pure propane composition consumed the least power when it came to the compressor (Fig. 11).

5 Conclusion

In our first approach of testing the TWO CONDENSING SYSTEM approach by utilizing the recycle cooler as a stage in condensing two important results, first the ability to achieve full propane condensation in hot climates (25–35 °C). Second, no liquid propane was discovered at the recycle cooler's exit under any tested pressure or temperature conditions. This makes the procedure safe for the compressor compartment in the event of a potential liquid escape from the compressor. In the second approach of modifying the propane composition, in terms of Air Cooler Duty, Pure propane showed the least Air cooler duty across the Propane condenser. However adding the Sub Cooling Duty, it favors lighter components. In terms of Heat Exchanger UA values, Pure Propane Showed and increased UA values in comparison with compositions that contains percentage of Methane refrigerant. In terms of Compressor Power consumption, Pure Propane was the least in terms of power consumption in comparison of other refrigerant compositions.

6 Recommendations

This study has examined certain approaches in improving the performance of the propane refrigerant during hot climate conditions and normal conditions. However further studies are to be considered for future work including the optimum refrigerant configuration taking into account economic analysis of Plant equipment's and operating cost, control System. However, Piping and installation study should be investigated and further study on the (CCC) surge protection system of the propane compressor.

References

1. Majzoub M (2012) Evaluation and selection of the precooling stage for LNG processes. Master's thesis, Institutt for energi-og prosessteknikk
2. Gas Processors Suppliers Association, Engineering Data Book (1998) Chapter 10: Air-cooled Exchangers. Eleventh Edition. Tulsa, Oklahoma 74145
3. Fathalla BM, Teknologi U, Bandar P, Iskandar S, Perak T, Ridzuan D (2013) Enhancing propane refrigerant performance at pre-cooling stage during hot climate conditions at LNG Plants-case study from Egypt
4. Campbell JM, Hubbard RA, Lilly LL (2000) Gas conditioning and processing. Vol. 2. Norman, Okla: Campbell Petroleum Series
5. Almeida-Trasvina F, Smith R (2023) Design and optimisation of novel cascade mixed refrigerant cycles for LNG production—Part I: Benchmark cascade cycles. Chem Eng Res Des 190:619–633. https://doi.org/10.1016/j.cherd.2022.12.046
6. He T, Lin W (2020) A novel propane pre-cooled mixed refrigerant process for coproduction of LNG and high purity ethane. Energy. https://doi.org/10.1016/j.energy.2020.117784
7. Qyyum MA, Ahmed F, Nawaz A, He T, Lee M (2021) Teaching-learning self-study approach for optimal retrofitting of dual mixed refrigerant LNG process: energy and exergy perspective. Appl Energy. https://doi.org/10.1016/j.apenergy.2021.117187
8. Qyyum MA, He T, Qadeer K, Mao N, Lee S, Lee M (2020) Dual-effect single-mixed refrigeration cycle: an innovative alternative process for energy-efficient and cost-effective natural gas liquefaction. Appl Energy. https://doi.org/10.1016/j.apenergy.2020.115022

Condition Monitoring as a Pathway for Sustainable Operation: A Case Study for Vibration Analysis on Centrifugal Pumps

Mahmoud Mostafa, Mohamed Elsakka, Mohamed S. Soliman, and Mohamed El-Ghandour

1 Introduction

Centrifugal pumps have many applications in our modern life. They are employed for home water supplies and as a booster. Slurries and sewage can be pumped using centrifugal pumps because of their unique design. These pumps are also employed in cooling and heating systems and fire protection systems. They are employed in the beverage sector to move bottled water, juice, and other drinks. Centrifugal pumps are used in the dairy sector to move dairy products including buttermilk, milk, and flavored milk. They are used for refrigerants and cryogenics in many industries, including manufacturing, industrial, chemicals, food processing, pharmaceutical, and aerospace.

They pump crude oil, mud, and slurry utilized by power plants in the oil energy sector. They are employed in the pharmaceutical and cosmetics industries to transfer lactose, glucose, as well as several other medications and medium-viscosity personal

M. Mostafa (✉)
Belayim Petroleum Company, Cairo, Egypt
e-mail: mahmoud.mst93@gmail.com

M. Mostafa · M. Elsakka · M. S. Soliman · M. El-Ghandour
Department of Mechanical Engineering, Faculty of Engineering, Port Said University, Port Said, Egypt
e-mail: Elsakka@eng.psu.edu.eg

M. S. Soliman
e-mail: eng_salo_0100@eng.psu.edu.eg

M. El-Ghandour
e-mail: mghandour@eng.psu.edu.eg

M. Elsakka
Energy Research and Studies Unit, Faculty of Engineering, Port Said University, Port Said, Egypt

care products. The global centrifugal pump market size was valued at 36.6 million dollars in 2021 and is expected to reach 48.8 billion dollars by 2026 [1].

Centrifugal pump has many advantages over other pumps, especially since it has less friction. Furthermore, if the magnetic coupling breaks, the pump won't be damaged or overloaded. The pumps enable manufacturers and processors to move a variety of fluids, including ones that might quickly corrode traditional pumps. When used appropriately, pumps can have a long service life. The pumps can withstand caustic substances. Compared to all other pumping technologies, centrifugal chemical pumps are among the most energy-efficient machines. Their effectiveness lowers costs during each unit's lifetime as well as in the immediate future. While some other pumps can provide a pulsating flow, centrifugal chemical pumps do not. Centrifugal chemical pumps come in a wide range of sizes.

Centrifugal Pumps suffer from cavitation that occurs when the system's net positive suction head NPSH for the chosen pump is too low. It can lead to high noise and vibration levels and reduced efficiency. Eventually, cavitation can limit the pump's operating range as well as the pump's lifetime.

Many researchers were interested in cavitation phenomena and its effect on centrifugal pumps, the following sections provide a summary of previous research relevant to this study and concerned with cavitation in centrifugal pumps and condition monitoring rules in the detection of pump mechanical faults like bearings faults and cavitation. Condition Monitoring is defined as the measurement and analysis of several equipment parameters, which are used to determine the current health of the equipment and thus the correct timing and extent of equipment maintenance.

There are many ways used by researchers to detect and study cavitation phenomena, of them is using audible sound. The noise generated by a centrifugal pump depends on its form and size on pump operating conditions. Other factors that can promote noise and pump instability are surge and stall. Stall and surge can occur when the pump operates below the design flow, however cavitation can occur within the entire operating regime. Cavitation can occur without stall and surge, and vice versa [2].

Experimental and theoretical studies held by Sánchez et al. [3], in 2018, investigated the cavitation phenomenon using vibration signals connected to a centrifugal pump at a speed of 3450 rpm in axial, horizontal, and radial directions and received by acceleration sensors using standard ISO 10816 of vibration severity. The results showed that the cavitation-induced collapse of bubbles produces a high-velocity micro-jet that erodes nearby surfaces like the impeller; all the measures taken were in accordance with the recommendations of the frequency of blade pitch (BPF), They discovered that, in addition to making loud noises and creating bubbles inside the storage tank, cavitation produces a change in vibrations by increasing vibration amplitude, reducing pumping capacity from 77.9 to 46.6 GPM, and changing pumping head from 6.4 to 2.9 m. Al-Obaidi [4], in 2019, used centrifugal pumps with a range of flow rates and vibration analysis to predict and study cavitation in centrifugal pumps. He recorded the trend of the peak, Root Mean Square (RMS), and minimum value for the head under flow rates ranging from 103 to 378 (L/min) with a pump rotational speed of 2755 rpm. Also, he discovered that cavitation occurs in

the broadband frequency region between 1 and 2 kHz. While the pump is running at less than 350 (L/min), there is no discernible change. The maximum RMS value was 0.088 m/s^2 at about 152 (L/min). Although, though the RMS value rises after 350 L/min to 0.113 m/s^2 at 365 L/min, the head also falls with flow rate due to mechanical and hydraulic losses and various stages of cavitation inside the pump, increasing the RMS percentage by 21.45%. He discovered that cavitation begins to happen when the flow rate is greater than 30 L/min, that cavitation does not occur at low flow rates because the pump head is higher than NPSH, that the amount of cavitation in centrifugal pumps is directly proportional to pump rotational speed and pump flow rate, and that cavitation most frequently begins near the leading edges of the blades or at the impeller eye. He also discovered that using low-frequency ranges between 1 and 2 kHz was more economic. Abdulaziz and Kotb [5] used a mixed flow and axial centrifugal pump with six vanes impellers in their test rig, in 2017, and they discovered that the pump choked during cavitation at a fixed speed of 2850 rpm and pressure variations between 10 and 78 kPa with a frequency range of 0–15 kHz. In addition, the highest overall vibration level at 2205 L/h is 2.19 g, followed by a sharp decrease at 2270 L/h to 0.84 g, then continue decreasing to 2.16 g at 2410 L/h. Cavitation starts at a flow rate of 508 L/h with an overall vibration level of 1.95 g. The vibration level decreases to a minimum of 1.4 g at 1672 L/h, but then increases to 1.66 g at a discharge flow rate of 1970 L/h. They also discovered that the sudden fluctuation of vibration can be used as a cavitation detector thus eliminating the need to follow harmonics of blade passing frequency. In 2012, Stopa et al. [6] used Load Torque Signature Analysis (LTSA) technique, using electrical signals of the motor to calculate the torque done by the pump and through its frequency spectrum determine the occurrence of cavitation and its intensity using load torque estimator and a Fast Fourier Transformation (FFT) and Spectrum Analyzer. Based on the principle that most load faults cause torque vibrations and/or oscillations transmitted directly to the driving motor through the shaft.

Using computational results, it was found that the LTSA tool showed a response pattern very close to those done by pressure and vibration sensors typically used to detect this application and the peaks of the vibration and torque were between 410 and 420 Hz.

In 2019, Yang et al. [7] used a three-axis accelerometer with a frequency range of 0 to 1000 Hz to measure the vibration characteristics of the mixed flow pump as part of an experimental setup that followed the ISO 5198 standard.

$$\text{Net positive suction head, } NPSH = \frac{P_{inlet} - P_{vapour}}{\rho g} \tag{1}$$

$$\text{Cavitation number, } \sigma = \frac{2gNPSH}{u_1^2} \tag{2}$$

where P_{inlet} is the total pressure at the pump inlet (Pa), P_{vapour} the saturation pressure of the liquid (Pa), ρ the density (kg/m^3), u_1 the tangential speed at the blade inlet (m/s) and g the acceleration gravity (m^2/s).

Experimental testing and computational fluid dynamics (CFD) simulation produced values of 0.95 and 0.73, respectively, for a 3% head drop. The entire head fell and there was a significant change in the magnitude of the pressure fluctuation and the vibration when the value was between 0.9 and 1.3; these phenomena are known to cause cavitation bubbles.

Li et al. [8], in 2018, used an improved algorithm-unified algorithm based on the Wigner-Ville distribution (WVD), the short time Fourier transform (STFT), then using vibration data obtained from the centrifugal pump, the STFT-WVD approach is evaluated. Using a single-stage, single-entry centrifugal pump with a head of 32 m, speed of 2900 rpm, and volume flow rate $= 60$ m^3/s. Several cavitation stages, from the free state to cavitation breakdown, were seen when the NPSHa dropped from 11.34 to 2.85 m. The results demonstrated a clear relationship between the development of cavitation and the intensification of vibration increase with a decrease in NPSHa, and they showed that the STFT algorithm cannot be used to detect the onset of cavitation; rather, it can only be used to confirm the presence of cavitation. In 2014, Zhang et al. [9] used a centrifugal pump with a sloped volute tongue in a closed loop connected to an accelerometer with a speed of 1450 rpm and a response range of 0.5 Hz to 5 kHz. With respect to the vertical axis, the diffusion section of the slope volute bears an acute angle of roughly 15°. Flow rate $Q = 48$ m^3/h, designed head 7.5 m, impeller inlet diameter 100 mm, impeller outlet diameter 172 mm, impeller outlet width 17 mm, and blade number 6. They discovered that vibration energy rose by 3 dB with a flow rate from 0.3 of the flow rate to a shutdown state. It is also determined that vibration signals can be utilized to monitor fully developed cavitation instead of the 3% head drop methods as the overall vibration level grows by roughly 1.83 dB and reaches a critical point at the intended mass flow rate. Tong et al. [10], in 2022, to prevent cavitation damage in water centrifugal pumps and detect it in an early-stage using vibration signal-based neural network with high-speed photography was used.

According to the previous research, researchers used different vibration analysis methods to detect cavitation inside pumps also searching for the root causes and trying to find control measures to reduce the effect of this phenomenon. In this case study, the effect of cavitation on an industrial feed water centrifugal pump is investigated using the vibration analyzer CSI 2140. Also, the root cause analysis of this phenomenon and how to avoid its occurrence again is explained to increase the health time of the rotating equipment (the pump).

Fig. 1 Pump model A2P BB2

2 Case Study on Cavitation Effect on Pump

The pump under investigation is a typical boiler feed water pump, model: A2P BB2, used in a certain industrial facility in Egypt, as shown in Fig. 1. The pump suffered from high noise and vibration, so it has been recommended to check the operating parameters for pump and ensure that it's working at best efficiency point (BEP) to eliminate cavitation problem. It was doing well from a process point of view during its early commissioning period, but over time after two years with the pump in service, it has low efficiency and there is a lack of performance. The decision was to dismantle the pump, inspect it internally and replace it with a new one.

3 Pump Information

Pump performance curve: this is the performance curve of the pump working in normal condition before cavitation (Fig. 2; Table 1).
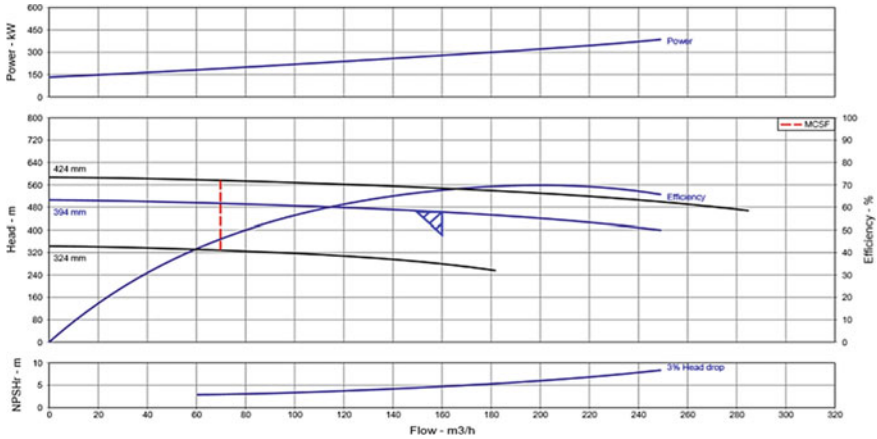
Fig. 2 Boiler feed pump performance curve [11]

Table 1 Pump data: this table for operating conditions of the pump, model and material

Model	A2P BB2
Service	Boiler feed water pump
Pump temp.	130 °C
Suction pressure	2.6 bar
Discharge press at rated capacity	45 bar
NPSH	10.3 m
Rated capacity	160 m^3/h
Power	279 kw
RPM	2980
No of impeller stage	Two
Impeller type	Closed
No of impeller blades	Four
Casing material	A216 WCB

In this investigation, the utilized vibration analyzer is Emerson's CSI 2140, as shown in Fig. 3. It's a four-channel machinery health analyzer with hazardous environment certification (SAFETY RATED CLASS I, DIV 2, GP A-D; T4 AND CLASS II, DIV 2, GROUPS F, G; T105 C).

Fig. 3 Vibration analyzer CSI 2140

4 Problem Description

While the pump was in service and based on condition monitoring vibration assessments, it was noticed a high noise (flow disturbance) and vibration as shown in Fig. 4.

After analyzing the vibration pattern (spectrum and time waveform TWF), the spectrum shows a peak at blade pass frequency (the number of impeller blades × RPM) with the harmonics shown in Fig. 4 (as green text). Furthermore, there is high noise floor on the spectrum and a random impact on the TWF pattern which indicates a
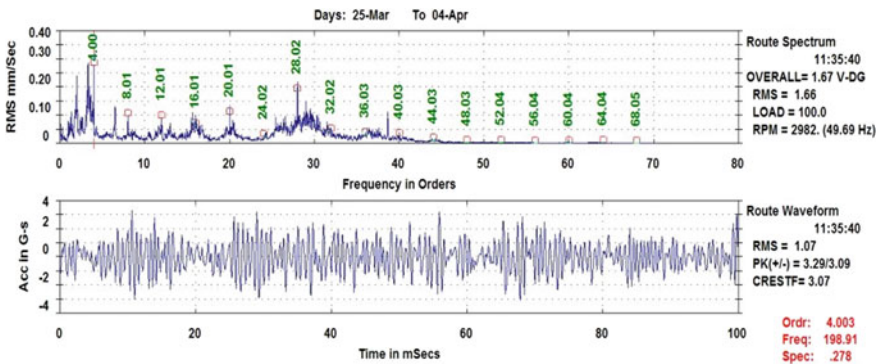
Fig. 4 Spectrum and time waveform for the pump

flow disturbance or cavitation problem. Therefore, a decision has been taken to check operating conditions to ensure the pump is working at its best efficiency point (BEP).

The pump performance deteriorated over time as the cavitation occurred and this affected the impeller and its casing. This is due to the fact that cavitation is a process in which a flowing liquid generates bubbles and then ruptures. If cavitation bubbles bursting does not occur at the flowing liquid but occur at the wall of the flow guiding assembly, the cavitation can cause the wall material to be etched, which highly contributes to deteriorating the performance of the pump.

5 Anomalies and Findings

Internal visual inspection has been performed for the casing of the pump after dismantling and found the following damages:

1. An eroded damaged wall casing between the two stages increased in the 2nd stage impeller as shown in Fig. 5.
2. Three plugs observed in the pump casing, between the two stages, are seen in Fig. 6.
3. A hole is found in the pump wall casing between the two stages as shown in Fig. 6.
4. A loose and wear of the casing wear ring of 1st impeller are shown in Fig. 7.
5. Thermal stress was observed in the pump casing and a hot spot on the bearing housing is detected as can be seen in Fig. 8.
6. A bend in the internal blades of the impeller can be shown in Fig. 9.

Fig. 5 An eroded wall between stages

Fig. 6 Three plugs in the wall between stages

Fig. 7 A loose and wear of the casing wear ring of 1st impeller

6 Discussions and Correcting Measures

The three plugs observed and the hole in the pump casing between the two stages may lead to minimizing the discharge pressure and efficiency of the pump. The hole in the casing, as well as the material deficient, are recommended to be filled with welding. Moreover, a magnetic test or dye penetrant test (MT or PT) shall be performed after the flush grinding of the surface prior to the welding built-up and after finishing the

Fig. 8 A thermal stress and hot spot on bearing housing

Fig. 9 A bend on the internal blades of the impeller

weld built-up to make sure there are no any cracks. In addition, the vendor should be contacted to give clarification regarding this material loss.

Also, during the stand-by pump startup, water vaporization is noticed. As the pump encloses water at ambient temperature, cavitation occurs and causes pitting and erosion on the pump casing. By referring to the operation and installation manual

of the pump. Warming up of the stand-by pump shall be ensured by continuously bleeding a small flow from the discharge side of the pump in operation, before starting a pump in cold conditions. And the pump shall be flushed by a small rate of flow to increase the casing temperature at a maximum rate of 3 °C/min. According to the manufacturing manual, the pump is considered ready to start-up if following conditions are fulfilled: (I) The difference between the temperature of the fluid to be pumped and the average temperature of the pump casing is lower than 100 °C. (II) The difference between the temperatures measured on the top and the bottom of the casing is lower than 20 °C.

7 Conclusion

Centrifugal pumps are very important in various aspects of household and industrial applications. These pumps may face cavitation issues that adversely affect their performance and can even lead to damage to their components. Condition monitoring, particularly through vibration analysis, could be employed in order to identify cavitation in pumps. This would enable the pump operator to take action and eliminate the cause of the cavitation before the pump becomes unusable. This would lead to an increase in the lifespan of the pump, a reduction in the need for new pump manufacturing, and a reduction in pollution during the production process. In this paper, a case study is considered where condition monitoring is employed on a particular centrifugal pump in an industrial facility that is experiencing cavitation. The vibration analyzer CSI 2140 is utilized, and a root cause analysis is performed. The utilization of condition monitoring, especially vibration analysis, assists in detecting cavitation in centrifugal pumps at early stages. Hence, by performing periodic vibration tests on pumps, it is expected to avoid losing more pumps due to cavitation and eliminate the high cost of maintenance.

8 Recommendation

1. A justification from the vendor about the metal erosion found in the three holes.
2. In case of repair hole in the wall between two stages by welding a magnetic test or dye penetrant test (MT or PT), the test shall be performed after the flush grinding of the surface prior to the welding built up and after finishing the weld built up to make sure there are not any cracks.
3. Machining pump non-drive end and drive-end bearing housings.
4. Checking the defective parts of the impeller and replacing them if needed.
5. After the repair and starting putting the pump in the service, warming up shall be ensured by continuously bleeding a small flow from the discharge side of the pump in operation. Before starting a pump from cold conditions, the pump shall be flushed with a small rate of flow in order to increase the casing temperature

at a maximum rate of 3 °C/min according to the operating installation manual of the pump.

References

1. Centrifugal pump market growth drivers and opportunities. MarketsandMarkets. [Online]. Available: www.marketsandmarkets.com/Market-Reports/centrifugal-pump-market-174 94785.html
2. Čdina M (2003) Detection of cavitation phenomenon in a centrifugal pump using audible sound. Mech Syst Signal Process 17(6):1335–1347
3. Sánchez W, Carvajal C, Poalacin J, Salazar E (2018, Apr) Detection of cavitation in centrifugal pump for vibration analysis. In: 2018 4th International conference on control, automation and robotics (ICCAR). IEEE, pp 460–464
4. Al-Obaidi AR (2019) Investigation of effect of pump rotational speed on performance and detection of cavitation within a centrifugal pump using vibration analysis. Heliyon 5(6):e01910
5. Abdulaziz AM, Kotb A (2017) Detection of pump cavitation by vibration signature. Aust J Mech Eng 15(2):103–110
6. Stopa MM, Cardoso Filho BJ, Martinez CB (2012, Oct) Detection of incipient cavitation phenomenon in a centrifugal pump. In: 2012 IEEE industry applications society annual meeting. IEEE, pp 1–6
7. Yang HM, Lee KY, Kim JH, Choi YS (2018) Analysis of performance variation with cavitation test for a mixed-flow pump. In: IOP Conference series: earth and environmental science, vol 163, no 1. IOP Publishing, p 012031
8. Li Y, Feng G, Li X, Si Q, Zhu Z (2018) An experimental study on the cavitation vibration characteristics of a centrifugal pump at normal flow rate. J Mech Sci Technol 32:4711–4720
9. Zhang N, Yang M, Gao B, Li Z (2015) Vibration characteristics induced by cavitation in a centrifugal pump with slope volute. Shock Vib
10. Tong, Z., Liu, H., Cao, X. E., Westerdahld, D., & Jin, X. (2023). Cavitation diagnosis for water distribution pumps: An early-stage approach combing vibration signal-based neural network with high-speed photography. Sustainable Energy Technologies and Assessments, 55, 102919.
11. A2P & A2PD BB2 type centrifugal pump from trillium flow technologies. https://www.trilli umflow.com/product/a2p-a2pd-bb2-type-api-610-centrifugal-pump/. Accessed 15 Mar 2023
12. Cucit V, Burlon F, Fenu G, Furlanetto R, Pellegrino FA, Simonato M (2018) A control system for preventing cavitation of centrifugal pumps. Energy Procedia 148:242–249

Maximization of Condensate Production in Gas-Oil Separation Plant in Gulf of Suez: Case Study

Mamdouh A. Gadalla, Ahmed A. Elsheemy, Hany A. Elazab, Thokozani Majozi, and Fatma H. Ashour

1   Introduction

Global energy consumption is expected to increase by about 56% over the next thirty years [1–4], which is a direct result of the huge population growth and the significant prosperity worldwide, particularly in the most advanced countries. Currently, fossil fuels (oil, gas and coal) represent around 80% of the total energy source, despite the fact that it will be depleted soon and hence, there are huge efforts to use renewable resources as an alternative in our energy systems [5–8].

It is expected that natural gas will become the most predominant fossil fuel in the coming decades according to The International Energy Agency [3, 9–14].

Crude oil could be light or heavy. This is dependent on the properties of crude oil vaporization when it is heated, or chemical agents added to it. It is light in case it is volatile and heavy oil if viscous. Most of the crude oil produced in the world is in the form of emulsion. The hydrocarbon fluids usually exist in a reservoir under

M. A. Gadalla (✉)
Department of Chemical Engineering, Faculty of Engineering, Port Said University, Port Said, Egypt
e-mail: m.gadalla@eng.psu.edu.eg

A. A. Elsheemy
AMAL Petroleum Company (AMAPETCO, an Egyptian General Petroleum Corporation Joint-Venture Company), Cairo, Egypt

H. A. Elazab
Chemical and Biochemical Engineering Department, Missouri University of Science and Technology, Rolla 65409, MO, USA

M. A. Gadalla · T. Majozi
Faculty of Engineering and the Built Environment, University of the Witwatersrand, Johannesburg, South Africa

F. H. Ashour
Department of Chemical Engineering, Faculty of Engineering, Cairo University, Giza, Egypt

high pressure and in a liquid or gaseous form. Hydrocarbon fluids usually co-exist with salty water in the reservoir and the way we produce and treat this fluid on surface depends on the fluid properties including pressure, temperature, density, type and quality of fluid, content of undesired components as hydrogen sulfide, carbon dioxide, and quantity of associated free water in the crude [15–18].

The composition of the hydrocarbon fluids that can be found in the reservoir ranges from nearly pure methane to heavy crude such as asphalt. Therefore, the main job of gas-oil production facilities is to separate the well stream into three components oil, gas and water [19–22].

The separation process often consists of two or three stages of decreasing pressure stages, especially in case of production from high-pressure wells. Staged separation is preferable for the numeral reasons, including the high efficiency separation [23–25].

This research is oriented towards the sustainable development goals (SDGs) related to health and well-being, affordable and clean energy, and the climate action. Specifically the SDG #12 is achieved in this research as production of valuable materials is maximized, i.e. natural gas and condensate, on one side. On the other side, energy (natural resources) is efficiently consumed through the optimization. The main objective of this study is to simulate a Gas-Oil Separation plant (GOSP) using Aspen-Tech HYSYS with an inlet crude composition (produced naturally from Kareem and Rudies reservoir formations located in Gulf of Suez) to obtain stabilized crude with maximum Reid Vapor Pressure (RVP) 12 psia for storage/export and maximize condensate production by proposing different revamping schemes for the existing GOSP referred to as base case. Therefore, to achieve the main aim, the following objectives needs to be achieved:

1. Process simulation (HYSYS) of GOSP using the actual plant data as the case study.
2. Validate the HYSYS simulation data with actual plant data.
3. Propose the different revamping schemes to maximize the condensate production.
4. Preliminary economic evaluation of the proposed schemes.
5. Recommend the best scheme technically and economically.

The diagram in Fig. 1 shows the general flow of this research study.

In order to simulate a practical plant and revamping schemes that can be implemented in the real word, the following rules of thumb for process design have been adapted. Compressors design aspects includes their materials of construction, seals, and lubricants, and it is recommended about 300 °F (150 °C) as a "good average" for outlet temperatures [18, 26–28].

The type of compressor is determined whether centrifuge or reciprocating based on the inlet flow rate and the compressor discharge pressure [29–35].

Figure 2 shows the general process simulation procedure that will be implemented in this research study.

The separated liquids flow to the inlet separator D-2010 under the action of level control, the free water separated in D-2010 will be directed to the corrugated plate separator D-9040. While the water–oil emulsion is directed to the inter-stage exchanger E-2410 where the emulsion is preheated against the hot treated oil from
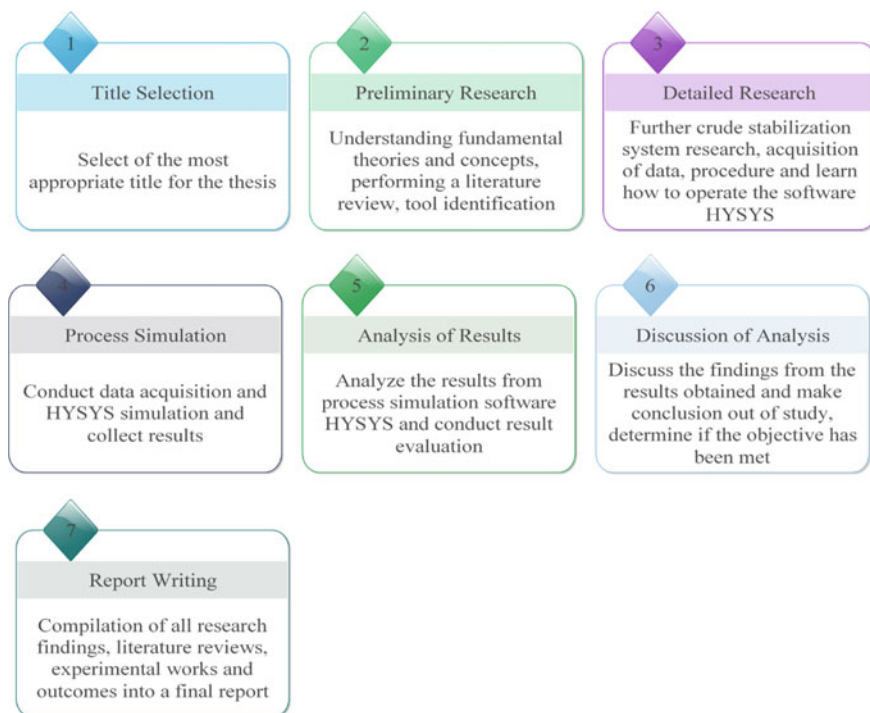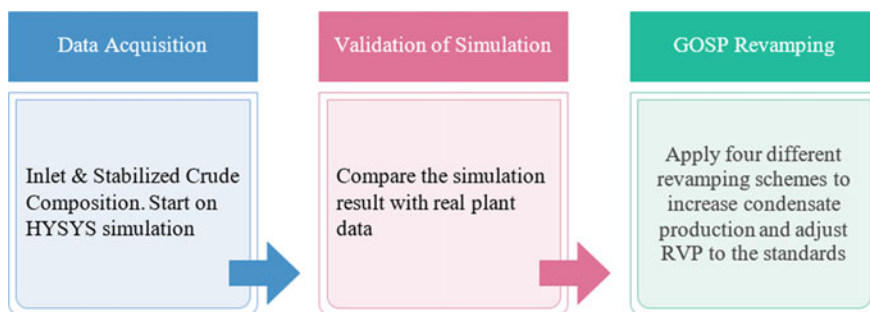
Fig. 1 Methodology flow diagram

Fig. 2 Flow chart of simulation, data validation and revamping steps

the second stage De-Salter D-2430 before entering the Inter-stage heater H-2060. In the modelling of the condensate stabilization unit, the main equipment that governs the process is the stabilization column. The GOSP is steady state simulated by Aspen HYSYS (v. 8.6) software. The feed used for the simulation is based on GOSP inlet crude composition. The crude composition is obtained from the recently recombined sample from the high pressure inlet separator. This feed is based on a GOR of

12143 SCF/BO & Water content (W.C.) of 30% as indicated by the company [36–38] (Fig. 3).

The simulation model of the GOSP is validated by comparing between Actual plant data and the HYSYS model data as shown in Fig. 4. This data includes the Gas and products' composition, flow rates, and their physical properties as molecular weight, mass density, viscosity, and low heating value for gas.

After the matching between the real and simulated data, four revamping schemes are applied on the validated simulation model.

The results of the revamping schemes are gathered such as the increase in condensate recovery, composition of the recovered condensate and gas, flow rates, and their physical properties.

All the revamping schemes are applied after the glycol contactor X-2530 for two reasons; the first reason is to ensure the inlet gas is dehydrated and avoid hydrate formation. And the second reason is that the maximum design pressure of the contactor is 21 bar(g) "gauge pressure" which means that it is not allowed to apply high compression stage before the contactor. Also, hydrate formation is checked for every stream while revamping the gas processing train to avoid hydrate formations at the applied very low temperatures and it is found ok.

2   Process Simulation

The self-refrigeration scheme illustrated in the literature review section is applied after the glycol contactor unit (X-2530) excluding the glycol separator unit as there is no need for it in the presence of the glycol contactor (X-2530).

To apply the self-refrigeration scheme, it is recommended that the inlet gas pressure should be high therefore, a compression stage is applied before conducting the aforementioned scheme. A stabilizer unit is added at the end of the scheme to adjust the RVP to 12 psia.

Similarly, revamp two constructed using the same above-mentioned design considerations except that two stage compression is introduced in this scheme instead of one.

The external refrigeration scheme demonstrated in the literature review section is applied after the glycol contactor unit (X-2530). No compression stages are required in this scheme as refrigeration depends on the transfer of the latent heat of propane from to the processed gas in the chiller at a nearly constant pressure.
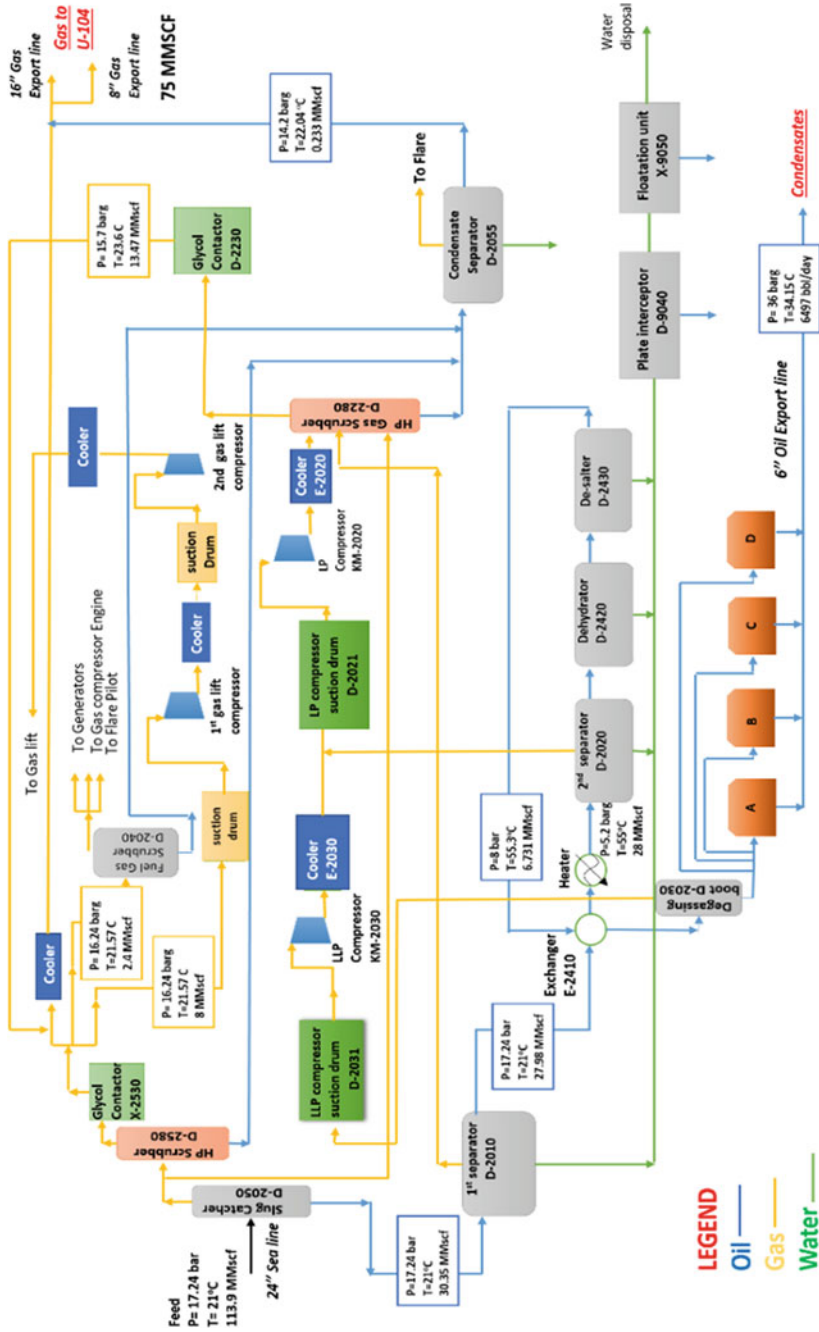
Fig. 3 Process-flow diagram of the GOSP before modification
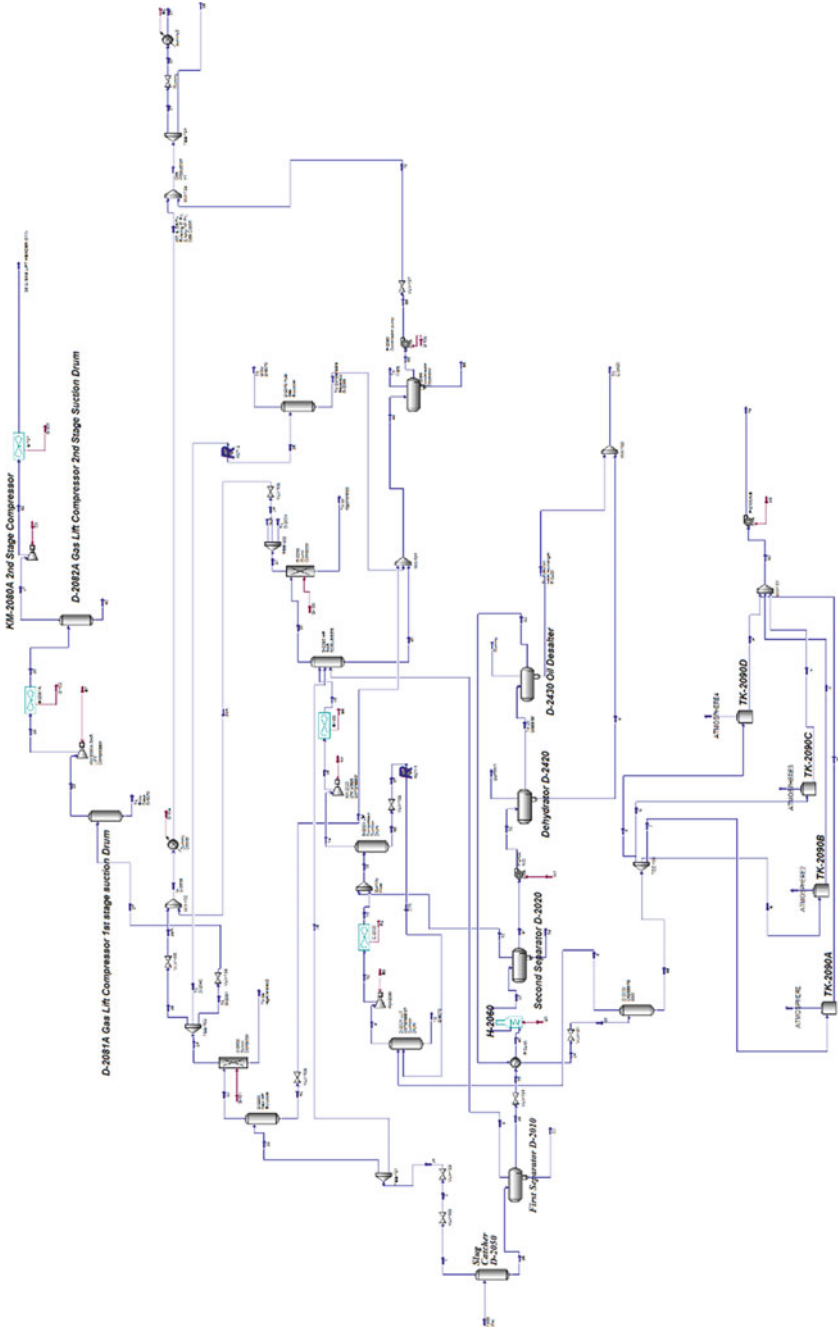
Fig. 4 GOSP HYSYS simulation before revamping (base case)
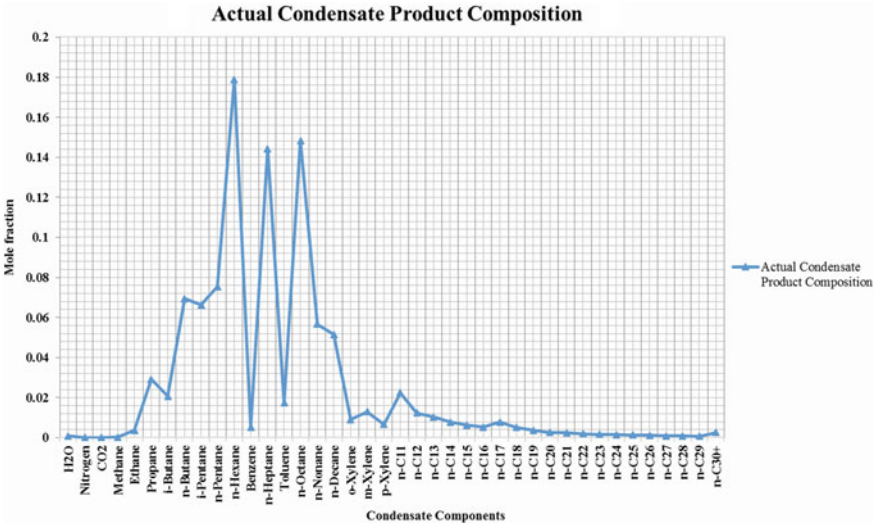
Fig. 5 GOSP Condensate product composition

3 Results and Discussion

3.1 GOSP Terminal Products Compositions

Figures 5 and 6 show a graph of stabilized condensate and gas compositions respectively at GOSP Terminal for the year 2015. The sample was taken at the transportation line of the terminal condensate and gas.

As shown in Fig. 5, most of the volatile components including methane, ethane, and propane (C1–C3) in the live crude have been flashed off during condensate stabilization system under high pressure different in the water separator vessels, oil, and gas.

3.2 Revamping Schemes

Four schemes (LTSUSR-1, LTSUSR-2, LTSUER and RRS) are suggested to maximize condensate production. The first and second schemes are based on low-temperature separation using Joule-Thompson valve. The third scheme utilizes low-temperature separation using propane refrigeration cycle. Finally, the fourth scheme suggests a slight modification in the base case flow sheet by directing the condensate product stream to the oil products stream. A preliminary economic study is performed on the suggested schemes to indicate their feasibility and which scheme is profitable economically.
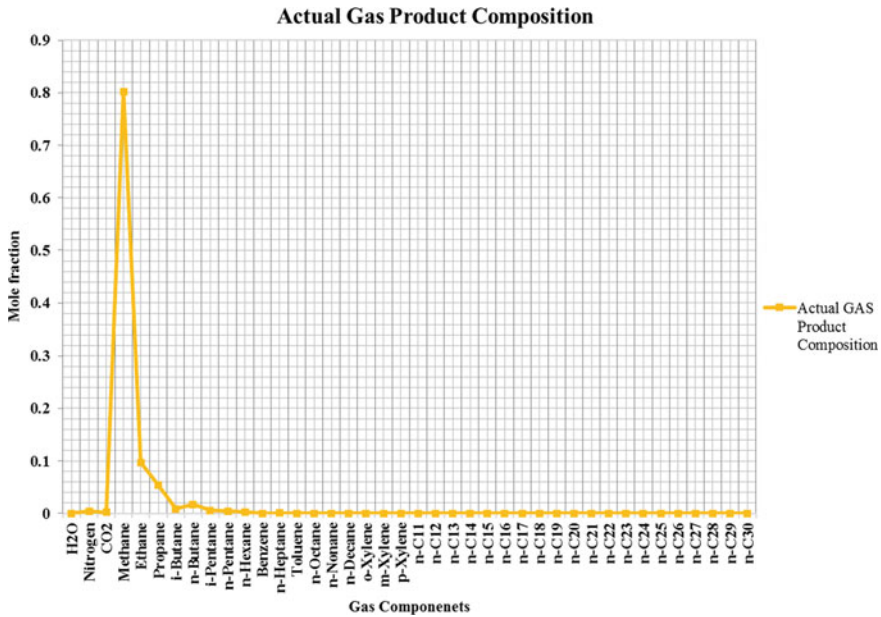
Fig. 6 GOSP gas export composition

The main step towards a good comparison for these different NGL recovery methods is to assess the details of the simulation for each process scheme [39–48].

3.2.1 Revamp One (LTSUSR-1)

Cooling in general can be achieved by Heat exchange with a cooler stream or Expansion (sudden pressure reduction) such as Throttling using Joule-Thompson effect (Isenthalpic expansion) and Turbine expanders (Isentropic expansion).

This scheme depends mainly on the concept of self-refrigeration by compressing the gas to a high pressure then lowering its temperature to the lowest temperature possible at constant enthalpy using Joule-Thompson throttling.

The reduction in pressure across the control valve (VLV-111) causes the condensate to undergo a partial vaporization referred to as a flash vaporization.

The thermodynamic pathway of LTSUSR-1 in Fig. 7 shows the phase behavior of a natural gas as a function of pressure and temperature. Obviously, the cooling process is outside the retrograde condensation zone (the shaded area) which induces condensation and yield NGL at − 28 °C and 16.3 barg.

Actually after applying the proposed scheme, the increase in condensate recovery is 465.4 bbl/day which correspond to 7.2% increase. Furthermore, Fig. 8 shows that
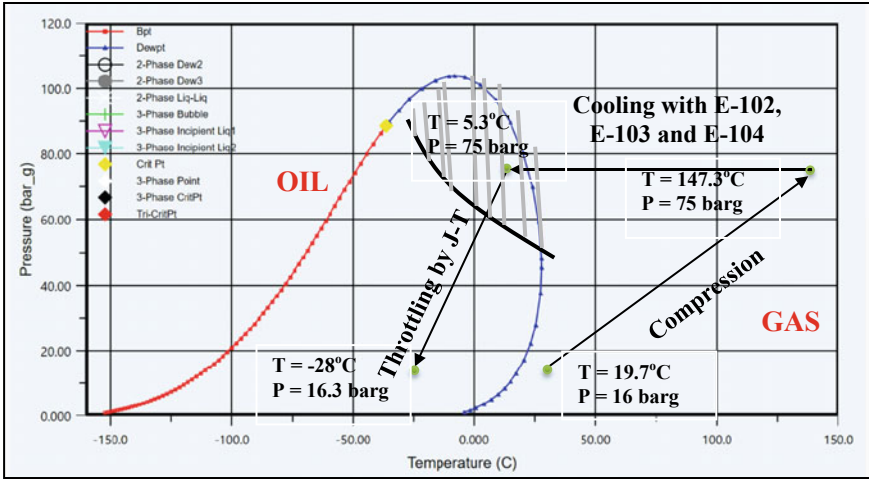
Fig. 7 LTSUSR-1 thermodynamic pathways of NGL recovery

the traces of propane removed from the gas due to adjusting the RVP, but significant amount of the butanes, pentanes and hexane are recovered in the condensate compared to the base case which is desirable.

3.2.2 Revamp Two (LTSUSR-2)

As shown in Fig. 9, two stage compression (K-100 and K-101) instead of one stage as in revamp one to raise the gas pressure to 102 bar. In this case, there is no need for the gas lift compression stages and a stream (stream 33) with rate 8 MMscf is branched by (TEE-101) from the main compressed gas stream and is sent directly for gas lift with 102 bars as in the GOSP base case. The reduction in pressure across the throttling valve (VLV-106) causes the condensate to undergo a partial vaporization referred to as flash vaporization.

The thermodynamic pathway of LTSUSR-2 as presented by Fig. 10, shows the phase behavior of a natural gas as a function of pressure and temperature. Obviously, the cooling process is outside the retrograde condensation zone (the shaded area) which induces condensation and yields NGL at − 45.6 °C and 16.3 barg. The increase in recovered condensate is about 628 bbl/day which corresponds 9.7% increase compared to base case.

3.2.3 Revamp Three (LTSUER)

This scheme based on the idea of external refrigeration in condensing the natural gas liquids. No compression stages are conducted on the gas coming from the glycol
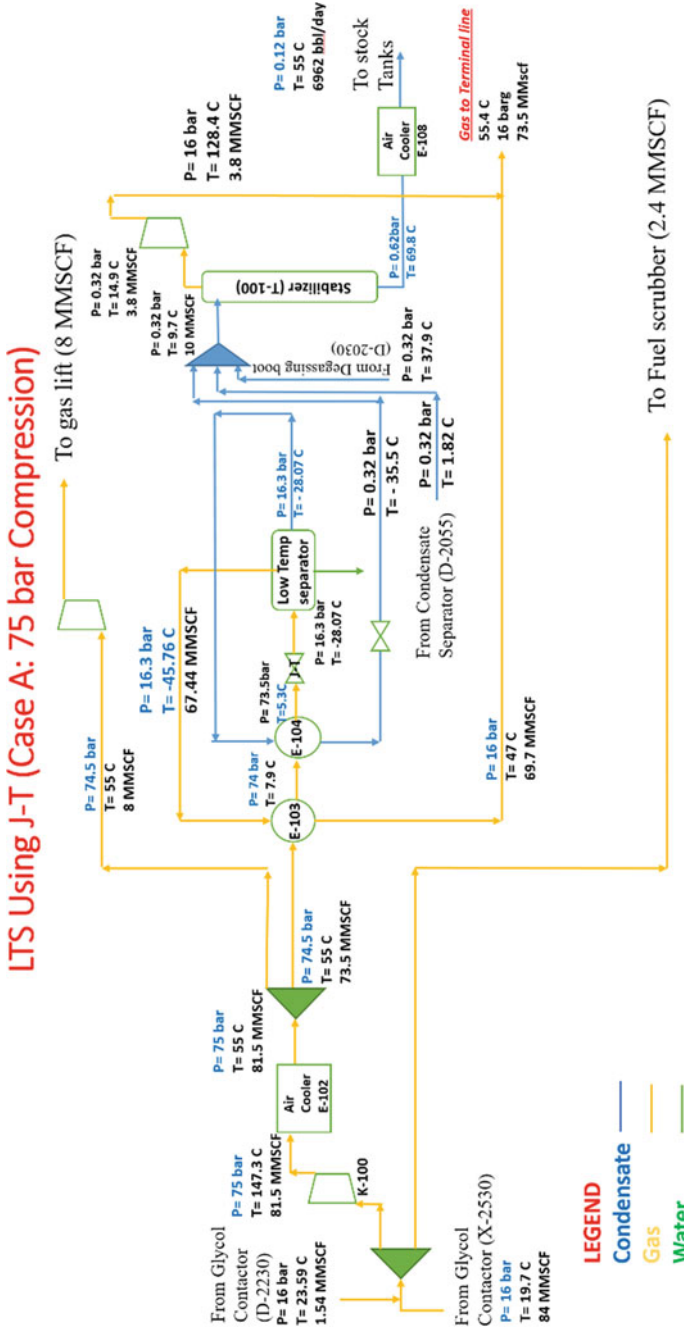
Fig. 8 Process flow diagram of LTSUSR-1
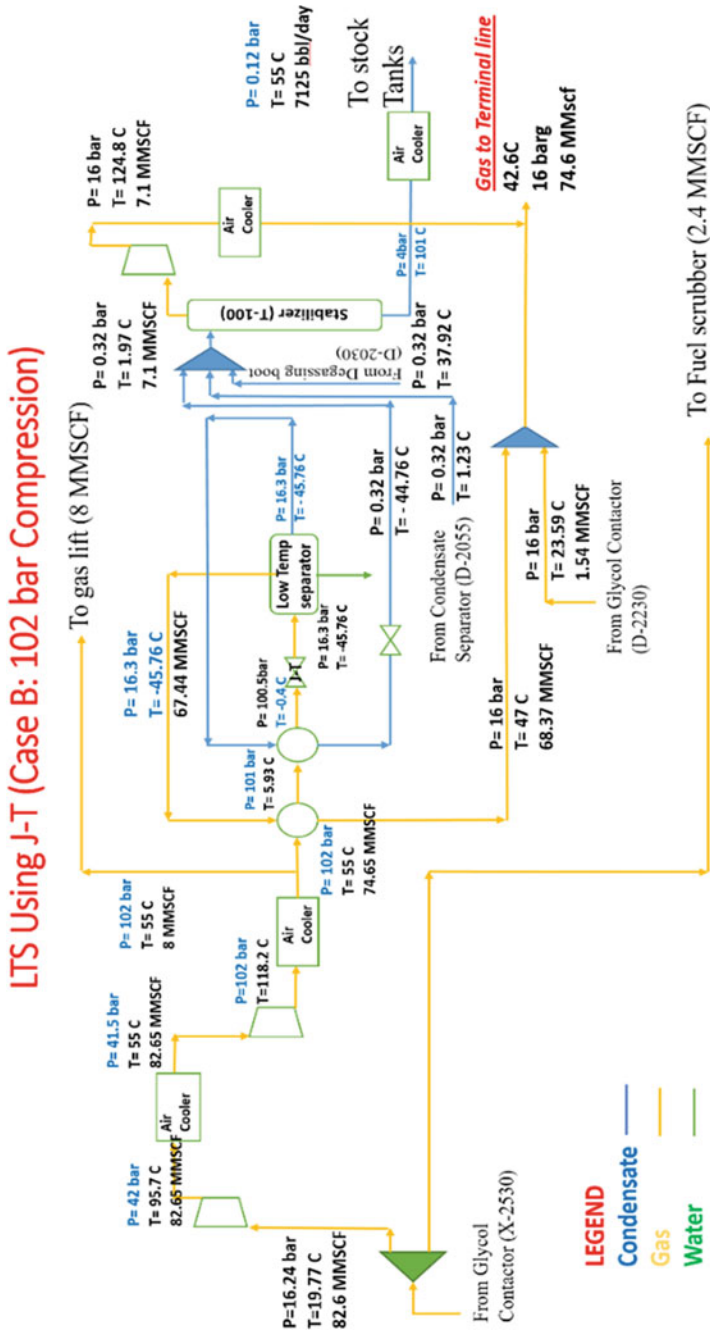
Fig. 9 Process flow diagram of LTSUSR-2
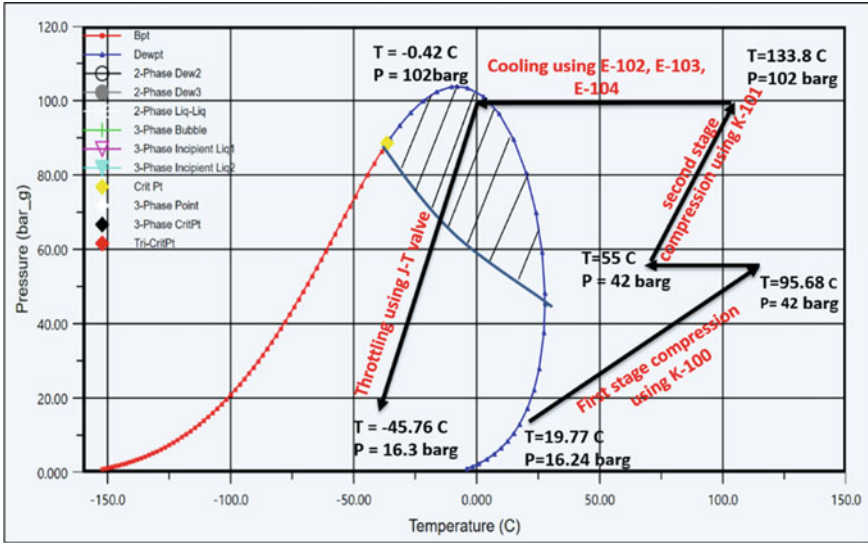
Fig. 10 LTSUSR-2 thermodynamic pathways

contactors (X-2530 and D-2230) and an external refrigeration "Propane cycle" is applied instead of cooling using J-T expansion. Revamp four (RRS).

It is a simple modification in the routing of the condensate outlet from the condensate separator D-2055. In the base case this stream is combined with gas export stream. Modification is done by re-routing of the condensate stream to be combined with the export condensate stream. The combined condensate stream is then directed to stabilization unit to adjust the RVP to export specifications (12 psia).

This modification as shown in Fig. 11 has increased the condensate production rate to 6618.73 bbl/day which is about 2% increase in recovery. The cost of this revamp is considered to be negligible compared to other schemes.

4 Conclusions

The main objective of this research study is maximization of condensate production and adjusting the RVP of the produced condensate to the standard export specifications (max RVP = 12 psia). After reviewing various textbooks and journals related to natural gas processing and condensate stabilization, it is concluded that the best way for maximizing the condensate of the studied GOSP is by the recovery of the natural gas liquids (NGLs) from the produced gas.

A novel NGL recovery configuration was introduced and are accomplished either by self-refrigeration, external refrigeration of raw gas.
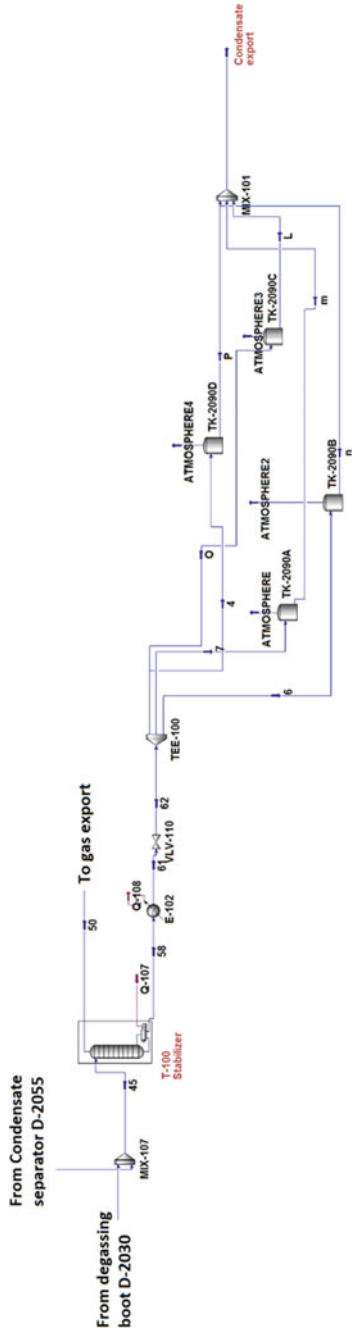
Fig. 11 Process flow diagram of RRS

References

1. Manning FS, Thompson RE (1991) Oilfield processing of petroleum: stabilization and sweetening of crude oil, vol 2. PennWell Books
2. Schlumberger (2016). http://articles.compressionjobs.com/articles/oilfield
3. Dainure MF (2013) Process simulation of crude oil stabilization system: an industrial case study
4. Abdel-Aal HK, Aggour MA, Fahim MA (2015) Petroleum and gas field processing. CRC Press
5. Burruss R, Ryder RT (2003) Composition of crude oil and natural gas. U.S Geological Survey
6. Arnold K, Stewart M (1999) Surface production operation: design of oil-handling system and facilities, vol 1. MA Butterworth-Heinemann
7. Rahmanian N, Jusoh LSB, Homayoonfard M, Nasrifar K, Moshfeghian M (2016) Simulation and optimization of a condensate stabilization process. J Nat Gas Sci Eng
8. Rahmanian N, Ilias IB, Nasrifar K (2015) Process simulation and assessment of a back-up condensate stabilization unit. J Nat Gas Sci Eng
9. Campbell JM (2014) Gas conditioning and processing. Campbell petroleum series, 9th edn, vol 2, Norman, OK
10. Benoy J, Kale RN (2010) Condensate stabilization, Offshore World. Chemtech Foundation, India
11. Geankoplis CJ (2003) Transport processes and separation process principles. Prentice Hall, New Jersey
12. Mokhatab S, Poe WA, Speight JG (2006) Handbook of natural gas transmission and processing. Gulf Professional Publishing, UK
13. Elazab HA, El-Idreesy TT (2019) Optimization of the catalytic performance of Pd/Fe$_3$O$_4$ nanoparticles prepared via microwave-assisted synthesis for pharmaceutical and catalysis applications. Biointerface Res Appl Chem 9(1):3794–3799
14. Elazab HA, Gadalla MA, Sadek MA, El-Idreesy TT (2019) Hydrothermal synthesis of graphene supported Pd/Fe$_3$O$_4$ nanoparticles as efficient magnetic catalysts for Suzuki cross—coupling 9(2):3906–3911
15. Radwan MA, Al-Sweasy O, Sadek MA, Elazab HA (2018) Investigating the agricultural applications of acryl amide-based hydrogel 7(4.29, special issue 29):168–171
16. Esmaeili A (2010) Optimization of effective parameters on Reid vapour pressure (RVP) in an Iranian condensate stabilization plant and a back-up unit. In: The 13th Asia Pacific confederation of chemical engineering congress. APCChE, Taipei
17. Piping-engineering website (2016). http://www.piping-engineering.com
18. (2004) Engineering data book. Hydrocarbon treating, 12th edn, sect 21. Gas Processors Supply Association, Tulsa
19. Kidnay AJ, Parrish WR, McCartney DG (2011) Fundamentals of natural gas processing, vol 218. CRC Press
20. Arnold K, Stewart M (2008) Surface production operations: design of oil handling systems and facilities. Elsevier
21. (2004) Engineering data book. Product specifications, 12th edn, sect 2. Gas Processors Supply Association, Tulsa
22. Klinkenbijl JM, Dillon ML, Heyman EC (1999) Gas pre-treatment and their impact on liquefaction processes. In: Proceedings of the seventy-eighth annual convention of the Gas Processors Association, Tulsa
23. Ghorbani B, Hamedi MH, Amidpour M (2016) Development and optimization of an integrated process configuration for natural gas liquefaction (LNG) and natural gas liquids (NGL) recovery with a nitrogen rejection unit (NRU). J Nat Gas Sci Eng 590–603
24. Geist J (1985) Refrigeration cycles for future base-load LNG plants need a close look. Oil Gas J (United States) 83(5)
25. (2004) Engineering data book. Refrigeration, gas processors supply, 12th edn, sect 14. Association, Tulsa

26. Brands DS, Rajani JB (2001) Comparison between low temperature separation (LTS) and SORDECO process for hydrocarbon dew pointing. Paper presented at the 18th GPA Europe annual conference, Amsterdam, The Netherlands
27. Russell T (2001) Gas processing basics. Paper presented at the 80th GPA annual convention, San Antonio, TX
28. Guthrie KM (1969) Capital cost estimating. Chem Eng NY 76(Mar 24th):114
29. Ewan DN, Laurence JB, Rambo CL, Tonne R (1975) Why cryogenic processing? Paper presented at the 54th GPA annual convention, Houston, TX
30. Sinnott RK (1999) Chemical engineering design. Coulson & Richardson's chemical engineering series, 3rd edn, vol 6
31. Aries RS, Newton RD (1955) Cost estimation. McGraw-Hill
32. Chilton CH (1960) Cost engineering in the process industries. McGraw-Hill
33. Winfield MD, Dryden CE (1962) Chart gives equipment, plant costs. Chem Eng NY 69(Dec 24th):100
34. Hall RS, Matley J, Mcnaughton J (1982) Current cost of process equipment. Chem Eng NY 89(Apr 5th):80
35. Ulrich GD (1984) A guide to chemical engineering process design and economics. Wiley
36. Garrett DE (1989) Chemical engineering economics. Van Norstrand Reinhold
37. Guthrie KM (1970) Capital and operating costs for 54 processes. Chem Eng Note: Correction, Dec 14th, 7NY 77(June 15th):140
38. Day MF (1979) Materials for high temperature use, engineering design guide, no 28, Oxford U.P.
39. Lai GY (1990) High temperature corrosion of engineering alloys. ASM International
40. Wigley DA (1978) Materials for low temperatures, engineering design guide, no 28, Oxford U.P.
41. Wells AA (1968) Fracture control of thick steels for pressure vessels. Br Weld J 15:221
42. Sinnott RK (2005) Chemical engineering design. Coulson & Richardson's chemical engineering series, vol 6
43. Lynch JT, Lousberg NB, Pierce CM (2007) How to compare cryogenic process design alternatives for a new NGL project. Presented at the 86th annual convention of the Gas Processors Association
44. Getu M, Mahadzir S, Long NVD, Lee M (2013) Techno-economic analysis of potential natural gas liquid (NGL) recovery processes under variations of feed compositions. Chem Eng Res Des 91(7):1272–1283
45. ENNPI (2010) Process control philosophy (3170-300-RT-001)
46. Chemical Engineering (2016). http://www.chemengonline.com/economic-indicators-3/?printmode=1
47. Towler G, Sinnott RK (2012) Chemical engineering design: principles, practice and economics of plant and process design. Elsevier
48. Schlumberger (2016). https://www.slb.com/~/media/Files/testing/other/epf_crude_oil_treatment.pd

Examining the Behaviour of Lubricating Oil Film Within Marine Journal Bearing Under Emergency and Critical Operational Conditions

Nour A. Marey, El-Sayed H. Hegazy, and Amman A. Ali

1 Introduction

Crash Stop has always been considered as one of the risky conditions that would, in certain cases, negatively affect the efficiency of lubrication within the journal bearing. Conducting such serious emergency maneuverability effectively leads to the prevention of potential marine collision. Such type of collisions is so detrimental as it poses a real threat to marine environment. Thus, it is of much importance to observe and take all essential precautions when resorting to crash stop so that sustainable marine life could be maintained.

Certain criteria plainly stated in the regulations of ship maneuverability ought to be observed, if the crash stop maneuvering is to be implemented successfully. Those criteria were issued by the Marine Safety Committee (MSC), illustrating the concept of stopping ability and stating that in the full astern stopping test the track reach should by no means exceed 15 ship's length [1]. Also, demonstrating the astern response characteristics has entailed subjecting the main propulsion system to certain tests during delivery sea trials of a new ship. It is noteworthy that for conducting the crash stop tests effectively, they have to be within the maneuvering range regarding the propulsion system, and encompassing all of the control positions. Also, the ship yard would provide a test plan that must be accepted by the surveyor. Furthermore,

N. A. Marey (✉) · A. A. Ali
Institute of Maritime Upgrading Studies, Arab Academy for Science, Technology and Maritime Transport, Alexandria, Egypt
e-mail: nour_marine@aast.edu

A. A. Ali
e-mail: amman_ali@aast.edu

E.-S. H. Hegazy
Naval Architecture and Marine Engineering Department, Faculty of Engineering, Port Said University, Port Said, Egypt
e-mail: elsayed.hussein@eng.psu.edu.eg

the test plan must include any definite operational characteristics defined by the manufacturer according to classification societies rules, such as the General Astern Characteristics American Bureau of Shipping (ABS) Steel Vessel Rules, Sec 4-1-1/7.5 ABS [2]. The following lines would shed light on some of the most crucial endeavors exerted for the sake of better identifying the consequences of conducting the crash stop procedure, regarding the oil film lubrication within the journal bearing. In order that the structural safety of the propeller could properly be evaluated, a study was implemented on the hydrodynamic propeller loads at crash stop by Hur et al. [3]. The study has comprised measuring the torques of propeller shafts at crash stop in the sea trials, with view to evaluating the structural safety of the propeller blade at initial design stage. On the other hand, considering the great importance of optimizing the Crash-Stop maneuver of vessels during crash stop critical moments, [4], has attempted to reduce the stopping distance in cases of emergencies. Besides, the researcher has attempted to enhance the engine speed at which pneumatic reversing could be conducted. Moreover, there has been another study on the crash-stop issue by Nowicki [5], that has basically aimed at offering a description of various possibilities, regarding stopping a large ship equipped with Azipods. They were found to offer a positive influence, regarding promoting propulsion efficiency and better maneuverability. Stopping by turning Azipods around was discovered to be the best technique, as it could reduce the non-dimensional track reach. In addition, crash stop procedure is often accompanied by certain failures, leading to excessive wear of the journal bearing white metal, and ultimately negatively affecting journal bearing performance. However, maneuvers required by IMO standards are known to include full astern stopping tests, which are unfortunately still neglected by many shipyards and class societies [6]. Such crucial issues were not likely given sufficient investigations in the previous studies dealing with the optimal performance relating to the journal bearing. Furthermore, several researches have been focused on tracing the consequences badly affecting the hydrodynamic journal bearing under non-steady state speeds. One such study has been conducted by Liu et al. [7]. On achieving the final steady speed, the film thickness rate was observed to reach its maximum regarding the startup/shutdown process. It was concluded that the film thickness could attain its steady value asymptotically during startup and shutdown process. Smaller load and lower speed maximum were found to help give longer time delay. Moreover, [8], have launched a study aiming at making a prediction relating to the crash stopping maneuvering performance. The researchers have attempted to predict, at design stage, the crash stop main characteristics, for the preliminary assessment of safety requirements imposed by the classification society. Nearly around the same year of 2017, and working on the ultimate goal of predicting ship maneuver for enhancing the crash stop procedure utilizing mathematical means, [9], has presented a novel mathematical framework, aiming at predicting ship maneuvers within a short time interval. Based on the derived outcomes, the predicted position and orientation information could be used for assessing of prior collision situations. Besides, [10] have conducted a study with view to better understanding the behavior of cylindrical journal bearing with two axial grooves, as being affected by the rotational speeds, as well as the applied static loads, under severe operating conditions. Further, the

deformation of the bearing housing, and the bending of the shaft were found out to make a large difference, providing the load was increased. Moreover, [11] have attempted to optimize bi-directional-rotation herringbone-grooved journal bearings, via applying stabilized term in free boundary problems. Such methodology appeared to have the advantage of optimizing textured groove appearance on applying Fluid Dynamic Bearings (FDBs) to spindle motors. Among the latest studies aiming at studying the influence played by the surface form deviation regarding the friction in mixed lubrication, [12] were concerned with measuring the overall form deviation of the test bearing by means of simulation procedures. The results obtained have manifested a significant effect of the surface form deviations on the pressure distribution of the lubricant, and hence on size of the asperity contact area. Also, parallel to the previous efforts, [13] focused on the effects occurring as a result of mixed friction and warming of the components of journal bearings during run-ups. It was found that the model boundaries were what predictions of heat flow within run-up strongly relied on. Noteworthy to say that a very important experimental study was implemented into surface texture effect on journal bearings performance by Galda et al. [14], with the aim of identifying the characteristic parameters, such as the sliding velocity, Hersey number and friction torque or friction coefficient, when the transition of lubrication regimes occurred for different journal bearing types. It was observed that during shut-down, the textured journal bearings remained in hydrodynamic lubrication for longer and moved to mixed lubrication at lower speeds, compared to the smooth journal bearing. Marey et al. [15–20] carried out a series of research programs for investigating and enhancing the oil film lubrication within journal bearing in marine application. Marey et al. [15] involved the design and setup of a journal bearing test rig (JBTR). The study made it possible to trace the oil film pressure distribution at different speeds and constant load. Marey et al. [16] conducted a numerical study to investigate the oil film pressure profile within journal bearing. A new Computational Fluid Dynamic (CFD) model has been built for coupling future experimental test trials with computerized ones. Based on the versatile conducted test trials, the validity of the newly constructed model has been ascertained and its potentials regarding conducting thorough investigations on the lubricating oil film within journal bearing has also been confirmed. Marey [17] Utilized different oil grades for experimentally investigating the pressure behavior of different lubricants within the hydrodynamic journal bearing, at different speeds ranging from 50 to 400 rpm at constant load. A positive relation has been concluded as between the oil film pressure distribution and both the rotation speed and the oil viscosity. Marey et al. [18] enlarged the capabilities of journal bearing to contain much more sophisticated experimental test trials, via comprehensive and continuous modifications. The modifications involved adding a hydraulic loading system and full monitoring process via Supervisory Control and Data Acquisition (SCADA) system [19]. The integrated systems have turned the structure into a Universal Journal Bearing Test Rig (UJBTR) that allowed for more extensive experiments for enhancing the performance of journal bearing and testing the most critical operational factors. Uncertainty and validation measurement analysis of UJBTR [20] has been carried out for ensuring the accuracy of the obtained outcomes.

Finally, it is of much importance to mention that resorting repeatedly to the crash stop procedure during emergency conditions related to ships can possibly damage the plain bearings. Consequently, carrying out such maneuver may trigger other complicated problems. Additionally, the literature has revealed that more experimental studies to investigate the oil film lubrication behavior within journal bearing during such critical conditions are certainly needed. Accordingly, the usefulness of such researches has not yet reached a satisfactory degree and the issue may still be seen as an open area in need of more investigations.

2   Case Study

The Universal Journal Bearing Test Rig (UJBTR) is characterized by assured validity. UJBTR validity was of topmost necessity for ensuring the accuracy and conformity of the results [20]. The following is an illustration of the different components of UJBTR structure. A structure that could help conduct versatile experiments at the time being or potentially in the future.

As is shown in Figs. 1, 2 and 3, the oil film lubricant is supplied to the bearing at an inlet port mounted on the vertical center line of the journal bearing. On the rotation of the journal shaft, pressure incurred inside is measured via the ten pressure transmitters. Those are distributed around the circumference of the Circumferential Grooved Bearing (CGB). Pressure values are hence displayed on the Programmable Logic Controller (PLC).

Also, an "Inverter" is integrated into JBTR so that speed could be manipulated and rotation direction could as well be easily reversed. Besides, many comparisons were to be held for proving the consistency of the obtained results with their previously derived theoretical counterparts. In addition, Table 1, provides the main dimensions of the JBTR at hand.
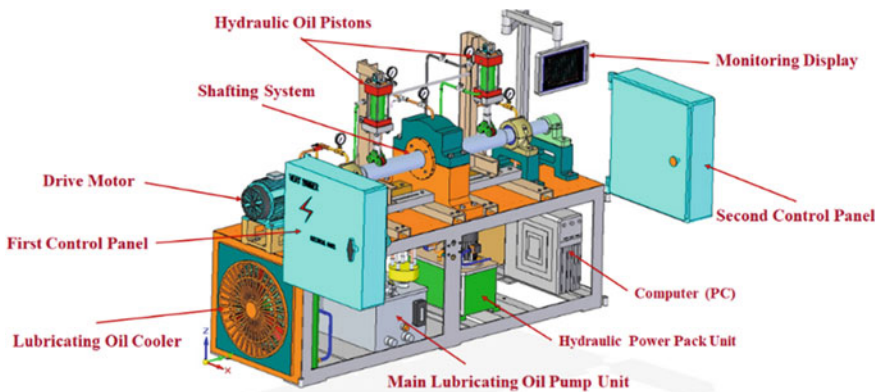
Fig. 1 A schematic of UJBTR full structure [18]

Fig. 2 The shafting system of UJBTR [18]
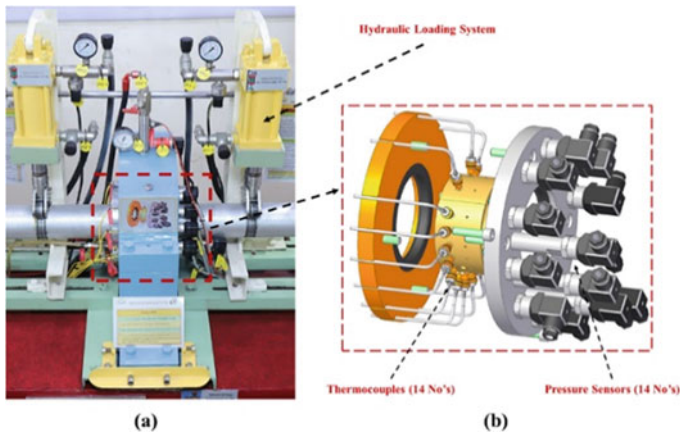
Fig. 3 **a** UJBTR main journal bearing and **b** pressure sensors and thermocouples distributed on grooved bearing circumference [18]

Table 1 Dimensional data of UJBTR

Description	Specifications
L, bearing length	58 mm
d, inner diameter for plain bearing	105.05 mm
Φ_s shaft diameter	104.97 mm
W, weight of journal shaft	727.65 N
C_0, total clearance	0.08 mm
C, radial clearance	0.04 mm
L/D ratio	0.5
Bearing material	White metal
Pressure transmitter range	0:10 bar

3 Crash Stop Tests Procedures

For tracing the impacts resulting from applying the "Crash stop" maneuvering on the journal bearing, different experimental test trials have been carried out utilizing UJBTR. In addition, launching such high-risk experiments on the journal bearing have necessitated taking all safety precautions. Continuous monitoring has been a must, so that journal bearing safety could be maintained throughout the conducted procedures.

The oil lubrication system has been prepared, checking that the oil level in the storage tank was always normal. Further, the oil supply pressure has been adjusted to be 2.0 bar, at a temperature degree of 40 °C. The journal shaft direction has initially been anticlockwise. A lubricant oil of grade SAE 20W50, as an optimal heavy-duty option, has been utilized. Properties of such oil grade are introduced in detail in Table 2. The different test trials with their set conditions have been carried out to investigate the oil film lubrication behavior under circumstances similar to those accompanying actual crash stop maneuverability. The different "Crash Stop" tests have comprised mainly three testing phases.

The first phase has involved a non-stop abrupt rapid speed alteration "from 50 rpm anticlockwise to 50 rpm clockwise", at a change rate of 100 rpm per second. The second phase has included a gradual, speed change that was "from 50 rpm anticlockwise to 50 rpm clockwise" at a change rate of 10 rpm per 20 s. The third phase has the same procedure under a speed limit of 200 rpm, and has initially comprised a non-stop rapid speed alteration (from 200 rpm anti-clockwise to 200 rpm clockwise). It was then followed by a deaccelerating stage, the duration of which has been of around 30 s, from 200 rpm and up to 0 rpm anticlockwise. It was then almost immediately followed by an acceleration from 0 rpm to reach 200 rpm clockwise of the same duration, the speed of which reflects the ship normal speed. The values of the oil film pressure distribution under these conditions were also recorded for further investigations. Versatile comparisons were then held among the results obtained for more valid and certified evidence in relation to the crash stop procedures.

Table 2 Properties of SAE 20W50 grade oil

| SAE 20W50 Properties	Specifications
Volumetric mass at 15 °C	895 kg/m^3
Kinematic viscosity at 40 °C	153 mm^2/s
Kinematic viscosity at 100 °C	17.0 mm^2/s
Viscosity index	120
Flash point	230 °C
Pour point	− 21 °C

4 Results and Discussions

The study at hand has involved conducting many test trials, related to crash stop, to identify its full impacts on the performance of the journal bearings. Furthermore, recognizing the oil film pressure distribution within CGB, in such critical phases, has been put into consideration on carrying out the procedures. In this way, the deterioration that might occur, due to the degradation of the lubrication oil film, could be identified. All results obtained based on the conducted test trials are introduced in the following polar diagrams.

4.1 Crash Stop at Non-stop Abrupt Rapid Speed Alteration

For such case, the polar diagrams, shown on Fig. 4, would reveal all the recorded values relating to the lubricating oil pressure distribution within CGB. Based on such polar diagrams, a number of observations could be derived as follows:

- Under a non-stop abrupt rapid speed alteration, the maximum value of the oil film pressure P_{max}, at anticlockwise direction at shaft speed of 50 rpm and an angle of 180°, has recorded 2.075 bar.

Fig. 4 Crash stop under a non-stop abrupt rapid speed alteration
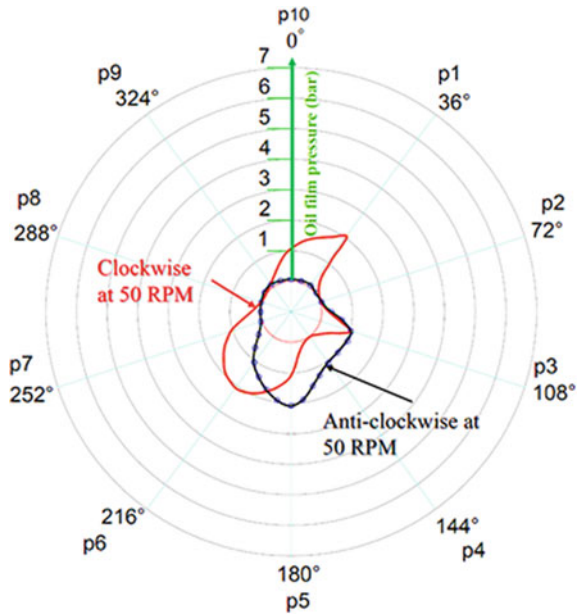
- Pressure values featured a significant fall at an angle of 144°, where they assumed the value of 0.036 bar. That was due to reversing the rotation direction in an abrupt and a sudden way.
- The deterioration of the lubricating oil film at this region means that lubrication has turned from hydrodynamic lubrication region to boundary one.
- Such sudden shift would result in the metal-to-metal contact and the failure of CGB.
- At an angle of 36°, the pressure value featured a sudden increase where it reached 2.065 bar. That would lead to increasing the upper load working on journal shaft.

4.2 Crash Stop with Gradual Speed Change

Experiments were conducted to investigate the behavior of oil film pressure distribution under crash stop procedures. They have initially been carried out under a gradual speed change from 50 rpm anti clockwise to 50 rpm clockwise, at a change rate of 10 rpm per 20 s Fig. 5.

The lubricating oil film pressure has featured a notable decrease on carrying out the test under a speed limit of 30 rpm in the basic rotation direction which is anticlockwise, Fig. 5c. That reduction would amount to 50%, indicating the existence of transient lubrication at this speed. To illustrate the deterioration of oil film pressure distribution with gradual speed reduction anticlockwise, all previously mentioned 10 rpm intervals have been collectively plotted as shown in Fig. 6. The pressure values are observed to remain constant up till a speed limit of 10 rpm in the same direction, Fig. 5c–e. The previously mentioned observations reflect the inefficient lubrication throughout this stage.

On reversing shaft rotation gradually in a clockwise direction, the oil film pressure distribution values were noted to remain constant from 10 rpm and up to 50 rpm. Also, P_{max} has featured some increases at an angle of 216°, where the oil pressure has acquired a value of 3.1 bar. However, the value of the lubricating oil film pressure was noted to suffer a complete failure at an angle of exactly 144°. Such sudden failure would lead to boundary lubrication with likelihood of metal-to-metal contact between the bearing angles of 108° and up till 180° as pointed out by Fig. 7. Furthermore, the steady-state condition would be reached after the passing of 4 min, where P_{max} would return to its original value of 2.07 bar. This occurs at an angle 180°, where boundary region at an angle of 144° would disappear, whereas the pressure would rise to return to its previous value of 1.07 bar.

Based on the outcomes of the test trials, it is obvious that the crash stop procedure is a major risk regarding the performance of the journal bearing. The reason is that carrying out crash stop negatively affects the lubricating oil film, which in turn, would ultimately lead to journal bearing failure.
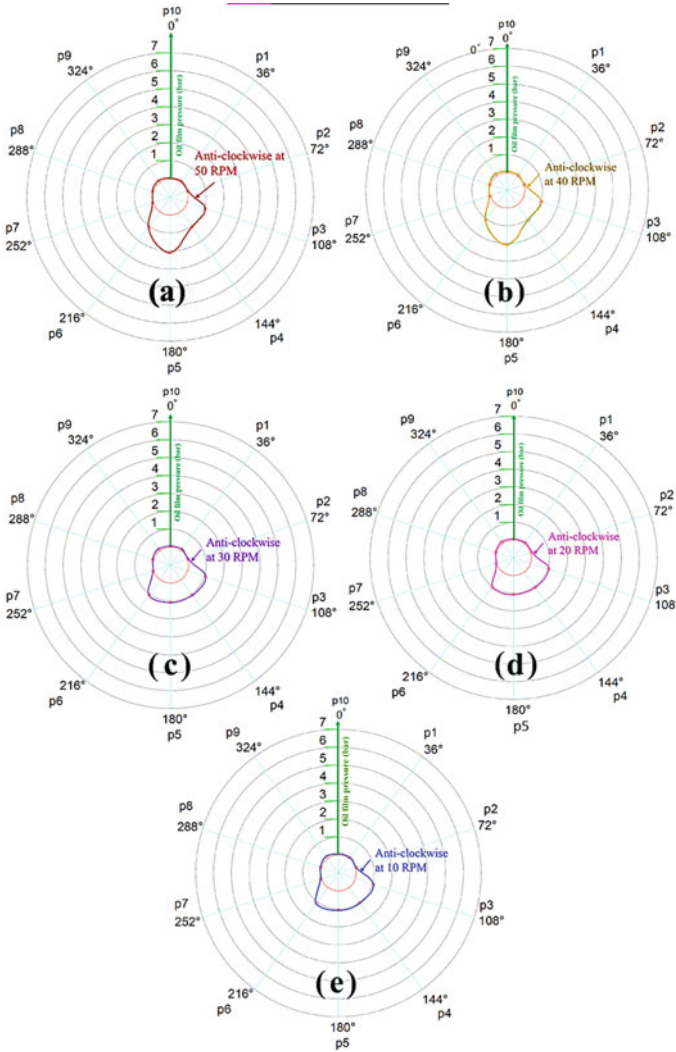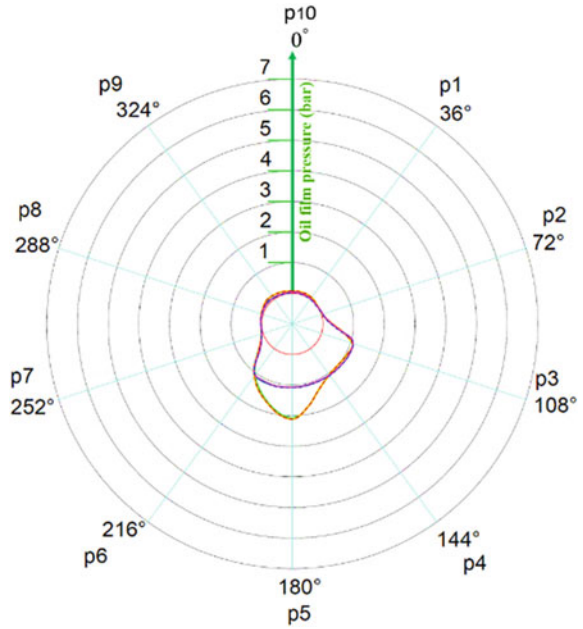
Fig. 5 a–e Oil film pressure distribution under a gradual, speed change from 50 rpm anti clockwise at a change rate of 10 rpm per 20 s
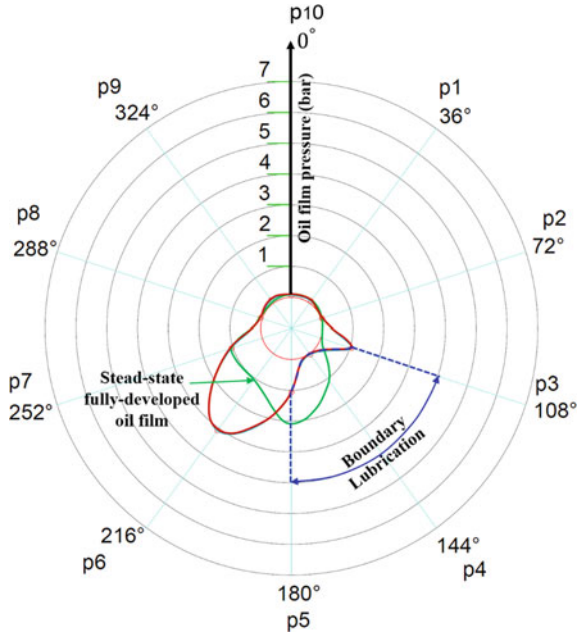
4.3 Crash Stop at a Non-stop Abrupt Rapid Speed Alteration Under 200 rpm

Under a non-stop abrupt rapid speed alteration of 200 rpm, the oil film pressure distribution would suffer an abrupt failure from the angle of 36° until just below the angle of 180°. It is here that boundary lubrication occurs and after that the oil film pressure rises to assume the maximum value of 6.164 bar at an angle of 216°. In light

Fig. 6 The deterioration of oil film pressure distribution with gradual speed reduction anticlockwise (from 50 rpm)

Fig. 7 Oil film pressure distribution build up in clockwise acceleration following direction reversing (up to 50 rpm)

Fig. 8 Crash stop under non-stop abrupt rapid speed alteration at 200 rpm
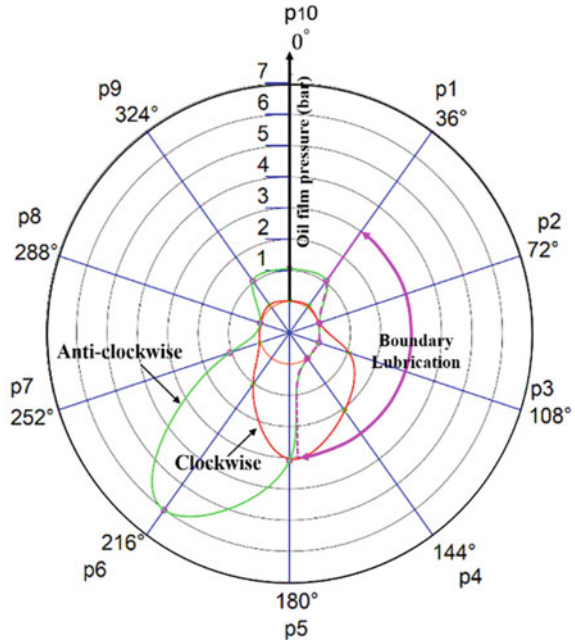
of the previously mentioned conducted procedures, it is concluded that the metal-to-metal contact region would be larger and riskier under 200 rpm, if compared with its peer obtained at a non-stop abrupt rapid speed alteration of 50 rpm, Fig. 8.

4.4 Crash Stop Behaviour at 200 rpm by De-acceleration and Acceleration

During the De-Acceleration moments from 200 rpm and down to 50 rpm in 30 s, the oil film pressure distribution values within CGB features a gradual reduction. Here, the risks related to oil profile failure would decrease, as clearly shown in Fig. 9.

Throughout the acceleration phase, also conducted in the course of thirty seconds in clockwise direction at 50 rpm, P_{max} has assumed a value of 2.085 bar, at an angle of 216°. In comparison, on conducting the De-acceleration experiment under the same speed but in an anticlockwise direction, P_{max} has recorded a value of 2.078 bar at an angle of 180°. It is thus noted that P_{max} angle has shifted by 36°. Also, P_{max} has obtained higher values corresponding to the increases in shaft speed, without changing P_{max} angle that has remained at 216°, Fig. 10.

Fig. 9 Oil film pressure distribution deterioration at an anticlockwise gradual speed reduction
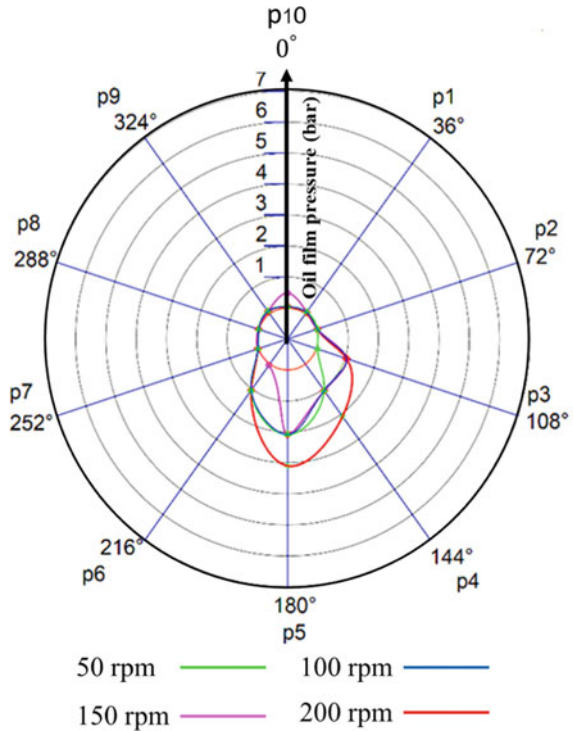
5   Conclusions

Crash Stop maneuver is thus concluded to have some very negative effects on the journal bearing lubricating oil film, working on separating the stationery surface from the moving surface. Such fact is true for all crash stop conditions, whether the change rate of movement at 50 rpm is rapid or gradual. Changing direction in a fast and abrupt way would lead to the failure of the shafting system, in charge of the ship transmission efficiency. Besides, minimizing the risks on the lubricating oil film could be achieved via carrying out the crash stop procedures at a gradual change rate. Such target could be carried out by slowing down shaft speed change rate until it reaches a complete stoppage, and then immediately reversing rotation direction.

On conducting crash stop at a non-stop abrupt rapid speed alteration of 50 rpm at both directions of rotation, the oil film pressure distribution values significantly decrease at the angles of 144° and 180°, which means a deterioration of oil pressure by 50%. Also, the deterioration of the oil film pressure distribution at the angle of 144° means that the value has recorded zero bar.

In addition, carrying out the crash stop procedure at a non-stop abrupt rapid speed alteration of 200 rpm at the angles of 108° and 144°, leads to the complete failure

Fig. 10 Behavior of oil profile during acceleration procedures (up to 200 rpm)
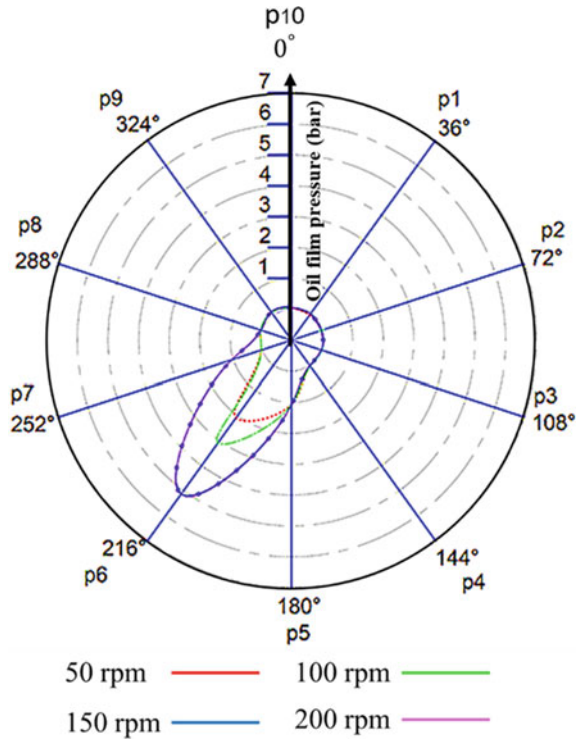
of oil profile. Such reductions result in the risky condition in which the journal shaft would come to a direct contact with the journal bearing.

Furthermore, conducting tests at 200 rpm, by both De-acceleration and acceleration, has been found out to represent less risk regarding the lubricating oil film. It is here that the lubricating oil film is more stable and is less likely to suffer, compared to the case of operating under non-stop and abrupt way at the same speed. The reason could be attributed to the rapid deterioration of the lubricating oil film of journal bearing. Finally, the lubricating oil film within journal bearing is in charge of the efficient performance of the shafting system of ship navigation. Consequently, the most important operational factors related to journal bearing must be maintained to ensure the safety of the shafting system as a whole.

6   Recommendations

To meet the requirements, clearly stated by The Marine Safety Committee (MSC) of the International Maritime Organization (IMO), and related to the safe navigation in case of crash stop procedures, the following recommendations are proposed:

1. The journal bearing of the shafting system should be provided with a fully controlled additional lubrication oil system. Such system could be activated at a shaft speed ranging from 0 up to 50 rpm in both directions, so that the lubrication process of the journal bearing could be carried out by force.
2. An oil feeding system is recommended to be provided in the mid bottom position of the journal bearings related to the shafting system.

References

1. Maritime Organization International (2002) Resolution Msc.137(76) standards for ship manoeuvrability. IMO, p 2018
2. American Bureau of Shipping (1994) Rules for building and classing steel vessels, v. <2>
3. Hur JW, Lee H, Chang BJ (2011) Propeller loads of large commercial vessels at crash stop. Time
4. Wirz D (2012) Optimisation of the crash-stop manoeuvre of vessels employing slow-speed two-stroke engines and fixed pitch propellers. J Mar Eng Technol 11:35–43. https://doi.org/10.1080/20464177.2012.11020259
5. Nowicki J (2014) Stopping of ships equipped with azipods. TransNav Int J Mar Navig Saf Sea Transp 8:373–376. https://doi.org/10.12716/1001.08.03.07
6. Babicz J (2015) Wärtsilä Encyclopedia of ship technology, 2nd edn. ISBN 978-952-93-5536-5 (PDF)
7. Liu HC, Guo F, Zhang BB, Wong PL (2016) Behavior of hydrodynamic lubrication films under non-steady state speeds. Tribol Int 93:347–354. https://doi.org/10.1016/j.triboint.2015.09.026
8. Oneto L, Coraddu A, Sanetti P, Karpenko O, Cipollini F, Cleophas T, Anguita D (2017) Marine safety and data analytics: vessel crash stop maneuvering performance prediction. In: Lecture notes in computer science (including subseries Lecture notes in artificial intelligence and Lecture notes in bioinformatics), pp 385–393
9. Perera LP (2017) Navigation vector based ship maneuvering prediction. Ocean Eng 138:151–160. https://doi.org/10.1016/j.oceaneng.2017.04.017
10. Chatterton S, Dang PV, Pennacchi P, De Luca A, Flumian F (2017) Experimental evidence of a two-axial groove hydrodynamic journal bearing under severe operation conditions. Tribol Int 109:416–427. https://doi.org/10.1016/j.triboint.2017.01.014
11. Chen CY, Liu CS, Tee CK, Li YC (2017) Application of stabilized term in free boundary problems for optimizing bi-directional-rotation herringbone-grooved journal bearings. Appl Math Model 47:826–838. https://doi.org/10.1016/j.apm.2016.11.002
12. Fricke S, Hager C, Solovyev S, Wangenheim M, Wallaschek J (2018) Influence of surface form deviations on friction in mixed lubrication. Tribol Int 118:491–499. https://doi.org/10.1016/j.triboint.2017.05.032
13. Prölß M, Schwarze H, Hagemann T, Zemella P, Winking P (2018) Theoretical and experimental investigations on transient run-up procedures of journal bearings including mixed friction conditions. Lubricants 6:105. https://doi.org/10.3390/lubricants6040105
14. Galda L, Sep J, Olszewski A, Zochowski T (2019) Experimental investigation into surface texture effect on journal bearings performance. Tribol Int 136:372–384. https://doi.org/10.1016/j.triboint.2019.03.073
15. Marey N, Hegazy E-S, Aly A (2018) Design and setup for a journal bearing universal test rig. Port-Said Eng Res J 22:101–106. https://doi.org/10.21608/pserj.2018.32472
16. Marey N, Aly A, Hegazy E-S (2018) Computational investigation of oil film pressure profile in journal bearings. Port-Said Eng Res J 22:40–45. https://doi.org/10.21608/PSERJ.2018.32095

17. Marey N (2019) An experimental investigation of hydrodynamic journal bearing with different oil grades. Port-Said Eng Res J 23:46–54. https://doi.org/10.21608/pserj.2019.49576
18. Marey N, Hegazy E, El-Gamal H, Ali A, Abd-El-Ghany R (2021) Development of a Universal Journal Bearing Test Rig (UJBTR) and experimental setup for oil film lubrication enhancement regarding marine applications. Port-Said Eng Res J 26:81–93. https://doi.org/10.21608/pserj.2021.100583.1149
19. Marey NA, Ali AA (2023) Novel measurement and control system of universal journal bearing test rig for marine applications. Alexandria Eng J 73:11–26. https://doi.org/10.1016/j.aej.2023.04.006
20. Marey N, Hegazy E, El-Gamal H, Ali A, Abd-El-Ghany R (2022) Universal journal bearing test rig uncertainty and validation measurement to enhance marine shafting performance. In: International maritime transport and logistics conference "Marlog 11", Alexandria, pp 258–275

Generalized Thermo-microstretch with Harmonic Wave for Mode-I Crack Problem Under Three Theories by Using a Laser Pulse with Non-Gaussian Form Temporal Profile

Wafaa Hassan and Khaled Lotfy

1 Introduction

Excitation of thermoelastic waves by a pulsed laser is of great interest due to extensive applications in material processing, non- destructive detecting and characterization. When a solid is illuminated with a laser pulse, absorption of the laser pulse results in a localized temperature increase, which in turn causes thermal expansion and generates a thermoelastic wave. In ultra-short pulsed laser heating, two effects become important. One is the non-Fourier's effect in heat conduction which is a modification of the Fourier heat conduction theory to account for the effect of mean free time (thermal relaxation time) in the energy carrier's collision process. Consideration of the non-Fourier effect also eliminates the paradox of the infinite heat propagation speed [1, 2]. The other is the dissipation of the stress wave due to coupling between temperature and strain rate, which causes transform of mechanical energy associated with the stress wave to the thermal energy of the material.

The elasticity linear theory is of paramount importance in the stress analysis of steel, which is the commonest engineering structural material. To a lesser extent, linear elasticity describes the mechanical behavior of the other common solid materials, e.g. concrete, wood and coal. However, the theory does not apply to the behavior of many of the new synthetic materials of the clastomer and polymer type, e.g. polymethyl-methacrylate, polyethylene and polyvinyl chloride. The linear theory of

W. Hassan (✉)
Physics and Mathematical Engineering Department, Faculty of Engineering, Port Said University, Port Said, Egypt
e-mail: wafaa.hassan@eng.psu.edu.eg

K. Lotfy
Mathematics Department, Faculty of Science, Zagazig University, Zagazig, Egypt
e-mail: khlotfy@zu.edu.eg

micropolar elasticity is adequate to represent the behavior of such materials. For ultrasonic waves i.e. for the case of elastic vibrations characterized by high frequencies and small wavelengths, the influence of the body microstructure becomes significant. This influence of microstructure results in the development of new types of waves which are not in the classical theory of elasticity. Metals, polymers, composites, solids, rocks, concrete are typical media with microstructures. More generally, most of the natural materials including engineering, geological and biological media possess a micro-structure. Eringen and Şuhubi [1] and Eringen [2] developed the linear theory of micropolar elasticity. Othman [3] studied the relaxation effects on thermal shock problems in elastic half space of generalized magneto-thermoelastic waves under three theories. Othman [4] constructed a model of the two-dimensional equations of generalized magneto-thermoelasticity with two relaxation times in an isotropic elastic medium with the modulus of elasticity being dependent on the reference temperature. Eringen [5] introduced the theory of microstretch elastic solids. This theory is a generalization of the theory of micropolar elasticity [2, 6] and a special case of the micromorphic theory. The material points of microstretch elastic solids can stretch and contract independently of their translations and rotations. The microstretch continua is used to characterize composite materials and various porous media [7]. The basic results in the theory of micro stretch elastic solids were obtained in the literature [8–11].

The theory of thermomicrostretch elastic solids was introduced by Eringen [7]. In the frame-work of the theory of thermomicrostretch solids Eringen established a uniqueness theorem for the mixed initial-boundary value problem. The theory was illustrated through the solution of one dimensional waves and compared with lattice dynamical results. The asymptotic behavior of solutions and an existence result were presented by Bofill and Quintanilla [12]. A reciprocal theorem and a representation of Galerkin type were presented by De Cicco and Nappa [13]. De Cicco and Nappa [14] extended a linear theory of thermomicrostretch elastic solids that permits the transmission of heat as thermal waves at finite speed. The theory is based on the entropy production inequality proposed by Green and Laws [15]. In [14], the uniqueness of the solution of the mixed initial-boundary-value problem is also investigated. The basic results and an extensive review on the theory of thermomicrostretch elastic solids can be found in the book of Eringen [8]. The coupled theory of thermoelasticity has been extended by including the thermal relaxanon time in the constitutive equations by Lord and Shulman [16] and Green and Lindsay [17]. These theories eliminate the paradox of infinite velocity of heat propagation and are termed generalized theories of thermoelasticity. A laser is a device that emits light through a process of optical amplification based on the stimulated emission of electromagnetic radiation.

Othman and Lotfy [18] studied two-dimensional problem of generalized magneto-thermoelasticity under the effect of temperature dependent properties. Othman and Lotfy [19] studied transient disturbance in a half-space under generalized magneto-thermoelasticity with moving internal heat source. Othman and Lotfy [20] studied the plane waves in generalized thermo-microstretch elastic half-space by using a

general model of the equations of generalized thermo-microstretch for a homogeneous isotropic elastic half space. Othman and Lotfy [21] studied the generalized thermo-microstretch elastic medium with temperature dependent properties for different theories. Othman and Lotfy [22] studied the effect of magnetic field and inclined load in micropolar thermoelastic medium possessing cubic symmetry under three theories. The normal mode analysis was used to obtain the exact expression for the temperature distribution, thermal stresses, and the displacement components.

In the recent years, considerable efforts have been devoted the study of failure and cracks in solids. This is due to the application of the latter generally in industry and particularly in the fabrication of electronic components. Most of the studies of dynamical crack problem are done using the equations of coupled or even uncoupled theories of thermoelasticity [23–31]. This is suitable for most situations where long time effects are sought. However, when short times are important, as in many practical situations, the full system of generalized thermoelastic equations must be used [16].

The Effect of Thermal Loading Due to Laser Pulse in Generalized Thermoelastic Medium with Voids in Dual Phase Lag Model is studied by [32, 33], they used A normal mode method is proposed to analyze the problem and obtain numerical solutions for the displacement components, stresses, temperature distribution and change in the volume fraction field in a material with homogeneous isotropic elastic half-space and heated by a non-Gaussian laser beam with pulse duration of 8 ps. the photothermal effects generated in a half-space semiconducting medium by a uniform laser radiation using the modified Green–Lindsay theory is studied by [34]. A new model based on the coupling of thermoelasticity, plasma, and microelongation effect under absorption of laser pulse having spatial and temporal Gaussian distributions are studied by [35]. They applied Three different thermoelasticity theories to construct the new model in a 2D thermoelastic semiconducting medium whose properties are temperature-dependent.

The purpose of the present paper is to obtain the normal displacement, temperature, normal force stress, and tangential couple stress in a microstretch elastic solid heated by a laser pulse with non-Gaussian form temporal profile $f(t)$. The normal mode analysis used for the problem of generalized thermo-microstretch for an infinite space weakened by a finite linear opening Mode-I crack is solving for the considered variables. The distributions of the considered variables are represented graphically.

A comparison is carried out among the temperature, stresses and displacements as calculated from the generalized thermoelasticity (LS), (GL) and (CD) theories for the propagation of waves in semi-infinite microstretch elastic solids.

2   The Non-Gaussian Laser Pulse

If we consider the medium is heated uniformly by a laser pulse with non-Gaussian form temporal profile $f(t)$ is represented as,

$$f(t) = \frac{I_0 t}{t_0^2} \exp\left(-\frac{t}{t_0}\right) \tag{1}$$

The conduction heat transfer in the medium can be modeled as a one-dimensional problem with an energy source Q near the surface, we can written in the form

$$Q = \frac{1 - R}{\delta} \exp\left(\frac{x - h/2}{\delta}\right) f(t) \tag{2}$$

where Q is the heat input of laser pulse. From Eqs. (1) and (2), we get

$$Q = \frac{B_a I_0}{\delta t_0^2} t \exp\left(\frac{x - h/2}{\delta} - \frac{t}{t_0}\right) \tag{3}$$

where t_0 is the pulse rise time, δ is the absorption depth of heating energy and B_a is the surface reflectivity. I_0 is the laser intensity which is defined as the total energy carried by a laser pulse per unit area of the laser beam.

When we consider the laser pulse lie on the surface of the medium when $x = 0$, we get the energy source in the form

$$Q = \frac{B_a I_0}{\delta t_0^2} t \exp\left(\frac{-h/2}{\delta} - \frac{t}{t_0}\right). \tag{4}$$

The model of heat conduction equation of two temperature subjected to the memory-dependent derivatives under the influence of laser pulse, can be written in the form

$$\left(1 + \tau_0 \frac{\partial}{\partial t}\right)\left(\rho C_E \frac{\partial T(x, t)}{\partial t} + \gamma T_0 \frac{\partial e(x, t)}{\partial t} - \rho Q\right) = K \nabla^2 T(x, t) \tag{5}$$

3   Formulation of Problem

Following Eringen [3], Green and Lindsay [15] and Lord and Şhulman [16], the constitutive equations and field equations for a linear isotropic generalized thermo-microstretch elastic solid in the absence of body forces are obtained. We consider Cartesian coordinate system (x, y, z) having origin on the surface y = 0 and z-axis pointing vertically into the medium, the region G given by G =
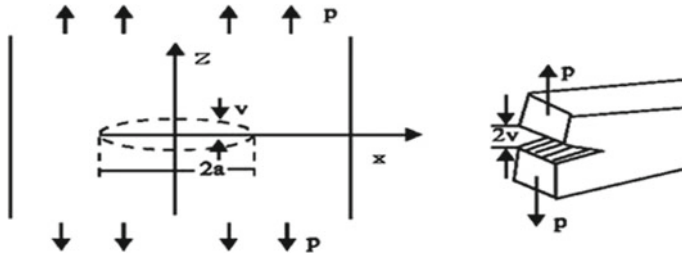
Fig. 1 Displacement of an external Mode-I crack

$\{(x, y, z)|, -\infty < x < \infty, -\infty < z < \infty\}$, with a crack on the x-axis, $|x| \leq a$, is considered. The crack surface is subjected to a known temperature and normal stresses distributions. There are many types of crack and this study will be devoted to Mode-I shown in Fig. 1.

The fundamental system of field equations consists of the equations of motion for a linear, isotropic generalized thermo-microstretch elastic soiled medium are given by

$$(\lambda + \mu)\nabla(\nabla.\vec{u}) + (\mu + k)\nabla^2 u + k(\nabla \times \vec{\varphi}) + \lambda_0 \nabla \varphi^* - \hat{\gamma}\left(1 + v_0\frac{\partial}{\partial t}\right)\nabla T = \rho\frac{\partial^2 \vec{u}}{\partial t^2} \qquad (6)$$

$$(\alpha + \beta + \gamma)\nabla(\nabla.\vec{\varphi}) - \gamma\nabla \times (\nabla \times \vec{\varphi}) + k(\nabla \times \vec{u}) - 2k\vec{\varphi} = j\rho\frac{\partial^2 \vec{\varphi}}{\partial t^2} \qquad (7)$$

$$\alpha_0\nabla^2\varphi^* - \frac{1}{3}\lambda_1\varphi^* - \frac{1}{3}\lambda_0(\nabla.\vec{u}) + \frac{1}{3}\hat{\gamma}_1\left(1 + v_0\frac{\partial}{\partial t}\right)T = \frac{3}{2}\rho j\frac{\partial^2\varphi^*}{\partial t^2} \qquad (8)$$

$$\left(1 + \tau_0\frac{\partial}{\partial t}\right)\left(\rho C_E\frac{\partial T(x, t)}{\partial t} + \gamma T_0\frac{\partial e(x, t)}{\partial t} - \rho Q\right) + \hat{\gamma}_1 T_0\frac{\partial\varphi^*}{\partial t} = K\nabla^2 T(x, t) \qquad (9)$$

$$K\nabla^2 T = \rho C_E\left(n_1 + \tau_0\frac{\partial}{\partial t}\right)\dot{T} + \hat{\gamma}_1 T_0\left(n_1 + n_0\tau_0\frac{\partial}{\partial t}\right)\dot{e}$$
$$+ \hat{\gamma}_1 T_0\frac{\partial.\varphi^*}{\partial t} + \rho\left(n_1 + n_0\tau_0\frac{\partial}{\partial t}\right)Q \qquad (10)$$

The constitutive law for the theory of generalized thermoelasticity with two relaxation times

$$\sigma_{il} = (\lambda_0\varphi^* + \lambda u_{r,r})\delta_{il} + (\mu + k)u_{l,i} + \mu u_{i,l} - k\varepsilon_{i,l,r}\varphi_r - \hat{\gamma}\left(1 + v_0\frac{\partial}{\partial t}\right)T\delta_{il} \qquad (11)$$

The field equations and constitutive relations for thermo-microstretch generalized thermoelastic medium

$$m_{il} = \alpha \varphi_{r,r} \delta_{il} + \beta \varphi_{i,l} + \gamma \varphi_{l,i} \tag{12}$$

$$\lambda_i = \alpha_0 \varphi_i^* \tag{13}$$

The relation between strain–displacement is:

$$e = \frac{\partial u}{\partial x} + \frac{\partial v}{\partial y} + \frac{\partial w}{\partial z}. \tag{14}$$

The state of plane strain parallel to the xz-plane is defined by

$$u_1 = u(x, z, t), \, u_2 = 0, \, u_3 = w(x, z, t), \, \varphi_1 = \varphi_3 = 0, \, \varphi_2 = \varphi_2(x, z, t),$$
$$\varphi^* = \varphi^*(x, z, t) \tag{15}$$

The field Eqs. (6)–(10) reduce to

$$(\lambda + \mu)\left(\frac{\partial^2 u}{\partial x^2} + \frac{\partial^2 w}{\partial x \partial z}\right) + (\mu + k)\left(\frac{\partial^2 u}{\partial x^2} + \frac{\partial^2 u}{\partial z^2}\right) - k\frac{\partial \phi_2}{\partial z} + \lambda_0 \frac{\partial \varphi^*}{\partial x}$$
$$- \hat{\gamma}\left(1 + v_0 \frac{\partial}{\partial t}\right)\frac{\partial T}{\partial t} = \rho \frac{\partial^2 u}{\partial t^2} \tag{16}$$

$$(\lambda + \mu)\left(\frac{\partial^2 u}{\partial x \partial z} + \frac{\partial^2 w}{\partial z^2}\right) + (\mu + k)\left(\frac{\partial^2 w}{\partial x^2} + \frac{\partial^2 w}{\partial z^2}\right) + k\frac{\partial \phi_2}{\partial x} + \lambda_0 \frac{\partial \varphi^*}{\partial z}$$
$$- \hat{\gamma}\left(1 + v_0 \frac{\partial}{\partial t}\right)\frac{\partial T}{\partial t} = \rho \frac{\partial^2 w}{\partial t^2} \tag{17}$$

$$\gamma\left(\frac{\partial^2 \phi_2}{\partial x^2} + \frac{\partial^2 \phi_2}{\partial z^2}\right) - 2k\phi_2 + k\left(\frac{\partial u}{\partial z} - \frac{\partial w}{\partial x}\right) = j\rho \frac{\partial^2 \phi_2}{\partial t^2} \tag{18}$$

$$\alpha_0\left(\frac{\partial^2 \varphi^*}{\partial x^2} + \frac{\partial^2 \varphi^*}{\partial z^2}\right) - \frac{1}{3}\lambda_1 \varphi^* - \frac{1}{3}\lambda_0\left(\frac{\partial u}{\partial x} - \frac{\partial w}{\partial z}\right) + \frac{1}{3}\hat{\gamma}_1\left(1 + v_0 \frac{\partial}{\partial t}\right)T = \frac{3}{2}\rho j \frac{\partial^2 \varphi^*}{\partial t^2} \tag{19}$$

$$K\left(\frac{\partial^2 T}{\partial x^2} + \frac{\partial^2 T}{\partial z^2}\right) = \rho C_E\left(n_1 + n_0 \tau_0 \frac{\partial}{\partial t}\right)\frac{\partial T}{\partial t} + \hat{\gamma}T_0\left(n_1 + n_0 \tau_0 \frac{\partial}{\partial t}\right)\frac{\partial e}{\partial t} + \hat{\gamma}_1 T_0 \frac{\partial \varphi^*}{\partial t}$$
$$- \rho\left(n_1 + n_0 \tau_0\left(\frac{1}{t} - \frac{1}{t_0}\right)\right)Q \tag{20}$$

where

$$\hat{\gamma} = (3\lambda + 2\mu + k)\alpha_{t_1}, \, \hat{\gamma}_1 = (3\lambda + 2\mu + k)\alpha_{t_2} \text{ and } \nabla^2 = \frac{\partial^2}{\partial x^2} + \frac{\partial^2}{\partial y^2} \tag{21}$$

The constants $\hat{\gamma}$ and $\hat{\gamma}_1$ depend on mechanical as well as the thermal properties of the body and the dot denotes the partial derivative with respect to time.

Equations (16)–(20) are the field equations of the generalized thermo-microstretch elastic solid, applicable to the (LS) theory, the (GL) theory, as well as the classical coupled theory (CD), as follows:

1. The equations of the coupled thermo-microstretch (CD) theory, when

$$n_0 = 0, \quad n_1 = 1, \quad \tau_0 = v_0 = 0 \tag{22}$$

Equations (16), (17), (19) and (20) has the form

$$\rho \ddot{u} = (\lambda + \mu)\left(\frac{\partial^2 u}{\partial x^2} + \frac{\partial^2 w}{\partial x \partial z}\right) + (\mu + k)\left(\frac{\partial^2 u}{\partial x^2} + \frac{\partial^2 u}{\partial z^2}\right) - k\frac{\partial \phi_2}{\partial z} + \lambda_0 \frac{\partial \varphi^*}{\partial x} - \hat{\gamma}\frac{\partial T}{\partial x}, \tag{23}$$

$$\rho \ddot{w} = (\lambda + \mu)\left(\frac{\partial^2 u}{\partial x \partial z} + \frac{\partial^2 w}{\partial z^2}\right) + (\mu + k)\left(\frac{\partial^2 w}{\partial x^2} + \frac{\partial^2 w}{\partial z^2}\right) + k\frac{\partial \phi_2}{\partial x} + \lambda_0 \frac{\partial \varphi^*}{\partial z} - \hat{\gamma}\frac{\partial T}{\partial z} \tag{24}$$

$$C_3^2\left(\frac{\partial^2 \varphi^*}{\partial x^2} + \frac{\partial^2 \varphi^*}{\partial z^2}\right) - C_4^2 \varphi^* - C_5^2\left(\frac{\partial u}{\partial x} + \frac{\partial w}{\partial z}\right) + C_6^2 T = \frac{\partial^2 \varphi^*}{\partial t^2} \tag{25}$$

$$K\left(\frac{\partial^2 T}{\partial x^2} + \frac{\partial^2 T}{\partial z^2}\right) = \rho C_E \frac{\partial T}{\partial t} + \hat{\gamma}T_0 \frac{\partial e}{\partial t} + \hat{\gamma}_1 T_0 \frac{\partial \varphi^*}{\partial t} - \rho Q \tag{26}$$

The constitutive relation can be written as

$$\sigma_{xx} = \lambda_0 \varphi^* + (\lambda + 2\mu + k)\frac{\partial u}{\partial x} + \lambda \frac{\partial w}{\partial z} - \hat{\gamma}T \tag{27}$$

$$\sigma_{zz} = \lambda_0 \varphi^* + (\lambda + 2\mu + k)\frac{\partial w}{\partial z} + \lambda \frac{\partial u}{\partial x} - \hat{\gamma}T \tag{28}$$

$$\sigma_{xz} = \mu\frac{\partial u}{\partial z} + (\mu + k)\frac{\partial w}{\partial x} + k\varphi_2 \tag{29}$$

$$\sigma_{zx} = \mu\frac{\partial w}{\partial x} + (\mu + k)\frac{\partial u}{\partial z} + k\varphi_2 \tag{30}$$

$$m_{xy} = \hat{\gamma}\frac{\partial \varphi_2}{\partial x} \tag{31}$$

$$m_{zy} = \hat{\gamma}\frac{\partial \varphi_2}{\partial z}. \tag{32}$$

where

$$c_3^2 = \frac{2\alpha_0}{3\rho j}, \quad c_4^2 = \frac{2\lambda_1}{9\rho j}, \quad c_5^2 = \frac{2\lambda_0}{9\rho j}, \quad c_6^2 = \frac{2\hat{\gamma}_1}{9\rho j} \tag{33}$$

2. Lord-Shulman (LS) theory, when

$$n_1 = n_0 = 1, \quad v_0 = 0, \quad \tau_0 > 0. \tag{34}$$

Equations (16), (17) and (19) are the same as Eqs. (23), (24) and (25) and Eq. (20) has the form

$$K\left(\frac{\partial^2 T}{\partial x^2} + \frac{\partial^2 T}{\partial z^2}\right) = \left(\frac{\partial}{\partial t} + \tau_0 \frac{\partial^2}{\partial t^2}\right)\{\rho C_E T + \hat{\gamma} T_0 e\} + \hat{\gamma}_1 T_0 \frac{\partial \varphi^*}{\partial t}$$

$$- \rho\left(1 + \tau_0\left(\frac{1}{t} - \frac{1}{t_0}\right)\right)Q \tag{35}$$

3. Green-Lindsay (G L) theory, when

$$n_1 = 1, \quad n_0 = 0, \quad v_0 \geq \tau_0 > 0 \tag{36}$$

Equations (16), (17) and (19) remain unchanged and Eq. (20) has the form

$$K\left(\frac{\partial^2 T}{\partial x^2} + \frac{\partial^2 T}{\partial z^2}\right) = \rho C_E\left(1 + \tau_0 \frac{\partial}{\partial t}\right)\frac{\partial T}{\partial t} + \hat{\gamma} T_0 \frac{\partial e}{\partial t} + \hat{\gamma}_1 T_0 \frac{\partial \varphi^*}{\partial t} - \rho Q \tag{37}$$

4. The corresponding equations for the generalized micropolar thermo-elasticity without stretch can be obtained from the above mentioned cases by taking:

$$\alpha_0 = \lambda_0 = \lambda_1 = \varphi^* = 0$$

For convenience, the following non-dimensional variables are used:

$$\bar{x}_i = \frac{\omega^*}{C_2}x_i, \quad \bar{u}_i = \frac{\rho C_2 \omega^*}{\hat{\gamma} T_0}u_i, \quad \bar{t} = \omega^* t,$$

$$\bar{\tau}_0 = \omega^* \tau_0, \quad \bar{v}_0 = \omega^* v_0, \quad \bar{T} = \frac{T}{T_0}, \quad \bar{\sigma}_{ij} = \frac{\sigma_{ij}}{\hat{\gamma} T_0}$$

$$\bar{m}_{ij} = \frac{\omega^*}{C_2 \hat{\gamma} T_0}m_{ij}, \quad \bar{\varphi}_2 = \frac{\rho C_2}{\hat{\gamma} T_0}\varphi_2, \quad \bar{\lambda}_3 = \frac{\omega^*}{C_2 \hat{\gamma} T_0}\lambda_3,$$

$$\bar{\varphi}^* = \frac{\rho C_2^2}{\hat{\gamma} T_0}\varphi^*, \quad \omega^* = \frac{\rho C_E C_2^2}{K}, \quad C_2^2 = \frac{\mu}{\rho} \tag{38}$$

Using Eq. (38), Eqs. (16)–(20) become (dropping the dashed for convenience)

$$\frac{\partial^2 u}{\partial t^2} = \frac{(\mu + k)}{\rho C_2^2}\nabla^2 u + \frac{(\mu + \lambda)}{\rho C_2^2}\frac{\partial e}{\partial x} - \frac{k}{\rho C_2^2}\frac{\partial \phi_2}{\partial z} + \frac{\lambda_0}{\rho C_2^2}\frac{\partial \varphi^*}{\partial x} - \left(1 + v_0 \frac{\partial}{\partial t}\right)\frac{\partial T}{\partial x} \tag{39}$$

$$\frac{\partial^2 w}{\partial t^2} = \frac{(\mu + k)}{\rho C_2^2} \nabla^2 w + \frac{(\mu + \lambda)}{\rho C_2^2} \frac{\partial e}{\partial z} + \frac{k}{\rho C_2^2} \frac{\partial \varphi_2}{\partial x} + \frac{\lambda_0}{\rho C_2^2} \frac{\partial \varphi^*}{\partial z} - \left(1 + v_0 \frac{\partial}{\partial t}\right) \frac{\partial T}{\partial z}$$
(40)

$$\frac{j \rho C_2^2}{\gamma} \frac{\partial^2 \phi_2}{\partial t^2} = \nabla^2 \phi_2 - \frac{2k C_2^2}{\hat{\gamma} \omega^*} \phi_2 + \frac{k C_2^2}{\gamma \omega^{*2}} \left(\frac{\partial u}{\partial z} - \frac{\partial w}{\partial x}\right)$$
(41)

$$\left(\frac{C_3^2}{C_2^2} \nabla^2 - \frac{C_4^2}{\omega^{*2}} - \frac{\partial^2}{\partial t^2}\right) \varphi^* - \frac{C_5^2}{\omega^{*2}} e + a_9 \left(1 + v_0 \frac{\partial}{\partial t}\right) T = 0$$
(42)

$$\nabla^2 T - \left(n_1 + n_0 \tau_0 \frac{\partial}{\partial t}\right) \frac{\partial T}{\partial t} + \frac{\hat{\gamma}^2 T_0}{\rho K \omega^*} \left(n_1 + n_0 \tau_0 \frac{\partial}{\partial t}\right) \frac{\partial e}{\partial t} = \frac{\hat{\gamma} \hat{\gamma}_1 T_0}{\rho K \omega^*} \frac{\partial \varphi^*}{\partial t}$$

$$- \frac{\rho}{K \omega^*} \left(n_1 + n_0 \tau_0 \left(\frac{1}{t} - \frac{1}{t_0}\right)\right) Q$$
(43)

Assuming the scalar potential functions $\varphi(x, z, t)$ and $\psi(x, z, t)$ defined by the relations in the non-dimensional form:

$$u = \frac{\partial \varphi}{\partial x} - \frac{\partial \psi}{\partial z}, \quad w = \frac{\partial \varphi}{\partial z} - \frac{\partial \psi}{\partial x}.$$
(44)

Using (38) in Eqs. (39)–(43), we obtain.

$$\left[\nabla^2 - a_0 \frac{\partial^2}{\partial t^2}\right] \varphi - a_0 \left(1 + v_0 \frac{\partial}{\partial t}\right) T + a_1 \varphi^* = 0$$
(45)

$$\left[\nabla^2 - a_2 \frac{\partial^2}{\partial t^2}\right] \psi - a_3 \phi_2 = 0$$
(46)

$$\left[\nabla^2 - 2a_4 - a_5 \frac{\partial^2}{\partial t^2}\right] \phi_2 - a_4 \nabla^2 \psi = 0$$
(47)

$$\left[a_6 \nabla^2 - a_7 - \frac{\partial^2}{\partial t^2}\right] \varphi^* - a_8 \nabla^2 \varphi + a_9 \left(1 + v_0 \frac{\partial}{\partial t}\right) T = 0$$
(48)

$$\left[\nabla^2 - \left(n_1 \frac{\partial}{\partial t} + n_0 \tau_0 \frac{\partial^2}{\partial t^2}\right)\right] T - \varepsilon \left(n_1 \frac{\partial}{\partial t} + n_0 \tau_0 \frac{\partial^2}{\partial t^2}\right) \nabla^2 \varphi - \varepsilon_1 \frac{\partial \varphi^*}{\partial t} = \varepsilon_2 Q \quad (49)$$

where

$$c_1^2 = \frac{\lambda + 2\mu + k}{\rho}, \quad a_0 = \frac{C_2^2}{C_1^2}, \quad a_1 = \frac{\lambda_0}{\lambda + 2\mu + k}, \quad a_2 = \frac{\rho C_2^2}{\mu + k}, \quad a_3 = \frac{k}{\mu + k},$$

$$a_4 = \frac{kC_2^2}{\gamma \omega^{*2}}, \quad a_5 = \frac{\rho j C_2^2}{\gamma}, \quad a_6 = \frac{C_3^2}{C_2^2}, \quad a_7 = \frac{C_4^2}{\omega^{*2}}, \quad a_8 = \frac{C_5^2}{\omega^{*2}}, \quad a_9 = \frac{2\hat{\gamma_1} C_2^2}{9\hat{\gamma} j \omega^{*2}},$$

$$\varepsilon = \frac{\hat{\gamma}^2 T_0}{\rho \omega^* K}, \quad \varepsilon_1 = \frac{\hat{\gamma} \hat{\gamma_1} T_0}{\rho \omega^* K}, \quad \varepsilon_2 = \frac{\rho}{K \omega^*} \left(n_1 + n_0 \tau_0 \left(\frac{1}{t} - \frac{1}{t_0} \right) \right). \tag{50}$$

The solution of the considered physical variables can be decomposed in terms of normal mode as the following form:

$$[\varphi, \psi, \varphi^*, \varphi_2, \sigma_{il}, m_{il}, T](x, z, t) = [\overline{\varphi}(x), \overline{\psi}(x), \overline{\varphi}^*(x), \overline{\varphi}_2(x), \overline{\sigma}_{il}(x), \overline{m}_{il}(x), \overline{T}(x)]$$
$$\times \exp(\omega t + i\, a\, z) \tag{51}$$

where $[\overline{\varphi}, \overline{\psi}, \overline{\varphi}^*, \overline{\varphi}_2, \overline{\sigma}_{il}, \overline{m}_{il}, \overline{T}](x)$ are the amplitude of the functions ω is a complex and a is the wave number in the z-direction.

Using Eq. (51), then Eqs. (45)–(49) become respectively,

$$(D^2 - A_1)\overline{\varphi} - A_2\overline{T} + a_1\overline{\varphi}^* = 0, \tag{52}$$

$$(D^2 - A_3)\overline{\psi} - a_3\overline{\varphi}_2 = 0 \tag{53}$$

$$(D^2 - A_4)\overline{\varphi}_2 - a_4(D^2 - a^2)\overline{\psi} = 0 \tag{54}$$

$$(a_6 D^2 - A_5)\overline{\varphi}^* - a_8(D^2 - a^2)\overline{\varphi} + A_8\overline{T} = 0 \tag{55}$$

$$\left[(D^2 - a^2) - A_6 \right]\overline{T} - A_7(D^2 - a^2)\overline{\varphi} - \varepsilon_1 \omega \overline{\varphi}^* = 0 \tag{56}$$

where

$$D = \frac{d}{dx}, \quad A_1 = a^2 + a_0 \omega^2 \tag{57}$$

$$A_2 = a_0(1 + v_0 \omega), \tag{58}$$

$$A_3 = a^2 + a_2 \omega^2 \tag{59}$$

$$A_4 = a^2 + 2a_4 + a_5 \omega^2 \tag{60}$$

$$A_5 = a^2 a_6 + a_7 + \omega^2, \tag{61}$$

$$A_6 = \omega(n_1 + \tau_0 \omega) \tag{62}$$

$$A_7 = \varepsilon \omega(n_1 + n_0 \tau_0 \omega) \tag{63}$$

$$A_8 = a_9(1 + v_0 \omega) \tag{64}$$

Eliminating $\overline{\varphi}_2$, $\overline{\psi}$ between Eqs. (53) and (54), we get the following fourth order ordinary differential equation satisfied by $\overline{\varphi}_2$ and $\overline{\psi}$

$$\left[D^4 - AD^2 + B\right]\{\overline{\varphi}_2(x), \overline{\psi}(x)\} = 0. \tag{65}$$

Eliminating $\overline{\varphi}$, $\overline{T}$ and $\overline{\varphi}^*$ between Eqs. (52) and (55) we obtain the following sixth order ordinary differential equation satisfied by $\overline{\varphi}^*(x)$, $\overline{\varphi}(x)$ and $\overline{T}(x)$

$$\left[D^6 - CD^4 + ED^2 - H\right]\{\overline{\varphi}^*(x), \overline{\varphi}(x), \overline{T}(x)\} = 0 \tag{66}$$

where

$$A = A_3 + A_4 + a_3 a_4 \tag{67}$$

$$B = A_3 A_4 + a^2 a_3 a_4 \tag{68}$$

$$C = \frac{g_3(g_7 + g_8) - g_5}{g_3} \tag{69}$$

$$E = \frac{a^2 g_3 g_8 + \varepsilon_1 \omega g_1 A_2 - g_6 - g_5 g_7 - g_4 g_8}{g_3} \tag{70}$$

$$H = \frac{a^2 g_4 g_8 + g_6 g_7 - \varepsilon_1 \omega g_2 A_2}{g_3} \tag{71}$$

$$g_1 = A_8 - a_8 A_2, \quad g_2 = a^2 a_8 A_2 - A_1 A_8, \quad g_3 = a_6 A_2, \quad g_4 = a_1 A_8 + A_5 A_2,$$
$$g_5 = g_4 - A_1 g_3 - a_1 g_1, \quad g_6 = A_1 g_4 + a_1 g_2, \quad g_7 = a^2 A_6 + A_7, \quad g_8 = A_2 A_8 \tag{72}$$

The solution of Eqs. (65) and (66), has the form

$$\overline{\psi}(x) = \sum_{j=1}^{2} M_j(a, \omega) e^{-k_j x} \tag{73}$$

$$\overline{\varphi}_2(x) = \sum_{j=1}^{2} M_j'(a, \omega)e^{-k_j x} \tag{74}$$

$$\overline{\varphi}(x) = \sum_{n=3}^{5} M_n(a, \omega)e^{-k_n x} \tag{75}$$

$$\overline{\varphi}^*(x) = \sum_{n=3}^{5} M_n'(a, \omega)e^{-k_n x} \tag{76}$$

$$\overline{T}(x) = \sum_{n=3}^{5} M_n''(a, \omega)e^{-k_n x} \tag{77}$$

where $M_j(a, \omega)$, $M_j'(a, \omega)$, $M_n(a, \omega)$, $M_n'(a, \omega)$ and $M_n''(a, \omega)$ are some parameters depending on a and ω. k_j^2, $(j = 1, 2)$ are the roots of the characteristic equation of Eq. (65) and k_n^2, $(n = 3, 4, 5)$ are the roots of the characteristic equation of Eq. (66).

Using Eqs. (73)–(77) into Eqs. (52) and (56) we get the following relations

$$\overline{\varphi}_2(x) = \sum_{j=1}^{2} a_j^* M_j(a, \omega)e^{-k_j x} \tag{78}$$

$$\overline{\varphi}^*(x) = \sum_{n=3}^{5} b_n^* M_n(a, \omega)e^{-k_n x} \tag{79}$$

$$\overline{T}(x) = \sum_{n=3}^{5} c_n^* M_n(a, \omega)e^{-k_n x}. \tag{80}$$

where

$$a_j^* = \frac{\left(k_j^2 - A_3\right)}{a_3}, \quad j = 1, 2, \tag{81}$$

$$b_n^* = \frac{g_1 k_n^2 + g_2}{g_3 k_n^2 + g_4}, \quad n = 3, 4, 5, \tag{82}$$

$$c_n^* = \frac{g_3 k_n^4 + g_5 k_n^2 - g_6}{A_2(g_3 k_n^2 + g_4)}, \quad n = 3, 4, 5 \tag{83}$$

4 Application

The plane boundary subjects to an instantaneous normal point force and the boundary surface is isothermal, the boundary conditions at the vertical plan $y = 0$ and in the beginning of the crack at $x = 0$ are

$$\sigma_{zz} = -p(x), \quad |x| < a \quad T = f(x), |x| < a \text{ and } \frac{\partial T}{\partial z} = 0 \quad |x| > a$$

$$\sigma_{xz} = 0, \quad -\infty < x < \infty \tag{84}$$

$$m_{xy} = 0, \quad -\infty < x < \infty$$
$$\lambda_z = 0, \quad -\infty < x < \infty$$

Using (38), (44), (45)–(49) with the non-dimensional boundary conditions and using (73), (75), (78)–(80), we obtain the expressions of displacement components, force stress, coupled stress and temperature distribution for microstretch generalized thermoelastic medium as follows:

$$\overline{u}(x) = ia(M_1 e^{-k_1 x} + M_2 e^{-k_2 x}) - k_3 M_3 e^{-k_3 x} - k_4 M_4 e^{-k_4 x} - k_5 M_5 e^{-k_5 x} \tag{85}$$

$$\overline{v}(x) = k_1 M_1 e^{-k_1 x} + k_2 M_2 e^{-k_2 x} + ia(M_3 e^{-k_3 x} + k_4 M_4 e^{-k_4 x} + k_5 M_5 e^{-k_5 x}) \tag{86}$$

$$\overline{\sigma}_{zz}(x) = s_1 M_1 e^{-k_1 x} + s_2 M_2 e^{-k_2 x} + s_3 M_3 e^{-k_3 x} + s_4 M_4 e^{-k_4 x} + s_5 M_5 e^{-k_5 x} \tag{87}$$

$$\overline{\sigma}_{xz}(x) = r_1 M_1 e^{-k_1 x} + r_2 M_2 e^{-k_2 x} + r_3 M_3 e^{-k_3 x} + r_4 M_4 e^{-k_4 x} + r_5 M_5 e^{-k_5 x} \tag{88}$$

$$\overline{m}_{xy}(x) = q_1 M_1 e^{-k_1 x} + q_2 M_2 e^{-k_2 x} \tag{89}$$

$$\overline{T}(x) = c_3^* M_3 e^{-k_3 x} + c_4^* M_4 e^{-k_4 x} + c_5^* M_5 e^{-k_5 x} \tag{90}$$

$$\lambda_z = f_8 (b_3^* M_3 e^{-k_3 x} + b_4^* M_4 e^{-k_4 x} + b_5^* M_5 e^{-k_5 x}) \tag{91}$$

where

$$s_1 = iak_1(f_2 - f_3), \quad s_2 = iak_2(f_2 - f_3), \quad s_3 = f_1 b_3^* - a^2 f_2 + f_3 k_3^2 - c_3^*(1 + v_0\omega),$$
$$s_4 = f_1 b_4^* - a^2 f_2 + f_3 k_4^2 - c_4^*(1 + v_0\omega), \quad s_5 = f_1 b_5^* - a^2 f_2 + f_3 k_5^2 - c_5^*(1 + v_0\omega),$$
$$r_1 = a_1^* f_6 - a^2 f_4 - f_5 k_1^2, \quad r_2 = a_2^* f_6 - a^2 f_4 - f_5 k_2^2, \quad r_3 = -iak_3(f_4 + f_5),$$
$$r_4 = -iak_4(f_4 + f_5), \quad r_5 = iak_5(f_4 + f_5), \quad q_1 = -f_7 a_1^* k_1, \quad q_2 = -f_7 a_2^* k_2,$$

$$f_1 = \frac{\lambda_0}{\rho c_2^2}, \quad f_2 = \frac{\lambda + 2\mu + k}{\rho c_2^2}, \quad f_3 = \frac{\lambda}{\rho c_2^2}, \quad f_4 = \frac{\mu}{\rho c_2^2},$$

$$f_5 = \frac{\mu + k}{\rho c_2^2}, \quad f_6 = \frac{k}{\rho c_2^2}, \quad f_7 = \frac{\gamma \omega^{*2}}{\rho c_2^4} \text{ and } f_8 = \frac{\alpha_0 \omega^{*2}}{\rho c_2^4}. \tag{92}$$

Applying the boundary conditions (84) at the surface $x = 0$ of the plate, we obtain a system of five equations. After applying the inverse of matrix method, we obtain the values of the five constants $M_j, j = 1, 2$, and $M_n, n = 3, 4, 5$. Hence, we obtain the expressions of displacements, force stress, couple stress and temperature distribution for microstretch generalized thermoelastic medium.

5 Numerical Result and Discussions

In order to illustrate our theoretical results obtained in the preceding section and to compare these in the context of various theories of thermoelasticity, we now present some numerical results. In the calculation process, we take the case of copper crystal as material subjected to mechanical and thermal disturbances for numerical calculations consider the material medium as that of copper. Since, ω is the complex constant then we taken $\omega = \omega_0 + i\varsigma$. The other constants of the problem are taken as $\omega_0 = -2; \varsigma = 1$; the physical constants used are:

$$\rho = 8954 \text{ kg m}^{-1}, \quad \lambda = 7.76 \times 10^{10} \text{ N/m}^2, \quad T_0 = 293 \text{ K},$$
$$\mu = 3.86 \times 10^{10} \text{ N/m}^2, \quad a = 1, \quad \alpha_t = 1.78 \times 10^{-5} \text{ K}^{-1}$$
$$K = 0.6 \times 10^{-2} \text{ cal/cm s } °C, \quad C_E = 383.1 \text{ J kg}^{-1} \text{ K}^{-1}.$$

The results are shown in Figs. 2, 3, 4, 5, 6, 7, 8, 9, 10, 11, 12, 13, 14 and 15. The graph shows the three curves predicted by different thermoelasticity theories. In these figures, the solid lines represent the solution in the Coupled theory, the dotted lines represent the solution in the generalized Lord and Shulman theory and dashed lines represent the solution derived using the Green and Lindsay theory. We notice that the results for the temperature, the displacement, and stress distribution when the relaxation time is including in the heat equation are distinctly different from those when the relaxation time is not mentioned in heat equation, because the thermal waves in the Fourier's theory of heat equation travel with the propagation infinite speed of as opposed to finite speed in the non-Fourier case. This demonstrates clearly the difference between the coupled and the generalized theories of thermoelasticity.

For the value of z, namely z = 0.1, were substituted in performing the computation. It should be noted (Fig. 2) that in this problem, the crack's size, x is taken to be the length in this problem so that $0 \le x \le 3$, $z = 0$ represents the plane of the crack that is symmetric with respect to the z-plane. It is clear from the graph that T has maximum value at the beginning of the crack ($x = 0$), it begins to fall just near the crack edge (x = 3), where it experiences sharp decreases (with maximum negative
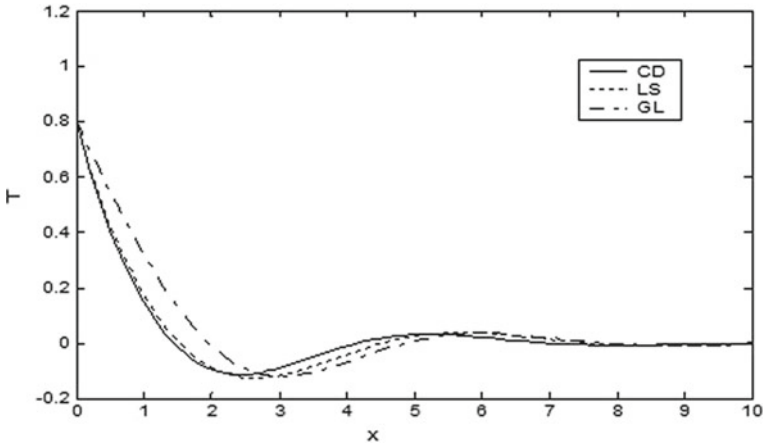
Fig. 2 Variation of temperature distribution T with different theories
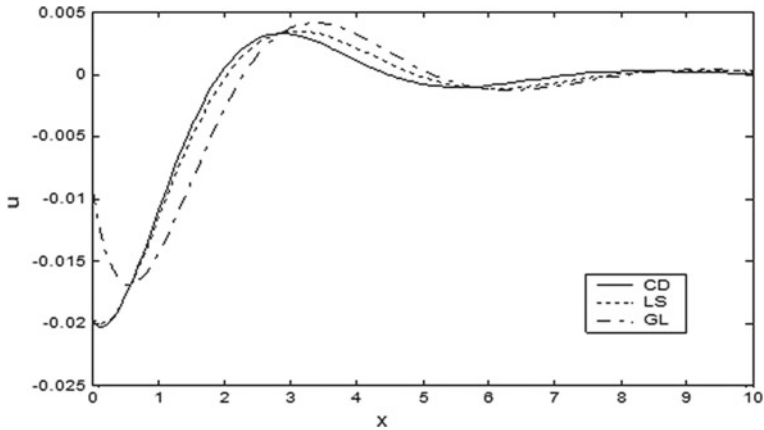
Fig. 3 Variation of displacement distribution u with different theories

gradient at the crack's end). The value of temperature quantity converges to zero with increasing the distance x.

In Fig. 3, the horizontal displacement, u, begins with decrease then smooth increases again to reach its maximum magnitude just at the crack end. Beyond it u falls again to try to retain zero at infinity.

In Fig. 4, the vertical displacement w, we see that the displacement component w always starts from the zero value and terminates at the zero value. Also, at the crack end to reach minimum value, beyond reaching zero at the double of the crack size (state of particles equilibrium).

The displacements u and w show different behaviours because of the elasticity of the solid tends to resist vertical displacements in the problem under investigation.
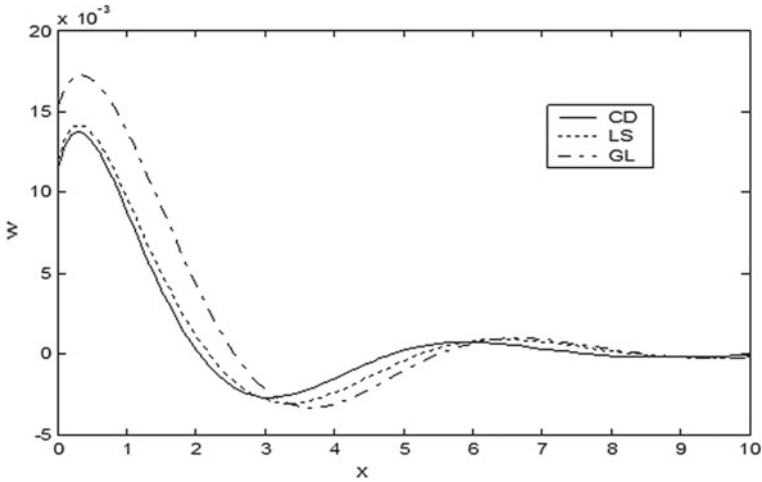
Fig. 4 Variation of displacement distribution w with different theories
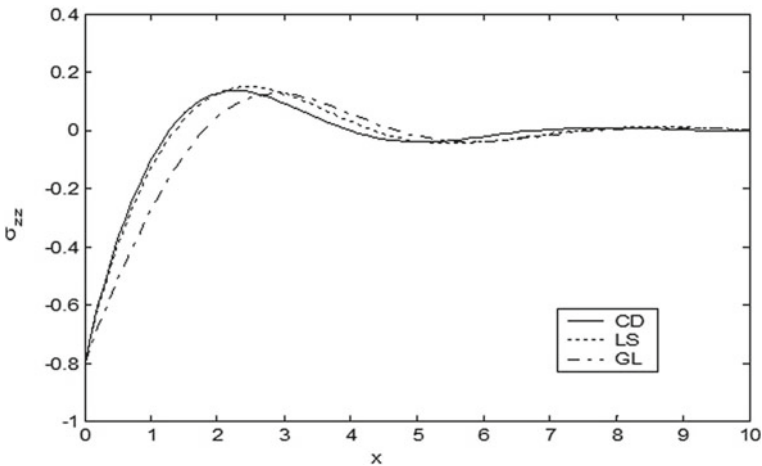
Fig. 5 Variation of stress distribution σ_{zz} with different theories

Both of the components show different behaviours, the former tends to increase to maximum just before the end of the crack. Then it falls to a minimum with a highly negative gradient. Afterwards it rises again to a maximum beyond about the crack end.

The stress component, σ_{zz} reaches coincidence with negative value (Fig. 5) and satisfies the boundary condition at $x = 0$, reaches the maximum value near the end of crack ($x \approx 3$) and converges to zero with increasing the distance x.

In Fig. 6, shows that the stress component σ_{xz} satisfies the boundary condition at x $= 0$ and has a different behaviour. It decreases in the start and decreases (maximum)
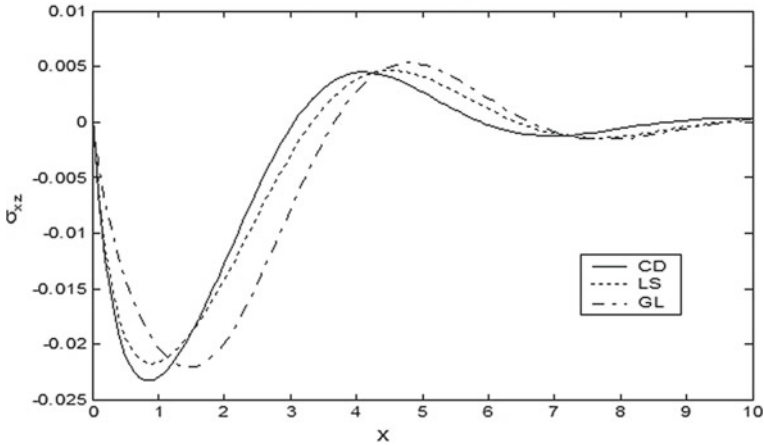
Fig. 6 Variation of stress distribution σ_{xz} with different theories
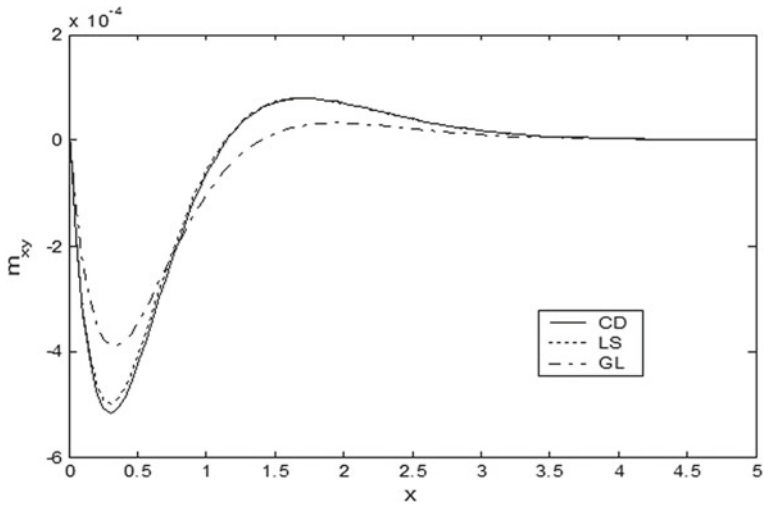
Fig. 7 Variation of tangential couple stress m_{xy} with different theories

in the context of the three theories until reaching the crack end. These trends obey elastic and thermoelastic properties of the solid under investigation.

In Fig. 7, the tangential coupled stress m_{xy} satisfies the boundary condition at x $= 0$.It decreases in the start and then start increases (maximum) in the context of the three theories until reaching the crack end. The value of microstress for λ_z satisfies the boundary condition at x $= 0$, begins with increase then decreases again to reach its minimum magnitude just near the crack end, beyond reaching zero at the double of the crack size (state of particles equilibrium), as depicted in Fig. 8.
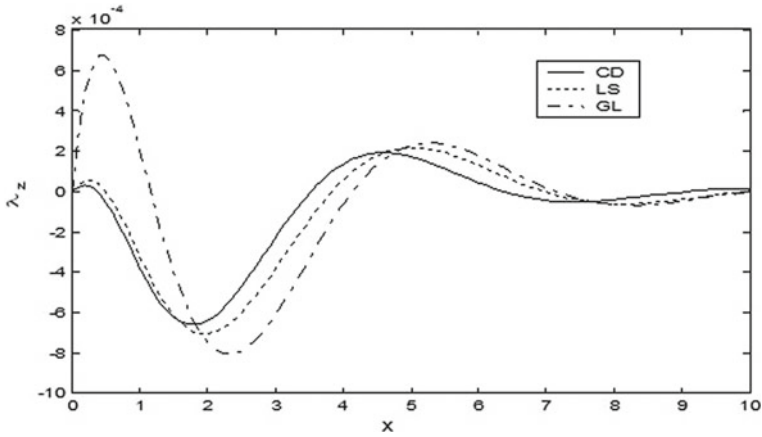
Fig. 8 Variation of microstress λ_z with different theories
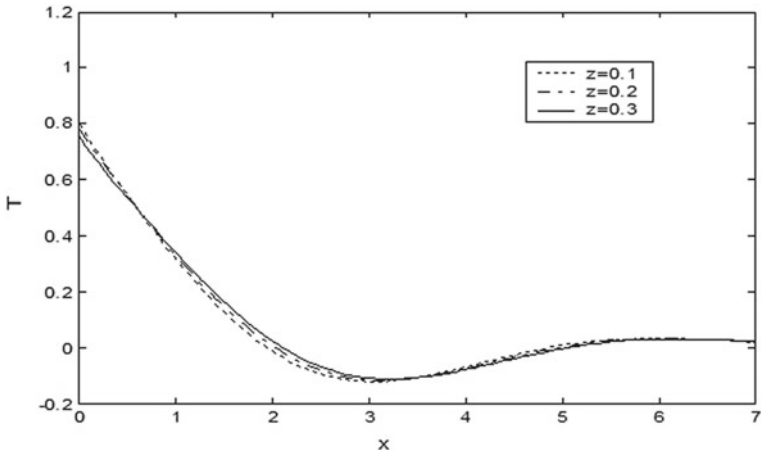
**Fig. 9** Variation of temperature distribution T for different vertical distances, under GL theory

Figures 9, 10, 11, 12, 13, 14 and 15 show the comparison between displacement components u, w, the temperature T, the force stresses components σ_{zz}, σ_{xz}, the tangential coupled stress m_{xy} and the microstress λ_z, the case of different three values of y, (namely z = 0.1, 0.2 and 0.3) under GL theory. It should be noted (Fig. 9) that in this problem. It is clear from the graph that T has maximum value at the beginning of the crack ($x = 0$), it begins to fall just near the crack edge ($x = 3$), where it experiences sharp decreases (with maximum negative gradient at the crack's end). Graph lines for both values of y show different slopes at crack ends according to y-values. In other words, the temperature line for z = 0.1 has the highest gradient when compared with that of z = 0.2 and 0.3 at the first of the range. In addition, all
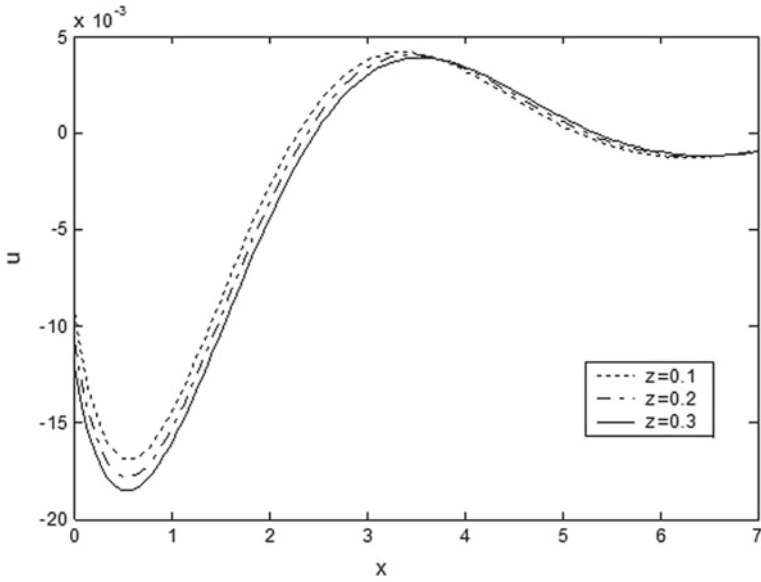
Fig. 10 Variation of displacement distribution u for different vertical distances, under GL theory
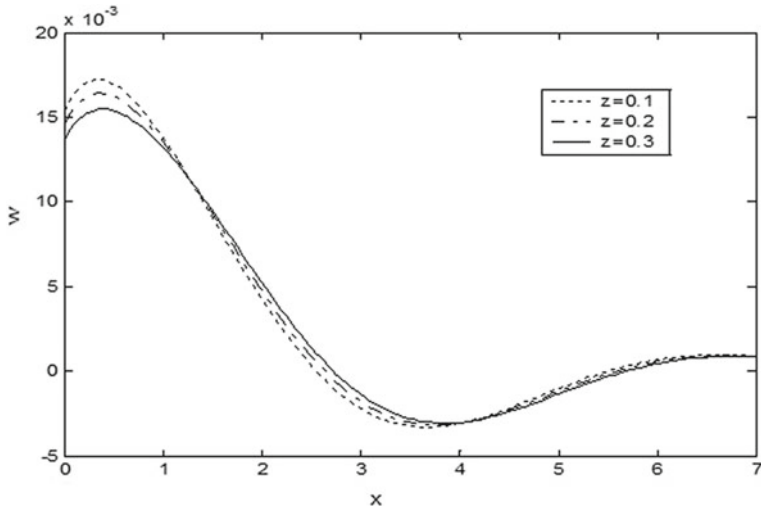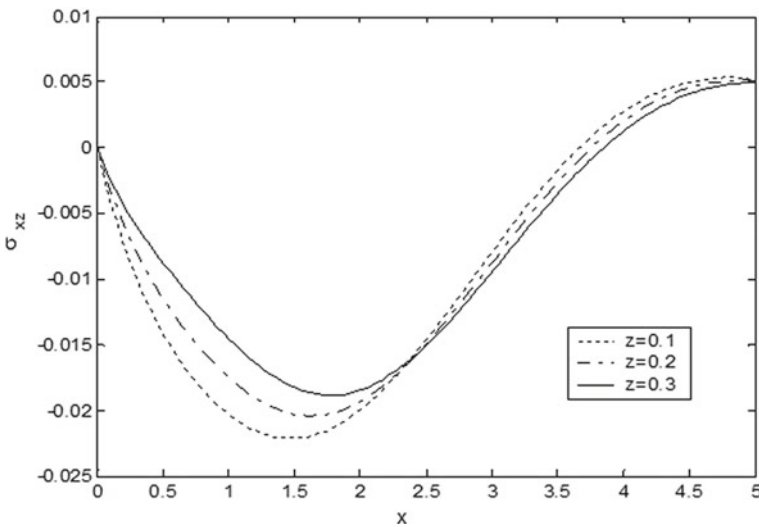

Fig. 11 Variation of displacement distribution w for different vertical distances, under GL theory

lines begin to coincide when the horizontal distance x is beyond the double of the crack size to reach the reference temperature of the solid. These results obey physical reality for the behaviour of copper as a polycrystalline solid.
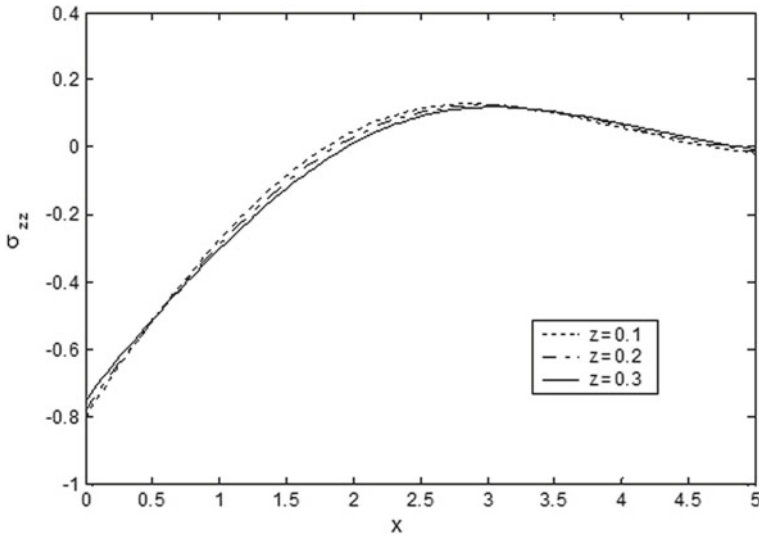
Fig. 12 Variation of stress distribution σ_{zz} for different vertical distances, under GL theory

Fig. 13 Variation of stress distribution σ_{xz} for different vertical distances, under GL theory

In Fig. 10, the horizontal displacement u, despite the peaks (for different vertical distances z = 0.1, 0.2 and 0.3) occur at equal value of x, the magnitude of the maximum displacement peak strongly depends on the vertical distance y. It is also clear that the rate of change of u increases with increasing y as we go farther apart from the crack.
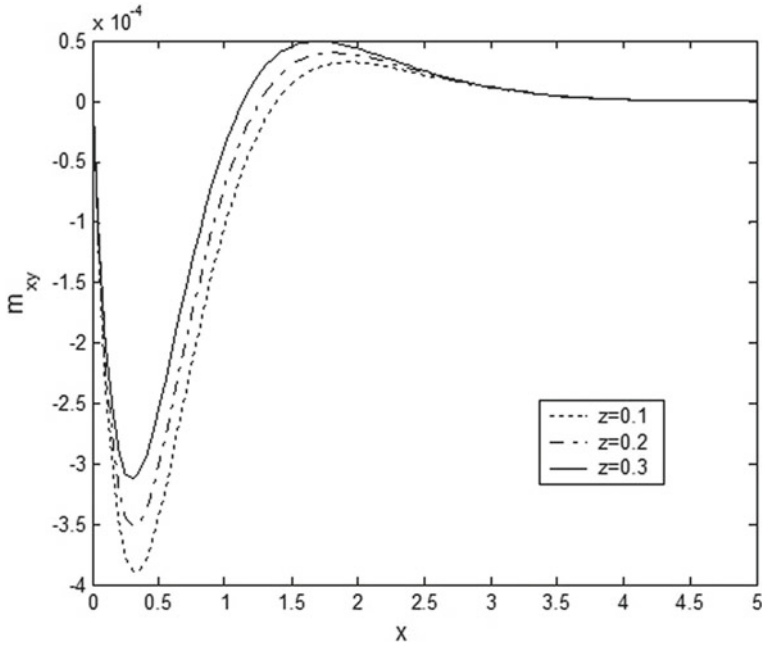
Fig. 14 Variation of tangential couple stress m_{xy} for different vertical distances, under GL theory
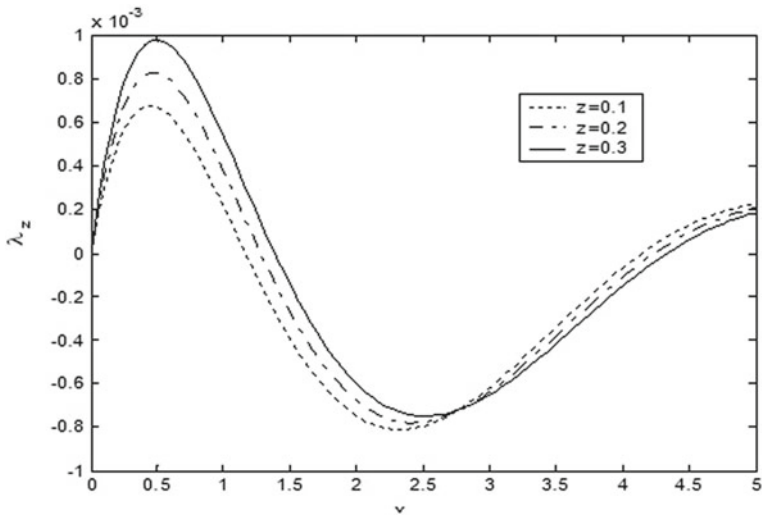
Fig. 15 Variation of microstress λ_z for different vertical distances, under GL theory

On the other hand, Fig. 11 shows atonable increase of the vertical displacement (w), near the crack end to reach minimum value beyond $x = 3$ reaching zero at the double of the crack size (state of particles equilibrium).

In Fig. 12, the vertical stresses σ_{zz} graph lines for both values of z show different slopes at crack ends according to z-values. In other words, the σ_{zz} component line for z = 0.1 has the highest gradient when compared with that of z = 0.2 and 0.3 at the edge of the crack. In addition, all lines begin to coincide when the horizontal distance x is beyond the double of the crack size to reach zero after their relaxations at infinity. Variation of y has a serious effect on both magnitudes of mechanical stresses. These trends obey elastic and thermoelastic properties of the solid under investigation.

Figure 13, shows that the stress component σ_{xz} satisfies the boundary condition, for z = 0.3 has the highest gradient when compared with that of z = 0.2 and 0.1 in the range $0 \leq x \leq 2.5$, the line for z = 0.1 has the highest gradient when compared with that of z = 0.2 and z = 0.3 in the range $2.5 \leq x \leq 5$ and converge to zero when $x > 5$. These trends obey elastic and thermoelastic properties of the solid.

In Fig. 14, the tangential coupled stress m_{xy} decreases in the start and increases (maximum) in the context of the three values of z until reaching the crack end, for z = 0.3 has the highest gradient when compared with that of z = 0.2 and 0.1 at the edge of the crack. All lines begin to coincide when the horizontal distance x is beyond the edge of the crack.

Figure 15, shows that the values of microstress for λ_z increases in the start and decreases (minimum) in the context of the three values of z until reaching nearly the crack end, for z = 0.3 has the highest gradient when compared with that of z = 0.2 and 0.1, at the edge of the crack.

All lines begin to coincide when the horizontal distance x is beyond the double of the crack size to reach zero after their relaxations at infinity.

6 Conclusions

We can conclude that:

1. The curves in the context of the (CD), (L-S) and (G-L) theories decrease exponentially with increasing x. This indicates that the thermoelastic waves are unattenuated and nondispersive, where purely thermoelastic waves undergo both attenuation and dispersion.
2. The presence of microstretch plays a significant role in all the physical quantities.
3. The curves of the physical quantities with (L-S) theory in most of the figures are lower in comparison with those under (G-L) theory, due to the relaxation times.
4. Normal mode Analytical solutions for thermoelastic problem in solids have been developed and utilized.
5. Mode-I crack has been investigated and studied for copper solid.

6. Temperature, radial and axial distributions were estimated at different distances from the crack edge.
7. The tangential coupled stress, the stresses distributions and the values of microstress were evaluated as functions of the distance from the crack edge.
8. Crack dimensions are significant to elucidate the mechanical structure of the solid.
9. Cracks are stationary and external stress is demanded to propagate such cracks.
10. The change of volume is attended by a change of the temperature while the effect of the deformation upon the temperature distribution is the subject of the theory of thermoelasticity.
11. All physical quantities value converges to zero with an increase in distance y and all functions are continuous.
12. Our studied problem has important applications for semiconductor nanocomposites in modern physics through a photothermal process in many industrial fields of Sustainable Development Goals. More applications of the considered problem are useful in researchers material science, designers of new materials and semiconductor materials, geophysics science, optics, acoustics, geomagnetic and earthquake engineering.

References

1. Eringen AC, Suhubi ES (1964) Non linear theory of simple micropolar solids. Int J Eng Sci 2:1–18
2. Eringen AC (1966) Linear theory of micropolar elasticity. J Math Mech 15:909–923
3. Othman MIA (2004) Relaxation effects on thermal shock problems in an elastic half-space of generalized magneto-thermoelastic waves. Mech Mech Eng 7:165–178
4. Othman MIA, Lotfy Kh, Farouk RM (2009) Transient disturbance in a half-space under generalized magneto-thermoelasticity with internal heat source. Acta Phys Polinca A 115:185–192
5. Eringen AC (1971)Micropolar elastic solids with stretch, vol 24. Ari Kitabevi Matbassi, Istanbul, pp 1–18
6. Eringen AC (1968) Theory of micropolar elasticity. In: Liebowitz H (ed) Fracture, vol II. Academic Press, New York, pp 621–729
7. Eringen AC (1990) Theory of thermo-microstretch elastic solids. Int J Eng Sci 28:291–1301
8. Eringen AC (1999) Microcontinuum field theories I: foundation and solids. Springer, New York
9. Iesau D, Nappa L (2001) On the plane strain of microstretch elastic solids. Int J Eng Sci 39:1815–1835
10. Iesau D, Pompei A (1995) On the equilibrium theory of microstretch elastic solids. Int J Eng Sci 33:399–410
11. De Cicco S (2003) Stress concentration effects in microstretch elastic bodies. Int J Eng Sci 41:187–199

12. Bofill F, Quintanilla R (1995) Some qualitative results for the linear theory of thermo-microstretch elastic solids. Int J Eng Sci 33:2115–2125
13. De Cicco S, Nappa L (2000) Some results in the linear theory of thermo-microstretch elastic solids. J Math Mech 5:467–482
14. De Cicco S, Nappa L (1999) On the theory of thermomicrostretch elastic solids. J Thermal Stresses 22:565–580
15. Green AE, Laws N (1972) On the entropy production inequality. Arch Ration Mech Anal 45:47–59
16. Lord HW, Şhulman Y (1967) A generalized dynamical theory of thermoelasticity. J Mech Phys Solid 15:299–306
17. Green AE, Lindsay KA (1972) Thermoelasticity. J Elast 2:1–7
18. Othman MIA, Lotfy KH (2009) Two-dimensional problem of generalized magneto-thermoelasticity under the effect of temperature dependent properties for different theories. MMMS 5:235–242
19. Othman MIA, Lotfy KH, Farouk RM (2009) Transient Disturbance in a half-space under generalized magneto-thermoelasticity due to moving internal heat source. Acta Phys Pol A 116:186–192
20. Othman MIA, Lotfy KH (2010) On the plane waves in generalized thermo-microstretch elastic half-space. In: International communication in heat and mass transfer, vol 37, pp 192–200
21. Othman MIA, Lotfy Kh (2009) Effect of magnetic field and inclined load in micropolar thermoelastic medium possessing cubic symmetry. Int J Ind Math 2:87–104
22. Othman MIA, Lotfy Kh (2010) Generalized thermo-microstretch elastic medium with temperature dependent properties for different theories. Eng Anal Bound Elem 34:229–237
23. Dhaliwal R (1980) External crack due to thermal effects in an infinite elastic solid with a cylindrical inclusion. Thermal Stresses in Server Environments Plenum Press, New York, pp 665–692
24. Hasanyan D, Librescu L, Qin Z, Young R (2005) Thermoelastic cracked plates carrying nonstationary electrical current. J Thermal Stresses 28:729–745
25. Ueda S (2003) Thermally induced fracture of a piezoelectric laminate with a crack normal to interfaces. J Thermal Stresses 26:311–323
26. Elfalaky A, Abdel-Halim AA (2006) A mode-I crack problem for an infinite space in thermoelasticity. J Appl Sci 6:598–606
27. Elsirafy IH, Abo-Dahab SM, Singh B (2011) Effects of voids and rotation on P wave in a thermoelastic half-space under Green-Naghdi theory. Math Mech Solids 17(3):243–253
28. Lotfy Kh (2012) Mode-I crack in a two-dimensional fibre reinforced generalized thermoelastic problem. Chin Phys B 21(1):014209
29. Lotfy Kh (2012) The effect of a magnetic field on a 2D problem of fibre-reinforced thermoelasticity rotation under three theories. Chin Phys B 21(6):064214
30. Sarkar N, Lahiri A (2012) A three-dimensional thermoelastic problem for a half-space without energy dissipation. Int J Eng Sci 5:310–325
31. Abd-alla AM (2010) Influences of rotation, magnetic field, initial stress and gravity on Rayleigh waves in a homogeneous orthotropic elastic half-space. Appl Math Sci 4(2):91–108
32. Othman MIA, Abd-Elaziz EM (2015) The effect of thermal loading due to laser pulse in generalized thermoelastic medium with voids in dual phase lag model. J Therm Stresses 38(9):1068–1082
33. Alshehri HM, Lotfy Kh (2022) Thermo-elastodifusive waves in semiconductor excitation medium with laser pulses under two temperature photo-thermoelasticity theory. Mathematics 10:4515

34. Mohammed MAY, Tayel IM (2022) Photothermal influences in semiconductors with temperature-dependent properties generated by laser radiation using strain–temperature rate-dependent theory. Eur Phys J Plus 137:703
35. Tayel IM, Alebraheem J, Lotfy Kh, Mohammed M, El Bary AA (2023) Volumetric absorption illumination induced by laser radiation in a 2D thermoelastic microelongated semiconductor body with temperature-dependent properties. Front Phys Sect Math Phys 11:1213440

In-Situ Fabrication of Poly (m-Phenylene Isophthalamide)/Fluorographene Nanocomposites and Their Properties

L. Elbayar, M. Abdelaty, S. A. Nosier, Abbas Anwar Ezzat, and F. Shokry

1 Introduction

With the rapid development of advanced technologies, more and more dielectric composites have been employed in sophisticated applications, such as energy storage devices [1, 2], aerospace power electronic systems [3] pulsed power systems [4], and film capacitors [5]. To meet the dielectric performance requirements of terminal electronic devices in the fields of high frequency, high-speed signal transmission networks and in the future, preparation of polymer materials with low dielectric constant and low dielectric loss has become a hot research direction in this field [6].

Poly (m-phenylene isophthalamide) (PMIA) is one of the most important aromatic polyamides with high crystallinity is shown in Fig. 1 [7, 8]. PMIA has been widely employed in the field of desalination and nanofiltration because of its high thermal resistivity (Tg = 270 °C), chemical stabilities, excellent mechanical properties, and homogeneous pore distribution [9–12], it can be also used in the field of electronics as separators for lithium-ion batteries due to excellent thermal stability, non-flammability, and excellent liquid electrolyte wettability [13–15]. In addition, it can

L. Elbayar · M. Abdelaty · A. A. Ezzat (✉)
Department of Petrochemical Engineering, Faculty of Engineering, Pharos University in Alexandria, Alexandria, Egypt
e-mail: abbas.ezzat@pua.edu.eg

M. Abdelaty
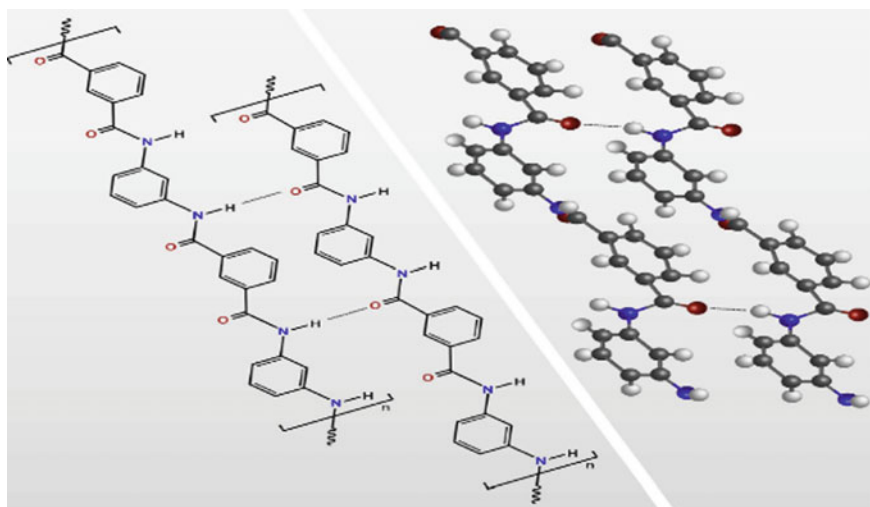e-mail: mahmoud.abdelaty@pua.edu.eg

S. A. Nosier
Department of Chemical Engineering, Faculty of Engineering, Alexandria University, Alexandria, Egypt

F. Shokry
Department of Chemical Engineering, Faculty of Engineering, Port Said University, Port Said, Egypt
e-mail: fathi.shokry@eng.psu.edu.eg

Fig. 1 The schematic of the chemical structure of PMIA [7]

also be applied to fire protective clothing, bulletproof products, and transformer insulation due to its mechanical performance and electrical insulation. The wide application of PMIA lies in their excellent properties, which are determined by their unique structures and molecular weights [16, 17].

PMIA materials exhibit better processability than inorganic solid-insulating materials commonly used in microelectronic fields [18–20]. However, traditional PMIA shows dielectric constants ($3 < \kappa < 4$) are still not low enough as an alternative to traditional insulators for future devices [21, 22]. As a result, significant research has been dedicated to reducing the dielectric constant of polyimide. One approach that was initially explored involved introducing controlled porosity to the material, as this was thought to be a promising way to develop low-κ substances due to air's naturally low dielectric constant [23, 24]. Porous polyimides are prepared by various methods [25]. However, this technique led to nano porous films with weak mechanical strength and Young's modulus only in the range of 0.4–0.6 GPa. To maintain strong mechanical properties, there are two primary routes available for reducing the material's dielectric constant. There are two main syntheses to this work. The first involves creating a fluorinated polyimide. Fluorine substitution tends to decrease electronic polarization due to the reduced electronic polarizability of the C–F bond compared to C–H, ultimately lowering the dielectric constant. Despite this, the majority of reported cases of fluorinated polyimide fall within a dielectric constant range of 2.6–3.0.

Fluorographene, a two-dimensional derivative of graphene, has recently gained attention [26–28]. It possesses unique interfacial and physicochemical properties due to its structural characteristics inherited from graphene and carbon material fluorides, providing opportunities for a variety of applications [29, 30]. Previous studies, including our own, have demonstrated that the high F/C ratio in fluorographene

results in a broad gap, increased hydrophobicity, and thermal stability. The goal of this study is to create PMIA/FG nanocomposites using in-situ interfacial polycondensation from m-phenylene diamine and isophthaloyl chloride to achieve the best results. The impact of various FG levels on the dielectric, mechanical, and thermal properties of PMIA was analyzed. Hybrid inorganic-polymer materials have unique properties at nanoscale [31].

The production of low dielectric constant Poly (m-phenylene isophthalamide)/ fluorographene (PMIA/FG) composite films demonstrates a sustainable approach to the development of integrated circuits. By utilizing FG nanoparticles, which are a form of carbon, the production of these films incorporates a renewable resource into the process. This process results in a significant enhancement of the mechanical, electrical, and thermal properties of the materials, reducing the need for frequent replacements and repairs. Additionally, the low dielectric constant of the resulting composite films can lead to more energy-efficient technology, contributing to sustainability.

2   Experimental Part

2.1   Materials

Isophthaloyl chloride (IPC) (> 98%) m-phenylene diamine (MPD) (> 97%) were supplied by Loba Chemie Reagent Co., India. N,N-dimethylacetamide (DMAC), (> 99%) was supplied by Sdfci Chemical Reagent Co., Ltd, Maharashtra. Tetrahydrofuran (THF) (> 99%), Lithium chloride, 2-Methylpyridine, sodium carbonate and sodium lauryl sulphate were supplied by Piochem Chemical Reagent Co., Ltd, Egypt. Lithium chloride was dried at 120 °C for 6 h before use. Sulphuric acid (> 99%) was supplied by Adwic Chemical Reagent Co., Ltd, Egypt, fluorographite (FGi) was purchased from Shanghai CarFluor Ltd., NMP ($\geq$ 98.0%) was purchased from Sinopharm Chemical Reagent Co. Ltd.

2.2   Preparation of FG Sonochemical Exfoliation Method

Figure 2 illustrates the process of preparing FG dispersions, whereby FGi was added to a round-bottomed flask containing 500 mL of NMP solution at an initial concentration of CFGi = 5 mg m L^{-1}, and refluxed at 60 °C for 2 h. Low-power ultra-sonication was then carried out in a sonic bath, after which samples were taken from the flask at various times. To ensure accuracy of the exfoliation process, the actual output power was determined to be 32 W by observing the temperature rise while ultra-sonicating 3 kg of water in similar experimental conditions. Furthermore, samples were prepared without the sonication process to evaluate the impact of NMP on fluorine coverage adjustment [32].
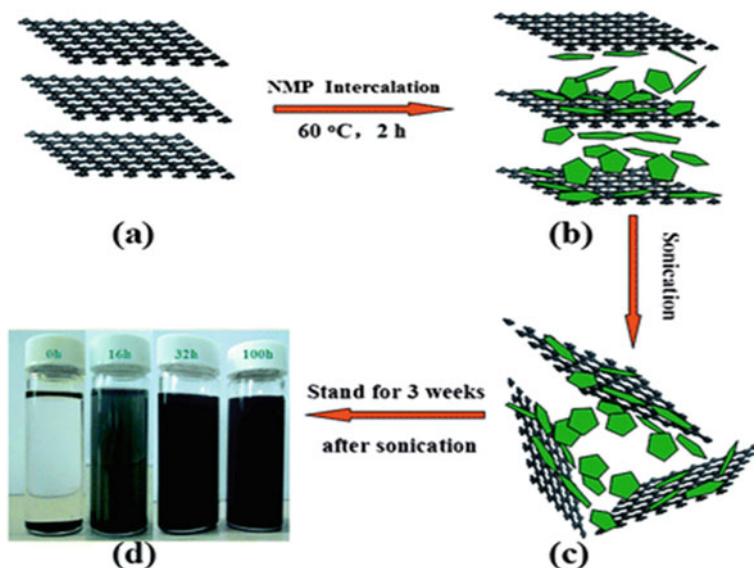
Fig. 2 NMP intercalation and exfoliation fabrication processes for FG dispersions: **a** pristine FGi; **b** intercalation of NMP into FGi interlayers; **c** sonication assisted exfoliation of FGi; **d** FG dispersions (obtained at different sonication times of 0, 16, 32 and 100 h, respectively) after standing for 3 weeks [32]

2.3 Preparation of PMIA/FG Nanocomposites Using In-Situ Interfacial Polycondensation

As illustrated in Fig. 3, polymerization was carried out in a 500 mL three-neck flask with a mechanical stirrer. A solution containing 5 g of m-phenylenediamine, 9.8 g of sodium carbonate, and 0.15 g of sodium lauryl sulphate in 125 ml of water was placed in three neck flasks. To form several solutions that contained 0.5, 0.75, 1, and 1.25 wt% of FG, differing weights of FG nanoparticles were added to the m-phenylenediamine solution. The m-phenylenediamine/FG mixtures were vigorously stirred for 1h, and a rapid addition of a solution containing 9.85 g of isophthaloyl chloride in 185 ml of tetrahydrofuran was carried out with moderate stirring. Agitation was then sustained for 12 min before filtering, washing the polymer composites three times with water and acetone, and finally drying at 100 °C for 12 h under vacuum. PMIA/FG composites with 0.5, 0.75, 1, and 1.25 wt% of FG were denoted as PMIA/FG 0.5%, PMIA/FG 0.75%, PMIA/FG 0.1%, and PMIA/FG 1.25%, respectively.
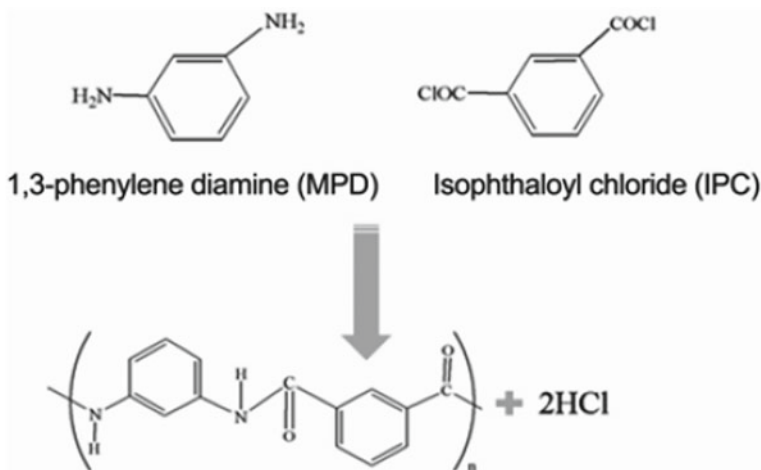
Fig. 3 Preparation of PMIA interfacial polymerization [33]

2.4 Preparation of Porous PMIA/FG Nano-composites Films

The method of preparing PMIA/FG nanocomposite films is clearly shown in Fig. 4. Initially, a combination of PMIA/FG (18 wt%) and lithium chloride (5 wt%) dissolved in N,N-dimethylacetamide was produced at 80 °C to obtain a homogeneous and transparent casting solution. The casting solution was positioned in an oven at 80 °C for 1h after being degassed. Both the glass plate and casting knife were preheated at 60 °C before casting. The polymer dope was then poured onto the glass plate and cast gradually with a gap of 150 μm by the casting knife. The glass plate containing the polymer wet film was subjected to an oven at 95 °C for 10 min, and finally, it was submerged into a water coagulation bath kept at 35 °C, and then the film was allowed to solidify and thereafter peeled off. A 24-h washing of the film with deionized water was performed to remove leftover solvent and lithium chloride. Non-solvent induced phase separation was used to prepare porous PMIA membranes [34].
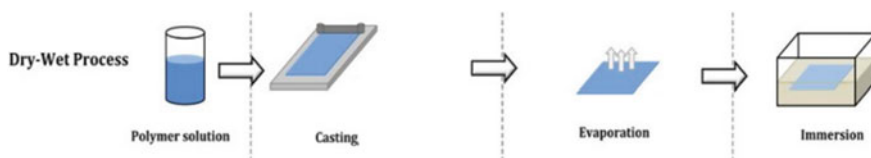

Fig. 4 The schematic illustration for the preparation of PMIA/FG film [35]

2.5   PMIA/FG Film Characterization

Fourier transform infrared (FTIR) spectra was acquired through Shimadzu FTIR-8400 S from Japan, covering the range of 400–4000 cm^{-1}.

The mechanical properties of polymer films were measured through a universal testing machine (SERVO PULSER, Simadzu EFH-EB20-40L) at a crosshead speed of 5 mm/min and ambient temperature. Five rectangular specimens measuring 40 mm in length, 10 mm in width, and 0.050 mm in thickness were tested for each sample, and their average values were taken.

The Nove-control Alpha broadband dielectric analyzer was utilized to measure the dielectric constants of PMIA and PMIA/FG films from 1 to 106 Hz at room temperature. Prior to measurement, the samples (4 cm × 4 cm) were coated with aluminum foil on both sides of the PMIA and PMIA/FG films to ensure proper electrode contact.

To examine the thermal stability of PMIA and PMIA/FG films, a Thermogravimetric Analyzer (Shimadzu Thermal Gravimetric Analysis (TGA)—50, Japan) was utilized. The recorders were conducted under a nitrogen environment with a flow rate of 10 ml/min. The material temperature was increased from 100 to 800 °C at a heating rate of 10 °C min^{-1}.

The surface morphologies of PMIA and PMIA/FG films were evaluated through a Scanning Electron Microscope (SEM, JEOL JSM-6360LA, Japan).

3   Results and Discussion

3.1   The Inherent Viscosity of PMIA/FG Nanocomposites

The synthesis of PMIA/FG nanocomposites was successfully carried out on a laboratory scale through in-situ interfacial polycondensation, resulting in a polymer yield of 93% of the theoretical value. In Table 1, it is shown that the inherent viscosity of PMIA and PMIA/FG nanocomposites ranges from 1.8 to 1.95, indicating a higher molecular weight. Additionally, there is a slight increase in the inherent viscosity of PMIA/FG nanocomposites as the content of FG increases. The presence of FG during the synthetic process of PMIA has minimal impact on the polymerization reaction of MPA and IPC.

### 3.2   FTIR Spectroscopy Characterization of PMIA/FG Nanocomposites

FTIR spectroscopy is a useful tool for identifying the functional group present in PMIA/FG nanocomposites. The FTIR spectra of both PMIA and PMIA/FG

Table 1 The inherent viscosity of PMIA and PMIA/FG

Sample	η_{inh} (dl/g)
PMIA	1.80
PMIA/FG 0.50%	1.85
PMIA/FG 0.75%	1.87
PMIA/FG 1.00%	1.90
PMIA/FG 1.25%	1.95

nanocomposites can be seen in Fig. 5. The peak at 3290 cm^{-1} corresponds to N–H stretching vibrations in a secondary amide with hydrogen bond. The 3000 cm^{-1} peak is attributed to the C–H stretching vibration in an unsaturated compound. The 1650 cm^{-1} peak is associated with the amide C=O group in hydrogen-bonded amides. The 1600 cm^{-1} group of closely related peaks is due to aromatic C=C stretching. The peak at 1415 cm^{-1} corresponds to N–H in-plane bending, while the peak at 1255 cm^{-1} corresponds to C–N stretching. These peaks differ from those observed in the pristine PMIA film [11, 36]. The stretching vibrations of the C–F covalent bonds and semi-ionic C–F bonds are represented by the absorption peaks at 1215 cm^{-1} and 1087 cm^{-1}, respectively. These observations indicate the presence of C–F bonds in the PMIA sample. The FTIR analysis validates the formation of C–F bonds on the PMIA [37].
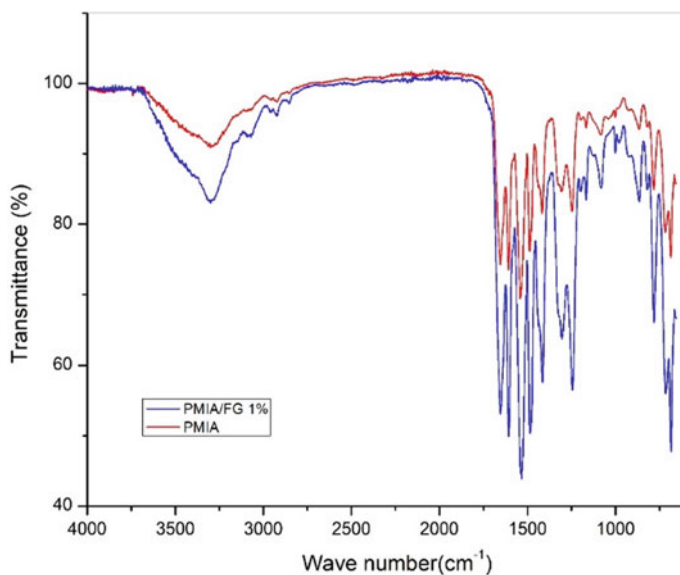
**Fig. 5** FTIR spectra of as-prepared PMIA and PMIA/FG 1% nanocomposite
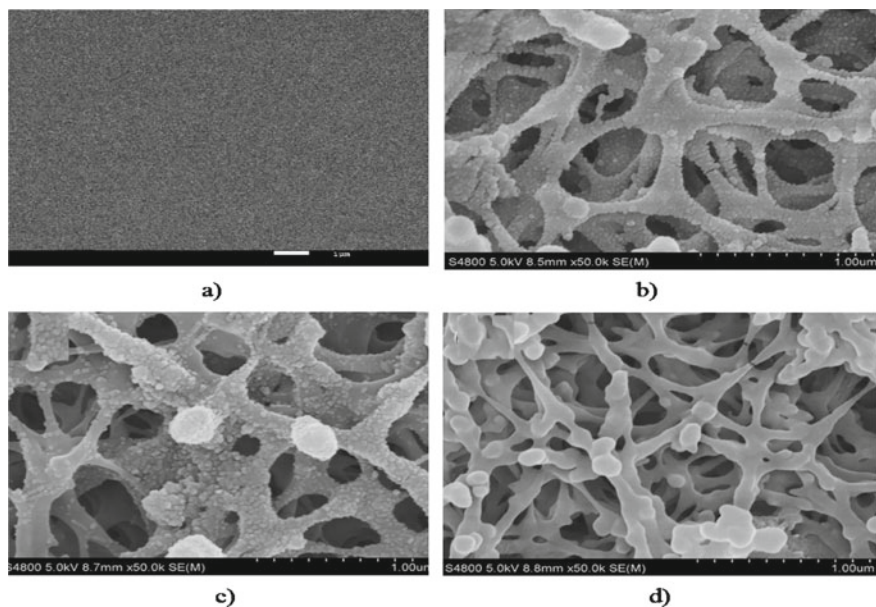
Fig. 6 SEM images of the surface of synthesized PMIA film **a** PMIA, **b** PMIA/FG 0.75%, **c** PMIA/FG 1%, and **d** PMIA/FG 1.25%

3.3 Morphologies of PMIA/FG Nanocomposites Films

The scanning electron microscope (SEM) was used to observe the surface morphology of the PMIA and PMIA/FG films. Figure 6 shows the SEM micrographs of the porous PMIA/FG films with 0.5, 0.75, 1, and 1.25% FG content. The smooth surfaces of PMIA were observed in Fig. 6a, while Fig. 6b–d revealed obvious pores in the porous PMIA/FG films. The size of the pores in the porous films formed using casting solution of PMIA/FG 18 wt% and LiCl 5 wt% with the phase inversion process at 25 °C was determined. The FG nanoparticles were monodispersed without any agglomerations even with an increased amount of 1.25 wt% in the PMIA polymer matrix. This result proves the strong interfacial interaction between FG and PMIA, and the good dispersal state of the FG nanoparticles in a PMIA polymer matrix.

3.4 The Dielectric Constants of Porous PMIA/FG Films

The dielectric constant (k) of the samples was analyzed, and Fig. 7 shows that k decreases with increasing frequency between 1 Hz and 1 MHz for all samples. Furthermore, the PMIA/FG nanocomposite films have lower k values compared to the PMIA film over the entire frequency range. It is a common phenomenon that the
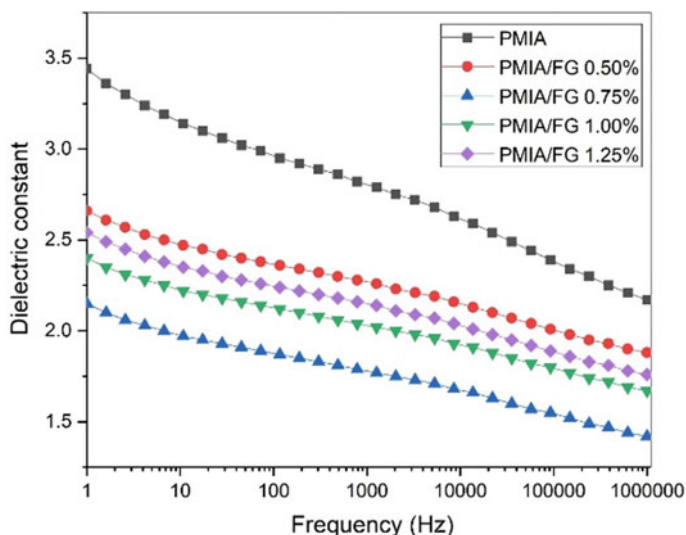
Fig. 7 The dielectric constant of as-prepared porous PMIA and PMIA/FG films with different FG content 0.5, 0.75, 1 and 1.25 wt% Number footnotes separately in superscript. Place the actual footnote at the bottom of the column in which it was mentioned. Do not put footnotes in the abstract or reference list

dielectric constant of materials decreases with increasing frequency. This is due to the lack of orientation of the dipolar polarizable units as they are unable to keep up with the high speed of the applied alternating current electric field at higher frequencies.

Results showed that the dielectric constant of PMIA/FG nanocomposite films decreased as the FG content increased. For instance, at 0.5 wt% FG content, the dielectric constant at 1 Hz decreased significantly from 3.44 for PMIA to 2.65. Furthermore, the dielectric constant of PMIA/FG 0.75% films decreased even further to 2.15. This phenomenon can be attributed to the low polarizability of C–F bonds in FG, which is well-dispersed through in situ polymerization and ultrasonic treatment. Additionally, FG with a vast surface area can interact with PMIA chains, which hinders the movement of dipoles in PMIA. However, the dielectric constant of these films started to increase gradually beyond 0.75 wt% FG concentration. This is primarily due to interfacial polarization enhancement resulting from the increased concentration of FG. It is understood that at lower frequencies, interfacial polarization is the dominant effect, as the large dipoles formed at the interfaces are unable to track the electric field at higher frequencies. Additionally, an increase in filler content results in the formation of more interfaces between the filler and polymer matrix, which in turn leads to a more significant interfacial polarization effect at frequencies around 1 kHz. However, it should be noted that excessive filler content may actually have counterproductive effects, as the resulting interfacial polarization can contribute to an increased dielectric constant [38, 39].
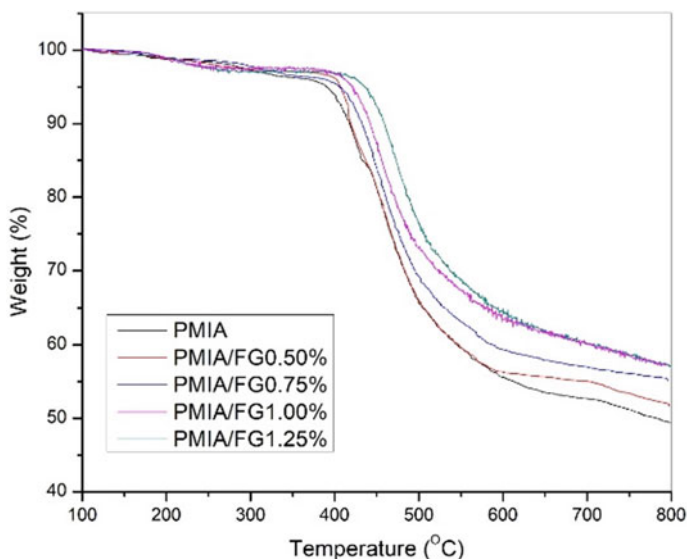
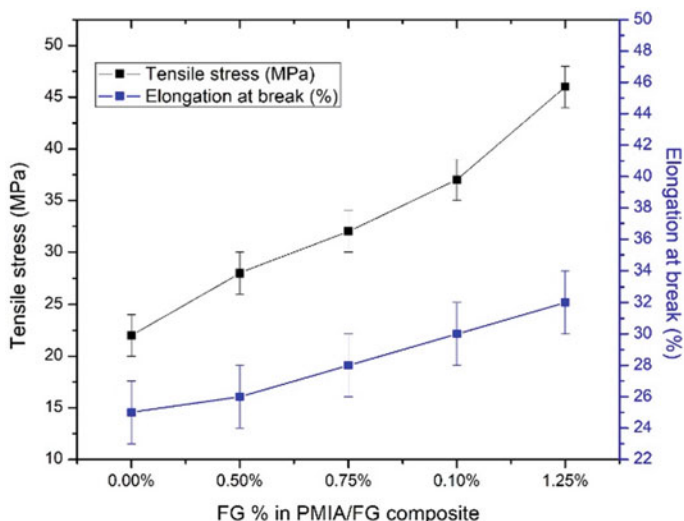**Fig. 8** TGA of as-prepared PMIA and PMIA/FG films with different FG content 0.5, 0.75, 1 and 1.25 wt%

3.5 Thermal Properties of Porous PMIA/FG Films

Figure 8 illustrates the results of thermal stability analysis of PMIA/FG nanocomposites. All samples showed high-temperature performance, with pure PMIA starting to decompose at 440 °C. However, the addition of FG resulted in a shift of the main thermal decomposition to a higher temperature region, indicating that FG can effectively slow down the thermal decomposition of PMIA. Specifically, the temperatures of the main thermal decomposition for PMIA/FG 0.5%, PMIA/FG 0.75%, PMIA/FG 1%, and PMIA/FG 1.25% are 447 °C, 453 °C, 457 °C, and 465 °C, respectively.

The excellent thermal stability of FG nanoparticles enables their uniform dispersion in PMIA. Moreover, the strong interaction between PMIA and FG molecular chains hinders molecular chain movement. FG with a large aspect ratio a brings out the "tortuous path" effect, acting as barrier in polymer matrices' to delay the permeation of oxygen and the escape of volatile degradation products and also char formation. As a result, improved thermal stability has been achieved for FG/PMIA composite films [40].

3.6 Mechanical Properties of PMIA/FG Films

The mechanical properties of as-prepared films of porous PMIA and PMIA/FG nanocomposites are presented in Fig. 9. The strain and tensile strength of the pure

Fig. 9 Tensile strength and elongation at break of as-prepared porous PMIA and PMIA/FG films with different FG content 0.5, 0.75, 1 and 1.25 wt%

porous PMIA film were found to be 15% and 22 MPa, respectively. Notably, both the tensile strength and elongation at break were observed to increase with increasing FG weight percentage. For instance, the tensile strength of porous PMIA/FG films containing 0.5%, 0.75%, 1%, and 1.25% FG were found to be 27.8, 32.5, 37.4, and 45.1 MPa, respectively, which were higher than that of porous PMIA. The corresponding elongation at break for these composites was found to be 16.4%, 18.3%, 21.5%, and 23.4%, respectively. These excellent mechanical properties resulted from the uniform distribution of FG in the PMIA matrix, as well as the excellent interfacial compatibility that effectively enhances the stress transfer at the interface.

4   Conclusions

In summary, the efficacy of using an in-situ interfacial polycondensation process for the successful fabrication of MIA and MIA/FG nanocomposites. Adding FG to PMIA is an efficient route for improving both the thermal stability and mechanical performance of the resulting composite. The study showed that the PMIA/G composites with 0.75 wt% FG exhibited the lowest dielectric constant at 1 Hz. The addition of 1.25 wt% FG resulted in a significant increase in the tensile strength and elongation at break compared to pure PI film. Composite films exhibited a high initial degradation temperature of 465 °C, indicating excellent thermal stability.

Overall, the in-situ fabrication of poly (m-phenylene isophthalamide)/ fluorographene nanocomposites and their properties have the potential to benefit the

community in numerous ways, including improved mechanical and flame-retardant properties, reduced environmental impact, and improved electrical properties. the development of these nanocomposites has the potential to revolutionize various industries and improve the lives of millions of people, making it a significant contribution to the betterment of society.

5　Recommendation

The use of fluorographene with different polyimides using in-situ interfacial poly-condensation is a promising method to obtain materials with low dielectric constants. Proper selection of polyimides, optimization of processing parameters, and characterization techniques are essential to obtain materials with tailored properties for various electronic applications. Moreover, application-specific properties should be taken into consideration while tailoring the properties of the composite material.

It is advisable to experiment with different types and proportions of additives to determine the optimum combination that will produce the desired outcome. This will help to achieve a balance between low dielectric constant and other desirable properties such as mechanical strength, thermal stability, and chemical resistance. Prioritize the use of additives that are known to be non-toxic, environmentally friendly, and cost-effective to ensure that the membrane is safe and economical to produce. Consider the application and environment the PMIA membrane will be used in, as this may impact the choice of additives. For example, if the membrane is intended for use in high-temperature environments, additives with good thermal stability should be selected.

References

1. Meng J, Cao Y, Suo Y, Liu Y, Zhang J, Zheng X (2015) Facile fabrication of 3D SiO_2 @graphene aerogel composites as anode material for lithium ion batteries. Electrochim Acta 176:1001–1009. https://doi.org/10.1016/j.electacta.2015.07.141

2. Han K, Li Q, Chanthad C, Gadinski MR, Zhang G, Wang Q (2015) A hybrid material approach toward solution-processable dielectrics exhibiting enhanced breakdown strength and high energy density. Adv Func Mater 25(23):3505–3513. https://doi.org/10.1002/adfm.201501070

3. Kumar B, Kim SH (2012) Energy harvesting based on semiconducting piezoelectric ZnO nanostructures. Nano Energy 1(3):342–355. https://doi.org/10.1016/j.nanoen.2012.02.001

4. Venkat N, Dang TD, Bai Z, McNier VK, DeCerbo JN, Tsao B, Stricker JT (2010) High temperature polymer film dielectrics for aerospace power conditioning capacitor applications. Mater Sci Eng B 168(1–3):16–21. https://doi.org/10.1016/j.mseb.2009.12.038

5. Li Q, Han K, Gadinski MR, Zhang G, Wang Q (2014) High energy and power density capacitors from solution-processed ternary ferroelectric polymer nanocomposites. Adv Mater 26(36):6244–6249. https://doi.org/10.1002/adma.201402106

6. Peng X, Xu W, Chen L, Ding Y, Xiong T, Chen S, Hou H (2016) Development of high dielectric polyimides containing bipyridine units for polymer film capacitor. React Funct Polym 106:93–98. https://doi.org/10.1016/j.reactfunctpolym.2016.07.017

7. Wang L (2005) Progress technology of aramid 1313 fiber. Shanghai Text Sci Technol 33:12–19

8. Xiongfei D, Hanwen Z, Yuxin Z (2022) J Taiwan Inst Chem Eng 139:104512–104529

9. Wang T, Zhao C, Li P, Li Y, Wang J (2015) Fabrication of novel poly(m-phenylene isophthalamide) hollow fiber nanofiltration membrane for effective removal of trace amount perfluorooctane sulfonate from water. J Membr Sci 477:74–85. https://doi.org/10.1016/j.memsci.2014.12.038

10. Wang T, Zhao C, Li P, Li Y, Wang J (2015) Effect of non-solvent additives on the morphology and separation performance of poly(m-phenylene isophthalamide) (PMIA) hollow fiber nanofiltration membrane. Desalination 365:293–307. https://doi.org/10.1016/j.desal.2015.03.016

11. Yang M, Zhao C, Zhang S, Li P, Hou D (2017) Preparation of graphene oxide modified poly(m-phenylene isophthalamide) nanofiltration membrane with improved water flux and antifouling property. Appl Surf Sci 394:149–159. https://doi.org/10.1016/j.apsusc.2016.10.069

12. Chen M, Xiao C, Wang C, Liu H, Naizhe H (2018) Preparation and characterization of a novel thermally stable thin film composite nanofiltration membrane with poly (m-phenyleneisophthalamide) (PMIA) substrate. J Membr Sci 550:36–44. https://doi.org/10.1016/j.memsci.2017.12.040

13. Zhai Y, Wang N, Mao X, Si Y, Yu J, Al-Deyab SS, Ding B (2014) Sandwich-structured PVdF/PMIA/PVdF nanofibrous separators with robust mechanical strength and thermal stability for lithium ion batteries. J Mater Chem A Mater Energy Sustain 2(35):14511–14518. https://doi.org/10.1039/c4ta02151g

14. Hua D, Japip S, Wang K, Chung T (2018) Green design of poly(m-phenylene isophthalamide)-based thin-film composite membranes for organic solvent nanofiltration and concentrating lecithin in hexane. ACS Sustain Chem Eng 6(8):10696–10705. https://doi.org/10.1021/acssuschemeng.8b02021

15. Zhang H, Zhang Y, Xu T, John AE, Li Y, Li W, Zhu B (2016) Poly(m-phenylene isophthalamide) separator for improving the heat resistance and power density of lithium-ion batteries. J Power Sources 329:8–16. https://doi.org/10.1016/j.jpowsour.2016.08.036

16. Huang Z, Chen Y, Han Q, Su M, Liu Y, Wang H, Wang H (2022) Vapor-induced phase inversion of poly (m-phenylene isophthalamide) modified polyethylene separator for high-performance lithium-ion batteries. Chem Eng J 429:132–429. https://doi.org/10.1016/j.cej.2021.132429

17. Huang J, Zhang K (2011) The high flux poly (m-phenylene isophthalamide) nanofiltration membrane for dye purification and desalination. Desalination 282:19–26. https://doi.org/10.1016/j.desal.2011.09.045

18. Hua C (2014) Performances of poly-m-phenylene isophthalamide and its application in individual protective clothing. J Saf Sci Technol 10

19. García JL, García F, Serna F, De La Peña JA (2010) High-performance aromatic polyamides. Prog Polym Sci 35(5):623–686. https://doi.org/10.1016/j.progpolymsci.2009.09.002

20. Wang X, Ding B, Wang X, Yang J, Chen L, Hu Z, Yu J (2013) Tuning hierarchically aligned structures for high-strength PMIA–MWCNT hybrid nanofibers. Nanoscale 5(3):886–889. https://doi.org/10.1039/c2nr33696k

21. Maex K, Baklanov MR, Shamiryan D, Lacopi F, Brongersma S, Yanovitskaya ZS (2003) Low dielectric constant materials for microelectronics. J Appl Phys 93(11):8793–8841. https://doi.org/10.1063/1.1567460

22. Maier G (2001) Low dielectric constant polymers for microelectronics. Prog Polym Sci 26(1):3–65. https://doi.org/10.1016/s0079-6700(00)00043-5

23. Huang Y, Economy J (2006) New high strength low-k spin-on thin films for IC application. Macromolecules 39(5):1850–1853. https://doi.org/10.1021/ma0518398

24. Yang S, Mirau PA, Pai C, Nalamasu O, Reichmanis E, Lin EK et al (2001) Molecular templating of nanoporous ultralow dielectric constant (≈ 1.5) organosilicates by tailoring the microphase separation of triblock copolymers. Chem Mater 13(9):2762–2764. https://doi.org/10.1021/cm0102786

25. Du X, Zheng H, Zhang Y, Zhao N, Chen M, Huang Q (2022) Pore structure design and optimization of electrospun PMIA nanofiber membrane. J Taiwan Inst Chem Eng 139:104512. https://doi.org/10.1016/j.jtice.2022.104512

26. Zboril R, Karlický F, Bourlinos AB, Steriotis T, Stubos AK, Georgakilas V et al (2010) Graphene fluoride: a stable stoichiometric graphene derivative and its chemical conversion to graphene. Small 6(24):2885–2891. https://doi.org/10.1002/smll.201001401

27. Zbořil R, Karlický F, Bourlinos AB (2010) Graphene fluoride: a stable stoichiometric graphene derivative and its chemical conversion to graphene. Small 6:2885−2891

28. Novoselov KS, Jiang D, Schedin F, Booth TC, Khotkevich VV, Morozov SV, Geim AK (2005) Two-dimensional atomic crystals. Proc Natl Acad Sci U S A 102(30):10451–10453. https://doi.org/10.1073/pnas.0502848102

29. Schrier J (2011) Fluorinated and nanoporous graphene materials as sorbents for gas separations. ACS Appl Mater Interfaces 3(11):4451–4458. https://doi.org/10.1021/am2011349

30. Mondal T, Bhowmick AK, Krishnamoorti R (2014) Stress generation and tailoring of electronic properties of expanded graphite by click chemistry. ACS Appl Mater Interfaces 6(10):7244–7253. https://doi.org/10.1021/am500471q

31. Basaki N, Kakanejadifard A, Faghihi K (2021) Preparation of new enforcement polyamide nanocomposite filled by ternary layer double hydroxide and investigation of electrochemical activity, optical and thermal properties. Polym Bull 78(11):6723–6741. https://doi.org/10.1007/s00289-020-03508-6

32. Gong P, Wang Z, Wang J, Wang H, Li Z, Fan Z et al (2012) One-pot sonochemical preparation of fluorographene and selective tuning of its fluorine coverage. J Mater Chem 22(33):16950. https://doi.org/10.1039/c2jm32294c

33. Kwolek SL, Morgan PS (1964) Preparation of polyamides, polyurethanes, polysulfonamides, and polyesters by low temperature solution polycondensation. J Polym Sci 2(6):2693–2703. https://doi.org/10.1002/pol.1964.100020619

34. Zhu H (2021) Preparation of porous aromatic polyamide membranes and their dielectric properties. Trans Beijing Inst Technol 41:1114–1119

35. Takeichi T, Zuo M, Ito A (1999) Preparation and properties of porous polyimide films. High Perform Polym 11(1):1–14. https://doi.org/10.1088/0954-083/11/1/001

36. Pramila J, Melbiah JB, Rana DS, Gandhi NN, Nagendran A, Mohan D (2018) Permeation characteristics of tailored poly (m-phenylene isophthalamide) ultrafiltration membranes and probing its efficacy on bovine serum albumin separation. Polym Testing 67:218–227. https://doi.org/10.1016/j.polymertesting.2018.03.006

37. Lee Y, Cho T, Lee B, Rho J, An KH, Lee YH (2003) Surface properties of fluorinated single-walled carbon nanotubes. J Fluorine Chem 120(2):99–104. https://doi.org/10.1016/s0022-1139(02)00316-0

38. Zhang P, Zhao J, Zhang K, Bai R, Wang Y, Hua C et al (2016) Fluorographene/polyimide composite films: mechanical, electrical, hydrophobic, thermal and low dielectric properties. Compos Part A Appl Sci Manuf 84:428–434. https://doi.org/10.1016/j.compositesa.2016.02.019
39. Wang X, Dai Y, Wang W, Ren M, Li B, Fan C (2014) Fluorographene with high fluorine/carbon ratio: a nanofiller for preparing low-κ polyimide hybrid films. ACS Appl Mater Interfaces 6(18):16182–16188. https://doi.org/10.1021/am5042516
40. Cao Y, Lai Z, Feng J, Wu P (2011) Graphene oxide sheets covalently functionalized with block copolymers via click chemistry as reinforcing fillers. J Mater Chem 21(25):9271. https://doi.org/10.1039/c1jm10420a

A Systematic Methodology for Retrofit Analysis of Refineries Preheat Trains with Variable Heat Capacity and Exchangers Fouling

Haya Kaled, Hany A. Elazab, Mamdouh Gadalla, Thokozani Majozi, Osama Abd El-Baari, and Fatma Ashour

1 Introduction

Energy efficiency has become one major factor to consider in chemical processes design because of high energy prices, fossil fuel limited resources and environmental restrictions applied worldwide to mitigate impact of climate changes. This research is oriented towards the sustainable development goals (SDGs) related to health and well-being, affordable and clean energy, and the climate action. Therefore, several process industries started to raise the awareness of energy conservation and improve the energy efficiency of processing plants to remain sustainable and competitive in the challenging global market. Energy integration is a key technique in enhancing energy efficiency to cut utility costs in the chemical industries. Several methods were established for exchanger network design. Heat integration in process industries intends to re-use all heat sources of the process streams and thus reduce heating demands overall [1]. The heat capacity (C_P) of process fluids is a function of temperature, which means that it isn't constant, and thus changes with the change of temperature. Fouling is also an important factor in revamping, as adding area without considering

H. Kaled · O. A. El-Baari · F. Ashour
Chemical Engineering Department, Faculty of Engineering, Cairo University, Giza, Egypt

H. A. Elazab
Chemical and Biochemical Engineering Department, Missouri University of Science and Technology, Rolla 65409, MO, USA

M. Gadalla (✉)
Chemical Engineering Department, Faculty of Engineering, Port Said University, Port Said, Egypt
e-mail: m.gadalla@eng.psu.edu.eg

M. Gadalla · T. Majozi
Faculty of Engineering and the Built Environment, University of the Witwatersrand, Johannesburg, South Africa

the fouling might not give the required duty. Most of retrofit studies in literature ignored the impact of heat capacities and fouling. Consequently, their modifications might not lead to a practical solution as the solution is not accurate as a result of ignoring the heat capacity and fouling effect [2]. Energy (or process) integration is important in chemical processes and crude oil refineries to reduce the consumption of fuel, as in some refineries part of the crude itself is used as fuel in the fired heater [1, 3].

Energy integration typically re-uses heat sources from processes to provide heat to cold sinks within the same process leading to minimum external heat requirement. As a result, adopting energy integration reduces the apparent cost of energy for a process. With less expensive energy, more resources will be used to improve, for example, the conversion of raw materials to products [4–10]. Process integration has two applications: (1) to optimally arrange exchangers and process facilities in processing plants for better heat exchange opportunities, and (2) to synthesize networks based on systematic techniques to maximize heat recovery and lessen the dependence on external utilities. In both applications, heat sources are optimally reused to provide heat to cold sinks. Efficient use of equipment is also part of the process integration scope [5, 11–14].

Heat exchanger networks (HENs) are necessary in the chemical plants to manage the heating and cooling requirement of the process, and minimize the external utility consumption through recovering process heat available with no operating costs [1, 3]. Process integration is tracked back to Hohmann. Linnhoff and Flower developed Hohmann's work, leading to the well-known Pinch Technology in 1977. This technique later become the solid foundation of most research done within the heat integration field till recent times [6, 15–17]. Pinch analysis (or technology) is a method for reducing energy consumption of industries by predicting energy targets ahead of complete design and reaching such targets by optimizing distribution between hot and cold resources through manipulating operational conditions. This research field is also known as "process integration", "heat integration", "energy integration" or "pinch technology" [6].

The concept of pinch analysis is originally discovered and further developed in late 70s by Hohmann, Huang and Elshout, Linnhoff et al. and Umeda et al. [10]. It presents a methodology for analyzing chemical processes and the surrounding utility systems depending on the first and second laws of thermodynamics.

Pinch analysis is applied in a systematic procedure: (1) energy targets are predicted at early stage of design for a given process conditions and minimum temperature approach, (2) minimum number of exchanger units and needed heat exchange areas are determined accordingly, (3) network is designed for minimum capital investment and utilities expenses [7].

As a result of process integration application, minimizing energy demands will lead to less environmental impact of climate change through less fuel combustion and less water resources consumed. Violating any one of the previous rules will result in increasing the energy requirements. Literature is rich in applications of Pinch Technology to a wide range of refining/gas processes, chemical plants and other related industries [8]. One main tool of Pinch Technology is Composite Curves to

predict energy targets for exchanger networks with any number of process streams. These curves are constructed typically for cold streams and hot streams, one for each type of streams. Composite curves are generated in temperature versus enthalpy (T/H) diagrams [8]. This technique is applicable for new network design and valid for analyzing existing ones for various objectives. The reuse or the revamping is essential for as energy saving, debottlenecking, capacity increase, carbon emissions cut, or changing feed or product specifications [1, 18–22]. Several methods for process integration and HEN revamping have been proposed aiming to fulfill process and plants' heating and cooling requirements. The use of heat exchanger networks design is a well-established tool for both new designs and retrofit situations, that has been developed over the years [22–26]. Research in process heat integration identifies systematic procedures that modifies process arrangements and operating conditions to improve overall energy efficiency of a plant. Most research reported in literature focused on retrofit of HENs in oil refiners ignored variation of heat capacities and fouling in equipment, leading to impractical results [1, 3, 6, 17, 18].

The aim of this work is to propose a design methodology for retrofit of preheat trains in petroleum refining industries for minimum energy requirements considering variable heat capacities of process streams and fouling in exchanger equipment. This objective serves to cut emissions of CO_2 gases and thus mitigate climate change's impact on the environment. In other words, the objective of the research helps to achieve SDG #13 focusing on Climate Action. In addition, the results of minimizing the dependence/consumption on the energy natural resources contribute to SDG #12 (Responsible Consumption and Production). In this case fuel burned as energy source for heating is efficiently consumed. The methodology is based on Pinch Analysis and process simulation.

2 Statement of the Problem

In order to reduce energy consumption in refineries and cut carbon emissions, the energy use in furnace should be decreased. A real refining plant, in Fig. 1, producing crude oil fractions and fuel products with a capacity of 85 thousand-barrels-per-day of crude oil feed is taken from the available library data of the simulator 'Aspen HYSYS®'. It includes atmospheric crude distillation tower and crude vacuum unit.

The crude oil is processed in several units to reach its final products like kerosene, diesel, gasoline, and other important fuels. At first it enters the atmospheric distillation unit at a relatively high temperature of approximately 343 °C. Raw crude oil is heated initially in a preheat train or HEN (Fig. 2) and then enters the furnace, where most of energy consumed. In order to decrease the energy consumption of the furnace, consequently decrease the overall energy consumption in the refinery [1, 18].

Figure 2 shows the preheat train of the crude oil feed stream, revealing details of heating crude oil stream from atmospheric temperature to target temperature by recovering heat from hot streams of the process. In this figure, crude oil stream
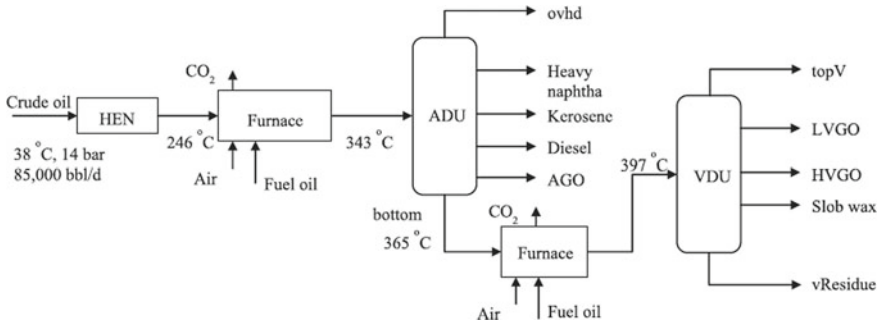
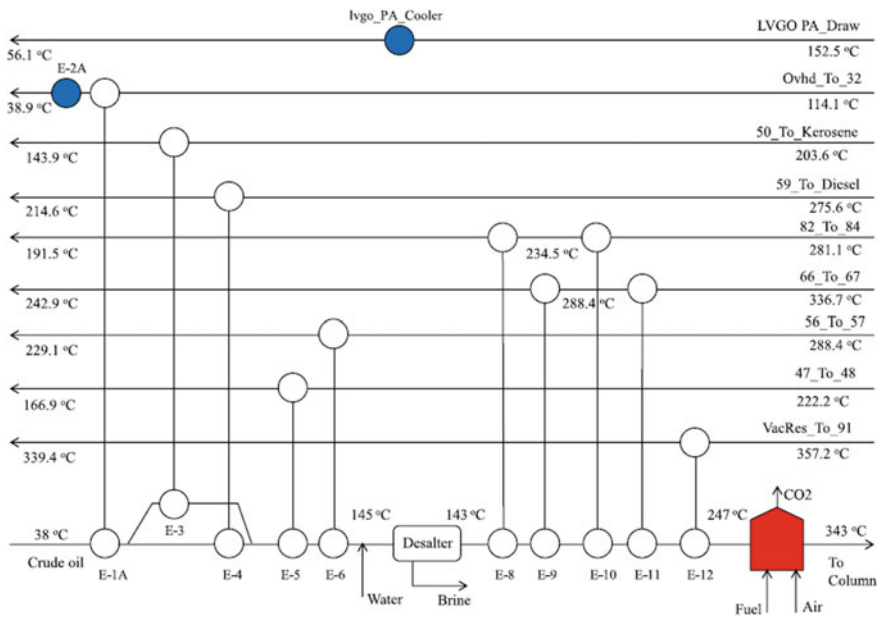**Fig. 1** Refining plant for crude oil distillation [1]

Fig. 2 An existing HEN including crude oil stream from the well to the distillation column [1]

is heated from atmospheric condition to 247 °C before entering the furnace to be heated further to 343 °C. A proposed revamping solution for the previous network was introduced by Gadalla [1] to increase the performance and the energy savings for the network. The temperature of crude oil feed to the fired heater increased from 247 to 275.7 °C, as shown in Fig. 3. The revamping solution comprises new exchanger unit and relocating a number of existing equipment, whose details can be found in literature [1]. The heat load on the fired heater for the revamping solution is 29.12 MW, to heat the crude oil stream from 275.7 °C before the furnace to the target temperature of 343 °C.
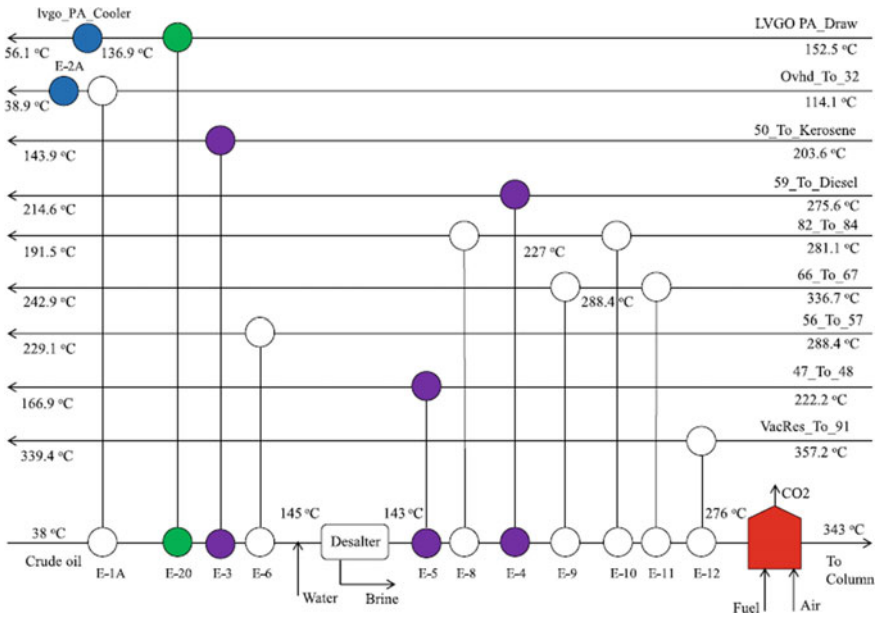
Fig. 3 A modified HEN for energy savings [1]

This revamping didn't take the variation of process fluids heat capacity and exchanger fouling into considerations. As a result, the solution when applied to the existing network might not lead to the predicted energy savings since heat capacity changes and exchangers suffer fouling. Therefore, the retrofit solution may seem impractical and results are not accurate. In this work, a systematic methodology will be proposed for the analysis of retrofit of a refinery's networks looking at the effect of heat capacities and exchanger fouling for minimizing energy consumption purposes.

3   Systematic Methodology

Figure 4 illustrates a systematic methodology to retrofit of refinery's heat exchanger network accounting for heat capacity and fouling. This systematic methodology for analysis is applicable in general to chemical process industries including oil and gas facilities. The systematic methodology starts with collecting the HEN data which includes temperatures, pressures, and flow rates. Once data are available, existing HEN is simulated using commercial packages such as Aspen HYSYS® and then validation of simulation results is performed against real data. Structure of existing network is fixed and fluid flow rates and temperatures are specified in the simulation to reproduce the real network. If the data validation is wrong, network simulation needs to be analyzed and checked. Otherwise, the retrofit methodology should proceed with
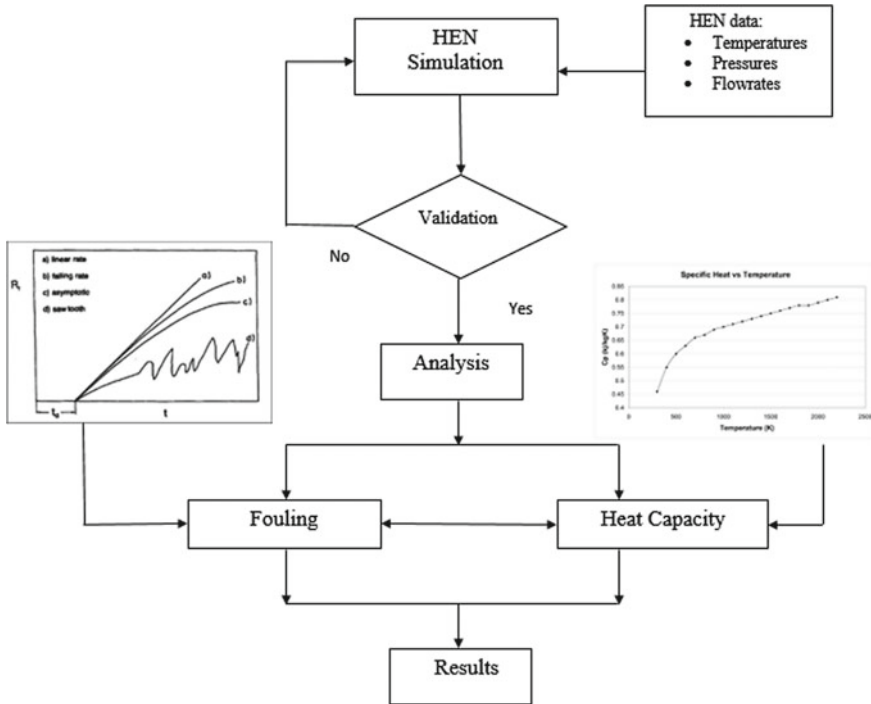
Fig. 4 A systematic methodology for retrofit of refinery's HEN

analysis. The retrofit analysis of HEN is divided into two sections: (1) heat capacity, and (2) fouling. The retrofit analysis is based on Pinch analysis as proposed by Gadalla [1], where energy targets are defined by composite curves and network is modified for minimum energy demands as shown by the simulated network of Fig. 5.

3.1 HEN Analysis with Variable Heat Capacity

When heat capacity C_P is considered in network analysis, the temperatures of process streams leaving exchangers seem different from proposed solutions with constant heat capacities. This is due to the fact that the heat duty differs according to the values of C_P (Fig. 6) [1, 3, 18]. Due to insufficient heat duty, temperature of hot outlet stream is higher than target, while outlet cold stream seems colder than target, leading to improper heat exchange (see Fig. 6). This is a result of underestimating or overestimating the value of heat capacity in the previous case study. Underestimating C_P is referred to the case that the values of heat capacities taken in calculations are smaller than the real values. Similarly, overestimating then implies that values considered are larger than real values. Commercial process simulators such
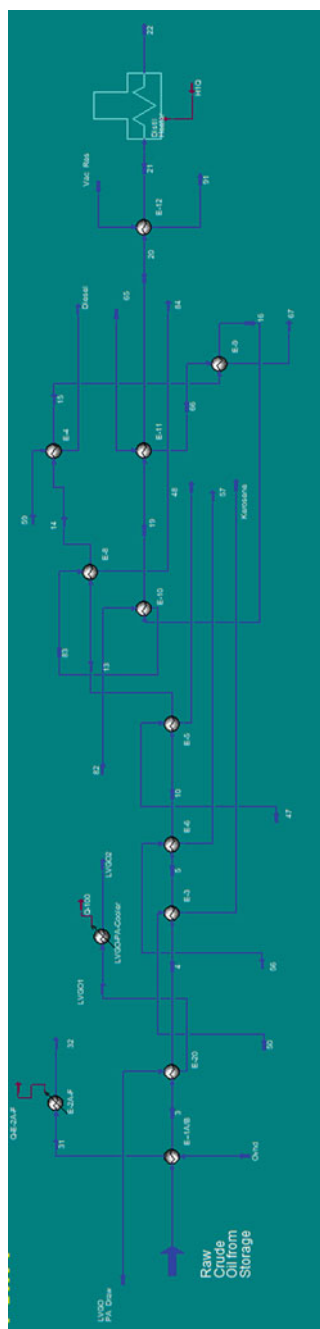
Fig. 5 HEN simulation on Aspen HYSYS®

as Aspen HYSYS® adopts thermodynamic models, such as the equation of state of Peng-Robinson, to calculate properties of fluids among which heat capacities are of importance. Therefore, such simulators are employed to address the variation of C_P of fluids during retrofit analysis. Both fluids into and from the exchanger equipment are taken into account with respect to their heat capacities, i.e. C_P for hot fluid and cold fluid (crude oil) is considered variable.

Results of heat capacities of fluids (such as crude oil stream) can be plotted against temperature ranges. Temperatures are classified according to the sensitivity of C_P with temperatures. A typical diagram for this dependence can be obtained as in Fig. 7. Two scenarios may be reached, one is underestimating C_P values and the other is overestimating C_P. For every fluid in the process, Fig. 7 can be constructed. However, experience tells that the main stream over wide range of temperature is of importance to consider such as crude oil feeds in petroleum refineries.
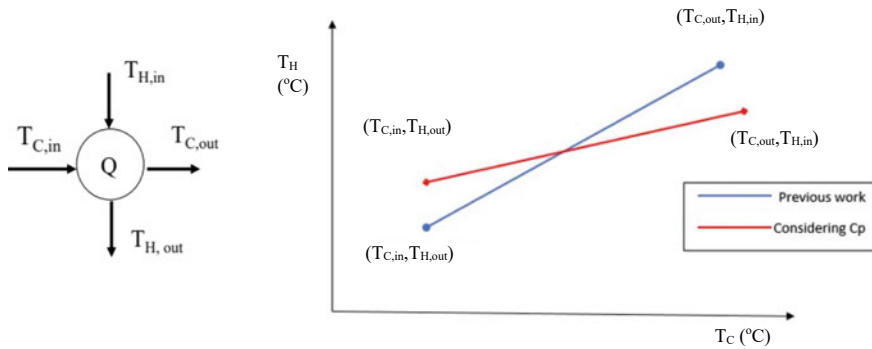

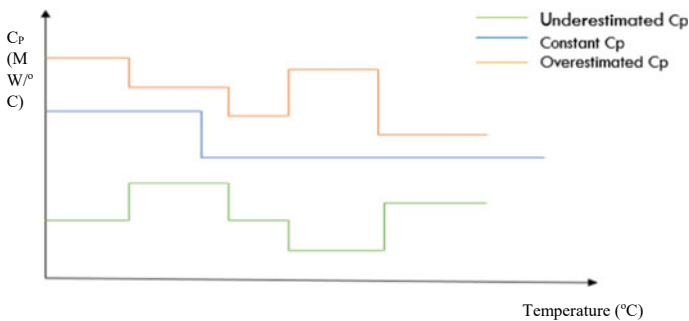**Fig. 6** Heat exchanger's temperatures diagram [1]

Fig. 7 Graphical representation for heat capacity versus temperature

3.2 HEN Analysis with Fouling

The outlet temperatures of process streams will be affected with fouling in the heat exchangers. So, the outlet temperatures of hot and cold streams are calculated for each exchanger considering the values of fouling according to the following equation: values of clean heat transfer coefficient (U_C) and fouling factor (f) are obtained from calculations and literature to get the values of dirt design coefficient (U_D). The fouling factor values vary from 0.001 to 0.003 ft^2 °F h/Btu [19].

$$\frac{1}{U_D} = \frac{1}{U_C} + f \tag{1}$$

Four scenarios are proposed in this work to calculate the values of U_D and hence the temperatures of outlet streams: (1) fouling factor of 0.003 ft^2 °F h/Btu, (2) fouling factor of 0.002 ft^2 °F h/Btu, (3) fouling factor of 0.001 ft^2 °F h/Btu and (4) variable fouling factor. For fluids of fouling tendencies, a fouling factor in exchangers is set to 0.003 ft^2 °F h/Btu, as in the case of crude oil streams. Then for less fouling fluids, fouling factors can be assumed as 0.0002 and 0.001 ft^2 °F h/Btu. Providing the values of U_D, the new heat duties are calculated to achieve the new set of outlet temperatures from Aspen HYSYS®, according to the following equation:

$$Q = U_D \times A \times \Delta T_m \tag{2}$$

where Q: heat duty, A: existing area of heat exchanger, ΔT_m: logarithmic mean temperature difference (or LMTD). Equation (2) can be applied also to calculate additional exchanger areas to keep the same heat duty before considering fouling as the difference between new area and existing one.

3.3 HEN Analysis with Variable Heat Capacity and Fouling

When the analysis is done considering both variable heat capacity and fouling simultaneously, we the previous steps are followed for fouling analysis such that the outlet temperatures are calculated with variable C_P as proposed by the simulator Aspen HYSYS®.

3.4 HEN Cost Analysis

Cost of energy savings and capital expenditure incurred by retrofit are calculated. Energy savings will equal the heat load on the fired heater after considering C_P and fouling minus the heat load of the original retrofit solution, i.e. not considering C_P

or fouling. It must be noted that this energy savings can be negative or positive. This implies that the original retrofit solution can be overestimating or underestimating the energy saving calculations. Nevertheless, the new methodology leads to robust and accurate solutions. Procedure to calculate energy costs is shown below:

(1) Get the energy difference for the furnace of the original case study and the Aspen HYSYS® simulator.
(2) Get the calorific value of this amount of energy as each barrel of oil burned has certain calorific value.
(3) Get the amount of fuel used by getting the number of barrels to be burned that give this energy difference.
(4) Calculate the number of barrels consumed annually.
(5) Multiply the number of barrels consumed annually by the cost of barrel of oil to give the cost of fuel consumed annually and thus annual savings.

Capital costs resulting from retrofit represent the cost of required area of additional areas needed to achieve the retrofit target. Cost of required area ($) can be calculated from the correlation proposed by Enríquez-Gutiérrez et al. [27], knowing the additional exchanger areas (m^2). Then, the payback time to recover this cost can be calculated from [1]:

$$\text{Cost of required area} = 1530 \times (\text{Additional area})^{0.63} \tag{3}$$

$$\text{Payback time} = \frac{\text{Cost of required area}}{\text{Annual savings}} \tag{4}$$

3.5 Greenhouse Gasses Emission

It is well known that environmental consequences of substantial consumption of fossil fuels contribute to global warming due to emissions of greenhouse gases. Emissions of CO_2 released from the combustion of petroleum-based fuels can increase the global warming significantly.

The flow rate of CO_2 (CO_2_Flow; kg/s) emitted can be determined as a result of burning fossil fuel in a fired heater to provide the necessary heating load (Q; kW) to the process from the following equation [28]:

$$CO_2\_\text{Flow} = \frac{1}{\eta}\left(\frac{Q}{NHV}\right)\left(\frac{\%C}{100}\right)\alpha \tag{5}$$

where η is the fired heater efficiency (90%) [28], α is the ratio of the molar masses of CO_2 and carbon (= 3.67), NHV is the net heating value of the fuel burned (kJ/kg). Net heating values (NHV) are assigned as 39,771 kJ/kg and 51,600 kJ/kg, and %C are set as 86.5 and 75.4 for heavy fuel oil and natural gas, respectively [28].

Accordingly, each megawatt of process heat required corresponds to the emissions of 2797 tons of CO_2 per annum.

4   Case Study and Results

The original network of case study presented in Fig. 2 [1] was simulated using Aspen HYSYS® simulator taking into account variable C_P provided by the simulator. Data were validated such as the heat duties of exchangers are fixed as the original case. Then, the outlet temperatures of the hot and cold streams for each heat exchanger were reported and compared with original case in Table 1.

Table 1 illustrates the difference between the inlet and outlet temperatures for hot and cold streams of the previous case study [1] and the simulation of Aspen HYSYS® with variable heat capacity. The crude oil stream, which is the main cold stream, outlet temperatures of Aspen HYSYS® is more than the temperatures mentioned in the previous case study. As shown in heat exchanger E-1 A/B, the outlet cold temperature in previous case study is 94.1 °C and the outlet temperature in current work considering C_P is 97.07 °C. Also, other heat exchangers have difference in their outlet cold and hot temperatures. Hence, a graphical figure was implemented for each heat exchanger in the HEN illustrating the comparison between the outlet temperatures of Aspen HYSYS® and the previous case as follows in Fig. 8. The difference in outlet temperatures is due to the variation of C_P with temperature. Given the new temperatures of Aspen HYSYS® and the heat duties, the variable heat capacities are calculated for each exchanger unit and shown in Fig. 9 compared with constant C_P of original case study [1].

Table 1 Temperatures of Aspen HYSYS® versus previous case study

Exchanger	$T_{c,in}$ (°C)	$T_{c,out}$ (°C)	$T_{h,in}$ (°C)	$T_{h,out}$ (°C)	$T_{c,out}$ with C_P (°C)	$T_{h,out}$ with C_P (°C)
E-1 A/B	37.8	94.1	114.1	72.8	97.07	78.5
E-20	94.1	99.6	152.5	136.9	102.5	138
E-3	99.6	110.1	203.6	143.9	112.6	143.9
E-6	110.1	145	288.4	229.1	144.8	229.1
E-5	142.6	168	222.2	166.9	169	166.9
E-8 A/B	167.9	194	227	191.5	197.5	191.5
E-4	194	201.3	275.6	214.6	205.7	214.6
E-9	201.3	211	288.4	242.9	217.7	242.9
E-10 A/B	210.9	250.6	281.1	227	259.7	228.3
E-11	250.6	261.5	336.7	288.4	263.3	288.4
E-12	261.5	275.7	357.2	339.4	281.2	339.4
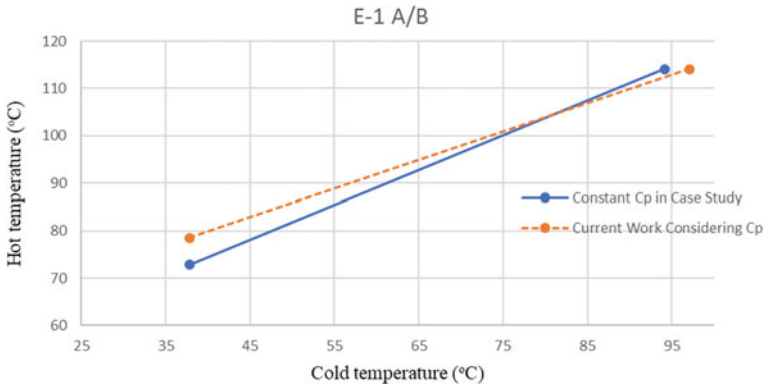
Fig. 8 Graphical presentation for the modified heat exchanger E-1 A/B
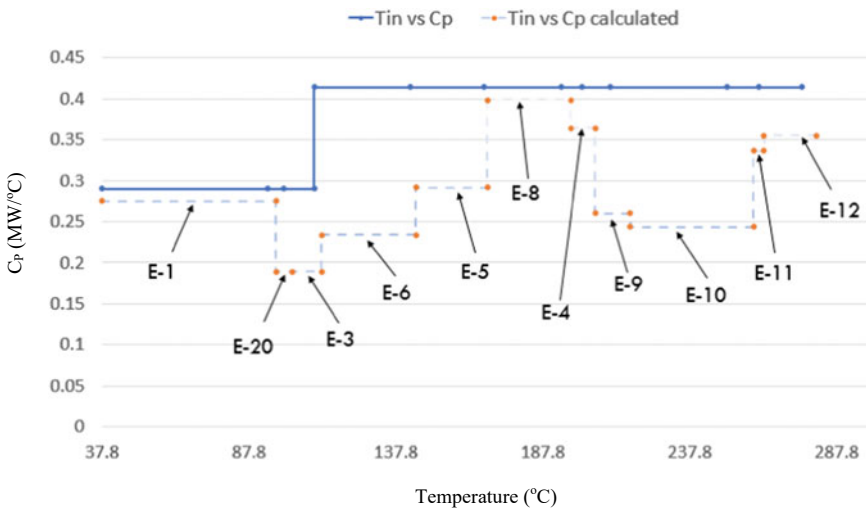
Fig. 9 C$_P$ versus temperature

In Fig. 9, it is noted that the value of old heat capacity for the crude oil cold stream constant during two intervals, from heat exchanger E-1 to E-6, and from heat exchanger E-5 to E-12. These two intervals are separated by the desalter, because of the heat capacity of the water. However, the new heat capacity calculated is change-able for each heat exchanger, as it is a function in many factors like the temperature and composition of each stream. It is clear that in many temperature intervals the original solution of previous case study [1] overestimated the C$_P$. This explains why in some exchangers the outlet temperature of crude oil is higher than that of the original retrofit solution. In overall, the temperature of the crude oil prior entering the furnace increased from 275.7 to 281.2 °C (see Fig. 9). As a consequence of

this finding, the heat exchange areas need to be increased further to accommodate the heat duties. It is clear that if the heat capacities were underestimated, the area required should be decreased as the heat duty will be more than required. Since the temperature before the furnace increased from 275.7 to 281.2 °C, the corresponding furnace heat load became 26.94 MW (compared with 29.12 MW for base case). Thus the energy savings are 2.18 MW.

Fouling consideration was performed following the procedure presented above by calculating the dirt design factor U_D, clean coefficient U_C and additional areas A, for the various scenarios mentioned earlier. Table 2 shows such results for scenario 4 as an example, i.e. for fouling factors as intervals of f = 0.0002 ft² °F h/Btu. Assuming that the starting value of fouling factor equals 0.003 ft² °F h/Btu, as crude oil enters the first exchanger full of dirt, and the value in the last exchanger is 0.001 ft² °F h/Btu, as it is the least value of fouling. As a result of fouling, the outlet stream temperature of E-1 A/B is shown in Fig. 10 compared with the original case and the case with variable C_P. As shown in figure, the temperature profile for the case of considering fouling lies to the left of the base case temperature profile on hot end, while it is above the base case on cold end. This is due to the exchanger fouling that resulted in a reduced head duty transferred across exchanger. Therefore, the cold stream is heated to a lower temperature than the base case target and correspondingly the hot stream is cooled to a little higher than the target.

The cost of the energy savings is calculated by estimating the fuel saved in the furnace. The energy saved from the furnace was found as mentioned previously to be 2.18 MW. This energy saving corresponds to a cut in CO_2 emissions of approximately 5594 tons/year (Eq. 5). As a result, the environmental consequences of global warming are thus relaxed and climate change impact is lessened. Therefore, the barrels-of-oil saved was calculated by knowing the calorific value of the fuel (1700 kWh/barrel) [21]. The fuel savings thus was obtained as 9412 barrels-per-year

Table 2 Fouling with interval difference 0.0002 ft² °F h/Btu

Exchanger	Existing area (m²)	Qold (MW)	Qnew (MW)	Delta Q (MW)	Area required (m²)	Area extra (m²)
E-1 A/B	328.0	16.30	15.50	0.79	344.88	16.88
E-3	98.7	3.03	3.00	0.03	99.84	1.14
E-6	209.5	10.12	10.03	0.08	211.24	1.73
E-5	320.2	10.52	10.33	0.19	326.08	5.88
E-8 A/B	651.6	10.77	10.64	0.12	659.24	7.64
E-4	58.6	3.03	2.97	0.06	59.87	1.27
E-9	108.0	4.00	3.95	0.04	109.09	1.09
E-10 A/B	759.3	16.40	16.16	0.23	770.43	11.13
E-11	126.5	4.50	4.47	0.03	127.44	0.94
E-12	146.1	5.88	5.85	0.028	146.81	0.71
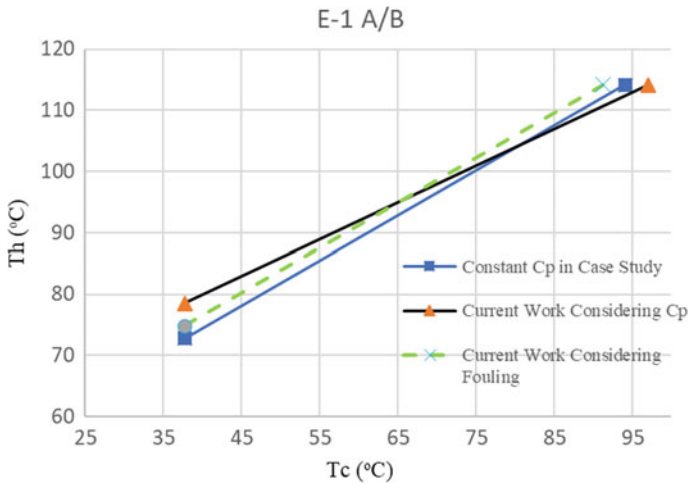
Fig. 10 Graphical presentation for the modified heat exchanger E-1 considering fouling

leading to annual savings of 508,719 $ since the cost-per-barrel; is 54.05 $ [23]. Capital costs of additional areas to existing network were estimated as stated earlier and found to be 285,983 $, leading to a payback time of almost 0.6 year [24, 25].

5   Conclusions and Recommendations

In this work, a systematic methodology study was proposed for the analysis and revamping of refinery's preheat trains taking variable heat capacities and heat exchangers' fouling into consideration. A real refining plant for producing crude oil fractions and fuel products with a capacity of 85 thousand-barrels-per-day of crude oil feed is taken from the available library data of the simulator 'Aspen HYSYS®'. The assumption of constant heat capacity is criticized and analyzed. This led to an increase in the inlet temperature to the furnace from 275.7 to 281.2 °C. In addition to take fouling into considerations the temperature will be 281.1 °C. However, the furnace duty will be decreased by 2 MW with carbon dioxide emissions cut of 5594 tons/year. This will cause a decrease in the cost of the furnace fuel by approximately 508,718.6 dollars/year. On the other hand, the payback time for the heat exchangers' cost will be 0.6 year to recover the capital investment of the modifications of nearly 286 k$. Both SDGs #12 and #13 are met through this research outcome since natural resources of energy fuels are efficiently consumed (SDG #12) and greenhouse gases are cut (SDG #13).

Nomenclature

A	Heat transfer area (m^2)
CO_2_Flow	Flow emissions of CO_2 (kg/s)
%C	Percentage carbon present in fuel (–)
C_P	Heat capacity of streams (kJ/kg K)
f	Fouling factor (ft^2 °F h/Btu)
NHV	Net heating value of fuel (kJ/kg)
U_C	Clean overall heat transfer coefficient (Btu/ft^2 °F h)
U_D	Design overall heat transfer coefficient (Btu/ft^2 °F h)
Q	Heat transfer rate or duty (kW)
Qnew	New heat transfer rate or duty (kW)
Qold	Old heat transfer rate or duty (kW)
T_C; T_c	Temperature of cold stream (°C)
$T_{C,in}$	Inlet temperature of cold stream (°C)
$T_{C,out}$	Outlet temperature of cold stream (°C)
T_H; T_h	Temperature of hot stream (°C)
$T_{H,in}$	Inlet temperature of hot stream (°C)
$T_{H,out}$	Outlet temperature of hot stream (°C)
η	Fired heater efficiency (–)
α	Ratio of molar masses of CO_2 and carbon (= 3.67)
ΔT_m	Logarithmic mean temperature difference or LMTD (°C)

References

1. Gadalla MA (2015) A new graphical method for pinch analysis applications: heat exchanger network retrofit and energy integration. Energy 81:159–174
2. IEA (2011) World energy outlook. Organisation for Economic Co-operation and Development (OECD)/International Energy Agency (IEA), Paris
3. Gadalla MA, Abdelaziz OY, Ashour FH (2016) Conceptual insights to debottleneck the network pinch in heat-integrated crude oil distillation systems without topology modifications. Energy Convers Manag 126:329–341
4. Westerberg AW (1992) An overview of process integration methodologies
5. Gundersen T (2013) Heat integration—targets and heat exchanger network design. 1 Introduction to key concepts and major topics, chap. 2.1. In: Handbook of process integration, pp 1–44
6. Piagbo BK, Dagde KK (2013) Heat exchanger network retrofit design by eliminating cross pinch heat exchangers. Am J Eng Res 2(05):11–18
7. Sahdev M (2010) Pinch technology: basics for the beginners. Chem Eng Resour 1–8
8. Kemp IC (2007) Pinch analysis and process integration: a user guide on process integration for the efficient use of energy. Pinch Anal Process Integr 416
9. CANMET Energy Technology Centre (2003) Pinch analysis: for the efficient use of energy, water and hydrogen, vol 11, no 4
10. Rangaiah GP (2016) Chemical process retrofitting and revamping: techniques and applications
11. Smith R (2005) Chemical process design and integration

12. Maloney JO (2007) Conversion factors and mathematical symbols
13. Awad MM, El-wahab IFA, Gad HE (2007) Effect of surface temperature on the fouling. In: Eleventh international water technology conference
14. Nptel (2006) Lecture 1: heat exchangers classifications. Chem Eng Des II 1–41
15. Al-Haj H (2012) Fouling in heat exchangers. MATLAB Fundam Tool Sci Comput Eng Appl 3
16. Wang B, Klemeš J, Li N, Zeng M, Varbanov P, Liang Y (2021) Heat exchanger network retrofit with heat exchanger and material type selection: a review and a novel method. Renew Sustain Energy Rev 138:1–26
17. Hogskola CT, View S, Nordman R (2015) New process integration methods for heat-saving retrofit projects in industrial systems new process integration methods for heat-saving retrofit projects in industrial systems, no Jan 2005
18. Kamel DA, Gadalla MA, Abdelaziz OY, Labib MA, Ashour FH (2017) Temperature driving force (TDF) curves for heat exchanger network retrofit—a case study and implications. Energy 123:283–295
19. Kern DQ (1965) Process heat transfer, p 757
20. http://www.essco.co.uk/Monitor/Detail_Output.html. Cited in May 2019
21. http://www.conversion-website.com/energy/barrel-of-oil-equivalent-to-kilowatt-hour.html. Cited in June 2019
22. https://www.engtips.com/viewthread.cfm?qid=389883. Cited in June 2019
23. https://oilprice.com/oil-price-charts/45. Cited in June 2019
24. https://matche.com/equipcost/Exchanger.html. Cited in Dec 2019
25. https://economictimes.indiatimes.com/wealth/tax/finance-ministry-notifies-cii-for-the-fy-2019-20-as-289/articleshow/71107063.cms?from=mdr. Cited in Dec 2019
26. Napitupulu FH et al (2023) Design and fabrication of shell and tube heat exchanger with one pass shell and two pass tube as a water heater with hot sulfur water. J Phys Conf Ser 2421, 012034
27. Enríquez-Gutiérrez VM, Jobson M, Ochoa-Estopier LM, Smith R (2015) Retrofit of heat-integrated crude oil distillation columns. Chem Eng Res Des 9(9):185–198
28. Abdelaziz OY, Hosny WM, Gadalla MA, Ashour FH, Ashour IA, Hulteberg CP (2017) Novel process technologies for conversion of carbon dioxide from industrial flue gas streams into methanol. J CO_2 Utilization 21:52–63

Maximizing Energy Efficiency in Petroleum Refining: Case Study—Delayed Coker Unit in an Egyptian Refinery

Mohamed Shahin, Hany A. Elazab, Mamdouh Gadalla, Thokozani Majozi, and Fatma Ashour

1 Introduction

The petroleum refining industry is considered one of the most critical industries that provides us with more products that are necessary for our daily activities including refinery gas, LPG gasoline, diesel, solar and asphalt. Despite these valuable products, the petroleum refining processes use more energy (heat and electricity) and such increase in the energy consumption will decrease the overall profit from the refinery plant. Environment impact is strongly related to energy consumption through the large quantities of carbon dioxide released in fuel combustion. Therefore, the common trend is to reduce the energy consumption and maximize energy efficiency for each unit involved in the petroleum refining flowsheet and also for rationalization in the used fuel with minimum emissions for the environment [1–5]. Petroleum refiners are massive facilities with including several physical equipment, reactors, columns, exchangers etc. to process a barrel of crude oil feed into valuable fuel products, light gases and chemicals. The 'bottom of the barrel' has become more of a problem for refiners because heavier crudes are being processed and the market for

M. Shahin · F. Ashour
Chemical Engineering Department, Faculty of Engineering, Cairo University, Giza, Egypt

H. A. Elazab
Chemical and Biochemical Engineering Department, Missouri University of Science and Technology, Rolla 65409, MO, USA

M. Gadalla (✉)
Chemical Engineering Department, Faculty of Engineering, Port Said University, Port Said, Egypt
e-mail: m.gadalla@eng.psu.edu.eg

M. Gadalla · T. Majozi
Faculty of Engineering and the Built Environment, University of the Witwatersrand, Johannesburg, South Africa

heavy residual fuel oils has been decreasing. Historically, the heavy residual fuel oils have been burned to produce electric power and to supply the energy needs of heavy industry, but more severe environmental restrictions have caused many of these users to switch to natural gas. Thus when more heavy residuals are in the crude there is more difficulty in economically disposing of them. Coking units convert heavy feedstocks into a solid coke and lower boiling hydrocarbon products which are suitable as feedstocks to other refinery units for conversion into higher value transportation fuels. In typical coking units, heavy residues from vacuum towers are thermally cracked under sever conditions to upgrade heavy residues into lighter products such as straight run gasoline and distillates. The process completely reduces hydrogen so that the residue is a form of carbon called 'coke'. The bottom of the barrel is heated to typically 440–500 °C and held in reactor drums for approximately 24 h 'delayed' at 2–5 bar until it cracks into light products leaving coke solids.

The process integration science is considered one of the most important inventions in the chemical industry in the last decades for reducing the used energy in the industry [6–8]. Several units belong to modern petroleum refiners; first process is the desalting system that uses heat to increase the crude oil and water mixture temperature to about 121 °C. Also it uses high potential electric field for the desalter and also electrical energy for the crude oil and water pumping [9–11]. Second refining process is the atmospheric distillation unit that consumes heat in a furnace to raise the crude oil temperature to about 375 °C, also uses steam for stripping purposes in the atmospheric column to increase the product purification and also using electrical energy for pumps [12–14]. The third refining process is the vacuum distillation unit that requires heat to increase the temperature of the bottom residue of the atmospheric distillation to about 445 °C. Steam is used in ejectors to create vacuum in the column. Then, one important unit is the delayed coking unit (DCU) that uses heat in furnace to raise the temperature of the feed from the bottom of the vacuum distillation unit to about 500 °C [15–17]. To run modern refiners, substantial quantities of fuels in furnaces and steam are consumed in the typical refinery processes to provide heat and electricity for operation. Consequently, environment is harmed with emissions of CO_2 and thus global warming problem becomes sever.

From the previous discussion, it is highlighted that energy is highly important in the petroleum refining processes, and that furnaces are needed to transfer heat to the process stream for large difference of operation temperatures. In addition, steam is used for many purposes such as heating the process streams in heat exchangers, as a stripping agent in the stripping columns to increase the purity of some products, as a heating source for some distillation columns, for driving the turbines, for creating vacuum through steam ejectors. Further, electrical energy is used for operating pumps, compressors, air coolers fans and for providing high potential electrical field in the desalting process [1, 5–7, 18–22].

This research considers an existing delayed coker of an Egyptian oil refinery to maximize energy efficiency and reduce fuel consumption as a driver to minimize greenhouse gases emitted from furnaces. This research is oriented towards the sustainable development goals (SDG's) related to health and well-being, affordable

and clean energy, and the climate action. In this context, process integration techniques are employed to identify process modification and optimum opportunities for heat integration between hot and cold sources within the plant. Revamping methods and approaches are very common in petroleum refining for several objectives, with more attention to crude atmospheric units and vacuum fractionation towers [23, 24]. In most of these research results, the exchanger network is considered for revamping studies for efficient reuse. However, little work is documented for delayed coker units in revamping applications. Not much recent work has been done on revamping of delayed coker; most reported research focus on the chemical processing of delayed coker [25] or revamping of a complete refining process including delayed coker among several units [26]. The expected results are more profit, less fuel consumption, lower greenhouse gas emissions, and more sustainable process. The SDGs of Climate Action (#13) and Responsible Consumption and Production (#12) are both achieved in this research are a result of lowering the tons released of CO_2 and through the efficient use of energy natural resources, i.e. fuel burned to provide heat for separation.

2 Research Methodology and Process Description

In this research study, a case study of an Egyptian delayed coker unit (DCU) is revamped. The revamping method is focusing on the efficient reuse of the existing network with the minimization of both energy and utility requirements. The revamping approach is based on the application of Pinch Analysis Principles [11] and the use of commercial process simulators (e.g. Aspen Energy Analyzer®). In the revamping method, the heat exchanger network (HEN) of the DCU is considered [12–14, 27]. The following is a systematic procedure on how to implement the revamping on HEN of the delayed coker unit:

(1) Data collection of process streams and heat exchangers.
(2) Energy targeting and pinch temperature calculations for existing ΔT_{min}.
(3) HEN simulation and data validation.
(4) Revamping methodology implementation.
(5) Calculation of total investment and energy saving costs.
(6) Selection of the optimum design.

In steps (2) and (3), Aspen Energy Analyzer® is employed for energy targeting, HEN simulation and validation. The data required for the HEN simulation is mainly the inlet and outlet temperatures of the heat exchangers, their heat loads and the outlet and inlet to the furnace. The simulation of HEN requires the entry of stream temperatures and heat loads across exchanger units. Pinch Analysis principles embedded in the simulator are applied to calculate the minimum heating and cooling requirement necessary for the process at the existing ΔT_{min} (minimum temperature driving force). Then the grid diagram of the existing HEN is constructed. For validation step, the simulation results are compared with the actual data of the existing HEN of DCU.

2.1 HEN Revamp Algorithm

Figure 1 summarizes the detailed steps for revamping method to be applied to the case study of the HEN of DCU. This algorithm is graphical based and applies to maximize the temperature of the cold fluid (e.g. bottom of barrel) before entering the furnace to reduce the heat load on the furnace and thus cut emissions and improve profit. Figure 2 [1] is constructed for the existing HEN to determine violation to Pinch Analysis and identity potential process modifications for better heat recovery opportunities. Areas (1) and (3) represent optimum feasible regions for relocating exchanger equipment. Such a graph is generated by knowing the exchanger streams terminal temperatures. Potential modifications can be identified, including additional areas, relocation of existing exchangers, repiping and resequencing of units. Capital investment is then incurred to provide modification solutions. Best economic design is selected with maximum energy efficiency.

2.2 Case Study and Process Description

In the present work, the developed methodology is applied to an actual case study of a heat exchanger network of a delayed coker of an Egyptian refinery (south Egypt). The data of the existing unit are confidential and the processing capacity is several tons per day of heavy bottoms from the vacuum distillation unit. The DCU produces LPG with flow of 6.6 t/h, Naphtha with 12.1 t/h, LGO with 35.6 t/h, HGO with 48.9 t/h and coke with flow of 44.1 t/h. Exchanger network data are available for different sections of the existing DCU, a sample of which is shown in Fig. 3 representing the network of the main fractionator.

The network shown in Fig. 3 represents a part of the total exchanger network of the DCU existing in the plant. As shown in figure, process hot streams run from left to right, while cold streams are shown to run from right to left. For example, stream 'LGO Product' is hot and available at 175 °C and is cooled using air cooler (E-16) to 55 °C. Some hot streams exchange heat with cold streams and this is displayed through the exchangers as circles connecting both streams. As an example, hot stream 'HGO Product' exchanges its heat with the cold stream 'Residue feed from storage' in the exchanger E-05.

2.3 HEN Simulation and Validation

Data collected from the different sections of the DCU are simulated using Aspen Energy Analyzer®, and results of simulation are shown in Fig. 4. The existing network contains some 29 exchanger unit. Data simulated include exchangers, heat loads, supply and target temperatures of process streams entering and leaving exchangers.
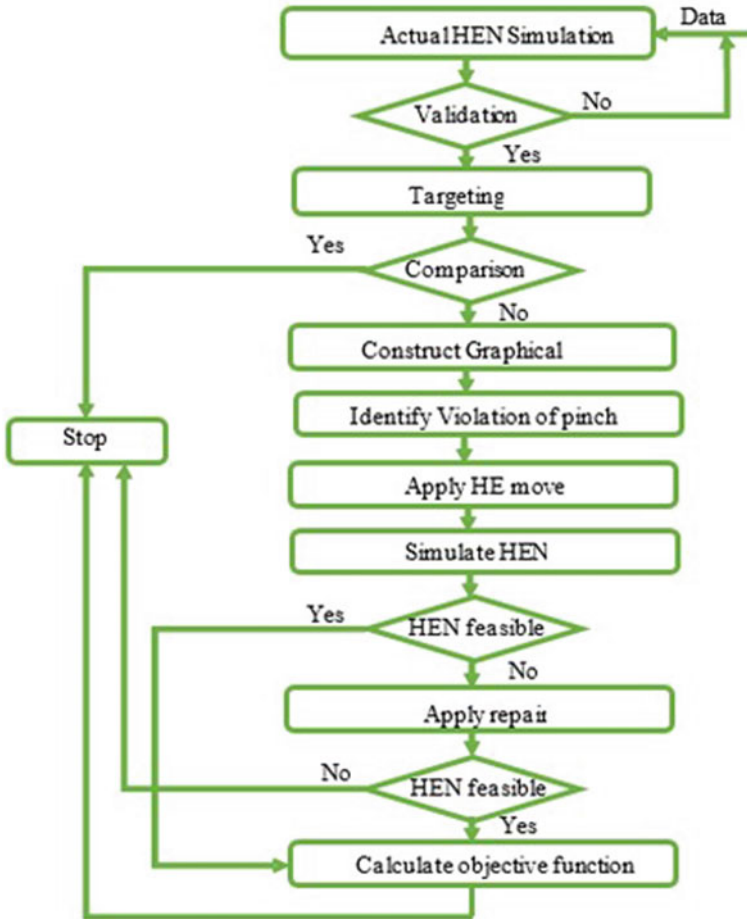
Fig. 1 HEN revamping algorithm

The existing DCU consumes total heating utility of $39(10)^6$ kcal/h and cooling utility of $81(10)^6$ kcal/h. The minimum temperature approach of the existing network (HEN) is given as 15 °C for the existing of the DCU. Simulation results are validated against actual data, as shown in Table 1. The data comparison between simulation and actual data reveal very good agreement (Table 1).

2.4 HEN Energy Analysis

At ΔT_{min} of 15 °C, Aspen Energy Analyzer® is employed to determine energy targets and to generate composite curves for the given/simulated HEN. Figure 5 displays
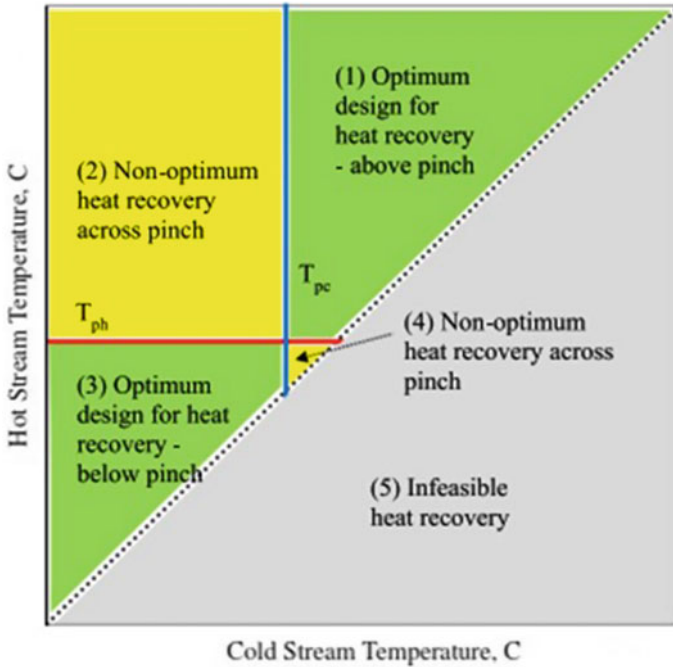
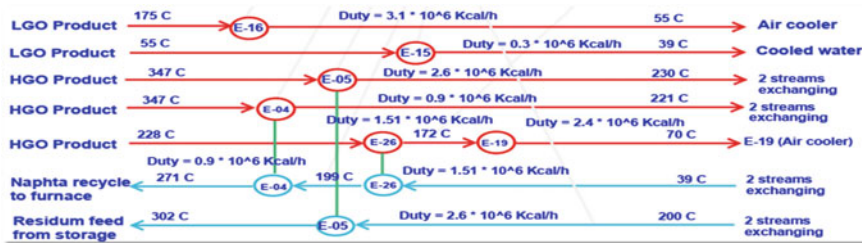**Fig. 2** Feasibility regions diagram for heat recovery [1]

Fig. 3 Data extraction for the main fractionator

the composite curve for the existing network. The energy targets can be extracted from Fig. 5; minimum heating duty is the heat required above 250 °C, and the minimum cooling duty is the cooling required below 160 °C. Energy targets are found to be $34.52(10)^6$ kcal and $70.43(10)^6$ kcal/h for heating and cooling respectively. Further, the pinch temperatures are 193 °C for the hot streams, and 173 °C for cold streams. Grid diagram for the existing HEN is constructed as shown in Fig. 6. It can be observed that the network comprises 36 process streams. The next step is to identify violations to Pinch Analysis principles which are: cooling above the pinch temperature, heating below the pinch temperature and exchanging heat from
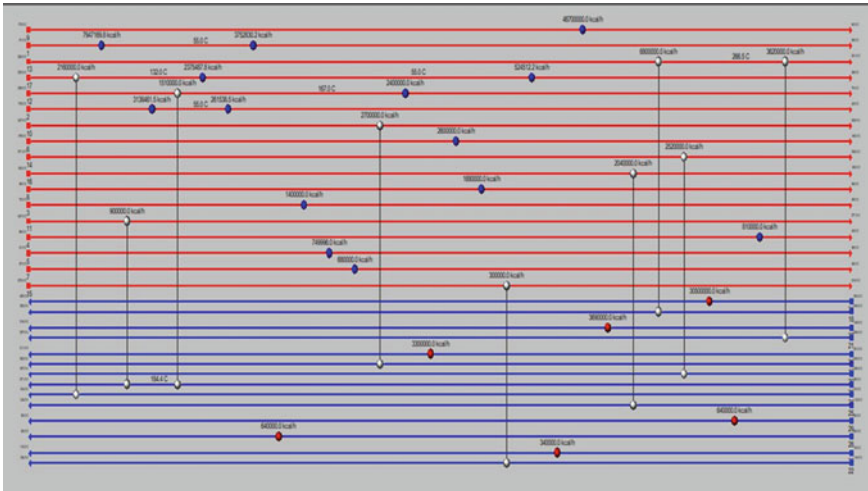
Fig. 4 HEN simulated using Aspen Energy Analyzer®

above the pinch to below or vice versa. By examining the grid diagram of Fig. 6, the following violations to Pinch Analysis are detected and on which revamping modifications are focused:

(1) Heating below the pinch in streams #32, #34 and #35.
(2) Exchangers across the pinch: E-26 between streams #14 and #27; E-06 between streams #18 and #26; and E-12 between streams #20 and #29.

3 Results and Discussion

Provided that the violations to Pinch Analysis Principles identified in Fig. 6 (Sect. 2.4), potential modifications are proposed to relax such violations. Figure 7 summarizes the design of these potential revamping modifications with the HEN grid diagram. The modifications focus on those exchangers crossing the pinch temperatures, i.e. E-26, E-06, and E-12. E-26 originally exchanges heat between streams #14 (hot) and #27 (cold) and as such it crosses the pinch. This hot stream is supposed to exchange heat with cold streams above the pinch/not below the pinch. Therefore, the revamping modification is to integrate the heat of stream #14 with the cold stream #32 in two stages, above the pinch in exchanger E-A and below the pinch in E-G, rather than with only one cold stream #27. Similarly, the hot stream #18 would better exchange heat with cold stream #27 (above the pinch) in exchanger E-B rather than with stream #26 (below the pinch). Hot stream #20 would exchange heat below the pinch with cold stream #29 in E-F. Therefore, these 4 new exchangers (E-A, E-B, E-F, E-G) will overcome the violation to Pinch Analysis and as such they fulfill the principles. Expectedly, the overall energy efficiency would improve.

Table 1 HEN simulation and validation

| Ex.	Actual HEN					HEN simulation				
	Q (MW)	Tube side streams		Shell side streams		Q (MW)	Tube side streams		Shell side streams	
		Tout (°C)	Tin (°C)	Tout (°C)	Tin (°C)		Tout (°C)	Tin (°C)	Tout (°C)	Tin (°C)
E-1	3.62	221	269	207	206	3.62	221	266.5	207	206
E-2	6.8	269	352	302	200	6.8	266.5	352	302	200
E-3	2.52	232	371	207	206	2.52	232	371	207	206
E-4	0.89	221	374	271	199	0.89	221	374	271	199
E-5	2.71	230	347	302	200	2.71	230	347	302	200
E-6	0.3	310	372	136	116	0.3	310	372	136	116
E-7	2.52	171	140	160	193	2.52	171	140	160	193
E-8	1.86	37	32	38	55	1.86	37	32	38	55
E-9	1.44	37	32	38	72	1.44	37	32	38	72
E-10	0.81	43	37	49	89	0.81	43	37	49	89
E-11	0.75	37	32	38	51	0.75	37	32	38	51
E-12	2.16	144	202	104	74	1.96	144	202	101.2	74
E-13	2.04	160	193	145	115	2.04	160	193	145	115
E-14	0.68	43	32	38	57	0.68	43	32	38	57
E-15	0.27	37	32	39	55	0.3	37	32	39	55
E-16	3.1	175	55	39	58.5	3.1	175	55	39	58.5
E-17	3.3	253	378	211	201	3.3	253	378	211	201
E-18	1.68	43	32	38	59	1.68	43	32	38	59
E-19	2.4	70	171	39	55.7	2.4	70	171	39	55.7
E-20	2.4	55	91	39	53.3	2.4	55	91	39	53.3
E-21	2.8	55	144	39	67.6	3	55	144	39	67.6
E-22	2.8	160	178	39	104.3	2.8	160	178	39	104.3
E-23	2.6	60	173	39	78.5	2.6	60	173	39	78.5
E-24	0.1	37	32	38	55	0.1	37	32	38	55
E-25	3.69	216	149	253	378	3.69	216	149	253	378
E-26	1.51	171	228	199	39	1.51	171	228	199	39
E-27	0.64	82	66	199	199	0.64	82	66	199	199
E-28	0.64	82	66	199	199	0.64	82	66	199	199
E-29	0.34	115	15	199	199	0.34	115	15	199	199
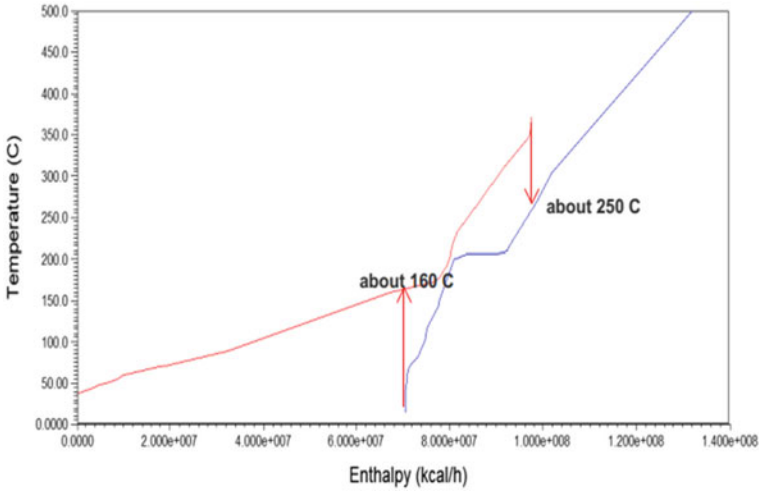
Fig. 5 HEN composite curve
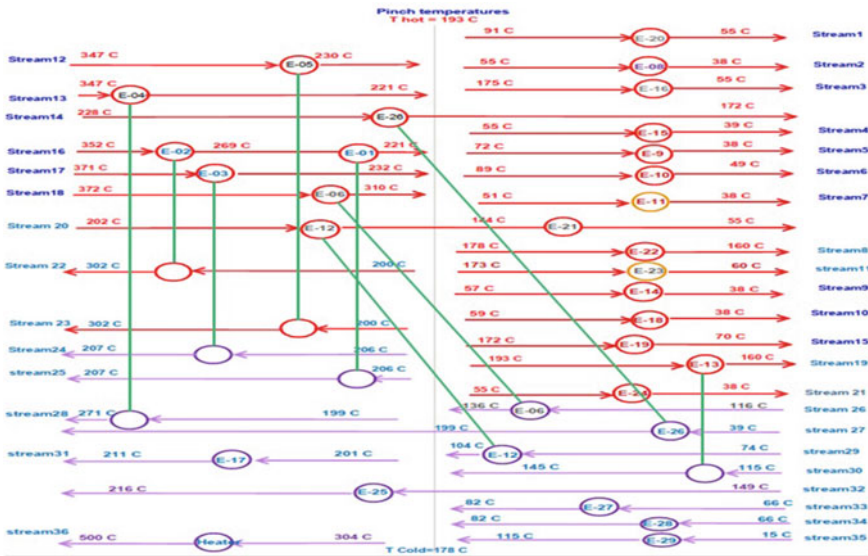
Fig. 6 HEN grid diagram

According to Fig. 6, streams #32, #34 and #35 are heated below the pinch in exchangers E-27 with 0.74 MW, E-28 with 0.74 MW and E-29 with 0.4 MW, respectively violating Pinch Analysis Principles. These cold streams should not be heated below the pinch and they optimally need heat integration with hot streams below the pinch. To solve this problem, these exchangers are relocated to exchange heat with
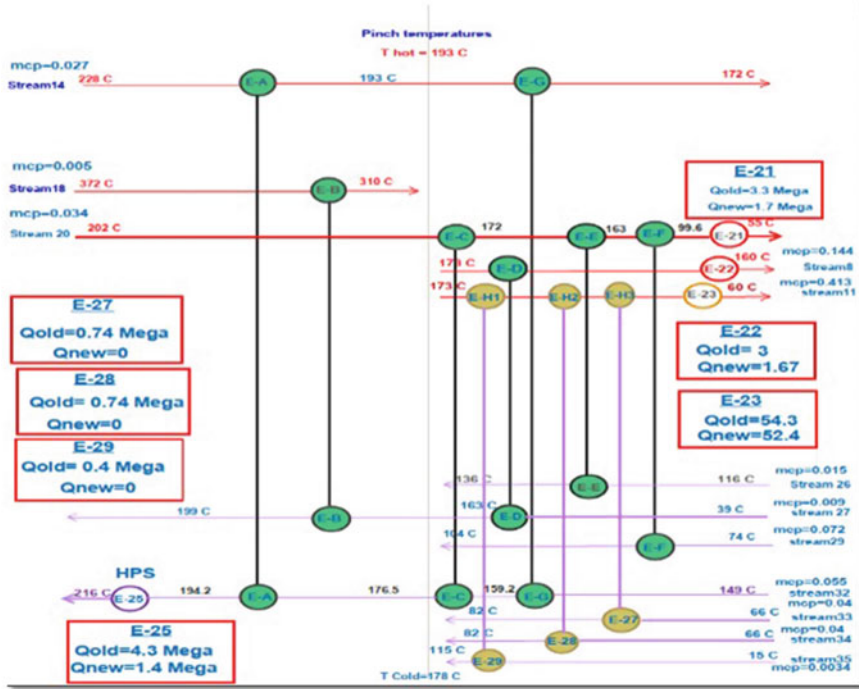
Fig. 7 HEN revamping modifications

one hot stream (#11) below the pinch, namely in exchangers E-H3, E-H2 and E-H1, as shown in Fig. 7. This relocation modification would necessitate some additional areas to existing equipment. As a result of these modifications, the heating duties of the heaters E-27, E-28 and E-29 are no more required leading to energy savings of 1.88 MW (= 0.74 + 0.74 + 0.40).

In the original network, hot stream #20 exchanges heat across the pinch with cold stream #29 (in E-12) as mentioned above, and then is cooled in a cooler (E-21). The revamping modification is shown in Fig. 7 as exchanging heat in exchangers E-C, E-E and E-F with cold streams #32, #26 and #29 respectively and finally is cooled in a cooler E-21. Further cold stream #32 is originally heated using heater from 149 to 216 °C with heating load of 4.3 MW in E-25 (see Fig. 7). As a result of the new modifications proposed in Fig. 7, this cold stream is preheated in exchangers E-G, E-C and E-A to a temperature of 194.2 °C before entering the heater to the final temperature (216 °C). The current heating load on the heater E-25 becomes 1.4 MW. This results in an energy saving of 2.9 MW (= 4.3–1.4). So the total heating energy savings will be 1.88 + 2.9 = 4.78 MW.

Another set of relocation modifications are proposed to improve the energy efficiency of the network which are relocating exchangers E-26, E-06 and E-12 to the new locations shown in Fig. 7; E-26 renamed as E-D between streams #8 and #27,

Table 2 Heat exchangers cost model

New heat exchanger cost ($)	$(6000 + A \times 200)$
Exchanger additional area cost ($)	$1530 \times (\text{additional area})^{61}$
Relocating and resequencing cost ($)	35,000

Table 3 Energy savings

	Actual case (MW)	Revamped case	Energy target (MW)	Energy savings (MW)
Hot utility consumption	45.3	40.5	40.1	4.8 (hot)
Cold utility consumption	94	89.5	82	4.5 (cold)
Hot utility saving %	–	–	–	10.6%
Cold utility saving %	–	–	–	5%

E-06 renamed as E-E between streams #20 and #26, and finally E-12 renamed as E-C between streams #20 and #32 (see Fig. 7). These relocation modifications are to integrate heat below the pinch and remove the violation of integrating heat across the pinch as identified in Fig. 6 previously.

Capital investment of the above modifications is calculated from Table 2, as new exchanger units, relocation costs, and additional costs. Energies of modified exchangers are shown in Fig. 7. It can be noted that the heating requirement of heater E-25 from 4.3 to 1.4 MW, while the heaters E-27 (0.74 MW), E-28 (0.74 MW) and E-29 (0.4 MW) are reduced to zero. Therefore, the total energy savings are 4.8 MW overall (see Table 3). A substantial cut in CO_2 emissions is expected as a result of this energy saving. The annual energy cost savings are estimated to be 3,128,854 $, while the total capital investment of exchangers is 321,819 $, leading to a payback time of 0.2 years.

4　Conclusion and Recommendations

A case study of delayed coker existing in a modern Egyptian refinery was considered for revamping application. A revamping method was proposed to modify existing HENs for maximum energy efficiency. The revamping method was based on Pinch Analysis and rigorous simulation. An algorithm for revamping has been proposed to modify existing networks of delayed coker units for maximum energy efficiency. The revamping procedure starts with data collection, network simulation and validation, after which energy targets are identified using Pinch Technology techniques.

Given the energy targets and composite curves, violations to Pinch Analysis can be detected leading to a number of potential modifications to overcome the violations in the existing network. Then, modifications are implemented to improve the energy integration within the network for reducing the external energy consumption and hence carbon emissions. The case study considered was a delayed coker unit producing LPG, naphtha, LGO, HGO and coke with total production capacity of 147.3 t/h. The existing network of the delayed coker consists of 29 exchangers with minimum temperature approach of 15 °C. The current heating and cooling loads are 39(10)6 kcal/h and 81(10)6 kcal/h respectively. The revamping of the case study proposed were 4 new exchangers, relocation of 3 exchanger units and additional areas to some existing equipment. The overall modification resulted in an energy saving of 4.8 MW, with corresponding cut in carbon emissions, and annual energy cost savings of 3,128,854 \$, and the payback time is less than a year. SDGs #12 and #13 are both achieved in this research resulting from maximizing energy efficiency and lowering the release of greenhouse gases to the atmosphere (CO_2).

References

1. Gadalla MA (2015) A new graphical method for pinch analysis applications: heat exchanger network retrofit and energy integration. Energy 81:159–174
2. Wang B, Klemeš JJ, Li N, Zeng M, Varbanov PS, Liang Y (2021) Heat exchanger network retrofit with heat exchanger and material type selection: a review and a novel method. Renew Sustain Energy Rev 138:1–26
3. Gadalla MA, Abdelaziz OY, Ashour FH (2016) Conceptual insights to debottleneck the network pinch in heat-integrated crude oil distillation systems without topology modifications. Energy Convers Manag 126:329–341
4. Alhajri IH, Gadalla MA, Abdelaziz OY, Ashour FH (2021) Retrofit of heat exchanger networks by graphical pinch analysis—a case study of a crude oil refinery in Kuwait. Case Stud Therm Eng 26:101130
5. Gundersen T (2013) Heat integration—targets and heat exchanger network design. 1 Introduction to key concepts and major topics, chap 2.1. In: Handbook of process integration, pp 1–44
6. Piagbo BK, Dagde KK (2013) Heat exchanger network retrofit design by eliminating cross pinch heat exchangers. Am J Eng Res 2(05):11–18
7. Smith R (2005) Chemical process: design and integration, 1st edn. Wiley
8. Kemp IC (2007) Pinch analysis and process integration: a user guide on process integration for the efficient use of energy. Pinch Anal Process Integr 416
9. CANMET Energy Technology Centre (2003) Pinch analysis: for the efficient use of energy, water and hydrogen vol 11, no 4
10. Safder U, Ifaei P, Yoo CK (2020) A novel approach for optimal energy recovery using pressure retarded osmosis technology: chemical exergy pinch analysis—case study in a sugar mill plant. Energy Convers Manage 213:112810
11. Ravi Kumar K, Krishna Chaitanya NVV, Sendhil Kumar N (2021) Solar thermal energy technologies and its applications for process heating and power generation—a review. J Cleaner Prod 282, 125296
12. Linnhoff B, Townsend D, Boland D, Hewitt G, Thomas B, Guy A, Marsland R (1982) User guide on process integration for the efficient use of energy. Institution of Chemical Engineers, Rugby, UK

13. Gai L, Varbanov PS, Klemeš JJ, Sun L (2020) Hierarchical targeting of hydrogen network system and heat integration in a refinery. Chem Eng Trans 81:217–222
14. Nptel (2006) Lecture 1: heat exchangers classifications. Chem Eng Des II 1–41
15. Bassiri R (2008) C and 600, vol 1509, no 5, pp 3503–3503
16. Hogskola CT, View S, Nordman R (2015) New process integration methods for heat-saving retrofit projects in industrial systems new process integration methods for heat-saving retrofit projects in industrial systems, no Jan 2005
17. Kamel DA, Gadalla MA, Abdelaziz OY, Labib MA, Ashour FH (2017) Temperature driving force (TDF) curves for heat exchanger network retrofit—a case study and implications. Energy 123:283–295
18. Gadalla M, Jobson M, Smith R (2003) Optimization of existing heat-integrated refinery distillation systems. Chem Eng Res Des 81(1):147–152
19. Klemeš JJ, Wang QW, Varbanov PS, Zeng M, Chin HH, Lal NS, Li NQ, Wang B, Wang XC, Walmsley TG (2020) Heat transfer enhancement, intensification and optimisation in heat exchanger network retrofit and operation. Renew Sustain Energy Rev 120:1–31
20. Li BH, Chota Castillo YE, Chang CT (2019) An improved design method for retrofitting industrial heat exchanger networks based on pinch analysis. Chem Eng Res Des 148:260–270
21. Gadalla MA (2015) A novel graphical technique for pinch analysis applications: energy targets and grassroots design. Energy Convers Manage 96:499–510
22. Gadalla MA (2015) A new graphical method for pinch analysis and energy integration. Chem Eng Trans 43:1291–1296
23. El-Halwagi MM (2012) Sustainable design through process integration: fundamentals and applications to industrial pollution prevention, resource conservation, and profitability enhancement. Elsevier Inc.
24. Clavijo Mesa MV, Patino-Rodriguez CE, Guevara Carazas FJ, Gunawan I, Droguett EL (2021) Asset management strategies using reliability, availability, and maintainability (RAM) analysis. J Braz Soc Mech Sci Eng 43(11)
25. Biao X, Lei Y, Jichang L, Xinglong Q, Wenxin Y, Jinquan X, Lixin H, Hangzhou W, Ye J, Diannan L, Jigang Z, Hui S, Hao L (2021) Reaction network of sulfur compounds in delayed coking process. Chem Eng J 422:129903
26. Lei Y, Xinglong Q, Alqubati M, Lixin H, Jichang L, Jinquan X, Wenxin Y, Xin P, Xin H, Jigang Z, Hui S, Hao L (2022) Coupling simulation of delayed coking and hydrotreating process at molecular level. Chem Eng J 449:137543
27. Al-Haj H (2012) Fouling in heat exchangers. MATLAB Fundam Tool Sci Comput Eng Appl 3